ICFM10

PROCEEDINGS OF THE

10th INTERNATIONAL CONFERENCE ON FLOOD MANAGEMENT

Adapting to Global Change:
Innovative Approaches to Flood Management and Resilience

London, Ontario, Canada
May 2026

Edited by
Slobodan P. Simonovic
Chairperson, ICFM Ad Hoc Committee

INTERNATIONAL CONFERENCES ON FLOOD MANAGEMENT (ICFM)

www.icfm10.com

Hosts: Western University Faculty of Engineering

Institute for Catastrophic Loss Reduction

Partners: Public Safety Canada

Natural Resources Canada

Introduction

The papers presented in these proceedings reflect the collective efforts of the international community engaged in advancing the science and practice of flood management. The 10th International Conference on Flood Management, held in London from May 20–22, 2026, continues a distinguished series of conferences that, since 2000, have provided a unique global platform for addressing one of the most pressing natural hazards affecting society.

Floods remain the most frequent and devastating natural disasters worldwide, with increasing impacts driven by climate change, rapid urbanization, land-use transformation, and socio-economic development. Addressing these challenges requires integrated, multidisciplinary approaches that combine advances in hydrology, engineering, environmental science, data analytics, policy, and community engagement. The ICFM series has consistently fostered such collaboration, bringing together researchers, practitioners, policymakers, and stakeholders to exchange knowledge and develop innovative solutions.

The theme of ICFM10, “Adapting to Global Change: Innovative Approaches to Flood Management and Resilience,” highlights the urgent need to transition from traditional flood control toward adaptive, risk-informed, and resilience-based strategies. Contributions in this volume address a wide range of topics, including flood hazard and risk assessment, forecasting and early warning systems, nature-based solutions, infrastructure resilience, climate change impacts, governance, and community-based adaptation.

These proceedings demonstrate the growing role of emerging technologies—such as high-resolution modeling, remote sensing, artificial intelligence, and impact-based forecasting—in improving our ability to anticipate and manage flood risks. At the same time, they emphasize that effective flood management must integrate technical innovation with social, institutional, and policy dimensions, recognizing the importance of stakeholder participation and local context.

The editors hope that this volume will serve as a valuable resource for researchers, practitioners, and decision-makers worldwide. By capturing the latest developments and lessons learned, it contributes to the ongoing effort to reduce flood risk, enhance resilience, and support sustainable development in an increasingly uncertain and changing world.

The editors would like to express their sincere appreciation to all authors for their valuable contributions to this volume and to the reviewers for their careful evaluations and dedicated efforts in maintaining the quality of the proceedings. We also extend our gratitude to the members of the Local Organizing Committee and the International Scientific Committee for their guidance and commitment in organizing the conference and preparing these proceedings. Special thanks are due to all administrative assistants and technical staff whose support made this work possible.

On behalf of the International Conference on Flood Management (ICFM),

Slobodan P. Simonovic

Chairperson, ICFM Ad Hoc Committee

London, Ontario, Canada

May 2026

Chapter 1 Global change and emerging flood risks

1.1 Changing flood regimes and extremes under climate change
1.2 Compound and cascading flood risks

Chapter 2 Flood risk assessment, data and modeling

2.1 Flood hazard and risk mapping across spatial scales
2.2 Advanced flood modelling
2.3 Use of emerging data sources
2.4 Flood forecasting and early warning systems, including ungauged basins
2.5 Uncertainty, causality, and confidence in flood risk information

Chapter 3 Urban flooding and infrastructure systems

3.1 Drivers of urban flooding and interactions with the urban water cycle
3.2 Urban flood mitigation and stormwater management strategies
3.3 Flood impacts on infrastructure and critical services, including cascading failures

Chapter 4 Flood resilience, adaptation, and recovery

4.1 Community, infrastructure, and system resilience to flooding
4.2 Adaptation strategies under increasing flood risk

Chapter 5 Governance, policy, and societal engagement

5.1 Flood risk governance, policy frameworks, and institutional coordination
5.2 Bridging science, policy, and practice through transdisciplinary approaches
5.3 Financing flood risk reduction, insurance, and risk transfer mechanisms
5.4 Role of communities, citizen science, and non-traditional actors in flood risk management

Chapter 1 - Global change and emerging flood risks

1.1 Changing flood regimes and extremes under climate change

ICFM 10
Adapting to Global Change:
Innovative Approaches to Flood Management and Resilience
May 20-22, 2026 | Western University, London, Ontario, Canada

Historical attribution and future projections of extreme flooding in the transboundary Saint John River Basin

Rajesh R. Shrestha, Alex J. Cannon, Carter Conboy
Climate Research Division, Environment and Climate Change Canada, Victoria, BC, Canada
E-mail: rajesh.shrestha@ec.gc.ca, alex.cannon@ec.gc.ca, carter.conboy@ec.gc.ca

ABSTRACT

The transboundary Saint John River Basin, which covers parts of the provinces of Quebec and New Brunswick in Canada and the state of Maine in the United States, experienced extreme flooding in 2008, 2018, and 2019, with the record-breaking 2018 flood event causing estimated damages of about $75 million in Canada. In this study, we employ a large-scale hydrologic modelling system to characterize these flood events in the context of historical, recent and future climates. Specifically, by conditioning the model on dominant hydroclimatic drivers, we identify anomalously high winter snowpack and spring precipitation as the main drivers of these floods. Furthermore, we show that the events would be even more severe when the two extreme drivers—namely, high winter snowpack and spring precipitation—co-occur. Additionally, by driving the model with an ensemble of statistically downscaled global climate models, we find a small decrease in the intensity of extreme events (e.g. 10–100-year return period) between the historical period (1955–1974) and the recent period (2001–2020). However, projections for the near-future period (2031–2050) suggest an intensification of extreme flooding beyond the most severe historical flood event. Future intensification of flooding occurs despite the projected decline in snowpack, suggesting an increasingly influential role of extreme spring precipitation in driving these floods. Overall, these results underscore the need for adaptation planning to address current and future flood hazards in the region.

KEYWORDS: extreme value analysis**,** future projections, hydroclimatic drivers, hydrological modelling, Saint John River Basin.

1 INTRODUCTION

The transboundary Saint John River, which flows through the provinces of Quebec and New Brunswick in Canada and the state of Maine in the United States within a drainage area of about 55,000 km^2 (Figure 1), is one of the most flood prone rivers in the region. Three large flood events occurred in the basin in 2008, 2018, and 2019, causing extensive property damage and economic losses (Newton and Burrell 2016; Rickard et al. 2025). Specifically, the 2008 flood event was the worst spring flooding in the preceding 35 years in New Brunswick, affecting about 1600 properties and causing damages exceeding Can$23 million (Newton and Burrell 2016; NBGELG 2025). Although the floodwater level in the 2018 event was lower than that of the 2008 event, estimated damages (about Can$75 million) in New Brunswick in 2018 were higher than in 2008 (NBGELG 2025; Rickard et al. 2025). The damages from the 2019 event were lower despite having the peak flow similar to 2018, which was attributed to better flood preparedness (NBGELG 2025). The flood events also caused disruptions to hydropower production from the Saint John River's seven run-of-the-river hydroelectric dams, with floodwater overwhelming the dams' capacity and freely flowing through the spillway, causing substantial financial losses for New Brunswick Power (Web-1). The economic losses and impacts on the communities underscore the need for a better understanding of current and future hazards in the basin.

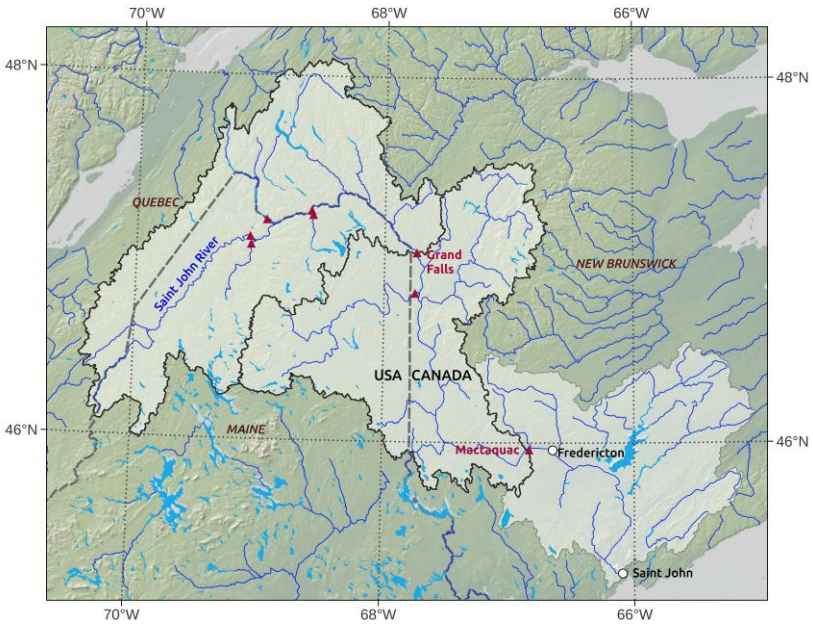

Figure 1. Location map of the Saint John River basin, including the hydrometric stations ▲ used for model calibration.

Floods in the Eastern Maritime region of Canada—where the Saint John River basin is located—primarily occur between March and May, generated by snowmelt, heavy spring precipitation, rain-on-snow events, and augmented by river ice-jamming (Buttle et al. 2016; Newton et al. 2024). Rickard et al. (2025) characterized the main drivers of the three flood events in terms of positive anomalies in winter and spring total precipitation and snow water equivalent (SWE), combined with spring rain-on-snow events. Furthermore, ongoing hydroclimatic changes, especially increasing trends in mean, minimum and maximum air temperature, together with some increases in precipitation, are affecting the magnitude and timing of spring high flows in the region (Caissie and El-Jabi 2024). Additionally, projected increases in precipitation and temperature in the basin can be expected to impact future flood flows and associated risks (El-Jabi et al. 2016; Yousfi et al. 2025).

In this study, we assess current and future flood hazards in the Saint John River basin by using a large-scale hydrological modelling system, the Community Water Model (CWatM) (Burek et al. 2020). Specifically, we drive CWatM with a combination of initial conditions and hydroclimatic drivers conditioned on recent flood events to characterize these events and assess the potential for more extreme events. Furthermore, we drive CWatM with an ensemble of statistically-downscaled Global Climate Models (GCMs) from the Coupled Model Intercomparison Project Phase 6 (Eyring et al. 2016) to assess changes in extreme flows from historical to recent and future climates.

2 METHODS

2.1 Hydrologic Modelling

We set up the CWatM hydrological model (Burek et al. 2020) to simulate historical and future flood response in the Saint John River basin. CWatM is a large-scale, semi-distributed hydrological model developed for global- to regional-scale applications, and the model has been used in previous assessments of historical and future floods (Boulange et al. 2021; Shrestha et al. 2025; Zhao et al. 2025). The model

includes a representation of cold-region processes, including snow accumulation and melt, as well as soil water movement through frozen soil. In this study, we used CWatM version 1.081 with the radiation-restricted degree-day factor snowmelt routine (Erlandsen et al. 2021), which has been modified to account for snow albedo decay (Shrestha et al. 2025).

We employed CWatM at a 5-arcmin resolution, with sub-grid variability in snow and land cover, using static geospatial data provided by the model developers (Web-2). We divided the CWatM setup for the Saint John River basin into upstream and downstream subbasins with outlets at the Grand Falls and Mactaquac hydrometric stations, respectively (Figure 1). We calibrated CWatM parameters for the upstream subbasin by sub-dividing it further into six sub-subbasins, and the downstream subbasin by subdividing it into two sub-subbasins and using flows at the Grand Falls station as inflow. We used flows from each of the six stations in the upstream basin and two stations in the downstream basin as objective functions for calibrating CWatM in a multi-objective framework using the non-dominated sorting genetic algorithm (NSGA-II) (Deb et al. 2002) as implemented in the Python DEAP package (Fortin et al. 2012). Calibration and validation periods consisted of the years 2007-2019 and 1995-2006, respectively.

2.2 Climate Data and Downscaling

We used daily maximum, minimum and mean temperature, total precipitation, downward longwave and shortwave radiation, relative humidity, surface pressure and wind speed from the Canadian Surface Reanalysis (CaSR) version 3.2 (Gasset et al. 2021) as forcing data to calibrate CWatM, and as target data for statistical downscaling. CaSR is a dynamically downscaled observational product based on the Regional Deterministic Reforecast System (RDRS). Gridded precipitation in CaSR is from an offline precipitation analysis using forecast values from RDRS as the background field. CaSR v3.2 has a spatial resolution of ~10 km, spans the period 1980-2024, and covers the entire North American domain. A key advantage of using CaSR for the transboundary Saint John basin is its spatial consistency, i.e. the dataset is not affected by discontinuity at the border.

We used six ensemble members from four CMIP6 GCMs that participated in the High Resolution Model Intercomparison Project (HighResMIP) (Haarsma et al. 2016). The HighResMIP GCMs were selected because of higher spatial resolution (at least 50 km in the atmosphere and 0.25° in the ocean), which reduces the scale of spatial disaggregation between the GCM and target CaSR dataset during downscaling. The selected GCMs span the historical period of 1950-2014 and the future period of 2015-2050 under the Shared Socioeconomic Pathways (SSP) 5-8.5 scenario.

We employed the n-dimensional probability density function transform and multivariate bias correction method (MBCn) (Cannon 2018) to spatially disaggregate and bias-correct GCM outputs to the resolution of the CaSR dataset. This method preserves the multivariate dependence of the target observational data, which is an important consideration for multivariate climate and hydrological extremes. The downscaling was done at the daily time step and includes all variables required for running CWatM, namely: maximum, minimum and mean temperature, total precipitation, downward longwave and shortwave radiation, relative humidity, surface pressure and wind speed.

We forced CWatM with the statistically downscaled GCM outputs and assessed the effect of long-term climate change on extreme flood events. We considered three periods: the historical period of 1955-1974, the recent period of 2001-2020, and the near-future period of 2031-2050 under the SSP5-8.5 scenario, which approximately correspond to 0.25 °C, 1.0 °C, and 2.0 °C of warming, respectively, since the preindustrial period of 1850-1900 (Forster et al. 2023).

2.3 Analyses

To assess the drivers of the flood events of 2008 and 2018, we ran conditional CWatM simulations by combining: i) April 1 initial condition of the flood year with April-August meteorological forcing from 2001-2020, and ii) April 1 initial condition from 2001-2020 with April-August meteorological forcing

from the flood year, excluding the drivers of the remaining flood events in all cases. For example, to assess the role of snowpack on 2008 flooding, we combined April 1 initial condition from 2008 with the 2001-2007, 2009-2017, and 2020 April-August meteorological drivers. Similarly, to assess the role of spring conditions on the 2008 flood, we combined the 2008 April-August meteorological drivers with April 1 initial condition from 2001-2007, 2009-2017 and 2020.

We analyzed extreme value statistics of annual maximum flows for each of the 20-year historical, recent and future periods, by assuming stationarity over each period, but non-stationarity across the three periods. Specifically, for each 20-year period, we combined all annual maximum flow values from the six-member GCM ensemble driven CWatM simulations and fitted the Generalized Extreme Value (GEV) distribution for the combined sample size of 120. The GEV distributions were fitted using the L-moments parameter estimation (Hosking 1990) (Hosking and Wallis, 1993), as implemented in the R extRemes package (Gilleland 2024).

3 RESULTS

3.1 CWatM calibration/validation

In this paper, we focus on the results for the Saint John River at Grand Falls station. The performance of the calibrated CWatM model generally indicates a good ability to represent the dynamics of streamflow hydrograph, with the Kling–Gupta efficiency (KGE) of 0.85 and 0.80 for the calibration and validation periods, respectively. However, the model had difficulty in replicating the peak flow magnitudes of some flood events, e.g. the 2019 event (Figure 2a). These discrepancies arise from a number of sources of uncertainties, including: i) forcing data, e.g. representativeness of precipitation and temperature in the CaSR reanalysis data; ii) observed streamflow data, e.g. estimated flows based on water levels, especially when affected by river ice; and iii) model structure, i.e. representation of underlying physical processes in the CWatM model. Nevertheless, the comparison of the quantiles of the observed versus simulated annual peak flows indicates a reasonable ability of the model to reproduce the distribution of extremes (Figure 2b), except for the maximum of all events.

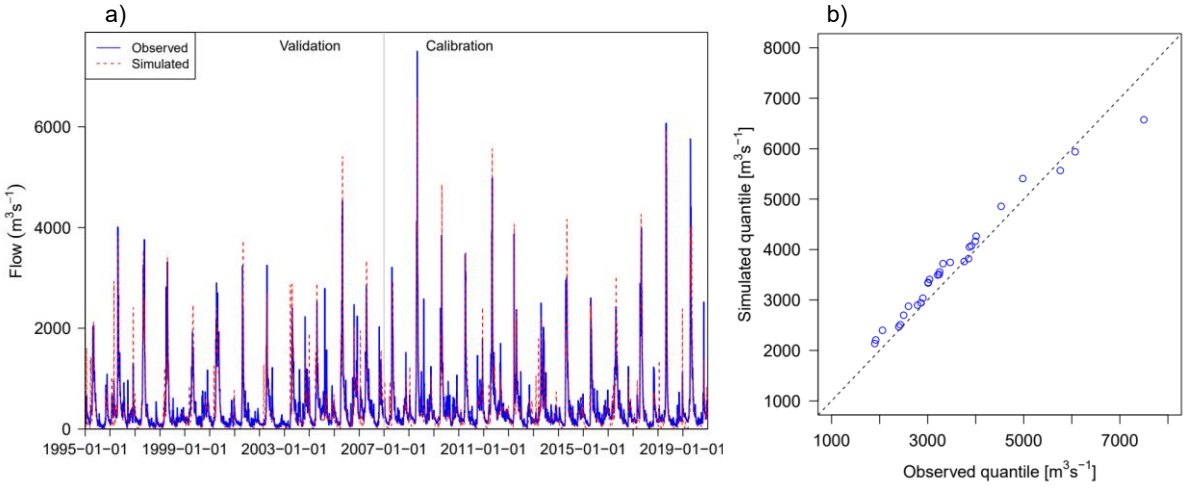

Figure 2: Observed vs. CWatM simulated discharge at the Saint John River at Grand Falls station: a) calibration (2007-2019) and validation (1995-2006) results; b) quantile–quantile plot of the distribution of observed vs. simulated annual peak flows over both calibration and validation period.

3.2 Effects of the drivers on the 2008 and 2018 flood events

The 2008 and 2018 flood events occurred between April 23 and May 12 (Rickard et al. 2025), and based on CWatM simulations, 2008 and 2018 April 1 SWE values are about 86% and 30% above 2001-2020 mean value, with the 2008 April 1 SWE value being highest over the entire period. April precipitation values were more variable, with the 2008 and 2018 values at about 8% and 35% of the 2001-2020 means, respectively.

The combined simulations i) and ii), corresponding to the drivers of the 2008 flood, revealed contrasting responses (Figure 3). Specifically, the simulations i) conditioned on the 2008 April 1 initial condition, show a substantial shift in the distribution of maximum flows, with the maximum of maximums about 29% higher, and 5 of 17 simulated flows higher than the 2008 event. This illustrates the potential for larger floods when the 2008 snowpack co-occurs with higher spring precipitation than in 2008. Furthermore, the large shift in the distribution of flows between 2001-2020 and simulations i), illustrate the dominant effect of the anomalously large snowpack on the 2008 flood event. The simulations ii), conditioned on the 2008 April-August meteorological drivers, resulted in a lower maximum of maximums and smaller shift in the distribution. This suggests limited effect of the spring meteorological conditions on the 2008 flood event.

The simulations i) and ii), corresponding to the 2018 flood event, both show maximum of maximums approximately equal to the 2018 event. Hence, the combinations of drivers of the 2018 flood event with 2001-2020 hydroclimatic conditions, excluding those from the 2008 and 2019 events, do not lead to a larger flood than in 2018. However, the differences in shifts in the distribution of maximum flows in the two sets of simulations indicate their differing influences on the 2018 flood event. Specifically, the smaller shift in simulations i) suggests smaller effect of the April 1 snowpack, while the larger shift in simulations ii) suggests larger effect of the spring meteorological drivers.

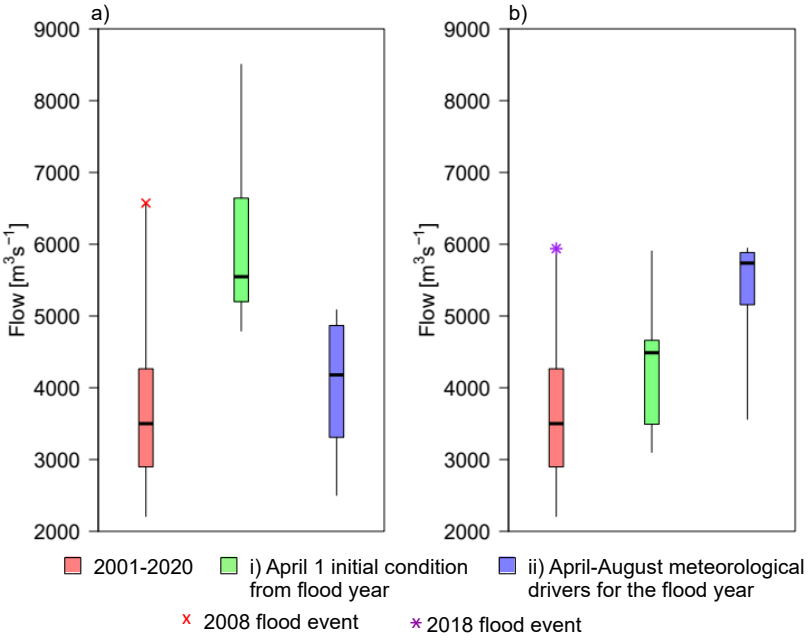

Figure 3: 2001-2020 simulated discharge together with simulations conditioned on: i) April 1 initial condition and, ii) April-August meteorological drivers corresponding to a) 2008 flood event and b) 2018 flood event. Boxplots depict interquartile ranges and whiskers depict maximum and minimum. The simulations i) and ii) for a) excludes the forcings from the 2018 and 2019 events and simulations i) and ii) for b) excludes forcings from the 2008 and 2019 events.

3.3 Comparison with historical and future simulations

The comparison of simulated April 1 SWE over the historical (1955-1974), recent (2001-2020) and near-future (2031-2050) periods generally shows successive declines over the three periods, indicating the influence of warming temperatures on snowpack storage in the basin. The decreases in snowpack occur despite increases in precipitation between each period, suggesting a warmer temperature-driven increase in the rainfall fraction of total precipitation. In general, maximum flows increase progressively from historical to recent to near-future periods. However, the maximum of the six-member ensemble for the recent period is lower than that of the historical period, indicating the variability across the ensembles used.

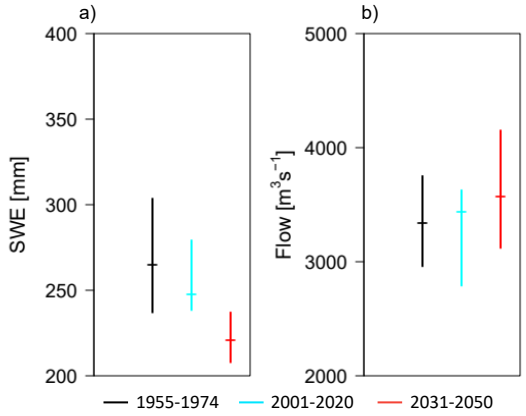

Figure 4: Comparison of simulated a) April 1 SWE and b) maximum flow over the historical (1955-1974), recent (2001-2020) and near-future (2031-2050) periods. The ranges show maximum, median and minimum values obtained from the 20-year means of each of the 6-member GCM driven CWatM simulations.

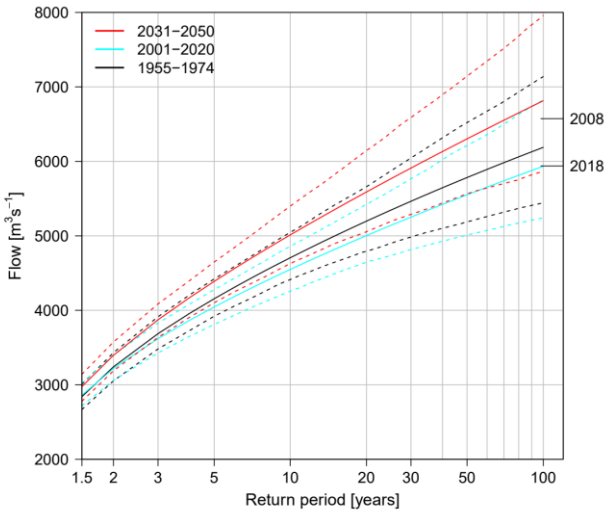

Figure 5. Flood frequency curves obtained by fitting the GEV distribution on the annual maximum flows. All GCM ensemble members are combined for the GEV fitting, and the dashed lines show the 95% confidence intervals of the fitted distribution. The years on the right axis indicate flows for two highest-recorded historical flood events.

We also analyzed the changes in flood frequencies across the three periods by fitting the GEV distribution to the annual maximum flows from all GCM ensemble members combined (Figure 5). The comparison of results between the historical and recent periods shows similar flows for floods of smaller

return periods (e.g. 1.5- and 2-year flood events). However, the curves diverge at higher return periods, which is consistent with the lower maximum for the recent period when the 20-year means of the GCM-driven simulations are compared (Figure 4). The projected flows for the 2031-2050 near-future period are higher than both the historical and recent periods at all return periods. Consequently, the return period of the 2018 flood event decreases from about 101-year to 31-year between the recent and near-future periods, respectively. Likewise, the return period of the 2008 flood event decreases from about 354-year to 72-year between the two periods, respectively. Hence, the model simulations suggest an intensification of extreme flooding in the near-future period, with flood events beyond the highest historical flood event of 2008 becoming increasingly common. Furthermore, future intensification of flooding occurs despite the projected decline in snowpack, suggesting an increasingly influential role of extreme spring precipitation in driving these floods.

4 CONCLUSION

This study provides an evaluation of historical, recent and future changes in flood hazard in the Saint John River basin in the context of the 2008, 2018 and 2019 flood events. We employ a large-scale hydrologic modelling system CWatM to characterize these flood events. Our evaluation identified the anomalously high snowpack as the main drivers of the 2008 flood event, and both high winter snowpack and spring precipitation as the drivers of the 2018 event. Furthermore, the results show the potential for flood events larger than the observed, under the compounding influence of high snowpack (such as in 2008), and high spring precipitation. Our evaluation also showed a general decrease in snowpack depth but an increase in maximum flows progressively from historical (1955-1974) to recent (2001-2020) to near-future (2031-2050) periods. In terms of the return periods of extreme maximum flow, the projections show small increases between the historical and recent periods, but larger decreases between the recent and future periods. This suggests future intensification of extreme flooding beyond the most severe historical flood events. Overall, these results underscore the need for an adaptation planning against current and future flood hazards in the region.

REFERENCES

Boulange J, Hanasaki N, Satoh Y, et al (2021) Validity of estimating flood and drought characteristics under equilibrium climates from transient simulations. Environ Res Lett 16:104028. https://doi.org/10.1088/1748-9326/ac27cc

Burek P, Satoh Y, Kahil T, et al (2020) Development of the Community Water Model (CWatM v1.04) – a high-resolution hydrological model for global and regional assessment of integrated water resources management. Geoscientific Model Development 13:3267–3298. https://doi.org/10.5194/gmd-13-3267-2020

Buttle JM, Allen DM, Caissie D, et al (2016) Flood processes in Canada: Regional and special aspects. Can Water Resour J 41:7–30. https://doi.org/10.1080/07011784.2015.1131629

Caissie D, El-Jabi N (2024) Hydrometeorological trends under a changing climate in New Brunswick Part 1 of 2: Final Report

Cannon AJ (2018) Multivariate quantile mapping bias correction: an N-dimensional probability density function transform for climate model simulations of multiple variables. Clim Dyn 50:31–49. https://doi.org/10.1007/s00382-017-3580-6

Deb K, Pratap A, Agarwal S, Meyarivan T (2002) A fast and elitist multiobjective genetic algorithm: NSGA-II. IEEE Transactions on Evolutionary Computation 6:182–197. https://doi.org/10.1109/4235.996017

El-Jabi N, Caissie D, Turkkan N (2016) Flood analysis and flood projections under climate change in New Brunswick. Canadian Water Resources Journal / Revue canadienne des ressources hydriques 41:319–330. https://doi.org/10.1080/07011784.2015.1071205

Erlandsen HB, Beldring S, Eisner S, et al (2021) Constraining the HBV model for robust water balance assessments in a cold climate. Hydrology Research 52:356–372. https://doi.org/10.2166/nh.2021.132

Eyring V, Bony S, Meehl GA, et al (2016) Overview of the Coupled Model Intercomparison Project Phase 6 (CMIP6) experimental design and organization. Geoscientific Model Development 9:1937–1958. https://doi.org/10.5194/gmd-9-1937-2016

Forster PM, Smith CJ, Walsh T, et al (2023) Indicators of Global Climate Change 2022: annual update of large-scale indicators of the state of the climate system and human influence. Earth System Science Data 15:2295–2327. https://doi.org/10.5194/essd-15-2295-2023

Fortin F-A, De Rainville F-M, Gardner M-AG, et al (2012) DEAP: evolutionary algorithms made easy. J Mach Learn Res 13:2171–2175

Gasset N, Fortin V, Dimitrijevic M, et al (2021) A 10 km North American precipitation and land-surface reanalysis based on the GEM atmospheric model. Hydrology and Earth System Sciences 25:4917–4945. https://doi.org/10.5194/hess-25-4917-2021

Gilleland E (2024) extRemes: Extreme Value Analysis

Haarsma RJ, Roberts MJ, Vidale PL, et al (2016) High Resolution Model Intercomparison Project (HighResMIP v1.0) for CMIP6. Geoscientific Model Development 9:4185–4208. https://doi.org/10.5194/gmd-9-4185-2016

Hosking JRM (1990) L-Moments: Analysis and Estimation of Distributions Using Linear Combinations of Order Statistics. Journal of the Royal Statistical Society: Series B (Methodological) 52:105–124. https://doi.org/10.1111/j.2517-6161.1990.tb01775.x

NBGELG (2025) Flood History Database, Saint John River (Watershed). https://www.elgegl.gnb.ca/0001/en/Flood/Search?LocationName=Saint+John+River+%28watershed%29. Accessed 3 Dec 2025

Newton B, Beltaos S, Burrell BC (2024) Ice regimes, ice jams, and a changing hydroclimate, Saint John (Wolastoq) River, New Brunswick, Canada. Nat Hazards 120:12613–12642. https://doi.org/10.1007/s11069-024-06736-5

Newton B, Burrell BC (2016) The April–May 2008 flood event in the Saint John River Basin: Causes, assessment and damages. Canadian Water Resources Journal / Revue canadienne des ressources hydriques 41:118–128. https://doi.org/10.1080/07011784.2015.1009950

Rickard LJ, Déry SJ, Stewart RE, Thériault JM (2025) Meteorologically Related Factors Leading to the 2008, 2018, and 2019 Major Spring Floods in the Transboundary Saint John River (Wolastoq) Basin. Journal of Hydrometeorology 26:201–220. https://doi.org/10.1175/JHM-D-24-0032.1

Shrestha RR, Cannon AJ, Hoffman S, et al (2025) Benchmarking historical performance and future projections from a large-scale hydrologic model with a watershed hydrologic model. Hydrology and Earth System Sciences 29:2881–2900. https://doi.org/10.5194/hess-29-2881-2025

Yousfi N, El Adlouni S, Gachon P (2025) Non-stationary and multivariate spring floods estimation of the Saint John River (eastern Canada). Stoch Environ Res Risk Assess 39:3063–3084. https://doi.org/10.1007/s00477-025-03008-x

Zhao F, Nie N, Liu Y, et al (2025) Benefits of Calibrating a Global Hydrological Model for Regional Analyses of Flood and Drought Projections: A Case Study of the Yangtze River Basin. Water Resources Research 61:e2024WR037153. https://doi.org/10.1029/2024WR037153

Web sites

Web-1 https://www.cbc.ca/news/canada/new-brunswick/mactaquac-dam-flood-2018-1.4948716, accessed 5 December 2025

Web-2 ftp://rcwatm:Water1090@ftp.iiasa.ac.at/, accessed 3 December 2025

Reframing resilience to guide indicator identification for index-based coastal flood resilience assessments within the UK's nuclear decommissioning sites

Michael Landry[1*], Sarah Percival[1], Joshua Griffiths[2,3], Nicholas Smith[1,2,3]
1 Liverpool John Moores University
2 United Kingdom National Nuclear Laboratory
3 University of Liverpool
Email: M.W.Landry@2024.ljmu.ac.uk

ABSTRACT

There is a significant lack of research regarding the coastal flood resilience of nuclear decommissioning sites, an issue that necessitates continuous assessment. As climate change associated sea level rise (SLR) projections are fuelling concerns about the long-term safe management of radiological inventory, and efficient progression of decommissioning, emphasised by the growing number of facilities entering decommissioning phases globally. A significant collection of literature was reviewed to collectively inform the reframing of resilience, which also aims to guide the development of coastal flood resilience index assessments through identification of indicators. Within this paper, resilience was reframed as the ability of the decommissioning site to maintain continuous essential operations, respond effectively, incorporate adaptations, and retain essential objectives. This approach presented decommissioning sites as systems, highlighting elements within dimensions that strongly influence resilience capabilities, further informed by the widely recognised framework (seismic resilience) that identifies key qualities required for sufficient resilience within a system. Focus on requirements of maintaining continuous essential operations was underpinned by the need to represent operational degradation and responses required to understand when resilience is being lost, and when it is no longer resilient, represented through thresholds. Overall, the synthesis of these elements into a reconceptualised resilience ability applicable for decommissioning contexts is significantly beneficial. As it provides a foundation not only for future research towards resilience in decommissioning sites, but for practical application, particularly in aiding index-based assessments with indicator identification within nuclear decommissioning sites for coastal flood and general natural hazard resilience.

1 INTRODUCTION:

Flooding is understood as the UK's most frequent and detrimental natural hazard, with coastal flooding ranked as the second highest risk for causing civil emergency, posing increasing risk for the UKs coastal zones (Hendry et al 2019), a significant issue that has impacted the UK previously. Such as the 1953 'North Sea Flood' storm surge that impacted the UKs east coast, causing approximately £1.2bn in damage (current value) and 307 deaths (Haigh et al 2017). In December 2013, the UK was hit by Storm Xaver, where extreme storm conditions generated comparable water levels to 1953 measurements, impacting coastlines on the Southwest of England and West of Wales (Kendon and McCarthy 2015). Future climate change induced SLR projections and associated increases in the frequency and severity of storms linked to amplification of extreme water levels are fuelling concerns for the UKs coastal zones (Perks et al 2023). As these zones are home to 9 operational reactors at 4 sites (Heysham 1 and 2, Sizewell B, Hartlepool, and Torness), with new reactors proposed across coastal positions, and Hinkley Point C (Somerset coast) and Sizewell C (Suffolk) under construction (Web 1). Yet there are 17 former sites that have ceased operations and are undergoing decommissioning by the Nuclear Decommissioning Authority (NDA), with most on the coastline and projected to take decades to complete due to engineering challenges associated with ageing assets and radiological inventory (Foster et al 2021). Consequentially, their coastal positions will further risk safety, security, and existing challenges.

There is significant focus on improving the natural hazard resilience for current and planned nuclear plants globally (Portugal-Perreira et al 2024), but a significant gap regarding the assessment of hazard

resilience at decommissioning sites. It is imperative to tackle this, not only for the UK but globally, as nuclear reactor fleets are continuously aging and reaching the end of their lifespans, soon coming offline and entering decommissioning phases at an increasing rate (Wimmers and Von Hirschhausen 2023). This trend will result in an increasing number of coastal nuclear decommissioning sites that must be equipped with the tools and knowledge to assess coastal flood resilience.

A commonly utilised technique to assess resilience are index-based tools, consisting of the identification of a context's elements and combination into a comprehensive index to quantify resilience, requiring indicator determination to represent these elements (Marzi et al 2019). Indicators are understood as *'inherent characteristics that quantitatively estimates the condition of a system; they usually focus on minor, feasible, palpable and telling piece of a system'* (Balica et al 2012). But a lack of past frameworks or research to assist index-based assessments for coastal flood resilience is absent. Hence, to support determination of potential indicators, this paper undertook the challenge of reframing resilience to aid guidance, repurposing previous definitions and approaches to resilience in literature to achieve this.

2 METHODOLOGY:

The requirement of reframing resilience for nuclear decommissioning sites requires the gathering of existing relevant research, encompassing the need for a literature review. This paper could not use a *'systematic'* approach for this paper due to the lack of literature surrounding the topic when the search string *'Nuclear Decommissioning'* AND *'Coastal Flooding'* AND *'Resilience'* produced minimal results with no eligibility. This paper utilised a '*narrative review'*, a more useful approach for researching topics with a lack of an extensive literature base, providing a comprehensive overview (Greenhalgh et al 2018). The narrative review provided an overview of links between associated resilience literature to synthesise knowledge across an array of research areas, providing a comprehensive understanding. This allowed a broad exploration of literature resulting from the combination of string searches that were utilised to infer applicable elements that can be utilised in conjunction to understand how resilience can be reframed for nuclear decommissioning sites. The array of existing literature was continuously refined and analysed that allowed categorisation into 4 stages in the discussion of findings, aiding reframing resilience for application into nuclear decommissioning sites, aiding guidance of index-based assessments.

3 DISCUSSION OF FINDINGS

Stage 3.1. Preliminary Review – Foundational resilience concepts relevant to nuclear decommissioning contexts:

There are many resilience definitions in literature, but the prominent theme remains the ability to withstand external disturbances and recover effectively (Haque and Doberstein 2021). But resilience is not an all-encompassing concept, and its effective application requires consideration of multiple context dependant factors (Jones 2019). Lack of relevant resilience research for decommissioning sites required an understanding of previous resilience approaches, to bolster how it can be reframed and effectively assist in indicator identification guidance. The most relevant identified resilience perspectives included engineering, ecological, social-ecological, adaptive capacity, and system resilience, presented below:

Engineering resilience entails the ability of a system to return to a singular equilibrium following disturbance, judging resilience capabilities by the speed of return to a singular stable state (Li et al 2020). The requirement to incorporate an ability of adaptation and preparedness implementation to reduce the likelihood of future failure is heavily present (Zevenbergen et al 2020). This perspective initially seems too simplistic for a heavily complex decommissioning site, but the aspect regarding recovery speed (i.e. operational restoration) was deemed highly applicable.

Ecological resilience was pioneered by *Holling (1973)*, focusing on the ability of ecosystems to withstand disturbance without changing self-organised structures and processes, where a system can exist in multiple stable states if essential structures are retained and resilience sufficient (Dakos and Kéfi 2022). Focus is on elements required to continuously support essential key processes, significant to consider in indicator identification guidance due to influence upon a system. However, despite relevant components,

further review had to be undertaken to understand how related knowledge can be translated to aid reframing of resilience in decommissioning sites, leading to the social-ecological perspective.

The social-ecological resilience approach builds upon ecological and engineering perspectives to recognise resilience as a system's capacity to absorb disturbance, reorganise, and retain essential processes, recognising the interactions between human/engineered systems (e.g. decommissioning site) and natural systems (coastal zones) (Chaffin and Scown 2018). Focus on the need to re-organise to improve resilience links heavily to engineering and ecological approaches, reinforcing the importance of adaptation and reorganisation. Furthermore, this concept highlights the influence of the *'social'* dimension, underlining how social factors can influence resilience and adaptation ability through organisation, reflected across and supported by social, governance, or institutional domains (Hahn and Nykvist 2017), important to consider as the ability to incorporate adaptations in a system underpins the sufficiency of continuous resilience.

The consistent mention of *systems* within these resilience perspectives is significant to consider, as it illustrates a decommissioning site as composed of a range of elements responsible for the continuity of essential operations (Mentges et al 2023). Resilience within systems is understood as the ability to withstand disturbance, recover, and adapt, underpinned by the capability to maintain vital functions, where understanding internal actions are crucial to comprehend resilience (Hosseini et al 2016). Thus, decommissioning sites could be perceived as *systems,* encompassing a significant array of internal interconnected and interacting components responsible for continuous essential operations, influenced by internal actions. Therefore, approaching decommissioning sites as systems could reduce the complexity of understanding what elements are responsible for resilience and operating capabilities, simplifying identification of elements that can be translated to indicators for index-based resilience assessments.

Preliminary Review findings summary:

When applicable aspects identified were combined, resilience for a decommissioning site is reframed as the ability to maintain continuous essential operations, respond effectively and efficiently, continuously incorporate adaptations, and retain original objectives. Further review simplified this approach by portraying nuclear decommissioning sites as engineered/human systems with an array of interacting elements responsible for the systems resilience capabilities, where the interaction with the natural system (coastal zone) must be recognised. Furthermore, this section presented the significance of considering the engineering, natural, and social aspects due to understood influence upon resilience capabilities, reflected within the organisational, environmental, and human dimensions. These findings provide guidance on what areas should be considered within indicator identification, signifying the importance of focusing on elements that influence the presented resilience capabilities and dimensions (organisation, environmental, human) that underpin its effectiveness. But these findings that have aided reframing resilience had to be deemed practical for real-life examples and synergise with literature regarding resilience in nuclear contexts, to reinforce applicability.

Stage 3.2. Applicability of preliminary review findings within nuclear context literature:

This section refines the preliminary review's findings through application of the reframed resilience capability to real-life examples, aiming to reinforce applicability. These examples revolve around the 2011 tsunami that impacted the Northeastern coast of Japan, specifically, the Fukushima Daiichi Plant, Tokai No.2, Onagawa, and Fukushima Daini plants. In 2011, Fukushima Daiichi was subject to the 2011 earthquake and induced tsunami, interrupting operations, causing failure in reactor cooling processes and triggering a chain reaction resulting in eventual explosions within reactor buildings and release of significant radiological material (Hasegawa et al 2014). Impacts were significant, resulting in the widespread contamination of the surrounding area that caused mass evacuations, leading to the plant's shutdown and decommissioning (Ono 2021). This practical example was found to link heavily to preliminary review findings, as the plant was unable to **maintain continuous essential operations, respond effectively** to operational loss, and **essential objectives were lost**. The other 3 plants were also impacted and operations interrupted, but these plants were able to **maintain continuous essential operations** to **respond effectively** and safely reach reactor shutdown (Ibrion et al 2020), reinforcing preliminary review findings. But only Onagawa unit 2 (a reactor within the site) is in active operation since

restart in 2024, and the rest are either undergoing decommissioning or awaiting restart (Web 2), reinforcing the requirement of retaining essential objectives to remain sufficiently resilient.

Maintaining continuous operation as a key resilience capability is furthered by the requirement of safe long-term management of radiological inventory to prevent consequence (Jenkins et al 2020). Focus can be directed to elements that influence safe-management, aiding identification of associated elements translation to indicators for index-based assessments. These concerns can be further fuelled by challenges associated with decommissioning sites, regarding engineering complexities management alongside radioactive inventory and secondary waste generated by decommissioning (Ngulimi 2025; Foster et al 2021). But despite this prominent concern, another significant consideration revolves around the ensuring of continuously efficient decommissioning progression (Wimmers and von Hirschhausen 2023), both this concern and inventory management identified the influence of organisation from the preliminary review.

Within Fukushima Daiichi, the Tokyo Electrical Power Company Holdings (TEPCO) and nuclear regulators organisational ineptitude hindered the ability to effectively respond and prepare, a result of inadequate emergency response training and lack of safeguards being implemented (Murata 2021). Technical issues also stemmed from organisational ineptitude, like locating many emergency generators underground resulting in their flooding and failure (Hollnagel and Fujita 2013). A relevant dimension as the technical dimension encompasses engineered components contributing to overall resilience capacity dependent on condition, a relevant concern in decommissioning sites due to deteriorating conditions. The influence of both the organisational and technical dimension is furthered by the example of the Kashiwazaki-Kariwa Nuclear Power Plant (KKNNP), Niigata Prefecture, Japan. Although only partially operating at the time, the Daiichi disaster sparked concerns, leading to reactors being shut down following the accident and the implementation of safety features within shutdown reactors, whereas unit 6 has been restarted with aims to return to operation in March 2026 (Web 3). Since previous damage from seismic events (2007), there has been positive organisational influence from TEPCO learning from the previous Fukushima Daiichi disaster, as enhanced safety measures have been mandated, leading to rigorous inspection and implementation of upgrades as of 2024 (Yamamoto and Yamamoto 2024). TEPCO implemented increasing safety investigations and upgrades like flood barriers to safeguard against tsunamis, whilst improving preparedness through response plans, training, and backup power systems (Web 3), highlighting positive organisational influence on resilience, alongside socio-economic and technical examples that can be taken to bolster resilience at nuclear sites.

This stage provides further evidence to the influence of dimensions and elements within, and when utilised in conjunction with previous findings, it provides further information regarding responsible components within a decommissioning site to further aid resilience indicator identification. However, further clarification to effectively guide indicator identification and reduce the complexity of reframing resilience ability was required, where further review found a plethora of aspects that could result in more specified and applicable aspects that must be considered (stage 3.3)

Stage 3.3: Further understanding the applicability of findings and influence on resilience capabilities:

Requirement of decommissioning sites to ensure safe long-term management of radiological inventories and efficient decommissioning progression led to evolution from systems to ‘high risk’ systems, an aspect linked to the critical infrastructure systems (CI). Like decommissioning sites, CI’s require continuous operation to support economic growth, governmental functions, and essential tasks (Ouyang 2014), as failure generates serious consequences (like Fukushima Daiichi) (Comes and Van de Walle 2014). Focus on continuous operation is prominent, and further research within CI literature heavily cited the framework of Bruneau et al (2003), a highly regarded, and relevant framework paper. Bruneau et al’s (2003) framework provides further understanding to disaster resilience, highlighting four properties, understood as qualities a system must possess to be resilient. Understood as **robustness** (strength of a system to endure disruption without functional degradation), **rapidity** (capacity or speed to recover and restore function if it falters), **resourcefulness** (ability to effectively apply resources to meet priorities), **redundancy** (extent to which systems components are substitutable).

Further highlighted are the idea of 4 dimensions, highlighting domains where resilience properties can be applied or expressed within a system, adding to the preliminary review’s findings regarding

dimensions. Within the framework they are understood as **technical** (covers an engineered system components ability to maintain acceptable essential operations during disturbance), **social** (represents human aspects and measures in place to less the extent of consequences for communities), **economic** (encompass financial aspects and the capacity to reduce economic losses), and **organisational** (capacity of managing organisations to take actions to enhance resilience properties effectiveness). These dimensions are evidently present and influential in real life examples, like the Fukushima Daiichi (2011) disaster, as resilience properties were impacted by organisational ineptitude, contributing to issues in the technical dimension, and inhibiting resilience capabilities of the site. In contrast, the influence of organisational dimension can have positive impacts on resilience, evident at the improved resilience capabilities of the KKNNP, improving the technical dimension. But dimensions have varying degrees of importance, dependent on the context they are applied to (Annarelli et al 2020), and based on previous findings, the technical and organisational dimensions are seemingly more important than social and economic dimensions within decommissioning sites. As the technical dimension can be linked to engineering domains, including infrastructure and technology responsible for continuous operations, and links to engineering concerns of ageing/deteriorating assets in decommissioning sites. Whereas the significance of the organisational dimension is supported by ineptitude at Fukushima Daiichi dampening resilience, whilst fostering resilience improvements at KKNNP. Evidently, the organisational dimension can be seen as the most influential upon resilience nuclear decommissioning sites, followed by the technical dimension, influencing resilience properties, and thus capabilities.

When applied to aid the guidance of indicator identification for index-based resilience assessments, the resilience properties provide further understanding of the influence of elements, as they can be recognised based on contribution to redundancy, robustness, resourcefulness, and rapidity. This is the same for the dimensions, presenting areas influencing resilience where elements are expressed, further reducing complexity and grouping them on a basic level to further aid potential indicator identification. But continued focus has been on retaining essential operations, resulting from the system composed of dimensions and components. This led to stage 3.4, as focus on operations highlights the need to understand when a decommissioning site is no longer resilient, and to understand periods of operational loss that require differing responses before critical loss, as highlighted in stage 3.2's examples.

Stage 3.4: Understanding operational degradation, response, and point of failure:

Focus on reframing resilience capability within decommissioning sites centres upon maintaining essential operations. Failure will result in consequence, thus operational loss and response required must be appropriately understood to effectively supplement practical application for guiding identification of indicators within index-based resilience assessments to reduce its complexity.

To represent operational loss effectively, the concept of *thresholds* is utilised, commonly present in resilience literature, and understood as the point a system can no longer withstand disturbance, transforming to an unrecognisable state (Forzieri et al 2022). Prominent aspects that must be understood for sufficient application revolve around the point disturbance can no longer be withstood, recovery, and state of the system post threshold crossing (Dakos et al 2015). Suggesting that threshold application can highlight resilience levels required for differing coastal flood scenarios, signifying its performance against hazard and the importance of adaptation incorporation to improve resilience. This is an imperative aspect to incorporate, due to climate change and associated increasing risk of coastal flood hazards (Portugal-Pereira et al 2024), necessitating a need for higher resilience to lower the possibility of threshold crossing during coastal flood hazards. However, focus on response effectiveness to restore operations signifies a single threshold representation does not accommodate the importance of restoration through rapidity of response, a key capability in reframing resilience within this paper. This led to considering multiple thresholds for appropriate representation of progressive periods of functional loss. As this bettered understanding of response requirements to highlight resilience at each threshold needed for operational restoration before critical failure is reached within a system (Liu et al 2019), significantly relevant for this paper's focus on coastal flood hazard resilience, and its reframing for decommissioning sites.

Incorporation of multiple thresholds highlights the sufficiency of resilience within a decommissioning site based upon how quickly thresholds are crossed and effectiveness of restoration. This

would aid indicator identification by magnifying focus to elements that influence operational degradation and thus response, signifying early warning signs, and suggesting improvements within the organisational and technical dimension. It is integral to map the potential stages of operational degradation across thresholds in coastal flood scenarios at nuclear decommissioning sites, highlighting response required and overall sufficiency of resilience, which can be translated into possible indicators.

4 COMPREHENSIVE SUMMARY:

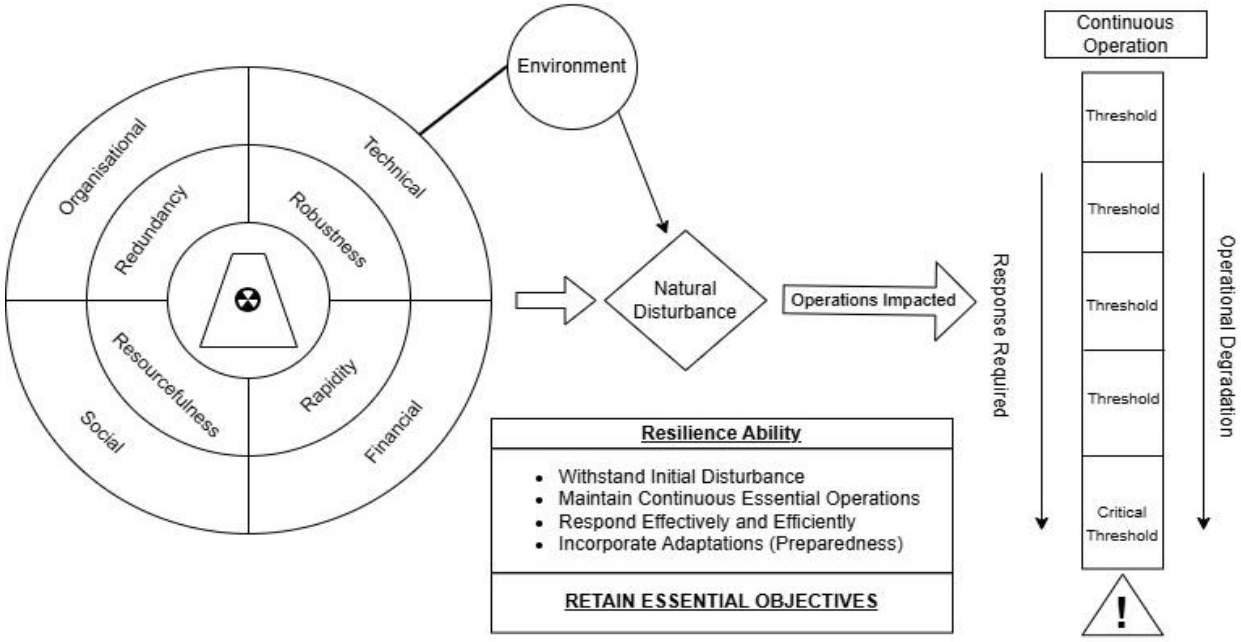

Figure 1, comprehensive illustrated representation of the reframed resilience ability.

Within figure 1 resilience capability is reframed as the ability to withstand initial disturbance, and failing that, maintain continuous essential operations, respond effectively, incorporate adaptations to improve preparedness, and **retain original essential objectives**. The capabilities to express this ability are dependent on the state of the system and resilience qualities/properties it possesses across elements, which are located within multiple dimensions that collectively shape the operational performance; organizational dimension is the most influential upon these properties. These *'systems'* (decommissioning sites) interact with the surrounding environment and if a coastal flood disturbance occurs it could interrupt essential operations. Operational loss or degradation will be represented through thresholds when applied to a site (figure 1), and dependent on the severity of the coastal flood disturbance, will result in the crossing of further thresholds and advancing operational degradation, requiring higher levels of response before a critical threshold (consequence) is reached. When this comprehensive reframed ability (figure 1) is applied within a nuclear decommissioning site, it will heavily aid the guidance of indicator selection for index-based resilience assessments, by reducing the complexity that exists within these vastly engineered sites. This will signify locations within a decommissioning site where indicators can be identified when this reframed resilience ability is applied. Providing a foundation of relevant knowledge for further reframing of resilience for nuclear decommissioning contexts to guide indicator selection in index-based coastal flood resilience assessments for decommissioning sites.

5 CONCLUSION:

To appropriately reframe resilience ability for nuclear decommissioning sites, concerns were understood through requirements of maintaining the long-term safety of radiological inventory and continuously progressing decommissioning operations without delay, underpinned by the capacity to

maintain continuous levels of operation and respond to disturbances. Collectively the repurposed aspects when encompassed into application at nuclear decommissioning sites highlight a range of dimensions, elements, and components that contribute towards resilience as the ability to maintain continuous essential operations, respond effectively, adapt, and retain original objectives. This will provide a beneficial structure within indicator identification and evaluation due to the structure it provides to seek out indicators across these areas, effectively establishing how resilience can be approached and how this influences the types of indicators that should be utilised to represent this. Further research should be undertaken to build on this foundation, encompassing further levels of research to understand in-depth how resilience can be more effectively approached to guide possible indicator identification for index-based resilience assessments with nuclear decommissioning sites. This could lead to the eventual practical execution of these findings which will ultimately assess the resilience of nuclear decommissioning sites to understand its current level and how that may cope with coastal flooding disturbances within the future.

REFERENCES

1. ANNARELLI, A., BATTISTELLA, C. & NONINO, F. 2020. A framework to evaluate the effects of organizational resilience on service quality. Sustainability, 12(3), 958. .
2. BALICA, S. F., WRIGHT, N. G. & VAN DER MEULEN, F. 2012. A flood vulnerability index for coastal cities and its use in assessing climate change impacts. Natural hazards, 64(1), 73–105. .
3. BRUNEAU, M., CHANG, S. E., EGUCHI, R. T., LEE, G. C., O'ROURKE, T. D., REINHORN, A. M., SHINOZUKA, M., TIERNEY, K., WALLACE, W. A. & VON WINTERFELDT, D. 2003. A Framework to Quantitatively Assess and Enhance the Seismic Resilience of Communities. Earthquake Spectra, 19(4), 733–752.
4. CHAFFIN, B. C. & SCOWN, M. 2018. Social-ecological resilience and geomorphic systems. Geomorphology, 305, 221–230.
5. COMES, T. & VAN DE WALLE, B. 2014. Measuring Disaster Resilience: The Impact of Hurricane Sandy on Critical Infrastructure Systems.
6. DAKOS, V., CARPENTER, S. R., VAN NES, E. H. & SCHEFFER, M. 2015. Resilience indicators: prospects and limitations for early warnings of regime shifts. Philosophical Transactions of the Royal Society B: Biological Sciences, 370(1659), 20130263.
7. DAKOS, V. & KÉFI, S. 2022. Ecological resilience: what to measure and how. Environmental Research Letters, 17(4), 043003.
8. FORZIERI, G., DAKOS, V., MCDOWELL, N. G., RAMDANE, A. & CESCATTI, A. 2022. Emerging signals of declining forest resilience under climate change. Nature, 608(7923), 534–539.
9. FOSTER, R. I., PARK, J. K., LEE, K. & SEO, B.-K. 2021. UK Civil Nuclear Decommissioning, a Blueprint for Korea's Nuclear Decommissioning Future?: Part I-Nuclear Legacy, Strategies, and the NDA. Journal of Nuclear Fuel Cycle and Waste Technology (JNFCWT), 19(3), 387–419.
10. GREENHALGH, T., THORNE, S. & MALTERUD, K. 2018. Time to challenge the spurious hierarchy of systematic over narrative reviews? Eur J Clin Invest, 48(6), e12931.
11. HAHN, T. & NYKVIST, B. 2017. Are adaptations self-organized, autonomous, and harmonious? Assessing the social–ecological resilience literature. Ecology and Society, 22(1).
12. HAIGH, I. D., OZSOY, O., WADEY, M. P., NICHOLLS, R. J., GALLOP, S. L., WAHL, T. & BROWN, J. M. 2017. An improved database of coastal flooding in the United Kingdom from 1915 to 2016. Scientific Data, 4(1), 170100.
13. HAQUE, C. E. & DOBERSTEIN, B. 2021. Adaptive governance and community resilience to cyclones in coastal Bangladesh: Addressing the problem of fit, social learning, and institutional collaboration. Environmental Science & Policy, 124, 580–592.
14. HASEGAWA, K. 2014. The Fukushima nuclear accident and Japan’s civil society: Context, reactions, and policy impacts. International Sociology, 29(4), 283–301.
15. HENDRY, A., HAIGH, I. D., NICHOLLS, R. J., WINTER, H., NEAL, R., WAHL, T., JOLY-LAUGEL, A. & DARBY, S. E. 2019. Assessing the characteristics and drivers of compound flooding

events around the UK coast. Hydrol. Earth Syst. Sci., 23(7), 3117–3139.
16. HOLLING, C. S. 1973. Resilience and Stability of Ecological Systems. Annual Review of Ecology and Systematics, 4, 1–23.
17. HOLLNAGEL, E. & FUJITA, Y. 2013. the Fukushima disaster – systemic failures as the lack of resilience. nuclear engineering and technology, 45(1), 13–20.
18. HOSSEINI, S., BARKER, K. & RAMIREZ-MARQUEZ, J. E. 2016. A review of definitions and measures of system resilience. Reliability Engineering & System Safety, 145, 47–61.
19. IBRION, M., PALTRINIERI, N. & NEJAD, A. R. 2020. Learning from non-failure of Onagawa nuclear power station: an accident investigation over its life cycle. Results in Engineering, 8, 100185.
20. JENKINS, L. M., ALVAREZ, R. & JORDAAN, S. M. 2020. Unmanaged climate risks to spent fuel from US nuclear power plants: The case of sea-level rise. Energy Policy, 137, 111106.
21. JONES, L. 2019. Resilience isn't the same for all: Comparing subjective and objective approaches to resilience measurement. Wiley Interdisciplinary Reviews: Climate Change, 10(1), e552.
22. KENDON, M. & MCCARTHY, M. 2015. The UK's wet and stormy winter of 2013/2014. Weather, 70(2), 40–47.
23. LI, T., DONG, Y. & LIU, Z. 2020. A review of social-ecological system resilience: Mechanism, assessment and management. Sci Total Environ, 723, 138113.
24. LIU, D., WU, Z., GUO, Q. & SHI, Y. 2019. Resilience and its thresholds of scientific collaboration network. IEEE Access, 7, 69339–69350.
25. MARZI, S., MYSIAK, J., ESSENFELDER, A. H., AMADIO, M., GIOVE, S. & FEKETE, A. 2019. Constructing a comprehensive disaster resilience index: The case of Italy. PloS one, 14(9), e0221585.
26. MENTGES, A., HALEKOTTE, L., SCHNEIDER, M., DEMMER, T. & LICHTE, D. 2023. A resilience glossary shaped by context: Reviewing resilience-related terms for critical infrastructures. International Journal of Disaster Risk Reduction, 96, 103893.
27. MURATA, A. 2021. Cultural aspects as a root cause of organizational failure in risk and crisis management in the Fukushima Daiichi disaster. Safety science, 135, 105091.
28. NGULIMI, M. F., KIM, S., ASGHAR, K., SEO, B. K. & ROH, C. 2025. Nuclear Decommissioning and Sustainable Environment: Insights on Decontamination Processes. Advanced Energy and Sustainability Research, 6(1), 2400243.
29. ONO, A. 2021. Fukushima Daiichi decontamination and decommissioning: status and challenges. Annals of the ICRP, 50(1), 24–30.
30. OUYANG, M. 2014. Review on modelling and simulation of interdependent critical infrastructure systems. Reliability engineering & System safety, 121, 43–60.
31. PERKS, R. J., BERNIE, D., LOWE, J. & NEAL, R. 2023. The influence of future weather pattern changes and projected sea-level rise on coastal flood impacts around the UK. Climatic Change, 176(3), 25.
32. PORTUGAL-PEREIRA, J., ESTEBAN, M. & ARAÚJO, K. 2024. Exposure of future nuclear energy infrastructure to climate change hazards: A review assessment. Energy Strategy Reviews, 53, 101365.
33. WIMMERS, A. & VON HIRSCHHAUSEN, C. 2023. Lessons for the organization of nuclear decommissioning from the UK and the US: risks, challenges, and opportunities. Safety of Nuclear Waste Disposal, 2, 7–8.
34. YAMAMOTO, D. & YAMAMOTO, Y. 2024. If it's in our backyard: the roles of local knowledge in the formation of a nuclear oversight organisation. Local Environment, 29(11), 1436–1450.
35. ZEVENBERGEN, C., GERSONIUS, B. & RADHAKRISHAN, M. 2020. Flood resilience. Philosophical Transactions of the Royal Society A: Mathematical, Physical and Engineering Sciences, 378(2168), 20190212.

Web1: https://researchbriefings.files.parliament.uk/documents/CDP-2024-0036/CDP-2024-0036.pdf
Web2: https://world-nuclear.org/nuclear-reactor-database/details/onagawa-2.
Web3: https://www.tepco.co.jp/en/hd/ourbusiness/nuclear/kashiwazaki-kariwa/overview/index-e.html

Determining climate change impacts across Australia

M Retallick[1], M Babister[1], N Dunning[1], H Babister[1] and B Jamali[1]
WMAwater Pty Ltd, Sydney, NSW, Australia[1]
E-mail: retallick@wmawater.com.au

ABSTRACT

In 2024 an update to Australia's national guidance on climate change and flooding was released to include the latest temperature projections from IPCC 6 and the latest research on how warming will affect flood producing rainfall and runoff generation. This update supersedes interim advice from 2015 that was included in 2016 version of Australian rainfall and runoff. In 2015 climate change was seen as a future problem with climate change results generally being treated as a sensitivity assessment and not be ing actively factored in planning levels and decision making. The new update dramatically increases impact of climate change and shows that the warming since 1990 has already significantly increased flood levels.

This has created an immediate need to factor climate change into current and future planning decisions. The implications of new guidance was not explored prior to its release. This paper outlines extensive testing that was carried out on the Eastern Australian states. The recommended guidelines were tested on 500 New South Wales, Queensland, and Victorian catchments representing rural and urban catchments. For each available catchment the rating curve was used to determine the impact level as well as flow. This allowed the impact of climate change on flood planning level to be assessed. A Climate Change Calculator has been developed which allows practitioners to easily understand how climate risk will change over time over the design life of a structure or with emissions pathway. The calculator allows users to upload design event flood level grids and interpolate design event grids factored by climate change reducing the need for model runs and allowing floodplain managers to effectively determine changes in flood risk. The development of this tool and demonstration of its application using a case study in Singleton NSW is presented.

KEYWORDS: flood, climate change, Australia, impacts, design floods, ARR, flood planning level

1 INTRODUCTION

Australian Rainfall and Runoff (ARR), the national design flood guideline in Australia (Ball et al, 2019) introduced Interim Climate Change rainfall adjustment factors based in temperature scaling of 5% per degree of warming for three representative concentration pathways (RCP). Results were available for RCP4.5, RCP6 and RCP8.5 but the RCP6 results were qualified due to the limited number of model results. Different Australian climate zones were used with different climate change temperature increases. Using the ARR 2019 rainfall adjustments, the estimated increases for year 2090 ranged from 7.2% - 10.8% for RCP4.5 and for 15.4% - 22.8% for RCP8.5. These results were based on the 5th IPCC (2013). While it was acknowledged climate change would also affect rainfall temporal patterns, antecedent conditions and baseflow regimes, no adjustment was proposed for these design inputs.

With the release of IPCC synthesis report (2023) the climate guidance within ARR (2024) was updated based on a climate science review (Wasko et al. 2023). The scaling of rainfall was based on a higher increase in temperature due to climate change and higher scaling factors (8% for 24 hours and 15% for 1-hour storms). The resultant rainfall increases are dramatically higher compared to the guideline they are

replacing and are constant across the country. Loss adjustments, which vary by region, were also provided.

This paper explores how the update to Australia's national climate change guidance for design flood estimation changes the frequency of flood producing rainfall. Using 343 test catchments and a series of tools developed to specifically aid the understanding of the impact of climate change on flooding this paper shows how the impacts of climate change can be assessed. These tools also allow floodplain managers to rapidly assess the impact of climate change, interpolate flood levels and determine vulnerable areas. More importantly, they allow floodplain managers to adjust policy and direct resources prior to undertaking detailed modelled.

2 DATA

2.1 Test catchments

A total of 343 catchments along the east coast of Australia were considered suitable for the study (WMAwater, 2019; Babister and Babister 2022, WMAwater 2021). A subset of 155 with high quality rating curve information and a long term at site record (WMAwater (2019)) were used for detailed assessment. Figure 1 shows the location of catchments included in the study, the catchment area to the gauge (yellow areas) and the distribution of catchment areas (right). The catchments ranged in size from 2 to 16000 km², with the majority falling between 50 and 500 km². Synthetic urban catchments were developed at 10 major cities with catchment areas 1, 5 and 10km^2 and varying levels of imperviousness. These additional urban catchments allow the impact of climate change in each major urban centre to be assessed. The locations of the urban catchments are show as red dots

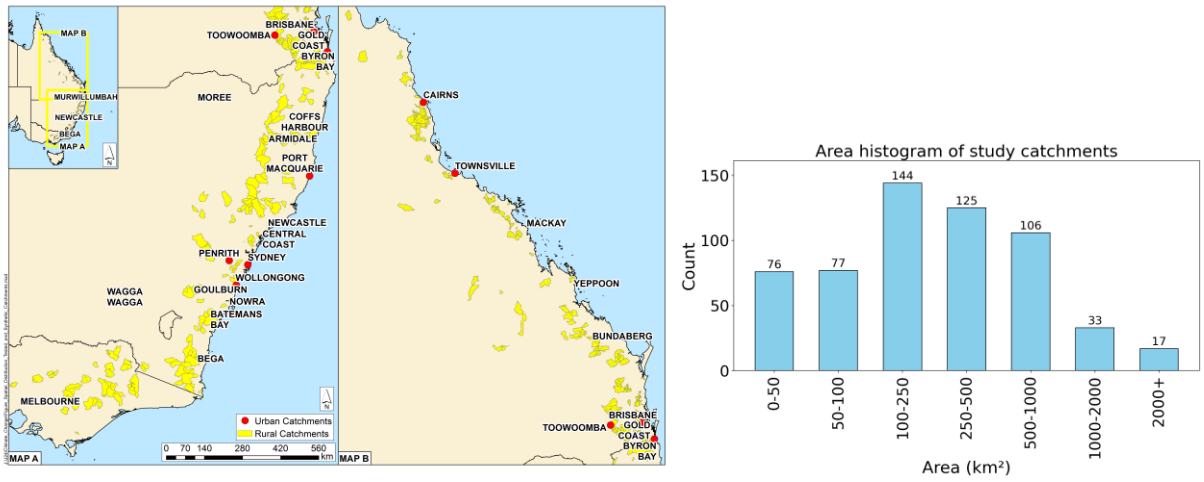

Figure 1: The location of study catchments (left) and histogram of study area (right)

2.2 Case Study- Singleton

Singleton was chosen as a case study due its population at risk due to a changing climate. Singleton is a town located on the Hunter River in New South Wales Australia. The population of the town is 17,500. Design flood level information (BMT WBM, 2023) in the form of an ascii grid for a range of Annual Exceedance Probability (AEP) shows that in a 1% AEP 2970 buildings are flooded.

3 METHODOLOGY

3.1 Impacts of climate change guidelines on flood planning levels

A hydrologic model was developed of each catchment (Section 2.1) using Watershed Bounded Network Model (WBNM). This is a widely used rainfall runoff model in Australia. The design inputs

(IFD, spatial and temporal patterns, losses) were applied as per ARR guidelines. The hydrologic models were run for the historic baseline conditions (1960-1990 baseline IFD, 2016 IFD (Bureau of Meteorology, 2016)) for durations from 1 Hour to 72 Hours and all ensemble temporal patterns. The standard design flood estimation process was used to produce historic baseline conditions flows. The same process was conducted for the climate change scenarios with the rainfall increases and loss adjustments made as per the ARR Climate change chapter. The critical duration was assumed not to change with climate change. For each scenario the peak flow for the climate change scenario was compared to the peak flow for the historic climate and the ratio of peak flow in climate scenario to historic peak flow calculated. For 155 catchments in New South Wales reliable rating curves were available that went past the 1% AEP level. For each scenario the peak flow was converted to a level using a rating curve. The change in level for the climate change scenario compared to the historic climate was then calculated.

3.2 Climate change calculator

Detailed hydrologic and hydraulic modelling of the catchment in order to estimate the shift in flood probability due to climate change provides a more robust estimate of the likely change.. Hydrologic and hydraulic modelling involves scaling of the rainfall, sampling other design inputs, identifying critical duration (through ensemble modelling). This amount of investment required for detailed modelling would preclude any routine estimation and would limit development of a tool that can quickly estimate the shift in flood probability due to climate change for any location in the country.

This limitation could be overcome by assuming that:

- a good approximation of critical duration can be estimated using the catchment area and 24 hr 1% AEP IFD (Babister et al, 2024a); and,
- using two design rainfall events with similar rainfall excess pattern and depth would result in the same peak flow.

That means a design rainfall with climate change scaling applied (to IFD, pre-burst, and losses), would produce the same flow as a historical climate design event with the same excess rainfall (Retallick et al, 2024b).

Using these assumptions the Climate Change Calculator was developed to estimate shifts in flood probability at any location in Australia using the available standard design rainfall inputs, and available at: ccc.wmawater.com.au. The Calculator is described in Babister et al (2024b), Babister et al (2024a), and Retallick et al (2024b). The tool can provide insights on how risk exposure over the life of the project changes. Knowing that exposure might change over time can potentially lead to more informed decision making. Current practice seems to relegate climate change assessment to sensitivity assessment that is often not factored into decision making (Retallick et al, 2024b). With climate change a present problem, this needs to change. The focus has often been too much on modelling and mapping a full range of design events under climate change and not enough on considering the current and future risk into decision making.

The climate change calculator includes a hydraulic interpolation function. Using ground elevation d from a hydraulic model, an upper water level grid and a lower water level grid with known AEPs, the user can choose a particular design event AEP between the upper and lower grid and estimate the flood extent using the hydraulic interpolator. During the interpolation, the lower design event grid is stretched, using the model terrain grid to match the extent of the upper grid. An interpolation is then applied to create the climate change design event grid within the stretched extent. The interpolated water levels lower than ground elevation grid levels are removed.

The method has been verified against calibrated hydraulic model design event results for a number of catchments using a leave one out analysis. For example, the 1% AEP design flood extent was interpolated (using the 5% AEP and 1 in 200 AEP) and compared to the existing flood extent. This analysis was conducted for all available AEPs (except for the rarest and most frequent AEP). Comparing

the interpolated extents to the existing design flood extents provided an indication of interpolation accuracy. The method was found to be suitable for purpose.

3.3 Comparison of the climate change calculator with traditional rainfall runoff modelling

In order to ensure the robustness of the assumptions of the climate change calculator, outputs were compared to the AEP shifts calculated by traditional rainfall runoff modelling. Traditional rainfall runoff modelling was undertaken for the rural test catchments described in Section 3.1 using WBNM. Design inputs, such as temporal patterns, areal reduction factors, and losses were downloaded from the ARR data hub. Design rainfalls were sourced from the Bureau of Meteorology. The climate change rainfall and loss factors from ARR V4.2 (Ball et al, 2019) were also applied. The AEP of the historical 1% AEP in the future was calculated for each climate change scenario. The historical 1 in X AEP event equivalent to the future 1% AEP event was also calculated.

4 RESULTS AND DISCUSSION

4.1 Impacts of climate change guidelines on flood planning levels

An assessment of the ratio of the flow for the historic climate and selected future climate change scenario found that design flows increased across all rural catchments with climate change. The ratio of climate change peak flows to historical flows did not vary significantly with catchment size, peak flow or catchment location (Figure 2). A small increase in flow ratio occurred in smaller catchments compared to large catchments, likely due to the higher climate change factors for smaller catchments. The average flow ratio for SSP3 2050 was 1.21. An increase in the 1% AEP flood level due to climate change can be used as a surrogate for the likely changes in flood planning levels used by local governments due to climate change. Figure 3 shows the 1% AEP increases in flood level compared to the historic climate. The increase in level is largely linear with some catchments showing a slight upwards curvature. Therefore, it can be concluded that a reasonable estimate of smaller increases in climate change and in flood level can be obtained by simply ratioing the 4.1 degree SSP5-2090 case.

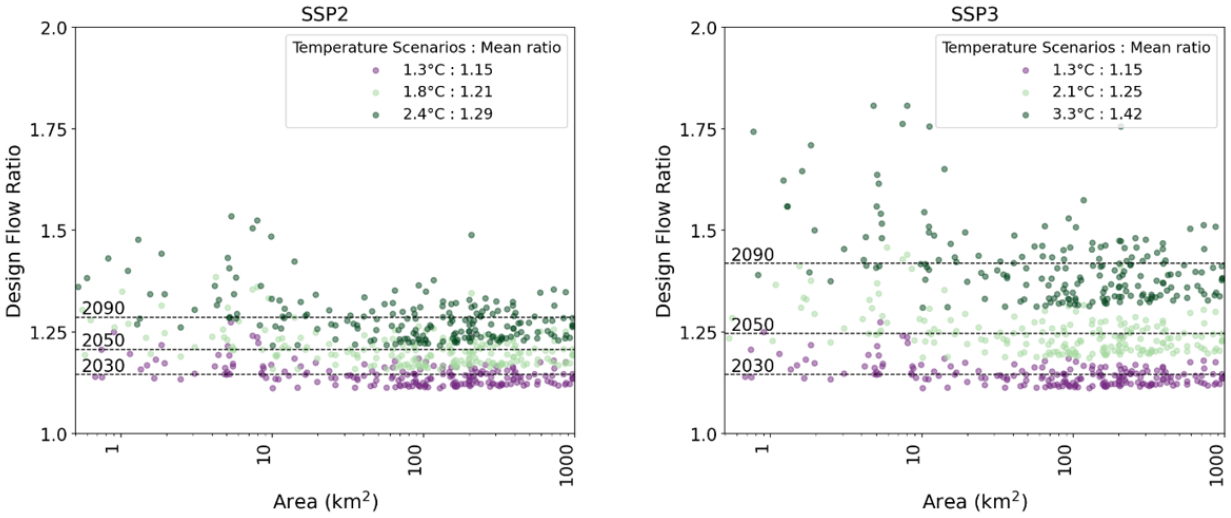

Figure 2: Outflow ratio for future climate scenarios sorted by SSP and catchment area. Mean ratio lines are added for the 2030, 2050 and 2090 time horizons.

4.2 Comparison of climate change calculator to traditional rainfall runoff modelling

Validation of the climate change calculator to traditional rainfall runoff method was undertaken for all test catchments. Figure 4 (left) shows the comparison of AEP estimates for the 1% AEP under various future climate scenarios for both methods for a catchment with an area of 325.6km^2. The calculator

produces similar answers to the rainfall runoff method. Figure 4 (right) shows what historical 1 in X AEP event that a Future 1% AEP is equivalent to for the same catchment. The climate change calculator slightly underestimates the AEP of events for higher temperature increases.

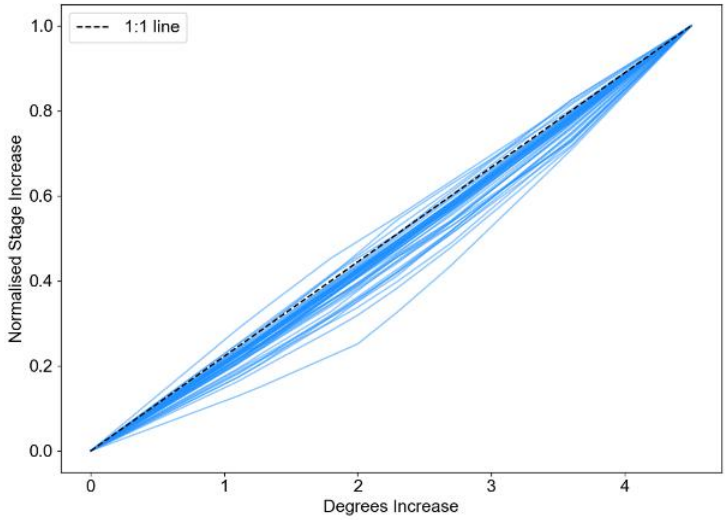

Figure 3: Normalised Increase in 1% AEP flood levels at NSW gauges with high quality rating curves

4.3 Case Study –Singleton

The application of the tool is demonstrated for the Hunter River catchment at Singleton. Figure 5 shows the input data and the processed catchment area . After locating the point, the catchment boundary is processed using the snap option (Figure 5). After submitting the query, a summary of the input, catchment map and several outputs are generated as follows.

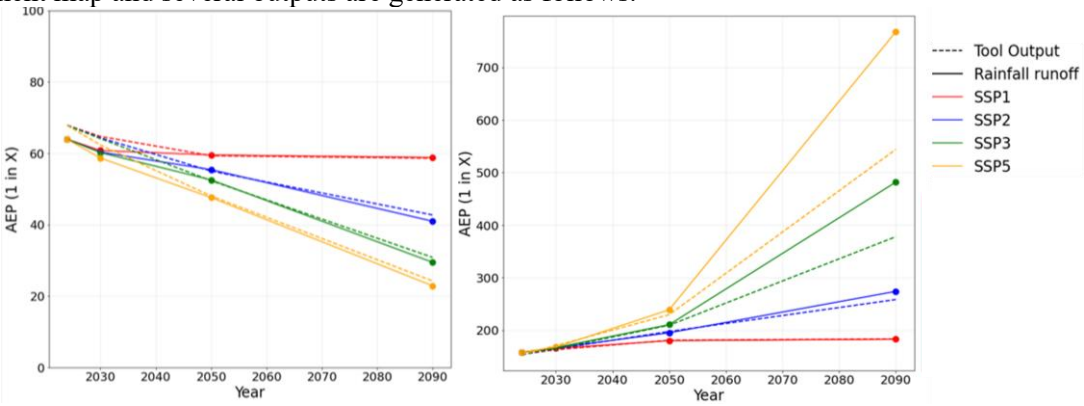

Figure 4: Comparison of annual exceedance probability (AEP) shifts between the climate change calculator (tool output) and traditional rainfall runoff method (left) and 1 in X AEP historical event that a future 1% AEP is equivalent to for various SSP scenarios (right)

Figure 6 shows outputs of the calculator relating to how the probability of a historical 1 in 100 AEP (BOM 2016 IFD) will be change with climate change in the future and vice versa. For example, for the Singleton, the catchment average 1 in 100 AEP rainfall will be equivalent to 1 in 65 AEP in 2025 (the current condition) under SSP1 scenario. Similarly, a 1 in 100 AEP in 2025 SSP1 scenario is equivalent to 1 in 140 AEP under historic climate. The "Mean over design exposure" is estimated by taking the geometric mean of the probability mass function over the design life (specified by the user). Other outputs include a graph of design rainfall under the different climate change scenarios and timeframes.

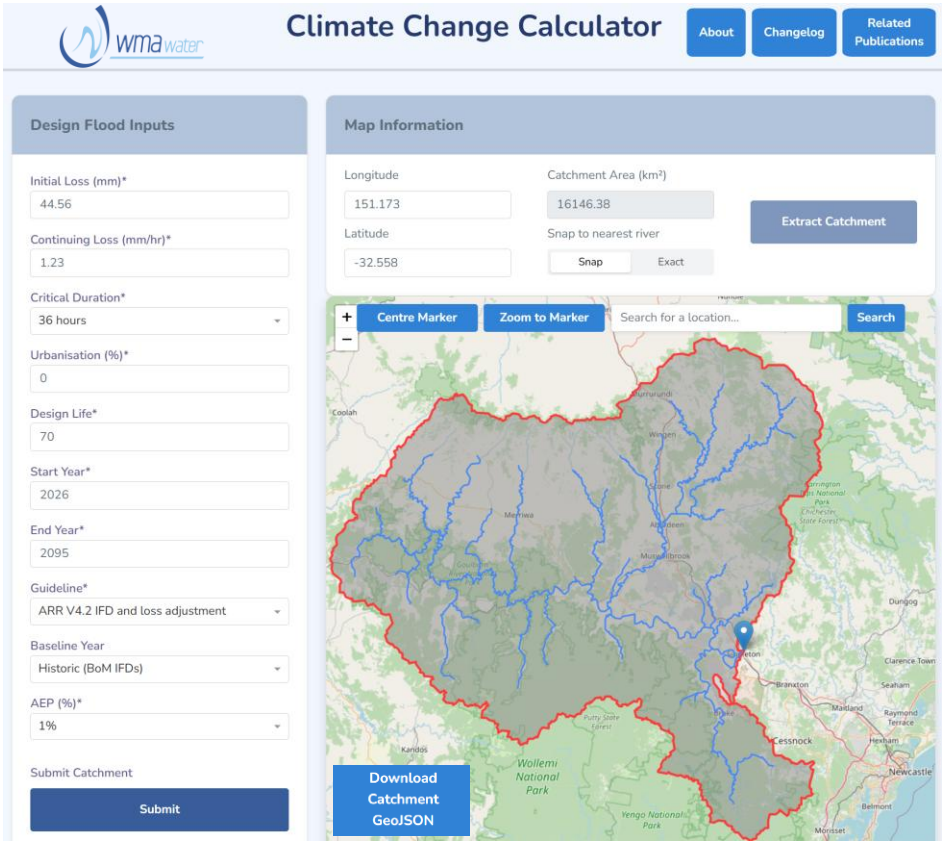

Figure 5: Extraction details of catchment and advanced parameters preparing for submitting the query

	SSP1	SSP2	SSP3	SSP5
2025	65	65	65	63
2030	62	62	61	59
2050	56	52	48	43
2090	55	38	26	19
Mean over design life	57	47	40	33

	SSP1	SSP2	SSP3	SSP5
2025	140	140	140	143
2030	145	146	147	151
2050	159	173	182	199
2090	161	224	332	475
Mean over Design Life	151	168	186	210

Figure 6: Changes in historical 1% AEP probability due to climate change and proxy events for future 1% AEP

Figure 7 shows the probability of a 1% AEP design event occurring exactly X many times (where X is zero, one, two, …) over the exposure period under historical and climate change conditions. Each section indicates the probability of a certain number of occurrences. In the case of Singleton there is a decrease in the likelihood of no 1% AEP flooding with climate change over a 70-year period. The probability of having no 1% AEP floods (zero occurrence) drops from around 50% under the historic climate to about 28.98% in SSP1. The chance of multiple exceedances increases in future scenarios. The

probability of one or more 1% AEP flood occurrence is 100% - 28.98% = 71.02 % under SSP1 shown by the lines on the secondary y axis.

The climate change calculator indicates that for Singleton under SSP2 scenario the 1 in 100 AEP design rainfall exceedance probability in year 2030 and 2050 is equivalent to 1 in 146 AEP and 1 in 173 AEP design rainfall based on historical series. Under SSP3 2050 the 1 in 100 AEP is equivalent to in 1 in 182 AEP. The flood study for the catchment includes the flood level grids for 1 in 100 and 1 in 200 AEP. Therefore, the climate change calculator was used to map SSP2 2030, 2050 and SSP3 2050 1 in 100 AEP flood level maps using the hydraulic interpolation. Figure 8 shows the change in flood extent for the SSP3 2050 as well as the 1 in 100 AEP flood extents used as an input in the hydraulic interpolation tool. The number of impacted buildings increases by 58% to 4708 in SSP2 2030, to 5212 in SSP 2 2050 and 5267 in SSP 3 2050.

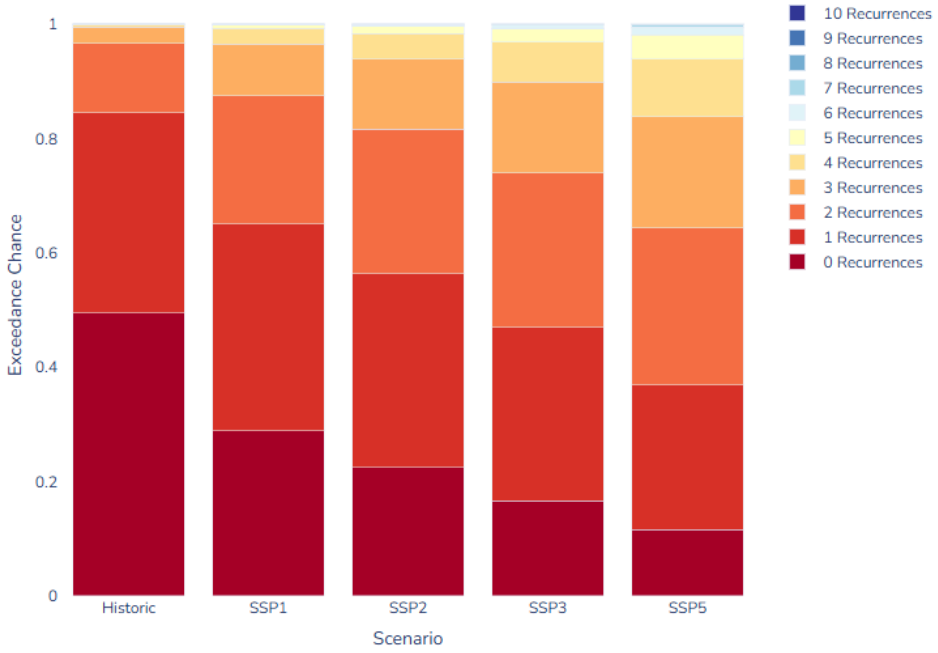

Figure 7: Expected exceedances over life time under various climate change scenarios compared to historical conditions

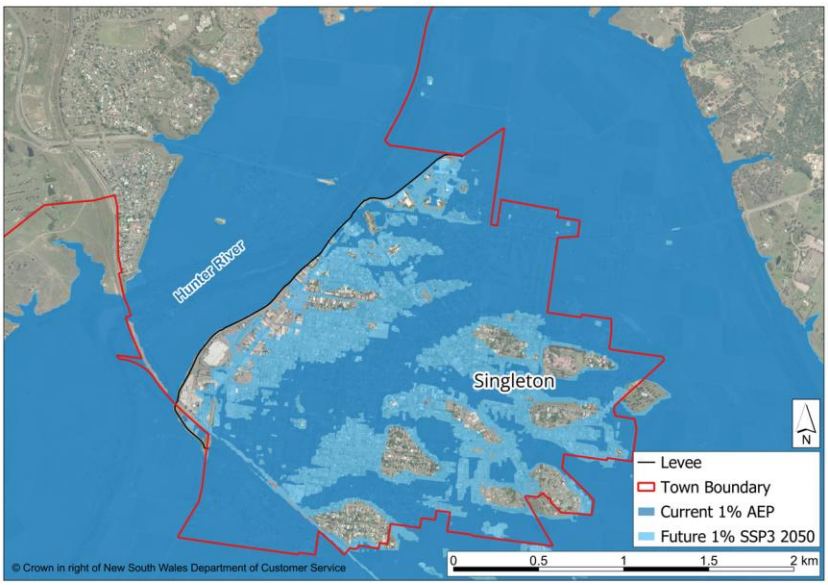

Figure 8: Singleton flood extents - current 1% AEP and interpolated 1% AEP SSP 3 2050

5 CONCLUSION

Australian Climate change guidelines provide factors for rainfall increases and losses under various climate scenarios. While the industry is keen to adopt the guidelines, no formal guidance has been provided by government agencies on which scenarios to adopt. The climate change calculator was developed to avoid unnecessary simulations and model runs. The new guidelines were tested on 500 catchments. The climate changes adjustments for current day warming (1 Degree) were found to increase the peak flow in the test catchments by approximately 10% compared to the baseline IFD. While there was a large variability in the magnitude of water level responded to temperature increase, the increase per degree of warming is generally linear. The climate change calculator allows practitioners, engineers, floodplain managers, planners and the general public to easily understand the change in climate risk. The tool has been compared against traditional rainfall runoff methods to ensure the estimates are robust. The hydraulic interpolation function available in the climate change calculator will reduce the need for costly two-dimensional model runs and allow floodplain managers to easily determine the change in flood risk in their catchment. The calculator can be used to estimate the number of buildings at risk of flooding under each future climate scenario. The interpolated grids identify the areas with the highest vulnerability to increases in flood levels due to climate change and can inform resource allocation.

REFERENCES

Babister H and Babister M, (2022) Assessing Underestimate Bias in the ARR2019 Design Rainfall Method in Queensland, HWRS 2022

Babister H, Babister M, Jamali B, Retallick M, Bodenlenz F, Dunning N, (2024a) Estimating Catchment Critical Duration Under Current and Future Climate critical duration, Hydrology and Water Resources Symposium, Melbourne 2024

Babister M, Babister H, Jamali B, Dunning N, Retallick M, Bodenlenz F, (2024b) The new climate change guideline: a novel and efficient approach to estimate lifetime exposure risk with changing flood probabilities, Hydrology and Water Resources Symposium, Melbourne 2024

Ball J, Babister M, Nathan R, Weeks W, Weinmann E, Retallick M, Testoni I, (Editors) (2019) Australian Rainfall and Runoff: A Guide to Flood Estimation, © Commonwealth of Australia (Geoscience Australia), Version 4.2

Bureau of Meteorology, (2016) "Design Rainfall Data System", available at http://www.bom.gov.au/water/designRainfalls/revised-ifd/ , 2016.

BMT WBM, (2023) Singleton Floodplain Risk Management Study and Plan

IPCC (2023). Climate Change 2023: Synthesis Report. Contribution of Working Groups I, II and III to the Sixth Assessment Report of the Intergovernmental Panel on Climate Change [Core Writing Team, H. Lee and J. Romero (eds.)]. IPCC, Geneva, Switzerland, 2023.

IPCC, 2013: Climate Change 2013: The Physical Science Basis. Contribution of Working Group I to the Fifth Assessment Report of the Intergovernmental Panel on Climate Change [Stocker, T.F., D. Qin, G.-K. Plattner, M. Tignor, S.K. Allen, J. Boschung, A. Nauels, Y. Xia, V. Bex and P.M. Midgley (eds.)]. Cambridge University Press, Cambridge, United Kingdom and New York, NY, USA, 1535 pp., 2013.

Retallick M, Babister M, Jamali B, Babister H, Bodenlenz F, (2024a) Assessing the Impact of Climate Change on Flood Risks: A Comprehensive Analysis of Updated ARR Guidelines Across Australian Catchments, Hydrology and Water Resources Symposium, Melbourne 2024

Retallick M, Babister M, Jamali B, Babister H, Dunning N, (2024b) The Australian Climate Change Calculator, Hydrology and Water Resources Symposium, Melbourne 2024

WMAwater, (2019) Review of ARR Design Inputs for NSW - Final Report- February 2019, Office of Environment and Heritage

WMAwater (2021) Regional Flood Frequency Estimation Model - 2021, https://rffe-2021.wmawater.com.au/

ICFM 10
Adapting to Global Change:
Innovative Approaches to Flood Management and Resilience
May 20-22, 2026 | Western University, London, Ontario, Canada

Finding Vulnerabilities to High Water Levels and Their Drivers in an Interconnected River Delta Under Climate Change

Niels M. Welsch[1], Jord J. Warmink[1], Suzanne J.M.H. Hulscher[1] and Denie C.M. Augustijn[1]
University of Twente, Drienerlolaan 5, Enschede, Netherlands[1]
E-mail: n.m.welsch@utwente.nl

ABSTRACT

Climate change poses great risks to flood safety in river deltas. However, the exact development of climate change and the effect on flood levels is deeply uncertain. In this paper we show the spatial extent and the contribution of various uncertainties (i.e. sea level rise, changing discharges and lake set-up) on system deficiencies in an interconnected river delta. System deficiencies are defined as unaccepted high-water levels. We do this by application of scenario discovery combined with a delta scale one-dimensional hydrodynamic model. Comparison of water levels with surrounding embankment heights show the spatial distribution of system deficiencies, which strongly differ across different river branches and largely depend on local river geometry. Scenario discovery furthermore provides insights in the spatial distribution of which boundary conditions drive the found deficiencies.

KEYWORDS: Scenario Discovery; Deep Uncertainty; Climate Change; River Delta; Interconnectivity

1 INTRODUCTION

There is consensus in scientific literature that climate change will increase the risk of flooding all around the world (te Linde et al., 2010; Haasnoot and Middelkoop, 2012). Flooding is mentioned to be the most devastating natural disaster for human societies. In the case of river deltas, the flood risk is shown to originate from both sea level rise, as well as increased river discharges due to climate change (Ericson et al., 2006; Klijn et al., 2015).

As deltas are often densely populated, reducing flood risk is of utmost importance. However, to reduce the flood risk, it requires thorough insight in the precise kind and extent of future problems (Klijn et al., 2015). In the light of climate change, this precision is rather difficult to achieve, as future developments of the worldwide climate are deeply uncertain (Lempert et al, 2006). Deep uncertainty is characterized by Lempert et al. (2006) as the conditions where the analysist cannot agree upon the probability distributions to represent uncertainty about key parameters in the models.

To incorporate such future uncertainty in policymaking, policymakers must get insights in the impact of the uncertainty on relevant policy domains. One of the possible methods to quantify the effect of deep uncertainty is through scenario discovery (Bryant and Lempert, 2010). Scenario discovery facilitates understanding the impact of future uncertainty by concisely summarizing a wide range of future states of the world in a way that helps decision makers more clearly understand the strengths and weaknesses of candidate strategies. Another approach when confronted by deep uncertainty, is to consider a large variety of scenarios, without assigning probabilities to them (Kwakkel et al., 2010). In such case one deviates from the possibilistic approach to a possibilistic approach. This possibilistic approach proves to counter one of the main limitations of the regular scenario approach, where scenario development processes tend to overlook discontinuities and surprising developments (Postma and Liebl, 2005; Kwakkel and Cunningham, 2016). For example, extreme conditions at the border of a considered domain not necessarily describe all extreme conditions inside the river delta.

The possibilistic approach is especially beneficial in complex interconnected river systems, where the interaction between confluencing and bifurcating rivers and canals may enhance or reduce effects of

boundary conditions (Welsch et al., under review). As studies regarding climate change in river deltas often only focus on either a single changing boundary (e.g. sea level rise) or on a part of the delta in isolation, the impact of discontinuities and combined effects might quickly be overlooked in a traditional scenario approach.

In this paper we make a first attempt to understand the impact of future developments affecting flood risk in an interconnected river delta. For this, we apply the scenario discovery methodology to determine which scenarios provide future vulnerabilities within the Dutch river delta. We define these future vulnerabilities as 'system deficiencies': scenarios in which the river system does not meet the desired criteria. We seek the answer to the following questions: (1) at which locations within the Dutch river delta are system deficiencies occurring due to uncertain future changes in hydrodynamics? and (2) which changing boundary conditions have most effect on the occurrence of these deficiencies?

1.1 Study area

In this study we focus on the rivers in the Dutch River Delta. This delta consists of the rivers Rhine and Meuse, Lake IJssel and a multitude of canals. The Rhine is the largest river and enters the Netherlands at Lobith, after which it bifurcates into the Waal and Pannerdensch Kanaal. The latter bifurcates again into the Nederrijn and the IJssel. The Waal and Nederrijn (which downstream becomes the Lek) both discharge in the North Sea. The IJssel culminates in Lake IJssel.

The river Waal receives the largest amount of discharge, roughly 2/3 of what is entering the Netherlands. The Nederrijn and IJssel split the remaining discharge in 2/3 and 1/3 respectively. This discharge distribution is set by law, as the flood safety standards are based on this distribution.

As flood protection measure, the Waal is confined at both sides by high dikes. The same holds for the IJssel, as almost the whole length of the river is embanked. Along the Nederrijn the embankments are mostly solely on the southern side, as the north side of the river is confined by higher terrain. The Lek is embanked on both sides again.

The Meuse enters the Netherlands at Borgharen. Shortly after entering the Netherlands, it splits into a free-flowing section and a shipping canal. Further downstream, both confluence again, after which the river enters the impounded section. In its final stretches, it becomes free flowing.

Figure 1. Rivers in the Dutch river delta and the embankments surrounding them.

2 METHOD

In line with the scenario discovery approach, first a large set of possible future scenarios is generated. Second, the scenarios are converted to water levels in the Dutch river delta using a 1D hydrodynamic model. Third, using the hydrodynamic conditions, the scenarios are filtered based on the occurrences of system deficiencies. Fourth, on the subset of scenarios where deficiencies occur, we apply a statistical data mining algorithm to find boundary conditions which produce clusters of scenarios leading to system deficiencies.

2.1 Scenarios

To draft a range of future conditions, we define a multitude of future scenarios. One scenario is defined by a unique combination of conditions at the four considered boundaries of our study area. E.g. a discharge for the Rhine and the Meuse, a given sea level and a storm surge set-up on Lake IJssel.

The scenarios are generated by sampling 2048 scenarios using a Sobol sampling scheme, assuming a uniform distribution for each sampled parameter. This uniform distribution is chosen, based on the comparisons and suggestions by Reis and Shortridge (2020) who assessed the impact of distribution choice for climate change under deep uncertainty. Since we adopted a possibilistic approach, all boundary conditions are assumed to vary independently from each other. An overview of boundary conditions is shown in Table 1.

The upstream river discharge boundary conditions are specified through two separate discharge hydrographs at the upstream model boundaries. These hydrographs are based on the Dutch standard discharge waves for the Rhine and Meuse (Hegnauer et al., 2023) (Figure 2a). We uniformly varied the peak discharge between the T100 and T10.000 return period for each river, where we accounted for the 95% uncertainty interval. The standard discharge hydrograph is scaled for each scenario based on the sampled peak discharge. For the Rhine this yields a discharge range of 11.167 m^3/s – 16.961 m^3/s and for the Meuse 2.430 – 5.120 m^3/s. We did not consider any cross-correlation between both river discharges when setting up scenarios. Additionally, on both the Rhine and Meuse, lateral inflows are neglected in this study since it is uncertain how they relate to the major rivers' discharges.

The downstream sea level is defined by an M2 water level tide, with a period of 12.25 hours and an amplitude of 100 cm, representative for the tidal amplitude at the river mouth. Since the three sea boundaries are in proximity to each other, we did not account for phase difference between the boundaries. To represent sea level rise, we superimpose the water level time series with a constant value. We thus consider climate change to only affect the base level (i.e. time-averaged water level). Changes in tidal periods and amplitudes are excluded. The range of sea level rise considered in this study is 0 – 5 m to capture future developments. A sea level increase of 5.15m is simultaneously the current T10.000 storm surge level at the river mouth.

The downstream boundary condition at Lake IJssel is defined as a stage-discharge relation (Figure 2b) where the stages are increased with a set-up based on the scenario. In case of prolonged periods of rain and/or strong winds, the water level in Lake IJssel rises at the mouth of the Ijssel. Additionally, the lake level might be increased in the future. This inclination in water level is represented in the scenarios by addition of a set-up on the stage-discharge relation. The set-up considered in this research is 0 – 2 m.

2.2 Hydrodynamic modelling

To translate the scenarios to water levels, we use a 1D hydrodynamic model, as developed by Welsch et al. (in press). To model the complete discharge hydrograph, we modelled 15 days before and after the peak discharge. To limit numerical effects, we included a spin-up period of 10 days, where the discharge is constant, equal to the discharge of the first day. We continued the simulation for ten days after the final step in the hydrograph (keeping the last river discharge constant), to let the complete discharge wave pass. In total this thus yielded a simulation time of 50 days.

Table 1. Overview of bounds used to uniformly sample boundary conditions.

	Unit	Lower bound	Upper bound
Rhine discharge	m^3/s	11.167	16.961
Meuse discharge	m^3/s	2.430	5.120
Sea level (rise)	m	0	5
Set-up Lake IJssel	m	0	2

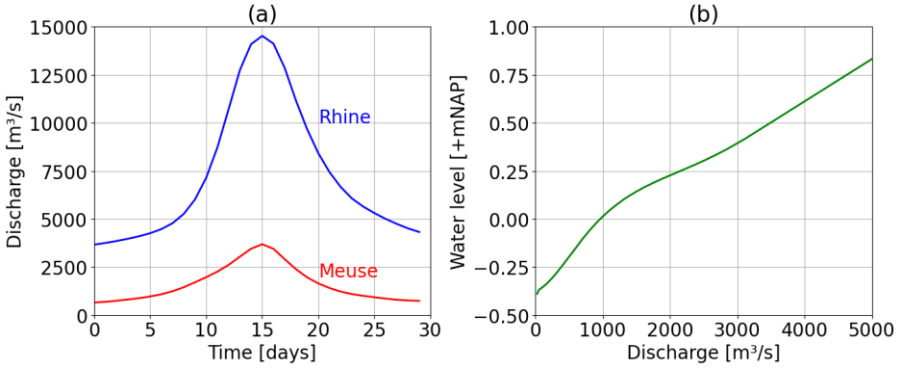

Figure 2. The reference boundary conditions in the model. (a) discharge hydrograph of the Rhine (blue) and the Meuse (red) and (b) the stage-discharge relation of the IJssel (river mouth).

2.3 System deficiencies

When defining our system deficiencies, we must determine in which cases the river system exceeds acceptable limits. As the focus of this study is on river flood modelling, we take the flood risk as indicator. Although flood risk assessment in the Netherlands is a complex method based on statistics, return periods and failure rates (Jongejan and Maaskant, 2015), we adopt a simpler approach as the scope of this research is to demonstrate application of scenario discovery in flood risk management. In this research, we consider the flood risk unacceptable in case the water level exceeds a certain threshold. This level is based on the minimum levee height along the river minus a safety margin. This safety margin consists of (a) a possible water level error due to modelling uncertainties (30 cm), and (b) a margin for wave run-up (20 cm). In summary, a system deficiency occurs if the water level along the river axis +50 cm exceeds the minimum crest height of the levee-transects in 500 m in up- and downstream direction.

2.4 Analysis

To find the combinations of boundary conditions which produce the most system deficiencies we apply the Patient Rule Induced Method (PRIM), first introduced by Friedman and Fisher (1999). The algorithm identifies subspaces (i.e. clusters) in the hyperspace spanned by the considered variables, which in this study are the boundary conditions. The subspaces are determined by hyperrectangular cubes with an upper- and lower bound for each variable which contributes to the bottlenecks. The PRIM algorithm uses a patient hill climbing optimization algorithm. In this study, we made use of the Exploratory Modelling Workbench (Kwakkel, 2017) to carry out the PRIM analysis.

In the analysis we first filtered the scenarios where deficiencies occur, as only these scenarios are of interest to us (see for example Figure 3a-b). Then, we let the PRIM algorithm find a box based on its internal optimization procedures by evaluating the peeling trajectory (e.g. Figure 3c). A balance must be found between the density (how many points within the box are of interest) and the coverage (how many of the total cases of interest are within the box) of the resulting box. This trade-off is characterized by a pareto-front: if one of them increases, the other one must decrease. For this analysis, the choice is made to select the box with the highest density, with the constraint that the marginal increase in density should be greater than the decrease in coverage (red circle in Figure 3c) along this peeling trajectory.

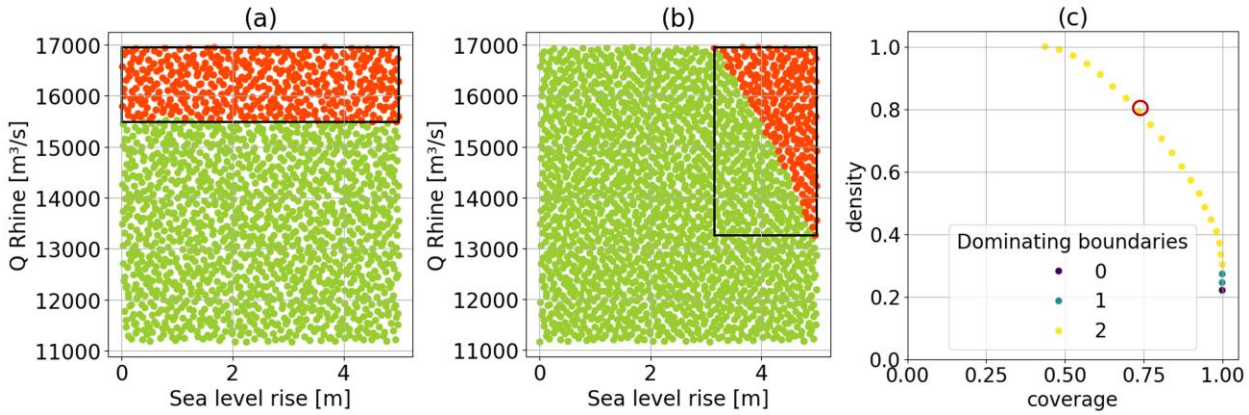

Figure 3. (a-b) Examples of scatter plots of Rhine discharge and sea level rise for two locations. The red dots represent a system deficiency. The boxes are drawn for a coverage of 1 (all deficiencies within the box). (a) shows a clear influence of only the Rhine discharge, while (b) shows dependence of both the Rhine discharge and the sea level. (c) An example peeling trajectory which displays the trade-off between coverage and density. The red circle shows the selected iteration based on the criteria in this study.

3 RESULTS

3.1 Spatial occurrence of system deficiencies

From the analysis (Figure 4) it becomes clear that system deficiencies occur along all rivers for the analysed scenarios. For each of the four major rivers, the spatial pattern differs. Most strikingly is the Meuse, where system deficiencies occur along the complete river stretch. The relative number of scenarios leading to deficiencies on this river is also very high, with the intensity centred in the northern part of the Meuse section. Partly, this might be an artefact of our analysis. This part of the Meuse naturally contains relatively few embankments as the river is constrained by higher grounds. However, at some places minor embankments are present to protect local areas (within the floodplains). As we do not consider natural elevation to be able to lead to deficiencies, only the local embankments are considered. Besides artefacts, the striking results can be explained by the design characteristics of the embankments. The embankments are designed based amongst others on a certain design discharge, based on a set return period. In this study, we vary the Meuse discharge between return periods of 100-10.000 years, while the current design discharge on the Meuse is in the lower regions of this range. It is thus to be expected that deficiencies occur for discharges which exceed the current design standard. Along the river Waal, system deficiencies also occur throughout the complete river stretch. Compared to the Meuse, the relative number of system deficiencies is much lower, but nevertheless still around 20-40%.

The patterns along the Nederrijn/Lek and IJssel differ in the sense that deficiencies occur locally. On the Nederrijn/Lek, the deficiencies mainly occur downstream. On the Nederrijn/Lek, the low percentage of scenarios leading to deficiencies is partly explained by the fact that this river stretch is only embanked at the south side of the river. In the north, the river is contained by natural higher grounds, which are not considered in this study. Thus, only a limited length of embankments is considered in this region of the analysis. On the IJssel, three very distinct clusters arise. Closer analysis shows that the deficiencies at these locations occur due to water level increase due to the local geometry of the river. The embankments do not show sudden descrease in height at these locations. At the first location, shortly after the bifurcation, the river has series of sharp bends, leading to water level set-up. At the middle and northernmost location, the water level set-up is due to a local narrowing of the river. The found deficiencies along the IJssel are thus not due to local decrease of levee heights.

The overall outcomes show that the scenario discovery approach provides insights in the spatial distributions of system deficiencies occurring on a large delta scale.

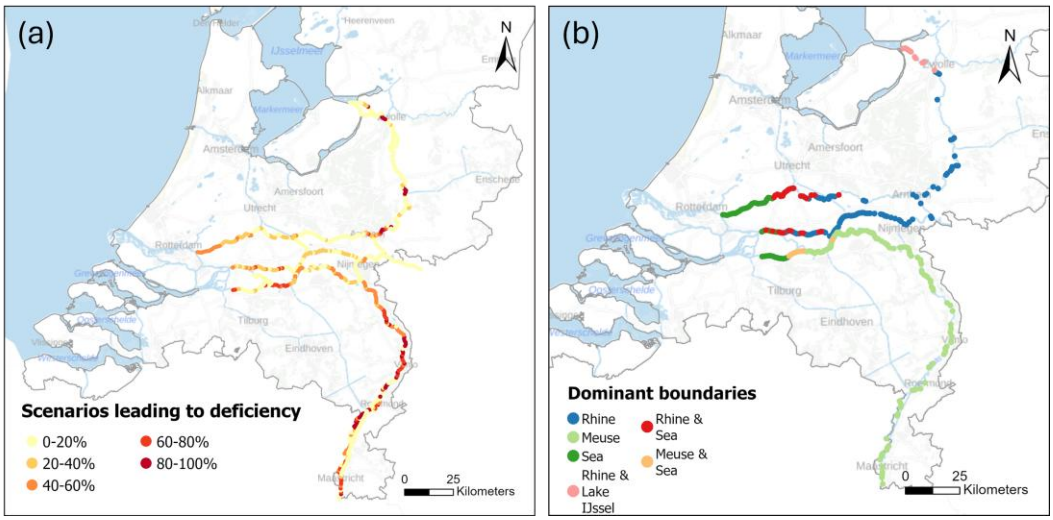

Figure 4. Outcomes of the scenario discovery: (a) fraction of scenarios leading to a system deficiency, (b) main contributors to the system deficiencies based on the PRIM algorithm.

3.2 Contributors to the system deficiencies

Application of the PRIM algorithm provides insight in the boundary conditions which contribute to the system deficiencies. Parameters which can be restricted to describe a cluster of system deficiencies in the overall outcome hyperspace are of importance. We apply this algorithm spatially as we carry out the analysis for each river kilometre independently of the others.

Outcomes show the spatial extent of the influence of boundary conditions on the occurrence of system deficiencies. In general, the arising pattern is in line with common expectations based on open channel hydraulics. In the upstream sections of the rivers, the deficiencies are determined by the upstream river discharge. At the downstream end, the occurrence of deficiencies is driven by the downstream sea level. In between both regions, there is a stretch where the deficiencies are driven both by the upstream as well as the downstream conditions. PRIM allows to spatially map out these different regions, showing explicitly where the upstream dominated zone ends and the downstream boundaries also determine the occurrence of deficiencies. However, there seems no mutual effect of both the Rhine and Meuse discharge in the downstream stretches of the Waal and Meuse. Possibly, the timing of both discharge wave is of importance here as well, which is not varied in the current study.

Another interesting observation is the difference in length of river stretch which is impacted by the sea when comparing the Nederrijn/Lek and Waal. In the flood scenarios considered, the deficiencies along the Waal are almost everywhere driven by, at least, the upstream discharge. Simultaneously, in the Nederrijn/Lek, a considerable stretch of river is mainly driven by the downstream sea level. For a physical explanation of this difference, open channel hydraulics again can provide answers. Due to the upstream bifurcations, the discharge on the Waal is trice the discharge of the Nederrijn/Lek (2/3 and 2/9 of the discharge at Lobith respectively. This larger discharge makes that the effect of the downstream boundary decreases. The PRIM analysis shows the spatial impact of this physical knowledge.

On all rivers, some isolated cases can be found as well. On the Waal for example, there are some locations where the sea level does seem to contribute to system deficiencies, while up- and downstream the deficiencies are mainly determined by the upstream Rhine discharge. Closer inspection shows the occurrence of these locations are of physical origin, due to the local geometry of the river.

One of the requirements for successful application of PRIM is that the hyperspace contains sufficient scenarios of interest. Along the rivers where only a small percentage of scenarios lead to system deficiencies, carrying out the analysis is thus not possible. Therefore, not for all considered locations outcomes are shown in Figure 4b. The locations along the river where no results are presented, contain too little number of scenarios of interest. This is in line with the lowest class shown in Figure 4a.

The opposite is also the case: the PRIM analysis shows the main drivers of the system deficiencies. As the algorithm is based on high-dimensional bump hunting, there must be made a trade-off between the coverage and density. Since we base this trade-off to favour a point somewhere along this trade-off, rather than always choosing a coverage of 1; scenarios leading to system deficiencies are excluded from the final boxes contained by the restricting boundary conditions. In other words, the presented outcomes in Figure 4b do not imply that the shown boundary conditions are the only drivers for system deficiencies at that specific location, but only the dominant drivers are shown.

4 DISCUSSION

Model wise, some remarks can be made to the presented works. As stated in the methods sections, lateral flows into the river systems are omitted. During peak flow situations, the impact of the additional discharges adds to the water levels, depending on the timing and the amount. Currently, little is known about the future developments of these lateral flows in relation to the discharge in the main river, making it difficult to assess the impact of omitting the laterals in this study. Based on analysis of a recent flood in the Meuse, the effect of the regional water system can be large. However, this was the case in an area with large gradients in elevation, which is not the case in most parts in the considered river delta.

As elucidated in section 1.1, the Dutch river delta is a complex network which can be operated to some extent through a collection of water management constructions. The hydrodynamic model operates these constructions based on the default operational rules. However, in the Netherlands, during impending floods, crisis teams at different levels of government assemble to act based on flood risks and (short-term) forecasts. Decisions taken by these crisis teams might deviate from default operations and are thus not incorporated in the presented results.

As stated in section 2.2, an oversimplification of the flood risk approach in the Netherlands has been made to illustrate the application of scenario discovery in an interconnected river delta case. In practice, flood risk design is a complex approach based on probabilities and assessment of different failure modes. The presented outcomes are thus also to be seen in that light: the presented system deficiencies do not represent dike overtopping locations or possible dike failures under future conditions. It does show the locations where the flood standards do not meet the requirements set in this study and shows its ability to relate these deficiencies to boundary conditions. For real-world applications, this definition of system deficiencies is advised to specify to better reflect design standards.

A general downside of the PRIM algorithm is that it uses a ‘patient’ hill climbing optimization procedure. Therefore, PRIM might only find a local optimum, while this is not the global optimum. To overcome this, different additional analysis techniques have been proposed (e.g. quasi p-values (Bryant and Lempert, 2010) or introducing machine learning (Kwakkel and Cunningham, 2016). Although we agree with this limitation in PRIM, we do not expect it to have major influence on the outcomes, as we do not expect multiple isolated local clusters in the outcomes. In general, increasing the considered boundary conditions leads to increased water levels. It is not expected that a further increase lowers the water levels again. Thus, this limitation is less of a concern in the presented outcomes.

The PRIM approach does add some room for interpretation for the researcher: as it is up to the user of the methodology to make the trade-off between coverage and density. In this research, a balance was strived for. However, for specific cases, the analyst, or the policy maker, might be interested in another balance: e.g. a coverage of 1 could be desired if no system deficiencies are allowed.

5 CONCLUSION

We assessed the occurrence of system deficiencies within an interconnected river delta by combining scenario discovery with a one-dimensional hydrodynamic model. We showed that on some rivers the deficiencies occur along the complete river stretch, while on other rivers the deficiencies occur only locally (driven by the river’s geometry). The most deficiencies occur along the complete Meuse. On

the IJssel, the deficiencies occur in clusters, due to local river geometry. On the Waal and Lek, the deficiencies also occur along the whole river.

Additionally, the presented methodology shows the spatial influence of the uncertain boundary conditions. Overall, most part of the considered river delta is mainly driven by the upstream river's discharge. Downstream it is an interplay between the discharge and the sea level rise. Surprisingly, the interaction between the Rhine and Meuse is not dominant in system deficiency occurrence.

The overall outcomes of this study show that the methodology has the potential of providing the basis for a structural stress testing procedure to prepare future deltas for the vulnerabilities against the effects of climate change.

6 ACKNOWLEDGEMENTS

This work is co-funded by Rijkswaterstaat within the framework of "Kennisimpuls Klimaatadaptatie, Rijkswaterstaat 225 jaar".

REFERENCES

Bryant, B. P., & Lempert, R. J. (2010). Thinking inside the box: A participatory, computer-assisted approach to scenario discovery. *Technological Forecasting and Social Change*, 77(1), 34–49.

Driessen, T. L. A., & van Ledden, M. (2013). The large-scale impact of climate change to Mississippi flood hazard in New Orleans. *Drinking Water Eng Sci*, 6(2), 81–87.

Ericson, J., Vorosmarty, C., Dingman, S., Ward, L., & Meybeck, M. (2006). Effective sea-level rise and deltas: Causes of change and human dimension implications. *Global Planet Change*, 50(1–2), 63–82.

Friedman, J. H., & Fisher, N. I. (1999). Bump hunting in high-dimensional data. *Statistics and Computing*, 9(2), 123–143.

Haasnoot, M., & Middelkoop, H. (2012). A history of futures: A review of scenario use in water policy studies in the Netherlands. *Environ Sci Policy*, 19–20(6), 108–120.

Hegnauer, M., Beersma, J., van den Brink, H., Leander, R. (2023). Generator of Rainfall and Discharge Extremes for the Rhine. (Publication No. 11205237-003-ZWS-0016)

Jongejan, R.B., & Maaskant, B. (2015). Quantifying flood risks in the Netherlands. *Risk Anal*, *35*(2), 252–264.

Klijn, F., Kreibich, H., de Moel, H., & Penning-Rowsell, E. (2015). Adaptive flood risk management planning based on a comprehensive flood risk conceptualisation. *Mitigation Adapt Strategies Global Change*, 20(6), 845–864.

Kwakkel, J.H. (2017). The Exploratory Modeling Workbench: An open-source toolkit for exploratory modeling, scenario discovery, and (multi-objective) robust decision making. *Env. Mod. Soft.*, *96*, 239–250.

Kwakkel, J. H., & Cunningham, S. C. (2016). Improving scenario discovery by bagging random boxes. *Technol Forecasting Social Change*, 111, 124–134.

Kwakkel, Jan H., Walker, W. E., & Marchau, V. A. W. J. (2010). Classifying and communicating uncertainties in model-based policy analysis. *Int J Technol Policy Manage*, 10(4), 299.

Lempert, R. J., Groves, D. G., Popper, S. W., & Bankes, S. C. (2006). A general, analytic method for generating robust strategies and narrative scenarios. *Manage Sci*, 52(4), 514–528.

Postma, T. J. B. M., & Liebl, F. (2005). How to improve scenario analysis as a strategic management tool? *Technol Forecasting Social Change*, 72(2), 161–173.

Reis, J., & Shortridge, J. (2020). Impact of uncertainty parameter distribution on robust decision-making outcomes for climate change adaptation under deep uncertainty. Risk Analysis: An Official Publication of the Society for Risk Analysis, 40(3), 494–511.

te Linde, A. H., Aerts, J. C. J. H., Bakker, A. M. R., & Kwadijk, J. C. J. (2010). Simulating low-probability peak discharges for the Rhine basin using resampled climate modeling data. *Water Resour Res*, 46(3).

Teng, J., Jakeman, A. J., Vaze, J., Croke, B. F. W., Dutta, D., & Kim, S. (2017). Flood inundation modelling: A review of methods, recent advances and uncertainty analysis. *Environ Modell Software*, 90, 201–216.

Welsch, N.M., Warmink, J.J., Hulscher, S.J.M.H., Augustijn, D.C.M. (*in press*) The importance of system interactions in hydrodynamic models of parts of complex interconnected deltas. *Env. Mod. Soft.*

ICFM 10
Adapting to Global Change:
Innovative Approaches to Flood Management and Resilience
May 20-22, 2026 | Western University, London, Ontario, Canada

Shifting Streamflow Regimes and Unusual Flood Events have an Impact on Flood Frequency Analysis for Cold Regions Watersheds

Donald H. Burn[1] and Paul H. Whitfield[2]
Dept. of Civil & Environmental Engineering, University of Waterloo, Waterloo, ON, Canada, N2L 3G1[1]
E-mail: donburn369@gmail.com

Center for Hydrology Coldwater Laboratory, University of Saskatchewan, Canmore, AB, Canada[2]
E-mail: paul.h.whitfield@gmail.com

ABSTRACT

Climate change is affecting flood events in complicated ways. In cold regions, the frequency of different flood drivers has shifted causing important changes in flood distributions that lead to challenges for flood frequency analysis (FFA). An assumption in FFA is that the flood series consists of independent events that are identically distributed. This assumption is unlikely to hold if there are i): changes occurring in the magnitude of flood events; ii) a mixture of flood generating processes; or iii) changes with time in the mixture of flood processes. A particular concern for FFA is when events that are large in magnitude occur outside the most common streamflow peak season. Such events can be characterized as Rogue events that are distinct from the commonly observed flood generating process in a watershed.

Significant changes in flood type fraction were found such that nival events decreased in frequency while mixed and pluvial events increased. These changes indicate a shift from nival events towards more pluvial dominated systems in other seasons. Flood frequency analysis using a combined distribution approach with the three flood types resulted in larger magnitude design flow estimates in comparison with the results from considering the data to be from a single population. The characteristics of Rogue events were explored using single dimension detection for magnitude and timing outliers, and multi-dimensional detection of magnitude/timing density outliers. The methods identify large events that are outliers in several distinct ways and are therefore considered Rogue events. The prevalence of Rogue events is explored by applying the methodology to more than 2100 hydrometric stations from Canada and the United States. The spatial and temporal distributions of these events are compared and the implications of the Rogue events for FFA are investigated.

KEYWORDS: cold regions hydrology; regime shifts; flood frequency analysis; rogue events

1 INTRODUCTION

Climate change is affecting flood events but the relationship between floods and climate change is complex. Recent research has demonstrated that the frequency of different flood drivers has shifted potentially causing changes in flood distributions (Mallakpour and Villarini 2015, Burn and Whitfield 2016). These shifts create challenges for FFA.

Changes in flood events have important ramifications for FFA, which forms the basis for the design and operation of flood protection systems and related infrastructure. An assumption in FFA is that the available flood series consists of independent events that are identically distributed (the IID assumption). The IID assumption is unlikely to hold if there are i): changes occurring in the magnitude of flood events as a function of a covariate, such as time; ii) a mixture of flood generating processes (e.g., Barth et al. 2017); or iii) changes with time in the mixture of flood processes (Burn and Whitfield 2023).

A variety of processes control the time of occurrence, duration, extent, and severity of river floods (Whitfield 2012) and the flood generating processes may change or shift over time. While no unified definition of causative mechanisms of flood events exists, Burn and Whitfield (2018) suggest viewing hydrologic regime as a nival-pluvial continuum with sites potentially moving over time from a purely nival regime towards a greater influence of pluvial events. Flood generating processes vary by region, season, and event severity. Changes in flood seasonality are most pronounced where snow accumulation and melt are the important flood generating processes (Köplin et al. 2014).

For the northern mid-latitude of North America, Burn and Whitfield (2023) showed changes in flood regime over time at 46 sites over an 80-year period. Strongly nival and pluvial watersheds show no changes, but stations with flood mixtures show an increasing influence of pluvial events. Tramblay et al. (2023) showed that changes in the flood generation mechanism, rather than trends, were occurring in the Mediterranean area based on annual peak flows from three rainfall types. In the UK, the duration and intensity of dry and wet spells increased with climate change, flash floods became less likely, but the probability of rain driven (pluvial) floods intensified (Rahmani and Fattahi 2023).

A method is presented (Burn and Whitfield, 2025) that uses circular statistics to cluster flood events and the clusters that are formed are linked to streamflow regime and climatology allowing separation of nival, mixed, and pluvial Peaks over Threshold (POT) events providing increased resolution of flood generating processes. The separation of event types allows the determination of changes in the frequency of event types over time and with temperature, precipitation, and climate indices.

Recently, emphasis has shifted to "strange" and "extreme" floods (Bertola et al. 2024). These extreme events often are not generated by the most commonly observed generating processes but rather may occur as a result of atmospheric rivers (Barth et al. 2017), hurricanes, or other large-scale processes (Whitfield and Pomeroy, 2016). The second part of this study presents a methodology to identify Rogue flood of record (FoR) events that are large in magnitude and occur outside the most common flood season or are simply different from the majority of observations. To identify Rogue R3-FoR events, the proposed method combines detection of [1] magnitude outliers, such as the flood-of-record, with [2] timing outliers, and [3] density outliers. Other "Interesting FoR" (R2-FoR) are detected when only two of the three conditions apply, specifically magnitude and timing or magnitude and density. While there is widespread familiarity with outliers in a single dimension, outliers in direction and multidimensions can be detected. These events are particularly interesting because they are outside the commonly observed generating process in a watershed, i.e., they are completely different to the 'regular' flood-generating mechanism, and may violate the IID assumption. An example would be a nival catchment where the annual peak is usually from snowmelt in spring/summer, but large events that occur in fall or winter are generated by an alternate process such as a hurricane or an atmospheric river. The proposed methodology is applied to more than 2100 reference and natural hydrometric stations across North America. The identified events are considered spatially and temporally to demonstrate that these are not random in space or time. This work is a step towards providing practitioners an approach that can be used to estimate appropriate design floods for cases where there are mixed flood generating processes, changes in the mixture of flood processes, or unusual flood events in the flood record.

2 METHODOLOGY

2.1 Changes in Flood Processes

All streamflow data used in the analysis were from gauging stations that are part of a Reference Hydrologic Network (RHN). Stations were selected from cold-region locations in Canada and the United States where nival or a mix of nival and pluvial flood events could be anticipated based on the location and the elevation of the gauging station. All stations were required to have an essentially complete data record for the 70-year period from 1951 to 2020. An essentially complete record was considered to entail no more than three missing years in a row, and no more than seven missing years in total where data for a year are considered to be missing if there are any days in the year with no data. A total of 202 stations

were analyzed with 49 stations from Canada and 153 from the United States. POT data were used in this research, rather than annual maximum data, since POT data will generally result in more flood events than annual maximum data and have been reported to be superior to annual maximum data for flood frequency analysis (Pan et al. 2022).

The first step is to assign a flood process to each over threshold event. The approach is based on clustering of the event dates and builds on the approach of Burn and Whitfield (2023). There is a strong link between the time of the year of flood events and the flood generating process for a flood event (Blöschl et al. 2017). The date of the maximum flow for the POT events for a site are grouped into clusters using circular clustering; circular clustering is described in Whitfield (2018). The clustering was conducted using partitioning around mediods (pam), with the implementation of the pam algorithm through the R package "cluster" (Maechler et al. 2019). Five clusters were used in the subsequent analysis as a consensus preferred number of clusters based on six clustering indices. See Burn and Whitfield (2025) for further details. The POT events in five clusters were regrouped into three flood types (nival, mixed, and pluvial) using median daily streamflow and monthly climatology. Nival events are associated with the spring freshet, pluvial events arise from rainfall and mixed events result from rainfall on a snowpack, or rain on snow (ROS), that did not occur during the freshet season. Three flood types are considered herein to increase the total number of events of each flood type and decrease the uncertainty in estimates of flood quantiles. The process of identifying a flood type for the events in each cluster used polar plots (Pewsey et al. 2014) to which information regarding the flood regime for each station was added. The polar plots, and ancillary information that included median daily flows as well as monthly climatology, were used to identify flood types for events. Monthly climatological variables used were temperature, precipitation depth and snow depth for the location of the gauging station, based on the 1961 – 1990 climate normal.

Changes in the fraction of flood events of a given type were evaluated using logistic regression (Frei and Schär 2001), with a correction for overdispersion. Logistic regression is used when the independent variable in a regression relationship is binary. The variable of interest is the fraction of flood events so the independent variable for this analysis is the count of flood events of the flood type of interest (e.g., nival) and the combined count of the other two flood types (e.g., mixed and pluvial). The model estimates the probability of an event of the flood type of interest as a function of a predictor variable. For each site, logistic regression was applied considering each flood type (nival, mixed, and pluvial) as the flood type of interest. Predictor variables considered were: time (year); mean annual temperature; mean annual precipitation; and four climate indices. Further details on the implementation of logistic regression can be found in Burn and Whitfield (2025).

The final step in the methodology was an application of FFA based on a combined, or mixed, distribution approach for sites with two or three identified flood types following the approach used by Waylen and Woo (1982). The combined distribution can be defined as:

$$F_C(x) = F_N(x) \times F_M(x) \times F_P(x) \quad (1)$$

where $F_C(x)$ is the combined distribution, subscripts N, M and P refer to the distribution fit to the nival, mixed and pluvial events, respectively, and x is the over threshold event. The Generalized Pareto Distribution (GDP) was used to fit a distribution to the nival, mixed and pluvial POT data using L-Moments. If a site does not have events of a given flood type, the corresponding term in Equation (1) is not included. The results from the combined distribution approach were compared to results from fitting a distribution to the entire dataset considered as a single population. A minimum data set size of 20 over threshold events for a flood type was selected as it was thought that 20 represents a reasonable balance between the number of sites for which analysis can be conducted and the uncertainty associated with the design flood estimates.

2.2 Rogue Flood Events

Rogue flood events were identified from daily streamflow data for sites with more than 50 years of data resulting in 2123 hydrometric stations in Canada and the US. For each site, the annual maximum daily discharge and the date on which it occurred were extracted for the daily flow record. Any year with only a partial record was removed.

Methods for outlier detection were used to identify different aspects of FoR extreme events. There are many different methods to determine outliers. Recently, data mining has produced several tests that can detect outliers with other attributes than available with a single variable. The exploration of outliers sought to find methods that were available and practical to implement. To describe these, it is useful to separate into three categories: magnitude, timing, and multidimensional density (timing and magnitude). Three methods were retained to identify N-FoR, R3-FoR or R2-FoR for the analysis presented here. These methods were focused on identifying three types of FoR outliers: [1] magnitude, [2] timing, and [3] combined magnitude and timing. The combination of these three provides the information to determine if a flood-of-record is 'normal' (N-FoR) implying similar to most floods at the site, but the largest, an R2-FoR, which is similar to 'normal' but not part of the distribution of 'normal' events, or, an R3-FoR, which is a flood event that is not 'normal' but larger, with different timing, and not part of the distribution of normal events. Further details on the methods used to identify outliers can be found in Whitfield and Burn (2026).

3 RESULTS

3.1 Changes in Flood Processes

The change in the fraction of events of a given flood type with time (year) are summarized in Table 1. The results indicate that, for some categories, there are substantively more changes than would be expected to occur by chance. Noteworthy is the decrease in the fraction of nival events with time. There is also an increase in the fraction of pluvial events. The decrease in the fraction of nival events and increase in the fraction of pluvial events suggests that a shift from nival towards pluvial events is a strong climate change signal for this data set. Mixed events are experiencing fewer changes over time. Fewer changes in the fraction of mixed events likely reflects the occurrence of more mixed events based on a shift from nival events balanced by fewer mixed events as mixed events shift to a pluvial flood response. Similar results were obtained for annual temperature or annual precipitation as the explanatory variable.

Table 1. Percent stations with changes in flood processes with time using logistic regression.

Significance Level	Nival	Mixed	Pluvial
Increase 5%	1.8%	5.0%	14.9%
Increase 10%	3.0%	8.3%	20.0%
Decrease 10%	21.5%	7.5%	1.7%
Decrease 5%	16.1%	4.2%	0.6%

The results from the combined frequency analysis approach are displayed in the form of boxplots of design flow ratios that are calculated as the design flow from the combined frequency analysis approach divided by the design flow from considering the entire data set as a single population. Figure 1 presents results for sites with three flood types. Sites were only included in the analysis if there was a minimum number of events for a flood type. For thresholds of 15, 20 and 25, the numbers of sites for 3 flood types were 74, 59 and 30, as shown on Figure 1.

The boxplots in Figure 1 are arranged by increasing return period values on the horizontal axis with three boxplots for each return period showing results, from left to right, for 15, 20 and 25 as the threshold for the minimum number of events for a flood type. The data points are superimposed on the boxplots in

3 columns with the left column (black upward triangles) for sites where the combined estimate is above the 95% confidence limit for the entire dataset estimate while the middle (grey circles) and right (black downward triangles) columns indicate sites that are, respectively, within and below the 95% confidence limits.

Values greater than one on the graphs indicate that the combined estimate (EQ 1) is larger than the single dataset estimate. It can be observed that the median design flow ratio is in the range of around 1.2 to 1.3 for all results presented indicating that a larger combined estimate is the norm. Increasing the minimum record length results in a narrower spread of the results. While the median design flow ratio is often slightly lower for the 15-event minimum record length, there is no systematic pattern in median design flow ratio as a function of the minimum record length in that the values for 20 and 25 record length minimum are generally quite similar. There is a preponderance of combined estimates of design flow that are above the 95% confidence limit of the single dataset estimate (black upward triangles) with this being more prevalent for shorter return periods. There are no combined estimates that are below the 95% confidence limit for the single dataset estimate.

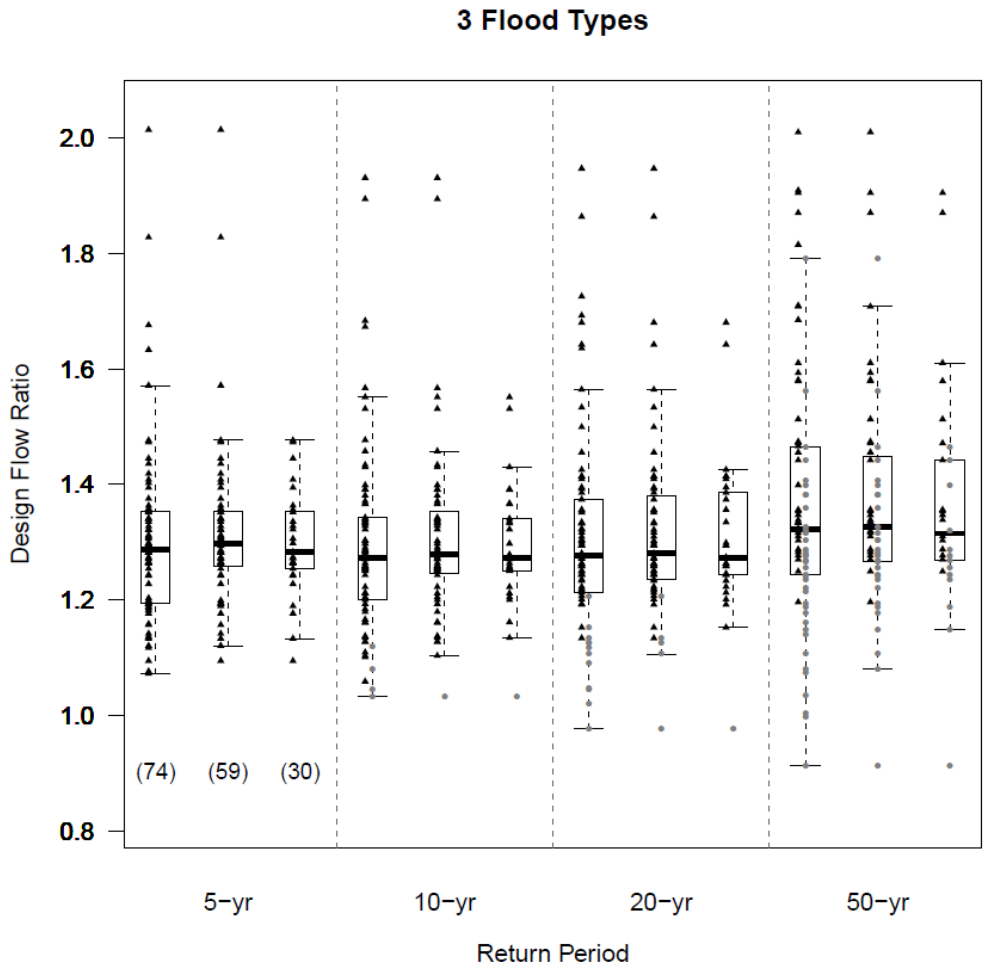

Figure 1: Boxplots of design flow ratio for sites with three flood types. The solid line inside the box indicates the median value and the box encompasses the 25th to the 75th percentile. The whiskers extend 1.5 times the interquartile range from the box. Points plotted as upwards black triangles, grey circles and downward black triangles indicate observed values that are above, within, and below the 95% confidence limits, respectively.

3.2 Rogue Flood Events

R3-FoR events, which are larger, with different timing, and not part of the distribution of normal events, are relatively rare, only about 10 % of the total number of cases (205/2123). R2-FoR events are more common as the selection is less stringent, constituting about 39 % (823) of the cases and N-FoR events represent 51 % (1095/2123).

The distribution of the flood-of-record events over time is shown in Figure 2. There are fewer FoR events in the early part of this plot because there were fewer stations in operation before 1960. There is no obvious trend in any of the N-FoR, R2-FoR, nor R3-FoR events, but a few years stick out as having more R3-FoR events such as 1937, 1954, and 2010 (Figure 2).

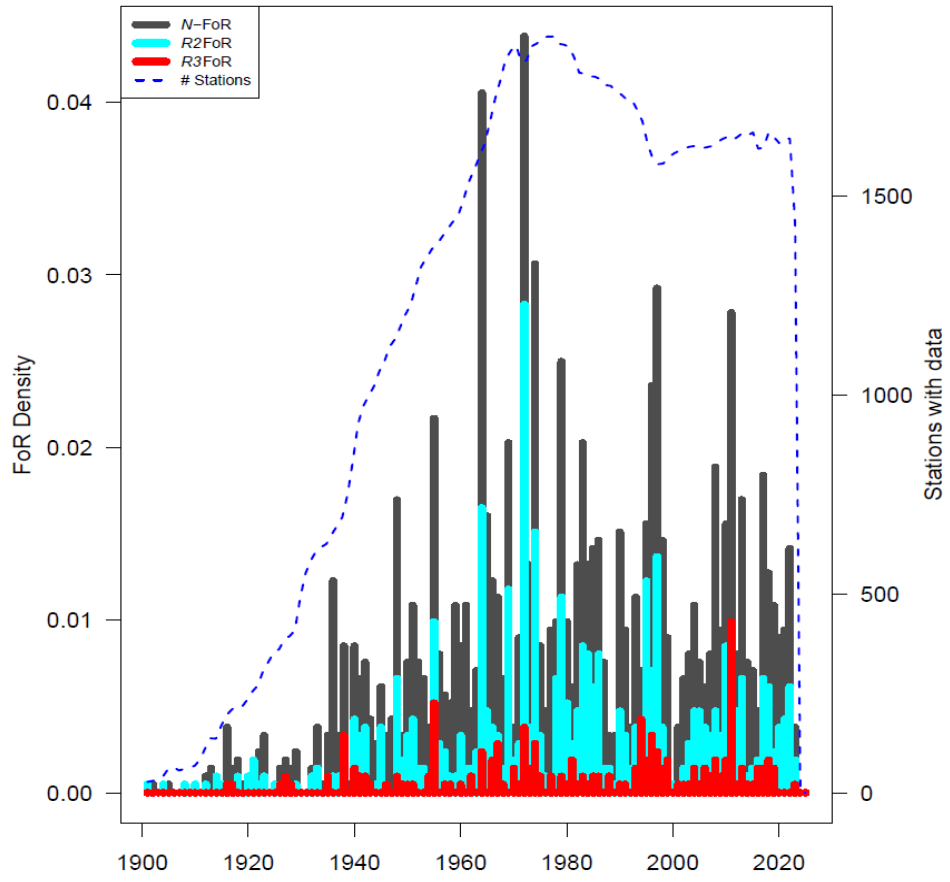

Figure 2: Histogram of flood-of-record (N-FoR), R2-FoR, R3-FoR events by year for the 2123 study stations. Also shown is the number of stations with data for each calendar year (dashed line)

4 DISCUSSION

The observed changes in the fraction of flood types have implications for FFA particularly since a comparison of design flow estimates in this work revealed that using the combined distribution approach generally resulted in higher estimates than those obtained from considering the entire data set as one population. The median increases in design flow estimates, for different return periods, were in the range of 20 to 30% (Figure 1). Large flood events are often not simply the largest of a common type of flood

event in a watershed (Bertola et al. 2024). Large flood events often originate from different processes than most of the observed floods for the basin having separate and distinct flood generation mechanisms such as hurricanes, atmospheric rivers and mesoscale events (Whitfield and Pomeroy 2016). Many sites have a limited number of floods from the subpopulation that generated the flood of record, which results in large uncertainty associated with estimates of design flows calculated using the combined distribution approach. A small number of events of the flood type responsible for the flood of record, as well as other large flood events, creates challenges for water professionals who must estimate design flow values for the design of critical infrastructure. Recent studies have considered extreme floods but have not addressed the issue of timing. We approach the study of large floods in this study by explicitly addressing the nature of the flood-of-record with respect to magnitude and timing. We adopt methods that identify outliers in large floods based on magnitude, timing, and magnitude with timing using three separate outlier detection methods.

Identifying Floods-of-Record that are not the result of the dominate flood generating process in a basin has several consequences. Most importantly, such events mean that the assumptions of FFA may be violated, but, unlike low outliers, these events cannot be censored.

5 CONCLUSION

This research emphasizes the importance of considering multiple flood types in flood frequency analysis. Flood frequency analysis using a combined distribution approach with three flood types resulted in larger magnitude design flow estimates with a median increase of 20 – 30 % in comparison with the results from considering the data set to be from a single population. Flood frequency analysis also needs to consider changes in the mix of flood types by adopting a broader definition of nonstationarity that considers more than just flood magnitudes. Challenges exist for designing flood protection works, and other critical infrastructure, due to short record lengths for less frequently occurring flood types, which may include the flood of record for a site. While there are no trends over time in the occurrence of Rogue events, they are expected to increase in a warming world where runoff events are becoming more common throughout the year. This too has important implications for flood frequency analysis.

6 ACKNOWLEDGEMENTS

This research was partially supported by funding provided by the Natural Sciences and Engineering Research Council of Canada (NSERC) and Global Water Futures.

REFERENCES

Barth, N.A., Villarini, G., Nayak, M.A. and White, K. (2017). Mixed populations and annual flood frequency estimates in the western United States: The role of atmospheric rivers. Water Resources Research, 53, 257-269.

Bertola, M., Castellarin, A., Viglione, A., Valtancoli, E. and Blöschl, G. (2024). Frequency and spatial variability of European record floods. Water Resources Research, 60(10), e2023WR036767.

Blöschl, G., Hall, J., Parajka, J., Perdigão, R.A.P., Merz, B., Arheimer, B., Aronica, G.T. et al. (2017). Changing climate shifts timing of European floods. Science, 357 (6351), 588-590.

Burn, D.H. and Whitfield, P.H. (2016). Changes in floods and flood regimes in Canada. Canadian Water Resources Journal, 41, 139-150.

Burn, D.H. and Whitfield, P.H. (2018). Changes in flood events inferred from centennial length streamflow data records. Advances in Water Resources, 121, 333-349.

Burn, D.H. and Whitfield, P.H. (2023). Climate related changes to flood regimes show an increasing rainfall influence. Journal of Hydrology, 617, 129075.

Burn, D.H. and Whitfield, P.H. (2025). Shifting cold regions streamflow regimes in North America affect flood frequency analysis. Hydrological Sciences Journal, 70, 51-70.
Frei, C., and Schär. C. (2001). Detection probability of trends in rare events: Theory and application to heavy precipitation in the Alpine region. Journal of Climate, 14, 1568-1584.
Köplin, N., Schädler, B., Viviroli, D. and Weingartner, R. (2014). Seasonality and magnitude of floods in Switzerland under future climate change. Hydrological Processes, 28, 2567-2578.
Maechler, M., Rousseeuw, P.J., Struyf, A., Hubert, M. and Hornik, K.M. (2019). cluster: Cluster Analysis Basics and Extensions. R package version 2 (0).
Mallakpour, I. and Villarini, G. (2015). The changing nature of flooding across the central United States. Nature Climate Change, 5, 250–254.
Rahmani, F. and Fattahi, M.H. (2023). Investigation of alterations in droughts and floods patterns induced by climate change. Acta Geophysica, 1-14.
Tramblay, Y., Arnaud, P., Artigue, G., Lang, M., Paquet, E., Neppel, L. and Sauquet, E. (2023). Changes in Mediterranean flood processes and seasonality. Hydrology and Earth System Sciences, 27, 2973–2987.
Whitfield, P.H. (2012). Floods in future climates: A review. Journal of Flood Risk Management, 5, 336-365.
Whitfield, P.H. (2018). Clustering of seasonal events: A simulation study using circular methods. Communications in Statistics - Simulation and Computation, 47, 3008-3030.
Whitfield, P.H. and Pomeroy, J.W. (2016). Changes to flood peaks of a mountain river: implications for analysis of the 2013 flood in the upper Bow River, Canada. Hydrological Processes, 30, 4657-4673.
Whitfield, P.H. and Burn, D.H. (2026). Rogue and Extreme Floods in North America, submitted to Journal of Hydrology.

ICFM 10
Adapting to Global Change:
Innovative Approaches to Flood Management and Resilience
May 20-22, 2026 | Western University, London, Ontario, Canada

Exploring Hydrologic Extremes in the Nicola River Watershed: Weaving Science and Traditional Knowledge Together

Reza Rezvani[1], Tamsin Lyle[1], Nikoletta Stamatatou[1], and Yinlue Wang[1]
Ebbwater Consulting Inc., Vancouver, British Columbia, V6B 1S5, Canada[1]
E-mail: tamsin@ebbwater.ca

ABSTRACT

Floods and droughts can adversely impact ecosystems and communities and are projected to intensify under climate change. The Nicola River watershed in British Columbia has experienced historic and recent hydrologic extremes, notably in November 2021. However, the limited understanding of the local weather and climatic drivers of past events has hindered understanding the future of the region.

Floods and droughts have occurred since time immemorial. However, western science is limited by written observations of weather and hydrometrics. To address this issue, we connected with local Indigenous communities to listen to and learn community stories to extend the spatial and temporal extent of the observation record.

These stories fed into quantitative analyses, for which we first developed a conceptual model comprising several drivers and modulators of floods and droughts. Drivers are the weather and climate processes that trigger floods or droughts (e.g., heavy rainfall). Modulators are the local watershed characteristics that can affect or amplify these conditions (e.g., watershed physical characteristics, land use changes, etc.). Then, we identified the main drivers using statistical methods. Results suggest the Nicola River watershed encompasses various hydrologic regimes.

We used the findings of this statistical analysis in a climate change assessment to evaluate projected changes for different drivers at 1.5°C and 4°C global warming levels. The main drivers of hydrologic extremes relate to snow and temperature processes. Rainfall is another important driver depending on the hydrologic regime. These main drivers could undergo considerable changes in a warming world. Our findings can support decision makers to better understand risks from floods and droughts under the changing climate to inform adaptation actions.

KEYWORDS: Flood, Drought, Hazard drivers and modulators, Correlation analysis, Climate change, Traditional Knowledge, Place-based knowledge

1 INTRODUCTION

Floods and droughts profoundly impact sectors such as water, ecosystems, and infrastructure. These events arise from complex interactions between hydrology, meteorology, and land surface features. Floods are often triggered by heavy rainfall, snowmelt, and/or high antecedent soil moisture, while droughts are linked to prolonged periods of low precipitation (Rezvani et al., 2023).

Flooding is Canada's most costly natural hazard. The Nicola River Watershed (NRW) in British Columbia is particularly susceptible to both floods and droughts. This area is home to the Scw̓ẽxmx (People of the Creeks). Historically, the watershed has experienced freshet, as well as flooding in fall, and winter. A recent, devastating flood followed an atmospheric river in November 2021 (City of Merritt, 2024). The region is also prone to drought, such as the event in 2019 caused by low snowpack and a dry summer (McCleary, 2019).

A limited understanding of the local drivers of past events hinders preparation for future extremes. Climate change is expected to intensify the hydrologic cycle, making this understanding crucial. To

address this, we examine the *drivers* and *modulators* of these events (Jiang et al., 2024). Drivers are the weather and climate processes that trigger floods or droughts. Modulators are the local watershed characteristics that can affect or amplify these conditions (e.g., watershed physical characteristics, land use changes, etc.).

Conventional quantitative analyses are limited by short observational records, typically 50-70 years. This makes evaluating rare, extreme events difficult. Furthermore, sparse data collection fails to capture the physical and environmental diversity across the NRW. To address these limitations, we incorporate place-based knowledge, from Indigenous communities. These narratives extend the historical record and provide a nuanced, hyper-local understanding of past events.

This project integrates place-based knowledge with quantitative methods. Our objective is to identify the dominant drivers of floods and droughts in the NRW. We then use these findings to assess how climate change may influence future conditions in the watershed. This combined approach provides a more comprehensive understanding of hydroclimatic extremes.

The structure of this paper is as follows: Section 2 introduces the study area and the datasets used, followed by a summary of the methods and limitations in Section 3. Results are presented and discussed in Section 4, and the study conclusions and recommendations are provided in Section 5.

2 STUDY AREA AND DATA

2.1 Study Area

The Nicola River watershed covers approximately 7,183 km² on the southwestern edge of BC's Interior Plateau (Figure 1). Its landscape includes rolling hills, pine forests, the Cascade Mountains, and four large lakes. The area is composed primarily of forest (75%) and grassland (11%) (Agriculture and Agri-food Canada, 2023).

The climate is arid, a result of the watershed's high altitude and its position in a rain shadow (Nicola WUMP Multi-Stakeholder Committee & Compass Resource Management, 2010). This leads to hot summers and cold winters. Average mean temperatures range from -3.9°C in January to 18.9°C in July. April is the driest month (15 mm), while December is the wettest (38 mm).

Streams in the watershed exhibit nival and mixed hydrological regimes (Figure 1). Nival regimes have low winter flows followed by a high spring freshet. In contrast, mixed regimes experience spring freshet in addition to high flows from fall and winter rainfall (Figure 2).

2.2 Data

We obtained historical data for precipitation, air temperature, Snow Water Equivalent (SWE), streamflow, land cover, land use, and land disturbance (wildfire) from various government agencies (Figure 1). The datasets varied in temporal coverage and completeness. We conducted a quality assessment, retaining stations with at least 30 years of complete records over the 1969–2010 period. Years with fewer than 10 missing days were considered complete. Due to data gaps, records from two climate stations outside the watershed were also included (Kamloops and Kelowna as shown in Figure 1).

Future hydroclimatic projections were obtained from the Pacific Climate Impacts Consortium (PCIC). This dataset included an ensemble of six downscaled and bias-adjusted (using the Bias Correction/Constructed Analogues and Quantile mapping technique) Global Climate Models (GCMs) from the 5th Phase of the Coupled Model Intercomparison Project (CMIP5). Each GCM was paired with two radiative forcing scenarios: RCP4.5 and RCP8.5. We also used hydrologic simulations from the Variable Infiltration Capacity (VIC) model, which was forced with the GCM ensemble to project future SWE, and streamflow.

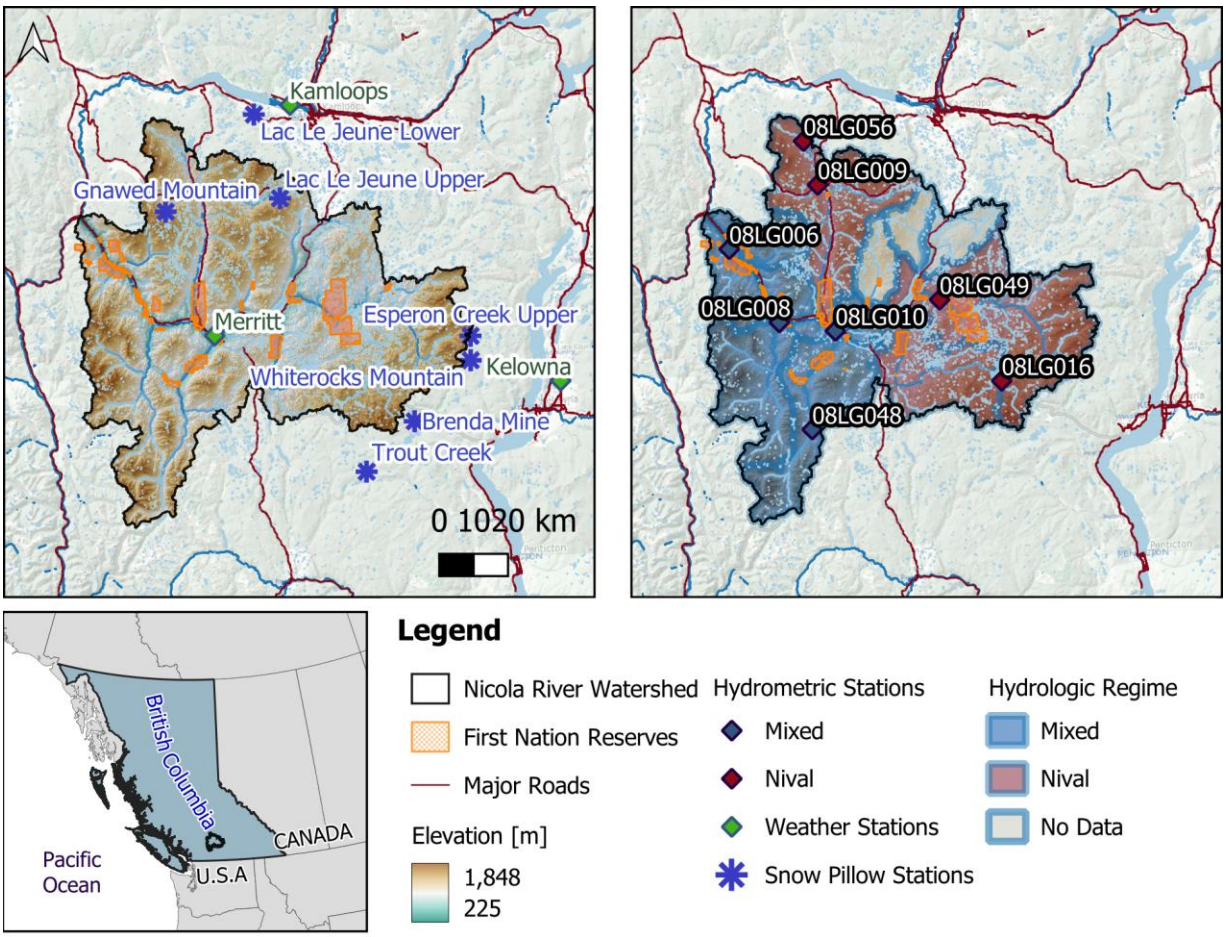

Figure 1: Location map of the Nicola River watershed, weather and hydrometric stations, and various hydrologic regimes in the watershed.

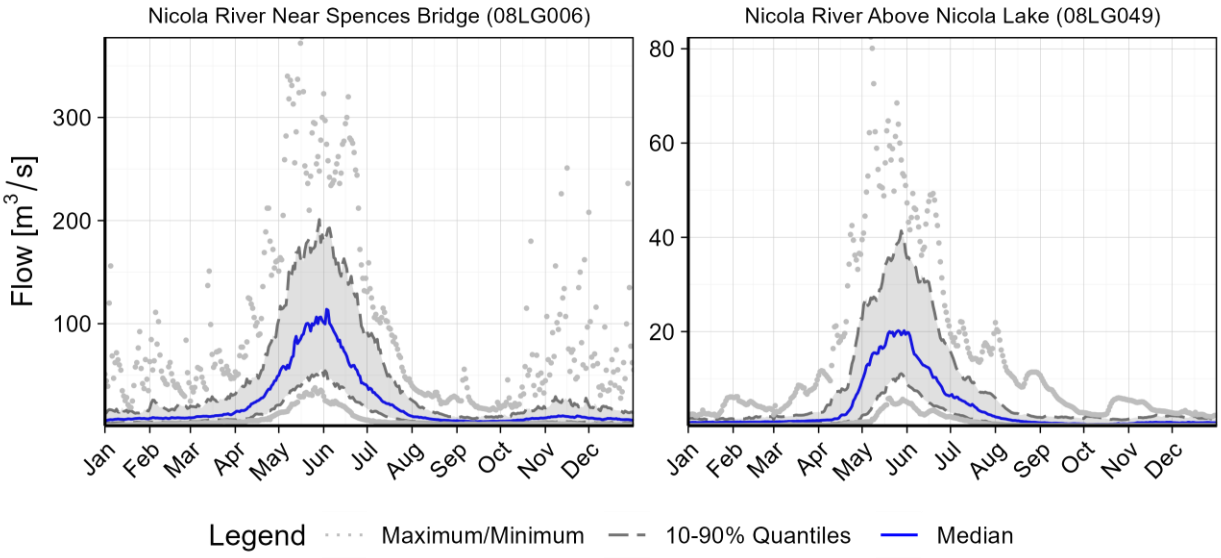

Figure 2: Example hydrographs of the creeks and rivers with mixed (left) and nival (right) hydrologic regimes in the Nicola River watershed (1969–2010).

3 METHODOLOGY

3.1 Identifying the Main Drivers of High and Low Flows

To identify the drivers of high and low flows, we conducted a correlation analysis similar to Curry and Zwiers (2018). This analysis assessed the relationship between seasonal high and low flow events and a set of hydroclimatic indices.

First, we defined seasonal flow events. Due to the watershed's seasonal hydrologic variability, we extracted the single highest and lowest streamflow for two six-month periods each water year: the *cold season* (October–March) and the *warm season* (April–September). This approach separates events generated by different processes, such as spring freshet and fall rainfall. These seasonal maxima and minima are distinct from hydrological floods or droughts, which are defined by sustained periods above or below a threshold.

Next, we defined several climatic indices to represent the hydroclimatic processes relevant to flood and drought generation (Table 1). The selection of these indices was informed by previous research and our understanding of the local hydroclimate.

Finally, we paired the seasonal high and low flows with each climatic index and used the nonparametric Spearman rank correlation to assess the relationship. The correlation coefficient indicates the strength and direction of this relationship. We tested these correlations for statistical significance at the 5% level, and only significant results are presented.

We classify the strength of correlations based on the coefficient value. Coefficients between 0 and ±0.2 are considered very weak. Values ranging from ±0.2 to ±0.4 are classified as weak. Correlations are moderate for values between ±0.4 and ±0.6. They are considered strong between ±0.6 and ±0.8. Finally, values from ±0.8 to ±1.0 indicate a very strong correlation.

Table 1: Climatic indices used to assess the importance of different driver groups on high and low flows in the Nicola River watershed.

Index	Description	Reference
Seasonal average temperature	Average of maximum daily temperatures over the season (warm or cold)	Dierauer et al. (2018)
Peak/Low Flow (PLF) rainfall	Total rainfall from X days before the seasonal peak/low flow to Y days after seasonal peak/low flow (see descriptions below)	Curry & Zwiers (2018)
Annual maximum snow	Annual maximum SWE	Curry & Zwiers (2018); Dibike et al. (2021); Jenicek et al. (2016)

3.2 Future Projections

We selected monthly values of air temperature, precipitation, and snowpack for analysis. This choice was informed by the correlation analysis that identified the key drivers of high and low flows in the watershed.

We report projected changes for these indicators at two Global Warming Levels (GWLs) of +1.5°C and +4°C, relative to the preindustrial era. We also use a 31-year baseline period of 1970–2000 as a reference for comparing past and future conditions. To ensure a consistent assessment, each GWL is defined for every model in our ensemble. A GWL is the centre of the first 31-year period during which the global mean temperature exceeds the target warming level. The timing for reaching each GWL varies between climate models and emission scenarios and is based on the ranges reported in Rezvani et al. (2023).

3.3 Traditional and Place-Based Knowledge

In this project, we applied the concept of knowledge weaving to combine the various knowledge systems (Henri et al., 2021; Indigenous Climate Hub, 2024). This approach has been applied to previous work of a similar nature in *Syilx* Territory (Ebbwater Consulting Inc. and Okanagan Nation Alliance, 2019). This integration ensures that management decisions are environmentally sustainable, culturally relevant, and socially acceptable to local communities (Berkes, 2017; Nicola Watershed Governance Partnership & POLIS Water Sustainability Project, 2024; Robinson et al., 2019).

3.4 Limitations

The datasets used and the methodology applied have several limitations. The climate and hydrologic models used (GCMs and VIC) are incomplete representations of reality and have known uncertainties. For example, our analysis indicates the VIC model tends to underestimate the magnitude of high flow events. Therefore, projections should be interpreted in terms of their direction and relative change rather than their absolute values. Furthermore, the daily timestep of the model does not fully capture sub-daily processes, meaning changes to instantaneous peak flows are likely greater than what is reported here.

The statistical methodology also has constraints. The correlation analysis used seasonal high and low flow values, which are not necessarily synonymous with hydrological flood or drought events. This approach was necessary to overcome methodological limitations but means the identified links are associative, not necessarily causative.

4 RESULTS AND DISCUSSION

4.1 Results

Figure 3 shows the correlation of the seasonal high/low flows in the NRW with annual maximum SWE, average of maximum temperature, and PLF rain.

The analysis shows that warm season high flows are strongly correlated with the annual maximum SWE. A moderate positive correlation also exists between SWE and warm season low flows (Figure 3). These findings mean a larger snowpack is associated with larger streamflows in the warm season. In contrast, SWE is negatively correlated with both high and low flows in the cold season. This may be because higher SWE indicates more water being stored as snow, resulting in less runoff during winter.

Warmer seasonal temperatures are negatively correlated with both high and low flows in the warm season (Figure 3). This means that warmer temperatures are associated with smaller streamflows during this period. The relationship is particularly strong for warm season low flows and is statistically significant at all assessed locations.

The results show a moderate positive correlation between short-term rainfall and cold season high flows in rivers with mixed regimes (Figure 3). This suggests that rainfall is a driver for high flows during this period. We also found a positive correlation between rainfall and cold season low flows. This indicates that larger rain events can lead to higher baseflows in winter.

The main drivers identified in the correlation analysis are projected to change in a warming climate (Figure 4).

Projections indicate seasonal changes in precipitation. Spring, fall, and winter are projected to become wetter, while summers are projected to be drier (Figure 4). Further, the precipitation regime is likely to shift from snowfall to rainfall, particularly between September and May (Figure 4).

Progressive decreases in SWE are projected across the watershed. This is due to reduced snowfall and increased snowmelt (Figure 4). The timing of peak SWE is projected to shift one month earlier, from March to February. Similarly, peak snowmelt is expected to shift from April to March. Consequently, snow-free periods may become longer by approximately one month.

These projected changes could impact the hydrologic regime (Figure 5). The annual peak flow, which occurs in May-June in the base period, is expected to shift to April-May, aligning with earlier snowmelt. The magnitude of this peak is projected to increase at the higher warming level (+4°C). Furthermore, extreme flows are projected to increase, with substantial changes in the fall (Figure 5). For example, at the +4°C warming level, the most extreme fall daily flow could increase from approximately 50 m³/s to 190 m³/s. This could indicate a greater likelihood of rain-on-snow events.

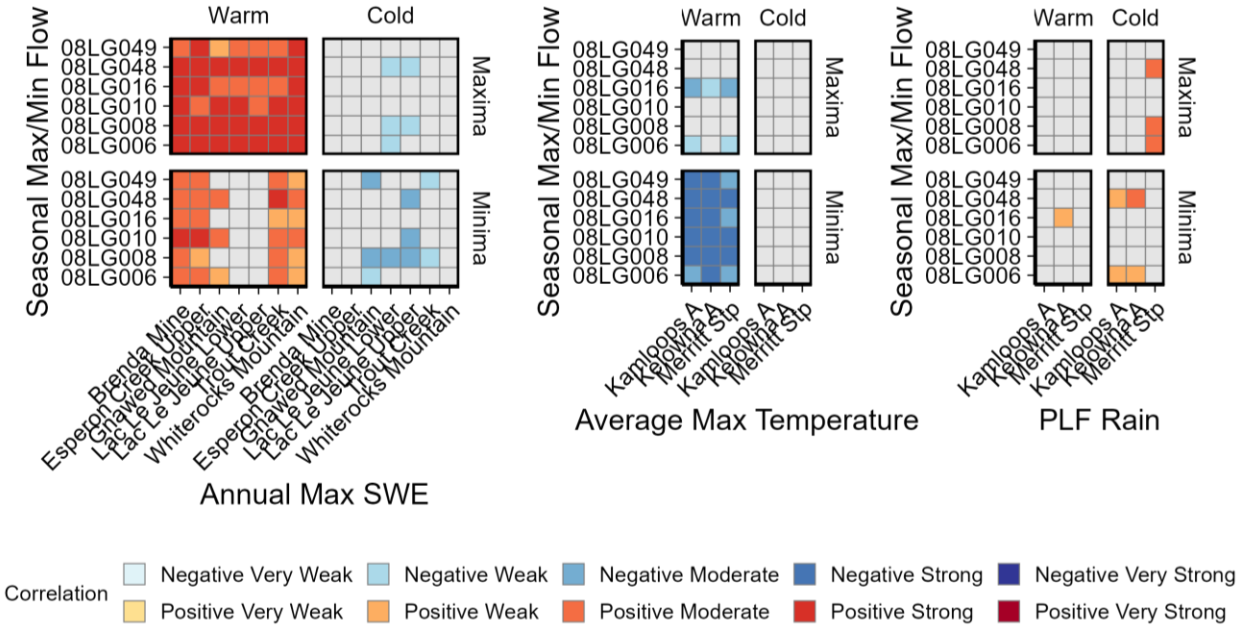

Figure 3: Correlation between snowpack (left), air temperature (middle), and rainfall (right) and seasonal high- and low-flow events (1969–2010). Squares are colored according to the correlation coefficient, with grey squares indicating correlations that are not statistically significant at the 5% level (p-value > 0.05).

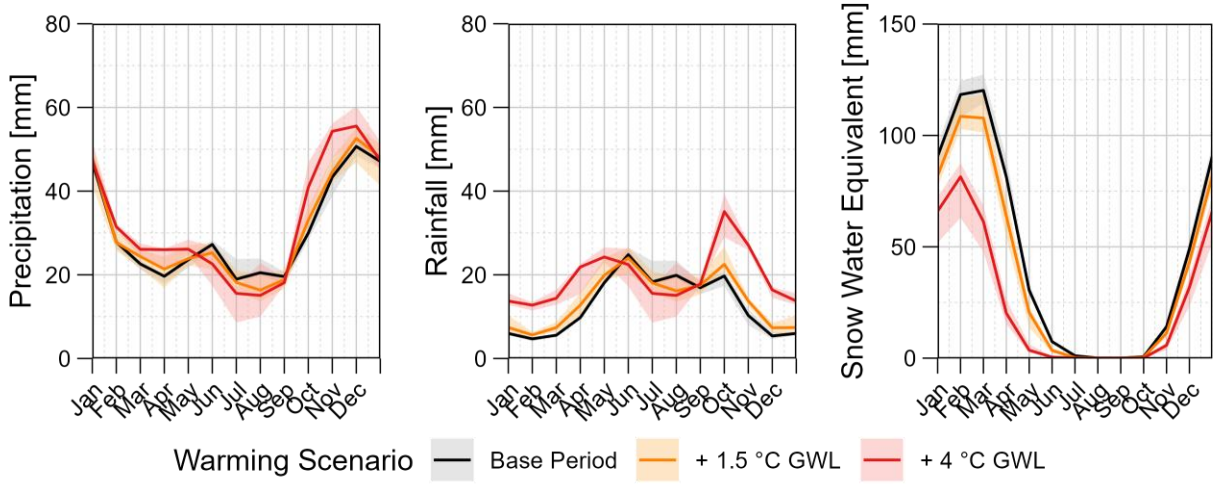

Figure 4: Monthly total precipitation (left), rainfall (middle), and Snow Water Equivalent (right) over the Nicola River watershed for the base period and future warming periods. Lines show the multi-model ensemble median, and the shading represents the ensemble's 80% confidence interval (ensemble's 10th - 90th percentiles range).

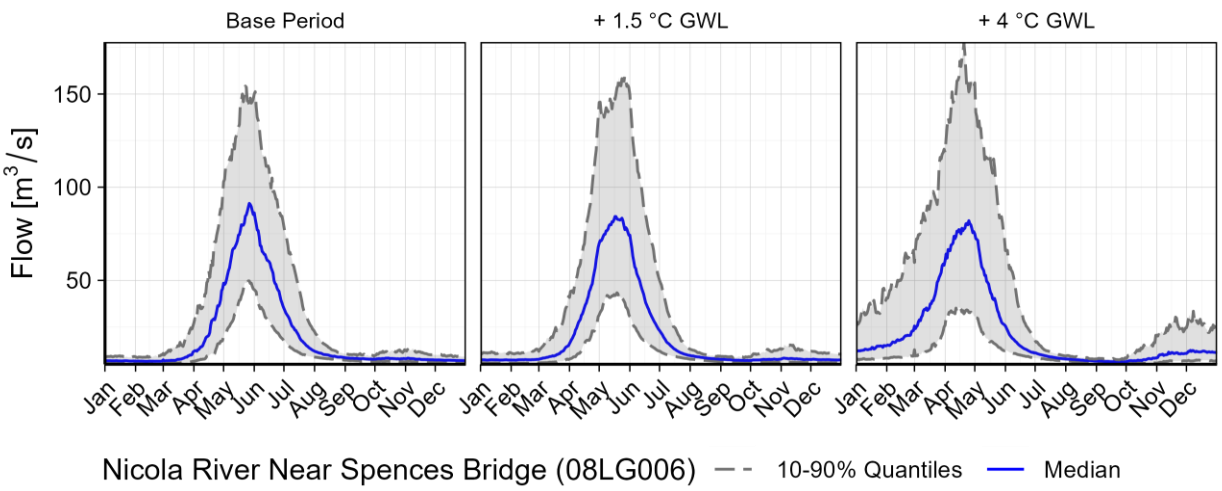

Figure 5: Projected daily hydrographs under warming scenarios at the Nicola River near Spencer Bridge hydrometric station based on daily simulations of the Variable Infiltration Capacity hydrologic model. For each day of the year, the multi-model ensemble's median and 80% confidence interval are presented.

Data gathering from place-based knowledge holders generally reflected the findings of the quantitative analysis. However, the qualitative research identified additional strong drivers of flood and drought, for which there was not adequate observed data to show a statistically significant correlation. Specifically, qualitative research identified the importance of land cover and land disturbance from anthropogenic activities (recreation, mining, etc.) and natural events (wildfire and mountain pine beetle infestations) as key drivers of change in hydrologic extremes.

4.2 Discussion

Our analysis shows that warmer summer temperatures are strongly correlated with lower summer flows. This suggests that cooler summers result in less evapotranspiration, which helps sustain streamflow. Precipitation patterns are also key drivers, with cold season rainfall linked to high flows and higher low flows. However, the strongest relationship identified is between annual maximum SWE and warm season flows. A larger snowpack results in both larger high flows during the spring freshet and more sustained low flows throughout the summer. Qualitative results, which are not repeatable with quantitative datasets due to sparse availability, highlight the importance of land disturbance as a key driver of meteorologic extremes.

Looking forward, climate projections indicate considerable changes for these drivers. Air temperature is projected to increase in all seasons, with the watershed warming at a higher rate than the global average. This warming will alter precipitation patterns, making fall, winter, and spring wetter while summers become drier. Further, a shift from snowfall to rainfall is also projected. This combination of wetter winters and existing snowpack increases the potential for rain-on-snow events, which can generate large floods. Despite increased winter precipitation, overall SWE is projected to decrease, especially at lower elevations.

These projected changes to temperature, precipitation, and snowpack will alter future streamflow patterns. The spring freshet peak is projected to shift approximately one month earlier. Increased fall rainfall will likely increase fall flows, shifting the river's hydrologic regime from nivo-pluvial to pluvio-nival. While the overall reduction in snowpack means that flood potential from snowmelt alone is likely to decrease in an average year, the risk of extreme floods will increase. The shift to rainfall, especially during years with high snowpack, heightens the risk of severe floods from rain-on-snow events.

Recognizing that climate change is largely outside the control of the communities in the NRW, the research identifies the importance of watershed stewardship to heal the land, and limit future land disturbance as a key tool to mitigate meteorologic extremes in the area.

5 CONCLUSION

The Nicola River watershed is vulnerable to floods and droughts. These hazards are expected to intensify with climate change. However, a limited understanding of the local drivers of past events hinders future preparedness. Therefore, this project used a two-pronged approach by weaving place-based knowledge with quantitative analyses to understand the historic, present, and future drivers of these hydroclimatic extremes. Our goal was to provide a local-level understanding of what climate change will mean for the region.

The technical analysis identified snowpack, temperature, and rainfall as the dominant local drivers of seasonal flows. The strongest relationship observed was between the annual maximum snowpack and warm season high and low flows. These key drivers are projected to undergo changes in a warming climate. Projections indicate a shift from snow to rain, a reduced overall snowpack, an earlier spring freshet, and more frequent rainfall-induced flooding in fall and winter. The qualitative analysis identified the importance of land cover and land disturbance as a key driver of meteorological extremes. Long-term watershed stewardship is identified as a pathway to mitigate this driver.

While the analyses are subject to data and methodological limitations, these findings provide a foundational understanding of future hydroclimatic conditions in the Nicola River watershed. The insights provide a basis for decisions that will support climate adaptation. Further work is required to build upon this analysis and continue to enhance the understanding of floods and droughts in the watershed.

6 ACKNOWLEDGEMENTS

The authors respectfully acknowledge the First Nations that have communities within the Nicola River watershed. These are the Coldwater Indian Band, the Lower Nicola Indian Band (LNIB), the Upper Nicola Band, the Nooaitch Indian Band, and the Shackan Indian Band.

The funding support for this project came from the Scw'exmx Tribal Council (STC), Indigenous Services Canada (ISC), and First Nation Adapt (FNA). The authors wish to thank the STC project manager, Neil Todd, who provided support throughout. Additionally, the authors wish to acknowledge the effort and resources provided by the steering committee including Robin Fenn, Susan Anderson Behn, Tom Duncan, Dylan Forrest, Brent Baron, Muhammad Naveed Khaliq, Sarah Simon, and Jeptha Ball.

REFERENCES

Agriculture and Agri-food Canada. (2023). *ISO 19131 Annual Crop Inventory-Data Product Specifications*.

Berkes, F. (2017). Sacred Ecology. Taylor & Francis. https://doi.org/https://doi.org/10.4324/9781315114644

City of Merritt. (2024). Flood 2021 Overview.

Curry, C. L., & Zwiers, F. W. (2018). Examining controls on peak annual streamflow and floods in the Fraser River Basin of British Columbia. Hydrology and Earth System Sciences, 22(4), 2285–2309. https://doi.org/10.5194/hess-22-2285-2018

Dibike, Y. B., Shrestha, R. R., Johnson, C., Bonsal, B., & Coulibaly, P. (2021). Assessing climatic drivers of spring mean and annual maximum flows in western canadian river basins. Water (Switzerland), 13(12). https://doi.org/10.3390/w13121617

Dierauer, J. R., Whitfield, P. H., & Allen, D. M. (2018). Climate Controls on Runoff and Low Flows in Mountain Catchments of Western North America. Water Resources Research, 54(10), 7495–7510. https://doi.org/10.1029/2018WR023087

Ebbwater Consulting Inc. and Okanagan Nation Alliance. (2019). Syilx Okanagan Flood and Debris Flow Risk Assessment Report 1 of 4: Synthesis and Recommendations. Prepared for and with the Okanagan Nation Alliance.

Henri, D. A., Steel, J., Rytwinski, T., Provencher, J. F., Popp, J. N., Mcgregor, D., … Ford, A. T. (2021). Weaving Indigenous knowledge systems and Western sciences in terrestrial research , monitoring and management in Canada : A protocol for a systematic map, (February), 1–9. https://doi.org/10.1002/2688-8319.12057

Indigenous Climate Hub. (2024). Bridging Two Worlds: Integrating Indigenous Knowledge and Western Science in Climate Policy. Retrieved from https://indigenousclimatehub.ca/2024/08/bridging-two-worlds-integrating-indigenous-knowledge-and-western-science-in-climate-policy/

Jenicek, M., Seibert, J., Zappa, M., Staudinger, M., & Jonas, T. (2016). Importance of maximum snow accumulation for summer low flows in humid catchments. Hydrology and Earth System Sciences, 20(2), 859–874. https://doi.org/10.5194/hess-20-859-2016

Jiang, S., Tarasova, L., Yu, G., & Zscheischler, J. (2024). Compounding effects in flood drivers challenge estimates of extreme river floods. *Science Advances*, *10*(13). https://doi.org/10.1126/sciadv.adl4005

McCleary, R. (2019). Overview of Drought Conditions in the Nicola. FLRNORD Thompson Okanagan Regional Drought Response Team.

Nicola Watershed Governance Partnership, & POLIS Water Sustainability Project. (2024). Successes in Joint Decisions for Drought Prevention and Response in the Nicola Watershed. Retrieved from https://poliswaterproject.org/wp-content/blogs.dir/162/files/sites/162/2024/02/Nicola-Case-Study-Final.pdf

Nicola WUMP Multi-Stakeholder Committee, & Compass Resource Management. (2010). Nicola Water Use Management Plan.

Rezvani, R., Na, W., & Najafi, M. R. (2023). Lagged compound dry and wet spells in Northwest North America under 1.5 °C–4 °C global warming levels. Atmospheric Research, 290, 106799. https://doi.org/10.1016/j.atmosres.2023.106799

Robinson, D., Bueno, P. de la C., Thompson, A., Olson, E., & Simpson, M. (2019). Nicola Watershed Characterization. Prepared for the Nicola Governance to Governance Forum by ESSA.

ICFM 10
Adapting to Global Change:
Innovative Approaches to Flood Management and Resilience
May 20-22, 2026 | Western University, London, Ontario, Canada

The Impact and outlook of Extreme Sea Level Rise on Flood Protection and Freshwater Systems in the Netherlands

Astrid Labrujere[1], Saskia van Gool[1], Jantine Hoekstra[1], Meinte Blaas[1] and Quirijn Lodder[1]
Rijkswaterstaat, Ministry of Infrastructure and Water Management, Griffioenlaan 2, 3526 LA Utrecht, The Netherlands[1]
E-mail: Astrid.labrujere@rws.nl

ABSTRACT

This paper synthesizes the national assessment of the impacts of up to 3 m sea level rise (SLR) on flood protection and freshwater availability in the Netherlands. Using exploratory, model-based analyses across coastal dunes, hard flood defenses along river-lake systems, and the Rhine–Meuse Estuary, the study finds that current flood safety levels can be technically and financially maintained up to 3 m SLR, though spatial and resource constraints intensify. Furthermore the supply of sand for coastal nourishments will be challenging due to other functions in potential sand winning areas in the North Sea (wind energy, shipping) and explosive remnants of war.

Freshwater systems are more vulnerable: salt intrusion and increased flushing demands grow sharply and ultimately exceed available river flows under severe drought and high SLR.

Key implications thus concern sand supply and logistics, reinforcement footprints in dense urban settings, barrier operation strategies, and trade-offs between salinity tolerance and water demand. To keep the flood protection and freshwaters systems up to standard, current safety activities can be prolonged but freshwater is more vulnerable.

KEYWORDS: climate adaptation; sea level rise; flood safety; freshwater

1 INTRODUCTION

The Netherlands is a low-lying, densely populated, heavily urbanized and cultivated delta of the Rhine, Meuse, Scheldt and Ems rivers. About 26% lies below mean sea level and ~60% is flood-prone. It is strongly exposed to the influences of the adjacent North Sea. Apart from flood risk and coastal erosion, the Netherlands is exposed to saltwater intrusion and salinization of its surface waters and groundwater. Due to salinization, around half of the country is dependent on freshwater supplied by the Rhine and Meuse distributed through the highly managed surface water system.

Climate observations show accelerating global and regional sea levels, with national scenarios exploring outcomes up to multiple meters by 2200 [1,2,3]. Projections of SLR derived by the Royal Dutch Meteorological Institute [3] showed an SLR of up to approximately 3 m in 2200 (83rd percentile of ensemble model results for the SSP5-8.5 emission scenario).

The Netherlands has developed and implemented a set of thorough strategies to manage flood risks and optimize freshwater supply [4–6]. The current strategies already consider an SLR of 0.85 in 2100 [7], and the recent insights raise the question of whether and how long these strategies for flood protection and freshwater can remain effective against extreme SLR.

While earlier methods have demonstrated their value in making complex issues with high degrees of uncertainty accessible to policy makers, model-based quantitative assessments of the impact of extreme SLR on flood protection and freshwater availability are not yet available for the Netherlands. The Dutch government hence initiated the national Sea Level Rise Knowledge Programme [8].

In earlier work bij Friocourt et al [43], a quantitative, model-based approach was applied to assess the impact of extreme SLR (up to 3 meters) on national strategies for flood protection and freshwater supply. The study demonstrated that current safety levels can be technically and financially maintained up to 3 meters of SLR, but spatial and logistical constraints—such as sand supply for coastal reinforcement and the operation of flood barriers—become increasingly critical. Moreover, the vulnerability of freshwater systems intensifies due to saltwater intrusion and rising flushing demands, especially during drought conditions. This work builds upon earlier publications [43] and provides additional insights and reflections on the measures which can be taken to extend the longevity of the national strategies.

This paper presents a part of the results of the Knowledge programme, trough the methodology and outcomes of the quantitative assessments of the impact of extreme SLR on the current flood protection and freshwater availability. Furthermore, we present an outlook for freshwater management and flood protection in possible adjustment to the system to keep up with the challenges SLR raises.

The work presented here is structured as follows: First, we provide an overview of the current strategies and consequential systems for flood protection and freshwater availability. We then describe our modeling approach for flood protection (both coastal sand nourishment requirements and structural safety) and freshwater availability (salinization of both groundwater and surface water), followed by the main outcomes of the assessments for current and future measures.

2 NATIONAL CLIMATE APPROACH

2.1. The Netherlands and the Dutch Delta Programme

Both flood safety and water availability are increasingly under pressure due to climate change. In 2010, the Netherlands, therefore, implemented a national policy program for adaptation to climate change: the Delta Programme [9,10]. It focuses on the themes of flood protection, freshwater availability, and spatial planning and works towards a climate-resilient design of urban and rural areas across the Netherlands through a so-called Adaptive Delta Management (ADM) approach [11]. This approach combines short-term plans with long-term delta strategies, as well as a monitoring and evaluation process. Every six years, decisions are reviewed and, if needed, updated. The Sea Level Rise Knowledge Programme [16], contributes to the update of 2026.

2.2. Flood Protection Strategy and System

The Dutch flood protection strategy is risk-based, considering both the probability of flood hazard and vulnerability (casualties and economic damage) [6]. The strategy focusses mainly on the first line of defense: preventing floods. The system consists of a network of primary flood defenses (over 3,600 km) with over 400 km2 of dunes, structural elements and about 25 barriers and dams. The required level of safety that primary flood defenses should provide is expressed as the probability of flooding per year for each segment of the enclosure.

A large part of the coastline is protected through natural dunes. Erosion in the coastal profile is compensated by regular sand nourishments on the shoreface and the beach. This aims to keep the coast line in its place and is intended to maintain the required safety level and leverage the natural, short- and long-term sediment transport dynamics cross-shore and alongshore in the beach zone and related aeolian sand transport in the dune zone [13]. This dynamic management is the preferred method for coastal protection in the Netherlands, with hard flood defenses (dikes and dams) and foreshore protection only in locations where nourishments or other sand-based solutions are technically or economically not feasible.

2.3. Freshwater Strategy and System

The Dutch freshwater strategy relies on managing and directing freshwater in the surface water system towards dedicated lakes, canals and river branches where important freshwater intakes are located. Apart from the main surface waters, reclaimed land (so-called polders) situated below sea level is prone to seepage of brackish groundwater. These polders are flushed with freshwater sourced from the main rivers [14]. The combined efforts to keep reservoirs fresh and up to required water levels and to flush saline groundwater seepage in polders put a considerable claim on freshwater resources, particularly during periods of low river flows and high evaporation. The volumetric water claim is expected to grow due to SLR. The overall freshwater policy ambition is to balance the overall water supply and demand such that actual water shortages only occur once per 20 years [15].

It is noted that, irrespective of climate change, low river discharges already lead to salt intrusion via the open river mouths of the Rhine–Meuse system [16]. Climate change is putting this freshwater management strategy further under pressure. Rising global temperatures lead to increased variability in seasonal precipitation and droughts, resulting in increasing summer water demand and periods of low river flows [12,18,19].

3 METHODS

3.1 The Modeling approach

In our modeling approach, we primarily focused on SLR but also considered other components of climate change, such as changes in temperature, precipitation and changing river flows. Timelines of SLR were used to allow a combination with other developments which influence flood protection and freshwater availability including developments in river flow and land subsidence [51]. More detail on all model input and assumptions can be found in the technical background reports [31–35].

3.2 Assessment of Flood Protection System Under SLR

3.2.1 Sand Nourishments to Maintain ‘Soft’ Flood Defenses

Required sand nourishment volumes to accommodate for SLR were modeled applying sediment budget analysis based on observational data [45]. The uncertainty in the sediment demand was assessed by taking into account multiple possible future areas (m^2) of nourishment sediment dispersal [46].

3.2.2 Assessing the Flood Safety of ‘Hard’ Flood Defenses

The modeling strategy was based on standardized methods for assessing primary flood defenses [7], the system for flood defenses. It involves comparing hydraulic loads (the forces exerted by water on flood defenses) with a failure model of the flood defense. The failure model includes the dike profile (including the immediate foreshore) besides revetments, inner dike materials, soil properties and the effect of water pressure in the dike. The hydraulic loads are modelled with a combination of hydrodynamic models and wave models for up to thousands of various circumstances. This study focused on three primary failure processes for flood defenses: dike height (overtopping and overflow), slope stability and piping. All failure processes are modelled with fragility curves.

The flood safety assessment followes a probabilistic approach using water level and wave load as the main stochastic variables. The total resulting hydraulic loads were simulated using several hydrodynamic models, including SOBEK3 [20] for rivers, IMPLIC [21] for the Eastern Scheldt and WAQUA for the Western Scheldt and Wadden Sea [43]. Waves were computed using the analytic 1-d model Bretschneider [22] for rivers or the spectral phase-averaged wave model SWAN [23,24]. These

models use statistics derived from previous frequency analyses on historical records of measured seawater levels, wind and river discharges as input [25]. Wind–water level correlation was added [26,27]. The statistical analysis described seawater levels, river discharges and wind spanning from short return periods (T = 2 years) to extreme return periods (T = 100,000 years) and beyond through extrapolation.

The model output includes physical parameters required for water levels and waves for all locations stored in a database of physical stochastic variables, which is input to the probabilistic modeling tool Hydra-NL [28,29]. Hydra-NL computes the probability of occurrence of the various combinations, with the exception of hydraulic loads to the dunes that were calculated using the Riskeer software, version 22.1.2 [47]. The stochastic variables considered vary per water system. Revetments were added as a cost factor for the total cost. For storm surge barriers and hard structures, a pragmatic approach based on height was employed, assuming that these structures will be replaced once before 2200, and the total cost for this was included.

The spatial and financial impact of strengthening flood safety structures has been further assessed with the cost model OKADER [30]. In places where available space was limited and a 'traditional' dike reinforcement was not possible, we assumed that either hard vertical structures will be constructed assuming a lifetime of 100 years, or buildings will be demolished to create space for dike reinforcement. In the latter case, the financial analyses included the cost of depreciation of existing houses.

To assess the impact of potential future measures, some adjustments to the system were analysed additionally.

3.3 Assessment of Freshwater Availability Under SLR

Due to the considerable differences between salinization processes in different Dutch local water systems, a combination of models was used to assess the impacts of SLR on freshwater resources: a nationwide groundwater flow model, different surface water models and a nationwide water balance model.

SLR impacts on *groundwater* were simulated with a high-resolution groundwater flow and salt transport model [14,36]. The model comprises a variable-density groundwater flow and salt transport. The impact of SLR is superimposed over ongoing groundwater salinization. The groundwater model was used to simulate the increase in saline seepage (or salt load) to the surface water systems in reclaimed land.

The *surface water* bodies of the Rhine–Meuse Estuary (RME) are characterized by a high salinity gradient that required a detailed 3D hydrodynamic model setup in the D-Hydro software release 2022.01 [37] including the tidal cycle. Critical for freshwater availability and salinization are long-term periods of drought with low river flows. The simulations were performed with river flows of 2000 m3/s (representative of summer average flows), 1000 m3/s (representative of current dry summers) and 500 m3/s (representative of low flows under future climate).

The other main freshwater systems in the Netherlands (Amsterdam-Rijn-Canal, Lake IJssel, and Lake Volkerak-Zoom) are closed off from the sea by dams that limit salinization. Salt intrusion, however, still occurs via groundwater and more importantly, through shipping locks. This type of saltwater intrusion is characterized by a semi-stationary horizontal salt gradient, which is largely controlled by river water inflow, water demand and saltwater leakage at the locks. The canal system has been approached by a quasi-stationary 3D hydrodynamic model, to account for the vertical stratification effects and geometric complexities. The lake systems have been approached by simpler 1-dimensional box models merely based on an advection–dispersion equation, building upon the concepts developed by Nolte et al. [38] and Bonte and Zwolsman [50].

4 RESULTS

4.1 Flood Protection

4.1.1 Sand Nourishments of 'Soft' Flood Defenses

The model results show that it is technically feasible to maintain the current shoreline for the majority of the coastline and maintain the current level of flood hazard protection (expressed as a probability of flooding or dike failure), even with extreme levels of SLR of up to 3 m. Additional strengthening is, however, required in built-up areas and cities situated in the dune area where constructions prevent the growth of dunes.

The sand balance simulations show that cumulative nourishment volumes will increase with a factor of 1.5 to 3 for a 1 m SLR, and with a factor of 3 to 6 for an SLR of 5 m, compared to a scenario with no SLR (Figure 1). These estimates have a considerable degree of uncertainty, which is related to the evolution of natural morphological processes in the North Sea due to SLR, in particular the development of the active coastal zone, and policy choices on nourishments. When compared to the sediment available for extraction in the North Sea, it was found that the current legislation and regulations will result in a shortage of sediment. Especially near the Wadden Islands and the estuarine coast of Zeeland, more sediment will be needed than what is currently available. Therefore, regulations regarding spatial reservations, unexploded ammunitions and mining depths should be changed to keep the feasibility of the nourishment strategy of the Netherlands.

Additionally, sand nourishments leverage the natural geomorphological coastal processes that allow very local sand nourishments to be subsequently distributed along the coastline by natural processes [39].

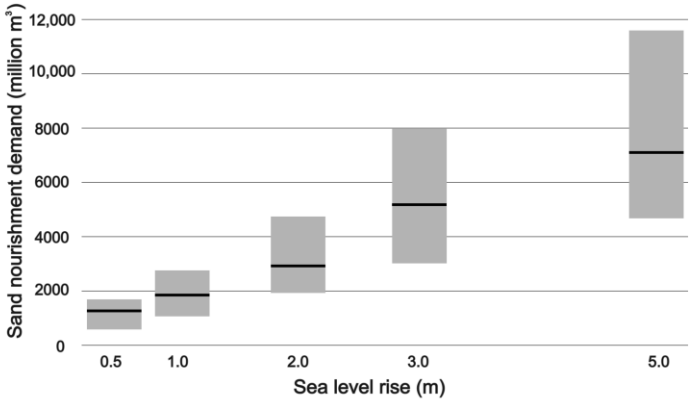

Figure 1. Sand nourishment volumes required under different levels of SLR. Grey bar indicates uncertainty range. Black line indicates expected sand nourishment volume.

4.1.2 Flood Safety of 'Hard' Flood Defenses

The simulations show that the required heightening and strengthening of dikes vary considerably (Figure 2). For an SLR of 3 m, dike segments that require heightening exceeding 5 m are found in the north of the Netherlands, decreasing to values between 1 and 4 m in the middle and south of the country, and gradually decreasing further inward along the Rhine and Meuse. Dike heightening exceeds the degree of SLR in areas where wave run-up is significant and wave growth is depth-limited, such as the northern Wadden Sea and the Western Scheldt. For instance, model results indicate that an increase of 7 m may be necessary in some places in the north of the country for an SLR of 3 m, of which about 5 m can be attributed to SLR, the remainder being due to the increased wave load (higher water heights mean that higher waves arrive at the dike; they are no longer attenuated by the foreshore).

Further inland along the Rhine and Meuse rivers, the influence of SLR gradually diminishes. However, the strengthening of the dikes remains necessary because of other effects such as soil subsidence and changes in peak river discharges. In these areas, the required increase in dike height is always smaller than SLR. Former sea dikes can cope with some level of SLR before they need to be strengthened again for higher SLR, since they were first robustly reinforced (1960–1980) before being (partially) closed off.

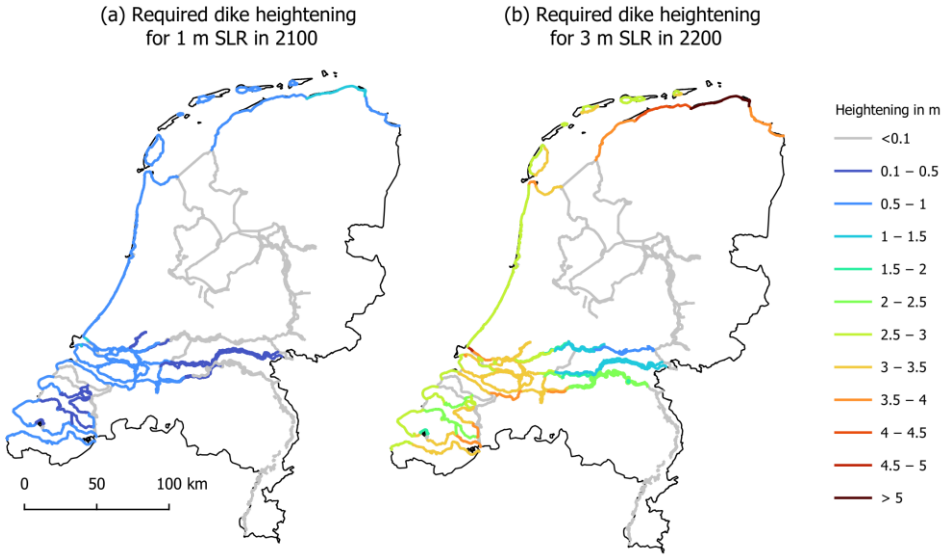

Figure 2. Required dike heightening for SLR of 1 m (left) and 3 m (right). These scenarios include dike heightening due to increasing river flows and land subsidence (modified from Zethof and Stijnen [35]).

As the sea level rises, the closure frequency of storm barriers increases if their closure level remains fixed. Eventually, the closure level can be reached at almost each high water, thereby making the concept of a barrier irrelevant. Storm barriers are designed to close only for very heavy storms (which occur rarely), to accommodate for other usages (shipping for the Europoort barriers, nature for the Eastern Scheldt barrier). For example, the closure frequency for the Europoort barrier is currently statistically once in 18 years and increases to every tidal cycle at 3 m SLR. In order to keep the closure frequency low enough, the closure level needs to increase with SLR. If the Europoort barrier closure level increases by 1.25 m under 2 m SLR, the closure frequency will become once per year. In that case, storm barriers still effectively close for extreme water levels corresponding to legal dike norms. However, the rising of the closure levels renders outer embankments more flood-prone.

Additional measures on top of current flood protection measures were analysed. The additional measures were found to be effective in bringing down the hydraulic loads, but were not found to be cost effective.

Although flood protection can be maintained at current safety levels through dike heightening, piping and stability berms, and strengthening of revetments, the implications for land use are considerable due to the space required for dike reinforcements. The footprint (width) of a dike increases by up to 90 m per meter of dike heightening, which can be difficult to achieve in densely built-up areas. Additionally, built-up areas located between dikes and open water (on relatively high areas of the floodplain) will be subject to more frequent flooding and increasing water depth. The cost analyses showed that the total cumulative nominal cost for 1 and 3 m SLR to maintain flood protection at the current safety level is around 1.5-2 times the current yearly cost for the dike enforcement program, compared to a baseline safety level in 2050. The total nominal annual costs are around EUR 0.3 and 0.5 billion per year, which is

in the same order of magnitude as the currently estimated annual budget for flood protection for the period 2023–2050, thereby showing that maintaining adequate flood protection is financially achievable. Not included are costs for regional water systems that have tot adept tot the changes in the main water system, and the costs caused by increased flooding of areas on the water side of the dikes.

4.2 Freshwater Availability

Many parts of the western half of the country already experience salinization of soil and groundwater due to the seepage of brackish groundwater. This seepage is a result of the geologic past and human intervention such as land reclamation [40]. The modeling results show that seepage rates are expected to increase with SLR. The increasing seepage results in increasing salt loads from groundwater to surface water in a zone of up to 20 km from the coastline and rising river branches. Behind the coastline, the current salt loads vary geographically between 100 and 10,000 kg/ha/year. Nationwide, the total load increases with 50% at 1m SLR and up to 250% for 3 m SLR. Salinization of *surface water* is mitigated by flushing with freshwater sourced from the rivers Rhine and Meuse. The required flushing volume in polder areas varies considerably geographically. The total flushing water demand, however, increases at a higher rate than the salt load itself: about 4.5-fold by 1 m SLR, about 14-fold by 3 m SLR.

In the open Rhine–Meuse Estuary, SLR leads to a change in the balance between sea-level-induced pressure and river-discharge-driven counterpressure on the salt gradient. This causes a shift in the salt-intrusion length, *i.e.*, the position of the transition zone between freshwater and saltwater. The increase in intrusion length per meter SLR varies between 2 to 5 km along the range of typical dry-season river-discharge values: the lower the discharge, the stronger the shift per meter SLR. The intrusion length is non-linearly dependent on variation in river discharge. Conversely, compensating the increase in intrusion length due to a 1 m increase in SLR by means of additional discharge would require about 50 m^3/s to about 200 m^3/s additional river discharge for extremely low flow and intermediate dry-season flow conditions, respectively. SLR essentially aggravates the sensitivity of the system to low discharge conditions, in line with sensitivity relations such as those presented by Wegman et al. 2024, Ralston [41] and data and model analyses reported by Dijkstra et al. [42]and Van den Brink et al. [16].

The modeling for the lakes and canals (the strategic freshwater reservoirs) indicates that salt intrusion through shipping locks is the largest salinization pressure, in contrast to the contribution of groundwater seepage. This salt pressure may be reduced through specific measures at locks [17].

As salt intrusion increases, the required flushing increases substantially, putting an additional demand on freshwater resources. With all these factors combined, continuing the current practice under SLR would result in a significant increase in the quantity of freshwater required for the flushing of polder areas and other water systems and mitigating saltwater intrusion in rivers. As climate change is expected to also result in warmer and drier summers with increased evaporation and lower freshwater inflow, it is quite evident that the amount of freshwater required for flushing will be increasingly unavailable during dry summers. The pressure on the national water balance due to flushing may in theory be alleviated by accepting higher chloride levels. This would, however, potentially impact agricultural productivity, drinking water production and freshwater ecosystems.

5 DISCUSSION

The study addresses whether strategies for flood defense and freshwater availability remain applicable under up to 3 m sea level rise over several centuries, despite deep uncertainty and evolving land use. Using exploratory modeling grounded in physical laws, validated operational and new models, and extensive expert involvement, including reviews by over 300 specialists and independent committees, the approach aimed to ensure robustness and mitigate bias. While results suggest technical feasibility at national scale, uncertainties persist regarding local dike stability, storm surge barrier strength, and societal acceptability, alongside ecological and resource considerations. Reviews by Dutch expert networks [39,48,49] confirm reliability but highlight limitations, emphasizing that long-term strategy depends on

more than technical measures. The findings provide quantitative input for adaptive planning within the Dutch Delta Programme's iterative cycle, acknowledging that refinements and broader climate pressures will shape future decisions.

6 CONCLUSION

This first nationwide quantitative assessment shows that sea level rise (SLR) will require significant reinforcement of flood defenses across the Netherlands, with dike height increases at least equal to SLR. No hydraulic tipping points were found up to 3 m, though spatial constraints, sand supply, and resource availability pose major challenges. Freshwater systems are more vulnerable: while increased flushing can initially counter salinization, beyond 2–3 m SLR river flows become insufficient to keep polders and surface waters fresh. The findings inform near-term decisions on dike upgrades and water diversions and feed into long-term adaptation pathways under Adaptive Delta Management. Future work will address technical, ecological, and socioeconomic aspects, including additional storage, new storm surge barriers, and land-use shifts toward salinity tolerance to extend strategy longevity and identify low-regret measures under deep uncertainty.

7 ACKNOWLEDGEMENTS

We acknowledge the support of the following colleagues, consultants and researchers during the research program: Matthijs Bonte, Marit Zethof, Jan Stijnen, Bastiaan Kuijper, Cees Oerlemand, David Knops of HKV; Maarten Jansen, Tim van Engelen, Bert van den Berg of Witteveen+Bos, Joost Delsman, Marcel Taal, Ilja America, Arno Nolte, Ymkje Huismans, Otto Weiler, Arnout Bijlsma, Bennie Minnema, Tobias Mulder, Ellen Quataert, Ad van der Spek, Bas Huisman, Edwin Elias, Zheng Bing Wang, Nienke Vermeer of Deltares; Maarten Spijker, Simon Muurman, Ruben Boelens, Meike Coonen, Jip Grootveld of Hydrologic; Michiel van Reen, Sanne van der Heijden, Jos van der Baan, Jelmer Cleveringa of Arcadis. We also thank the many experts that have been consulted throughout this research.

REFERENCES

1. IPCC *The Ocean and Cryosphere in a Changing Climate: Special Report of the Intergovernmental Panel on Climate Change*; 1st ed.; Cambridge University Press: Cambridge, UK, 2022; ISBN 978-1-009-15796-4.
2. Stolte, W.; Baart, F.; Muis, S.; Hijma, M.; Taal, M.; Le Bars, D.; Drijfhout, S. *Zeespiegelmonitor 2022*; Deltares: Delft, The Netherlands, 2023;
3. Van Dorland, R.; Beersma, J.; Bessembinder, J.; Bloemendaal, N.; Drijfhout, S.; Groenland, R.; Haarsma, R.; Homan, C.; Keizer, I.; Krikken, F.; et al. *KNMI National Climate Scenarios 2023 for the Netherlands - Version 2*; KNMI: De Bilt, The Netherlands, 2024; p. 374;.
4. ENW *Fundamentals of Flood Protection*; 2017; ISBN 978-90-8902-160-1.
5. Ministry of Infrastructure and Water Management *Now for the Future - National Delta Program 2024*; Ministry of Infrastructure and Water Management: The Hague, the Netherlands, 2023;
6. Ten Brinke, W.B.M.; Bannink, B.A.; Ligtvoet, W. The Evaluation of Flood Risk Policy in the Netherlands. *Proceedings of the Institution of Civil Engineers - Water Management* **2008**, *161*, 181–188, doi:10.1680/wama.2008.161.4.181.
7. Slomp, R. *Flood Risk and Water Management in the Netherlands - A 2012 Update*; Rijkswaterstaat: Utrecht, The Netherlands, 2012;
8. Ministry of Infrastructure and Water Management Kennisprogramma Zeespiegelstijging - Deltaprogramma Available online: https://www.deltaprogramma.nl/kennisprogramma-zeespiegelstijging (accessed on 7 February 2025).

9. Van Alphen, J.; Haasnoot, M.; Diermanse, F. Uncertain Accelerated Sea-Level Rise, Potential Consequences, and Adaptive Strategies in The Netherlands. *Water* **2022**, *14*, 1527, doi:10.3390/w14101527.

10. Zevenbergen, C.; Khan, S.A.; van Alphen, J.; Terwisscha van Scheltinga, C.; Veerbeek, W. Adaptive Delta Management: A Comparison between the Netherlands and Bangladesh Delta Program. *International Journal of River Basin Management* **2018**, *16*, 299–305, doi:10.1080/15715124.2018.1433185.

11. Bloemen, P.J.; Hammer, F.; van der Vlist, M.J.; Grinwis, P.; van Alphen, J. DMDU into Practice: Adaptive Delta Management in the Netherlands. In *Decision making under deep uncertainty: From theory to practice*; Marchau, V., AWJ., Walker, W.E., Bloemen, P.J., Popper, S.W., Eds.; Springer International Publishing: Cham, Switzerland, 2019; pp. 321–351.

12. Van Der Wiel, K.; Beersma, J.; Van Den Brink, H.; Krikken, F.; Selten, F.; Severijns, C.; Sterl, A.; Van Meijgaard, E.; Reerink, T.; Van Dorland, R. KNMI'23 Climate Scenarios for the Netherlands: Storyline Scenarios of Regional Climate Change. *Earth's Future* **2024**, *12*, e2023EF003983, doi:10.1029/2023EF003983.

13. Lodder, Q.; Huismans, Y.; Elias, E.; de Looff, H.; Wang, Z.B. Future Sediment Exchange between the Dutch Wadden Sea and North Sea Coast-Insights Based on ASMITA Modelling. *Ocean & Coastal Management* **2022**, *219*, 106067.

14. Delsman, J.R.; Mulder, T.; Verastegui, B.R.; Bootsma, H.; Zitman, P.; Huizer, S.; Essink, G.H.O. Reproducible Construction of a High-Resolution National Variable-Density Groundwater Salinity Model for the Netherlands. *Environmental Modelling & Software* **2023**, *164*, 105683.

15. Ministerie van Infrastructuur en Waterstaat *Strategiedocument Zoetwater Hoofdwatersysteem 2021 - Publicatie - Deltaprogramma*; Ministerie van Infrastructuur en Waterstaat: The Hague, The Netherlands, 2021;

16. Van den Brink, M.; Huismans, Y.; Blaas, M.; Zwolsman, G. Climate Change Induced Salinization of Drinking Water Inlets along a Tidal Branch of the Rhine River: Impact Assessment and an Adaptive Strategy for Water Resources Management. *Climate* **2019**, *7*, 49, doi:10.3390/cli7040049.

17. PIANC *Saltwater Intrusion in Inland Waterways*; PIANC: Brussels, Belgium, 2021; ISBN ISBN 978-2-87223-014-3.

18. Buitink, J.; Tsiokanos, A.; Geertsema, T.; ten Velden, C.; Bouaziz, L.; Weiland, F.S. *Implications of the KNMI'23 Climate Scenarios for the Discharge of the Rhine and Meuse*; Deltares: Delft, The Netherlands, 2023;

19. IPCC *Climate Change 2022 – Impacts, Adaptation and Vulnerability: Working Group II Contribution to the Sixth Assessment Report of the Intergovernmental Panel on Climate Change*; Pörtner, H.-O., Roberts, D.C., Eds.; 1st ed.; Cambridge University Press: Cambridge, UK, 2022; ISBN 978-1-009-32584-4.

20. Wesselius, C.; Fujisaki, A. *Landelijk SOBEK model in SOBEK 3 (LSM3)*; Deltares: Delft, The Netherlands, 2020;

21. Schrijver, M.; Saman, K.; Lievense, P. *Het Gebruik van Het Model Implic Bij Het Bepalen van de Prestatiepeilen*; Rijkswaterstaat: The Hague, The Netherlands, 2009;

22. Bretschneider, C.L. *Generation of Waves by Wind: State of the Art*; National Engineering Science Company, 1964;

23. Anonymous SWAN–User Manual, SWAN Cycle III, Version 41.20 AB Available online: https://swanmodel.sourceforge.io/online_doc/swanuse/swanuse.html accessed 18-3-2025.

24. Holthuijsen, L.H. *Waves in Oceanic and Coastal Waters*; Cambridge university press: Cambridge, UK, 2010;

25. Roscoe, K. *Assessment of the Still-Water-Level 1/10,000 Years Return Values Used in the Current Hydraulic Boundary Conditions*; Deltares: Delft, The Netherlands, 2009;

26. Geerse, C.P.M.; Duits, M.T.; Kalk, H.J.; Lammers, I.B.M. *Wind-Waterstandstatistiek Hoek van Holland*; HKV en Rijkswaterstaat: Lelystad, The Netherlands, 2002;

27. Caires, S. *Extreme Wind Statistics for the Hydraulic Boundary Conditions for the Dutch Primary Water Defences. SBW-Belastingen: Phase 2 of Subproject 'Wind Modelling';* Deltares: Delft, The Netherlands, 2009; pp. 1200264–005;.

28. Duits, M. *Hydra-NL Voor Kennisprogramma Zeespiegelstijging. Testrapport – Versie 2.8.1*; HKV, 2021;

29. Geerse, C.P. Hydra-Zoet for the Fresh Water Systems in the Netherlands-Probabilistic Model for the Assessment of Dike Heights. *PR2168 HKV rapport voor Rijkswaterstaat, Waterdienst;* **2011**.

30. Kolen, B.; Capsers, J.; Pol, J. *Actualisatie OKADER*; HKV: Lelystad, The Netherlands, 2021;

31. Zethof, M.; Stijnen, J.; Kuijper, B.; Knops, D.; Van Den Berg, B. *Systeemanalyse Waterveiligheid - Deelrapport Rijn-Maasmonding En Rivierengebied*; HKV,: Lelystad, The Netherlands: Rijkswaterstaat: The Hague, The Netherlands, 2023;

32. Zethof, M.; Stijnen, J.; Kuijper, B.; Oerlemans, C.; Jansen, M.; Van Engelen, T.; Knops, D.; Van Den Berg, B. *Systeemanalyse waterveiligheid Zuidwestelijke Delta - KP ZSS - Publicatie - Deltaprogramma*; HKV,: Lelystad, The Netherlands: Rijkswaterstaat: The Hague, The Netherlands, 2023;

33. Zethof, M.; Jansen, M.; Van Engelen, T.; Knops, D.; Stijnen, J.; Van Den Berg, B. *Systeemanalyse waterveiligheid Waddenzee en Eems-Dollard - KP ZSS - Publicatie - Deltaprogramma*; HKV,: Lelystad, The Netherlands: Rijkswaterstaat: The Hague, The Netherlands, 2023;

34. Zethof, M.; Jansen, M.; Van Den Berg, B.; Knops, D.; Stijnen, J. *Systeemanalyse waterveiligheid Harde waterkeringen kust - KP ZSS - Publicatie - Deltaprogramma*; HKV,: Lelystad, The Netherlands: Rijkswaterstaat: The Hague, The Netherlands, 2023;

35. Zethof, M.; Stijnen, J. *Systeemanalyse Waterveiligheid Bovenregionale Synthese - KPZSS - Publicatie - Deltaprogramma*; HKV,: Lelystad, The Netherlands: Rijkswaterstaat: The Hague, The Netherlands, 2023;

36. Delsman, J.; America, I.; Mulder, T. *Kennisprogramma Zeespiegelstijging, Spoor II: Grondwaterverzilting En Watervraag Bij Een Stijgende Zeespiegel*; Deltares: Utrecht, The Netherlands, 2022;

37. Deltares *Specificaties Zesde-Generatie Modellen Met D-HYDRO*; Deltares: Delft, The Netherlands, 2019;

38. Nolte, A.; Weeber, M.; Geurts, D.; Pans, S.; Vreeken, D.; Weiler, O. *Klimaatrobuustheid van het waterbeheer van het Volkerak-Zoommeer*; Deltares: Delft, The Netherlands, 2020;

39. van Slobbe, E.; de Vriend, H.J.; Aarninkhof, S.; Lulofs, K.; de Vries, M.; Dircke, P. Building with Nature: In Search of Resilient Storm Surge Protection Strategies. *Nat Hazards* **2013**, *66*, 1461–1480, doi:10.1007/s11069-013-0612-3.

40. Post, V.E.A. Groundwater Salinization Processes in the Coastal Area of the Netherlands Due to Transgressions during the Holocene, Vrije Universiteit Amsterdam: Amsterdam, The Netherlands, 2004.

41. Ralston, D.K.; Geyer, W.R.; Lerczak, J.A. Subtidal Salinity and Velocity in the Hudson River Estuary: Observations and Modeling. *Journal of Physical Oceanography* **2008**, *38*, 753–770, doi:10.1175/2007JPO3808.1.

42. Dijkstra, Y.M.; Schuttelaars, H.M.; Kranenburg, W.M. Salt Transport Regimes Caused by Tidal and Subtidal Processes in Narrow Estuaries. *Journal of Geophysical Research: Oceans* **2022**, *127*, e2021JC018391, doi:10.1029/2021JC018391.

43. Friocourt Y.; Blaas M.; Bonte M.; Vos R.; Slomp R.; Wilmink R.; Lodder Q.; Brakenhoff L.; van Gool S. The Impact of Extreme Sea Lever Rise on the National Strategies for Flood Protection and Freshwater in the Netherlands, Water 2025, 10.3390/w17070919

44. Wegman, T. M., Pietrzak, J. D., Horner-Devine, A. R., Dijkstra, H. A., & Ralston, D. K. (2024). Observations of Estuarine Salt Intrusion Dynamics During a Prolonged Drought Event in the Rhine-Meuse Delta. Journal of Geophysical Research: Oceans, 130(1).

45. Rijkswaterstaat *Kustgenese 2.0 : kennis voor een veilige kust*; Rijkswaterstaat: The Hague, 2020;

46. Taal, M.; Quataert, E.; Van der Spek, A.; Huisman, B.; Elias, E.; Wang, S.; Vermeer, N. *Eindrapport fase 1 Zandige kust: Sedimentbehoefte Nederlands kustsysteem - Publicatie - Deltaprogramma*; Rijkswaterstaat: Utrecht, The Netherlands: Deltares: Delft, The Netherlands, 2023;
47. Deltares *Riskeer*; Deltares: Delft, 2023;
48. ENW *Advies Tussenbalans Kennisprogramma Zeespiegelstijging*; Expertise Netwerk Waterveiligheid: Utrecht, The Netherlands, 2023;
49. ENZD *Kennisprogramma Zeespiegelstijging*; Expertise Netwerk Zoetwater en Droogte: Utrecht, The Netherlands, 2024;
50. Bonte, M.; Zwolsman, J.J.G. Climate Change Induced Salinisation of Artificial Lakes in the Netherlands and Consequences for Drinking Water Production. *Water Research* 2010, *44*, 4411–4424, doi:10.1016/j.watres.2010.06.004.
51. Vos, R. *Time Lines for Track 2 of the Knowledge Program Sea Level Rise (in Dutch)*; Rijkswaterstaat: Lelystad, The Netherlands, 2021;

ICFM 10
Adapting to Global Change:
Innovative Approaches to Flood Management and Resilience
May 20-22, 2026 | Western University, London, Ontario, Canada

Bridging Climate Information and Stakeholder Decisions: A Co-Design Approach for Regional Climate Change Adaptation

Gamze Koç[1*] and Changxing Lan[1]
Karlsruhe Institute of Technology – KIT, Institute of Meteorology and Climate Research Atmospheric Environmental Research (IMKIFU), Campus Alpin, Kreuzeckbahnstrasse 19, 82467 Garmisch-Partenkirchen, Bavaria - GERMANY
*Correspondence: gamze.koc@kit.edu

ABSTRACT

Climate change poses a significant threat to communities at both regional and global scales, with adaptation being particularly urgent for small- and medium-sized communities. However, a persistent knowledge gap limits their capacity to adapt effectively. The lack of accessible, tailored climate information and services further increases vulnerability. This study therefore aims to address this gap by developing effective science communication strategies using a co-design approach, with a focus on the regional scale through the implementation of Regional Climate Information Platforms. The selected case study area, Oberland (Upper Bavaria, Germany), is characterized by complex terrain encompassing Alpine and Pre-Alpine regions, where three distinct climate zones occur in close proximity. This diverse topography presents specific challenges, as climate change impacts may vary spatially, particularly with regard to hydro-meteorological extremes. In addition, the region is highly dependent on tourism, rendering it economically sensitive to changing climate conditions and increasing extreme events such as heavy precipitation, flooding, summer heatwaves, and decreasing snowfall affecting tourism-related activities. The study follows a comprehensive workflow, beginning with the identification of stakeholder needs and followed by the analysis of relevant climate information. The resulting climate information on hydro-meteorological extremes will provide essential input for stakeholders and decision-makers. These results will be visualized as maps and integrated into the digital decision support system Platform Oberland within the KARE (Klimawandelanpassung auf regionaler Ebene) project. Beyond its scientific objectives, the study emphasizes stakeholder interaction and co-design to ensure the relevance and usability of the generated information. Furthermore, it aims to identify best-practice approaches for translating scientific workflows and results into actionable climate adaptation measures for small- and medium-sized communities. The case study may serve as a regional model for effective science communication and adaptation strategies addressing hydro-meteorological extremes.

KEYWORDS: Climate information, science communication, co-design, floods, extreme heat

1 INTRODUCTION

In recent decades, there has been a significant advancement in scientific understanding of climate change and its regional impacts, in parallel with technological and computational developments (Pan et al., 2022), (Karetnikov and Ruth, 2014), (IPCC, 2023). Despite the increasing body of knowledge, a persistent gap remains between climate research and its effective application in policy and decision making, particularly among small and medium-sized communities (Selseng and Gjertsen, 2024), (Fünfgeld et al., 2023), (Ricciardi et al., 2023), (Buschmann et al., 2022), (Fila et al., 2024). Key barriers include the disconnect between researchers and policymakers (Thompson et al., 2017), (Briley et al., 2015), the limited accessibility and relevance of climate information, institutional and financial constraints (Fila et al., 2024), and the lack of participatory processes that involve local stakeholders in the

design and implementation of adaptation measures (Ricciardi et al., 2023), (Jones et al., 2017), (Thompson et al., 2017). Although small and medium-sized municipalities are not less affected by climate change, they are underrepresented in research, in contrast to larger cities and metropolitan areas (Ricciardi et al., 2023). In particular, the gap between the production of climate information and how it is used in the real world is a major challenge in developing resilient and inclusive climate adaptation strategies (Mabon, 2020), (Lemos and Rood, 2010). Local and regional stakeholders often find it difficult to incorporate scientific climate information into their planning and decision-making processes. This difficulty arises from several interrelated factors. Firstly, climate information is often presented in formats that are too technical or abstract for non-experts to interpret and apply directly (Mabon, 2020), (Briley et al., 2015). The use of specialized indices, probabilistic language, and complex visualizations can lead to confusion or underestimate of climate risks. Secondly, the relevance of the information is not always clear as scientific studies often focus on broad or global scales, whereas local stakeholders require insights that are tailored to their specific context (Briley et al., 2015), (Roberts et al., 2018). Third, the channels through which climate knowledge is communicated may not align with local actors' information seeking behaviours (Thompson et al., 2017), (Briley et al., 2015), further reducing the likelihood that available information will influence local decision-making (Jones et al., 2017), (Lemos and Rood, 2010). These challenges have highlighted the need for easy-to-use and decision-relevant climate information, which could also help bridging the gap between scientific production and practical application.

In order to enhance access to climate data and support adaptation planning, a number national and regional institutions in Germany have developed climate information platforms and services. At the national level, institutions such as the Deutscher Wetterdienst (DWD, 2025a), the Climate Service Center Germany (GERICS, 2025) and the German Environment Agency (UBA, 2025a) provide essential climate datasets, projections, and adaptation tools. These services are underpinned by high-resolution observational data and downscaled climate projections derived from international ensembles such as EURO-CORDEX (UBA, 2025b). The Climate Data Center (CDC) of DWD (DWD, 2025b), for instance, supplies gridded climate variables, while GERICS supports decision-making in sectors such as urban planning through tailored regional scenarios and vulnerability assessments (GERICS, 2025a; 2025b). At federal state level, Bavaria has developed its own specialised services to address the impacts of climate change at a more localised level. The Bavarian Climate Information System (BAYKIS), which is operated by the Bayerisches Landesamt für Umwelt (LfU), provides downscaled climate projections and impact indicators via a central platform (LFU, 2025). These datasets are statistically refined using outputs from the EURO-CORDEX regional climate model, DWD observations and LfU post-processing techniques. The LfU's portal also disseminates complementary tools, such as municipal climate checks and adaptation guidelines, facilitating the integration of climate considerations into local and regional governance structures (LFU, 2025). In addition to these services, several regional initiatives based on different research projects provide place-based climate information tailored to urban and sub-regional contexts for different federal states in Germany (i.e. KliVO Portal Hessen, Klimaatlas BW, Umweltatlas Berlin, etc.) (UBA, 2025c; LUBW, 2025, Landes Berlin, 2025). ReKIS (Regionales Klimainformationssystem), for example, is a regional climate information platform providing climate information to the eastern German states of Saxony, Saxony-Anhalt and Thuringia (REKIS, 2025). It provides high-resolution climate data and projections related to extreme weather events and long-term trends, as well as indicators. Similarly, The NRW Climate Atlas (Klimaatlas Nordrhein-Westfalen) provides regional climate change projections with a focus on temperature, precipitation, and extreme events across North Rhine-Westphalia Landesamt für Natur, Umwelt und Klima Nordrhein-Westfalen (LANUK, 2025).

Despite the wide range of climate information platforms and services available in Germany, they remain limited in their practical applicability for small and medium-sized communities. The multitude of providers, diverse data formats and differing methodological assumptions and time periods often cause confusion which pose challenges for non-specialist users in local administrations. Furthermore, while many existing services rely on downscaled regional climate projections with different ensembles, these are often insufficiently detailed to capture local extreme events and locally relevant impacts, which are

critical for municipal-level adaptation planning. Therefore, this study aims to address these limitations using NUKLEUS - Nutzbare lokale Klimainformationen für Deutschland, high-resolution, user-oriented climate information specifically tailored to the needs collected during the transfer meetings of medium- and small-sized communities. By bridging the gap between national and regional climate services and local decision-making requirements, the study aims to make climate data easily understandable, more usable, and relevant to effective, place-based adaptation planning.

2 STUDY AREA, DATA & METHODS

2.1 Study Area

The study area, Oberland, is located in the southern German province of Upper Bavaria, which is characterised by the presence of three distinct climate zones within the Alpine foreland. The area is renowned for its high level of tourism (for example, ski tourism) and is economically dependent on tourism due to its scenic landscape. Moreover, the region is considered to be one of the most economically dynamic areas in the country. However, the region is also known for its frequency of extreme convective precipitation events, which have been responsible for numerous floods in the past. Climate predictions indicate a continuation of the observed trend of rising event frequency, suggesting that the impacts of climate change are already evident and are expected to intensify further in the region.

2.2 Data

The NUKLEUS dataset is a comprehensive, high-resolution ensemble of regional climate model simulations developed within the "NUKLEUS - Nutzbare Lokale Klimainformationen für Deutschland" project, a cross-cutting activity of the RegIKlim research initiative. The core objective of NUKLEUS is to generate, evaluate, and provision spatially and temporally refined climate information tailored to regional climate impact assessments, adaptation planning, and climate service applications for Germany. The dataset under consideration comprises dynamically downscaled climate projections derived from multiple combinations of global climate models (GCMs) and regional climate models (RCMs). Initially, three CMIP6 GCMs (e.g., EC-EARTH3-Veg, MIROC6, MPI-ESM1-2-HR) are downscaled to an intermediate European grid (EUR-11, ~12 km), and subsequently to a convection-permitting scale (~3 km; CEU-3) over Germany via RCMs including COSMO-CLM, ICON-CLM, and REMO. The simulation types include evaluation runs against ERA5 reanalysis, historical runs, and future transient scenario projections under standardized SSP forcing pathways (NUKLEUS, 2025).

For the analysis of this study, ICON-CLM, EC-EARTH3-Veg, CEU-3 simulations were used due to the availability of three different future transient scenario projections under standardized SSP forcing pathways (SSP2-4.5, SSP3-7.0, SSP8-5.5) under two different global warming levels (GWL) (GWL2K, GWL 3K).

2.3 Method

Global warming, driven primarily by anthropogenic greenhouse gas emissions, exerts profound influences on regional climate dynamics through changes in key meteorological and hydrological variables. To assess these impacts and evaluate the associated risks to small- and medium-sized communities that are often characterized by limited adaptive capacity, resource constraints, and strong dependence on local ecosystems, it is essential to examine variations in air temperature, precipitation, and snow depth, which serve as fundamental indicators of regional climate change. Air temperature is a primary metric due to its direct link to the enhanced greenhouse effect, whereby increased atmospheric concentrations of greenhouse gases trap outgoing longwave radiation and raise surface temperatures. At the regional scale, this manifests as amplified warming trends, including more frequent and intense heatwaves. For small- and medium-sized communities, which often lack robust cooling infrastructure or

diversified economic structures, such warming poses significant risks, including increased heat-related mortality, reduced agricultural productivity through altered growing seasons, and higher energy demand for cooling. Precipitation represents another critical climate variable, as global warming intensifies the hydrological cycle. Warmer air masses can hold more moisture, leading to shifts toward more extreme precipitation regimes—characterized by heavier rainfall events in some regions and prolonged droughts in others. These changes affect water availability, flood frequency, and soil moisture, with cascading impacts on food security, infrastructure resilience, and public health. Small- and medium-sized communities are particularly vulnerable due to their reliance on rain-fed agriculture and local water resources. For example, increased flood frequency can overwhelm drainage systems and cause urban flooding, while drought conditions may lead to water scarcity that directly constrains agricultural and domestic water use. Snow depth, particularly in the Alpin region, provides insights into cryospheric responses to warming, including accelerated snowmelt and reduced accumulation. Global warming diminishes snowpack through elevated freezing levels and earlier spring thaw, altering seasonal hydrology and water storage. In addition, reduced snow cover affects winter economies (e.g., tourism) and ecosystems, potentially triggering feedback loops such as albedo reduction that further amplify regional warming.

Apart from the changes in the average annual temperature, precipitation, and winter average snow depth, we focus on the occurrence of extreme events, including yearly extreme heat days, heatwaves, heavy rain days, and snow days. Extreme heat days are defined as those days with daily maximum temperature exceeding 30°C. A heatwave event is defined as at least consecutive 3 days with daily mean temperature exceeding 95% of the historical reference temperature derived using CEU-3 output. Heavy rain days and snow days are defined as those days with precipitation exceeding 30 mm and with snow depth exceeding 1 cm, respectively.

The indicators and the final output formats were determined based on the results of a mini survey titled 'Climate Information Requests and Data Formats' that was conducted with all stakeholders in the project area during a project meeting on 20 June 2024. The research questions were then determined in line with this using a co-design approach.

3 RESULTS

The future climate projections for the Oberland region were evaluated under multiple SSP (SSP245, SSP370, and SSP585) and at two GWLs, +2K and +3K relative to pre-industrial conditions. Accordingly, annual mean temperature shows a linear and consistent increase across all SSP scenarios as the level of global warming increases; for example, in the SSP245 scenario, increases at low warming levels remain around +1.4°C (+3K), while in the SSP585 scenario, this increase exceeds +4 °C at high warming levels (+3K) (Table 1). Maximum temperatures and hot extremes respond more strongly than the average; increases in the number of hot days reach 12 days average in the high emissions scenario. In contrast, with the increase in minimum temperatures, cold extremes are decreasing significantly; for example, the number of cold days or cold nights decreases by a few days per year even at low warming levels, and by more than 20 days at high warming levels (SSP585, +3K) (Table 1).

The precipitation analysis based on NUKLEUS projections for Oberland shows that, annual total precipitation increases in relative terms across all SSPs and warming levels. We can see the strongest relative increase for SSP370 reaching up to %10.5 (+2K) and %5.5 (+3K), but with a large inter-model spread (up to %40, +3K) (Table 1). When we look at the seasonal precipitation changes, we can see that spring and autumn mean precipitation have a constant increase up to %25 (SSP245, +3K), where the change in autumn has high variability. The results for winter and summer precipitation values give more mixed responses and highly uncertain. Mean precipitation in winter decreases under SSP245 (%12.6, +2K), where it has near neutral changes for SSP370, and has a consistent decrease under SSP585. For summer, mean changes are comparatively small or negative for SSP245 and SSP585, where they are positive for SSP370 scenario (Table 1). Large min-max ranges (up to %70) shows high uncertainty and indicate strong model disagreement.

Table 1. Changes of climate indicators in Oberland region based on NUKLEUS data (ICON-CLM, EC-EARTH3-Veg, CEU-3)

	Historical	SSP245						SSP370						SSP585					
		GWL-2K			GWL-3K			GWL-2K			GWL-3K			GWL-2K			GWL-3K		
	Mean	Mean	Min	Max	Mean	Min	Max	Mean	Min	Max	Mean	Min	Max	Mean	Min	Max	Mean	Min	Max
Annual Mean Temperature (°C)	6.82	1.93	0.9	3.02	2.85	1.39	4.02	1.77	0.26	3.74	3.07	0.63	4.58	1.94	0.64	3	3.41	1.97	4.95
Winter (DJF) Mean Temperature (°C)	-1.41	2.42	0.79	5.38	2.77	-0.39	4.81	1.89	-1.5	4.2	3.07	0.76	5.46	2.4	0.24	4.47	3.6	0.95	6.18
Spring (MAM) Mean Temperature (°C)	6.26	1.12	-2.46	3.23	1.73	-1.24	3.56	1.14	-3.11	4.3	2.43	-1.22	4.53	1.33	-0.73	3.75	2.62	-0.27	5.63
Summer (JJA) Mean Temperature (°C)	14.83	2.39	0.34	4.78	3.84	1.9	6.03	2.22	-0.05	4.86	3.87	1.61	6.03	1.9	0.37	4.04	3.93	1.1	7.07
Autumn (SON) Mean Temperature (°C)	7.44	1.79	0.34	4.78	3.05	1.9	6.03	1.84	-0.05	4.86	2.92	1.61	6.03	2.11	0.37	4.04	3.5	1.1	7.07
Number of Summer Days (Tmax > 25°C) per Year	16.03	15.47	-0.03	40.97	29.17	4.97	65.97	15.43	-4.03	47.97	28.87	1.97	65.97	11.67	-6.03	38.97	31.9	8.97	77.97
Number of Heat Days (Tmax > 30 °C) per Year	1.03	3.6	-16.03	6.97	10.3	-14.03	18.97	4.03	-16.03	8.97	9.3	-15.03	10.97	3.3	-16.03	-2.03	12.1	-15.03	29.97
Number of Tropical Nights (Tmin > 20°C) per Year	0	0.1	-16.03	-14.03	1.13	-16.03	-7.03	0.4	-16.03	-12.03	1.2	-16.03	-9.03	0.13	-16.03	-14.03	2.07	-16.03	-4.03
Number of Heatwaves per Year	7.73	-0.8	-13.03	-0.03	-0.77	-13.03	-5.03	-0.07	-11.03	-5.03	-1.13	-13.03	-6.03	-0.9	-12.03	-2.03	-0.43	-12.03	-1.03
Number of Cold Days per Year	20.67	22.53	9.97	49.97	40.37	19.97	76.97	22.07	2.97	52.97	40.97	16.97	85.97	18.33	0.97	45.97	42.6	18.97	84.97
Number of Heating Days (Tmean > 15°C) per Year	309.1	-32.1	228.97	287.97	-50.87	223.97	265.97	-29.7	230.97	287.97	-53.4	205.97	272.97	-29.4	231.97	299.97	-54.97	193.97	271.97
Number of Frost Days (Tmin < 0°C) per Year	124.17	-27.7	45.97	116.97	-40.67	31.97	94.97	-26.6	47.97	122.97	-46.87	29.97	122.97	-29.6	34.97	100.97	-52.67	17.97	90.97
Number of Ice Days (Tmax < 0°C) per Year	35.97	-16.63	-15.03	30.97	-19.9	-15.03	25.97	-12.17	-9.03	45.97	-20.3	-13.03	16.97	-16.67	-12.03	24.97	-24.37	-13.03	19.97
Annual Total Precipitation	1511.96 mm	4.62%	-22.99%	25.80%	6.55%	-30.88%	32.53%	10.53%	-14.51%	36.77%	5.49%	-20.94%	43.97%	5.51%	-25.13%	31.80%	2.06%	-17.96%	33.25%
Winter (DJF)Total Precipitation	353.03 mm	-12.61%	-60.45%	39.17%	-2.12%	-47.58%	85.70%	0.81%	-55.67%	74.32%	-0.64%	-52.26%	71.23%	-9.26%	-50.22%	32.04%	-4.41%	-48.94%	32.05%
Spring (MAM)Total Precipitation	378.72 mm	16.11%	-21.51%	73.46%	25.03%	-26.40%	77.96%	15.95%	-42.89%	77.75%	15.54%	-32.72%	47.84%	12.17%	-34.41%	68.85%	9.68%	-44.35%	59.65%
Summer (JJA)Total Precipitation	475.99 mm	-1.24%	-34.98%	55.23%	-9.21%	-47.25%	37.42%	9.84%	-45.68%	66.96%	1.18%	-44.00%	72.31%	3.38%	-50.62%	53.28%	-7.86%	-56.55%	44.03%
Autumn (SON)Total Precipitation	304.22 mm	19.49%	-51.63%	96.39%	18.26%	-43.00%	116.13%	16.11%	-59.33%	76.59%	6.84%	-57.05%	99.91%	17.69%	-29.93%	96.44%	15.63%	-33.72%	92.66%
Before Growing Season Total Precipitation	445.16 mm	8.22%	-27.46%	33.56%	13.33%	-28.01%	64.75%	18.87%	-21.54%	65.23%	15.99%	-18.81%	54.16%	9.76%	-25.62%	61.92%	5.16%	-55.14%	76.28%
After Growing Season Total Precipitation	415.63 mm	4.03%	-52.74%	62.72%	-7.80%	-63.02%	48.96%	9.86%	-35.69%	62.75%	-4.00%	-68.60%	37.43%	3.16%	-53.54%	49.63%	-8.66%	-57.61%	49.61%
Number of Heavy Rain Days per Year	3.3	2.1	-3.3	7.7	2.2	-2.3	6.7	2.77	-1.3	6.7	1.4	-2.3	7.7	2.2	-2.3	6.7	1.9	-3.3	5.7
Number of Dry Days per Year	6.23	0.23	-2.23	4.77	1.3	-2.23	6.77	-0.2	-5.23	5.77	0.43	-4.23	3.77	0.43	-3.23	5.77	0.87	-3.23	3.77
Number of Dry Days Before Growing Season per Year	0.67	-0.03	-0.67	2.33	0.4	-0.67	2.33	-0.23	-0.67	1.33	0.03	-0.67	1.33	0.3	-0.67	3.33	0.57	-0.67	2.33
Number of Dry Days After Growing Season per Year	1.67	-0.1	-1.67	2.33	0.9	-0.67	3.33	-0.03	-1.67	2.33	0.3	-1.67	2.33	0.17	-1.67	1.33	0.4	-1.67	3.33
Number of Wet Days per Year	0.83	0.07	-0.83	3.17	0.47	-0.83	3.17	0.3	-0.83	2.17	0.17	-0.83	1.17	-0.13	-0.83	2.17	0.23	-0.83	4.17
Number of Wet Days Before Growing Season per Year	0.27	-0.07	-0.27	1.73	0.37	-0.27	1.73	0.27	-0.27	2.73	0.13	-0.27	0.73	0.03	-0.27	1.73	0.17	-0.27	2.73
Number of Wet Days After Growing Season per Year	0.33	0.03	-0.33	1.67	0.07	-0.33	1.67	0.07	-0.33	1.67	-0.03	-0.33	1.67	-0.07	-0.33	0.67	-0.03	-0.33	1.67
Mean Snow Depth (cm)	21.96	-12.81	-82.7	12.28	-13.27	-89.63	4.43	-10.02	-88.29	40.92	-11.41	-88.69	35.81	-12.08	-90.34	3.78	-15.77	-90.41	-43.49
Number of Snow Days per Year	87.77	-7.6	-26.77	3.23	-8.03	-32.77	3.23	-6.53	-26.77	3.23	-15	-45.77	2.23	-6.47	-48.77	3.23	-17.47	-48.77	3.23
Number of Heavy Snow Days per Year	23.6	-20.73	-23.6	2.4	-20	-23.6	14.4	-15.6	-23.6	28.4	-15.33	-23.6	22.4	-19.97	-23.6	8.4	-23.2	-23.6	-20.6
Number of Snowstorm Days per Year	2.07	0.33	-1.07	2.93	0.03	-2.07	1.93	0.1	-2.07	2.93	-0.33	-2.07	1.93	0.33	-2.07	2.93	0.6	-1.07	3.93

When we look at the extremes, heavy rain days increase robustly across all SSPs. Number of heavy precipitation days increase of 2-3 days per year in average, with maxima up to 7.7 days. This situation might indicate the intensification of extreme precipitation, even where total rainfall changes are moderate. When we analyse the changes in number of dry days, we see slight increases in total dry days especially under SSP245, +3K (6.7 days). However, seasonally change in number of dry days shows high variability but no strong systematic trend (Table 1). Number of wet days have positive changes in overall (< 0.5 days per year) suggesting that increased precipitation is driven more by intensity than frequency.

In addition to changes in temperature and precipitation, projected warming also affects snow-related variables. Winter snow conditions are projected to decrease under all warming levels and emission scenarios. Mean snow depth is reduced by about 10–16 cm on average, with mean changes ranging from −12.8 to −15.8 cm across scenarios and warming levels, and with some model projections showing much larger reductions, indicating that seasonal snow cover could become very limited under warmer conditions. The number of snow days per year also becomes lower, with mean reductions of about −6 to −17 days per year, corresponding to losses of approximately 7 to 17 snow days per year compared to the historical period. Heavy snow days show the strongest response, with average reductions of roughly −15 to −21 days, and some projections suggesting the complete loss of heavy snowfall events (Table 1). In contrast, changes in the number of snowstorm days are small, with mean changes between 0 and +0.6 day and a wide uncertainty range, indicating that snowstorms may still occur but will contribute less to overall snow accumulation.

Overall, the results show that the Oberland region will become steadily warmer, with more frequent heat extremes, heavier rainfall events, and a strong decline in snow cover, while seasonal precipitation changes remain uncertain, highlighting increasing climate-related challenges under higher warming levels and emission scenarios.

4 DISCUSSION

The projections indicate that rising temperatures, together with changing precipitation patterns, lead to more frequent heat extremes, stronger rainfall intensity, and substantially weaker snow conditions under future warming. A shift toward more intense but less evenly distributed precipitation, characterized by wetter springs and autumns, uncertain summers, and more frequent heavy rainfall events, particularly under intermediate to high forcing scenarios. This pattern suggests enhanced precipitation intensity and seasonality rather than uniform wetting, increasing the likelihood of hydrological extremes such as flooding and seasonal water stress, especially during and after the growing season. These conditions are significant for this region, which currently experiences heavy rainfall and has suffered flooding on numerous occasions. In parallel with the expected increase in rainfall intensity, short-term extreme rainfall, combined with the topography of this region at the foothills of the Alps, makes it more prone to flooding.

The analysis also shows that a systematic decline in snow accumulation, duration, and intensity, with snow depth and heavy snowfall being particularly sensitive to warming. While isolated snowstorm events may persist, the overall snow regime shifts toward shallower, shorter-lived, and less intense snow conditions, especially under higher warming levels. These conditions could pose a long-term risk for the local population, which is particularly dependent on ski tourism during the ski season in the region.

On the other hand, the results show that model uncertainty differs between variables and generally becomes larger at higher warming levels. Changes in annual and seasonal mean temperature are consistent across models, indicating good agreement on the overall warming trend. In contrast, temperature extremes, such as the number of summer days, heat days, and tropical nights, show a much wider range of projections, reflecting higher uncertainty. Precipitation changes are more uncertain, especially at the seasonal scale, where models project both strong increases and decreases, leading to low confidence in the direction of change. Precipitation extremes, represented by the number of heavy rain days, are more consistent across models and point to an increase in rainfall intensity. Snow-related variables show the highest uncertainty, with very large reductions in some projections and smaller

changes in others, reflecting the strong sensitivity of snow to temperature. Overall, while the warming trend is robust, the size of changes in precipitation and snow becomes increasingly uncertain at higher warming levels. Climate indices obtained through NUKLEUS simulations provide information about the region's future. However, since these results are model-dependent, any uncertainty should also be taken into account when communicating with stakeholders.

In order to improve the practical use of the presented indicators for decision-making purposes, it is also crucial to explicitly link projected climate changes with sector-specific adaptation measures. Despite uncertainties mentioned above in seasonal mean precipitation, the robust increase in heavy precipitation days suggests an intensification of short-duration rainfall events. For the Oberland region, which is characterised by complex topography and documented flood exposure, this translates into heightened risk of flash flooding and pluvial flooding. Adaptation responses should therefore prioritise the creation of flood retention areas, the enhancement of drainage infrastructure, the implementation of nature-based solutions and the improved integration of early warning systems into municipal planning tools. Similarly, the projected increase in extreme heat days and heatwave frequency implies elevated risks of heat stress, particularly for vulnerable populations (such as kids or elderly people) and outdoor workers. Municipal adaptation strategies may therefore include developing heat action plans, expanding urban green infrastructure to mitigate the urban heat island effect, integrating cooling centres into emergency planning and incorporating passive cooling standards into building regulations considering the vulnerable groups and climate information together. The projected decline in snow depth and days under all warming levels has significant implications for winter tourism, a key economic pillar of the region. Therefore, adaptation strategies may involve diversifying towards year-round tourism concepts, investing in climate-resilient infrastructure, and engaging in strategic economic planning to reduce dependence on snow-reliant activities. By linking quantified climate indicators into clearly defined risk factors and adaptation options, the study could help to provide more relevant information on regional scale for municipal authorities.

5 CONCLUSION & OUTLOOK

This study demonstrates the added value of combining high-resolution regional climate modelling in the region for the first time using the NUKLEUS dataset with a co-design approach to support climate change adaptation at regional and municipal levels. The analysis of the Oberland region as a case study reveals robust warming trends, an obvious increase in heat extremes and heavy precipitation events, and a significant decrease in snow depth and days with snow under all considered warming levels and emission scenarios. These changes highlight an increasing risk of heat stress, flooding, issues with water management and problems with winter tourism. This is particularly relevant for small and medium-sized communities with limited adaptive capacity and a strong dependence on local environmental conditions.

The results provide climate information that is relevant for decision-making and can directly support stakeholders and policymakers in regional planning and adaptation processes. By translating complex climate projections into specific indicators, such as the number of days with extreme heat, heavy precipitation, and snow-related metrics, the study enables an assessment of climate risks and supports the prioritization of adaptation measures in sectors such as disaster risk management, infrastructure planning, tourism, and land use. The co-design process ensures that the selected indicators and data formats align with stakeholder needs, thereby increasing their usability and trustworthiness and the likelihood of their integration into practical decision-making processes.

As a next step, the derived climate indicators will be visualized in the form of maps and to integrate them into the digital decision-support system within the KARE project. Beyond the regional scale, the methodology and results will be transferred and upscaled to the federal state level of Bavaria, and then to the national level in Germany. The objective is to ensure consistency across governance levels while preserving regional characteristics, thereby contributing to a more consistent and applicable climate information framework. Conducting this analysis will also facilitate the comparison of those previously conducted at national and federal state levels with analyses using NUKLEUS data, thereby providing a comparative overview. This approach can provide a transferable example for strengthening the interface

between science and policy and for improving climate adaptation planning in regions with diverse climatic and socio-economic conditions.

6 ACKNOWLEDGEMENTS

This study was undertaken as part of KARE II - Klimawandelanpassung auf regionaler Ebene Project, funded by Bundesministerium für Forschung, Technologie und Raumfahrt (BMFTR) under grant number 01LR2006D1.

Author contributions

GK: Funding acquisition, conceptualization, methodology, writing - original draft, writing - review and editing.

CL: Methodology; formal analysis; writing – review and editing.

REFERENCES

Briley, L., Brown, D. and Kalafatis, S. E. (2015), 'Overcoming barriers during the co-production of climate information for decision-making', Climate Risk Management 9, 41–49. Boundary Organizations. URL: https://www.sciencedirect.com/science/article/pii/S2212096315000157

Buschmann, D., Koziol, K., Bausch, T. and Reinhard, S. (2022), 'Adaptation to climate change in small German municipalities: Sparse knowledge and weak adaptive capacities', Natural Resources Forum 46(4), 377–392. URL: https://onlinelibrary.wiley.com/doi/abs/10.1111/1477-8947.12262

DWD (2025a), Wetter und Klima, Deutscher Wetterdienst. Available at: www.dwd.de (Accessed: 12 November 2025).

DWD (2025b), CDC - Climate Data Center, Deutscher Wetterdienst. Available at: www.dwd.de (Accessed: 17 November 2025).

Fila, D., Fünfgeld, H. and Dahlmann, H. (2024), 'Climate change adaptation with limited resources: adaptive capacity and action in small- and medium-sized municipalities', Environment, Development and Sustainability 26(3), 5607–5627. URL: https://doi.org/10.1007/s10668-023-02999-3

Fünfgeld, H., Fila, D. and Dahlmann, H. (2023), 'Upscaling climate change adaptation in small- and medium-sized municipalities: current barriers and future potentials', Current Opinion in Environmental Sustainability 61, 101263. URL: https://www.sciencedirect.com/science/article/pii/S1877343523000106

GERICS (2025a), Climate Service Center Germany. Available at: www.gerics.de (Accessed: 27 December 2025).

GERICS (2025b), Climate Service Center Germany, Klimanavigator. Available at: www.klimanavigator.eu (Accessed: 29 December 2025).

IPCC (2023), Climate Change 2023: Synthesis Report. Contribution of Working Groups I, II and III to the Sixth Assessment Report of the Intergovernmental Panel on Climate Change, IPCC, Geneva, Switzerland. URL: https://www.ipcc.ch/report/ar6/syr/

Jones, L., Champalle, C., Chesterman, S., Cramer, L. and Crane, T. A. (2017), 'Constraining and enabling factors to using long-term climate information in decision-making', Climate Policy 17(5), 551–572, https://doi.org/10.1080/14693062.2016.1191008

Karetnikov, D. A. and Ruth, M. (2014), Climate Change and Regional Impacts, In: Fischer, M., Nijkamp, P. (eds) Handbook of Regional Science. Springer, Berlin, Heidelberg. https://doi.org/10.1007/978-3-642-23430-9_57

Landes Berlin (2025), Umweltatlas Berlin. Available at: www.berlin.de/umweltatlas (Accessed: 29.12.2025).

LANUK (2025), Landesamt für Natur, Umwelt und Klima Nordrhein-Westfalen, Klimaatlas Nordrhein-Westfalen. Available at: www.klimaatlas.nrw.de (Accessed: 29.12.2025).

Lemos, M. C. and Rood, R. B. (2010), 'Climate projections and their impact on policy and practice', WIREs Climate Change 1(5), 670–682. URL: https://wires.onlinelibrary.wiley.com/doi/abs/10.1002/wcc.71

LFU (2025), Bayerisches Landesamt für Umwelt, Bayerisches Klimainformationssystem. Available at: https://klimainformationssystem.bayern.de/ (Accessed: 29 December 2025).

LUBW (2025), Landesanstalt für Umwelt Baden-Württemberg, Klimaatlas BW. Available at: www.klimaatlas-bw.de/klimaatlasbw (Accessed: 29.12.2025).

Mabon, L. (2020), 'Making climate information services accessible to communities: What can we learn from environmental risk communication research?', Urban Climate 31, 100537. URL: https://www.sciencedirect.com/science/article/pii/S2212095518303493

NUKLEUS (2025), NUKLEUS – Nutzbare Lokale Klimainformationen für Deutschland. Available at: https://ch1187.gitlab-pages.dkrz.de/Information/# (Accessed: 31 December 2025)

Pan, S. L., Carter, L., Tim, Y. and Sandeep, M. (2022), 'Digital sustainability, climate change, and information systems solutions: Opportunities for future research', International Journal of Information Management 63, 102444. URL: https://www.sciencedirect.com/science/article/pii/S0268401221001377

REKIS (2025), ReKIS – Regionales Klimainformationssystem Sachsen, Sachsen-Anhalt, Thüringen. Available at: rekis.hydro.tu-dresden.de (Accessed: 29 December 2025).

Ricciardi, G., Ellena, M., Barbato, G., Giugliano, G., Schiano, P., Leporati, S., Traina, C. and Mercogliano, P. (2023), 'Climate change adaptation cycle for pilot projects development in small municipalities: The north western Italian regions case study', City and Environment Interactions 17, 100097. URL: https://www.sciencedirect.com/science/article/pii/S2590252022000198

Roberts, M. J., Vidale, P. L., Senior, C., Hewitt, H. T., Bates, C., Berthou, S., Chang, P., Christensen, H. M., Danilov, S., Demory, M.-E., Griffies, S. M., Haarsma, R., Jung, T., Martin, G., Minobe, S., Ringler, T., Satoh, M., Schiemann, R., Scoccimarro, E., Stephens, G. and Wehner, M. F. (2018), 'The benefits of global high resolution for climate simulation: Process understanding and the enabling of stakeholder decisions at the regional scale', Bulletin of the American Meteorological Society 99(11), 2341 – 2359. URL: https://journals.ametsoc.org/view/journals/bams/99/11/bams-d-15-00320.1.xml

Selseng, T. and Gjertsen, A. (2024), 'What drives sustainable climate change adaptation at the local level? approaching three knowledge gaps', Sustainable Development 32(6), 6504–6519, https://doi.org/10.1002/sd.3043

Thompson, M. A., Owen, S., Lindsay, J. M., Leonard, G. S. and Cronin, S. J. (2017), 'Scientist and stakeholder perspectives of transdisciplinary research: Early attitudes, expectations, and tensions', Environmental Science Policy 74, 30–39. URL: https://www.sciencedirect.com/science/article/pii/S1462901116307493

UBA (2025a), Umweltbundesamt, Daten zur Umwelt: Umweltzustand und Trends, Klima. Available at: www.umweltbundesamt.de/daten/klima (Accessed: 27 December 2025).

UBA (2025b), Umweltbundesamt, Einführung in Klimaprojektionen. Available at: www.umweltbundesamt.de/themen/klima-energie/klimafolgen-anpassung/folgen-des-klimawandels/klimamodelle-szenarien-neu/einfuehrung-in-klimaprojektionen (Accessed: 29 December 2025).

UBA (2025c), Umweltbundesamt, Kompetenzzentrum Klimafolgen und Anpassung, Das Deutsche Klimavorsorgeportal - KLiVO. Available at: www.klivoportal.de (Accessed: 29 December 2025).

ICFM 10
Adapting to Global Change:
Innovative Approaches to Flood Management and Resilience
May 20-22, 2026 | Western University, London, Ontario, Canada

Simulating the Influence of the Agulhas Current on Cut-Off Low-Induced Flooding in KwaZulu-Natal, South Africa

Akintunde I. Makinde[1,2] and Babatunde J. Abiodun[1,2]
Email: mckynde@gmail.com, babatunde.abiodun@uct.ac.za

[1]Department of Environmental and Geographical Sciences, University of Cape Town, Cape Town, South Africa
[2]Nansen-Tutu Research Centre for Marine Environment, Department of Oceanography, University of Cape Town, South Africa

ABSTRACT

Cut-off low-induced floods are a threat to socio-economic activities in the KwaZulu-Natal (KZN) province of South Africa due to the associated landslides and high-impact disasters. When cut-off lows (COLs) track over southeastern Africa, they may interact with the Agulhas Current (AC). While studies have shown that the Agulhas Current plays a crucial role in rainfall over South Africa, there is no information on how the current affects floods over KZN, especially through COLs. The present study examines the impact of the Agulhas Current System (ACS) on COL-induced floods in KZN, with a focus on the specific event of the April 2022 Cut-Off Low. For the study, a flood prediction system called the Africa Flood Prediction System (AFPS) was developed by coupling atmospheric, hydrologic, and hydraulic models. First, we evaluate the AFPS model and quantify the sensitivity of COL-driven precipitation to ACS-modulated sea surface temperature anomalies and then evaluate how COL-driven rainfall propagates into basin-scale streamflow response. Thereafter, we assess how precipitation and streamflow translate into flood extent and inundation dynamics.

Results show that the AFPS provides credible simulations of the COLs and their associated extreme rainfalls, peak streamflow, and flood hazards over KZN. Also, it demonstrates that ocean-modulated atmospheric forcing strongly induces rainfall intensity and spatial organisation, while hydrological and hydraulic responses exhibit nonlinear sensitivity to precipitation magnitude and timing. Although explicit ACS sensitivity experiments are applied only at the atmospheric level in this phase, the cross-scale evaluation establishes a robust baseline for forthcoming end-to-end flood sensitivity attribution. The findings highlight the importance of explicitly representing ocean–atmosphere interactions in flood prediction and risk assessment frameworks for coastal southern Africa.

KEYWORDS: Flooding, Cut-off low, Extreme rainfall, Agulhas Current, Atmosphere-ocean interaction, regional modelling, KwaZulu-Natal, Southern Africa.

1 INTRODUCTION

Cut-off lows (COLs) are recurrent synoptic-scale systems over southern Africa and are frequently associated with prolonged and spatially extensive rainfall. In KwaZulu-Natal, such systems have been responsible for several high-impact flood events (Holloway et al. 2010; Favre et al. 2013; Molekwa et al. 2014), including the catastrophic April 2022 disaster. The extreme rainfall of April 2022, which battered towns in the region, resulted in a catastrophic flood which left 40,000 people displaced, 88 people missing, and at least 443 dead (Thoithi et al. 2022; Grab and Nash 2023). Despite the regular occurrence of COLs, only a subset generates extreme precipitation (Molekwa 2013; Abba Omar and Abiodun 2020), indicating

that regional-scale environmental controls play a decisive role in modulating rainfall intensity. Therefore, improving our understanding of various local-scale features in the vicinity of South Africa is essential for assessing their influence on COL-induced precipitation.

Previous studies have highlighted the importance of mesoscale interactions, including low-level jets, coastal mesolows and mesoscale convective systems, in shaping COL rainfall distribution (Jury 2015; Imbol Nkwinkwa et al. 2021; Thoithi et al. 2022). More recently, attention has turned towards the potential influence of the Agulhas Current System (Reason 2001; Rouault et al. 2002; Jury 2015), a warm western boundary current that enhances surface fluxes and onshore moisture transport. While observational and modelling studies suggest that the ACS may amplify storm systems along South Africa's east coast, its direct contribution to COL-induced flood has not been explicitly quantified. This study addresses this gap by isolating the influence of the ACS on a well-documented extreme COL event using the coupled atmosphere-hydrology-hydraulic model, with specific emphasis on implications for flood hazard assessment.

2 DATA AND METHODOLOGY

The analysis focuses on the April 2022 cut-off low that produced exceptional rainfall and flooding over KwaZulu-Natal. A top-down modelling framework was developed to simulate the April 2022 COL-induced flood event over KZN, integrating atmospheric, hydrological, and hydraulic components. Atmospheric simulations were conducted using the Model for Prediction Across Scales (MPAS), configured with variable-resolution meshes to resolve mesoscale circulation features over southern Africa and the adjacent southwest Indian Ocean. The model configuration enables explicit representation of moisture transport pathways associated with COL systems.

Hydrological simulations were performed using the Soil and Water Assessment Tool Plus (SWAT+) over the uMlazi River Basin, which experienced severe flooding during the April 2022 event. The model incorporates spatially distributed representations of land use, soil properties, topography, and river networks. Meteorological forcing was derived from MPAS precipitation outputs combined with reanalysis-based variables. A multi-month spin-up period was applied to stabilise soil moisture and groundwater storage before event-scale simulations. Model performance was evaluated against observed streamflow using standard statistical diagnostics, with emphasis on hydrograph timing, peak discharge magnitude, and overall flow dynamics.

Flood propagation and inundation dynamics were simulated using the Hydrology Engineering Centre's River Analysis System (HEC-RAS) hydraulic model over a critical downstream reach of the uMlazi River. Both observed and SWAT+-simulated hydrographs were applied as upstream boundary conditions to assess sensitivity to discharge magnitude and timing. Model outputs were evaluated against satellite-derived flood extent maps and post-event observational evidence. Additional idealised hydraulic experiments employing synthetic hydrographs were conducted to explore nonlinear floodplain responses to increasing peak discharge, providing a controlled framework for sensitivity assessment.

To assess sensitivity to oceanic forcing, a suite of idealised SST perturbation experiments is conducted over the Agulhas Current region using the MPAS model. These include a control simulation with unmodified SSTs, a cooling experiment that limits warm SST anomalies, and a warming experiment that amplifies them. This framework enables isolation of the ACS influence on moisture supply, latent heat fluxes and convective instability during the COL event.

3 RESULT AND DISCUSSION

3.1 Evaluation of the Coupled Modelling Framework

The AFPS framework was first evaluated by simulating the April 2022 cut-off low (COL) event in a component-wise manner, beginning with atmospheric processes and propagating the resulting forcing through hydrological and hydraulic components. This approach allows assessment of the internal consistency of the modelling chain before attribution or sensitivity analysis.

MPAS successfully captures the synoptic evolution of the April 2022 COL, including its cold-core structure, slow south-eastward progression, and the characteristic concentration of rainfall along the eastern flank of the system (Fig. 1). At coarse horizontal resolution, the model reproduces the broad-scale rainfall signal but exhibits spatially diffuse precipitation patterns and timing biases over KwaZulu-Natal. Increasing horizontal resolution to convection-permitting scales substantially improves the representation of low-level moisture convergence and orographically enhanced rainfall, resulting in more realistic coastal precipitation maxima. These results demonstrate that MPAS provides physically consistent atmospheric forcing suitable for downstream hydrological applications.

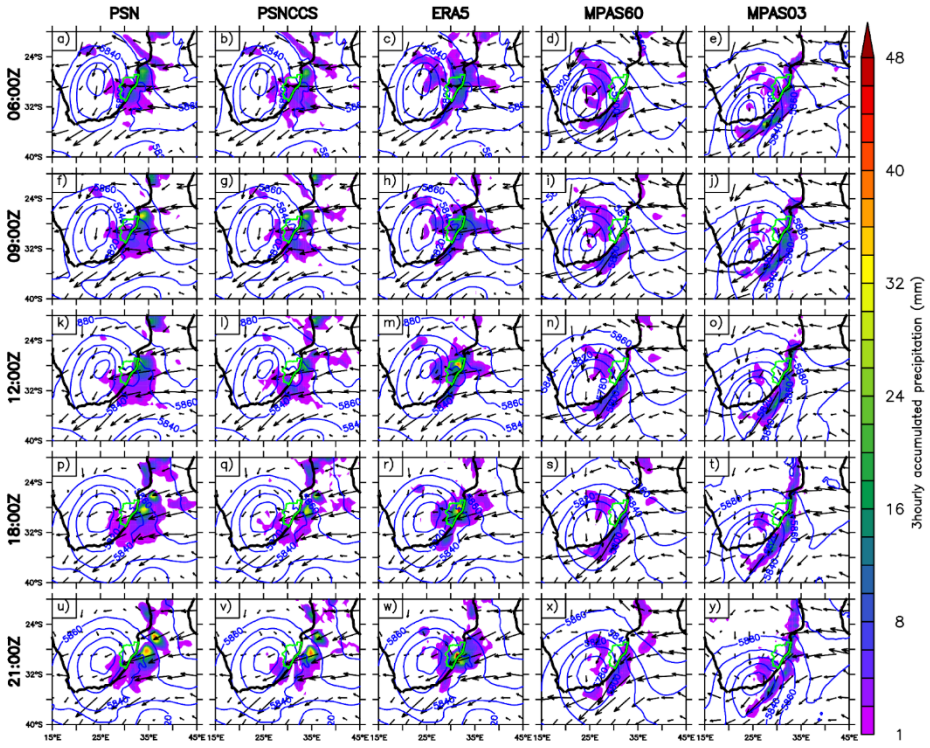

Figure 1: 500 hPa geopotential Height (blue contour; m), 850 hPa wind field (black vector; ms^{-1}) and the COL-associated 3-hourly accumulated precipitation (shaded, mm) as represented by the observation (PSN, PSNCCS), ERA5 reanalysis and MPAS simulations (MPAS60 and MPAS03). The green polygon represents the KwaZulu-Natal province of South Africa.

The simulated precipitation fields were subsequently used to force the SWAT+ hydrological model over the uMlazi River Basin. The simulated hydrographs reproduce the general timing and structure of observed streamflow, with peak discharge broadly coinciding with periods of extreme rainfall (Fig. 2). However, peak flows are systematically overestimated and exhibit secondary maxima, indicating sensitivity

to biases in precipitation magnitude and temporal phasing. The combined precipitation–streamflow diagnostics (combined Figures 4.4 and 4.6) illustrate both the capacity of SWAT+ to translate mesoscale rainfall forcing into runoff and the importance of targeted calibration when coupling atmospheric and hydrological models.

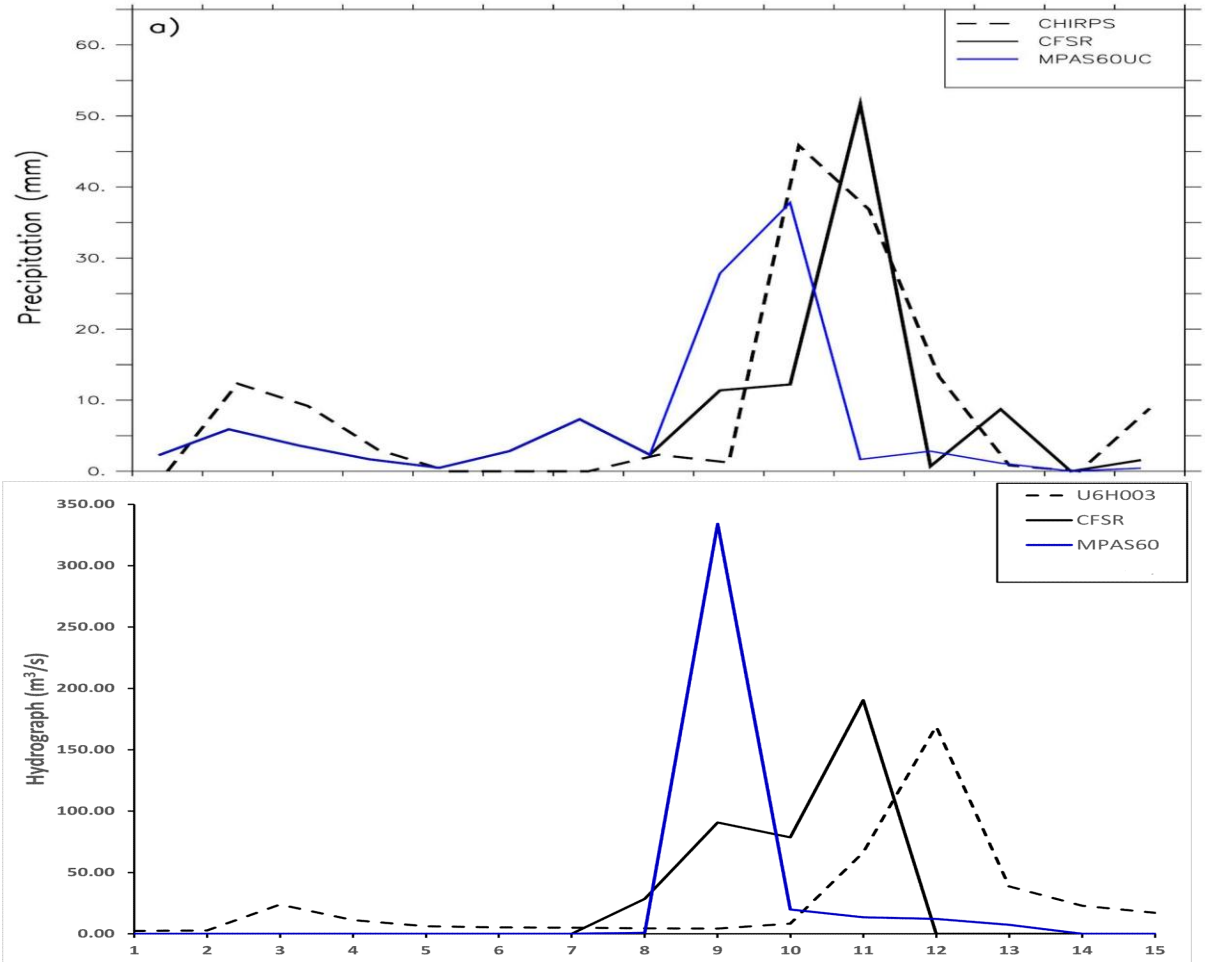

Figure 2: Temporal distribution of (a) daily precipitation over the study region from the period 1 - 15 April 2022 as depicted by CHIRPs, CFSR reanalyses, and MPAS 60 km simulation, and (b) daily hydrograph of SWAT+ initialised with CFSR and MPAS60 simulation.

Hydrological outputs were then passed to the HEC-RAS hydraulic model to simulate flood propagation and inundation over a vulnerable reach of the uMlazi River. Using both observed and SWAT+-derived hydrographs as boundary conditions, the model reproduces the main zones of flood inundation along the river corridor. Bias correction of simulated inflows improves agreement with satellite-observed inundation patterns, particularly along the main channel and adjacent low-lying floodplains. Nevertheless, inundation is underestimated in some urban areas, reflecting uncertainties in digital elevation data resolution and channel representation. Comparisons of observed and simulated flood extents and depths (Fig. 3) confirm that hydraulic outcomes are highly sensitive to upstream discharge magnitude and timing.

A key advantage of the sequential evaluation presented above is that it establishes confidence in the internal consistency of the coupled modelling framework, thereby providing a physically defensible basis for isolating and interpreting the influence of oceanic forcing on atmospheric processes.

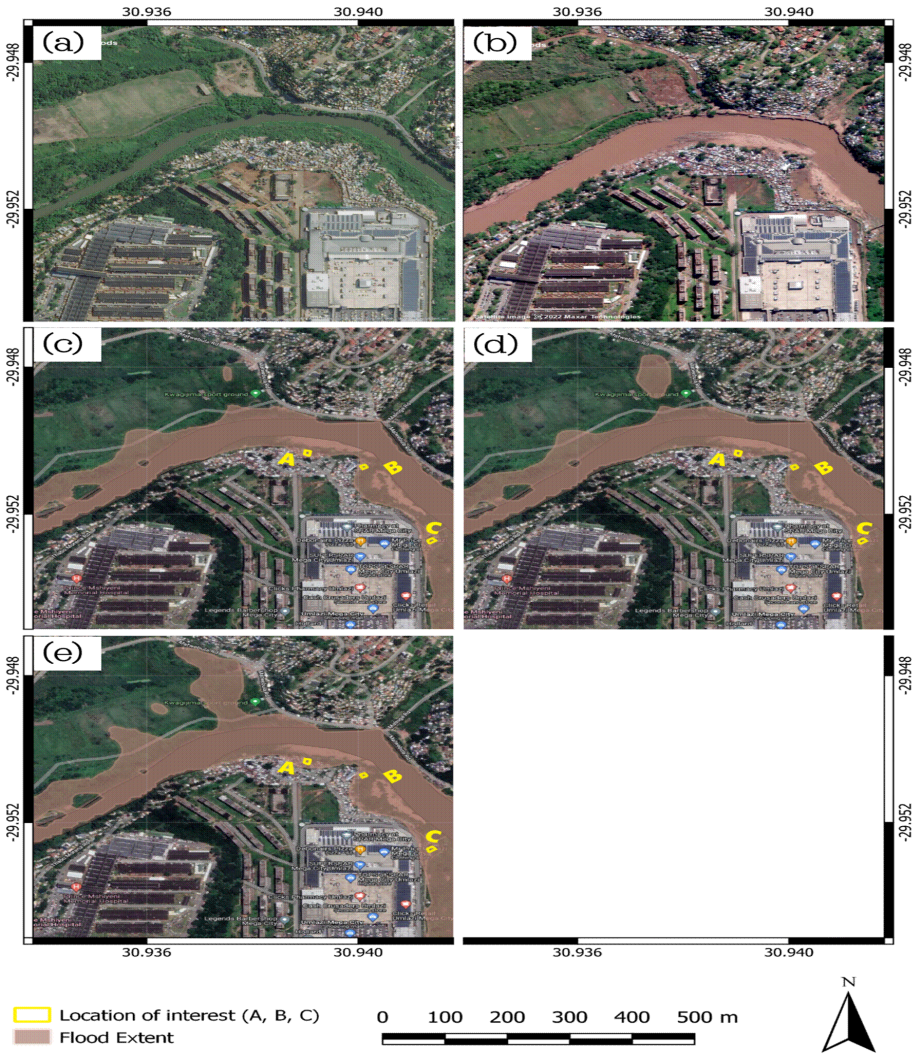

Figure 3: The map of the uMlazi area showing the area before the flood (a) and flood extent of the 10 -13 April 2022 flood as observed (b) and simulated with (c) U6H003, (d) CFSR, and (e) MPAS60 hydrographs. The yellow letters and small boxes indicate the locations of interest.

3.2 Sensitivity of COL-Induced Precipitation to the Agulhas Current System

Following evaluation of the coupled framework, sensitivity experiments were conducted to examine the influence of the Agulhas Current System (ACS) on COL-induced precipitation. Analysis of moisture fluxes confirms that the dominant moisture source for the April 2022 event originates over the southwest Indian Ocean, consistent with reanalysis diagnostics. Perturbations to ACS thermal conditions reveal a strong dependence of COL rainfall on oceanic forcing.

Cooling the Agulhas Current substantially weakens low-level moisture advection and surface latent heat fluxes, leading to a marked reduction in coastal rainfall and a displacement of convective activity offshore. In contrast, warming the current enhances near-surface moisture supply and convective buoyancy, resulting in increased coastal precipitation, although the inland rainfall response remains comparatively muted. This asymmetric rainfall response highlights nonlinear feedback between sea surface temperature anomalies, boundary-layer moisture availability, and convective dynamics. These results demonstrate that

the Agulhas Current acts as an effective regulator of COL-induced rainfall intensity, with direct implications for flood forecasting in coastal and adjacent inland catchments.

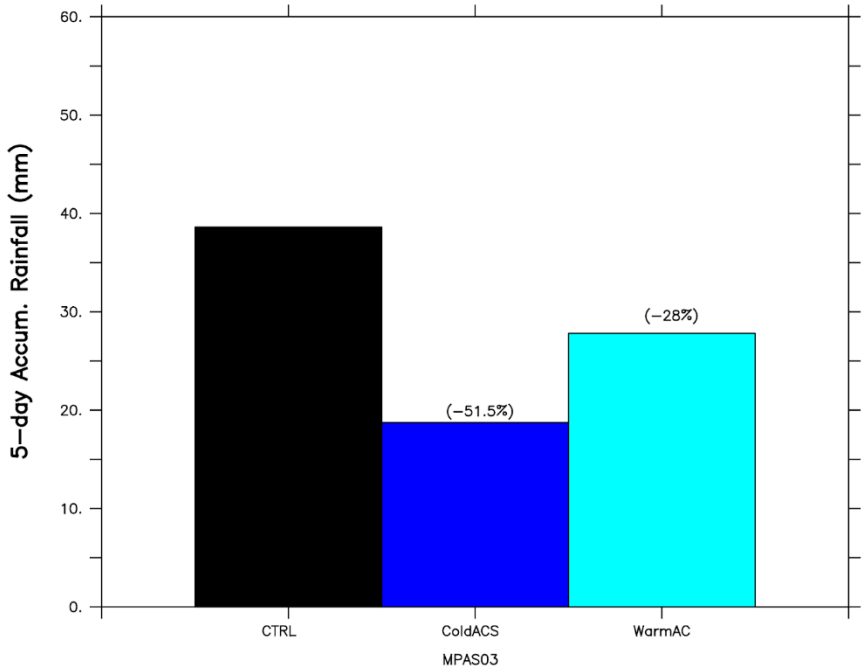

Figure 4: Accumulated precipitation (over 5 days from 8 - 12 April 2022) over the KwaZulu-Natal province (shown as green contour in Figure 1) as simulated in the control (CTRL; black bar) and the two scenarios (ColdACS; blue bar and WarmACS; cyan bars) for MPAS03. The values in brackets quantify the percentage error related to the control (CTRL) over the KwaZulu-Natal.

4 CONCLUSIONS

This extended abstract synthesises the first three objectives of a broader investigation into ACS–COL–flood interactions over KwaZulu-Natal. The results demonstrate that ocean-modulated atmospheric forcing substantially conditions extreme rainfall during COL events, while downstream hydrological and hydraulic responses exhibit nonlinear sensitivity to precipitation magnitude and timing. By establishing a coherent end-to-end modelling framework, the study provides a foundation for explicit attribution of ocean–atmosphere influences on flood hazards in coastal southern Africa. Ongoing sensitivity experiments will further quantify the role of the Agulhas Current in shaping flood risk and will be presented at the conference.

5 ACKNOWLEDGEMENTS

This research was supported by the Water Research Commission (WRC) of South Africa, the Pan-African and Transdisciplinary Lens in the Margins: Tackling the Risks of Extreme Events (PALM-TREEs) programme, and by the Nansen–Tutu Centre for Marine Environmental Research. The authors gratefully acknowledge the contributions of colleagues involved in related postgraduate research activities. The provision of computational resources and data support by the respective institutions is also acknowledged.

REFERENCES

Abba Omar, S., & Abiodun, B. J. (2020). Characteristics of cut-off lows during the 2015–2017 drought in the Western Cape, South Africa. Atmospheric Research, 235, pp1-16. https://doi.org/10.1016/j.atmosres.2019.104772

Favre, A., Hewitson, B., Lennard, C., Cerezo-Mota, R., & Tadross, M. (2013). Cut-off Lows in the South Africa region and their contribution to precipitation. Climate Dynamics, 41(9-10), pp2331–2351. https://doi.org/10.1007/s00382-012-1579-6

Grab, S. W., & Nash, D. J. (2023). A new flood chronology for KwaZulu-Natal (1836–2022): the April 2022 Durban floods in historical context. The South African Geographical Journal, Being a Record of the Proceedings of the South African Geographical Society, pp1–22. https://doi.org/10.1080/03736245.2023.2193758

Holloway, A. J., Fortune, G., Chasi, V., Beckman, T., Pharoah, R., Poolman, E., Punt, C., Zweig, P., & Others. (2010). RADAR Western Cape 2010: Risk and development annual review. PeriPeri Publications, pp1-117. https://www.researchgate.net/publication/305992362_RADAR_Western_Cape_2010_Risk_and_Development_Annual_Review

Imbol Nkwinkwa, A. S. N., Rouault, M., Keenlyside, N., & Koseki, S. (2021). Impact of the Agulhas Current on southern Africa precipitation: a modelling study. Journal of Climate, pp1–50. https://doi.org/10.1175/jcli-d-20-0627.1

Jury, M. R. (2015). Passive suppression of South African rainfall by the Agulhas Current. Earth Interactions, 19(13), pp1–14. https://doi.org/10.1175/ei-d-15-0017.1

Molekwa, S. (2013). Cut-off lows over South Africa and their contribution to the total rainfall of the Eastern Cape Province. https://repository.up.ac.za/handle/2263/36767

Molekwa, S., Engelbrecht, C. J., & Rautenbach, C. J. D. (2014). Attributes of cut-off low-induced rainfall over the Eastern Cape Province of South Africa. Theoretical and Applied Climatology, 118(1), pp307–318. https://doi.org/10.1007/s00704-013-1061-3

Reason, C. J. C. (2001). Evidence for the influence of the Agulhas current on regional atmospheric circulation patterns. Journal of Climate, 14(12), pp2769–2778. https://doi.org/10.1175/1520-0442(2001)014<2769:eftiot>2.0.co;2

Rouault, M., White, S. A., Reason, C. J. C., Lutjeharms, J. R. E., & Jobard, I. (2002). Ocean–atmosphere interaction in the Agulhas current region and a South African extreme weather event. Weather and Forecasting, 17(4), pp655–669. https://doi.org/10.1175/1520-0434(2002)017<0655:oaiita>2.0.co;2

Thoithi, W., Blamey, R. C., & Reason, C. J. C. (2022). April 2022 Floods over East Coast South Africa: Interactions between a Mesoscale Convective System and a Coastal Meso-Low. Atmosphere, 14(1), pp78-78. https://doi.org/10.3390/atmos14010078

ICFM 10
Adapting to Global Change:
Innovative Approaches to Flood Management and Resilience
May 20-22, 2026 | Western University, London, Ontario, Canada

Analysis of Hydroclimatic Extremes in the Great Lakes Basin Under Climate Change Using WRF-Hydro

Jiajin Feng[1], M. Reza Najafi[1], and Melika RahimiMovaghar[1]
Department of Civil and Environmental Engineering, Western University, London, Ontario, N6A 5B9, Canada[1]
E-mail: jfeng366@uwo.ca, mnajafi7@uwo.ca, mrahimim@uwo.ca

ABSTRACT

Floods are among the most frequent and damaging natural hazards, and their characteristics are evolving under climate change. This study investigates projected changes in flood magnitude, frequency, and seasonality across the Great Lakes Basin (GLB), an important freshwater resource of North America. We employed streamflow simulations from the WRF-Hydro model, driven by an ensemble of eight CMIP6 climate models under the SSP5-8.5 scenario. Future projections indicate basin-scale increases in flood magnitudes that are concentrated in the southern and eastern GLB, while northern subbasins show smaller increases or localized decreases. Seasonal analysis reveals pronounced increases in winter floods, especially in northern snow-influenced regions, alongside declining summer floods in the north. These findings highlight a significant reorganization of flood regimes driven by combined effects of intensified precipitation and altered snowmelt dynamics.

KEYWORDS: Climate Change, The Great Lakes Basin, WRF-Hydro, Flood frequency analysis

1 INTRODUCTION

Floods account for roughly 35–40% of weather-related disasters worldwide, causing substantial human and economic losses. Under climate change, flood characteristics such as magnitude, frequency, and seasonality are expected to evolve significantly, posing challenges for flood risk assessment and infrastructure design. The Great Lakes Basin (GLB) exhibits strong hydroclimatic gradients, including snowmelt-dominated regimes in the north and rainfall-dominated regimes in the south. While previous studies have examined parts of the GLB, basin-wide assessments of future flood magnitude, frequency, and seasonality remain scarce. This study addresses these gaps by integrating physically based hydrological simulations from WRF-Hydro and an ensemble of CMIP6 climate projections under a high-emission scenario. The objectives are to quantify projected changes in flood magnitude across the GLB, and assess shifts in the seasonal distribution of floods under future climate conditions.

2 STUDY AREA AND DATA

2.1 Study Area

The study focuses on the Great Lakes Basin, which spans approximately 1.4 million km^2 across the United States and Canada and comprises six major subbasins: Lake Superior, Lake Michigan, Lake Huron, Lake Erie, Lake Ontario, and the St. Lawrence River (Figure 1). The basin experiences a humid continental climate with strong seasonal temperature contrasts and a pronounced north-south gradient in snow influence.

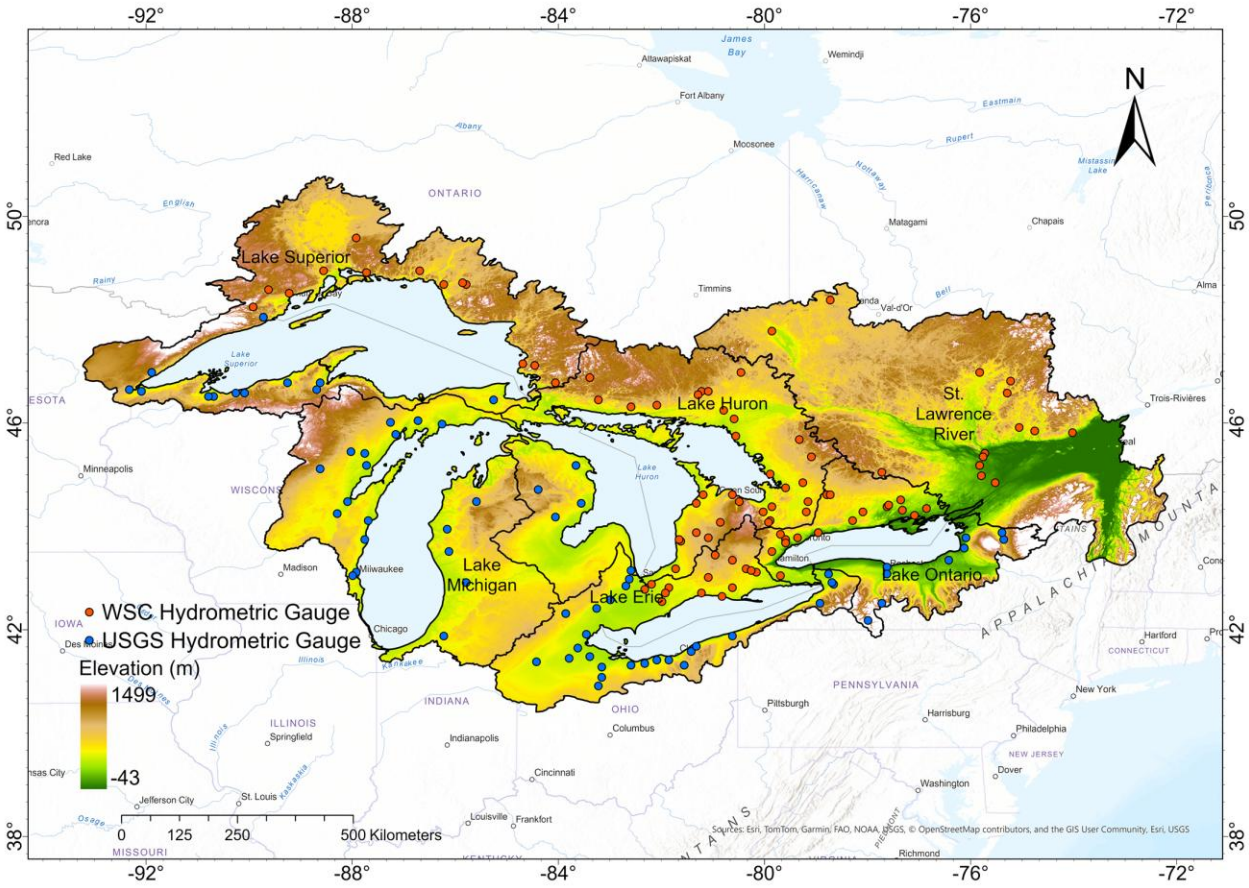

Figure 1: Location and topography of the Great Lakes Basin in North America, and the hydrometric gauges used in this study.

2.2 Hydrometric and Meteorological Data

Daily streamflow observations were obtained from the Water Survey of Canada (WSC) and the United States Geological Survey (USGS). After quality control and data availability screening, which requires at least 30 years of record and at least 90% completeness per year, 160 gauges were retained for analysis.

Meteorological forcing for hydrological simulations during the historical period was derived from the Regional Deterministic Reanalysis System v2 (RDRS-V2 reanalysis), which provides hourly precipitation, temperature, radiation, wind, humidity, and surface pressure fields at high spatial resolution.

2.3 Climate Model Projections

An ensemble of eight CMIP6 Global Climate Models was selected under the SSP5-8.5 scenario. Daily precipitation and temperature variables were bias-corrected and downscaled using the Multivariate Bias Correction (MBCn) method, which preserves inter-variable dependence (Cannon, 2018). Climate simulations span 1960–2100, with historical and future periods defined as 1985–2014 and 2071–2100, respectively.

2.4 Geophysical Data

Land cover, soil texture, and topography were obtained from the North American Land Change Monitoring System (NALCMS), Global Soil Dataset for use in Earth System Models (GSDE), and 2-

minute Gridded Global Relief Data v2 (ETOPO2) datasets and used to parameterize the hydrological model.

3 METHODOLOGY

The WRF-Hydro model (version 5.1.1) was implemented in standalone mode with the Noah-MP land surface model at approximately 3.7 km spatial resolution (Gochis et al., 2020). The model was calibrated and validated against observed streamflow using the Kling-Gupta Efficiency metric. The calibrated model was subsequently driven by bias-corrected CMIP6 climate projections to simulate streamflow for historical and future periods (Rahimimovaghar, 2024).

Multiple statistical distributions, which include GEV, GPD, Log-Pearson III, Metastatistical Extreme Value, and Extended GPD, were employed for flood frequency analysis. A Monte Carlo cross-validation experiment was conducted independently at each gauge. In each of 1000 realizations, a 10-year subset of data was randomly selected for calibration, while the remaining years were used for validation. Model performance was evaluated using a skill score computed for return periods exceeding the calibration length, focusing on extrapolation capability rather than in-sample fit. For each hydrometric gauge, the best-fitting distribution is used for estimating flood quantiles for different return periods.

4 RESULTS

Future projections indicate widespread increases in flood magnitude across the GLB, particularly in southern and eastern subbasins (Figure 2). Ensemble median increases frequently exceed 50% and locally surpass 100% for both 5-year and 100-year floods. Northern subbasins show smaller increases and occasional decreases, especially for more moderate floods. Uncertainty, quantified by the interquartile range across climate models, increases with return period, indicating greater uncertainty for rarer events.

Seasonal flood frequency analysis shows pronounced increases in winter floods (DJF), especially in northern snow-influenced regions (Figure 3). Spring (MAM) and autumn (SON) floods generally increase moderately across most of the basin. In contrast, summer floods (JJA) are projected to decrease in northern subbasins, notably in the Lake Superior and St. Lawrence River basins, while southern regions exhibit smaller changes or increases.

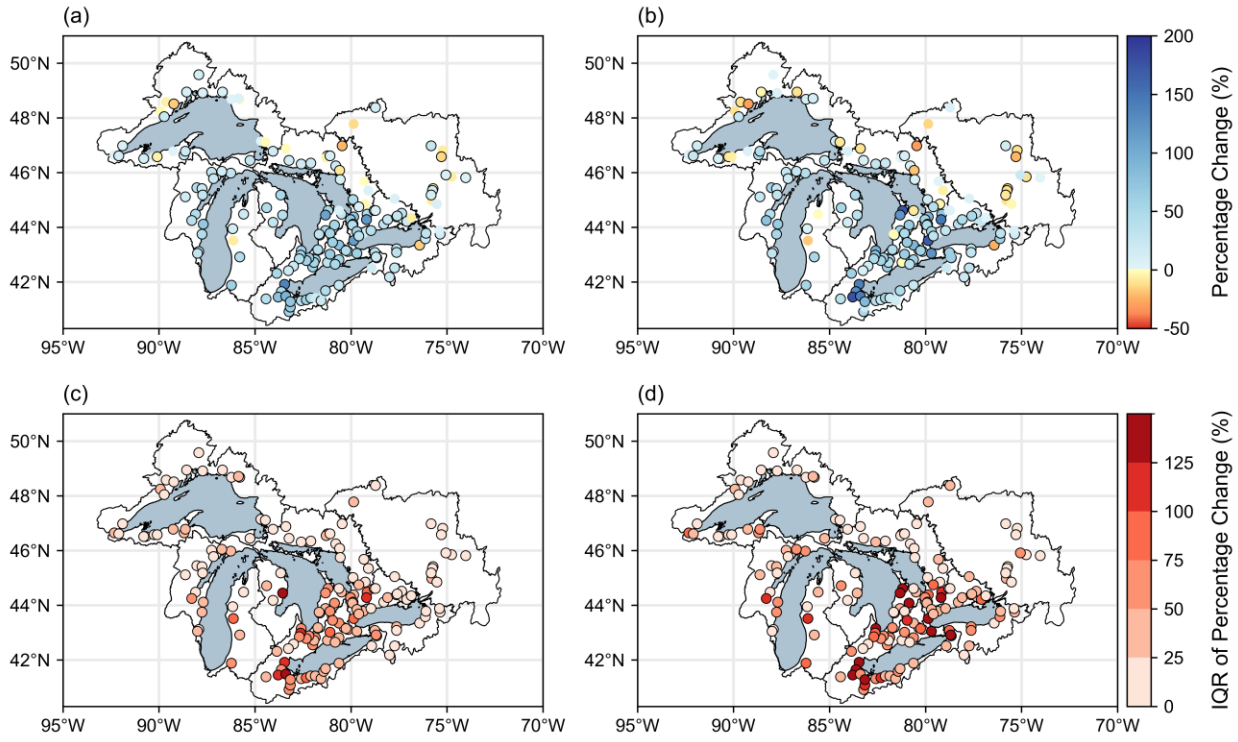

Figure 2: Spatial distribution of projected changes in flood magnitude across the Great Lakes basin. Panels (a) and (b) show the multi-model ensemble median (from 8 GCMs) of the percentage change in flood magnitude between the historical period (1985–2014) and the future period (2071–2100) for the (a) 5-year and (b) 100-year return periods, respectively. Dots outlined in black indicate gauges where the projected change meets the model agreement threshold (≥67% of GCMs). Panels (c) and (d) show the corresponding IQR of percentage change across the 8 GCMs for the (c) 5-year and (d) 100-year return periods.

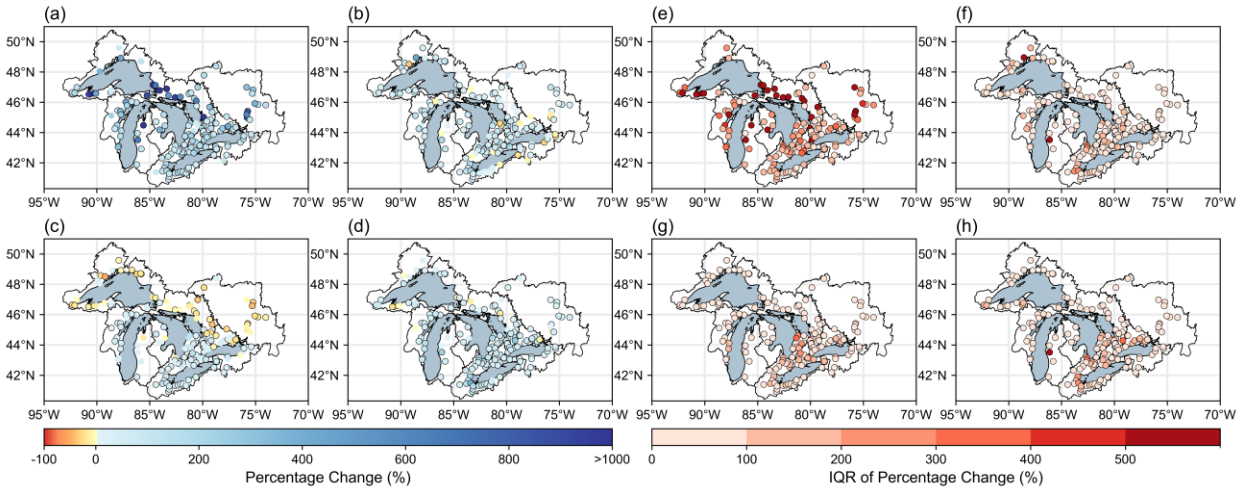

Figure 3: Seasonal projections of changes in the 100-year flood across the Great Lakes basin. Panels (a)–(d) show the multi-model ensemble median (from 8 GCMs) of the percentage change in the 100-year flood between the historical period (1985–2014) and the future period (2071–2100) for the four seasons: (a) DJF, (b) MAM, (c) JJA, and (d) SON. Dots outlined in black indicate gauges where the projected changes meet the model agreement threshold (≥67% of GCMs). Panels (e)–(h) show the corresponding IQR of percentage change across the 8 GCMs for (e) DJF, (f) MAM, (g) JJA, and (h) SON.

5 CONCLUSIONS

This study reveals a substantial reorganization of flood regimes across the Great Lakes Basin under climate change. Projected changes include widespread increases in flood magnitude concentrated in southern and eastern subbasins, with smaller or declining floods in some northern regions. There is a pronounced shift toward more winter-dominated flooding accompanied by declining summer floods in snowmelt-dominated areas. These changes reflect the combined influence of intensified precipitation and altered snowmelt dynamics. Overall, the findings underscore the importance of integrated modeling approaches for flood risk assessment in regions with complex hydroclimatic controls.

6 REFERENCES

Cannon, A. J. (2018). Multivariate quantile mapping bias correction: An N-dimensional probability density function transform for climate model simulations of multiple variables. *Climate Dynamics*, *50*(1), 31–49. https://doi.org/10.1007/s00382-017-3580-6

Gochis, D. J., Barlage, M., Cabell, R., Casali, M., Dugger, A., FitzGerald, K., McAllister, M., McCreight, J., RafieeiNasab, A., Read, L., Sampson, K., Yates, D., & Zhang, Y. (2020). *The NCAR WRF-Hydro® Modeling System Technical Description, (Version 5.1.1)*. NCAR Technical Note. https://ral.ucar.edu/sites/default/files/public/WRFHydroV511TechnicalDescription.pdf

Rahimimovaghar, M. (2024). *Analysis of Lagged Compound Droughts and Floods in the Great Lakes Basin: Historical Patterns and Future Projections under Climate Change*. Western University.

ICFM 10
Adapting to Global Change:
Innovative Approaches to Flood Management and Resilience
May 20-22, 2026 | Western University, London, Ontario, Canada

Isochrone-Based Screening of Watershed Hydraulic Response to Land-Use Change

Heather McGrath[1] , Sabrina Draude[2], Steven Weijs[3]
Natural Resources Canada, Ottawa ON, K15 2K5 Canada[1]
formerly at Natural Resources Canada, Ottawa ON, K15 2K5 Canada[2]
University of British Columbia, Vancouver, BC, V6T 1Z4, Canada[3]
E-mail: Heather.McGrath@nrcan-rncan-gc.ca

ABSTRACT

Land-use (LU) changes can modify watershed hydraulics by modifying surface roughness, infiltration capacity, and flow pathways, thereby affecting runoff timing and hydrograph characteristics. This study evaluates the spatiotemporal effects of LU change on surface-water drainage efficiency upstream of Merritt, British Columbia, along the Coldwater and Nicola Rivers between 2000 and 2020. Isochrone maps representing spatial zones of equal travel potential were generated for all years using composite cost surfaces that integrate LU-dependent surface resistance proxy and terrain-derived flow potential. To support screening-level assessments, we introduce a Connectivity and Hydraulic Shift (CHaS) score, a dimensionless indicator that summarizes relative changes in upstream travel potential and surface resistance proxy at points of interest. Hydrograph observations from nearby river gauges were analysed to contextualize the CHaS score. Preliminary results show that forest loss and urban expansion reorganize flow pathways, reduce surface resistance proxy in key areas, and increase variability in peak timing. Based on the river gauge measurements, rising-limb behaviour exhibits greater event dependence rather than uniform acceleration, indicating structural changes in hydraulic connectivity rather than consistent amplification of peak flows. These early results demonstrate potential value, yet the approach requires further validation and multi-site testing to determine its robustness and suitability for informing decisions about when hydrologic/hydraulic model updates or flood-hazard remapping may be justified.

KEYWORDS: isochrone analysis, hydraulic connectivity, land use land cover change, cost-distance analysis

1 INTRODUCTION

Land-use (LU) changes influence flood behaviour by altering surface roughness, infiltration capacity and flow routing. These effects are often most pronounced at fine spatial scales and for relatively frequent events but increasingly contribute to altered runoff dynamics and pluvial flooding in larger basins as well (Brody et al., 2008). Urban expansion and deforestation can increase imperviousness or modify natural flow paths, reducing infiltration and accelerating surface runoff (Alshammari et al., 2023). At the same time, loss or fragmentation of natural flood-mitigating features such as forests and wetlands reduces storage capacity and flow attenuation, collectively affecting hydrograph peak magnitude, timing and rising-limb stability.

Flood hazard maps are widely regarded as primary tools for assessing and communicating flood risk. Derived from physics-based hydraulic models that enforce conservation of mass and momentum, these maps integrate topography, land cover and hydraulic parameters to simulate inundation extent and depth. They underpin land-use planning, infrastructure design, regulatory compliance, and insurance assessments. However, assumptions embedded in these models, particularly those related to surface resistance and flow connectivity, may become outdated as landscapes evolve. Substantial LU change can therefore modify watershed hydraulic response in ways that are not reflected in existing flood hazard products, potentially reducing their reliability (Canada, 2023; Hounkpè et al., 2019).

Updating flood hazard maps is resource-intensive and existing guidelines provide limited direction on how to determine when landscape change is sufficiently significant to warrant re-evaluation (Canada, 2024). As a result, there is a need for efficient, diagnostic approaches that can screen for LU-driven changes in hydrologic and hydraulic behaviour prior to undertaking full model recalibration or remapping.

This study investigates a screening-level framework that applies spatiotemporal isochrone analysis to detect LU-induced changes in watershed hydraulic response, with river-gauge observations used solely as external validation rather than as components of the method.

2 DATA AND STUDY AREA

The study area surrounds Merritt, British Columbia located in the Nicola Valley and drained by the Coldwater and Nicola Rivers. The watershed was selected based on several criteria: a relatively small catchment exhibiting urbanization and deforestation over the past 20 years, a history of flooding, and the availability of essential datasets, including a digital terrain model (DTM), multiple LU maps, and long-term hydrometric data. Past floods in 2006 and 2012 resulted from heavy rainfall and rapid snowmelt, while the 2021 atmospheric river event caused the Coldwater River to overtop its banks, due to failure of the dikes and pluvial defences, leading to extensive inundation, road closures and evacuations (Emergency Management and Climate, 2025).

LU for 2000 and 2005 were obtained from Agriculture and Agri-Food Canada's land classification maps, available through the Open Government of Canada (OGC) data portal (Agriculture and Agri-Food Canada, 2025). The classifications are derived from Landsat 5 TM and/or 7 ETM+ multi-spectral imagery by inputting imagery and ground reference training data into a decision-tree or supervised image classification process. For 2010, 2015, and 2020, publicly available national-scale LU maps with 30 m spatial resolution were retrieved from the OGC (Canada, 2022). The 2010 LU is derived using observation from Thematic Mapper (TM) and Enhanced Thematic Mapper (ETM+) Landsat sensors, while 2015 and 2020 are from Operational Land Imager (OLI) Landsat sensor at 30 m x 30 m resolution.

A medium-resolution DTM serves as the basis for terrain analysis (Canada, 2025; McGrath et al., 2025). National Hydro Network (NHN) Work Units were used to define the watershed extent for the analysis (Secretariat and Secretariat, 2023). In this work, NHN WU 08LG002, which contains Merritt BC is used as the initial boundary condition, Figure 1. Historic river gauge data from the Water Office and the HYDAT database (Canada, 2010) were used to validate the isochrone-based indicators and provide context for the results. Specifically, for this work the Coldwater River at Merritt (08LG010) station and Nicola River at outlet of Nicola Lake (08LG065) gauge stations were used. 08LG010 has been operational, on and off since 1911 measuring primarily flow. There is a gap in the observations at this gauge between 1995 and 2005, and since 2011 a gauge recorder has been recording both flow and level (Government of Canada, 2026). For 08LG065, a station recorder has been measuring flow from 1983 to 2010 and from 2011 to 2026 both flow and level have been continuously measured, providing a continuous record length of 44 years.

3 METHOD

Figure 2 outlines the workflow used to generate the Connectivity and Hydraulic Shift (CHaS) score for the upstream areas of the two points of interest, river gauges 08LG010 and 08LG065 and is described in detail below.

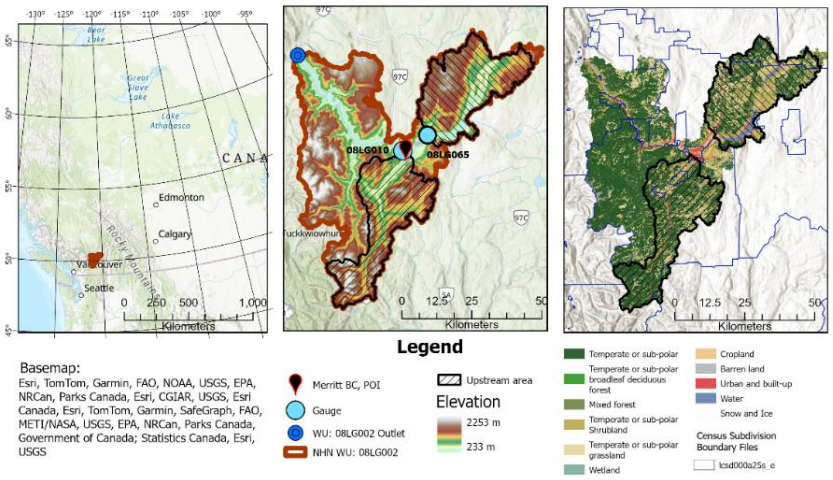

Figure 1 Study area location overview in western Canada, point of interest in Merritt, BC, river gauge 08LG010 on Coldwater River, Nicola River at outlet of Nicola Lake (08LG065) river gauge, their respective upstream areas and 2020 Land Use

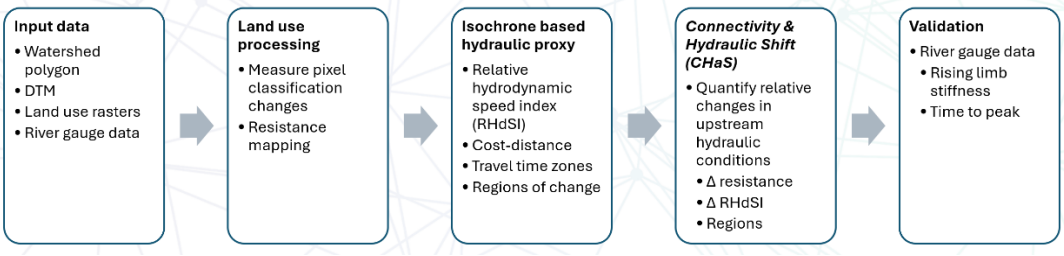

Figure 2 Overall method

3.1 Land Use Change Processing

LU data for the years 2000 to 2020 were acquired from national scale datasets (see Section 2). All rasters were clipped to the watershed area of interest (AOI) and reprojected to UTM Zone 10N. To facilitate comparison across years, the rasters were resampled to a common spatial resolution (30 m). Because classification schemes differed between datasets, a lookup table was created to harmonize classes across years. The remap table contains the original LU pixel values, class name descriptor and resistance values.

Resistance values were informed by Holt (Holt et al., 2015) and refined through literature review in hydrological modelling and landscape connectivity studies (Simpkins et al., 2018). Lower resistance values (e.g., water, open wetlands) facilitate flow while higher values (e.g. dense forests) impede movement.

The temporal changes were quantified by comparing the classified rasters, enabling identification of areas experiencing significant LU transitions over the 20-year period.

3.2 Isochrone-Based Hydraulic Proxy

To evaluate the potential hydro-dynamic effects of LU change, isochrone maps were generated to represent zones of equal travel potential to points of interest (POIs).

The DTM was hydrologically conditioned by filling pits, breaching depressions, and enforcing realistic drainage pathways using tools from Whitebox Geospatial (Whitebox Geospatial Inc., 2025). From the hydro-conditioned surface, flow direction, flow accumulation, slope, and stream networks were generated. Upstream contributing areas for each river gauge were then delineated, creating two distinct

AOIs upstream of Merritt, and all DTM derivatives were clipped or regenerated, as appropriate, to align with each AOI boundary for subsequent processing.

First, a relative velocity surrogate, Relative Hydro-dynamic Speed Index (RHdSI), is created by combining terrain derivatives (slope and flow accumulation). RHdSI is conceptually related to SPI (erosive power) and TWI (wetness), but differs in targeting relative flow speed. RHdSI is dimensionless and computed as Eq. 1-2, (Esri, 2026).

$$SlopeArea = SA = \sqrt{Sg} * \sqrt{A} \quad (1)$$

$$\text{RHdSI} = 0.1 * \frac{SA}{mean_{(SA)}}((1 + \text{w}) * \text{S}) \quad (2)$$

Where Sg = tan(β) is slope as hydraulic gradient (unitless), A is the upslope contributing areas in m^2 (flow accumulation * cell area), S is a stream mask (1 for channel cells, 0 otherwise), and w=0.5 applies a modest velocity-enhancement in channels, which were not sensitivity tested in this work. The square-root transform moderates extreme values while preserving monotonicity, and normalization by $mean_{(SA)}$ in the AOI and yields a dimensionless index. RHdSI is intended as a screening/routing layer under steady, uniform rainfall assumptions; incorporation of path-wise hydraulic resistance and event-specific runoff (IDF-based) is a value extension, but beyond the scope of this study.

Relative "travel-potential-cost" was then estimated by dividing the LU-based resistance values by the stream-boosted unitless RHdSI, which reflects relative flow potential rather than actual time. Higher resistance slows flow and higher RHdSI indicates faster movement. A cost-distance algorithm was then applied to each pixel to estimate cumulative "travel time" across the AOI to the POI. Finally, isochrones were created by reclassifying these cumulative costs into discrete zones.

3.3 Connectivity & Hydraulic Shift (CHaS)

The CHaS was developed to quantify relative changes in upstream hydraulic conditions. The score combines unitless resistance values, the RHdSI and connected patches/regions of change. For each gauge (POI), and its AOI the differences in cost-distance (ΔC) and resistance (ΔR) between consecutive time steps were evaluated. The resulting CHaS provides a dimensionless, screening-level proxy for altered hydraulic connectivity and flow pathways.

$$\Delta C_{obs} = \frac{\Delta C(t_1) - \Delta C(t_0)}{\Delta C(t_0)} \quad (3)$$

$$\Delta C_{\text{exp}=} \sum_{j \in U} w_j \, \Delta R_j, \quad w_j \propto \frac{1}{1 + d_j}, \sum_j w_j = 1 \quad (4)$$

$$F10 = \frac{\sum_{j \in top10\%}(w_j \, \Delta R_j)}{\sum_j (w_j \, \Delta R_j)} \quad (5)$$

$$U = SD(\sum_j w_j \Delta R_j^{\backslash * b})_{b=1}^{B} \quad (6)$$

$$CHaS = \alpha |\Delta C_{obs}| + \beta \Delta C_{exp} + \gamma \text{F10} - \delta \text{U} \quad (7)$$

(defaults α=β=γ=1, δ=0.5)

The observed relative change (C_{obs}) between the baseline and latest year and expected change from surrounding patches (C_{exp}) along with weights: α, β, γ, δ allow tuning - depending on priorities. Where α adjusts absolute observed change, higher α more sensitivity to local changes at the point. β influences the weight of surrounding patches, γ multiplies F10, which measures whether the expected change is concentrated in a few patches, and δ multiplies U the standard deviation of bootstrapped expected changes.

3.4 Validation

Validation was performed by comparing CHaS-derived indicators with observed hydrograph characteristics from nearby river gauges to assess consistency between modelled hydraulic change and measured streamflow behaviour. Daily discharge values were extracted from each gauge record, and

high-flow events were identified using a 95th-percentile threshold applied to the full daily time series for the analysis period. Each continuous sequence of days exceeding this threshold was treated as a distinct hydrologic event for the early (2010–2015) and late (2015–2020) intervals. For each event, the peak discharge was located, and the rising-limb start time (t_0) was determined using an inflection-based algorithm that selects the last point of non-increasing discharge prior to a sustained rise toward the event peak. Baseflow during the rising limb was defined as the fixed discharge at t_0 (constant baseflow), and direct runoff was computed as the positive difference between observed discharge and this baseflow from t_0 to the time of peak (t_p). Event-scale metrics of rising-limb stiffness and time-to-peak were then summarised for each interval.

These station-based metrics serve as an observational check on the CHaS results, as increased rising-limb stiffness, shifts in peak timing, or changes in event characteristics may provide independent evidence of altered hydrologic response. However, these indicators do not isolate the effects of land-use change from weather-driven variability or storm-type differences, which remains an important limitation.

4 RESULTS

4.1 Land Use Change

LU transitions between 2000 and 2020 are illustrated across four time periods using chord diagrams that visualize both the persistence and conversion of land classes, for the upstream areas of 08LG010 and 08LG065, Figure 3.

In the upstream area of gauge 08LG010 along the Coldwater River, LU changes between 2000 and 2005 were relatively minor, resulting in only a small increase in urban area (0.04% or 0.308 km²). During this interval, forest cover remained largely stable, with most transitions occurring toward grassland and shrubland. In contrast, the period from 2005 to 2010 exhibited substantially greater shifts. These changes may partly reflect differences in sensor type or classification methodology between LU datasets, but they may also represent genuine change. Over this period, urbanization increased by 2.1%, and forest loss reached 14.83%. From 2010 to 2015 urban growth is 0.10% while 2015 to 2020 decreased by 0.15% which may represent errors in classification or enhancements in the classification methods of the LU. Over the entire period 2000-2020, deforestation of 25.51% and urban growth of 2.08% are measured in this AOI.

In 08LG065 a similar change in urbanization and deforestation are computed over the time period: deforestation of 30.86% and urbanization of 2.78%. Initially, 75.48% of the upstream area is considered forested. From 2000 to 2005 there is some shuffling between classifications, with grassland and shrubland classes appearing, but the largest changes are again found between 2005 and 2010. During this time forest pixels decreased by 22.89% and there is minimal urban growth, 1.07%, Figure 3.

4.2 CHaS

Pairwise temporal comparisons of CHaS and F10 (spatial concentration of change) were computed for the upstream areas of 08LG010 and 08LG065, Figure 4, Table 1. F10 quantifies how concentrated the weighted Δ-signal is in space: higher values indicate that a small subset of upstream cells dominates, while lower values indicate diffuse change.

In 08LG010, lowest CHaS occurs in 2000–2005 (CHaS 1.0214, F10 1.0103, U 0.000395), consistent with minor, diffuse LU change. The highest CHaS is in 2015–2020 (CHaS 1.6847, F10 1.4631, U 0.002306). The combination of a very high F10 and moderate U (smaller than the longest-span U values) indicates that a concentrated subset of upstream cells strongly influenced the weighted Δ-signal while the uncertainty penalty remained limited. Across all intervals, F10 ranges widely from 0.8099 (2000–2020) to 1.4631 (2015–2020), reinforcing the interpretation that long spans capture diffuse, cumulative change (low F10) whereas shorter spans can reveal spatially focused changes (high F10).

In 08LG065 the highest CHaS is observed for the 2000–2020 span (CHaS 1.5704) together with the lowest F10 (0.7516) and the largest U (0.003098), pointing to broadly distributed change that accumulated

over the 20-year period. The lowest CHaS appears again during 2000–2005 (CHaS 1.0949, F10 1.0011, U 0.000810), consistent with relatively minor change. For shorter intervals (e.g., 2010–2015 and 2015–2020), F10 remains near 1.15–1.18 (1.1454–1.1786), whereas for long spans (2000–2020, 2005–2020) F10 drops to ~0.75–0.81 (0.7516–0.8105), underscoring the contrast between diffuse long-period signals and more concentrated short-period signals.

Intervals with higher CHaS align with times when mapped LU changes are more hydraulically well-positioned (closer to fast travel pathways and/or more spatially concentrated), while F10 neatly distinguishes whether the signal arises from concentrated patches (high F10; e.g., 08LG010, 2015–2020) or from spatially diffuse, cumulative changes over long spans (low F10; e.g., 08LG065, 2000–2020).

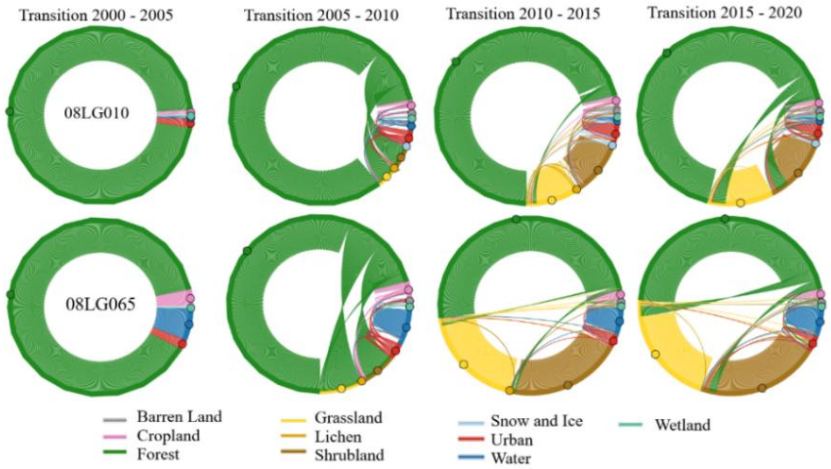

Figure 3 LU transitions in five-year increments for upstream areas of river gauges: 08LG010 (top) and 08LG065 (bottom)

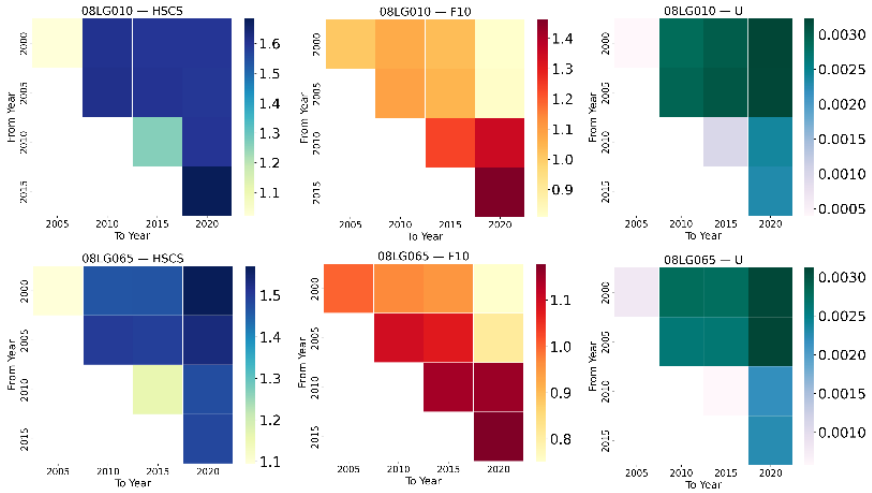

Figure 4 Heatmap of all year change pairs for upstream areas of 08LG010 (top) and 08LG065 (bottom), showing: (i) left: CHaS (yellow to blue) and (ii) middle: F10 values (yellow to red), (iii) right: U (purple-blue-green)

4.3 Validation

To contextualize the CHaS scores, we analyzed daily streamflow at two river gauges and compared two intervals (2010–2015 vs 2015–2020) to test for concurrent hydrologic change in event timing and rising-limb shape. For 08LG010, which lacks usable data in 2000–2005, the 2015–2020 interval shows higher mean rising-limb stiffness and a heavier upper tail of stiffness than 2010–2015. Stiffness describes

how sharply and quickly runoff responds to rainfall and is used here as a preliminary validation metric to assess whether the CHaS score preserves physically realistic catchment response dynamics. For 08LG065, comparing the two time intervals, CHaS and F10 increase together, showing mutual agreement, but here the increase in stiffness is much larger, indicating a substantially steeper rising limb in the later period and the time-to-peak increases strongly, 4.5 to 11.667, suggesting events are not just steeper, but also more prolonged.

Across both basins, CHaS and F10 increases align with the observed stiffness increases Table 1, supporting the interpretation that recent LU changes have altered hydraulic connectivity and flow pathways, producing sharper high-flow responses. While these signals are consistent with the CHaS hypothesis, fuller confirmation will benefit from expanded interval sampling and targeted hydrodynamic modeling.

Table 1 Summarizes CHaS, F10 and rising-limb stiffness ($m^3/s/day$) and time-to-peak (TTP) measured in days, detection uses a 95th-percentile flow threshold on each temporal subseries

	2010-2015				2015-2020			
Station	**CHaS**	**F10**	**Stiffness**	**TTP**	**CHaS**	**F10**	**Stiffness**	**TTP**
08LG010	1.264	1.235	3.7856	1.972	1.684	1.463	3.9803	2.275
08LG065	1.161	1.145	0.7068	4.500	1.484	1.179	2.0592	11.667

5 CONCLUSION

This study introduces a screening-level framework to identify areas where LU changes may be altering watershed hydraulic response. By combining LU-derived resistance values with terrain-based flow potential, the Hydraulic Signal Change Score (CHaS) captures shifts in hydraulic connectivity and potential travel pathways. Comparison with river-gauge hydrographs indicates that increases in CHaS and F10 correspond to observable changes in rising-limb behaviour, suggesting that recent LU change has reorganized upstream flow pathways. While the framework shows promise as a screening tool, broader multisite testing is required to assess robustness and determine where flood hazard remapping may be prioritized and/or justified.

We plan to extend the analysis to additional watersheds and points of interest to test whether CHaS thresholds can function as practical triggers for targeted flood-hazard map updates. We will also benchmark screening results against 1D/2D hydraulic models to evaluate whether the isochrone method efficiently identifies locations where flood-hazard products may be outdated. To move from relative to event-aware timing, we will incorporate IDF-based event forcing and Curve Number–based runoff scaling so that the framework can convert relative travel potential into event-specific travel time, supporting direct, storm-by-storm comparison with hydrodynamic simulations.

ACKNOWLEDGEMENTS

The authors wish to acknowledge funding from Natural Resources Canada Flood Hazard Identification and Mapping Program (FHIMP).

REFERENCES

Agriculture and Agri-Food Canada, 2025. AAFC Land Use - Open Government Portal [WWW Document]. AAFC Land Use. URL https://open.canada.ca/data/en/dataset/fa84a70f-03ad-4946-b0f8-a3b481dd5248 (accessed 3.13.26).

Alshammari, E., Rahman, A.A., Rainis, R., Seri, N.A., Fuzi, N.F.A., 2023. The Impacts of Land Use Changes in Urban Hydrology, Runoff and Flooding: A Review. Current Urban Studies 11, 120–141. https://doi.org/10.4236/cus.2023.111007

Brody, S.D., Zahran, S., Highfield, W.E., Grover, H., Vedlitz, A., 2008. Identifying the impact of the built environment on flood damage in Texas. Disasters 32, 1–18. https://doi.org/10.1111/j.1467-7717.2007.01024.x

Canada, E. and C.C., 2010. National Water Data Archive: HYDAT [WWW Document]. URL https://www.canada.ca/en/environment-climate-change/services/water-overview/quantity/monitoring/survey/data-products-services/national-archive-hydat.html (accessed 10.2.25).

Canada, N.R., 2025. Medium Resolution Digital Elevation Model (MRDEM) - CanElevation Series - Open Government Portal [WWW Document]. Medium Resolution Digital Elevation Model (MRDEM) - CanElevation Series. URL https://open.canada.ca/data/en/dataset/18752265-bda3-498c-a4ba-9dfe68cb98da (accessed 8.28.25).

Canada, N.R., 2024. Federal Hydrologic and Hydraulic Procedures for Flood Hazard Delineation [WWW Document]. URL https://natural-resources.canada.ca/science-data/science-research/natural-hazards/flood-mapping/federal-hydrologic-hydraulic-procedures-flood-hazard-delineation (accessed 11.19.25).

Canada, N.R., 2023. Federal Land Use Guide for Flood Risk Areas [WWW Document]. URL https://natural-resources.canada.ca/science-data/science-research/natural-hazards/flood-mapping/federal-land-use-guide-flood-risk-areas (accessed 11.19.25).

Canada, N.R., 2022. 2020 Land Cover of Canada - Open Government Portal [WWW Document]. 2020 Land Cover of Canada. URL https://open.canada.ca/data/en/dataset/ee1580ab-a23d-4f86-a09b-79763677eb47 (accessed 12.3.25).

Emergency Management and Climate, 2025. Province funds replacement of flood-damaged dikes in Merritt [WWW Document]. BC Gov News. URL https://news.gov.bc.ca/releases/2025EMCR0008-000251 (accessed 12.3.25).

Esri, 2026. Predict floods with unit hydrographs | Documentation [WWW Document]. Predict floods with unit hydrographs. URL https://learn.arcgis.com/en/projects/predict-floods-with-unit-hydrographs/ (accessed 3.18.26).

Government of Canada, 2026. Daily Discharge Graph for COLDWATER RIVER AT MERRITT (08LG010) [BC] [WWW Document]. Daily Discharge Graph for COLDWATER RIVER AT MERRITT (08LG010) [BC]. URL https://wateroffice.ec.gc.ca/report/historical_e.html?stn=08LG010 (accessed 2.25.26).

Holt, A.R., Mears, M., Maltby, L., Warren, P., 2015. Understanding spatial patterns in the production of multiple urban ecosystem services. Ecosystem Services 16, 33–46. https://doi.org/10.1016/j.ecoser.2015.08.007

Hounkpè, J., Diekkrüger, B., Afouda, A.A., Sintondji, L.O.C., 2019. Land use change increases flood hazard: a multi-modelling approach to assess change in flood characteristics driven by socio-economic land use change scenarios. Nat Hazards 98, 1021–1050. https://doi.org/10.1007/s11069-018-3557-8

McGrath, H., Papasodoro, C., Moreau, J.S., Bourgon, J.F., Fortin, M., Fuss, C., Perry, B., Tardif, P., 2025. Descriptor: Medium Resolution Digital Elevation Model From Natural Resources Canada's CanElevation Series (MRDEM-30). IEEE Data Descriptions 2, 211–217. https://doi.org/10.1109/IEEEDATA.2025.3576318

Secretariat, T.B. of C., Secretariat, T.B. of C., 2023. National Hydro Network - NHN - GeoBase Series - Open Government Portal [WWW Document]. URL https://open.canada.ca/data/en/dataset/a4b190fe-e090-4e6d-881e-b87956c07977 (accessed 7.28.23).

Simpkins, C.E., Dennis, T.E., Etherington, T.R., Perry, G.L.W., 2018. Assessing the performance of common landscape connectivity metrics using a virtual ecologist approach. Ecological Modelling 367, 13–23. https://doi.org/10.1016/j.ecolmodel.2017.11.001

Whitebox Geospatial Inc., 2025. Whitebox Geospatial [WWW Document]. Whitebox Geospatial Inc. URL https://www.whiteboxgeo.com/ (accessed 9.16.25).

Chapter 1 Global change and emerging flood risks

1.2 Compound and cascading flood risks

ICFM 10
Adapting to Global Change:
Innovative Approaches to Flood Management and Resilience
May 20-22, 2026 | Western University, London, Ontario, Canada

Efficient Compound Flooding Scenario Evaluation via Hydrodynamic Modelling and Coordinate Based Neural Surrogates

Afshin Shaygani[1], Yasaman Taleghani[1], Mohammad Reza Najafi[1], Merce Casas Prat[2] and Julien Cousineau[3]
Western University, 1151 Richmond Street, London, ON N6A 3K7, Canada[1]
E-mail: ashaygan@uwo.ca; E-mail: ytalegha@uwo.ca; E-mail: mnajafi7@uwo.ca
Environment and Climate Change Canada, Ottawa, ON, Canada[2]
E-mail: merce.casasprat@ec.gc.ca
National Research Council Canada, Ottawa, ON, Canada[3]
E-mail: julien.cousineau@nrc-cnrc.gc.ca

ABSTRACT

Compound flooding is an increasing challenge for coastal resilience because coincident drivers can amplify inundation beyond what single driver analyses capture. Focusing on Tofino on the outer coast of Vancouver Island, we develop a scenario-based framework that combines joint extreme characterization of coastal water levels and precipitation with physics-based inundation modelling and a machine learning surrogate for rapid evaluation. Joint compound scenarios are derived from ERA5 reanalysis (1970 to 2019) (Hersbach et al., 2020) and simulated with LISFLOOD FP (Sharifian et al., 2023; Bates et al., 2013) to produce high resolution flood depth and extent fields. A coordinate based neural surrogate is then trained to emulate these inundation outcomes directly from compound forcing, enabling orders of magnitude faster scenario screening than full hydrodynamic simulation. The approach supports efficient exploration of joint return period conditions and provides a practical basis for compound flood risk assessment and climate informed stress testing.

KEYWORDS: Compound flooding; surrogate modelling; LISFLOOD-FP; Copula dependence modelling; storm surge; precipitation

1 INTRODUCTION AND BACKGROUND

Compound flooding occurs when multiple flood drivers coincide and interact through synergistic effects, producing impacts greater than those expected from any driver acting alone. In coastal communities, a common and particularly damaging combination is intense precipitation occurring near the time of elevated coastal water levels driven by storm surges and tides. For Tofino, British Columbia (Figure 1), this interaction is highly relevant because Pacific storm systems can generate both heavy rainfall and elevated coastal water levels, while the local shoreline geometry and low-lying infrastructure can amplify inundation pathways.

A central difficulty in compound flood risk assessment is that the hazard space is inherently multivariate. It is not enough to characterize extreme rainfall or extreme coastal water levels independently. What matters for inundation is their joint behaviour, including dependence, timing, and how these combined boundary conditions translate into overland flow across complex topography. This has direct implications for planning and design because risk estimates can be biased if joint extremes are under sampled or treated as independent, and because the most consequential impacts often arise from plausible combinations rather than record breaking single driver events.

Physics based hydrodynamic models can represent these interactions credibly, but compound flooding assessments quickly become computationally demanding when they require large scenario ensembles across a range of joint return periods or when they are used for stress testing under future climate conditions. As a result, there is a practical need for workflows that preserve physical realism while enabling rapid exploration of compound scenarios and clear interpretation for risk assessment.

In this study, we present a scenario-based framework for compound flooding in Tofino that combines joint extreme characterization with physics-based inundation modelling and a machine learning surrogate. We use historical reanalysis (1970 to 2019) to generate synthetic compound scenarios that represent the co-occurrence of precipitation and elevated coastal water levels, then simulate inundation with LISFLOOD FP v8.2 (Sharifian et al., 2023; Bates et al., 2013) on a 5 m digital elevation model. A coordinate based neural surrogate is trained on the resulting inundation fields to provide fast reconstruction of flood depth and extent for new compound scenarios. The purpose of the surrogate is not to replace the hydrodynamic model, but to enable rapid screening of compound flood risk across many scenarios, support sensitivity studies, and make joint return period analysis more tractable for decision making.

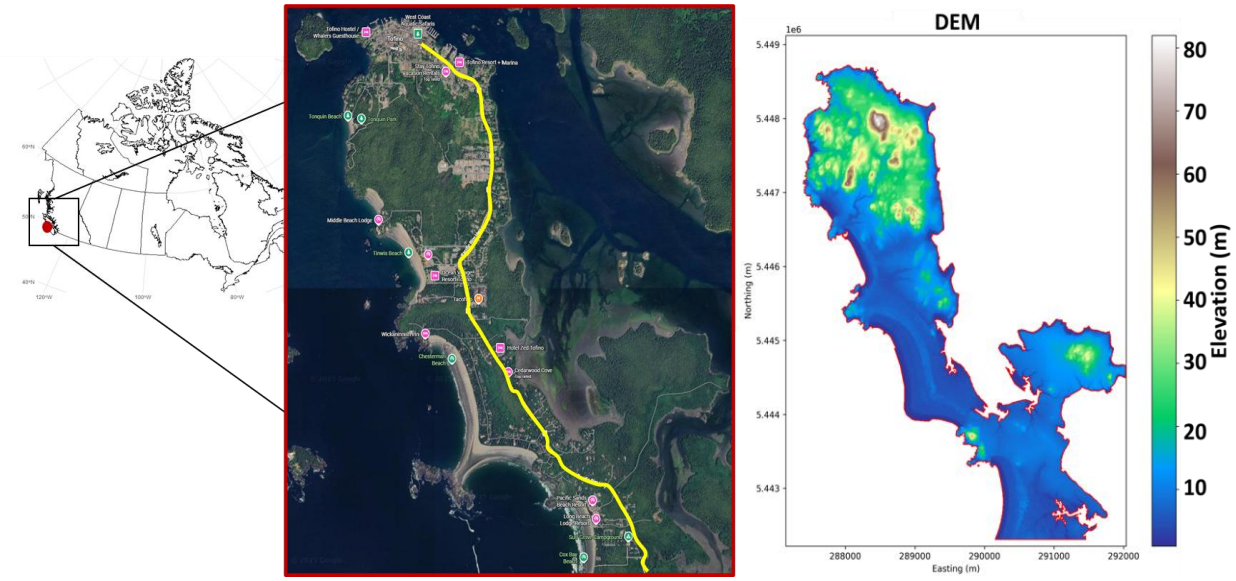

Figure 1: Tofino study area: location in North America, model domain, and DEM

2 METHODOLOGY

We developed a scenario-based workflow for compound flooding in Tofino that links joint extreme characterization of the compound drivers to physics-based inundation modelling and rapid emulation for efficient risk assessment. Historical reanalysis (1970 to 2019) (Hersbach et al., 2020) was used to describe extremes in precipitation and storm surge using a peaks-over-threshold approach, and dependence between drivers was represented with a copula-based model. This enabled sampling of synthetic compound scenarios across the joint space and joint return period regimes. Each scenario was translated into three-day time series boundary conditions so that the hydrodynamic model is forced by physically meaningful temporal evolution of both rainfall and coastal water levels.

Inundation was simulated with LISFLOOD FP v8.2 over a 5 m digital elevation model of Tofino referenced to CGVD2013. Simulations were run for a three-day window using the local inertial formulation with adaptive time stepping and GPU acceleration through the CUDA solver. The physics-based ensemble was executed on HPC as a SLURM job array to support large scenario counts while

keeping runs traceable and computationally manageable. The resulting outputs are spatial flood depth and extent fields for each compound scenario.

To enable rapid scenario exploration for flood risk assessment, we trained a machine learning surrogate, specifically a coordinate based neural implicit model with event conditioning, to emulate LISFLOOD FP inundation outcomes from the compound forcing. The surrogate's role in this conference paper is pragmatic: it provides near real time reconstruction of flood maps for new compound scenarios so that joint return period conditions can be screened efficiently, sensitivity to compound forcing can be explored, and risk relevant summaries can be generated without repeatedly running the full hydrodynamic model. Detailed architectural and training choices are beyond the scope of this conference paper and are reserved for journal publication.

Figure 2 summarizes this Physics–AI framework and should be interpreted as follows: the only observational information enters through the event-based context used for evaluation, while the flood depth and inundation fields shown are model outputs. Where 2018 and 2021 events are referenced, the observations consist of documented impacts and reported flooding extents from Department of Transportation reports and publicly available news sources, and these are used to corroborate plausibility of the modelled inundation patterns rather than to directly provide gridded water depth observations.

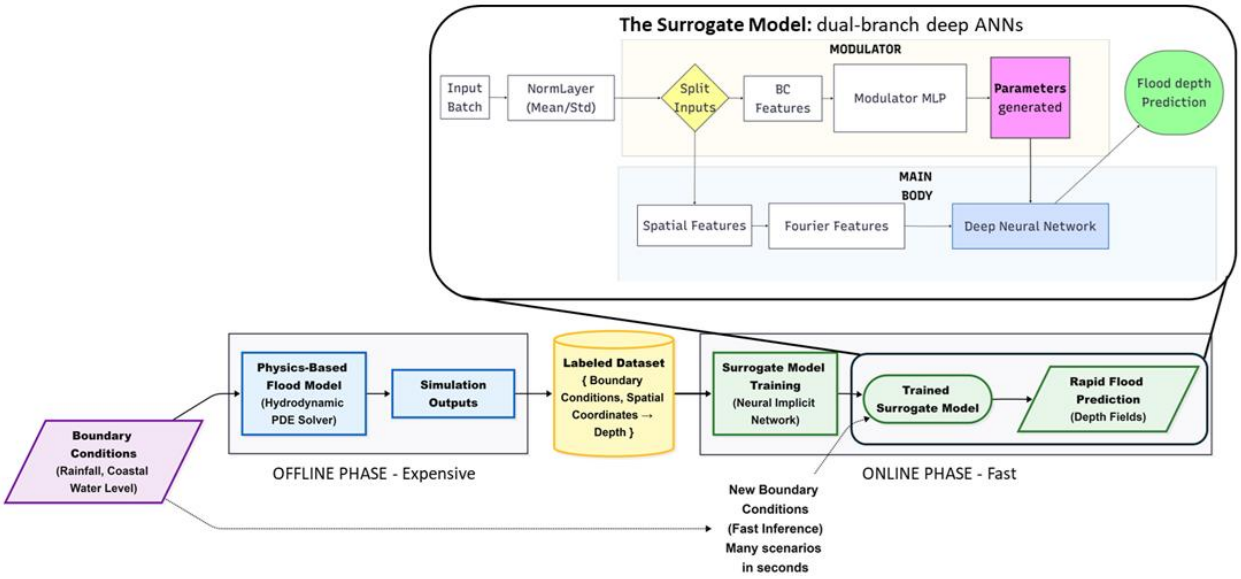

Figure 2: Physics–AI framework for compound flood inundation modelling

3 KEY RESULTS

Key results are summarized in Figure 3 (a–e) and emphasize the main implication for flood risk assessment: the framework enables rapid, scenario-based screening of compound flood hazard across a wide range of joint conditions while preserving the spatial patterns needed for local decision making. The physics-based ensemble provides a consistent mapping from compound forcing to inundation outcomes, allowing flood depth and extent to be evaluated in terms of both spatial footprint and distributional behaviour. Figure 3a and 3b illustrate a representative event and the corresponding depth statistics from the physics-based model, which together highlight how compound scenarios can shift not only maximum depths but also the proportion of the domain that becomes inundated. Figure 3c and 3d then show that the surrogate reproduces the key inundation pathways and extents of the physics-based simulation under the same forcing, making it practical to sweep large numbers of joint return period scenarios that would otherwise be computationally prohibitive. Figure 3e indicates that differences between the surrogate and

the physics-based solution remain small for the evaluated case, supporting the use of the surrogate as an efficient front end for compound flood risk screening. Event based context from the 2018 and 2021 floods, supported by District of Tofino reports and publicly available news sources, provides an external check that the simulated inundation patterns are plausible for real world events.

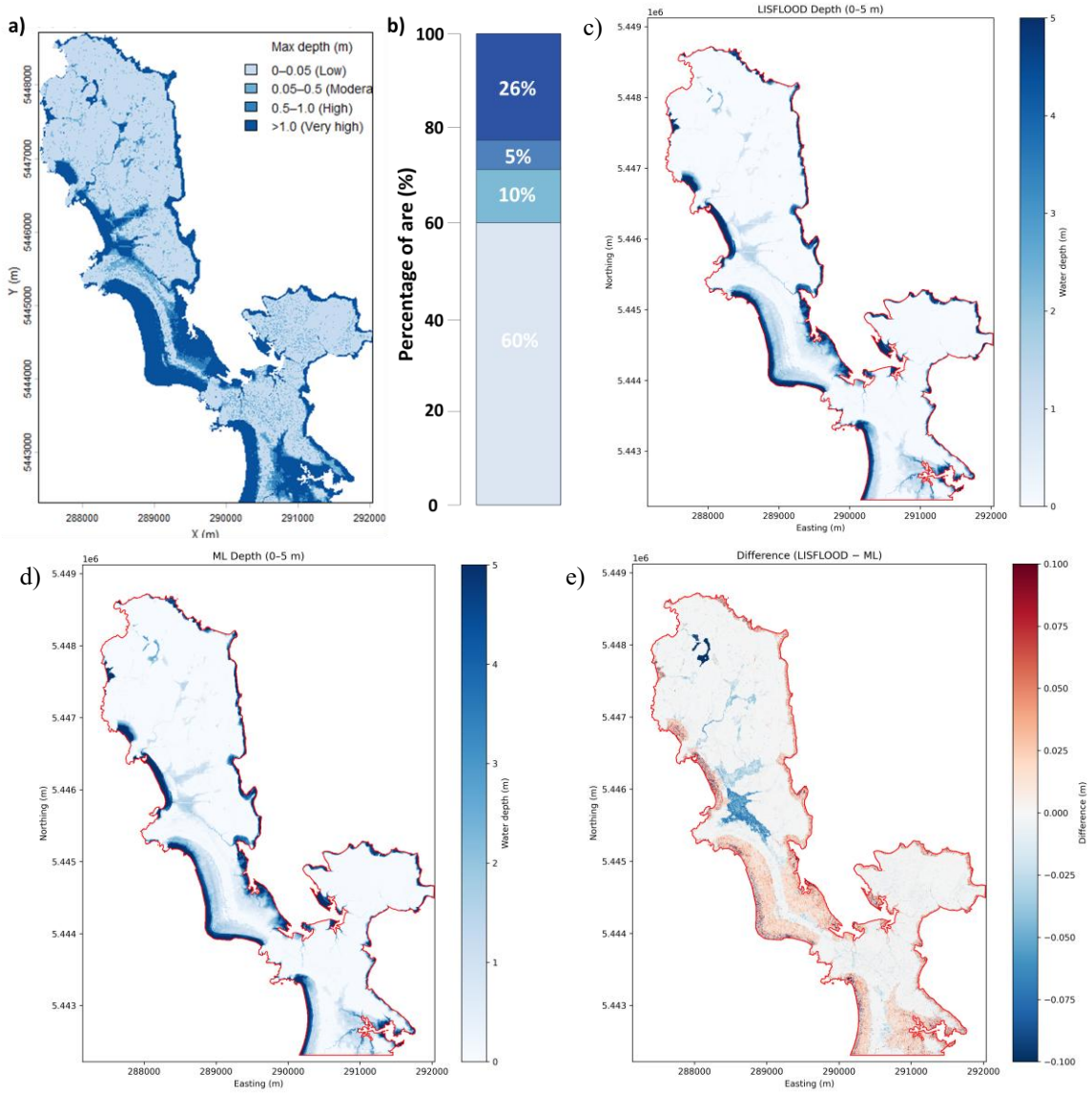

Figure 3: Validation of physics based and surrogate compound flood modeling for a representative event. (a) Physics based flood depth field. (b) Statistical descriptors of simulated flood depths from the physics-based model. (c) Inundation extent from LISFLOOD FP. (d) Inundation extent for the same event predicted by the surrogate. (e) Flood depth error (surrogate minus physics) showing differences within a 10 cm bound

4 CONCLUSION

In conclusion, this study presents a practical framework for scenario-based compound flood risk assessment in Tofino that links joint extreme characterization to physics-based inundation modelling and rapid emulation. The key outcome is that compound flooding can be explored across a wide range of joint conditions and return period regimes without the prohibitive computational cost of running a full hydrodynamic model for every scenario. LISFLOOD FP provides physically consistent inundation maps for representative compound events, and a machine learning surrogate, implemented as a coordinate based neural implicit model, is used to rapidly reproduce flood depth and extent fields for additional scenarios. Comparisons against the 2018 and 2021 events, supported by documented impacts and publicly available reports, indicate that the modelled inundation patterns are plausible at the event scale. Overall, the framework enables efficient screening, sensitivity analysis, and stress testing of compound flood hazard while retaining the spatial detail needed for local decision making and prioritization.

5 ACKNOWLEDGEMENTS

The authors acknowledge the support of the National Research Council Canada (NRC, CNRC) and Environment and Climate Change Canada (ECCC). The large ensemble simulations and surrogate model training were enabled by compute resources provided through the Digital Research Alliance of Canada.

REFERENCES

Bates, P., Trigg, M., Neal, J. and Dabrowa, A. (2013). LISFLOOD-FP User Manual, Code Release 6.1.1. School of Geographical Sciences, University of Bristol, UK, 25 November 2013.

Hersbach, H., Bell, B., Berrisford, P., Hirahara, S., Horányi, A., Muñoz-Sabater, J., Nicolas, J., Peubey, C., Radu, R., Schepers, D., Simmons, A., Soci, C., Dee, D. and Thépaut, J.-N. (2020). The ERA5 global reanalysis. Quarterly Journal of the Royal Meteorological Society, 146(730), 1999–2049. https://doi.org/10.1002/qj.3803

Sharifian, M.K., Kesserwani, G., Chowdhury, A.A., Neal, J. and Bates, P. (2023). LISFLOOD-FP 8.1: New GPU-accelerated solvers for faster fluvial/pluvial flood simulations. Geoscientific Model Development, 16, 2391–2413. https://doi.org/10.5194/gmd-16-2391-2023

ICFM 10
Adapting to Global Change:
Innovative Approaches to Flood Management and Resilience
May 20-22, 2026 | Western University, London, Ontario, Canada

Improving flood monitoring and forecasting in High Mountain Asia using remote sensing of glacier lake outbursts

Qiuhong Tang[1*], Li He[2], Gang Zhao[2], Chi Zhang[2], Ximeng Xu[2], Jie Wang[3], Xiaobo Yun[4], Xingcai Liu[2] and Yuanyuan Zhou[2]

Department of Earth System Sciences, Tsinghua University, Beijing, 100084, China[1]
E-mail: tangqh@gmail.com[*]

Key Laboratory of Water Cycle and Related Land Surface Processes, Institute of Geographic Sciences and Natural Resources Research, Chinese Academy of Sciences, Beijing 100101, China[2]

Lanzhou University, Gansu 730000, China[3]

National Meteorological Centre, China Meteorological Administration, Beijing 730000, China[4]

ABSTRACT

A flood and drought monitoring and forecasting system with high spatiotemporal resolution (up to 500 m, 30 min) using satellite and climate model data has been developed for China. The system uses a combination of the Variable Infiltration Capacity (VIC) and Catchment-Based Macro-scale Floodplain (CaMa-Flood) models to simulate hydrologic-hydrodynamic processes over large basins. Satellite precipitation data such as NASA's Integrated Multi-satellitE Retrievals for GPM (IMERG) have been used to drive the models in near real time, enabling the implementation of the system over ungauged regions such as the transboundary Lancang-Mekong, Ganges-Brahmaputra-Meghna (GBM), and Aksu river basins. Although the system can monitor the rainfall and snow induced floods, it cannot predict the glacier lake outburst floods (GLOF) because the current framework does not take into account of the glacier lakes, which hinders its application in the High Mountain Asia where GLOF frequently occurs. A simple approach is therefore proposed to monitor glacier lake change and detect glacier lake outburst using remote sensing, and to simulate the downstream impacts of the glacier lake outburst floods. Glacial lake volume was estimated by combining lake area data derived from satellite imagery with the 1-meter resolution bathymetric data. When a decrease in glacial lake volume was detected, the suspicious GLOF warning was initiated and the GLOF simulation was triggered. An ensemble of water release processes of glacier lake outburst was formed using the water release processes in the historical periods, and the ensemble GLOF predictions are made by adding glacial lake outburst water release to the hydrological-hydrodynamic simulations. The system successfully detected the decrease of glacier lake storage in July 2024, enabling reliable nowcasting of GLOF risk for Aksu city. The improved flood monitoring and forecasting framework can greatly benefit flood assessment and early warning in other rivers with glacier lakes in High Mountain Asia.

KEYWORDS: Hydrological monitoring and forecasting; Glacier lake outburst floods; Satellite remote sensing; High Mountain Asia

1 INTRODUCTION

Large-scale hydrological monitoring and forecasting systems are essential for managing water resources and providing early warnings of floods and droughts. Satellite-based hydrological monitoring typically involves long-term hydrological simulations that provide a reference database. It also includes a

hydrological monitoring component that processes real-time observations and a hydrological forecasting component that offers future predictions based on initial hydrological states provided by the monitoring component. Previous studies have developed long-term land surface hydrologic flux and state datasets for China (Zhang et al., 2014; Miao and Wang, 2020; Gou, et al., 2021). A probability mapping method was used to integrate real-time satellite precipitation into long-term, gauge-based retrospective products by matching cumulative probability functions. This enabled near-real-time hydrological monitoring consistent with long-term retrospective simulations (Zhang and Tang, 2015). Using initialization states from satellite-assisted hydrological monitoring, a hydrological forecast based on climate forecasts and ensemble streamflow predictions was developed (Zhang et al., 2017). This hydrological monitoring system has been applied in China and in various transboundary river basins surrounding China (Jia et al., 2020; Yang et al., 2020; Wang et al., 2021). However, these hydrological models did not account for glacial lake outburst floods (GLOFs). Although the hydrological monitoring system can capture floods induced by rainfall and snowmelt, it cannot predict GLOFs because the current framework lacks an explicit representation of glacial lakes. This hinders its application in High Mountain Asia, where GLOFs frequently occur. Remote sensing monitoring techniques for GLOFs could improve hydrological predictions for rivers in High Mountain Asia. This paper proposes an improved framework for monitoring and forecasting floods in High Mountain Asia by remotely sensing glacier lake outbursts. The Aksu River Basin, where GLOFs occasionally occur, was selected as the case study area. We tested the improved hydrological monitoring and forecasting system to predict GLOF risk in the Aksu River Basin.

2 SATELLITE-BASED HYDROLOGICAL MONITORING

2.1 Framework of Improved Monitoring and Forecasting System

The proposed framework is an improved ensemble GLOF prediction approach built on the ensemble streamflow prediction-based hydrological forecasting framework, with the addition of ensemble GLOF processes. It uses satellite remote sensing techniques to acquire information on glacier lake changes and glacier lake outbursts. Once a glacier lake outburst is detected, an ensemble of water-releasing processes is used to release the water from the glacier lake outburst into the river network. A hydrodynamic model is used to simulate flood propagation and assess the downstream impacts of GLOFs (Figure 1). The original, satellite-based, large-scale hydrological monitoring framework provides the platform, and the GLOF ensemble provides a range of possible water-releasing processes during a GLOF that cannot be observed by satellite remote sensing (Figure 1). The improved framework is described in details below.

The satellite-based hydrological monitoring system employs a combination of the Variable Infiltration Capacity (VIC) and Catchment-Based Macro-scale Floodplain (CaMa-Flood) models to simulate hydrological and hydrodynamic processes in large basins (Zhang and Tang, 2015; Wang et al., 2021). The system provides flood and drought monitoring and forecasting with high spatiotemporal resolution (up to 500 meters and 30 minutes). The models are primarily driven by near-real-time satellite precipitation data, such as NASA's Integrated Multi-satellitE Retrievals for GPM (IMERG) Early Run. This enables implementation of the system over ungauged regions (Tang and Lettenmaier, 2010).

To enable the system to predict GLOF in High Mountain Asia, where it frequently occurs, variations in glacial lakes are monitored using remote sensing. The minimum lake area prior to a GLOF event in historical records was used to determine the warning threshold. The lake area usually increases from winter to summer. When the lake area approaches the warning threshold, there is an increased risk of outburst, so the remotely sensed lake imagery is checked manually every day. Glacial lake volume is estimated by combining lake area data derived from satellite imagery with 1-metre resolution bathymetric data. When a sharp decrease in glacial lake volume is detected, suspicious GLOF warning is initiated and the GLOF simulation is triggered. An ensemble of glacier lake outburst water-releasing processes was formed using those in historical years, and ensemble GLOF predictions were made by adding the released water to hydrological-hydrodynamic simulations.

Although satellite remote sensing can detect GLOF events, it cannot capture the timing of the event or the process by which water is released due to the low revisit frequency of satellites, which is usually 2–5 days. Similar to ensemble streamflow prediction, an ensemble GLOF prediction approach was adopted. Firstly, the ensemble members of the GLOF water-release process were formed based on discharge records following GLOF events in previous years. Most GLOF water-release processes take about 70 hours, but some last less than 40 hours. The volume of water released by the GLOF is obtained from remote sensing estimates, and the total volume is redistributed across the time series in line with the water-release process. Climate sequences resampled from the past will be used as model inputs to perform the ensemble GLOF prediction. Secondly, ensemble GLOF predictions were made by adding glacial lake outburst water release to hydrological-hydrodynamic simulations.

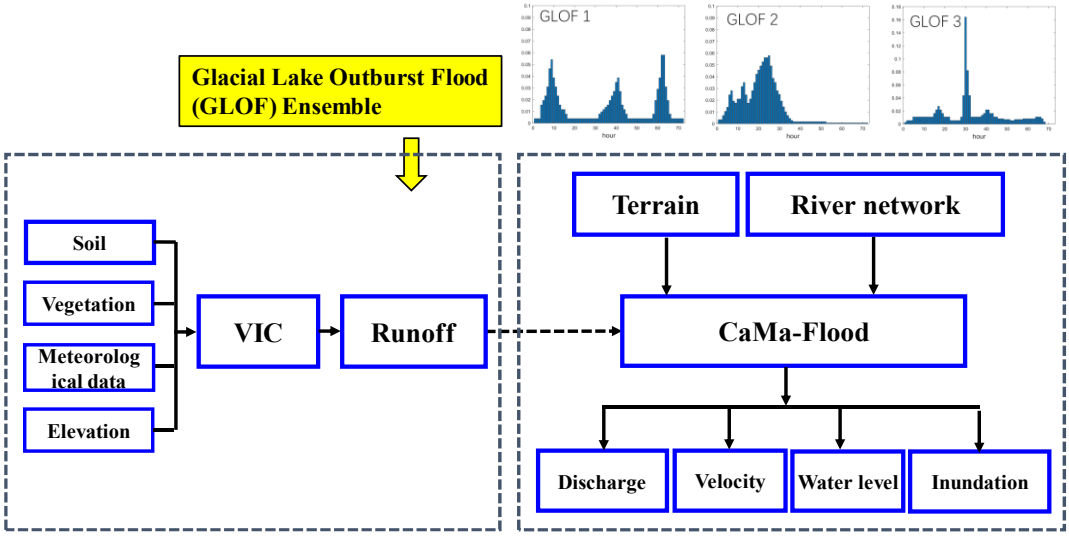

Figure 1: Framework of the improved flood monitoring and forecasting system using remote sensing of glacier lake outbursts

In summary, satellite remote sensing is used to detect the approximate timing and total volume of water released by GLOFs. Information about the water-releasing process, which cannot be obtained from satellite data, was obtained from an ensemble of past GLOF events. This approach involves generating multiple model simulations based on plausible GLOF water-release scenarios in order to produce a range of possible future river flows following a GLOF. This provides probabilistic forecasts rather than a single estimate. The uncertainty of GLOF impact prediction can therefore be quantified.

3 APPLICATION IN HIGH MOUNTAIN ASIA

The Aksu River Basin was chosen as the case study area in which to test the performance of an improved hydrological monitoring and forecasting system. The Merzbacher glacier lake, located upstream of the Aksu River, was monitored and the impact of a glacier lake outburst was predicted.

3.1 Aksu River Basin

The upper reaches of the Aksu River basin possess a complete set of cryospheric elements, with glacial lake outburst floods having a significant impact on the city of Aksu downstream (Figure 1a). Merzbacher glacial lake, located in the upper Sarez River, is a large-to-medium-sized glacial lake formed by the melting of the northern branch of the Irchek Glacier and the blockage of its southern branch by an ice dam (Figure 1b). Each year during spring and summer, as the glaciers melt, the lake gradually fills,

generating hydrostatic pressure on the downstream ice dam and promoting the formation of subglacial drainage channels. Following significant accumulation of lake water, the southern ice dam lifts and bursts, causing flooding. This dynamic interplay between hydrostatic pressure and drainage channel adjustment (Figure 1c) makes Merzbacher Lake highly suspicious to outburst hazards.

Although the glacier is located in Kyrgyzstan, its outburst floods affect the Aksu oasis in China every year. In recent years, climate warming has accelerated glacial melt, continuously increasing the lake's volume. This has, in turn, heightened the frequency and peak intensity of downstream floods. An improved monitoring and forecasting system has been implemented to monitor changes in the Merzbacher glacial lake and predict the risk of GLOFs in Aksu city.

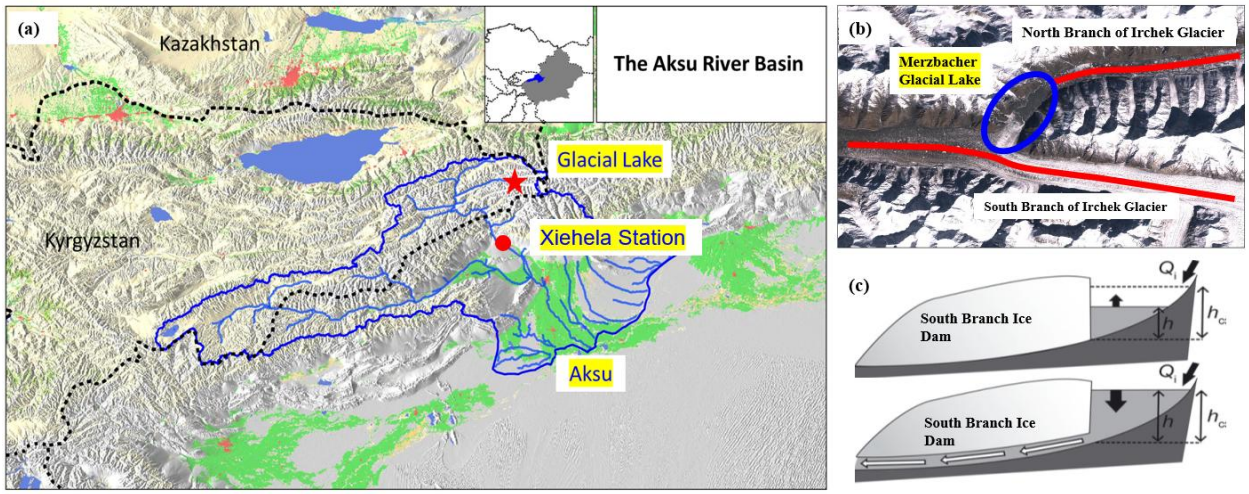

Figure 2: Merzbacher glacial lake and Aksu River basin (a), the two branches of the Merzbacher glacial lake (b), and an illustration of the dynamic interplay of these two branches (c).

3.2 Monitoring Glacial Lakes and Detecting GLOFs

Sentinel-2 satellite imagery with a resolution of 10 m and a revisit time of 2–5 days was used to extract the lake area (see Figures 3a and 3c). The minimum lake area prior to GLOFs in previous years, when satellite data was available, can be used to determine the lake area warming threshold. The estimated lake area was converted to lake storage volume using bathymetric data with a resolution of 1 metre (Figures 3b and 3d). Monitoring began in April 2024 and lasted for more than two months. Monitoring of the lake shows that the lake area increased to 2.5 km² by 30 June 2024, while the corresponding storage volume increased to 80×10^6 m³. Subsequently, the lake storage volume decreased sharply after 7 July 2024 and the GLOF impact simulation was triggered.

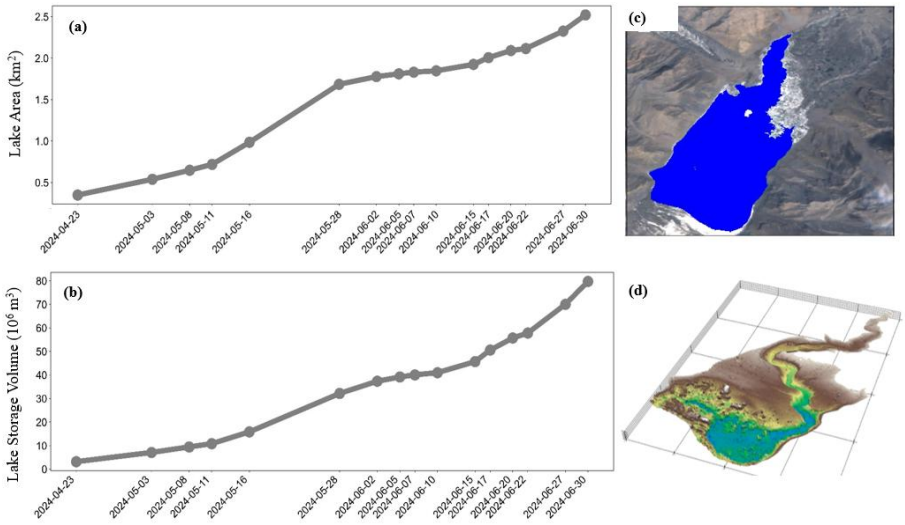

Figure 3: Panel (a) shows the lake area and panel (b) shows the lake storage volume of the Merzbacher glacial lake in 2024. Panel (c) shows the lake area on 7 July 2024 and panel (d) shows the bathymetry data at a resolution of 1 metre.

3.3 The GLOF Ensemble

Based on discharge records at the Xiehela hydrological station from previous years, an ensemble of GLOF water release processes has been formed for GLOF flow prediction in the Aksu river basin. Three ensemble members are shown as an example, and the flood volume is redistributed across the time series in line with the water-release process, resulting in different peak discharges. The ensemble members differ from each other greatly with different numbers of peaks and peaking time. The flood peak could be three times higher in some ensemble members than in others (Figure 4), suggesting significant uncertainty in GLOF flow predictions.

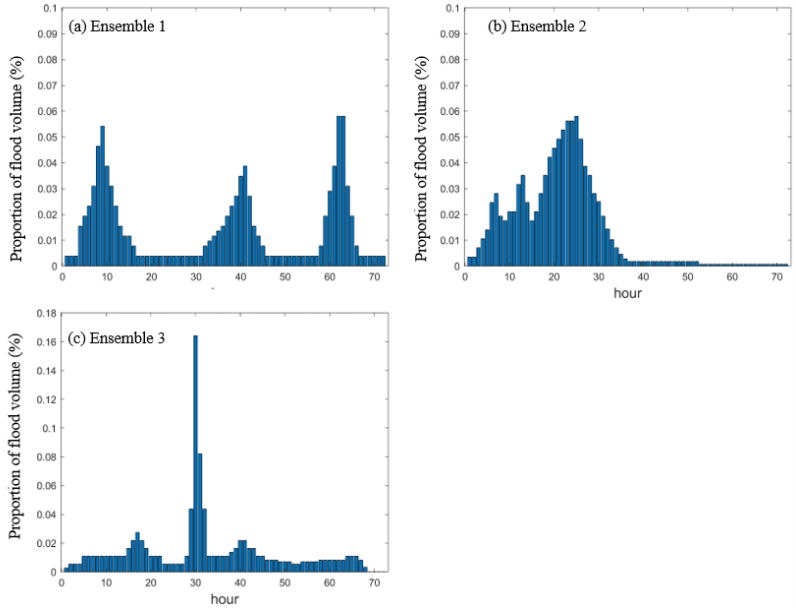

Figure 4: Ensemble of GLOF water release processes in the AKsu River

3.4 Nowcasting of GLOF Hazards

Figure 5 shows the ensemble GLOF forecast at the Xiehela hydrological station, including the simulated water elevation, river discharge and flow velocity. Although there is significant uncertainty regarding the timing of the peak, the forecasting system successfully predicted a flood peak that would not have been anticipated if GLOF had not been explicitly incorporated into the hydrological monitoring and forecasting framework. According to the forecast, the GLOF started on 7 July, with the release of the lake's stored volume taking place over a period of approximately three days, ending on 9 July. According to observations at the hydrological station, the peak discharge occurred on 8 July, which is quite close to the prediction. This suggests that the most likely forecasted GLOF process fairly agrees with the after-event report, except for the slightly overestimated flood volume.

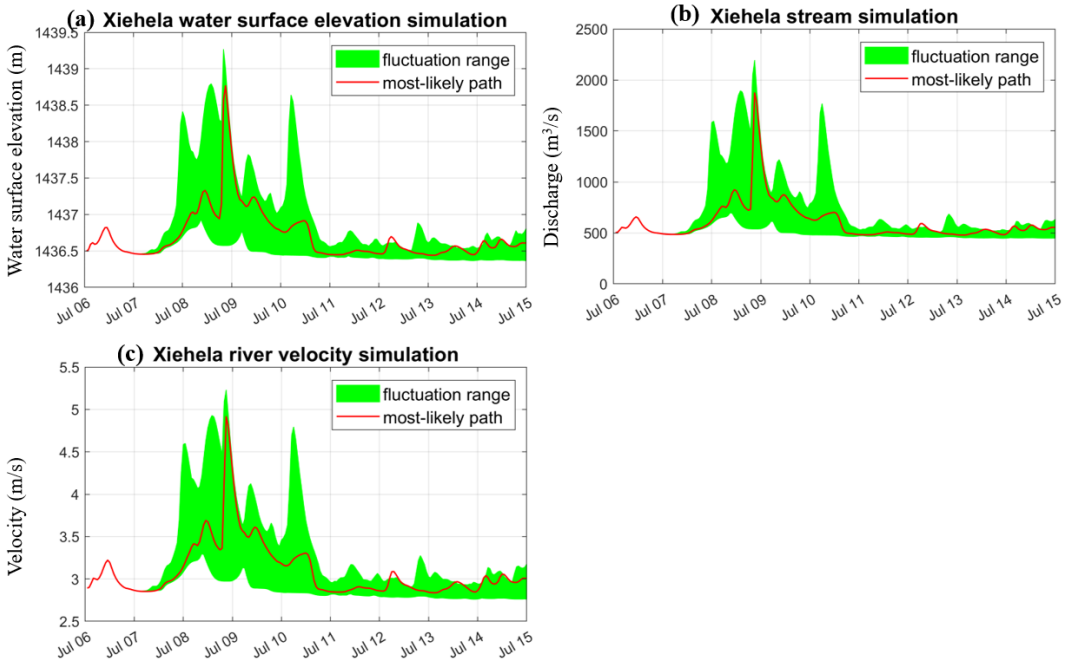

Figure 5: Ensemble GLOF forecast in 2024 at Xiehela Station (with all GLOF ensemble members)

4 CONCLUSION

This paper presents an improved satellite-based hydrological monitoring and forecasting system that uses remote sensing to detect glacier lake outbursts. The approach involves monitoring changes to glacier lakes and detecting outbursts using remote sensing, as well as simulating the downstream impacts of glacier lake outburst floods. Glacial lake volumes were estimated by combining lake area data derived from satellite imagery with 1-metre resolution bathymetric data. When a sharp decrease in glacial lake volume was detected, a GLOF warning was issued and a GLOF simulation was triggered. The system successfully detected a sharp decrease in glacial lake storage in July 2024, enabling reliable nowcasting of the GLOF hazard in the city of Aksu. This improved flood monitoring and forecasting framework could greatly benefit flood assessment and early warning systems in other rivers with glacier lakes in High Mountain Asia.

REFERENCES

Gou J.J., Miao C.Y., Samaniego L., Xiao M., WU J.W. and Guo X.Y. (2021). CNRD v1.0: A High-Quality Natural Runoff Dataset for Hydrological and Climate Studies in China. Bulletin of the American Meteorological Society, 102(5), E929-E947.

Jia G.Q., Tang Q.H. and Xu X.M. (2020). Evaluating the performances of satellite-based rainfall data for global rainfall-induced landslide warnings. Landslides, 17(2), 283-299.

Miao Y. and Wang A.H. (2020). Evaluation of Routed-Runoff from Land Surface Models and Reanalyses Using Observed Streamflow in Chinese River Basins. Journal of Meteorological Research, 34(1), 73-87.

Tang Q.H. and Lettenmaier D.P. (2010). Use of satellite snow-cover data for streamflow prediction in the Feather River Basin, California. International Journal of Remote Sensing, 3(14), 3745-3762.

Wang J., Yun X.B., Pokhrel Y., Yamazaki D., Zhao Q.D., Chen A.F. and Tang Q.H. (2021). Modeling Daily Floods in the Lancang-Mekong River Basin Using an Improved Hydrological-Hydrodynamic Model. Water Resources Research, 57(8), e2021WR029734.

Yang Q.Q, Huang X. and Tang Q.H. (2020). Irrigation cooling effect on land surface temperature across China based on satellite observations. Science of the Total Environment. 705, 135984.

Zhang X.J. and Tang Q.H. (2015). Combining satellite precipitation and long-term ground observations for hydrological monitoring in China. Journal of Geophysical Research-Atmospheres, 120(13), 6426-6443.

Zhang X.J., Tang Q.H., Leng, G.Y., Liu, X.C., Li, Z. and Huang Z.W. (2017). On the Dominant Factor Controlling Seasonal Hydrological Forecast Skill in China. Water, 9(11), 902.

Zhang X.J., Tang Q.H., Pan M. and Tang Y. (2014). A Long-Term Land Surface Hydrologic Fluxes and States Dataset for China. Journal of Hydrometeorology, 15(5), 2067-2084.

ICFM 10
Adapting to Global Change:
Innovative Approaches to Flood Management and Resilience
May 20-22, 2026 | Western University, London, Ontario, Canada

Assessing Future Compound Coastal Flooding Along the Pacific Coast of North America Using Multi-model Projections

Yasaman Taleghani[1], Mohammad Reza Najafi[1], Mercè Casas-Prat[2], Julien Cousineau[3], Mohammad Fereshtehpour[1]

University of Western Ontario, 1151 Richmond Street, London, Ontario, Canada[1]
E-mail: ytalegha@uwo.ca
Environment and Climate Change Canada (ECCC), Canada[2]
National Research Council (NRC), Canada[3]

ABSTRACT

Compound coastal flooding from storm surge and waves is a growing risk along the Pacific coast of North America, yet changes in their dependence under climate change remain unclear. Using multi-model projections (2006–2100, RCP8.5), extreme events were extracted via a Peak-Over-Threshold approach and analysed using Kendall's tau and copula-based joint return periods. Results show a strengthening surge–wave dependence across Alaska, British Columbia, and the western U.S. coast, leading to reduced joint return periods and more frequent compound flooding events. These findings highlight the importance of incorporating evolving multivariate dependence into coastal risk assessments to avoid underestimating future flood hazards.

Keywords: Compound coastal flooding, Wave–surge interaction, Climate change projections, Copula modelling, Peak-Over-Threshold (POT)

1 INTRODUCTION

Coastal flooding is one of the most frequent and costly natural hazards worldwide, with risk increasing as populations and infrastructure concentrate in low-lying coastal zones and the climate change intensifies extreme events. Flooding is often driven by the combined influence of storm surge, waves, and precipitation occurring simultaneously or in close sequence, producing compound events whose impacts exceed those estimated from single-driver or independence-based assumptions. Along energetic Pacific coastlines, wave–storm surge interactions are particularly important, as large offshore wave fields associated with extratropical cyclones can coincide with elevated surge levels, enhancing coastal water levels through wave setup, runup, and overtopping. These processes strongly influence flood extent but are inadequately represented when wave and surge hazards are treated independently. The changes in wave–surge dependence can substantially alter compound flood probabilities and design exceedance risk. Despite recent advances in compound hazard research, significant gaps remain in understanding multivariate dependencies and their potential evolution under climate change, especially along the Canadian Pacific coastline where evidence is limited. Given projected changes in storm tracks, cyclone intensity, and wave climate in the Northeast Pacific, wave–surge dependence itself may evolve, with important implications for future coastal flood risk. This study examines how wave–storm surge dependence, may change under climate change, with a focus on impacts relevant to compound coastal flooding and adaptation planning.

2 DATA

Hourly time series for storm surge and significant wave height were extracted at 500 coastal nodes along the Pacific Ocean from 2006 to 2100. The dataset comprises TELEMAC model outputs forced by three Regional Climate Models (RCMs) with four realizations under the RCP8.5 emissions scenario by (Cousineau & Murphy, 2022). To support regional interpretation, nodes were grouped into four latitude-based zones: Alaska (54.49°–60.21° N), British Columbia (48.0°–54.5° N), Northwest (42.0°–48.0° N), and West (35.77°–42.0° N). For consistent temporal comparison, the analysis period was partitioned into four windows: Baseline (2006–2025), Near Future (2031–2060), Mid Future (2061–2080), and Far Future (2081–2099).

3 METHODOLOGY

We identified extreme events for each driver using a univariate Peak-Over-Threshold (POT) approach with a 95th-percentile threshold. We declustered the series and chose only the maximum value from each event, helping to ensure that the extracted extremes are independent. Compound events between two drivers were then constructed by pairing these event maxima within a ±1-day time window. We quantified interdependence of compound events using Kendall's tau and examined how this dependence varies across the defined analysis periods. For the marginal behaviour of each extreme series, we fitted a Generalized Pareto Distribution (GPD), consistent with the POT framework. Joint dependence was modelled using a suite of copula families; their goodness of fit was evaluated using the Cramér–von Mises test, and the best-performing copula at each node was selected based on the Akaike Information Criterion (AIC). Finally, we calculated the joint return period using AND scenario as shown in equation1.

$$T_{AND} = \frac{\mu}{P(X > x, Y > y)} = \frac{\mu}{1 - F_X(x) - F_Y(y) + C\big(F_X(x), F_Y(y)\big)} \quad (2)$$

We quantified natural variability in joint return periods by generating 1000 bootstrap-resampled present-day annual blocks and using these to construct a 95% confidence interval. Projected return period changes were considered robust when they fell outside this interval and at least three of four models agreed on the direction of change (Bevacqua et al, 2020).

4 RESULTS

The interdependence analysis indicates that Kendall's tau for surge–wave compound events increase over the 21st century in Alaska, British Columbia, and the West as is shown in figure 1. This strengthening of dependence indicates that extreme storm surges are increasingly likely to coincide with high-energy wave conditions, enhancing total coastal water levels through wave setup, runup, and overtopping processes. While the interactions between storm surge and precipitation are more variable, they remain important for understanding flood risks in certain areas. The multi model median return period change and significance of surge-wave compound events in figure 2 shows that the percentage of nodes with negative significant return period change is increasing in Alaska and West regions. This shift implies that compound surge–wave extremes are projected to occur more frequently, effectively shortening the recurrence interval of high-impact coastal flooding events. Together, these results highlight the need to incorporate evolving multivariate dependence into future coastal flood risk assessments and adaptation planning along the Canadian Pacific coast, as reliance on stationary or independence-based assumptions may substantially underestimate future flood frequency and design exceedance risks.

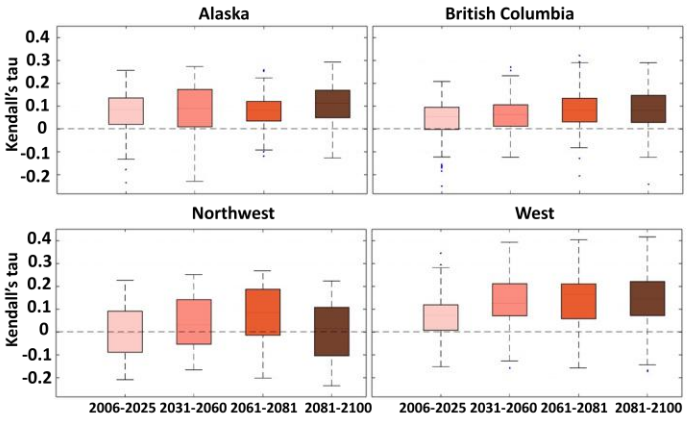

Figure 1. Multi model mean Kendall's tau of surge–wave events

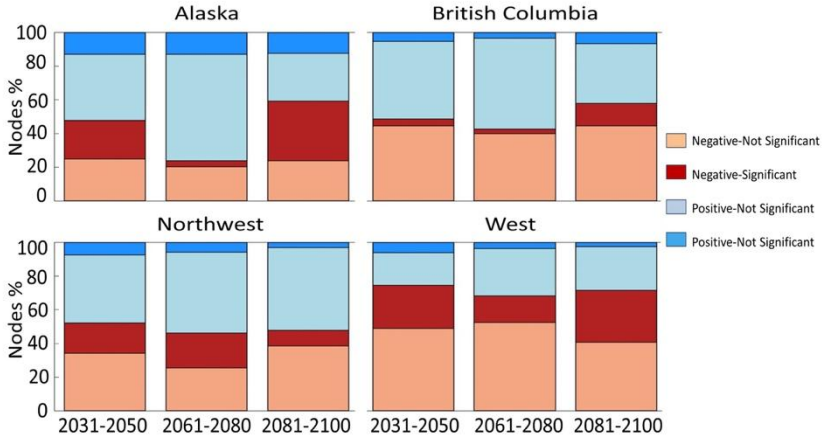

Figure 2. Multi model median return period change and significance of surge–wave events

5 CONCLUSION

Overall, our results suggest a strengthening dependence between storm surge and wave extremes and an increase in the frequency of compound surge–wave events along parts of the Pacific coastline, particularly in Alaska and the West. These changes imply that coastal flooding hazards may intensify not only because individual drivers become more extreme, but also because their joint occurrence becomes more likely under future climate conditions. This highlights the importance of moving beyond single-driver or stationary assumptions and adopting multivariate, climate-informed risk assessment frameworks that explicitly account for evolving dependence structures. Incorporating these dynamics into coastal planning, design standards, and adaptation strategies is critical to avoid underestimating future flood risk and to support more resilient coastal infrastructure and management decisions.

REFERENCES

1. Cousineau, Julien & Murphy, Enda. (2022). Numerical Investigation of Climate Change Effects on Storm Surges and Extreme Waves on Canada's Pacific Coast. Atmosphere. 13. 311. 10.3390/atmos13020311.

2. Bevacqua, E., Vousdoukas, M.I., Zappa, G. et al. More meteorological events that drive compound coastal flooding are projected under climate change. Commun Earth Environ 1, 47 (2020). https://doi.org/10.1038/s43247-020-00044-z

ICFM 10
Adapting to Global Change:
Innovative Approaches to Flood Management and Resilience
May 20-22, 2026 | Western University, London, Ontario, Canada

Compound Flooding and the Role of Nature-Based Solutions in Coastal and Estuarine Systems

Rose Cook, Nigel Wright, and Xilin Xia
School of Engineering, University of Birmingham, Birmingham, United Kingdom
E-mail: rxc124@student.bham.ac.uk

Abstract

Compound flooding arises from the interaction of multiple drivers such as elevated coastal water levels (tide–surge), high river discharge, and intense rainfall, and can produce hazards that differ nonlinearly from those expected under single-driver assumptions. In parallel, nature-based solutions (NbS) including floodplain reconnection, managed realignment/saltmarsh restoration, peatland restoration, and urban green infrastructure, are increasingly promoted as sustainable alternatives or complements to engineered defences. However, NbS performance under compound flooding remains weakly quantified, in part because many modelling studies focus on reconstructing a small number of historical events rather than testing interventions across a standardised range of compound severities and dominance regimes.

We present a transferable compound design-event generator that links historical observations, bivariate extreme-value modelling, and process-based hydrodynamic simulation. The framework harmonises 15-min coastal water level, rainfall, and multi-gauge river inflow series; extracts and declusters multi-day compound events and computes event features including peaks and river–coast timing; fits peaks-over-threshold (POT/GPD) marginals and a copula-based dependence model for event-scale peak coastal level (H) and peak total inflow (Q); generates return-period design peak pairs and selects representative coastal-dominant, fluvial-dominant, and balanced scenarios; and converts design peaks into SynxFlow-ready time-series.

The approach is illustrated through a pilot application to the Humber Estuary, UK, one of the country's most compound flood-prone systems. Preliminary outputs include an automated event catalogue (1993–2016), a compact baseline design suite for five return periods (5–200 years; 15 events total), and dependence diagnostics indicating very weak association between H_{peak} and Q_{peak} in the Humber record (Kendall's $\tau \approx 0$), motivating explicit regime and phasing exploration. Historical reconstructions provide additional end-to-end pipeline checks. Baseline batch simulations and subsequent NbS scenario comparisons are ongoing. The framework provides a foundation for more realistic assessment of NbS performance under compound flooding and supports evidence-based development of resilient, hybrid flood risk management strategies.

Keywords: compound flooding; nature-based solutions; hydrodynamic modelling; estuaries; flood risk

1 Introduction

Flooding is one of the most damaging natural hazards globally, with risks projected to increase due to climate change, sea-level rise, and continued urbanisation (Hallegatte et al., 2013; Paprotny et al., 2018). In coastal and estuarine environments, flooding is rarely driven by a single process. Instead, storm surge, high astronomical tides, river discharge, and intense precipitation often occur simultaneously or sequentially, producing compound flood events that amplify hazard and impact.

While recent research has improved understanding of compound flood drivers and their statistical dependence, many flood risk assessments remain single driver focused (Svensson and Jones, 2002; Hendry et al., 2019). This limits their ability to represent real-world flood dynamics and can lead to systematic underestimation of risk. At the same time, nature-based solutions (NbS), including wetlands, floodplains, and managed realignment schemes, are increasingly promoted as sustainable approaches to flood risk reduction. Although NbS have demonstrated benefits under individual hazards, their role under compound flooding remains insufficiently understood.

This paper addresses this gap by presenting a modelling framework to evaluate NbS performance under compound flood scenarios using process-based hydrodynamic models. The framework is illustrated through a pilot case study in the Humber Estuary, UK, a system characterised by strong compound flood drivers and significant NbS implementation. The key methodological contribution is a transferable design-event generator that links multivariate extremes (return periods), event sequencing (phasing) and process-based 2D modelling, enabling systematic testing of NbS performance across compound scenarios rather than single-driver events.

1.1 Compound flooding

Compound flooding refers to flood events that arise from the co-occurrence or interaction of two or more flood drivers, or from the interaction between extreme events and preconditioning factors that amplify impacts (Seneviratne et al., 2012). In coastal regions, compound floods are driven by combinations of storm surge, tide, river discharge, and rainfall (Hendry et al., 2019; Kumbier et al., 2018). These drivers are often physically linked through shared meteorological forcing, such as deep low-pressure systems that generate both storm surges and extreme precipitation. Elevated coastal water levels can also impede river drainage, producing backwater effects that exacerbate inland flooding.

The relevance of compound flooding has increased in recent decades due to observed and projected changes in climate extremes, sea-level rise, and catchment conditions (Bevacqua et al., 2018; Ward et al., 2018). Rising mean sea levels elevate baseline coastal water levels, increasing the likelihood that moderate surges coincide with high tides, while changes in precipitation intensity and antecedent soil moisture influence river and surface runoff contributions. Historical events, including Hurricane Harvey (USA, 2017), the Bristol Avon flood (UK, 2014), and flooding in Ravenna, Italy (2015), demonstrate the severe impacts that can arise from compound interactions (Hendry et al., 2019; Ganguli and Merz, 2019). Projections of increasing extreme rainfall and rising mean sea levels suggest that the frequency and severity of such events will continue to grow. As a result, compound flooding is now recognised as a key research priority for flood risk science and management.

Analysis of compound flooding events has traditionally relied on statistical methods to quantify dependence between flood drivers, including copula-based techniques (Granger, 1959; Svensson and Jones, 2002; Chebana and Ouarda, 2019). While valuable for estimating joint probabilities and return periods, these approaches provide limited insight into flood dynamics, such as water depths, velocities, and inundation extents. Numerical hydrodynamic models offer a complementary approach by explicitly simulating the physical processes governing compound flooding. Two-dimensional and coupled 1D–2D models are increasingly used to represent interactions between rivers, floodplains, tides, and rainfall (Pasquier *et al.,* 2019; Xu *et al.,* 2023). When driven by compound boundary conditions or scenario-based storylines, these models can provide spatially explicit hazard information directly relevant to flood risk management.

In this study we address a practical gap in the compound-flood literature: many modelling studies use a single hydrodynamic modelling set-up to reconstruct one (or a small number of) historical compound events, rather than generating a repeatable suite of compound boundary conditions across return periods. For example, Kumbier *et al.* (2018) simulate compound flooding in the Shoalhaven Estuary using Delft3D for the June 2016 storm event, forcing model boundaries with observed water levels and discharge and validating against observations such as satellite data. Similarly, Eilander *et al.* (2023) develop an automated compound-flood modelling framework centred on a 2D hydrodynamic model (SFINCS) and test it by simulating two historical compound events (Tropical Cyclones Idai and Eloise) and comparing flood extents with satellite-derived observations. Other studies do explore severity classes, but often by tying return periods to specific historical storms: for instance, Liu *et al.* (2022) use Delft3D Flexible Mesh and treat particular historical tropical cyclones as 5–100 year events based on the storm-tide probability distribution. Similarly, Lian *et al.* (2013) used a single hydraulic modelling framework (HEC-RAS river-network model) to explore combinations of rainfall and tidal-level severities, deriving design rainfall processes and tidal hydrographs for multiple return periods; however, this approach is tailored to their case-study set-up. While these approaches are highly valuable for event understanding and validation, they typically do not provide a standardised procedure to generate a repeatable design suite of compound time-series boundary conditions across return periods. We therefore develop and demonstrate a design-event generator that produces a structured set of compound scenarios (coastal-dominant, fluvial-dominant and balanced, with explicit lag/sequence information) that can be applied consistently when evaluating NbS interventions.

1.2 Nature-based solutions and ecosystem buffering

Nature-based solutions (NbS) encompass measures that utilise or restore natural processes to reduce flood risk while delivering co-benefits for biodiversity, climate mitigation, and human well-being. In coastal and estuarine environments, NbS include tidal wetlands, saltmarshes, mangroves, dunes, and managed realignment schemes. Inland examples include floodplain reconnection, riparian woodland, peatland restoration, and soil and land management interventions (Sayers et al., 2025; Radfar et al., 2024). In the UK, NbS examples are illustrated in figure 1.

The flood risk reduction benefits of NbS arise through several mechanisms (Narayan et al.,

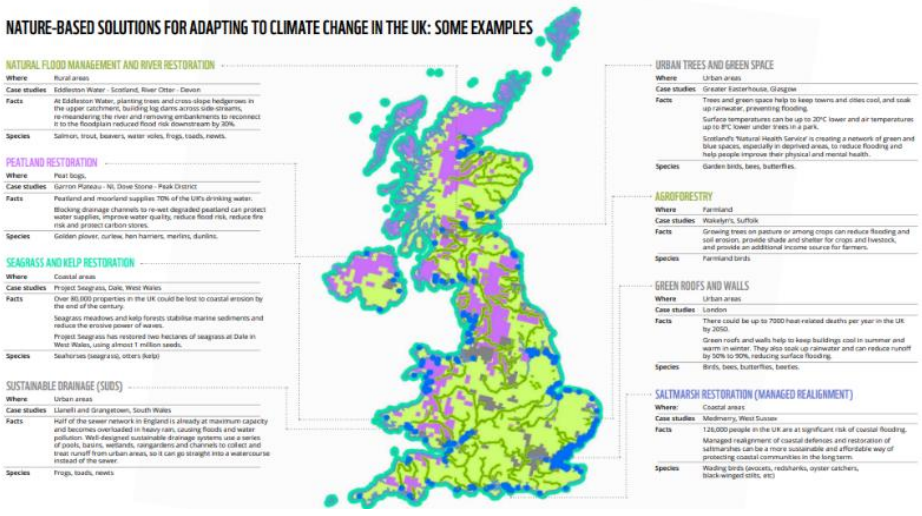

Figure 1. NbS examples in the UK. Source: Smith &

2017; Menéndez et al., 2020; Radfar et al., 2024). These include the attenuation of wave energy

and storm surge through vegetation drag, increased hydraulic roughness that slows overland flow, enhanced storage capacity, and delayed runoff generation. For example, coastal wetlands in the United States were estimated to have avoided approximately USD 625 million in direct flood damages during Hurricane Sandy (Narayan et al., 2017). Similarly, mangroves globally are estimated to avert over USD 65 billion in flood damages annually, protecting more than 15 million people (Menéndez et al., 2020). Unlike fixed engineered structures, NbS can adapt dynamically to changing conditions, although their effectiveness may vary under extreme or prolonged loading. Quantifying NbS effects in hydraulic models remains challenging because interventions can influence multiple processes simultaneously (storage, roughness/drag, conveyance and timing) and their effectiveness may be non-linear under extreme loading. Many studies therefore rely on simplified parameter changes or single-driver forcing, which makes it difficult to identify thresholds and trade-offs under compound conditions.

1.3 NbS and compound flooding

Despite strong evidence of NbS benefits under individual flood drivers, relatively few studies explicitly examine their role under compound flood conditions. Existing modelling efforts often simplify forcing or neglect interactions between drivers, limiting understanding of how NbS perform when exposed to simultaneous surge, river, and rainfall inputs (Radfar et al., 2024; Green et al., 2024). Key uncertainties remain regarding performance thresholds, resilience under extreme events, and the conditions under which NbS should be combined with engineered defences. Addressing these gaps requires modelling frameworks that explicitly represent compound flooding and NbS strategies within the same system, enabling evaluation of both hazard reduction and potential failure modes.

Key knowledge gaps include limited understanding of NbS performance thresholds under extreme compound events, insufficient representation of non-linear interactions between drivers, and weak links between hydrodynamic benefits and risk-based metrics (Radfar et al., 2024; Green et al., 2024; Marino et al., 2025). Addressing these gaps requires integrated, process-based modelling frameworks capable of representing compound flooding and ecosystem buffering simultaneously. The framework presented here is designed to be reproducible for other estuaries where long time series of tide, river flow and rainfall are available, providing a pathway from data to a historical compound-event catalogue, return-period design peaks, and physically consistent time-series inputs for hydrodynamic models. This enables NbS testing under controlled compound scenarios and supports comparison of performance across event severity and sequencing.

2 Study site: Humber estuary, UK

The Humber Estuary is one of the UK's most compound flood-prone systems, influenced by North Sea storm surges, high astronomical tides, river inflows from the Trent and Ouse, and heavy rainfall (Hendry et al., 2019). The estuary includes major NbS interventions, most notably the Alkborough Flats managed realignment scheme, which provides intertidal storage and surge attenuation.

The availability of high-resolution LiDAR, tide gauge records, river flow data, and monitoring reports makes the Humber a suitable pilot site. An estuary-scale model, outlined in figure 1, is used to assess NbS buffering under compound flooding, with scope for nested urban modelling in Hull to evaluate downstream impacts.

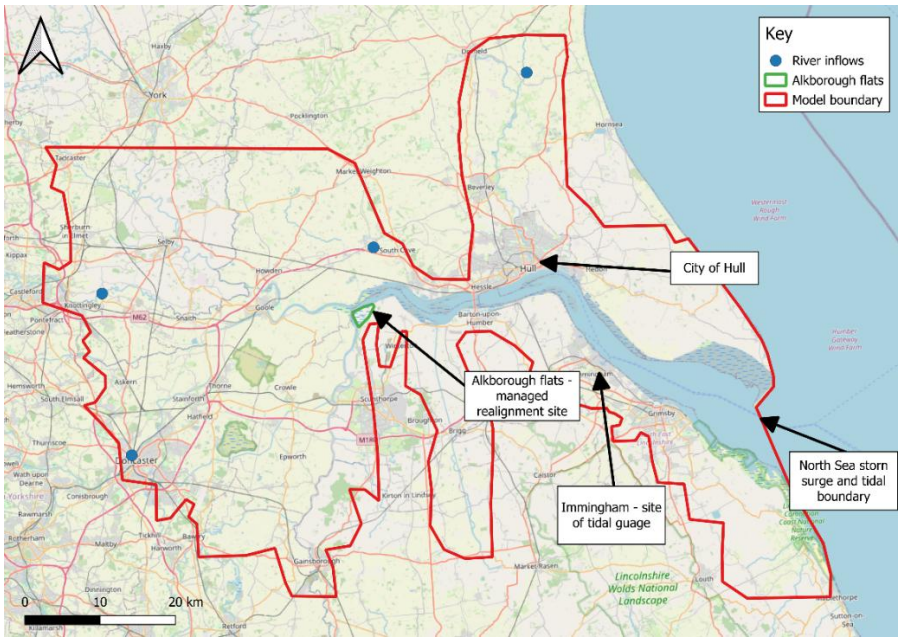

Figure 2. Location of the Humber Estuary pilot site

3 Methodology

3.1 Overview

We developed a compound design-event generator that links multi-driver observations, bivariate extreme-value modelling, and hydrodynamic simulation in SynxFlow. The generator outputs a reproducible set of return-period design events as time-series forcing (storm tide, multiple river inflows, and rainfall) suitable for batch simulation under baseline and nature-based solution (NbS) configurations. The workflow comprises: data preparation; compound event catalogue construction; bivariate peaks-over-threshold (POT) design modelling for peak coastal level (H) and peak total inflow (Q); selection of representative design peak pairs for each return period; and conversion of design peaks into SynxFlow-ready time series using historical templates.

3.2 Observational forcing data and harmonisation

We compiled 15-minute time series of coastal water level, rainfall, and discharge at four upstream gauges. All series were parsed and aligned to a strict 15-minute grid (UTC) without gap-filling to preserve extremes and event peaks. Coastal water levels were converted to ODN to ensure vertical datum consistency with the DEM. Rainfall is represented as 15-minute depth increments (mm per 15 min) and converted to rainfall rate (m s^{-1}).

3.3 Historical compound event catalogue

We identified historical compound events using a peaks-over-threshold approach anchored initially on coastal water level and applied declustering via a minimum temporal separation between retained peaks to reduce dependence between events. For each retained event time, a fixed multi-day window (centred on the anchor time) was extracted to capture tidal cycling and the river hydrograph response.

For each event window we computed peak coastal level and timing, peak discharge and timing at each gauge and for the aggregated inflow ($Q_{tot}=\sum_k Q^{(k)}$), rainfall totals and peak

intensities, and a simple phasing metric defined as the lag between the peak aggregated inflow and peak coastal level. The resulting event catalogue (1993–2016) provides a sample for extreme-value modelling and dependence diagnostics and a library of historical time-series templates for constructing design events.

3.5 Bivariate design model for peak coastal and fluvial drivers

We constructed a bivariate design model for event-scale peak coastal level (H_{peak}) and peak aggregated inflow ($Q_{tot,\ peak}$). Marginal extremes were modelled using a POT framework with Generalised Pareto distributions fitted to exceedances above selected thresholds. Thresholds were chosen as quantiles of the event-peak samples and adjusted to ensure sufficient exceedance counts for stable fitting. Exceedance rates were estimated from the 1993–2016 record length and used to map return periods to annual exceedance probabilities under a Poisson exceedance assumption. Dependence between H_{peak} and $Q_{\text{tot, peak}}$ was characterised using Kendall's τ and a Gaussian copula parameterisation.

3.6 Design peak pairs and dominance regimes

For each target return period (T), candidate design peak pairs (H, Q) were generated by sampling from the fitted bivariate model and mapping samples back to physical space using the fitted marginal transforms. For each T, we retained three representative design points spanning: coastal-dominant (relatively larger coastal contribution), fluvial-dominant (relatively larger fluvial contribution), and balanced conditions. This yields a compact baseline suite of design peak pairs for time-series construction and simulation.

3.7 Converting design peaks to SynxFlow-ready time series

Each design peak pair is converted into a full set of time series by selecting a historical template event from the catalogue. The template provides realistic within-event shapes for storm tide, river hydrographs, and rainfall.

The coastal time series is adjusted using an additive shift so that the template peak matches the design peak. SynxFlow requires boundary water depth, so coastal water level (ODN) is converted to depth using a representative downstream bed elevation (z_b) derived from the DEM within the downstream boundary box. Depth is computed as:

$$h(t) = \max(0,\ H(t) - z_b)$$

River inflow hydrographs at each gauge are scaled multiplicatively using a single factor so that the peak of the aggregated inflow matches the target design (Q), while preserving within-event timing and hydrograph shape across gauges.

Rainfall depth increments are converted to rainfall rate for SynxFlow forcing:

$$R(t) = \frac{P(t)}{1000\,\Delta t}$$

where $P(t)$ is rainfall depth in mm per 15 minutes and Δt=900 s.

Each design event is written to a dedicated folder containing downstream depth forcing, four upstream inflow time series, rainfall forcing, and metadata (template ID, scaling factors, and phasing). These folders enable automated batch execution of baseline simulations across return periods and dominance regimes.

3.8 Historical event reconstructions (2007 and 2013)

To establish confidence in the domain configuration and forcing pipeline, we also simulated two historical compound events (June 2007 and December 2013) using observed 15-minute river inflows, rainfall, and coastal water levels. These reconstructions use the same DEM and boundary box definitions as the design-event simulations, with boundary time series taken directly from observations for the corresponding event periods. The historical reconstructions provide an additional check that the modelling setup can reproduce plausible inundation behaviour under real multi-driver forcing, prior to systematic testing of synthetic return-period design events and NbS scenarios.

3.9 Scenario structure, NbS parameterisation, and evaluation (planned)

Baseline simulations are first executed for the full design-event suite. NbS interventions are then represented as scenario modifications affecting one or more of: topography/connectivity (e.g., managed realignment), hydraulic resistance (e.g., saltmarsh/woodland/urban greening), and effective rainfall–runoff response (e.g., peatland restoration, green roofs). Each NbS scenario is run under identical design-event forcing to isolate intervention effects. Evaluation focuses on hazard-based metrics extracted consistently across runs, including maximum inundation depth and inundation extent above a depth threshold, with additional metrics (e.g., duration or velocity) available for extension.

3.10 Uncertainty and sensitivity analysis plan

Sensitivity analyses are planned around event declustering settings, POT threshold selection, event-window length, and phasing assumptions. Additional uncertainty arises from data quality and datum conversion of coastal water levels and from tail extrapolation in POT fitting; these are addressed through quality control of the observational record and threshold sensitivity tests. The design-event generator is structured to facilitate these tests by regenerating design suites under alternative parameter choices and rerunning identical simulation batches.

4 Results and discussion

We established an end-to-end design-event generator for compound flooding that converts multi-driver observations (15-min tide, rainfall, and four river inflows) into SynxFlow-ready design-event time series for batch simulation. After conversion and basic plausibility screening, event-scale coastal peaks fall predominantly within a physically realistic range for the site, and remaining anomalous values were treated as artefacts during extremes fitting via screening/capping.

A historical compound-event catalogue was constructed using a peaks-over-threshold identification and declustering approach, with fixed multi-day windows extracted around each event. For each event we computed peak coastal level (H), peak aggregated inflow (Q) (and per-gauge peaks), rainfall totals/intensities, and the lag between Q and H peaks. This catalogue supports both statistical design modelling (via event peaks) and time-series template selection (via event windows).

Dependence diagnostics show weak peak dependence between coastal and fluvial drivers in the Humber estuary record. Scatter plots (figure 3) of H_{peak} versus $Q_{tot,\,peak}$ coloured by season show a narrow band of coastal peaks (mostly ~3.6–4.3 m ODN) across which river peaks span a wide range (tens to >500 $m^3\ s^{-1}$), and Kendall's τ is close to zero. This indicates that, for this site and event definition, compound hazard is unlikely to be dominated by systematic co-occurrence of the largest coastal and fluvial peaks; instead, phasing/timing and moderately high co-occurring drivers are expected to be key controls. This motivates the design suite structure adopted here (coastal-dominant, fluvial-dominant, balanced) and supports planned extensions to explicitly test

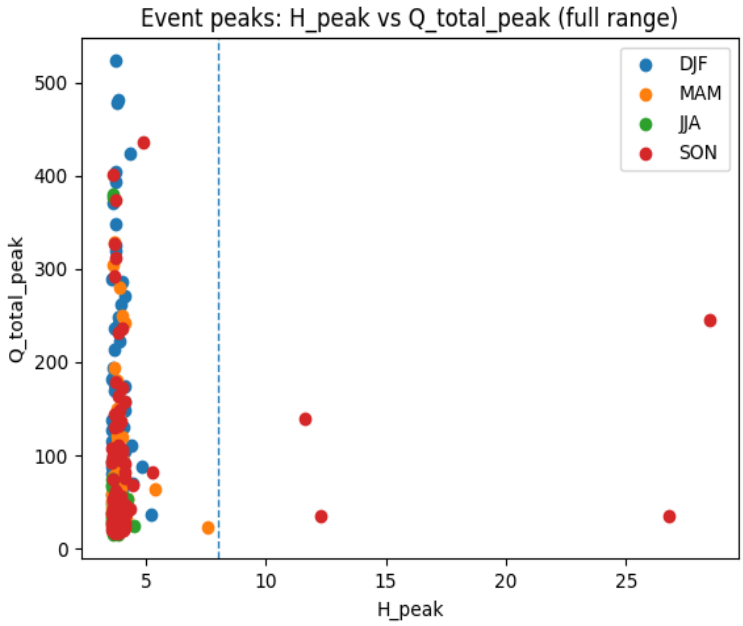

Figure 3. Dependence diagnostics: scatter of H_{peak} versus

lag scenarios.

Using POT/GPD marginals and copula sampling, we generated a compact baseline design suite of return-period peak pairs for five return periods (5, 20, 50, 100, 200 years) with three regimes per return period (coastal-dominant, fluvial-dominant, balanced; 15 events total).

Two historical multi-driver reconstructions were also simulated using observed 15-minute forcing to check the model domain configuration and end-to-end forcing pipeline prior to full NbS evaluation. Ongoing work is now focused on robust extraction and summarisation of maximum inundation depth and inundation extent outputs across all baseline design events, followed by systematic NbS scenario testing under identical forcing. The expected outcome is a set of regime- and severity-dependent NbS performance curves and maps, highlighting where NbS benefits are robust and where effectiveness diminishes under increasingly coastal-controlled compound loading.

5 Conclusions

Compound flooding represents a growing challenge for coastal and estuarine flood risk management. While nature-based solutions offer clear benefits, their performance under compound flood scenarios remains poorly quantified. As well as this, a standardised method to

model compound flood scenarios across different return periods was lacking. This paper presents a process-based modelling framework to address this gap, illustrated through a pilot application to the Humber Estuary. Ongoing work will generate quantitative results to support evidence-based implementation of NbS within integrated flood risk strategies.

References

Bevacqua, E., Maraun, D., Hobæk Haff, I., Widmann, M., & Vrac, M. (2019). Multivariate statistical modelling of compound events via pair-copula constructions: Analysis of floods in Ravenna. *Hydrology and Earth System Sciences*, 23(6), 2701–2723.

Bevacqua, E., Zscheischler, J., & Seneviratne, S. I. (2018). Methods to improve statistical modelling of compound events. *Climatic Change*, 147(1–2), 1–15.

Chebana, F., & Ouarda, T. B. M. J. (2019). Multivariate quantiles in hydrological frequency analysis. *Encyclopedia of Water*, 1–10.

Couasnon, A., Eilander, D., Muis, S., Veldkamp, T. I. E., Haigh, I. D., Wahl, T., & Ward, P. J. (2020). Measuring compound flood potential from river discharge and storm surge extremes at the global scale. *Natural Hazards and Earth System Sciences*, 20(2), 489–504.

Eilander, D., Couasnon, A., Leijnse, T., Ikeuchi, H., Yamazaki, D., Muis, S., Dullaart, J., Haag, A., Winsemius, H.C. & Ward, P.J. (2023). A globally applicable framework for compound flood hazard modeling. Natural Hazards and Earth System Sciences, 23, 823–846.

Ganguli, P., & Merz, B. (2019). Extreme compound flooding in north-western Europe. *Natural Hazards and Earth System Sciences*, 19(9), 1945–1956.

Green, D., Sayers, P., Penning-Rowsell, E., & Ashley, R. (2024). Advancing nature-based solutions for flood risk management: Evidence, challenges and future directions. *Philosophical Transactions of the Royal Society A*, 382, 20230234.

Hallegatte, S., Green, C., Nicholls, R. J., & Corfee-Morlot, J. (2013). Future flood losses in major coastal cities. *Nature Climate Change*, 3(9), 802–806.

Hendry, A., Haigh, I. D., Nicholls, R. J., Winter, H., Neal, R., Wahl, T., Joly-Laugel, A., & Darby, S. E. (2019). Assessing the characteristics and drivers of compound flooding events around the UK coast. *Hydrology and Earth System Sciences*, 23(7), 3117–3139.

Kumbier, K., Carvalho, R. C., Vafeidis, A. T., Woodroffe, C. D., & Karunarathna, H. (2018). The influence of extreme sea levels on coastal flood hazard in Southeast Australia. *Natural Hazards and Earth System Sciences*, 18(3), 875–888.

Lian, J.J., Xu, K. & Ma, C. (2013). Joint impact of rainfall and tidal level on flood risk in a coastal city with a complex river network: a case study of Fuzhou City, China. Hydrology and Earth System Sciences, 17, 679–689.

Liu, Q., Xu, H. & Wang, J. (2022). Assessing tropical cyclone compound flood risk using hydrodynamic modelling: a case study in Haikou City, China. Natural Hazards and Earth System Sciences, 22, 665–675.

Marino, E., Radfar, M., & Castelle, B. (2025). Modelling the performance of nature-based solutions under compound coastal flooding. *Coastal Engineering*, 190, 104482.

Menéndez, P., Losada, I. J., Torres-Ortega, S., Narayan, S., & Beck, M. W. (2020). The global flood protection benefits of mangroves. *Scientific Reports*, 10, 4404.

Moftakhari, H. R., Schubert, J. E., AghaKouchak, A., Matthew, R. A., & Sanders, B. F. (2019). Linking statistical and hydrodynamic modeling for compound flood hazard assessment in tidal channels and estuaries. *Advances in Water Resources*, 128, 28–38.

Narayan, S., Beck, M. W., Reguero, B. G., Losada, I. J., Van Wesenbeeck, B. K., Pontee, N., Sanchirico, J. N., Ingram, J. C., Lange, G.-M., & Burks-Copes, K. A. (2017). The effectiveness, costs and coastal protection benefits of natural and nature-based defences. *PLOS ONE*, 12(5), e0174735.

Paprotny, D., Sebastian, A., Morales-Nápoles, O., & Jonkman, S. N. (2018). Trends in flood losses in Europe over the past 150 years. *Nature Communications*, 9, 1985.

Pasquier, U., He, Y., Hooton, E. W., Gouldby, B., & Panzeri, M. (2019). Coupled 1D–2D hydrodynamic modelling with dynamic linking. *Journal of Flood Risk Management*, 12(S2), e12582.

Radfar, M., Marino, E., Green, D., & Castelle, B. (2024). Assessing nature-based solutions for flood mitigation under compound coastal flooding. *Water Resources Research*, 60(2), e2023WR035214.

Sayers, P., Penning-Rowsell, E., & Horritt, M. (2025). *Flood risk management: Governance, policy and practice*. Routledge.

Seneviratne, S. I., Nicholls, N., Easterling, D., Goodess, C. M., Kanae, S., Kossin, J., Luo, Y., Marengo, J., McInnes, K., Rahimi, M., Reichstein, M., Sorteberg, A., Vera, C., & Zhang, X. (2012). Changes in climate extremes and their impacts on the natural physical environment. *IPCC Special Report on Managing the Risks of Extreme Events and Disasters to Advance Climate Change Adaptation (SREX)*.

Svensson, C., & Jones, D. A. (2002). Dependence between sea surge, river flow and precipitation in south and west Britain. *Hydrology and Earth System Sciences*, 6(6), 973–992.

Ward, P. J., Couasnon, A., Eilander, D., Haigh, I. D., Hendry, A., Muis, S., Veldkamp, T. I. E., Winsemius, H. C., & Wahl, T. (2018). Dependence between high sea-level and high river discharge increases flood hazard in global deltas and estuaries. *Environmental Research Letters*, 13(8), 084012.

Xu, H., Li, Z., Wang, H., & Chen, Y. (2023). Integrated 2D hydrodynamic modelling of compound flooding in estuarine environments. *Journal of Hydrology*, 620, 129373.

Yang, Z., Wang, H., & Xu, Y. (2023). Compound flood hazard under climate change: A review of drivers, impacts, and modelling approaches. *Earth-Science Reviews*, 240, 104378.

Zscheischler, J., Westra, S., van den Hurk, B. J. J. M., Seneviratne, S. I., Ward, P. J., Pitman, A., AghaKouchak, A., Bresch, D. N., Leonard, M., Wahl, T., & Zhang, X. (2018). Future climate risk from compound events. *Nature Climate Change*, 8(6), 469–477.

Geomorphic Controls on Cascading Flood–Landslide Multi-Hazard Susceptibility Revealed by Machine Learning and Explainable AI in a Fragile Biodiversity Hotspot of India

Sabirul Sk[1], Nirul Ranjan Patra[2], Subimal Ghosh[3], Subhankar Karmakar[1, 2]
[1]Centre for Climate Studies, Indian Institute of Technology Bombay, Mumbai 400076, India
[2]Environmental Science and Engineering Department, Indian Institute of Technology Bombay, Mumbai 400076, India
[3]Department of Civil Engineering, Indian Institute of Technology Bombay, Mumbai 400076, India
Email of first and corresponding author: sabirul@iitb.ac.in/ sabirulgis@gmail.com
Email of co-authors: nirul.iiserb@gmail.com; subimalghosh@gmail.com; subhankar.karmakar@gmail.com

Abstract

Floods and landslides frequently co-occur in steep tropical mountain belts, generating cascading hazards that threaten human societies and fragile ecosystems. The Western Ghats (WG) of India, a globally recognised biodiversity hotspot and one of the most monsoon-affected regions in the tropics, are highly susceptible to such compound events. However, the geomorphic controls linking floods and landslides remain poorly quantified at regional scales. Here, we develop the first integrated flood–landslide multi-hazard susceptibility framework for the WG by utilising high-resolution digital elevation model-derived geomorphic descriptors with multi-decadal hazard inventories. Six machine-learning models are evaluated, and an ensemble of XGBoost, LightGBM, and CatBoost yields the highest predictive performance for both hazards. Explainable AI highlighting flood susceptibility (FS) is primarily associated with downslope index, convexity, geomorphic flood index, and overland-flow distance, whereas landslide susceptibility (LS) is strongly influenced by structural lineaments, flow accumulation, stream power, and plan curvature. Spatial analysis reveals distinct regional hotspots where geomorphic conditions promote the co-occurrence of floods and landslides across parts of Maharashtra, Kerala, and Karnataka states. Extreme rainfall analysis further identifies the IMD-defined very heavy rainfall threshold (115.6 mm day^{-1}) as a critical trigger beyond which cascading hazard intensity increases sharply. Overall, the results demonstrate that geomorphology provides a robust predictive template for cascading flood–landslide hazards and underscore the importance of terrain-informed early-warning systems and sustainable land-use planning in fragile mountain regions.

Keywords: Digital elevation model, flood susceptibility, geomorphic descriptors, landslide susceptibility, machine learning, multi-hazard, Western Ghats

1 INTRODUCTION

Extreme precipitation in mountainous regions frequently triggers cascading hydrogeomorphic hazards, including landslides and flooding (Acosta-Quesada and Quesada-Román, 2024; Deijns et al., 2024; Mani et al., 2023). These processes are tightly coupled: intense rainfall, steep slopes, saturated soils, and confined channels interact to amplify impacts beyond those of individual hazards (Kappes et al., 2012; Kharismalatri et al., 2025; Leonard et al., 2014). Under climate change, increasing rainfall intensity in tropical mountain belts is expected to intensify such compound events (Encalada et al., 2019).

The geomorphic response of mountain catchments is governed by terrain configuration, lithology, structural discontinuities, and sediment connectivity (Mani et al., 2023). These controls regulate whether rainfall generates slope failure, rapid runoff and flooding, or coupled flood–landslide cascades (Arango-Carmona et al., 2025; Croissant et al., 2017; Fan et al., 2025; Zhang et al., 2024). In humid tropical mountains, strong hillslope–channel connectivity promotes sediment delivery that alters channel morphology, while flood undercutting destabilises saturated slopes (Rusk et al., 2022). Despite their significance, regional-scale quantification of these geomorphic–hydrological linkages remains limited.

The Western Ghats (WG) of India represent a highly susceptible monsoon-dominated escarpment (Encalada et al., 2019). The 2018 Kerala disaster illustrated the coupled nature of flood–landslide processes under prolonged extreme rainfall (Hao et al., 2020; Tripathy et al., 2020). However, most regional assessments treat floods and landslides independently, overlooking shared terrain controls.

Recent advances in machine learning (ML) and deep learning (DL) offer new opportunities to characterise such complex, nonlinear hazard systems (Liu et al., 2025; Luo et al., 2025; Rusk et al., 2022). ML models have shown strong predictive skill for individual hazards, including floods and landslides (Deijns et al., 2024; Deroliya et al., 2022; Ibebuchi and Abu, 2025), while DL approaches can capture latent spatial patterns and interactions among geomorphic and hydrological variables (Pourghasemi et al., 2020; Tiggeloven et al., 2025; Ullah et al., 2022; Wang et al., 2020; Youssef et al., 2023). However, ML- and DL-based multi-hazard susceptibility assessments remain limited, particularly in monsoon-dominated mountain belts where compound flood–landslide processes are frequent and highly damaging.

Here, we develop a geomorphologically informed multi-hazard susceptibility framework for the WG. Specifically, we: (i) derive DEM-based geomorphic drivers conditioning both hazards; (ii) model flood and landslide susceptibility using ML; (iii) integrate outputs to map compound hotspots; and (iv) evaluate rainfall exceedance thresholds activating cascading hazard zones. This study links terrain configuration with rainfall forcing to improve terrain-informed risk assessment in humid tropical mountains.

2 STUDY AREA AND DATA

2.1 Study Area

The Western Ghats (WG), also known as the Sahyadri Mountains, form a 1,600 km orographic escarpment along India's southwest coast (8°–21°N) (Encalada et al., 2019). Elevations exceed 2,500 m, generating strong monsoon–orographic interactions (Fig.1). Steep slopes, deep valley incision, and structurally weakened bedrock contribute to recurrent floods, landslides, and cascading hazard interactions (Das, 2020).

.

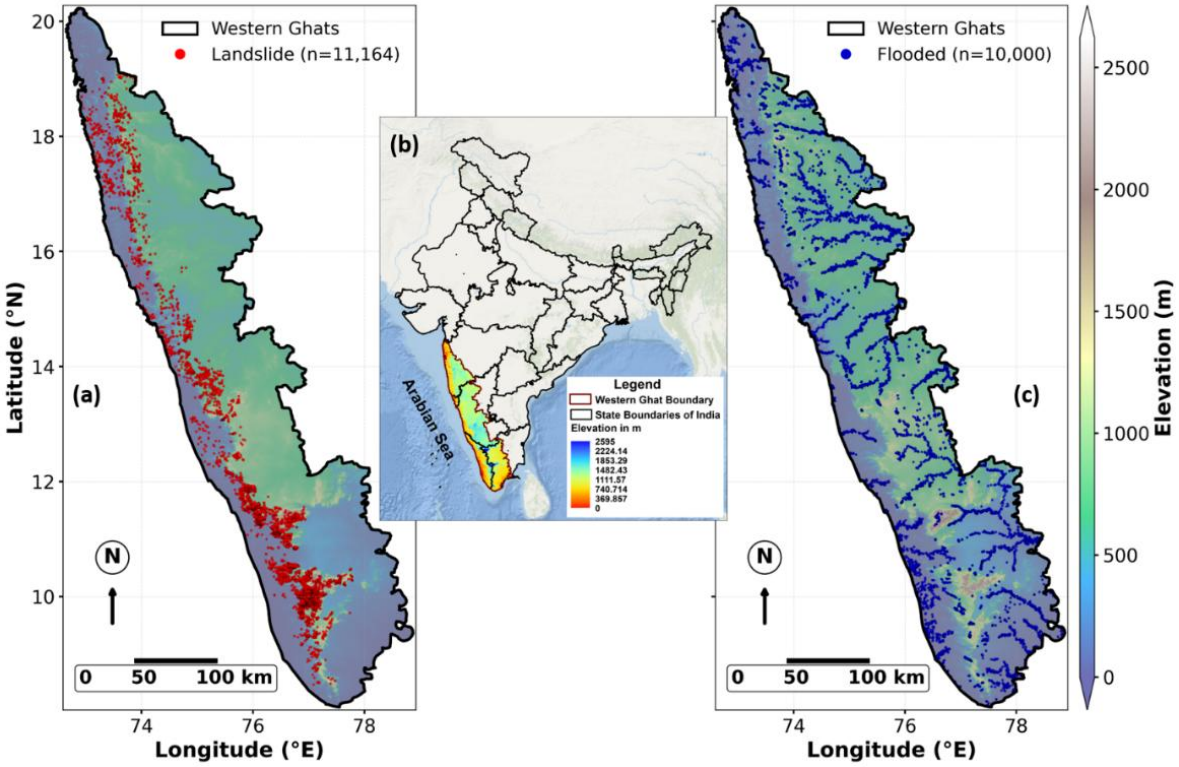

Figure 1. Location map of the Western Ghats (WG) mountain range and the spatial distribution of observed hazards. (a) Elevation map of the WG overlaid with documented landslide occurrences (n = 11,164) obtained from the Geological Survey of India. (b) Regional context map showing the position of the Western Ghats along the western margin of India, spanning the states of Maharashtra, Goa, Karnataka, Kerala, and Tamil Nadu. (c) Elevation map overlaid with observed flood-affected locations (n = 10,000), illustrating the distribution of recent flood impacts across the WG.

2.2 Data

2.2.1 Geomorphic and Geological Data

We derived a suite of geomorphic descriptors from the 90-m hydrologically corrected Shuttle Radar Topography Mission (SRTM) DEM, including slope, relief, curvature, LS factor, topographic wetness index, flow accumulation, multi-resolution valley bottom flatness, valley depth, ridge–valley distance, and terrain ruggedness. These metrics capture hydrologic convergence, slope stability, and geomorphic confinement, which are relevant to both flood and landslide processes (Bernard et al., 2022; Deroliya et al., 2022; Luo et al., 2025; Pourghasemi et al., 2020; Rusk et al., 2022; Ullah et al., 2022; Youssef et al., 2023). Geological and structural datasets from the Geological Survey of India (GSI; https://bhukosh.gsi.gov.in/Bhukosh) were integrated, including lithology, faults, thrusts, lineaments, and regolith units. All vector layers were rasterised to 90-m resolution. Distance-to-fault and lineament-density surfaces were computed to represent structural weakening.

2.2.2 Hazard Inventories

Flood occurrence was derived from the Global Flood Database (2000–2018) (https://global-flood-database.cloudtostreet.ai/), generating a binary presence–absence layer. Landslide inventories (2010–2021) were compiled from NRSC and GSI datasets and rasterised to 90 m resolution.

3 METHODS

Figure 2 shows the overall methodological workflow adopted in this study, outlining the complete sequence from data acquisition and pre-processing to predictor selection, ML model development, and susceptibility map generation. The framework integrates multi-source geospatial datasets, DEM-derived geomorphic descriptors, geological and structural information, and long-term hazard inventories to produce high-resolution flood and landslide susceptibility models for the WG. The major components of the methodology are described below.

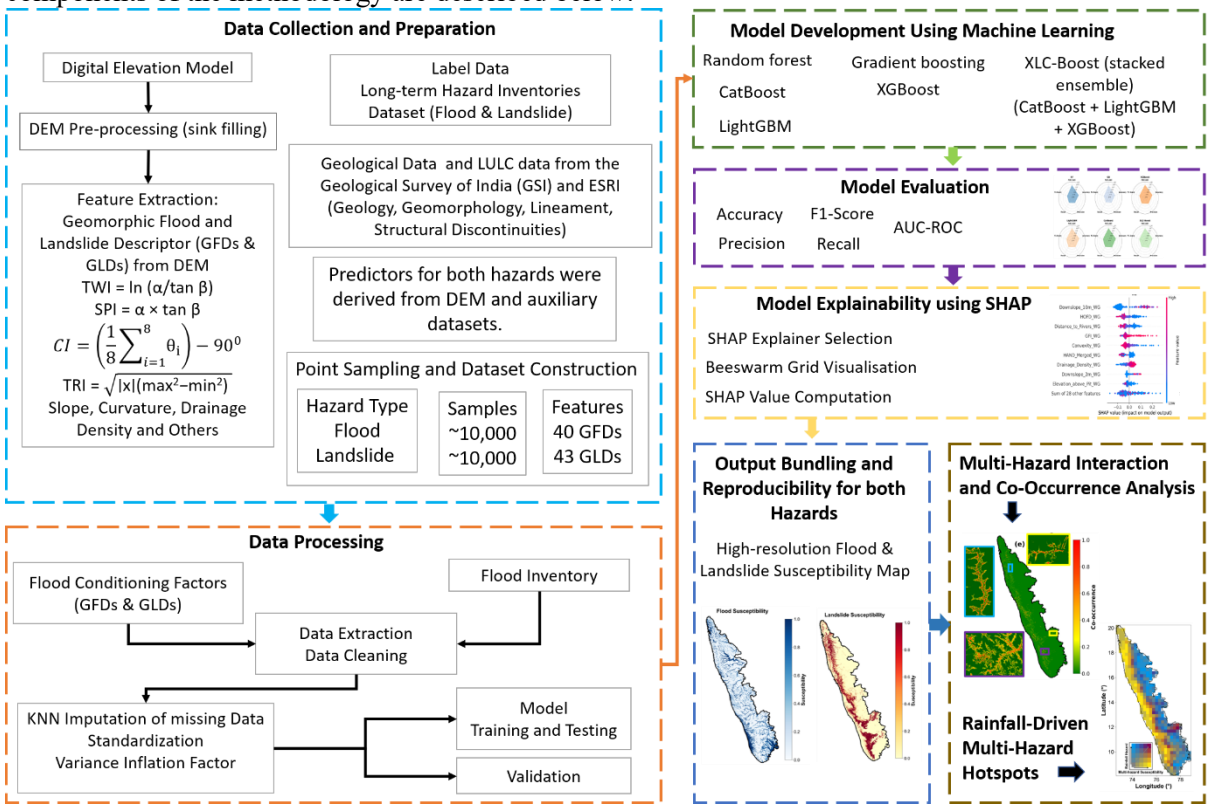

Figure 2. Overall methodological workflow for developing flood and landslide susceptibility models in the WG. The framework integrates multi-source geospatial datasets, geomorphic conditioning factors, long-term hazard inventories, and ML modelling to derive high-resolution susceptibility maps.

Predictor Selection and Multicollinearity Assessment

To reduce redundancy and avoid unstable model behaviour, we quantified multicollinearity among predictors using the Variance Inflation Factor (VIF) (Deroliya et al., 2022; Mansfield and Helms, 1982):

$$VIF = \frac{1}{1-R_i^2} \quad (1)$$

where R_i^2 is the coefficient of determination when predictor i is regressed against all other predictors. Higher VIF values indicate stronger collinearity, which can inflate model variance and distort the relative influence of predictors. A threshold of VIF < 2 was applied for landslides and VIF < 5 for floods. After iterative filtering, 33 flood predictors and 29 landslide predictors were retained (Fg.3).

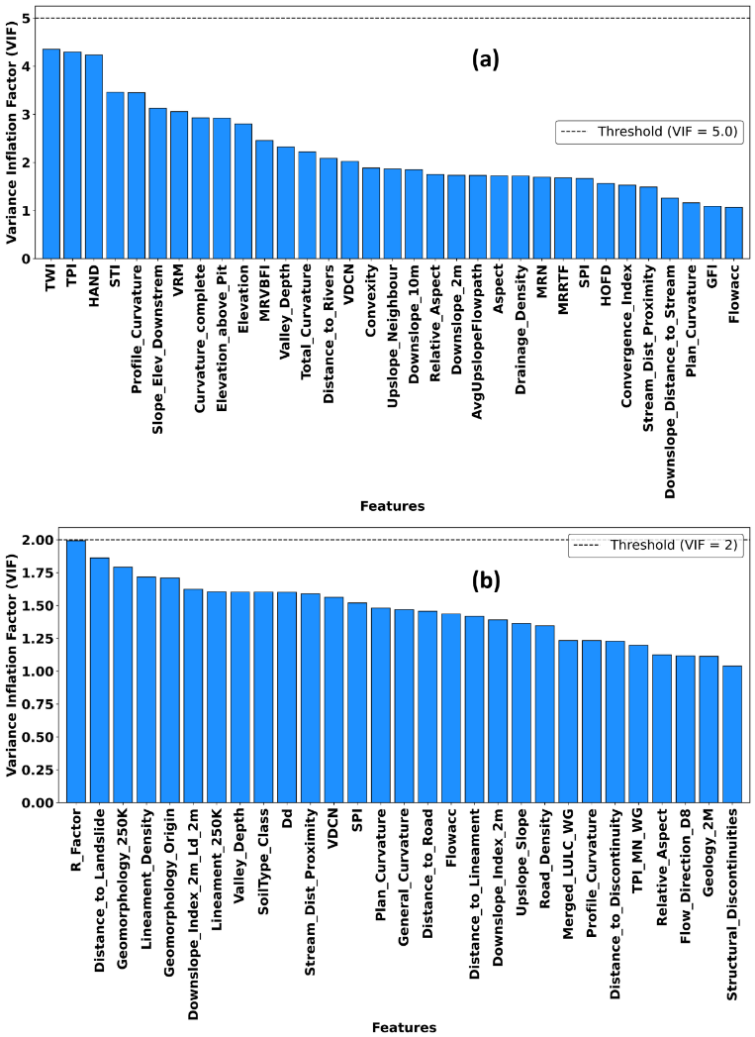

Figure 3. Variance Inflation Factor (VIF) analysis for flood (a) and landslide (b) geomorphic drivers. For the flood dataset, 40 initial predictors were screened using a VIF threshold of 5, resulting in a reduced set of 33 non-collinear variables. For the landslide dataset, 43 geomorphic and geological drivers were evaluated using a stricter VIF threshold of 2, yielding 29 retained indicators. Dashed horizontal lines denote the respective VIF thresholds.

Machine-Learning-Based Susceptibility Modelling

Flood and landslide susceptibility were modelled independently using Random Forest, Gradient Boosting, XGBoost, LightGBM, CatBoost, and a soft-voting ensemble (XLC-Boost) (Murphy, 2013; Waleed and Sajjad, 2025). Spatially balanced sampling and a 70/30 spatially stratified train–test split were applied (Rusk et al., 2022). The ensemble susceptibility was computed as:

$$S_{ensemble} = \frac{S_{Cat} + S_{XGB} + S_{LGBM}}{3} \quad (2)$$

where S_{Cat}, S_{XGB}, and S_{LGBM} denote the susceptibility scores estimated by the CatBoost, XGBoost, and LightGBM models, respectively, each representing the model-estimated probability of a location being susceptible to the corresponding hazard. Model performance was evaluated using the area under the receiver operating characteristic curve (ROC–AUC) and confusion-matrix-based metrics.

Multi-Hazard Susceptibility

To characterise cascading or concurrent hazard potential, we combined flood susceptibility (FS) and landslide susceptibility (LS) using three formulations:

$$MH_{mean} = (LS + FS)/2 \quad (3)$$

$$MH_{max} = \max(LS, FS) \quad (4)$$

$$MH_{prod} = LS \times FS \quad (5)$$

The product index (MH_{prod}) highlights areas where both hazards co-occur with high intensity, a diagnostic for cascading hazard pathways.

Rainfall Data and Exceedance Analysis

Daily India Meteorological Department (IMD) rainfall (1982–2021) was used to compute the exceedance probability of Very Heavy Rainfall (≥115.6 mm/day) (IMD, 2021; Pai et al., 2014). Exceedance probability was calculated as the proportion of days exceeding this threshold. A bivariate choropleth was constructed by jointly mapping rainfall exceedance probability and multi-hazard susceptibility to identify rainfall–terrain activation zones.

4 RESULTS

Model Performance

All machine learning algorithms demonstrated strong predictive performance for both flood and landslide susceptibility (Fig. 4). For floods, XLC-Boost achieved the highest discrimination (AUC = 0.945), followed closely by XGBoost (0.943), CatBoost (0.943), and LightGBM (0.941). Random Forest (0.929) and Gradient Boosting (0.924) showed slightly lower but robust performance. For landslides, performance was higher overall, with XLC-Boost achieving an AUC of 0.988 and all boosting-based models exceeding 0.98. Random Forest and Gradient Boosting achieved AUC values of 0.984 and 0.981. These results indicate strong and stable classification across hazards under spatial validation.

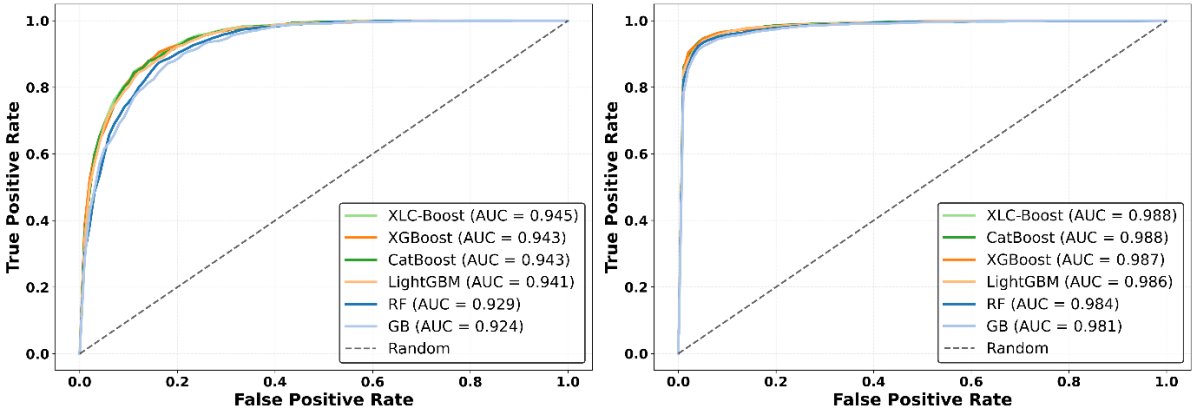

Figure 4. Receiver Operating Characteristic (ROC) curves showing the predictive performance of six machine learning algorithms for flood susceptibility (left) and landslide susceptibility (right) in the Western Ghats. Boosting-based models demonstrate the highest discrimination ability, with XLC-Boost achieving the best performance for floods (AUC = 0.945) and landslides (AUC ≈ 0.988). Random Forest and Gradient Boosting show slightly lower but still strong predictive skill. The dashed line represents random classification.

Flood and Landslide Susceptibility Patterns

The flood and landslide models reveal distinct yet complementary spatial patterns (Fig. 5). Landslide susceptibility concentrates along steep escarpments, deeply incised valleys, and structurally weakened

bedrock, particularly in Idukki, Wayanad, central Kerala, and interior Karnataka (Fig. 5a). In contrast, flood susceptibility highlights hydrologically convergent valleys and low-relief basin floors, with pronounced hotspots in Alappuzha, Thrissur, Ernakulam, and river floodplains of Maharashtra (Fig. 5b). These contrasting patterns reflect the different geomorphic settings predisposing the landscape to each hazard.

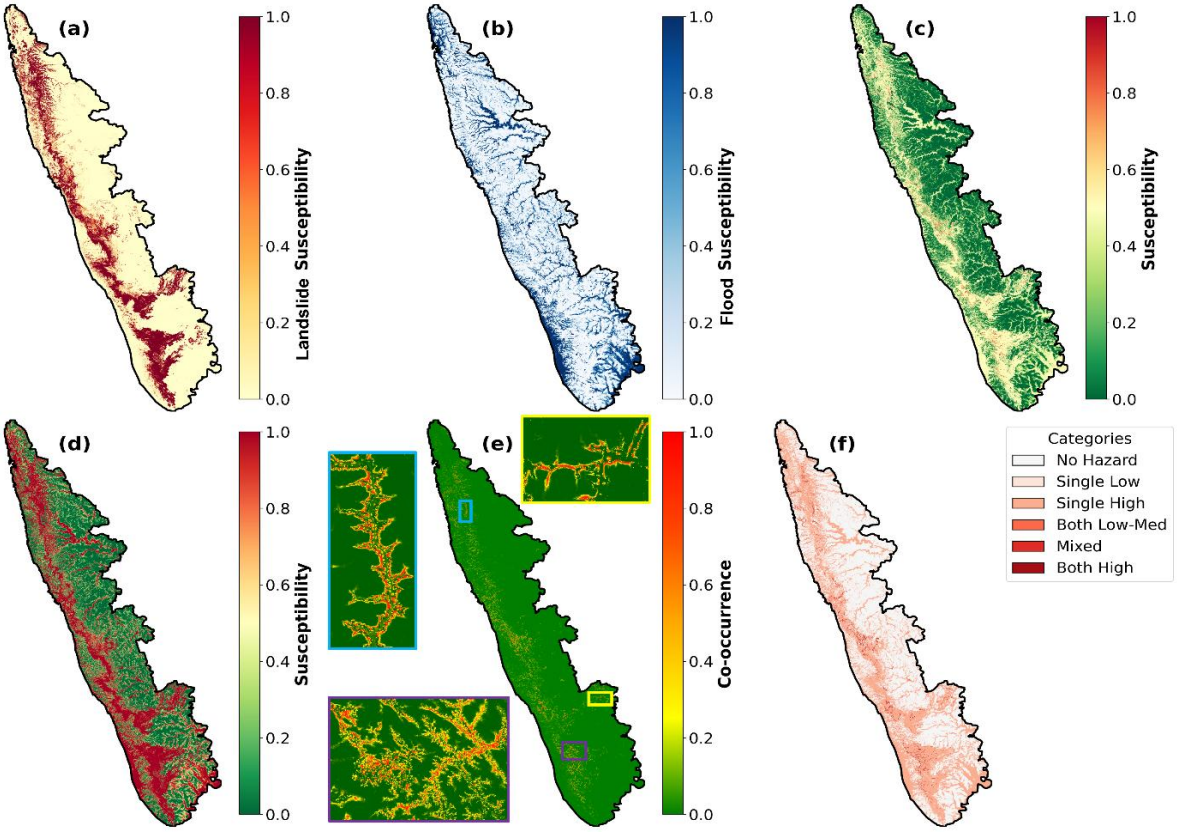

Figure 5. Flood, landslide, and multi-hazard susceptibility across the Western Ghats. (a) & (b) Landslide and flood susceptibility map derived from high-resolution geomorphic and geological descriptors. (c) Mean multi-hazard surface showing areas where both hazards maintain moderate–high susceptibility. (d) Maximum hazard envelope representing the dominant hazard at each pixel. (e) Multiplicative co-occurrence index highlighting zones where flood and landslide susceptibility simultaneously intensify; insets show fine-scale channel–hillslope coupling. (f) Categorical multi-hazard classification delineating six compound hazard states ranging from no hazard to "both high." Together, these panels identify spatial hotspots where steep slopes, structural discontinuities, and concentrated monsoon runoff interact to produce cascading multi-hazard risk.

Multi-Hazard Co-occurrence and Cascading Hotspots

Multi-hazard metrics reveal clear spatial interaction between floods and landslides. The mean surface (Fig. 5c) identifies regions where moderate-to-high susceptibility overlaps, particularly along hillslope–channel interfaces. The multiplicative co-occurrence index (Fig. 5e) isolates cascading hotspots in Idukki, parts of Wayanad, northern Kerala, and the high-relief belts of Karnataka. These zones align with areas where steep slopes intersect confined drainage networks, indicating strong terrain-driven coupling. The categorical classification (Fig. 5f) shows that "Both High" zones are spatially restricted to regions combining extreme relief, structural discontinuities, and concentrated runoff, confirming that geomorphology governs cascading hazard amplification.

Geomorphic Controls and Rainfall Triggering of Cascading Hazards

SHapley Additive exPlanations (SHAP) demonstrates contrasting controls for each hazard (Fig. 6). Flood susceptibility is dominated by hydrologic convergence metrics (downslope index, drainage density, geomorphic flood index), whereas landslides are strongly influenced by slope steepness, rainfall erosivity, curvature, and structural indicators. The consistency of dominant predictors across algorithms confirms robust geomorphic control.

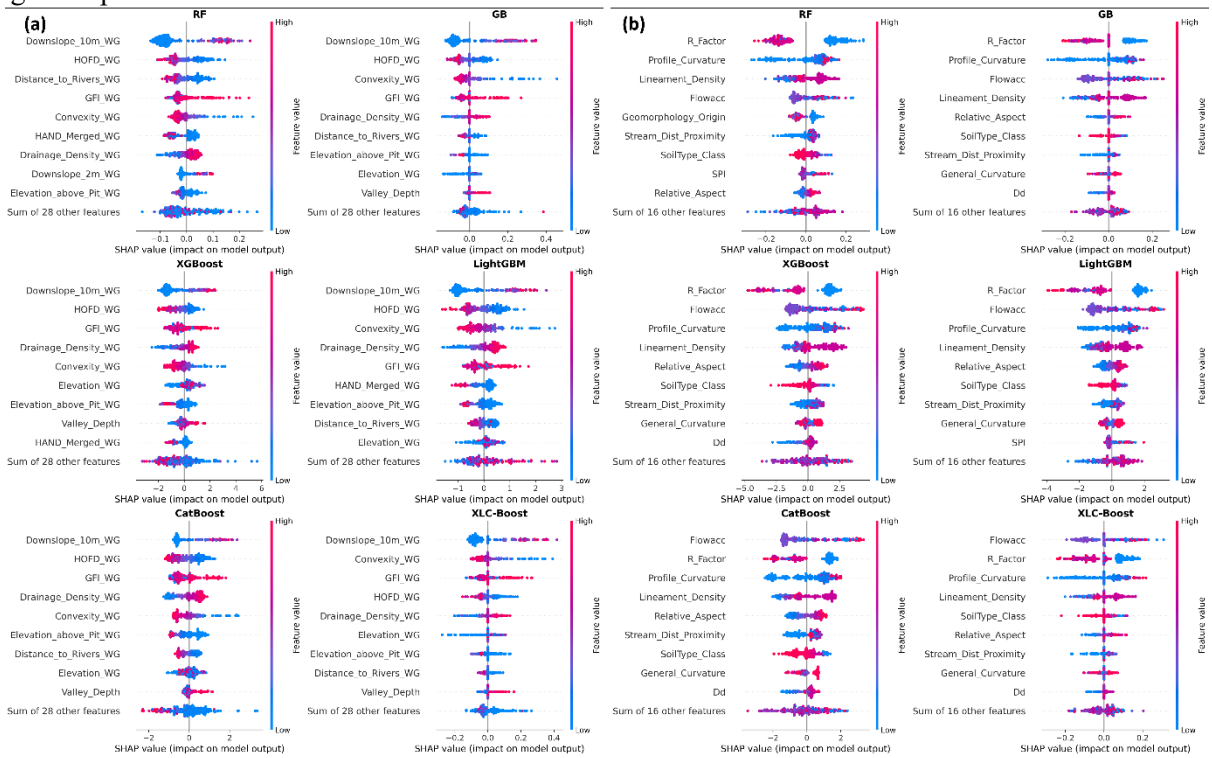

Figure 6. SHAP-based feature importance for flood (a) and landslide (b) susceptibility models across six machine-learning algorithms.

Extreme rainfall analysis identifies 115.6 mm/day (IMD “very heavy rainfall”) as a critical activation threshold. The bivariate rainfall–multi-hazard map (Fig. 7) shows strong spatial coupling between high rainfall exceedance and elevated multi-hazard susceptibility, particularly in the southern and central Western Ghats. Areas with low rainfall exceedance correspond to predominantly low multi-hazard intensity, indicating that extreme rainfall acts as a climatic trigger superimposed on terrain predisposition.

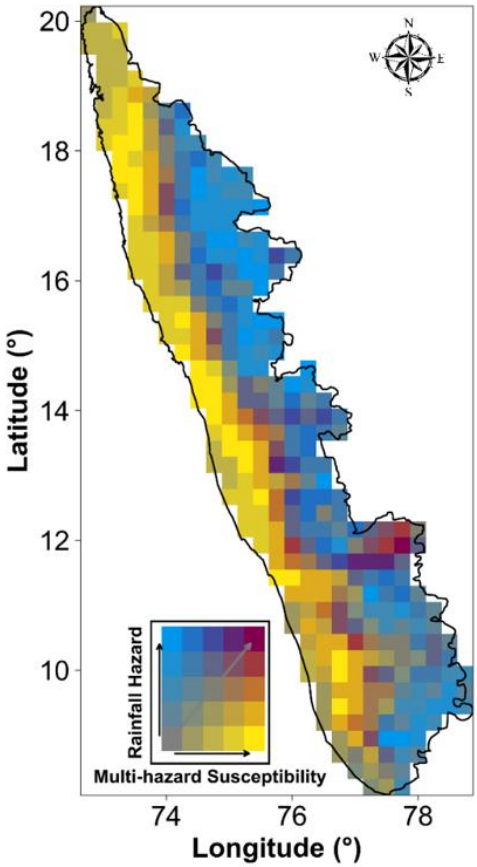

Figure 7. Bivariate rainfall–multi-hazard map for the Western Ghats. The 2D colour space shows how multi-hazard susceptibility varies with increasing rainfall hazard. Warmer colours indicate areas where very heavy rainfall coincides with high flood–landslide susceptibility, highlighting climatically triggered multi-hazard hotspots across southern and central Western Ghats.

5 DISCUSSION

This study shows that cascading flood–landslide hazards in the Western Ghats arise from the spatial alignment of geomorphic predisposition and extreme monsoon rainfall. Steep slopes, valley incision, and litho-structural discontinuities promote landsliding (Youssef et al., 2023; Zhang et al., 2024), while hydrologic convergence and drainage confinement enhance flood susceptibility (Das, 2020; Deroliya et al., 2022). Where these controls overlap, particularly along hillslope–channel interfaces, distinct multi-hazard hotspots emerge across Idukki, Wayanad, and the central escarpment.

SHAP-based analysis reveals contrasting yet complementary controls: floods are primarily governed by flow routing and accumulation (Ibebuchi and Abu, 2025; Li et al., 2025; Waleed and Sajjad, 2025), whereas landslides respond strongly to slope steepness and structural weakening (Liu et al., 2025; Pradhan et al., 2023; Youssef et al., 2023). Their interaction is intensified where steep terrain directly connects to hydrologically active channels, facilitating cascading processes.

Extreme rainfall acts as a nonlinear trigger superimposed on terrain susceptibility. Exceedance of the IMD very heavy rainfall threshold (115.6 mm/day) corresponds to a sharp increase in multi-hazard intensity, consistent with observations from the 2018 Kerala event (Hao et al., 2020; Tripathy et al., 2020). . These findings indicate that extreme rainfall preferentially activates hazards in geomorphically predisposed terrain rather than uniformly across the landscape.

Despite the strong predictive performance, some uncertainties remain. Flood and landslide inventories may contain spatial incompleteness, particularly in remote mountainous areas. In addition,

susceptibility modelling primarily relies on static geomorphic predictors, while dynamic factors such as antecedent rainfall and soil moisture were not explicitly considered. Although spatial cross-validation was used to reduce spatial bias, uncertainty related to DEM resolution and predictor scale may persist. Future work could incorporate higher-resolution terrain data and event-based rainfall information to further improve model reliability.

6 CONCLUSIONS

This study develops an integrated flood–landslide susceptibility framework for the Western Ghats, demonstrating that cascading hazards are governed by the interaction between terrain configuration and extreme rainfall thresholds. Floods and landslides are controlled by distinct but spatially complementary geomorphic drivers, and their co-occurrence intensifies in zones of strong hillslope–channel coupling. By incorporating persistent geomorphic controls into a multi-hazard framework, this approach provides a robust basis for identifying terrain prone to cascading impacts under extreme monsoon events. The methodology offers a transferable foundation for terrain-informed early warning and climate-resilient hazard planning in tropical mountain regions.

ACKNOWLEDGEMENTS

This research was supported by the Department of Science and Technology (DST), Government of India, under the SPLICE–Climate Change Programme (DST/CCP/CoE/140/2018), and by the Green Energy and Sustainability Research Hub (GESH), IIT Bombay (DO/2024-RHUB004-003; Grant No. 0000000000050004495). IIT Bombay provided computational facilities for this study. We acknowledge the India Meteorological Department (IMD) for rainfall datasets and the Geological Survey of India (GSI) for geological and landslide data. Additional geospatial resources were obtained from the Survey of India (SOI) and ESRI.

References

Acosta-Quesada, M., Quesada-Román, A., 2024. Landslides and flood hazard mapping using geomorphological methods in Santa Ana, Costa Rica. International Journal of Disaster Risk Reduction 113, 104882. https://doi.org/10.1016/j.ijdrr.2024.104882

Arango-Carmona, M.I., Voit, P., Hürlimann, M., Aristizábal, E., Korup, O., 2025. Hillslope-Torrential Hazard Cascades in Tropical Mountains. https://doi.org/10.5194/egusphere-2025-1698

Bernard, T.G., Davy, P., Lague, D., 2022. Hydro-Geomorphic Metrics for High Resolution Fluvial Landscape Analysis. JGR Earth Surface 127, e2021JF006535. https://doi.org/10.1029/2021JF006535

Croissant, T., Lague, D., Steer, P., Davy, P., 2017. Rapid post-seismic landslide evacuation boosted by dynamic river width. Nature Geosci 10, 680–684. https://doi.org/10.1038/ngeo3005

Das, S., 2020. Flood susceptibility mapping of the Western Ghat coastal belt using multi-source geospatial data and analytical hierarchy process (AHP). Remote Sensing Applications: Society and Environment 20, 100379. https://doi.org/10.1016/j.rsase.2020.100379

Deijns, A.A.J., Michéa, D., Déprez, A., Malet, J.-P., Kervyn, F., Thiery, W., Dewitte, O., 2024. A semi-supervised multi-temporal landslide and flash flood event detection methodology for unexplored regions using massive satellite image time series. ISPRS Journal of Photogrammetry and Remote Sensing 215, 400–418. https://doi.org/10.1016/j.isprsjprs.2024.07.010

Deroliya, P., Ghosh, M., Mohanty, M.P., Ghosh, S., Rao, K.H.V.D., Karmakar, S., 2022. A novel flood risk mapping approach with machine learning considering geomorphic and socio-economic vulnerability dimensions. Science of The Total Environment 851, 158002. https://doi.org/10.1016/j.scitotenv.2022.158002

Encalada, A.C., Flecker, A.S., Poff, N.L., Suárez, E., Herrera-R, G.A., Ríos-Touma, B., Jumani, S., Larson, E.I., Anderson, E.P., 2019. A global perspective on tropical montane rivers. Science 365, 1124–1129. https://doi.org/10.1126/science.aax1682

Fan, X., Bhuyan, K., Wang, X., Cook, K.L., Ozturk, U., Loew, S., Gyamtsho, P., Jansen, J.D., Xu, Q., 2025. Rethinking policy on high mountain cascading hazards. Nat. Geosci. 18, 1066–1067. https://doi.org/10.1038/s41561-025-01834-w

Hao, L., Rajaneesh A., Van Westen, C., Sajinkumar K. S., Martha, T.R., Jaiswal, P., McAdoo, B.G., 2020. Constructing a complete landslide inventory dataset for the 2018 monsoon disaster in Kerala, India, for land use change analysis. Earth Syst. Sci. Data 12, 2899–2918. https://doi.org/10.5194/essd-12-2899-2020

Ibebuchi, C.C., Abu, I.-O., 2025. Probabilistic flood susceptibility mapping using explainable AI for the Western United States. Environ. Res. Commun. 7, 105008. https://doi.org/10.1088/2515-7620/ae0c5c

IMD, 2021, 2021. Standard operation procedure: weather forecasting and warning services.

Kappes, M.S., Keiler, M., Von Elverfeldt, K., Glade, T., 2012. Challenges of analyzing multi-hazard risk: a review. Nat Hazards 64, 1925–1958. https://doi.org/10.1007/s11069-012-0294-2

Kharismalatri, H.S., Gomi, T., Sidle, R.C., 2025. Geomorphic thresholds for cascading hazards of debris flows and natural dam formation caused by large landslides. Nat Hazards 121, 15537–15552. https://doi.org/10.1007/s11069-025-07402-0

Leonard, M., Westra, S., Phatak, A., Lambert, M., Van Den Hurk, B., McInnes, K., Risbey, J., Schuster, S., Jakob, D., Stafford-Smith, M., 2014. A compound event framework for understanding extreme impacts. WIREs Climate Change 5, 113–128. https://doi.org/10.1002/wcc.252

Li, K., Guo, L., Wang, G., Gao, J., Ma, J., Li, J., Huang, P., Zhai, B., Sun, X., 2025. A novel hybrid framework of high-resolution flood susceptibility mapping in ungauged mountainous regions. Weather and Climate Extremes 50, 100822. https://doi.org/10.1016/j.wace.2025.100822

Liu, L.-L., Duan, C., Gao, J.-H., Xiao, H., Zhu, W.-Q., Yang, C., 2025. Landslide susceptibility assessment using machine learning with a novel SHAP-based sampling strategy. Geoscience Frontiers 102188. https://doi.org/10.1016/j.gsf.2025.102188

Luo, W., Qiu, H., Wei, Y., Huangfu, W., Yang, D., 2025. A proposed method for landslide detection based on transfer learning and graph neural network. Geoscience Frontiers 16, 102171. https://doi.org/10.1016/j.gsf.2025.102171

Mani, P., Allen, S., Evans, S.G., Kargel, J.S., Mergili, M., Petrakov, D., Stoffel, M., 2023. Geomorphic Process Chains in High-Mountain Regions—A Review and Classification Approach for Natural Hazards Assessment. Reviews of Geophysics 61, e2022RG000791. https://doi.org/10.1029/2022RG000791

Mansfield, E.R., Helms, B.P., 1982. Detecting Multicollinearity. The American Statistician 36, 158–160. https://doi.org/10.1080/00031305.1982.10482818

Murphy, K.P., 2013. Machine learning: a probabilistic perspective, 4. print. (fixed many typos). ed, Adaptive computation and machine learning series. MIT Press, Cambridge, Mass.

Pai, D.S., Rajeevan, M., Sreejith, O.P., Mukhopadhyay, B., Satbha, N.S., 2014. Development of a new high spatial resolution (0.25° × 0.25°) long period (1901-2010) daily gridded rainfall data set over India and its comparison with existing data sets over the region. MAUSAM 65, 1–18. https://doi.org/10.54302/mausam.v65i1.851

Pourghasemi, H.R., Kariminejad, N., Amiri, M., Edalat, M., Zarafshar, M., Blaschke, T., Cerda, A., 2020. Assessing and mapping multi-hazard risk susceptibility using a machine learning technique. Sci Rep 10, 3203. https://doi.org/10.1038/s41598-020-60191-3

Pradhan, B., Dikshit, A., Lee, S., Kim, H., 2023. An explainable AI (XAI) model for landslide susceptibility modeling. Applied Soft Computing 142, 110324. https://doi.org/10.1016/j.asoc.2023.110324

Rusk, J., Maharjan, A., Tiwari, P., Chen, T.-H.K., Shneiderman, S., Turin, M., Seto, K.C., 2022. Multi-hazard susceptibility and exposure assessment of the Hindu Kush Himalaya. Science of The Total Environment 804, 150039. https://doi.org/10.1016/j.scitotenv.2021.150039

Tiggeloven, T., Ferrario, D.M., Claassen, J.N., Jäger, W.S., Shapovalova, Y., Koyama, M., De Ruiter, M.C., Daniell, J.E., Torresan, S., Ward, P.J., 2025. A Global Approach for Mapping Multi-Hazard Susceptibility Using Deep Learning: A Case Study in Japan. Artificial Intelligence for the Earth Systems 4, 250039. https://doi.org/10.1175/AIES-D-25-0039.1

Tripathy, S.S., Vittal, H., Karmakar, S., Ghosh, S., 2020. Flood risk forecasting at weather to medium range incorporating weather model, topography, socio-economic information and land use exposure. Advances in Water Resources 146, 103785. https://doi.org/10.1016/j.advwatres.2020.103785

Ullah, K., Wang, Y., Fang, Z., Wang, L., Rahman, M., 2022. Multi-hazard susceptibility mapping based on Convolutional Neural Networks. Geoscience Frontiers 13, 101425. https://doi.org/10.1016/j.gsf.2022.101425

Waleed, M., Sajjad, M., 2025. Advancing flood susceptibility prediction: A comparative assessment and scalability analysis of machine learning algorithms via artificial intelligence in high-risk regions of Pakistan. J Flood Risk Management 18, e13047. https://doi.org/10.1111/jfr3.13047

Wang, Y., Fang, Z., Hong, H., Peng, L., 2020. Flood susceptibility mapping using convolutional neural network frameworks. Journal of Hydrology 582, 124482. https://doi.org/10.1016/j.jhydrol.2019.124482

Youssef, K., Shao, K., Moon, S., Bouchard, L.-S., 2023. Landslide susceptibility modeling by interpretable neural network. Commun Earth Environ 4, 162. https://doi.org/10.1038/s43247-023-00806-5

Zhang, Z., Liu, M., Tan, Y.J., Walter, F., He, S., Chmiel, M., Su, J., 2024. Landslide hazard cascades can trigger earthquakes. Nat Commun 15, 2878. https://doi.org/10.1038/s41467-024-47130-w

ICFM 10
Adapting to Global Change:
Innovative Approaches to Flood Management and Resilience
May 20-22, 2026 | Western University, London, Ontario, Canada

An Innovative Camera-based Flow Monitoring and Flood Early Warning System

Issa Hansen[1], Salvador Peña-Haro[2] and Beat Lüthi[2]

[1]SEBA Hydrometrie GmbH & Co. KG, Gewerbestr. 61A, 87600 Kaufbeuren, Germany
[2]Photrack AG, Ankerstr. 16a, 8004 Zurich, Switzerland

Contact: Dr. Issa Hansen
e-mail: hansen@seba.de
Phone: +49 (0) 834196480
Fax: +49 (0) 8341964848

Abstract

Particularly during extreme events, precise knowledge of the discharges in flowing waters is of great and decisive interest. Conventional measurement methods, however, reach their limits precisely then, as they often rely on a sensor that is not contactless. Image-based flow measurement systems offer a flexible non-intrusive alternative with real time measurement. Unlike conventional measurement methods, the ratio of measurement signal to measurement noise is optimal for extreme events. In the present paper, two extreme flood events are presented, which occurred under completely different conditions. A camera-based discharge system (DischargeKeeper) is permanently installed in northern Spain on the northern slopes of the Pyrenees. In November 2021, an event with a 500-year return period was recorded there. Most of the conventional measuring systems installed at this station were destroyed during the flood event but the camera-based system remained intact because it could be mounted on the side of the cross-section far enough away from the flood water. The measured discharge at the flood peak was 980 m^3/s.
The second case study is about an event in a wadi in the United Arab Emirates (UAE). Wadis are completely dry during most of the time. However, flash floods must then be expected during the very rare but equally heavy rainfall. In April 2021, a DischargeKeeper system was installed in Wadi Naqab in the northern UAE. The wadi is about 100m wide and was completely dry for two years. In January 2022, a first such event was recorded. Within 15 minutes, the flow increased from 0 m^3/s to 78 m^3/s.
The specific requirements and challenges in such extreme flood situations are presented in this paper.

1. Introduction

Real-time flood monitoring is becoming more and more important in recent years. Reliable river water level and discharge data are crucial for flood monitoring and for the design of flood protection measures. However, discharge measurements during flood events are difficult to obtain resulting in a lack of data during those events. Many discharge measuring systems with different measuring principles can be implemented for this purpose. However conventional discharge systems must be installed within the stream cross-section or on a bridge above the water surface. Therefore, these systems are mostly impaired or fail completely during flood events.

In the last years several image-based methods were developed and have been successfully applied to a variety of situations. (Fujita et al., 1998; Hauet et al., 2008; Muste et al., 2008; Dramais et al., 2011). In recent years, camera-based technologies for water level, velocity and discharge measurements have become very robust (Peña-Haro et al., 2021). Image velocimetry showed clear advantages against conventional systems for flow measurement under high flow conditions (Jodeau et al., 2008; Le Coz et al., 2010; Fujita and Kunita, 2011), especially because they are not in contact with water. Even more, these technologies have been used to analyse video from social media (Le Boursicaud et al., 2016) and surface velocity and stream discharge had been measured from video footage acquired with unmanned aerial vehicles (Detert and Weitbrecht, 2015; Tauro et al., 2016).
Herein, the application of image-based methods during flood events are presented here are based on two case studies. In both cases a stationary camera-based discharge system (DischargeKeeper) is installed. The first site is in northern Spain where a 500-year flood event was measured. During that event other installed devices, which were in contact with the water, were flooded away. Since the camera was far enough from the water it was not damaged, and it measured the whole extreme flood event. In the second case study, the system was installed in very different environment, in a Wadi in the United Arab Emirates. Wadis are dry almost all year round, but they are prone to flash flood events. In the one recorded, the peak of the event arrived just 15 minutes after the water started flowing and lasted for some hours before coming dry again.

2. Methods

Camera-based technologies apply the velocity-area method for discharge calculation: $Q=A\cdot v_b$, where A is the wetted area (m^2) and v_b is the bulk velocity (m/s). The current cross-section and the water level are required to calculate the flow area. The bulk velocity is calculated based on the measured surface velocity measured by image analysis. To obtain the surface velocity using images, different methods are available such as Large-Scale Particle Tracking Velocimetry (LSPTV), Kanade-Lucas Tomasi Image Velocimetry (KLTIV), Optical Tracking Velocimetry (OTV), Surface Structure Image Velocimetry (SSIV), or Space Time Image Velocimetry (STIV). In this work, it was used the camera-based measuring system DischargeKeeper (DK) developed by SEBA Hydrometrie GmbH & Co. KG and Photrack AG , which has implemented the SSIV (Lüthi et al., 2018) . The measuring system consists of an IP-camera, an infrared beamer for measuring at night and a central unit with remote data transmission. The implemented algorithm is running in real-time on the device to provide on-site measurement and evaluation. The measuring process including recording image streams takes less than one minute. This enables very short measuring intervals which is very beneficial for flood monitoring.

In addition to the digitized measured values, proof images and videos are stored and can be transmitted to an FTP server. Independently of the method implemented, to obtain the discharge from videos the following main steps are required: the first step is Camera calibration, which allows to make transformation between image space and the real world, during these procedure the camera's internal and external parameters are obtained. Camera calibration is done by positioning Ground Control Points, getting its 3D coordinates and its correspondence on the image.
The second step is image orthorectification. Once the correspondence between image space and object space has been established via camera calibration, the images are orthorectified and at the same time, they can be corrected for lens distortion. The third step is water level estimation. Water level is a key quantity when calculating the discharge, together with the cross-section, it is needed to obtain area to be used in for the discharge calculation. There are several ways to obtain the water level, from image-methods (see Peña-Haro et al., 2021) or it can be gotten from external sensors.

The fourth step is surface velocity calculation. The system presented herein have implemented the SSIV method (Lüthi et al., 2018) which is based on a cross correlation technique and has several common features with LSPIV. SSIV applies a filter to the images prior the cross correlation to reduce the influence of glare and shadows and to enhance structures that are present on the free flow surface. All analysed images are subdivided into interrogation windows on which the cross-correlation algorithm is applied, yielding a displacement field. Then, using the camera calibration, the displacement field can be transformed into velocities in metric units. The fifth step is depth average velocity and discharge calculation. Once the surface velocity is obtained, and assuming the cross section of the stream and river stage are known, it is then possible to calculate the discharge by integrating the depth-averaged velocity over the width of the river. To calculate the depth-averaged velocity several approaches are available, from physically-based models to fully empiric models. In the systems shown here, the ISO 748 (2007) was used. Image-base methods are very flexible, since the sensor is a camera which can be mounted anywhere as far as it has a view of the full width of the flow and good resolution. The camera can be mounted in almost any position relative to the flow.

3. Results and discussion

The discharge measuring system of the first case study in northern Spain was installed in February 2021. A 500-year return event was measured at the first site in Spain. The measuring system was installed at a monitoring station, together with other systems for measuring the discharge. The monitoring station is located at a control canal. The IP-camera was mounted on the wall of a house outside the canal cross-section area. In November 2021 a 500-year event took place, the high flows destroyed much of the equipment which was in contact with the river. The water even reached the house, but not the camera. Figure 1 shows three different flow conditions with discharge values from 100m^3/s to 980 m^3/s withing the year 2021. While the left image shows a sudden water level increase occurred at night, the image in the middle shows a relatively moderate flood event with about 200 m^3/s discharge. The image on the far right shows the maximum condition with about 975 m^3/s discharge close to the flood peak. It was possible to get the river stage using an existing water level sensor which is housed inside the monitoring station and was not affected by the flood.

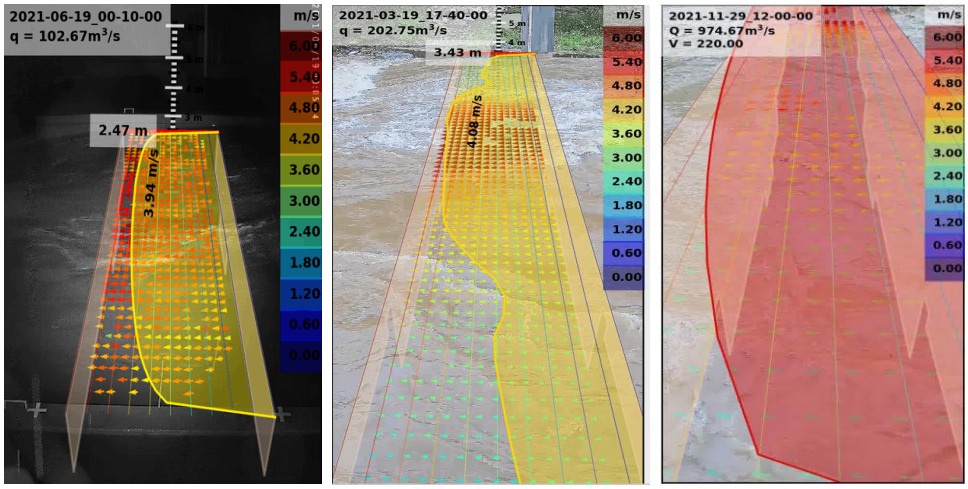

Figure 1. proof images at different flow and lighting conditions on a DischargeKeeper site in Spain

The hydrograph of the event is shown in Figure 3, the maximum measured discharge was 980 m^3/s.

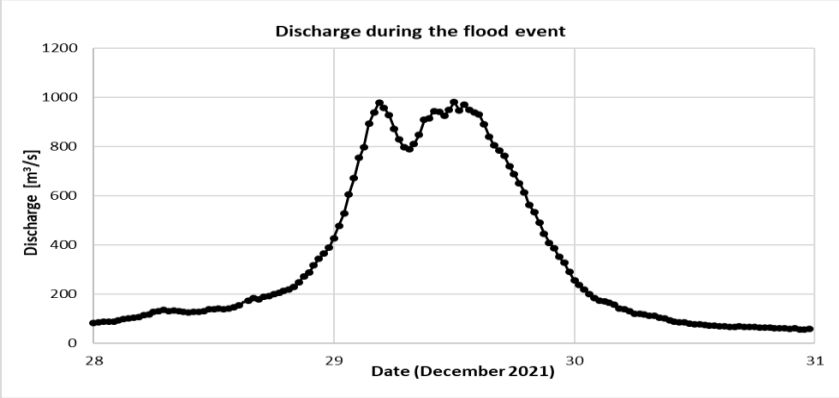

Figure 2. hydrograph of the flood event measured by the DischargeKeeper site in Spain

The second case study is about a flash flood event in a wadi in the United Arab Emirates (UAE). Wadis are completely dry during most of the time. However, flash floods must then be expected during the very rare but equally heavy rainfall. In April 2021, a DischargeKeeper system was installed in Wadi Naqab in the northern UAE. The wadi is about 100m wide and was completely dry for two years. The camera installed on this site is a PTZ-camera (Pan-Tilt-Zoom) with a range >200m and the measuring system is solar-powered.
In January 2022, a first flood event was recorded. Within 15 minutes, the flow increased from 0 m^3/s to 78 m^3/s (see Figure 3). Discharge measurement in semi-arid regions is a major challenge due to their harsh and continuously changing environment. Wadis are normally dry except after a rain event, often resulting in flash floods events with flood peak values occurring in the first few minutes of the event. In April 2021 a DK was installed at the Wadi Naqab located in northern United Arab Emirates. The Wadi is approximately 50m wide and has been dry for most of the time. One event occurred at the beginning of January 2022, reaching a peak discharge of 78 m^3/s with surface velocities around 3 m/s just 15 minutes after water started flowing. Figure 3 shows an image (left) one hour before the flood and one image during the flash flood event (right).

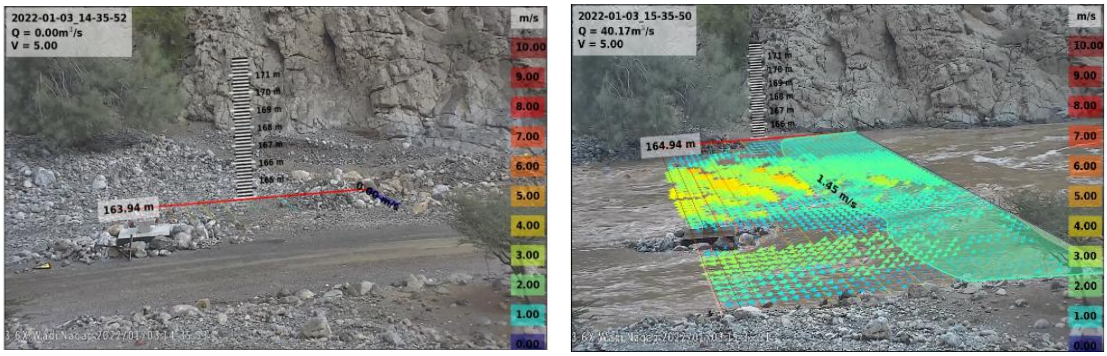

Figure 3. proof images before and during a flash flood event on a DischargeKeeper site in Wadi

Figure 4 shows the hydrograph of the discharge values measured by the camera-based system on the day of the flash flood event.

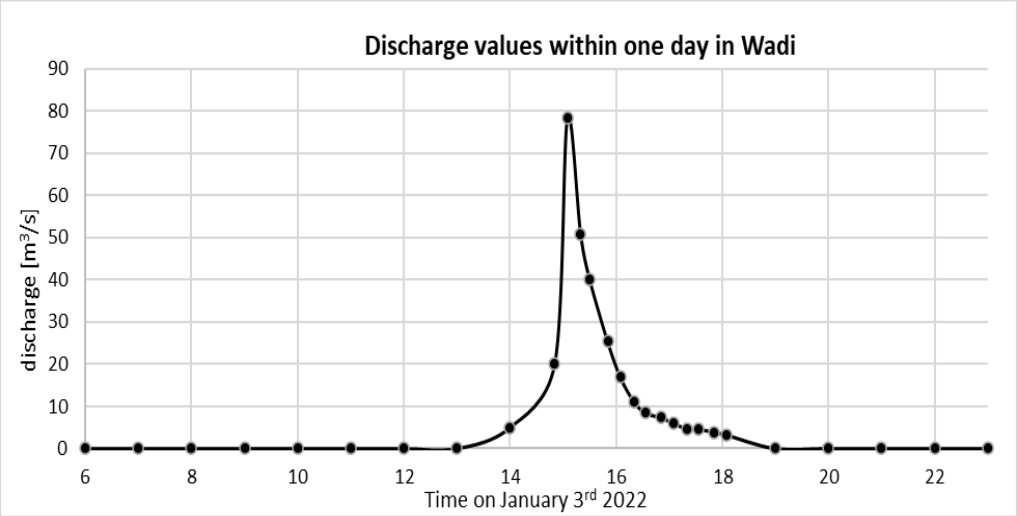

Figure 4. Discharge hydrograph of the flash flood event on a DischargeKeeper site in Wadi

4. Conclusions

The camera-based system installed on both sites of the case studies presented could continuously provide reliable measured data. The transmitted proof images were very helpful for the optical verification of the measurement especially during the flood events. Furthermore, the camera used can be installed at almost any position with respect to the flow, regardless of the presence of a bridge, as far as the flow is in the view of the camera with a good resolution.

There were no measurement limitations even during the extreme flood events on both sites. This is mainly because the sensor is a camera which can be permanently mounted at a safe distance from the flow outside the cross-section and the flood area. Due to the image processing method, the measuring system does not need to come into contact with the measured medium, which means that mud or flotsam do not affect the operation of the implemented measuring system. Only the camera lenses and the glass of the illumination unit must be free of dirt. Thus, the measuring system is almost maintenance-free and causes hardly any operating costs.

Furthermore, it is possible to install either one camera with one image view, several cameras with one image view each or one PTZ camera with several image views. Therefore, the DischargeKeeper can be used for rivers or canals with a width of a few metres up to several hundred metres. The infrared illumination of the measuring system enables operation in the most varied weather and light conditions.

A special feature of the technology is that no detectable tracers or floating objects need to be present to measure the flow velocity. Sufficient roughness on the water surface and profile data are the only requirements of the measuring system.

References

1. **Fujita, I., Muste, M., and Kruger, A.** (1998). Large-scale particle image velocimetry for flow analysis in hydraulic engineering applications. J. Hydr. Res. 36, 397–414. doi: 10.1080/00221689809498626
2. **Fujita, I., and Kunita, Y.** (2011). Application of aerial LSPIV to the 2002 flood of the yodo river using a helicopter mounted high density video camera. J. Hydro-Environ. Res. 5, 323–331. doi: 10.1016/j.jher.2011.05.003
3. **Hauet, A., Kruger, A., Krajewski, W., Bradley, A., Muste, M., Creutin, J., et al.** (2008). Experimental system for real-time discharge estimation using an image-based method. J. Hydrol. Eng. 13, 105–110. doi: 10.1061/(ASCE)1084-0699(2008)13:2(105)
4. **ISO (2007).** Hydrometry—Measurement of Liquid Flow in Open Channels Using Current-Meters or Floats. Vol. 748. ISO
5. **Jodeau, M., Hauet, A., Paquier, A., Le Coz, J., and Dramais, G.** (2008). Application and evaluation of LS-PIV technique for the monitoring of river surface velocities in high flow conditions. Flow Meas. Instr. 19, 117–127. doi: 10.1016/j.flowmeasinst.2007.11.004
6. **Le Boursicaud, R., Pénard, L., Hauet, A., Thollet, F., and Le Coz, J.** (2016). Gauging extreme floods on YouTube: application of LSPIV to home movies for the post-event determination of stream discharges. Hydrol. Proc. 30, 90–105. doi: 10.1002/hyp.10532
7. **Le Coz, J., Hauet, A., Pierrefeu, G., Dramais, G., and Camenen, B.** (2010). Performance of image-based velocimetry (LSPIV) applied to flash-flood discharge measurements in mediterranean rivers. J. Hydrol. 394, 42–52. doi: 10.1016/j.jhydrol.2010.05.049
8. **Lüthi, B., Philippe, T., and Peña-Haro, S.** (2018). Method and System for Determining the Velocity and Level of a Moving Fluid Surface. European Union. Available online at: https://patents.google.com/patent/EP3018483B1/en?q=photrack&oq=photrack (accessed September 21, 2022).
9. **Muste, M., Fujita, I., and Hauet, A.** (2008). Large-scale particle image velocimetry for measurements in riverine environments. Water Res. Res. 44:W00D19. doi: 10.1029/2008WR006950
10. **Peña-Haro S., Carrel M., Lüthi B., Hansen I. and Lukes R.** (2021) Robust Image-Based Streamflow Measurements for Real-Time Continuous Monitoring. Front. Water 3:766918. doi: 10.3389/frwa.2021.766918
11. **Perks, M. T., Russell, A. J., & Large, A. R. G.** (2016). Technical note: Advances in flash flood monitoring using unmanned aerial vehicles (UAVs). Hydrology and Earth System Sciences, 20, 4005– 4015.
12. **Tauro, F., Porfiri, M., and Grimaldi, S.** (2016). Surface flow measurements from drones. J. Hydrol. 540, 240–245. doi: 10.1016/j.jhydrol.2016.06.012

ICFM 10
Adapting to Global Change:
Innovative Approaches to Flood Management and Resilience
May 20-22, 2026 | Western University, London, Ontario, Canada

Investigating the Behavior of Hail, Wind, and Extreme Rainfall Events and Their Impact on Urban Flooding in Alberta

Issam Mohamed*[1], Yasaman Masaeli[1], Mohammad Reza Najafi[1]

Department of Civil and Environmental Engineering, Faculty of Engineering, Western University, London, Ontario, Canada N6A 5B91
E-mail: * imoham2@uwo.ca * ymasaeli@uwo.ca

ABSTRACT
Flooding is a major natural hazard that poses serious threats to lives and property safety, which is increasingly driven by compound weather extremes rather than isolated hazards. In regions such as Alberta's "hail alley," intense rainfall is often accompanied by hail accumulation and strong winds, which together may reduce urban drainage capacity, increase surface runoff, and amplify flood- related damages. Hailstones can clog stormwater inlets and conveyance systems, while strong winds enhance rainfall-driven runoff and debris transport, jointly exacerbating urban flooding impacts. Therefore, understanding the inter-dependencies and joint behaviour of these hazards in both historical and future periods is crucial for developing effective flood risk mitigation strategies. In this study, we conduct a multivariate probabilistic assessment of concurrent hail, wind, and rainfall extremes over Alberta's "hail alley" using radar and ground-based observations to investigate the joint occurrence of these extreme events in the historical period. Moreover, the changes in the behaviour of these compound events are investigated under future global changes.

KEYWORDS: compound weather extremes, hail and rainfall and wind, urban flooding, probabilistic analysis, copula, joint return period.

1 INTRODUCTION

Flooding is one of the most devastating natural disasters worldwide, resulting in more than half a million deaths over the past 30 years (Liu et al., 2022) and annual damage of around US$50 billion worldwide (Jalili Pirani and Najafi, 2023). Multiple interacting drivers may jointly influence flood magnitude and impacts rather than individual drivers alone. Recent studies have shown that the concurrence of extreme climate events can exacerbate the consequences of urban flooding, resulting in significant damage and human fatality due to the potential associated (non)linear interactions (Zhong et al., 2021, Jalili Pirani and Najafi, 2023, AghaKouchak et al., 2014; Chang et al., 2016). For example, hailstorms, can be significantly more hazardous when accompanied by extreme rainfall and wind, leading to increased risks of urban flooding. The accumulation of large hailstones can potentially clog rain drains, reducing their capacity to manage runoff effectively. This, combined with intense rainfall, may increases surface runoff, which overwhelms drainage systems, exacerbating urban flooding and causing damage to infrastructure, property, and public safety (Mohamed et al., 2024).

The June 13, 2020's flood in Alberta, Canada, which cost at least $1.2 billion in insured damages, was caused by the concurrence of large hailstones, intense short-duration rainfall, and strong wind gusts. Observations and post-event assessments indicated that hail accumulation obstructed stormwater inlets and reduced drainage efficiency, while strong winds and heavy rainfall enhanced surface runoff. This event highlights the critical role of compound climate extreme events analysis in flood risk management (Mohamed et al., 2024).

This study conducts a multivariate probabilistic assessment of concurrent hail, wind and extreme rainfall events in Alberta's 'hail alley' Using radar data and data from Western University's Northern Hail

Project (NHP), including ground surveys, drone observations, and hail pad data. We analyse individual and joint hazard scenarios through a copula-based approach for the historical period. The study quantifies individual and joint return periods to evaluate the compound risk of hail and extreme rainfall during 2008-2020. Moreover, projected changes in the characteristics of concurrent rainfall, wind and hail extremes are investigated using CMIP6 RCMs. Furthermore, a copula-based approach is applied to assess the interdependence between these extremes and to estimate the joint return periods of theses compound events in the future and under different global warming levels.

2 METHODOLOGY

A comprehensive multivariate statistical framework is developed to quantify risk of compound urban flooding events. For each variable (hail, wind, and rainfall), extreme events are identified using the Peaks-Over-Threshold (POT) method, with the 90th percentile threshold selected to isolate the most impactful events. Suitable marginal distributions are fitted individually for each variable using maximum likelihood estimation, and the optimal distributions are selected based on the Akaike Information Criterion (AIC) and Kolmogorov–Smirnov goodness-of-fit tests.

Dependence between hazard components is first explored using rank-based measures, including Kendall's τ and Spearman's ρ, confirming statistically significant positive dependence among hail, wind, and rainfall extremes. To capture nonlinear and potentially asymmetric dependence structures, a copula-based modeling approach is adopted. Multiple copula families—Gaussian, Student-t, Clayton, Gumbel, Frank, and Joe—are evaluated, and the best-fitting copulas are identified through likelihood-based criteria and goodness-of-fit diagnostics.

The analysis is conducted at both bivariate and trivariate levels. While bivariate copulas are used to model paired combinations of hazards, a vine copula construction is implemented for the trivariate case to flexibly represent complex interdependencies that cannot be adequately captured by standard multivariate copulas. Using the fitted copula models, joint probabilities and joint return periods are calculated under both "AND" (simultaneous exceedance of all variables) and "OR" (exceedance of at least one variable) definitions.

3 RESULTS

The analysis of various return periods during the historical period has highlighted the importance of quantifying the trivariate return periods of compound hailstorm variables to accurately assess the projected risks of urban flooding and the potential impact if they occur simultaneously. According to Table 1, Joint return periods for trivariate and bivariate OR and AND cases are smaller than those of the independent cases for all scenarios, indicating a high correlation between variables and a higher likelihood of simultaneous occurrence of such extreme events.

The trivariate analysis indicates that although the concurrent occurrence of extreme hail, wind gust, and rainfall events is less frequent than univariate and bivariate extremes, it represents substantially higher risk when such events occur. Using a trivariate C-vine copula framework applied to peak-over-threshold samples (90th percentile), the nonlinear dependence structure among hail intensity (max_VIL), maximum wind gust (WGust), and rainfall rate (PRate) is explicitly quantified.

Table 1 demonstrates that the trivariate AND return periods during the historical period derived from the copula-based framework are markedly shorter than those obtained under the assumption of independence. This nearly 80% reduction in return period relative to the independence assumption demonstrates that neglecting dependence among the three drivers leads to a substantial underestimation of compound flood risk. Therefore, the trivariate return period provides a more realistic estimate of how often urban drainage systems may be exposed to simultaneous extreme rainfall, reduced drainage capacity due to hail accumulation, and wind-enhanced runoff conditions that are critical for urban flooding management.

Table 1 Univariate, bivariate and tri-variate joint return periods estimated for quantile 90 using the tri-variate sample of observations

Hazard quantiles estimated using the inverse of the best fitted marginal cumulative distribution functions (CDFs)			Univariate joint return periods (Years)			Bivariate joint return periods (Years)				Tri-variate joint return Periods		Independent cases		
max_VIL (X) (kg/m2)	Prate (Y) (mm/hr)	WGust (Z) (km/hr)	Tx	Ty	Tz	T_{XY}^{OR}	T_{XY}^{AND}	T_{XZ}^{OR}	T_{XZ}^{AND}	T_{XYZ}^{OR}	T_{XYZ}^{AND}	T_{XY}^{IND}	T_{XZ}^{IND}	T_{XYZ}^{IND}
96.19	19.59	89.97	3.6	3.3	4.10	1.16	4.8	1.0	10	1.7	55.4	16.32	12.59	285

4 CONCLUSION

The results demonstrate that ignoring dependence among hail, wind, and rainfall extremes leads to a substantial underestimation of return periods of compound urban floods. Joint return periods derived under an independence assumption are underestimated by up to approximately 70% compared to copula-based estimates during the historical period. In the trivariate case, the joint AND return period of concurrent hail–wind–rainfall extremes is approximately 55 years, compared to about 285 years under the assumption of independence.

These findings highlight the importance of trivariate dependence analysis for flood risk assessment and emphasize the need to consider compound-event analysis into stormwater infrastructure design and urban flood management, particularly in regions such as Alberta where severe convective storms are common.

REFERENCES

AghaKouchak, A., Cheng, L., Mazdiyasni, O., Farahmand, A., 2014. Global warming and changes in risk of concurrent climate extremes: Insights from the 2014 California drought. Geophys. Res. Lett. 41, 8847–8852. https://doi.org/10.1002/2014GL062308

Chang, J., Li, Y., Wang, Y., Yuan, M., 2016. Copula-based drought risk assessment combined with an integrated index in the Wei River Basin, China. J. Hydrol. 540, 824–834. https://doi.org/10.1016/j.jhydrol.2016.06.064

Liu, J., Feng, S., Gu, X., Zhang, Y., Beck, H.E., Zhang, J., Yan, S., 2022. Global changes in floods and their drivers. J. Hydrol. 614, 128553. https://doi.org/10.1016/j.jhydrol.2022.128553

Mohamed, I., Najafi, M.R., Joe, P., Brimelow, J., 2024. Multivariate analysis of compound hail, wind and rainfall extremes in Alberta's hail alley. Weather Clim. Extrem. 46, 100718. https://doi.org/10.1016/j.wace.2024.100718

Pirani, F.J., Najafi, M.R., 2023b. Nonstationary frequency analysis of compound flooding in Canada ' s coastal zones. Coastal Engineering 182 (March). https://doi.org/ 10.1016

Zhong, M., Zeng, T., Jiang, T., Wu, H., Chen, X., Hong, Y., 2021. A copula-based multivariate probability analysis for flash flood risk under the compound effect of soil moisture and rainfall. Water Resour. Manag. 35 (1), 83–98. https://doi.org/ 10.1007/s11269-020-02709-y

Chapter 2 - Flood risk assessment, data and modeling

2.1 Flood hazard and risk mapping across spatial scales

Integrated Methodologies for Flood Susceptibility Mapping and Urban Flood Prediction

Maria Clara Fava[1], Marcos Roberto Benso[2], Maurício Jonas Ferreira[3], Marina Batalini de Macedo[4], Anaí Floriano Vasconcelos[5], Beliana Cavalcante Sawada de Carvalho[6], Alan Vaz Lopes[7], Maria Elisa Leite Costa[8], Thiago Biscaro[9], Javier Tomasella[10]

Federal University of São Carlos, São Carlos, São Paulo, Brazil[1]
E-mail: mcfava@ufscar.br

University of São Paulo, São Carlos, Piracicaba, Brazil[2]
E-mail: marcosbenso@usp.br

University of São Paulo, São Carlos, São Paulo, Brazil[3]
E-mail: mjferradura@hotmail.com

Federal University of Itajubá, Itajubá, Minas Gerais, Brazil[4]
E-mail: marinamacedo@unifei.edu.br

Federal University of São Carlos, São Carlos, São Paulo, Brazil[5]
E-mail: anai.vasconcelos@ufscar.br

National Institute for Space Research, São José dos Campos, São Paulo, Brazil[6]
E-mail: beliana.sawada@unesp.br

National Water and Basic Sanitation Agency, Brasília, Distrito Federal, Brazil[7]
E-mail: alanvazlopes@gmail.com

Ministry of Cities, Brasília, Distrito Federal, Brazil[8]
E-mail: elisa.costa@cidades.gov.br

National Institute for Space Research, Cachoeira Paulista, São Paulo, Brazil[9]
E-mail: thiago.biscaro@inpe.br

National Institute for Space Research, Cachoeira Paulista, São Paulo, Brazil[10]
E-mail: javier.tomasella@inpe.br

ABSTRACT

Extreme precipitation events, such as urban flooding and flash floods, represent major challenges for risk management, particularly in rapidly urbanized regions. Climate change has increased the frequency and intensity of these events, resulting in significant social and economic impacts. In Brazil, many cities are marked by dense urbanization, unplanned expansion, and extensive impervious surfaces, which intensify flood risks. These characteristics underscore the need for reliable, robust, and easily replicable methodologies to support flood prediction and mitigation, especially in data-scarce contexts. This study focuses on the Metropolitan Area of São Paulo, a megacity highly vulnerable to urban flooding, aiming to develop integrated methodologies that combine flood prediction with susceptibility mapping. The hydrological component employs historical flood records and modeling tools to simulate surface runoff processes and estimate flood extents under different scenarios. In parallel, data-driven approaches are applied to produce detailed flood susceptibility maps. Using Geographic Information Systems (GIS) and statistical analyses, the study evaluates key physical and socioeconomic drivers of flood risk, including land use, slope, proximity to water bodies, population density, and socioeconomic vulnerability indicators. These variables are correlated with historical flood occurrences to develop predictive susceptibility models

that can support urban planning and risk reduction strategies. The outcomes include high-resolution flood susceptibility maps and predictive tools suitable for integration into operational early warning systems. These products are intended to support city planners and disaster management agencies by providing actionable information to improve preparedness, response, and long-term resilience. Moreover, the methodological framework developed in this research can be transferred to other Brazilian municipalities, particularly those with limited hydrometeorological data availability.

KEYWORDS: Urban flooding; Hydrological modeling; Machine learning; GIS-based analysis; Data-scarce environments.

1 INTRODUCTION

The consequences of high-intensity precipitation events, including urban flooding and flash floods, pose significant challenges for risk management. The impact of these events is even more concerning in vulnerable communities (Deria et al., 2020). The increasing frequency and intensity of these events, driven by climate change (Simonovic and Peck, 2022), have led to severe social and economic impacts (Chaudhary and Piracha, 2021), particularly in densely populated areas with limited infrastructure (IPCC, 2022). Many Brazilian cities and countries in the Global South are characterized by high levels of urbanization, unplanned expansion, and significant impervious surface coverage, which exacerbate flood risks (Adelekan, 2016; Tadesse et al., 2024; Shatanawia et al., 2024; Zhang et al., 2025). These conditions highlight the urgent need for reliable and easily replicable methodologies to predict and mitigate the impacts of urban flooding.

This study focuses on the Metropolitan Area of São Paulo, a megacity highly vulnerable to urban flooding, to develop integrated methodologies that combine flood prediction and susceptibility mapping. The city of São Paulo is the most populous municipality in Brazil, with a population of approximately 11.4 million inhabitants in 2022 (IBGE, 2022). Every summer, the megacity experiences flooding in various locations throughout its urban area (Haddad, 2015). Situated among three major rivers, Tietê, Pinheiros, and Tamanduateí, São Paulo's municipal territory encompasses around 1,521 km² and contains 166 sub-basins within its urban landscape (Gouveia, 2016). Considering the city's flood history, the heterogeneity of areas exposed to flood risk, and São Paulo's significant social and economic importance, this study adopts an integrated methodological approach. For the pilot case study, the assessments were conducted in the Aricanduva catchment, a highly urbanized catchment with frequent flood events.

In this context, this study aims to develop and evaluate an integrated and replicable framework for urban flood assessment in data-scarce environments. Two hydrological models with different levels of complexity, HYMOD and HEC-HMS, are applied and compared to assess the trade-off between model performance, computational cost, and data requirements. In parallel, flood susceptibility mapping is conducted using machine-learning classification algorithms, including Random Forest, Regularized Random Forest, and XGBoost, trained with historical flood occurrence data. By integrating hydrological modeling and data-driven susceptibility analysis, this study seeks to provide a cost-effective and robust methodology to support flood risk management in urban basins, particularly in large metropolitan areas of the Global South.

2 METHODOLOGY

The methodological framework of this study integrates hydrological modeling and data-driven susceptibility mapping to assess and predict urban flooding in a highly urbanized catchment. The approach combines physically based rainfall–runoff simulations with machine learning classification techniques, allowing both the dynamic representation of flood-generating processes and the spatial identification of areas prone to flooding. The following sections describe the study area, the hydrological modeling procedures, and the flood susceptibility assessment.

2.1 Case Study

The study area is the Aricanduva River basin, located in the eastern zone of the municipality of São Paulo, Brazil (Figure 1). The catchment covers an area of approximately 102.5 km² and is fully urbanized, with a high population density and a long history of recurrent flood events, including flash floods.

The region is characterized by a humid subtropical climate, with average monthly temperatures ranging from 17.2 °C in July to 23.5 °C in February. Mean monthly precipitation varies markedly throughout the year, from 32.3 mm in August to 292.1 mm in January, reflecting strong seasonal rainfall patterns (INMET, 2020).

According to the most recent demographic data, the basin has a population density of approximately 7,400 inhabitants per square kilometer (IBGE, 2022), which significantly increases exposure to flood-related hazards, including population displacement, injuries, and economic losses (Simas, 2017). In addition, the Aricanduva basin is well instrumented, with continuous monitoring of rainfall, streamflow (Gauge control in Fig. 1), and water level (Gauges at Fig. 1) at 10-minute intervals over a period of approximately ten years, providing a robust dataset for modeling and flood analysis.

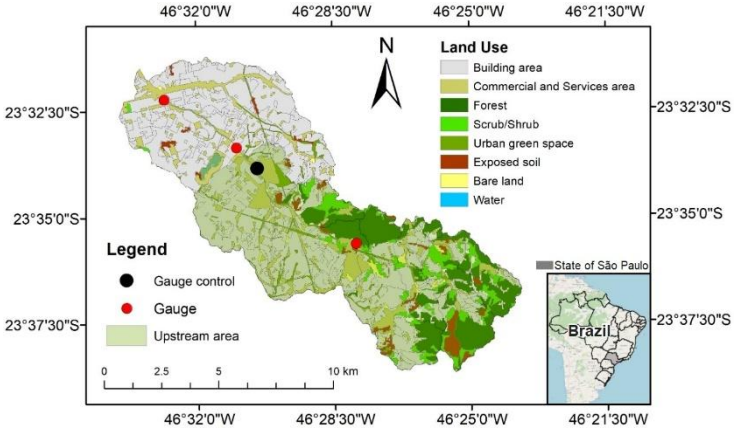

Figure 1: Land use and land cover were mapped using high-resolution orthorectified imagery

2.2 Hydrological Modeling

Hydrological modeling was carried out to simulate rainfall–runoff processes and support flood forecasting in the Aricanduva River catchment. Two widely used rainfall–runoff models with different levels of complexity were applied and adjusted: the conceptual HYMOD model and the semi-distributed HEC-HMS model. The joint use of these models allows the comparison of hydrological responses derived from simplified and spatially distributed representations of urban catchment processes.

Both models were calibrated and validated using the same observational dataset, consisting of precipitation and streamflow records collected within the catchment. Precipitation data were obtained from four monitoring stations, while discharge data were measured at a control section of the Aricanduva stream. All time series were processed at a 10-minute time step, allowing the representation of short-duration, high-intensity rainfall events typical of urban flooding.

Model calibration was performed utilizing automatic optimization techniques complemented by manual adjustments as needed. Additional details regarding model structure, parameterization, calibration strategies, and performance assessment are presented separately for each model in Sections 2.1.1 and 2.1.2, which describe the configuration of the HYMOD and HEC-HMS models, respectively.

2.2.1 HYMOD Model Configuration and Calibration

The HYMOD model was applied as a lumped conceptual rainfall–runoff model to simulate streamflow response in the catchment. The model was forced with time series of precipitation (P), potential evapotranspiration (PET), and calibrated using observed discharge (Q_{obs}).

The canonical five-parameter structure of HYMOD was adopted, including the maximum soil moisture storage capacity (C_{max}), the spatial variability of soil moisture storage (B_{exp}), the fraction of excess rainfall routed to the fast flow component (α), and the recession coefficients of the slow (Rs) and fast (Rq) flow reservoirs. Excess rainfall was computed using a probabilistic soil moisture capacity distribution and partitioned between fast and slow flow paths, represented by a cascade of linear reservoirs.

Parameter calibration was performed using the SciPy Optimize Minimize function with the L-BFGS-B algorithm, constrained by physically plausible parameter bounds reported in previous studies. Automatic calibration was complemented by manual adjustments when necessary to improve model performance. The optimized parameter set was subsequently applied to the full dataset for validation, and model performance was assessed by comparing simulated and observed discharges using standard statistical performance metrics.

2.2.2 HEC-HMS Model Configuration and Calibration

The HEC-HMS model was implemented as a semi-distributed hydrological model to represent spatial variability in land use and hydrological response across the catchment. Initial estimates of the Initial Loss (IL) and Constant Rate (CR) parameters were derived from HEC-HMS application guidelines and hydrological handbooks for urban catchments. The impervious area fraction (IM) was defined based on land use and land cover classification, while basin lag time (LT) was estimated during model pre-processing according to the spatial distribution of urban occupation. The basin was subdivided into 13 sub-catchments, allowing localized calibration of hydrological parameters.

Automatic calibration was conducted using the Univariate Gradient optimization method, with a maximum of 100 iterations and a convergence tolerance of 0.01. In cases where automatic calibration did not yield satisfactory results, manual calibration was applied. Final parameter values for IL, CR, IM, and LT were optimized for each sub-catchment based on the Runoff Curve Number (RCN) methodology and selected to maximize agreement between simulated and observed streamflow, following established statistical performance criteria.

2.3 Susceptibility Assessment

The study employs classification-based machine learning models to map urban flood susceptibility. The Random Forest, Regularized Random Forest, and XGBoost algorithms were employed and trained using flood occurrence data recorded between 2013 and 2024, classified into three categories: non-susceptible (1,000 data points), waterlogging of drainage system (196 data points), and fluvial flooding (207 data points), totaling 1,403 data points (Figure 2). Explanatory variables were derived from LiDAR data originally acquired at 0.5 m spatial resolution and resampled to 5 m for computational efficiency, using a Triangulated Irregular Network (TIN). From this dataset, the following topographic and hydrological factors were calculated: slope, slope length, slope steepness, Topographic Position Index (TPI), Topographic Index (TI), Height Above the Nearest Drainage (HAND), Profile Convergence Index (TCI), Stream Power Index (SPI), aspect, and drainage direction. The dataset was split into training (80%) and testing (20%) samples, and model performance was assessed using repeated 10-fold cross-validation. Model accuracy and Cohen's Kappa coefficient were used as evaluation metrics, allowing for both performance evaluation and identification of the most relevant factors influencing flood susceptibility.

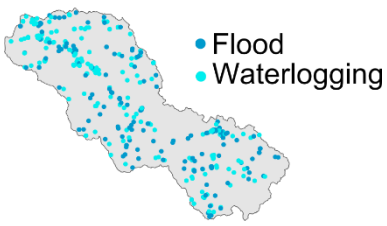

Figure 2: Flood occurrence data used in the susceptibility analysis (2013–2024; n = 1,403)

3 RESULTS AND DISCUSSION

3.1 Flood Modeling

The calibration and validation results of the HYMOD and HEC-HMS models showed a high level of agreement between simulated and observed hydrographs, particularly with respect to peak discharge and runoff volume. During the validation stage, both models were executed using the same calibrated parameters, demonstrating a consistent ability to reproduce the main hydrological characteristics of the analyzed events (Figure 3).

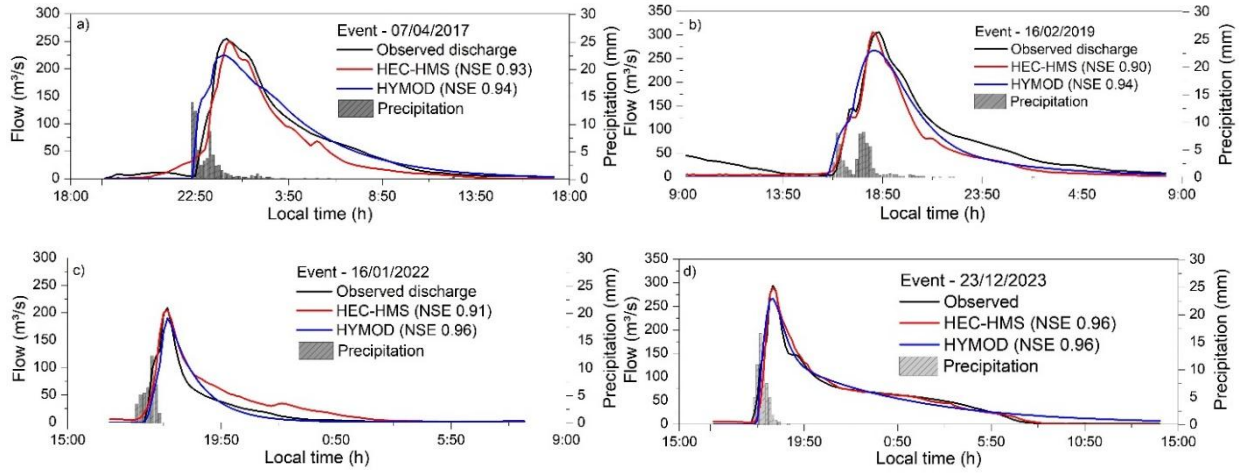

Figure 3: Measured and simulated discharge ($m^3\ s^{-1}$) for calibration (a–c) and validation (d).

Table 1: Statistic index of HEC-HMS and HYMOD calibration (dark grey) and validation (light grey)

Statistic index	Calibration/Validation									
	Date/time (duration of rain)									
	07Apr2017/ (22:50h to 04:00h)		16Feb2019/ (16:00 to 20:50h)		16Jan2022/ (16:00h to 17:10h)		23Dez2023/ (17:10h to 19:00h)		Performance Rating Moriasi et al. (2007)	
	HEC-HMS	HYMOD	HEC-HMS	HYMOD	HEC-HMS	HYMOD	HEC-HMS	HYMOD		
PEV (%)	**17.48**	**1.18**	**19.89**	**21.46**	**7.80**	**4.90**	**0.64**	**4.98**	Very good	<±10
									Good	±10–±15
									Satisfactory	±15–±25
									Unsatisfactory	>±25
PEPF (%)	**1.91**	**11.54**	**0.19**	**12.53**	**1.98**	**9.23**	**1.33**	**9.22**	Very good	<15
									Good	15 to 30
									Satisfactory	30 to 40
									Unsatisfactory	>40
R^2	**0.97**	**0.94**	**0.96**	**0.95**	**0.95**	**0.92**	**0.97**	**0.96**	Very good	0.75 to 1
									Good	0.65 to 0.75
									Satisfactory	0.50 to 0.65
									Unsatisfactory	<0.50
RMSE	**0.22**	**0.24**	**0.32**	**0.29**	**0.25**	**0.28**	**0.19**	**0.20**	Very good	0 to 0.5
									Good	0.5 to 0.6
									Satisfactory	0.6 to 0.7
									Unsatisfactory	> 0.7
NSE	**0.93**	**0.94**	**0.90**	**0.94**	**0.91**	**0.96**	**0.96**	**0.96**	Very good	0.75 to Unity
									Good	0.65 to 0.75
									Satisfactory	0.50 to 0.65
									Unsatisfactory	<0.50
PBIAS (%)	**17.48**	**-1.18**	**19.89**	**21.46**	**7.80**	**4.90**	**-0.64**	**-4.98**	Very good	<±10
									Good	±10 to ±15
									Satisfactory	±15 to ±25
									Unsatisfactory	>±25

Model performance was evaluated using six statistical indices (Table 1), allowing a comprehensive assessment of simulation accuracy. Across all simulations, R^2 values exceeded 0.90, and NSE ranged from 0.90 to 0.96, classifying the performance of both models as very good according to the criteria proposed by Moriasi et al. (2007). Low RMSE values, RSR values below 0.33, and reduced PBIAS further confirm the high reliability of the simulations.

In terms of runoff volume, HYMOD exhibited better overall performance, with percentage errors (PEV) below ±5% in three of the four analyzed events and satisfactory performance in only one event. HEC-HMS presented higher volumetric errors in earlier events, but achieved very good performance in the most recent events.

Peak discharge reproduction was satisfactory for both models, with percentage errors below 15% in all cases. HEC-HMS showed superior performance in this aspect, with consistently low errors (below 2%), while HYMOD exhibited slightly higher errors, although still classified as very good.

Overall, the results demonstrate that the HYMOD model, despite its simpler conceptual structure, was able to simulate urban flood events satisfactorily, accurately reproducing both peak flows and runoff volumes, and confirming its suitability for flood modeling in highly urbanized catchments.

3.2 Susceptibility Mapping

The susceptibility models achieved high predictive performance, with accuracy values above 0.80 and Kappa coefficients indicating good to substantial agreement across calibration and validation stages (Figure 4a). Random Forest-based models showed slightly better generalization capability compared to XGBoost. Variable importance analysis revealed that HAND and elevation were the dominant predictors, highlighting the critical role of relative topographic position with respect to the drainage network in controlling urban flood susceptibility (Figure 4b). Secondary variables related to flow convergence and hydraulic energy contributed to model performance, while slope length and flow direction showed limited influence, reflecting the strong impact of urban infrastructure on runoff dynamics.

Figure 4: a) Evaluation indices for calibration and validation of ML models, b) Variable importance

a)

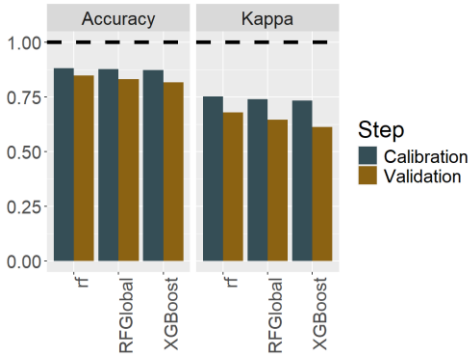

b)

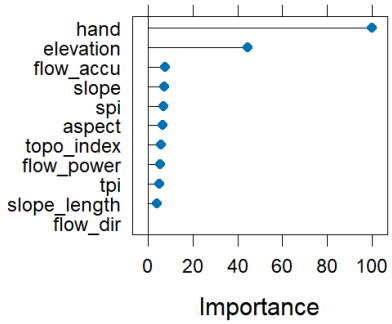

Figure 5 shows the flood susceptibility maps generated by the Random Forest, XGBoost, and Regularized Random Forest models. Despite methodological differences, all models consistently identify high-susceptibility areas along the main drainage network and low-lying regions of the basin, indicating robust spatial patterns. Minor differences are observed in the spatial continuity of susceptible areas, with XGBoost producing more fragmented patterns and Random Forest-based models yielding smoother susceptibility gradients. These patterns are consistent with the dominance of HAND and elevation identified in the variable importance analysis, reinforcing the physical interpretability of the results. Areas classified as highly susceptible by all models represent priority zones for flood risk management and urban drainage interventions.

Figure 5: Flood susceptibility maps of the Aricanduva catchment – red areas are the most susceptible

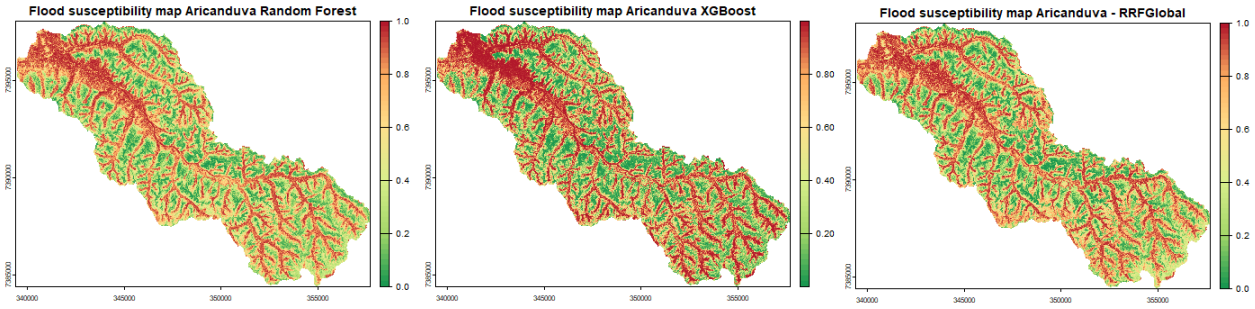

4 CONCLUSION

This study investigated hydrological modeling and flood susceptibility mapping to support flood risk assessment in a highly urbanized catchment. The results demonstrated that both HYMOD and HEC-HMS models were able to accurately reproduce urban flood events, with very good performance in terms of peak discharge and runoff volume. Despite its simpler conceptual structure, HYMOD showed reliable results, highlighting its potential for operational flood forecasting in urban basins.

The susceptibility mapping complemented the hydrological analysis by providing a spatially explicit identification of flood-prone areas. Machine learning models consistently highlighted low-lying areas near the drainage network as highly susceptible, with physically interpretable patterns strongly controlled by HAND and elevation. The convergence of results across different algorithms reinforces the robustness of the susceptibility maps and their applicability for urban flood management.

The combined use of hydrological modeling and susceptibility mapping offers a practical framework for urban flood risk mitigation. While high-resolution hydraulic models are computationally demanding for real-time applications in large urban areas, susceptibility maps can be used to pre-identify priority zones. In this context, when alert discharges are issued by the hydrological model, hydraulic simulations can be selectively applied to the most susceptible areas, enabling faster and more targeted flood response and decision-making.

Some limitations should be acknowledged. The hydrological models rely on lumped or semi-distributed representations, which may not fully capture the localized effects of urban drainage infrastructure. The susceptibility mapping is based on historical flood occurrences and static topographic variables, not explicitly accounting for temporal changes in land use, drainage capacity, or rainfall characteristics. Additionally, uncertainties associated with input data resolution and event reporting may affect model performance. Future research should focus on integrating dynamic rainfall forecasts, improving the representation of urban drainage systems, and coupling the proposed framework with real-time hydraulic simulations for operational flood warning systems.

5 ACKNOWLEDGEMENTS

The authors acknowledge the support of the National Council for Scientific and Technological Development (CNPq) through research grants (processes 381989/2024-0 and 174232/2023-3) and funding provided by the CNPq/MCTI Call No. 15/2023 – *Extreme Meteorological Events: Natural Disaster Prevention and Damage Minimization* (process 446029/2023-8).

REFERENCES

Adelekan I. O. (2010). Vulnerability of poor urban coastal communities to flooding in Lagos, Nigeria. Environment and urbanization, 22(2), 433-450. https://doi.org/10.1177/09562478103801

Chaudhary M. T. and Piracha A. Natural Disasters—Origins, Impacts, Management. Encyclopedia 1, no. 4 (2021): 1101–1131. https://doi.org/10.3390/encyclopedia1040084

Gouveia I. C. M. C. (2016). A cidade de São Paulo e seus rios: uma história repleta de paradoxos. Confins. Revue franco-brésilienne de géographie/Revista franco-brasilera de geografia, (27).

Haddad E. A. and Teixeira E. (2015). Economic impacts of natural disasters in megacities: The case of floods in São Paulo, Brazil. Habitat International, 45, 106-113. https://doi.org/10.1016/j.habitatint.2014.06.023

Intergovernmental Panel on Climate Change. (2022). Climate change 2022: Impacts, adaptation and vulnerability. Contribution of Working Group II to the Sixth Assessment Report of the Intergovernmental Panel on Climate Change. Cambridge University Press. https://www.ipcc.ch/report/ar6/wg2/

INMET - Instituto Nacional de Meteorologia [National Meteorology Institute]. (2020). Normais climatológicas do Brasil [Brazilian climate normal]. Available at: https://portal.inmet.gov.br/normais#

IBGE - Instituto Brasileiro de Geografia e Estatística [Brazilian Institute of Geography and Statistics], https://www.ibge.gov.br/cidades-e-estados/sp/sao-paulo.html, consulted 19 December 2025.

Moriasi D.N. et al. (2007). Model evaluation guidelines for systematic quantification of accuracy in watershed simulations. Trans. ASABE 50, 885–900. https://doi.org/ 10.13031/2013.23153.

Shatanawia K., Al-Weshaha R., Ta'anyc R., Mohammadd A. H., Kassaba G. and Halalshehd M. Assessment and mapping of flash flood hazard and risk at wadi yuyum basin in jordan: integrating hydrological modeling techniques. Water Conservation & Management (WCM) 8(3) (2024) 315-325. http://doi.org/10.26480/wcm.03.2024.315.325

Simas I. T. H. (2017). Análise retrospectiva de episódios de inundações na Bacia Hidrográfica do Rio Aricanduva – São Paulo [Retrospective analysis of flooding episodes in the Aricanduva River catchment – São Paulo]. Thesis, Universidade de São Paulo, São Paulo. https://doi.org/10.11606/D.8.2017.tde-21072017-162915

Simonovic S. P. and Peck, A. (2022). Resilience to climate change-caused flooding—Metro Vancouver case study. River, 1(1), 47-59. https://doi.org/10.1002/rvr2.6

Tadesse D., Suryabhagavan K. V., Nedaw D. and Hailu B. T. (2024). A model-based flood hazard mapping in Itang District of the Gambella region, Ethiopia. Geology, Ecology, and Landscapes, 8(1), 8-25. https://doi.org/10.1080/24749508.2021.2022833

Zhang Q., Li C., Wen D., Kang J., Chen T., Zhang B. and Slater L. (2025). Global South shows higher urban flood exposures than the Global North under current and future scenarios. Communications Earth & Environment, 6(1), 594. https://doi.org/10.1038/s43247-025-02585-7

Comparative Analysis of DEM Products for Flood Susceptibility Mapping in Urban Areas using Machine Learning

Marcos Roberto Benso[1], Maria Clara Fava[2], Anaí Floriano Vasconcellos[3], Marina Batalini[4], Beliana Cavalcante Sawada de Carvalho[5], Alan Vaz Lopes[6], Maria Elisa Leite Costa[7], Thiago Souza Biscaro[8], Javier Tomasella[9]
Luiz de Queiroz College of Agriculture, University of São Paulo, Piracicaba, 50200, Brazil[1]
E-mail: marcosbenso@usp.br
Federal University of São Carlos, São Carlos, São Paulo, Brazil[2]
E-mail: mcfava@ufscar.br
Federal University of São Carlos, São Carlos, São Paulo, Brazil[3]
E-mail: anai.vasconcelos@ufscar.br
Federal University of Itajubá, Itajubá, Minas Gerais, Brazil[4]
E-mail: marinamacedo@unifei.edu.br
National Institute for Space Research, São José dos Campos, São Paulo, Brazil[5]
E-mail: beliana.sawada@unesp.br
National Water and Basic Sanitation Agency, Brasília, Distrito Federal, Brazil[6]
E-mail: alanvazlopes@gmail.com
Ministry of Cities, Brasília, Distrito Federal, Brazil[7]
E-mail: elisa.costa@cidades.gov.br
National Institute for Space Research, Cachoeira Paulista, São Paulo, Brazil[8]
E-mail: thiago.biscaro@inpe.br
National Institute for Space Research, Cachoeira Paulista, São Paulo, Brazil[9]
E-mail: javier.tomasella@inpe.br

ABSTRACT

Data-driven flood susceptibility mapping derived from flood inventories help to evaluate the relationship between influencing factors and occurrence of urban floods. Despite recent efforts, the role of different digital elevation models has been poorly described in the literature, which have practical applications that are relevant for regions that are poorly covered by high resolution digital elevation models. This study has the objective of analysing the impact of different digital elevation models on flood susceptibility mapping using random forest. The main methodological challenge is that flood inventories usually only have positive points (flooded), but machine learning models require also negative points (non-flooded). This issue was addressed using a positive and unlabeled learning method in two steps. The first step is aimed to identify a set of relatively reliable negative (RRN) from a randomly generated set of points within the area, and the second step aims to create flood maps using the flood inventory and RRN dataset. The best model results were achieved with LiDAR 5m (Kappa 0.99); AlosPalsar, LiDAR 30m, ANADEM, and SRTM compose a middle tier (Kappa 0.92); LiDAR 10 m presents a lower performance suggesting the impact of noise in the aggregation process (Kappa 0.89); and ASTER presents the worst performance (Kappa 0.75). Considering the average of the machine learning models, the most important flood conditioning factors were Height Above Nearest Drainage (HAND) and Topographic Position Index (TPI) with windows of 35 and 25. The results suggest that the most common globally available digital elevation models can produce reliable flood susceptibility maps and that the PUL applied in this study can be successfully applied to other flood susceptible urban areas.

KEYWORDS: random forest, positive and unlabeled learning, variable importance

1 INTRODUCTION

The current state of climate change has imposed great challenge for urban water management. A warmer atmosphere can hold more water, hence the increase in the frequency and occurrence of severe heavy rainfall, especially in the tropics. From a practice point of view, urban planners and decision-makers have the hard task to continuously update the flood susceptibility maps and monitor urban areas with higher risk of floods. The flood risk mapping requires in upfront the correct description of the terrain with high resolution topographic data and digital elevation models (Tehrany et al., 2019).

Terrain analysis derived from digital elevation models (DEMs) provides a fundamental basis for identifying areas that are more likely to experience urban flooding. However, flood impacts are not determined by topography alone; exposure of human lives and assets plays a central role in shaping flood risk (Rentchler et al., 2022). Flood modeling supports the characterization of flood propagation beyond the river channel, yet flow measurements are typically confined to the channel itself, which increases uncertainty in representing flood dynamics once water spreads across the floodplain (Huang & Qin, 2014). Flood inventories have therefore been widely used to document areas affected by flooding, particularly those with the greatest impacts on the population. Although these datasets depend on civil defense reporting and response capacity, they offer significant potential for mapping flood-susceptible areas and complementing model-based approaches.

Data-driven methods can improve the flood map susceptibility with the use of flood inventories. Several studies have demonstrated the potential of machine learning algorithms for binary classification such as Random Forest, Support Vector Machine (Mukomberanwa & Madamombe, 2025), and Artificial Neural Networks (Li et al., 2022). One of the main bottlenecks of training a classification algorithm is that flood inventories only report the flood occurrence points, which leaves the non-occurrence points not reported. For binary classification, the model requires both negative and positive examples to be trained. Another question is whether the digital elevation model plays a significant role in the model training. The terrain characterization has been shown to be of great relevance for flood modeling, however, does play the same role in a1 data-driven model?

In the context of data-driven models, this study aims to assess the effect of different digital elevation models on flood susceptibility mapping using positive and unlabeled (PUB) methods for random forest. A case study is built in the Aricanduva Catchment, São Paulo, Brazil, by comparing the predictive performance of Random Forest (RF) models.

2 METHODOLOGY

The model framework was implemented in R environment (R Core Team, 2024) using the packages terra with methods for working with raster data and spatial data analysis (Hijmans, 2025) and sf for working with simple features providing a standardized way to encode and analyze spatial vector data (Pebesma & Bivand, 2023). The processing of terrain metrics was also performed using Whitebox tools front end interface in R (Lindsay, 2016; Wu & Brown, 2022). The machine learning models were implemented using the package caret (Classification and Regression Training) with provides functions for training and plotting classification and regression models (Kuhn, 2008). The random forest was implemented using the package randomForest (Liaw & Wiener, 2002).

2.1 Case study and datasets

The present study was conducted in the Aricanduva Catchment, São Paulo Metropolitan Region, Brazil, which is predominantly urban (ca. 86% according to MapBiomas). The study area covers 103 km², characterized with dense urban development and poor natural land used. The average altitude above the sea level is 750 meters.

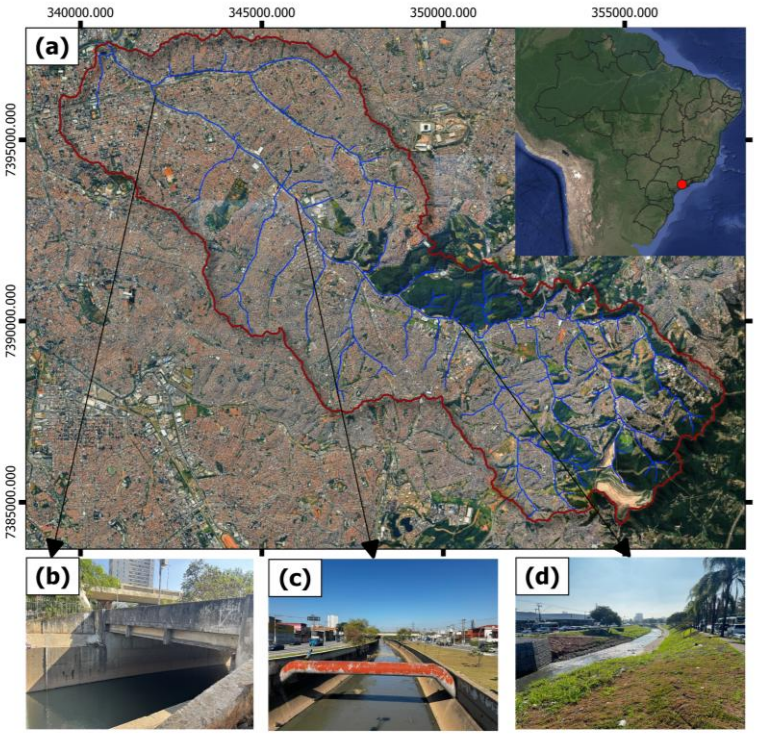

Figure 1: (a) Delineation of the Aricanduva Catchment area with highlights of (b) channel nearby the catchment outlet in the Tietê River, channel (c) in the middle part and (d) in the upper part of the catchment.

The flood inventory database was collected from São Paulo Municipal Geographic Data (Web-1). The flood inventory is collected by the civil defence since 2013 considering the official definition of drainage system overflow and floods. The drainage system overflow could be related to the fluvial processing during floods and inefficiencies of the drainage system during heavy rainfall. In the time from of 2013 to now, 593 flood occurrences were registered in the Aricanduva catchment area with most of the events being concentrated the month of February (Figure 2). The wet period is from October to March, where most occurrences were registered.

This study evaluates a set of widely used and freely available Digital Elevation Model (DEM) products. ANADEM, SRTM, NASADEM, and ALOS PALSAR. alongside LiDAR-derived DEMs generated at different spatial resolutions (5 m, 10 m, and 30 m). These datasets span a range of sensor technologies, processing methodologies, and levels of vertical and horizontal accuracy, offering a representative basis for comparison in flood modeling applications.

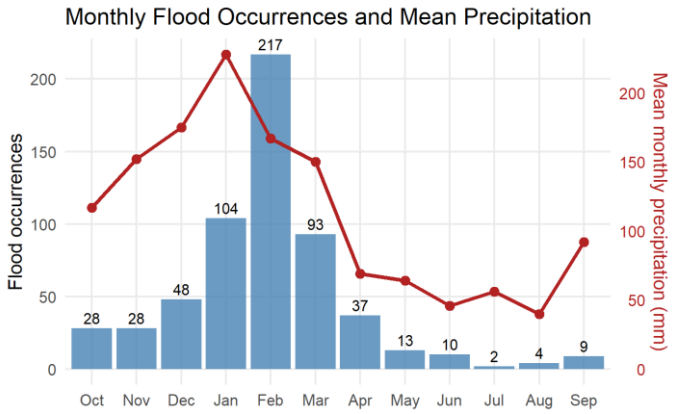

Figure 2: Annual distribution of monthly count of flood occurrences and historic mean precipitation in the Aricanduva Catchment

2.2 Flood conditioning factors

The conditioning factors considered in this study include a set of topographic and hydrological variables derived from the digital elevation model. Slope (°) expresses the terrain inclination in degrees, while Aspect (°) indicates the compass direction or azimuth that the terrain surface faces; both are continuous variables.

To characterize terrain morphology, several indices were used. The Terrain Ruggedness Index (TRI) (°) quantifies terrain roughness and is continuous. The Topographic Position Index (TPI) (°) describes the relative position of a pixel in relation to its surroundings and was computed using different moving window sizes: 8 × 8 pixels (Queen case), 3 × 3 pixels (TPI 3), 15 × 15 pixels (TPI 15), 25 × 25 pixels (TPI 25), and 35 × 35 pixels (TPI 35). All TPI-derived variables are continuous. Roughness (°), representing terrain roughness measured in degrees, is also a continuous variable.

Hydrological characteristics were represented by Flow Direction (FLD) and Eight Flow Direction (D8), are discrete variables that indicates the direction of surface runoff, and HAND (m), which expresses the height above the nearest drainage channel and is treated as a continuous variable.

2.3 Positive and unlabeled classification of flood susceptibility

The problem of positive and unlabeled classification is common to flood inventory data where only the positive, i.e., the point of flood occurrence is known ($y = 1$). The negative data, which are the points where the flood did not occur, generally are not recorded. The methodology proposed is divided into two steps: (i) the first step is designed to obtain a set of relatively reliable negative (RRN) points using a machine learning model, and (ii) the second step has the objective of using the new dataset composed of RRN to train a new machine learning model to generate the flood susceptibility maps. The models in the two steps were trained using random forest and the hyperparameter tunning considere1d leave-one-out cross-validation (LOOCV) to maximize data usage and reduce bias associated with limited positive samples. Class probabilities $P(s = 1|x)$ were estimated for each sample, and model performance was evaluated using two-class summary statistics based on receiver operating characteristic (ROC) analysis.

Model performance was evaluated using precision, accuracy, and Cohen's Kappa. Precision was computed as the ratio of correctly predicted flooded locations to all predicted flooded locations. Accuracy represents the proportion of correctly classified samples, while Cohen's Kappa measures the agreement between predictions and observations corrected for chance.

In the step-one, a set of random points (s) is generated over the study area. There is a chance of each random point being a flood point ($s = 1$) and non-flood point ($s = 0$). The random points were generated 10 times the number of flood points. For training the model, an unbalanced dataset was created considering 80% of the positive dataset and 2% of the random points. The test dataset was composed only with the 20% of the positive dataset. The main goal of the first model is to create a bias towards the positive prediction. The trained model is then used to classify the rest of 98% of random points into 0 and 1 probabilistically. The probabilistic prediction over the observed flood points is compared with the observed positive points, that is, the model predicts $p(x) = P(y = 1|x)$ for the cases we know the flood points. To choose the RNN points, a threshold representing the minimum probability required for a point to be considered flooded is given by equation 1. The RRN are given by the $P(s = 1|x) \leq c$, that is, all predictions made over the random points that were classified with a probability lower than the threshold.

$$c = \min_{x \in P} P(y = 1|x) \quad (1)$$

In the step-two, a new dataset is created to train random forest models to perform flood susceptibility mapping. The division of the observed positive data (flood points) is maintained the same as the step-one. The same 80% of positive labels is used for training and 20% used for testing the model in step-one was used for the models in step-two. The difference is that the RRN points were now randomly sample in 80% for training and 20% for testing.

3 RESULTS AND DISCUSSION

A comparison of model performance for test set for step-one and step-two is presented on Table 1. The test set is the 20% portion of the dataset that was never used for training the machine learning models. When considering precision, both steps presented a high performance. Step-one presented an equivalent or higher precision than step-two. This is because we introduced a bias towards classification of positive cases in the step-one. This result shows that the models were overoptimistic toward positive classification, which indicates a good classification of relatively reliable negatives. When comparing accuracy and kappa, it is clear that step-two presented a highly superior performance than step-one when considering both classes, positive and RRN.

The reduction of LiDAR resolution impacts model performance, however, there is an especial attention that must be paid to the impact of noise that can be introduced by the aggregation method. LiDAR 5m presented the highest performance with almost perfect classification metrics and was able to classify the highest number of relatively reliable negatives. The changes in precision in the two steps of LiDAR 5m indicate that the RRN did not reduced the ability of the model of classifying positive correctly and the increase in accuracy and kappa corroborate that there was an overall improvement of the model.

Considering a balance among the performance metrics, there is a middle tier with very similar performance models LiDAR 30m, ANADEM, SRTM and ALOSPALSAR. ALOSPALSAR presents a lower precision, which is related to the ability of the model predict correctly positive points. The worst performing model was trained with ASTER.

Table 1: performances of random forest model trained with different digital elevation models

Name	Precision		Accuracy		Kappa		Nº of RRN
	Step-one	Step-two	Step-one	Step-two	Step-one	Step-two	
LiDAR 5 m	0.999	0.994	0.258	0.996	0.013	0.993	167
LiDAR 10 m	0.997	0.868	0.364	0.955	0.019	0.896	46
LiDAR 30 m	0.997	0.907	0.386	0.962	0.020	0.920	49

ANADEM	0.995	0.912	0.339	0.959	0.015	0.917	62
SRTM	0.994	0.914	0.360	0.956	0.015	0.911	74
ASTER	0.996	0.636	0.190	0.956	0.006	0.755	7
ALOSPALSAR	0.996	0.892	0.189	0.972	0.007	0.924	33

The probabilistic binary predictions, that is, the probability of a prediction being a flooded point, for all digital elevation models are shown in Figure 3. The Aricanduva catchment was classified into five susceptibility classes; very low, low, moderate, high and very high. The visual analysis show that the high and very high flood susceptibility areas are located around the main channel of the Aricanduva and around the outlet.

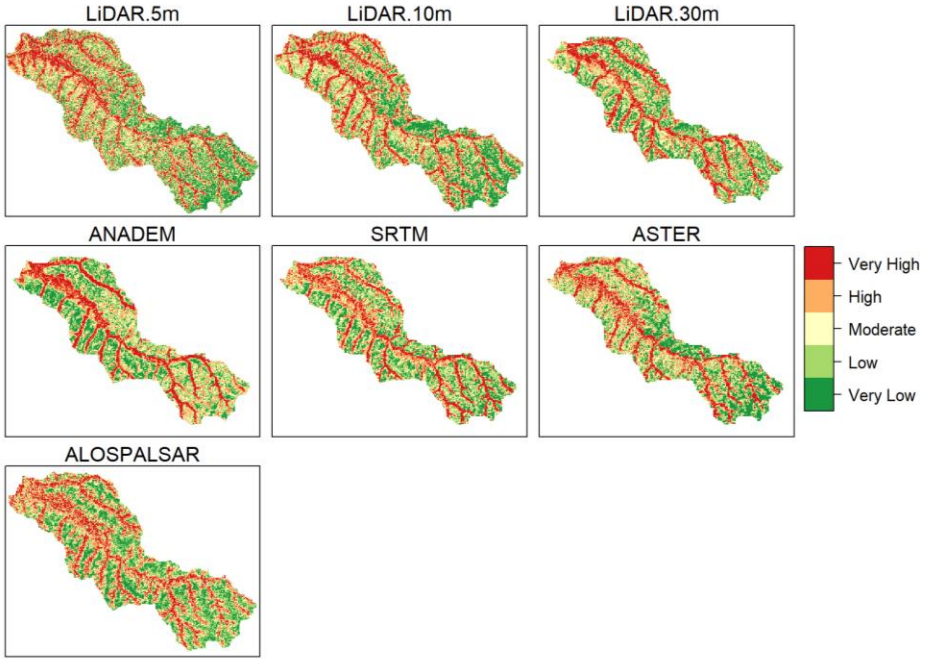

Figure 3: Flood susceptibility predictions produced by random forest model.

The variable importance that is extracted from the trained random forest in the step-two. The most important variable for all models was the height above the nearest drainage (HAND). The topographic position index (TPI) also played a significant role in model predictions. The number 35, 25 and 15 are the number of neighbouring cells, and, as observed in Table 2, the larger the number of neighbouring cells the more importance in model prediction. For all models, the D8 and flow direction (FLD) are not significatively important for model prediction and, for most models, FLD was unused for model predictions.

Table 2: Relative importance of terrain covariates (ordered by mean importance) extracted from the step-two random forest

Covariate	**LiDAR 5 m**	**LiDAR 10 m**	**LiDAR 30 m**	**ANADEM**	**SRTM**	**ASTER**	**ALOS PALSAR**	**Mean**
HAND	100.0	100.0	100.0	100.0	100.0	100.0	100.0	**100.0**
TPI_35	62.3	45.4	52.7	58.3	84.3	89.3	61.5	**64.8**

TPI_25	56.9	26.3	32.4	50.0	58.5	94.4	49.4	**52.6**
TPI_15	42.7	25.1	28.3	57.4	59.1	78.9	41.3	**47.5**
TRI	53.8	31.8	42.5	35.5	33.9	55.9	17.8	**38.7**
ROUGH	60.7	29.4	24.7	32.0	38.8	57.0	0.0	**34.7**
SLOPE	58.2	24.6	19.2	31.0	35.8	53.6	44.7	**38.2**
TPI	45.0	15.0	40.4	30.8	42.6	64.0	9.7	**35.4**
TPI_3	38.4	16.1	36.0	29.9	44.4	46.5	34.5	**35.1**
ASPECT	32.6	22.1	27.5	20.1	31.8	41.3	32.5	**29.7**
D8	9.6	5.8	9.1	7.7	9.7	13.3	15.4	**10.1**
FLD	0.0	0.0	0.0	0.0	0.0	0.0	2.4	**0.3**

4 CONCLUSION

This study investigated the use of different digital elevation models for flood susceptibility mapping using random forest. The machine learning models were developed in positive in unlabeled learning framework divided into two steps that is typical of flood inventory data that usually has only the positive cases (flooded points). The step-one generated a set of relatively reliable negative data points that were used the step-two to predict flood susceptibility. The results indicate that the random forest were able to correctly classify flood-prone areas, that were mostly controlled by the height above the nearest drainage and topographic position index that consider the influence of higher number of neighbouring cells.

The comparison of products indicates that LiDAR 5m, which was the lowest resolution, presented the best performance with precision, accuracy and kappa of 0.99. The reduction of horizontal resolution impacted model results, however, there was a good agreement that most used global digital models ALOS PALSAR, and SRTM and the Brazilian model ANADEM, presented high performance metrics with precision close to 0.90, accuracy to 0.96 and kappa close to 0.92. The results indicate that these models can be used for reliable flood mapping based on flood inventory in other study areas. The weakest model was produced by ASTER data with precision of 0.63, accuracy of 0.95 and kappa of 0.75.

Flood susceptibility mapping relies on historical flood records and static topographic variables and therefore does not explicitly represent temporal changes in land use, urban drainage capacity, or rainfall characteristics. Moreover, uncertainties related to input data resolution and the completeness of reported flood events may influence model performance. Future research should prioritize the integration of dynamic rainfall information, enhanced representation of urban drainage networks, and the coupling of the proposed framework with real-time hydraulic simulations to support operational flood early warning systems.

5 ACKNOWLEDGEMENTS

The authors acknowledge the support of the National Council for Scientific and Technological Development (CNPq) through research grants (processes 381989/2024-0 and 174232/2023-3) and funding provided by the CNPq/MCTI Call No. 15/2023 – Extreme Meteorological Events: Natural Disaster Prevention and Damage Minimization (process 446029/2023-8).

REFERENCES

Hijmans R (2025). _terra: Spatial Data Analysis. R package version 1.8-54, <https://CRAN.R-project.org/package=terra>.

Huang, Y., & Qin, X. (2014). Uncertainty analysis for flood inundation modelling with a random floodplain roughness field. Environmental Systems Research, 3(1), 9. https://doi.org/10.1186/2193-2697-3-9.
Kuhn, M. (2008). Building Predictive Models in R Using the caret Package. Journal of Statistical Software, 28(5), 1–26. https://doi.org/10.18637/jss.v028.i05.
Li, W., Liu, Y., Liu, Z., Gao, Z., Huang, H., & Huang, W. (2022). A Positive-Unlabeled Learning Algorithm for Urban Flood Susceptibility Modeling. Land, 11(11), 1971. https://doi.org/10.3390/land11111971
Liaw, A. and Wiener, M. (2002). Classification and Regression by randomForest. R News 2(3), 18--22.
Lindsay, J. B. (2016). Whitebox GAT: A case study in geomorphometric analysis. Computers & Geosciences, 95, 75-84. doi: http://dx.doi.org/10.1016/j.cageo.2016.07.003.
Mukomberanwa, N. T., & Madamombe, H. K. (2025). Next generation data-driven flood susceptibility modelling with spatial machine learning. Scientific African, e03082. https://doi.org/10.1016/j.sciaf.2025.e03082.
Pebesma, E., & Bivand, R. (2023). Spatial Data Science: With Applications in R. Chapman and Hall/CRC. https://doi.org/10.1201/9780429459016
R Core Team (2024). _R: A Language and Environment for Statistical Computing. R Foundation for Statistical Computing, Vienna, Austria. <https://www.R-project.org/>.
Rentschler, J., Salhab, M., & Jafino, B. A. (2022). Flood exposure and poverty in 188 countries. Nature communications, 13(1), 3527. https://doi.org/10.1038/s41467-022-30727-4.
Tehrany, M. S., Jones, S., & Shabani, F. (2019). Identifying the essential flood conditioning factors for flood prone area mapping using machine learning techniques. Catena, 175, 174-192. https://doi.org/10.1016/j.catena.2018.12.011.
Wu, Q., Brown, A. (2022). whitebox: 'WhiteboxTools' R Frontend. R package version 2.2.0 <https://CRAN.R-project.org/package=whitebox>

Web sites:
Web-1: https://metadados.geosampa.prefeitura.sp.gov.br/geonetwork/srv/por/catalog.search#/home, consulted 18 December 2025.

ICFM 10
Adapting to Global Change:
Innovative Approaches to Flood Management and Resilience
May 20-22, 2026 | Western University, London, Ontario, Canada

Next Generation Flood Model for Canada: A Comprehensive Approach by Impact Forecasting

Ladislav Palán[1], Martin Salaj[1], Petr Punčochář[1], Vít Kovačka[1], Tomáš Račoch, Vojtěch Sýs[1], Jan Vele[1]
Aon Impact Forecasting, Aon, Václavské náměstí 19, Praha 1, 110 00, Czechia[1]
E-mail: ladislav.palan@aon.com

ABSTRACT

Flooding is one of the most consequential natural hazards in Canada, regularly causing major economic losses. Catastrophic events in Alberta and Ontario in 2013 or in British Columbia in 2021 highlight the need for advanced, physically based and climate-aware flood risk tools for the insurance sector and others. Impact Forecasting, Aon's catastrophe model development center, has been developing a dedicated flood model for Canada since 2015, with successive updates including a pluvial component and a climate change view. The latest generation, Impact Forecasting Flood Model for Canada 3.0, is a complete rebuild using new datasets and modelling approaches. It covers the entire Canadian territory of roughly 10 million km²; integrates fluvial and pluvial flooding and storm surge. Hazard and vulnerability components are combined with detailed property information to estimate losses at high spatial resolution.

Flood maps are derived from large sets of 2D hydrodynamic simulations using high-resolution Digital Elevation Models with grid resolutions from 0.5m to 10m in areas containing over 95% of the population, complemented by 30m MRDEM and 2m ArcticDEM elsewhere. Simulations are performed in TUFLOW, producing flood depths, velocities at resolutions up to 5m. Hydraulic conditioning of DEMs includes artefact removal and explicit representation of channels and defenses, while pluvial simulations account for variable rainfall intensities, soil infiltration properties and urban stormwater drainage.

An atmospherically driven stochastic event catalog combines pluvial and fluvial events derived from long-term rainfall–runoff simulations. Forcing data include historical reanalyzes and CMIP5/CMIP6 climate model runs, which are bias-corrected and downscaled using machine learning to produce thousands of years of daily precipitation and temperature for present and future climates. The HYPE rainfall–runoff model is calibrated for Canadian conditions, including prairie hydrology, snow processes and ice jams, to generate stochastic river flows. In parallel, a storm surge component based on the SFINCS model simulates coastal and Great Lakes flooding from cyclone-driven events, enabling a consistent representation of multiple flood drivers within a single catastrophe modelling framework.

KEYWORDS: flood risk; Canada; fluvial flooding; pluvial flooding; storm surge; climate change; catastrophe model; hydrodynamic modelling

1 INTRODUCTION

Flooding is one of the most damaging natural hazards in Canada, causing large economic losses and social disruption. Recent events, such as the 2013 floods in Alberta and Ontario, the 2021 floods in British Columbia, and the 2024 floods in Quebec, have shown that Canadian flood risk is driven by multiple mechanisms, including river flooding, intense rainfall, snowmelt, ice jam and storm driven events. These events underline the need for physically based and climate aware tools to support flood risk management and decision making, especially in the insurance and reinsurance sectors.

Impact Forecasting, Aon's catastrophe model development center, has maintained a dedicated flood model for Canada since 2015. The original version focused mainly on fluvial flooding and was gradually enhanced by adding a pluvial component and a climate change view. However, advances in topographic data, hydrological and hydrodynamic models and climate information have created both the opportunity and the need to redesign the model more fundamentally.

The Impact Forecasting Flood Model for Canada 3.0 represents this next generation step. It is a complete rebuild that combines new high resolution Digital Elevation Models (DEMs), updated 2D hydrodynamic simulations and an atmospherically driven stochastic event catalog. The model covers the entire Canadian territory of about 10 million km² and explicitly represents fluvial and pluvial flooding and storm surge along the coasts and the Great Lakes. Hazard and vulnerability components are designed to be used with detailed property exposure data to estimate flood losses at high spatial resolution.

The aim of this paper is to present the methodological framework and overall architecture of the Impact Forecasting Flood Model for Canada 3.0, rather than to provide a full quantitative evaluation. We describe how the different hazard components are modelled, how long climate simulations and rainfall–runoff modelling are used to construct a stochastic event catalog, and how these elements fit within a catastrophe modelling context. Selected illustrative hazard outputs are shown, while full calibration and validation are left for future work.

2 MODEL ARCHITECTURE AND COVERAGE

The Impact Forecasting Flood Model for Canada 3.0 follows a standard catastrophe modelling structure (Figure 1). It combines a hazard component, representing physical flood processes, with a vulnerability component describing damage to exposed assets and an exposure component describing the spatial distribution and characteristics of insured property. Together, these components provide probabilistic estimates of flood losses for individual locations, portfolios and aggregated regions.

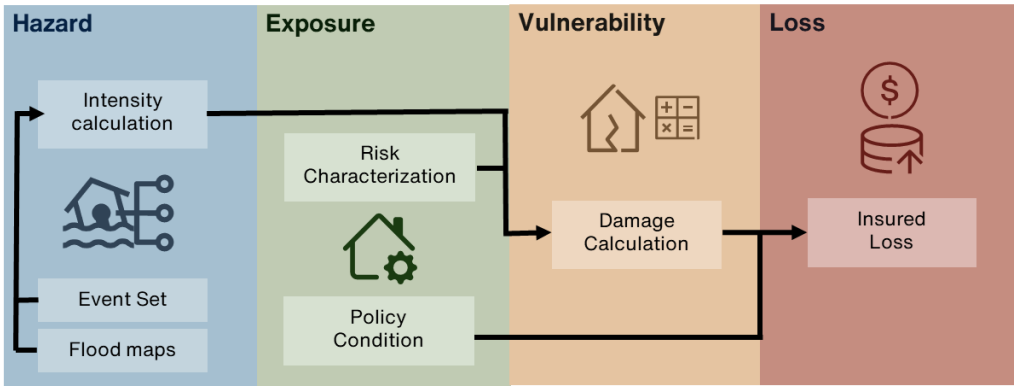

Figure 1: Scheme of catastrophe flood model

At the hazard level, the model integrates three main flood perils. Fluvial represents riverine inundation on the floodplain and in adjacent off floodplain areas. Pluvial flooding represents surface water accumulation driven by intense rainfall, including urban flooding where drainage capacity is exceeded. A storm surge component captures coastal and Great Lakes flooding caused by tropical cyclone driven events. All three components are built on a common terrain and hydrological basis.

The model covers the entire Canadian territory of approximately 10 million km². High resolution Digital Elevation Models HRDEM (Government of Canada, Natural Resources Canada, 2025) with grid resolutions between 0.5 m and 10 m are used in areas containing more than 95% of the population, enabling detailed representation of terrain, drainage features and flood defences. For the remaining areas, 30 m MRDEM (Government of Canada & Natural Resources Canada, 2025) and 2 m ArcticDEM (Morin et al., 2016) ensure full national coverage. Hydrodynamic simulations are run on these DEMs and hazard layers such as flood depths are generated at resolutions up to 5m, and can be aggregated to coarser resolutions when required.

On the loss side, hazard outputs are combined with regional and occupancy-specific vulnerability functions and detailed property exposure information. This allows the model to provide loss estimates for individual buildings where coordinates and attributes are available, as well as for aggregated administrative units. While this paper focuses on the hazard and event catalog components, the overall architecture in Figure 1 is designed to support end-to-end flood risk assessment across Canada.

3 HAZARD MAPS MODELLING METHODOLOGY

3.1 Digital Elevation Models and terrain processing

The hazard maps are modelled using HRDEM, MRDEM and ArcticDEM. All DEM sources are harmonized and converted to resolutions suitable for 2D hydrodynamic simulations, typically 5 m or 10 m. Before simulations, the terrain is hydraulically conditioned by removing artefacts, correcting artificial barriers and explicitly representing river channels, drainage features and known flood defenses. In urban areas, additional processing represents key conveyance elements such as canals, culverts and major overland flow routes, so that both fluvial and pluvial processes are consistently captured.

3.2 Fluvial flooding (floodplain and off-floodplain)

Fluvial hazard maps are based on a combination of hydrological analysis and 2D hydrodynamic simulations in TUFLOW (TUFLOW, 2025). Canada has a dense hydrometric network, with more than 7,000 discharge gauges in the national HYDAT database (Water Survey of Canada, 2025), particularly in populated regions. This network was used to perform frequency analysis of observed flows, derive design discharges for a range of return periods and characterize regional hydrological behavior. Several probability distributions were fitted at each station, including Lognormal (LN3), Gamma, General Extreme Value (GEV), Gumbel (GUM) and Weibull (WEI). To obtain design flows along the entire river network, graph theory concepts were applied to propagate and interpolate design discharges from gauged to ungauged basins. For ungauged catchments, hydrological similarity methods group basins based on multiple hydrological, topographic, morphological and climatological attributes and transfer information from better observed to data poor regions. The resulting design discharges provide consistent inputs for hydraulic simulations across the full model domain.

Hydrodynamic simulations in TUFLOW are then performed on the conditioned DEMs, using a Sub Grid Sampling approach (TUFLOW, 2025) that preserves fine scale terrain structure even when the computational grid is coarser, for example allowing 1m LiDAR information to be used in 5 m simulations. The fluvial component explicitly distinguishes between floodplain and off-floodplain areas. Floodplain maps represent direct river inundation for the design flows. The off-floodplain component captures damage mechanisms commonly observed in claims data outside the main inundation footprint, such as losses related to elevated groundwater levels causing seepage through basement walls or flooding caused by failure or absence of backflow protection on sewer connections. Information on flood protection measures, such as dikes and levees, and their indicative levels of protection is incorporated where available from municipalities or governmental sources, hydrological analyses or flood protection manuals, and complemented by automated ML detection methods where explicit defense data are limited.

3.3 Pluvial flooding

Pluvial hazard maps represent surface water flooding driven by intense rainfall events. Design rainfall is derived from intensity–duration–frequency (IDF) curves constructed using multiple datasets. Gridded products such as the Ensemble Meteorological Dataset for North America (EMDNA) (Tang et al., 2020a) are combined with station data from the Serially Complete Dataset for North America (SCDNA) (Tang et al., 2020b) and other Canadian sources to derive spatially consistent IDF curves across Canada. These curves provide design rainfall depths for a range of durations and return periods.

For hydrodynamic modelling, these IDF based design depths are converted into spatially distributed design storms using constructed hyetographs. A modified Chicago method (Keifer & Chu, 1957) is applied to generate temporal rainfall patterns consistent with the target IDF curves while concentrating peak intensities around a specified time within the storm. This allows the simulations to represent both total storm depth and realistic temporal clustering of intense rainfall, which is critical for pluvial flooding in urban catchments.

The same DEM as in the fluvial component is used, supplemented by land use and soil information that define spatially variable roughness and infiltration parameters. Infiltration is parameterized using soil and land surface datasets to distinguish between permeable and impervious areas and to reflect regional differences in soil properties. Pluvial simulations are carried out as 2D hydrodynamic simulations forced

by the design storms and represent key processes such as infiltration, surface storage and runoff concentration. Urban stormwater drainage systems are represented in the model with assumption of the location of inlets, outlets and their capacity capturing the onset of surface flooding once system capacity is exceeded. The resulting maps quantify the depth and extent of pluvial flooding, which can be combined with fluvial and off floodplain components in an integrated hazard view.

3.4 Storm surge

Coastal and Great Lakes flooding driven by storm surge is represented using the SFINCS model (Leijnse et al., 2021). This component simulates water level setup and overland inundation associated with severe storms and cyclone driven events along the Canadian coasts and selected Great Lakes shorelines. The simulations use the same DEM as the fluvial and pluvial components, ensuring consistent representation of topography, coastal defenses and low-lying areas. Storm surge hazard layers are produced for a set of tropical cyclones used in the US hurricane model certified by the Florida Commission and are later linked to the inland flooding event catalog. This allows storm surge events to be considered together with fluvial and pluvial events in a unified catastrophe modelling framework and supports analyses of multiple flood drivers affecting coastal areas.

4 CLIMATE FORCING AND STOCHASTIC EVENT CATALOG

4.1 Atmospheric forcing data

The stochastic event catalog is driven by long, consistent time series of precipitation and temperature compiled from several climate and reanalysis products. To represent present day variability, a 50 year window from 1987 to 2036 is used wherever possible, yielding more than 10,000 simulation years of daily forcing in total. For future climate conditions, multiple SSP scenarios with time windows from 2030 to 2100 are used. As a physically based reference, the ERA5 reanalysis (Hersbach et al., 2020) provides a baseline reconstruction of historical precipitation and temperature fields. It is complemented by the Ensemble Meteorological Dataset for North America (EMDNA) (Tang et al., 2020a), a station based, reanalysis infused product that blends gauge information with large scale fields. To extend the range of climate conditions and scenarios, bias corrected and downscaled outputs from global and regional climate models are included, in particular the CanLEAD (Cannon et al., 2022) and CanDCS M6 (Sobie et al., 2024) ensembles and dynamically downscaled simulations from the NA CORDEX framework for North America (Mearns et al., 2017).

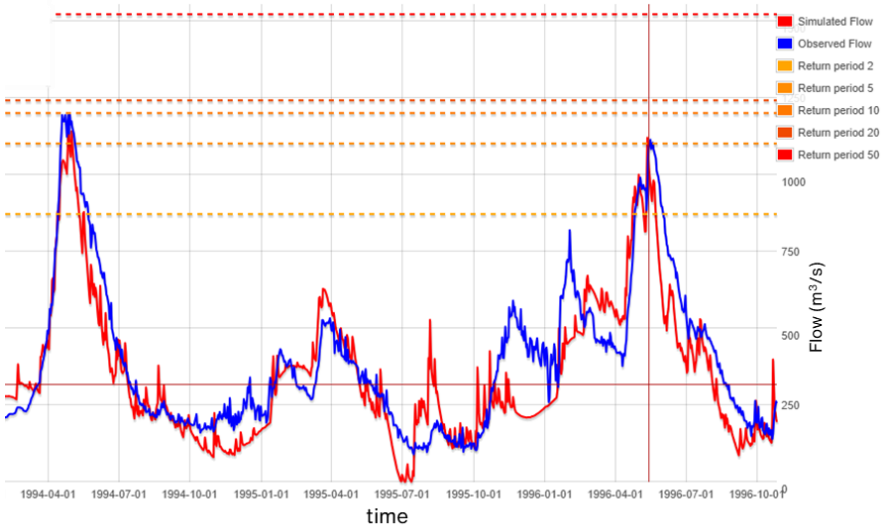

Figure 2: Example of HYPE–mizuRoute calibration at a selected HYDAT gauge, showing observed and simulated daily discharge and demonstrating the ability of the model to reproduce seasonal regimes and high-flow events.

4.2 Rainfall–runoff modelling

The hydrological transformation from precipitation and temperature to river flows is performed using the HYPE rainfall–runoff model (Lindström et al., 2010) with routing via the mizuRoute framework (Mizukami et al., 2016). HYPE is applied over the Canadian domain with parameterizations tailored to regional conditions, including prairie hydrology, snow accumulation and melt and other cold climate processes. Calibration is based on discharge observations from the national HYDAT network and other sources, with a focus on capturing both seasonal regimes and high flow behavior relevant for flooding and the insurance sector. An example of the calibration performance for one representative gauge is shown in Figure 2. The simulated hydrograph closely follows the observed discharge, capturing both the seasonal regime and individual high flow events, which is essential for reproducing the timing and magnitude of flood peaks relevant for hazard and loss modelling. The stochastic forcing is then run through the calibrated HYPE setup to generate long synthetic time series of river discharge along the river network. These simulations provide a consistent representation of hydrological variability and extremes under present and future climate conditions and form the basis for constructing the fluvial component of the stochastic event catalog. For selected regions and processes, additional hydrological components, such as ice jams, are incorporated where relevant to Canadian flood regimes.

4.3 Construction of the event catalog

The atmospherically driven stochastic event catalog is constructed by identifying flood relevant events within the long term hydrological and meteorological simulations. For fluvial flooding, candidate events are detected based on river discharge peaks exceeding specified thresholds or return period levels (RP 1 in 2 years with potential to cause insured losses) at locations across the river network, and spatial–temporal clustering algorithms group related peaks into basin scale or multi basin flood events. For pluvial flooding, events are identified from precipitation fields, focusing on high intensity and short duration rainfall critical for surface water flooding. Thresholds are applied to accumulated rainfall over relevant durations, and spatial clustering is used to define pluvial. The identification of pluvial and fluvial events is done together so that concurrent or causally related phenomena (e.g. storms producing both heavy rainfall and elevated river flows) are represented as combined events in the catalog. Each event in the catalog is associated with a set of hazard maps generated by hydrodynamic simulations.

4.4 Integration with storm surge events

Storm surge events are integrated into the same catalog to enable a multi-peril view of flood risk. For coastal and Great Lakes regions, cyclone-driven systems are identified within the climate and reanalysis datasets based on metrics such as low pressure, strong winds and elevated water levels. Stochastic catalog of TC events is used to drive SFINCS simulations of storm surge and coastal inundation, producing hazard layers that are linked to corresponding atmospheric conditions.

5 RESULTS AND DISCUSSION

5.1 Fluvial and pluvial flood extents

To demonstrate the capabilities of the fluvial component, Figure 3 presents an example of simulated flood extents and depths for a selected river reach in a densely populated area. The map shows a 1 in 100-year fluvial event derived from the hydrological frequency analysis.

The final flood extents highlight several key features of the model. High resolution terrain allows floodplain geometry, local depressions and flow paths to be represented in detail, which is reflected in the spatial variability of flood depths near the channel and in adjacent low-lying areas. The inclusion of flood protection measures is visible in the way defences constrain or redirect inundation. These aspects are essential for reproducing observed claim patterns during large river floods. In addition, the same combination of high-resolution terrain, spatially variable infiltration and an aggregated representation of stormwater drainage leads to realistic patterns of urban flooding. Water accumulates in local depressions,

behind transport embankments and along streets that act as flow conduits, and even where river flooding is minor, pluvial processes can generate significant surface water depths and associated losses.

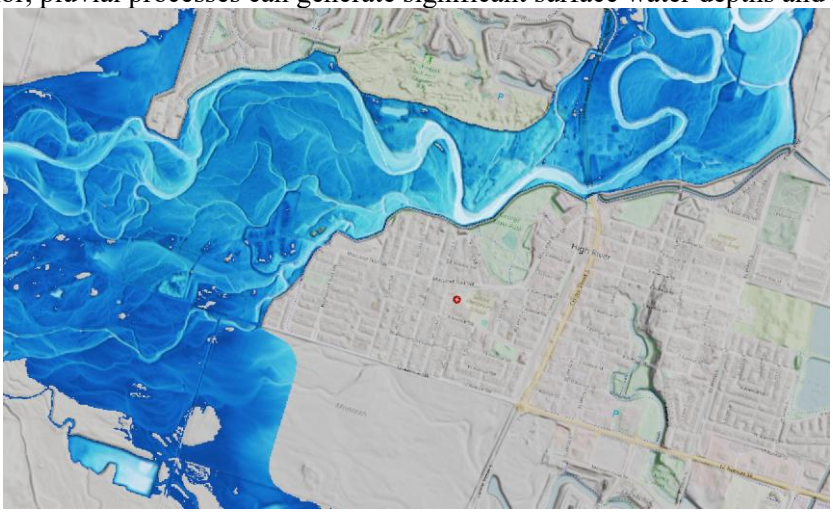

Figure 3: Example of simulated fluvial flood depths for return period 1 in 100 years, close to High Rivers with all design protection included in simulation

5.2 Combined multi-peril perspective

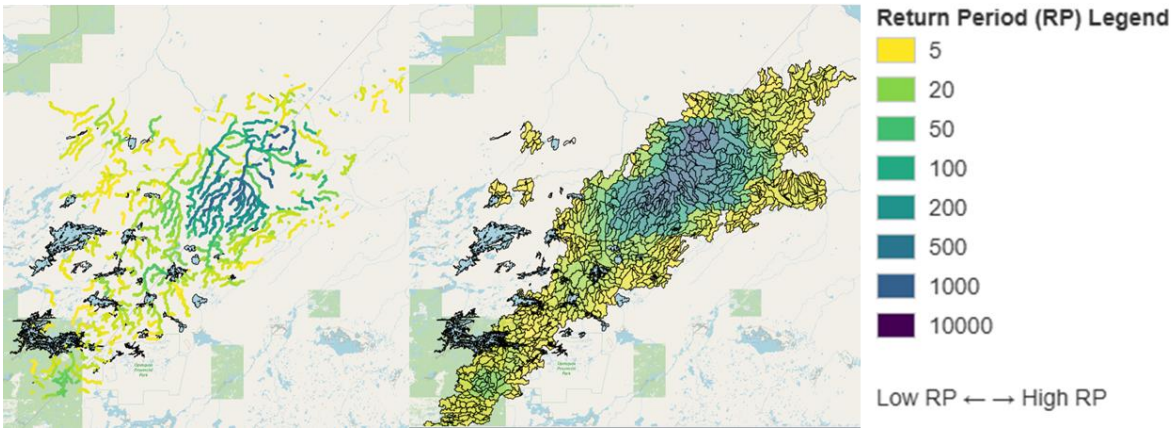

Figure 5: Combined view of fluvial and pluvial event close to Nelson and Severn, event duration is 6 days, max return period of flows is higher than 1 in 1000 years.

Although a full multi-peril analysis is beyond the scope of this paper, the integrated design of the hazard components and the stochastic event catalog enables combined views of fluvial, pluvial and storm surge flooding. In coastal or Great Lakes regions, pluvial flooding driven by intense rainfall can coincide with elevated water levels and overland inundation from storm surge, while widespread storm systems may generate both high river flows inland and pluvial flooding in urban centers. Within the catastrophe modelling framework, such combined situations are represented by single catalog events that carry consistent hazard layers from all relevant components. This allows analyses of compound flooding scenarios and provides a more realistic picture of potential losses for portfolios exposed simultaneously to river, surface water and coastal flooding.

5.3 Methodological strengths and current limitations

The presented examples illustrate several methodological strengths of the Canada Flood Model 3.0. High resolution DEMs and detailed terrain conditioning improve the realism of simulated flow paths and

local inundation patterns. The integration of an extensive hydrometric network, frequency analysis and graph-based extrapolation for design flows supports a consistent representation of fluvial hazard across gauged and ungauged catchments. For pluvial, the use of EMDNA, SCDNA to derive spatially consistent IDF curves, combined with design storms constructed using a Chicago type method, allows urban surface water flooding to be represented in a physically meaningful way. The atmospherically driven event catalog, based on long climate simulations and HYPE rainfall–runoff modelling, provides a coherent framework for simulating a broad range of events under current and future climates.

At the same time, several limitations and ongoing developments need to be acknowledged. Calibration and validation against historical flood events and claims data are still in progress and will be documented separately as well as detailed description of entire Vulnerability component framework with unique calculation of loss ratios based on both water depths and velocities. In some regions, especially in sparsely monitored or data poor areas, uncertainties in input datasets and hydrological parameters remain higher. The representation of urban drainage systems is necessarily simplified and may not capture all local infrastructure details. Finally, while the integration of storm surge with pluvial and fluvial components is conceptually implemented, further work is required to fully characterize compound flooding and associated dependencies in a probabilistic way.

Overall, the preliminary results suggest that the methodological choices underlying the Canada Flood Model 3.0 provide a solid basis for detailed, multi-peril flood hazard assessment across Canada, while also indicating where additional data and model refinements can further improve performance.

6 CONCLUSION

This paper presented the methodological framework and architecture of the Impact Forecasting Flood Model for Canada 3.0. The model combines high resolution terrain data, hydrological analysis and 2D hydrodynamic simulations to represent fluvial, pluvial and storm surge flooding across the entire Canadian territory of about 10 million km².

A key element of the approach is the integration of dense hydrometric observations, frequency analysis and graph-based extrapolation of design flows for fluvial hazard, together with IDF based design storms and Chicago type hyetographs for pluvial hazard. These components are driven by long, bias corrected and downscaled climate forcing, transformed into river flows using the HYPE model and organised into an atmospherically driven stochastic event catalog.

Illustrative examples show how the model captures detailed floodplain inundation, urban pluvial flooding and combined fluvial–pluvial impacts, providing a consistent basis for multi-peril flood risk assessment. Ongoing and future work focuses on systematic calibration and validation against observed events and claims data, refinement of urban drainage representation and more detailed treatment of compound flooding, including interactions with storm surge.

7 ACKNOWLEDGEMENTS

The authors would like to thank their colleagues at Aon Impact Forecasting in Prague, Bengaluru and Singapore, who have contributed to the development of the Canada Flood Model 3.0, from data processing and hydrodynamic modelling to software implementation and testing. We also acknowledge Aon colleagues in Toronto for their input on market needs, client use cases and historical event experience, which has helped to align the model design with practical applications in the insurance and reinsurance industry. Finally, we are grateful to Professor Alain Pietroniro and his team at the University of Calgary for their collaboration on the methodological development of the rainfall–runoff component.

REFERENCES

Cannon, A. J., Alford, H., Shrestha, R. R., Kirchmeier-Young, M. C., & Najafi, M. R. (2022, November). Canadian Large Ensembles Adjusted Dataset version 1 (CanLEADv1): Multivariate bias-corrected

climate model out puts for terrestrial modelling and attribution studies in North America. Geoscience Data Journal , 9 (2), 288–303, from https://rmets.onlinelibrary.wiley.com/doi/10.1002/gdj3.142 doi: 10.1002/gdj3.142

Government of Canada, Environment and Climate Change Canada, Water Survey of Canada. (2025,Environment and Climate Change Canada, Water Survey of Canada. (2019). HYDAT: National Water Data Archive. Government of Canada. https://www.canada.ca/en/environment-climate-change/services/water-overview/quantity/monitoring/survey/data-products-services/national-archive-hydat.html (canada.ca)

Government of Canada, Natural Resources Canada. (2025). Medium Resolution Digital Elevation Model (MRDEM) – CanElevation Series – Product specifications (Edition 1.2). Government of Canada. https://ftp.maps.canada.ca/pub/elevation/dem_mne/MRDEM_MNEMR/CanElevation-MRDEM-Product-Specifications.pdf

Government of Canada, Natural Resources Canada. (2025). High Resolution Digital Elevation Model (HRDEM) – CanElevation Series – Product specifications (Edition 1.6). Government of Canada. https://ftp.maps.canada.ca/pub/elevation/dem_mne/highresolution_hauteresolution/HRDEM_Product_Specification.pdf

Hersbach, H., Bell, B., Berrisford, P., Hirahara, S., Horanyi, A., Munoz-Sabater, J.,. . . Thepaut, J. (2020, July). The ERA5 global reanalysis. Quarterly Journal of the Royal Meteorological Society, 146 (730), 1999–2049., from https://onlinelibrary.wiley.com/doi/10.1002/qj.3803 doi:10.1002/qj.3803

Keifer, C. J., & Chu, H. H. (1957). Synthetic storm pattern for drainage design. Journal of the Hydraulics Division, ASCE, 83 (4), 1–25.

Lindström, G., Pers, C., Rosberg, J., Strömqvist, J., & Arheimer, B. (2010, June). Development and testing of the HYPE (Hydrological Predictions for the Environment) water quality model for different spatial scales. Hydrology Research,41 (3-4), 295–319., from https://iwaponline.com/ hr/article/41/3-4/295/822/Development-and-testing-of-the-HYPE

Leijnse, T., van Ormondt, M., Nederhoff, K., & van Dongeren, A. (2021). Modeling compound flooding in coastal systems using a computationally efficient reduced-physics solver: Including fluvial, pluvial, tidal, wind- and wave-driven processes. Coastal Engineering, 163, 103796. https://doi.org/10.1016/j.coastaleng.2020.103796

Mizukami, N., Clark, M. P., Sampson, K., Nijssen, B., Mao, Y., McMillan, H., . . .Brekke, L. D. (2016). mizuroute version 1: a river network routing tool for a continental domain water resources applications. Geoscientific Model Development , 9 (6), 2223–2238. https://gmd.copernicus.org/articles/9/2223/2016/ doi: 10.5194/gmd-9-2223-2016

Mearns, L., McGinnis, S., Korytina, D., Arritt, R., Biner, S., Bukovsky, M., . . .Kessenich, L. (2017). The NA-CORDEX dataset. UCAR/NCAR. https://na-cordex.org/ doi: 10.5065/D6SJ1JCH

Sobie, S. R., Ouali, D., Curry, C. L., & Zwiers, F. W. (2024, July). Multi variate Canadian Downscaled Climate Scenarios for CMIP6 (CanDCS955

M6). Geoscience Data Journal , gdj3.257. Retrieved 2025-10-24, from https://rmets.onlinelibrary.wiley.com/doi/10.1002/gdj3.257 doi:10.1002/gdj3.257

Morin, P., Porter, C., Cloutier, M., Howat, I., Noh, M. J., Willis, M., ... & Peterman, K. (2016, April). ArcticDEM; a publically available, high resolution elevation model of the Arctic. In Egu general assembly conference abstracts (Vol. 18, p. 8396).

Tang, G., Clark, M. P., Papalexiou, S. M., & Knutti, R. (2020a). Ensemble meteorological dataset for north america (emdna). Earth System Science Data, 12 ,3571–3580. doi: 10.5194/essd-12-3571-2020

Tang, G., Clark, M. P., Newman, A. J., Wood, A. W., Papalexiou, S. M., Vionnet, V., & Whitfield, P. H. (2020b). SCDNA: a serially complete precipitation and temperature dataset for North America from 1979 to 2018. Earth System Science Data, 12 (4), 2381–2409. https://essd.copernicus.

TUFLOW. (2025). TUFLOW Classic/HPC User Manual 2025.2 (Version 2025.2). BMT Commercial Australia Pty Ltd. https://docs.tuflow.com/classic-hpc/manual/2025.2/overview.html

ICFM 10
Adapting to Global Change:
Innovative Approaches to Flood Management and Resilience
May 20-22, 2026 | Western University, London, Ontario, Canada

Accounting for Reasonably Plausible Flood Conditions, such as Bridge Obstruction, in Floodplain Mapping

Sophia Eugeni[1], Vanessa McMaster[1], and Dale Muir[1]
Northwest Hydraulic Consultants Ltd., 30 Gostick Place, North Vancouver, Canada[1]
E-mail: SEugeni@nhcwater.com

ABSTRACT

Often, floodplain mapping is based on existing channel conditions, as observed. However, conditions may change during a flood, such as obstruction and sedimentation at bridges, which can substantially increase flood levels for a given flood flow. It is argued that consideration of reasonably plausible flood conditions must be given in the development of floodplain maps. NHC prepared floodplain maps for a 62 km reach of the Salmon River in southern British Columbia, Canada, using a HEC-RAS 2D numerical hydraulic model. The study reach contained 55 bridge crossings. Although channel obstruction can occur at a variety of locations along a channel, such as from slope failure or from debris or ice jams at constrictions, sharp bends or changes in slope, the greatest likelihood and sensitivity to channel obstruction within the study reach were at these bridge crossings. Using this sample project, an investigation into approaches to assess and incorporate the influence of potential obstructions at crossings in floodplain mapping is presented.

KEYWORDS: Floodplain Mapping, Hydraulic Modelling, Bridge Blockage

1 INTRODUCTION

Bridge crossings can influence hydraulic behaviour in a river by introducing substantial hydraulic losses, causing increased upstream flood levels and extents and in some cases attenuating unsteady flows, resulting in measurable reduction in downstream peak flows. These influences are greater when crossings are obstructed. The potential variable condition of bridge crossings and their hydraulic performance during a flood increases uncertainty in flood results, which needs to be accounted for in hydraulic modelling and ultimately in floodplain mapping.

For the purposes of floodplain mapping, bridges are typically modelled without any obstruction and, as such, may underestimate upstream flood levels and extents. During the recent Shuswap Region Floodplain Mapping Project, conducted for the Fraser Basin Council, the impacts of bridge obstruction on floodplain mapping were investigated using a case study analysis of the Salmon River (NHC, 2025).

2 CASE STUDY CONTEXT

The study area is the 62 km long reach of the Salmon River from the town of Falkland to Salmon Arm. The study reach includes 55 bridges (Figure 2.1). Likelihood of obstruction and sensitivity of flood extents to crossing obstruction varied across the set of crossings within the study reach. Some of the structures were well above the channel with a clear span much larger than the channel's width and larger than the length of riparian trees. However, other crossings had multiple piers, trestle support, or relatively low farm-access crossings with little clearance between the soffit and the typical high water level.

Fieldwork for the study included aerial survey, ground survey, and ground observations. These were conducted during the spring of 2023, at which time a flood occurred with a peak flow similar to a five to ten-year average return period event. Flow was obstructed by debris at a number of the structures.

The Railway Bridge (Figure 2.1d) was identified as highly sensitive to obstruction. Accordingly, further analysis was conducted of this structure to quantify the potential impacts of obstruction at this structure on inundation extents and levels.

a) Multi-pier bridge with debris being removed

b) Typical low clearance farm bridge.

c) Low clearance farm bridge experiencing pressurized flow.

d) Wood trestle bridge accumulating debris.

Figure 2.1 Sample of Bridges along the Salmon River

3 APPROACH

Within the context of floodplain maps in British Columbia, Canada, flood levels are calculated for a specific design flood event, typically the 200-year flood event, with a freeboard applied to this level to establish the flood construction level and accompanying flood extents. The freeboard is a vertical allowance used to account for local variations in water level (i.e., surging, superelevation, local

turbulence) and uncertainty in the data, analysis, and mapping. This methodology allows the hydrotechnical engineer the ability to establish both expected suitable design conditions – to calculate the 200-year flood level – and the level of uncertainty – to establish a suitable freeboard.

Numerical modelling was used to evaluate the hydraulic response of the channel and floodplain to the hydrologic design event. The same numerical model was used to evaluate the influence of bridge obstructions on flood level and extent to support a quantified assessment of uncertainty. The two-dimensional numerical hydraulic model was developed in HEC-RAS 6.4.1. Three scenarios of bridge obstructions were simulated: clear (0% obstruction), partial obstruction (20% blocked), and near complete blockage (80% blocked).

3.1 Simulation Scenarios

Since the study reach included a large quantity of bridges, it wouldn't be practical to individually assess the sensitivity of the results at each bridge, one by one. Therefore, to understand the range of influence of the crossings on the resulting floodplain maps, obstructions were simulated using the three severities of obstruction at all bridges and then evaluated in greater detail at the crossings identified as probable for obstruction and where flooding is most sensitive to crossing obstruction.

Comparison of flood levels and extents between the clear conditions and the obstructed scenarios enabled identification of the bridges most sensitive to obstruction.

The Railway Bridge was determined to be highly likely to be obstructed given the trestle style of bridge, the observed upstream large overhanging, and in some cases undermined and failing, trees, and extent of debris caused obstruction observed during field investigations. The Railway Bridge was also determined to be highly sensitive to obstruction. The structure spans a localized deeply confined floodplain within a low gradient reach, and as shown through the modelling, slight increases in obstruction can result in large increases in upstream flood level and flood extent. Therefore, the Railway Bridge was one of the bridges where obstructions were further investigated.

3.2 Methods to Simulate Bridge Obstructions at a Single Crossing

Further analysis was conducted at crossings identified as sensitive to obstruction (from model results) and relatively likely to be obstructed (from crossing span, clearance, style, and upstream supply for potential debris recruitment). Debris blockage at hydraulic structures is impactful because it reduces the cross-sectional area in the channel section available to convey streamflow. There are several ways to represent this mechanism in the hydraulic model, such as:

1. Applying the HEC-RAS Floating Pier Debris tool.
2. Extending the bridge abutment from the left or right to narrow the channel section.
3. Extending the bridge abutment from both sides of the channel to narrow the channel section.
4. Lowering the low chord of the bridge deck.
5. Raising the channel bed to reduce the channel cross-section.

The approach(es) selected depends on the style of bridge and expected mechanism of flooding obstruction (e.g., debris, ice, sedimentation).

For Scenario 1: Clear Conditions and the final design scenario for the project, the Railway Bridge was simulated as blocked by 20% to represent existing conditions, as it is never expected to be fully clear of debris. Calibration data was collected for this hydraulic structure, upstream and downstream of the crossing, where the debris obstruction effects were causing a difference in water surface elevation of approximately 1 m. The calibration data was used to validate the application of the floating pier debris tool at this crossing. In the design scenario, the floating pier debris tool was used to simulate the obstruction effects of the debris. This was an example of a structure in the study area which required a detailed assessment of the impacts of obstruction.

However, to assess the model sensitivity to debris obstruction at the hydraulic crossings, the obstructions were simulated as simply and efficiently as possible, for the purpose of evaluating the impact at all bridge locations in the model. It was noted that during the site investigation, the Railway Bridge was blocked from the left bank towards the center of the crossing, with debris floating at the waterline on the upstream side of the bridge. Following this observation, the obstruction modelling Option 2 (as listed above) was used to block the structures from the left bank when debris blockages were applied to bridges in the model, as in Scenario 2 (Expected Conditions) and Scenario 3 (Extreme Conditions) (Figure 3.1).

Since the Railway Bridge had a high sensitivity to blockage, different methods of blocking the bridge were tested and compared. In addition to the floating pier debris tool, blockages from the left bank and both banks were simulated. The results of this analysis are compared in the next section.

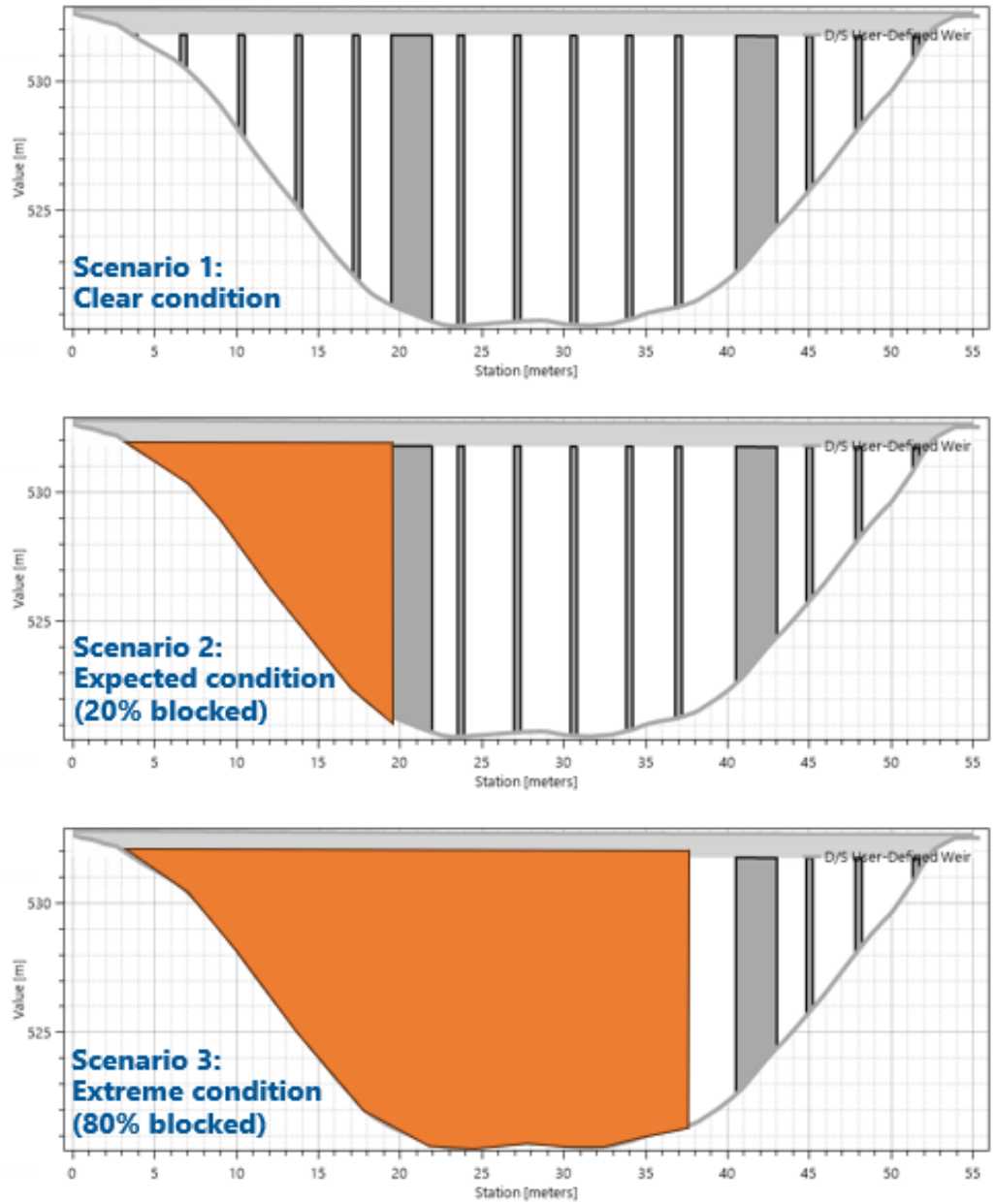

Figure 3.1 Hydraulic Model Bridge Blockage Scenarios presented on the model-simplified Railway Bridge

4 RESULTS

To evaluate the sensitivity of bridges to obstruction, both changes in water surface elevations and inundation extents were compared across the three obstruction simulation scenarios.

The profile plot (Figure 4.1) of the water surface elevations of each simulated scenario demonstrates a noticeable increase from the Scenario 1: Clear Conditions profile at some bridge locations, with a substantial increase in simulated flood water surface elevations at the railway bridge (circled in orange). This increase in water surface elevation indicates that flow is being constricted at these structures.

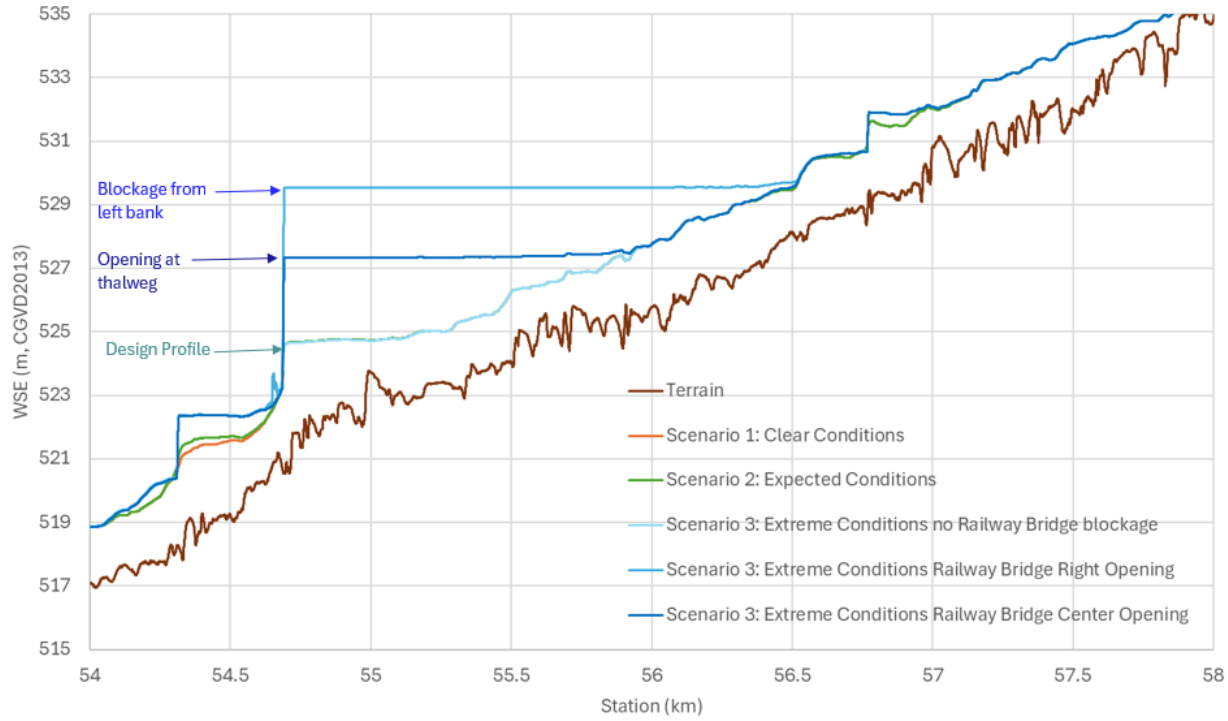

Figure 4.1 Profile plot comparing blockage scenarios at the Railway Bridge.

A closer view of the profile plot (Figure 4.1) at the Railway Bridge emphasizes that the manner in which the bridge is blocked can make a substantial difference in the ability of the crossing to convey flow without influencing hydraulic behaviour. The plot shows the difference between blocking the railway bridge 80% from the left bank versus narrowing the channel from both sides and leaving the thalweg of the channel at the bridge open for conveyance. The difference in modelling blockage technique resulted in a difference in water surface elevations over 2 m upstream of the bridge, and a much farther backwater influence upstream (~ 1 km from the crossing).

The increase in inundation extents once the Railway Bridge is 80% blocked is displayed on the left in Figure 4.2. The backwatering effects caused an increase in inundation extents upstream of the bridge, for over 1 km.

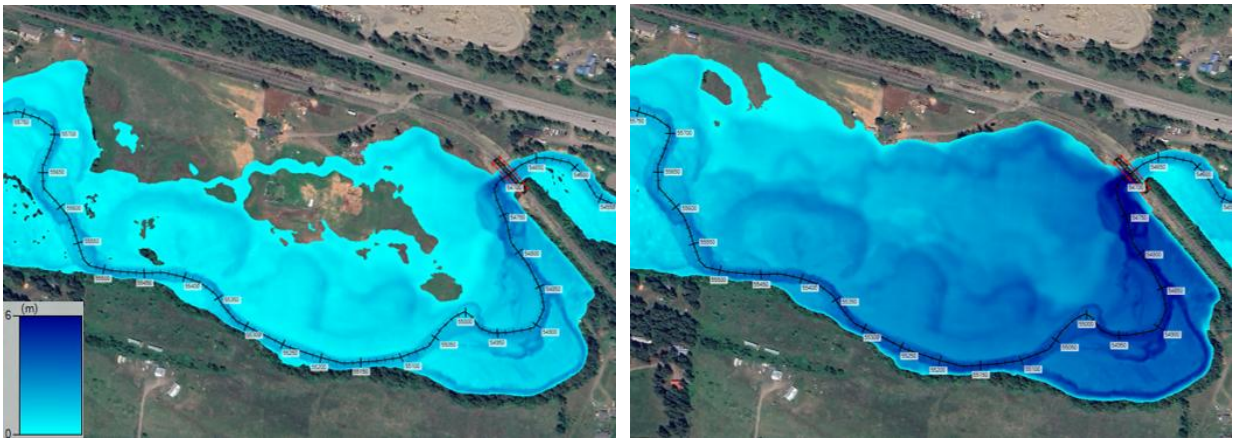

Figure 4.2 Railway Bridge flood extent comparison. Scenario 2: Expected Conditions (left), Scenario 3: Extreme Conditions (right).

The project identified five bridges vulnerable to obstruction along the reach to be investigated individually. Scenario 3: Extreme Conditions was used to compare the increase in blockage depth to a critical increase in depth (study-specific, in this case, 1.5 m was used) from the design scenario to determine which bridges in the study reach would be identified as sensitive to debris blockage.

5 CONCLUSIONS

The blockage scenario comparisons confirmed that bridge obstructions can have substantial impacts (exceeding 1.5 m) on the surrounding flood levels, highlighting the need for consideration during floodplain mapping projects. As was done in this case study, assessing multiple bridge blockages simultaneously is a useful approach to efficiently identify which structures are likely to have a higher flood response to blockage. Once these structures are identified, further analysis can be conducted to evaluate the sensitivity of the surrounding water elevations to blockage at specific structures.

Based on the general level of uncertainty identified at the 55 bridge crossings, a freeboard of 0.6 m was applied to the study. Ultimately, the study demonstrated that the sensitivity of some bridges to obstruction in the floodplain mapping model exceeds the uncertainty accounted for by the freeboard in the project maps. In these situations, rather than overconservatively raising the freeboard for the entire project, the approach of blocking the identified sensitive bridges (as determined by the potential to cause increases in flood level above the design flood event of greater than 1.5 m) in the model accounts for the inherent increase in uncertainty at the structures which are likely to be blocked.

Especially in regions which do not include freeboard in their floodplain maps, the differences caused by bridge obstruction can have implications on results and should be accounted for in floodplain mapping analysis.

6 ACKNOWLEDGEMENTS

The case study project was the Shuswap Region Floodplain Mapping project, which was funded by the Government of Canada and the Province of British Columbia through the Flood Hazard Identification and Mapping Program (FHIMP). It was administered and coordinated by Fraser Basin Council (FBC) and supported by a technical committee including representatives from FBC, Environment and Climate Change Canada (ECCC), Natural Resources Canada (NRCan), and the BC Ministry of Water, Land and Resource Stewardship (WLRS).

REFERENCES

NHC (2025). Shuswap Region Floodplain Maps - Riverine and Coastal Hydraulics. Final Report. Prepared for Fraser Basin Council by Northwest Hydraulic Consultants Ltd., North Vancouver, BC.

ICFM 10
Adapting to Global Change:
Innovative Approaches to Flood Management and Resilience
May 20-22, 2026 | Western University, London, Ontario, Canada

Estimating Flood Damages in Data-Sparse Regions: Challenges, Uncertainties, and Strategies for Efficient Field Data Collection

Nathan Valsangkar[1] and Ben Humphreys[2]
Northwest Hydraulic Consultants Ltd. (NHC), North Vancouver, BC, Canada

E-mail[1]: NValsangkar@nhcwater.com
E-mail[2]: BHumphreys@nhcwater.com

ABSTRACT

Flood risk assessments are powerful tools for supporting flood management decisions. These assessments often rely on flood damage estimates to quantify potential economic losses, evaluate mitigation strategies, and understand community vulnerability. However, accurate flood damage estimation requires detailed information on flood hazards and the characteristics of exposed assets. In data-sparse regions, practitioners must often rely on simplifying assumptions or undertake field data collection for site-specific analysis. Both have limitations: simplifying assumptions may introduce uncertainty, while data collection in remote communities poses financial and logistical challenges. A critical evaluation of uncertainty sources is needed to guide decisions on balancing study accuracy and data collection costs. This study conducts an uncertainty analysis of flood damage estimates for a First Nation community in Northern BC using the open-source NRCan CanFlood software. The analysis relies on flood damage estimates from a highly detailed building dataset for the community, which serves as a reference case for relatively low uncertainty. To assess the impact of data limitations, we remove layers of information from the detailed dataset, replace them with simplifying assumptions, and quantify the associated change in damage estimates. We also assess, through sub-sampling of the building dataset, how uncertainty may change with differing community sizes from 5 to 100 buildings. Uncertainty ranges are compared to other sources of uncertainty such as hydrology, hydraulics, and the use of depth-damage vulnerability curves. The findings highlight key uncertainty sources affecting flood damage estimates and inform efficient field data collection strategies to balance cost against acceptable levels of study uncertainty. These insights can support more reliable flood risk assessments in data-sparse regions.

KEYWORDS: Flood, risk, CanFlood, uncertainty, sensitivity, vulnerability, Nass, Nisga'a

1 INTRODUCTION

The shift toward risk-based flood management has elevated the importance of quantitative flood risk models. These models integrate four key components to estimate flood risk, whether at the event level (e.g., 200-year flood) or annualized: flood hazard (primarily inundation depth), exposure (e.g., asset inventories), asset value, and vulnerability (e.g., depth–damage relationships). Each component introduces uncertainty, which propagates through the analysis and accumulates in the final damage estimates (de Moel & Aerts, 2011). Understanding and managing these uncertainties is critical for producing reliable risk assessments and supporting decision making.

While flood risk uncertainties have been examined in prior studies (e.g., Ward et al., 2011), a bibliometric review by Diez-Herrero and Garrote (2020) found that only one-sixth of published flood risk assessments examine uncertainty as a key topic. Existing research largely focuses on urban or regional scales with high-quality data. In British Columbia (BC), recent policy shifts aim to extend flood risk assessments to remote and Indigenous communities (BC, 2024), where data scarcity is common. These

assessments often depend on assumptions or limited datasets, which can significantly affect study outcomes (Rrokaj et al., 2025). Collecting additional data may be costly or infeasible. Identifying dominant uncertainty sources in small-scale, data-limited contexts is essential to guide efficient data collection strategies and use of reasonable assumptions.

The purpose of this study is to determine whether the detail of a building asset inventory can be reduced to significantly lower data collection requirements for future studies. The question arose after a detailed building asset inventory was developed for a flood risk assessment of Nisg̲a'a villages in northwest BC. The objectives of this study are to determine whether simplified building assumptions are sufficient for the calculation of annualized flood risk, whether these yield results that are within acceptable uncertainty bounds, and how this uncertainty compares to other sources of uncertainty inherent in the risk assessment.

2 STUDY AREA AND DATA SOURCES

The study area consists of the villages of Lax̲galts'ap and Gitwinksihlkw in the Nass River Valley, in Northwestern BC, Canada. Figure 1 shows the village locations, as well as the distribution of buildings and floodplain extents. Gitwinksihlkw is subject to riverine flooding from the Nass River, has a population of 207 people (as of the 2021 census), and contains 70 buildings. Lax̲galts'ap is subject to riverine flooding from both the Nass River and Greenville Creek, has a population of 248, and contains 186 buildings. The buildings in both villages are primarily residential, with some being commercial and institutional (of both the Nisg̲a'a Lisims Government and Village governments).

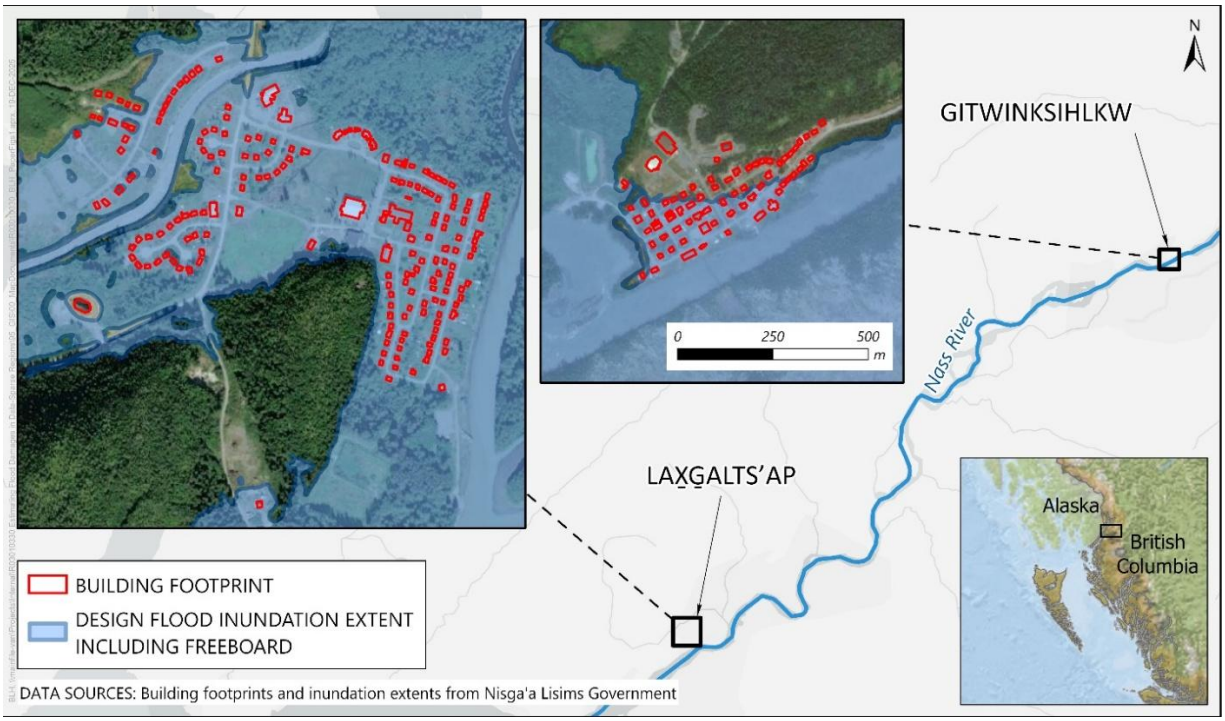

Figure 1: Location of Nisg̲a'a Villages within study area.

2.1 Flood Hazards

This study focuses on flood hazards and risks primarily associated with the Nass River. The Nass River originates in the Skeena Mountains and has the third largest watershed entirely contained in British Columbia, draining an area of roughly 20,500 km^2 (Cascadia, 1997). Peak flood flows typically occur in June due to spring freshet; however, the largest floods have been generated by extreme fall precipitation. Detailed flood hazard data for Gitwinksihlkw and Lax̲galts'ap was developed from local hydrologic and floodplain mapping studies completed for the Nisg̲a'a Lisims Government (NHC, 2022). Those studies

used gauge flood frequency analysis (93-year record period, spanning back to 1917) to estimate Nass River discharges at the two villages for return periods up to 500 years. Greenhouse gas emission scenarios from CMIP6, SSP5-8.5 were also modelled to assess increased flood discharges for the mid- (2041-2070) and end-of-century (2071-2100) climate periods. Flood discharges were input to a calibrated two-dimensional numerical model (HEC-RAS 6.1) to simulate floodplain hydraulics. Key outputs utilized included floodplain limits and raster files of flood elevation, depth, and velocity. For the present study, we used hydraulic model outputs from the end-of-century climate period as those produced the greatest inundation extents and a larger sample size of buildings for uncertainty analysis. Return periods evaluated included the 5-, 10-, 25-, 50-, 100-, 200-, and 500-year events.

2.2 Building Inventory

The detailed building asset inventory dataset consisted of attributed building footprint polygons in a GIS format. The polygon boundaries were derived from full-feature lidar data, with manual modifications based on imagery and photogrammetry-derived point cloud data where applicable (see description below, and overview of the point cloud for the Village of Gitwinksihlkw in Figure 2). Manual modifications included the removal of outbuildings (e.g., sheds), and the addition and removal of buildings that were not correctly represented or did not exist at the time of the lidar data collection.

Figure 2: Overview of photogrammetry-derived point cloud for the Village of Gitwinksihlkw.

Open-source 3D imagery such as Google Street View is often used for building attribution (Ho et al., 2024) but is unavailable for large portions of this remote study area. To address this, we used a combination of drone- and mobile ground camera-based imagery to develop a detailed 3D model of the two villages, georeferenced using lidar tie points. The drone imagery provides a good overview of the study area and coverage of the building roofs, streets, and some building faces, but not significant detail. The ground-based imagery provides greater detail of the building faces, but lacks overall areal context and makes 3D construction difficult. Integrating the datasets mitigated these limitations and produced a complete 3D model.

The building footprints were attributed with data from a variety of open and closed data sources, including BC Assessment data, lidar, and the photogrammetry-derived point cloud. Main attributes include building type (e.g., single family home, mobile home, commercial), floor area, foundation type (e.g., crawlspace, basement, slab), first floor elevation, and adjacent ground elevation. The process of collecting data and attributing the buildings to this level of detail requires a significant amount of time and effort. The opportunity to use simplifying assumptions would greatly reduce the level of effort required for this stage of flood risk assessment projects.

3 METHODOLOGY

The uncertainty analysis focused on tangible direct damages to building structures and contents. A baseline risk assessment used the full building inventory and hazard datasets, calculating both event-level and annualized risk. Next, sensitivity runs explored the impact of simplified building inventory assumptions on the risk results. Finally, the influence of sample size was explored by resampling the baseline and sensitivity scenario results to determine the threshold at which a lesser number of buildings cause simplifying assumptions to introduce large magnitudes of uncertainty.

3.1 Using CanFlood for Risk Analysis

Natural Resources Canada's CanFlood V1.2.2 flood risk modelling toolbox was utilized for the building risk modelling (NRCan, 2024). CanFlood is an open source QGIS plugin that contains tools to automate modelling tasks and utilizes a standardized data format to enhance reproducibility and future expansion of the assessment. Asset data inventories and water surface elevation rasters are input to determine the exposure and risk of the structures in the study area.

Building depth-damage vulnerability functions were taken from previous flood risk studies in BC's Lower Mainland (IBI Group, 2020) and Okanagan Valley (Arcadis IBI Group and NHC, 2023). The curves represent the replacement value of flood damages, rather than the depreciated value, and include minimum, maximum, and "typical" damage values based on flood depth. The base curves were scaled up by 25% to account for inflation and regional differences in construction costs (NRCan, 2021). Despite being derived from other regions, the curves provide a reasonable approximation of potential flood damages considering the existing building stock in the Nass Valley. Previous work by NHC (unpublished, confidential data) compared these vulnerability curves to actual flood damages in another BC Indigenous community, and found that the minimum and maximum curves generally enveloped the reported flood damages across eight homes. Vulnerability functions were applied to each asset to estimate losses associated with building structures and contents. Structural losses include repairs to basements, common areas, garages, and main floors for residential and non-residential buildings. Content losses cover household items and equipment or stock for non-residential properties. Contents were not verified in the field and rely on curve-based estimates. Both structural and content damage estimates are highly sensitive to small changes in water surface elevation, as illustrated in Figure 3.

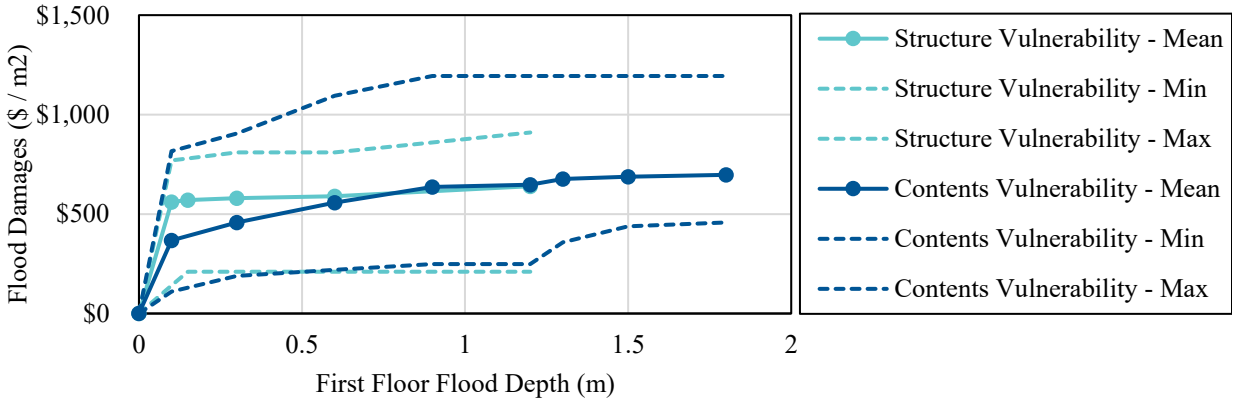

Figure 3: Example of structural and contents damage curves for single-family residential buildings

3.2 Baseline Risk Assessment

The baseline risk assessment utilized the fully detailed building asset inventory (Section 2.2), vulnerability curves (Section 3.1), and the set of seven flood hazard return periods (Section 2.1). Damages were calculated for each return period and integrated over the damage–frequency distribution to estimate expected annualized damage (EAD), assuming zero damage for the 2-year event and a maximum of 120% of the 500-year damages for the upper tail.

3.3 Sensitivity Scenarios

Eight sensitivity scenarios evaluated how simplified assumptions regarding the building inventory influence flood risk estimates and associated uncertainty. The analysis emphasized quantifying the magnitude of uncertainty introduced by these assumptions in comparison to other contributing sources of uncertainty.

Scenario 1. Building type (e.g., single family, commercial, institutional) was set from zoning data, and structures that visually appeared to be outbuildings (e.g., sheds) were removed from the inventory. Building main floor elevations were set from the following assumptions: all single-family dwellings have basements, and the first floor is 0.6 m above adjacent ground; all mobile homes are 0.6 m above adjacent ground; all other buildings are slab-on-grade, with the first floor 0.2 m above adjacent ground. This represents a scenario where the building type and footprint are known, but where the main floor elevation and foundation status are unknown. The 0.6 m assumption is based on engineering judgement and typical stair heights to the front door.

Scenario 2. All buildings are set as single family dwellings with basements, and the first floor is 0.6 m above adjacent ground. This represents a further simplification of Scenario 1, where the building type or zoning information are unknown.

Scenario 3. Building main floor elevations were set as per Scenario 1, but foundation conditions (basement vs. crawlspace vs. slab) and building type (main building vs. outbuilding) were updated based on BC Assessment data, where available. This represents a scenario where building information is available for the majority of buildings, other than the main floor elevation.

Scenario 4. Hydrologic uncertainty was assessed by recalculating baseline risk using the 90% confidence limits from the Nass River flood frequency analysis (NHC, 2022). To minimize additional hydraulic runs, scenarios adjusted the return periods for given discharges when computing EAD. For example, the 100-year discharge at Gitwinksihlkw has a 90% confidence range of 44-233 years. This represents a lower estimate of the hydrologic uncertainty, which is further influenced by gauge measurement error, choice of statistical distribution, and climate change effects.

Scenario 5. Hydraulic uncertainty was assessed by uniformly adjusting flood depths in CanFlood by ±0.3 m, based on hydraulic model calibration errors (0.1-0.4 m) identified for the June 2021 freshet (NHC, 2022). This approach does not capture the spatial variability in hydraulic uncertainty and may underestimate damage, as higher depths could expand flood extents and the number of impacted properties beyond the baseline scenario.

Scenario 6. Uncertainty in the building vulnerability curves was evaluated by applying the minimum and maximum curve values contained in the CanFlood inventory, rather than the mean value used for the baseline risk scenario. This is a simplified approach to evaluating uncertainty. A more fulsome assessment would require the development of site-specific curves, or a comparison of estimated damages to actual damages from recent floods. However, local data to support either approach is not available.

Scenario 7. Uncertainty in the EAD calculation was first assessed by reducing the number of computed return periods from seven (5, 10, 25, 50, 100, 200, 500 year) to four (10, 50, 100, 500 year). Extrapolation of the risk curve tails was done under the same assumptions as the baseline assessment.

Scenario 8. Uncertainty in the EAD calculation was further assessed by modifying assumptions around the upper risk curve tail. Rather than setting the tail value to 120% of the 500-year flood damages, additional tests were conducted at 150% and 200%.

3.4 Effect of Building Sample Size

For sensitivity Scenarios 1-3, applying simplified assumptions to a small set of buildings could introduce proportionally greater uncertainty than when applied to a larger dataset. This effect is most pronounced for first-floor elevation, which strongly influences flood depth and resulting damage estimates. In smaller samples, elevation assumptions are more likely to skew results, whereas with larger samples the effect could be smoothed out over the building inventory. To evaluate the influence of sample size, 1,000 randomized building subsets were generated, with replacement, for sample sizes of 5, 10, 20, 50, and 100

buildings. For each subset, percentage differences in damage estimates were calculated relative to the baseline scenario for sensitivity Scenarios 1-3. Percentile statistics were then computed to characterize the distribution of errors.

4 RESULTS AND DISCUSSION

In the baseline risk scenario, for the 500-year return period, there were 93 buildings exposed to flooding at Laxgalts'ap, and 38 at Gitwinksihlkw. Integration over the risk curve yielded an EAD of $551,197. Table 1 compares the sensitivity scenarios' EAD to the baseline risk scenario, in absolute and percentage terms. Figure 4 illustrates the event-level risk curves for the baseline scenario and sensitivity Scenarios 1-3.

Simplifying assumptions in Scenarios 1-3 produced errors of about ±20% in total EAD. Scenario 1 underestimated damages due to assumed floor elevations (0.6 m above grade) being, on average, higher than surveyed values (Figure 4). Scenario 2 overestimated damages because all buildings were treated as single-family homes, which have greater vulnerability than mobile or commercial structures. Scenario 3 improved accuracy in Laxgalts'ap by using BC Assessment data for foundation types; however, it introduced large errors in Gitwinksihlkw, where BC Assessment data contained errors such as missing buildings, or misclassification of main structures as outbuildings.

Table 1: Comparison of sensitivity scenarios EAD to baseline risk

Scenario	Flood Damages EAD			Difference from Baseline Risk		
	Laxgalts'ap	Gitwinksihlkw	Total	Laxgalts'ap	Gitwinksihlkw	Total
Baseline	$475,633	$75,565	$551,197	-	-	-
1	$410,375	$65,135	$475,510	-14%	-14%	-14%
2	$559,466	$89,929	$649,396	18%	19%	18%
3	$445,849	$14,243	$460,092	-6%	-81%	-17%
4 (lower)	$287,521	$36,030	$323,551	-40%	-52%	-41%
4 (upper)	$801,761	$170,281	$972,042	69%	125%	76%
5 (lower)	$342,594	$48,983	$391,577	-28%	-35%	-29%
5 (upper)	$629,855	$100,352	$730,207	32%	33%	32%
6 (lower)	$190,914	$34,987	$225,900	-60%	-54%	-59%
6 (upper)	$768,254	$123,903	$892,156	62%	64%	62%
7	$637,112	$84,835	$721,947	34%	12%	31%
8 (150%)	$481,779	$78,136	$559,915	1%	3%	2%
8 (200%)	$492,023	$82,422	$574,445	3%	9%	4%

Uncertainty from hydrologic (Scenario 4), hydraulic (Scenario 5), and vulnerability curve (Scenario 6) inputs was substantially greater than that from the simplifying assumptions of Scenarios 1-3. Hydrologic uncertainty was particularly influential due to the wide confidence intervals for high-return-period floods extrapolated from the 93-year gauge record. This finding is likely applicable to other remote locations in BC where gauge records are often short or non-existent. Vulnerability curve uncertainty was approximately twice that of hydraulic uncertainty and comparable to hydrologic uncertainty. Developing site-specific vulnerability curves could reduce this error source but would not significantly reduce overall EAD uncertainty because of the underlying hydrology and hydraulics.

A reduction in the number of modelled flood return periods from 7 to 4 (Scenario 7) increased the overall EAD by 31% compared to the baseline risk. This result is similar to previous work by Ward et al (2011) on the Meuse River, Netherlands, where the use of only three return periods overestimated EAD by 33% to 100%. Guidance from Messner et al (2007) based on a literature review recommends using at least three and preferably six flood return periods. Because EAD is computed over discrete return periods, even

the use of seven return periods could result in overestimation of EAD; however, it is not possible to quantify that error without completing additional hydraulic model simulations.

Increasing the maximum damage for the tail of risk curve (Scenario 8) somewhat increased the EAD, though the change was substantially less than for other sources of uncertainty. The true uncertainty in tail assumptions could only be assessed by modelling additional flood scenarios beyond the 500-year event. In BC, provincial guidelines do recommend including additional return periods (1,000-year, 2,500-year) in locations of very high flood risk (EGBC, 2018). However, at those return periods, the degree of hydrologic uncertainty would be substantial and may not provide significant gains in EAD understanding, though there could be other gains in understanding event-based damages for specific discharges.

Overall, the sensitivity analysis indicates that simplifying assumptions introduce uncertainty, but their effect is less than uncertainties from the hydrologic, hydraulic, and vulnerability curve inputs, provided that EAD is integrated over an adequate number of return periods. Scenario 1 is particularly straightforward to apply if building types and ground elevations are known. However, this finding is specific to the local building stock and sample size and may not hold true in all cases.

An analysis of sample size effects (Figure 5) shows that uncertainty from Scenarios 1-3 is highly sensitive to the number of buildings. Small subsamples (n = 5, 10) produce uncertainty ranges comparable to or exceeding hydrologic, hydraulic, and vulnerability curve uncertainty. At intermediate sizes (n = 20, 50), uncertainty decreases substantially, and for large samples (n = 100) it becomes minimal. Scenarios 1 and 2 consistently introduce negative and positive bias, respectively, particularly for $n \geq 20$. These biases reflect local building stock and foundation height assumptions (see Section 3.3). In practice, the height assumptions could be "tuned" to reduce bias by reviewing photos of the typical building stock.

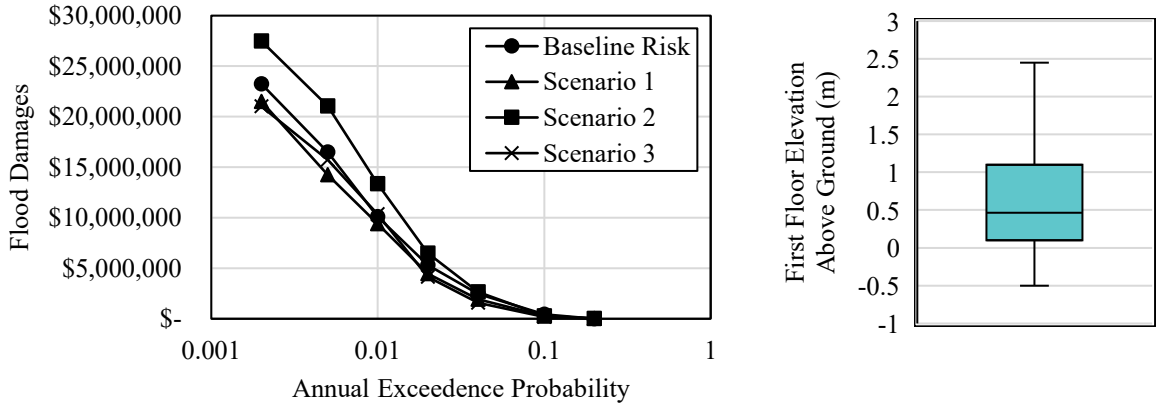

Figure 4: Left panel: Comparison of total flood risk curves for baseline and Scenarios 1-3. Right panel: First-floor elevation differences relative to adjacent ground for the baseline building inventory.

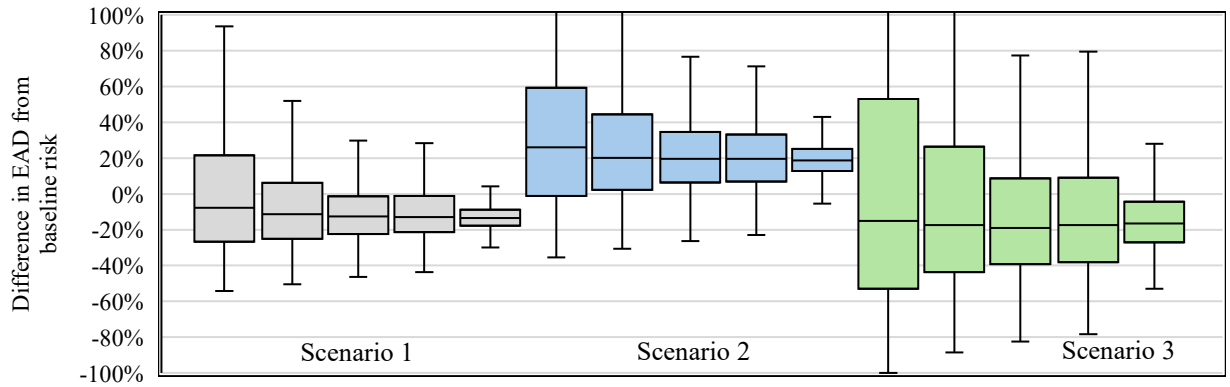

Figure 5: Effect of sample size on distribution of EAD differences between baseline and Scenarios 1-3

5 CONCLUSIONS

Flood damage estimates are inherently uncertain, with major influence from hydrologic and hydraulic variability and uncertainty, particularly in data-sparse regions where gauge records are short or non-existent, and model calibration is limited. Our findings indicate that while simplifying building inventory assumptions introduces error, its impact is generally smaller than uncertainties from hydrologic, hydraulic, and vulnerability curve inputs when annualized damages are computed over adequate numbers of return periods. For larger inventories (~50 buildings or more), generalized assumptions can provide acceptable accuracy and significantly reduce data collection effort. However, detailed building inventories remain critical when estimating structure-specific damages, designing lot-level mitigation measures, or addressing atypical building characteristics. The findings of this study support prioritizing hydrologic and hydraulic data quality while applying simplified asset assumptions judiciously to balance cost and reliability in remote or resource-limited contexts.

6 ACKNOWLEDGEMENTS

We gratefully acknowledge the Nisga'a Lisims Government, and in particular, David Cassidy, for agreeing to their data being used in this study. We would also like to recognize input of Julie Van de Valk, Robin Bourke, and Karl Chastko of Public Safety Canada for their valuable collaboration and contributions to the methodology and results analysis of this project. Finally, we thank Piotr Kuras of Northwest Hydraulic Consultants Ltd. for his review and input on this paper.

REFERENCES

Province of British Columbia (2024). From flood risk to resilience: a B.C. flood strategy to 2035, pp. 1-44.

Cascadia Natural Resources (1997). Water Survey of Canada stations pertaining to the Nass habitat capability model. Prepared for BC Ministry of Environment, Land, and Parks, pp. 1-23.

Diez-Herrero A. and Garrote J. (2020). Flood risk analysis and assessment, applications, and uncertainties: a bibliometric review. Water, 12(7), 2050.

Engineers and Geoscientists BC (2018). Legislated flood assessments in a changing climate in BC, version 2.1, pp. 1-175.

Ho et al. (2024). ELEV-VISION: automated lowest floor elevation estimation from segmenting street view images. ACM J. Comput. Sustain. Soc., 2(2), pp. 1-18.

IBI Group (2020). Flood risk assessment for BC's Lower Mainland. Prepared for Fraser Basin Council.

Arcadis IBI Group and NHC (2023). Flood risk mapping for the Okanagan Valley Watershed. Prepared for the Okanagan Basin Water Board Flood Risk Mapping for the Okanagan Valley Watershed – Okanagan Basin Water Board.

Messner F. et al (2007). Evaluating flood damages: guidance and recommendations on principles and methods. FLOODsite Report Number T09-06-01.

de Moel H. and Aerts, J.C.J.H. (2011). Effect of uncertainty in land use, damage models, and inundation depth on flood damage estimates. Nat. Hazards Earth Syst. Sci, 58, pp. 407-425.

Natural Resources Canada (2021). Federal flood damage estimation guidelines for buildings and infrastructure, Version 1.0.

Natural Resources Canada (2024). Documentation for CanFlood user manual.

NHC (2022). Adaptation of the Nisga'a Nation to the impacts of climate change: hydraulic modelling. Prepared for Nisga'a Lisims Government.

Rrokaj S. et al (2025). Flood risk assessment and participative process in the data-scarce Metuge district of Mozambique: an exportable approach. Int. J. Disaster Risk Reduct., 116, 105163

Ward P.J., de Moel, H. and Aerts, J.C.J.H. (2011). How are flood risk estimates affected by the choice of return periods? Nat. Hazards Earth Syst. Sci., 11, pp. 3181-3195

ICFM 10
Adapting to Global Change:
Innovative Approaches to Flood Management and Resilience
May 20-22, 2026 | Western University, London, Ontario, Canada

Comprehensive Risk-Perspective for Flood Defence System Management

Frank den Heijer
HAN University of Applied Sciences, Ruitenberglaan 26, Arnhem, The Netherlands
E-mail: Frank.denHeijer@han.nl

ABSTRACT

This paper synthesizes recent elaborations for comprehensive risk analyses for flood defence system management in den Heijer (2025). Since risk is a key parameter for asset management, risk management capabilities are important for the maturity and quality of flood defence asset management. The elaboration's main objective is *to develop and test methods for risk analysis in flood defence system management subject to deterioration and climate change*.

Asset management of flood defences systems includes strategic, tactic and operational decision levels. On the operational decision level, a novel integrated risk analysis enables to assess structural robustness caused by ductile dike behaviour. This behaviour may be provided by a clay core, eroding slowly after occurrence of initial dike damage due to a failure mechanism. On the tactical decision level, a systems risk approach has been set up to compare different tactical plans to prioritize and plan measures in interdependent systems, like dikes along rivers. This enables to reduce system risks most effectively and efficiently, dependent of specific tactical preferences such as the risk metric or planning conditions. On the strategic level a simple analytical relationship is derived to tune the economic optimal reliability of a flood defence based on its structural robustness, in combination with its optimal design horizon. This enables to adapt the optimal reliability to a specific dike design.

Today, mostly the decision levels are mutually disconnected for practical reasons. The presented approach differs from today's practice because of the opportunities for coherent use in between the decision levels: the dike design relates to its optimal reliability and to the optimal planning of its reinforcement in system. This concept is called a 'dynamic connected risk analysis'. This provides a comprehensive perspective for the utilization of risk analysis as a tool supporting efficient flood defence system management.

KEYWORDS: flood risk, flood defence, reliability, system management, risk-based planning

1 INTRODUCTION

'Flood risk management' can be defined as the continuous and holistic societal analysis, assessment and reduction of flood risk. From all opportune flood risk reduction measures, structural and non-structural, flood defence management is the most important for those areas protected by a system of flood defence assets like dikes. Asset management of flood defences systems includes strategic, tactic and operational decision levels. Since risk is a key parameter for asset management, risk management capabilities are important for the maturity and quality of flood defence asset management.

Flood risk concerns both the probability of flooding and its consequences. For flood risk in low lying areas protected by dikes, the undesired event is a flooding, most likely due to dike breach caused by natural hazards anywhere along the flood defence protecting the area. The assessment of probabilities of flood defence failure depends on the hydraulic loads and the flood defence strength. The consequences are dependent on failure-, breach- and flood characteristics, and on the exposed values in the considered

area. Consequences of flooding are mostly expressed in economic damage, number of victims and number of affected people.

This paper synthesizes the thesis (den Heijer, 2025) which main objective is to develop and test methods for risk analysis in flood defence system management subject to deterioration and climate change. While the thesis and previously published work (den Heijer & Kok, 2022, 2024; den Heijer et al., 2023, 2025) provide an in-depth comprehensive treatment, the present paper integrates the main aspects to support and enhance knowledge transfer to the flood risk management community. It focuses on three questions which elaboration can improve the risk-based management of flood defences, one at each of the three asset management decision levels. Together these questions refer to the asset managers needs to find out why, when, where and how to intervene.

At operational decision level it concerns optimization of dike design, to assess how to intervene: How can the structural robustness of the flood defence contribute to flood risk reduction? This paper introduces the opportunities of ductile dike behaviour to value structural robustness of designs.

At tactical decision level it concerns portfolio prioritisation of measures in system, to assess when and where to intervene: How can planning of measures contribute to effective system risk reduction? Different asset managers may differently develop and apply intervention criteria and conditions, leading to different plans. In this paper the interventions are narrowed to dike reinforcements, since its objective concerns flood defences.

At strategic decision level it concerns flood risk standards, to assess why to intervene: How can risk-based standards for flood defences reflect the benefits of structural robust designs? Individual and economical risks provide a risk-based target or standard to keep a system safe under changing conditions.

The choices in the different decision levels interact. First, in this paper the structural robustness is outlined (paragraph 2), because the 'how' of the design is input for the adapted standardization, the strategic topic. Second, the tactical planning is outlined (paragraph 3), because the 'when' and 'where' is input for the adapted standardization as well. Third, the updating of the standardization is outlined (paragraph 4). Then the dynamic connected risk analysis is outlined, as well a proposed organisation to benefit from this approach (paragraph 5). Finally, paragraph 6 presents the conclusions.

2 STRUCTURAL-ROBUST FLOOD DEFENCES MAY REDUCE RISK CONSIDERABLY

Increase of structural robustness focuses on risk reduction. It differs from strength increase, which primarily aims at reducing the probability of failure. A dike's design not only influences its failure probability, but it may also significantly impact the scale of floodings consequences, especially when the dike exhibits structural robustness due to its ductile behavior. Ductile behavior is defined as a slow failure process of a dike, characterized by relatively slow or depth-limited breach growth, which ultimately leads to reduced breach dimensions and lower flood impacts. This is contrasted with brittle behavior, where a breach occurs suddenly, leading to increased flood impacts. The key insight is that a more ductile dike is not necessarily larger but rather employs different construction, such as a clay core instead of a sand core, to mitigate flood impacts.

To evaluate this, an integrated risk analysis method is developed (den Heijer & Kok, 2022). This method models the entire chain of events in an integral and time-dependent manner: from initial dike failure mechanisms and failure path development to breach growth and the resulting consequences. This comprehensive approach allows for valuing the risk reduction achieved due to the structural robustness of a specific construction type.

The methodology is applied to a case study on the Grebbedijk along the Rhine River in the Netherlands. Based on a database with flood consequence simulations (Helpdesk, 2020), the total volume of water entering the polder is used as a proxy for consequences. This enables a direct link between dike design and flood impacts. Probabilistic software (Brinkman, 2021) for Monte Carlo Importance Sampling (MC-IS) is employed to calculate probabilities of exceedance of polder water levels (F_H-curves). Six different dike construction types, representing variations in core material (sand or clay) and structural

elements (with or without a sheet pile, or with extra width), are analyzed. Figure 1 provides the F_H-curves for various construction types for the same dike dimensions (crest height, slope and berm). Since the polder water level is directly related to the consequences, the surface below the curves represents the flood risk.

Elaborating a variety of combinations of dimensions, the economic optimal dimensions per construction type led to different dimensions, footprint and corresponding costs. A brittle sand dike might require larger dimensions than a more ductile dike with a clay core to achieve similar risk levels. The total societal costs and individual risks to victims strongly depend on the construction type. The study shows that optimizing the structural robustness dike construction can lead to substantial reductions in both societal costs and individual risks. In the case study, a dike with a sheet pile could reduce individual risk by a factor of 10. The additional budget needed is relatively small, because the sheet pile prevents dike height increase and the construction of a berm.

In conclusion, next to load reduction, strength increase, and consequence reduction, structural robust dike design is a fourth category of flood risk reduction measures. The integrated risk analysis approach provides valuable insights for comparing alternative designs, fostering decisions that go beyond mere compliance with probability standards to achieve optimal societal benefits, particularly in densely populated areas where flood consequences are high.

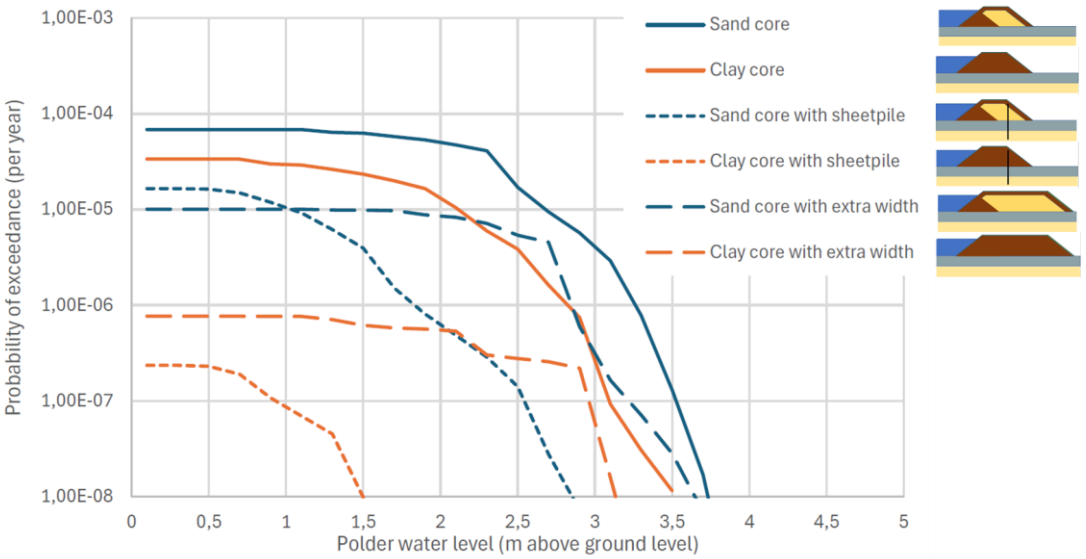

Figure 1: Examples of a series of probabilities of exceedance of polder water level H (F_H-curves), for different construction types at location Grebbedijk. Crest height = 12.2 m+ NAP, berm width = 10m, berm height = 0.75m, inner slope 1:2.5. Source: adapted from (den Heijer & Kok, 2022).

3 PROPER TACTIC PLANS REDUCE TIME-AGGREGATED SYSTEM RISKS

Tactical plans define the planning of consecutive measures (interventions) required to implement a flood risk reduction strategy, a process which may take decades. Tactical plans may consist of several features, such as a planning metric, the budget and specific planning constraints. Planning these costly measures requires proper insight into system risk effects. The tactical decision level concerns the portfolio prioritization of interventions in the dike system. Dike systems require continuous intervention to mitigate changes such as ageing and climate change.

In (den Heijer & Kok, 2024) a method was developed to compare different tactics to prioritize and plan measures in interdependent systems of dikes to reduce risks most effectively and efficiently. The time-aggregated system flood risk (TAR) is introduced as a novel measure. Existing measures consider

different types of risk separately, and mostly per polder and per year. The TAR is the combination of the total economic and individual risk in a system of polders over a reference period of time, in (den Heijer & Kok, 2024) taken over 100 years. The TAR enables comparison of different tactics, because it identifies the effectivity of the man-induced changes like dike reinforcements during the reference period, with respect to the system risk reduction. The importance of tactical planning is underscored by the finding that time-aggregated risk reduction can be introduced as a decision variable for plan evaluation.

A case study, meant as a proof of concept, was carried out for the reinforcement of approximately 500 km of dikes along the Rhine River branches in the Netherlands. The research studied the effects of 12 different tactical plans on the aggregated risks over time. The results demonstrated that tactical planning decisions are critical for reducing time-aggregated flood risks. Specifically, the present value of the sum of costs and economic risks differed by up to about 40% between the plans, while the risks on victims differed by up to 70%. Figure 2 summarizes these outcomes by plotting expected victims (individual risk) against the total present value of costs (investments and economic risk), for the 12 tactical plans. This illustration revealed that combining a risk-based prioritization metric with a priority condition for the top 3 ranked dike segments (filled red and green triangles) yields a comparable effect on reducing total costs and risks as doubling the budget when using a safety-level based metric (open yellow dot). The case study underlines the crucial role of tactical planning decisions, alongside prioritization metrics and budget constraints, influencing the resulting risk pattern.

By aligning fragility curves with ductile designs, the tactical planning analysis can balance the structural robustness of designs against the optimal time-aggregated system risk reduction, supporting efficient and well-considered reinforcement decisions.

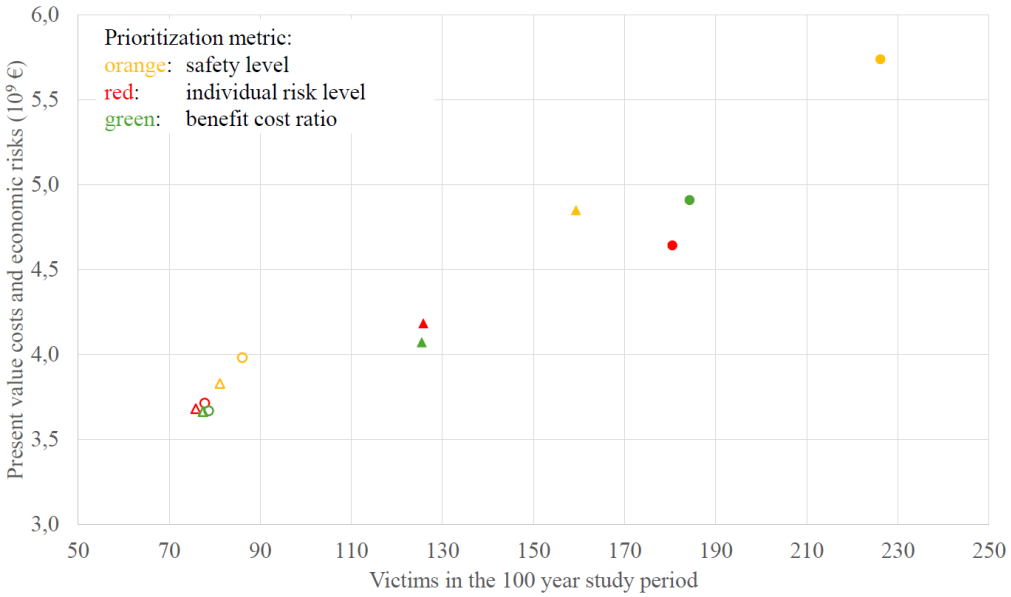

Figure 2 Model result for 12 tactical plans in the case study. Prioritization metric denoted by color. Budget and priority condition by marker shape: proportional budget (filled marker), doubled budget (open marker), no priority condition (dot), top 3 first (triangle). Source: (den Heijer & Kok, 2024).

4 UPDATING FLOOD RISK STANDARDS

A standard defines the performance requirement for flood defences, typically expressed as an acceptable probability of flooding per year, to keep a system safe under changing conditions. These standards provide the rationale for organizations to invest in a complex portfolio of risk-reducing assets.

In the Netherlands, standards are based on acceptable limits for individual and economic risks. Despite being risk-based, formal standards are generally static, set in law.

The optimal standard is derived based on the principle of minimizing total societal costs, which comprises the sum of investment costs and the present value of risks. The methodology to update the standard consists of an adapted analytical approach developed by Van Dantzig (1956) and Kind (2014), whose work provided the numerical basis for the current formalized Dutch standards (2017). The Adapted Van Dantzig method includes the dynamic effects of relative water level rise (due to subsidence and climate change) and reinforcement interventions over time (den Heijer et al., 2025). The analysis focused on the failure mechanism of wave overtopping. To account for structural robust dike behavior (ductility) in the Adapted Van Dantzig method, a translation factor was proposed to update existing probability standards to risk-optimal probability that reflects a specific design. This factor translates the marginal investment costs and the economic damage corresponding to the proposed design against the reference values used for standardization in Kind (2014). Since ductile designs reduce consequences after a breach, this allows a structural robust construction to be associated with a less stringent reliability standard than a less robust construction.

The methodology was compared with Kind (2014). The comparison focused on the middle probabilities (the average of the intervention limit and the design limit) for over 70 dike segments. The agreement was considered to be sufficiently convincing, see Figure 3

. Specifically, the results for the adapted analytical approach were comparable to the detailed numerical study, showing the average difference in return periods was only about 5%. This convergence supports the use of the simpler analytical model in (den Heijer, 2025) for standard estimations and its updates due to dike design or new information.

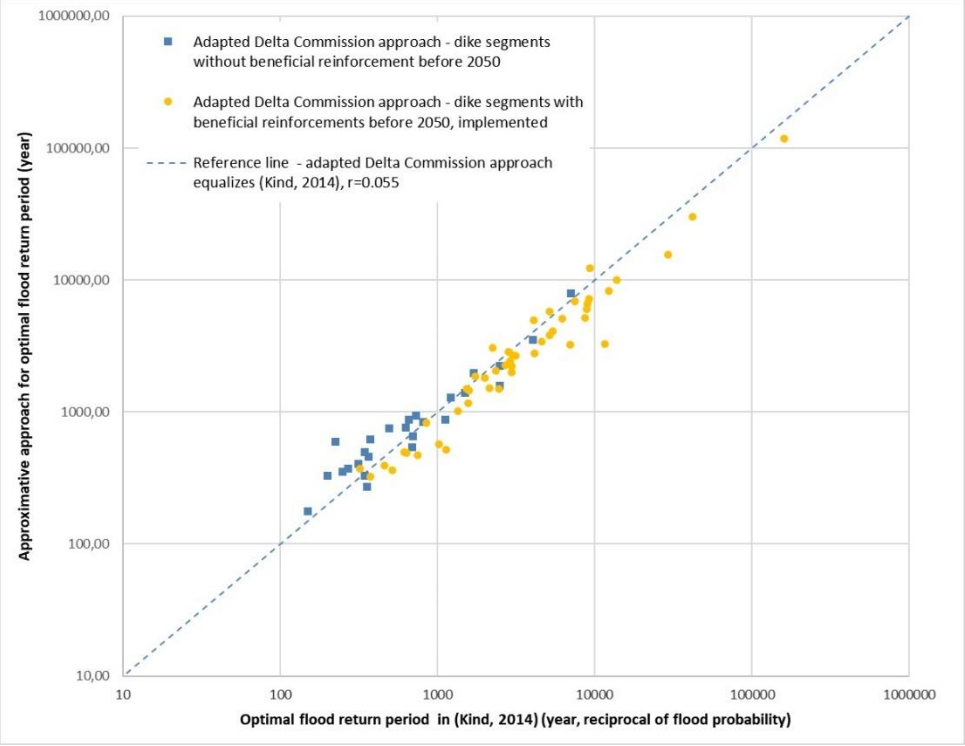

Figure 3 Comparison of adapted Delta Commission approach with the results of (Kind, 2014). Source: (den Heijer et al., 2025).

Regarding the optimal design horizon, the study developed an analytical relation for the economically optimal intervention timing. The analysis showed that the optimal life cycles (design horizons) for the dike segments averaged around 40 years. However, for a number of dike segments, the

economically optimal life cycle was shorter than 25 years. This finding indicates that the typical design horizon of 50 years is not universally optimal, and shorter design horizons may be economically optimal.

In conclusion, the derived method makes it practically possible to update the flood defence performance requirement, enabling a dynamic focus on optimal risk reduction dependent on the intervention timing and the chosen design construction type. This capacity to risk-aware update standards is crucial because it allows the benefits of structural robustness to be valued and utilized in efficient asset management and reinforcement decisions.

5 ORGANISING A DYNAMIC CONNECTED RISK ANALYSIS: HOW IT COULD WORK

Dynamic risk analysis is defined as enabling the involvement of changes over time on the time scale appropriate for the considered decision level. This forward-looking approach is indispensable because risks develop in time. This affects each decision level. At the operational level (see paragraph 2 in this paper), analysis must be time dependent and integrated to model the consecutive occurrence of dike failure paths, breach growth, and consequences during a single flood event, which is necessary to value structural robustness accurately. For tactical planning (see paragraph 3), where interventions span decades, a dynamic approach is crucial to assess time-aggregated system flood risk under deterioration and climate change. Finally, at the strategic level (see paragraph 4), dynamic analysis allows reliability standards to be updated, reflecting both the effects of time-dependent parameters and the economic optimal design horizons.

A connected risk analysis links involved technical disciplines and spatial system effects in the physical domain to bridge practical disconnections between asset management decision levels. Practical disconnections may be, among others, the distinction of individual dike segments, individual failure mechanisms, loads and strength calculations.

When combined with a connected risk analysis it forms a dynamic connected risk analysis. This integrated method facilitates efficient and comprehensive flood risk management. Its application supports risk management practices across operational, tactical, and strategic decision levels. This coherent approach is key to improving flood defence management. It enhances risk communication and supports continuous capability improvement.

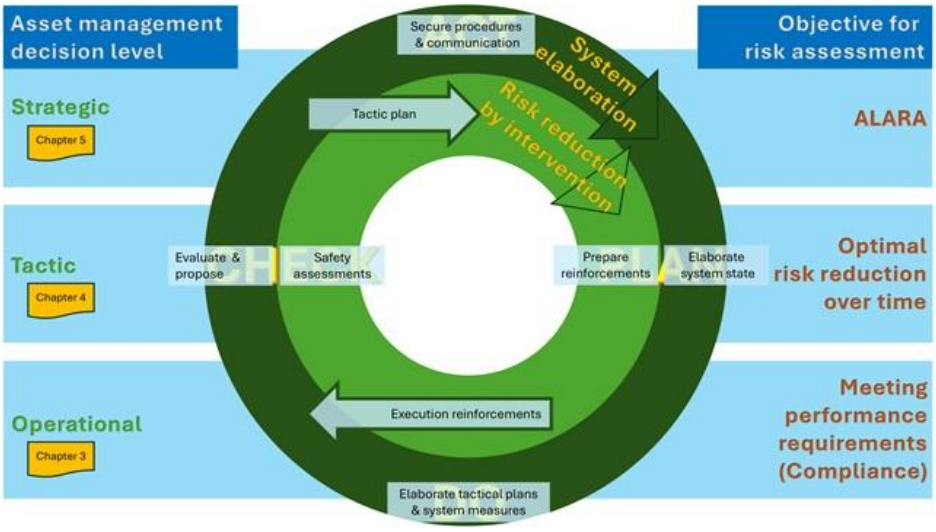

Figure 4: Schematic overview of dynamic concept for flood defence asset management. Source and reference to Chapters: (den Heijer, 2025).

Below a storyline is described for how the process could work, following the Deming circle (Deming, 1986), introducing the repeating process of PLAN, DO, CHECK and ACT for continuous

improvement. Figure 4 presents the three decision levels (left) and the corresponding risk management objectives (right), with a double Deming circle for system elaboration (outer) and intervention (inner). Please note, the Deming's circles are turned a bit to better align with the decision levels.

Starting the process in the outer circle in Figure 4 at the strategic decision level (ACT), 'Secure procedures' is mainly about providing starting points for system development on the relevant sectors (e.g. technical, spatial, capacity, capability), as well as about communication of choices and investigating societal acceptability. One of the procedures can be the prescription of the Adapted Van Dantzig method for derivation of an economic optimal safety level, see paragraph 4. Most relevant for utilizing the risk analysis in a dynamic connected way are the starting points for tactical planning providing room for a series of tactical plans.

The system elaboration process continues with 'elaboration system state' (PLAN), inventorying the present system condition as a starter. For each dike segment a preliminary assessment is performed based on a preliminary safety level as the performance requirement. Further elaboration of interventions can be done without the dikes which reinforcements are certainly out of programme horizon. For the remaining dike segments an inventory of several reinforcement alternatives is made, including alternatives changing the construction type, and including future projections of ageing. NB. Performance requirements appropriate to alternative construction types can be based on the Adapted Van Dantzig method (paragraph 4).

With 'elaborate tactical plans & system measures' (DO) potential intervention programmes are composed based on a series of tactical plans fitting which fit the strategic starting points, including potential system measures. For each dike in system reinforcement alternatives are analysed, for several structural robustnesses. For each tactical plan the initial safety level for the dike segments in system is derived based on actual assessments, and the intended safety level is based on the prescribed method from the strategic decision level in combination with and the structural robustness of the reinforcement alternative. Therewith, the time-aggregated risk reductions corresponding to the tactical plans and corresponding interventions can be calculated, see paragraph 3.

With 'Evaluate & propose' (CHECK) these time-aggregated risk reductions are weighed and a proposal has been made for a tactical plan, to be decided for at strategic level. At strategic level the proposal is confirmed or rejected (ACT).

In case it is confirmed the choice for a tactical plan is the start of the inner intervention circle in Figure 4 (ACT). In case it is rejected the argument for the rejection is added to the set of starting points provided to the next step in the outer system elaboration circle. In that case, a next iteration in the outer circle may lead to confirmation of a proposed plan, entering the intervention circle.

Following the strategic choice for a tactical plan, with 'prepare reinforcements' (PLAN) the corresponding intervention programme is set-up. The programme is based on actual assessments and the confirmed tactical plan including the budget. Therewith, the timing, construction type, safety performance requirement and design horizons are determined.

Following the system programme, the first upcoming reinforcements need a formal decision after which they cannot be withdrawn by programme considerations without loss. Then, the reinforcement can be executed (DO). Note, the formal reinforcement decision contains not only earmarking the dike segments to be reinforced, but the reinforcement plan as well, including construction type and safety level, because of its effect on the system.

Finally, the last step in the intervention circle is to update the 'actual assessments' for all flood defences in system (CHECK) based on the actual system and status of the interventions. These actual assessments are input for 'communication' (ACT) and for the next steps in the outer circle for system elaboration, evaluating interventions to continuously find the best coherent tactical plans.

In this way the executed reinforcements are tuned on their direct effects, reducing the risk in polders they protect, and on their system effects, due to the increased loads (e.g. in a river: for downstream located dikes). For each of the asset management decision levels the risk management objectives are met. Individually, the executed reinforcements meet the required safety levels, they are compliant. Due to the thoroughly evaluated tactical plans, the time aggregated flood risk in system is optimally reduced over time, within the strategic boundaries. At strategic level, due to the thorough

consideration and communication on the progress, the process is related to societal acceptability, meeting the ALARA principle. For this process, cooperation between the actors is crucial (den Heijer et al., 2023).

6 CONCLUSION

The main objective of the thesis (den Heijer, 2025) synthesized in this paper is to develop and test methods for coherent risk analysis in flood defence system management, addressing deterioration and climate change. The primary contribution is providing a comprehensive perspective for the utilization of risk analysis as a tool supporting efficient flood defence system management. The conclusions address the three decision levels of asset management.

For dike design, regarding the operational level, the structural robustness of the flood defence contributes to flood risk reduction. A risk analysis was set up, time dependent integrating the disciplines loads, strength, breach growth and consequences. This allows for valuing the risk reduction provided by ductile behavior (e.g., by a dike with clay core). Case study results show that total societal costs and individual risks on victims strongly depend on the construction type.

For system planning, regarding the tactical level, the tactical plan of consecutive measures is crucial for effective and efficient reduction of time-aggregated system flood risks. The time-aggregated risk reduction can be introduced as a decision variable for plan evaluation. The effects of different tactical plans showed that economic risks can differ significantly.

For risk-aware updating of standards, regarding the strategic level, failure probability standards can reflect the benefits of structural robust designs. An easy-to-use analytical translation enables to maintain a dynamic and risk-aware focus on the economic optimal probability of failure, dependent on the design and planning of the intervention.

A dynamic process can be introduced to continuously focus on effective and efficient risk reduction, for which sound cooperation among flood defence system management actors is indispensable.

REFERENCES

den Heijer, F., & Kok, M. (2022). Assessment of ductile dike behavior as a novel flood risk reduction measure. Risk Analysis, 1–16. https://doi.org/10.1111/risa.14071

den Heijer, F., Rijke, J., Bosch-Rekveldt, M., de Leeuw, A., & Barciela-Rial, M. (2023). Asset management of flood defences as a co-production – An analysis of cooperation in five situations in the Netherlands. Journal of Flood Risk Management. https://doi.org/10.1111/jfr3.12909

den Heijer, F., & Kok, M. (2024). Risk-based portfolio planning of dike reinforcements. Reliability Engineering & System Safety, 242, 109737. https://doi.org/10.1016/J.RESS.2023.109737

den Heijer, F., van Gelder, P. H. A. J. M., & Kok, M. (2025). Risk-Aware Updating of Reliability Standards for Flood Defences. Journal of Flood Risk Management, 4, 17. https://doi.org/doi.org/10.1111/jfr3.70134

den Heijer, F. (2025). Comprehensive risk-perspective for flood defence system management. ISBN 978-94-6384-803-9, Delft University of Technology.

Brinkman, R. (2021). Probabilistic Toolkit (2.1.24.2006). Deltares. https://www.deltares.nl/en/software/probabilistic-toolkit-ptk/

van Dantzig, D. (1956). Economic Decision Problems for Flood Prevention. Econometrica, 24(3), 276. https://doi.org/10.2307/1911632

Kind, J. M. (2014). Economically efficient flood protection standards for the Netherlands. Journal of Flood Risk Management, 7(2), 103–117. https://doi.org/10.1111/jfr3.12026

Helpdesk Water. (2020). National database flood simulations. https://www.helpdeskwater.nl/onderwerpen/wetgeving-beleid/europese-richtlijn-overstromingsrisico/overstromingsgevaar-overstromingsrisicokaarten/

Deming, W. E. (1986). *Out of the crisis* (C. for A. E. S. Massachusetts Institute of Technology (ed.)).

ICFM 10
Adapting to Global Change:
Innovative Approaches to Flood Management and Resilience
May 20-22, 2026 | Western University, London, Ontario, Canada

Urban Flood Risk Management: Mapping Potential Impacts of Pluvial Flooding on Elements at Risk

Sarah Lindenlaub[1,2], Guilherme Samprogna Mohor[1,2], Benjamin Creutzfeldt[3], Hanna M. Floto[2], Annegret H. Thieken[1]
Institute of Environmental Science and Geography, University of Potsdam,
Karl-Liebknecht-Str. 24-25, 14476 Potsdam, Germany[1]
E-mail: sarah.lindenlaub@uni-potsdam.de
E-mail: guilherme.samprogna.mohor@uni-potsdam.de
E-mail: annegret.thieken@uni-potsdam.de

UP Transfer GmbH, Am Neuen Palais 10, 14469 Potsdam, Germany[2]
E-mail: hanna.marleen.floto@uni-potsdam.de

Senate Department for Urban Mobility, Transport, Climate Action and the Environment (SenMVKU),
Brückenstrasse 6, 10179 Berlin, Germany[3]
E-mail: benjamin.creutzfeldt@senmvku.berlin.de

ABSTRACT

Urban areas are susceptible to damage caused by pluvial flooding due to sealed surfaces and high property assets in a small area. Pluvial flooding can occur anywhere and is not bound to water bodies, making its impacts hard to predict. Furthermore, the risk posed by such floods is not clearly understood by the general public, which can regularly be observed from citizens careless behaviour, such as driving or walking through flooded areas and underpasses, leading to dangerous situations, injuries and even fatalities. Pluvial flooding cannot only have a negative impact on people, but also cause damage to buildings, disrupt infrastructure services and cause cascading effects. Communicating the potential impacts to raise awareness is therefore an important task, often performed at the municipal level in Germany. One way to translate hydraulic parameters of floods into impact and visual information, is the mapping of its potential results on elements at risk. To operationalize such an impact mapping for the city of Berlin a joined project was established, based on close cooperation of local decision-makers and research. The here presented project results are a further development of the approach by Lindenlaub et al. (2025, https://doi.org/10.5675/HyWa_2025.6_5), focusing on people, buildings, vehicles and points of interest.

KEYWORDS: urban pluvial flooding, hazard maps, impact visualisation, hotspots, risk management, hazard to people, building damage

1 INTRODUCTION

Urban pluvial floods occur frequently after heavy rainfall events and cause huge damages, like in the city of Berlin, where pluvial floods led to damage of €174 million between 2002 and 2021 (Web-1), making Berlin the most frequently and heaviest affected German city (Nikogosian et al., 2021). Although the flow velocity is lower than in mountainous regions, considerable damage is caused, due to Berlin's high density of tangible assets, like buildings, cultural institutions and critical infrastructure.

Currently there is no regulation in place for a standardized development of pluvial risk or impact maps in Germany. An approach applicable throughout the whole country can make an important contribution not only to the technical but also to the political discussion, which is becoming particularly important in the context of the upcoming revision of the German Federal Water Act (WHG). The current draft of the new Flood Protection Act III (HWSG III) no longer only covers fluvial flooding but also defines

pluvial flooding as risk and focusses with §79 (Draft WHG) on establishing flood risk maps and detailed analysis of impacts on human health, the environment, cultural heritage, economy and tangible assets (BMUKN, 2024). However, the methodological approach remains unclear. Therefore, research on this topic is of high interest for the municipal pluvial flood risk management.

Here, a methodology towards a more comprehensive impact and risk mapping is presented, addressing several aspects of pluvial flood risks and complementing risk communication. The methodology was developed in close cooperation with local stakeholders and implemented for all of Berlin. The impact analysis was carried out for various elements at risk, namely: people, buildings, vehicles, and points of interest on the micro- (e.g. individual houses) and meso-scale (i.e. indicators aggregated per urban quarter).

Both the micro- and meso-scale provide useful information for various users, such as civil protection, city planning as well as for risk communication towards the general public. Additionally, a cluster analysis on the meso-scale was performed to identify possible hotspot areas. One central aspect during the methodological development was the use of mostly open-source data and of a nationwide standardized pluvial flood scenario (Web-2) to ensure transferability to other German municipalities.

2 METHOD

2.1 Data

The impact analysis is based on an indicative map for pluvial flood hazards published by the German Federal Agency for Cartography and Geodesy (Web-2). This raster map offers modelled maximum water depth and flow velocity for two rainfall scenarios. Our analysis was carried for the extreme event scenario, with a precipitation of 100 mm in 60 min (block rain distribution). The two-dimensional model of the surface runoff incorporates a digital terrain model, cadastral data and the precipitation scenario but does not account for the local sewer network or infiltration into the soil. In addition, terrain details such as culverts beneath roads are not always fully represented. Since the maximum water depth and velocity do not necessarily occur simultaneously, along with the extreme precipitation, it can be assumed that the scenario represents an overestimation and the impact mapping can therefore be considered a “worst case scenario”. The BKG map is the first German-wide approach of mapping pluvial flood hazards that has been agreed upon between all federal states and will be made publicly available.

In addition, official open-source data for buildings, street areas, population density, locations of fire brigades, hospitals, kinder gardens, schools and other points of interest were retrieved from the geoportal of Berlin (Web-3 to -10). Data on cultural sites and non-public data on past flood events were provided by personal communications (SenKultGZ, 2024, BWB, 2025).

2.2 Risk to People

Three factors are important, when analysing the risk to people by pluvial floods: 1) risk to people outdoors (e.g., people stability), 2) risk inside of buildings (i.e., limited vertical evacuation) and 3) the distribution of vulnerable groups (e.g., children and elderlies) (DEFRA, 2006).

1) Flow velocity and water depth are hydraulic parameters that determine people’s stability outside of buildings. The used hazard curves are based on experimental stability tests in water channels summarized by Martinez-Gomariz et al. (2016), describing four hazard classes. The hazard class “low” describes an area where there is generally no hazard and it’s safe also for children. The zone is limited by a water depth (WD) of 0.5 m and a flow velocity (V) of 3 m/s. Additionally the class is limited by the combination of water depth and velocity (WD * V = DV), along the curve of DV = 0.22 m/s^2. The class “moderate” displays an area, where there is a threat to some people, e.g., elderly people with low mobility or kids, which is limited by a) WD = 1.2 m and DV = 0.22 m/s^2, b) WD = 0.5 m, V = 3 m/s and DV = 0.6 m/s^2. In an area with a significant threat is dangerous for most people and the class is limited by WD = 1.2 m, V = 3 m/s and DV= 1.2 m/s^2. Everything above these limits is classified as an extreme threat (for all).

2) Being trapped during a flood in an affected part of a building, such as the basement or the ground floor, and subsequently drowning is a leading cause of death inside of buildings (Thieken et al., 2023).

Being able to evacuate vertically to a non-affected building level can thus reduce this risk. Berlin's flat topography allows a wide horizontal spread of flood water (with exception of local depressions). Therefore, we considered buildings with only one level as "dangerous". This means that houses such as bungalows, which have no vertical evacuation option, are classified as high-risk locations .

3) In case there is a need to evacuate affected buildings it is crucial for civil protection operators to know how many individuals are living in the affected area and how many might need special assistance, e.g. due to mobility issues. There is no clear definition of vulnerable groups based on age limits. In the context of flooding, people over the age of 65 can be considered a vulnerable group, given that this age group is overrepresented among flood fatalities in Germany and several other European countries (FFEM-DB; Papagiannaki et al., 2022, Thieken et al., 2023). Therefore, the age threshold of 65 years is used in the impact analysis. For children, the threshold of (up to) 10 years is used, based on the relationship between body weight and height and data availability in Berlin (DEFRA, Web-5). On the micro-scale (per living block) the total number of residents, children and elderly people can be depicted at once in the following format: XXX|XXX|XXX

2.3 Building Damage

The damage to residential buildings was estimated using the Flood Damage Estimation Tool (FlooDEsT) by Samprogna Mohor et al. (2025). The tool was developed specifically for the estimation of building damage caused by pluvial flooding, given that other damage models, developed for fluvial floods, often lead to an overestimation of the damage for pluvial flood scenarios due to the difference in hydraulic conditions between the two flood types. The recursive partitioning algorithm (XGBoost, Chen & Guestrin, 2016) was trained using household survey data from past pluvial flood events (Thieken et al., 2017; Kellermann et al., 2020).

In its application FlooDEsT uses the hydraulic parameters from the scenario, building polygons and, if possible, building information. In the case of Berlin, the building data is derived from the ALKIS dataset (Web-3). Building damage is only calculated with FlooDEsT for residential buildings and not for objects classified as points of interest (see section 2.5). Missing information and further needed parameters are supplemented by data imputation from the household survey data, which are representative of urban pluvial flooding. As a result, FlooDEsT delivers a relative building damage (percentage of building value) per building. The loss ratios are grouped into four damage classes: low (> 0 bis 3 %), medium (> 3 bis 9 %), high (> 9 bis 16 %), and very high (> 16 %).

2.4 Damage to Vehicles

Driving through flooded area is a commonly observed though dangerous behaviour, which can lead to damage of the engine or electrical system or the loss of a vehicle's stability and can cause injuries and fatalities (Haynes et al., 2009; Thieken et al., 2023). For the impact mapping in Berlin a quite conservative approach was developed together with experts from the local fire brigade.

We distinguished four groups of vehicles, 1) typical civilian vehicles for which the hazard classes 'low', 'medium', 'high' and 'very high' are established; 2) "geländefähig" which are vehicles with a required wading depth of at least 30 cm, commonly used by fire brigades; 3) "geländegängig" which are vehicles with a minimum required wading depth of 60 cm; and 4) special vehicles with an advanced wading depth of up to 1 m. The differentiation of street accessibility based on wading depth between civilian and organizational vehicles is an important information for local civil protection, for example in case of evacuations or emergency calls, while it is possible at the same time to communicate a rather conservative trafficability to the general public.

The four hazard classes for civil vehicles are based on the stability curves summarized and published by Martínez-Gomariz et al. (2017) and are depicted in Figure 1. Aquaplaning is a form of stability loss which is often not included in stability curves and is here represented in the 'low' hazard class. In addition, water can damage the technical system of a vehicle already at reasonably low water depths, therefore the General German Automobile Club (ADAC) suggests a max. trafficable water depth of 20 cm for all vehicles

(Web-11). This aligns with the water depth threshold for the 'very high' hazard class (Figure 1). As the trafficability in general is bound to streets, the street area was derived via a buffer from polyline network data (Web-4).

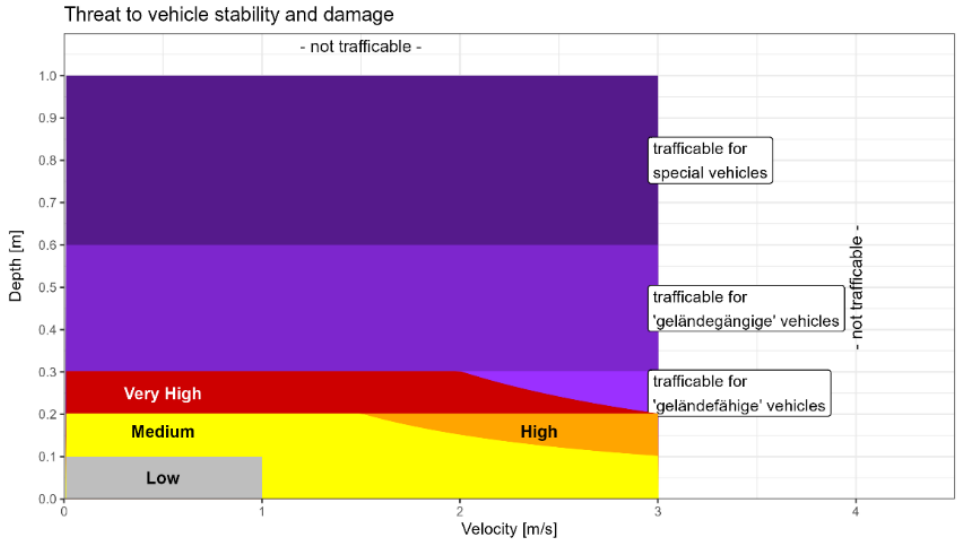

Figure 1: Classification for vehicle stability and damage for civil and organizational vehicles

2.5 Points of Interest

Apart from residential buildings, buildings of public interest or requiring special protection, such as critical infrastructure or cultural and religious buildings, can also be affected by pluvial flooding. Since damage to these "points of interest" (PoI) could either cause cascading effects or require special emergency measures, such as an evacuation of zoo animals or rescuing artworks, the impact on these PoI was determined separately. The assessment was carried out for polygon shapes from the ALKIS buildings data set (Web-3). Here certain buildings were classified as PoI based on their attribute table ("BEZGFK"). The classification was developed in cooperation between local stakeholders as it combines not only critical infrastructure but also other critical objects. Additional locations of PoI were acquired from further official point data (Web-6 to Web-10, SenKultGZ, 2024).

The impact assessment is based on the approach from LUBW (2019) for critical objects, which uses the water depth and flow velocity as criteria and distinguishes four hazard classes (low, moderate, high and very high) as shown in Table 1.

Table 1: Hazard matrix for critical objects, adapted from LUBW (2019)

		Velocity			
		< 0.2 m/s	0.2 to 0.5 m/s	0.5 to 2 m/s	> 2 m/s
Water Depth	< 5 cm	low	low	low	low
	5 to 10 cm	moderate	moderate	high	very high
	10 to 50 cm	high	high	very high	very high
	50 to 100 cm	high	very high	very high	very high
	> 100 cm	very high	very high	very high	very high

2.6 Aggregation on Meso-Scale (Indicators)

An aggregation of indicators on a larger scale, e.g., urban quarters ("LOR-Prognoseräume" by Web-12) offers the opportunity to compare impacts on a meso-scale and allow a hotspot mapping. The following four indicators were calculated per urban quarter based on the results from the micro-scale analyses:

1. Indicator “People Stability”: percentage of area with a classification of ‘moderate’ to ‘extreme’ threat to people’s stability, outdoors (excluding water surfaces and building footprints);
2. Indicator “Building Damage”: percentage of buildings with an estimated damage class of ‘high’ or ‘very high’;
3. Indicator “Vehicle Stability”: percentage of street area classified ‘high’ or more severe threat to civil vehicles;
4. Indicator “Points of Interest”: percentage of PoI with hazard classes ‘high’ or ‘very high’.

2.7 Cluster Analysis

To identify hotspot areas within the city, a cluster analysis was performed, using the four indicators per urban quarter. To overcome their different dimensions, all values were scaled to a range from 0 to 1 per indicator by their minimal and maximal values. In addition to the indicators, deployment data from the fire brigade operations and other reports during past pluvial flood events (BWB, 2025) were considered. The indicator “Report Density” was calculated from the number of reports, divided by the number of inhabitants (Web-5, Web-12) for every urban quarter and afterwards normalized to a scale of 0 to 1.

The cluster analysis was carried out following the procedure proposed by Backhaus et al. (2018). The “Complete Linkage” (farthest neighbor) agglomerative clustering with squared Euclidian distances delivered the best plausible cluster solution. The number of clusters was selected based on the elbow criterion, the increase in the measure of heterogeneity, the dendrogram and Mojena's test (see Backhaus et al., 2018).

3 RESULTS AND DISCUSSION

3.1 Results on Meso-Scale (Aggregation)

The results on the meso-scale (indicators, see section 2.6) show the distribution of potential impacts of pluvial flooding on all elements at risk in the 58 urban quarters in the form of choropleth maps. As an example, the indicator for potential building damage is shown in Figure 2. A maximum of 14% of all buildings are estimated to suffer a ‘high’ or ‘very high’ loss ratio in the urban quarter of “Wilmersdorf Süd”. In ten more quarters at least 5% of the buildings are estimated to show ‘high’ or ‘very high’ loss ratios, while the median value across all 58 areas is 3% for the used scenario.

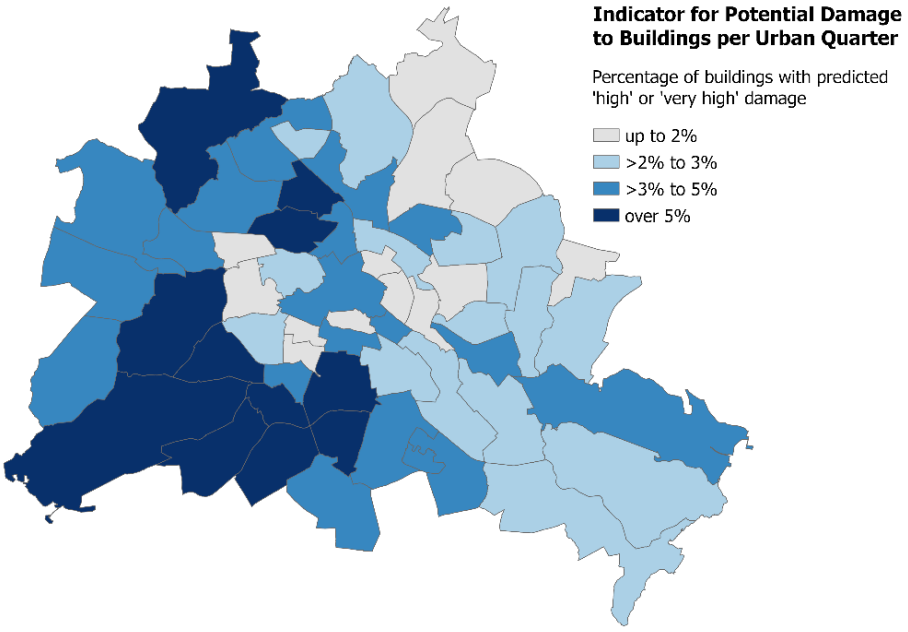

Figure 2: Choropleth map for the indicator “Building Damage” for all 58 urban quarters

3.2 Hotspot Identification

For the „Complete Linkage“ clustering, a five cluster solution was chosen, consisting of three bigger and two smaller clusters. Figure 3 depicts the urban quarters per cluster alongside the mean indicators of each cluster. Cluster 1, with 25 urban quarters, shows below-average values for all variables and is therefore designated as ‘low impact’ (Figure 3). Cluster 2 (20 urban quarter) shows high indicator values for people, vehicles and points of interest. In comparison, cluster 3 shows higher building loss ratios for residential buildings and also high values for PoI and people. Both clusters are therefore labelled ‘medium to high impact’, but show differences in building loss ratios due to the different building structures in the quarters (predominance of one-family versus multi-family homes). The urban quarter “Grüner Norden” was separated into an own cluster, since here the value for the report density is especially high, while the other values are comparatively low.

Cluster 4 shows the hotspots with ‘very high’ potential for pluvial flood impacts for people, vehicles and points of interest, while at the same time also showing medium values for report density. Only the building loss ratio is estimated as low, as the three urban quarters of the cluster “Friedenau”, “Schöneberg Nord“ and “Kreuzberg Süd“ mostly consist of large buildings, where the relative damage is quite low due to the large building sizes.

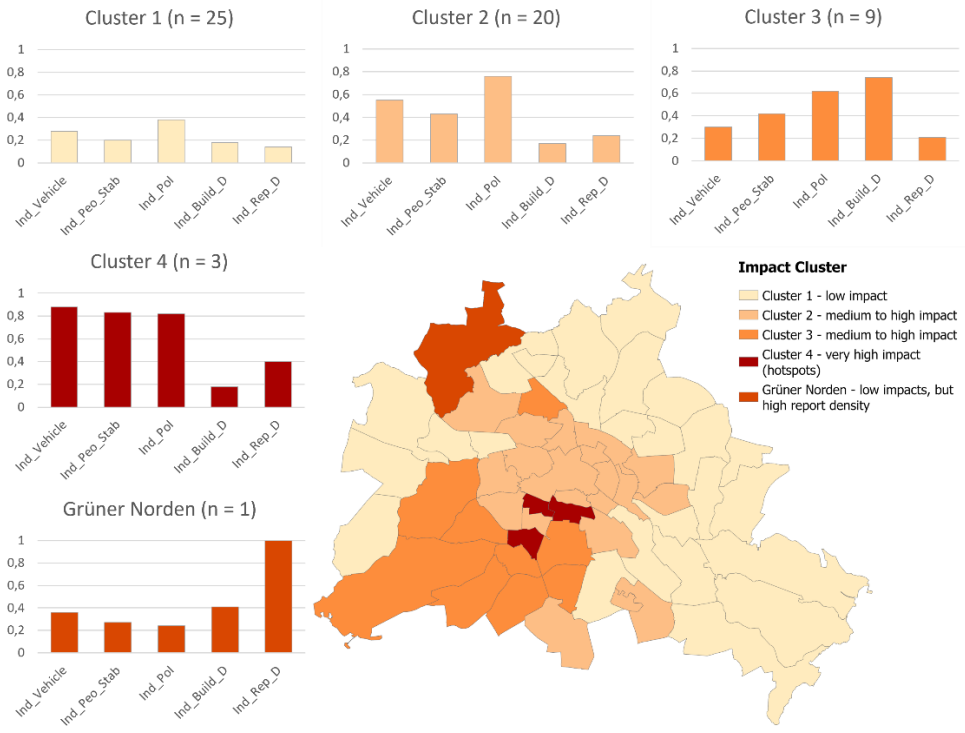

Figure 3: Results of the cluster analysis considering the five indicators: Vehicle Stability (Ind_Vehicle), People Stability (Ind_Peo_Stab), Points of Interest (Ind_PoI), Building Damage (Ind_Build_D), and Report Density (Ind_Rep_D); for all 58 urban quarters

3.3 Results on Micro-Scale

The visualization on the micro-scale can serve for risk communication and for crisis management operations, as it shows possible impacts in more detail. As an example, the combination of the three hazard to people variables are displayed in the hotspot region of “Friedenau“ (see Figure 4). Friedenau is a highly populated urban quarter with a high threat to the people’s stability due to a local depression. An evacuation for this extreme scenario would be very complicated, as there is not only a high risk to people’s stability but also to the vehicle’s stability. In case of an evacuation, the number of residents and of vulnerable people has to be considered, too. At least the vertical evacuation is available in most buildings. Risk

communication of urban pluvial flood impacts in this quarter should be one of the central measures, especially because Friedenau has been highly affected by pluvial flooding before (BWB, 2025).

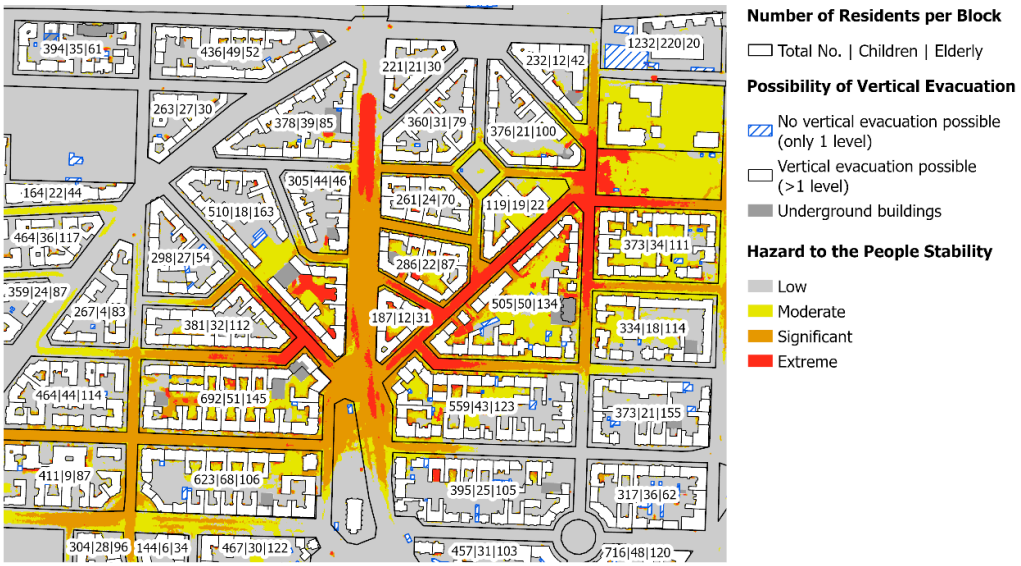

Figure 4: Example of the visualization on the micro-scale, showing the distribution of vulnerable people, the possibility for vertical evacuation and the hazard to the people stability in the hotspot region of Friedenau

3.4 Limitations and Transferability

The impact mapping is bound to up-to-date data, its availability and resolution, which might change when applying the methodology elsewhere. The BKG (Web-2) map on pluvial flooding is the first harmonized, German-wide approach, which is currently the best data basis for a transferable impact mapping, but the map has some limitations. The uncertainties in the results (only max. water levels are provided) and the low level of detail of the hydraulic approach (e.g. no consideration of sewer network) lead to problems in areas such as underpasses and an overestimation of the event's impacts. In regions where more detailed risk maps, with several scenarios, are available, these should be used instead. Still the BKG (Web-2) map can be used for a first impact mapping.

When applying the methodology to other regions some data sources have to be supplemented. Population density data in Berlin is accessible on a very high resolution, which might lead to privacy issues in other regions. Nonetheless, for all of Germany the Census data at 100 x 100 m resolution (Web-13) could be used. The ALKIS building data should also be available in all federal states, but the data availability and quality varies. Building data and information on PoI could be derived from OpenStreetMap data instead.

Due to a lack of data no information can be provided on other vulnerable groups, such as people with long-term illnesses or those in shared accommodations for people needing intensive care, although this would be of great importance for operational crisis management.

There is a high risk in underground parts of buildings, such as basements and underground car parks (Thieken et al. 2023). However, data sets on this topic are incomplete or unavailable and their specific flood impacts therefore cannot be mapped. Nevertheless, information on this risk should be included in any risk and crisis communication as a precautionary measure.

4 CONCLUSION

Pluvial flooding after heavy rainfall is becoming an increasing problem for urban areas. Mapping its impacts can support a better understanding of the potential challenges involved in dealing with such events. As part of the methodological approach, potential impacts on various elements at risk were assessed for an

extreme rainfall scenario. Along the micro-scale, a meso-scale assessment was carried out at the level of urban quarters, resulting in the identification of three hotspot areas through a cluster analysis. The quarters "Friedenau", "Schöneberg Nord" and "Kreuzberg Süd" would potentially suffer very high impacts if such an extreme precipitation occurred. Both the micro- and meso-scale results can provide useful information for different users, such as municipal flood risk management (spatial planning and risk communication) and crisis management operators. The approach can easily be transferred to other municipalities, adding value to the current gap of pluvial impact mapping in Germany.

5 ACKNOWLEDGEMENTS

For financing the project, we would like to thank the Senate Department for Urban Mobility, Transport, Climate Action and the Environment (SenMVKU) of Berlin. Additionally, we would like to thank SenMVKU, the Berlin Water Suppliers (Berliner Wasserbetriebe), the fire brigade of Berlin (Berliner Feuerwehr), the Senate Department for the Interior and Sports (SenInn), and the Senate Department for Urban Development, Building and Housing (SenStadt) for supporting this project with their expert knowledge and by providing additional data. The original approach (Lindenlaub et al., 2025) was developed within the Inno_MAUS project, for financial support of this work we would like to thank the Germany Federal Ministry of Research, Technology and Space (BMFTR; FKZ 02WEE1632A).

REFERENCES

Backhaus, K., B. Erichson, W. Plinke and Weiber, R. (2018). Multivariate Analysenmethoden. Springer: Berlin, Heidelberg, 15. Auflage, Kapitel 8, S. 435-496, https://doi.org/10.1007/978-3-662-56655-8_9

BMUKN, Bundesministerium für Umwelt, Klimaschutz, Naturschutz und nukleare Sicherheit (2024): Referentenentwurf eines Gesetzes zur Verbesserung des Hochwasserschutzes und des Schutzes vor Starkregenereignissen sowie zur Beschleunigung von Verfahren des Hochwasserschutzes. https://www.bundesumweltministerium.de/gesetz/referentenentwurf-hochwasserschutzgesetz-iii.

Chen, T. and Guestrin, C. (2016). XGBoost: A Scalable Tree Boosting System. Proceedings of the 22nd ACM SIGKDD International Conference on Knowledge Discovery and Data Mining. 785-794. DOI: 10.1145/2939672.2939785.

DEFRA, Department for Environment, Food and Rural Affairs (2006). Flood Risks to People - Phase 2 - FD2321/TR1, The Flood Risks to People Methodology. Technical Report. Flood and Coastal Defence R&D Program. https://assets.publishing.service.gov.uk/media/602bbc768fa8f50383c41f80/Flood_risks_to_people_-_Phase_2_The_flood_risks_to_people_methodology_technical_report.pdf

Haynes, K., Coates, L., Leigh, R., Handmer, J., Whittaker, J., Gissing, A., McAneney, J. and Opper, S. (2009). „Shelter-in-place" vs. evacuation in flash floods. Environmental Hazards. 8. 291–303. DOI: 10.3763/ehaz.2009.0022

Kellermann, P., Schröter, K., Thieken, A.H., Haubrock, S.N. and Kreibich, H. (2020). The object-specific flood damage database HOWAS 21. Natural Hazards and Earth System Sciences, 20(9), 2503-2519. DOI: 10.5194/nhess-20-2503-2020

Lindenlaub, S., Samprogna Mohor, G., Creutzfeldt, B. and Thieken, A.H. (2025). Neue Impulse für das kommunale Starkregenrisikomanagement: Kartierung potenzieller Auswirkungen auf ausgewählte Risikoelemente. Hydrologie und Wasserbewirtschaftung 69(6), 349-364. https://doi.org/10.5675/HyWa_2025.6_5

LUBW, Landesanstalt für Umwelt, Messungen und Naturschutz Baden-Württemberg (2019). Leitfaden Kommunales Starkregenrisikomanagement in Baden-Württemberg - Risikoanalyse. Anhang. https://pudi.lubw.de/detailseite/-/publication/47871

Martínez-Gomariz, E., Gómez, M. and Russo, B. (2016). Experimental study of the stability of pedestrians exposed to urban pluvial flooding. Nat Hazards 82, 1259–1278. https://doi.org/10.1007/s11069-016-2242-z

Martínez-Gomariz, E., Gómez, M., Russo, B., and Djordjević, S. (2017). A new experiments-based

methodology to define the stability threshold for any vehicle exposed to flooding. Urban Water Journal 14(9), 930–939. https://doi.org/10.1080/1573062X.2017.1301501

Nikogosian, C., Winterrath, T., Walawander, E., Fischer, I., Schmitz-Kröll, D. and Wischott, V. (2021). Klassifikation meteorologischer Extremereignisse zur Risikovorsorge gegenüber Starkregen für den Bevölkerungsschutz und die Stadtentwicklung (KlamEx) - Projekt der Strategischen Behördenallianz „Anpassung an den Klimawandel“. Abschlussbericht. (hrsg.) Bundesamt für Bevölkerungsschutz und Katastrophenhilfe. https://www.dwd.de/DE/fachnutzer/wasserwirtschaft/kooperationen/klamex/pdf/abschlussbericht_klamex.pdf?__blob=publicationFile&v=1

Papagiannaki, K., Petrucci, O., Diakakis, M. et al. (2022). Developing a large-scale dataset of flood fatalities for territories in the Euro-Mediterranean region. FFEM-DB. Sci Data 9, 166. https://doi.org/10.1038/s41597-022-01273-x

Samprogna Mohor, G., Lindenlaub, S. and Thieken, A. H. (2025). Fast and operational building damage estimation tool for urban pluvial flooding. EGU Abstracts. https://doi.org/10.5194/egusphere-egu25-10095

Thieken, A. H., Bubeck, P. and Zenker, M. L. (2023). Flood-related fatalities during the flood of July 2021 in North Rhine-Westphalia, Germany: what can be learnt for future flood risk management?. J. Coast. Riverine Flood Risk 2. https://doi.org/10.59490/jcrfr.2023.0005

Thieken, A. H., Kreibich, H, Müller, M. and Lamond, J. (2017). Data Collection for a Better Understanding of What Causes Flood Damage – Experiences with Telephone Surveys. In: Molinari, D., Mononi, S. & Ballio, F.: Flood damage survey and assessment. American Geophysical Union, 95-106.

Web sites:

Web-1: https://www.gdv.de/gdv/medien/medieninformationen/starkregenbilanz-2002-bis-2021-bundesweit-12-6-milliarden-euro-schaeden-137444, consulted 17 February 2025.

Web-2: https://sgx.geodatenzentrum.de/web_public/gdz/datenquellen/datenquellen_hwk_srg.pdf, consulted 28 August 2025.

Web-3: https://www.berlin.de/sen/sbw/stadtdaten/geoinformation/liegenschaftskataster/, consulted 15 October 2025.

Web-4: https://gdi.berlin.de/services/wfs/atkis?REQUEST=GetCapabilities&SERVICE=wfs, consulted 15 October 2025.

Web-5: https://gdi.berlin.de/services/wfs/ua_einwohnerdichte_2024?REQUEST=GetCapabilities&SERVICE=wfs, consulted 15 October 2025.

Web-6: https://gdi.berlin.de/services/wfs/feuerwehr?REQUEST=GetCapabilities&SERVICE=wfs, consulted 15 October 2025.

Web-7: https://gdi.berlin.de/services/wfs/krankenhaeuser?REQUEST=GetCapabilities&SERVICE=wfs, consulted 15 October 2025.

Web-8: https://gdi.berlin.de/services/wfs/kita?REQUEST=GetCapabilities&SERVICE=wfs, consulted 15 October 2025.

Web-9: https://gdi.berlin.de/services/wfs/schulen?REQUEST=GetCapabilities&SERVICE=wfs, consulted 15 October 2025.

Web-10: https://gdi.berlin.de/services/wfs/bimschg?REQUEST=GetCapabilities&SERVICE=wfs, consulted 15 October 2025.

Web-11: https://presse.adac.de/meldungen/adac-ev/technik/vorsicht-bei-wasserschaeden.html, consulted 11 December 2025.

Web-12: https://www.berlin.de/sen/sbw/stadtdaten/stadtwissen/sozialraumorientierte-planungsgrundlagen/lebensweltlich-orientierte-raeume/, consulted 26 November 2025.

Web-13: https://atlas.zensus2022.de/, consulted 30 December 2025.

Non-public

SenKultGZ (2024): dataset cultural sites, private communication 16 October 2025.

BWB (2025): dataset fire brigade deployment, private communication 09 October 2025.

ICFM 10
Adapting to Global Change:
Innovative Approaches to Flood Management and Resilience
May 20-22, 2026 | Western University, London, Ontario, Canada

Deployment of a Machine Learning Model for North America-wide Hydrometric Flow Forecasting with LiDAR-based Floodplain Mapping Capabilities

R. Mark Palmer[1], Trevor Boston[2], Steven French[3], and Hamid Mohebzadeh[4]

Greenland International Consulting Ltd., Collingwood, ON, L9Y 1V5, Canada[1]
E-mail: mpalmer@grnland.com
Greenland International Consulting Ltd., Collingwood, ON, L9Y 1V5, Canada[2]
E-mail: tboston@grnland.com
Greenland International Consulting Ltd., Collingwood, ON, L9Y 1V5, Canada[3]
E-mail: sfrench@grnland.com
Greenland International Consulting Ltd., Collingwood, ON, L9Y 1V5, Canada[4]
E-mail: hmohebzadeh@grnland.com

ABSTRACT

The Integrated Science and Watershed Management System (ISWMS™) incorporates a temporal fusion transformer-based machine learning model designed to generate hydrometric flow forecasts across North America. Trained on an extensive archive of flow measurements from thousands of gauging stations, the model integrates real-time hydrometric observations, climate inputs, and catchment characteristics to produce localized probabilistic flow predictions. Alongside forecasting capability, ISWMS™ includes a Flood-Frequency Analysis (FFA) functionality used to derive return-period design flows. Together, these components support operational decision-making by providing both real-time forecasts and long-term hydrologic design information. The decision support system is deployed within The Healthy Rivers Ecosystem AssessmenT System (THREATS™), a web-based platform that includes tools for watershed data access, visualization, and analysis.

To translate forecasted or design flows into actionable flood intelligence, ISWMS™ requires flow forecasting and hydraulic model / flood mapping components capable of rapidly equating discharge inputs into inundation extents that can be rendered on a map. To address this need, we evaluated the Blackbird hydraulic model and results of cross validation of the TFT flow forecasting model. Blackbird has an efficient, reach-integrated, hydraulic framework that has been designed for large-scale, regional flood line mapping. Blackbird's potential for use in ISWMS™ was assessed by comparing its predicted flood extents to those generated by the widely used HEC-RAS 1D model for the Mattagami River Basin under 25-, 50-, and 100-year return periods and the Timmins storm event. Validation employed nine statistical measures.

By integrating a continental-scale machine learning forecasting engine, flood-frequency analysis functionality, and a computationally efficient hydraulic flood mapping model, ISWMS™ will provide a scalable and operational system for real-time and design-based flood risk assessment. This combined approach enables timely, geographically extensive flood intelligence, particularly valuable for remote regions where conventional hydraulic modelling is impractical.

KEYWORDS: ISWMS™, Temporal Fusion Transformer, Flood risk, Blackbird, Inundation mapping, real-time flow forecasting

1 INTRODUCTION

Although floods can play an important ecological role by sustaining riverine and wetland ecosystems during periodic scouring events, their increasing impacts on human communities highlight the urgent need for reliable flood risk assessment and mapping tools (Aristizabal et al., 2023; Bhupsingh et al., 2022). Flood inundation models have therefore become essential for hazard mapping, flood forecasting, damage assessment, and water resources planning (Apel et al., 2022; Arduino et al., 2005).

Hydraulic models, such as HEC-RAS, have been widely used to generate flood maps based on numerical solutions of the shallow-water equations (Brunner and RAS, 2008). In practice, both 1D and 2D versions of HEC-RAS are applied, but each has notable drawbacks. The 1D approach requires detailed cross-sectional data and relies on interpolation between sections, which can lead to unrealistic predictions of inundation in areas lacking hydraulic connectivity (Hashim et al., 2021; Yang et al., 2006). While 2D models generally provide higher accuracy, they demand significant computational resources and extensive setup effort, making them difficult to implement at large scales or for real-time applications (Ghimire et al., 2022; Teng et al., 2017). These limitations often result in flood maps that are outdated or unavailable in many high-risk regions.

To address these challenges, the Integrated Science and Watershed Management System (ISWMS™) originally developed by GREENLAND® International Consulting Ltd. (Greenland) over 2 decades ago, was re-developed as a multi-component platform that integrates hydrometric flow prediction and hydrologic analysis with hydraulic flood mapping capabilities. The ISWMS™ decision support system is now deployed within the Healthy Rivers Ecosystem AssessmenT System (THREATS™), a web-based platform, developed and maintained by Greenland, that offers tools for watershed data access, visualization and analysis.

A key element of ISWMS™ is a Temporal Fusion Transformer (TFT) deep learning model capable of producing real-time probabilistic flow forecasts across North America, with prediction horizons of up to 14 days. Complementing this forecasting capability, ISWMS™ incorporates flood-frequency analysis for deriving design flows used in regulatory and planning contexts. Together, these functions allow ISWMS™ to characterize both short-term forecasted extremes and long-term risk. To translate either forecasted or design flows into inundation extents, ISWMS™ requires a hydraulic mapping tool that is both computationally efficient and readily scalable.

Blackbird, developed by Chlumsky et al. (2024), is a reach-integrated hydraulic model that combines the Geospatially Augmented Standard Step (GASS) method with the Height Above Nearest Drainage (HAND), eliminating the need for cross-sectional data, streamlining model development, and producing flood maps orders of magnitude faster than comparable 2D models while maintaining reasonable accuracy relative to hydrodynamic benchmarks. Its efficiency and reduced data requirements make it particularly suitable for large-scale and real-time flood mapping, as well as for remote locations where traditional hydraulic modelling may be infeasible.

In this study, we present evaluation results from both the TFT and the Blackbird models and consider how their combined use could provide a comprehensive visualization of flood inundation for emergency preparedness and long-term planning.

2 MATERIALS AND METHODS

2.1 Study area and data

The Mattagami River is a major riverine system in northern Ontario, Canada. Its watershed encompasses approximately 36,800 km² (Clavet-Gaumont et al., 2017), draining a diverse landscape of lakes, wetlands, and forested terrain before flowing northward through the City of Timmins and eventually joining the Moose River system located within the “Ring of Fire” natural resources economic region. The latter was designated recently by the Government of Ontario as a Special Economic Zone (SPZ). The river reach

examined plays a critical role in drinking water supply, hydroelectric generation, and flood management for the region. Figure 1 illustrates the portion of Mattagami River Basin that was used for the study.

In this study, LIDAR-derived digital elevation model (DEM) data with 2-m resolution was employed to ensure accurate representation of terrain and channel geometry in the Mattagami River watershed. The DEM was used to compute flow accumulation, flow direction, and HAND layers, as well as channel polylines, which are critical inputs for reach-integrated hydraulic property calculations. A high-resolution DEM was necessary to preserve landscape connectivity, minimize interpolation errors, and improve the accuracy of flood depth mapping across complex terrain. For hydrological input, the Mattagami River hydrometric station 04LA002, located upstream of the City of Timmins, was used. This station provides a continuous record of daily flow data from 1969 to 2025, making it suitable for flood frequency analysis. The long record length allows for robust statistical fitting of probability distributions to estimate return period flows (e.g., 25-, 50-, and 100-year floods). These return period discharges were applied as boundary conditions in both HEC-RAS 1D and Blackbird simulations to generate flood inundation maps for comparison.

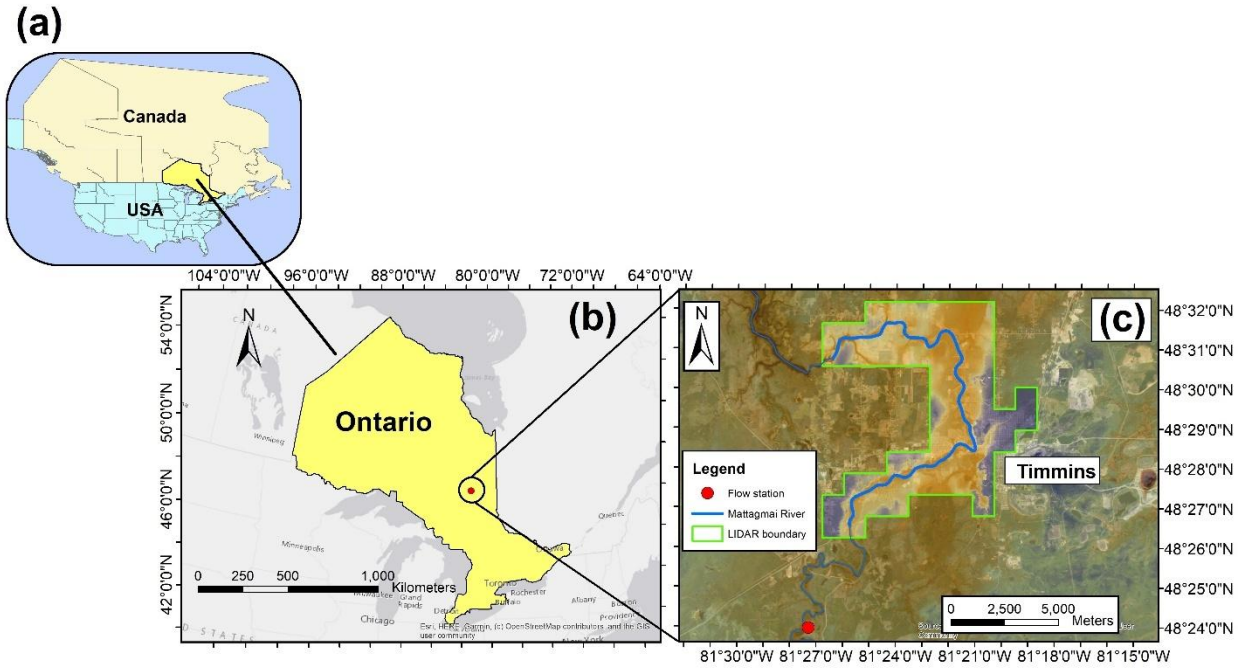

Figure 1: Location and hydrological context of the study area in northern Ontario: (a) National overview showing Ontario within North America, (b) Regional map of Ontario highlighting the Timmins area, (c) Detailed map of the Mattagami River near the City of Timmins, including the LiDAR survey boundary, the river channel, and the upstream hydrometric station 04LA002.

2.2 Methodology

2.2.1 ISWMS™ machine learning flow forecasting model

The machine learning component of ISWMS™ is based on the Temporal Fusion Transformer (TFT) architecture developed and evaluated by French (2023). The TFT is a sequence-to-sequence deep learning model designed for multivariate time-series forecasting and can learn complex temporal relationships among climate variables, catchment attributes, and historical streamflow. The model was trained on several decades of hydrometric and climate data from thousands of stations across North America, using large datasets such as Hydrological Streamflow Extent Time Series (HYSETS), Global Land Data Assimilation System (GLDAS), Canada's National Water Data Archive (HYDAT), Natural Resources Canada (NRCAN), and numerical weather prediction products.

Key features of the TFT include attention mechanisms, gating layers, and variable-selection networks, which allow the model to identify the most influential predictors at each timestep and to provide interpretable probabilistic forecasts. Within ISWMS™, the TFT model generates real-time flow predictions with 14-day lead times. These forecasts can serve as inputs to a hydraulic inundation model, enabling rapid flood extent mapping when elevated flows are predicted. Figure 2 shows real-time probabilistic discharge forecasts generated by the TFT-based prediction system alongside Mattagami River high-flow event thresholds.

2.2.2 Flood Frequency Analysis

Within ISWMS™, flow forecast analysis is implemented as a dedicated function that provides design flows for regulatory and planning applications. This functionality was used to derive return-period discharges for the Mattagami River. The analysis was based on annual maximum series extracted from long-term daily discharge records. These annual maxima were fitted to a Generalized Extreme Value (GEV) distribution using the L-moments method, which offers stable parameter estimation for extreme value distributions commonly applied in hydrologic studies. To quantify uncertainty in the estimated flood quantiles, ISWMS™ employs a bootstrap resampling procedure that repeatedly samples the annual maxima to approximate the sampling distribution of return-period flows.

This approach yields robust 95% confidence intervals for each return period. Flood quantiles were subsequently derived for the 25-, 50-, and 100-year return periods, with three values reported for each: the lower confidence bound, the median estimate, and the upper confidence bound. By integrating L-moments-based GEV fitting with bootstrap uncertainty analysis, the ISWMS™ flood-frequency function provides both point estimates and confidence ranges, enabling a reliable characterization of flood risk at the station. These design flows served as the hydraulic inputs for evaluating the Blackbird model in this study, complementing the broader ISWMS™ framework including flow forecasting.

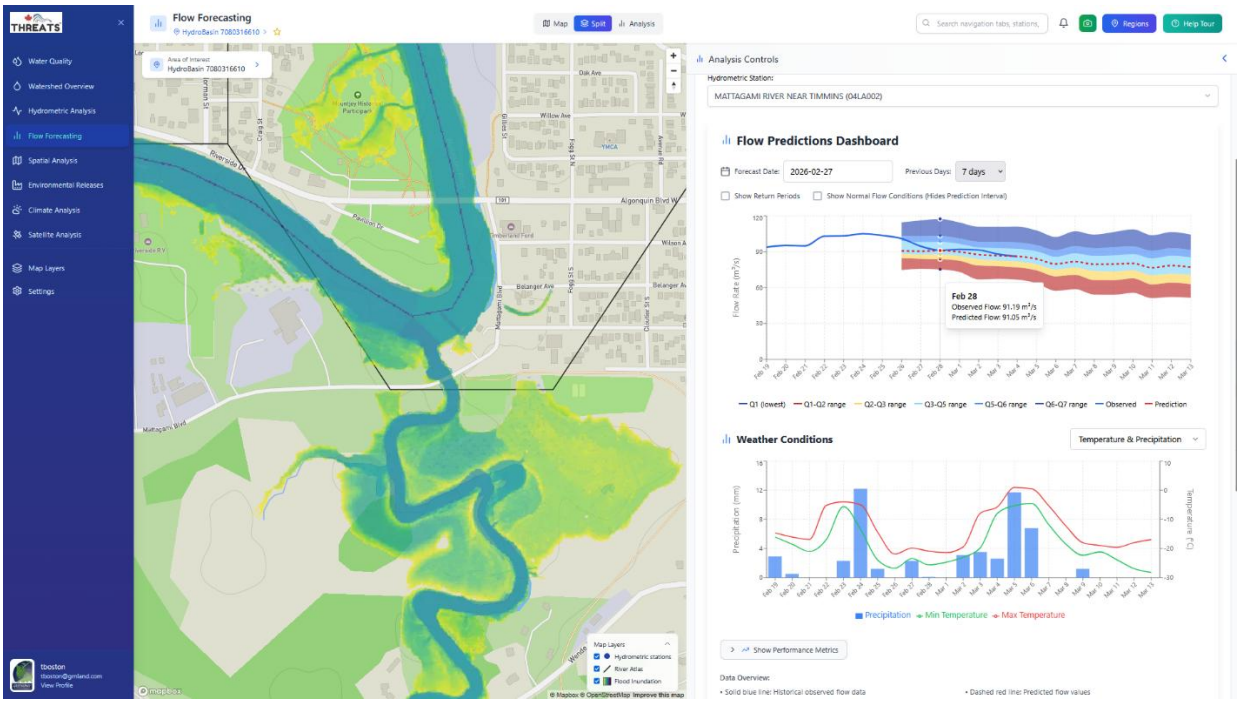

Figure 2: ISWMS™ flow prediction interface showing probabilistic discharge forecasts for the Mattagami River. The right panel displays predicted flows and confidence bands with meteorological forecast data, while the left panel shows locations of any flood inundation for forecast flows or return period events.

2.2.3 HEC-RAS 1D model development

The HEC-RAS hydraulic model for the Mattagami River was developed using high-resolution digital elevation data and detailed field survey information to construct river geometry, cross-sections, culverts, and bridge structures. All hydraulic structures such as bridge decks were incorporated based on direct field verification. The model was run under steady-state conditions using flow values for selected return period floods derived from Flood Frequency Analysis (FFA) of the long-term record at hydrometric station 04LA002. The resulting flood extents were then used as references for validation of the Blackbird model simulations.

2.2.4 Blackbird model description

Blackbird applies the Geospatially Augmented Standard Step (GASS) method, which integrates geospatial data directly into hydraulic calculations. A central concept is conveyance, representing the ability of a river reach to carry flow under a given stage. Unlike traditional cross-sectional models, Blackbird computes conveyance by aggregating contributions from raster cells across the reach, ensuring hydraulic capacity is calculated consistently across the terrain.

The hydraulic solver is based on the standard step method, which balances energy between successive stream nodes:

$$z_j + d_j + \alpha_2 \frac{\overline{u}_j^2}{2g} = z_{j-1} + d_{j-1} + \alpha_1 \frac{\overline{u}_{j-1}^2}{2g} + \Delta h_j \tag{1}$$

where z is channel invert, d is depth, α is the velocity coefficient, $\overline{u}$ is mean velocity, g is acceleration due to gravity, and Δh_j is head loss.

Head loss is expressed as:

$$\Delta h_j = L_{e_j} S_{f_j} + C_j \left(\frac{\alpha_j \overline{u}_j^2}{2g} - \frac{\alpha_{j-1} \overline{u}_{j-1}^2}{2g} \right) \tag{2}$$

with L_{e_j} the effective reach length, S_{f_j} the friction slope, and C_j contraction or expansion coefficients. The friction slope is linked to conveyance:

$$S_{f_j} = \left(\frac{Q_j}{K_j} \right)^2 \tag{3}$$

where Q_j is discharge and K_j is conveyance.

Flood depths are mapped using the Height Above Nearest Drainage (HAND) algorithm, which preserves terrain connectivity. Cell depth is determined by:

$$d_i = \max(d_j - H_i, 0) \tag{4}$$

where H_i is the HAND value for cell *i*.

Together, these formulations allow Blackbird to compute flood extents rapidly while maintaining hydraulic realism, with outputs provided as spatially distributed flood depth rasters.

2.2.5 Accuracy assessment

To evaluate the accuracy of Blackbird in flood inundation mapping, we applied nine statistical performance measures, namely the Critical Success Index (CSI), Probability of Detection (POD), False Alarm Ratio (FAR), True Positive Rate (TPR), F1 score (F1), Overall Accuracy (ACC), Hit Rate (HR), Cohen's Kappa (Kappa), and Bias using results from previous modelling using HEC-RAS as a standard. The application of Blackbird was an out-of-the-box application on a single length of the Mattagami River. There was no calibration and no adjustments were made to address constrictions at bridges or the influence of tributaries joining the main reach.

3 RESULTS

3.1 ISWMS™ machine-learning flow forecasting model

The performance of the TFT model integrated into ISWMS™ was evaluated extensively by French (2023). Across approximately 8,500 North American catchments, the model demonstrated strong hindcasting skill and reliable short-term forecasting performance through cross-validation.

Forecast accuracy was highest within the first several days of prediction, decreasing toward the 14-day horizon due to increasing meteorological forecast uncertainty. Table 1 summarizes the forecasting performance metrics, including NSE, R^2, and PBIAS across the full validation dataset. These results show that the TFT model consistently achieved high predictive skill for short-term flow forecasting across approximately 8,500 hydrometric stations, with reasonable performance in capturing peak flows, an essential requirement for operational flood forecasting. Results showed regional variation in performance with regulated watersheds being harder to predict reliably. These findings support the informed use of the TFT model as the real-time forecasting engine within ISWMS™ and justify its integration with a hydraulic mapping tool for rapid flood extent prediction during forecast flow events.

Table 1 Quantification of prediction performance and thresholds (hindcasting) (French (2023)).

R^2 Median	NSE Median	PBias Median	KGE Median
0.86	0.81	-3.25	0.78

Statistic	Unsatisfactory	Satisfactory	Good	Very Good
R^2	12%	13%	22%	53%
NSE	15%	14%	17%	54%
PBias	35%	15%	22%	28%

Thresholds used

Metric	Not satisfactory	Satisfactory	Good	Very Good
R^2	≤0.60	(0.6,0.75]	(0.75,0.85]	>0.85
NSE	≤0.50	(0.5,0.7]	(0.7,0.8]	>0.8
PBIAS	$(-\infty, -15] \cup [15, \infty)$	(-15,-10] ∪[10, 15)	(-10,-5] ∪[5, 10)	(-5,5)

3.2 Flood Frequency Analysis

Design flow conditions estimated from the fitted GEV distribution yielded peak flow values of 396.1 m^3/s, 426.5 m^3/s, and 450.46 m^3/s for the 25-, 50-, and 100-year return periods, respectively. These values represent the expected magnitude of flow events based on statistical extrapolation of annual maxima. The Timmins Storm, an observed extreme event, produced a peak discharge of 707.92 m^3/s, as reported by the Mattagami Region Conservation Authority. This observed flow substantially exceeds the 100-year estimate, underscoring the severity of the event and its relevance for model validation. Both Blackbird and HEC-RAS 1D were executed using the four design flows. Results from Blackbird were evaluated against HEC-RAS 1D, which served as the reference model for validation.

3.3 Blackbird Hydraulic Model Assessment

Table 2 presents the performance metrics derived from spatial intersection between Blackbird and HEC-RAS 1D flood inundation maps across four flood scenarios: 25-year, 50-year, 100-year, and the Timmins Storm. These metrics quantify Blackbird's ability to replicate HEC-RAS predictions using statistical measures. From Table 2, Blackbird demonstrates consistently high performance for the 25-, 50-, and 100-year flood events. CSI ranged narrowly from 0.85 to 0.87, and POD and TPR remained stable at 0.95 across these three scenarios. F1 scores were similarly strong (0.92–0.93), and ACC was exceptionally high at 0.99. Cohen's Kappa values (0.91–0.93) indicated substantial agreement with HEC-RAS, and Bias values close to 1 (1.08, 1.06, 1.03) suggested minimal overprediction.

Performance declined under the Timmins Storm. CSI dropped to 0.73, and POD/TPR fell to 0.74, indicating reduced detection of flooded areas. The F1 score decreased to 0.85, and Kappa dropped to 0.83, reflecting weaker agreement. Notably, Bias fell to 0.75, suggesting underprediction of flood extent. Despite this, HR increased to 0.99, indicating that Blackbird correctly identified most of the areas flagged by HEC-RAS as flooded, but with reduced precision.

Table 2 Performance metrics of Blackbird flood inundation mapping under multiple flood events.

Performance metrics	25-year Flood	50-year Flood	100-year Flood	Timmins Storm	Average
CSI	0.85	0.86	0.87	0.73	0.83
POD	0.95	0.95	0.95	0.74	0.90
FAR	0.12	0.10	0.08	0.01	0.08
TPR	0.95	0.95	0.95	0.74	0.90
F1 Score	0.92	0.93	0.93	0.85	0.91
ACC	0.99	0.99	0.99	0.97	0.98
HR	0.88	0.90	0.92	0.99	0.92
Kappa	0.91	0.92	0.93	0.83	0.90
Bias	1.08	1.06	1.03	0.75	0.98

Figure 3 illustrates the spatial agreement between Blackbird and HEC-RAS flood extents across four flood scenarios. For the 25-, 50-, and 100-year floods, True Positive areas dominate, with minimal False Positives and False Negatives, indicating strong spatial accuracy.

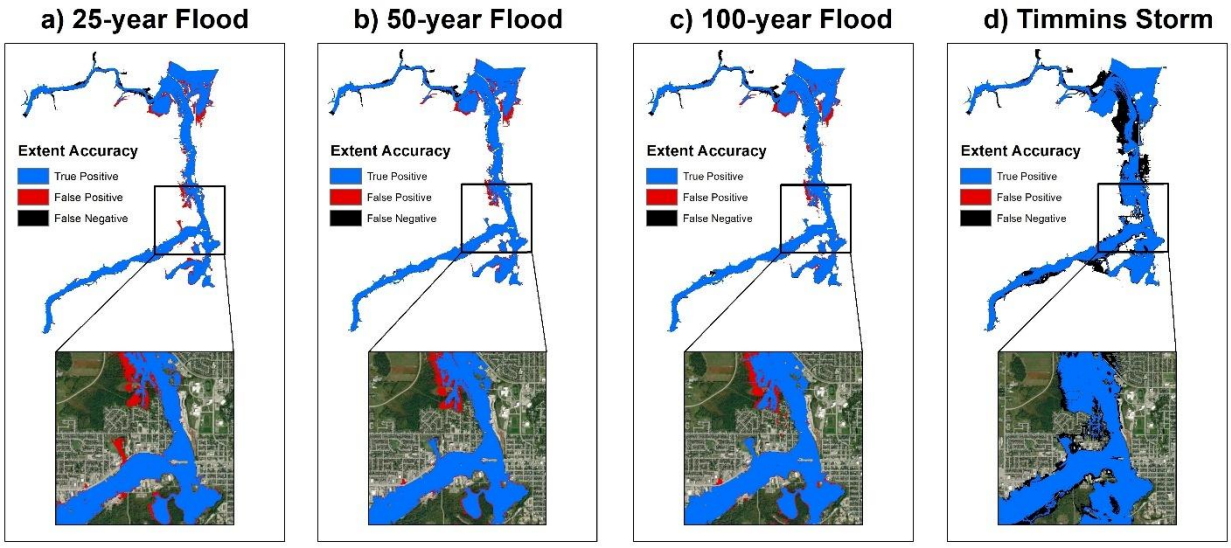

Figure 3: Spatial distribution of flood extent accuracy for four flood scenarios: (a) 25-year, (b) 50-year, (c) 100-year, and (d) Timmins Storm. Each panel shows areas correctly predicted as flooded (True Positives, blue), areas incorrectly predicted as flooded (False Positives, red), and areas that flooded but were not predicted (False Negatives, black).

4 DISCUSSION

Blackbird achieved strong agreement with HEC-RAS for the 25-, 50-, and 100-year floods, with consistently high CSI, POD, F1, and accuracy values. Its performance declined under the Timmins Storm, where detection rates dropped and false negatives increased. The reasons for this divergence are likely tied to the structural and hydraulic complexities of extreme events that were not adequately addressed in the model setup. Blackbird does not explicitly simulate bridges, culverts, or other hydraulic controls, which play a critical role in shaping flow patterns during high-magnitude floods. When discharge levels rise substantially, as in the Timmins Storm (≈707 m^3/s compared to ≈450.46 m^3/s for the 100-year flood), these structures and other tributaries influence backwater effects, channel conveyance, and localized inundation to a greater degree. Without their representation, Blackbird tends to underestimate flood extent, as reflected in the lower Bias and higher false negative rate. Similar limitations of simplified flood models have been documented in prior studies, which emphasize that neglecting urban features and hydraulic structures can reduce predictive skill in complex scenarios (Fewtrell et al., 2008; Neal et al., 2012; Schubert and Sanders, 2012).

An import distinction is that the Blackbird model was uncalibrated. Several adjustments could have been made to improve its performance for the Timmins Storm, but this would have deviated from the study goal of doing an "out-of-the-box" comparison to see how it might perform without additional information being coded into the model.

While the flow inputs used in this study were derived from flood frequency analysis rather than machine learning forecasts, they represent the types of high-flow conditions that ISWMS™ aims to predict operationally. The machine learning algorithms within ISWMS™ can forecast discharge up to 14 days ahead, enabling early detection of potential flood events. By validating Blackbird against benchmark flood extents using design flows and a historical storm, we demonstrated its capability to rapidly generate inundation maps under conditions consistent to those forecasted by ISWMS™ algorithms. This confirms Blackbird's suitability for integration into the ISWMS™ workflow, where it will support real-time flood mapping triggered by TFT model flow predictions. The consistently high accuracy for design floods demonstrates that Blackbird is reliable for typical hazard assessment. Its computational efficiency makes it particularly valuable in remote regions, where developing detailed hydraulic models like HEC-RAS 1D or 2D may be impractical. Thus, while refinement in model approach and application technique is needed to

improve performance under extreme events, Blackbird already offers a practical balance between accuracy and speed for operational flood mapping.

5 CONCLUSION

The TFT based algorithms used in ISWMS™ provides access to stream flow forecasting across North America at approximately 8,500 hydrometric stations. The wide availability of forecasting data creates a strong potential for wide-spread, cost effective adoption of the system for extreme event prediction. The model was found to perform well in cross-validation across thousands of hydrometric stations where weather forcing data was accurate and there was limited influence on flows due to regulation.

The Blackbird hydraulic mapping model using flood frequency analysis derived flows and a regulatory storm event, demonstrated strong agreement with HEC-RAS 1D for return period flood events with strong agreement across statistical metrics and very low misclassification rates. It struggled with the Regional Timmins storm event likely due to inadequate handling of bridge constrictions and tributary inflows.

Since ISWMS™ can forecast discharge, integrating Blackbird offers a practical solution for rapidly rendering forecasted flows into flood extent maps in real-time. Scenario flows can be used for planning and mitigation purposes. The result will be a fully operational deployment of ISWMS™ within the THREATS web platform, supporting its broader goal of scalable, efficient, real-time flood risk assessment. Future applications could include:

- Flood and drought forecasting to protect vulnerable floodplain communities.
- Flow predictions to reduce risks in operating hydropower and other utility facilities.
- Flow predictions to protect the operations of resource industry (mining) projects.
- Flow predictions for infrastructure assets at risk from flooding or accelerated erosion processes, including: 1) Wastewater Treatment Plants (with or without CSO storage or overflow capabilities) affected by floodplains; 2) stream/river road crossing structures monitoring; 3) road/highway construction & community servicing retrofit projects susceptible to “flash flood” events; and, 4) oil/gas pipeline and telecommunication underground floodplain crossings impacted by severe flow - erosion induced events.

6 ACKNOWLEDGEMENTS

The authors gratefully acknowledge the support of David Vallier, General Manager of the Mattagami Region Conservation Authority, for his cooperation and for providing access to high-resolution LiDAR data essential to this study. We also thank Nicole Scott (Greenland) for her assistance in integrating the Blackbird model into the web-based THREATS™ application, which enables broader accessibility and operational deployment. The authors further acknowledge George Yang (Greenland) for providing the HEC-RAS 1D flood inundation maps used as reference datasets in this validation study. We also extend our appreciation to Robert Chlumsky, developer of the Blackbird model, for his valuable comments and guidance that supported the application and refinement of the model for the Mattagami River case study. MITACS is a partial funder of this research with Greenland International Consulting Ltd. as an industry partner.

REFERENCES

Apel H.Vorogushyn S.Merz B. (2022). Brief communication–Impact forecasting could substantially improve the emergency management of deadly floods: Case study July 2021 floods in Germany. Nat. Hazards Earth Syst. Sci, 2022: 1-10.

Arduino G.Reggiani P.Todini E. (2005). Recent advances in flood forecasting and flood risk assessment. Hydrol. Earth Syst. Sci, 9(4): 280-284.

Aristizabal F. et al. (2023). Extending height above nearest drainage to model multiple fluvial sources in flood inundation mapping applications for the US National Water Model. Water Resour. Res, 59(5): e2022WR032039.
Bhupsingh T. et al. (2022). Adapting to rising flood risk–an analysis of insurance solutions for Canada.
Brunner G.RAS H. (2008). River analysis system hydraulic reference manual. Do Defense, Davis.
Chlumsky R.Craig J.R.Tolson B.A. (2024). A reach-integrated hydraulic modelling approach for large-scale and real-time inundation mapping. Geosci. Model Dev. Discuss, 2024: 1-28.
Clavet-Gaumont J. et al. (2017). Probable maximum flood in a changing climate: An overview for Canadian basins. J. Hydrol. Reg. Stud, 13: 11-25.
Fewtrell T.Bates P.D.Horritt M.Hunter N. (2008). Evaluating the effect of scale in flood inundation modelling in urban environments. Hydrol. Process, 22(26): 5107-5118.
French S. (2023). Temporal Fusion Transformers: A Novel Approach to Streamflow Prediction, University of Guelph.
Ghimire E.Sharma S.Lamichhane N. (2022). Evaluation of one-dimensional and two-dimensional HEC-RAS models to predict flood travel time and inundation area for flood warning system. ISH J. Hydraul. Eng, 28(1): 110-126.
Hashim S. et al. (2021). Cross section intervals of flood intervals of flood inundation mapping at ungauged area, IOP Conference Series: Earth and Environmental Science. IOP Publishing, pp. 012003.
Neal J. et al. (2012). How much physical complexity is needed to model flood inundation? Hydrol. Process, 26(15): 2264-2282.
Schubert J.E.Sanders B.F. (2012). Building treatments for urban flood inundation models and implications for predictive skill and modeling efficiency. Adv. Water Resour, 41: 49-64.
Teng J. et al. (2017). Flood inundation modelling: A review of methods, recent advances and uncertainty analysis. Environ. Model. Softw, 90: 201-216.
Yang J.Townsend R.D.Daneshfar B. (2006). Applying the HEC-RAS model and GIS techniques in river network floodplain delineation. Can. J. Civ. Eng, 33(1): 19-28.

ICFM 10
Adapting to Global Change:
Innovative Approaches to Flood Management and Resilience
May 20-22, 2026 | Western University, London, Ontario, Canada

Flood Mapping for Small Creeks on the Canadian Prairies: Challenges and Strategies - Stettler Flood Mapping Case Study

Md Makamum Mahmood[1], Hammad Javid[2], Robyn Andrishak[1], Can Hua (Ken) Zhao[1], Michael Brayall[2], Muhammad Durrani[2], and Peter Onyshko[2]

Northwest Hydraulic Consultants Ltd. (NHC), 9819-12 Avenue SW, Edmonton, AB, T6X 0E3, Canada[1]
E-mail: mmahmood@nhcwater.com, randrishak@nhcwater.com, kzhao@nhcwater.com

River Engineering and Technical Services, Watershed Resilience and Predictions Branch, Alberta Environment and Protected Areas (EPA), 9820 106 Street NW, Edmonton, AB, T5K 2J6, Canada [2]
E-mail: hammad.javid@gov.ab.ca, michael.brayall@gov.ab.ca, muhammad.durrani@gov.ab.ca, peter.onyshko@gov.ab.ca

ABSTRACT

Effective flood risk management and land-use planning depend on accurate, realistic flood mapping. In a country as large and diverse as Canada, flood mapping must account for varied landscapes, multiple flood mechanisms, different land uses, and a broad range of waterbody types. These factors create unique challenges that demand site-specific methodologies. This paper examines two challenges encountered in flood mapping along small prairie creeks: estimating flood frequency flows for ungauged small streams and delineating inundation maps at road crossings with limited culvert capacity. It then introduces strategies to improve flood mapping accuracy. Using the study for the town of Stettler, Alberta as a case, we demonstrate the importance of site-specific analyses, often overlooked in large-scale or regional studies.

Flood frequency analysis was challenged by limited hydrometric data available, floodplain attenuation, and lake storage effects in the basin upstream of the study site. To overcome this, we developed a site-specific, physical process-based approach that integrates local knowledge into a regional flood frequency analysis, accounting for flood flow attenuation due to upstream lake and floodplain storage. This produced more reliable flood frequency estimates than standard statistical methods and more accurate inundation and hazard maps.

In the Stettler study, accurately representing potential road overtopping and flood inundation at 27 culvert crossings was another challenge. Inundation mapping at culvert crossings typically employs a sloped water surface across road embankments. However, this approach can produce unrealistic results at a crossing where the downstream water level is well below the road crest while the upstream water is significantly higher. To address this issue, we employed GIS techniques that better represent the local hydraulic condition without more complex numerical modelling. This method accurately mapped road overtopping at several locations where the conventional mapping approach failed to identify it.

KEYWORDS: Flood Mapping, Flood Hydrology, Inundation Mapping at Culvert Crossing

1 INTRODUCTION

The Canadian Prairies, spanning Alberta, Saskatchewan, and Manitoba, feature flat to gently rolling terrain, small low-gradient streams, and wide floodplains that are highly susceptible to flooding from spring snowmelt and intense rainfall. This paper focuses on the Stettler Flood Study, which was completed in 2022-2025 by Northwest Hydraulic Consultants (NHC) for Alberta Environment and Protected Areas (EPA). Flood maps were developed for 30 km of Redwillow Creek and 4 km of an unnamed tributary

flowing through the town of Stettler and surrounding areas of Stettler County in east-central Alberta.

Flood mapping is essential for rural communities like Stettler, supporting flood protection, emergency preparedness, land-use planning, and infrastructure design. Past events, most notably the 1974 flood (which affected many prairie communities in Alberta and Saskatchewan), have demonstrated the region's vulnerability. Prairie flood studies also face some site-specific challenges which are unique to this landscape. In Stettler, these included difficult surveying conditions due to poorly defined channels, intermittent flows, marshy areas, and deep-water pools created by beaver dams; complex hydrology in ungauged basins; mapping limitations at culvert crossings; and Digital Terrain Model (DTM) distortions caused by floodplain vegetation. This paper focuses on two technical challenges: developing hydrology for ungauged prairie streams and mapping roadway overtopping at culvert crossings.

2 FLOOD HYDROLOGY

Reliable flood mapping requires accurate peak flow estimation. Studies like the Stettler Flood Study require modelling and mapping multiple flood frequencies based on careful assessment of basin responses under different flood magnitudes. This section summarizes the challenges and methods used to develop flood hydrology for Redwillow Creek and the unnamed tributary in the Stettler Flood Study. Local knowledge indicated that peak flow estimates from some previous studies in the region were unrealistically high, prompting a refined, evidence-based approach for more accurate flood mapping.

2.1 Watershed Characteristics

Flood hydrology assessment in ungauged watersheds typically relies on regional flood frequency analyses because local flow measurements are not available. This approach demands accurate delineation of the basin area and its physiographic characteristics. In prairie basins, flat terrain with numerous lakes and wetlands complicate basin delineation and the determination of contributing areas. Overcoming these challenges requires local knowledge, high-resolution topographic data, and representative regional hydrologic data to refine and verify basin contributing areas, as outlined below for the Stettler Flood Study.

The Redwillow Creek basin, including the unnamed tributary, is shown in Figure 1. The basin features flat terrain with extensive wetlands and sloughs that are typical of prairie landscapes. Agriculture is the dominant land use. Redwillow Creek flows northwest through Stettler and is ungauged within the study reach. A discontinued gauge near its downstream end operated from 1962-1991. Available data show that annual peak flows usually occurred during spring snowmelt. The largest recorded flood occurred in spring 1974 (AEP, 1995). Another notable flood event occurred in July 1999 and was attributed to a local rainstorm, though no measurements were taken (Stantec, 2004).

Basin delineation for this study was completed using Water Survey of Canada (WSC) data, Agriculture and Agri-Food Canada (AAFC) watershed information, and LiDAR topography. Although published sources report a gross drainage area of 825 km² upstream of the discontinued Redwillow Creek gauge (WSC Station 05FC005), detailed hydrologic and topographic assessments showed that the Lonepine Lake subbasin (Figure 1) is a self-contained area and does not contribute flows to Redwillow Creek under typical conditions. It was estimated that spillover from the Lonepine subbasin would require approximately 120 mm of runoff. This greatly exceeds the design runoff depth of 35 mm for this region determined by Alberta Transportation (AT, 2006) from regional runoff envelop curves. Historical flow data from the nearby WSC Bigknife Creek gauge (Figure 1) indicate a runoff depth of only 30 mm in this gauged similar basin corresponding to the 1974 flood, the largest event on record. Because these values fall far below the estimated threshold required for spilling, the Lonepine Lake subbasin was excluded, resulting in a 228 km^2 reduction in the contributing area for Redwillow Creek at the discontinued gauge (05FC005). Moreover, the high-resolution LiDAR data indicate that, if the Lonepine Lake subbasin were to spill during an extreme event, overflow would run northeast, bypassing the Stettler study reach, and join Redwillow Creek at a downstream location. This analysis further confirmed the need to exclude Lonepine Lake subbasin in this study, a critical step to improving flood peak estimation and producing reliable flood mapping.

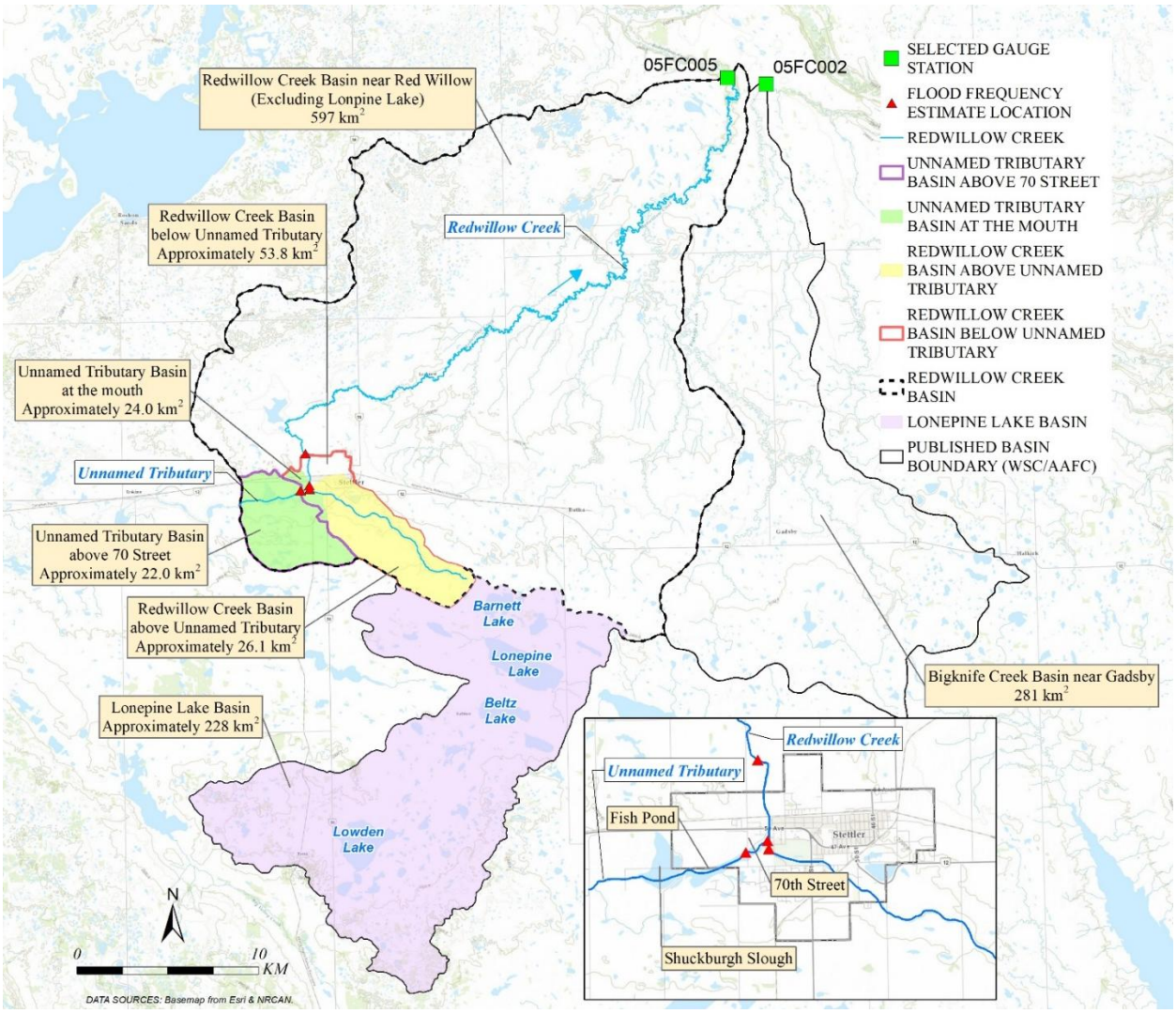

Figure 1: Redwillow Creek basin overview and selected flood frequency estimate locations

2.2 Regional Analysis

Flood frequency estimates for Redwillow Creek and the unnamed tributary were developed using a regional analysis approach, as neither stream is gauged within the study reach. Key challenges included identifying hydrologically representative basins, addressing limited gauge record lengths, and selecting a reliable relationship. Regional reference stations were chosen based on proximity, climatic and physiographic similarity, basin size, record length, and topographic characteristics. Instantaneous peak discharges from these stations were used in the analysis, with missing values estimated through correlations between instantaneous and daily peaks from overlapping years. The regional analysis produced instantaneous peak discharge estimates for multiple open water return periods (2-, 20-, 100-, 200-, and 1000-year floods presented in this paper) at two locations on Redwillow Creek and two on the unnamed tributary within the town of Stettler.

The annual peak instantaneous discharges (Q_p) for each of the selected regional stations were normalized by their mean value (Q_{pm}) and are plotted in Figure 2 (a) against their empirical return periods based on the Cunnane formula. Different theoretical probability distributions were tested for each individual station. The Pearson type III (P3) distribution generally provides the best fit for all selected stations. As such, a normalized P3 curve was used to fit the normalized regional flow data. The normalized P3 curve

shown in Figure 2 (a) was computed by varying the standard deviation and coefficient of skewness within the respective ranges of the values for the selected gauge stations until the total Sum of Standard Error (SSE) values (Equation 1) for the regional stations become minimum. The SSE measures the root mean square difference between observed value (x_i) and predicted value (y_i), adjusted for the degrees of freedom ($n - m$).

$$\text{SSE} = \sqrt{\frac{1}{n-m}\sum_{i=1}^{n}(x_i - y_i)^2} \tag{1}$$

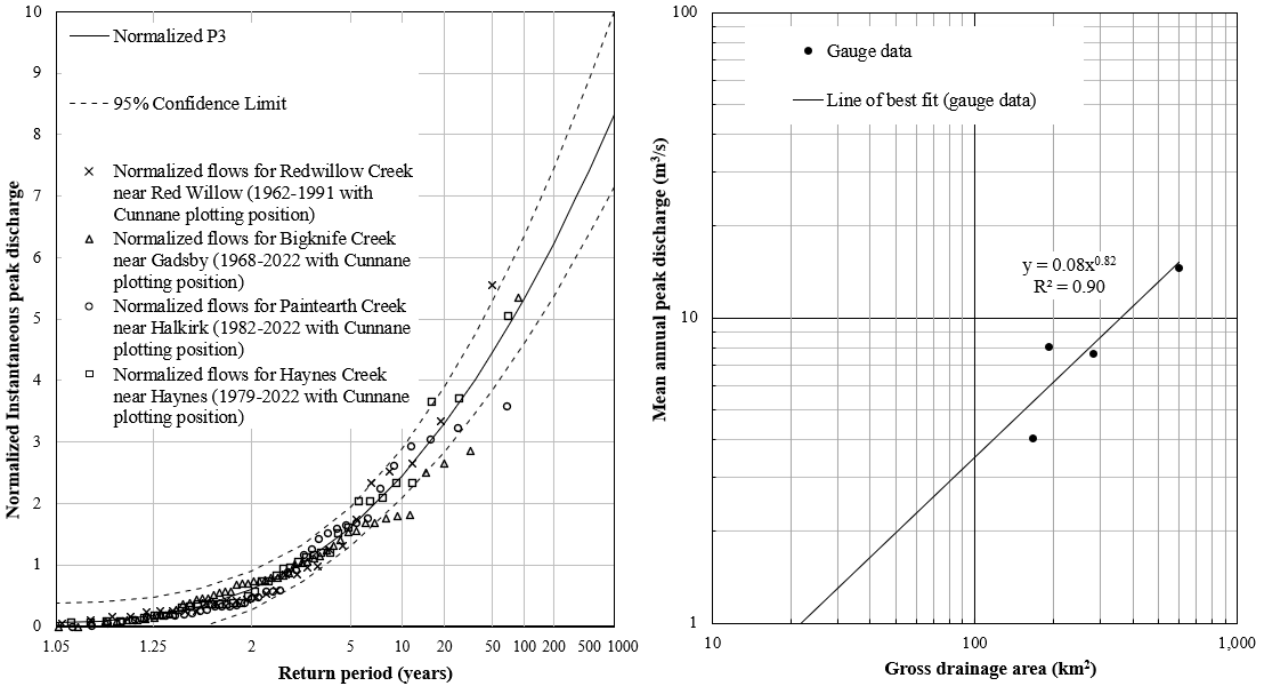

Figure 2: (a-left) Adopted P3 frequency distribution for normalized flood peak discharges and (b-right) Relationship between mean annual peak discharge and drainage area

As shown in the figure above, the curve fits all data points reasonably well. Figure 2 (a) also shows the 95% confidence limits for the normalized P3 curve, which were estimated based on the average length of the regional flood data series (41 years). Figure 2 (b) above on right side, shows the relationship between the mean annual peak discharges (Q_{pm}) and gross drainage areas for the selected regional stations. The peak discharge is proportional to the gross drainage area to the power of 0.82. Using the normalized P3 curve from Figure 2 (a) and the relationship of mean peak discharge versus drainage area from Figure 2 (b), flood frequency estimates can be developed.

To reduce uncertainty, the regional analysis used a rigorous gauge selection process and an appropriate flood frequency analysis method. A flood-index approach with normalized flows reduced bias from differing record lengths, and the best-fit curve was statistically optimized. Confidence limits were determined based on the average record length. These refinements improved the consistency and reliability of the estimates, which are summarized later in the paper.

2.3 Flood Hydrograph Routing

Steady flow modelling is typically preferred for flood mapping studies. However, it is important to assess whether channel or floodplain storage could significantly attenuate downstream flood peaks, particularly at road crossings with elevated roadways and limited culvert flow capacities that can cause significant upstream impoundment. This condition is common in small prairie streams and was encountered

in the Stettler Flood Study. Within the study area, the unnamed tributary flows through a relatively large slough (known as Shuckburgh Slough) and a stormwater management facility (known as Fish Pond) before joining Redwillow Creek (Figure 1). Local observations from the 1999 flood event as documented in Stantec (2004) suggest that Redwillow Creek back flowed into this tributary and constrained tributary contributions. The LiDAR data analysis confirmed a substantial storage capacity available in Shuckburgh Slough. Within the study reach, flows move through the slough, pass through an undersized 600 mm CSP culvert at 70 Street, enter Fish Pond, and then discharge to Redwillow Creek via a 1.1 m × 1.7 m box culvert and a 750 mm CSP culvert before reaching Redwillow Creek. To account for attenuation of flood flows through this tributary, synthetic hydrographs were developed and routed through these features.

The synthetic hydrographs were developed from the gauged data for Bigknife Creek (WSC Station 05FC002). Daily flows for the five largest flood events on record, including the 1974 event, were used. These events had peak flows from 13.7 to 37.7 m^3/s with times to peak from 3 to 5 days (average 3.6 days). The recorded hydrographs were normalized by corresponding peak discharges (Q_p) and times to peak (T_p). The normalized hydrographs were then represented with a dimensionless hydrograph shape featuring a linear rising limb and an exponential recession limb (Figure 3). The recession limb follows the standard exponential decay as discussed in Chow et al. (1988) and is expressed by Equation 2.

$$Q_* = e^{(T_*-1)b} \tag{2}$$

Where Q_* is the dimensionless discharge (Q/Q_p); T_* is the dimensionless time (T/T_p); b is the recession constant, for which a value of -0.95 was adopted to fit the data. While the hydrograph shape is transferable, the time to peak scales with basin size. Based on comparisons of basin area, slope, and length, the time to peak for the unnamed tributary (basin area: 24 km^2) was estimated to be approximately 1 day, or one-third of the value for Bigknife Creek (basin area: 281 km^2). This was used along with flood peak estimates from regional analysis for Unnamed Tributary above 70 Street presented in Table 1 (discussed later) to generate synthetic flood hydrographs for the unnamed tributary (Figure 3 (b)).

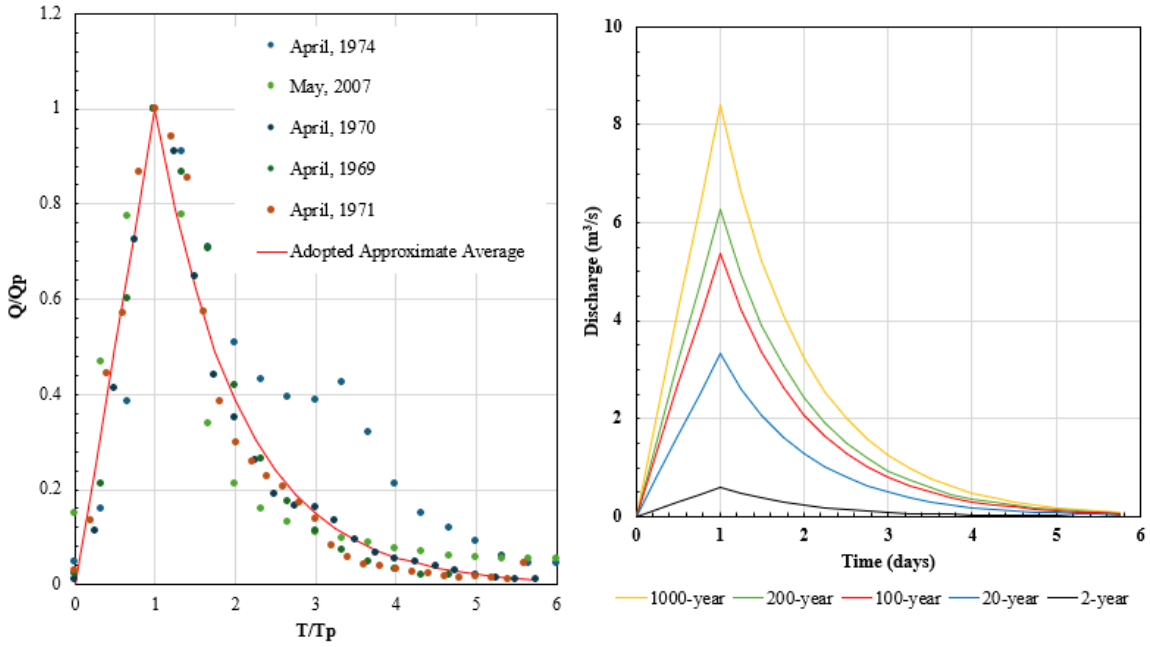

Figure 3: (a -left) Dimensionless hydrograph for the unnamed tributary (b-right) Synthetic flood hydrographs for Unnamed Tributary above 70 Street

The synthetic hydrographs for the unnamed tributary were routed through the 70 Street culvert and Fish Pond using level pool routing. The analysis indicated that the peak discharges of all flood hydrographs

attenuated by 90% to 95% as flowing across 70 Street due to the limited capacity of the existing culvert and significant upstream storage. Subsequent routing through Fish Pond resulted in negligible attenuation. The routing results determined flood peak discharges from the unnamed tributary to Redwillow Creek (estimates for Unnamed Tributary at the mouth as listed in Table 1).

2.4 Adopted Flood Frequency Estimates

Table 1 presents the final adopted flood frequency estimates. Regional estimates were applied directly at Redwillow Creek above the Unnamed Tributary and at the Unnamed Tributary above 70 Street. However, because the flows in Unnamed Tributary attenuated significantly above 70 Street, adjustments were required for Redwillow Creek below Unnamed Tributary and for Unnamed Tributary at the mouth.

Table 1 Flood frequency estimates

Return period	Peak instantaneous discharge (m^3/s)							
	Redwillow Creek above Unnamed Tributary		Redwillow Creek below Unnamed Tributary		Unnamed Tributary above 70 Street		Unnamed Tributary at the mouth	
	Adopted	Without Routing	Adopted	Without Routing	Adopted	Without Routing	Adopted	Without Routing
1000-yr	9.7	9.7	11.8	17.5	8.4	8.4	1.6	9.0
200-yr	7.2	7.2	8.9	13.1	6.3	6.3	1.2	6.7
100-yr	6.2	6.2	7.6	11.2	5.4	5.4	1.1	5.8
20-yr	3.8	3.8	4.8	6.9	3.3	3.3	0.7	3.6
2-yr	0.7	0.7	0.9	1.3	0.6	0.6	0.2	0.7

For Redwillow Creek downstream of the unnamed tributary, peak flows were estimated using regional frequency curves for the reduced drainage area (excluding Unnamed Tributary above 70 Street) and then combined with the routed flows for the unnamed tributary. At the mouth of the unnamed tributary, flood peaks were determined by adding the routed outflows from the 70 Street culvert to locally generated runoff between 70 Street and the creek mouth, based on regional analysis.

Table 1 also lists flood frequency estimates based solely on the regional relationship without adjustments for routing effects. Compared with the results based on routing analysis, these estimates are noticeably higher and inconsistent with local observations at two locations. This comparison demonstrates the importance of considering site-specific conditions to develop reliable flood estimates for flood mapping.

3 MAPPING ROAD OVERTOPPING

Mapping road overtopping for various flood events is important for assessing impacts on transportation infrastructure and supporting emergency planning. Prairie creeks commonly cross small bridges and culverts that are not designed to convey 50-year or larger floods, which can complicate inundation mapping using standard 1D hydraulic modelling. The Stettler study illustrates this issue, with 27 culvert crossings along a 34 km reach, many with limited hydraulic capacity. A 1D steady-state hydraulic model was used to compute flood levels and culvert hydraulics, with the results used to inundation mapping.

3.1 Culvert Hydraulics

Culvert hydraulics directly affect upstream water levels, roadway overtopping, and local inundation. Mapping is straightforward when culvert is not overtopped or where the roadway is fully submerged; but it becomes challenging when there is a large difference between upstream headwater (HW) and downstream tailwater (TW) levels at a surcharged culvert crossing. Figure 4, adapted from WSDOT (2025), illustrates

these scenarios, where HW is headwater elevation, TW is tailwater elevation, Q and Q_T denote total discharge, Q_c is culvert discharge, and Q_o is overtopping discharge.

3.2 Mapping Challenges

Inundation mapping at road crossings based on 1D modelling results is typically produced through interpolation of water surface elevations between the upstream and downstream cross sections, which can produce incorrect mapping for overtopped road crossings where the downstream tailwater level is significantly lower than the road crest. Figure 5 shows the modelled flood conditions at the 38 Avenue crossing in Stettler as an example. Because the tailwater level was too low, the interpolated water surface across the road embankment fell below the road crest. As a result, the map incorrectly shows no/partially overtopping at this road crossing, even though the hydraulic model indicated overtopping.

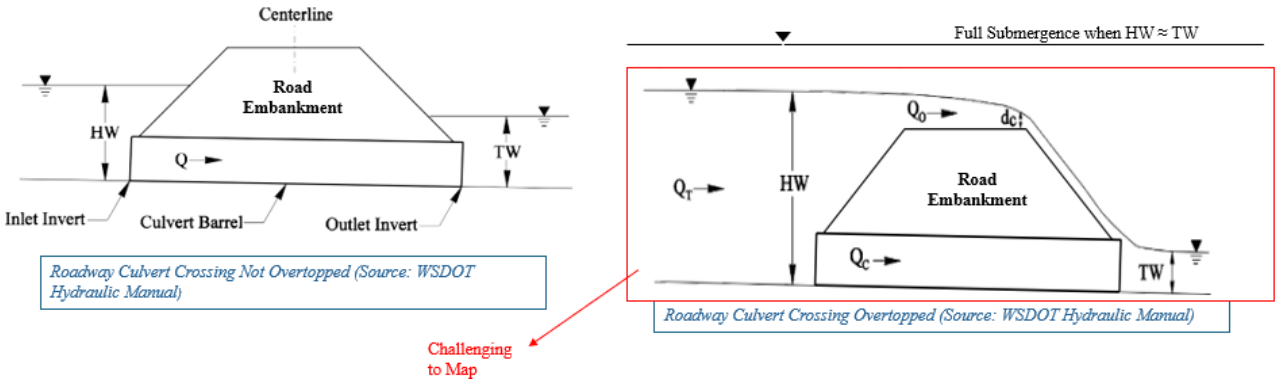

Figure 4: Submerged culvert hydraulics without and with road overtopping (Source: WSDOT, 2025)

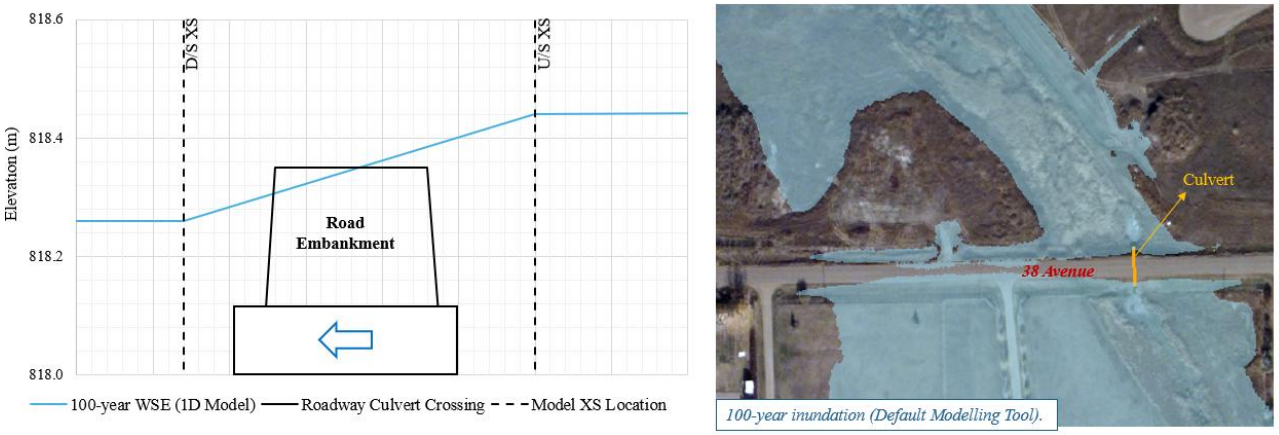

Figure 5: Roadway culvert overtopping mapping using standard modelling and mapping tools

3.3 Hydraulic Modelling and GIS Integration

The Stettler Flood Study used an integrated hydraulic modelling and GIS approach to accurately map roadway overtopping. Overtopping was identified in the model by weir flows, and at each identified location, a breakline was added at the downstream road edge with the upstream water level assigned (Figure 6). A modified water-surface TIN was created from cross sections and the breakline, then converted to elevation and depth raster to generate inundation polygons. This ensured the water surface remained high across the road crest for accurate overtopping representation.

3.4 Improved Inundation Mapping

The proposed approach produced an improved inundation map for the 38 Avenue crossing in Stettler, Alberta (Figure 6), providing more accurate delineation of inundation extents and road overtopping and greater efficiency than manual editing, particularly in areas with numerous culvert crossings. Using this method, flood depths computed on the downstream side of the roadway embankment (Figure 6) may be overestimated. However, this limitation has minimal effect on overall flood mapping, as this localized area does not typically influence hazard delineation, floodplain interpretation, or emergency planning decisions.

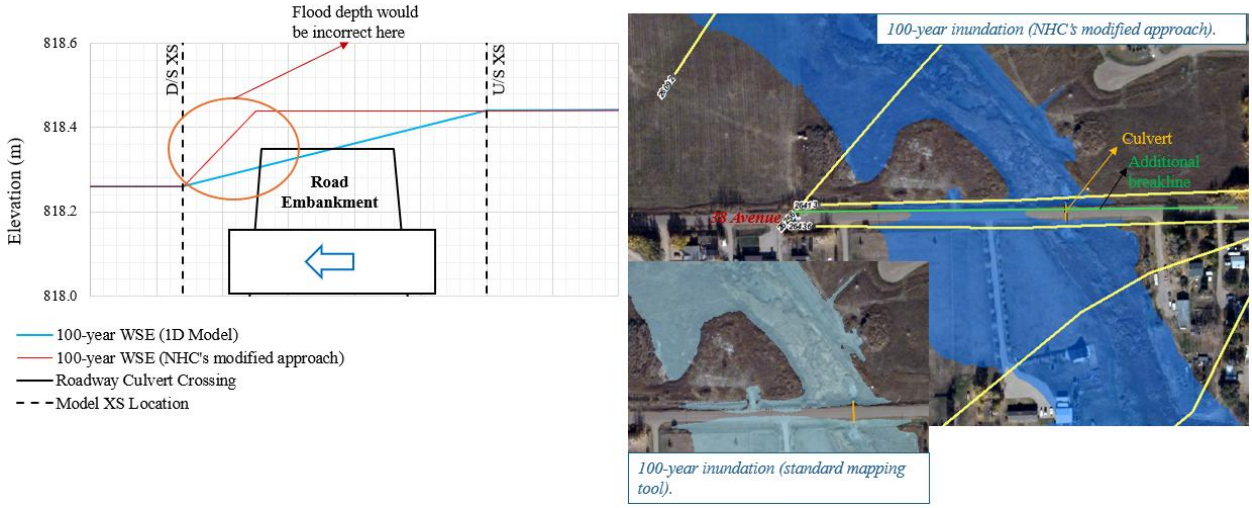

Figure 6: Improved flood mapping adopting the advanced integrated approach

4 CONCLUSION

This paper highlights two main challenges in flood mapping studies for small prairie streams, using the Stettler Flood Study as an example. First, it addresses the difficulty of developing flood hydrology in a flat prairie basin with limited data and significant basin and floodplain storage capacity. The results illustrate the importance of accounting for site-specific conditions, basin storage, and floodplain detention for more accurate flood frequency estimates and reliable inundation mapping. Second, it demonstrates the challenge of mapping roadway overtopping at culvert crossings with large differences between headwater and tailwater levels. A GIS processing approach was developed to resolve this issue, providing more accurate overtopping representation than the standard linear interpolation approach. Together, these hydrologic and mapping approaches improved floodplain mapping in the Stettler Flood Study.

REFERENCES

Alberta Environmental Protection (AEP) (1995). Flood Frequency Analyses: Stettler Floodplain Study. Surface Water Assessment Branch, Technical Services & Monitoring Division, Water Resources Services, Alberta Environmental Protection, Edmonton, AB, March 1995.

Alberta Transportation (AT) (2006). Development of Runoff Depth Map for Alberta. September 2006.

Chow V.T., Maidment D.R. and Mays L.W. “Applied Hydrology”. McGraw-Hill Book Company, New York, NY (1988) pp. 134.

Stantec (2004). Town of Stettler Redwillow Creek Flood Risk Mapping Study. Developed for Alberta Environment River Engineering and Water Monitoring, Edmonton, AB, February 2004.

Washington State Department of Transportation (WSDOT) (2025). Hydraulics Manual, M 23-03.11, Olympia, WA, April 2025, 312 pp 3-8 – 3-9.

ICFM 10
Adapting to Global Change:
Innovative Approaches to Flood Management
May 20-22, 2026 | Western University, London, Onta

Inclusion of Geomorphic Hazards in Floodplain Mapping and Land Use Regulation

Dale Muir[1], Ryan McQueen[1], and Vanessa McMaster[1]
Northwest Hydraulic Consultants, North Vancouver, BC, V7M 3G3, Canada [1]
E-mail: dmuir@nhcwater.com, rmcqueen@nhcwater.com, and vmcmaster@nhcwater.com

ABSTRACT

Floodplain maps for land use regulation are generally based on the hydraulic level and extent during a design flood event. Geomorphic channel changes during large and even moderate flood events can lead to equal or greater damages than seen from inundation alone. Geomorphic hazards, such as lateral channel migration, channel aggradation or degradation, channel widening, avulsion, sediment and debris loading, and debris damming with potential outburst floods, can result in erosion and undermining of dikes, infrastructure, and homes with complete loss of property and infrastructure.

We present how geomorphic hazards have been identified and incorporated into floodplain mapping and how this information has been used to inform regulators and public for land use regulation. An example of the approach applied during recent floodplain mapping projects in the province of British Columbia, Canada, is presented.

KEYWORDS: Floodplain mapping, geomorphic hazards, land use regulation

1 INTRODUCTION

Flood level and extent derived from local hydrology and hydraulics are the foundational information presented in the majority of floodplain maps for land use regulation. This information illustrates the inundation hazard but often neglects the geomorphic hazard. In dynamic riverine environments, geomorphic channel processes can have a sizable influence on the hydrology and hydraulics as well as impose additional hazards to property and infrastructure along the floodplain.

This paper presents an approach to evaluate geomorphic influence on flood hazards, illustrate the geomorphic information, and apply the information to land use regulation. Floodplain mapping conducted within British Columbia, Canada is used to demonstrate the methodology.

1.1 Background and Motivation

Geomorphic hazard analysis and understanding of the local river channel forms and processes are essential for floodplain mapping within a dynamic riverine environment to (1) ensure a comprehensive representation of present hydrotechnical hazards are presented in the floodplain maps and (2) to extend the useful life of the floodplain maps through evaluation and incorporation of the range of reasonably plausible future conditions. Upstream geomorphic events can affect floodplain hazards through rapidly and sizably altering the supply of sediment and debris (*e.g., sediment laden floods, debris floods, debris flows*) or the supply of streamflow (*e.g., landslide generated channel blockage and subsequent outburst*). Within a study reach flood hazards can be exacerbated by geomorphic processes such as deposition, aggradation, degradation, channel migration, erosion, scour, and avulsion. These can alter flood profiles, flood extents, or undermine, fail, or completely remove dikes, embankments, roads, rails, homes or other near-channel infrastructure. Flood profiles can also be influenced by downstream geomorphic processes

that influence channel gradient, such as channel obstructions, alignment changes, or aggradation and channel encroachment. These geomorphic processes can occur during flood events less extreme than the typical design flood event yet can impose a greater hazard and loss than flood inundation on its own.

Due to the level of risk potentially imposed, geomorphic hazards are increasingly being considered during community and land use planning and subsequently incorporated into floodplain mapping. For example, geomorphic hazards are included in the soon to be released British Columbia floodplain mapping guidelines, are to be included in future publications under the Natural Resources Canada Federal Flood Mapping Guideline Series (NRCan and ECCC, 2023), and are already considered in the states of Colorado (Blazewicz et al., 2020), Washington (Rapp and Abbe, 2003), and Vermont (VT ANR, 2017).

1.2 Definitions

Geomorphology is the study of landforms and the processes that influence their development and evolution. Within this document, geomorphology is for the most part referring to fluvial geomorphology; that is, those landforms and processes related to rivers and streams.
Land use regulation refers to governmental laws and policies that control how land can be developed.
Development refers to issuance of building permits or approval of subdivision (dividing property into multiple lots).

2 ASSESSMENT METHODS

Assessment of geomorphic hazards often follows the approach of (1) delineate and characterize geomorphic study reaches; (2) identify and assess fluvial geomorphic hazards; and (3) characterize hydrologic and hydraulic implications. A generalized approach to these three steps is presented in the following paragraphs. Detailed refinement of the approach can become challenging when applied over a range of landforms, and risks producing guidance to land use regulation that lacks consistency and transparency. Focus is therefore directed towards a consistent meaning of hazard classifications instead of a rigid definition of the classification or approach.

2.1 Delineate and Characterize Geomorphic Study Reaches

This step involves segmenting the river into discrete reaches of similar form and process to establish a suitable scale for analysis. The delineation should sufficiently extend upstream and downstream to capture potential influences on flood hazard within the study reach. Characterization of the reaches should consider valley setting, channel characteristics, source and characteristics of sediment, anthropogenic influences, as well as the local geology, hydrology, and hydraulics. This step is conducted through review of maps, historic and present air photographs, field observations, regional hydrology and watershed delineation, and preliminary hydraulic modelling results (*e.g., relative elevation model*).

2.2 Identify and Assess Fluvial Geomorphic Hazards

Identify and assess the processes that may influence flood hazards through the characterized reaches from upstream to downstream. This should consider past events, present day hazards, and influence of reasonably foreseeable future conditions (*e.g., climate change, development, logging, forest fires*). Within the broader study area (*including upstream and downstream of the flood study reach*), identify locations of existing or potential obstruction (*e.g., landslide and debris flow paths, channel constrictions, steep bends, shallows, debris jams, and channel crossings)* and sources of sediment and debris that can contribute to obstructions. Evaluate their influence on hydrology (*e.g., outburst flood or bulking of flow*), flood profiles, or geomorphic hazards (*e.g., deposition, redirection of flow, or channel degradation*).

Delineate the hazard corridors for each geomorphic reach within the flood study. This often includes consideration of multiple geomorphic process corridors or hazard zones. Such as, (1) high hazard zone, where channel migration (*e.g., channel widening, erosion, or avulsion*) is reasonably plausible to

reach during a single event or over 10 to 30 years if unmitigated; (2) moderate hazard zones, where most unmitigated channel migration is expected to remain over a time horizon of roughly 100 years; and (3) low hazard zones, where topographic, geologic, or ecological evidence suggests the river occupied this area under present hydroclimate conditions but the river is not expected to reach even over 100 year time horizon (*often defined as the modern valley bottom*).

In addition to the geomorphic process corridors along the study water course, adjacent geomorphic hazards may be identified and incorporated in the mapping. This can include steep banks along the river margins that extend above the mapped floodplain or geomorphic process corridors. These locations may warrant delineation if channel scour, erosion, or migration could undermine and destabilize these banks, particularly if the banks support developable land. Instead of assessing the geotechnical stability of these slopes, a geotechnical flag or warning may be used.

Alluvial fans adjacent to or intersecting the river floodplain are often delineated and where possible classified as active, non-active, or unclassified. Within steep mountain valley terrain, alluvial fans have historically been preferentially selected for development, as they often provide gently sloping ground above the surrounding floodplain. However, fans may be at risk of rapid increases in flow; deep overland flow of water, sediment, and debris; or sudden changes in flow paths. Due to this particularly extreme hazard and relatively small effort to delineate, it is often appropriate to delineate the adjacent fans.

2.3 Characterize Hydrologic and Hydraulic Implications

Hazards located upstream, downstream, or within the study reach that have the potential to influence the hydrology or hydraulics of the flood are communicated with the hydrologic and hydraulic modelling team to incorporate in model runs for the design or sensitivity simulations used to establish the hydraulic floodplain mapping extents and levels. This could include changes to flow, such as from an outburst obstruction, channel and crossing obstructions, or alternative channel geometries.

3 MAPPING OF GEOMORPHIC HAZARDS

Information from the geomorphic assessment can be used as supporting information for the development of the floodplain maps, presented as a separate set of geomorphic hazard maps, or presented within a geomorphic atlas. These three approaches are presented below followed by examples.

3.1 Floodplain Maps

Potential geomorphic events and hazards can be used as additional information to establish the typical floodplain map flood construction levels (FCL), flood extents, and setbacks. For example, flow, flow path, or channel geometry influenced by reasonably expected geomorphic conditions can be used to establish the conditions simulated to prepare the floodplain map or used in the sensitivity analysis where uncertainty is accounted for, such as with a safety factor, freeboard, or through use of probabilistic outputs.

Within the British Columbia context, a freeboard is applied to the calculated design flood profile prior to establishing the FCL and floodplain extents. The freeboard is used to account for local water level variations (*e.g., surge, superelevation, standing waves*) as well as uncertainty in the data and analysis. The freeboard may therefore take account for the uncertainty in channel geometry, streamflow, sediment supply, or obstructions within a geomorphically active environment; provided adequate study has been conducted to establish a suitable freeboard, appropriate setbacks, and understanding of residual risk. To maintain consistency the probability of incorporated geomorphic hazards should be of similar probability to the design flood event, i.e., the 200-year flood event in British Columbia. Events that are substantially less likely to occur, would typically not be included in the development of the floodplain map to guide land use regulation, at least not without careful consideration and communication of the risk and cost of using a sizably more extreme event.

3.2 Geomorphic Hazard Maps

Additional geomorphic context pertaining to the characterization, identification, and assessment of the hazards can be explicitly presented within a set of geomorphic hazard maps. These maps often present the various hazard corridors and potential sources of hazards. For example, geomorphic hazard maps can illustrate historic channel alignments, meander migration zones, avulsion routes, and other specifically identified geomorphic hazards. These maps illustrate the geomorphic hazard elements resulting from the analysis that have supported the development of the floodplain map. These maps are analogous to flood velocity and depth maps that occasionally accompany standard floodplain maps.

To maintain transparency and consistency the meaning of the hazard zones should be clear and appropriate to guide land use regulation. Continuing the with the British Columbia example;
High Hazard Zone supports the delineation of the no-build setback, indicating where most (>50%) of the unmitigated channel migration is expected in the near future (e.g. within 30 years). This hazard zone should also consider, and ideally include, the corridor required to allow for expected geomorphic processes without transferring risk to other properties.
Moderate Hazard Zone indicates areas where development may occur with the expectation that future mitigation may be required, that is areas outside the high hazard zone where most (>50%) of unmitigated channel migration is expected over the project lifetime (e.g., within 100 years).
Low Hazard Zone indicates areas where unmitigated channel migration may eventually occur but may still be suitable for development as it is outside of the high and moderate hazard zones.

3.3 Geomorphic Atlas

Further details can be provided in the form of a geomorphic atlas. Atlases provide the underlying data and analysis used to develop the geomorphic hazard maps. Atlases illustrate information such as historic air photos, delineated historic channel alignments (*i.e., banklines*), rates of channel migration, the delineated geomorphic reaches, avulsion pathways, alluvial fans, sediment sources, geologic anomalies, etc. Photographs are included to provide evidence of materials, grain size, sources of sediment and debris, active processes (*e.g., undermined banks, degradation, bar or island growth*), or past processes (*e.g., debris lobes, layered deposition, poorly sorted deposition*). Text is incorporated with the atlas to describe past events, present processes, potential future conditions (e.g., following development, forest harvesting, climate change, forest fire), and geomorphic interpretation for each geomorphic reach. Geomorphic atlases provide detailed information with a blend of text and figures well suited for storybook or other printed or digital formats. This level of detail is typically warranted in areas of high risk, complex geomorphic setting, or under substantial development pressure.

4 EXAMPLES

Following are some examples of floodplain maps prepared with consideration of geomorphic conditions. The first example (Figure 1) illustrates a typical floodplain map with the simulated design condition and freeboard applied to the resulting flood profile partially derived from the geomorphic analysis. The setback (yellow line) was added as the recommended no-build zone to limit loss and avoid notable transfer of flood risk. The setback was based on the greater of the floodway and the high geomorphic hazard corridor. For this example, the floodway was defined as the portion of floodplain that conveys the majority of flow during the design flood event, as determined using the hydraulic model. This figure also illustrates the delineated adjacent alluvial fans and geotechnical flags. The geotechnical flags were used to identify where the river potentially threatens high, steep adjacent banks.

The second example (Figure 2) illustrates a geomorphic hazard map that depicts high, medium, and low hazards zones as well as alluvial fans and geomorphic flags. The third example (**Error! Reference source not found.**) is a page from the geomorphic atlas, providing a sample of photographs, historic bankline delineation, and characterization of local sediments; elements often included in a

geomorphic atlas.

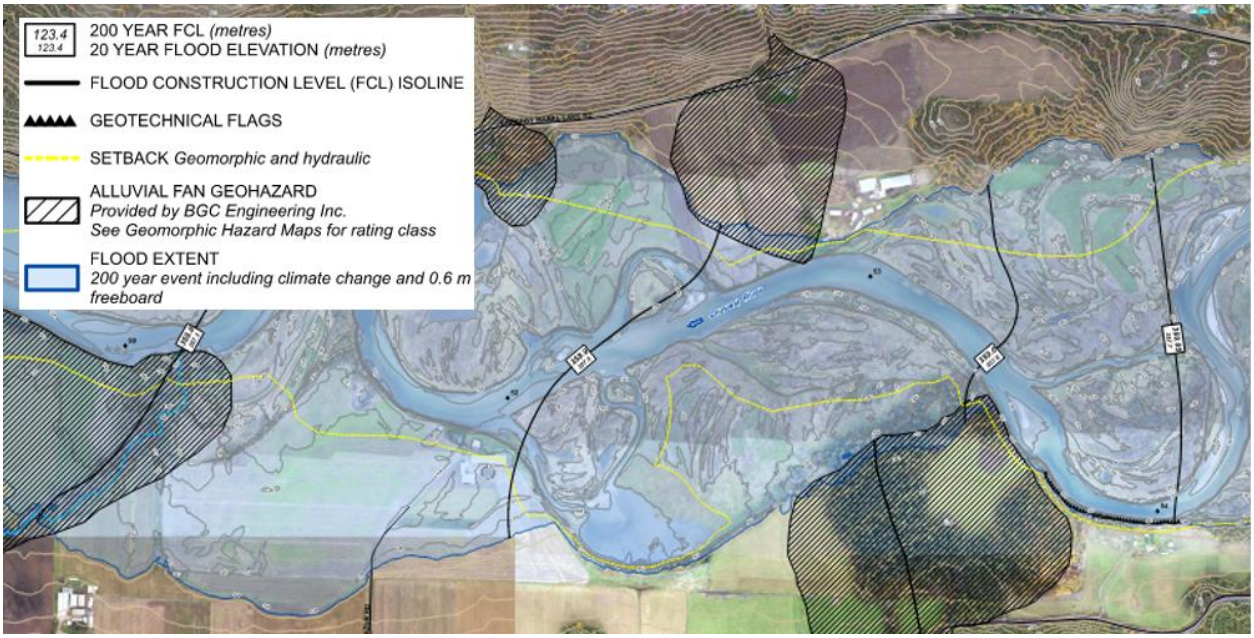

Figure 1: Sample floodplain map, Shuswap River, illustrating the flood extents (blue hatch), FCL (isolines with elevations in accompanying text box), no-build setback (yellow lines established from area of primary flow conveyance and high geomorphic hazard), and adjacent alluvial fans (diagonal hatching) (NHC, 2025)

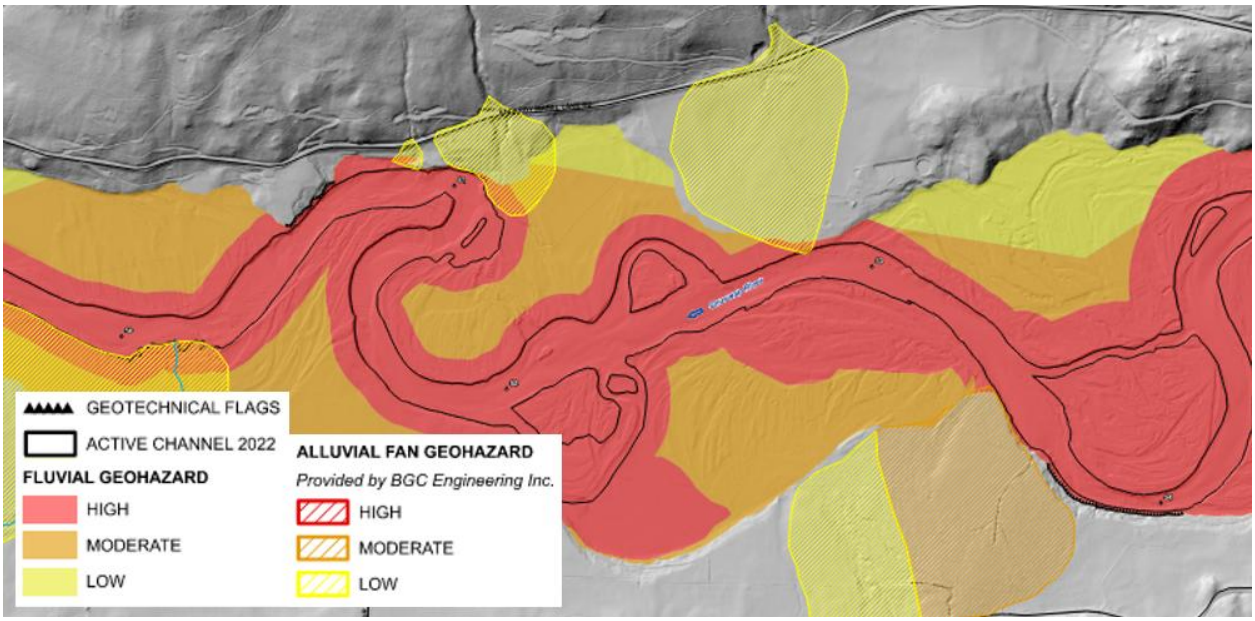

Figure 2: Sample geomorphic hazard map, Shuswap River, illustrating the classified geomorphic (colour filled) and alluvial (diagonal hatching) hazard zones for the corresponding floodplain map of Figure 1 with the high geomorphic hazard zone used in the development of the no-build setback of Figure 1, (NHC, 2025)

Fluvial Hazard Assessment - Lower Shuswap River
RKM 59.5 to 53.5

nhc

- From RKM 59.5 to 53.5, the Lower Shuswap River is laterally unconfined and forms an island braided or anabranching morphology. This area encompasses the Shuswap River Islands Provincial Park.
- The morphology of the river in this reach is strongly influenced by the interaction between flow and LWD. Accumulations of LWD are deposited through this reach, typically on bars and at the inlet to side channels, controlling the location and frequency of channel avulsions.
- The riverbed is composed of coarse to very coarse gravels within this reach, reflecting a reduction in grain size from that observed upstream.

▲ An accumulation of LWD at the inlet to a side channel (RKM 59.2).

▲ View of the island braided channel morphology at RKM 58.8.

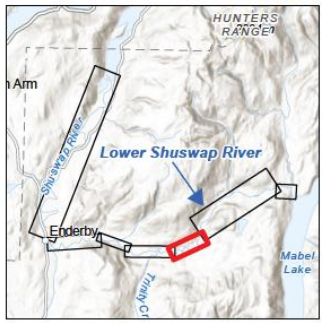

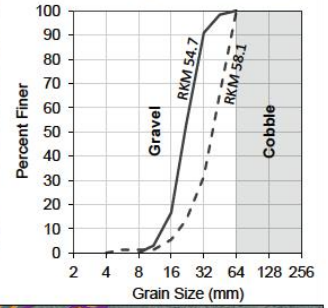

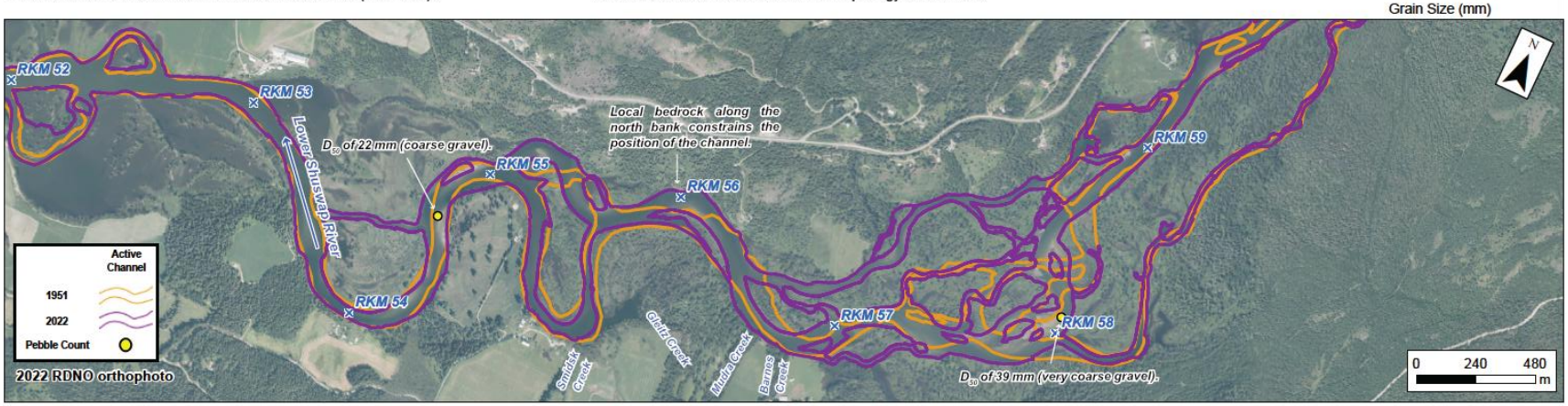

Figure 3: Sample geomorphic atlas, Shuswap River, illustrating the presentation of the underlying data and analysis used to establish the geomorphic hazard zones (NHC, 2025)

5 APPLICATION TO LAND USE REGULATION

Within a strict definition of land use regulation, maps and associated information can be used to define areas of fluvial geomorphic hazard in which future development should be constrained, controlled or avoided. In the British Columbia context, development is locally regulated by designating floodplains, establishing minimum FCL and watercourse setbacks (*no build zones*) (*e.g., using flood bylaws*), regulating the type of land use and development (*e.g., zoning*), and requiring site-specific engineering studies prior to development (*e.g., development permit areas*).

Within this context the study of geomorphic hazards must provide the delineated zones of hazard and suitable land use regulation to mitigate the hazard, such as zones of no-build, FCL, suitable type or density of industrial, commercial, institutional, or habitable development, or requirement for project specific engineering study. These zones of hazard and suitable development restrictions are typically illustrated as zoning maps, delineated development permit areas, and floodplain maps with FCL and setbacks.

Additional maps and information illustrating specific geomorphic and hydraulic hazards typically do not alter the land use regulation but can substantially improve the quality and consistency in conducting (*by developer*) and review (*by local government*) of project specific engineering studies to meet development requirements (*e.g., development permit area*) or secure an exemption (*e.g., from a flood bylaw*).

Adopting a broader definition of land use regulation, to incorporate community planning, can further benefit from additional maps and information on specific geomorphic and hydraulic hazards. Detailed information can support non-structural flood mitigation (*e.g., education, emergency planning, long-term retreat and relocations, sediment maintenance removal or nourishment*), structural flood mitigation (*e.g., justification for dikes, revetments, grade controls, sediment and debris basin*), establishment of environmental corridors (*e.g., riparian setback for present and projected future conditions*), and locating engineering works (*e.g., road and utility alignments*).

6 CONCLUSION

Geomorphic hazards can substantially alter or exacerbate flood hazards beyond that defined solely using hydrology and hydraulics. When mapping flood hazards along a dynamic river system the geomorphic setting and hazards must be considered in order to account for the range of present and future hazards. This paper presents a generalized approach to evaluate, assess, and map the geomorphic hazards in support of developing maps that are more inclusive and have a longer applicable life, and subsequently of greater value to support land use regulation.

7 ACKNOWLEDGEMENTS

We respectfully acknowledge that the Shuswap Region Floodplain Mapping project used here as an example, lie within the traditional territories of the Secwepemcúl'ecw (Secwépemc), Ĩyãħé Nakón mąkóce (Stoney), Syilx (Okanagan), Ktunaxa ʔamakʔis, snʕickstx tmxʷúlaʔxʷ (Sinixt), and the Confederated Tribes of the Colville Reservation. Northwest Hydraulic Consultants Ltd. (NHC) would like to thank Fraser Basin Council (FBC) for initiating and supporting the Shuswap Region Floodplain study as well as the British Columbia Ministry of Water, Land and Resource Stewardship (WLRS), Environment and Climate Change Canada (ECCC), and Natural Resources Canada (NRCan) for providing support during the Shuswap project.

REFERENCES

Blazewicz, M., Jagt, K., and Sholtes, J. (2020). *Colorado Fluvial Hazard Zone Delineation Protocol v1.0*. Department of Natural Resources.

NHC (2025). *Shuswap Region Floodplain Maps - Region 5: Lower Shuswap River*. Final Report. Prepared for Fraser Basin Council by Northwest Hydraulic Consultants Ltd., North Vancouver, BC.

NRCan, and ECCC (2023). *Federal Hydrologic and Hydraulic Procedures for Flood Hazard Delineation, Version 2.0* (General Information Product 113e). Government of Canada. 169 pp.

Rapp, C., and Abbe, T. B. (2003). *A Framework for Delineating Channel Migration Zones* (#03-06-027). Ecology Publication. Washington State Department of Transportation and Washington State Department of Ecology.

VT ANR (2017). *Flood Hazard Area and River Corridor Protection Procedure*. Prepared by Vermont Agency of Natural Resources, Department of Environmental Conservation. 40 pp.

Next generation watershed and subwatershed planning to inform flood mitigation in the context of urbanization and climate change

Wilfred Ho, Melanie Randolph, Elizabeth Speller, Namrata Shrestha
Toronto and Region Conservation Authority, 5 Shoreham Drive, Toronto, ON, M3N 1S4, Canada
E-mail: Namrata.shrestha@trca.ca

ABSTRACT

Next-generation watershed and subwatershed planning in the Greater Toronto Area increasingly integrates comprehensive baseline data, historical environmental records, and advanced flood and predictive modelling. These approaches improve the integrated assessment of watershed-scale impacts and support the prioritization of mitigation measures, particularly for downstream communities most vulnerable to flooding.

This presentation outlines the techniques that leverage diversity of data sources including field monitoring networks, LiDAR, multi-spectral imagery, climate data, hydrologic modelling, and engagement with partners and the public to evaluate potential future management scenarios and their implications on flood risk management. The results help identify priority actions and areas that most effectively reduce off-site impacts to flood-prone areas and protect key eco-hydrological features and functions. These findings inform watershed and subwatershed scale policy and planning decisions and guide implementation of green and grey infrastructure enhancements aimed at strengthening community resilience to flooding and climate change.

Using examples from several watersheds within the jurisdiction of Toronto and Region Conservation Authority (TRCA) such as Carruthers Creek, Etobicoke Creek, and Humber River, this presentation will illustrate the importance of integrated watershed planning processes and partnerships to advance flood risk management. This will be done within the larger framework of building climate resilience, ecosystem enhancement, and effective engagement of the public, governments, and agencies on flood risk management.

KEYWORDS: Flood Management, Watershed planning, Collaborative, Modelling, Climate Resilience

1 INTRODUCTION

1.1 Watershed Context

A watershed is the land area that drains rainfall and snowmelt into a river system and its tributaries. Everything that happens within a watershed is interconnected through the movement of water above and below ground, meaning actions upstream directly influence conditions downstream.

Healthy watersheds deliver critical ecosystem services, including reducing flood and erosion risks, protecting water quality and supply, supporting biodiversity, and strengthening climate resilience. Because of their central role in community safety, environmental health, and economic stability, watersheds require coordinated, cross-sector collaboration to ensure their long-term sustainability and resilience including effective flood risk management.

Toronto and Region Conservation Authority (TRCA) watersheds encompass one of the most highly urbanized and fastest-growing regions in Canada, with substantial population and infrastructure growth projected over the coming decades. Managing this growth in a way that avoids, minimizes, and mitigates natural hazard risks - particularly flooding - while maximizing the benefits of nature-based solutions requires an integrated watershed approach.

Integrated Watershed Management (IWM) provides a systematic framework to accomplish this, especially in the face of climate change, as nature often provides the most effective and cost-efficient solutions for building resilience. Effective flood risk reduction and climate adaptation are closely linked to the protection and restoration of natural systems along with the human designed systems. Achieving these outcomes depends on a holistic understanding of the complex interactions among land use, hydrology, infrastructure, and ecosystems across the watershed (Figure 1).

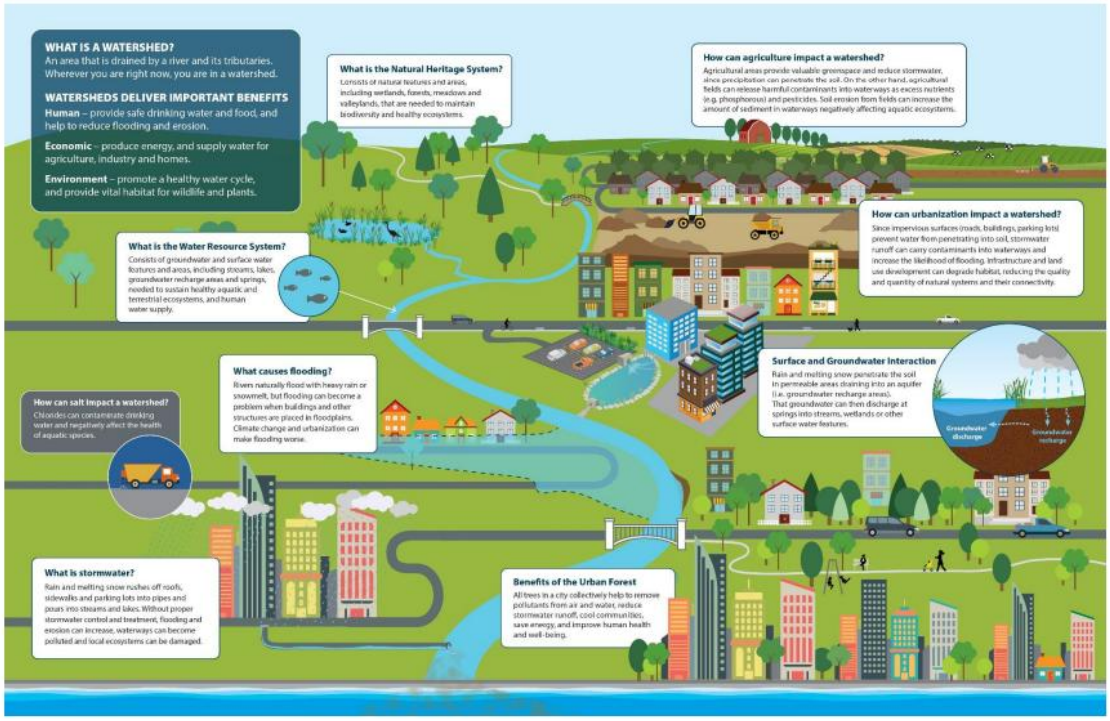

Figure 1: Integrated nature of watershed components, their inter-connections, and benefits

1.2 Watershed Planning

One of the main ways by which TRCA and partners comprehensively undertake IWM is by integrating the information from all our science-based programs and engagements through the development and periodic update of the watershed plans.

The watershed planning process provides a systematic and comprehensive framework to characterize current watershed conditions, assess future implications under potential future land use and climate conditions, and identify measures to protect, restore, and enhance the health of the watershed and build resiliency to land use and climate changes.

The development of watershed plans has been a collaborative effort between TRCA, local and regional municipalities, First Nations and Indigenous Communities, stakeholders, and public. Watershed plans do not make land use and infrastructure planning decisions. Rather, they are intended to help municipalities make informed decisions on where and how to grow in a way that minimizes and/or mitigates impacts to watershed health. Watershed plans also help inform other initiatives including ecosystem restoration and management, land management and acquisition, best practices for rural land uses, low impact development and green infrastructure implementation, and climate adaptation.

The watershed planning process at TRCA is initiated by scoping, building partnerships, and data gap filling. This is followed by watershed characterization to understand current conditions and trends in the watersheds, future management scenario analysis to help understand implications of potential future land use and climate conditions, and implementation planning to develop a management framework to identify priority measures and areas to strategically plan for mitigation and adaptation in the watershed (Figure 2). The final watershed plan provides a comprehensive blueprint for all participating organizations to endorse and implement identified actions.

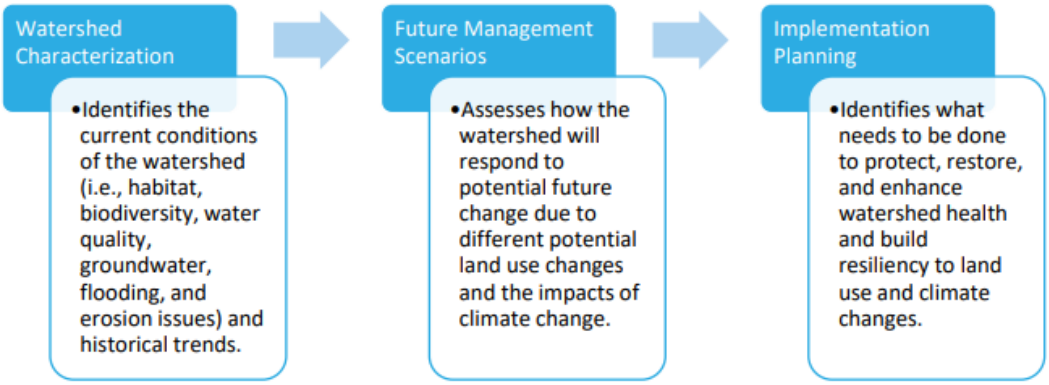

Figure 2: Overview of the watershed planning process

The watershed plans at TRCA focus on four broad thematic areas that are critical components for the health and safety of watersheds and their residents (Figure 3). These include Natural Hazards (i.e., flooding and erosion), Water Resources (i.e., surface water, groundwater, aquatic habitat, in-stream barriers), Water Quality (i.e., surface water quality), and Natural Heritage and Urban Forest (i.e., terrestrial habitat quantity, quality, and connectivity, tree canopy, and sensitive species). These four components are assessed within the broader context of land use and climate scenarios, and various policy and on-the-ground interventions such as restoration and other enhancements.

Figure 3: The four key components of the integrated watershed plans

1.3 Flood Risk Management and Key Concepts

At TRCA, a flood is defined as an overflow or inundation that comes from a river or other body of water and causes or threatens damage. Within a riverine system, floods are a natural process that occur as the result of relatively high flow of water overtopping the channel within a valley system. TRCA defines flood risk in its jurisdiction through extensive mapping of the flood plain.

1.3.1 Flood plain mapping

TRCA's flood plain maps identify the areas on normally dry land that may be covered by water during flood events. These maps can identify the specific risk of flooding to structures, people, and assets. The extent of the flood plain is determined through flood plain mapping studies. These are technical assessments prepared and approved for TRCA by qualified engineers, using standards and criteria established by the Ontario Ministry of Natural Resources.

Flood plain mapping studies use topographical information, surveys of infrastructure (e.g., bridges and culverts), land use and land cover information, weather, and stream flow data to create detailed hydraulic and hydrologic models of each watershed. A hydrology model simulates the effect of this amount of rainfall falling over each watershed, accounting for topography, soil type, land use, and other characteristics to determine how much water would be conveyed to rivers and streams. A hydraulic model then looks at where this water would go, and what areas would be inundated. The inundated area for the Regional storm is called the Regulatory Flood Plain.

Within TRCA's jurisdiction it is standard practice to complete comprehensive flood plain mapping updates on a 10-year cycle. This ensures that flood plain maps and associated hydrology and hydraulic modelling incorporate the latest land use and land cover information, and incorporate technological advancements in modelling software and techniques so that the resulting flood plain maps remain current and state of the art.

1.3.2 Flood Vulnerable Areas/Clusters

Through its flood plain mapping program, TRCA identified approximately 10,000 flood vulnerable roads and buildings in the Regulatory Flood Plain. These Flood Vulnerable Areas (FVAs) include Special Policy Areas, as well as historical flood damage centres. To help agencies allocate attention and resources, the FVAs have been grouped into 41 ranked Flood Vulnerable Clusters (FVCs), for each of which a single, comprehensive flood remediation approach may be viable. The FVCs represent urban areas that are at an elevated risk of flooding and are areas that have historically experienced riverine flooding under less

extreme events than the Regional storm and may continue to do so without remediation. This work has also enabled TRCA to develop site specific plans for emergency response and digital handbooks with information and resources for residents living in FVCs.

1.3.3 Peak flow estimates

To support TRCA's Regulatory flood Plain mapping program, a hydrology study is conducted for each watershed, which includes watershed-scale hydrologic modelling. These hydrologic models use the Regional storm, as well as design storms typically at the 2-, 5-, 10-, 25-, 50-, and 100-year return periods as precipitation inputs. These models generate flow hydrographs at various points along the rivers within the watershed, and the peaks from these hydrographs are input to hydraulic models of the river systems, resulting in flood depth, velocity, and water surface elevations for regulatory and design purposes.

2 FLOOD RISK ASSESSMENT IN WATERSHED PLANNING

One of the main responsibilities of TRCA is to protect life and property from natural hazards including riverine flooding and erosion risks. Riverine flood risk is well understood within the watersheds through flood plain mapping and the underlying hydrology models described in Section 1.3. These are mostly updated every decade at the regional scale and further refinements are completed, as needed, to align with watershed and subwatershed needs.

Riverine flooding occurs when water levels rise, and the streams overtop their banks. Urban flooding, on the other hand, is caused by limited capacity of stormwater infrastructure or drainage systems. Historically, urbanization has generally increased flood risk by altering the volume, intensity, and timing of runoff to streams. This is especially true for areas that were built without stormwater management features in place (i.e., developments pre-1980s).

The flood plain mapping leads to development of the Regulatory Flood Plain, which is the approved standard used in a particular watershed to define the limit of the flood hazard for regulatory purposes. Within TRCA's jurisdiction, the Regulatory Flood Plain is based on the greater of the Regional storm (i.e., Hurricane Hazel) or the 100-year return period applied to the watershed developed to an approved future planning horizon (e.g., 2051) without controls.

Hypothetically, flood risk as defined by the Regulatory Flood Plain should not significantly change between the baseline and current periods because it is based on future development conditions; however, data-driven techniques such as model recalibration, validation, and general refinement (e.g., higher resolution topographic information), as well as policy-driven processes such as Official Plan Amendments, may result in a current Regulatory Flood Plain that is somewhat different than the previous versions used to regulate land use in years past. Looking at TRCA's identified FVCs can provide a nuanced understanding of how urbanization impacts flood risk during the baseline and current conditions, as these areas have historically experienced, or are likely to experience, flooding during less intense events than the Regional storm.

2.1 Case Example: Humber River Watershed Plan

At 90,258 hectares in size, the Humber River watershed is the largest watershed in TRCA's jurisdiction. The upper portions of the watershed are largely rural and the middle and lower parts are mostly urbanized. The watershed consists of five subwatersheds including Main Humber, East Humber, West Humber, Lower Humber, and Black Creek (Figure 4).

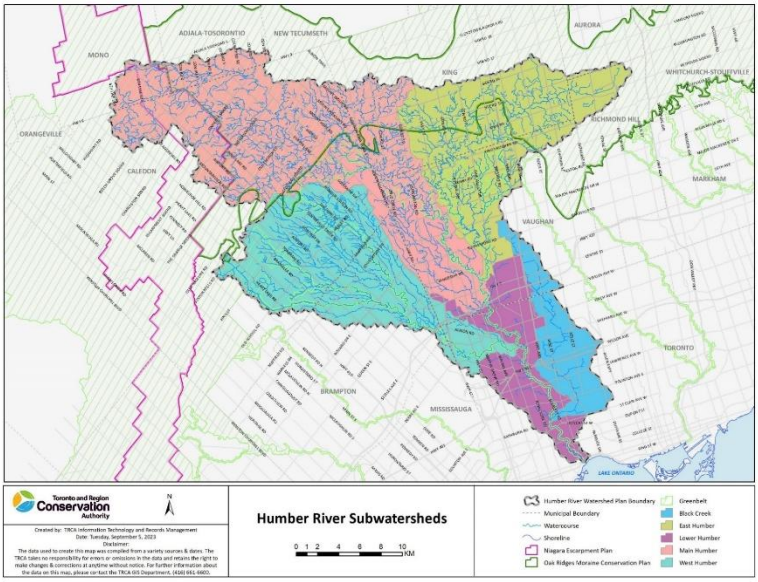

Figure 4: Humber River Watershed and Subwatersheds

2.1.1 Data and Methods

Land use changes between baseline and current periods alter watershed hydrologic response, which can influence flows to FVCs and associated flood risk. To quantify these impacts, baseline and current-conditions hydrologic models were developed using the 2015 Humber River Hydrology Update and 2017 addendum (Civica Infrastructure Inc.) as the base hydrologic model, built on the Visual OTTHYMO (VO) platform. This base model was rigorously calibrated and validated using streamflow gauges and flood frequency analysis to select appropriate return-period Atmospheric Environment Service (AES) design storms.

The model subdivides the watershed into 714 subcatchments (about 4–860 ha, avg. ~126 ha) using topography and sewershed data, and incorporates stormwater quantity control ponds. For the Humber River Watershed Plan (HRWP), the model was updated to represent 2002, 2012, and 2020 development conditions using land use mapping, historic orthophotography, and municipal/TRCA stormwater management (SWM) datasets.

Hydrologic response was parameterized using total imperviousness (TIMP) and effective imperviousness (XIMP), where subcatchments with ≥20% TIMP were treated as urban and modelled using the STANDHYD routine. TIMP and XIMP were calculated through ArcGIS preprocessing, intersecting land-use datasets with subcatchments, and further refined in Excel before being batch-assigned in VO.

Hydraulic features such as SWM ponds, dams, and reservoir-like structures were represented using the RouteReservoir command, which applies discharge–storage relationships. The model includes 79 SWM ponds, Claireville Dam, Lake Wilcox, and additional reservoir-type features—such as the Black Creek Dam, where two storage–discharge curves were used to reflect capacity changes between 2002 and 2020.

After model updates, simulated historical rainfall events were used to verify hydrologic parameters. The models were then run using 2-, 5-, 10-, 25-, 50-, and 100-year return-period AES design storms (6- or 12-hour). Because the baseline and current models share consistent structure, flows extracted at common nodes allow direct comparison of hydrologic changes over time. These flow results were then applied to assess effects on FVCs across the Humber River watershed to characterize the current conditions.

In addition to current conditions, three potential future land use scenarios reflecting the range of urbanization and enhancements in the watershed were assessed as part of the future management scenarios analysis. These scenarios were tested using a hydrology model for flood risk assessment.

- Scenario 1 looked at the full build out of the areas in the watershed that are yet to be developed, controlled peak flows using TRCA's SWM criteria, and minimal on-site retention targets and natural cover enhancement.
- Scenario 2 looked at urban expansion based on Official Plans (OPs), controlled peak flows using enhanced stormwater quantity control criteria, local on-site retention targets, and moderate natural cover enhancements.
- Scenario 3 also looked at OP urban expansion with the same enhanced quantity control as Scenario 2, but with broader on-site retention targets, and optimal natural cover enhancements.

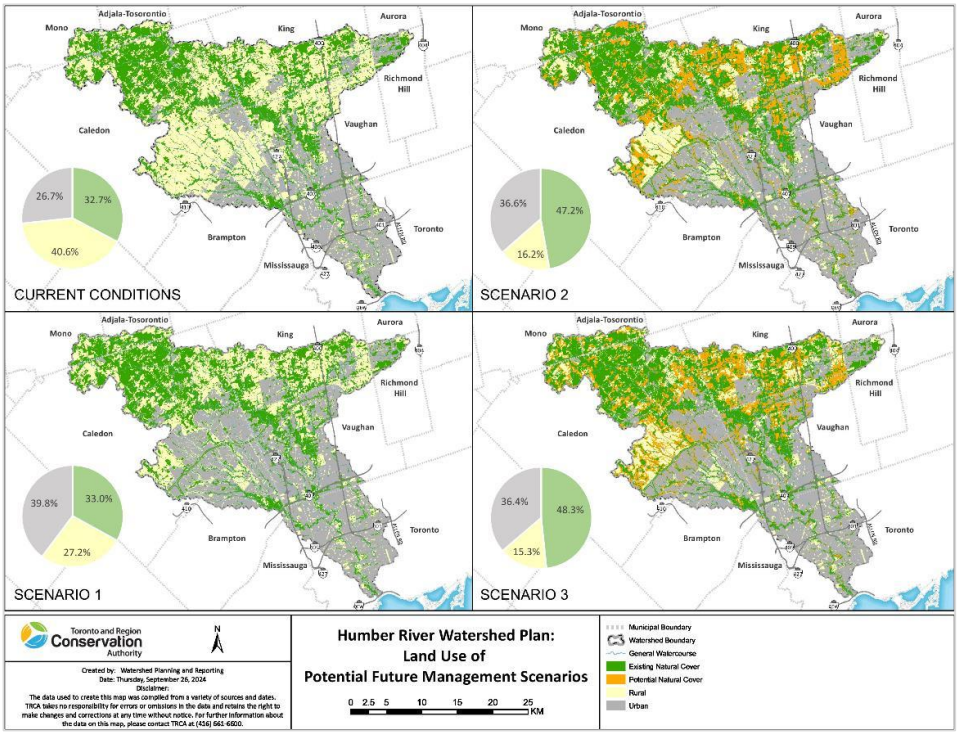

Figure 3: Current and three future land use scenarios for Humber River Watershed

Two illustrative climate scenarios were selected for future scenario analysis including the very high emissions (SSP5-8.5) and moderate emissions (SSP2-4.5) scenarios. The future climate data used in the scenario analysis was derived from downscaled global climate models (GCMs). Modelled historical and future climate data were retrieved through the Power Analytics and Visualization for Climate Science (PAVICS) portal for the two climate scenarios. PAVICS is part of a national suite of climate data portals that have been developed with support from the Canadian Centre for Climate Services. It offers future climate data at a resolution of approximately 10 km. Statistically downscaled daily data from 26 GCMs were used to derive almost all of the 52 climate variables for the HRWP scenario analysis, except the Humidex variables which were based on 19 GCMs.

As part of scenario analysis, hydrologic modelling was completed to examine how flood risk (i.e., peak flows) in the seven Humber FVCs and the broader watershed may change between current (2020 land use) conditions and the three potential future land use scenarios with varying degrees of watershed enhancements/management and without and with climate change. Climate change scenarios were tested by

upscaling standard design storms and applying them to the future management scenario models. Each future management scenario was run without and with climate change.

Peak flow results for each of the seven FVCs and design storms from the 2 to 100-year return period and the Regional storm were obtained. The inflow locations to the seven FVCs were chosen as observation points for changes in flood risk because these areas experience riverine flood conditions under less extreme events than the Regional storm or the 100-year storm, and are therefore sensitive to upstream development and management interventions. Figure 4 shows the locations of the inflows to the 7 FVCs within the Humber River watershed.

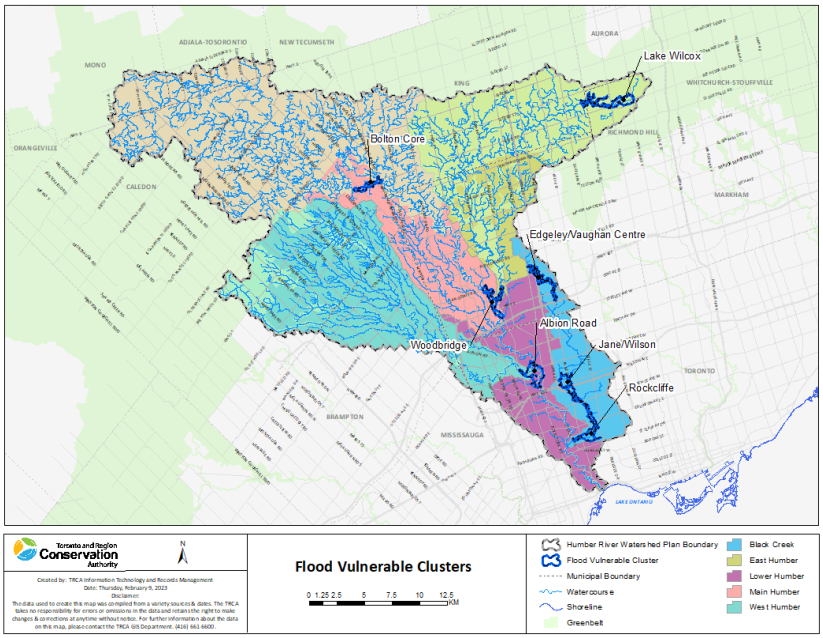

Figure 4: Humber River Watershed and Seven Flood Vulnerable Clusters

2.1.2 Results

Historically, flood risk has generally increased due to urbanization, which alters the volume, intensity, and timing of runoff to watercourses. This is especially true for areas that were built without SWM features in place, such as quantity control ponds.

Based on the results of a hydrologic modelling exercise, this technical report will examine how flood risk in the seven FVCs and the broader watershed may change between current (2020 land use) conditions and potential future urban expansion and climate change scenarios with varying degrees of management.

The key findings of the flood risk assessment indicated that where the standard or enhanced SWM criteria were able to maintain peak flows at the FVCs to current levels or lower, the on-site retention targets for each of the future management scenarios generally trimmed the event peaks further. Where standard SWM criteria were not sufficient to control peak flows to current levels or reduce them, both enhanced quantity control and greater on-site retention targets were needed to bring peak flows down to current levels at the FVCs. In areas where standard or enhanced SWM criteria are not widely distributed or not applied, downstream FVCs generally benefitted more from the Scenario 2 and 3 retention targets than the Scenario 1 targets. The natural cover enhancements generally did not have a significant impact on the volume of stormwater in urbanized areas. The climate change scenarios were tested by upscaling standard design storms and applying them to the future management models; the previously noted trends were magnified and consequently the 100-year peak flows were significantly higher than current levels at all FVCs regardless of the management strategy. An example of this is illustrated in Figure 5 below, which compares

the peak flows at FVCs under current and future climate (high emission) scenarios for the 100-year return period storm in land use Scenario 1 (minimal enhancement) and Scenario 3 (optimal enhancement).

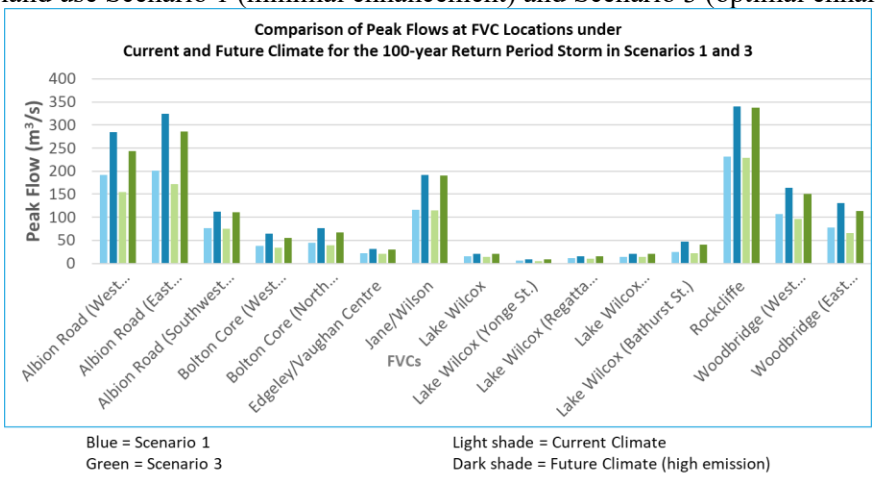

Figure 5: Humber River Watershed and Seven Flood Vulnerable Clusters

Regional storm peak flows from all three future management scenarios were near the current levels at the southwest tributary of the Albion Road FVC and the Black Creek FVCs likely because the contributing drainage areas were currently considered built out and were not expected to undergo significant future development. To an extent, this trend is also seen at the Oak Ridges and Bolton Core FVCs because the potential future land uses were mostly consistent with current conditions. Notably, the west tributary to the Bolton Core FVC saw significant decreases in peak flows for Scenarios 1 to 3. In contrast, inflows to the west tributary of the Albion Road FVC significantly increased for all three future management scenarios likely because of the expansive potential future development across the West Humber and Rainbow Creek subwatersheds. For similar reasons, but to a lesser extent, peak flow increases were also seen in the future management scenarios in the east tributary to the Woodbridge FVC, which was the entirety of the East Humber subwatershed.

The potential future development in the East Humber did not cut across the subwatershed to the extent that it did in the West Humber and Rainbow Creek. Rather, it was concentrated mostly in one tributary. In the case of development occurring across a subwatershed, the timing of peak flows from the various development areas coincided and compounded farther downstream. However, in the case of concentrated development, the timing of peak flows was staggered, with flows from relatively undeveloped areas tending to lag behind flows from the potential future development areas in reaching the main branch of the East Humber. At the confluence of the Woodbridge east and west tributaries, the flow increases from the East Humber seemed to be dampened by flows from the Upper Main Humber, which remained largely unchanged between current and future conditions. In addition, a lower increase in peak flows was seen on the downstream receiving end at the east tributary of the Albion Road FVC for Scenario 1 while Scenario 2 saw somewhat significant reductions and Scenario 3 was reasonably consistent with current levels.

For more information on the results refer to the TRCA's Humber Future Scenarios Analysis Report (2025).

3 CONCLUSION

The flood risk assessment in TRCA's watershed planning framework incorporated site level field information and integrated the hydrology and hydraulic modelling with watershed scale information on potential future land use change, climate change, various management interventions such as natural cover enhancements and implementation of low impact development and urban canopy enhancements to understand their potential implications on the peak flows at the FVCs in the watershed. This provides insights into other areas that may be affected in terms of flood risk across the watershed. The watershed

planning framework and data allowed for the decision makers to identify potential measures and priority catchments to enhance flood risk management in a proactive way for watershed health and community resilience.

ICFM 10
Adapting to Global Change:
Innovative Approaches to Flood Management and Resilience
May 20-22, 2026 | Western University, London, Ontario, Canada

Approach for Assessing Land-Cover Changes using Satellite Imagery and their Impact on Risk of Flooding

Badri Bhakta Shrestha[1,*], Mohamed Rasmy[1], Katsunori Tamakawa[2], Sauhardra Joshi[3] and Daisuke Kuribayashi[1]

International Centre for Water Hazard and Risk Management (ICHARM), Public Works Research Institute (PWRI), Tsukuba, 305-8516, Japan[1]

[*]Correspondence E-mail: shrestha@icharm.org

Global Environment Data Commons, The University of Tokyo, Tokyo, 153-8505, Japan[2]

Department of Hydrology and Meteorology, Ministry of Energy, Water Resources and Irrigation, Kathmandu, 44600, Nepal[3]

ABSTRACT

It is crucial to understand land-cover changes and their impacts on society because land-use and land-cover (LULC) changes have recently become a key component in flood risk management. Most previous studies mainly analyzed the impact of land-cover changes on surface runoff or river discharge, and limited research investigated their impact on flood risk, including flood extent and volume. This study thus aimed to analyze land-cover changes and their impact on flood risk and hydrological responses, including flood runoff, inundation, and volume, in the Bagmati River basin of Nepal. Land-cover maps for historical years (2014, 2019, and 2024) were generated using Landsat satellite imagery in the Google Earth Engine Platform, and land-cover maps for future years were projected using machine learning techniques. After preparing land-cover maps, flood simulations were conducted for flood events of different return periods using a diffusive-wave based distributed hydrologic-hydraulic model named the Rainfall Runoff Inundation (RRI) model with the land-cover maps for different years. Then, we analyzed the impact of LULC changes on flood runoff, flood inundation, flood inundation volume, and flood risk. The results show that the built-up area may increase by 73% in the future, while the cropland area may decrease by 28%. The flood inundation extent and the peak inundation volume for a 100-year flood may increase by 2.5% and 4.7% in the future. The inundated built-up area may increase by more than 79% under LULC conditions in 2049, while the flood-exposed area of cropland may decrease by 6.3%. The results of this study can be useful for planning and implementing effective flood risk reduction measures and for establishing land use planning and regulations.

KEYWORDS: land use/land cover, flood inundation, exposure, RRI model, Nepal flood

1 INTRODUCTION

Floods are one of the most common water-related disasters in the world. Flood risk has been increasing in many countries (Zhai et al., 2005), particularly developing ones, due to rapidly growing settlement areas, poorly planned development activities, continuous land-use and land-cover (LULC) changes, and ongoing climate change. Among these, LULC changes have recently been recognized as a major environmental issue, affecting hydrological characteristics and society. They are regarded as significantly altering the natural water cycle and the spatial distribution of surface runoff, thereby impacting flow discharge and, consequently, increasing flood risk. In addition, changes in the land system in flood-prone areas may expose them to even greater environmental risks. It is thus crucial to understand

land-cover changes and their impacts on hydrological responses and society to better manage flood risk in the future and establish effective land-use regulations.

Accurately understanding flood characteristics and flood risk levels while considering potential LULC changes provides useful information to effectively carry out future flood management and establish land use regulations. Moreover, urbanization and LULC changes may have significant impacts on hydrological responses in the watershed (e.g., river runoff and flood inundation) and on flood risk (Martínez-Retureta et al., 2020). LULC changes can be analyzed using satellite imagery (Shrestha, 2019a), and their impact on hydrological responses can be assessed by incorporating land-cover maps for different years into hydrological model simulations. Numerous studies have focused on the analysis of LULC impact on hydrological responses (Shrestha, 2019a; Martínez-Retureta et al., 2020; Wudineh, 2023; Banjara et al., 2024). However, most of them have mainly analyzed its impact on river runoff, and limited research has investigated its impact on flood inundation (Shrestha, 2019a). Understanding the impact of LULC changes while considering potential future land-use changes is crucial to implementing better land-use management practices and providing policy- and decision-makers with useful information to identify flood risk levels and plan and enforce appropriate land-use regulations.

This study presents a novel integration of machine learning–based future land-cover projections with hydrological flood modeling to assess the impacts of LULC changes on flood dynamics and risk. We analyzed LULC changes and their impacts on flood risk and hydrological responses, including flood runoff, inundation, and volume, in the Bagmati River basin of Nepal. The land-cover maps for 2014, 2019, and 2024 were generated from Landsat satellite imagery using the Google Earth Engine (GEE) Platform. The land-cover changes were analyzed using a Geographic Information System (GIS), and future land-cover maps were projected using machine learning techniques with a QGIS plugin called the Modules of Land Use Change Evaluation (MOLUSCE). After preparing land-cover maps, flood simulations were conducted for flood events of different return periods using the Rainfall-Runoff-Inundation (RRI) model with the land-cover maps generated for the past years and projected maps for the future years. Then, we investigated the impact of LULC changes on flood runoff, inundation, and volume. By overlaying the land-cover maps with delineated flood inundation maps in GIS, we also estimated the flood-exposed area for each land-cover class to assess their flood risk.

2 STUDY AREA

Figure 1 shows the location of the Bagmati River basin of Nepal and its topographical features. The watershed area within the study boundary is approximately 4723 km^2, including the Lal Bakaiya River basin. The figure also shows the location of the water level stations. The elevation of the basin ranges from 72.4 to 2843 m. The average annual precipitation in the basin is approximately 1805 mm, and more than 81% rainfall occurs in the monsoon season (June-September). The Bagmati River basin is important in Nepal for its cultural, religious and economic significance. However, this basin has recently been experiencing severe flooding, resulting in significant physical damage and agricultural crop losses. Therefore, it is crucial to understand LULC changes and their impacts on flooding and flood risk in the basin to manage future flood risk better.

3 DATA AND METHODOLOGY

The key terminologies in this study are defined as follows: (i) *hydrology* refers to the study of the occurrence, distribution, and movement of water within the Earth system, including processes such as precipitation, runoff, infiltration, and river discharge; (ii) *hazard* refers to the potential occurrence of flood inundation under different scenarios; (iii) *inundation* refers to the resulting flooding of normally dry land and is characterized by the spatial extent and depth of floodwater; and (iv) *risk* is defined as a function of hazard probability and exposure, where exposure is influenced by LULC dynamics. This study consisted of two components: (i) analysis of land-cover changes and projection of future land-cover

maps, and (ii) assessment of the impact of LULC changes on flood risk and hydrological responses, including flood runoff, inundation, and volume (Figure 2). The methodology and data used for this study are described in the following subsections.

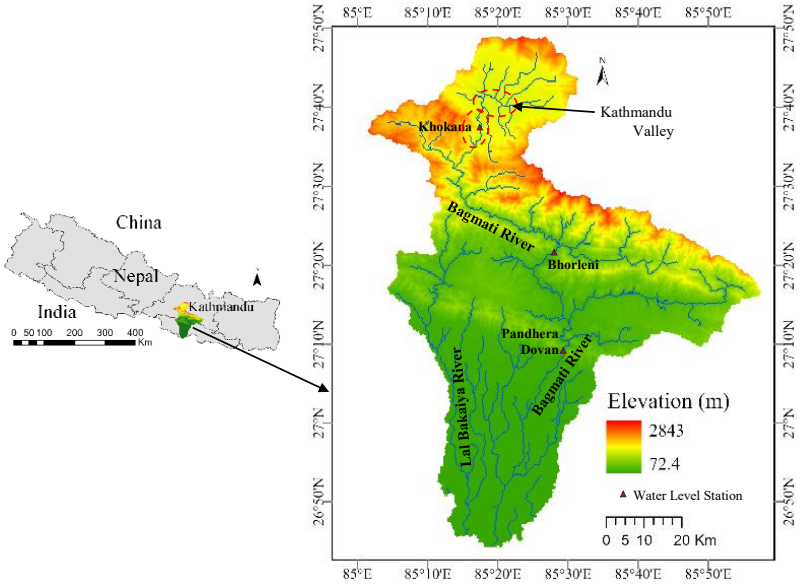

Figure 1: Location of the Bagmati River basin, Nepal

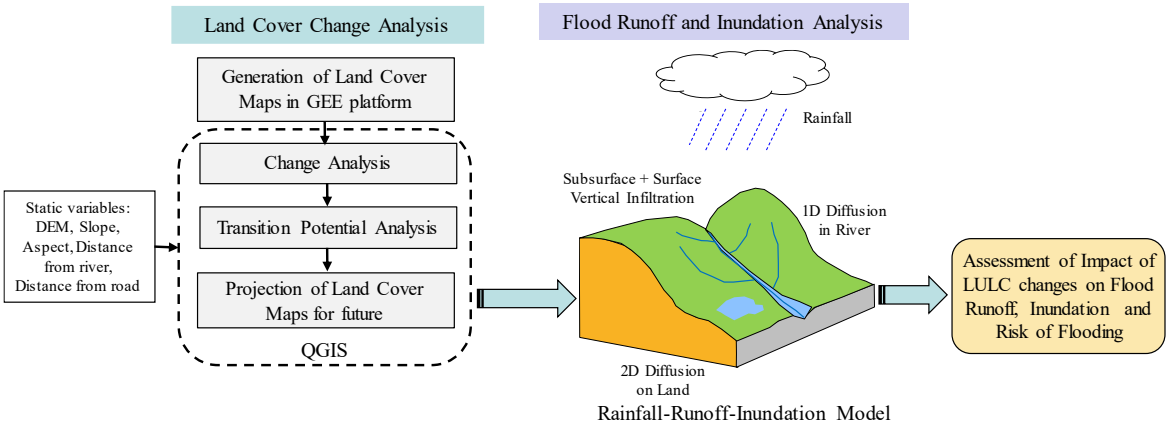

Figure 2: Methodology used in this study

3.1 Analysis of Land-Use and Land-Cover Changes

We generated land-cover maps for 2014, 2019, and 2024 using Landsat 8 surface reflectance images (USGS Landsat 8 Level 2, Collection 2, Tier 1) of 1 arc-second spatial resolution with the GEE Platform (Earth Resources Observation and Science Center, 2020). Images with less than 4% cloud cover were collected. To generate training and validation samples, true-color (RGB bands 432) and false-color (RGB bands 543) composite images were created using the multiband Landsat images. This study used a supervised classification method, which requires the development of training sites. The land-cover categories in the basin were classified into six classes: 1) Water bodies, 2) Forest, 3) Vegetation, 4) Bare land, 5) Cropland, and 6) Built-up areas. Training and validation samples for each land-cover class in 2014, 2019, and 2024 were created throughout the entire image based on composite and Google Earth images. Total number of selected training samples for land cover class for 2014, 2019, and 2024 was about 800, 812, and 885, respectively, while the total selected validation samples were 180 for 2014, 184 for 2019, and 215 for 2024. The random forest classifier available in the GEE platform was used to

generate a land-cover map from the training samples. Accuracy assessment was conducted using the validation samples for each generated map. A land-cover map for 2004 was also generated for calibrating hydrologic-hydraulic model simulations. The spatial resolution of the generated land-cover maps for the past years was upscaled from 1 arc-second to 9 arc-seconds, which is the same resolution as the hydrologic-hydraulic model simulations.

To analyze LULC changes and project future land-cover maps, we used a QGIS plugin called the MOLUSCE. The land cover maps for 2014 and 2019 were used to train the MOLUSCE model, and the land cover map for 2024 was used to validate the model. The cellular automata-artificial neural network model in the MOLUSCE was used for projecting future land-cover maps. The transition matrix and change map of the land-cover maps between 2014 and 2019, as well as static variables, such as digital elevation model (DEM), slope, aspect, distance from the river, and distance from the major road, were used to train the model. The DEM data were downloaded from the HydroSHEDS (Lehner et al., 2008). The slope and aspect were calculated using DEM in GIS. The river network data were delineated by referring to Google Earth images in GIS. The road data were downloaded from the Humanitarian Data Exchange of UN-OCHA, which was developed by the Overture Maps Organization (Overture Maps Foundation, 2025). First, a land-cover map for 2024 was projected and validated with the generated land-cover map using the validation module in the MOLUSCE. The LULC projected model performance was in an acceptable range with 77% overall accuracy and 0.65 kappa values. Then, land-cover maps for future years, 2039 and 2049, were projected.

3.2 Analysis of the Impact of Land-Use and Land-Cover Changes on Flood Risk

Flood simulations were conducted using the RRI model, a diffusive-wave based distributed hydrologic-hydraulic model, with the land-cover maps generated for past years and projected maps for the future years. To simulate past flood events, observed rainfall from ground-gauge stations across the basin was used as input to the model. The values of the model parameters were defined considering land-cover classes to analyze the impact of LULC changes on flooding and hydrological responses in the study basin. The RRI model is a two-dimensional hydrologic-hydraulic model capable of simulating rainfall-runoff, infiltration process, and flood inundation simultaneously (Sayama et al., 2012). The model was set up for the basin with DEM data of 9 arc-seconds (approximately 270 m spatial resolution). The HydroSHEDS DEM of 3 arc-seconds was upscaled to 9 arc-seconds for smooth simulations of the RRI model. The model was calibrated and validated using past flood data by comparing calculated and observed discharges (calibration used 2004 flood data; validation used 2002, 2014, and 2019 flood data). The model was also validated by comparing calculated flood extent areas with satellite based flood observation. Then, flood simulations were conducted for a recent severe flood event in 2024 (11-year flood) and flood events of different return periods (50- and 100-year floods), using the land-cover map created for 2024 and the land-cover maps projected for 2039 and 2049. For designing the spatial and temporal rainfall for different return periods, flood frequency analysis was performed using basin average 2-day annual maximum rainfall data from 1976 to 2024, based on the Generalized Extreme Value (GEV) distribution. Rainfall for specific return periods (e.g., 50- and 100-year floods) was generated using the spatial and temporal pattern of the September 2024 flood, a recent severe flood event in the study area. The return-period rainfall was estimated by multiplying the ground-gauge rainfall data of the September 2024 flood event by a conversion factor, calculated as the ratio of the return-period rainfall from the frequency curve to the 2-day annual maximum rainfall of the 2024 flood. The flood simulations for each return period were conducted using the rainfall estimated for the corresponding return period.

The impacts of LULC changes on flood runoff, inundation, and volume were analyzed under different LULC scenarios. By overlaying the land-cover maps with delineated flood inundation maps in GIS, the flood-exposed area for each land-cover class was estimated, and the impact of land-cover changes on flood risk was assessed. The calculated flood inundation extent was overlaid on the LULC map to identify areas where different LULC types were exposed to flooding. Subsequently, the area and percentage of each LULC category affected by floods were calculated to quantify flood exposure.

4 RESULTS AND DISCUSSION

4.1 Land-Use and Land-Cover Changes

Figure 3 shows the land-cover maps generated for 2014, 2019, and 2024. Table 1 shows the calculated area of each land-cover class and the changes in area between 2014–2019, 2019–2024, and 2014–2024. The results indicated that the cropland area rapidly decreased, while the built-up area rapidly expanded during the study periods. The built-up area rapidly expanded in the Kathmandu valley, which is located in the upper part of the basin. The cropland area decreased from 1758 km^2 in 2014 to 1731 km^2 in 2019 and to 1560 km^2 in 2024, while the built-up area increased from 104 km^2 in 2014 to 139.7 km^2 in 2019 and to 212 km^2 in 2024. The percentage of the cropland area decreased by 11% from 2014 to 2024, while the percentage of the built-up area increased by 105% from 2014 to 2024. The forest area decreased from 2726 km^2 to 2692 km^2 from 2014 to 2019. However, it increased from 2692 km^2 to 2779 km^2 from 2019 to 2024, because of recent reforestation and conservation efforts in the basin.

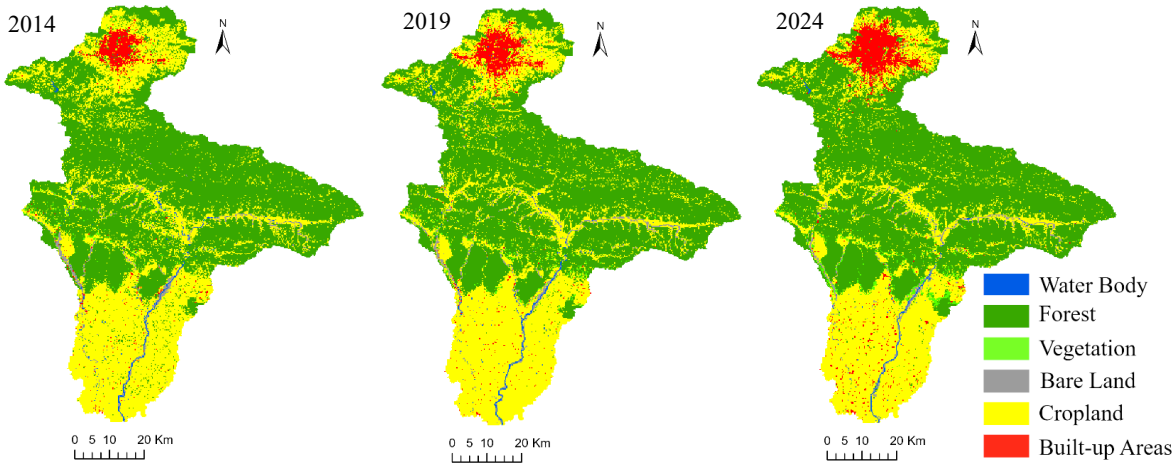

Figure 3: Land-cover maps created for 2014, 2019, and 2024

Figure 4 shows the land-cover maps projected for 2039 and 2049, and Table 2 shows the estimated area of each land-cover class and the estimated changes in area in the future years in comparison with the 2024 data. The cropland area may decrease by 23% in 2039 and by 28% in 2049, compared with the 2024 cropland area, while the built-up area may increase by 66% in 2039 and by 73% in 2049. The lost cropland area was mainly converted to the built-up area. The projected LULC maps for future were based on change trends in LULC for historical periods. The significant changes observed in projected LUCL are based on current change trends that may shift due to socio-economic, climatic, or land use regulation and policy factors.

Table 1 Area of land-cover classes and changes in area between 2014 and 2024

LULC type	Area (km^2)			Change in area (km^2)		
	2014	2019	2024	2014–2019	2019–2024	2014–2024
Water Bodies	34.6	29.5	21	−5.1	−8.5	−13.6
Forest	2726	2692	2779	−34	87	53
Vegetation	36.3	51	85.7	14.7	34.7	49.4
Bare Land	63.8	79.5	65	15.7	−14.5	1.2
Cropland	1758	1731	1560	−27	−171	−198
Built-up Areas	104	139.7	212	35.7	72.3	108

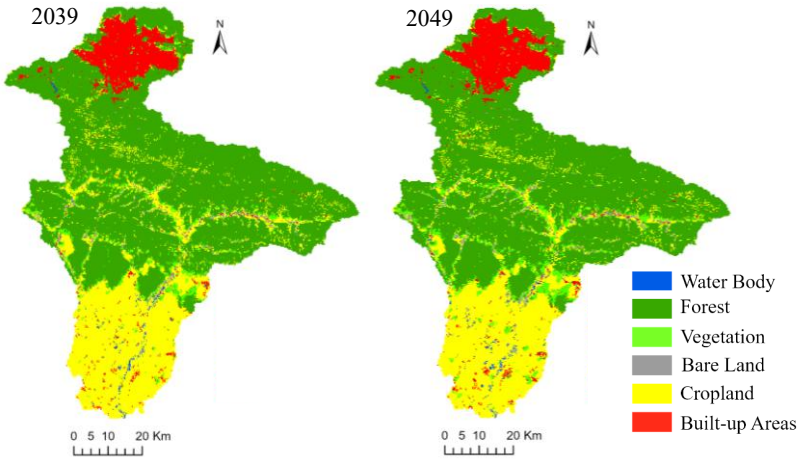

Figure 4: Land-cover maps projected for 2039 and 2049

Table 2 Area of land-cover classes in 2039 and 2049 and comparison with 2024

LULC type	Area (km^2)		Change in area from 2024 (km^2)	
	2039	2049	2024−2039	2024−2049
Water Bodies	19.4	20.9	−1.6	− 0.1
Forest	2896	2898	117	119
Vegetation	180	239	94.3	153
Bare Land	71.3	80.7	6.3	15.5
Cropland	1204	1116	−356	−444
Built-up Areas	352	368	140	156

4.2 Impact of Land-Cover Changes on Flood Risk

Figure 5 compares calculated and observed discharges at the Pandhera Dovan gauging station (calibration with 2004 flood data and validation with 2002, 2014, and 2019 flood data). The results show that the calculated discharges reasonably agree with the observed discharges, indicating high Nash-Sutcliffe Efficiency (NSE) and r-squared values. However, discrepancies between the calculated and observed peak discharges were identified for the 2014 and the second peak in 2019. These discrepancies may be attributed to several possible factors, such as the use of daily rainfall data as model input, limitations in spatial rainfall representation, the quality of topographical data, and potential uncertainties in the discharge-rating curve at high flows. For validation of flood inundation extent, we compared the calculated areas with satellite-based flood observations. Figure 6 shows a comparison between the calculated flood extent area for 2002 flood event and the observed flood inundation extent derived from Moderate Resolution Imaging Spectroradiometer (MODIS) satellite remote sensing (Shrestha, 2019b). The calculated flood inundation extents were very similar to the observed extents by MODIS satellite remote sensing.

Figure 7 compares the calculated discharges using LULC in 2024 and 2049 for the 2024, 50-year, and 100-year floods. The changes in river discharge due to LULC changes are significantly greater at the Khokana station compared with those at the Pandhera Dovan station. Figure 8 shows the time-series inundation volume over the basin, using LULC estimates in 2024 and 2049. The results indicated that the flood inundation volume might also increase in the future due to LULC changes. LULC changes, particularly due to urbanization, lead to increases in river discharge and inundation volume not only during peak flow periods but also during non-peak flow periods. Table 3 summarizes the calculated results of the inundation area and peak inundation volume using LULC estimates in 2024, 2039, and 2049

in the cases of the 2024, 50-year, and 100-year flood events. The rate of increase in flood inundation volume due to LULC changes is comparatively higher than that of flood inundation area, which indicates that most areas of the basin will be flooded to greater depths in the future. In the study area, particularly the Kathmandu valley, located in the upper part of the basin, the built-up area has been significantly expanding, thereby leading to increased river channel encroachment and a higher risk of flooding. The rapid urbanization in the Kathmandu valley may increase river runoff, resulting in greater inundation area and flood inundation volume. The expansion of settlement in flood-prone areas increases the exposure of people and assets to flood damage. Moreover, a significant reduction in cropland has further worsened the flooding situation. LULC changes due to factors such as urbanization, deforestation, and conversion of pervious land to impervious land significantly alter flooding characteristics, increasing the frequency and magnitude of flood events. As a result, the flood risk levels will also change.

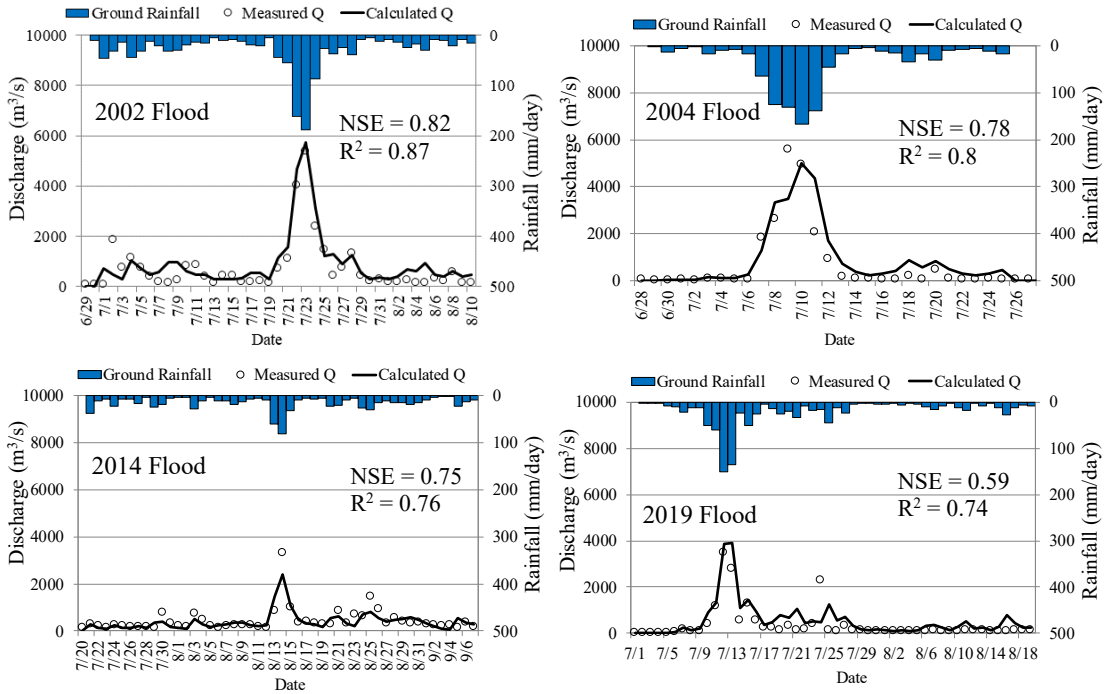

Figure 5: Comparison of calculated and observed discharges at the Pandhera Dovan station (see Fig. 1 for the location of the station

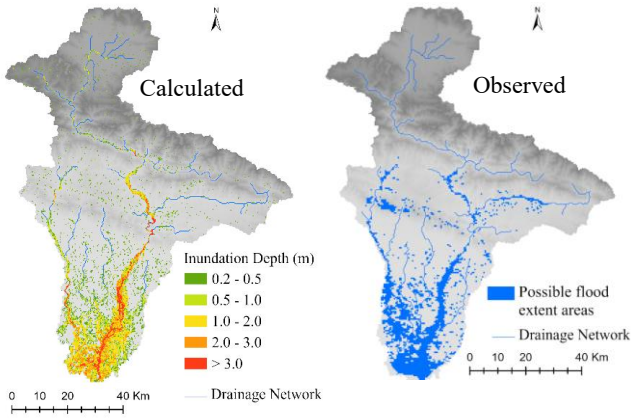

Figure 6: Calculated and satellite-based observed flood extent areas for 2002 flood (Data source for observation: Shrestha, 2019b)

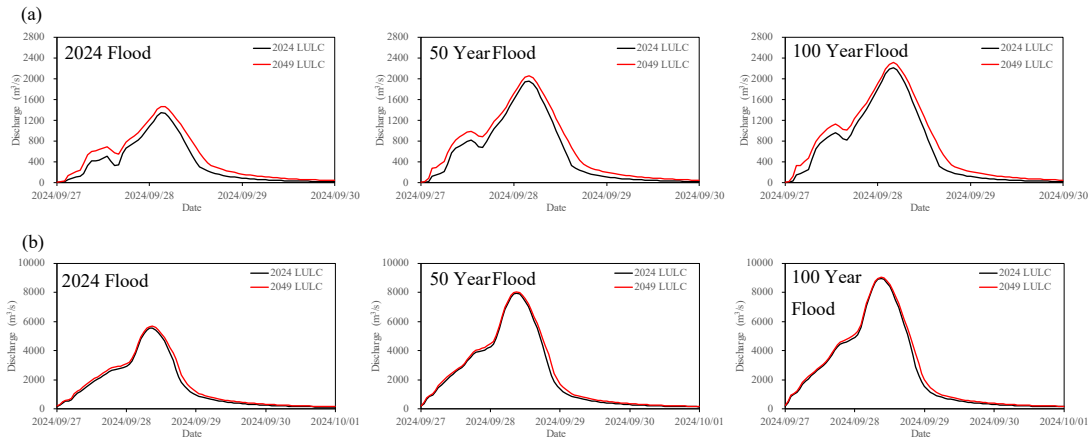

Figure 7: Calculated discharges at the (a) Khokana and (b) Pandhera Dovan stations, using the land-cover maps for 2024 and 2049 (see Figure 1 for the locations)

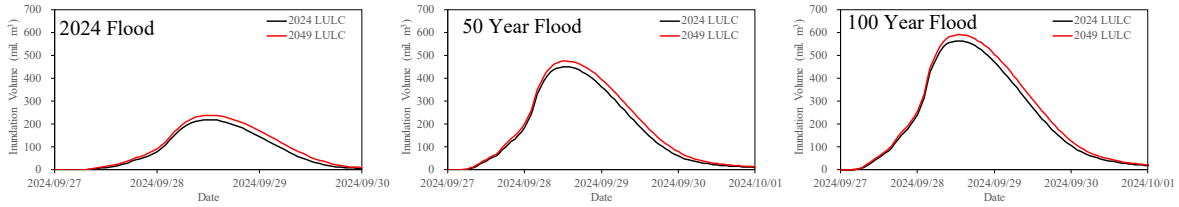

Figure 8: Calculated time-series inundation volumes in the basin, using the land-cover maps for 2024 and 2049

After flood simulations considering the effect of LULC changes, we also estimated inundated area for each land-cover class by overlaying the land-cover maps generated for past and future years with delineated flood inundation maps in GIS. Then, we analyzed the impact of land-cover changes on flood risk. Figure 9 shows the calculated inundated area of each land-cover class for a 100-year flood event under LULC conditions in 2024 and 2049. The results indicated that inundated built-up area may increase by more than 79% under LULC conditions in 2049, because of increases in both flood inundation and exposures in the flood-prone areas, while the flood exposure area of cropland may decrease in the future by 6.3%. This reduction is due to the conversion of cropland to settlement or other land use. The results also indicated that the inundated area of forest and vegetation may also increase in the future.

Table 3 Calculated inundation area and peak inundation volume under current and future land-use and land-cover conditions

LULC year	2024 Flood (11-Year Flood)				50-Year Flood				100-Year Flood			
	Inundation Area		Peak Inundation Volume		Inundation Area		Peak Inundation Volume		Inundation Area		Peak Inundation Volume	
	km^2	% increase with base case	mil. m^3	% increase with base case	km^2	% increase with base case	mil. m^3	% increase with base case	km^2	% increase with base case	mil. m^3	% increase with base case
Using 2024 LULC (base case)	289.5	-	219.1	-	537.4	-	450.2	-	634.9	-	564.8	-
Using 2039 LULC	305.4	5.5	236.3	7.9	551.4	2.6	472.3	4.9	648.8	2.2	588.2	4.2
Using 2049 LULC	307.3	6.2	238.2	8.7	554.5	3.2	474.8	5.5	650.6	2.5	591.2	4.7

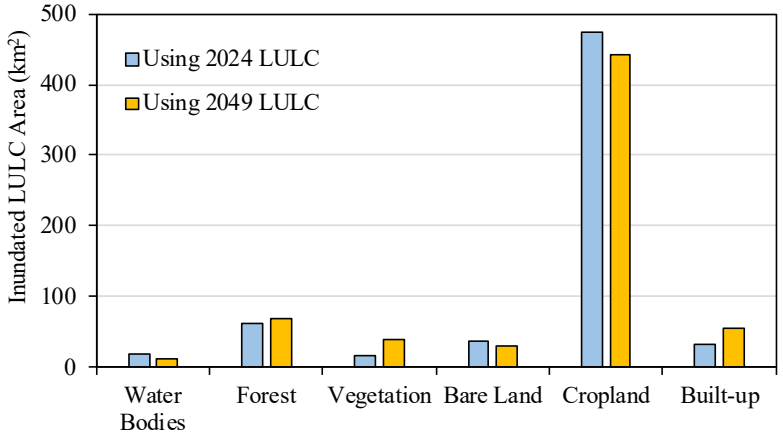

Figure 9: Calculated inundated area of each land-cover class for a 100-year flood under the 2024 and 2049 LULC conditions for flood simulation and exposure assessment

5 CONCLUSIONS

This study analyzed LULC changes in the Bagmati River basin of Nepal using satellite imagery. Land-cover maps for future years were projected using machine learning techniques. Then, the impacts of LULC changes on flooding and flood risk were assessed by coupling hydrologic-hydraulic modelling with exposure assessments under past and future land-cover conditions.

The results indicated that the built-up area, particularly in the Kathmandu valley, located in the upper part of the study basin, is rapidly expanding and may further expand in the future. The percentage of built-up area increased by 105% from 2014 to 2024, and may further increase by 66% in 2039 and by 73% in 2049, compared with the 2024 built-up area. The cropland area is in a declining trend and may continue to decline. The percentage of cropland area decreased by 11% from 2014 to 2024, and may further decrease by 23% in 2039 and by 28% in 2049, compared with the 2024 cropland area. Recently, the forest area in the basin has increased due to reforestation and conservation efforts.

LULC changes in the basin can worsen flooding and increase flood risk. The expansion of the built-up area and the reduction of the cropland area will increase river runoff, flood extent, and flood inundation volume. Changes in river discharge due to LULC changes are significantly greater at the Khokana station, located at the upstream part of the basin, compared with those at the Pandhera Dovan station, located at the middle stream of the basin. The flood inundation extent and the peak inundation volume for a 100-year flood may increase in the future by 2.5% and 4.7%, respectively, due to LULC changes, while they were estimated at 6.2% and 8.7% in the case of the flood scale similar to the recent 2024 event. The inundated built-up area may increase by more than 79% under LULC conditions in 2049, while the flood-exposed cropland area may decrease by 6.3% in the future.

The results indicated that flood runoff, flood extent, and flood inundation volume may increase in the future due to land-cover changes in the basin. The built-up area in the Kathmandu Valley is likely to be exposed to more severe flooding and become more vulnerable to floods due to rapid urbanization, river channel encroachment, and inadequate drainage systems. A large part of cropland is also expected to be exposed to flooding, especially in floodplains in the downstream areas of the basin. This study provides more detailed quantitative link between land-cover changes and hydrological response or risk, and the combined approach of projecting future LULC, analyzing flood impacts, and evaluating class-specific exposure advances current methodologies by linking landscape change directly to flood vulnerability and decision-making. The findings of this study provide useful information for establishing effective land use regulations and flood prevention and adaptation measures.

This study predicted future LULC based on historical LULC change trends. However, future studies should incorporate land-use policies, regulatory or restricted zones, and socio-economic factors to

improve the prediction of future LULC patterns. Furthermore, this study used globally available topographical data for flood simulations across the entire catchment of the study area. The reliability of the simulated flood inundation depth and extent could be improved by incorporating ground-based elevation data.

6 ACKNOWLEDGEMENTS

This work was supported by the Japan Society for the Promotion of Science (JSPS), KAKENHI Research Grant Number 24K07692.

REFERENCES

Banjara M., Bhusal A., Ghimire A.B. and Karla A. (2024). Impact of land use and land cover change on hydrological processes in urban watersheds: analysis and forecasting for flood risk management. Geosciences, 14, 40.

Earth Resources Observation and Science (EROS) Center. (2020). Landsat 8-9 Operational Land Imager / Thermal Infrared Sensor Level-2, Collection 2 [dataset]. U.S. Geological Survey.

Lehner B., Verdin K., Jarvis A. (2008). New global hydrography derived from spaceborne elevation data. Eos, Transactions, American Geophysical Union, 89(10): 93–94.

Martínez-Retureta R., Aguayo M., Stehr A., Sauvage S., Echeverría C. and Sánchez-Pérez J.-M. (2020). Effect of land use/cover change on the hydrological response of a southern center basin of Chile. Water, 12, 302.

Overture Maps Foundation (OMF). (2025). Overture Maps Open Data, https://data.humdata.org/dataset/osgeonepal_npl_roads [accessed on 4 March 2026]

Sayama T., Ozawa G., Kawakami T., Nabesaka S. and Fukami K. (2012). Rainfall-runoff-inundation analysis of the 2010 Pakistan flood 2010 in the Kabul River basin. Hydrol. Sc. J., 57, 298-312.

Shrestha B.B. (2019a). Approach for analysis of land-cover changes and their impact on flooding regime. Quaternary, 2, 27.

Shrestha B.B. (2019b). Assessment of flood hazard and agriculture damage under climate change in the Bagmati River basin of Nepal. Int. J. Environ., 8(2), 55-69.

Wudineh F.A. (2023). Land-use and land-cover change and its impact on flood hazard occurrence in Wabi Shebele River basin of Ethiopia. Hydrology Research, 54(6), 756.

Zhai G., Fukuzono T. and Ikeda S. (2005). Modeling flood damage: case of Tokai Flood 2000. J. Am. Water Resour. Assoc., 41(1), 77-92.

ICFM 10
Adapting to Global Change:
Innovative Approaches to Flood Management and Resilience
May 20-22, 2026 | Western University, London, Ontario, Canada

Enhancing Flood Vulnerability Assessment: Integrating Flow Velocity, Duration, and Debris Flow into a Component-Level Framework

Mohammad Shoraka, Ph.D., CEEM[1]; Raulina Wojtkiewicz, M.S.[1]; Karthik Ramanathan, Ph.D.[1]; Ahmed Abdelhady, Ph.D., CEEM[1]
Verisk Catastrophe & Risk Solutions, Boston, MA 02111, USA[1]
E-mail: mshoraka@verisk.com

ABSTRACT

Recent extreme flood events have highlighted the limitations of traditional flood vulnerability models that rely predominantly on inundation depth as the sole hazard intensity metric. Observations from events such as the July 2021 European floods and prolonged rainfall-induced flooding in recent years demonstrate that flow velocity, flood duration, and debris flow play a decisive role in driving structural damage and economic losses. This paper presents an enhanced flood vulnerability framework that explicitly integrates these additional hazard-intensity parameters into an engineering-based, component-level modeling approach. The framework introduces four flow-velocity classes, two flood-duration categories, and an explicit treatment of debris flow, resulting in twelve distinct hazard intensity combinations. Component-level damage functions are developed and then aggregated to create building mean damage ratios (MDRs) using floor-level cost distributions, allowing the model to explicitly capture hydrostatic and hydrodynamic forces, prolonged saturation effects, and debris-induced load amplification.

KEYWORDS: Flood vulnerability; component-level modeling; flow velocity; flood duration; debris flow; mean damage ratio; hydrodynamic forces; catastrophe modeling

1 INTRODUCTION

Flood catastrophe models have become essential tools for quantifying and managing flood risk across insurance, reinsurance, and public-sector applications. These models typically consist of four integrated modules: hazard, exposure, vulnerability, and financial modules. Each module contributes to the estimation of physical damage and economic loss. Traditional models generally categorize events into storm surge and precipitation-induced flooding, with the latter further divided into on-plain (fluvial) and off-plain (pluvial) flooding. Historically, for all types of flood events, flood vulnerability modules have relied almost exclusively on inundation depth as the primary determinant of damage. While depth remains the dominant factor in many flood scenarios, recent flood events have highlighted the limitations of depth-only representations for capturing the full range of flood-induced damage mechanisms.

Recent extreme events, such as the July 2021 Bernd flood in Germany and neighbouring European countries, were characterized by high flow velocities and substantial debris flow, leading to severe structural damage, bridge clogging, and rapid escalation of flood levels. Conversely, long-duration rainfall events, such as the April 2023 flooding in South Florida, demonstrated that prolonged exposure to relatively shallow water can also result in significant losses through prolonged wetting, material degradation, and delayed recovery. These contrasting event types underscore the need for vulnerability models that distinguish among fundamentally different flood processes rather than treating all floods as having equivalent depth–damage relationships.

In response to these challenges, Verisk has developed an enhanced flood vulnerability framework that extends hazard intensity parameters beyond inundation depth. Leveraging nearly two decades of probabilistic flood modeling experience across multiple regions, this framework integrates additional

hazard parameters such as flood velocity, flood duration, and debris flow into a unified, component-level vulnerability methodology. The objective is to enhance the physical realism of damage estimates while maintaining consistency with observed insured loss experience and established engineering principles.

2 METHODOLOGY

2.1 Overview of the Vulnerability Framework

The enhanced vulnerability framework is embedded within a standard catastrophe modeling architecture and focuses on the engineering-based estimation of physical damage. Damage is expressed in terms of the mean damage ratio (MDR), defined as the ratio of repair cost to replacement value for a given asset (see Figure 1). Separate damage functions are developed for buildings and contents, with additional functions to support loss-of-use and business-interruption estimation.

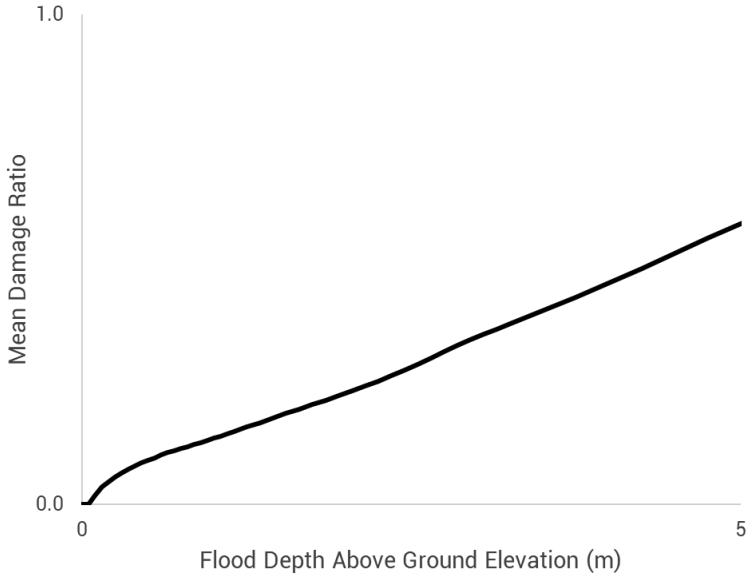

Figure 1: Sample flood damage function, showing the relationship between flood intensity and the mean damage ratio for a given building type

Unlike traditional depth-only approaches, the local flood intensity in this framework is defined by four parameters: inundation depth, flow velocity, flood duration, and the presence of debris flow. Damage functions are conditioned on combinations of these parameters and on a detailed representation of building characteristics.

2.2 Hazard Intensity Parameters

Flood Depth: The on-plain and off-plain depths are modeled for each event and location to account for the hydrostatic forces. On-floodplain flood depths are computed using a computational algorithm similar to the steady-state mode of HEC-RAS (HEC-RAS, 2002). To explicitly determine off-floodplain inundation depths, Verisk researchers developed a Graphics Processing Unit (GPU)-based 2D shallow-water wave model that uses 24-hour precipitation accumulation to compute inundation depths.

Flood Velocity: Flow and runoff velocity are explicitly modeled for each event and location to account for hydrodynamic forces exerted by moving water. As velocity increases, hydrodynamic forces acting on structural and non-structural components increase nonlinearly, increasing the potential for damage (FEMA, 2011). To represent this effect, flood velocity is classified into four discrete classes: low (0-0.5 m/s), normal (0.5-1.5 m/s), moderate (1.5-2.5 m/s), and high velocity (2.5 m/s or higher).

Flood Duration: Flood duration captures the length of time a structure remains exposed to inundation above a critical depth threshold. Duration is estimated using event-specific hydrographs and classified into two categories: short (less than 24 hours) and long-duration (24 hours or longer). Prolonged exposure increases the likelihood of water penetration, material saturation, mold growth, and damage to porous components, such as interior finishes and fixtures (Hall et al., 1984).

Debris Flow: Debris flow is the transport of solid materials such as sediment, soil, vegetation, and man-made objects by moving floodwater, which amplifies hydrostatic and hydrodynamic forces and increases structural damage beyond that caused by water depth and velocity alone. Its occurrence is driven by a combination of debris susceptibility (derived from slope/topography and land use/cover), event-level soil moisture, and flood velocity. Debris flow is applied only to moderate- and high-velocity classes, reflecting the minimum energy required to mobilize and transport debris.

The combination of four velocity classes, two duration classes, and the presence or absence of debris flow results in 12 distinct hazard-intensity combinations. Each combination is associated with a unique set of damage functions.

2.3 Component-Level Damage Functions

The framework employs a component-based approach to vulnerability modeling, in which buildings are decomposed into discrete physical components. The model considers ten key building components, plus clean-up and miscellaneous costs, to determine the total replacement cost (see Table 1).

Table 1: Building component breakdown

Component Name	Component Description
Foundation	The foundation forms part of the building that transmits the loads from the building to the ground below. The types of foundations used for residential buildings vary and may be in the form of a basement, crawlspace, slab, or others.
Structural Frame	The structural frame includes all load-carrying parts of the building, including the columns, beams, joists, and studs.
Exterior	The exterior forms the outer parts of a building, including the exterior walls and siding.
Openings	The opening includes the building's doors and windows.
Roof	The roof includes the roof frame, roof decking, and roof covering.
Interior	The interior component refers to walls inside the building (e.g., partition walls and drywall), flooring and floor coverings, and other interior finishes.
Fixtures	Fixture components of a house include items like light fixtures, faucets, sinks, toilets, built-in cabinets, door handles, window coverings, ceiling fans, and any other item permanently attached to the structure of the house, meaning they are considered part of the property.
Mechanical Systems	Mechanical systems typically include heating, ventilation, and air conditioning (HVAC), ducts, and elevators.
Electrical Systems	The electrical systems component includes electrical switchboards, meters, distribution panels, switches, circuit breakers, and control and utilization systems (e.g., lighting and wiring).
Plumbing Systems	Plumbing systems consist of water piping and sewage treatment and disposal systems, including septic tanks, bathroom drains, sinks, and interior pipes.
Clean-Up and Miscellaneous	This component includes remediation and other activities associated with repair and mold removal.

For each component, damage functions are developed as functions of flood depth relative to the floor level, conditioned on the applicable velocity and duration class (see Figure 2). To build the

component damage functions, Verisk engineers used the results of studies conducted by the New Orleans District of the USACE, as well as other studies, on flood losses to single-family homes and commercial buildings (e.g., Babbitt et al., 2010; Dottori et al., 2016; FEMA, 2006; Kelman, I., 2003; Kelman, I., & Spence, R., 2004; Penning-Rowsell et al., 2005, 2005; Priest et al., 2021; Shrubsole et al., 1993; USACE, 1992; USACE, 2006). Velocity effects influence most components, primarily load-bearing and envelope components, while duration effects are most pronounced for porous interior components and fixtures (see Figure 3). The presence of debris flow is represented through an amplification factor applied at the building level.

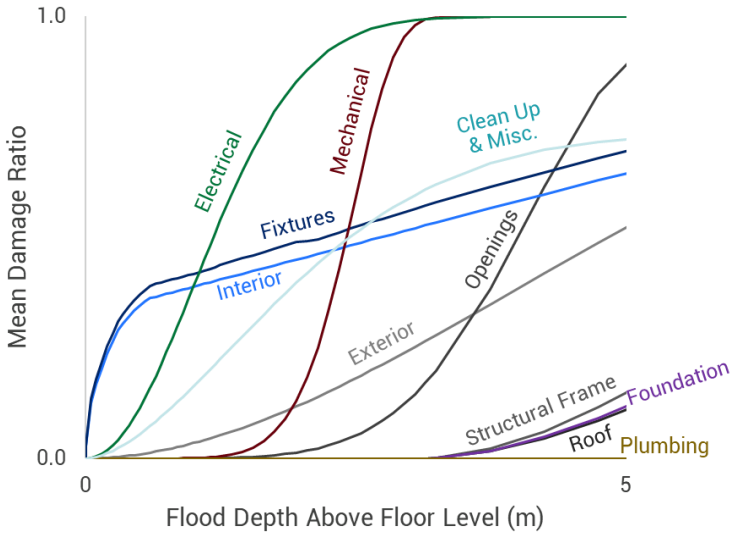

Figure 2: Sample component damage functions for a given building type, susceptible to a low velocity, short-duration flood event

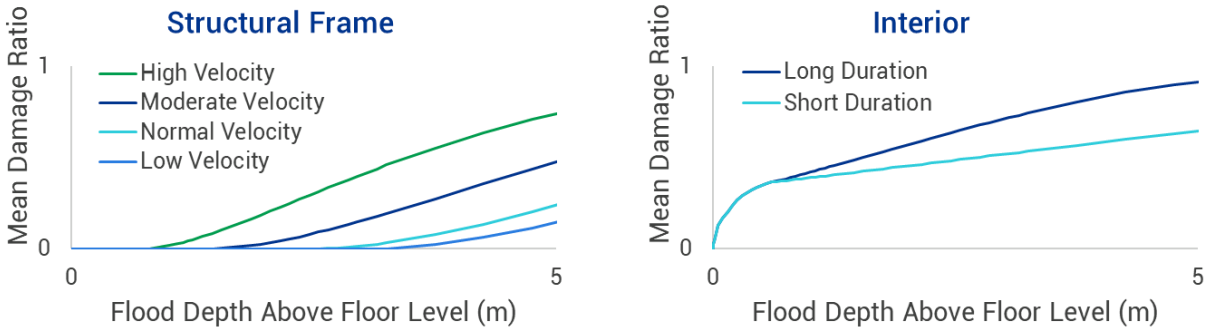

Figure 3: The effect of flow velocity and flood duration on different components

2.4 Aggregation to Building-Level Damage

Component-level damage functions are aggregated to produce story-level damage functions using component cost ratios and vertical distribution factors (Ramanathan and Kafali, 2014). These story-level functions are then aggregated across the building's height to obtain an overall building damage function. The aggregation explicitly accounts for building height, number of stories, foundation type, and the vertical location of vulnerable components, such as mechanical and electrical systems. The mathematical formulation for the building damage function ($DF_{Building}$) is (1):

$$DF_{Building} = \sum_{j=1}^{N} \sum_{i=1}^{M} \alpha_i \beta_{i-j} DF_{component,i} \quad (1)$$

Where:

- N is the number of stories.
- M is the number of components.
- α_i is the $i-th$ component cost breakdown.
- β_{i-j} is the floor cost distribution factor for the $i-th$ component at the $j-th$ story.
- $DF_{component,i}$ is the $i-th$ component-level damage function.

Component cost ratios and floor cost distributions are informed by Verisk 360-Value (a subsidiary of Verisk) and local sources. This formulation enables the model to capture key vulnerability drivers, including the presence of a basement and the concentration of value in lower floors. For instance, in multi-story residential buildings, mechanical and electrical fittings are often located on lower floors, increasing their vulnerability. In such cases, the values of β_{i-j} will be higher in lower floors, exacerbating the vulnerability of such buildings. Figure 4 shows the resulting building-level MDR for a one-story masonry single-family home (see Figure 4-a) and a five-story office building (see Figure 4-b) expressed as a function of flood depth relative to ground level, ensuring compatibility with hazard outputs.

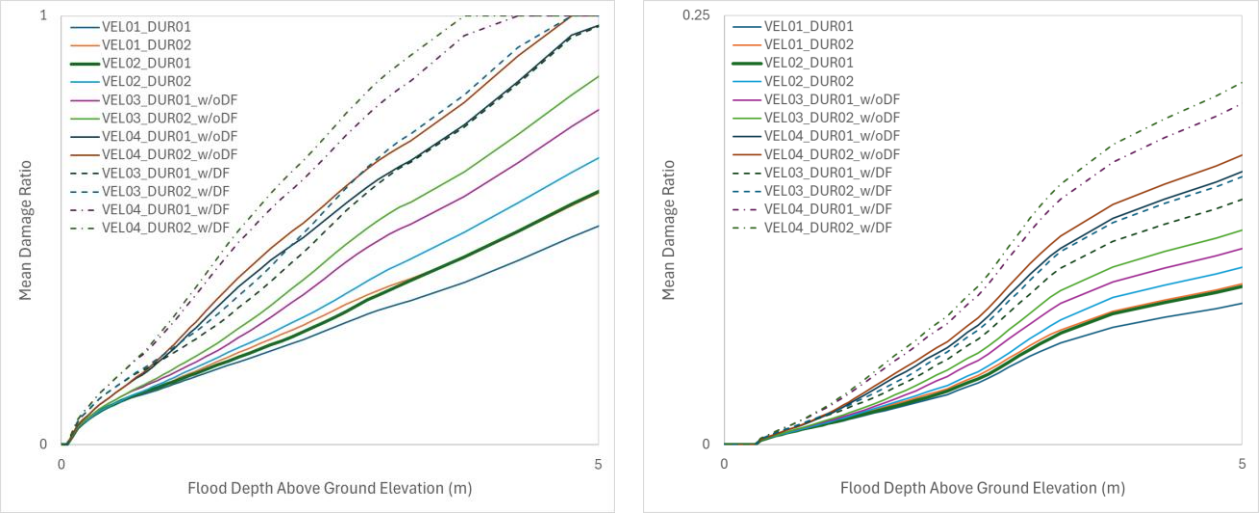

(a) (b)

Figure 4: Sample building level damage functions for twelve distinct hazard combinations, showing the range of damage for a given inundation depth depending on the velocity (VEL01-VEL04) and duration class (DUR01-DUR02), and the debris flow presence (without debris flow - w/oDF, and with debris flow - w/DF) for a one-story masonry single-family home (a) and a five-story concrete office building (b). The thicker line depicts the damage function for normal velocity (VEL02) and short duration (DUR01).

2.5 Building Characteristics and Unknown Attributes

Building vulnerability is conditioned by a set of primary risk characteristics, including occupancy, construction type, and height, as well as secondary characteristics such as foundation type and first-floor

height. For the Verisk United Kingdom (UK) and Republic of Ireland (ROI) inland flood model, researchers utilized 142 occupancies, 129 construction types, and height classifications up to 30 stories to create hundreds of thousands of unique archetypes.

For cases where exposure attributes are missing, such as unknown construction types, the number of stories, or foundation type, the model employs CRESTA[1]-level weighted damage functions derived from industry exposure databases (IEDs) and proprietary datasets, such as the Verisk UKBuildings data, another subsidiary of Verisk. This approach preserves regional variability in vulnerability and avoids reliance on national-average assumptions.

Example: Building Height in the UK: The IED analysis shows distinct regional variations. As an example, London is characterized mainly by high-rise apartments, while Bath consists of low- and mid-rise buildings. Since vulnerability decreases as the number of stories increases (due to value distribution), applying a country-wide average would misrepresent the risk. By using CRESTA-level unknown-height damage functions, the model correctly identifies Bath as more vulnerable than London for undefined apartment risks (see Figure 5).

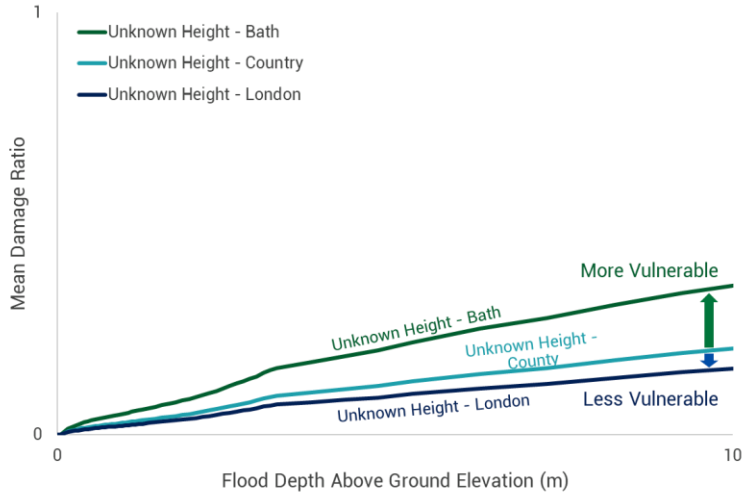

Figure 5: Verisk's UK industry exposure database informs highly granular assumptions on primary risk characteristics – building height in the UK

Example: Basements – Foundation Type: Basements significantly increase flood vulnerability. Using the UKBuildings Database, we determined the likelihood of basement presence based on occupancy, year built, height, and CRESTA, resulting in 72 specific combinations per CRESTA zone. For instance, buildings constructed before 1914 are significantly more likely to have a basement. Figure 6 shows the percentage of commercial mid-rise (4 to 7 stories) buildings with a basement constructed before 1914 (Figure 6-a) and after 1914 (Figure 6-b), per CRESTA.

For example, for CRESTA Leeds, the percentages of commercial mid-rise buildings with a basement constructed before and after 1914 are 83% and 38%, respectively. Using this CRESTA-year built-level information, we can develop known and unknown foundation damage functions per year-built class for 5-story commercial buildings susceptible to normal velocity and short-duration events in a sample CRESTA, Leeds, as shown in Figure 7.

[1] A standardized geographic zoning system developed by the Catastrophe Risk Evaluating and Standardizing Target Accumulations initiative, used by the insurance industry to consistently aggregate and manage catastrophe risk exposure and losses at a subnational regional level.

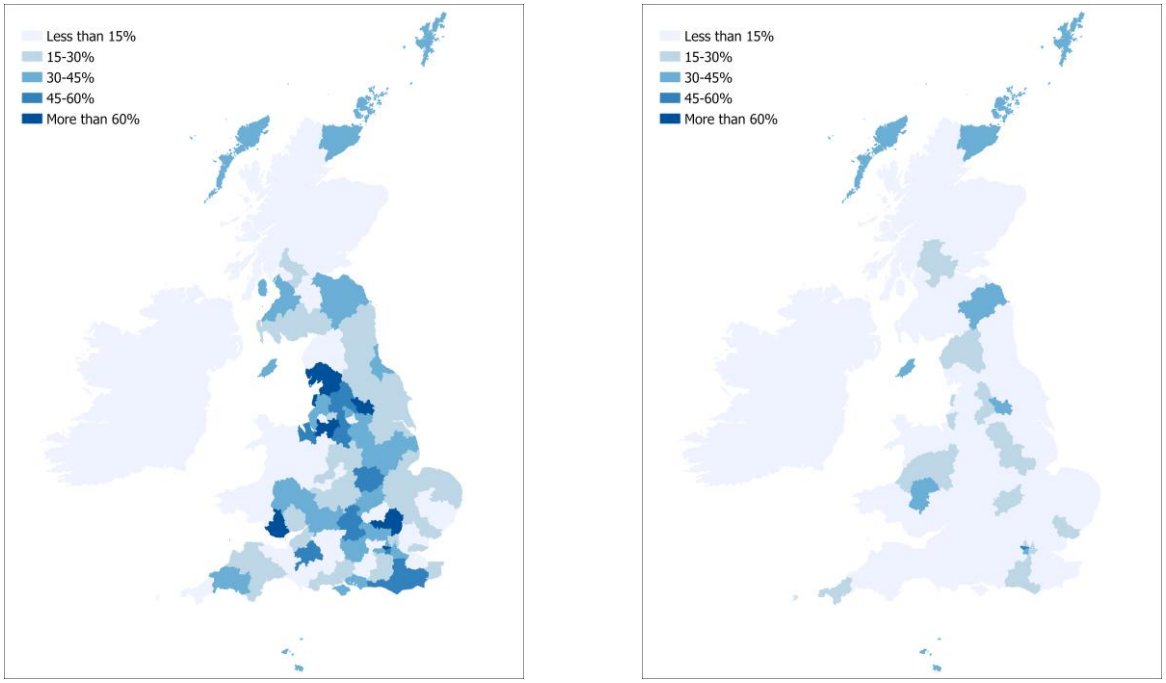

(a) (b)

Figure 6: Verisk's UK Buildings database offers highly granular assumptions on the presence of basements. (a) shows the percentage of commercial mid-rise buildings constructed before 1914 with a basement per CRESTA, and (b) shows the percentage of commercial mid-rise buildings constructed after 1914 with a basement per CRESTA

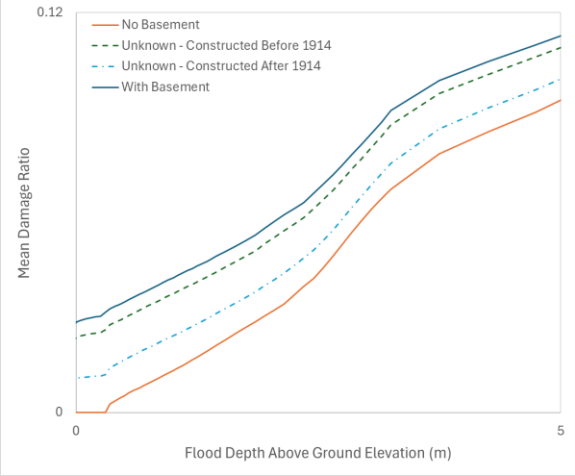

Figure 7: Basement, no basement, and unknown basement damage function for 5-story commercial buildings susceptible to normal velocity and short duration in CRESTA Leeds

2.6 Model Calibration and Validation

Validating the entire model, from hazard to vulnerability to loss, is essential. For our UK and ROI inland flood model, we validated our component-level damage functions against established external sources, including the Multi-Coloured Manual (MCM; Priest et al., 2021), INSYDE (Dottori et al., 2016), and various loss data sets.

Comparisons show that Verisk-derived damage functions closely mirror MCM functions, with expected deviations at lower depths, where our model accounts for uncertainties in building characteristics and hazard (see Figure 8).

While the framework does not explicitly model all secondary damage mechanisms (e.g., contamination or erosion), these effects are implicitly captured through calibration and validation.

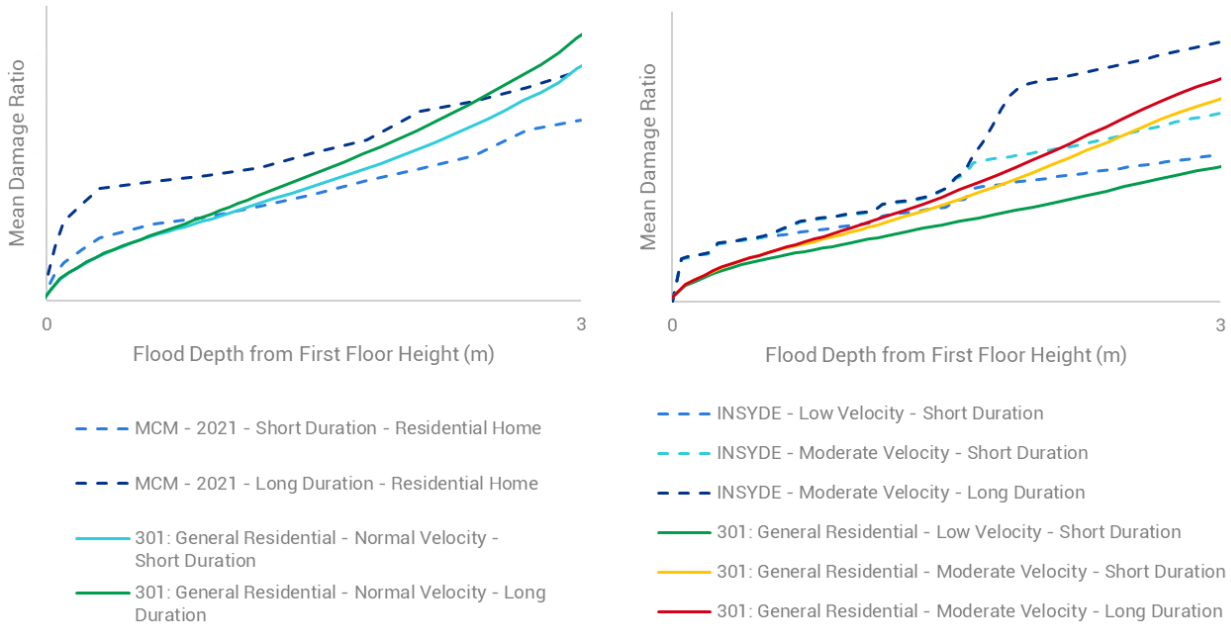

Figure 8: Comparison of Verisk flood damage functions (solid lines) with external sources (dashed lines)

3 RESULTS

The introduction of additional hazard intensity parameters substantially broadens the range of damage outcomes that can be represented at a given flood depth (see Figure 4). When averaged over depth, modeled MDRs for low-velocity, short-duration floods are approximately 5–10% lower than those associated with the baseline normal-velocity, short-duration case. In contrast, high-velocity, long-duration floods with debris flow can produce MDR increases on the order of 130–140% relative to the baseline.

These differences reflect the cumulative effects of hydrodynamic loading, prolonged wetting, and debris-induced force amplification. Notably, the framework enables consistent modeling of both slow-rising, long-duration floods and short-duration, high-energy flash floods within a single vulnerability modeling framework.

4 DISCUSSION

The enhanced vulnerability framework demonstrates that explicitly incorporating flood velocity, duration, and debris flow materially improves flood damage functions. By operating at the component level, the model effectively captures key primary characteristics, such as occupancy and number of stories, as well as secondary features, including foundation type and first-floor height. This approach enables differential sensitivity analysis across various building systems and facilitates a detailed understanding of how specific building features influence loss outcomes.

The use of highly granular exposure and building inventory data allows the model to move beyond an "average building" representation and instead reflect regional construction practices and exposure

distributions. This capability is significant for flood risk, where slight differences in first-floor elevation, foundation type, or building height can result in substantial differences in damage.

5 CONCLUSION

This paper presents a component-level flood vulnerability framework that extends traditional depth-based modeling by incorporating flood velocity, duration, and debris flow as explicit parameters of hazard intensity. By defining twelve distinct hazard combinations and developing component-specific damage functions, the framework captures key physical processes that drive flood damage across diverse event types.

Application of the framework demonstrates significant variation in modeled damage outcomes at a given flood depth, highlighting the importance of distinguishing between slow-rising inundation and high-energy, debris-laden floods. The results suggest that vulnerability models incorporating these additional parameters can provide a more accurate and differentiated view of flood risk, supporting improved risk management, pricing, and resilience planning. The framework is designed to be extensible and suitable for application across regions, providing a robust foundation for future enhancements and potential journal-level extensions.

The inclusion of granular "unknown" damage functions further refines risk assessment for portfolios with incomplete data. We encourage the scientific community to continue researching the complexities of the flood peril to further refine these engineering frameworks.

6 ACKNOWLEDGEMENTS

This manuscript reflects the work of the Atmospheric Perils Vulnerability Group at Verisk Catastrophe and Risk Solutions, as presented by Mohammad Shoraka at ICFM10. All technical terminology and assumptions are preserved from the internal documentation, with clarifications added only for the conference audience.

REFERENCES

Babbitt, C., Baker, T., & Robert, A. (2010). RSMeans Square Foot Costs (ed 32). RSMeans Company, Kingston, MA, December 1, 2010.

Dottori, F., Figueiredo, R., Martina, M. L. V., Molinari, D., & Scorzini, A. R. (2016). INSYDE: a synthetic, probabilistic flood damage model based on explicit cost analysis. Natural Hazards and Earth System Sciences, 16(12), 2577–2591, December 2, 2016.

Federal Emergency Management Agency (FEMA; 2006). HAZUS-MH MR2, Multi-Hazard Loss Estimation Methodology, Technical Manual, Federal Emergency Management Agency, National Institute of Building Sciences, Washington, D.C.

FEMA (2011). Coastal Construction Manual Volume II (4th ed.): Principles and Practices of Planning, Siting, Designing, Constructing, and Maintaining Residential Buildings in Coastal Areas. FEMA P-55, 400 pp., August 2011.

Hall, C., Hoff, W. D., & Nixon, M. R. (1984). Water Movement in Porous Building Materials-VI. Evaporation and Drying in Brick and Block Materials. Building and Environment, 19(1), 13–20.

Hydrologic Engineering Centers River Analysis System (HEC-RAS; 2002). Hydraulic Reference Manual, Version 3.1. U.S. Army Corps of Engineers, HEC (Davis, California).

Kelman, I. (2003). Physical Flood Vulnerability of Residential Properties in Coastal, Eastern England. Doctoral dissertation, University of Cambridge.

Kelman, I., & Spence, R. (2004). An overview of flood actions on buildings. Engineering Geology, 73(3–4), 297–309, June 2004.

Penning-Rowsell, E., Johnson, C., Tunstall, S., Tapsell, S., Morris, J., Chatterton, J., & Green, C. (2005). The Benefits of Flood and Coastal Risk Management: A Manual of Assessment Techniques. London: Middlesex University Press, 238 pp., January 2005.

Priest, S., Viavattene, C., Penning-Rowsell, E., Parker, D., Hardman, D., Joyce, J., Morris, J., & Chatterton, J. (2021). Multi-Coloured Handbook. Flood and Coastal Erosion Risk Management. Middlesex University, Flood Hazard Research Council (FHRC), Environment Agency, and the Department for Environment and Rural Affairs (Defra).

Ramanathan, K. & Kafali, C. (2014). Component Level Framework for Developing Storm Surge Damage Functions for Application in Catastrophe Models. 1415–1425. 10.1061/9780784413357.125.

U.S. Army Corps of Engineers (USACE; 1992). Catalog of Residential Depth-Damage Functions used by Army Corps of Engineers in Flood Damage Estimations. IWR Report 92-R-3, Army Engineer Institute for Water Resources, Fort Belvoir, Virginia, May 1992.

USACE. (2006). Depth-Damage Relationships for Structures, Contents, and Vehicles and Content-to-Structure Value Ratios (CSVR) in Support of the Donaldsonville to the Gulf, Louisiana, Feasibility Study. USACE, New Orleans District, New Orleans, LA, 163 pp., March 2006.

ICFM 10
Adapting to Global Change:
Innovative Approaches to Flood Management and Resilience
May 20-22, 2026 | Western University, London, Ontario, Canada

FLOOD HAZARD FORECASTING WITH CONVOLUTIONAL NEURAL NETWORK BASED SPATIO-TEMPORAL FLOOD PREDICTION

Yoshua Widijatmoko[1], Xilin Xia[1], and Nigel Wright[1]
School of Engineering, University of Birmingham, Birmingham, United Kingdom[1]
E-mail: yxw1385@student.bham.ac.uk

ABSTRACT

Real time flood hazard forecasting is critical part of early warning systems, and machine learning approach has emerged as viable way for rapid flood prediction, but generalisability and explainability is still a challenge. This study aims to develop a surrogate model for flood prediction using machine learning approach that can generalise to different resolution. The model is developed using a physics informed neural network (PINN), and a physics guided approach to attain generalisability. Flood events of Birmingham and Carlisle in England are used as study area to develop the model. The model is trained and validated using flood model at 50m resolution and tested on 10m resolution. The results show that the model manages to maintain the performance at lower resolution on higher resolution, and is faster than hydrodynamic model, whilst also being computationally inexpensive to be developed at commercially accessible platforms.

KEYWORDS: Rapid flood prediction, Surrogate models, CNN, Physics informed

1 INTRODUCTION

Over the years, a machine learning approach has offered an option to speedup the flood modelling process to real-time level at the cost of lower accuracy, but generalisability and nature of the model hinder its application (Karim et al., 2023; Teng et al., 2017). Fraehr et al. (2024) developed a model for converting flood map from low to high resolution, and a surrogate model for direct flood prediction. Model for converting resolution is flexible, while surrogate model has better speed, but both apply black box approach that is difficult to explain (Fraehr et al., 2024). Despite the drawbacks, surrogate model offers practicality for rapid flood prediction, especially for early warning system (Cao et al., 2024).

The development a flexible surrogate model is reflected through much research in the area (Karim et al., 2023). However, none has been as versatile as a hydrodynamic model that can generalise to different case or resolution. While the attempt to explain such model led to approach such as physics informed neural network (PINN) that aims to guide black box model using the continuity equation of physics law as part of the training loss function (Donnelly et al., 2024). However, the guiding model to follow physics law can also be done via imposing physics knowledge in framework formulation (Muralidhar et al., 2020).

Ideally, a surrogate model should be able to predict the temporal evolution of flood water depths and velocities. It should also generalise to any case at any resolution, and operate in line with the governing physics law, while maintaining a much lower computational burden. Such a surrogate model is beneficial for preliminary rapid flood prediction, especially within the framework of early warning system. To this end, this study seeks to contribute to the field of flood hazard forecasting by exploring surrogate model generalisability to different resolution to answer the following research questions: Can a surrogate model generalise to different resolution of the same case while maintaining performance? How to facilitate the development of such a model?

To answer these questions, a new framework of surrogate model will be developed by applying PINN and physics guided approach. Both physics approaches leverage physics knowledge on model

framework to allow generalisability across resolution. The rest of the paper is organised as follows: section 2 will discuss the materials and methodology applied, section 3 shows the result and discussion of the model, and finally conclusion is drawn in section 4.

2 MATERIALS AND METHODS

2.1 Study Area and Scenarios

Surrogate model is typically developed with single flood driver, either from rainfall or river flow (Fraehr et al., 2024; Situ et al., 2024), but in this study both are considered and the area of Birmingham and Carlisle in England are chosen as study area. From Birmingham, the watershed of River Rea is chosen, it has drainage area of 88 km^2 and flood is driven solely by rainfall. While from Carlisle, urban area along the River Eden is chosen, it has a domain of 109 km^2 and driven by both rainfall as well as river flow from four upstream. Figure 1 shows the location of both study area.

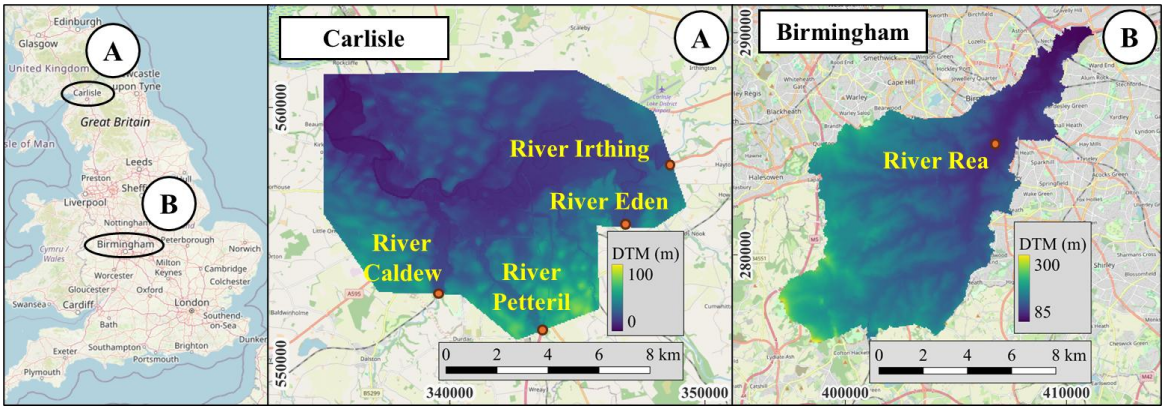

Figure 1: Location of Study Area

Aside from historical data, synthetic data is commonly used to increase availability and variability (Liao et al., 2023; Wang et al., 2024), and it is often generated from historical analysis or design pattern (Situ et al., 2024; Song et al., 2025). In this study, terrain and boundary condition data is collected from UK Department of Environment Food and Rural Affairs, synthetic data is generated from return period analysis, and flood is simulated using SynxFlow that solve 2D Shallow Water Equations (Xia and Ming, 2025). The data used in the study are summarised in Table 1.

Synthetic hyetograph is applied in pluvial and compound flood cases, but not for dry state and fluvial cases. Friction coefficient is uniformly set in all simulation to simplify modelling process as the focus of this study is replicating hydrodynamic modeller performance. Moreover, only simulation output from the 24 hours duration of synthetic flood event is included as data pool to reduce computational burden of training stage while maintaining key learning feature. Furthermore, data within training, validation, and testing set are engineered to optimise model development. Training set contain wide range of flood case and return periods to encourage generalisability. Validation set is engineered to validate performance at interpolating storm conditions. While testing set is to test model performance at unknown resolution.

2.2 Surrogate Model

In this study, fully convolutional network (CNN) is used as the framework since it allows processing of different input sizes (Wang et al., 2024) and therefore also applicable for different resolution since different resolution can be interpreted as expressing the same case over different size. The underpinning principle applied within the model is image-to-image translation where image output

and input are different but still maintain a level of resemblance (Guo et al., 2021). Hence the input and output of the model is limited to 2D format, and 1D inputs are processed into 2D spatial data that resembles hydrodynamic output to allow model to learn better. Accordingly, hyetograph and hydrograph are processed into 2D spatial data by imposing inversed min-max scaled DTM as spatial distribution pattern. This enables lower elevation to have more distribution weight than higher elevation that resemble hydrodynamic model water depth output since area near river channel will have deeper water than flood plain. Hyetograph is processed into rain intensity distribution map by calculating total rainfall inflow and distribute it according to the distribution pattern. While hydrograph is processed into river flow distribution map by identifying elevation bellow inlet surface elevation as inundation extend, then scaling distribution pattern within extend with discharge value. Hydrograph transformation does not maintain mass conservation due to technical difficulties and is left for the machine learning framework to resolve. Figure 2 shows example of rain intensity distribution map and river flow distribution map.

Table 1 Summary of Data Used in the Study

Description	Birmingham	Carlisle
Data Collected		
Terrain data	2022 LiDAR DTM at 2 m resolution	2022 LiDAR DTM at 2 m resolution
Daily rainfall	2003-2024 Saltley, Waseley Hills, Alvechurch, and	1997-2024 Willow Holme and Cumwhinton
15 min rainfall	2003-2024 Frankley	1997-2024
15 min hydrograph		1997-2024 Cummersdale - River Caldew (E: 339489; N: 552735)
		2006-2024 Newbiggin Bridge - River Petteril (E: 343561; N: 551259)
		1996-2024 Great Corby - River Eden (E: 346825; N: 555339)
		1975-2024 Greenholme - River Irthing (E: 348618; N: 558072)
Synthetic Data		
Terrain data	Averaging DTM data to 50m and 10m resolution	Averaging DTM data to 50m and 10m resolution
Return Period	2, 5, 8, 10, 20, 50, 80, 100, 200, 500 years	2, 5, 8, 10, 20, 50, 80, 100, 200, 500 years
Simulation		
Output	Hourly Water Depth (m) and Velocity at x and y directions (m/s)	Hourly Water Depth (m) and Velocity at x and y directions (m/s)
Total simulation time	72 hours (24 leads, 24 floods, 24 lags)	72 hours (24 leads, 24 floods, 24 lags)
Manning's (n)	0.055 $sm^{(-1/3)}$	0.055 $sm^{(-1/3)}$
Flood Scenarios	70 Pluvial Floodings, 56 Dry State	70 Compund Floodings, 56 Fluvial Floodings
Data Pool		
Training Set	112 data	112 data
- Resolution	50 m	50 m
- Return period	2, 5, 10, 20, 50, 100, 200, 500 years	2, 5, 10, 20, 50, 100, 200, 500 years
- Scenarios	56 Pluvial Floodings, 56 Dry State	56 Compund Floodings, 56 Fluvial Floodings
Validation Set	14 data	14 data
- Resolution	50 m	50 m
- Return period	8, 80 years	8, 80 years
- Scenarios	14 Pluvial Floodings	14 Compund Floodings
Testing Set	14 data	14 data
- Resolution	10 m	10 m
- Return period	8, 80 years	8, 80 years
- Scenarios	14 Pluvial Floodings	14 Compund Floodings

Aligning with physics guided approach (Muralidhar et al., 2020), this study proposes context convolution mechanism where terrain data is projected into context vectors that later are used as kernel weights within a convolutional layer operation. Moreover, to embody the concept that flood depth

increases rapidly within river channel and slower as it flows out to flood plain, a custom output function is proposed and shown in Eqs. (1). Figure 3 shows the framework used in this study.

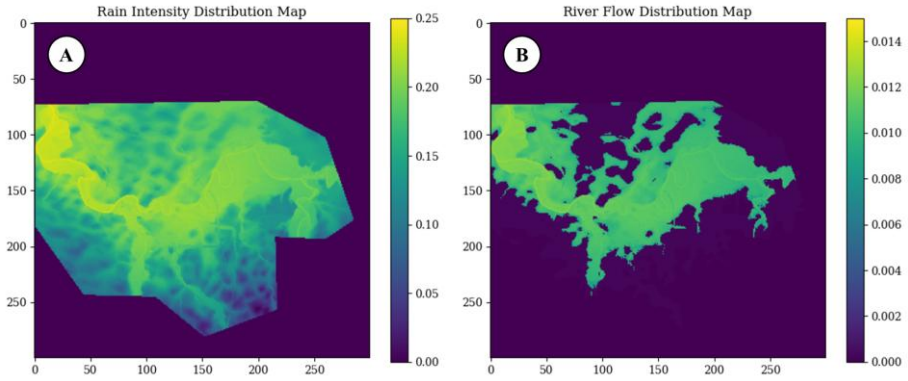

Figure 2: Rain Intensity Distribution Map (a) and River flow Distribution Map (b) of Carlisle Study Area

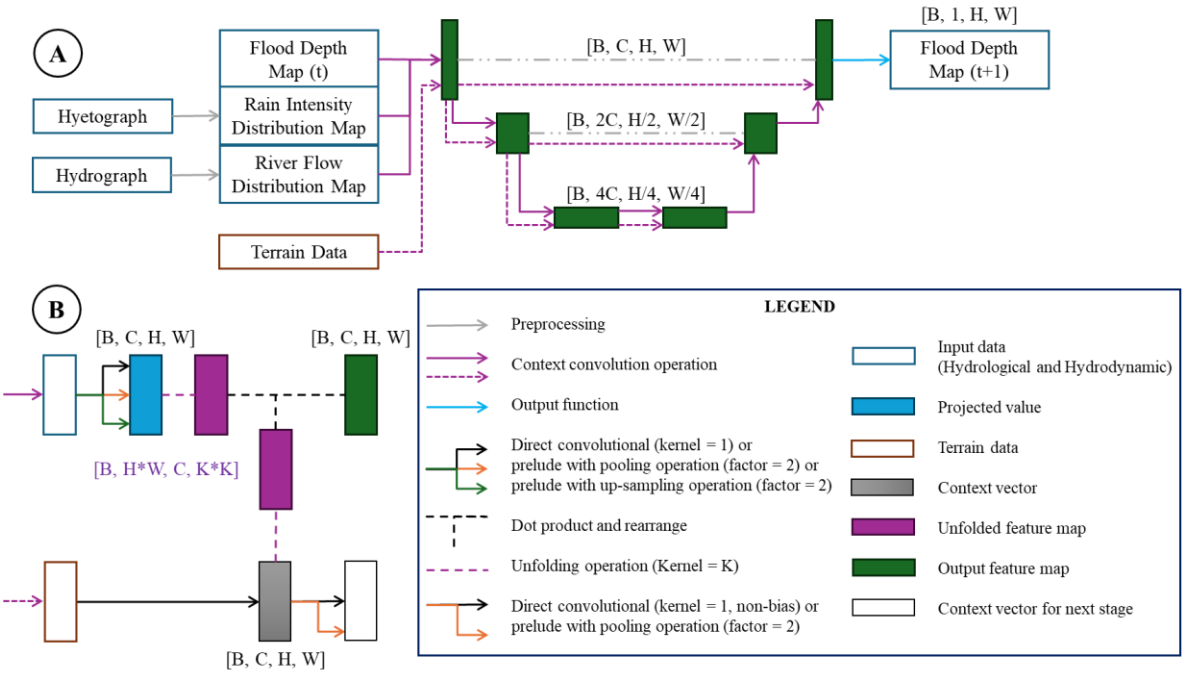

Figure 3: Surrogate Model Framework (a) and Context Convolutional Mechanism (b)

$$f(\boldsymbol{X}) = ReLU\left(W_2 \frac{\ln(ReLU(\boldsymbol{X}) + 1)}{\ln(W_1)}\right) \quad (1)$$

Where $ReLU$ is rectified linear function, $\boldsymbol{X}$ is the input tensor, W_1 and W_2 are learnable weights. The model receive input that consist of water depth map, rain intensity distribution map, and river flow distribution map of current time step together with DTM data to predict the next time step of water depth map. Furthermore, the model works autoregressively with hourly time step where the output of previous step is used as input for current step until the prescribe time step is finished.

To further develop model performance, PINN is also implemented by directly applying law of conservation of mass in shallow water equations (Eleuterio, 2001) to form the PINN loss function (L_{PINN}). Eqs. (2) - (3) shows the PINN loss function implemented. The model is also trained separately using

Mean Square Error (MSE) loss function (L_{MSE}) to explore the effectiveness of PINN (Donnelly et al., 2024).

$$S_{(i,j)} = \frac{1}{\Delta t}\left(h^{t+1}_{(i,j)} - h^{t}_{(i,j)}\right) + \frac{1}{\Delta x}\left(hu^{t}_{\left(i+\frac{1}{2},j\right)} - hu^{t}_{\left(i-\frac{1}{2},j\right)}\right) + \frac{1}{\Delta y}\left(hv^{t}_{\left(i,j+\frac{1}{2}\right)} - hv^{t}_{\left(i,j-\frac{1}{2}\right)}\right) \quad (2)$$

$$L_{PINN} = \frac{1}{|\Omega|}\sum_{(i,j)\in\Omega}\left(\left(h^{t+1}_{(i,j)} - \hat{h}^{t}_{(i,j)}\right) + \frac{\Delta t}{\Delta x}\left(\hat{h}u^{t}_{\left(i+\frac{1}{2},j\right)} - \hat{h}u^{t}_{\left(i-\frac{1}{2},j\right)}\right) + \frac{\Delta t}{\Delta y}\left(\hat{h}v^{t}_{\left(i,j+\frac{1}{2}\right)} - \hat{h}v^{t}_{\left(i,j-\frac{1}{2}\right)}\right) - \Delta t S_{(i,j)}\right)^{2} \quad (3)$$

Where $\hat{h}$ is predicted water depth, h, u, and v are ground truth value of water depth, velocity due x and y direction respectively, Ω is valid region of cell coordinate (i, j), t and Δt are time step and its duration, Δx and Δy are grid cell size.

2.3 Experiment Setup

The surrogate model is developed using Python in Google Colab using PyTorch libraries and details of model setups are summarised in Table 2. All input data are pre-processed to value between 0 to 1 to ensure learning stability (Wang et al., 2024). DTM data is pre-processed differently for the same reason stated in Section 2.2 concerning spatial distribution pattern. Furthermore, training regulations are imposed to safeguard learning failure due to overfitting and gradient explosion or vanishing (Zhao et al., 2024). During development stage, it is found that PINN loss function only works well when trained with input that involve hyetograph, hence PINN model is trained using half of the training set data with pluvial and compound flood cases only (see Table 1).

Table 2 Summary of Model Setup in the Study

Description	MSE Model	PINN Model
Traning Strategy	Stochastic gradient descent	Stochastic gradient descent
Optimiser	Adaptive moment estimation (Adam)	Adaptive moment estimation (Adam)
Training Regulation	Batch processing, Batch normalisation, Early stopping	Batch processing, Batch normalisation, Early stopping
Loss Function	MSE	PINN
Learning Rate	0.0001	0.001
Learning Epoch	25	25
Preprocessing Data		
- DTM Data	Inverse min-max scaling	Inverse min-max scaling
- Other Input Data	Min-max scaling	Min-max scaling
Hyperparameter Optimisation		
- Batch Size	12	12
- Base Channel Size	64	64
- Framework Depth	2	2
- Kernel Size K	3	3

3 RESULTS AND DISCUSSION

During development of the model, it is found that loss value calculated for MSE and PINN model had different scales of magnitude, therefore both training and validation loss graph are ploted at log scale for better comparison and is shown in Figure 4. Comparing Figure 4a and 4b, training and validation loss graph of PINN model is more similar in trend with each other than MSE model, this indicates that PINN loss function allows the model to corelate better to unknown storm conditions than MSE loss function. This is expected since PINN is based on shallow water equations while MSE is purely a statistical evaluation. Based on validation loss, the best performing models are both found at 15 epochs at loss value of 2.260 and 7.765 point for MSE and PINN model respectively and is used for subsequent evaluation.

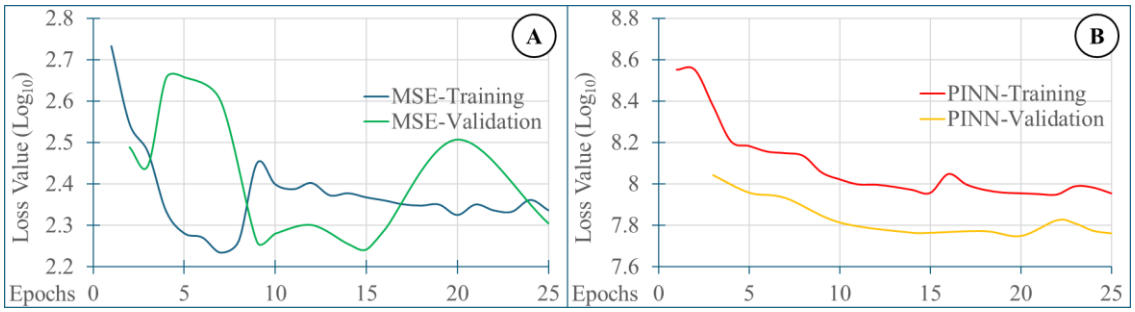

Figure 4: Comparing training and validation loss for MSE model (a) and PINN model (b)

The model performance is evaluated by using regression metrics of Root Mean Square Error (RMSE) and Mean Absolute Error (MAE), and classification metrics of precision, recall, and F1 value with 0.05 m threshold to screen wet and dry cells. Performance is evaluated on validation and testing set and the results are given in Table 3. Based on the results, model trained with MSE loss function outperform model with PINN, but compared with other studies (Donnelly et al., 2022; Guo et al., 2021; Liao et al., 2023), the regression performance is limited while classification performance is decent. The failure to perform better can be attributed to the level of generalisability that the model aim to achieve and the inability of the framework to accommodate it. However, as performane only declined within the range of 2.1~10.4% when resolution increase from 50 to 10 m, this shows that the model maintain initial performance across different resolution reasonably well.

Table 3 Surrogate Model Performance Summary

Case Set	Cases	Duration (hr)	Resolution (m)	Loss Function	RMSE (m)	MAE (m)	Precision	Recall	F1
Validation	28	24	50	MSE	2.405	1.548	0.685	0.784	0.725
Test			10		2.656	1.659	0.639	0.744	0.681
Percentage Difference					10.40%	7.20%	6.70%	5.10%	6.10%
Validation	28	24	50	PINN	4.378	2.968	0.827	0.672	0.714
Test			10		4.685	3.277	0.844	0.625	0.684
Percentage Difference					7.00%	10.40%	2.10%	7.00%	4.20%

Figure 5 shows prediction sample of CNN model trained with MSE loss function compared to ground truth water depth map from SynxFlow. Inline with the performance report, prediction results resemble the outputs from SynxFlow but with lower accuracy. Comparing predictions at 50m and 10m resolution (Figure 5b-c and 5e-f), the model maintain visual coherency when tested at higher resolution. Moreover, considering flood flows towards Northeast in Birmingham (Figure 5a-c) and Northwest in Carlisle (Figure 5d-f), this shows that model can also recognise river direction. These overall success can be atributed to the use of DTM data within the model framework, as effectively the model predict flood in the image of DTM data. However, the use of DTM data within the framework also impose limitation along the boundry region near the outlet area as shown by Figure 5a-c. Boundary region around outlet area are clearly predicted as flooded by the CNN model but not so by SynxFlow, these can be caused by elevation around the oulet area that are mostly very low when compared to the rest of the domain area and therefore have unrealistic distribution weight during prediction process. Nonetheless, this limitation is deemed acceptable as the framework has allowed surrogate model to emulate the ability of hydrodynamic model to generalise different resolution and river direction. This also reasonably improve explainability of the model since it now behave similarly to hydrodynamic model.

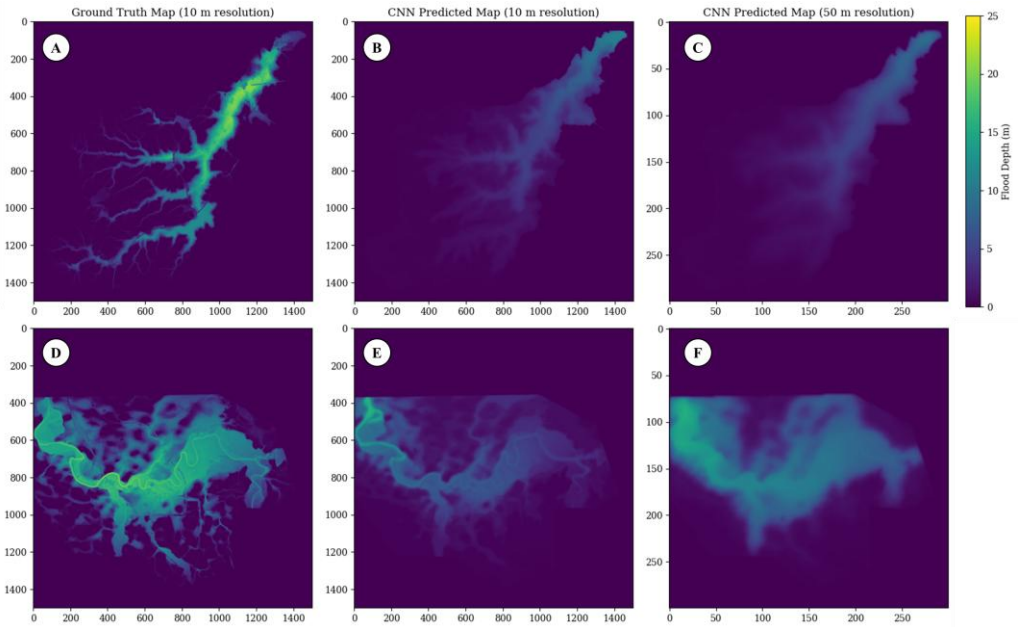

Figure 5: Prediction at t = 11 hour of return period 80 years for Birmingham (a-c) and Carlisle (d-f)

Computational burden of the model is compared to SynxFlow and results are shown in Table 4. The CNN model is faster than SynxFlow, and speed factor increases as resolution incease. This can be atributed due to the exponential increase in computing cell when moving from 50 m to 10 m resolution. Although faster, the time needed to train the model takes up to 137.6 hours excluding the time needed to generate data pool, which shows that substantial amount of preparation is needed. However, since it only required once, it can be argued that the model is still faster than hydrodynamic model and is suitable for rapid flood prediction. Furthermore, as the model is successfully developed in Google Colab, this shows that resources required to develop the model is not prohibitively expensive.

Table 4 Computational Burden Evaluation

Model	Device (Google Colab)	Training Time (hr)	Simulation Duration (hr)	Resolution (m)	Simulation Time (min)	Speed Factor
SynxFlow	T4 GPU	-	72	50	1.64	1
				10	111.47	1
CNN	CPU High Ram (Training)	137.6	24	50	0.12	4.6
	v5e-1 TPU (Validation & Testing)	-		10	3.7	10.03

4 CONCLUSION

This study shows that surrogate model can be developed to generalise different resolution of the same case while maintaining performance. The model manages to achieve this by leveraging terrain data to guide the process and mechanism within the framework. The model is computationally inexpensive to be developed on Google Colab platform and faster than hydrodynamic model, showing that it is accessible for stakeholders with limited resources while allowing certain degrees of rapid flood predictions. However, the model has limited predictive ability at water depth predictions but arguably functional at inundation extend. Nonetheless, this study has contributed to improve generalisability of surrogate model across resolution for flood predictions and open the possibility of training such model with low resolution to predict high resolution case. Future study should focus on improving ways to process data, enhance framework ability to predict accurately, and expand prediction to include velocity.

5 ACKNOWLEDGEMENTS

The first author acknowledges the support of the Indonesia Endowment Fund for Education LPDP (Grant No. 202407120105809).

REFERENCES

Cao, A., Nakamura, S., Otsuyama, K., Namba, M., & Yoshimura, K. (2024). Current status and challenges in operating flood early warning systems at the local level in Japan. International Journal of Disaster Risk Reduction, 112. https://doi.org/10.1016/j.ijdrr.2024.104802

Donnelly, J., Daneshkhah, A., & Abolfathi, S. (2024). Physics-informed neural networks as surrogate models of hydrodynamic simulators. Science of the Total Environment, 912. https://doi.org/10.1016/j.scitotenv.2023.168814

Eleuterio, F. T. (2001). Shock-Capturing Methods for Free-Surface Shallow Flows. Wiley.

Fraehr, N., Wang, Q. J., Wu, W., & Nathan, R. (2024). Assessment of surrogate models for flood inundation: The physics-guided LSG model vs. state-of-the-art machine learning models. Water Research, 252. https://doi.org/10.1016/j.watres.2024.121202

Guo, Z., Leitão, J. P., Simões, N. E., & Moosavi, V. (2021). Data-driven flood emulation: Speeding up urban flood predictions by deep convolutional neural networks. Journal of Flood Risk Management, 14(1). https://doi.org/10.1111/jfr3.12684

Karim, F., Armin, M. A., Ahmedt-Aristizabal, D., Tychsen-Smith, L., & Petersson, L. (2023). A Review of Hydrodynamic and Machine Learning Approaches for Flood Inundation Modeling. In Water (Switzerland) (Vol. 15, Number 3). MDPI. https://doi.org/10.3390/w15030566

Liao, Y., Wang, Z., Chen, X., & Lai, C. (2023). Fast simulation and prediction of urban pluvial floods using a deep convolutional neural network model. Journal of Hydrology, 624. https://doi.org/10.1016/j.jhydrol.2023.129945

Muralidhar, N., Bu, J., Cao, Z., He, L., Ramakrishnan, N., Tafti, D., & Karpatne, A. (2020). PhyNet: Physics Guided Neural Networks for Particle Drag Force Prediction in Assembly. In Proceedings of the 2020 SIAM International Conference on Data Mining (pp. 559–567). Society for Industrial and Applied Mathematics. https://doi.org/10.1137/1.9781611976236.63

Situ, Z., Wang, Q., Teng, S., Feng, W., Chen, G., Zhou, Q., & Fu, G. (2024). Improving urban flood prediction using LSTM-DeepLabv3+ and Bayesian optimization with spatiotemporal feature fusion. Journal of Hydrology, 630. https://doi.org/10.1016/j.jhydrol.2024.130743

Song, W., Guan, M., & Yu, D. (2025). SwinFlood: A hybrid CNN-Swin Transformer model for rapid spatiotemporal flood simulation. Journal of Hydrology, 660. https://doi.org/10.1016/j.jhydrol.2025.133280

Teng, J., Jakeman, A. J., Vaze, J., Croke, B. F. W., Dutta, D., & Kim, S. (2017). Flood inundation modelling: A review of methods, recent advances and uncertainty analysis. In Environmental Modelling and Software (Vol. 90, pp. 201–216). Elsevier Ltd. https://doi.org/10.1016/j.envsoft.2017.01.006

Wang, Z., Lyu, H., Fu, G., & Zhang, C. (2024). Time-guided convolutional neural networks for spatiotemporal urban flood modelling. Journal of Hydrology, 645. https://doi.org/10.1016/j.jhydrol.2024.132250

Xia, X., & Ming, X. (2025). SynxFlow: A GPU-accelerated Python package for multi-hazard simulations. Journal of Open Source Software, 10(111), 7586. https://doi.org/10.21105/joss.07586

Zhao, X., Wang, L., Zhang, Y., Han, X., Deveci, M., & Parmar, M. (2024). A review of convolutional neural networks in computer vision. Artificial Intelligence Review, 57(4). https://doi.org/10.1007/s10462-024-10721-6

ICFM 10
Adapting to Global Change:
Innovative Approaches to Flood Management and Resilience
May 20-22, 2026 | Western University, London, Ontario, Canada

The Relationship Between Peak Flow and Flood Volume for Deriving Probable Maximum Flood Hydrographs in Ontario

Dequan Zhou[1] and Diana Sankar[2]
Hatch Ltd. Ontario, Canada[1]
E-mail: dequan.zhou@hatch.com

Hatch Ltd., 80 Hebron Way, Suite 100, St. John's, NL, Canada[2]
E-mail: diana.sankar@hatch.com

ABSTRACT

In dam safety assessments the Inflow Design Flood (IDF) may be the Probable Maximum Flood (PMF) according to the current regulations and guidelines in both the Canadian Dam Association (CDA) and the Lakes and River Improvement Act (LRIA) of Ontario. This IDF is set to be the PMF when there are extreme hazards imposed to downstream communities in the event of a dam failure. A dam must be designed (or be modified if an existing dam does not have the spillway capability) to safely pass the IDF. The peak flow, flood volume, the shape of the hydrograph and flood duration are important components of the PMF hydrograph. A PMF hydrograph, not just a PMF peak flow, is important when determining the hydrological risk of dams where a dam has significant storage capacity. Traditionally, these parameters of the PMF are obtained by rainfall-runoff modelling based on Probable Maximum Precipitation (PMP). The processes of the analyses may take considerable time and resources. This paper proposes an alternative approach using regional relationships based on streamflow statistics and envelope curves of peak flow and flood volume for Ontario, Canada. The approach is similar to the Hershfield (1961, 1965) method for the derivation of PMP. A database of 396 flow stations was analyzed to derive the relationship between the PMF peak flows and the corresponding volumes. A PMF hydrograph can be developed for ungauged locations within Ontario using the proposed method.

KEYWORDS: PMF, Flood, Hydrology, Dam Safety, Regional Technique, Flood Frequency, Risk, Hydrograph

1. Dequan Zhou, P. Eng. Hatch Ltd.
2. Diana Sankar, P. Eng. Hatch Ltd.

1 INTRODUCTION

As part of a dam safety assessment, an Inflow Design Flood (IDF) is used to determine the size of a spillway and the hydrological hazards of a dam. If a dam break event would lead to incrementally large losses of life, high social, cultural and economical damages and severe environmental consequences, the dam has a high to very high Hazard Potential Classification (HPC) (Ontario Ministry of Natura Resources, 2011). In this case, the IDF could be the Probable Maximum Flood (PMF) based on standard dam safety guidelines (CDA, 2013 and Ontario Ministry of Natural Resources, 2011). All dams must be able to safely pass the IDF to meet the safety requirement in a standard based regulation system.

Various methods exist for the derivation of IDF less than the PMF event. These approaches include: 1) rainfall-runoff modeling (FEH, 1999). 2) flood frequency analyses based on historical flood records (for dam's IDF much less than the PMF) (Moin, S. and M. Shaw (1985)), and 3) regional flood estimation techniques (Nathan, et. al., 1994, Abrahamson et. al., 2010, and Zhou, 2023).

The most popular method is through a Probable Maximum Precipitation (PMP) – Probable Maximum Flood (PMF) approach. The first step is to determine the PMP by site specific study. The PMP can be derived by regional PMP maps or by statistical (e.g. Hershfield, 1961, 1965) methods (WMO, 2009). The PMP will then be used in a rainfall-runoff model to obtain the PMF. Various hydrological models are used in rainfall-runoff simulations.

The rainfall-runoff modeling approach is considered a reliable after the model was calibrated and validated properly. However, this approach takes considerable time to undertake. The advantage of the rainfall-runoff simulation approach is that many of the processes are physically based and hence are supported by physical laws. This is also a disadvantage at the same time since lack of data may often lead to misuse of these models.

Flood frequency analysis is another option for IDF derivation. There are two obvious drawbacks in using the flood frequency analysis in deriving the IDF. The IDF has a recurrence interval at least in a period of hundreds, thousands or even millions (e.g. PMF) of years but the length of available historical data rarely extends past 100 years. Therefore, the frequency curve must be extrapolated to a length significantly longer than the data recording period. This will introduce significant errors and lead to unreliability in predictions of the magnitude of the IDF. The second drawback is that flood frequency analyses are often done only for the peak flows. However, the flood volumes, time to peak and durations are also important controlling factors that are needed in dam safety assessments (especially for dams with storage reservoirs). Univariate frequency analysis does not solve the full IDF problem. Due to the need for the other variables, multivariate frequency analysis techniques have been developed. The common approach is bivariate (peak flow and total flood volume) frequency analysis applying copulas techniques (Chowdhary et.al. 2011, Gaál et.al, 2015 and Zhou, 2006, 2015). This type of frequency analysis requires new definitions of return period in bivariate or multivariate conditions (Gräler et al 2013).

In recent years, some regional and empirical equations were developed to simplify the processes in PMF estimation. Nathan et. al. (1994) developed an equation for south-eastern Australia for the estimation of peak PMF flow. Abrahamson and Pentland (2009, 2010) developed a series of empirical equations for British Columbia streams. Zhou (2023) used 92 sites specific PMF in Ontario and derived an empirical equation for Ontario streams. Zhou and Sankar (2025) developed a PMF peak flow derivation procedure based on historical statistics similar to the Hershfield method for PMP. The regional approach provides an effective way for the determination of PMF peak flows.

These methods have the same disadvantage as univariate flood frequency analysis, only the peak flows are estimated. For small reservoirs or run-of-river dam sites, knowing the peak flow will be sufficient to determine the IDF peak water levels. When the storage capacity of a dam or reservoir is large enough to lead to certain levels of peak flow reduction, the peak flow, flood volume and the shape of the flood hydrograph will be important variables in the flood routing processes. Therefore, there is a need to estimate the corresponding flood runoff volume as well as the shape of the hydrograph in a full dam safety assessment.

This paper describes a procedure to derive the PMF hydrograph using historical recorded relationship between peak flows and the total flood volumes of extreme floods from 396 flow stations located in Ontario. The assessment of the dataset demonstrated that there are very strong correlations between peak flows and total runoff volumes in Ontario streams. The high dependence between the two variables established a solid foundation on the framework for derivation of IDF hydrographs.

2 DATABASE

In 2014, the Ontario Ministry of Natural Resources published a database of peak flows for 297 streamflow stations of the Great Lakes-St. Lawrence watersheds. The stations covered a large portion of Central and Southern Ontario, but excluded Northern Ontario. To make the dataset representative of the entire province an additional 99 stations in Northern Ontario were added into the database from the Hydrometric Historical Data (HYDAT) from Environment Canada, increasing the number of stations to 396. The database contained the variables of drainage area, maximum flood records, mean, standard deviation, coefficient of skewness and kurtosis for each station. All of the stations have at least 10 years of extreme flow data. In the database, the size of the drainage areas ranged from 0.07 km^2 to 118,000 km^2. The peak floods ranged between 0.36 m^3/s to 8270.0 m^3/s (Table 1).

The spatial distributions of the stations are plotted in Figure 1.

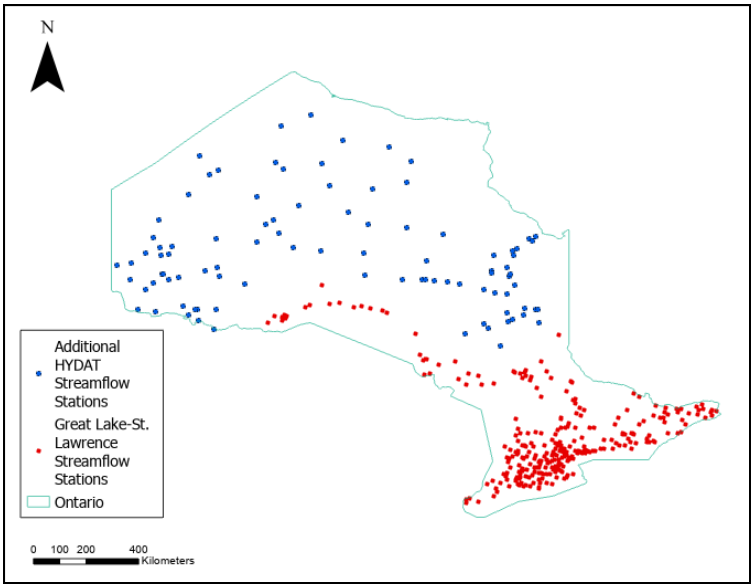

Figure 1 The spatial distribution of stations within the database

In Figure 1, the stations represented by red dots are the 297 Great Lake watersheds (Ontario, 2014). The 99 stations represented by blue triangles are the stations added based on HYDAT. As can be seen from Figure 1, the stations cover the province of Ontario well. The database contains historical maximum peak flows, but did not contain maximum flood volumes. For the purpose of this assessment, the maximum flood volumes were derived based on the following procedure:

1) Using the long-term streamflow records to find the year and date of the highest peak flow in the records of each station; 2) find the starting and the ending dates corresponding to the historical maximum flood; 3) identify the baseflow portion (as shown in Figure 2); 4) estimate the total flood runoff volume (with baseflow excluded). Figure 2 illustrates the baseflow separation from the flood volume estimate and the definitions of time to peak (T_p), flood duration (D) and the peak flow (Q_p) are also shown graphically.

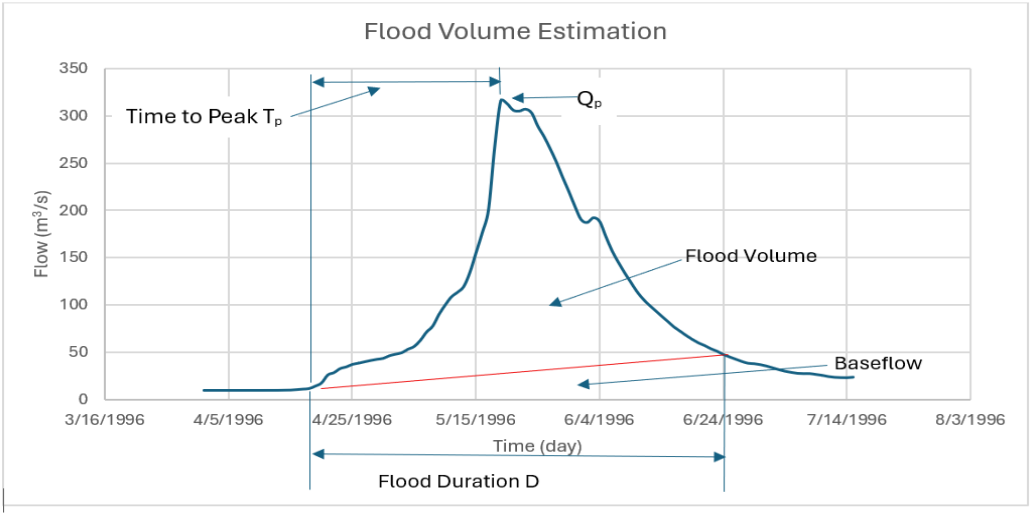

Figure 2 Determination of Flood Volume

The main statistics of the database are presented in Table 1. This database is used in the analysis of the relationship between the peak flow and total flood volume. Statistical analysis shows that the two variables are highly correlated with a R^2 of 0.79.

Table 1 Summary of Watershed Database

	Drainage Area	Peak Flow	Flood Volume	T_p/D
	km^2	m^3/s	Million m^3	
Min	0.1	0.36	.04	0.21
Max	118000.0	8270.0	17529.3	0.83
Mean	4043.4	410.7	575.8	0.41
StDev	12171.7	936.2	1973.7	0.11

Zhou (2024) used the database to derive a new method for predicting the PMF peak flows by the concept developed by Hershfield for PMP (1960, 1965). However, as discussed in the previous sections, a hydrograph is necessary to adequately assess the IDF when the dam impounds a reservoir with significant storage, and only a peak flow is not sufficient. The flood volume and flood shape are also important to describe the full hydrograph. The proposed approach to estimate the PMF hydrograph is described in Section 3.

3 METHODOLOGY

3.1 Peak Flow Estimation

The estimation of PMF peak flows can be obtained by three simplified methods in Ontario, such as 1) empirical equation (Zhou, 2023), 2) Statistical method (Zhou and Sankar 2025), and 3) Creager equation (Creager, 1945).

3.1.1 Empirical Equation

In 2023, Zhou developed an empirical equation for the estimation of PMF peak flows in Ontario using a regional approach. Based on 92 PMF peak flows estimated for dam sites in Ontario, the equation with the following form was obtained:

$$Q_{PMF} = 12.8312DA^{0.63564} \qquad (1)$$

Where Q_{PMF} is the PMF peak flow in m^3/s, DA is the drainage area in km^2. The regression equation has a $R^2 = 0.863$ and adjusted $R^2 = 0.861$. This equation has been accepted by the Ontario Ministry of Natural Resources (MNR) for the quick estimation of PMF peak flows for some of their dam sites. This empirical equation can be applied to sites where a quick peak of PMF is required and there are no available streamflow records.

3.1.2 Statistical Method

This method was developed for a site where there are long term flow records. Statistics of historical stream floods can be used for the estimation of PMF. The first step is to do the statistical assessment of the historical flood time series, the second step is to obtain the mean ($Q_{p,mean}$) and standard deviation (Std_p) of the peak flows, the third step is to estimate the frequency factor of the PMF (K_{PMF}). Zhou and Sankar (2025) found that this factor can be defined by an empirical equation calculated as a function of the historical average peak flow ($Q_{p,mean}$) of a site as follows:

$$K_{PMF} = 112.4514Q_{p,Mean}^{-0.34974} \qquad (2)$$

Where, K_{PMF} is the frequency factor for PMF estimation and $Q_{p,mean}$ is the mean peak flow (in m^3/s) estimated by the statistics of the site. Then the peak flow of the PMF can be calculated by:

$$Q_{PMF} = Q_{p,mean} + K_{PMF}Std_p \qquad (3)$$

Where Q_{PMF} is the peak flow of the PMF event (m^3/s), Std_p is the standard deviation of the peak flow statistics, and K_{PMF} is the frequency factor defined by equation (2).

3.1.3 Creager Equation

The Creager equation was derived by Creager et. al. (1945) and has been used as a method to validate the PMF peak flow used in many engineering works. Zhou (2023) found that all of the 92 PMF peak flows previously estimated in Ontario sites fall into the Creager curves with the coefficient C value between 5 to 45. For this reason, the peak flow estimated by the Creager equation with C value between 5 and 45 could be viewed as a good approximation of PMF peak flow for a site. The Creager equation has the following form:

$$Q_{PMF} = 46\ C\ DA^{0.984DA^{-0.048}} \quad \text{(original equation in imperial units)} \qquad (4)$$

Where drainage area DA is in $mile^2$ and Q_{PMF} is the peak of the PMF flow in ft^3/s.
This equation can be expressed as

$$Q_{PMF} = 1.303 * C * (0.386 * DA)^{0.936DA^{-0.048}} \quad \text{(in SI units)} \qquad (5)$$

Where DA is in km^2 and Q_{PMF} is in m^3/s.
Using an average C value of 25 can provide a reasonable first approximation of the Q_{PMF} in Ontario.

3.2 Relationship between Peak Flow and Flood Volume

As has been discussed previously, peak flow is only one of the variables that describes a PMF event. For dam safety assessment sites with storage reservoirs, the peak flow, flood runoff volume and the shape of the hydrograph are needed. Based on the database of 396 streamflow stations, the historical maximum flood peak flows and their corresponding flood volumes were obtained. A relationship between the maximum peak flows and the peak flood volumes was then derived as follows:

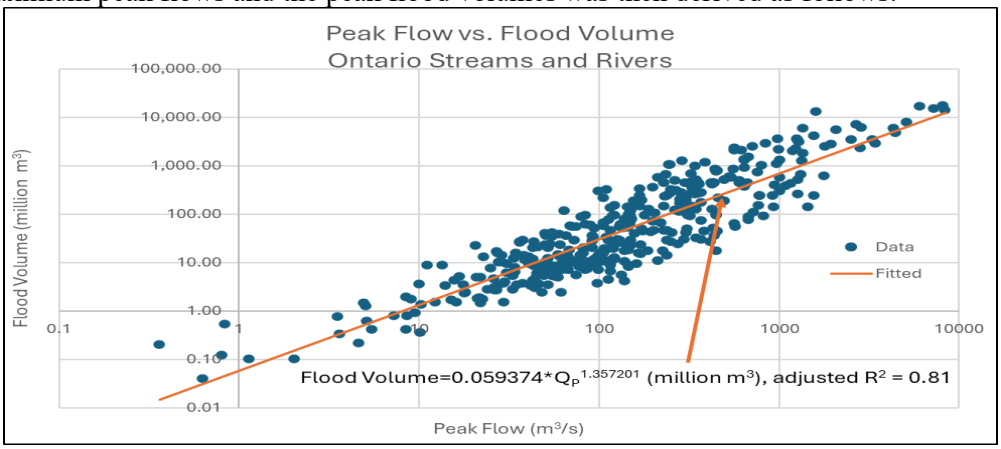

Figure 3 Relationships between historical maximum Peak Flow and Flood Volume (396 stations)

$$Vol_{p,Max} = 0.059374 Q_{p,Max}^{1.357201} \qquad (6)$$

Where $Vol_{p,Max}$ is the peak flood volume in million m^3 and $Q_{p,max}$ in m^3/s for the historical maximum peak flood. The regression has a $R^2 = 0.9$ and an adjusted $R^2 = 0.81$ which means that there is a strong relationship between the peak flow and flood volume in Ontario streams. The relationship is plotted in Figure 3.

3.3 Time to Peak

Another important factor in the determination of PMF and IDF hydrographs is time to peak. This variable in principle is a function of drainage area, basin land use, density of channel network, the main channel geometry, slope, roughness and bed materials. A statistical analysis of time to peak to flood duration ratio, T_p/D, was performed for the 396 Ontario stream's historical flood events. The results are presented in Table 2 and Figure 4. Referring to Table 2, most of Ontario stream have T_p/D ratio between 0.4 to 0.45 (81 stations). More than 60% of the stations have T_p/D ratio between 0.25 to 0.50. This indicates that the peak floods are mainly front loaded (i.e. the peak flow occurs in the first half of the flooding process). This table can be used to guide the selection of T_p/D ratio in extreme flood analysis. Therefore, it is reasonable to select a T_p/D ratio between 0.25 to 0.50 for ungauged locations.

Table 2 Tp/D Ratio Distribution (396 Stations)

Tp/D range		Number of Stations	Percentage %	Cumulation %
0.20	0.25	27	6.8	6.8
0.25	0.3	56	14.1	21.0
0.30	0.35	46	11.6	32.6
0.35	0.4	63	15.9	48.5
0.40	0.45	81	20.5	68.9
0.45	0.5	62	15.7	84.6
0.50	0.55	17	4.3	88.9
0.55	0.6	23	5.8	94.7
0.60	0.65	9	2.3	97.0
0.65	0.7	9	2.3	99.2
0.70	0.75	2	0.5	99.7
0.75	0.8	1	0.3	100.0

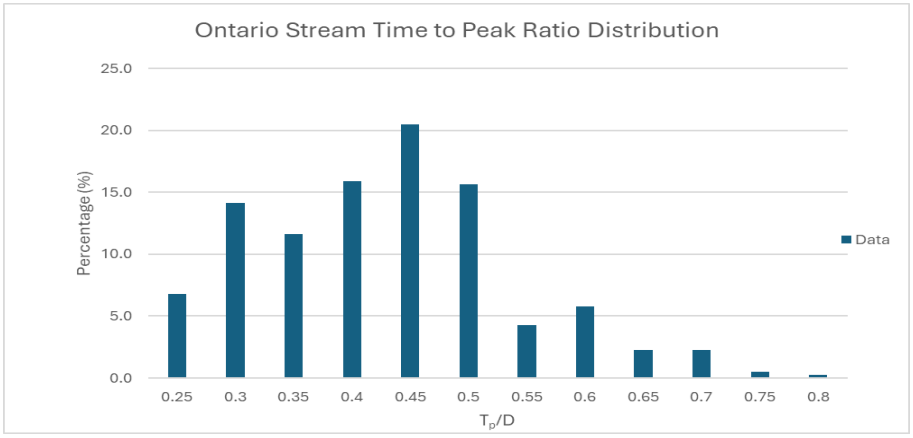

Figure 4 Time-to-Peak Distribution (396 Ontario Streams)

However, for gauged sites, the time-to-peak/flood duration (T_p/D) can be determined by historical data.

The total duration, D, can be estimated by dividing the flow volume by the peak flow using a triangular hydrograph, Figure 5**.**

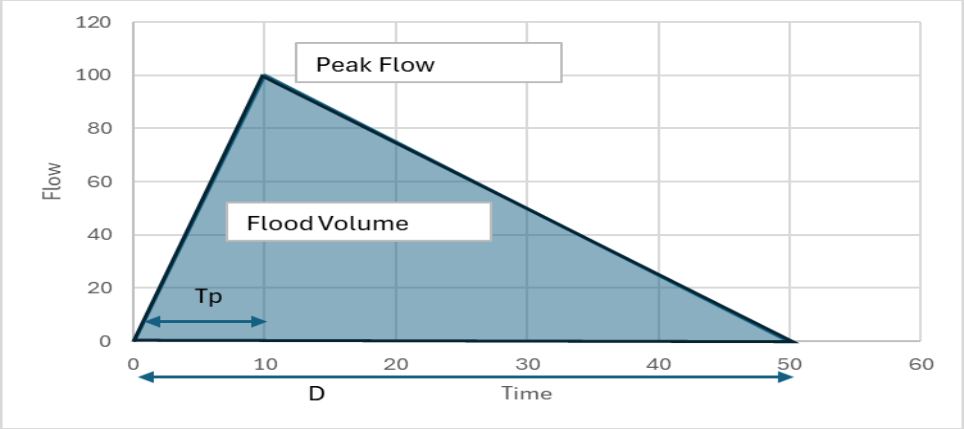

Figure 5: Derivation of D, Time of Flood Duration

3.4 PMF Hydrograph Derivation

In sections 3.1, 3.2, and 3.3 three of the important variables, peak flow Q_{PMF}, flood volume Vol_{PMF}, and T_p, time to peak were estimated. This section discusses the remaining steps for fully defining the shape of the PMF hydrograph using these variables.

There have been numerous studies in the development of design flood hydrographs. The use of statistical distribution functions in a synthetic design flood hydrograph has been widely accepted as a general way of representing design flood processes. Probability distributions employed for this purpose include Gamma distribution (Yue, et. al. (2002), Bhunya et. al. 2003), Weibull Distribution (Bhynya, et. al. (2007), Log-normal (Bhattacharjya, 2004), Beta distribution (Johnson and Kotz 1970), and other types of distributions. Rai and Singh (2008) summarized the method of parameter estimation for these probability distributions given the time-to-peak (T_p) and the peak flow (Q_p). All of these probability distributions can be applied for synthetic design flood hydrograph representations. However, based on the simulation results, the goodness-of-fit to the natural flood hydrographs to match the peak flow, total runoff volume and the shape by these probability distributions are not consistent. For some river's data, the fittings are acceptable. But for other rivers, the fittings are poor. This might be due to the fact that the parameter estimations are only based on time to peak (T_p) and peak flow (Q_p), while the total flood volume was not considered.

Reitz and Kreps (1945) developed a general hydrograph model that can be used for the estimation of design flood hydrographs. Their design hydrograph consists of two portions. For time steps before the time-to-peak (T_p), the hydrograph follows:

$$Q_t = Q_p sin^2(\frac{\pi t}{2T_p}) \qquad \text{for } t \leq T_p \qquad (7)$$

And for time after the time to peak T_p:

$$Q_t = \exp(-\alpha(t - T_p)) \qquad \text{for } t > T_p \qquad (8)$$

The Reitz and Kreps model has only one parameter α and α can be first estimated by the time to peak, peak flow and flood volume (Strupczewski et. al. 2011) as:

$$\alpha = \frac{2Q_p}{2Vol - Q_p T_p} \qquad (9)$$

Where Q_p is the peak flow (m^3/s), Vol is the flood volume (m^3) and T_p is in seconds or hour. Normally parameter α obtained by equation 9 requires adjustments given Q_p, T_p and Vol of the flood so

that the integrated total volume under the hydrograph equal to the given volume (Vol). It was found that the Reitz and Kreps model can fit the general shape of historical maximum flood hydrographs in Ontario well. Figure 5 shows one example of the recorded and fitted flood hydrographs for station 02MB006. This station has flow records from 1970 to 2022. The historical maximum flood occurred in 2017 with a peak flow of 55.2 m^3/s (55.0 m^3/s after baseflow removal). The total flood volume in the 7 days (approximately 150 hours) is estimated to be about 1.04 million m^3. The time-to-peak occurred on the third day or about 50 hours after the beginning of the flood. Figure 6 presents the comparison of the recorded and fitted flood hydrographs.

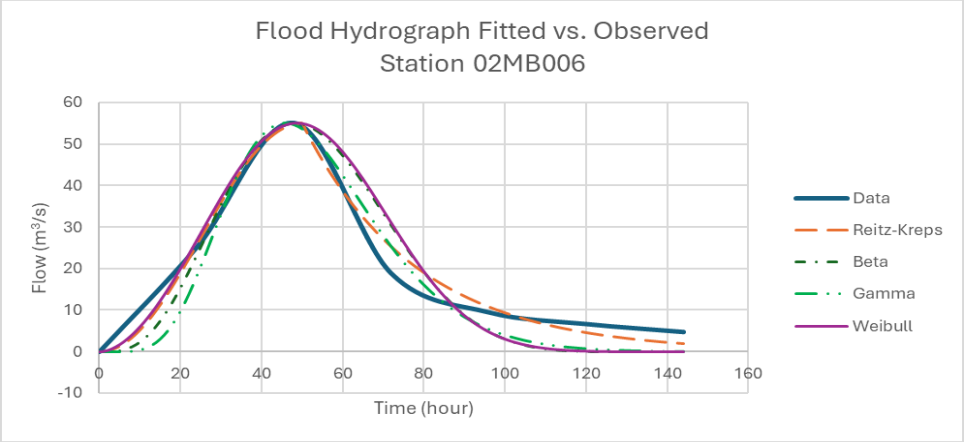

Figure 6 Comparison of Recorded and Fitted Historical Maximum Flood Hydrographs using Various Models

It can be seen that the shape of the flood hydrograph was simulated well by the Reitz and Kreps design hydrograph model, especially from the start of the hydrograph up to the peak flow. Between 62 hours to 108 hours the two hydrographs show some deviations, however the total volumes matched very well.

The flood hydrographs derived from equations 7, 8 and 9 require baseflow adjustments. Baseflow is not directly generated from the excess rainfall during a storm event. The baseflow portion can be estimated based on baseflow index (BFI). A constant baseflow during a flood event, see Figure 2 for an example, can be used and added into the PMF hydrograph.

The comparisons of goodness-of-fitting shown in Figure 6 show that the Reitz-Kreps model fits the data best. The other distributions do not work well for the tail area. But all of the models show reasonable agreement with the peak flow. Overall, the Reitz-Kreps model is recommended for use for streams in Ontario. However, the other types of models (Beta and Gamma) can be applied to create a flood hydrograph depending on conditions and response observed at the site of interest.

4 SUMMARY OF PMF DERIVATION

Based on the methodology described in Section 3, the PMF hydrograph derivation procedure is summarized below:

A) Determination of project drainage area,

B) Estimation of PMF peak flow. Depending on the availability of data, this can be undertaken by:

B.1) If the site does not have any streamflow records, the PMF peak flow are calculated by Zhou's empirical equation (equation 1) or Creager Curve (equation 5)

B.2 If the site has reliable streamflow records, the method described by Zhou and Sankar (2025) or equation 2 and equation 3, or the empirical equation and Creager equation

C) Estimate the flood runoff volume using equation 6

D) Estimate the time to peak T_p/D

E) Calculation of the PMF hydrograph using equations 7, 8 and 9. It shall be noted that equation 9 is only an approximation of the parameter α. α shall be adjusted by setting the difference between the given flood volume and the volume under the hydrograph to zero through changing α value by iterations.

The flood hydrograph developed following the procedure provides the full information for PMF flood (i.e. peak flow, time to peak, flood hydrograph for the entire duration.

5 CONCLUSIONS

In Ontario dam safety assessments, a PMF is needed determine the risk level of a dam to meet regulatory requirements. However, PMF determination has proven to be a difficult task with respect to technical effort and budget limitations. Currently, a lack of suitable methods to derive the PMF hydrograph is still a problem faced by the engineers.

In the past, there were a few methods for PMF peak flow estimation. However, peak flow alone does not fully define the PMF, especially for dam sites with considerable storage capacity. Other variables such as time to peak, shape of the flood hydrograph and the total volume of flood are also important.

This paper described a complete method to provide relatively accurate but quick techniques for PMF hydrograph development for Ontario streams, based on a database with 396 stations across the province.

An equation between peak flow and flood volume was constructed based on the data sets of the historical maximum floods.

Once both the peak flow and the flood volume are determined for the PMF event, a flood hydrograph can be calculated based on the Reitz and Kreps (1945) model or other suitable methods.

It shall be noted that the hydrograph needs to be adjusted by adding the baseflow into the time series.

A sensitivity analysis will help to determine the impacts of changing some of the variables, such as peak flow, flood volume and time-to-peak, in the PMF hydrograph to the safety of dams.

6 REFERENCES

Abrahamson B. T. and Pentland R. S., 2010, Probable Maximum Flood Estimators for British Columbia, Prepared For: Agriculture and Agri-Foods Canada Agri-Environment Services Branch, ©HER MAJESTY THE QUEEN IN RIGHT OF CANADA (2010) as represented by the Minister of Agriculture and Agri-Food.

Beven, K.J. Rainfall-Runoff Modelling: The Primer; John Wiley & Sons: Hoboken, NJ, USA, 2011

Bhunya, P.K.; Mishra, S.K.; Berndtsson, R. Simplified two parameter gamma distribution for derivation of synthetic unit hydrograph. J. Hydrol. Eng. **2003**, 8, 226–230.

Bhunya, P.K.; Berndtsson, R.; Ojha, C.S.P.; Mishra, S.K. Suitability of gamma, chi-square, weibull and beta distributins as synthetic unit hydrographs. J. Hydrol. **2007**, 334, 28–38.

Bhattacharjya, R.K. Optimal design of unit hydrographs using probability distribution and genetic algorithms. Sadhana **2004**, 29,499–508.

Canadian Dam Association, 2013, Dam Safety Guidelines, Canadian Dam Association

Chowdhary, H., Escobar, L. and Singh, V.P., 2011, Identification of suitable copulas for bivariate frequency analysis of flood peak and flood volume data, Hydrology Research, 42. 2-3

Committee on Modernizing Probable Maximum Precipitation Estimation, 2024, Modernizing Probable Maximum Precipitation Estimation, National Academies Press, Washington, DC.

Flood Estimation Handbook, 1999, Centre for Ecology and Hydrology, Wallingford, Oxfordshire (formerly the Institute of Hydrology). December 1999. ISBN 0 948540 94 X.

Gaál, L., Szolgay, J., S. Kohnová, K. Hlavčová, J. Parajka, A. Viglione, R. Merz & G. Blöschl, Dependence between flood peaks and volumes: a case study on climate and hydrological controls, 2015, Hydrological Science Journal, Volume 60, 2015 - Issue 6

Gräler, B., et al., 2013. Multivariate return periods in hydrology: acritical and practical review focusing on synthetic designhydrograph estimation. Hydrology and Earth System Sciences, 17, 1281–1296. doi:10.5194/hess-17-1281-2013

Hershfield, D. M., Estimating the probable maximum precipitation, J. Hydraulic Div. Am. Soc. Civ. Eng., 87(HY5), 99-106, 1961.

Hershfield, D. M., Method for estimating probable maximum precipitation, J. Am. Waterworks Assoc., 57, 965-972, 1965.

Johnson, N. L., and Kotz, S. ~1970!. Distributions in statistics: Continuous univariate distribution, Vol. II, Wiley, New York.

Moin, S. and M. Shaw (1985). "Canada/Ontario Flood Damage Reduction Program - Regional Flood Frequency Analysis for Ontario Streams", Volume 1, 2, and 3, Environment Canada, Ontario, Canada

Nathan, R. J., Weinmann, P. E. and Gato, S. A., 1994: "A quick method for estimating the Probable Maximum Flood in south-eastern Australia", I. E. Aust., National Conf. Publ. 94/15, pp.229-234.

Ontario Ministry of Natural Resources, 2011, Lakes and Rivers Improvement Act, Administrative Guide, Ontario Ministry of Natural Resources

Pan, X., Rahman, A., Haddad, K., and Ouarda, T., 2022, Peaks-over-Threshold Model, in Flood Frequency Analysis: a Scoping Review, Stochastic Environmental Research and Risk Assessment (2022) 36:2419–2435 https://doi.org/10.1007/s00477-022-02174-6

Rai, R.K., and Singh, V.P., 2009, Evaluation of the Adequacy of Statistical Distribution Functions, for Derivation of Unit Hydrograph, Water Resources Management, 2009, 23:899-929, DOI 10.1007/s11269-008-9306-0

Reitz, W.; Kreps, H. Näherungsverfahren zur Berechnung des Erforderlichen Struraumes für Zwecke des Hochwasserschutzes; Deutsche Wasserwirtschaft: Hennef, Germany, 1945

Strupczewski, W. G., Bogdanowicz, E. and Kochanek, K. 2013, Discussion of "Synthetic Design Hydrographs Based on Distribution Functions with Finite Support" by Francesco Serinaldi and Salvatore Grimaldi, J. Hydrol. Eng., 2013, 18(1): 126-129

World Meteorological Organization, 2009, Manual on Estimation of Probable Maximum Precipitation (PMP), WMO-No. 1045, Chairperson, Publications Board World Meteorological Organization (WMO)

Zhou, D. and C. Donnelly, 2006, Copulas: a new way for inflow design flood determination, Canadian Dam Association 2015 Conference, Quebec City Canada

Zhou, D. 2015, The difference between univariate and bivariate flood frequency analysis models for the inflow design flood in dam safety analysis, Canadian Dam Association 2015 Conference, Mississauga Ontario

Zhou, D. 2023, An Empirical Equation for Estimation of Probable Maximum Floods in Ontario, 56th International Conference on Water management Modeling (ICWMM2023)

Zhou, D and Sankar, D., 2025, A Statistical Method Similar to the Hershfield Procedure for Estimating Probable Maximum Flood in Ontario, 58th International Conference on Water management Modeling (ICWMM2025)

Yue, S.; Taha, B.M.J.; Bobee, B.; Legendre, P.; Bruneau, P. Approach for describing statistical properties of flood hydrograph. J. Hydrol. Eng. 2002, 7, 147–153.

ICFM 10
Adapting to Global Change:
Innovative Approaches to Flood Management and Resilience
May 20-22, 2026 | Western University, London, Ontario, Canada

Mosaic Model Map (M³): Hong Kong's Cutting-edge Solution for Real-time City-wide Flood Risk Visualisation

Leonard Chek Yuet Wong[1], **Wah Sang Eddy Chiang**[1],
Wing Sze Winsy Choi[1], **And Chi Hung Philip Tsang**[1]
Drainage Services Department,
The Government of the Hong Kong Special Administrative Region of the People's Republic of China,
8/F, Drainage Services Tower, 8 Ying Wa Street, Cheung Sha Wan, Kowloon, Hong Kong[1]
E-mail: wschiang02@dsd.gov.hk

ABSTRACT

Hong Kong's steep topography, rapid urbanisation, and exposure to both extreme rainfall and storm surges create one of the most challenging environments for real-time flood forecasting. Traditional hydrodynamic modelling, while physically robust, is too computationally intensive for operational use during fast-evolving events. The Drainage Services Department (DSD) of the Hong Kong Special Administrative Region Government of the People's Republic of China, has therefore developed the Mosaic Model Map (M³), an innovative system that achieves territory-wide, street-level flood visualisation in near real time by pre-running thousands of high-resolution 1D/2D scenarios and dynamically selecting and mosaicking the most relevant results. This paper presents the system architecture, its three-stage methodology (pre-run, scenario mapping, mosaic compilation), implementation details, and its proven operational value as exemplified during Super Typhoon Ragasa in September 2025.

KEYWORDS: Flood Risk Mapping, GIS, Hydrodynamic Modelling, Drainage Master Plan, Hydrometric Information System, Real-time Visualisation, Flood Forecasting

1 INTRODUCTION

Hong Kong receives an average annual rainfall of approximately 2,400 mm, concentrated mainly in the wet season from May to September. The combination of steep catchments, limited natural storage, and extensive impervious cover results in extremely short times of concentration—often less than one hour. When heavy rain coincides with high astronomical tides or tropical-cyclone-induced storm surges, compound flooding develops rapidly, leaving little margin for conventional forecasting approaches.

Despite substantial drainage upgrades since the establishment of the DSD in 1989 and the progressive implementation of Drainage Master Plan Review (DMPR) recommendations, the intensification of extreme weather under climate change continues to test the city's resilience. Effective real-time forecasting has remained challenging because detailed 1D/2D hydrodynamic simulations of the entire territory typically require several hours—far exceeding the available decision window.

2 CHALLENGES OF REAL-TIME FLOOD FORECASTING IN HONG KONG

In Hong Kong, real-time flood forecasting has historically been constrained by four principal factors. First, the city's extremely rapid catchment response means that even moderate rainfall can lead to flash flooding with minimal warning time. Second, rainfall patterns are highly localised due to convective storms influenced by complex topography, making uniform predictions unreliable. Third, as a coastal city,

Hong Kong frequently experiences coupled flooding from simultaneous rainstorms and elevated sea levels, requiring models that integrate hydrological and oceanographic dynamics. Fourth, the computational demands of territory-wide coupled 1D/2D hydrodynamic modelling prohibit on-the-fly simulations during storms, as runtimes often exceed the critical response window. Flood forecasting is one crucial topic where different methodologies were proposed and discussed as it enables timely predictions to mitigate flood impacts and may allow timely and appropriate follow up measures (Byaruhanga et al. 2024). The above-mentioned challenges render traditional approaches impractical for operational use.

3 LEVERAGING AVAILABLE ASSETS FOR ENHANCED FLOOD FORECASTING

The M³ system capitalises on decades of prior investment in stormwater planning and monitoring infrastructure since the 1990s. In particular, the detailed 1D/2D hydrodynamic models from twelve comprehensive DMPR studies provide a consistently calibrated, high-resolution representation of Hong Kong's territory-wide drainage networks and overland flow paths.

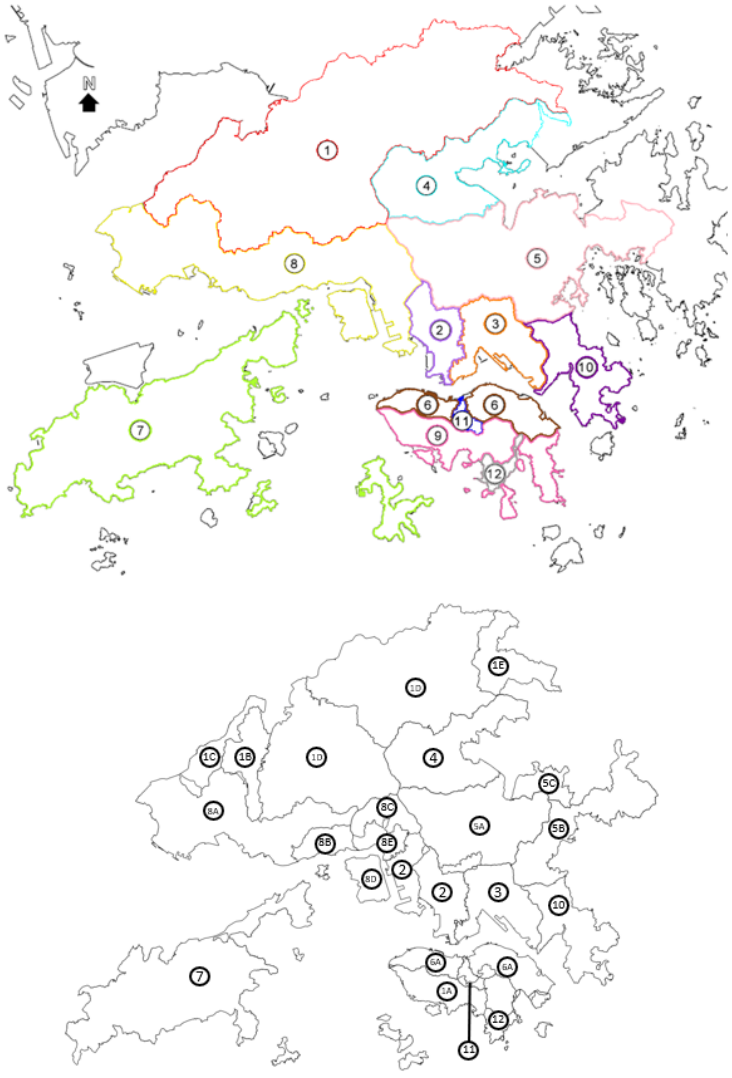

Drainage Master Plan Review (DMPR) Studies	
1	Yuen Long & North District
2	West Kowloon
3	East Kowloon
4	Tai Po
5	Shatin & Sai Kung
6	Northern Hong Kong Island
7	Lantau & Outlying Islands
8	Tuen Mun, Tsuen Wan & Kwai Tsing
9	Southern Hong Kong Island
10	Tseung Kwan O
11	Happy Valley

M³ Catchments	
1A	Yuen Long Town & Kam Tin
1B	Tin Shui Wai
1C	Lau Fau Shan
1D	North District
1E	Sha Tau Kok
2	West Kowloon
3	East Kowloon
4	Tai Po
5A	Shatin
5B	Sai Kung
5C	Ma On Shan
6A	Northern Hong Kong Island - East
6B	Northern Hong Kong Island - West
7	Lantau & Outlying Islands
8A	Tuen Mun
8B	Sam Tseng
8C	Tsuen Wan
8D	Tsing Yi
8E	Kwai Chung
9	Southern Hong Kong Island
10	Tseung Kwan O
11	Happy Valley
12	Repulse Bay & Tai Tam

Figure 1 –23 M³ catchments evolved from the existing models developed under 12 drainage planning studies

These models, built with InfoWorks ICM, utilises 1D and 2D finite volume models based on well-established hydraulic principles, such as the St. Venant equations, and Navier-Stokes equations (Autodesk, 2025). These models provide detailed hydrodynamic analysis with a holistic consideration of various factors, including rainfall, downstream sea-water levels, and specific catchment characteristics such as topography and land use. These models incorporated the latest infrastructure upgrades and climate-change allowances. Complementing these are the real-time observations from the Hydrometric Information System (HIS), a dense telemetric network established in the 1990s that comprises more than 300 gauging with sensors including rain gauges, river level stations, and tide gauges delivering data every minute. Additionally, high-resolution radar-based rainfall nowcasts (updated every 6 minutes) and combined astronomical tide plus storm-surge predictions are sourced from the Hong Kong Observatory, ensuring that M³ operates with reliable meteorological inputs.

4 METHODOLOGY

The system is built by a three-step mythology with model pre-run, scenario mapping and mosaic compilation as detailed in following sub-sections and as illustrated in Figure 2.

4.1 Model Pre-run

Hong Kong is divided into 23 hydrological catchments following DMPR boundaries (Figure 1). For each catchment, a matrix of 12 rainfall intensities (30–160 mm/h) × 20 boundary water levels (2.0–6.2 mPD) was simulated offline, yielding more than 5,000 scenarios territory-wide. Flood extents and depths from each simulation were exported as GIS shapefiles and stored as “mosaic tiles” in a relational database.

4.2 Scenario Mapping

Every six minutes, the system automatically evaluates current and forecasted hydrometeorological conditions across all 23 catchments to produce four standard outputs: one real-time map and three short-range forecast maps at 60, 90, and 120 minutes ahead. Real-time rainfall intensity is derived from surrounding HIS rain gauges, whereas forecast intensities for the forward horizons are based on the statistical distribution of the Hong Kong Observatory’s high-resolution gridded nowcast data, thereby accounting for the highly localised nature of the upcoming rainstorm. Tide and storm-surge levels are similarly derived from real-time HIS tide gauges and Observatory astronomical-plus-surge predictions. For each catchment and each time horizon, the mosaic tile whose rainfall intensity class and tide/surge class most closely matches — or deliberately exceeds to prioritise safety — the observed or forecasted values is selected.

In addition to this fully autonomous mode, M³ offers a manual “what-if” capability that is particularly valuable for medium- to longer-range planning. Authorised users may specify any custom rainfall hyetograph (uniform, spatially varying, or a full design storm) and any tide/surge boundary condition, including multi-day ensemble surge forecasts issued several days in advance. The system then identifies and retrieves the corresponding pre-computed tiles for all 23 catchments according to the same conservative matching logic used in the autonomous mode.

4.3 Mosaic Compilation

Once the appropriate tiles have been selected — whether through the automatic six-minute cycle or through a user-defined manual "what-if" scenario — the 23 individual catchment tiles are automatically merged in QGIS to create a seamless territory-wide flood risk map. The resulting GIS layers (flood extent and depth) are instantly published on the internal web portal, together with supporting layers such as forecasted rainfall contours and tide graphs (Figure 5 and Figure 3).

4.4 Implementation

Its continuous operation is driven by a Python-based module known as the "M³ Integrated Data Keeper", which continuously harvests and harmonises inputs from the HIS and the Hong Kong Observatory. The core processing engine, running within QGIS on standard office workstations, handles scenario selection and mosaic compilation, completing each full cycle well within the six-minute update interval. Since its full deployment in early 2025, M³ has been providing 24/7 real-time flood risk visualisation, integrated directly into DSD's Emergency Control Centre workflows.

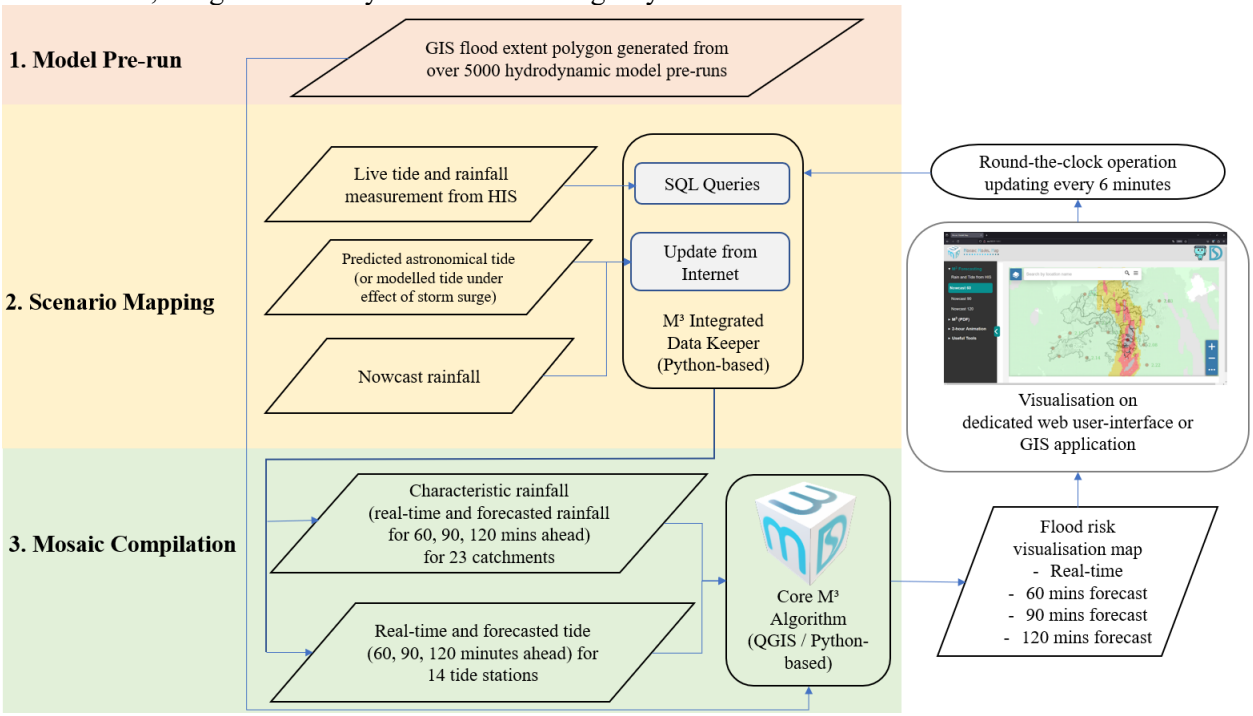

Figure 4 - Schematic workflow of the M³ system under the autonomous mode

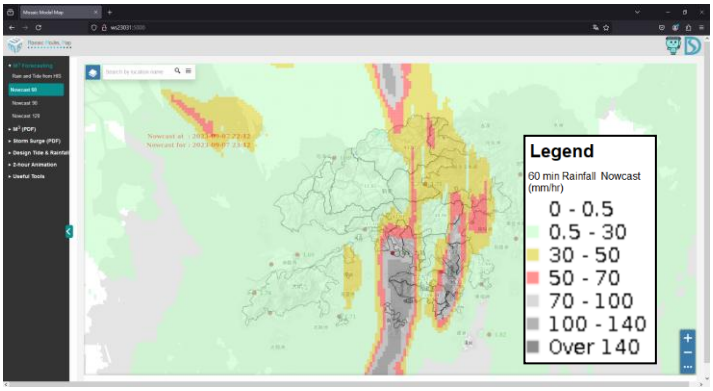

Figure 5 – Screenshot of M³'s user interface accessed through web browser, showing the city-wide layers of modelled flood extent, forecasted rainfall contour, predicted tide levels and flood extent at one glance

Figure 6 – When hiding layers on gridded rainfall forecast and tide levels, modelled flood extent at different levels of modelled flood depth may be more clearly displayed

5 OPERATIONAL APPLICATION: SUPER TYPHOON RAGASA (SEPTEMBER 2025)

Since its official deployment in early 2025, M³ has been continuously supporting DSD emergency operations throughout an exceptionally severe wet season. Hong Kong experienced multiple black rainstorm warnings, with August 2025 recording the highest monthly rainfall since records began in 1884 (>500 mm) and a daily peak of 355.7 mm on 5 August 2025. During these intense rainstorm events, M³'s six-minute autonomous updates provided real-time flood extent forecasts, enabling rapid deployment of up to 180 emergency teams and pumping robots to more than 240 flood-prone and reported locations.

The system's most widely publicised application occurred during Super Typhoon Ragasa, which passed ~120 km south of Hong Kong on the morning of 24 September 2025, triggering Hurricane Signal No. 10 — only the second such signal of the year. The typhoon brought over 200 mm of rainfall and a storm surge peaking at 3.4 m above Chart Datum at Quarry Bay, comparable to Super Typhoon Hato (2017). The manual "what-if" mode was intensively used with ensemble surge forecasts to generate worst-case inundation scenarios days in advance. In view of Super Typhoon Ragasa edging closer to the coast of Guangdong, the Authorities held an inter-departmental joint press conference on 22 September 2025 to inform the public of areas with heightened risk for major flooding with the use of the M³ flood risk maps. The maps clearly highlighted low-lying areas or windy residential areas with higher risks including Tai O, Lei Yue Mun, Tai Po and Yuen Long etc., prompting pre-emptive measures that included increased emergency crews, pre-positioned pumping robots, additional sandbag distribution, temporary shelter arrangements, and early closure of vulnerable underpasses. These actions, taken more than 24 hours before peak surge, significantly reduced flooding impacts across the territory.

6 COMPARISON WITH OTHER FORECASTING APPROACHES

Real-time flood forecasting globally has evolved through several paradigms, each addressing the tension between computational speed and physical accuracy. Data-driven models, particularly artificial neural networks (ANN) and other machine-learning techniques, have gained significant traction in recent years due to their ability to deliver rapid predictions from historical data patterns (Byaruhanga et al., 2024). These approaches excel in environments with abundant training datasets and can achieve sub-minute runtimes, making them suitable for large-scale applications. However, they often require extensive calibration, specialised data-science expertise, and substantial computational resources for training.

Moreover, ANN models can exhibit reduced transparency and reliability during extreme events that fall outside the training envelope, potentially leading to opaque decision-making in high-stakes scenarios.

In contrast, physically-based hydrodynamic models grounded in equations like Saint-Venant equations provide interpretable, robust simulations but at the cost of lengthy runtimes. A notable hybrid solution is the pre-computed inundation library approach demonstrated by Bhola et al. (2018) for the 11.5 km² catchment in Kulmbach, Germany. Their framework refreshed flood forecasts every three hours by matching observed discharge rates to a pre-run library of MIKE-11/MIKE-21 simulations, achieving operational efficiency without sacrificing physical fidelity. This method proved effective for a single, relatively small catchment but highlighted scalability challenges for larger, heterogeneous urban areas.

The M³ system builds directly on this pre-run philosophy while addressing its limitations through several key advancements. It extends coverage from a single catchment to an entire megacity encompassing 23 diverse hydrological units, enabling true territory-wide analysis. Unlike the discharge-focused matching in Kulmbach, M³ uses direct rainfall and tide levels as indices, which are more readily available and responsive in real time, particularly for compound flooding scenarios. Furthermore, by leveraging high-resolution gridded nowcasts and a conservative percentile-based selection, M³ captures spatial rainfall variability more effectively. Most critically, its six-minute refresh rate aligns with Hong Kong's ultra-rapid catchment dynamics, providing actionable insights during the narrow warning windows of flash floods. The combination of physically-based modelling, territory-wide coverage, compound tide-rainfall effects, and a six-minute update cycle appears unique among currently operational systems, marking M³ as an important contribution to real-time flood risk visualisation.

7 LIMITATIONS AND ONGOING DEVELOPMENTS

Despite its strengths, the M³ system incorporates a deliberately conservative scenario-selection logic that rounds up to the nearest higher rainfall or tide class, which may occasionally result in slight overestimation of flood risks to prioritise safety. The underlying DMPR models, while regularly updated for major infrastructure changes, are primarily planning-grade and may not immediately reflect minor site alterations, such as temporary construction or natural sediment shifts. Additionally, the system focuses on capacity-based flooding and does not yet account for localised incidents like drainage blockages from debris, which are common triggers in urban Hong Kong. Forecast accuracy remains contingent on the inherent uncertainties in short-range rainfall nowcasts and storm-surge predictions, particularly during tropical cyclones. To address these, ongoing developments include the integration of IoT-based blockage detection sensors, incorporation of higher-resolution digital twins for dynamic model updates, and hybrid enhancements using machine learning to refine tile selection without compromising physical interpretability.

8 CONCLUSION

The Mosaic Model Map (M³) demonstrates that real-time, physically-based, territory-wide flood visualisation is achievable without requiring supercomputing infrastructure or entirely new data ecosystems. By reorganising existing high-quality hydrodynamic models into a pre-run mosaic framework matched against live observations and forecasts, M³ overcomes the four fundamental barriers—rapid response times, rainfall localisation, compound effects, and computational delays—that have long hindered operational flood forecasting in Hong Kong. Its proven performance during Super Typhoon Ragasa illustrates tangible benefits for emergency preparedness, resource deployment, and public communication, ultimately contributing to reduced flood impacts on communities and infrastructure. The methodology is inherently scalable and offers a cost-effective blueprint for other steep, densely developed coastal cities worldwide grappling with intensifying climate-driven flood risks.

9 ACKNOWLEDGEMENTS

This work is supported by the DSD, the Government of the Hong Kong Special Administrative Region of the People's Republic of China. We also acknowledge the Hong Kong Observatory for continuous support in making available the tide data and high-resolution rainfall forecast to make this project possible.

REFERENCES

Autodesk (2025) Understanding the ICM simulation engine. Available at: https://www.autodesk.com/learn/ondemand/tutorial/understanding-the-icm-simulation-engine (Accessed: 12 December 2025).

Bhola, P.K.; Bacci, M.; Barroco, J.; Ribeiro, L.; Fernandes, L.; Leandro, J. (2018). *Flood inundation and flood depth mapping using ensemble of global numerical weather prediction models: A case study for Super Typhoon Mangkhut (2018). Geosciences, 8(9), 346. https://doi.org/10.3390/geosciences8090346*

Byaruhanga, N.; Kibirige, D.;Gokool, S.; Mkhonta, G. (2024) *Evolution of Flood Prediction and Forecasting Models for Flood Early Warning Systems: A Scoping Review.* Water 2024, 16, 1763. https://doi.org/10.3390/w16131763

Chui, S. K.; LEUNG, John K. Y.; CHU, C. K. (2006) *The development of a comprehensive flood prevention strategy for Hong Kong. International journal of river basin management.* Available at: https://www.dsd.gov.hk/EN/Files/Technical_Manual/technical_papers/LD0601.pdf

Drainage Services Department (2019) *Sewerage and flood protection : drainage services, 1841-2018.* Hong Kong: Drainage Services Department.

Web sites:

Web-1: https://www.dsd.gov.hk/EN/Files/Technical_Manual/technical_manuals/Stormwater_Drainage_Manual_Eurocodes.pdf, consulted 12 December 2025.

Web-2: https://www.dsd.gov.hk/EN/Flood_Prevention/Long_Term_Improvement_Measures/Drainage_Master_Plan_Studies_and_Drainage_Studies/index.html, consulted 12 December 2025.

Web-3: http://www.dsd.gov.hk/EN/Flood_Prevention/Our_Flooding_Situation/Flooding_Problems/index.html, consulted 12 December 2025.

Web-4: https://www.dsd.gov.hk/EN/What_s_New/What_s_New/news31014.html, consulted 12 December 2025.

Chapter 2 - Flood risk assessment, data and modeling

2.2 Advanced flood modelling

ICFM 10
Adapting to Global Change:
Innovative Approaches to Flood Management and Resilience
May 20-22, 2026 | Western University, London, Ontario, Canada

Flash flood assessment for economic losses in an urban basin of the São Paulo metropolitan region – Brazil

Marina Batalini de Macedo[1*], Priscilla Mota Costa[1], Samuel Marcos Tavares[1], Marcos Roberto Benso[2], Maria Clara Fava[3], Anaí Floriano Vasconcelos[4], Beliana Cavalcante Sawada de Carvalho[5], Javier Tomasella[5]

Federal University of Itajubá, Institute of Natural Resources, Itajubá, Brazil [1]

University of São Paulo, Superior School of Agriculture "Luiz de Queiroz", Piracicaba, Brazil [2]

Federal University of São Carlos, Department of Civil Engineering, São Carlos, Brazil [3]

Federal University of São Carlos, Department of Environmental Sciences, São Carlos, Brazil [4]

National Institute for Space Research – Center for Weather Forecasting and Climate Studies (INPE/CPTEC), Cachoeira Paulista, Brazil [5]

*E-mail contact author: marinamacedo@unifei.edu.br

ABSTRACT

Megacities in developing countries frequently experience severe flooding, generating significant social and economic impacts. Assessing flood scenarios and their consequences is essential to support evidence-based mitigation and adaptation strategies that reduce exposure and vulnerability. This study evaluates flash-flood scenarios in the Aricanduva River catchment, located in the metropolitan region of São Paulo, Brazil. The 102.5 km² catchment is fully urbanized, highly flood-prone, and characterized by a population density of approximately 7,400 inhabitants per km², with January presenting an average monthly precipitation of 292.1 mm. The objective of this study is to estimate flood-related economic losses and quantify the socioeconomic vulnerability of the population. Flood hazard maps were generated using the CADDIES cellular automata–based hydraulic model under extreme precipitation events, employing a LiDAR-derived digital terrain model aggregated to 10 m resolution. Simulated flood extents and water depths were combined with census-based socioeconomic data and information on public infrastructure to identify exposed assets, residential units, income levels, and socioeconomic classes. Economic losses were estimated using depth–damage functions relating floodwater depth to proportional losses in buildings, contents, and infrastructure. Results indicate that losses associated with household and commercial contents represent the largest share of total damage, followed by infrastructure and structural losses. Average damages per exposed building were estimated at approximately US$ 1,244 for construction, US$ 4,089 for contents, and US$ 1,599 for infrastructure, while maximum sector-level losses reached US$ 1.27 million, US$ 2.12 million, and US$ 1.01 million, respectively. Although higher-income classes exhibit greater individual losses, total damage is concentrated in lower-income sectors due to their higher spatial prevalence, highlighting the importance of integrating high-resolution flood modelling with socioeconomic data for urban flood-risk management.

KEYWORDS: Flood damage assessment; Socioeconomic vulnerability; Megacities; Flood risk management

1 INTRODUCTION

Flood risk arises from the interaction between hazard, exposure, and vulnerability, and effective flood management therefore requires integrated assessments of these components (IPCC, 2014). In rapidly urbanizing regions, particularly in Latin America, informal settlements, weak land-use regulation, socioeconomic inequalities, and deficits in basic infrastructure significantly increase exposure and vulnerability to flooding (Der Sarkissian et al., 2022). As a result, populations in megacities such as São Paulo remain highly susceptible to recurrent hydrometeorological disasters, especially where urban expansion has outpaced the implementation of adequate mitigation and adaptation measures (UN-Habitat, 2020).

The Metropolitan Region of São Paulo exemplifies these challenges, where intense rainfall combined with dense urban occupation, topographic constraints, and widespread impervious cover results in frequent flash floods and riverine flooding (Borba et al., 2016). Within this region, the Aricanduva River catchment stands out due to its high flood recurrence and demographic density. Flood events in this catchment regularly cause population displacement, damage to infrastructure, traffic disruption, and considerable economic losses (Simas, 2017; Haddad & Teixeira, 2015), highlighting the need for detailed and spatially explicit flood hazard assessments.

Recent advances in flood modelling, supported by LiDAR-derived digital elevation models and computationally efficient algorithms, have improved the representation of flood dynamics in urban environments (Vashit & Singh, 2024). Cellular automata–based models, such as CAFlood, offer an efficient alternative for simulating flood scenarios in densely urbanized catchments, where detailed topography plays a key role in flow propagation. When integrated with socioeconomic data, these models enable the estimation of direct economic losses and the assessment of community vulnerability (Merz et al., 2010).

In this context, the Aricanduva catchment provides a valuable case study for combining high-resolution flood modelling with census-based socioeconomic information. By integrating extreme rainfall scenarios, automated hydraulic modelling, and economic loss estimation through depth–damage functions, this study contributes to a more robust understanding of flood impacts in megacities of the Global South and supports evidence-based flood-risk management and urban planning strategies.

2 METHODOLOGY

2.1 Study area

The Aricanduva catchment is located in the eastern portion of São Paulo, Brazil, covering approximately 102.5–103 km² of highly urbanized territory (Figure 1). The catchment is characterized by dense built-up areas, limited natural vegetation, and a history of recurrent flooding. These conditions make it a representative setting for studies focused on hydrological processes and flood dynamics in megacities.

The climate of the region is classified as humid subtropical (Köppen), with an average annual temperature of around 19 °C. Seasonal variability is marked: temperatures range from 17.2 °C in July to 23.5 °C in February, while rainfall varies from 32.3 mm during the dry month of August to 292.1 mm in January, the peak of the wet season (INMET, 2020). The average annual discharge of the Aricanduva River is about 5.6 m³/s, and its channel width ranges from 13.3 m near the headwaters to 18.3 m near the outlet.

In addition to its hydrological relevance, the catchment presents significant socioeconomic vulnerability. With a population density of roughly 7,400 inhabitants/km^2 (IBGE, 2022), flash flooding events pose substantial risks of displacement, injuries, and economic losses (Simas, 2017). The area is also well monitored with rainfall, streamflow, and water-level measurements collected at 10-minute intervals over a 10-year period. This extensive monitoring network provides a robust basis for detailed flood modelling and risk assessment.

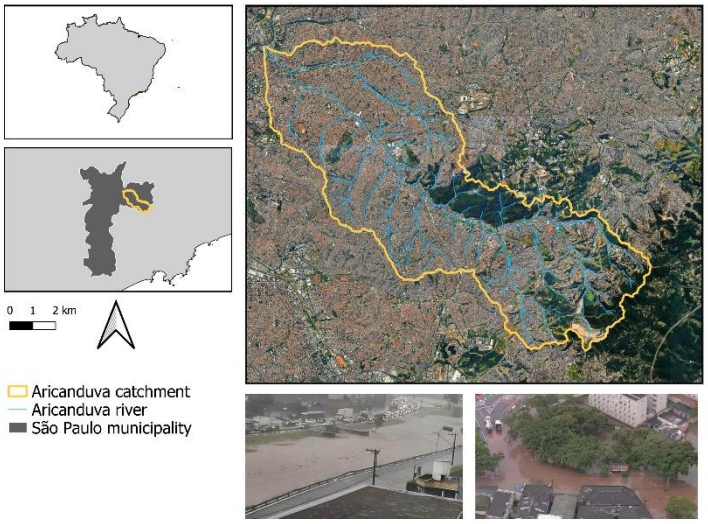

Figure 1: Aricanduva catchment location and pictures of flooding events

2.2 Flood modelling and mapping

Flood modelling for the Aricanduva catchment was conducted using hydrological time series, spatial rainfall interpolation, and two-dimensional hydraulic simulations. Hydrological data were obtained from the telemetric network of the São Paulo Metropolitan Region Flood Warning System (SAISP), which provides rainfall intensity and water level measurements at 10-minute intervals. For this study, one historical rainfall event was selected based on its magnitude and documented impacts on the catchment. The event happened on 2017-04-06, with 84 mm of total rainfall depth and 66 mm/h of peak rainfall intensity. Water depths recorded at four stream gauges distributed across the basin were used to support model assessment, while rainfall data from 12 gauges were interpolated using inverse distance weighting (IDW) with a power coefficient of 2.

Surface flooding dynamics were simulated using the Cellular Automata Dual Drainage System (CADDIES), also known as CAFLOOD a two-dimensional hydraulic model based on Weighted Cellular Automata (WCA2D). The model operates on a grid using a Von Neumann neighborhood structure and applies a ranking technique to determine the volume of water moving between cells. Flow propagation follows the diffusive-wave approximation of the Saint Venant equations combined with Manning's equation, providing a physically based upper limit for intercell flow exchange. Although the simplification omits inertial terms found in full hydrodynamic models, it offers a practical balance between accuracy and computational efficiency, particularly suitable for shallow and slowly varying flows in dense urban environments such as Aricanduva.

The model requires inputs including a digital elevation model (DEM), spatially averaged precipitation, and inflow or water-level boundary conditions. Given the catchment's 103 km² urbanized extent and high imperviousness, precipitation was aggregated to 10-minute intervals for simulation. A single Manning roughness coefficient was applied across the domain, and numerical stability parameters, such as timestep limits, tolerance thresholds, and iteration limits, were maintained at standard recommended values.

2.3 Economic valuation of affected assets and goods

The economic valuation of affected assets exposed to flooding in the Aricanduva River catchment considered damages related to building structures, goods and basic public infrastructure. To this end, data regarding hazard and exposure were integrated using geoprocessing procedures implemented in QGIS. These procedures included the extraction and association of hazard data, i.e. flood maps obtained from hydrodynamic modelling, socioeconomic indicators and the estimation of the number and type of buildings

per area, obtained from the Brazilian Census of 2022 (IBGE, 2022). The workflow was structured to integrate flood-depth raster produced by flood modelling with Census and building-footprint layers, enabling a spatially explicit assessment of economic exposure.

For the socioeconomic indicators, Census data provide information on the average household income per census sector. Based on this information, sectors were classified into socioeconomic classes according to income thresholds commonly used in Brazil. These thresholds are expressed in multiples of the national minimum wage, a legally defined monthly income reference used for socioeconomic classification. At the time of analysis, one minimum wage corresponded to approximately R$ 1,412 per month (≈ US$ 270, considering the current conversion rate of R$ 1 ≈ US$ 0.193). The resulting classes were defined as: A (more than 20 minimum wages), B (10–20 minimum wages), C (4–10 minimum wages), D (2–4 minimum wages), and E (less than 2 minimum wages). Additionally, the Census microdata allow the identification of the location and type of each building, which were aggregated at the sector level and categorized as residential or non-residential buildings by summing their occurrences within each sector.

At the end of the workflow, each census sector contained integrated information on flood-depth values, total residential and non-residential buildings, average income, associated socioeconomic class and percentage of the sector area affected by the flood.

Based on the standardized data for each census sector, the estimation of building damages was carried out by cross-referencing the affected built-up area corresponding to each socioeconomic class (standardized according to the construction type defined by NBR 12.721/2006 with the basic unit construction cost provided by the Civil Construction Industry Union (updated in March 2025) for each construction standard category (Table 1).

In addition to structural damages, economic losses associated with the contents of each building were also considered. For this purpose, we used an adaptation of the study by Cançado (2009), presented in PDAU-RMGV (2021), which establishes content costs according to socioeconomic class. These values were updated using the Extended National Consumer Price Index (IPCA) for March 2025 (Table 1).

Table 1: Values of construction and goods' content according to different economic classes

Economic class	Building standard	Category (NBR 12.721/2006)	Basic Unit Cost (US$/m²)	Content value (US$)
A	High	R1-A	677.32	26975.16
B	Normal	R1-N	543.05	11313.45
C	Low	R1-B	453.35	3487.91
D and E	Popular	RP1Q	464.05	2723.89

Finally, the estimation of the proportion of damages to buildings and their goods' contents as a function of flood depth was based on Equations 1 and 2, proposed from the work of Machado (2005) and adapted by PDAU-RMGV (2021), where h represents the flood-depth.

$$PercentualDamage_{building} = 0.0125h + 0.0819 \quad (1)$$

$$PercentualDamage_{goods} = 0.2183\ln(h) + 0.4986 \quad (2)$$

As for the damages concerning the public basic infrastructure, according to data from the World Bank, based on actual flood occurrences in Brazilian states, losses in basic infrastructure represent between 12.5% and 30% of the total damage costs. To ensure a more conservative risk assessment, a percentage of 30% of the total estimated losses will be adopted.

3 RESULTS AND DISCUSSION

The flood extent simulated by the CADDIES model for the analyzed event in the Aricanduva catchment is presented in Figure 2. The results indicate that the model is able to realistically represent the basin's hydrodynamics, with well-defined river channels and clear representation of urban features such as buildings, street layout, and detention basins constructed as flood mitigation measures. High flood-depth values within some areas reflect water accumulation in detention basins, confirming that these structures are explicitly accounted for in the model framework. A critical assessment and validation of CADDIES for the Aricanduva catchment, including the event analyzed in this study, is provided by Benso et al. (2024).

Despite the presence of detention basins, Figure 2 shows that these structures are insufficient to fully attenuate flooding during events of this magnitude. Floodwaters still extend over large portions of the basin, particularly in downstream areas (highlighted by the red zoom in Figure 2), where flood depths outside the main channel reach approximately 2 to 4 m. Similar limitations of detention-based mitigation measures under extreme rainfall conditions have also been reported in other studies of highly urbanized basins, where storage capacity is often exceeded during high-intensity storms (e.g., Bhusal et al., 2023). In the Aricanduva catchment, these downstream areas also coincide with higher concentrations of commercial buildings and higher average income levels, increasing the potential for significant economic losses.

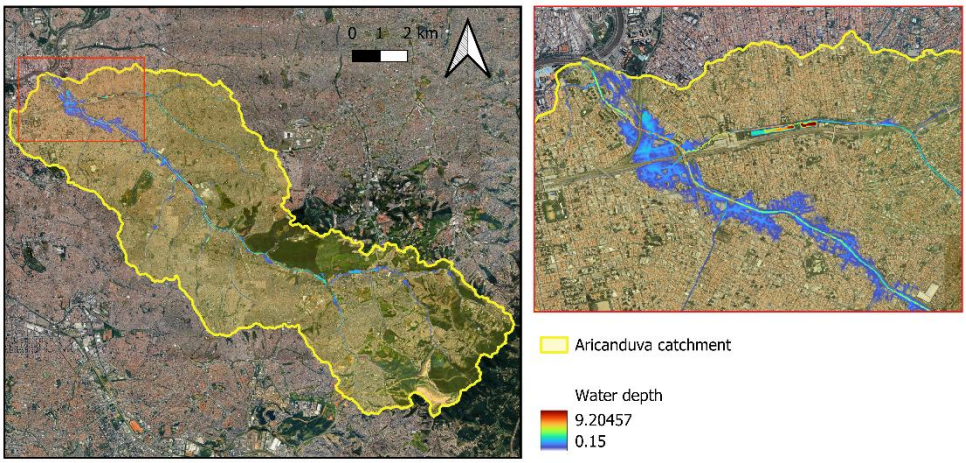

Figure 2: Flood extent and water depth obtained through CADDIES - in the right, it is shown a zoom in the most affected part of the catchment

By intersecting the simulated flood extent with 2022 Census data for the city of São Paulo, restricted to the Aricanduva catchment, economic losses associated with structural damage, infrastructure impacts, and losses of goods within buildings were estimated as a function of flood depth. Aggregated results for the entire basin are shown in Table 2. Losses related to goods and contents represent the largest share of total damages, followed by infrastructure and, finally, building structures. This damage hierarchy is consistent with findings from flood loss assessments in Europe and Asia, where contents often account for a substantial proportion of total urban flood losses, particularly in areas with moderate to high water depths (Merz et al., 2010). At the census-sector scale, maximum estimated losses reached US$ 1.28 million for construction damage, US$ 2.13 million for goods, and US$ 1.02 million for infrastructure, while several sectors experienced negligible losses.

For a more detailed assessment at the building level, average damages per structure (including residential and commercial buildings) were calculated across all census sectors. The mean losses were US$ 1,255 for construction, US$ 4,126 for goods, and US$ 1,615 for infrastructure per building. Figure 3 presents the distribution of individual building losses by census sector and socioeconomic class. As expected, individual losses related to construction and goods are higher for class B, reflecting the higher asset values associated with this group. These are followed by classes C, D, and E, with relatively small differences among the latter classes. Similar patterns have been documented in international studies, where higher-income

groups exhibit larger per-asset losses, while lower-income groups tend to experience smaller individual losses but higher cumulative impacts due to greater exposure (Kreibich et al., 2014). Infrastructure losses remain nearly constant across socioeconomic classes, reflecting the relatively homogeneous provision of basic urban infrastructure across income groups in large cities.

Table 2: Statistics of economic damages for the Aricanduva catchment

	Economic damages (mi US$)		
	Construction	**Goods**	**Infrastructure**
Total	1123.03	3693.76	1444.45
Average	0.03	0.11	0.04
Min	0.00	0.00	0.00
Max	1.28	2.13	1.02
Standard deviation	0.09	0.16	0.07

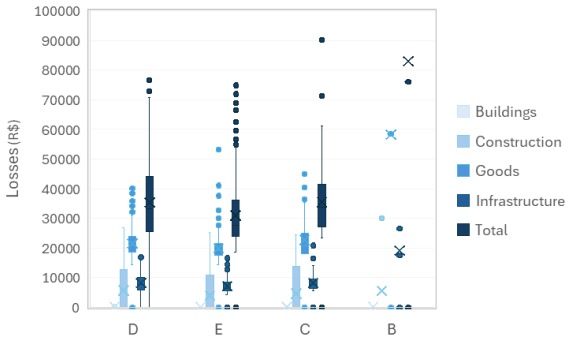

Figure 3: Flood damages per economic class and losses' type in the Aricanduva catchment. Conversion rate: R$ 1 ≈ US$ 0.193

Although class B exhibits the highest individual losses, class D accounts for the largest total losses at the catchment scale, as it is the most numerous socioeconomic group in the Aricanduva basin. This finding underscores the importance of population distribution in shaping aggregate flood impacts and aligns with international evidence showing that middle- and lower-middle-income groups often bear a disproportionate share of total urban flood losses (Winsemius et al., 2016).

Figure 4 focuses on sectors where total losses exceed US$ 1.94 million, classified here as extreme losses. While Figure 4 does not reveal a strong spatial pattern, Figure 4 shows that extreme losses are predominantly concentrated in downstream areas of the catchment. These sectors correspond to locations with higher simulated flood depths outside the river channel or detention basins (Figure 2) and a higher density of commercial establishments. Comparable spatial clustering of extreme flood losses in downstream or low-lying urban areas has been reported in studies of large cities worldwide, emphasizing the combined role of hazard intensity and economic concentration in amplifying flood risk (Hallegatte et al., 2013). This spatial variability reflects the combined effects of local flood depth, building density, and socioeconomic characteristics, as also observed in other large metropolitan areas (Jongman et al., 2012; Tellman et al., 2021).

Overall, the results highlight that flood risk in the Aricanduva catchment is governed not only by hydrological processes but also by the spatial distribution of socioeconomic assets and urban infrastructure. While detention basins provide localized benefits, they are insufficient to prevent significant losses during extreme events, particularly in economically dense downstream areas. These findings reinforce international evidence advocating for integrated flood risk management approaches that combine structural measures with land-use planning, asset-level protection, and targeted adaptation strategies to reduce exposure and vulnerability in megacities.

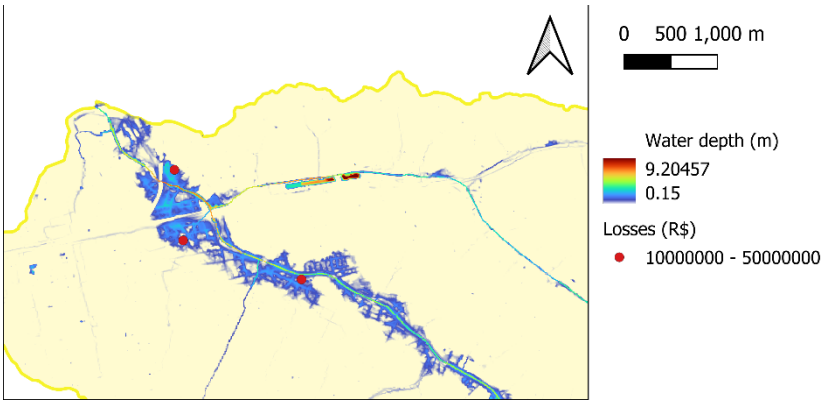

Figure 4: Zoom in the three most damaged points

4 CONCLUSION

This study highlights the value of integrating high-resolution two-dimensional flood modelling with socioeconomic data to support detailed flood impact assessments in highly urbanized catchments. The application of the CADDIES model in the Aricanduva basin successfully represented key hydrodynamic processes, including channelized flow, floodplain inundation, and the effects of detention basins. By combining simulated flood depths with census-based indicators, the results show that losses associated with household and commercial goods constitute the largest share of total damages, followed by infrastructure and structural impacts. While higher-income classes present greater individual losses, total damages are concentrated in lower-income classes due to their greater spatial extent and population density. These findings reinforce the importance of coupling physical flood modelling with socioeconomic vulnerability indicators to inform urban planning and flood risk management strategies.

Nevertheless, this study is limited to the estimation of direct tangible damages and does not account for indirect flood impacts. Losses related to disrupted economic activities, reduced mobility, loss of working hours and income, as well as health-related effects that impair labor capacity were not considered. Such impacts can significantly increase the overall cost of flooding in urban areas. Future research should aim to incorporate these indirect and intangible dimensions, potentially through the integration of economic, mobility, and public health data, to provide a more comprehensive assessment of flood risk and its socioeconomic consequences.

5 ACKNOWLEDGEMENTS

The authors would like to acknowledge the financial support of Brazilian National Council for Scientific and Technological Development CNPq (Grant n. 446029/2023-8.) and Federal University of Itajubá for the grant of Scientific Initiation 2025/2026.

REFERENCES

Benso, M. R., de Macedo, M. B., Lopes, A. V., Floriano, A., Vasconcelos, B. C. S. D. C., Costa, M. E. L., ... & Fava, M. C. (2024). Efeito da resolução de modelos digitais de elevação na acurácia de modelagem hidráulica em áreas urbanas. Proceedings of XV Encontro Nacional de Águas Urbanas, Recife – PE, 2024.

Bhusal, A., Kalra, A., & Shin, S. (2023). Resilience effect of decentralized detention system to extreme flooding events. Journal of Hydroinformatics, 25(3), 971-988. https://doi.org/10.2166/hydro.2023.176

Borba, M. L., Warner, J. F., & Porto, M. F. A. (2016). Urban stormwater flood management in the Cordeiro watershed, São Paulo, Brazil: does the interaction between socio-political and technical aspects create an opportunity to attain community resilience?. Journal of Flood Risk Management, 9(3), 234-242. https://doi.org/10.1111/jfr3.12172

Der Sarkissian, R., Al Sayah, M. J., Abdallah, C., Zaninetti, J. M., & Nedjai, R. (2022). Land use planning to reduce flood risk: opportunities, challenges and uncertainties in developing countries. Sensors, 22(18), 6957. https://doi.org/10.3390/s22186957

Haddad, E. A., & Teixeira, E. (2015). Economic impacts of natural disasters in megacities: The case of floods in São Paulo, Brazil. Habitat International, 45, 106-113. https://doi.org/10.1016/j.habitatint.2014.06.023

Hallegatte, S., Green, C., Nicholls, R. J., & Corfee-Morlot, J. (2013). Future flood losses in major coastal cities. Nature Climate Change, 3, 802–806. https://doi.org/10.1038/nclimate1979

IBGE – Instituto Brasileiro de Geografia e Estatística [Brazilian Institute of Geography and Statistics]. Municípios [Municipalities]. (2022). Available at: https://cidades.ibge.gov.br/brasil/sp/sao-paulo/panorama

INMET - Instituto Nacional de Meteorologia [National Meteorology Institute]. (2020). Normais climatológicas do Brasil [Brazilian climate normal]. Available at: https://portal.inmet.gov.br/normais#

Jongman, B., Kreibich, H., Apel, H., Barredo, J. I., & Aerts, J. C. J. H. (2012). Comparing flood damage models: Towards a European approach. Natural Hazards and Earth System Sciences, 12, 3733–3742. https://doi.org/10.5194/nhess-12-3733-2012

Kreibich, H., Van Den Bergh, J. C. J. M., Bouwer, L. M., Bubeck, P., Ciavola, P., Green, C., Hallegatte, S., Kreibich, H., Kuhlicke, C., Logar, I., Meyer, V., Michaelis, S., Papyrakis, E., Pfurtscheller, C., Poussin, J., Przyluski, V., Thieken, A. H., & Viavattene, C. (2014). Costing natural hazards. Nature Climate Change, 4, 303–306. https://doi.org/10.1038/nclimate2182

Machado, M. L., Nascimento, N., Baptista, M., Gonçalves, M., Silva, A., Lima, J. D., ... & Fernandes, W. (2005). Curvas de danos de inundação versus profundidade de submersão: desenvolvimento de metodologia. Revista de Gestão de Água da América Latina, 2(1), 35-52.

Merz, B., Kreibich, H., Schwarze, R., & Thieken, A. H. (2010). Assessment of economic flood damage. Natural Hazards and Earth System Sciences, 10, 1697–1724. https://doi.org/10.5194/nhess-10-1697-2010

PDAU-RGMV. (2021). Plano Diretor de Águas Urbanas da Região Metropolitana da Grande Vitória. Vitória, 2021.

Tellman, B., Sullivan, J. A., Kuhn, C., Kettner, A. J., Doyle, C. S., Brakenridge, G. R., Erickson, T. A., & Slayback, D. A. (2021). Satellite imaging reveals increased human exposure to floods globally. Nature, 596, 80–86. https://doi.org/10.1038/s41586-021-03695-w

UN-Habitat (2020). World Cities Report 2020: The value of sustainable urbanization. United Nations. Available at: https://unhabitat.org/world-cities-report-2020-the-value-of-sustainable-urbanization

Vashist, K., & Singh, K. K. (2024). Flood Inundation Modeling: A Brief Review. Sustainable Management of Land, Water and Pollution of Built-up Area, 87-97. https://doi.org/10.1007/978-3-031-56176-4_7

Winsemius, H. C., Aerts, J. C. J. H., Van Beek, L. P. H., Bierkens, M. F. P., Bouwman, A., Jongman, B., Kwadijk, J. C. J., Ligtvoet, W., Lucas, P. L., Van Vuuren, D. P., & Ward, P. J. (2016). Global drivers of future river flood risk. Nature Climate Change, 6, 381–385. https://doi.org/10.1038/nclimate2893

ICFM 10
Adapting to Global Change:
Innovative Approaches to Flood Management and Resilience
May 20-22, 2026 | Western University, London, Ontario, Canada

Damage Prognosis of Dynamic Flood Events Using a System of Harmonized Damage Grades and Considering Uncertainties

Holger Maiwald[1] and Jochen Schwarz[2]
Earthquake Damage Analysis Center (EDAC), Bauhaus-Universität Weimar, Weimar, 99423, Germany[1]
E-mail: holger.maiwald@uni-weimar.de

Earthquake Damage Analysis Center (EDAC), Bauhaus-Universität Weimar, Weimar, 99423, Germany[2]
E-mail: schwarz@uni-weimar.de

ABSTRACT

The “century flood events” of 2002, 2013 and 2021 in Germany show that extreme events with very low probabilities of occurrence are possible in a short time and can cause devastating damage. The events of 2002 and 2021 in particular indicated that, in addition to pure moisture damage, serious structural damage to the buildings could also occur.

Starting with the 2002 flood in Saxony, the Earthquake Damage Analysis Center (EDAC) at the Bauhaus-Universität Weimar has repeatedly carried out damage surveys after flood events over the past 20 years. The basis for the EDAC flood damage model was derived from the obtained damage cases.

In contrast to conventional flood damage models, the updated EDAC flood damage model allows not only the prediction of the financial losses, but also the prognosis of structural damage, including collapsed or even washed-away buildings. The analyses of the damage recordings after the flood of July 2021 in the federal states Rhineland-Palatinate and North Rhine-Westphalia also fall into this context.

The paper presents "fragility functions", which reflect the probability of exceedance of certain damage grades depending on water level and flow velocity. Using Monte Carlo simulations, these “fragility functions” also enable the identification of uncertainties in the prognosis of structural damage. In the past, these functions were successfully verified for low to moderate flow velocities during the 2002 flood in six investigation areas in the federal state of Saxony.

Evidence for high water levels in connection with high flow velocities has not been provided, yet. This article shows the verification of the derived “fragility functions” using the example of the extremely severe structural damage caused by the 2021 floods in the Ahr valley. The uncertainties of the prognosis can be expressed by selection of the mean or values for 50%, 84% or other fractile as starting points.

KEYWORDS: Vulnerability, types of structure, dynamic flood events, damage grades, fragility functions, Monte Carlo simulations, damage prognosis, scenarios

1 INTRODUCTION

The Earthquake Damage Analysis Center at the Bauhaus University Weimar (EDAC) has repeatedly conducted damage surveys immediately after flood events over the past 20 years, beginning with the 2002 floods in Saxony. The damage cases obtained in the process were used to derive the basis for the EDAC flood damage model (Maiwald and Schwarz, 2023). In this damage model, the elements of the European Macroseismic Scale 1998 (Grünthal et al., 1998) were applied to the natural hazard of flooding. The specific vulnerability of building types is considered by the assignment of vulnerability classes, depending on the materials of the load-bearing walls and the specific construction design. These vulnerability classes combine different building types with the same susceptibility to damage in an engineering-oriented approach (Schwarz and Maiwald, 2007).

In contrast to conventional flood damage models (see the overviews by Jongman et al., 2012; Gerl et al., 2016), the EDAC flood damage model allows the prognosis of structural damage, including collapsed or even washed-away buildings.

Analyses of the current damage assessments following the July 2021 floods in Rhineland-Palatinate and North Rhine-Westphalia also support this view. The event caused 184 casualties in Germany (134 in the Ahr Valley) and exceptionally high losses in the affected regions. Munich Re estimates total flood-related damages across Europe at €46 billion, with Germany alone accounting for €33 billion (Web-1). This means that the damage exceeds that caused by the floods of 2002, which amounted to €11.5 billion (Deutsche Rück, 2005) – equivalent to approximately €18.8 billion in 2021 prices based on the Federal Statistical Office's building price index (Statistisches Bundesamt, 2022). The 2021 floods were marked by exceptionally high inundation levels and flow velocities, causing severe structural damage to buildings and infrastructure, particularly in the Ahr Valley.

For the prognosis of structural damage, the EDAC flood damage model provides various vulnerability functions. They have been validated in different investigation areas in the Free State of Saxony based on the damage caused by the 2002 floods for low to moderate flow velocities (Maiwald and Schwarz, 2015, Maiwald et al., 2022a, Schwarz and Maiwald, 2008). Validation outside Saxony and for high flow velocities is still pending. A continuation of the analyses of damage survey following the floods in July 2021 in the Federal States of Rhineland-Palatinate and North Rhine-Westphalia (Maiwald et al., 2022b) enables a validation for a special type of fragility functions; results are given in the paper.

2 DATA

2.1 Damage Database

The damage database underlying the vulnerability and damage functions of the current version of the EDAC flood damage model is presented in detail in Maiwald et al (2022a). The unified compilation of damage cases is the result of an extensive review of damage data from the 2002 floods at the Saxonian Relief Bank. The database contains data from approximately 5,000 damaged buildings with the relevant structural parameters, the inundation levels, the descriptions of the structural damage and the actual recovery costs. For approximately 1,000 damage cases, hydraulic simulations of water levels were used to assign flow velocities. The calculated flow velocities do not exceed the value of $v_{fl} = 2.5$ m/s, meaning that a different data source had to be used for high flow velocities.

Therefore, to derive the vulnerability functions presented in Maiwald et al. (2022a) for the prognosis of the expected value of structural damage and the fragility functions validated here, damage data from the tsunami caused by the Tohoku earthquake (2011) were also used covering high inundation levels and flow velocities (cf. Suppasri et al., 2013). Further explanations on the data background of fragility functions can also be found in Maiwald and Schwarz (2022).

2.2 Field Survey of the 2021 Flood

Based on and continuing similar operations, researchers of EDAC carried out several damage surveys in the Ahr Valley in Rhineland-Palatinate between July 19 and August 5, 2021 (Figure 1). The objective was the documentation of damage to affected building stock. In addition to the elaboration of observed damage patterns, relevant building characteristics and structural parameters (e.g., building use, number of stories, inlet heights, wall construction type, basement configuration, roof structure) were collected on site or subsequently assigned during plausibility checks and data enhancement, following the system developed in Schwarz et al. (2019). Consistent with the EDAC flood damage model (Maiwald and Schwarz, 2023), each damage case was classified into a corresponding damage grade, representing the extent of structural damage (cf. Section 3.1). In total, damage cases ranging from light structural damage to collapsed or washed-away buildings caused by high inundation levels and flow velocities in combination with bank erosion and foundation scouring contribute to a significant extension of the database.

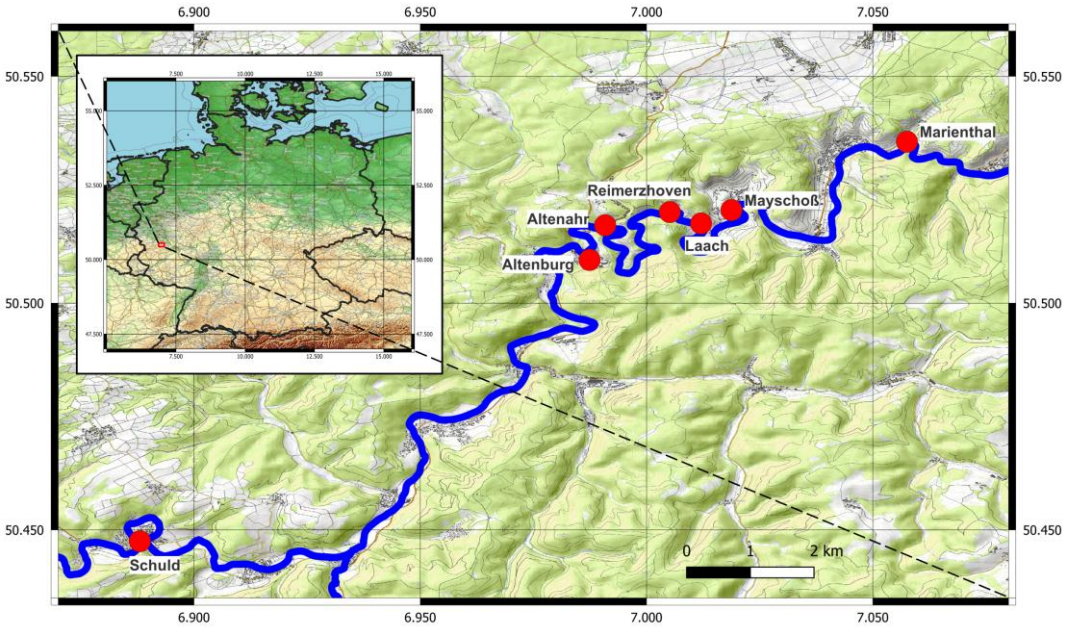

Figure 1: Investigation areas of the 2021 flood in the Ahr Valley (Basemap: OpenTopoMap)

A detailed evaluation of the collected building and damage data can be found in Maiwald et al. (2022b). The documented building data form the basis of the resistance parameters for the simulations in Section 4.

2.3 Flood Scenario

As part of a scientific collaboration directed to the re-interpretation of the flood scenario for the 2021 floods in the Ahr Valley the hydrodynamic model calculated using the RIM2D (Apel et al., 2022) has been made available for this study. The program offers the modelling of pluvial (rain-induced) and fluvial (river) floods in urban and rural areas. It uses graphics processing units (GPUs) for fast and efficient calculations, enabling rapid simulation of flood dynamics. This makes it suitable for advanced applications such as probabilistic flood risk analysis and operational flood forecasting.

Background of the simulation is the official Digital Elevation Model (DEM 10 m resolution: © GeoBasis-DE/BKG 2012). The model used in the paper consists of two sections: Müsch to Altenahr and from the Altenahr gauge to Sinzig. In the investigation areas, the model was further adapted to the actual existing structures. The water levels (h_{gl}) and flow velocities ($_{vfl}$) determined from the Grid files were assigned to the buildings in QGIS. Since there are no impact values in the grids calculated in the areas of the building floor plans themselves, a 5 m buffer was placed around the structures and the mean values for h_{gl} and v_{fl} were calculated in the buffer areas. In the investigation areas, high inundation levels of up to 8 m and high flow velocities of more than 9 m/s were calculated for individual buildings. These values are applied as impact parameters for the simulative flood damage modelling in Section 4.

3 ELEMENTS OF THE EDAC FLOOD DAMAGE MODEL

3.1 Damage Grades

Based on the documented building stock and building damage in August 2002, Schwarz and Maiwald (2007) introduced an initial five-stage differentiation of damage grades ranging from simple moisture penetration (D1) to complete collapse of the building (D5). In Maiwald and Schwarz (2019), this damage scale was extended by an additional damage grade D6 in order to distinguish between buildings that were washed away or displaced from their foundations and collapsed buildings (D5).

Table 1: Applied flood damage scale (complete description c.f. Maiwald and Schwarz, 2019)

Damage grade		D1	D2	D3	D4	D5	D6
Damage	structural	none	light	moderate	heavy	very heavy	complete
	non-structural	light	moderate	heavy	very heavy	very heavy	complete

The six-stage damage scale (Table 1) represents one of the basic elements of the EDAC flood damage model (Maiwald and Schwarz, 2023).

3.2 Vulnerability Classes

The concept of vulnerability classes refers to the European Macroseismic Scale EMS-98 (Grünthal et al., 1998); it is one of innovative aspects to classify the observed shaking effects of higher earthquake intensities systematically on the basis of damage pattern for pre-classified types of structures (buildings). The vulnerability classes summarize building types that exhibit similar structural damage under comparable impact intensity (see Table 2). Schwarz and Maiwald (2007) successfully adapted this concept to flood damage and risk assessment; an advance state in methodology, tool development and application is presented by Schwarz et al. (2018). The Vulnerability Table (Table 2) is a key element of the EDAC damage model (Maiwald and Schwarz, 2023). Flood vulnerability class HW-A represents the most vulnerable building category, buildings of vulnerability class HW-F are expected to withstand even high impact levels with minimal or no significant structural damage (Maiwald et al., 2022a).

Table 2: Classification of building types into vulnerability classes (Schwarz et al., 2018)

Building type	Flood vulnerability class HW-					
	A	B	C	D	E	F
Clay	○					
Prefabricated timber frame	⊢○⊣					
Timber frame with masonry or clay infills	⊢○┈⊣					
Masonry	┈—○┈					
Reinforced concrete			┈○			
Flood resistant design				⊢○		
Flood evasive design						○

○ Most likely vulnerability class — Probable range ┈ Range of less probable, exceptional cases

4 SIMULATIVE FLOOD DAMAGE MODELLING

4.1 Fragility Functions for Dynamic Floods Considering Water Level and Flow Velocity

The EDAC flood damage model (Maiwald and Schwarz, 2023) provides different types of vulnerability functions for calculating the expected Mean damage grade (D_m). The term fragility functions mean functions with which the probability of exceedance a certain damage grade D_i can be determined depending on the intensity of impact. In general, the cumulative logarithmic normal distribution (Eqn. 1) is used to describe the functions mathematically.

$F_{Di}(x)$ is the conditional probability that the structure will reach or exceed the damage grade D_i, depending on the action parameter x. The parameters μ and σ are to be derived for each building type, vulnerability class and damage grade. From Eqn. (2) the probability that a building will be damaged up to the damage grade D_i is calculated.

$$F_{D_i}(x) = \Phi\left(\frac{\ln(x) - \mu}{\sigma}\right) \quad (1)$$

$$P[D_i \mid x] = F_{D_i}(x) - F_{D_i+1}(x) \quad (2)$$

x - impact parameter ($x = h_{gl} + h_{gl} \cdot v_{fl}^2$), not true in units
h_{gl} - waler level above ground level
μ - logarithmic mean
Φ - standard normal distribution
v_{fl} - flow velocity
σ - logarithmic standard deviation

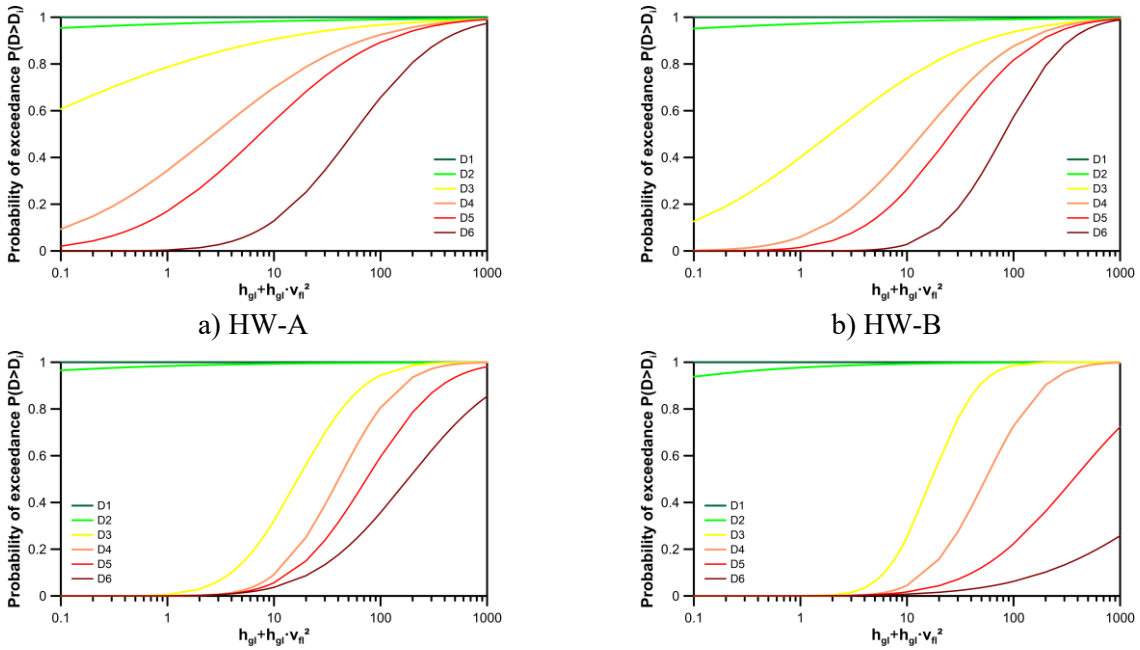

Figure 2: Fragility function considering water level and flow velocity (Maiwald and Schwarz, 2022)

The fragility functions for vulnerability classes (Figure 2) used in this study were first presented in Maiwald and Schwarz (2022) and validated for six Saxon investigation areas for low and moderate flow velocities. The parameter $x = h_{gl} + h_{gl} \cdot v_{fl}^2$, has been proven as an effective impact factor. Preliminary and successful application of the fragility functions in the Ahr Valley - limited to the investigation areas of Altenburg and Altenahr and using a different hydraulic model - can be found in Schwarz et al. (2023).

Table 3 lists the fragility function control parameters. Preliminary and successful application of the fragility functions in the Ahr Valley - limited to the investigation areas of Altenburg and Altenahr and using a different hydraulic model - can be found in Schwarz et al. (2023).

Table 3: Control parameter of the fragility functions (Maiwald and Schwarz, 2023)

Damage Grade	HW-A		HW-B		HW-C		HW-D	
	μ	σ	μ	σ	μ	σ	μ	σ
D2	-20.00	10.50	-18.05	9.49	-15.00	7.00	-10.00	5.00
D3	-3.50	4.40	0.65	2.58	2.82	1.12	2.84	0.80
D4	1.00	2.50	2.64	1.70	3.70	1.05	4.00	1.00
D5	2.00	2.10	3.25	1.50	4.30	1.26	5.90	1.70
D6	4.00	1.50	4.40	1.10	5.20	1.62	8.60	2.60

4.2 Application to 2021 Flood in the Ahr Valley

For the re-interpretation of the observed damage, the flood-damage simulation methodology based on the fragility functions presented in Section 4.1 is applied. The mean values for the water level and the flow velocity on each building are considered. Structural damage is simulated by generating 1,000 random realizations using a Monte Carlo approach. This simulation-based approach enables the quantification of the probable scatter of the structural damage. Table 4 provides the outcome of error analysis for residential buildings in each of the investigation areas in the Ahr Valley in terms of the Mean Error (ME), the Mean Absolute Error (MAE), and Root Mean Square Error (RMSE).

Table 4: Error analysis of the simulations for residential buildings

Investigation area	No.	50 % fractile			84 % fractile			Mean		
		ME	MAE	RMSE	ME	MAE	RMSE	ME	MAE	RMSE
Altenahr	59	0.49	0.73	1.24	0.19	0.69	1.14	0.40	0.71	1.14
Altenburg	171	0.05	0.15	0.47	-0.07	0.21	0.57	0.00	0.19	0.44
Laach	43	0.26	0.44	0.85	-0.37	0.70	1.06	0.09	0.51	0.78
Marienthal	43	0.42	0.51	1.03	0.19	0.56	1.06	0.29	0.53	0.98
Mayschoß	146	-0.10	0.30	0.71	-0.31	0.46	0.95	-0.13	0.35	0.70
Reimerzhoven	23	-0.48	0.48	0.81	-1.00	1.00	1.37	-0.50	0.55	0.78
Schuld	138	-0.33	0.62	1.00	-0.76	0.96	1.40	-0.41	0.70	0.98
Combined	623	**-0.01**	0.40	0.83	-0.29	0.57	1.04	**-0.08**	0.45	0.80

The maps in the Figures 3 and 4 give insight in the simulated 50% and 84% fractiles of the damage grades in Altenburg and Mayschoß. For comparison maps for observed damage grades are given. Results follow the studies by Maiwald et al. (2022b) to support the pending planning decisions.

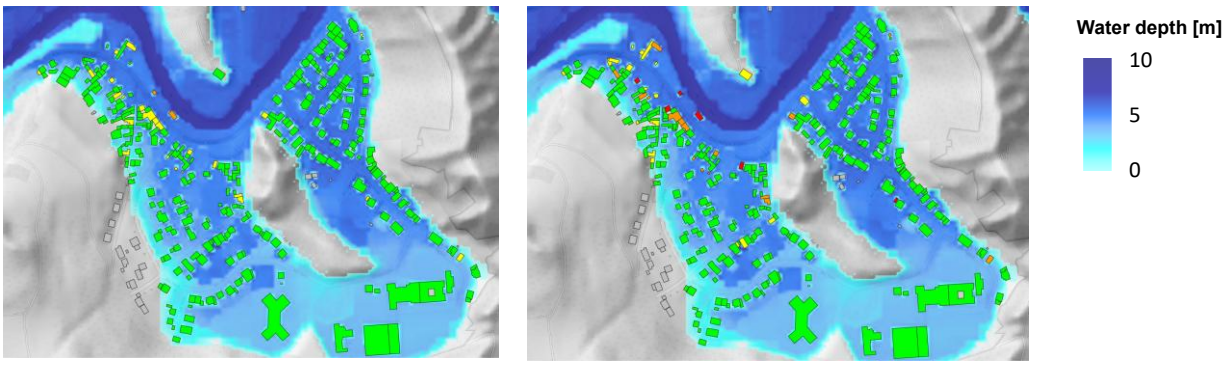

a) 50% fractile b) 84% fractile

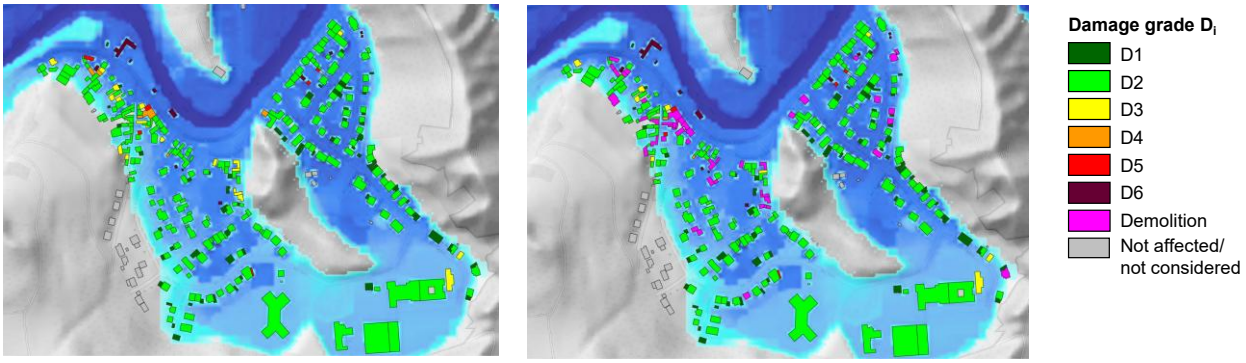

c) Observed damage d) Observed damage, incl. demolitions

Figure 3: Comparison of simulated and observed damage grades for the investigation area Altenburg

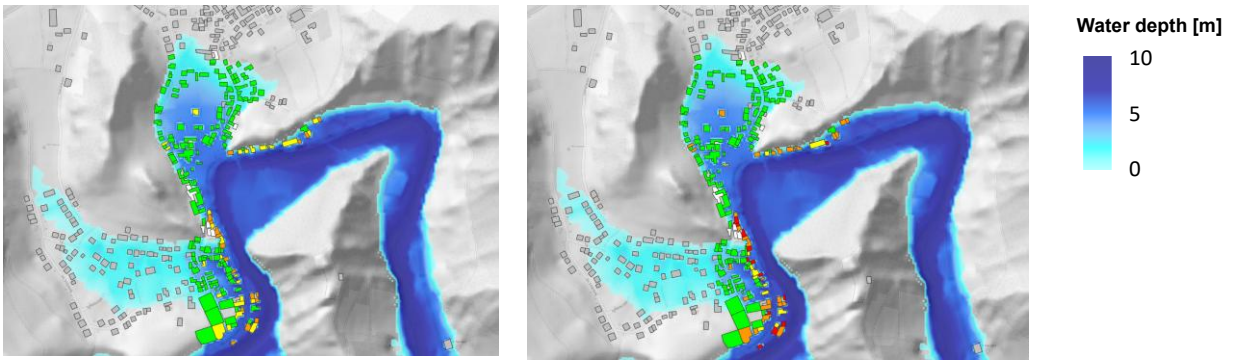

a) 50% fractile b) 84% fractile

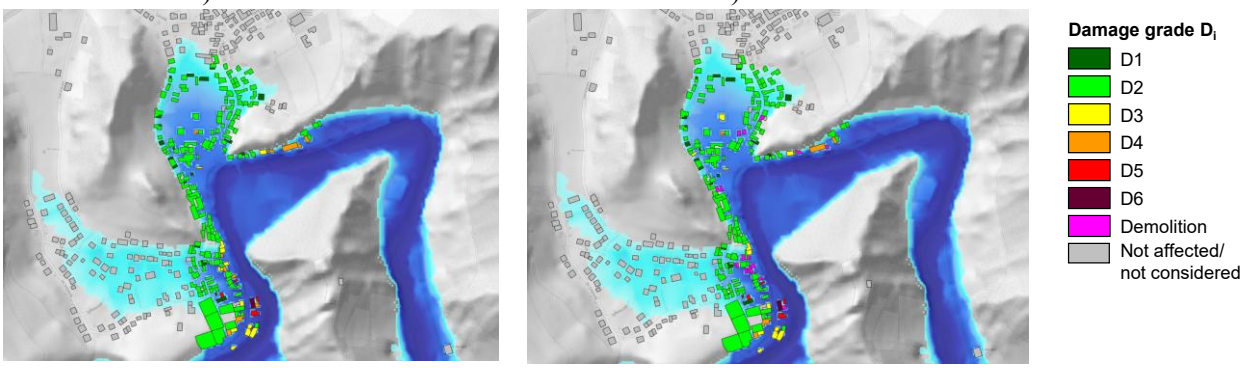

c) Observed damage d) Observed damage, incl. demolitions

Figure 4: Comparison of simulated and observed damage grades for the investigation area Mayschoß

5 CONCLUSIONS AND OUTLOOK

As it can be concluded from Table 4, the 50% fractiles and mean values show the lowest ME values. In general, the slight over- and underestimations in the investigation areas indicate a remarkable prognosis quality. As the low ME values in the "combined" row show, the deviations balance each other out across the entire area. The RMSE values for the entire area are almost twice as high as the values determined for the Saxon investigation areas in Maiwald et al. (2022a). And the MAE values for the entire area are only slightly higher (10 – 15%). Recognizing that the uncertainties (in hydraulic modelling and in the assignment of structural parameters) will remain, the results are encouraging. Not at least, it has to be emphasized that the damage model was derived from empirical data from other flood affected regions and that extremely high flow velocities occurred 2021 in the Ahr Valley. Figures 3 and 4 show

also a good visible spatial correlation between the 50% fractiles of the simulated and the observed damage. It is noteworthy that the later demolitions are partially reflected in the 84% fractile values.

The initial results of the investigations in the Ahr Valley confirm the effectiveness and transferability of the vulnerability-oriented approach for the prognosis of structural damage caused by extreme flooding events. As demonstrated by Maiwald and Schwarz (2022), realistic prognosis of financial losses can also be generated, along with estimates of the expected ranges of scatter.

Due to the sensitivity of the topic and the non-availability of reliable data on the actual losses for the individual investigation areas in the Ahr Valley, any comparison between the simulated losses (including their ranges of scatter) and the observed losses will have to be deferred to subsequent studies.

6 ACKNOWLEDGEMENTS

We thank the colleagues of Section 4.4. Hydrology at the GFZ Helmholtz Centre for Geosciences Potsdam for sharing the hydraulic model for the 2021 flood in the Ahr Valley in ongoing joint efforts.

REFERENCES

Apel, H., Vorogushyn, S. and Merz, B. (2022). Brief communication: Impact forecasting could substantially improve the emergency management of deadly floods: case study July 2021 floods in Germany. Nat. Haz. Earth Syst. Sci., 22, 9, 3005-3014. https://doi.org/10.5194/nhess-22-3005-2022

Deutsche Rückversicherung AG (2005). Sturmdokumentation Deutschland 1997-2004, Düsseldorf. https://www.deutscherueck.de/fileadmin/Downloads/Sturmdoku_1997_2004_web.pdf

Gerl, T., Kreibich, H., Franco, G., Marechal, D. and Schroter, K. (2016). A Review of Flood Loss Models as Basis for Harmonization and Benchmarking. PloS one. 11(7), e0159791. https://doi.org/10.1371/journal.pone.0159791

Grünthal, G., Musson, R., Schwarz, J. and Stucchi, M. (1998). European Macroseismic Scale 1998. Cahiers de Centre Européen de Géodynamique et de Seismologie, Volume 15, Luxembourg.

Jongman, B., Kreibich, H., Apel, H., Barredo, J.I., Bates, P.D., Feyen, L., and Gericke, A. Neal, J., Aerts, J. C. J. H. and Ward P. J. (2012). Comparative flood damage model assessment: towards a European approach. Nat. Haz. Earth Syst. Sci., 12, 12, 3733-3752. https://doi.org/10.5194/nhess-12-3733-2012

Maiwald, H. and Schwarz, J. (2015). Damage And Loss Prognosis Tools Correlating Flood Action And Building's Resistance-type Parameters, Int. J. of Safety and Security Engineering, 5, 3, 222 - 250. dx.doi.org/10.2495/SAFE-V5-N3-222-250

Maiwald, H. and Schwarz, J. (2022). Simulative flood damage modelling taking into account inundation level and flow velocity: Uncertainties and strategies for further refinement. 8th Int. Conf. on Flood and Urban Water Management, FRIAR 2022, Online, 6–8 July 2022. doi.org/10.2495/FRIAR220031

Maiwald, H., Schwarz, J., Kaufmann, C., Langhammer, T., Golz, S. and Wehner, T. (2022a). Innovative Vulnerability and Risk Assessment of Urban Areas against Flood Events: Prognosis of Structural Damage with a New Approach Considering Flow Velocity. Water 14, 2793, 28 pages. doi.org/10.3390/w14182793

Maiwald, H., Schwarz, J., Kaufmann, Ch. and Abrahamczyk, L. (2022b). Das Hochwasser 2021 - Ingenieuranalyse der Bauwerksschäden. Bautechnik 99, 12, 878-890. doi.org/10.1002/bate.202200062.

Maiwald, H. and Schwarz, J. (2023). Ermittlung von Hochwasserschäden unter Berücksichtigung der Bauwerksverletzbarkeit, Erweitertes EDAC-Hochwasserschadensmodell, scientific technical reports 01-22, Bauhaus-Universitätsverlag, ISBN: 978-3-95773-305-4

Schwarz, J. and Maiwald, H. (2007). Prognose der Bauwerksschädigung unter Hochwassereinwirkung. Bautechnik 84, 7, 450–464. https://doi.org/10.1002/bate.200710039

Schwarz, J. and Maiwald, H. (2008). Damage and loss prediction model based on the vulnerability of building types, in Proc. 4th Int. Symp. on Flood Defence (ISDF), 6 – 8 May 2008, Toronto, Canada.

Schwarz, J., Maiwald, H., Kaufmann, C., Langhammer, T. and Beinersdorf, S. (2019). Conceptual basics and tools to assess the multi hazard vulnerability of existing buildings. Europ. J. of Masonry, 23, 4, 246-264. doi.org/10.1002/dama.201910025

Schwarz, J., Maiwald, H., Abrahamczyk, L., Morgenthal, G. and Hallermann, N. (2023). Methoden für digitale 3D-Lagebilder: Erfahrungen aus dem Hochwasser 2021, Bautechnik, 100, 7, 358-373. doi.org/10.1002/bate.202300003.

Statistisches Bundesamt (2022). Preisindizes für die Bauwirtschaft. Fachserie 17, 4, Febr. 2022

Suppasri, A., Mas, E., Charvet, I., Gunasekera, R., Imai, K., Fukutani, Y., Abe, Y. and Imamura, F. (2013). Building damage characteristics based on surveyed data and fragility curves of the 2011 Great East Japan Tsunami. Nat. Haz., 66, 319–341. https://doi.org/10.1007/s11069-012-0487-8.

Web sites:

Web-1: https://www.munichre.com/de/unternehmen/media-relations/medieninformationen-und-unternehmensnachrichten/medieninformationen/2022/bilanz-naturkatastrophen-2021.html, consulted 17 November 2025

ICFM 10
Adapting to Global Change:
Innovative Approaches to Flood Management and Resilience
May 20-22, 2026 | Western University, London, Ontario, Canada

Assessment of water and food security nexus under climate change using a seamless modelling framework

Mohamed Rasmy[1], Koki Homma[2], Miho Ohara[1], Tomoki Ushiyama[1], Ralph Acierto[1], and Toshio Koike[1]
International Centre for Water Hazard and Risk Management (ICHARM), Public Work Research Institute, Japan[1]
E-mail: abdul@pwri.go.jp
Graduate School of Agricultural Science, Tohoku University, Japan [2]
E-mail: koki.homma.d6@tohoku.ac.jp

ABSTRACT

Climate change has led to an increase in hydro-meteorological extremes, which have significant and often devastating impacts on lives, economies and agricultural production. It is crucial to quantify the impact of climate change on water availability, hydro-climatic extremes and agricultural productivity for sustainable basin-scale planning. Previous studies have not fully investigated the impact on the water-food nexus using an integrated approach. To address this, the research project has developed a seamless modelling framework that integrates the latest scientific and technological advances, such as Global Climate Model (GCM) outputs and downscaling techniques, as well as seamless hydrological and crop modelling. This research therefore presents a reliable method of quantifying the impact of climate change on water and food security, taking advantage of the latest scientific and technological advances. These include GCM outputs for past (1979–2003) and future (2075–2099) climates under two scenarios (RCP2.6 and RCP8.5); downscaling techniques; and a seamless Water and Energy Budget-based Rainfall-Runoff-Inundation (WEB-RRI) model coupled with a Simulation Model for Rice–Weather Relations (SIMRIW) model. The results indicated an increase in annual and seasonal rainfall under both RCP2.6 and RCP8.5 scenarios, particularly during the wet season, with enhanced intra-basin variability. The basin's hydrological response showed increased river discharge, with the future scenarios indicating higher mean flows, greater seasonal peaks, and an amplification of extreme high-flow events. Projections of rice yield reveal that the future climate under RCP2.6 will produce relatively minor yield reductions, whereas RCP8.5 will lead to widespread yield declines due to the combined effects of rising temperatures, altered rainfall patterns and increased hydrological extremes. The results of this study show that hydro-climatic extremes will increase significantly under higher emission pathways (RCP8.5). This threatens food security and highlights the importance of climate-informed strategies for managing water and agriculture in the basin, in order to enhance resilience and sustainability.

KEYWORDS: Climate change, hydrological modelling, crop modelling, crop yield change

1 INTRODUCTION

Climate change threatens water security by disrupting the water cycle and accelerating extreme weather events such as floods and droughts. Water is also central to agriculture, a key driver of sustainable socio-economic growth, livelihoods and food security. Food production depends heavily on water availability, as irrigation accounts for a significant proportion of global water withdrawals, and is often affected by hydro-meteorological extremes. As climate change continues to exacerbate water and food insecurity (IPCC, 2022), it is crucial to develop disaster risk reduction (DRR) policies in a changing climate to ensure sustainable development. The development of DRR policies relies on the reliable quantification of the impact of climate change on water availability, water-related disasters and agricultural production. Previous studies have used simulation models to quantify the impact of climate change on water-related disasters and crop damage separately. However, no studies have investigated the combined effects of floods, droughts and water availability on crop yield under changing climatic conditions simultaneously. Consequently, this research proposes a method to reliably quantify the impact of climate change on water and food security, leveraging the latest scientific and technological advancements such as Global Climate Model (GCM) outputs, downscaling techniques, and integrated hydrological and crop modelling.

GCMs are fundamental tools for projecting future climate changes; however, their outputs cannot be utilised directly in basin-scale hydro-crop models due to model-related uncertainties, coarse resolutions and unrealistic representations of basin-scale precipitation information (Zhang et al., 2016). Studies have shown that high-resolution GCMs (i.e. with a resolution of ~20–60 km or less) improve rainfall simulation (Kusunoki, 2015). However, the outputs of these models are still too coarse for climate change impact assessment studies on water availability and food production at relatively small and medium-sized basins. To address these resolution issues, regional climate models (RCMs) can be employed to enhance atmospheric variables, including extreme rainfall events (Rockel, 2015). To further improve bias originating from the parent GCM and parameterisation processes, statistical bias correction methods are employed, involving the derivation of statistical transfer functions from long-term ground data and past GCM outputs (Moghim et al., 2017). Therefore, using bias-corrected, high-resolution RCM rainfall outputs for climate change impact studies is preferable given their superior performance in simulating rainfall amounts and distributions.

Moreover, distributed hydrological models (DHMs) are essential tools for simulating various hydrological processes under past and future climatic conditions. They provide policymakers with evidence-based information on water resources and water-related disasters (Sayama et al., 2010; Zheng et al., 2021). As floods and droughts are likely to intensify and often occur in succession in a warming climate, it is necessary to manage these two extremes in an integrated way rather than addressing them as separate hazards. In order to seamlessly simulate floods and droughts as well as assess their impact on crop production, the hydrological model must be physically based and capable of addressing parameters related to floods (e.g. peak flood discharge and inundation), droughts (e.g. soil moisture, evapotranspiration (ET) and low flow discharges) and crop growth (e.g. soil moisture and temperature) simultaneously. Rasmy et al. (2019) developed the Water and Energy Budget-Based Rainfall-Runoff-Inundation (WEB-RRI) model, which considers water- and energy-related processes, as well as soil moisture dynamics, ET and runoff and inundation processes. It is an appropriate model for reliably simulating basin hydrological responses under water cycle variability and climate change.

Furthermore, paddy rice is a staple food globally and its cultivation occupies a significant portion of food production systems worldwide. In this study, we adopted the SIMRIW-Rain-fed model (Homma and Horie, 2009), a simplified, process-based model for simulating the growth and yield of irrigated rice. The model simulates three major processes: plant ontogenetic development; leaf area expansion; and dry matter accumulation. It has been validated in many regions, including Japan, the USA, Thailand, Indonesia and Lao PDR (Homma and Horie, 2009; Homma et al., 2017; Maki et al., 2017; Raksapatcharawong et al., 2020).

Consequently, this paper assessed the impact of climate change on hydro-meteorological characteristics and their effect on paddy yields, using high-resolution climate model outputs from MRI-AGCM-3.2H (with a resolution of ~60 km) for two extreme Representative Concentration Pathway (RCP) scenarios (i.e. RCP2.6 and RCP8.5). This was achieved through RCM downscaling of MRI-AGCM-3.2H data, as well as using the WEB-RRI and SIMRIW models in the Pampanga River basin in the Philippines.

2 METHOD, STUDY AREA, DATA, AND MODEL SET-UP

2.1 Method

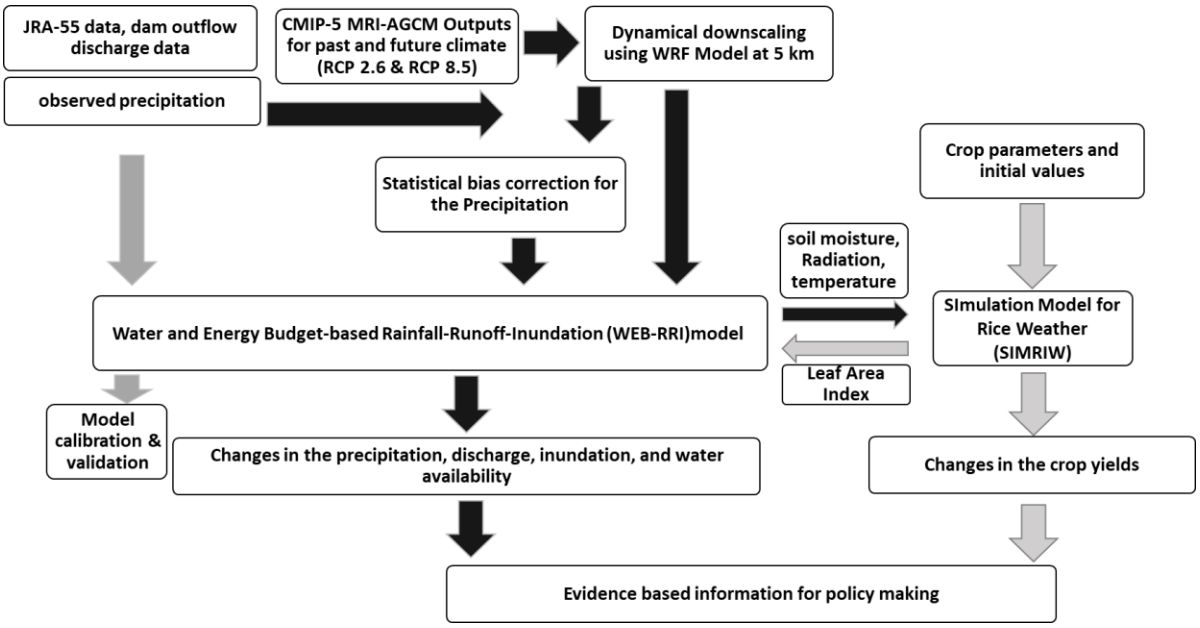

Figure 1. The research framework of climate change impact assessment on the water resources and paddy rice production

This research presents a method of assessing the impact of climate change on water and food security (Fig. 1). The proposed method involves dynamical downscaling of the MRI-AGCM from a horizontal resolution of 60 km to 5 km, and the statistical bias correction of the resulting rainfall data using long-term daily rainfall observations from several gauging stations. A hybrid WEB-RRI-SIMRIW model was developed, calibrated and validated using in situ data. This model was then used to evaluate changes in water resources, water-related disasters and paddy yield in future climates. The following subsections briefly describe the major components and procedures shown in Fig. 2.

2.2 Study area and Data

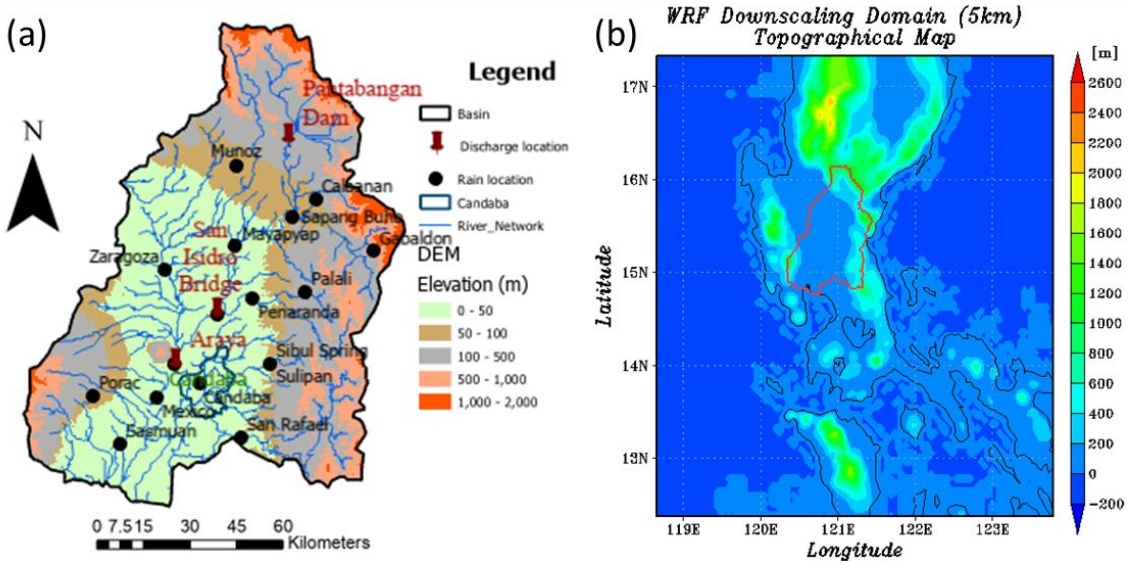

Figure 2: Study area, gauge locations, and simulation domain: (a) a map of the Pampanga River basin and the locations of rain gauges, the Pantabangan dam, and the discharge gauging points, and b) a WRF-downscaling domain and topographical map at the 5-km spatial resolution.

The Pampanga River basin (Fig. 2a) is located in Central Luzon of the Philippines and the basin covers an area of 10,434 km^2. The basin receives an average annual rainfall of 2,155 mm. Due to its rich soil and water, the basin is a vital agricultural hub in the country and plays a crucial role in regional and national food security. However, the basin frequently faces threats from water-related disasters due to climate change. On average, the basin experiences at least one flood event per year, causing severe damage to agriculture, housing and infrastructure (Shrestha et al., 2016). For this study, hourly rainfall data were collected from 17 stations inside and outside the basin from 2009 to 2023 from the Philippine Atmospheric, Geophysical and Astronomical Services Administration (PAGASA). Figure 2a shows the locations of the daily rain gauges and their spatial distribution. To calibrate and validate the model of simulated streamflow, this research used discharge data collected at the San Isidro station during 2022–2023 (Fig. 2a).

The topographic data for the basin (i.e. digital elevation models, flow directions and flow accumulation) were obtained from the U.S. Geological Survey's (USGS) Hydrological Data and Maps Based on Shuttle Elevation Derivatives at Multiple Scales (HydroSHEDS). Figure 2 shows the spatial distribution of the DEM data used in the WEB-RRI modelling. The reclassified land-use data for the SiB2 model were obtained from USGS global datasets. Soil-type distribution data and related soil-water parameters, including three-layer saturated hydraulic conductivity values (i.e. surface soil, root zone and groundwater zone), soil porosity, residual soil moisture content and Van Genuchten parameters, were obtained from the Food and Agriculture Organization (FAO). The leaf area index (LAI) and the fraction of photosynthetically active radiation (FPAR) for incorporating vegetation phenology in the estimation of surface energy, water and carbon budget processes were obtained from the Moderate Resolution Imaging Spectroradiometer (MODIS) global products (MOD15A2) on the Terra satellite. Paddy area data for simulating the SIMRIW model were obtained from the Global Land Cover by National Mapping Organizations (GLCNMO). In addition to rainfall, meteorological forcing inputs such as air temperature, shortwave and longwave radiation, specific humidity, wind speed and surface pressure were obtained from the 55-year Japanese Reanalysis (JRA-55) products prepared by the Japan Meteorological Agency (JMA). This is one of the highest-quality, most homogeneous climate datasets covering the entire globe

for the last half-century (Kobayashi et al., 2015). All of these gridded data were interpolated to model grid resolutions of ~450 m and temporal resolutions of ~1 hour.

2.3 Model setup

This study used climate outputs from the MRI-AGCM3.2H model (~60 km) and scaled these down to a 5 km grid using the Weather Research and Forecasting (WRF) model. The WRF model domain comprised 100 × 100 horizontal grids and 40 vertical layers (see Fig. 2b). It was calibrated using the WRF single-moment 3-class cloud microphysics scheme, the Mellor-Yamada-Nakanishi-Niino (MYNN) surface layer scheme, the unified Noah land-surface model and the MYNN level 2.5 boundary layer scheme. The study adopted the combined scaling and quantile mapping method proposed by Inomata et al. (2009) to correct the bias in the WRF-downscaled rainfall outputs.

The WEB-RRI model was adopted to simulate the basin's hydrological responses. It takes into account the dominant hydrological processes of a catchment area in a fully distributed manner (Rasmy et al., 2019), incorporating water and energy budget processes, land-vegetation-atmosphere interactions, multi-layer soil moisture dynamics and two-dimensional lateral water flow. This improves the simulation of processes such as interception, evaporation and transpiration, infiltration, groundwater flow, surface runoff and inundation. Due to its implicit treatment of basin-scale processes, the model is well-suited to long-term climate change simulations, enabling more accurate reproduction of hydrological responses to past climates, future projections and hydrological extremes.

This study also adopted the SIMRIW-Rainfed model, taking into account N-uptake and water stress (Homma and Horie, 2009). Additionally, the research implemented a formulation to consider the impact of flood depth and duration on rice damage and yield estimation. Although many factors change from the present to the future and affect rice production, this study only considered changes in meteorological factors such as rainfall, temperature, radiation and soil moisture. No changes were assumed in CO_2 concentration, fertiliser, irrigation and rice cultivars in the past or future. Only single cropping in the rainy season under rainfed conditions (no irrigation) was considered. The hybrid model exchanges radiation, temperature, root-zone soil moisture and inundation water depth, as calculated by the WEB-RRI model, for the SIMRIW-rainfed model at each identified paddy grid to simulate water stress, plant growth, damage due to water stress and flooding, and net yield. Conversely, the leaf area index (LAI) simulated by the SIMRIW-rainfed model is passed to the WEB-RRI model to simulate evapotranspiration processes and changes in soil moisture at each paddy grid.

2.4 3.3 Model performance evaluation indices

The Mean Bias Error (MBE), the Root Mean Square Error (RMSE), and the Nash-Sutcliffe Efficiency Coefficient (Nash), and spread (i.e. unbiased estimator of the standard deviation) were used for evaluating model performance on deterministic and ensemble mean estimation.

MBE is defined as:

$$MBE = \frac{\sum(o_i - \bar{o})}{N} \quad (1)$$

RMSE is defined as:

$$RMSE = \sqrt{\frac{\sum(o_i - s_i)^2}{N}} \quad (2)$$

Nash is defined as:

$$Nash = \frac{\sum(o_i - \bar{o})^2 - \sum(o_i - s_i)^2}{\sum(o_i - \bar{o})^2} \quad (3)$$

where O_i is the observation at i^{th} time, $\bar{O}$ is the average observation, S_i is the simulated value at i^{th} time, and N is the number of data.

3 RESULTS AND DISCUSSIONS

3.1 Future changes in temperature and rainfall

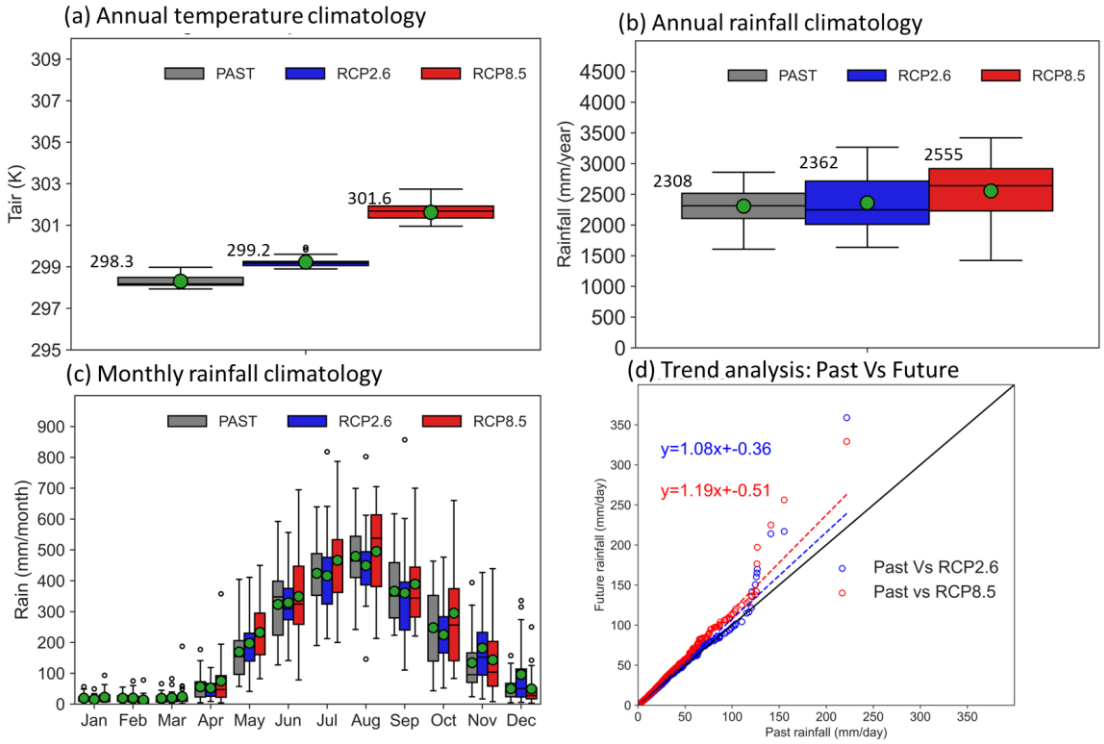

Figure 3: Comparison of basin-averaged climatology and extremes between historical and RCP scenario; (a) annual temperature climatology, b) annual rainfall climatology, c) monthly rainfall climatology, and c) rainfall trend analysis. The green circle in the box-whisker plot represents the mean values.

Figure 3a shows the comparison of the basin-averaged annual 2-meter air temperature climatology between the historical climate and the future climate projections under the RCP 2.6 and RCP 8.5 scenarios. The results show that the future climate will be warmer than the past climate. In particular, the warming is substantially greater under the RCP8.5 scenario (~3.3 K) than under the RCP2.6 scenario (~1 K) across the basin.

Figure 3b shows a comparison of the annual rainfall amounts in the past and future. The mean annual precipitation increases from approximately 2,308 mm/year in the historical period to approximately 2,362 mm/year under the RCP2.6 scenario (a 2.5% increase) and to approximately 2,555 mm/year under the RCP8.5 scenario (a 10.7% increase). In addition to the increase in mean rainfall, the RCP8.5 scenario exhibits greater variability, suggesting a higher likelihood of wet and dry years. The monthly rainfall climatology (Fig. 3c) shows that dry-season rainfall remains relatively low across all scenarios. In contrast, wet-season rainfall exhibits notable variations in median rainfall and increased variability in the future. Specifically, mean rainfall increases from April to June, indicating a stronger monsoon onset over the basin. Additionally, mean rainfall will decrease from July to October under the RCP2.6 scenario, while the RCP8.5 scenario shows increased mean rainfall during that period. Moreover, daily rainfall trend analysis shows that the intensity of rainfall (mm/day) will increase relative to the past. The regression slopes are 1.08 for RCP2.6 and 1.19 for RCP8.5, both of which exceed unity. Notably, the number of events with an intensity greater than 100 mm/day will be significantly higher under RCP8.5 than under RCP2.6, indicating more frequent and intense flooding events under RCP8.5.

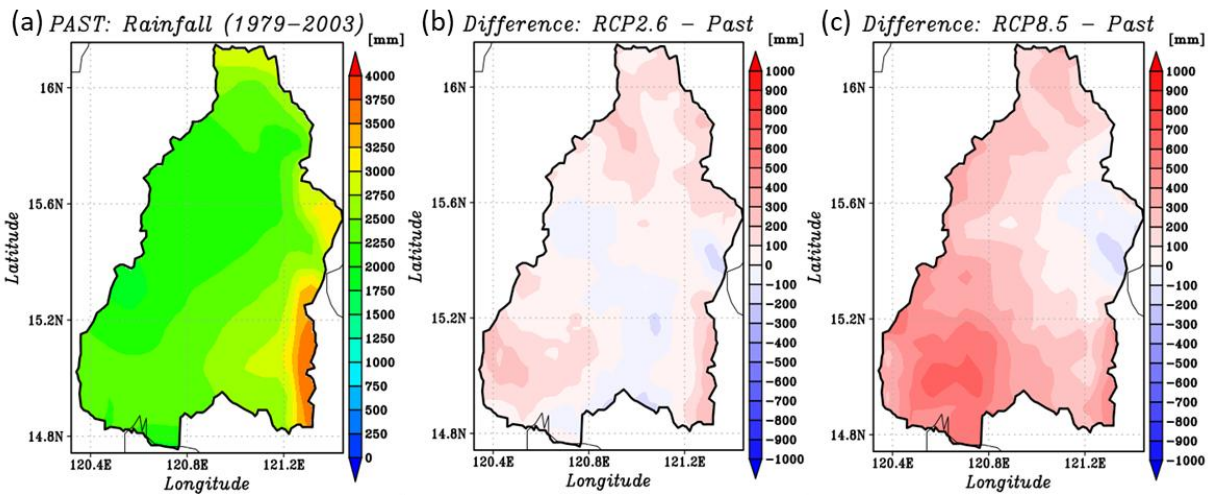

Figure 4: Comparison of spatial distribution of past and future annual rainfall climatology; a) past climate, b) changes in RCP2.6 scenario compared to past climatology, and c) changes in RCP8.5 scenario compared to past climatology

Figure 4a shows the spatial distribution of mean annual rainfall over the past period. It exhibits spatial variability, with localized zones of higher rainfall amounts along the eastern and southeastern parts of the basin. Figures 4b and 4c show the projected changes under the RCP2.6 and RCP8.5 scenarios, respectively, relative to past climate. The results suggest that under the RCP2.6 scenario, future rainfall will marginally change in the middle of the basin and moderately increase (by ~100–300 mm/year) in the rest of the region. Conversely, under RCP8.5, annual rainfall will increase more widely and significantly (~300–600 mm/year), particularly over the central and southern portions of the basin. Additionally, it should be noted that rainfall will decrease in the eastern part of the basin by ~100–200 mm/year, indicating the importance of developing sub-catchment-based water resource management policies for sustainable development.

3.2 WEB-RRI and SIMRIW model development, calibration, and validation

We developed the WEB-RRI-SIMRIW coupled model to assess the impact of meteorological changes under past and future Representative Concentration Pathway (RCP) climates on the basin's hydrological responses and rice yield. Based on our investigation, reliable discharge data from 2022 to 2023 was used for calibration and validation. Additionally, rain-fed crop yield data from the Pampanga province was limited and only available from 2017 to 2019. We simulated the WEB-RRI and SIMRIW models from 2017 to 2023, using Pantabangan dam outflow records as boundary conditions.

Figure 5(a) compares observed and WEB-RRI model-simulated discharges from January 1 to December 31, 2002. This period includes the recorded flood event and was used for model calibration. As shown in the figure, the WEB-RRI model was reasonably well calibrated (Nash = 0.6, RMSE = 84 m^3/s). Though the model captured the peak flow during the typhoon period well, it underestimated it. This could be due to uncertainties in heavy rainfall observations and measurement techniques. Furthermore, Fig. 7(b) shows that the model simulated river low and peak discharges during the validation period that matched the observed discharges well (Nash = 0.68, RMSE = 82 m^3/s).

Figure 6 compares recorded and simulated rice yield data under non-irrigated conditions in the Pampanga province from 2015 to 2019. Observed yields remained relatively stable at approximately 410–430 g/m^2, and the SIMRIW simulations captured the yield estimation relatively well, comparable to the observations (MBE = -9.6 g/m^2 and RMSE = 41.5 g/m^2). Though the observed records are limited to five

years, these simulations provide valuable insights into the mean and variability of yields, highlighting the potential of the SIMRIW rain-fed model for assessing rice productivity in the context of climate change.

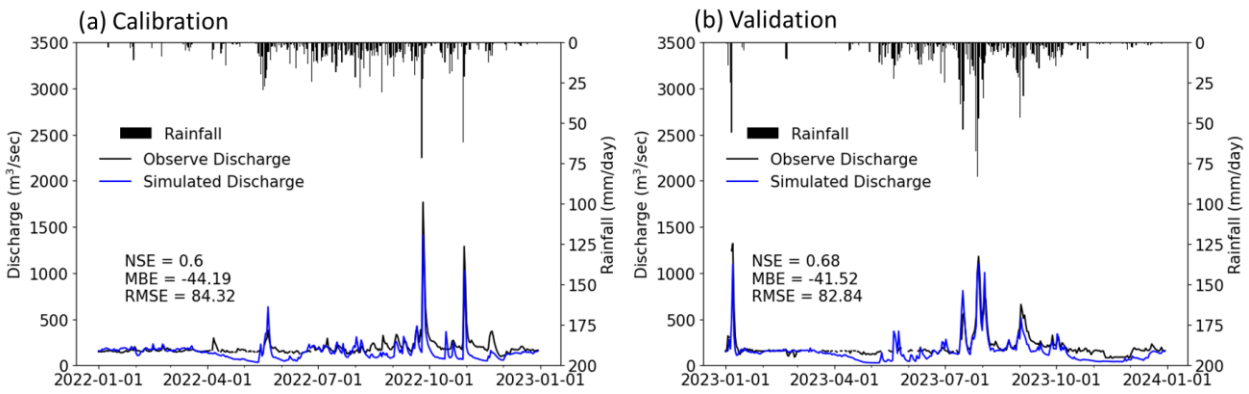

Figure 5: Comparison between observed discharge and simulated discharge at the SanIsidro gauging station: (a) model calibration for 2002 and (b) model validation for 2023

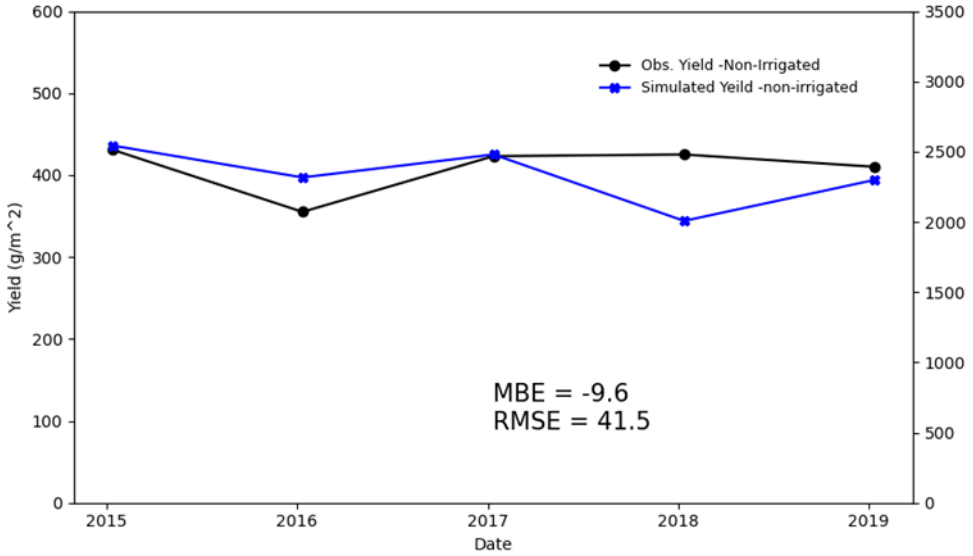

Figure 6: Comparison between reported and simulated yields of non-irrigated paddy from 2015 to 2019

3.3 Future changes in hydrological parameters

Figure 7(a) compares the annual climatology of river discharge at the San Isidro gauging station for past climates and future projections under the RCP 2.6 and RCP 8.5 scenarios. The results indicate a marginal (~1%) increase in mean discharge under RCP2.6 and a moderate (~5%) increase under RCP8.5. More importantly, the RCP8.5 scenarios exhibit greater variability and a higher probability of extreme high and low flow conditions. At the same time, the mean monthly climatology of river discharge (Fig. 7b) increases at the onset of the wet season (i.e., May–July), with the strongest amplification observed under RCP8.5. This implies an elevated risk of seasonal flooding and crop cultivation damage, as this period coincides with sowing and the early stages of crop growth. Additionally, it can be noted that the monthly mean and median discharges decrease under both future projections during August–October, highlighting the trend of water scarcity for food production. Trend analysis of daily discharges (Fig. 7c) reveals that hydrological events with a flow rate greater than 1,000 m³/s will be more frequent under

RCP8.5. However, flow rates greater than 2,000 m³/s will be more frequent under RCP2.6 than in the past. Therefore, these results further highlight the amplification of extremes in the future climate under both projections. Specifically, there will be more flood events, and low-flow events (<50 m³/s) will be more frequent (Fig. 7d) under RCP8.5.

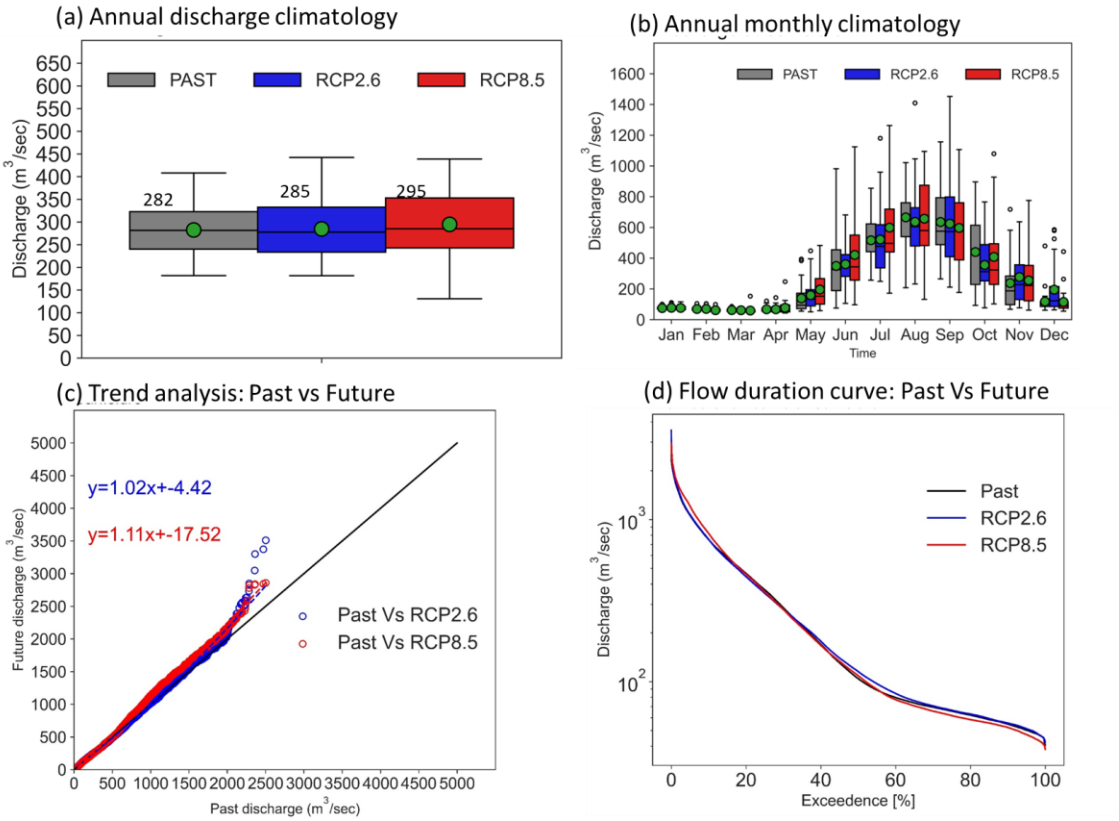

Figure 7: Comparison of basin-averaged discharge climatology and extremes at San-Isidro gauging station between historical and RCP scenario; (a) annual discharge climatology, b) annual monthly climatology, c) trend analysis of daily discharges, and d) flow duration curve. The green circle in the box-whisker plot represents the mean values.

3.4 Future changes in paddy yield

We used the calibrated WEB-RRI-SIMRIW model to simulate crop yields at the basin scale, and investigated the model outputs to assess the simultaneous impact of temperature increases, water stress, and flood inundation on paddy yields. Figure 8(a) shows the spatial distribution of rice yields across the basin under past climate conditions. As the figure shows, the simulation results indicate an average yield of around 500 g/m² in the basin and around 350 g/m² in the frequently flooding Candaba region. Figure 8(b) presents the projected mean change in yield under RCP2.6 relative to past climate conditions. Most of the basin exhibits marginal yield reductions (20 to 100 g/m²), while localized yield gains (50 to 100 g/m²) are evident in the Candaba area. Conversely, Fig. 8c shows that the projected mean yield change under RCP8.5 is more widespread and severe. Extensive areas show losses of up to 50-150 g/m².

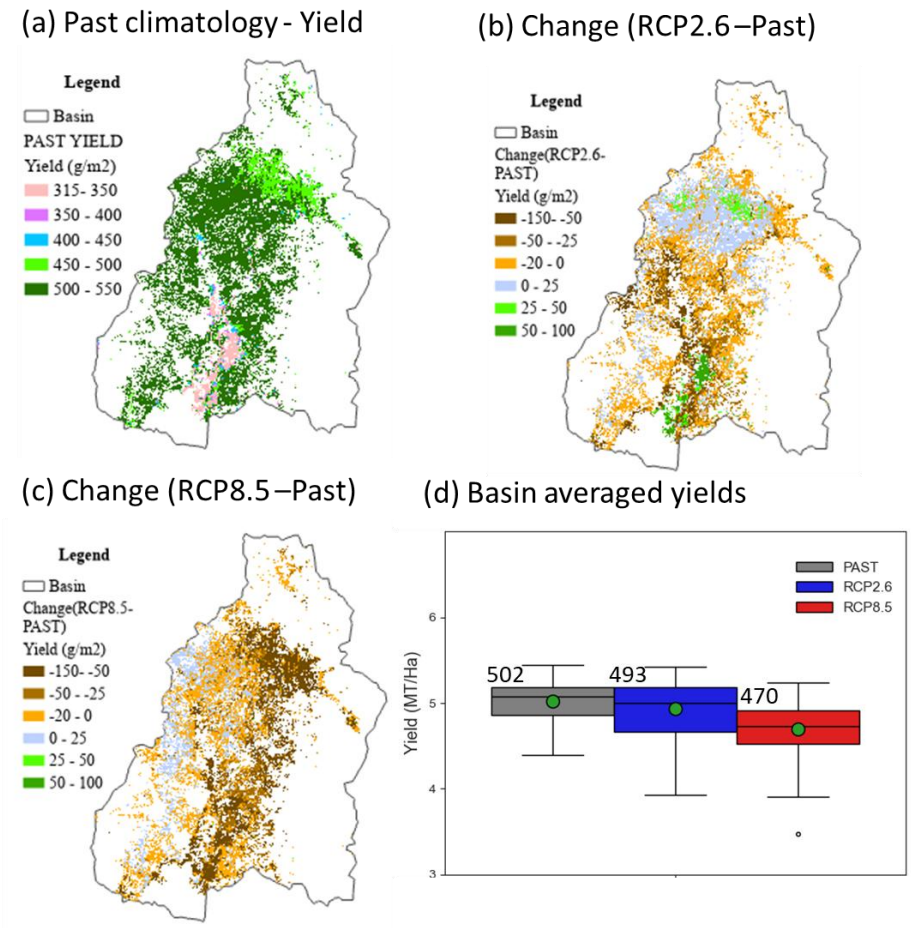

Figure 8: Comparison in annual average rain-fed -paddy yield between historical and RCP8.5 scenario; a) past climatology (g/m^2), b) changes in RCP2.6 projection compared to past (g/m^2), and c) changes in RCP8.5 projection compared to past (g/m^2), and d) basin averaged yield (MT/Ha)

The box plots (Fig. 8d) summarize basin-wide yield statistics for the historical period and future projections. The mean yield is expected to decrease by ~1.6% under RCP2.6 and by an additional 6.3% under RCP8.5 compared to past climate yields. Notably, the variability of yields under future RCPs shifts toward lower values, not only the mean values. The future climate under RCP8.5 shows that intensified climate change leads to reduced average productivity and greater uncertainty. This intensified climate change includes warming, increased flood intensity and frequency, and decreased low flow rates. Overall, these results demonstrate that average yields will not only reduce under emission scenarios but also exhibit greater risk and uncertainty, which are critical concerns for agricultural resilience and food security in the basin.

4 CONCLUSIONS

Reliably assessing the impacts of climate change on the water-food nexus is crucial for developing policies that build climate-resilient and sustainable societies. This study provides a thorough evaluation of climate change's effects on rainfall, river discharge, and water yield at the basin level, considering two different climate projections (RCP2.6 and RCP8.5), in the Pampanga basin. Projected results for the future climate show an intensification of the hydrological cycle with increased annual rainfall, an intensified monsoon onset, and amplified extreme rainfall events and intensity. We translated

these meteorological changes using a seamless Water and Energy Budget-based Rainfall-Runoff-Inundation (WEB-RRI) model coupled with the Simulation Model for Rice-Weather Relations (SIMRIW) model. This allowed us to produce a basin response with respect to water availability, hydrological extremes, and food production. The results indicate that annual river discharge at the San-Isidro gauging station will increase, especially during monsoon onset, and that the frequency and intensity of extreme high-discharge events will increase, which highlights the amplified flood risk under future climate conditions. Crop yield projections show a predominantly negative response to climate change. Moderate emissions (i.e., RCP2.6) result in relatively minor yield reductions, while high emissions (i.e., RCP8.5) lead to significant and widespread yield losses across the basin. The combined effects of climate change, including rising temperatures, altered rainfall seasonality, and increased hydrological extremes, will likely exacerbate stress on water and food security and threaten the long-term sustainability of the basin. The findings of this study provide valuable scientific evidence to support climate-informed planning, disaster risk reduction, and adaptive water and agriculture policies in the basin.

5 ACKNOWLEDGEMENTS

This research was supported by the Science and Technology Research Partnership for Sustainable Development (SATREPS) program, which is implemented in collaboration with Japan and the Philippines. The authors would like to thank the University of Tokyo for providing resources for data archiving, processing, model simulations, and evaluation through the Data Integration and Analysis System (DIAS), as well as PAGASA for providing the necessary data for developing and validating the hydrological model.

REFERENCES

IPCC, 2022: Climate Change 2022: Impacts, Adaptation, and Vulnerability. Contribution of Working Group II to the Sixth Assessment Report of the Intergovernmental Panel on Climate Change [H.-O. Pörtner, D.C. Roberts, M. Tignor, E.S. Poloczanska, K. Mintenbeck, A. Alegría, M. Craig, S. Langsdorf, S. Löschke, V. Möller, A. Okem, B. Rama (eds.)]. Cambridge University Press. Cambridge University Press, Cambridge, UK and New York, NY, USA, 3056 pp., doi:10.1017/9781009325844

Kusunoki, S. and O. Arakawa, 2015: Are CMIP5 models better than CMIP3 models in simulating rainfall over East Asia? J. Clim. 28, 5601–5621

Rockel, B., 2015: The regional downscaling approach: A brief history and recent advances, Curr. Clim. Change Rep., 1(1), 22–29

Moghim, S., Bras, R.L., 2017: Bias Correction of Climate Modeled Temperature and Precipitation Using Artificial Neural Networks. J. Hydrometeorology, 18, 1867–1884.

Sayama, T, G. Ozawa, T. Kawakami, S. Nabesaka, and K. Fukami, 2012: Rainfall-Runoff-Inundation Analysis of Pakistan Flood 2010 at the Kabul River Basin, Hydrological Sciences Journal, 57(2), pp. 298-312.

Zheng, Y., J. Li, T. Zhang, Y. Rong, and P. Feng, 2021: Exploring the Application of Flood Scaling Property in Hydrological Model Calibration, Journal of Hydrometeorology, 22(12), 3255-3274

Rasmy, M., T. Sayama, T. Koike, 2019: Development of water and energy Budget-based Rainfall-Runoff -Inundation model (WEB-RRI) and its verification in the Kalu and Mundeni River Basins, Sri Lanka. J. Hydrol. 579, 124163

Horie, T., Nakagawa, H., Centeno, H., Kropff, M., 1995: The rice crop simulation model SIMRIW and its testing. In: Matthews, R.B., Kropff, M.J., Bachelet, D., van Laar, H.H.

(Eds.), Modeling the Impact of Climate Change On Rice Production. CAB International, AsiaOxon, U.K., pp. 51–66.

Homma, K., Maki, M., Hirooka, Y., 2017: Development of a rice simulation model for remote-sensing (SIMRIW-RS). J. Agric. Meteorol. 73, 9–15. https://doi.org/10.2480/agrmet.d-14-00022.

Maki, M., Sekiguchi, K., Homma, K., Hirooka, Y., Oki, K., 2017. Estimation of rice yield by SIMRIW-RS, a model that integrates remote sensing data into a crop growth model. J. Agric. Meteorol. 73, 2–8. https://doi.org/10.2480/agrmet.D-14-00023.

Raksapatcharawong, M., Veerakachen, W., Homma, K., Maki, M., & Oki, K., 2020: Satellite-Based Drought Impact Assessment on Rice Yield in Thailand with SIMRIW-RS. Remote Sensing, 12(13), 2099. https://doi.org/10.3390/rs12132099

Inomata, H., K. Takeuchi, K. Fukami, 2009: Development of a statistical bias correction method for daily rainfall data of GCM20. Annu J Hydraul Eng 55, 247–252

ICFM 10
Adapting to Global Change:
Innovative Approaches to Flood Management and Resilience
May 20-22, 2026 | Western University, London, Ontario, Canada

Identifying boundaries that enhance system resilience in an integrated FRM project

Max C.J. de Vries[1], Joanne Vinke-de Kruijf[1], Leentje Volker[1], and Denie C.M. Augustijn[1]
University of Twente, the Netherlands[1]
Corresponding author e-mail: m.c.j.devries@utwente.nl

ABSTRACT

Traditionally, flood risk management (FRM) has relied on engineered structures to prevent floods. However, this strategy does not enhance system resilience as it only reduces the probability of flooding, focusing on the capacity to resist floods and neglecting the absorptive capacity of a landscape. Therefore, there have been calls for more integrated FRM, where flood prevention is viewed as interdependent with other spatial challenges. However, considering system interdependencies is complex. To manage this complexity, system boundaries have to be drawn. Setting boundaries is a balancing act; both too tight and too wide boundaries may cause problems. This study, therefore, asks: *To what extent do boundaries applied in FRM projects contribute to or hinder system resilience?* To analyse these boundaries and their impact on resilience, we combine insights about system and resilience thinking with insights from the literature on forward-looking decision-making. The latter allows us to account for the temporal aspects of resilience, which is key in FRM projects, given their high uncertainty and infrastructure systems with long lifespans. We developed a conceptualisation of boundaries that distinguishes between spatial, domain, hazard, participation, and temporal boundaries. We apply this conceptual framework to a project that aimed to reduce flood risks while improving spatial quality in the Netherlands. In this case, most boundaries were neither tight nor wide. As such, the project balanced between complexity and manageability. One boundary that was drawn notably tight concerns hazards, focusing solely on resilience to flooding without considering other disturbances. The participation boundary was relatively wide, encompassing diverse stakeholders, multiple levels, and various types. This research provides a practical framework for boundaries to consider in integrated FRM projects, acknowledging the need to balance complexity by drawing boundaries that are manageable yet supportive of system resilience.

KEYWORDS: Flood risk management, system thinking, flood resilience, spatial planning, system boundaries

1 INTRODUCTION

For several decades, flood risk management (FRM) in the Netherlands has relied on engineered structures that reduce the probability of flooding (Tempels & Hartmann, 2014; Verweij et al., 2021). Notable examples include the Dutch Delta Works, constructed after the 1953 storm surge that affected major parts of the Netherlands. This prevention-based FRM strategy is an illustrative example of the Netherlands' century-long fight against water. However, climate change is increasingly impacting urban and rural areas, intensifying extreme weather events and sea-level rise and increasing flood risks. The expected increase in both flood frequency and severity, coupled with spatial challenges such as urbanisation, suggests that an FRM strategy relying solely on engineered structures is unlikely to be the remedy to future flooding (IPCC, 2023; Van Buuren et al., 2016). Around the world, policies reflect a growing awareness of shifting towards innovative, more integrated FRM concepts. This shift is also referred to as the diversification of FRM strategies, in which flood resilience is enhanced not only by resisting to floods, but also by enabling the capacity to absorb, recover, transform and adapt to them (Hegger et al., 2016). Despite existing international and national policies on integrated FRM, the implementation of

integrated FRM – which would generally enhance resilience – remains challenging (Bosoni et al., 2023; Hartmann & Spit, 2016).

An underlying factor is the complexity involved in enhancing system resilience. Thinking in terms of system resilience often implies taking a holistic view, acknowledging interdependencies between and within system elements (Helfgott, 2018). This increases complexity and potentially leads to 'paralysis by analysis' as more and more elements and interconnections are taken into account (De Loë & Patterson, 2017). Therefore, when considering resilience, one is always drawing boundaries regarding resilience of what, to what, for whom and over what timeframe (Helfgott, 2018). Resilience thinking, therefore, involves balancing boundaries and acknowledging the difficulty of fully understanding all interdependencies within an entire system.

In response to calls for integrated FRM, which requires actors to collaborate across more and diverse domains (Willems et al., 2022), and which spans a longer time frame (Pot et al., 2019), this study highlights the importance of balancing system boundaries that enhance resilience. We consider that integrated FRM has a pivotal role in enhancing resilience (Doornkamp et al., 2024) and that its implementation requires making forward-looking decisions to address uncertainty. However, the extent to which boundaries in integrated FRM enhance resilience, and whether these boundaries support forward-looking decisions, remains understudied. To address this knowledge gap, we address the following question: *To what extent do boundaries applied in FRM projects contribute to or hinder system resilience?* To answer this question, we develop and apply a framework to assess boundaries in integrated FRM projects. Empirically, we focus on a regional project in the Netherlands that integrated two objectives: ensuring flood safety and enhancing spatial quality. Based on the analysis of the implemented Polder Project, we identify the extent to which boundaries are supportive or restrictive of contributing to system resilience. Consequently, this research offers guidance on balancing boundaries to enhance flood resilience.

2 THEORY

In this section, we further explore the concept of system boundaries, which addresses the ever-increasing complexity of interdependent systems, and explain resilience and forward-looking decisions in relation to these boundaries. We conclude with a conceptualisation of boundaries in integrated FRM.

2.1 Balancing boundaries in flood risk management

Although integrating a wide range of environmental challenges brings co-benefits (Bakhanova et al., 2025), involving more domains, expanding the scope, and extending the time horizon generally also increases complexity. To manage the growing interdependence and complexity within and between systems, practitioners, experts, researchers, and individuals tend to draw – sometimes explicitly but oftentimes implicitly – system boundaries, to reduce complexity (Meadows, 2009). These boundaries typically reflect different transition zones. In the social sphere, boundaries may refer to the need to bridge between differing values and perspectives among individuals, organisations, or domains. Boundaries can also be physical, for example, marking transitions in land use, ecosystems, or hydrological systems (Van den Brink et al., 2022).

These system boundaries may be drawn rather tightly or too widely. Tight boundaries oversee potential adverse outcomes in adjacent systems, which are on 'the other side' of the boundary but enable more manageable analysis and demand fewer resources from actors. On the other hand, wider boundaries increase complexity as they may overwhelm system analysts by complicating the analysis of numerous potential interdependencies, while still allowing for system interconnections (De Loë & Patterson, 2017; Meadows, 2009). For FRM, boundaries were rather clear, as the focus was on engineered and sectoral solutions to flooding (Van Buuren et al., 2016). However, interdependent climate and spatial challenges emphasise the need for more integrative FRM that enhances flood resilience, for example, by acknowledging the need to address the consequences of flooding in spatial planning. The boundaries in FRM are therefore broadening, as flood solutions are increasingly considered as an interdependent social,

ecological, and technological system (Markolf et al., 2018). This calls for more balanced boundaries that recognise increasing complexity, without simplifying the challenges at hand.

Various studies show that in FRM and the water sector in general, system boundaries are often defined quite tightly (De Loë & Patterson, 2017; Van Meerkerk et al., 2013; Vinke-de Kruijf et al., 2024). Previous research in the Netherlands, which conceptualises boundary judgements as the explicit and implicit decisions made about who and what to include in FRM projects, confirms this. It shows that regional water authorities, accustomed to making decisions independently, tend to draw tight boundaries, hindering cross-sectoral collaboration, reducing participation, limiting the scope, and lacking adaptability (Van Meerkerk et al., 2013; Vinke-de Kruijf et al., 2024). Other studies employ the concept of boundaries differently, emphasising the inherently subjective and value-laden character of boundary judgements, which arises when analysing the roles of specific actors. For example, Van den Brink et al. (2019) emphasise the crucial role of actors in integrated FRM: the earlier actors are involved, the more crucial their role is in spanning boundaries and converging values and perspectives within integrated FRM.

2.2 Resilience and forward-looking system boundaries

Resilience thinking is generally characterised by a holistic philosophy that considers everything within and between systems (Helfgott, 2018). To analyse system resilience and make it more manageable and less complex, system boundaries are drawn. This also applies to the context of FRM, where we acknowledge the need to balance boundaries to enhance flood resilience. This is often associated with the alignment of three capacities of a system to 1) resist floods, 2) absorb and recover from floods, and 3) transform and adapt to floods (Hegger et al., 2016). This view necessitates a comprehensive systemic perspective, wherein resistance-oriented structures, such as dikes, throughout the entire flood-prone area are considered alongside required institutional changes to transform and adapt to future floods (ibid.). However, adopting this perspective not only requires drawing boundaries related to geographic scale or the involvement of various domains in integrated FRM (Willems et al., 2022), but also to temporal boundaries.

In times of great uncertainty, making forward-looking decisions is crucially important. Such decisions consider adaptability (Pot et al., 2018) but also consider future developments. As such, they enable the selection of adaptive alternatives that are suited to changing circumstances (Pot et al., 2019). We further build on the *forward-looking* element of integrated FRM projects, since integrated FRM generally encompasses a longer time frame compared to traditional FRM (Pot et al., 2019). We build upon the forward-looking decision framework to analyse the extent to which integrated FRM is forward-looking. This framework considers whether the problem at hand, the proposed solution, and the justification are forward-looking (Pot et al., 2018).

In the subsequent section, we conceptualise system boundaries in integrated FRM in relation to resilience and forward-looking decision-making.

2.3 Conceptualising boundaries in integrated FRM

To operationalise boundaries that enhance system resilience in FRM, we use the four framing questions identified by Helfgott (2018) which specify resilience *of what*, *to what*, *for whom*, and *over what timeframe.* We enrich this framework with criteria for making forward-looking decisions (Pot et al., 2018). In the context of FRM, we further build on boundary typologies identified in adaptive water governance and integrated FRM projects (Van Meerkerk et al., 2013; Vinke-de Kruijf et al., 2024) and distinguish five system boundaries: spatial, domain, hazard, participation, and temporal (Table 1).

Spatial scale refers to '*resilience of what*' and concerns which geographical boundaries of the system are of interest. This indicates whether the geographical system boundaries are tight or wide. For instance, do boundaries reflect the hydrological properties and dike trajectory alongside the river, the potentially affected flood-prone area, or an entire catchment?

The **domain** boundary, considers the extent to which multiple domains are involved (Vinke-de Kruijf et al., 2024), which also relates to '*resilience of what*'. We use 'domain' instead of sector, as the former is broader and also refers to expertise and knowledge, while sectors are mainly considered as a specific subset

of a larger system or economy. For this conceptualisation, we ask whether only the flood protection domain is involved, or whether broader water-related domains or adjacent areas such as housing or agriculture are also considered.

We define a **hazard** boundary considering the '*resilience to what*' disturbance. To make forward-looking decisions, a problem definition should include consideration of future challenges to which resilience is enhanced (Pot et al., 2018). We assess where boundaries are drawn and which challenges are considered. For instance, does the integrated FRM project include flood-related disturbances only, or does it also address drought or external disturbances (Van Meerkerk et al., 2013)?

The fourth boundary relates to stakeholder **participation**, focusing on '*resilience for whom*' and questioning the extent to which system features need to be preserved for whom. A tight boundary involves only one stakeholder group, such as experts, government organisations, and citizens (Vinke-de Kruijf et al., 2024). Expanding boundaries to include a broader and more diverse range of stakeholders, both horizontally and vertically, increases complexity but allows for a greater variety of perspectives to be heard.

The last boundary concerns '*resilience over what time frame*', addressing the often longer timespan of integrated FRM, and the necessity to take forward-looking decisions (Pot et al., 2018). The **temporal** boundary defines the time horizon considered, with tight boundaries representing a few years, and wider boundaries contributing to resilience that extend at least 100 years. (Vinke-de Kruijf et al., 2024). It also touched upon the adaptability of the solution over the considered time frame, i.e., can it be adapted to changing circumstances, and to what extent the decision-making process is adaptive (Pot et al., 2018). A rigid, less adaptable solution and process are less capable of dealing with changing circumstances.

Table 1: Five categories of system boundaries in integrated FRM.

Category	**Explanation**	**Resilience framing**
Spatial	Geographical scale of the implemented project.	*Resilience of what?*
Domain	Involved domains in the project.	*Resilience of what?*
Hazard	External disturbances considered.	*Resilience to what?*
Participation	Involved stakeholders in project phases.	*Resilience for whom?*
Temporal	Time horizon and adaptability of the solution and process.	*Resilience over what time frame?*

3 METHODOLOGY

To answer our research question, we use empirical evidence derived from a single case. Based on the distinction between system boundaries, we examine the extent to which these boundaries support or restrict system resilience in an integrated FRM project in the Netherlands. We first describe the Dutch context and our case. Finally, we elaborate on data collection and analysis.

3.1 Case description and context

We focus empirically on the Polder Project, where an existing dike protecting a low-lying polder was opened to allow water to flow freely in the event of high discharges in the surrounding rivers (Figure 1). This project was part of the Space for the River programme, which was initiated in response to the 1993 and 1995 extreme water levels in the major rivers in the Netherlands (Bosoni et al., 2023; Hegger et al., 2020; Pot et al., 2024). Compared to engineered FRM, which focuses on flood prevention by heightening dikes and resisting floods (Hegger et al., 2016), the Space for the River programme aimed to create more space for the river with two key objectives: flood safety and spatial quality (Van den Brink et al., 2019).

Completed in 2015, the Polder Project employed a co-creative design approach that involved extensive participation from local stakeholders. After involving local stakeholders, a design was proposed that protected inhabited areas in the polder with mounds, while transportation routes were elevated on smaller levees within the landscape. The project introduced a special programme structure that included a team focused specifically on spatial quality, ensuring that the double objective could be achieved (Berenschot, 2018).

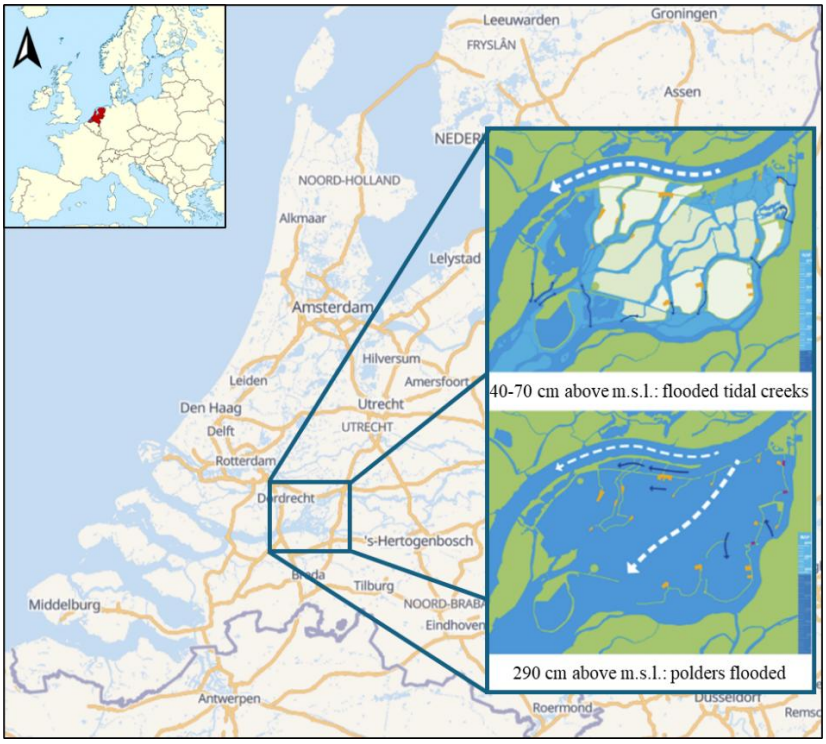

Figure 1: The Polder Project situated within the Netherlands, displaying a situation where the tidal creeks are flooded, and a situation where all polders, except the mounds and levees, are flooded (adapted from Bralts (2024)).

3.2 Data collection and operationalisation

Data were collected through document analysis and seven 90-minute-long semi-structured interviews (Bralts, 2024). The document analysis included action plans, policy and design documents, news articles and evaluations. The interviewees were selected based on their background, role, and expertise, and included representatives from governmental institutes, a research institute, and the Space for the River programme management. All interviews were recorded, fully transcribed, and the interviewees signed a consent form to inform them that they could withdraw at any time. The interviews were analysed in Atlas.ti using deductive thematic analysis with predefined codes related to, e.g., forward-looking decision-making.

Building on the distinction of system boundaries as presented in Table 2, we empirically identify the system boundaries of the implemented integrated FRM project. We use a three-point scale to assess whether system boundaries are tight, wide, or moderate, as shown in Table 2. In consideration of resilience thinking, which requires a holistic perspective, we regard wide boundaries as those that more accurately support system resilience. We associate tight boundaries with a sectoral, expert-centred and short-term approach.

Table 2: Assessment of system boundaries.

Category	Tight	Moderate	Wide
Spatial	Dike trajectory	Flood-prone area	River catchment
Domain	Flood protection	Water-related	Beyond the water domains
Hazard	Flood-related disturbance	Water-related disturbance	Water and external disturbances
Participation	Expert-centred stakeholder involvement	Horizontal **or** vertical involvement of diverse stakeholders	Horizontal **and** vertical involvement of diverse stakeholders
Temporal	Short-term (years) and rigid solutions and process	Medium-term (decades) and adaptable solution or process	Long-term (century) and adaptable solution and process

4 CASE STUDY RESULTS

This section presents the preliminary results of spatial, domain, hazard, participation, and temporal boundaries in the integrated FRM project and discusses the extent to which the drawn boundaries are supportive or restrictive to system resilience.

4.1 Assessment of boundaries

In the Polder Project, the **spatial boundary** was **moderate**. The project extended beyond a traditional dike reinforcement project, involving the depoldering of an area of approximately 2,000 hectares. However, it did not evaluate the potentially affected land in the river catchment. Multiple alternatives were considered, starting with a side channel through the area. This solution was rather tight and lacked support from local stakeholders. This led to a broader scope, involving the replacement of dikes and depoldering the area.

The **domain boundary** was also **moderate**. Primarily, the flood protection domain was considered without accounting for droughts and sea level rise. Nevertheless, flood safety was integrated with spatial quality as part of the project's dual objective, which involved domains as diverse as archaeology and cultural history. Although the dual objective of the project led to the involvement of various disciplines, only flood protection was considered in relation to water.

The **hazard boundary** was **tight**, since boundaries were only drawn in relation to resilience to flooding, without considering other water-related or external disturbances explicitly. The primary focus of the Polder Project was on addressing flood-related disturbances associated with riverine discharges, while overlooking droughts, sea level rise, and other water-related disturbances. For the spatial quality objective, no long-term goals or other external disturbances were explicitly considered.

The **participation boundary** was **wide** due to the inclusion of a diverse range of stakeholders, both horizontally and vertically. The project involved experts, regional governments, and national government bodies, which covered most costs and risks, thereby promoting collaboration among various stakeholders. Additionally, inhabitants had an active say in the project, and responsibilities were distributed among multiple national ministries.

The **temporal boundary** was **moderate**. As a long-term problem, only potential increases in river discharges have been considered, without accounting for potential long-term sea-level rise. To evaluate the integrated FRM solution for extreme flood events, hydraulic models have been utilised to assess its long-term effectiveness. Long-term spatial design has not been developed, as land-use claims in the Netherlands are affected by the constantly changing political climate. Instead, improvements in spatial quality for the Polder Project have focused on the short and medium term, with the flexible development of biodiversity and nature explicitly considered for future development. While adaptability to future development is considered dual – both in terms of flood safety and spatial quality – the project structure no longer exists, hindering adaptation to future changes.

4.2 How boundaries contributed to or hindered resilience

In this paragraph, we briefly reflect on whether the applied boundaries were contributing to system resilience or not. First, we observe that regarding resilience '*of what*', relating to spatial scale and domain involvement, moderate boundaries were applied, indicating that complexity is balanced between adopting a holistic perspective and maintaining manageable analysis. Resilience '*to what*' is considered tight, encompassing only flood-related disturbances. Conversely, resilience '*to whom*' is assessed widely, reflecting the participation of a wide range of stakeholders both horizontally and vertically. Lastly, resilience '*over what time frame*' is assessed as moderate, since neither a long-term (century) perspective was incorporated into flood protection nor spatial planning. Despite the solution being adaptable, the programme structure has been abolished, thereby impeding an adaptive decision-making process should a river catchment-wide disturbance recur. When conceptualising resilience based on these four framing categories, we consider the boundaries drawn in the Polder Project to be rather diverse, balancing complexity in considering disturbances with a holistic perspective of stakeholder involvement.

5 CONCLUSION AND OUTLOOK

Bringing together insights from systems thinking, resilience, and forward-looking decision-making, this study designed a framework to evaluate the extent to which system boundaries contribute to or hinder system resilience within an integrated FRM project in the Netherlands. We operationalised five boundaries, each framed by questions that specify system resilience in distinct ways, with wider boundaries reflecting a more holistic view but also adding complexity. Overall, we observe that the boundaries drawn in the considered integrated FRM project are rather moderate or wide. Considering that thinking in terms of system resilience typically involves a holistic perspective, and given that only one boundary in the Polder Project was tightly defined, we conclude that the Polder Project may potentially contribute to resilience regarding flooding. Nevertheless, because the assessment of hazards was tight due to its primary emphasis on flood protection, further research is required to determine how the project enhances system resilience to other disturbances.

Looking ahead, we would like to discuss some future research considerations. Firstly, operationalising resilience and setting boundaries involve values, as organisations and individuals draw boundaries based on their own perspectives and values. Further research into how experts or institutions perceive resilience and boundaries could reveal important insights into the informal mechanisms behind system analysis. Secondly, we note that some boundaries overlap; for example, in our case, stakeholder involvement and domain inclusion coexist. Therefore, we recommend further research into how boundary categories interact, creating synergies or trade-offs. Finally, as the project relied heavily on informal citizen involvement to facilitate a spatial solution, we suggest further study into the importance of including informal relations that usually remain outside formal institutional frameworks.

Acknowledgements.

We thank Ruben Bralts for thoroughly documenting the Polder Project case in light of his MSc Thesis research on spatial approaches to flood resilience. We also thank Anicia Touraine Andersson for proofreading an earlier version.

REFERENCES

Bakhanova, E., Vinke-de Kruijf, J., Wöhler, L., Warbroek, B., & Arentsen, M. (2025). Integrative Approaches to Interconnected Environmental Challenges: How Institutional Factors Influence Cross-Sector Integration in Dutch Rural Areas. *Environmental Management*, *75*(5), 1308–1321. https://doi.org/10.1007/s00267-025-02140-2

Berenschot. (2018). *Ruimte voor de rivier. Sturen en ruimte geven. Eindevaluatie.*

Bosoni, M., Tempels, B., & Hartmann, T. (2023). Understanding integration within the Dutch multi-layer safety approach to flood risk management. *International Journal of River Basin Management*, *21*(1), 81–87. https://doi.org/10.1080/15715124.2021.1915321

Bralts, R. (2024). *Flood resilience through spatial approaches: Preparing for the future* [MSc Thesis]. University of Twente.

De Loë, R. C., & Patterson, J. J. (2017). Rethinking water governance: Moving beyond water-centric perspectives in a connected and changing world. *Natural Resources Journal*, *57*(1), 75–100.

Doornkamp, T. J. L., Vinke-de Kruijf, J., Pahlow, M., & Matheson, D. (2024). How flood risk management projects can improve urban resilience: A combined assessment approach of functional resilience and adaptive capacity. *Australasian Journal of Water Resources*, *29*(1), 8–18. https://doi.org/10.1080/13241583.2024.2429226

Hartmann, T., & Spit, T. (2016). Implementing the European flood risk management plan. *Journal of Environmental Planning and Management*, *59*(2), 360–377. https://doi.org/10.1080/09640568.2015.1012581

Hegger, D. L. T., Alexander, M., Raadgever, T., Priest, S., & Bruzzone, S. (2020). Shaping flood risk governance through science-policy interfaces: Insights from England, France and the Netherlands. *Environmental Science & Policy*, *106*, 157–165. https://doi.org/10.1016/j.envsci.2020.02.002

Hegger, D. L. T., Driessen, P. P. J., Wiering, M., van Rijswick, H. F. M. W., Kundzewicz, Z. W., Matczak, P., Crabbé, A., Raadgever, G. T., Bakker, M. H. N., Priest, S. J., Larrue, C., & Ek, K. (2016). Toward more flood resilience: Is a diversification of flood risk management strategies the way forward? *Ecology and Society*, *21*(4). https://doi.org/10.5751/es-08854-210452

Helfgott, A. (2018). Operationalising systemic resilience. *European Journal of Operational Research*, *268*(3), 852–864. https://doi.org/10.1016/j.ejor.2017.11.056

IPCC. (2023). *Climate Change 2023: Synthesis Report* (Core Writing Team, H. Lee, & J. Romero, Eds). IPCC, Geneva, Switzerland.

Markolf, S. A., Chester, M. V., Eisenberg, D. A., Iwaniec, D. M., Davidson, C. I., Zimmerman, R., Miller, T. R., Ruddell, B. L., & Chang, H. (2018). Interdependent Infrastructure as Linked Social, Ecological, and Technological Systems (SETSs) to Address Lock-in and Enhance Resilience. *Earth's Future*, *6*(12), 1638–1659. https://doi.org/10.1029/2018ef000926

Meadows, D. H. (2009). *Thinking in systems: A primer*. Earthscan.

Pot, W. D., de Ridder, Y., & Dewulf, A. (2024). Avoiding future surprises after acute shocks: Long-term flood risk lessons catalysed by the 2021 summer flood in the Netherlands. *Environmental Sciences Europe*, *36*(1). https://doi.org/10.1186/s12302-024-00960-3

Pot, W. D., Dewulf, A., Biesbroek, G. R., & Verweij, S. (2019). What makes decisions about urban water infrastructure forward looking? A fuzzy-set qualitative comparative analysis of investment decisions in 40 Dutch municipalities. *Land Use Policy*, *82*, 781–795. https://doi.org/10.1016/j.landusepol.2018.12.012

Pot, W. D., Dewulf, A., Biesbroek, G. R., Vlist, M. J. van der, & Termeer, C. J. A. M. (2018). What makes long-term investment decisions forward looking: A framework applied to the case of Amsterdam's new sea lock. *Technological Forecasting & Social Change*, *132*, 174–190. https://doi.org/10.1016/j.techfore.2018.01.031

Tempels, B., & Hartmann, T. (2014). A co-evolving frontier between land and water: Dilemmas of flexibility versus robustness in flood risk management. *Water International*, *39*(6), 872–883. https://doi.org/10.1080/02508060.2014.958797

Van Buuren, A., Ellen, G. J., & Warner, J. F. (2016). Path-dependency and policy learning in the Dutch delta: Toward more resilient flood risk management in the Netherlands? *Ecology and Society*, *21*(4). https://doi.org/10.5751/es-08765-210443

Van den Brink, M., Edelenbos, J., Van den Brink, A., Verweij, S., van Etteger, R., & Busscher, T. (2019). To draw or to cross the line? The landscape architect as boundary spanner in Dutch river management. *Landscape and Urban Planning*, *186*, 13–23. https://doi.org/10.1016/j.landurbplan.2019.02.018

Van den Brink, M., Van den Brink, A., & Bruns, D. (2022). Boundary thinking in landscape architecture and boundary-spanning roles of landscape architects. *Landscape Research*, *47*(8), 1087–1099. https://doi.org/10.1080/01426397.2022.2091121

Van Meerkerk, I., van Buuren, A., & Edelenbos, J. (2013). Water Managers' Boundary Judgments and Adaptive Water Governance. An Analysis of the Dutch Haringvliet Sluices Case. *Water Resources Management*, *27*(7), 2179–2194. https://doi.org/10.1007/s11269-013-0282-7

Verweij, S., Busscher, T., & van den Brink, M. (2021). Effective policy instrument mixes for implementing integrated flood risk management: An analysis of the 'Room for the River' program. *Environmental Science & Policy*, *116*, 204–212. https://doi.org/10.1016/j.envsci.2020.12.003

Vinke-de Kruijf, J., Groefsema, L., & Snel, K. A. W. (2024). Diversification of flood risk management in the Netherlands: Implications for boundary judgement practices. *Journal of Flood Risk Management*. https://doi.org/10.1111/jfr3.13028

Willems, J. J., Kuitert, L., & Van Buuren, A. (2022). Policy integration in urban living labs: Delivering multi-functional blue-green infrastructure in Antwerp, Dordrecht, and Gothenburg. *Environmental Policy and Governance*. https://doi.org/10.1002/eet.2028

ICFM 10
Adapting to Global Change:
Innovative Approaches to Flood Management and Resilience
May 20-22, 2026 | Western University, London, Ontario, Canada

Forecast-Informed Reservoir Operations (FIRO): A Roadmap of Lessons Learned for Implementation

Joe Forbis[1], Cary Talbot[2], Cuong Ly[3]
US Army Corps of Engineers, Engineer Research and Development Center, Coastal and Hydraulics Laboratory, Sacramento, CA United States[1]
E-mail: joseph.c.forbis@usace.army.mil

US Army Corps of Engineers, Engineer Research and Development Center, Coastal and Hydraulics Laboratory, Vicksburg, MS United States[2]
E-mail: cary.a.talbot@usace.army.mil

US Army Corps of Engineers, South Pacific Division, Los Angeles, CA United States[3]
E-mail: cuong.ly@usace.army.mil

ABSTRACT

Population increases have led to dramatic changes in water demand. For over a decade, the U.S. Army Corps of Engineers (USACE) and the Center for Western Weather and Water Extremes (CW3E) has led the multi-agency, multi-disciplinary research and development initiative called Forecast-Informed Reservoir Operations (FIRO) that explores the potential of enhanced forecast skill, advanced hydrologic modelling, and improved observational networks to optimize water management decisions in reservoir operations. Traditional reservoir management strategies solely rely on historical hydrologic data, which can be insufficient for capturing the dynamic nature of extreme weather events and long-term climate variability. FIRO addresses this limitation by integrating real-time and forecasted hydrometeorological information to inform reservoir release decisions, balancing competing demands for water management purposes such water supply and conservation, flood risk management, and environmental benefits. Pilot implementations of FIRO at various sites in the United States have demonstrated its capacity to significantly improve water availability, particularly during drought periods, while simultaneously enhancing flood risk management by strategically releasing water prior to major storm events. Furthermore, FIRO can be leveraged to optimize flows for environmental benefits, such as maintaining suitable water temperatures and flow regimes for aquatic species. These improvements have been achieved without requiring substantial and costly infrastructure modifications. Lessons have been learned from years of research and development focused on assessing FIRO viability and its integration into water control manuals, the USACE guidance documents that prescribe the rules for reservoir operations. The research included advancements in forecasting techniques, hydrologic model calibration and validation, and the utilization of decision support tools tailored to specific reservoir characteristics and operational objectives. Diverse pathways for FIRO implementation were developed, considering factors such as regional climate, regulatory frameworks, and stakeholder engagement. The status of FIRO implementation at various pilot sites shows the successes, challenges, and ongoing research.

KEYWORDS: forecast-informed reservoir operations, flood risk management, reservoir management, atmospheric rivers

1 INTRODUCTION

The U.S. Army Corps of Engineers (USACE) prescribes flood control operations in water control manuals (WCMs). Many of these WCMs are decades old and may not fully capture changed conditions in watersheds or include the benefit of state-of-the-science weather and streamflow prediction. Historically, reservoir operations have been governed by rule curves primarily derived from climatology, prioritizing "water on the ground" observations. However, the stationary climate assumption is increasingly challenged by climate variability, characterized by vacillations between extreme drought and severe flooding.

Forecast-Informed Reservoir Operations (FIRO) is a reservoir-operations strategy that better informs decisions to retain or release water by integrating additional flexibility in operational policies and rules with enhanced monitoring and improved weather and water forecasts (Jasperse et al, 2020). By integrating forecast information, FIRO may show it is appropriate for reservoir operators to encroach into flood control pools to store water for supply when forecasts are dry, or to release water ahead of extreme events to create additional flood storage capacity.

1.1 USACE Policy Update

The exploration of potential FIRO viability is supported by updates to USACE policy, specifically ER 1110-2-240 (Water Control Management). The 2016 update allowed for the use of forecasted conditions in planning future operations, provided that such operations do not compromise dam safety or flood risk management objectives (USACE, 2016). This change in guidance enabled the FIRO pilot projects to test and validate new FIRO strategies through temporary deviations to reservoir operations, laying the groundwork for permanent updates to WCMs.

1.2 Atmospheric Rivers and Forecast Skill

The viability of FIRO in the western U.S. is linked to the predictability of atmospheric rivers (ARs), which drive both water supply and flood risks in the region. Research by the Center for Western Weather and Water Extremes (CW3E) and partners has focused on improving the forecast skill for AR landfall, intensity, and duration. The premise is that improved forecast lead times support better water management decisions, such as knowing when it is safe to evacuate reservoir storage ahead of storm events. The integration of data from AR reconnaissance (AR Recon) campaigns into global models has been shown to improve precipitation forecast accuracy over the U.S., thereby enhancing FIRO operations (Zheng, M., et al, 2021).

2 VIABILITY ASSESSMENT METHODOLOGY

To operationalize FIRO, USACE and the partners in the FIRO program developed a structured, scalable framework known as the viability assessment (VA) process. This framework mirrors the rigor of a USACE feasibility study and uses a Hydrologic Engineering Management Plan (HEMP) to ensure systematic and defensible evaluation of reservoir operations strategies. The HEMP dictates a multi-step process for every VA, including objective definition, constraint identification, metric development, simulation, and comparison of alternatives (USACE, 1994).

2.1 FIRO Screening Process

To efficiently scale FIRO implementation beyond the initial pilots, USACE has developed a national FIRO Screening Process. This three-stage effort evaluates all dams in the USACE portfolio for potential FIRO suitability. The screening process examines factors such as forecast skill, reservoir infrastructure constraints, environmental considerations, and collaboration potential, and it categorizes dams into four recommendation categories:

- Strongly consider pursuing FIRO,

- Consider pursuing FIRO,
- Make improvements before pursuing FIRO, and
- Barriers to FIRO may be prohibitive – do not pursue until challenges are addressed (Yeates et al, 2023).

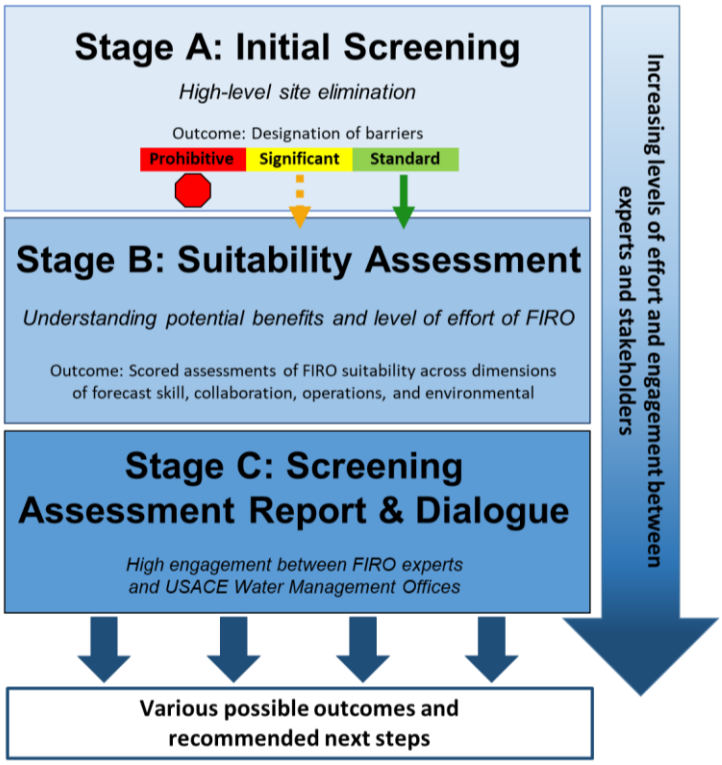

Figure 1: FIRO Screening Process Framework (Yeates et al, 2023)

2.2 Viability Assessment Pathways

For projects identified as being suitable for a VA, a set of three viability ability assessment pathways has been developed to match the level of analysis to the complexity of the site. Table 1 below summarizes key characteristics of each pathway.

Table 1 Characteristics of FIRO Viability Assessment Pathways

Pathway	Complexity	Primary Driver	Duration	Key Components
Expedited	Low	Consensus on benefits; minimal conflict	1–2 years	No PVA; uses existing models
Streamlined	Moderate	Some complexities; no major barriers	1–3 years	No PVA; minor model refinements
Full	High	Significant technical or stakeholder challenges	2–4 years	Full PVA and FVA; substantial model development

The Expedited track targets the reservoirs with the relatively lowest level of effort where minor operational changes yield benefits with low risk. The Streamlined track addresses projects with moderate complexity and allows for broader exploration of FIRO strategies without the requirement of allocate the

research resources typical of a full VA. The Full track is reserved for high-complexity environments and includes a Preliminary Viability Assessment (PVA) and a Final Viability Assessment (FVA).

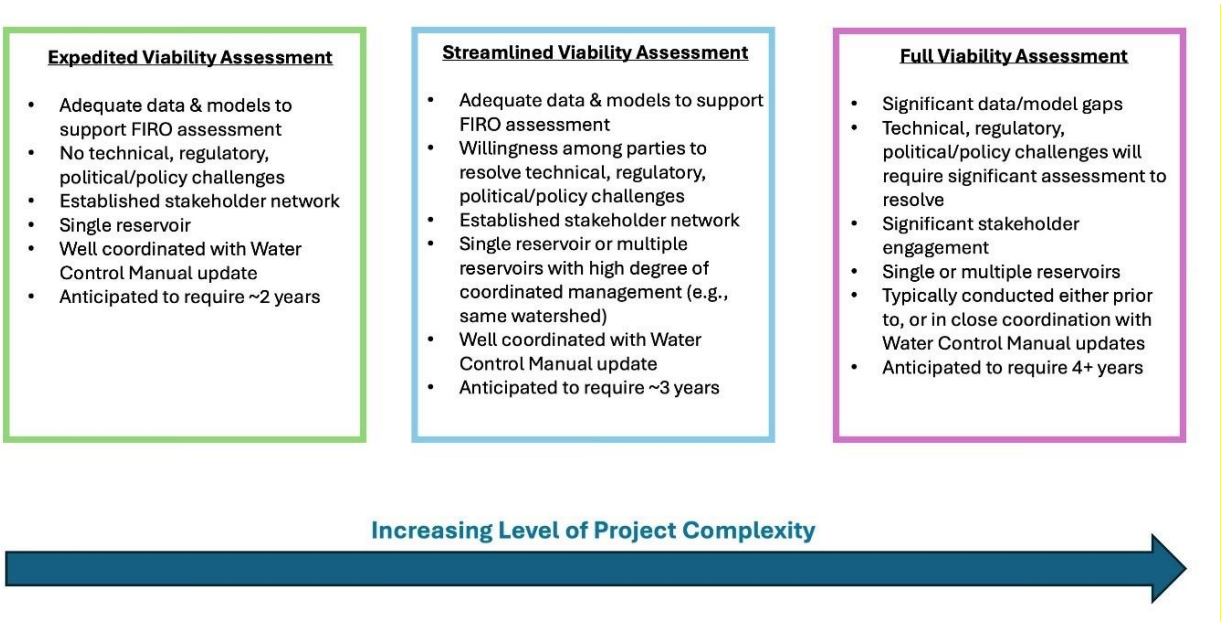

Figure 2: FIRO pathway options with increasing project complexity

3 PROGRAMMATIC LESSONS LEARNED

With the expansion of the FIRO program, several lessons can be learned regarding the processes and frameworks developed and evolved over time, going from one isolated pilot project to several pilot projects going on concurrently.

3.1 Research and Operations Partnership

A key factor in the success of FIRO has been the Research and Operations Partnership (RAOP). This approach bridges the gap between meteorologists developing numerical weather prediction models and the water managers operating the dams. By embedding researchers directly into the decision-making structure via Steering Committees, researchers gain insight into operational constraints (e.g., specific lead time requirements for safe evacuation), while operators gain a sophisticated understanding of forecast uncertainty. This bidirectional feedback loop was essential in the Lake Mendocino pilot, allowing operators to move from binary "rain/no rain" decisions to risk-based probabilistic assessments (Jasperse et al, 2020).

3.2 VA-WCM Alignment

The primary outcome of a VA is a recommendation for implementation of a FIRO strategy in a WCM update. Through the various pilot projects, there have been different alignment opportunities for VAs and WCM updates.

- Sequential Alignment (VA then WCM): In this model, the VA is completed before the WCM update begins. This allows the VA to act as a "sandbox" for innovation, unconstrained by the schedule and resourcing required of the WCM update process, but it significantly elongates the timeline for implementation.

- Concurrent Alignment (VA with WCM): In this model, the VA and WCM update proceed simultaneously. It is the fastest model by finding efficiencies in schedules. Challenges include the WCM update process requiring defined alternatives for environmental review before the VA work has fully developed them. Early coordination is identified as a critical lesson to minimize friction between these processes.

3.3 Water Control Plan (WCP) Deviations for FIRO Testing

Planned temporary deviations from the existing WCP have proven to be an essential mechanism for testing and validating FIRO strategies. A WCP is a plan of regulation for a reservoir in the interest of flood control, navigation, and other authorized purposes, and a deviation is a temporary change to a reservoir's approved WCP that can be made to respond to an unforeseen circumstance or realize opportunities to increase project benefits. These deviations allow the reservoir to implement FIRO concepts in real-time for a set period (potentially up to 5 years) while pursuing a permanent change to the WCM. This provides immediate benefits and allows operators to stress test the new rules, exposing operational challenges that models might not capture.

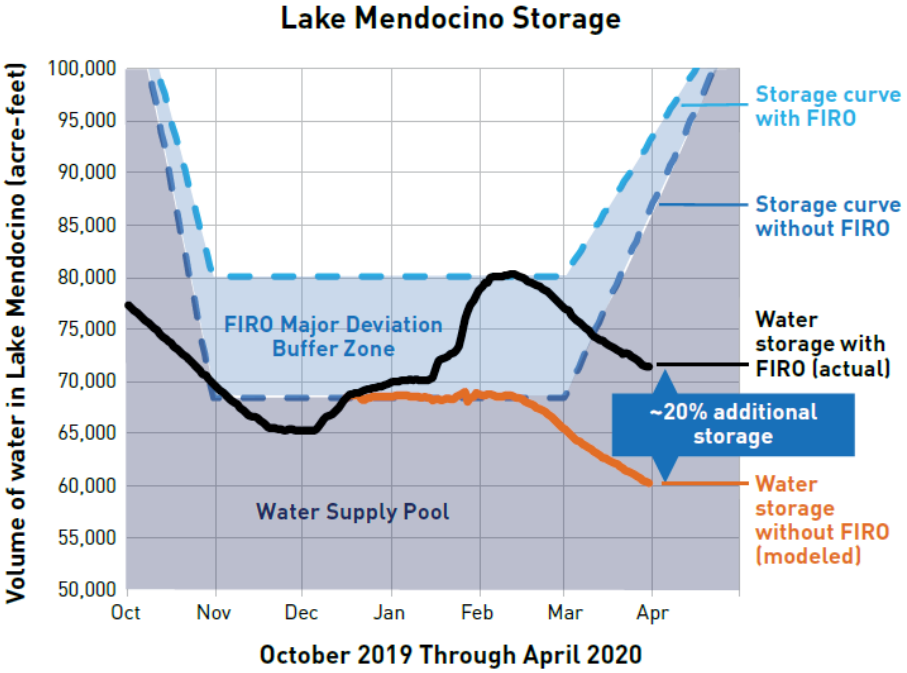

Figure 3: Water year storage graph showing 20% increase to storage due to temporary implementation of FIRO (Jasperse et al, 2020)

4 TECHNICAL FRAMEWORK AND MODELLING

The translation of FIRO from a research concept into operational reality requires a robust software infrastructure. To ensure that FIRO strategies are sustainable and safe for nationwide implementation in USACE, the USACE Hydrologic Engineering Center (HEC) has established strict standards for software compatibility, which in turn drive the development of specific modelling architectures.

4.1 Corps Water Management System (CWMS) Compatibility Standard

A formal definition of CWMS compatibility has been developed to ensure that any FIRO strategy proposed in a VA can be seamlessly transitioned into a permanent WCM update. To be considered compatible, a method must meet three criteria:

- Documentation: The operational method must be describable in Chapter 7 of the WCM in terms clear enough for future water managers to understand and execute.
- Standard Software: It must run fully within the standard CWMS modelling suite.
- Supportability: Any methods involving scripting must be developed, supported, maintained, documented, and understood by USACE district water management staff. It also must be approved by the CWMS software development team and Program Manager.

4.2 Real-Time Operations: CWMS and the Ensemble Forecast Processor

To meet the supportability and standardization requirements of the CWMS compatibility definition, HEC has adapted the Corps Water Management System (CWMS)—the USACE standard for real-time decision support—to natively handle probabilistic data.

A key technological capability in CWMS is the Ensemble Forecast Processor (EFP). This allows CWMS to natively handle probabilistic forecast information, such as the ensemble streamflow traces produced by National Weather Service's Hydrologic Ensemble Forecast System (HEFS). The EFP computes statistical metrics from the ensemble forecast and passes these metrics to the reservoir simulation model HEC-ResSim to inform logic rules, allowing water management decision-making to better account for probability, risk, and uncertainty.

4.3 Planning and Robustness: HEC-WAT and Synthetic Ensembles

While CWMS manages real-time operations, HEC-WAT (Watershed Analysis Tool) can be utilized for planning and risk analysis. Using this tool in FIRO VAs is a more recent development, and current pilot projects are developing standard operating procedures on how best to utilize HEC-WAT to support FIRO strategy development and evaluation.

A major limitation in early studies was the relatively short record of the hindcasts, the retrospective approach used to simulate and analyse past weather conditions, which often missed extreme events necessary to stress-test FIRO rules. To address this, researchers developed the Synthetic Forecast Ensemble generator (Brodeur et al., 2024). This technique creates thousands of years of plausible synthetic forecasts based on the statistical error characteristics of the actual forecast system, which allows the FIRO strategies to be tested using extreme events and quantify the risk of scenarios occurring where a forecast fails to predict a flood (CW3E, 2025).

5 RESULTS AND DISCUSSION: PILOT PROJECTS

The FIRO program has progressed from theoretical research to operational validation across several major pilot sites in the western United States.

5.1 Lake Mendocino (Russian River)

Lake Mendocino served as the proof-of-concept for the FIRO program, testing the direct use of inflow forecasts improved by AR reconnaissance work. The VA confirmed that FIRO could safely increase water supply reliability. During the 2020 water year (a drought year), operations under a planned deviation allowed the reservoir to retain approximately 13.6 Mm^3 (11,000 acre-feet) of additional storage compared to the baseline rule curve (Jasperse et al., 2020). Pertaining to flood risk, detailed modelling demonstrated

that by pre-releasing water based on AR forecasts, FIRO could reduce peak reservoir stages during extreme events, thereby improving flood risk management and dam safety.

5.2 Prado Dam (Santa Ana River)

Prado Dam operates in a highly constrained urban environment and provides critical habitat for the endangered bird species Least Bell's Vireo. Water conservation was a primary focus area for the Prado Dam FIRO project, and the VA demonstrated that FIRO strategies could increase groundwater recharge by an average of 8.6 Mm^3 (7,000 acre-feet) per year. Another major achievement was the integration of ecological metrics into HEC-WAT. The model simulated inundation frequencies to ensure that higher water conservation pools did not negatively impact vireo nesting habitat. The study also identified that while precipitation gauges were adequate, stream gauge improvements were necessary to support the proposed operations (Ralph et al., 2023).

5.3 Yuba-Feather System

This system involves the coordinated operation of New Bullards Bar Reservoir and Lake Oroville to protect the downstream communities of Marysville and Yuba City. One unique characteristic of the Yuba-Feather pilot project is that it is a two-reservoir system. The VA showed that coordinated FIRO operations could significantly reduce peak flows at the confluence of the Yuba and Feather rivers. Unlike single-reservoir pilots, this project emphasized the timing of releases between two independent dams to better manage peak flows downstream. The project also highlighted the critical need to align FIRO VA timelines with concurrent WCM updates for the two reservoirs. Early coordination allowed the FIRO VA results to directly inform the ongoing comprehensive WCM update for the system (Ralph et al., 2022).

5.4 Other Ongoing FIRO Pilots

A priority at new FIRO pilot project sites is to. The FIRO program identified three sites, each in a different phase of the VA process, to better integrate HEC resourcing and tools into the project teams – Lake Sonoma (Russian River), Howard A. Hanson Dam (Green River), and the Willamette Valley in Oregon. By more comprehensively utilizing CWMS and WAT, as well as collaborating with HEC personnel as part of the work teams, best practices can be identified, and standard operating procedures can be updated and leveraged on future FIRO VAs.

6 CONCLUSION

There have been three completed FIRO pilot projects in California, each evaluating reservoirs with varying characteristics and performance objectives. Each project has shown that FIRO has the potential to be an effective reservoir operations strategy. The technical accomplishments, including utilization of the EFP and synthetic ensemble generation, have provided the necessary tools to quantify and manage forecast uncertainty.

Lessons learned from these projects are currently being used to implement FIRO across the USACE inventory. The establishment of tiered VA pathways (Expedited, Streamlined, Full) allows USACE to efficiently assess which reservoirs show the most promise. As the program expands to sites like Lake Sonoma, and Howard Hanson Dam and the Willamette Valley, the focus remains on standardizing implementation through CWMS-compatible methods, ensuring that the benefits of forecast-informed operations can be realized broadly to improve water supply reliability, flood risk management, and other authorized purposes.

REFERENCES

Brodeur, Z., Taylor, W., Herman, J. D., and Steinschneider, S. (2024). Synthetic Forecast Ensembles for Evaluating FIRO. Water Resources Research.

Forbis, J. & Ly, C. (2024). Application of forecast-informed reservoir operations at US Army Corps of Engineers dams in California. Journal of Flood Risk Management. 18. 10.1111/jfr3.13051.

Jasperse, J., et al. (2020). Lake Mendocino Forecast Informed Reservoir Operations Final Viability Assessment. Lake Mendocino FIRO Steering Committee.

Ralph, F. M., et al. (2023). Prado Dam Forecast Informed Reservoir Operations Final Viability Assessment. Prado Dam FIRO Steering Committee.

Ralph, F. M., et al. (2025). Yuba-Feather Forecast Informed Reservoir Operations Final Viability Assessment. Yuba-Feather FIRO Steering Committee.

USACE (1994). Engineer Pamphlet 1110-2-9: Hydrologic Engineering Studies Design. U.S. Army Corps of Engineers.

USACE (2016). Engineer Regulation 1110-2-240: Water Control Management. U.S. Army Corps of Engineers.

Yeates, E., Barber, C., & Rodman, N. (2023). Forecast-Informed Reservoir Operations FIRO Screening Process Stage A Development and SPD Results. U.S. Army Engineering Research and Development Center (ERDC) Library. https://erdclibrary.on.worldcat.org/discovery

Zheng, M., et al. (2021). Improved forecast skill through assimilating dropsonde observations from Atmospheric River Reconnaissance. J. of Geophys. Res. – Atmosphere, 126, e2021JD034967

Web sites:

Web-1: https://glossary.ametsoc.org/wiki/Forecast-informed_reservoir_operations, consulted 21 January 2026.

ICFM 10
Adapting to Global Change:
Innovative Approaches to Flood Management and Resilience
May 20-22, 2026 | Western University, London, Ontario, Canada

Hydrodynamic Modelling of Lake Ontario for Flood Resilience

Mehrdad Jafarzadeh Khoshroudi[1], Mohammad Reza Najafi[2], and Kelly Anne Ogden[1]

Department of Mechanical and Materials Engineering, Western University, London, ON, Canada[1]
E-mail: mjafarz@uwo.ca
Department of Civil and Environmental Engineering, Western University, London, Canada[2]

EXTENDED ABSTRACT

1 INTRODUCTION AND MOTIVATION

Lake Ontario's highly urbanized shoreline is exposed to large seasonal-interannual lake-level variability and episodic high-water events that can stress coastal infrastructure and complicate shoreline risk management. Recent extreme seasons (International Joint Commission, 2020) underscored the need for long, physically based reconstructions of water levels that are both quantitatively evaluated and suitable for flood-resilience applications. This study develops and evaluates a long-term, depth-averaged hydrodynamic hindcast of Lake Ontario using TELEMAC-2D over 1992-2021 (Ata et al., 2014), forced by observed boundary conditions and reanalysis-based atmospheric drivers. The scientific contribution is to quantify, in a consistent modelling framework, how well a single optimized 2D configuration can reproduce multi-decadal water-level variability and historical high-water extremes that are directly relevant to flood-resilience planning.

2 MODEL SETUP AND FORCING

TELEMAC-2D solves the depth-averaged Saint-Venant (shallow-water) equations using an unstructured finite-element mesh, which enables targeted refinement along complex shorelines and boundary corridors while remaining computationally feasible at the lake scale.

The model is forced with (i) daily Niagara River discharge at Queenston (upstream inflow), (ii) prescribed downstream water levels at the St. Lawrence outlet near Brockville, and (iii) hourly wind forcing from ERA5 reanalysis (Hersbach et al., 2020). A wetting-drying scheme is activated in shallow nearshore areas to represent exposure/inundation dynamics; evaluation focuses on lake-wide water-level skill at the gauge network.

2.1 Mesh sensitivity, scenario definition, and calibration approach

Mesh sensitivity was first examined using three baseline meshes coarse (52,243 nodes), medium (115,866 nodes), and finest (234,474 nodes) under consistent forcing and the same calibration window.

To refine the accuracy cost trade-off beyond the baseline three meshes, six additional candidate meshes (Scenarios 4-9) were generated between the medium and finest grids by redistributing resolution primarily in the Niagara inflow and St. Lawrence outflow corridors (Table 1). Screening was based on station-based performance metrics (RMSE, R^2, and Nash–Sutcliffe Efficiency) computed against observed water levels at five stations (Kingston, Cobourg, Toronto, Burlington, Port Weller) during the 2021 calibration period, together with numerical robustness (stable convergence) and feasibility for multi-decadal simulation.

Scenario 7 (125,109 nodes) was selected for the long hindcast because it provided a defensible balance between skill and runtime. The final mesh applies targeted refinement consistent with the basin

physics: ~75 m resolution near the Niagara inflow, 225-675 m transition bands, ~180 m near the St. Lawrence outflow with a 450 m transition, and ~945 m in the lake interior.

3 VALIDATION RESULTS (1992–2021) AND EXTREME-EVENT PERFORMANCE

Across 1992-2021, the calibrated model reproduces observed water levels at the five validation stations with strong overall agreement. Burlington is used here as an illustrative example: daily simulated versus observed levels show high correspondence, with $R^2 = 0.89$, RMSE = 0.10 m, and Nash-Sutcliffe = 0.89 (Moriasi et al., 2007), indicating that the model captures the dominant variance in observed water-level variability over the full 30-year period at this station. For flood-relevant extremes, event-scale agreement was evaluated for the high-water seasons of 2017 and 2019 at Burlington. In 2017, the simulation reproduces the observed high-water plateau with a simulated peak of approximately 75.9-76.0 m and an event RMSE of 0.11 m, supporting close agreement in both magnitude and hydrograph evolution during the extreme season. The 2019 high-water season shows similarly strong correspondence, with event RMSE = 0.11 m, indicating that the calibrated configuration remains performant during a second major extreme period.

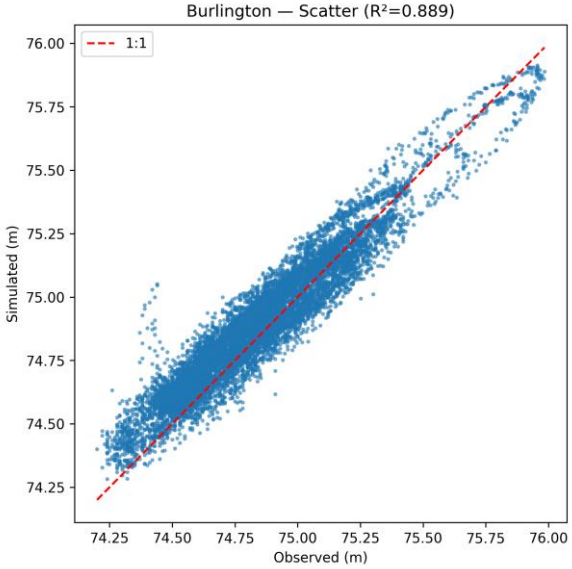

Figure 1: Daily simulated versus observed water levels at Burlington for 1992-2021.

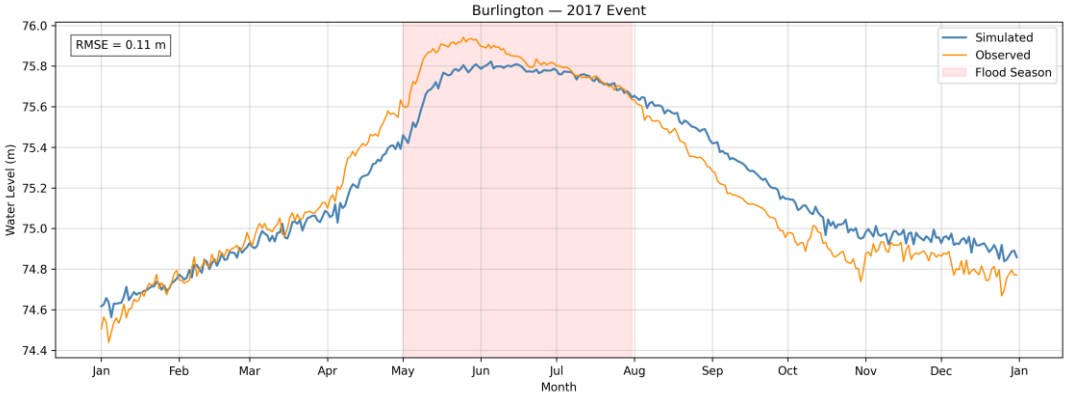

Figure 2: Burlington 2017 high-water season hydrograph: observed and modelled daily water levels (time series comparison).

4 CONCLUSIONS AND FLOOD-MANAGEMENT IMPLICATIONS

This study demonstrates a practical workflow for producing a quantitatively evaluated, multi-decadal Lake Ontario hindcast using TELEMAC-2D, and for identifying an accuracy–cost mesh choice suitable for long simulations.

The mesh sensitivity and scenario screening indicate that a sub-kilometre-scale unstructured mesh (Scenario 7) provides a defensible balance between station-based skill and computational cost for multi-decadal application. At Burlington (illustrative example), the configuration maintains low error during major high-water seasons (2017 and 2019), supporting its use for analysing historical extremes central to flood-risk management.

From a flood-resilience perspective, the validated hindcast provides a physically based reconstruction of historical lake-level variability and extremes that can support shoreline risk communication, resilience benchmarking, and evaluation of adaptation strategies that require credible historical water-level behaviour. The framework is suitable for extension to future analyses (e.g., scenario forcing, climate-change impact assessment, and hydrodynamic baselines for compound flooding and statistical risk assessment). These results provide a defensible hydrodynamic baseline for subsequent compound-event and probabilistic flood-risk analyses along the Lake Ontario shoreline.

5 REFERENCES

Hersbach, H., Bell, B., Berrisford, P., Hirahara, S., Horányi, A., Muñoz-Sabater, J., Nicolas, J., Peubey, C., Radu, R., Schepers, D., Simmons, A., Soci, C., Abdalla, S., Abellan, X., Balsamo, G., Bechtold, P., Biavati, G., Bidlot, J., Bonavita, M., … Thépaut, J.-N. (2020). The ERA5 global reanalysis. Quarterly Journal of the Royal Meteorological Society, 146(730), 1999–2049. https://doi.org/10.1002/qj.3803

Moriasi, D. N., Arnold, J. G., Van Liew, M. W., Bingner, R. L., Harmel, R. D., & Veith, T. L. (2007). Model evaluation guidelines for systematic quantification of accuracy in watershed simulations. Transactions of the ASABE, 50(3), 885–900. https://doi.org/10.13031/2013.23153

International Joint Commission. (2020, January 23). Background paper answers key questions on 2019 Lake Ontario and St. Lawrence River flooding. https://ijc.org/en/loslrb/background-paper-answers-key-questions-2019-lake-ontario-and-st-lawrence-river-flooding

Ata, R., Goeury, C., & Hervouet, J.-M. (2014). *TELEMAC modelling system: 2D hydrodynamics, TELEMAC-2D software (Release 7.0): User manual*. EDF R&D. https://www.opentelemac.org/downloads/MANUALS/TELEMAC-2D/telemac-2d_user_manual_en_v7p0.pdf

ICFM 10
Adapting to Global Change:
Innovative Approaches to Flood Management and Resilience
May 20-22, 2026 | Western University, London, Ontario, Canada

Comparing Engineering and Resilience Strategies for urban Flood Control: A Case Study of the "23·7" Flood in Mentougou, Beijing

Minglong Fei[1, 2], Baoyi Wei[1, 2], Yi Zhang[1, 2] and Xiaoxin Zhang[1, 2, 3]
Beijing Municipal Institute of City Planning and Design, Beijing, 100045, P. R. China[1]
Beijing Key Laboratory of Urban Hydrological Cycle and Sponge City Technology, 100045, P. R. China[2]
School of Environment,Tsinghua University, Beijing, 100084, P. R. China[3]
E-mail: mfei16@163.com

ABSTRACT

Frequent extreme rainfall due to global climate change has heightened challenges for urban flood control. The "23·7" extreme rainfall in July 2023 in Beijing's Mentougou District caused severe mountain flash floods. Post-disaster analysis suggests that enhancing flood control systems, such as building peripheral flood interception ditches, and adopting resilience strategies like improved urban vertical planning, can boost flood response and reduce losses. Using 2-D shallow water numerical model associated with measured data from the "23·7" rainfall event and high-resolution terrain models, this study revisits the disaster in the Mentougou River Basin and simulates the effects of engineering measures (e.g., flood interception ditches) and resilience strategies (e.g., urban vertical planning). Simulations reveal that both strategies reduce urban flood impacts, but the engineering approach alters water catchment patterns in urban area, significantly increasing downstream peak flows for rapid discharge, while the resilience strategy mainly modifies the spatial distribution of flood-affected areas with minimal impact on catchment characteristics. Furthermore, the paper discusses the applicability of various flood control strategies in urban flood planning based on the findings.

KEYWORDS: Extreme rainfall; Urban flood disasters; Engineering solutions; Resilience strategies

1 INTRODUCTION

Under the combined influence of Typhoon Doksuri moving northward and a cold air mass, from late July to early August 2023, the Haihe River Basin, which is located in northern China and encompasses megacities such as Beijing and Tianjin, experienced heavy rainfall, leading to a basin-wide catastrophic flood. The cumulative areal rainfall reached 155.3 mm, with 22 rivers in the Haihe River Basin exceeding warning levels, and 8 rivers recording their highest flood levels since data collection began. This event marked the largest flood in the Haihe River Basin since 1963(Web-1).

From 20:00 on July 29 to 07:00 on August 2, Beijing encountered an exceptionally heavy rainstorm lasting 83 hours, with an average rainfall of 331 mm across the city, accounting for 57% of its multi-year average annual rainfall of 585 mm. The extreme rainfall triggered historic floods in multiple tributaries and main streams of river basins, including the Yongding River, Dashi River, and Juma River. The floods were characterized by rapid onset, high volume, and peak intensity. For instance, the flow discharge at Lugou Bridge on the Yongding River surged from 1,000 m^3/s to a peak of 4,650 m^3/s within just two hours, exceeding the once-in-50-year flood standard and marking the highest peak flow recorded since 1925 (Web-2, Junmei et al., 2024).

The Mentougou District, which is a distant suburb in western Beijing, with mountainous areas accounting for 98.5% of its total land area (Web-3), was severely affected by the catastrophic "23·7" flooding. The catastrophic torrential rains caused comprehensive damage across all 178 administrative

villages and 126 residential communities in Mentougou District. Approximately 310,000 people were affected, accounting for about 77% of the district's total population. A total of 7,787 houses collapsed, with an additional 12,925 severely damaged (Mentougou District People's Government of Beijing Municipality, 2024). In the urban area of Mentougou, gullies served as flood discharge channels, causing severe damage to river courses, roads, buildings, and other infrastructure along both sides, flatter areas with lower elevation experienced varying degrees of inundation.

Post-disaster assessment indicated that, a major engineering shortcoming was the lack of a comprehensive flood interception system, particularly on the upstream side of the urban built-up area. In the absence of functional interception ditches, floodwaters from the mountains flowed directly into the urban area along natural drainage channels and roads, causing severe damage. Furthermore, resilience measures such as the urban grading and emergency management were insufficient, roads intersecting the river channel essentially functioned as flood dispersal pathways once overtopping occurred. The failure to implement timely emergency interventions, such as deploying barriers at critical road-river intersections, allowed floodwaters to spread unchecked into the urban area, thereby expanding the impact.

In this work, a 2-D flood simulation is carried out to revisit the disaster in the Mentougou River Basin, Urban area of Mentougou. Furthermore, effects of engineering measures (e.g., flood interception ditches) and resilience strategies (e.g., urban vertical planning) on resisting "23·7" flood are tested.

2 SIMULATION

2.1 Basin information

In this work, we focus on the Mentougou River Basin in the middle of the Mentougou urban area, as shown below in Figure 1. Mentougou River is a tributary of Yongding River, it's also one of the four main flood rivers of Mentougou urban area. Mentougou River Basin is isolated by mountains around on the north, west and south, and the east of the basin stands the right bank of the Yongding River. Mentougou River flows from west to the east, river length is 10.3 kilometers, river slope ranges from 1‰ to 5‰, basin area is 22 square kilometers,

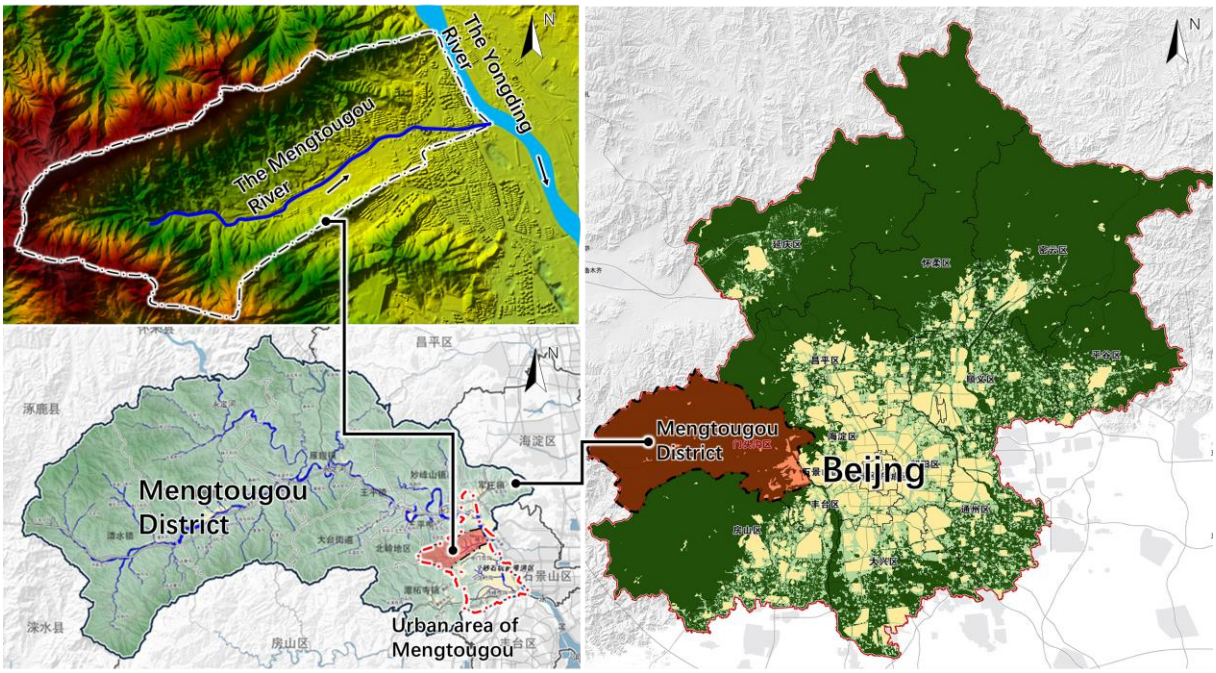

Figure 1: Mentougou river base and it's location in Beijing (Web-4)

According to the rainfall data of the Beijing Geological Hazard Monitoring Rainfall Stations, during the "23·7" extreme rainfall, the 24 hours and 72 hours averaged rainfall in the urban area of Mentougou are 426 mm and 595 mm, and the maximum rainfall occurred at the Dongxinfang station (Mentougou River basin), with average accumulations amounting to 665 mm in 24 hours and 928 mm in 72 hours. Heaviest rainfall happened at about 10:45, July 31st, 2023.

2.2 Model and parameters

The Hec-Ras 2-D flow model (Hydrologic Engineering Center, 2024) is chosen to carry out the simulation of the "23·7" flood in Mentougou River Basin. Terrain DEM of Mentougou River Basin with 2-meter resolution is applied in the model. Basic calculation mesh scale in the model is about 100 m * 100 m, while mesh along the river and roads are refined to 2 m * 2 m to get a better simulation detail. About 125 thousands meshes in total are used in the calculation.

In this work, the simulation directly incorporates rainfall data recorded by the Beijing Geological Hazard Monitoring Rainfall Stations. This dataset has a 5-minute temporal resolution and covers the period from 00:00 on July 29th to 24:00 on August 2nd. The Thiessen polygon method is used to determine the areal distribution of rainfall. The Deficit and Constant loss method is used for runoff calculation, loss rate is calculated according to the *Beijing Hydrologic Manual* (Beijing Water Authority, 2005), which is 5mm/h in this work.

Land use in the basin is divided into 3 types and related roughness coefficients are listed below.

Table 1 Land use classification and related roughness coefficients in Mentougou Basin

Land use classification	roughness coefficients
Urban development land	0.015~0.035
Forest land	0.035~0.25
River and water land	0.035

2.3 Validation

Due to the limited hydrological monitoring facilities in Mentougou District during the disaster, data on inundation depth and flow discharge collected from post-disaster investigations were used to calibrate the model.

Quantitative water depth measurements were unavailable during the flood event, although qualitative calibration of this model was conducted based on the video footage and photographs documenting the inundation extent and depth (Yi et al. (2024)). However, a post-disaster field survey identified a flood level marker at the entrance of a downstream community along the Mentougou River, which recorded the maximum inundation depth from the "23·7" event. This recorded depth (0.75 m) was subsequently used as a benchmark for the quantitative calibration of the model, by comparison with the simulated depth at the same location.

As shown in Figure 2, the simulated inundation depth at the community gate peaked at 11:20 on July 31st, exhibiting a lag of approximately half an hour behind the rainfall peak. The maximum simulated depth is approximately 0.86 m, showing good agreement with the post-disaster measurement of 0.75 m.

The flow hydrograph for the outlet section of the Mentougou Basin was also used to calibrate the model. The simulated flow hydrograph at the outlet section of the Mentougou Basin is shown in

Figure 3. The simulated peak flow occurred at about 11:40 am July 31st, 2023, reaching 452.5 m^3/s. This value is close to the post-disaster estimate of 512.6 m^3/s by Jiahong et al. (2024). Considering the complexity of the actual underlying surface conditions, the discrepancy is within an acceptable range, demonstrating that the models and parameters used in this study are reliable for reproducing the flood event.

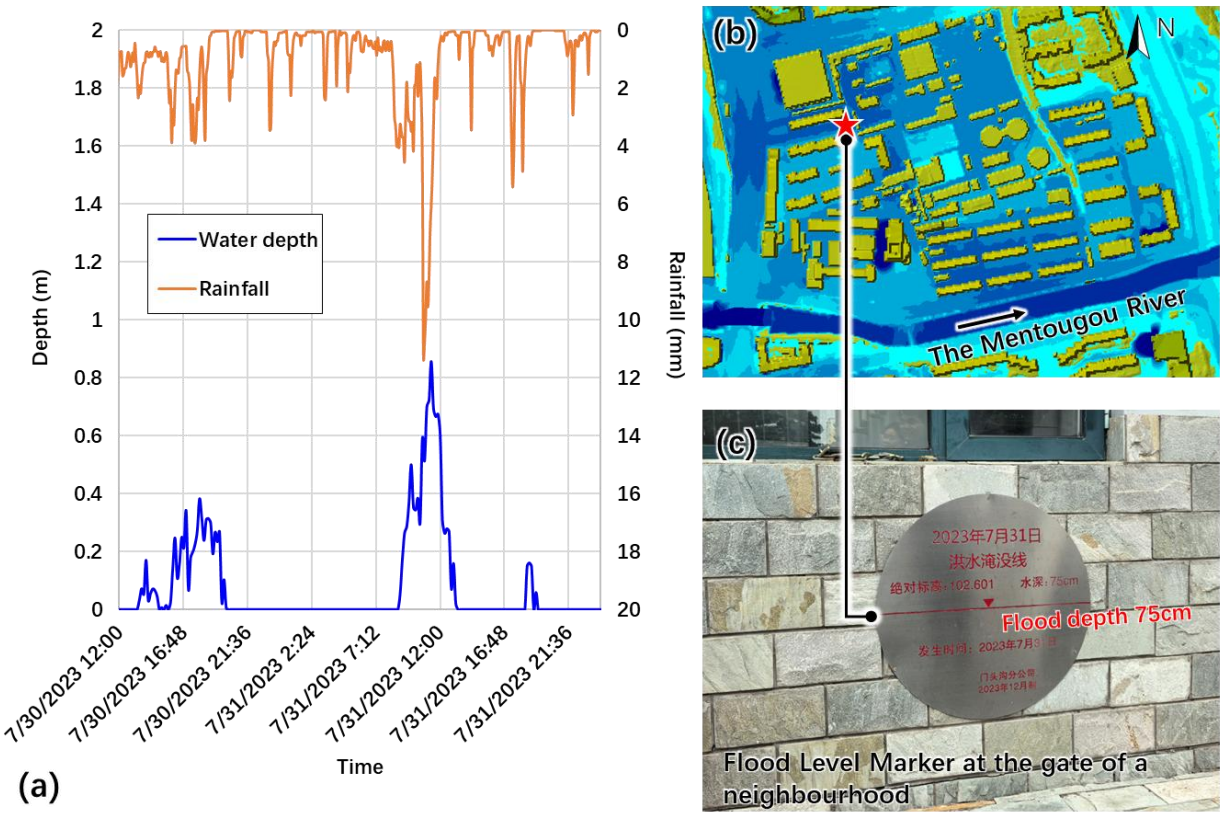

Figure 2: (a) Temporal variation of simulated flood depth and rainfall at a flood level marker during the "23·7" flood in the downstream of Mentougou River. (b) Location of the flood level marker. (c) The picture of the flood level marker.

2.4 Case study

During the “23·7” flood event, the lack of flood interception ditches allowed mountain floodwaters to flow directly into adjacent built-up areas. Meanwhile, roads perpendicular to the river acted as conduits for flood dispersal, channeling water toward the city center. Therefore, constructing flood interception ditches around built-up areas, and elevating key road junctions near rivers to prevent flood ingress, would be effective in reducing flood damage.

This study investigates the performance of engineering measures (e.g., flood interception ditches) and resilience strategies (e.g., urban vertical planning) during the “23·7” extreme rainfall event. To this end, two simulation scenarios are established, as illustrated in

Figure 3.

Case 1: Implementation of planned ditches. Flood interception ditches, which were planned but not constructed before the disaster, are added to the model around the built-up area of the Mentougou River Basin to control mountain floodwaters.

Case 2: Deployment of temporary barriers. As a resilience strategy to modify local topography and block flood ingress, 1-meter-high temporary barriers are placed around the most flooded downstream region as well as the nearby road intersections with the river channel.

The inundation area with maximum flood depth in

Figure 3 (a) to (c) is 3.2 km², 3.5 km² and 3.8 km², respectively. The flood interception ditches in case 1 effectively direct mountain floodwaters into the downstream river, resulting in less inundation compared to both the original scenario and Case 2; On the other hand, the flood barriers in case 2 also

perform well in protecting the core built-up area. Flood barriers around core built-up area altered the flow direction, reducing the inundation area from 0.89 km² in the original case to 0.76 km² in Case 2. Furthermore, the maximum flood depth decreased by approximately 0.2-0.6 m within areas surrounded by flood barriers, as shown in Figure 4.

The flood flow volume hydrographs for all three cases are also presented in

Figure 3 (d). As we can see, the engineering measures implemented in case 1 significantly altered the watershed confluence characteristics. At the outlet section of Mentougou river, the peak discharge and flood volume in case 1 is 753.8 m^3/s and 8,672.1 m^3, respectively, representing increases of approximately 66% and 62% compared to the original scenario. This is because the ditches directed floodwaters from the upstream mountainous areas to the downstream river more efficiently, resulting in a substantial increase in both peak discharge and total flood volume.

In contrast, the resilience strategies in case 2 had little effects on the flood hydrograph, both the maximum discharge and flood volume in case 2 are comparable to those of the original simulation.

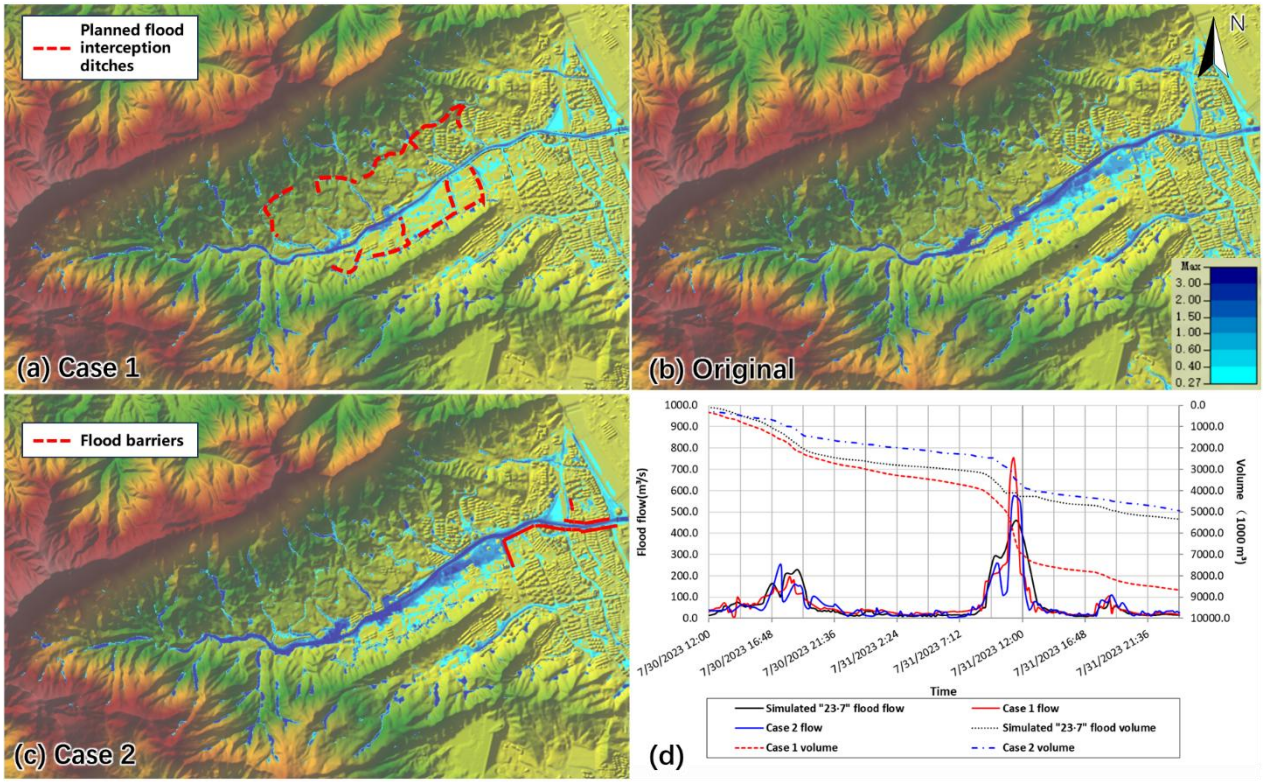

Figure 3: Simulation results of case 1 & 2, and the comparison with original "23·7" flood simulation. (a) ~ (c) are the maximum inundation depth maps of Mentougou river basin in case 1, original "23·7" flood simulation and case 2, respectively. (d) Comparison of flood flow volume hydrographs at the outlet section of Mentougou river between these cases.

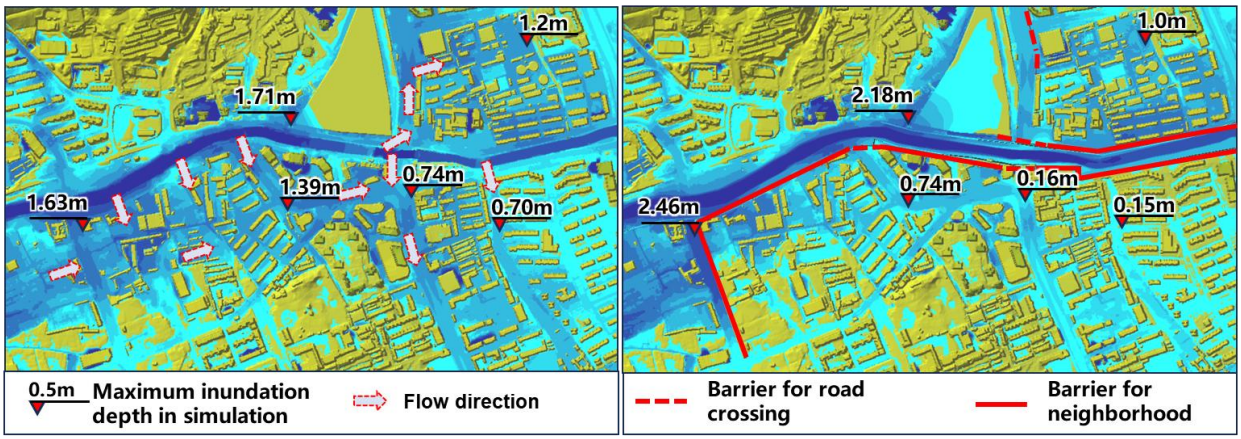

Figure 4: Simulation results in downstream built-up area of Mentougou: (left) original "23·7" flood simulation and (right) Case 2.

3 DISCUSSION AND CONCLUSION

In this work, engineering measures (e.g., flood interception ditches) and resilience strategies (e.g., urban vertical modification) are simulated to mitigate the "23·7" flood in the simulation. Both prove effective in reducing the inundation area and maximum flood depth in built-up areas. However, the flood interception ditches reduced flow resistance, allowing mountain flood to drain into the downstream river more easily. This led to a significant increase in peak discharge and flood volume downstream. In contrast, setting flood barriers around the most severely flooded built-up region—acting as a temporary elevation barrier—successfully blocked the flood but raised the local water depth, as shown in Figure 4.

The simulation results indicate that engineering measures such as flood interception ditches around built-up areas are more effective for flood risk mitigation in general. However, their implementation must be incorporated into an integrated flood control strategy, which requires concurrently strengthening the downstream flood defence system. On the other hand, resilience strategies like blocking flood by temporary flood barrier may be more suitable for areas with sufficient surrounding open space, given their potential to cause adverse impacts on adjacent zones.

In this study, the spatial configurations of the two simulation cases were determined based on the layout of flood interception ditches as planned in the urban flood control plan and the spatial distribution of urban built-up areas. Specifically, the engineering measures were primarily concentrated in the mountainous areas of the upstream basin, while the resilience strategies were mainly focused on the concentrated built-up areas in the downstream basin. The impact of this spatial disparity in the two types of measures on the hydrological processes of the river basin has not been fully explored in this paper and warrants further investigation in future research.

REFERENCES

Beijing Water Authority. (2005) Beijing Hydrologic Manual, Part 2, 31-32. (In Chinese)

Hydrologic Engineering Center, U.S. Army Corps of Engineers. (2024) HEC-RAS 2D User's Manual Version 6.6, 51-140.

Jiahong L., Chao M., Jia W. et al. (2023) "23·7"heavy rain in Mentougou Watershed of Beijing[J].China Flood & Drought Management, 33(9), 50-55. (In Chinese)

Junmei L., Yi Y., Jinyan G. et al. (2024). Investigation and Analysis of the Yongding River July 2023 Catastrophic Flood and Recommendations for Flood Control Engineering Design. China Flood & Drought Management, 34(1), 52-57. (In Chinese)

Mentougou District People's Government of Beijing Municipality. (2024) The Overall Plan for Post-Disaster Recovery and Reconstruction in Mentougou District, 7. (In Chinese)
Yi Z., Baoyi W., Minglong F. et al. (2024). Retrospective simulation and planning strategies study of "23·7"flood for New Downtown in Mentougou District of Beijing City. China Flood & Drought Management, 34(10), 15-19. (In Chinese)

Web sites:
Web-1: https://mp.weixin.qq.com/s/yb3fVkcIaQZ9azCqdqVTtQ,2023-08-21
Web-2: https://m.thepaper.cn/newsDetail_forward_24169894.
Web-3:
https://ghzrzyw.beijing.gov.cn/ziranziyuanguanli/gyxdzzl/mtg_gyxdzzl/201912/t20191213_1721982.html.
Web-4: https://www.beijing.gov.cn/gongkai/guihua/wngh/cqgh/201907/t20190701_100008.html

ICFM 10
Adapting to Global Change:
Innovative Approaches to Flood Management and Resilience
May 20-22, 2026 | Western University, London, Ontario, Canada

Data-Centric ML-based flood forecasting system of the Drina-Lim hydropower system (south-east Europe)

Milan Stojković[1,2], Luka Vinokić[1], Milan Dotlić[1], Ana Samac[1], Vanja Švenda[1], Veljko Prodanović[1,3]
The Institute for Artificial Intelligence R&D, Fruškogorska 1, 21000 Novi Sad, Serbia[1]
E-mail: milan.stojkovic@ivi.ac.rs
E-mail: luka.vinokic@ivi.ac.rs
E-mail: milan.dotlic@ivi.ac.rs
E-mail: ana.samac@ivi.ac.rs
E-mail: vanja.svenda@ivi.ac.rs
E-mail: veljko.prodanovic@ivi.ac.rs

Faculty of Civil Engineering, University of Novi Sad, Kozaračka 2a, 24000 Subotica, Serbia[2]
E-mail: milan.stojkovic@gf.uns.ac.rs
University of South Wales (UNSW), School of Civil and Environmental Engineering, Sydney, NSW 2052, Australia[3]
E-mail: v.prodanovic@unsw.edu.au

ABSTRACT

Climate change has intensified extreme hydrological events in South-East Europe, increasing flood risk in the Sava River Basin. The Drina River, a key hydroenergetic system within the Sava River basin, requires reliable inflow forecasting to support hydropower operations and flood management. Existing platforms rely on physics-based models that face limitations under non-stationary climatic conditions. This study introduces the first data-centric, ML-based operational inflow forecasting system for the Drina–Lim hydropower cascade. The framework integrates hydrological observations, ERA5 reanalysis data, satellite-derived inputs, and bias-corrected meteorological fields to enhance data quality prior to model training. Four ML architectures (LSTM, TCN, TKAN, GNN) were evaluated using assimilated meteorological variables for the 2019–2023 period. All models achieved high predictive accuracy, with NSE values between 0.86 and 0.90 and low MAPE across reservoirs. Upstream HPPs exhibited particularly low absolute errors, while downstream stations maintained strong performance despite larger flow magnitudes. The results show that ML-based forecasting provides a robust and accurate alternative to traditional hydrological models and is well-suited for operational flood risk management in the Drina River Basin.

KEYWORDS: ML flood forecasting, hydropower plants, ERA5, data-centric approach, river flow

1 INTRODUCTION

Climate change and climate variability have intensified the frequency and severity of hydrometeorological extremes across southeastern Europe, leading to more frequent heavy-rainfall events, accelerated snowmelt episodes, and prolonged wet periods (Stojković et al. 2014;

Stojković et al. 2017a; Stojković at al. 2017b; Stojković and Simonović, 2020). These shifts have significantly increased flood risk in river basins, within the considered area, where mountainous terrain and rapid runoff magnify the impacts of extreme precipitation.

Within this context, the Sava River Basin is recognized as one of the most flood-prone regions in the area (Brilly et al., 2014). Due to its complex hydrological regime, steep tributaries, and recurrent extreme precipitation, the basin experiences regular and often severe flooding, threatening local communities, infrastructure, and hydropower operations across multiple countries. A major sub-basin of the Sava is the Drina River catchment, which contains one of the most important hydroenergetic systems in South-East Europe (Stojković and Simonović, 2019, Milivojević at al. 2014). The river hosts a cascade of hydropower plants (HPPs) whose reliable and safe operation critically depends on accurate inflow forecasting. Over the past decade, several forecasting and monitoring platforms have been developed to support water authorities and hydropower operators. The HIS Drina system (Milivojević et al, 2014) provides integrated acquisition and visualization of meteorological and hydrological data, and streamflow forecast while the Sava FEWS system (ISRBC, 2018), built on the Delft-FEWS platform, delivers operational hydrological forecasts for the entire Sava Basin and supports transboundary flood management

However, these systems rely on physics-based hydrological models, which can struggle to maintain performance under non-stationary climate conditions. Increased variability in precipitation patterns, increased air temperatures, and shifts in seasonal runoff have made model calibration more challenging and increased predictive uncertainty. In response to these challenges, this study presents the first ML-based operational inflow forecasting system developed for the Drina–Lim hydropower cascade, marking an advancement in flood forecasting for South-East Europe. The system adopts a data-centric design philosophy (Ng, 2021; Liu et al. 2023), where the quality, completeness, and representativeness of input data are prioritized as key drivers of model performance. To achieve this, the framework integrates not only recent hydrological observations and ERA5 (Hersbach et al. 2020) climate reanalysis datasets but also enhanced input data produced through satellite-derived observations (Ilić et al., 2025) and bias-correction procedures (Vinokić et al., 2023; Stojković et al, 2019). As a result, the ML models operate on higher quality, harmonized datasets that more accurately represent real hydrometeorological conditions.

Unlike traditional models, the proposed ML flood forecasting system demonstrates high predictive accuracy, strong robustness to reanalysis-driven meteorological inputs, and stable performance across varying hydrological regimes, including conditions influenced by climate variability and extremes. These results highlight the potential of ML-based forecasting as both a complement and a viable alternative to classical hydrological modeling approaches in complex river systems.

2 MATERIALS & METHODS

2.1 Data collection

In the Drina River basin, there are 9 reservoirs with their corresponding hydropower plants (Figure 1). The most upstream reservoir is Mratinje on the Piva River, equipped with a storage hydropower plant. Along the main course of the Drina River, three reservoirs with storage hydropower plants are located: Višegrad, Bajina Bašta, and Zvornik. An additional reservoir, Lazići, represents the upper reservoir of the Bajina Bašta pumped-storage hydropower plant. In

the Lim River basin, there are four reservoirs in total. Three of them are situated on the Uvac River (Kokin Brod, Uvac, and Radojna), while the Potpeć reservoir is located on the Lim River. All reservoirs are associated with storage hydropower plants, while the Radojna reservoir is directly connected to the Bistrica diversion hydropower plant. In Table 1, the HPPs located at the Drina-Lim hydropower systems are presented, along with their catchment areas.

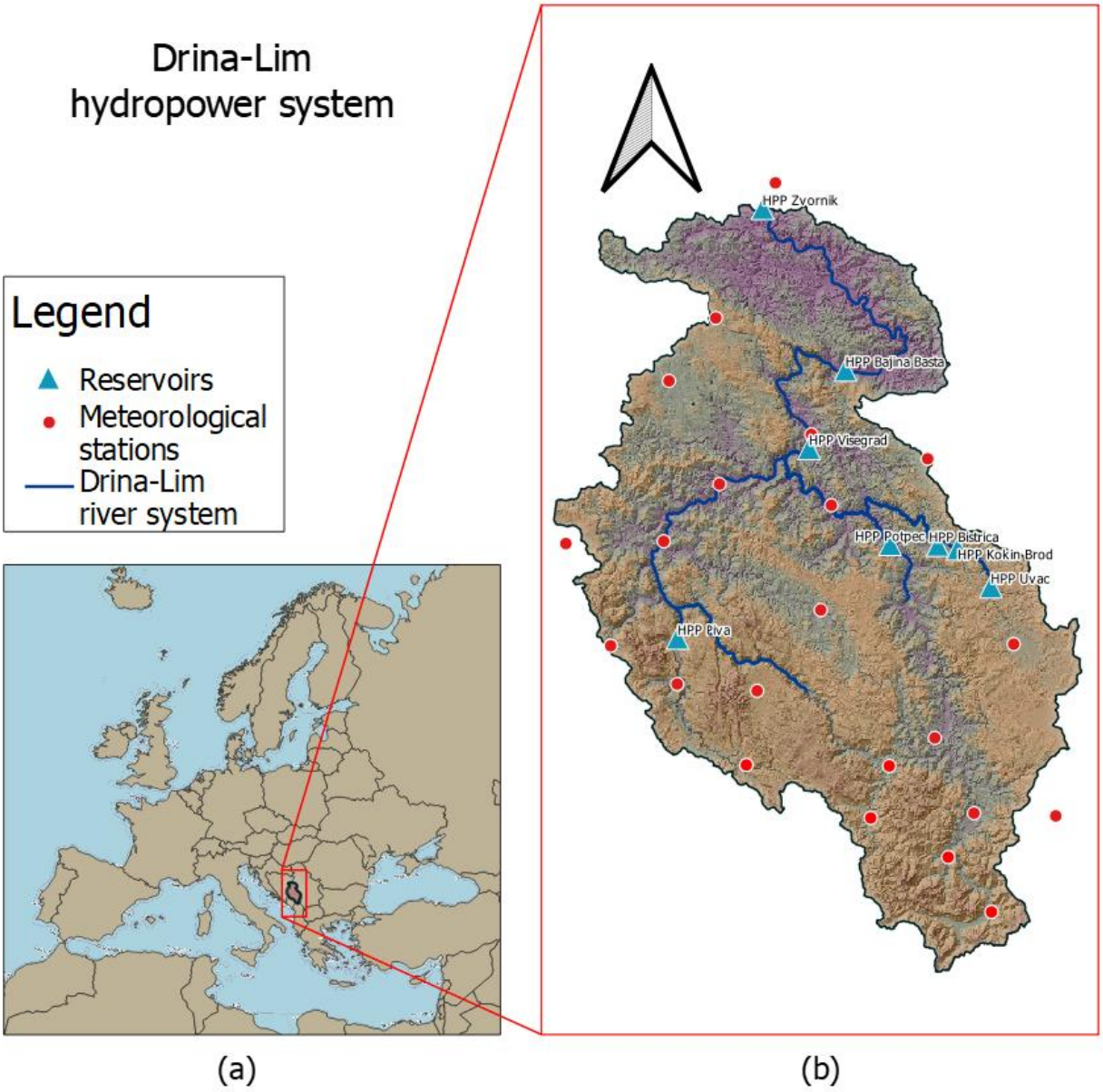

Figure 1. Drina-Lim hydropower system river basin based with associated HPPs.

Table 1. Reservoirs at the Drina-Lim hydropower system alongside catchment area.

Reservoir:	**River:**	**Catchment Area (km²):**
Mratinje	Piva	1500
Višegrad	Drina	13300
Bajina Bašta	Drina	15200

Zvornik	Drina	17400
Uvac	Uvac	1050
Kokin Brod	Uvac	1300
Radojnja	Uvac	1400
Potpeć	Lim	3600

Naturalized inflows in reservoirs, precipitation and air temperature are collected for ML model developing and functioning in real time. Hydrological data are collected from: HPP Višegrad, HPP Bajina Bašta, HPP Zvornik, HPP Piva, HPP Uvac, HPP Kokin Brod, HPP Bistrica, and HPP Potpeć (Figure 1, Table 1). Meteorological data (precipitation and air temperature) with stations equipped with real-time data acquisition, are collected within the Drina river basin covering each representative part (Figure 1).

2.2 A methodology for flood forecasting at the Drina-Lim hydropower system

A core component of the flood-forecasting system of Drina-Lim hydropower system (Figure 2) is the acquisition of recently observed historical hydrological releases under the naturalized river regime, together with key meteorological parameters (precipitation and air temperature). In addition, the system collects meteorological forecasts (precipitation and air temperature). All collected data are stored in a central database and formatted into the required structure, after which the previously trained ML models are executed. A description of the developed models is provided in Table 2, while the data needed for ML model operation can be specified as follows:

- Daily Air Temperature – historical data for the previous two days;
- Daily Air Temperature – forecast for five days ahead, including the current day (ECMWF (2025), GFS (2025), Open-Meteo ensemble (2025));
- Daily precipitation sums – historical data for the previous two days;
- Daily precipitation sums – forecast for five days ahead, including the current day;
- Naturalized streamflows from HPPs – historical data for the previous seven days.

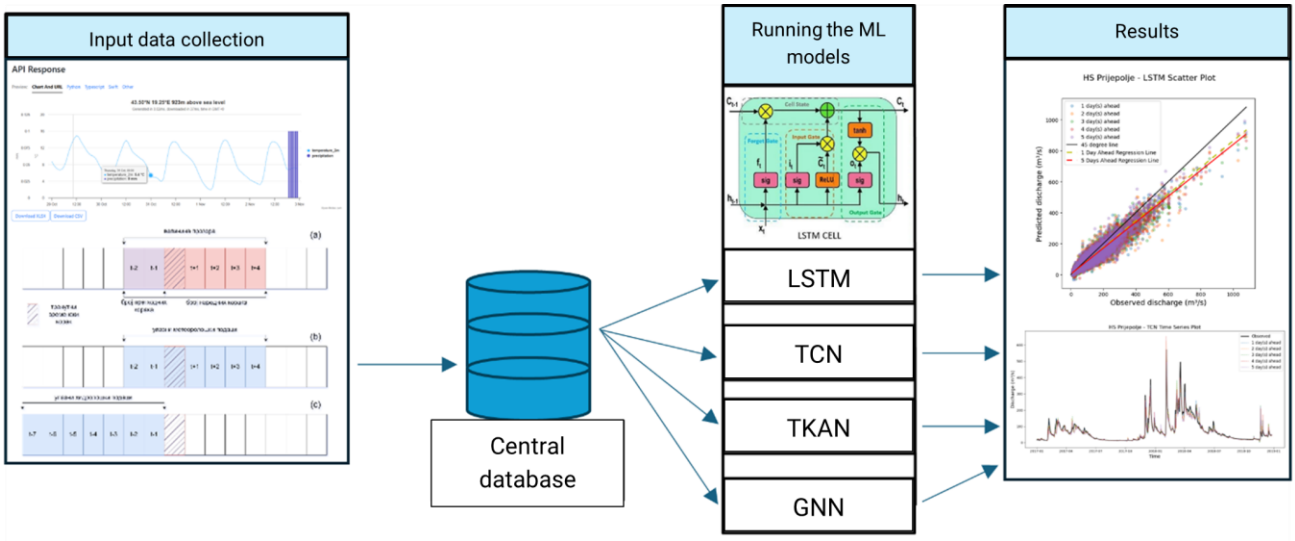

Figure 2. Data-centric flood forecasting system: Drina-Lim hydropower system.

Table 2. Overview of ML Models used in the Drina-Lim flood forecasting system.

ML models	Full name	Key underlying mechanism	Relevance for hydrological predictions	References
LSTM	Long Short-Term Memory	Recurrent neural network with memory cells governed by input, forget, and output gates that regulate information flow over long sequences.	Captures long-term temporal dependencies; effective for delayed hydrological responses (e.g., runoff after precipitation).	Vinokić et al. (2025)
TCN	Temporal Convolutional Network	Uses 1D dilated causal convolutions and residual connections to model sequential data while ensuring temporal causality.	Learns both short- and long-range temporal patterns; stable training and strong performance in time-series forecasting.	Vinokić et al. (2025)
TKAN	Temporal Kolmogorov–Arnold Network	Extends KANs by using learnable univariate functions on edges and adapting them for temporal dependencies.	Highly flexible nonlinear transformations with fewer parameters; promising for hydrological forecasting.	Vinokić et al. (2025)
GNN	Graph Neural Network	Encodes spatial dependencies using graph structures where nodes represent stations and edges represent hydrological or spatial connectivity.	Explicitly models spatial interactions; captures basin-wide spatiotemporal dynamics.	Dodig et al. (2025)

3 RESULTS

The verification period does not belong to the measured dataset. Instead, the period from 2019 through 2023 without available datasets was selected. During this period, meteorological data from the ERA5 dataset is used. ERA5 provides assimilated meteorological parameters for the European domain, based on observational data collected by hydrometeorological institutes across the region. For the hydrological data required for verification, the estimated naturalized streamflows of the Drina–Lim hydropower plants are used.

The model performance is presented through visualizations and metrics (MAE- Mean Absolute, MAPE- Mean Absolute Percentage Error; RMSE- Root Mean Square Error; NSE - Nash–Sutcliffe Efficiency) that enable a comprehensive assessment of predictive skill. Comparative scatter plots are provided for the Lim river example, showing the dynamics of predicted and observed values (Figure 3).

Table 3. Performance metrics for each ML model estimated using the ERA5 meteorological datasets from 2019 to 2023.

HPPs:	MAE (m3/s)	MAPE (-)	RMSE (m3/s)	NSE (-)
Uvac	0.95	0.17	1.85	0.88
Kokin Brod	1.07	0.12	2.28	0.89
Bistrica	1.20	0.13	2.70	0.86
Potpeć	17.08	0.21	27.32	0.88
Piva	8.11	0.14	18.49	0.89
Višegrad	46.75	0.17	71.53	0.89
Bajina Bašta	55.01	0.32	75.64	0.90
Zvornik	65.77	0.24	88.46	0.87

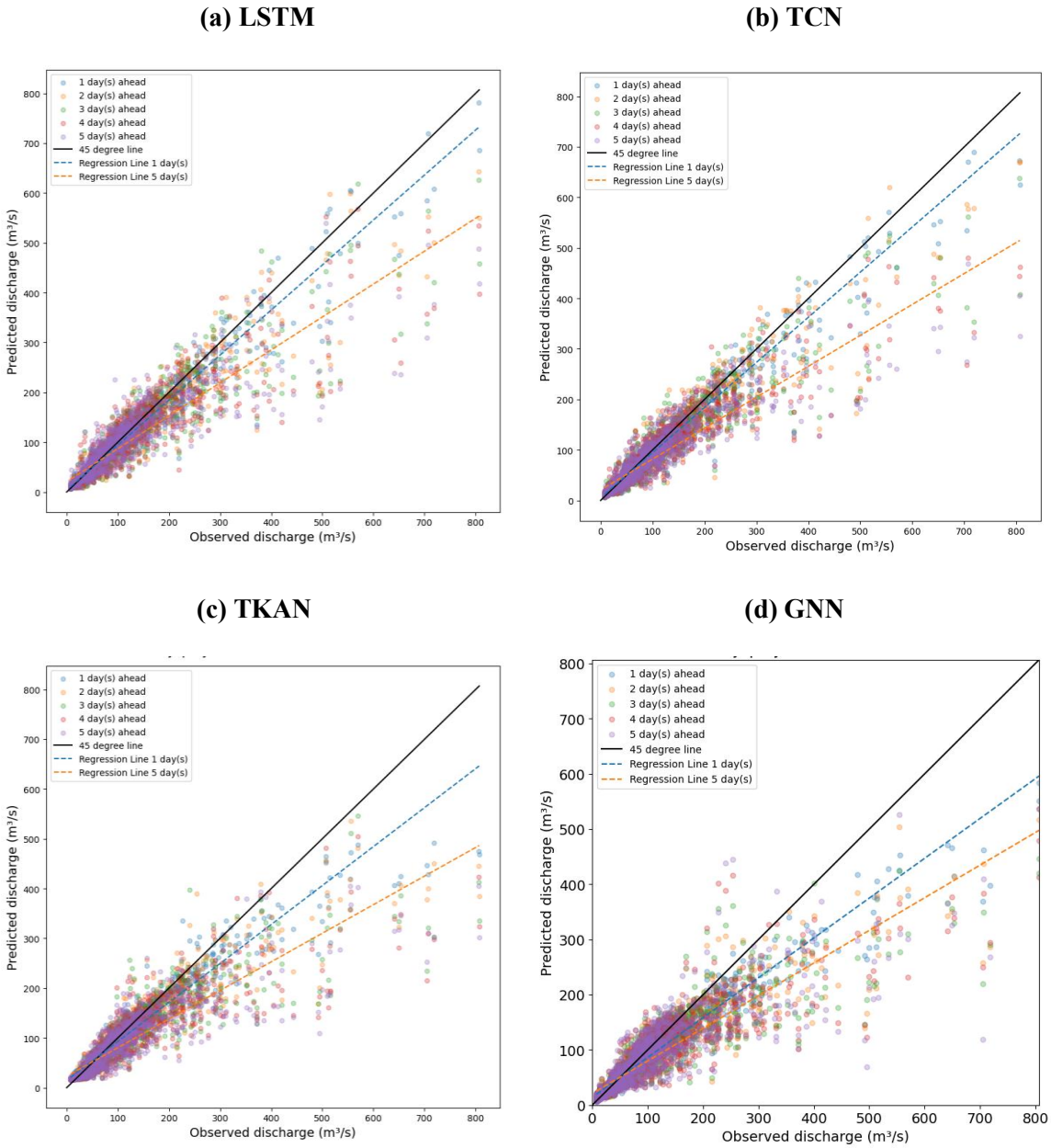

Figure 3. Example of model verification for the Drina-Lim hydropower system using LSTM, TCN, TKAN, and GNN.

The results from Table 3 and Figure 3 demonstrate high predictive skill of ML models, with NSE values ranging from 0.86 to 0.90, indicating that the models reproduce observed inflows with strong fidelity. The upstream HPPs (Uvac, Kokin Brod, Bistrica) exhibit very low absolute errors (MAE between 0.95 and 1.20 m³/s). Correspondingly low RMSE values further confirm high model precision in these sub-basins. For mid- to downstream reservoirs (Potpeć, Piva, Višegrad, Bajina Bašta, Zvornik), the models maintain consistently strong performance despite

substantially larger flow magnitudes. Although MAE and RMSE naturally increase with the scale of the system, the models continue to show excellent relative accuracy, with MAPE ranging between 0.14 and 0.32 and NSE values ≥ 0.87. The highest absolute errors occur at Bajina Bašta and Zvornik due to the cumulative upstream contributions and larger catchment variability, yet their NSE values (0.90 and 0.87, respectively) confirm high reliability.

4 CONCLUSIONS

The results demonstrate that a data-centric, ML-based inflow forecasting framework can substantially enhance predictive accuracy within the Drina–Lim hydropower system. By integrating multiple sources of meteorological and hydrological information, including ERA5 reanalysis data, satellite-derived observations, and bias-corrected datasets, the system effectively overcomes limitations associated with traditional physics-based hydrological models, particularly under conditions influenced by climate variability and extremes. All evaluated ML architectures exhibited strong performance across both upstream and downstream reservoirs, confirming the robustness of the proposed approach for real-time flood forecasting and hydropower decision support in complex mountainous catchments. The key conclusions may be summarized as follows:

- the ML-based forecasting system achieves high predictive skill (NSE 0.86–0.90) and outperforms classical hydrological models.
- the data-centric approach, incorporating data assimilation, satellite inputs, and bias correction, significantly improves input data quality and model robustness.
- the framework is operationally suitable for flood forecasting and hydropower management, even when driven by reanalysis datasets rather than direct measurements.

Despite these promising results, several limitations should be acknowledged. The ML models are trained on historical data that may not fully capture the statistical properties of unprecedented extreme events, raising questions about transferability to flood scenarios under a shifting climate. Additionally, operational deployment introduces constraints related to quality of real-time meteorological inputs, where forecast uncertainty propagates through the ML pipeline and may degrade prediction skill at longer lead times. Finally, the relatively short training record may restrict the ability to learn the full range of hydrological variability, particularly for rare, high-magnitude events.

5 ACKNOLIGEMENT

The research presented herein received financial support from the European Union's Horizon Europe project ARTIFACT, under Grant Agreement 101159480. We also extend our gratitude to Joint Stock Company Elektroprivreda Srbije for support in the project "Prediction of Daily Reservoir Inflows at the Drina–Lim Hydropower Plants Using Artificial Intelligence Techniques." Their collaboration and funding were instrumental in enabling the research activities and achieved outcomes.

REFERENCES

Brilly, M., Šraj, M., Vidmar, A., Primožič, M., & Koprivšek, M. (2014). Climate change impact on flood hazard in the Sava River Basin. In The Sava River (pp. 27-52). Berlin, Heidelberg: Springer Berlin Heidelberg.

Hersbach, Hans, et al. The ERA5 global reanalysis. *Quarterly journal of the royal meteorological society*, 2020, 146.730: 1999-2049.

Dodig, A., Stankovic, V., Stankovic, L., & Stojkovic, M. Enhancement of Hydrological Time Series Prediction with Real-World Time Series Generative Adversarial Network-Based Synthetic Data and Deep Learning Models. *Available at SSRN 5246048*.

ECMF (2025) https://www.ecmwf.int/en/publications/ifs-documentation?utm_source=chatgpt.com (available on 4 December 2025)

GFS (2025) https://www.ncei.noaa.gov/products/weather-climate-models/global-forecast (available on 4 December 2025)

OpenMETEO (2025) https://open-meteo.com/en/docs/ensemble-api (available on 4 December 2025)

Liu, G., Savic, D., & Fu, G. (2023). Short-term water demand forecasting using data-centric machine learning approaches. Journal of Hydroinformatics, 25(3), 895-911.

Stojkovic, M., & Simonovic, S. P. (2019). Mixed General Extreme Value Distribution for Estimation of Future Precipitation Quantiles Using a Weighted Ensemble - Case Study of the Lim River Basin (Serbia). Water Resources Management.

Stojković, M., Ilić, A., Prohaska, S., & Plavšić, J. (2014). Multi-temporal analysis of mean annual and seasonal stream flow trends, including periodicity and multiple non-linear regression. *Water resources management*, *28*(12), 4319-4335.

Stojković, M., Kostić, S., Prohaska, S., Plavšić, J., & Tripković, V. (2017a). A new approach for trend assessment of annual streamflows: A case study of hydropower plants in Serbia. *Water Resources Management*, *31*(4), 1089-1103.

Stojković, M., Prohaska, S., & Zlatanović, N. (2017b). Estimation of flood frequencies from data sets with outliers using mixed distribution functions. *Journal of Applied Statistics*, *44*(11), 2017-2035.

Stojkovic, M., & Simonovic, S. P. (2019). System dynamics approach for assessing the behaviour of the Lim Reservoir system (Serbia) under changing climate conditions. *Water*, *11*(8), 1620.

Milivojević, V., Milivojević, N., Stojković, M., Ćirović, V., & Divac, D. (2014). Development of distributed hydro-information system for the Drina river basin. *ICIST 2014*.

ISRBC (2018) International Sava River Basin Commission *Sava Flood Forecasting and Warning System (Sava FFWS) — Final Report* (1220579-000-ZWS-0066, Version 2.0, October 25, 2018).

Ng, A. (2021). MLOps: From Model-centric to Data-centric AI. *DeepLearning.AI*, Landing AI.

Stojković, M., Plavšić, J., Prohaska, S., Pavlović, D., & Despotović, J. (2020). A two-stage time series model for monthly hydrological projections under climate change in the Lim River basin (southeast Europe). *Hydrological Sciences Journal*, *65*(3), 387-400.

Stojkovic, M., & Simonovic, S. P. (2020). Understanding the uncertainty of the Lim river basin response to changing climate. *Journal of Hydrologic Engineering*, *25*(9), 05020023.

Ilic, V., Sekulic, M. T., Brboric, M., Radonic, J., Dmitrasinovic, S., & Stojkovic, M. (2025). Enhancing the monitoring system for river water quality: harnessing the power of satellite data and machine learning. *Blue-Green Systems*, *7*(2), 338-352.

Vinokić, L., Stojković, M., Kolaković, S. (2023). Bias correction and weighting methods to shape precipitation under the climate change options. Proceedings of the International Conference Synergy of Architecture & Civil Engineering. SINARG 2023. Niš, Serbia.

Vinokić, L., Dotlić, M., Prodanović, V., Kolaković, S., Simonovic, S. P., & Stojković, M. (2025). Effectiveness of three machine learning models for prediction of daily streamflow and uncertainty assessment. *Water Research X*, *27*, 100297.

ICFM 10
Adapting to Global Change:
Innovative Approaches to Flood Management and Resilience
May 20-22, 2026 | Western University, London, Ontario, Canada

Enhancing Flood Management and Resilience in Somalia's Riverine Zones

Author: Ir. Abdulaziz Mohamed Abdullahi
Founder and Director, African Research Centre
Email: irmataan@icloud.com
London, United Kingdom.

Abstract

Flooding in Somalia's Riverine zones—particularly along the Juba and Shabelle rivers—has emerged as one of the most persistent natural disasters threatening rural livelihoods, food security, and socio-economic stability. This study investigates the existing flood management mechanisms and explores strategies to enhance community resilience in these flood-prone areas. Using a mixed-method approach, data were gathered from local communities, agricultural extension officers, and government institutions to assess current adaptation practices, infrastructural capacities, and institutional challenges. The findings reveal that while traditional coping mechanisms such as elevated housing, seasonal migration, and indigenous flood forecasting persist, structural weaknesses in governance, poor maintenance of river embankments, and the absence of early warning systems exacerbate vulnerability. The study underscores the need for integrated flood management approaches that combine ecosystem-based solutions, community participation, and climate-smart technologies. The research concludes with policy recommendations aimed at embedding flood risk reduction into Somalia's national climate adaptation framework and fostering sustainable resilience in riverine livelihoods.

Keywords: Flood management, Resilience, Riverine zones, Climate adaptation, Somalia, disaster risk reduction.

1. Introduction

Flooding represents one of the most significant environmental challenges facing Somalia's riverine communities. The twin river systems—Juba and Shabelle—support a majority of the nation's irrigated agriculture and serve as essential lifelines for food production. However, due to erratic rainfall patterns, deforestation in upper catchments, and inadequate water management infrastructure, these rivers frequently overflow, leading to destructive floods that threaten livelihoods and erode resilience.

According to the United Nations Office for the Coordination of Humanitarian Affairs (OCHA), seasonal flooding in Somalia displaces tens of thousands annually and destroys critical assets such as farmland, livestock, and housing. Recurrent floods also contribute to food insecurity and poverty, particularly in Lower and Middle Shabelle, Juba, and Hiraan regions. The situation is worsened by climate change, which intensifies extreme rainfall and increases river discharge variability.

While numerous humanitarian and government-led flood responses exist, most are reactive and short-term. There remains a critical gap in long-term, integrated flood management frameworks that combine community engagement, early warning systems, and sustainable ecosystem restoration. This paper explores these challenges and opportunities by proposing multi-level strategies for enhancing flood management and resilience in Somalia's riverine zones.

2. Problem Statement

Somalia's riverine regions have become increasingly prone to destructive floods that hinder agricultural productivity and human security. Despite the importance of these areas to national food supply and trade, flood management remains fragmented and under-resourced. The lack of coordinated policies, weak institutional frameworks, and overreliance on emergency responses perpetuate a cycle of vulnerability. Deforestation, unplanned settlement in floodplains, and sedimentation further exacerbate the problem.

In this context, understanding the socio-ecological drivers of flooding and identifying context-specific management solutions are vital. The absence of robust flood control infrastructure, coupled with limited community preparedness and early warning systems, continues to place rural livelihoods at risk.

3. Objectives of the Study

1. To assess the current state of flood management systems and community-based coping strategies in Somalia's riverine regions.
2. To analyze environmental, socio-economic, and institutional factors contributing to flood vulnerability.
3. To evaluate the effectiveness of existing flood mitigation measures and identify gaps in governance.
4. To propose integrated flood management strategies aligned with Somalia's climate adaptation policies.
5. To recommend policy actions that enhance resilience through participatory and ecosystem-based approaches.

4. Research Questions

1. What are the main drivers of recurrent flooding in Somalia's riverine zones?
2. How effective are current flood management and adaptation measures in mitigating disaster impacts?
3. What institutional and policy gaps hinder effective flood risk reduction?
4. How can ecosystem-based and community-led approaches strengthen flood resilience? 5. What policy frameworks can integrate flood management into Somalia's broader climate adaptation strategy?

5. Methodology

This study employed qualitative research approach to capture the complexities and depth of local; experiences and beliefs and strategies related to flood resilience.

- *Study Area*: The research focused on three major flood-prone regions: Lower Shabelle, Middle Juba, and Hiiraan. These areas are characterized by intensive farming along riverbanks and recurring flood events.

- *Data Collection:* the research utilizes a desktop based method or secondary data from a variety of credible sources.

6. Study frameworks

a) Conceptual Framework

This study is grounded in the understanding that effective flood management in Somalia's riverine zones requires the integration of environmental, institutional, and community-based components into a unified resilience framework. The conceptual framework (Figure 1) illustrates the dynamic interaction between flood hazards, exposure, vulnerability, and adaptive capacity—key elements that determine community resilience.

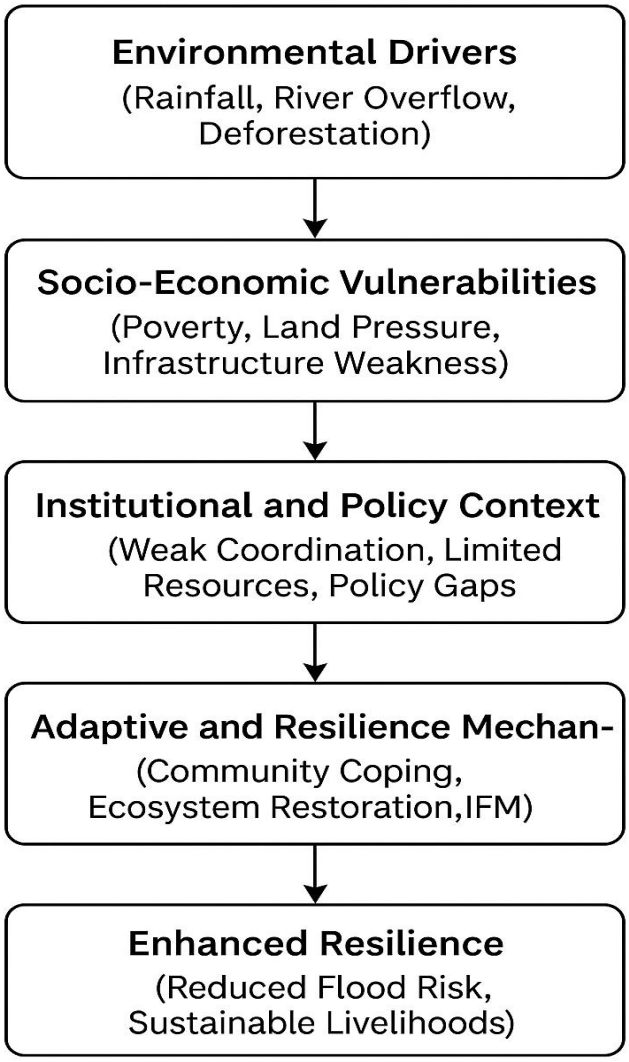

Figure1. Conceptual Framework of Flood Management

B) Theoretical Framework

The theoretical underpinning of this study draws on two complementary theories: the Pressure and Release (PAR) Model and the Resilience Theory.

Applying the PAR model thus highlights the systemic factors behind flood risk and underscores the need for transformative policy interventions beyond emergency response.

Resilience Theory helps to analyze how communities combine indigenous knowledge and external interventions to manage floods and sustain livelihoods. It also supports the design of interventions that enhance adaptive governance, ecosystem restoration, and participatory decision-making, thereby promoting sustainable flood resilience.

The synthesis of these theories provides a robust analytical foundation for understanding the socio-ecological dimensions of flood management in Somalia.

c) Analytical Framework Summary

Component	Key Focus	Relevance to the Study
Hazard	Flood intensity and frequency (river overflow, rainfall patterns)	Identifies hydrological risks in Juba and Shabelle basins
Exposure	Populations, farmlands, and infrastructure in flood zones	Determines degree of risk and target for mitigation
Vulnerability	Poverty, land degradation, weak governance	Explains why some communities experience greater losses
Adaptive	Capacity Knowledge, social networks, early warning, livelihood diversity	Central to resilience building and policy design
Resilience	Outcome Recovery, adaptation, and reduced future risk	

7. Literature Review

Flooding is one of the most pervasive environmental hazards affecting human settlements, agriculture, and ecosystems globally (Kundzewicz et al., 2019). Riverine floods occur when rivers overflow their banks due to excessive rainfall, upstream runoff, or structural failure of embankments. In many parts of sub-Saharan Africa, floods have intensified due to climate change, land degradation, and poor watershed management (Di Baldassarre et al., 2018). Somalia's riverine regions—particularly the Juba and Shabelle basins—represent a classic case where hydrological variability and weak institutional capacity converge to produce recurring disasters. Studies by the Food and Agriculture Organization (FAO, 2023) and the United Nations

Office for the Coordination of Humanitarian Affairs (OCHA, 2022) have documented the increasing frequency and magnitude of floods, often linked to erratic rainfall patterns associated with El Niño–Southern Oscillation events.

Overall, the reviewed literature identifies five key gaps:

1. Weak institutional coordination between federal and regional bodies.
2. Limited integration of local knowledge into formal flood management systems.
3. Absence of a national flood policy and long-term investment framework.
4. Underutilization of ecosystem-based adaptation and transboundary cooperation.
5. Insufficient early warning dissemination and community participation.

This synthesis demonstrates that addressing Somalia's flood challenges requires a multidimensional approach—combining hydrological, ecological, institutional, and socio-cultural perspectives. Building resilience thus depends on linking scientific knowledge with local adaptive practices within an inclusive governance framework.

8. Results

The findings indicate several interrelated drivers of flooding and vulnerability in Somalia's riverine zones:

- *Hydrological and Environmental Drivers*: Deforestation in the upper catchments and siltation of riverbeds has reduced water-holding capacity, while the absence of dredging and weak embankments increases overflow risks.
- *Socio-Economic Factors*: Poverty and dependence on riverbank agriculture force communities to settle in flood-prone areas. Low income limits the adoption of adaptive technologies such as raised granaries or flood-tolerant crops.
- *Institutional Weaknesses*: Fragmentation between national and regional agencies results in poor coordination of flood response and early warning dissemination.
- *Traditional Adaptations*: Communities employ local techniques—such as planting on elevated ridges, seasonal migration, and reliance on indigenous weather knowledge—but these are increasingly insufficient due to climate variability.

Overall, 73% of surveyed households reported significant crop loss in the last five years, and 62% indicated receiving no early warning before major flood events.

9. Policy Implications and Recommendations

1. *Develop a National Flood Management Strategy*: Integrate disaster risk reduction into Somalia's National Adaptation Plan (NAP) and Climate Change Policy.
2. *Invest in Early Warning Systems*: Establish decentralized hydrometeorological monitoring and community alert networks using mobile-based technologies.
3. *Rehabilitate Infrastructure*: Repair and maintain embankments, canals, and drainage systems along the Juba and Shabelle rivers.
4. *Promote Ecosystem-Based Adaptation*: Reforest upstream areas, restore wetlands, and regulate land use along floodplains to reduce runoff and sedimentation.
5. *Strengthen Institutional Coordination*: Create a River Basin Management Authority to coordinate between ministries, donors, and regional administrations.
6. *Enhance Community Capacity*: Implement participatory flood management and awareness campaigns, integrating local knowledge with modern science.
7. *Regional Collaboration*: Foster cross-border water-sharing and early warning coordination with Ethiopia for improved flood forecasting.

10. References:

1. Aden, M. A., & Roble, F. H. (2023). Transboundary water management and flood risk in the Juba–Shabelle Basin: Challenges and cooperation opportunities. Journal of African Water Policy, 14(2), 101–117.
2. Blaikie, P., Cannon, T., Davis, I., & Wisner, B. (1994). At risk: Natural hazards, people's vulnerability, and disasters. Routledge.
3. Di Baldassarre, G., Kooy, M., Kemerink, J. S., & Brandimarte, L. (2018). Towards understanding the dynamic behaviour of floodplains as human–water systems. Hydrology and Earth System Sciences, 22(1), 267–284. https://doi.org/10.5194/hess22-267-2018
4. Elmi, A. H., & Ahmed, I. M. (2020). Flood risk and response strategies in Somalia: A policy gap analysis. Somali Institute for Development Studies. Enhancing Flood Management in Somalia riverine Zones no 311 16
5. Food and Agriculture Organization (FAO). (2023). Somalia: Integrated flood management and climate resilience report. FAO Somalia.
6. FAO-SWALIM. (2023). Flood early warning systems in the Juba and Shabelle river basins. Somalia Water and Land Information Management Unit.
7. Haile, A. M., & Barre, M. A. (2022). Community-based early warning and response mechanisms for flood management in Somalia. Disaster Prevention and Management, 31(4), 512–526. https://doi.org/10.1108/DPM-01-2022-0012
8. Hassan, S. M., & Warsame, A. A. (2021). Environmental degradation and flood vulnerability in the Shabelle basin of Somalia. African Journal of Environmental Studies, 9(3), 88–102.
9. Holling, C. S. (1973). Resilience and stability of ecological systems. Annual Review of Ecology and Systematics, 4(1), 1–23. https://doi.org/10.1146/annurev.es.04.110173.000245
10. Intergovernmental Panel on Climate Change (IPCC). (2021). Climate change 2021: The physical science basis. Cambridge University Press.
11. Kundzewicz, Z. W., Kanae, S., Seneviratne, S. I., Handmer, J., & Nicholls, N. (2019). Flood risk and climate change: Global and regional perspectives. Hydrological Sciences Journal, 64(9), 1234–1247. https://doi.org/10.1080/02626667.2019.1620500
12. Mohamed, A. H., & Farah, A. M. (2022). Traditional flood coping strategies and adaptation among riverine farmers in Somalia. Somali Journal of Agricultural Research, 7(1), 35–49.
13. Muktar, Y. M., & Osman, A. I. (2022). Institutional fragmentation and flood risk governance in Somalia: Lessons for climate adaptation. African Governance Review, 11(2), 59–77.
14. Munang, R., Thiaw, I., Alverson, K., Mumba, M., Liu, J., & Rivington, M. (2019). Ecosystem-based adaptation: A cost-effective approach to climate change adaptation and food security. Environmental Science & Policy, 93, 93–101. https://doi.org/10.1016/j.envsci.2018.12.011 Enhancing Flood Management in Somalia riverine Zones no 311 17
15. Mwangi, J. M., Otieno, V. O., & Were, G. M. (2020). Nature-based solutions for flood mitigation in Kenya's Tana River Basin. Sustainability Science, 15(4), 991–1005. https://doi.org/10.1007/s11625-020-00810-1

16. United Nations Development Programme (UNDP). (2020). Community-based disaster risk reduction and resilience in the Horn of Africa. UNDP Regional Bureau for Africa.
17. United Nations Office for the Coordination of Humanitarian Affairs (OCHA). (2022). Somalia humanitarian response plan 2022. OCHA Somalia.
18. Walker, B., Holling, C. S., Carpenter, S. R., & Kinzig, A. (2004). Resilience, adaptability and transformability in social–ecological systems. Ecology and Society, 9(2), 5. https://doi.org/10.5751/ES-00650-090205
19. World Bank. (2021). Building resilience in fragile states: Climate and disaster risk management in Somalia. World Bank Group.

ICFM 10
Adapting to Global Change:
Innovative Approaches to Flood Management and Resilience
May 20-22, 2026 | Western University, London, Ontario, Canada

Uncertainties in ML-based Daily Reservoir Inflow Forecasting: A Case Study on Drina-Lim Hydropower Plants

Luka Vinokić[1], Milan Dotlić[1], Ana Samac[1], Vanja Švenda[1], Veljko Prodanović[1,2], Milan Stojković[1,3]
The Institute for Artificial Intelligence R&D, Fruškogorska 1, 21000 Novi Sad, Serbia[1]
E-mail: luka.vinokic@ivi.ac.rs
E-mail: milan.dotlic@ivi.ac.rs
E-mail: ana.samac@ivi.ac.rs
E-mail: vanja.svenda@ivi.ac.rs
E-mail: veljko.prodanovic@ivi.ac.rs
E-mail: milan.stojkovic@ivi.ac.rs

University of South Wales (UNSW), School of Civil and Environmental Engineering, Sydney, NSW 2052, Australia [2]
E-mail: v.prodanovic@unsw.edu.au

Faculty of Civil Engineering, University of Novi Sad, Kozaračka 2a, 24000 Subotica, Serbia[3]
E-mail: milan.stojkovic@gf.uns.ac.rs

ABSTRACT

Accurate streamflow forecasting is essential for hydropower optimization and flood risk reduction. This study develops an operational, data-centric forecasting framework integrating three machine learning architectures—LSTM, TCN, and TKAN—trained on long-term hydrometeorological data and driven by numerical weather predictions from IFS, GFS and OM. Two bias correction methods, delta-scaling and quantile mapping, are applied to address systematic NWP biases. An ensemble of 27 model-forcing-bias correction combinations is used for each station to quantify predictive uncertainty, while factorial ANOVA decomposes contributions from ML model choice, NWP source, and BCM (with additional insight into variability in performance by stations). Results show that uncertainty is predominantly governed by model choice and station (location) effects, which together account for the majority of total variance, whereas the influence of NWP and BCM remains marginal. These findings highlight key vulnerabilities in operational inflow forecasting chains and provide actionable guidance for strengthening system resilience under real-time conditions.

KEYWORDS: uncertainty, forecast, machine learning, inflow, data-centric, hydrology

1 INTRODUCTION

The hydropower plants within the Drina and Lim River networks generate around 3295 GWh of electricity annually, contributing roughly 10% of Serbia's total electricity production (Web-1). These reservoirs play a crucial role in balancing the country's energy supply, especially during peak demand periods, as hydropower provides a flexible and renewable energy source. Efficient management of reservoir operations and water resources is essential for maintaining grid stability, optimizing generation schedules, and ensuring cost-effective electricity production. In addition, the Drina-Lim water system is vital for flood management and regional water security. High-flow events, which can be caused by extreme weather patterns, prolonged rainfall, or snowmelt, pose significant risks by potentially exceeding reservoir capacities and leading to flooding, endangering infrastructure, agricultural land, and local communities, resulting in substantial economic losses.

As climate change increases the frequency and severity of extreme hydrological events, the need for accurate and reliable streamflow forecasting has become more critical than ever. Advanced predictions of river flow and reservoir levels enable stakeholders to optimize hydropower production while simultaneously reducing flood risks. Machine learning (ML) models have shown significant capabilities for river flow prediction (Kratzert et al., 2018; Vinokić et al., 2025). Even though ML models can deliver highly accurate results efficiently, data inconsistencies can reduce their effectiveness (AL-Jarrah et al., 2015). Adopting a data-centric approach, we focus on the quality and reliability of model inputs, as well as the uncertainties they introduce into the system. By understanding these uncertainties and their cascade effects, hydropower operators gain deeper insights into informed decision-making. Furthermore, these insights serve as a blueprint for strengthening the system at its most vulnerable points, creating a more resilient forecasting system.

Our approach leverages global datasets, such as ECMWF ReAnalysis v5 (ERA5) (Web-2), as well as operational weather forecasts such as Integrated Forecasting System (IFS), Global Forecasting System (GFS), and Open Meteo (OM) weather forecast. Since these global numerical weather simulation models exhibit inherent biases at localized scales, two bias correction techniques are investigated: a pragmatic delta-scaling approach and empirical quantile mapping. To ensure robust predictions, three state-of-the-art machine-learning models—LSTM, TCN, and TKAN—are trained on pre-processed data, each offering unique perspectives in capturing hydrological patterns. A detailed uncertainty propagation analysis is conducted, dissecting each step to identify weak links and areas of high variability.

By systematically addressing key sources of uncertainty and integrating advanced AI-driven forecasting models, system operators and policymakers can make more informed decisions, enhance system resilience, and improve the long-term sustainability of energy and water resource management. This comprehensive approach highlights the critical role of uncertainty assessment in developing robust streamflow forecasting systems, ensuring efficient water resource utilization, infrastructure protection, and public safety amid escalating environmental challenges.

2 MATERIALS & METHODS

As mentioned in the previous section, the study area is the Drina-Lim river system (Figure 1a), located in Southeastern Europe, where the forecasting system is developed for total of 8 hydropower plants (HPP), where the unregulated reservoir inflow was estimated. This reservoir system is a multipurpose system, primarily used for hydropower generation, river regulation, and flood management. The catchment area of Drina river basin is characterized by predominantly mountain region, where rainfall-runoff process yields significant contributions to river flow dynamics and flood formation.

The general workflow of the study (Figure 1b) consists of five main steps: (1) preparing historical data for model training, (2) ML model development, (3) acquiring forcing data from different NWPs for the verification period, (4) implementing bias correction techniques, and (5) assessing uncertainty.

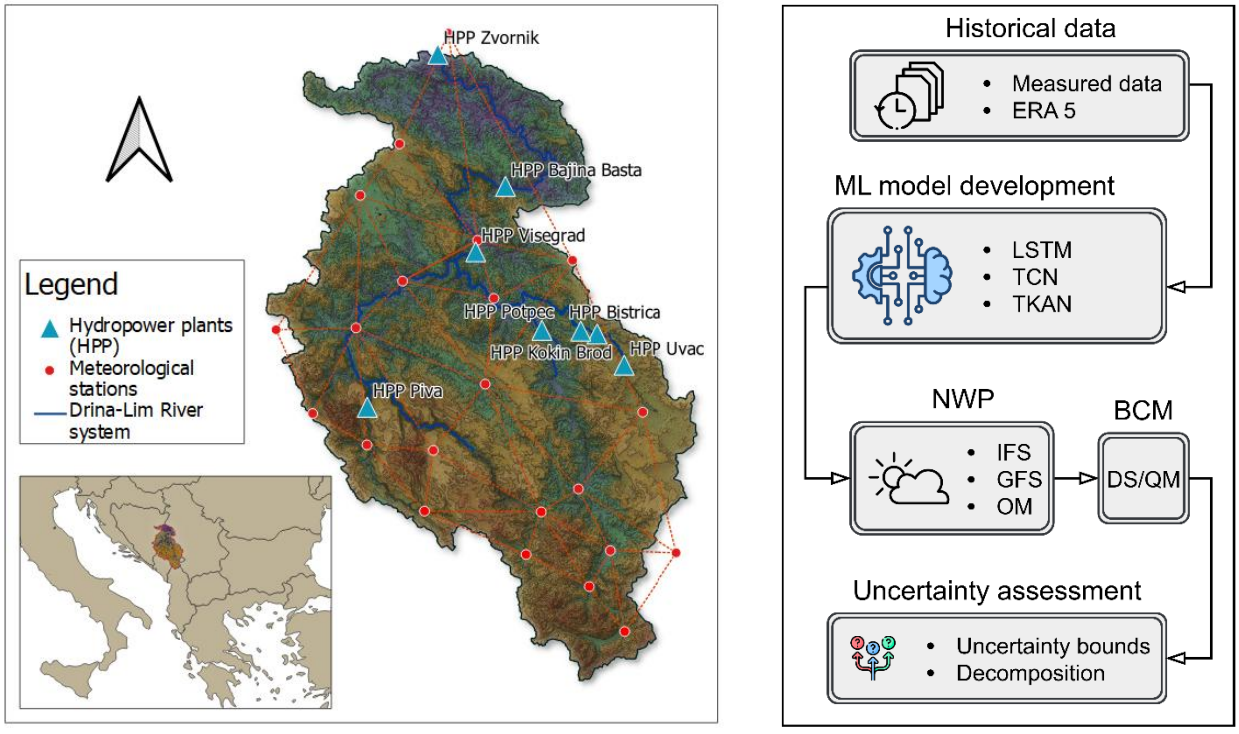

(a) (b)

Figure 1: (a) Case study and (b) study workflow

2.1 Data collection and processing

The dataset comprises daily time series data collected from 8 HPPs and 22 meteorological stations located in the Drina River basin, shown in more detail in Table 1. Data is structured in windowed features, consisting of several previous steps and forecast horizon. Lagged streamflow from previous 7 days is taken, along with precipitation and air temperature from 2 days before and 5 days ahead (referencing to forecast horizon). In training, this "future" data is taken from the existing observed dataset, while this data is taken from numerical weather predictions (NWPs) in inference.

Table 1: List of datasets used in the study

Type of data	Variable	Source
Hydrological data	Reservoir inflow data	EPS
Meteorological data	Precipitation sum	RHMSS (Web-3), ZHMS (Web-4)
	Air temperature	
Weather forecast data	Precipitation sum	IFS, GFS, UKMO
	Air temperature	IFS, GFS, UKMO

When ML models are operational and ready for real-time use, the weather forecast data must be transformed into daily time series data, and re-gridded onto the coordinates of meteorological measuring stations. This is achieved with spatial interpolation via inverse distance weighting (IDW) between a station location and the four nearest centres of the NWP grid. Equation (1) is used to determine the weights of neighboring center points, while Equation (2) calculates the interpolated value of a variable $\tilde{x}$ for a given x for 4 nearest neighbors:

$$w_j = \frac{{d_j}^{-\alpha}}{\sum_j {d_j}^{-\alpha}}; \quad (1)$$

$$\bar{x} = \sum_j w_j x_j; \quad (2)$$

where w_j represents weight of j-th center point, d_j its distance, and α denotes an order of an inverse distance (Atiah et al., 2023). For this study, inverse squared distance is used, which means that $\alpha = 2$.

Since the availability of data depends on location, models that are trained on specific HPPs utilize maximum available data (earliest time series begins in 1949 and latest in 1968, limited by dam construction / reservoir creation).

2.2 Bias correction methods (BCMs)

Two fundamentally different BCMs are used to estimate the impact of the use of bias correction in real-time operational conditions: delta scaling (DS), also known as delta change; and quantile mapping (QM). DS is a pragmatic method that utilizes, a principle of equating the mean monthly air temperature and precipitation sums. The strengths of this approach are its simplicity and cumulative volumetric consistency. However, its limiting factor is the assumption of linearity, effectively ignoring tails of distributions, which is of utmost importance for precipitation, as flattening the spike of heavy rainfall can produce underpredictions in river flow (Stojkovic & Simonovic, 2019). DS approach can be described as follows:

$$\Delta(\text{month}) = \begin{cases} \frac{\bar{x}_{obs}(\text{month})}{\bar{x}_{mod}(\text{month})}, & x = \text{precipitation} \\ \bar{x}_{obs}(\text{month}) - \bar{x}_{mod}(\text{month}), & x = \text{air temperature} \end{cases} \quad (3)$$

$$\hat{x}_{mod} = \begin{cases} \Delta * x, & x = \text{precipitation} \\ x + \Delta, & x = \text{air temperature} \end{cases} \quad (4)$$

where *obs* subscript represent observed, and *mod* modelled values, $\bar{x}$ denotes mean value of a variable, and $\hat{x}$ a bias corrected value. Quantile mapping (QM), on the other hand, suits precipitation data better, where cumulative distribution function (CDF) is mapped onto the reference CDF, correcting the entire probability distribution (Stojkovic & Simonovic, 2019). This is especially useful in situations with extreme events, such as extreme precipitation because of the high sensitivity to such occurrences (Vinokić et al., 2023). QM is generally expressed through following function:

$$\hat{x}_{mod}(q) = F_{obs}^{-1}(F_{mod}[x_{mod}(q)]). \quad (5)$$

Transfer functions are calculated from the only available period where NWP and observed values overlap, which is from 2022, limiting the period from which a transfer function can be extracted.

2.3 Machine Learning models

Three state-of-the-art ML model architectures are used, including Long Short-Term Memory (LSTM), Temporal Convolutional Network (TCN), and Temporal Kolmogorov Arnold Network (TKAN).

LSTMs (Hochreiter & Schmidhuber, 1997) augment traditional recurrent neural networks by incorporating a memory cell regulated by input, forget, and output gates. These components enable effective preservation and updating of long-term temporal information, making LSTMs particularly suitable for modelling hydrological phenomena with delayed responses, such as runoff generation following precipitation (Kratzert et al., 2018). TCNs (Lea et al., 2016) model sequences using 1D dilated causal convolutions, allowing them to capture long-range dependencies while maintaining strict temporal causality. Residual connections facilitate the training of deep models, mitigating vanishing gradients. TCNs have shown strong performance in time-series forecasting due to their ability to model both short-term and long-term temporal patterns (Bai et al., 2017). TKANs extend Kolmogorov–Arnold Networks (KANs), which replace fixed activation functions with learnable univariate functions (often splines) applied on edges rather than nodes (Liu et al., 2024). By modifying KANs to incorporate temporal dependencies, TKANs adapt this flexible functional representation to sequence modelling. Their ability to learn expressive nonlinear transformations with fewer parameters makes them a promising emerging architecture for hydrological time-series forecasting (Vinokić et al, 2025).

ML models are trained on data from different periods, from the earliest 1949, to the latest 1968, to the year 2014, while the following two years used for validation, and 2017 and 2018 for testing. However, for the testing of operational conditions an estimation of uncertainty in real-time forecasting scenarios, a verification set is selected to be year 2023, as the only remaining year with available data, after using pre previous one for extracting the transfer functions.

2.4 Uncertainty decomposition

The uncertainty bounds are derived from an ensemble of 27 model predictions. Each prediction differs from the others in terms of the numerical weather prediction (NWP) forcing, bias-correction method (BCM), or machine-learning (ML) model employed. This structured ensemble enables the decomposition of predictive uncertainty across these three sources by treating them as independent factors. The uncertainty decomposition is performed using factorial ANOVA, as illustrated in Figure 2.

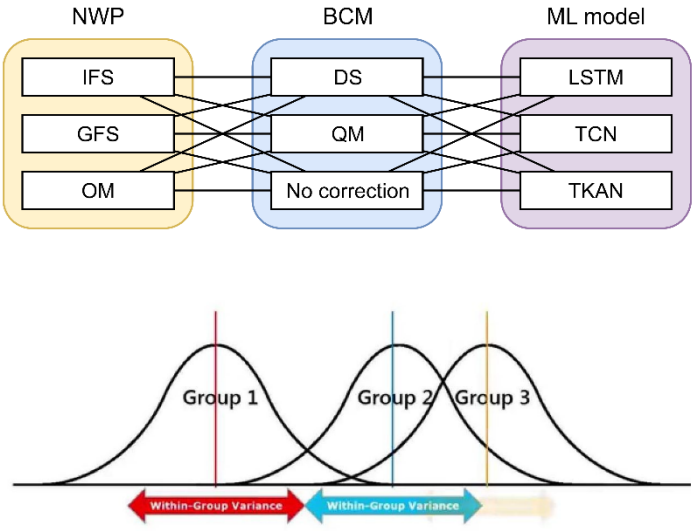

Figure 2: Uncertainty decomposition scheme

The ANOVA-derived variance corresponds to interpretable uncertainty contributions for each of the three factors, where the proportion of total explained variance by a given factor R_i is computed as follows:

$$R_i = \frac{v_i}{v_{total}} \times 100, \quad (6)$$

ANOVA-based uncertainty decomposition is run on multiple scalar metrics to capture different dimensions of model behaviour, together providing a comprehensive decomposition across factors, by averaging their respective results.

2.5 Performance metrics

ANOVA is applied to scalar performance metric or a scalar characteristic, computed for every factor combination, indicating model performance. Since the analysis is performed on multiple different HPPs, the relative or normalized metrics are applied for comparability across stations, as shown in Table 2.

Table 2: Overview of used performance metrics

Performance metric	Equation	Use
Normalized Root Mean Squared Error (NRMSE)	$NRMSE = \frac{1}{n}\sqrt{\frac{\sum_i^n \left(Q_i^{mod} - Q_i^{obs}\right)^2}{\overline{Q}^{obs}}}$	Skill metrics for ANOVA
Nash-Sutcliffe Efficiency (NSE)	$NSE = \frac{\sum_i^n \left(Q_i^{obs} - Q_i^{mod}\right)^2}{\sum_j^n \left(Q_i^{obs} - \overline{Q}^{obs}\right)^2}$	
Prediction Interval Coverage Percentage (PICP)	$PICP = \frac{1}{N}\sum_{i=1}^{N} \mathbb{I}(y_i \in [\hat{Q}_i^{\,L}, \hat{Q}_i^{\,U}])$	Uncertainty bounds

* Q_i^{mod} and Q_i^{obs} represent the predicted and measured discharge for i-th time-step respectfully, $\overline{Q}^{obs}$ denotes the mean measured river flow for the period, while n denotes the number of time-steps. $\hat{Q}_i^{\,L}$ and $\hat{Q}_i^{\,U}$ represent the lower and upper value of uncertainty bounds for a single time-step.

3 RESULTS & DISCUSSION

Ensemble forecasting provides a significant insight into uncertainty, while also providing reliable forecasting bounds. Depending on the station, the prediction envelope covers from 65% to 93% observed values within the 10% margin of error, measured with PICP. Note that reservoir inflow estimates can be inaccurate, impacted with the reservoir system operation. Therefore, heavily regulated inflows, such as on HPP Zvornik or HPP Bajina Bašta, where PICP was the lowest (65% and 70%), can be difficult to estimate natural flow, resulting in somewhat noisy data, especially in low flow periods. Ensemble forecast in verification (operational-like) setting are shown in Figure 3. The distribution of uncertainty is quite different for each of the stations, indicating a high level of uncertainty is connected to catchment-specifics and river inflows that are not considered as a factor, since there is only one source of inflow data. Upon analyzing the results that include HPPs (location) as a factor, the variability attributed to station factor is 31% to 65% depending on chosen metric, confirming that the large portion of the uncertainty spread is location-based.

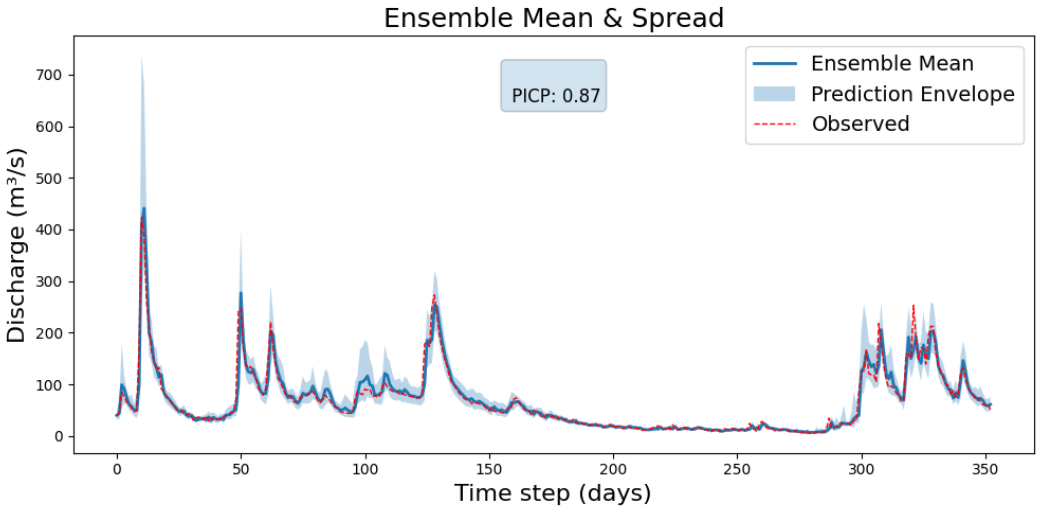

Figure 3: Example of ensemble forecasting with uncertainty bounds on the verification set.

As shown in Table 3, model choice emerges as the dominant contributor to total uncertainty, explaining between 57% and 96% of the overall variance. By comparison, NWP and BCM selections exhibit mostly marginal influence, under 10% combined for the majority of HPPs, while the unexplained variance spans from 3% to 31%.

Table 3: Uncertainty contributions for each reservoir inflow forecast averaged for three skill scores

Factor	Uvac	Kokin Brod	Bistrica	Piva	Potpeć	Višegrad	Bajina Bašta	Zvornik
NWP	4.2%	3.8%	11.6%	3.1%	0.7%	0.3%	1.1%	0.5%
BCM	1.1%	3.6%	2.6%	14.5%	13.1%	1.0%	2.0%	1.5%
ML	81.4%	61.8%	64.5%	57.4%	66.5%	95.5%	91.7%	94.8%
Residual	13.3%	30.8%	21.3%	25.0%	19.7%	3.1%	5.2%	3.2%

4 CONCLUSION

This study confirms that uncertainty in ML-based daily reservoir inflow forecasting on the Drina-Lim system is dominated by model structure and location-specific characteristics, particularly under strong hydraulic regulation. While ensemble forecasts provide reliable predictive bounds, a substantial share of uncertainty remains inherently station-dependent, highlighting the critical role of local hydrological and operational influences.

When considering station-specific models, the largest share of the explained variance is attributed to the ML model architecture. This is expected given the design of this study, where variability is introduced primarily through the operational setting rather than the training process. The absence of variability in training data and optimization constrains the contribution of other uncertainty sources, thereby emphasizing structural differences between model types. These findings highlight a clear direction for future research, where variability should be systematically introduced at the training stage by employing substantially larger ensembles of models trained on different data realizations, architectures, and hyperparameter configurations.

5 ACKNOWLEDGEMENTS

The research presented herein received financial support from the European Union's Horizon Europe project ARTIFACT, under Grant Agreement 101159480. We also extend our gratitude to Joint Stock Company Elektroprivreda Srbije for their trust and support in the project "Prediction of Daily Reservoir Inflows at the Drina–Lim Hydropower Plants Using Artificial Intelligence Techniques." Their collaboration and funding were instrumental in enabling the research activities and achieved outcomes.

REFERENCES

Al-Jarrah, O. Y., Yoo, P. D., Muhaidat, S., Karagiannidis, G. K., & Taha, K. (2015). Efficient machine learning for big data: A review. Big Data Research, 2(3), 87-93.

C. Lea, M. D. Flynn, R. Vidal, A. Reiter, and G. D. Hager, "Temporal Convolutional Networks for Action Segmentation and Detection," Nov. 16, 2016, arXiv: arXiv:1611.05267. Accessed: Jul. 14, 2024. [Online]. Available: http://arxiv.org/abs/1611.05267.

F. Kratzert, D. Klotz, C. Brenner, K. Schulz, and M. Herrnegger, "Rainfall–runoff modelling using Long Short-Term Memory (LSTM) networks," Hydrol. Earth Syst. Sci., vol. 22, no. 11, pp. 6005–6022, Nov. 2018, doi: 10.5194/hess-22-6005-2018.

S. Ahmad and S. P. Simonovic, "System Dynamics Modeling of Reservoir Operations for Flood Management," J. Comput. Civ. Eng., vol. 14, no. 3, pp. 190–198, Jul. 2000, doi: 10.1061/(ASCE)0887-3801(2000)14:3(190).

S. Bai, J. Z. Kolter, and V. Koltun, "An Empirical Evaluation of Generic Convolutional and Recurrent Networks for Sequence Modeling," Apr. 19, 2018, arXiv: arXiv:1803.01271. Accessed: Jul. 14, 2024. [Online]. Available: http://arxiv.org/abs/1803.01271

S. Hochreiter and J. Schmidhuber, "Long Short-Term Memory," Neural Comput., vol. 9, no. 8, pp. 1735–1780, Nov. 1997, doi: 10.1162/neco.1997.9.8.1735.

Stojkovic, M., & Simonovic, S. P. (2019). Mixed General Extreme Value Distribution for Estimation of Future Precipitation Quantiles Using a Weighted Ensemble - Case Study of the Lim River Basin (Serbia). Water Resources Management.

Vinokić, L., Dotlić, M., Prodanović, V., Kolaković, S., Simonovic, S. P., & Stojković, M. (2025). Effectiveness of three machine learning models for prediction of daily streamflow and uncertainty assessment. *Water Research X*, *27*, 100297.

Vinokić, L., Stojković, M., Kolaković, S. (2023). Bias correction and weighting methods to shape precipitation under the climate change options. Proceedings of the International Conference Synergy of Architecture & Civil Engineering. SINARG 2023. Niš, Serbia.

W. A. Atiah et al., "Bias correction and spatial disaggregation of satellite-based data for the detection of rainfall seasonality indices," Heliyon, vol. 9, no. 7, p. e17604, Jul. 2023, doi: 10.1016/j.heliyon.2023.e17604.

Z. Liu et al., "KAN: Kolmogorov-Arnold Networks," Jun. 16, 2024, arXiv: arXiv:2404.19756. Accessed: Jul. 14, 2024. [Online]. Available: http://arxiv.org/abs/2404.19756

Web sites:

Web-1: https://www.eps.rs/cir/dlhe/Pages/default.aspx, consulted 10 December, 2025

Web-2: https://cds.climate.copernicus.eu/cdsapp#!/dataset/reanalysis-era5-complete, consulted 15 July, 2024.

Web-3: https://www.hidmet.gov.rs/index_eng.php, consulted 11 September 2025.

Web-4: https://www.meteo.co.me/, consulted 15 July, 2024.

ICFM 10
Adapting to Global Change:
Innovative Approaches to Flood Management and Resilience
May 20-22, 2026 | Western University, London, Ontario, Canada

Digital Twin for Urban Flood Resilience: Integrating Four-Pre Modules into Digital Infrastructure

Sien Liu[1], Fan Yang[1], Xuan Huang[1], Jinjin Gao[1], Jingxiu Wu[1], Guoqing Liu[1], Benyou Jia[1], Ziwu Fan[1, *]
Nanjing Hydraulic Research Institute, Nanjing 210029, Jiangsu, China
E-mail: seliu@nhri.cn

ABSTRACT

Climate change and rapid urbanization have significantly amplified flood risks from extreme rainfall events, exposing critical limitations in conventional flood management systems. Traditional approaches often fail to address systemic challenges such as fragmented data integration, computationally heavy forecast models, and static emergency protocols lacking dynamic adaptability. This study proposes an innovative digital twin framework that integrates "Four-Pre" modules (Forecasting, Warning, Rehearsal, Planning) into urban flood resilience infrastructure. The framework employs a unified digital baseboard to aggregate multi-source spatial-temporal data, extending beyond traditional IoT sensors to include urban crowdsourced monitoring. A novel hybrid dual-engine architecture, utilizing multi-layer grid overlay analysis and decoupled interpolation, is established to overcome computational bottlenecks. This hybrid approach accelerates 72-hour flood simulations to merely 1/12 of the time required by traditional models, while maintaining sub-5cm inundation depth accuracy. Furthermore, enhanced by advanced Knowledge Graph technologies and a multi-scenario rainstorm waterlogging scheme library, the platform shifts from direct physical interventions to an intelligent decision-support ecosystem, enabling dynamic map visualization and rapid one-click scheme invocations. The Nanjing case study demonstrates the framework's effectiveness in upgrading urban flood standards through cyber-physical convergence, aligning with national strategies for digital twin basin development.

KEYWORDS: Digital Twin; Urban Flood Resilience; “Four-Pre” Modules; Hydro-hydraulic Coupled Modelling; Computational Acceleration

1 INTRODUCTION

The confluence of shifting climate patterns and rapid urban expansion has led to a marked rise in extreme rainfall, placing immense strain on urban public safety and infrastructure (Fan et al., 2025, Zhang et al., 2025). High-density urban environments, characterized by vast impervious surfaces and shrunken natural retention areas, have become highly sensitive to flash floods that frequently overwhelm traditional drainage systems (Bakhtiari et al., 2023, Zeng et al., 2025). The transition from natural landscapes to built environments has fundamentally altered the urban water cycle, resulting in higher runoff coefficients and shortened concentration times (Song et al., 2024).

Despite continuous engineering advancements, conventional flood management often hits technical and operational ceilings. A primary obstacle is the existence of fragmented data silos across meteorological, hydrological, and municipal planning departments (Ge et al., 2025). Critical information remains isolated within disparate administrative units, complicating unified response efforts during a crisis (Liu et al., 2024). Furthermore, older forecasting models frequently struggle to reflect the complex, non-linear water flow changes seen during intense cloudbursts (Zeng et al., 2025). While broad-scale models offer discharge estimates, they often lack the granularity required to simulate dynamic inundation

at the street or building level (Zhang et al., 2025, Qi et al., 2021). Perhaps most importantly, current emergency protocols rely heavily on static plans that lack the flexibility to adapt to rapidly evolving flood conditions in real time (Liu et al., 2024).

To address these vulnerabilities, Digital Twin technology provides a way to bridge these disconnected elements. Defined as a virtual mirror of physical entities that undergoes continuous updates via real-time data, a Digital Twin facilitates the visualization, analysis, and simulation of complex system behaviour (Kaynak et al. 2025, Chen et al., 2024). In the context of urban flooding, DT technology allows for the fusion of multi-source data—including satellite imagery, Internet of Things (IoT) sensors, and 3D city models (BIM/GIS)—into a cohesive digital baseboard (Li Q, 2022, Ge et al., 2025). Recent strategic initiatives, such as the "Digital Twin Basin" development framework, have underscored the necessity of moving toward proactive, intelligence-driven management (Zhang et al. 2024, Cai Y. 2022, Zhu et al., 2025).

The operational heart of this framework is the "Four-Pre" logic: Forecasting, Warning, Rehearsal, and Planning (Li, et al., 2022). In this cycle, Forecasting establishes the empirical basis through rolling data updates; Warning serves as a sentinel, identifying risk thresholds before a disaster manifests; Rehearsal acts as an essential tool for "what-if" testing, enabling managers to evaluate the efficacy of various interventions in a virtual environment; and Planning represents the final objective, translating simulation-derived insights into actionable, optimized emergency responses (Mao, et al., 2024).

Realizing a functional urban flooding digital twin, however, requires overcoming substantial modelling and computational hurdles. High-resolution simulations that couple one-dimensional pipe networks with two-dimensional surface flow are notoriously resource-intensive (Yang, et al., 2024, Wang, et al., 2025). To provide results within the "minute-level" windows needed for emergency decision-making, advanced acceleration techniques—such as GPU-based parallel computing and Local Time Step (LTS) algorithms—are essential to minimize calculation overhead without compromising precision (Fan et al., 2025, Wang, et al., 2023). Moreover, the integration of advanced Knowledge Graph technologies transforms the platform from a passive monitoring tool into an intelligent decision-support ecosystem, enabling rapid multi-scenario visualization and actionable emergency planning.

The following sections provide a systematic exploration of the framework, beginning with Methods and System Architecture and the protocols for Data Fusion and Digital Baseboard Construction. Subsequent chapters focus on Coupled Hydro-Hydraulic Modelling and Computational Acceleration, followed by an analysis of forecasting precision in Results and Case Studies. Finally, Discussion and Conclusions reflect on the framework's contribution to urban resilience.

2 METHODS AND SYSTEM ARCHITECTURE

The proposed framework implements a hierarchical configuration to maintain a direct correspondence between physical watershed processes and their virtual representations. This methodological approach ensures that the digital twin functions not merely as a visualization tool, but as an active management infrastructure capable of autonomous response and predictive analysis.

2.1 Hierarchical Framework and Layered Architecture

The proposed framework implements a decoupled five-layer architecture to establish a high-fidelity mapping between the physical watershed and its digital twin.

The Physical Layer represents the baseline urban topography and hydraulic infrastructure such as pipe networks, pump stations, and sluice gates. Overlying this, the Perception Layer utilizes IoT sensors and rain radars to capture real-time dynamic boundary conditions, such as rainfall intensity and water levels. These streams are integrated into the Data Layer, which fuses static 3D city models via LiDAR and oblique photography with real-time sensor data into a unified spatiotemporal database.

The Model Layer serves as the simulation core. Unlike conventional digital twins that rely either on computationally heavy traditional models which lack timeliness or pure-AI algorithms which often yield

unstable and low-precision results, this framework distinguishes itself through a novel hybrid dual-engine architecture. It tightly couples physically-based 1D-2D hydro-hydraulic solvers with a rapid forecasting module utilizing multi-layer grid overlay analysis and static-dynamic variable decoupled interpolation. This hybrid innovation resolves the inherent conflict between simulation speed and physical accuracy, reducing computational time to 1/12 of classic models while maintaining an absolute inundation depth error of less than 5 cm. Finally, the Application Layer acts as the executive interface for urban flood management.

Crucially, this hierarchical design establishes a Data-Model-Decision Closed-loop. Rather than acting solely as a passive observation tool, the digital twin empowers operators with a domain-specific Knowledge Graph and a scheme library. This ensures that simulation insights are rapidly translated into optimized, actionable emergency scheduling strategies.

2.2 The "Four-Pre" Operational Cycle

The operational efficacy of the proposed framework is governed by the "Four-Pre" operational cycle, which systematizes the dynamic transition from environmental data to proactive risk mitigation through Forecasting, Warning, Rehearsal, and Planning (Figure 1). Forecasting serves as the empirical foundation, utilizing rolling data ingestion to generate high-resolution hydrological projections across a 72-hour horizon. When simulated water stages breach safety thresholds, the Warning module automatically triggers multi-level risk alerts, ensuring critical information is rapidly disseminated to administrative authorities.

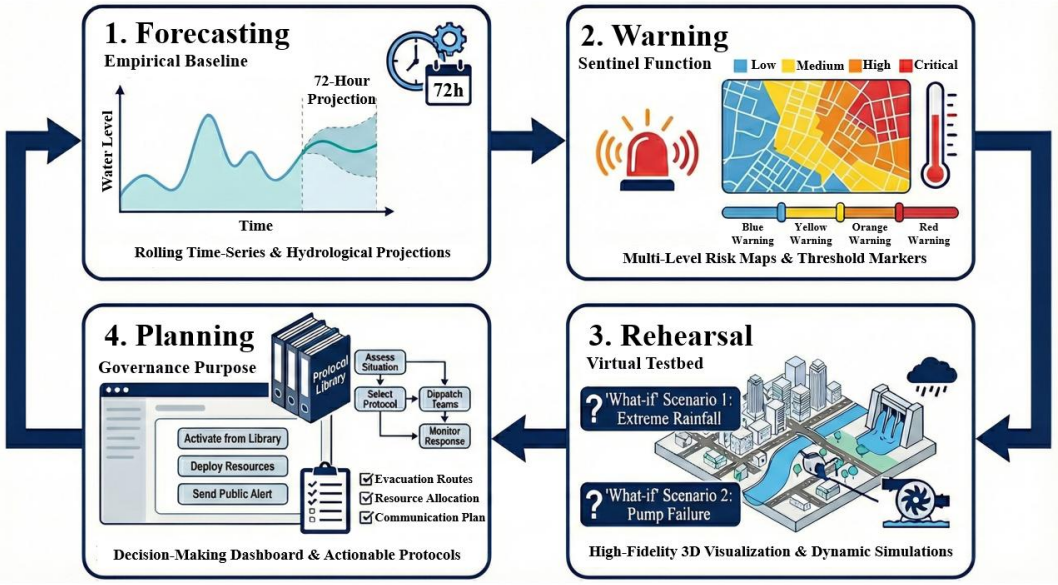

Figure 1: the “Four-Pre” Operational Logic

Building on these predictions, the Rehearsal component functions as a virtual testbed. It utilizes optimization algorithms to evaluate diverse scheduling schemes—such as varying sluice gate openings or pump station configurations—under extreme rainfall scenarios prior to physical deployment. Finally, the Planning phase translates these simulation-derived insights into optimized, actionable emergency protocols. This continuous cycle shifts urban flood management from a reactive, experience-based crisis response to a proactive, evidence-based governance paradigm.

3 DATA FUSION AND DIGITAL BASEBOARD CONSTRUCTION

The framework establishes a unified digital baseboard that is deeply integrated with the broader Smart City framework, dismantling traditional data silos across municipal departments. It fuses multi-

source spatiotemporal data into comprehensive dimensions: hydrological sensing, engineering facility status, space-air-ground integrated perception, and urban crowdsourced monitoring (Figure 2).

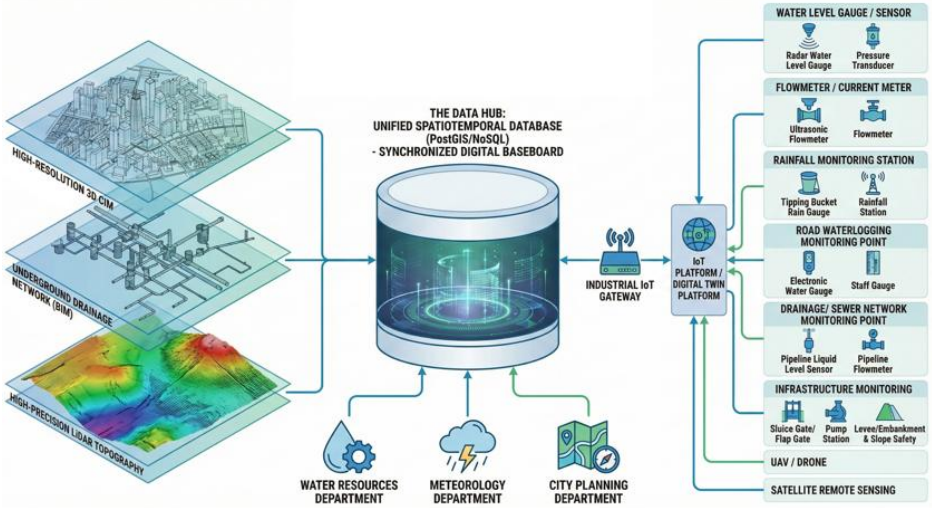

Figure 2: Multi-source Data Fusion

At the ground and subterranean levels, an extensive IoT network captures dynamic boundary conditions via radar water gauges, pipeline sensors, and geotechnical monitors. Crucially, moving beyond conventional water-centric data, the system ingests cross-departmental and public data streams. This includes real-time traffic information and crowdsourced data from social media platforms (e.g., Weibo, WeChat, and Douyin). These non-traditional data sources serve as vital auxiliary indicators, enabling the system to rapidly detect, verify, and assess the severity of urban waterlogging on streets and underpasses in real time.

To achieve space-air-ground integration, the system fuses high-resolution 3D city models with X-band rain radar data. Synchronized via robust industrial IoT gateways and protocols (e.g., 5G, NB-IoT, SCADA), these multimodal streams are continuously ingested into a distributed spatiotemporal database. This comprehensive data fusion provides the high-fidelity empirical foundation necessary to drive the "Four-Pre" operational cycle.

4 COUPLED HYDRO-HYDRAULIC MODELLING AND COMPUTATIONAL ACCELERATION

The simulation core of the framework is built upon a dual-engine modelling architecture that integrates a high-fidelity hydrodynamic solver with a novel rapid forecasting system based on multi-layer grid overlay analysis. The mechanistic component employs a refined 1D-2D coupled model to simulate flood propagation across urban surfaces, river networks, and subsurface drainage systems. Flow dynamics in channels and conduits are governed by the Saint-Venant equations. To represent intricate surface inundation processes typical of dense urban settings, the 1D drainage network is bidirectionally coupled with a 2D shallow-water solver. The model employs dynamic mesh refinement and local time-stepping methods to handle complex micro-topography, enabling the pre-simulation of historic and synthetic 72-hour flood events to populate a comprehensive model scenario library.

While this study is conceptualized under the macro-framework of China's 'Digital Twin Basin' strategic initiative, the specific hybrid dual-engine methodology and the Nanjing demonstrative case study presented herein represent our original, previously unpublished adaptations and technical enhancements.

Complementing the physics-based engine, a data-driven rapid forecasting module provides near-immediate projections. Unlike conventional approaches, this module executes a multi-layer grid overlay analysis across three distinct spatial scales: meteorological grids, catchment grids, and hydrodynamic model grids. Through GIS-based geometric intersection, the system dynamically calculates the rainfall allocated to each catchment unit using the intersection area between meteorological grid points and catchment zones as the distribution weight.

To achieve massive computational acceleration, the system leverages a distributed spatiotemporal database (e.g., PostgreSQL with Postgres-BDR) and employs a static-dynamic variable decoupled interpolation method. The dynamically calculated catchment rainfall is rapidly queried via database indexes against the pre-computed scenario library to identify the matching historical rainfall intervals. Subsequently, utilizing barycentric coordinate linear interpolation within a parallel computing environment, the maximum inundation depth for each hydrodynamic grid cell is rapidly calculated.

Within the platform, the two engines operate cooperatively: the mechanistic solver ensures physical consistency, while the multi-layer grid matching module supplies low-latency forecasts. Quantitative evaluations demonstrate that this hybrid innovation effectively resolves the inherent conflict between simulation speed and physical accuracy. It reduces computational time to merely 1/12 of classic hydro-dynamic models, while maintaining an absolute inundation depth error of less than 5 cm. This coupled mechanism transforms the digital twin into an active operational infrastructure capable of driving minute-level emergency decision-making.

5 RESULTS AND CASE STUDIES

The practical efficacy of the proposed framework is demonstrated by the Nanjing Extreme Rainstorm Flood Prevention and Drainage Platform, which integrates multi-source spatiotemporal data to maintain a high-fidelity digital representation of the urban watershed. A central technical achievement of the Nanjing project is the realization of synchronous operation between mechanistic hydro-hydraulic solvers and data-driven predictive models, augmented by advanced knowledge graph technologies.

5.1 Performance of the Dual-Engine Architecture

By coupling physically-based 1D-2D solvers with the multi-layer grid overlay algorithm, the system bypasses the computational bottlenecks inherent in traditional numerical schemes while preserving physical consistency. Supported by distributed databases and parallel computing, this dual-engine architecture facilitates rolling forecast-update mechanisms. Quantitative evaluations in the Nanjing platform demonstrate that this hybrid approach reduces the computational time required for simulating a 72-hour flood process to merely 1/12 of classic hydro-dynamic models. Furthermore, the framework maintains an absolute inundation depth error of less than 5 cm, with over 97.7% of hydrodynamic grid cells exhibiting absolute errors below 0.25 cm, ensuring granular and highly reliable situational awareness.

5.2 Multi-Scenario Visualization and Optimization

The Rehearsal component serves as a high-fidelity virtual testbed utilizing a comprehensive multi-scenario rainstorm waterlogging scheme library. To demonstrate its practicality, an extreme rainfall event in Nanjing was utilized as a case study. The platform simulated diverse precipitation scenarios and their corresponding inundation evolution across the urban terrain. Through intelligent data analysis and map visualization, administrators could visually assess the dynamic distribution of waterlogging risks. Within minutes, the platform retrieved the most appropriate scheduling schemes—such as optimal pump operation

sequences—allowing decision-makers to execute one-click scheme invocations. This visual demonstration of effects ensures that the generated emergency protocols are both scientifically rigorous and practically actionable.

5.3 Knowledge Graph-Driven Intelligent Decision Support

Rather than relying on direct physical interventions, the platform emphasizes holistic, system-level decision-making supported by a domain-specific Knowledge Graph. Specifically, the system established the "Nanjing City Main Urban Area River and Hydraulic Engineering Topological Relationship Knowledge Graph". This semantic network extracts and integrates multi-dimensional entities—including spatial relationships, historical flood scenarios, and operational rules.

By fusing this Knowledge Graph with an expert experience library and a business rule library, the digital twin transforms massive, unstructured historical disaster records into structured, reusable reasoning paths. During extreme events, the reasoning engine automatically correlates real-time hydrodynamic predictions with the Knowledge Graph to recommend optimized, scenario-specific scheduling strategies. This intelligent visualization of entities, rules, and predicted outcomes equips urban managers with a comprehensive and practical decision-support ecosystem, fundamentally upgrading the city's proactive flood resilience.

6 DISCUSSION AND CONCLUSIONS

The successful implementation of the Nanjing Extreme Rainstorm Flood Prevention and Drainage Platform confirms that the integration of the "Four-Pre" operational logic transforms urban flood management into a proactive, evidence-based governance paradigm. By utilizing a high-fidelity digital baseboard, the platform effectively dismantles fragmented data silos across meteorological, hydrological, municipal departments, and crowdsourced social platforms, achieving a comprehensive spatiotemporal representation of the urban watershed.

A pivotal milestone of this framework is the development of a hybrid dual-engine modelling architecture that couples mechanistic 1D-2D solvers with a rapid forecasting module based on multi-layer grid overlay analysis. This hybrid innovation dramatically accelerates computational speeds—reducing simulation time to merely 1/12 of classic hydro-dynamic models—while maintaining an absolute inundation depth error of less than 5 cm. Furthermore, by establishing a domain-specific Knowledge Graph and a multi-scenario scheme library, the digital twin has upgraded its cyber-physical integration. Instead of relying solely on manual physical infrastructure adjustments, the system provides an intelligent decision-support ecosystem capable of multi-scenario visualization and one-click scheme invocations. This transition from reactive intervention to an automated, model-driven strategy is critical for high-density urban environments where the lead time for effective crisis mitigation is exceptionally narrow.

To further advance this capability, future iterations will integrate Graph Neural Networks to better capture the complex spatial dependencies inherent in interconnected river and pipe networks. By incorporating Physics-Informed Neural Networks, the system can ensure that data-driven outputs strictly adhere to fundamental hydraulic laws. Furthermore, the emergence of Generative AI offers the potential for on-the-fly scenario synthesis to overcome the limitations of sparse historical datasets.

Ultimately, this study establishes a scalable blueprint for urban resilience in direct alignment with China’s “Digital Twin Basin” strategic initiative. Future research will prioritize Federated Learning to facilitate secure, multi-agency data collaboration, alongside Large Language Models to provide semantic reasoning for emergency responders. By converging high-performance computing clusters with these frontier AI technologies, the urban flood digital twin framework will serve as a robust foundation for the next generation of smart water management.

REFERENCES

Bakhtiari, V., Piadeh, F., Behzadian, K., & Kapelan, Z. (2023). A critical review for the application of cutting-edge digital visualisation technologies for effective urban flood risk management. Sustainable Cities and Society, *99*, 104958.

Cai Y. (2022) Establishing a smart water system with "forecast, early-warning, rehearsal and plan" functions by focusing on the construction of digital twin basin (in Chinese). China Water Research. 2022(20), 2-6.

Chen, M. Y., Huang, C. Y., Liu, C. Y., Jang, J. H., Chang, T. H., & Hsu, S. C. (2024). A Digital Twin Urban Flood Forecasting System Integrating a Weather Forecast Model and an Urban Flood Model. In 45th Asian Conference on Remote Sensing, ACRS 2024.

Fan, C., Hou, J., Li, X., Song, G., Yang, Y., Liang, X., ... & Lu, P. (2025). Efficient urban flood control and drainage management framework based on digital twin technology and optimization scheduling algorithm. Water Research, 123711.

Ge, C., & Qin, S. (2025). Urban flooding digital twin system framework. Systems Science & Control Engineering, 13(1), 2460432.

Kaynak, S., Kaynak, B., Mermer, O., & Demir, I. (2025). City-scale digital twin framework for flood impact analysis: Integrating urban infrastructure and real-time data analytics. Urban climate, 64, 102640.

Li, L., Liu, G., Yang, G., Li, D., Fan, Z., and Ma, Q. (2022) Development and application of Yongding River flood forecasting and dispatching system based on "four forecasts" system (in Chinese). Hydro-Science and Engineering. 2022(12), 45-53.

Li Q. (2022) Analysis of the Evaluation and Pre-warning System of the Urban Flood Disaster Based on the Digital Twin Technology (in Chinese). Journal of Beijing University of Technology. 48(5), 476-484.

Liu, J., Mei, C., Liu, H., Fang X., Ni, G., and Jin, W. (2023) Key scientific and technological issues of joint prevention and control of river flood and urban waterlogging disaster chain in megacities (in Chinese). Advance in Water Science,34(2), 172-181

Mao, X., Xu, Z., Lu, H., Lin, B., Tong, A., and Chen, G. (2024) Practice of "Four Preventions" digital twin application for Qiantang River (in Chinese). Water Resources Informatization, 2024(10), 1-7.

Qi, W., Ma, C., Xu, H., Chen, Z., Zhao, K., & Han, H. (2021). A review on applications of urban flood models in flood mitigation strategies. Natural Hazards, 108(1), 31-62.

Song, X., Xu, N., Zhang, J., & He, R. (2024) Urban flooding in China: current status, causes and challenges (in Chinese). Advance in Water Science,35(3), 357-373

Wang, K., Xu, S., Liu, C., Hu, Y., Ren, M., and Chen, S. (2023) Key technology of "four pre" system for flood control of digital twin Huaihe River (in Chinese). Water Resources Informatization. 2023(6), 1-4.

Yang, F., Hu, Y., Song, L., and Zhao, J. (2024) Acceleration method of the urban flood model based on the dynamic grid system and local time step technology (in Chinese). Journal of Tsinghua University (Science and Technology). 64(12), 2132-2143.

Zeng, B., Huang, G., & Chen, W. (2025). Research progress and prospects of urban flooding simulation: From traditional numerical models to deep learning approaches. Environmental Modelling & Software, 183, 106213.

Zhang, D. M., Bai, H., Zheng, C. Z., Huang, H. W., Ayyub, B. M., & Cao, W. J. (2025). Extreme rainfall induced risk mapping for metro transit systems: Shanghai metro network as a case. Reliability Engineering & System Safety, 111234.

Zhang, J., Luo, Q., Wang, B., Li, R., Gai, Y., and Chen C. (2024) Research progress on causes and countermeasures for extreme rainstorm-induced urban flood disasters (in Chinese), Water Resources Protection, 40(01),6-15

Zhang, L., Yang, M., Fan, Z., Kong, X., & Zhang, J. (2024, May). Jining City Si River Digital Twin Watershed Management Platform Construction Practice. In Proceedings of the 2024 International Conference on Smart City and Information System (pp. 268-274).
Zhu, S., Zhang, W., and Wang, G. (2025) Research on the application of the “four pre” system for flood control and drainage in a basin of Shenzhen City based on digital twins (in Chinese). Technical Supervision in Water Resources. 2025(3), 38-41

ICFM 10
Adapting to Global Change:
Innovative Approaches to Flood Management and Resilience
May 20-22, 2026 | Western University, London, Ontario, Canada

PHLASH: A Physics-Informed Hybrid Learning Framework for Enhanced Short-Duration Flash Flood Forecasting

Farrukh A. Chishtie[1,2], Rana U. Ali[1], Abdolreza Bahremand[3], Mujtaba Hassan[4], John J. Clague[5]

[1]Peaceful Society, Science and Innovation Foundation, Vancouver BC, Canada

[2]Department of Occupational Science and Occupational Therapy, University of British Columbia, Vancouver BC, Canada

[3]Department of Watershed Management, Gorgan University of Agricultural Sciences and Natural Resources, Gorgan, Iran

[4]Department of Space Science, Institute of Space Technology, Islamabad, Pakistan

[5]Centre for Natural Hazard Research, Simon Fraser University, Burnaby BC, Canada

E-mail: fachisht@uwo.ca

ABSTRACT

We introduce PHLASH (PHysics-informed Hybrid Learning for Accelerated Short-duration Hazards), an open framework designed to integrate short-duration, high-intensity rainfall data with terrain and soil factors for both flash flood susceptibility mapping and near-real-time forecasting. Using Google Earth Engine (GEE), we fuse hourly precipitation accumulations, meteorological data, MERIT DEM-derived terrain metrics such as HAND (Height Above Nearest Drainage) and slope, MODIS-based landcover/NDVI products, and daily soil moisture fields. The resulting unified dataset assigns pixel-level flood labels based on short-duration rainfall and local saturation thresholds. In trials conducted in Nova Scotia, Canada, we evaluated multiple machine learning algorithms with comprehensive metrics appropriate for imbalanced classification. We demonstrate that conventional metrics - overall accuracy and AUC - are misleading for rare event prediction, with models achieving 94% accuracy while missing 40% of flood events. An Artificial Neural Network with distribution-informed features achieves 90% recall and 90.6% balanced accuracy. SHAP analysis reveals that the intensity-duration product dominates predictions, validating fundamental hydrological understanding. PHLASH incorporates physics-based constraints including infiltration capacity and runoff routing directly into the learning pipeline. Although initially tailored for Nova Scotia, PHLASH is readily adaptable to other regions worldwide, delivering a robust, scalable early warning system that balances machine learning flexibility with physics-informed constraints.

KEYWORDS: PHLASH, Flash floods, Machine learning, Physics-informed learning, Google Earth Engine, Class imbalance, SHAP interpretability

1. INTRODUCTION

Climate change has increased the frequency and intensity of extreme weather events across all inhabited continents (IPCC, 2021). Among climate-related hazards, flash floods stand out as one of the most dangerous phenomena, distinguished by their rapid onset, localized intensity, and minimal warning time available for protective action (Jonkman, 2005). Addressing this challenge requires frameworks that integrate multi-source Earth observations with machine learning while incorporating physics-based constraints. We introduce PHLASH (PHysics-informed Hybrid Learning for Accelerated Short-duration Hazards), an open framework designed to fuse short-duration, high-intensity rainfall data with terrain and soil factors for both susceptibility mapping and near-real-time forecasting. Between 2000 and 2019, floods accounted for 44% of all disaster events, affecting over 1.65 billion people worldwide (CRED, 2020).

Recent catastrophic events underscore flash floods' devastating potential. On July 21-22, 2023, an atmospheric river delivered over 250 mm of rainfall to parts of Nova Scotia in less than 24 hours, killing four people and causing over $257 million in insured damages (IBC, 2024). The recurrence of fatal flash flooding in July 2024 demonstrates the persistent and escalating nature of this hazard.

Applying machine learning to flash flood prediction faces a fundamental challenge that is pervasively inadequately addressed: extreme class imbalance. Flash floods are rare events - occurring on perhaps 1-10% of days at any given location. In our dataset, flash flood events constitute 9% of observations. Yet this seemingly modest imbalance creates a critical evaluation problem. A model that predicts "no flood" for every instance achieves 91% accuracy while being completely useless for flood warning.

The flood prediction literature frequently reports AUC values exceeding 0.90 as evidence of model success (Band et al., 2020; He et al., 2025). However, examination of class-specific metrics often reveals a troubling pattern: high AUC coexists with inadequate minority class detection. A flood warning system that achieves 95% AUC but detects only 60% of actual floods provides a false sense of security.

The PHLASH framework incorporates distribution theory-informed feature generation through Weibull Extreme Value Theory analysis, building on the Distribution-Informed Graph Neural Network framework (Chishtie et al., 2024). Rather than manually constructing features through intuitive transformations, we derive features systematically from rigorous statistical characterization of the data-generating process. Our objectives are: (1) demonstrate the failure of conventional metrics, (2) introduce physics-informed feature generation using GEE, (3) evaluate multiple ML architectures with comprehensive metrics, and (4) provide interpretability through SHAP analysis.

2. MATERIALS AND METHODS

2.1 Study Area and Data

Nova Scotia, Canada, provides an ideal setting for flash flood susceptibility analysis (Figure 1). The province's complex terrain - ranging from coastal lowlands to interior highlands exceeding 270 m elevation - creates diverse hydrological conditions. The PHLASH framework uses Google Earth Engine (GEE) to fuse hourly precipitation accumulations covering 1-12 hour windows, meteorological data from ERA5-Land, MERIT DEM-derived terrain metrics including HAND (Height Above Nearest Drainage) and slope, MODIS-based landcover/NDVI products, and daily soil moisture fields. Flash flood susceptibility events were identified using Environment and Climate Change Canada (ECCC) operational warning thresholds combined with soil saturation criteria.

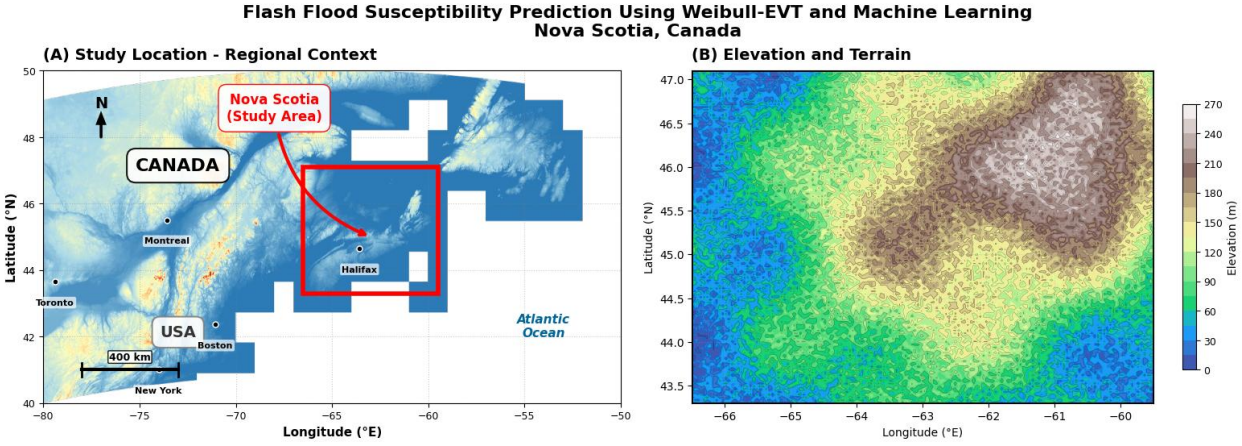

Figure 1: Study area overview for flash flood susceptibility prediction in Nova Scotia, Canada. (A) Regional context showing Nova Scotia's location in Atlantic Canada. (B) Digital elevation model revealing terrain variability across the study region, with elevations ranging from sea level through coastal plains to interior highlands exceeding 270 m.

The final dataset contains 1,117 samples: 100 flash flood events (9.0%) and 1,017 non-flood observations (91.0%). We constructed 28 baseline features comprising static terrain characteristics (slope, flow accumulation, Topographic Wetness Index, HAND) and dynamic meteorological variables from ERA5-Land (precipitation, soil moisture, runoff).

2.2 Physics-Informed Feature Generation

PHLASH incorporates physics-based constraints directly into the learning pipeline. Extreme Value Theory provides the mathematical framework for characterizing distribution tails where rare events occur (Coles, 2001). Preliminary analysis revealed bounded tail behavior in Nova Scotia precipitation data, indicating the Weibull distribution is appropriate. The two-parameter Weibull distribution is defined by $F(x; k, \lambda) = 1 - \exp[-(x/\lambda)^k]$, where k is the shape parameter and lambda is the scale parameter representing the characteristic extreme value.

From pooled precipitation data, we computed Weibull shape k = 2.71 and scale lambda = 279.87 mm. The scale parameter represents the approximate physical upper bound for daily precipitation - consistent with maximum observed precipitation during intense extratropical cyclones. From the fitted distribution, we derived 24 features including exceedance probabilities, return periods, threshold-relative metrics, and physical process interactions such as intensity-duration product and rain-on-saturated-soil.

2.3 Machine Learning Models

We evaluated three architectures: Random Forest (100 trees, depth 12, balanced sample weights), Support Vector Machine (RBF kernel, C = 0.1, balanced class weights), and Artificial Neural Network (128-64-32-1 architecture with focal loss). Data were split 80%/20% with stratification. Feature selection using mutual information identified the top 20 features, balancing model complexity against generalization.

2.4 Evaluation Metrics

For imbalanced classification, we report balanced accuracy (arithmetic mean of class-specific accuracies), precision, recall, F1-score, Critical Success Index, and bias score. These metrics directly characterize minority class performance that accuracy and AUC obscure. SHAP analysis was applied to quantify feature contributions to individual predictions.

3. RESULTS

3.1 Demonstration of Metric Failure

Table 1 presents comprehensive performance across all model configurations, revealing how conventional metrics mask operational failures.

Table 1: Comprehensive model performance on test set (224 samples: 20 floods, 204 non-floods)

Model	Acc.	Bal.Acc.	Prec.	Recall	F1	AUC
RF Base	0.942	0.788	0.706	0.600	0.649	0.975
RF Selected	0.929	0.826	0.583	0.700	0.636	0.967
SVM Base	0.786	0.882	0.294	1.000	0.455	0.949
SVM Selected	0.826	0.904	0.339	1.000	0.506	0.946
ANN Weibull	0.911	0.816	0.500	0.700	0.583	0.936
ANN Selected	**0.911**	**0.906**	**0.500**	**0.900**	**0.643**	**0.950**

The results demonstrate that RF Base achieves the highest accuracy (94.2%) and AUC (0.975) while detecting only 60% of flood events. Conversely, SVM models achieve lower accuracy (78.6-82.6%) but

detect all 20 flood events. The model with highest accuracy misses 8 flood events; the model with lowest accuracy misses none. AUC rankings are inversely related to operational flood detection performance.

3.2 Best-Performing Model

The ANN with selected features achieves the best balance: 90% recall (detecting 18 of 20 floods), 90.6% balanced accuracy, and generating approximately equal numbers of true positives and false positives. This performance represents viable operational deployment, detecting the vast majority of flood events while maintaining acceptable precision.

3.3 SHAP Interpretability

SHAP analysis reveals that the intensity-duration product dominates predictions with mean |SHAP| = 0.127 - more than triple the second-ranked feature (Figure 2). This compound variable captures total rainfall energy delivered to the landscape, validating fundamental hydrological understanding. Four of the top seven SHAP-ranked features are distribution-informed (intensity-duration product, runoff ratio, distance from bound, precipitation excess), demonstrating that physics-informed features provide predictive value beyond conventional meteorological variables.

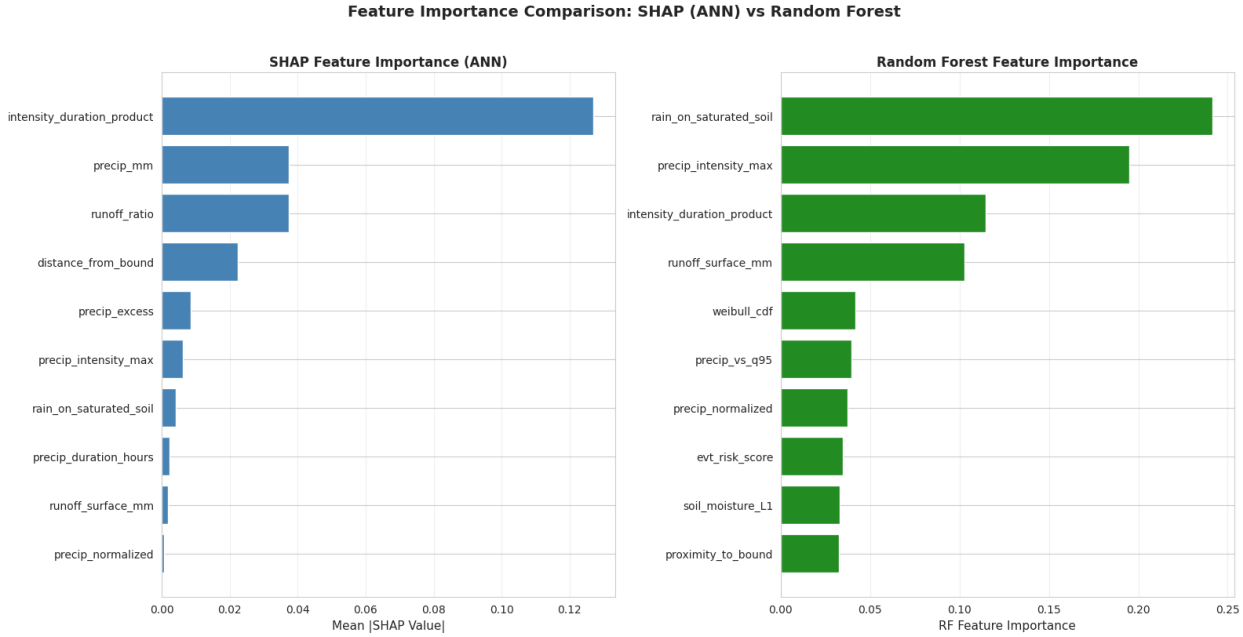

Figure 2: Feature importance comparison between SHAP analysis of the ANN model (left) and Random Forest permutation importance (right). The intensity-duration product dominates ANN predictions with mean |SHAP| = 0.127. Both algorithms identify physical process features as dominant predictors, validating the PHLASH framework.

4. DISCUSSION

Our results provide compelling empirical evidence for the failure of conventional metrics in imbalanced classification. Overall accuracy's failure stems from its domination by majority class performance. With 91% non-flood observations, accuracy = 0.91 x Specificity + 0.09 x Recall - systematically penalizing flood detection. AUC measures ranking quality rather than operational performance at any specific threshold, explaining why the model with highest AUC (0.975) achieves lowest recall (0.60).

The PHLASH framework demonstrates both theoretical and practical value by incorporating physics-based constraints directly into the learning pipeline. By fitting the Weibull distribution to precipitation

extremes, we obtain principled features: the threshold u = 125.15 mm formally defines "extreme" precipitation; the scale parameter lambda = 279.87 mm provides the physical upper bound; exceedance probabilities give precise likelihood estimates. These features are interpretable characterizations of extreme behavior rather than intuitive approximations.

For practitioners, we recommend: (1) report balanced accuracy, precision, recall, and confusion matrices for all rare event prediction models; (2) do not rely on accuracy or AUC as primary evaluation measures; (3) incorporate physics-informed features including HAND, infiltration capacity, and runoff routing; (4) use physical process interactions that combine distribution-derived normalization with hydrological understanding.

5. CONCLUSION

This study introduces PHLASH (PHysics-informed Hybrid Learning for Accelerated Short-duration Hazards), advancing flash flood susceptibility prediction through three contributions. First, we demonstrate empirically that both accuracy and AUC are fundamentally misleading for imbalanced classification - models achieving 94% accuracy and AUC exceeding 0.97 simultaneously miss 40% of flood events. Second, we integrate physics-based constraints including terrain metrics, infiltration capacity, and runoff routing directly into the learning pipeline using Google Earth Engine. Third, SHAP analysis provides interpretability essential for operational deployment, with the intensity-duration product emerging as the dominant predictor.

Our best-performing model achieves 90% recall and 91% balanced accuracy, detecting 18 of 20 flood events. Although initially tailored for Nova Scotia's short-duration flood hazards, PHLASH is readily adaptable to other regions worldwide, provided suitable hourly precipitation, DEM, and landcover datasets are available within GEE. The framework delivers a robust, scalable early warning system that balances machine learning flexibility with physics-informed constraints, addressing the critical demand for accurate, timely, and interpretable flood hazard mapping.

6. ACKNOWLEDGEMENTS

F.A.C. acknowledges funding from Vancouver Foundation via their Recovery and Resilience grant awarded to Peaceful Society, Science and Innovation Foundation. ERA5-Land data were accessed through Google Earth Engine.

7. REFERENCES

Band S.S., Janizadeh S., Chandra Pal S., Saha A., Chakrabortty R., Shokri M. and Mosavi A. (2020). Flash flood susceptibility modeling using new approaches of hybrid and ensemble tree-based machine learning algorithms. Remote Sensing, 12(21), 3568.

Chishtie F.A., Chishtie F., Mushtaq H., Lam A.C.L. and Hsieh W.W. (2024). Advancing heatwave forecasting via distribution informed-graph neural networks: Integrating extreme value theory with GNNs. arXiv preprint arXiv:2411.13496.

Coles S. (2001). An Introduction to Statistical Modeling of Extreme Values. Springer-Verlag, London.

CRED (2020). EM-DAT: The International Disaster Database. Centre for Research on the Epidemiology of Disasters, Brussels.

He F., Liu S., Mo X. and Wang Z. (2025). Interpretable flash flood susceptibility mapping in Yarlung Tsangpo River Basin using H2O Auto-ML. Scientific Reports, 15, 1702.

IBC (2024). Anniversary of Nova Scotia's deadly flash flood provides sombre reminder of the impacts of severe weather. Insurance Bureau of Canada.

IPCC (2021). Climate Change 2021: The Physical Science Basis. Cambridge University Press, Cambridge.

Jonkman S.N. (2005). Global perspectives on loss of human life caused by floods. Natural Hazards, 34(2), 151-175.

ICFM 10
Adapting to Global Change:
Innovative Approaches to Flood Management and Resilience
May 20-22, 2026 | Western University, London, Ontario, Canada

Hydrologic Modelling to Investigate Flood Mitigation Measures in the Muskoka River Watershed using SWAT+

Elisabeth Bowering[1], Sarah Irwin[1], Allyson Bingeman[1], and Glenn Cunnington[2]
GHD Ltd., Waterloo, Ontario, Canada[1]
E-mail: Lisa.Bowering@ghd.com, Allyson.Bingeman@ghd.com, Sarah.Irwin@ghd.com

District Municipality of Muskoka, Bracebridge, Ontario, Canada[2]
E-mail: Glenn.Cunnington@muskoka.on.ca

ABSTRACT

Recent significant flooding events in the Muskoka River Watershed in Ontario, Canada prompted the provincial government to provide funding for research to help reduce the impact of flooding and improve the watershed's health while considering implications of social, environmental, and economic factors in decision-making processes. This study comprises the development, calibration, and validation of a hydrologic model of the 5,100 square kilometres watershed using the Soil and Water Assessment Tool (SWAT+) to better understand the sensitivity of watershed response to changes in climate and land-use.

The model was calibrated at a daily timestep over five years and further validated using a separate five-year period. It was then run for 30-years under changing climate, land-use, and potential flood mitigation measure scenarios. Scenarios included varying levels of wetland enhancement, forest reduction, and online reservoirs, to evaluate their role in the Muskoka River watershed response and to test local response to increased storage.

The results showed that the additional reservoirs effectively reduce peak flows in the area local to the reservoir, but they did not have a significant impact on reducing flood risk downstream in the main system. At a local level, increasing wetland cover reduced peak flows in tributary channels, particularly in summer months. Similarly, a reduction in forest cover was associated with an increase in summer runoff and a faster hydrologic response, impacting local peak flows. The study also identified an existing park that likely provides flow attenuation in the early spring, which may be a key area to protect from future development.

The results demonstrate the importance of protecting natural wetlands and forests to manage local riverine flooding in the Muskoka River Watershed. The developed hydrologic model and scenario analysis results can inform future planning and watershed management and can be used to evaluate potential local flood mitigation measures.

KEYWORDS: Flood mitigation, Hydrologic modelling, watershed response, scenario analysis

1 INTRODUCTION AND BACKGROUND

The Muskoka River Watershed has experienced several major flooding events in recent years, most notably in 2019, 2016, 2013, and 2008. These events affected multiple parts of the system, including the Big East River north of Huntsville, the North Branch of the Muskoka River between Huntsville and Bracebridge, the South Branch of the Muskoka River near Purbrook, the Lake Rosseau–Lake Joseph system, and Lake Muskoka. Across the District, road washouts and widespread damage to public and private infrastructure highlighted the need for a clearer understanding of the watershed's flood dynamics.

The Muskoka River Watershed Hydrologic Modelling Study was undertaken to develop a hydrologic model of the Muskoka River Watershed capable of identifying the drivers of flooding in the system with a

focus on the main river branches. The modelling was performed using the SWAT+ software. A calibrated baseline model was first established to represent existing hydrologic conditions. Building on this foundation, a scenario analysis was completed to evaluate how three major categories of change could alter flood behaviour across the watershed, including climate change, land use change, and reservoir storage. Although this paper focuses on the reservoir storage category, brief summaries of the climate and land-use results are included to provide context for interpreting the reservoir findings and to support a discussion in the conclusion of this paper.

The baseline modelling confirmed that flooding in the Muskoka River system is primarily driven by snowmelt and multi-day rainfall events in the spring season. Climate change scenarios significantly alter the watershed's flow regime. Higher winter temperatures reduced snowfall and increased the frequency of mid-winter melt events, leading to a smaller snowpack and lower spring peak flows across much of the system. The freshet shifted earlier in the year. Summer peak flows increased modestly due to more frequent high-intensity short-duration storms, which the watershed generally absorbs more effectively than freshet flows. Overall, climate change produced a redistribution of peak flows rather than a consistent increase in the maximum annual flood magnitude. Land use change scenarios resulted in small changes in peak flows relative to baseline conditions. Population growth, deforestation, and wetland enhancement scenarios produced small but measurable changes in flow in summer months, generally proportional to the extent of land cover alteration, and had a negligible impact on larger spring flood flows.

This paper focuses on reservoir storage as it remains the most operationally relevant aspect of flood behaviour in the Muskoka River system. The scenarios presented here are strictly exploratory: they are not intended to recommend new reservoir construction, which would require extensive environmental, cultural, and infrastructure assessment. Instead, the analysis is meant to improve the understanding of how additional storage, whether hypothetical or through adjustments to existing reservoir operations, could influence flood attenuation.

The objective of this paper is therefore to present the methodology and results of the reservoir storage scenarios and to assess their potential effectiveness as a flood mitigation strategy within the Muskoka River Watershed.

2 STUDY AREA

The Muskoka River Watershed covers approximately 5,100 km² on the Canadian Shield in central Ontario. The watershed is divided into three major subbasins: the North Branch Muskoka River (including the towns of Huntsville and Bracebridge), the South Branch Muskoka River (including the town of Gravenhurst), and the Lower Muskoka River (extending toward the villages of Port Carling and Bala). The landscape is predominantly forested outside of the urban centres, with thin soils, exposed bedrock, and a dense network of lakes and wetlands typical of the Shield.

The watershed contains more than 2,000 lakes, including 650 lakes larger than eight hectares, and 38 provincially significant wetlands. Water levels and flows are influenced by an extensive system of water control structures: 65 dams operate throughout the watershed, including 23 major control structures. Although none of these dams were originally constructed for flood control – most were built to support log driving and commercial navigation – their roles have evolved to include recreation, fisheries management, and, to some extent, flood moderation.

Hydrologic response in the watershed is shaped by the interaction of rainfall, snow accumulation and melt, lake storage, and operational decisions at the control structures (which are driven by the Muskoka River Water Management Plan). The combination of large lake storage volumes, complex channel networks, and variable winter conditions makes the Muskoka River system particularly sensitive to changes in climate, land use, and control structure operations, underscoring the need for a comprehensive modelling approach.

3 MODEL DEVELOPMENT

A hydrologic model of the Muskoka River Watershed was built, calibrated, and validated using SWAT+. The continuous model runs on a daily timestep for 32 years, including 2 warm-up years.

3.1 Model Setup

Provincial datasets for soil (Gao et al. 2007), watercourses and elevation were used along with District LiDAR (Hatch, 2023), and land cover mapping (Dougan & Associates, 2022) to set up the physical parameters in the model. These parameters were not subjected to calibration, as they are physical characteristics of the watershed, assigned using measured data. This is a common approach, especially considering detailed models with over 100 parameters, such as SWAT+ (e.g., Kumarasamy and Belmont, 2018). Climate data was input as daily maximum and minimum temperature and daily precipitation, using five Environment and Climate Change Canada (ECCC) stations. Future projected climate data for climate change scenario analysis was downloaded from ClimateData.ca (Web-1).

Major lakes were modelled as reservoirs that are online to the channel network. The Ministry of Natural Resources and Foresty (MNRF) Operations Manual (2007), dam geometry files, and dam safety assessments were used to characterize the reservoirs. The manual includes details for each reservoir such as operating level curves based on the watershed management plan, and stage-storage curves. The reservoirs typically have seasonal operating rules according to the watershed management plan, to manage water levels in the lakes throughout the year. The principal spillway of the reservoir is the level at which water begins to flow out of the reservoir in a controlled manner, which is adjusted seasonally to maintain target lake levels. The emergency spillway is the level at which water overflows the outlet – and is considered the maximum lake level.

In the model, reservoirs are characterized by the surface area and volume required to fill them up to the principal spillway and the emergency spillway elevations. The volume at the principal spillway elevation is equivalent to the normal reservoir storage volume, and the volume at the emergency spillway elevation is equivalent to the maximum reservoir storage volume. These measurements define the stage storage relationship for each reservoir, which is used to calculate reservoir storage based on the change in inflow and outflow volumes at each timestep.

The outflow volumes are calculated by a set of rules defined in the reservoir release decision tables that are based on the volume of water relative to the defined principal and emergency spillway volumes at each timestep. The decision tables can be coded to release varying outflow rates depending on the time of year to simulate seasonal operational rules at the dam control structures. The reservoir geometries and release decision tables were characterized using the most recent Water Level Operating Zone Limits graphs for the corresponding dam structure, provided by the MNRF through the Muskoka River Water Management Plan.

The principal and emergency spillway elevations were set equal to the minimum and maximum water surface elevations of the target operating level curve. The surface areas and volumes were determined from the corresponding lake storage table, provided by the MNRF. Twelve reservoir release equations were developed (one for each month of the year) to simulate the seasonal operating rules at the dam. The equations relate the average volume of the normal operating zone and target release rate in the form of a rating curve, represented by the number of drawdown days that would be required to lower the average storage volume over the spillway elevation (or top of stop log elevation). The drawdown days are calculated as half the maximum storage volume (*evol*) minus the storage volume at the specified spillway elevation (*vol*), divided by the target release rate for that month, as shown in Equation 1.

$$drawdown\ days\ = \frac{0.5 \times (evol - vol)}{target\ release\ rate} \quad (1)$$

The target release rates were obtained from the Downstream River Flow Operating Zone Limits graphs provided by the MNRF for each dam. A thirteenth equation was included to calculate the release rate when the reservoir storage volume exceeds the emergency storage volume, which results in a faster release. The drawdown days of the reservoir volume over the emergency storage volume is included as a calibration parameter.

3.2 Calibration and Validation

To evaluate model performance over a variety of conditions, it is considered best practice to select calibration and validation periods that include wet, dry, and average years (Arnold, J.G., et. al., 2012). The calibration and validation periods were each selected to be 5 years in length to include variation in precipitation.

The model was calibrated using a split sample technique, both spatially and temporally. Spatially, the model was divided into five basins, and each basin was calibrated and validated separately, beginning upstream, and working downstream to the model outlet. The basins were delineated based on five Water Survey of Canada (WSC) gauges with available flow data during the calibration and validation period. Temporally, the calibration and validation periods were separated as described above.

A sensitivity analysis was performed on over 20 model parameters (2 were reservoir based) to determine the parameters of the hydrological processes that impact streamflow from which 11 were selected. Hydrological parameters that could be measured and assigned with a higher level of certainty were excluded from the calibration process – this included many of the reservoir parameters. Of the 11 parameters chosen to calibrate the model, five control snow accumulation and melt, four are related to infiltration and baseflow processes, and two are related to reservoir release. The model was highly sensitive to the reservoir release parameters.

Once the model was calibrated, each basin was validated. The results of the calibration and validation procedures were evaluated using both graphical and statistical methods, including percent bias (PBIAS), Nash Sutcliffe Efficiency (NSE), and the Coefficient of Determination (R^2). Results for basin 5, which is located at the downstream southwestern end of the watershed, with an outlet downstream of Bala Dams, are shown in Figure 1. Basin 5 shows how well the model followed the Bala Lake (reservoir) rules as it achieved good calibration results across all seasons.

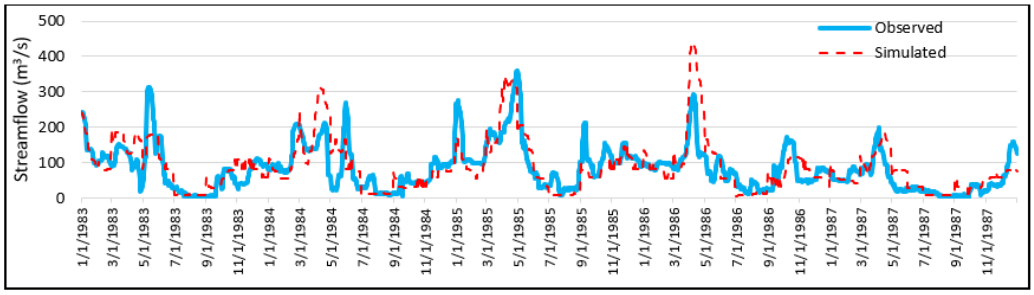

Basin 5 Observed and Modelled Streamflow During Calibration Period

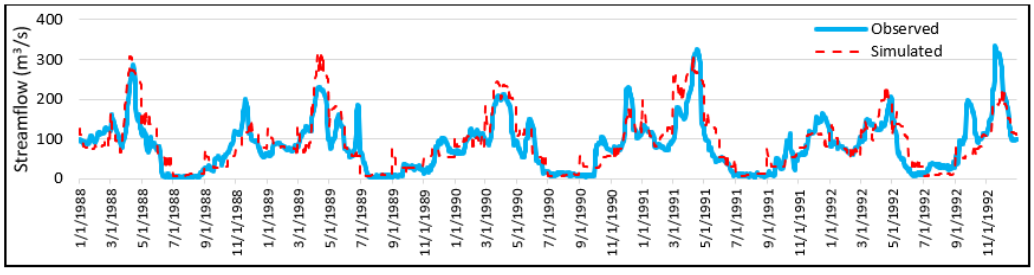

Basin 5 Observed and Modelled Streamflow During Validation Period

Figure 1: Calibration and validation results for basin 5

4 RESERVOIR SCENARIO ANALYSIS

A scenario analysis was performed to assess the ability of the reservoir storage to attenuate peak flow rates and reduce flood risk in the system. To assess the potential for reservoir storage to reduce peak flows in the Muskoka River system, a targeted analysis was conducted focusing on the hydrologic response to hypothetical reservoirs. This section outlines the approach used for site selection and reservoir routing of the hypothetical reservoirs to evaluate their influence on flood attenuation.

4.1 Site Selection

Potential reservoir sites were identified through a spatial analysis of high-resolution LiDAR data. The objective was to locate suitable locations where a dam could theoretically be constructed at a natural constriction in the river, with sufficient upstream width to provide meaningful storage. Sites were selected to ensure that impounded water would not propagate excessively far upstream, thereby avoiding large-scale alterations to the flow regime or inundation of long river reaches. As part of this screening, efforts were made to minimize potential impacts to existing infrastructure such as roads, bridges, and developed areas.

For each candidate site, LiDAR-derived elevation data were used to delineate the potential reservoir footprint and to develop a stage–storage relationship up to a maximum containing elevation. This provided a realistic estimate of the storage volume available at each site and formed the basis for subsequent reservoir-routing simulations. Figure 2 shows the hypothetical reservoir locations and Table 1 describes their location and purpose in terms of flood mitigation.

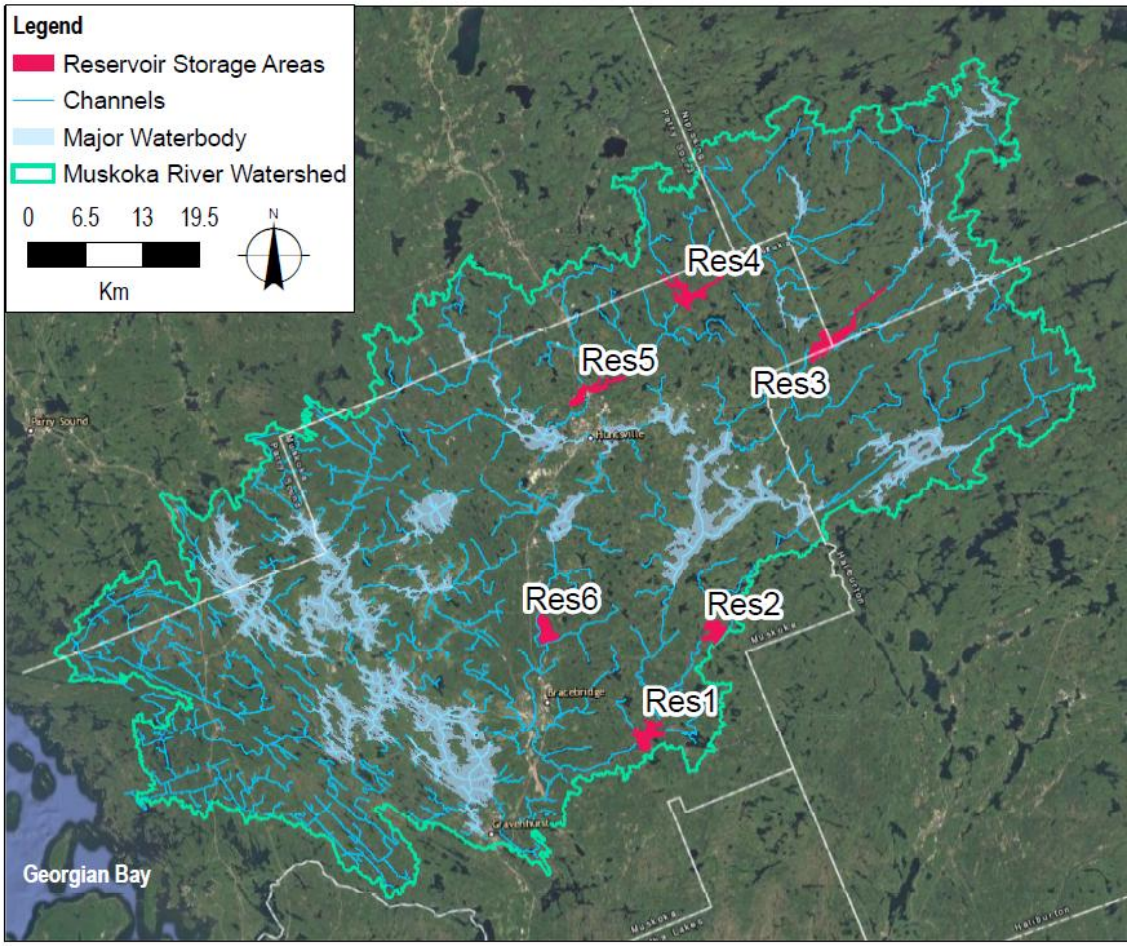

Figure 2: Hypothetical reservoir locations

Table 1 Site Selection of Hypothetical Reservoirs for Analysis

Reservoir	Location	Description
Res1	South Branch Muskoka River near Purbrook	Intended to mitigate flood risk on the South Branch Muskoka River near the Purbrook community, an area identified as high risk (DMM Floodline and LiDAR Mapping 2.0 (Web-2))
Res2	Tributary of the South Branch Muskoka River upstream of Purbrook	Located further upstream than Res1, with a larger storage volume. Intended to reduce flood risk on the South Branch Muskoka River near Purbook.
Res3	Oxtongue River upstream of the community of Dwight and Lake of Bays	Located further upstream in the watershed, with a larger storage volume. Intended to reduce downstream flood risk on the South Branch Muskoka River near Purbook.
Res4	Big East River at the site of the historic Distress Dam	Reinstatement of the historic Distress Dam on the Big East River, which currently functions as a low-capacity weir. Intended to mitigate existing flood risk on the Big East River near Highway 11 and downstream on the North Branch Muskoka River.
Res5	Big East River near Highway 11	Intended to mitigate existing flood risk on the Big East River near Highway 11 and downstream in the North Branch Muskoka River.
Res6	North Branch Muskoka River between Port Sydney and Springdale Park	Use of an existing quarry pit as flood storage to reduce downstream flood risk on the North Branch Muskoka River, particularly for the Town of Bracebridge. The quarry is currently active, so the scenario reflects a theoretical closure plan with storage maximized within property, topographic, and infrastructure constraints.

4.2 Reservoir Routing

For each hypothetical site, reservoir routing was performed using a historical flood event and the stage-storage relationship derived from the LiDAR-based topography. Simple weir and gated weir outlet structures were used to control the release flow.

Historical flood events were selected based on their relevance to different parts of the watershed. The 2019 and 2013 events represent the largest observed floods on the main river branches, with the dominant event varying by subbasin. For each candidate reservoir site, the flood hydrograph corresponding to the most representative event was used as the inflow condition for routing. The 2013 flood event was applied to assess flood impacts and mitigation measures on the Big East River and Oxtongue River, and the 2019 flood event was applied on the north and south branches of the Muskoka River. The 2013 and 2019 floods were classified as milti-day rain-on-snow events, which produced peak flow rates in April and May of these years. The design flood events were obtained from the nearest Water Survey Canada hydrometric station and prorated to the reservoir locations.

Routing simulations were performed using SWMM-based software to estimate the maximum potential reduction in peak flow at the reservoir outlet. Reservoirs that demonstrated meaningful peak flow reduction at the local scale were retained for the scenario analysis. SWMM was used for the initial reservoir routing because of its functionality and ease-of-use, which allowed for multiple reservoir locations to be tested quickly to identify the best options for inclusion in the SWAT+ model and scenario analysis. Table 2 summarizes the available storage and performance in peak flow reduction.

The results show that the peak inflow rate at Res5 on the Big East River is higher than at Res6 on the North Branch Muskoka River, even though Res6 is located much further downstream on the same system

where the contributing catchment area is larger. While the peak flow rate at Res6 is lower, the total flood volume is substantially greater, meaning far more storage would be required to meaningfully reduce the peak. This pattern of lower peak flows but larger flood volumes downstream is driven by the attenuating influence of the Huntsville Lakes and Mary Lake, which lie between Res5 and Res6 and moderate flows as water moves through the system.

Table 2 Reservoir Capacity and Performance in Peak Flow Reduction

Reservoir	Maximum Storage Volume Available (1000 m^3)	Maximum Available Depth (m)	Design Flood Peak Inflow Rate (m^3/s)	Effective Design Flood Peak Flow Reduction
Res1	14,900	4	192.8	Less than 1 m^3/s
Res2	6,400	4	15.1	Approximately 10 m^3/s
Res3	11,000	8	107.1	Approximately 25 m^3/s
Res4	10,000	11	176.4	Approximately 120 m^3/s
Res5	2,800	4	277.4	Less than 10 m^3/s
Res6	22,800	6	247.9	Approximately 5 m^3/s

Figure 3 compares the inflow (Quarry Lake) and outflow (Outlet) hydrograph immediately downstream of Res6, the hypothetical quarry reservoir on the North Branch Muskoka River from the reservoir-routing exercise performed using the SWMM model. The design flood hydrograph spans roughly one month, illustrating the challenge of attenuating such a long-duration event. Any reservoir storage located on the main river system – particularly downstream of the Huntsville Lakes on the North Branch or Lake of Bays on the South Branch – would require very large storage volumes to achieve meaningful peak flow reduction.

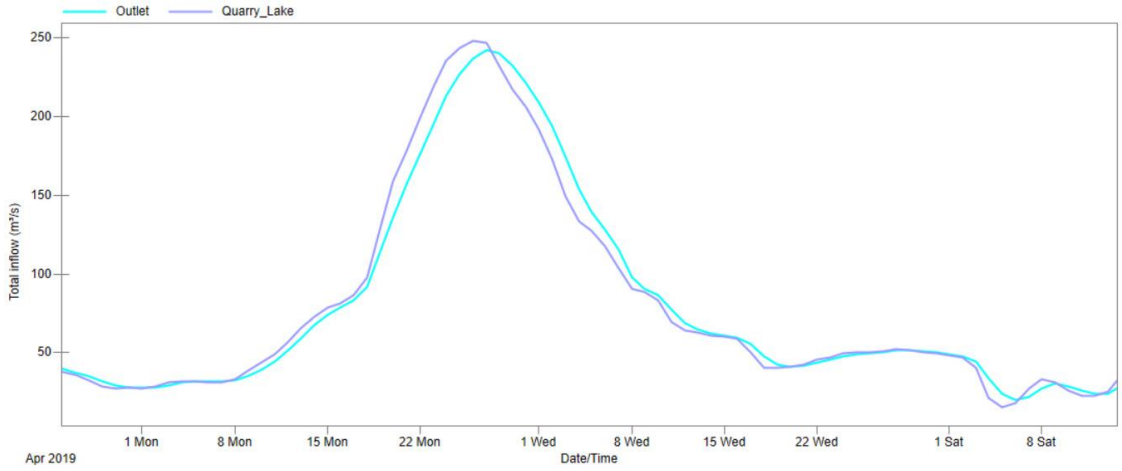

Figure 3 – Res 6 (Quarry Lake) Design Flood Peak Flow Rate Reduction

Among the sites assessed, Res2, Res3, and Res4 provided the greatest peak flow reduction and were carried forward into the SWAT+ scenario analysis. Res5 was not included because it is located close to Res4 (the Distress Dam reinstatement scenario) but offers significantly less attenuation and is therefore considered redundant.

4.3 Scenario Analysis

The reservoirs selected for the scenario analysis were incorporated into the SWAT+ model to evaluate their system wide effects. This step allowed assessment of how attenuation at individual sites propagates downstream, interacts with other branches, and influences peak flows at key locations throughout the Muskoka River system. The impacts of reservoir storage on peak flow rates through the Muskoka River system are summarized in Table 3.

Table 3 Reservoir Performance in Peak Flow Reduction on Muskoka River System

Location	Associated WSC Station ID	Peak Flow % Change from Existing Conditions		
		Res2	Res3	Res4
Big East River near Huntsville	02EB013	0%	0%	**-6%**
North Branch Muskoka River at Port Sydney	02EB004	0%	0%	**-1%**
South Branch Muskoka River at Baysville	02EB008	0%	0%	0%
Indian River (Port Carling)	02EB020	0%	0%	0%
Muskoka River below Bala	02EB006	0%	0%	0%
Oxtongue River near Dwight	02EB014	0%	**-11%**	0%
South Branch Muskoka River near Purbrook	n/a	0%	0%	0%
Big East River near Williamsport Road	n/a	0%	**-31%**	0%

5 DISCUSSION

The results demonstrate that larger reservoirs can reduce peak flow rates locally; however, their ability to reduce peak flow rates is diminished further downstream in the system as the river receives runoff from larger contributing drainage areas and flows through the operated major lakes. This is most evident in the results for Res3 and the Res4. Res3 provides an 11% reduction in peak flow rate on the Oxtongue River near the village of Dwight, and no change on the South Branch Muskoka River at Baysville. Res4 provides a 31% reduction in peak flow rate in the Big East River near Williamsport Road; however, as the river gains more runoff from the downstream contributing drainage areas, and meanders through wetlands and under roads toward Lake Vernon, the flow reduction is diminished to 6%, and reduces to 1% downstream of the Huntsville Lakes and Mary Lake at Port Sydney.

Res2 has the capacity to significantly attenuate the peak flow rate on the tributary where it is located as shown in Table 2; however, it provides negligible impact on the main branches of the Muskoka River system as shown in Table 3 due to the relatively high flow rates in the main branch compared to the volume of the reservoir. Res2 and Res3 demonstrate how online storage can be an effective way of reducing peak flow rates on the tributaries and upper reaches of the river system. It is important to note that there may be other locations within the watershed where online storage could effectively mitigate flooding at a local level. To mitigate flooding on the main branches of the Muskoka River, very large reservoirs would be required, or many relatively smaller reservoirs would need to be constructed on the tributaries and upper reaches of the river system to reduce the peak flow rates contributing to the main stems.

6 CONCLUSIONS

The study assessed the potential for flood storage to reduce peak flow rates in the Muskoka River system by evaluating the performance of six hypothetical reservoirs. Reservoir sites were selected based on conceptual feasibility, considering topographic constraints and the need to avoid major impacts to existing

infrastructure. Reservoirs located on the Big East River (upstream of the Huntsville Lakes) and on the Oxtongue River (upstream of Lake of Bays) provided the greatest local peak flow reduction. However, their effectiveness diminished downstream due to the large volume and long duration of the flood hydrographs moving through the system.

The broader study's climate change analysis showed that flood flows in the watershed are highly sensitive to warming temperatures and shifting precipitation patterns. For this reason, any future assessment of reservoir storage should be paired with a range of climate change scenarios. Given the required storage volumes, it may not be feasible to add new reservoirs to the system for the purpose of flood control on the main branches of the Muskoka River. Therefore, there may also be value in examining adjustments to existing structures and operating rules on existing reservoirs and dams. Their performance under changing climate conditions and ability for flood control warrants further evaluation.

Overall, the results suggest that reservoir storage could provide meaningful peak flow reduction and flood mitigation in the upper parts of the watershed, particularly on the Big East River near Highway 11 where hydrographs are shorter and less attenuated. Any further consideration of reservoir storage would need to weigh these potential benefits against significant environmental, cultural, infrastructure, and cost implications, and may not be feasible in the downstream reaches.

ACKNOWLEDGEMENTS

This work was made possible through funding from the District Municipality of Muskoka and the Government of Ontario. The authors would like to thank ClimateData.ca for providing the climate information used in this study. ClimateData.ca was created through a collaboration between the Pacific Climate Impacts Consortium (PCIC), Ouranos Inc., the Prairie Climate Centre (PCC), Environment and Climate Change Canada (ECCC), Centre de Recherche -20.0 Informatique de Montréal (CRIM) and Habitat7.

REFERENCES

Arnold, J.G., Moriasi, D.N., Gassman, P.W., Abbaspour, K.C., White, M.J., Srinivasan, R. Santhi, C., Harmel, R.D., van Griensven, A., Van Liew, M.W., Kannan, N., Jha, M. K. (2012). SWAT: Model Use, Calibration and Validation. American Society of Agricultural and Biological Engineers, 55(4), 1491 1508.

Dougan & Associates Ecological Consulting & Design (2022). Muskoka River Watershed IWM Natural Capital Inventory: Phase 2 Final Report: Data Enhancements, New Data & Verification.

Gao, Cunhai & Shirota, Jiro & Kelly, Ross & Brunton, Frank & Haaften, Steve. (2007). Bedrock Topography And Overburden Thickness Mapping, Southern Ontario. Diamond Jubilee Proceedings of the 60th Canadian Geotechnical Conference and the 8th Joint CGS/IAH CNC Groundwater Conference: Ottawa, Ontario, Canada.

Hatch (2023). Floodplain Mapping Technical Report for Floodplain Mapping Study (H366496-0000-200-230-0002).

Kumarasamy, K, and Belmont, P. (2018). Calibration Parameter Selection and Watershed Hydrology Model Evaluation in Time and Frequency Domains. Water, 10(6), 710.

Ministry of Natural Resources and Forestry, MNRF (2007). Muskoka River Dam Operation Manual.

Web sites:

Web-1: https://climatedata.ca, consulted 20 July 2023.

Web-2: https://experience.arcgis.com/experience/4aefea73e8684812a2e3d0bf8006ca50/page/2D, consulted 5 December 2025.

ICFM 10
Adapting to Global Change:
Innovative Approaches to Flood Management and Resilience
May 20-22, 2026 | Western University, London, Ontario, Canada

Prophet-driven AI Modeling for Flood Prediction in the Bow River, Canada

Adya Aiswarya Dash[1] and Edward McBean[2]
PhD Student, College of Engineering, University of Guelph, Guelph, Canada, ON N1G 2W1[1]
E-mail: adash@uoguelph.ca

University Professor Emeritus, College of Engineering, University of Guelph, Guelph, Canada, ON N1G 2W1[2]
E-mail: emcbean@uoguelph.ca

ABSTRACT

Flooding remains one of the most damaging natural hazards in Canada, with the June 2013 Bow River flood causing widespread disruption in southern Alberta and highlighting the critical need for reliable early warning systems. This study presents an artificial intelligence-based flood forecasting approach using the Prophet time-series model to predict streamflow in the Bow River at Banff, a snowmelt-dominated mountainous watershed. Prophet is particularly suited for hydrological applications due to its ability to capture nonlinear trends, strong seasonal patterns, and abrupt changes in time-series data while remaining computationally efficient and robust to missing values.

Historical daily streamflow, precipitation, snowfall, and temperature data were used to develop the forecasting framework. The model was evaluated for multiple lead times, including 15-day, 10-day, 5-day, and 1-day ahead predictions, with a specific focus on the extreme flood event of June 21, 2013. Results demonstrate that Prophet performs exceptionally well at short lead times, accurately reproducing both the timing and magnitude of peak flows during the extreme event. Forecast accuracy decreases with increasing lead time; however, the model retains useful predictive skill for advance warning purposes.

The findings indicate that Prophet-based forecasting can provide valuable lead time for flood preparedness and emergency response in cold-region river basins. The approach offers a practical and interpretable tool for supporting operational flood forecasting and risk management, particularly in watersheds where snowmelt and seasonal variability play a dominant role.

KEYWORDS: Flood forecasting; Bow River; Prophet model; Early warning systems; AI in hydrology; Extreme events

1 INTRODUCTION

Flooding remains one of the most damaging natural hazards worldwide, with increasing impacts on communities, infrastructure, and economies. In Canada, floods are the most frequent natural disaster, and recent extreme events have highlighted the growing need for reliable and timely flood forecasting systems. Mountainous, snowmelt-dominated river basins are particularly vulnerable, as rapid snowmelt combined with intense precipitation can lead to sudden and severe flooding with limited warning time.

The Bow River in southern Alberta exemplifies these challenges. The June 2013 flood caused widespread damage across the region, including large scale evacuations and significant economic losses, emphasizing the importance of early warning and preparedness. Accurate short to medium-term streamflow forecasting is therefore essential to support emergency response, operational decision making, and risk mitigation in such basins.

Traditional flood forecasting approaches often rely on physically based hydrological models, which can be computationally intensive and require extensive data and calibration. In contrast, data driven and artificial intelligence (AI) approaches have gained increasing attention due to their ability to learn complex patterns directly from historical data. However, many machine learning models are difficult to interpret and require substantial tuning, which can limit their adoption in operational settings.

This study investigates the use of the Prophet time-series forecasting model for flood prediction in the Bow River at Banff. Prophet is an additive forecasting framework designed to capture nonlinear trends, strong seasonality, and abrupt changes in time-series data, while remaining computationally efficient and robust to missing values. Using historical hydrometeorological data, Prophet is applied to generate streamflow forecasts at multiple lead times, ranging from 15-days to 1-day ahead, with a specific focus on the June 2013 extreme flood event.

The objective of this work is to evaluate the suitability of Prophet as a practical flood forecasting tool for snowmelt dominated river basins. By assessing forecast performance across multiple lead times, this study demonstrates the potential of Prophet to support early warning systems and improve flood preparedness in cold region watersheds.

2 STUDY AREA AND DATA

The Bow River is a major river system in southern Alberta, Canada, originating in the Canadian Rocky Mountains and flowing eastward through Banff National Park toward the city of Calgary. The study area focuses on the Bow River at Banff hydrometric station, located in a mountainous, snowmelt-dominated watershed characterized by glaciers, icefields, and steep topography. The surrounding landscape consists primarily of montane, subalpine, and alpine ecosystems, with forested areas concentrated in valley bottoms and lower slopes.

The hydrology of the Bow River basin is strongly influenced by climatic conditions typical of cold regions, including long winters and short summers. Annual precipitation in the upper basin ranges from approximately 500 to 700 mm, with nearly half falling as snow. Peak streamflow typically occurs between May and June due to the combined effects of seasonal snowmelt and spring rainfall. These conditions make the basin particularly susceptible to rapid increases in discharge and extreme flooding.

The Bow River at Banff station has been operational since 1909, providing one of the longest continuous streamflow records in western Canada. For this study, daily streamflow data were obtained from Environment and Climate Change Canada (ECCC), complemented by historical records compiled by Alberta Environment and Parks. In addition, daily precipitation (rainfall and snowfall) and temperature data were used to support the forecasting framework. The analysis focuses on the extreme flood event of June 2013, with model training based exclusively on data available prior to the forecast dates in order to replicate realistic forecasting conditions.

Figure 1 illustrates the location of the Bow River basin, highlighting the study reach and the monitoring station used in this analysis.

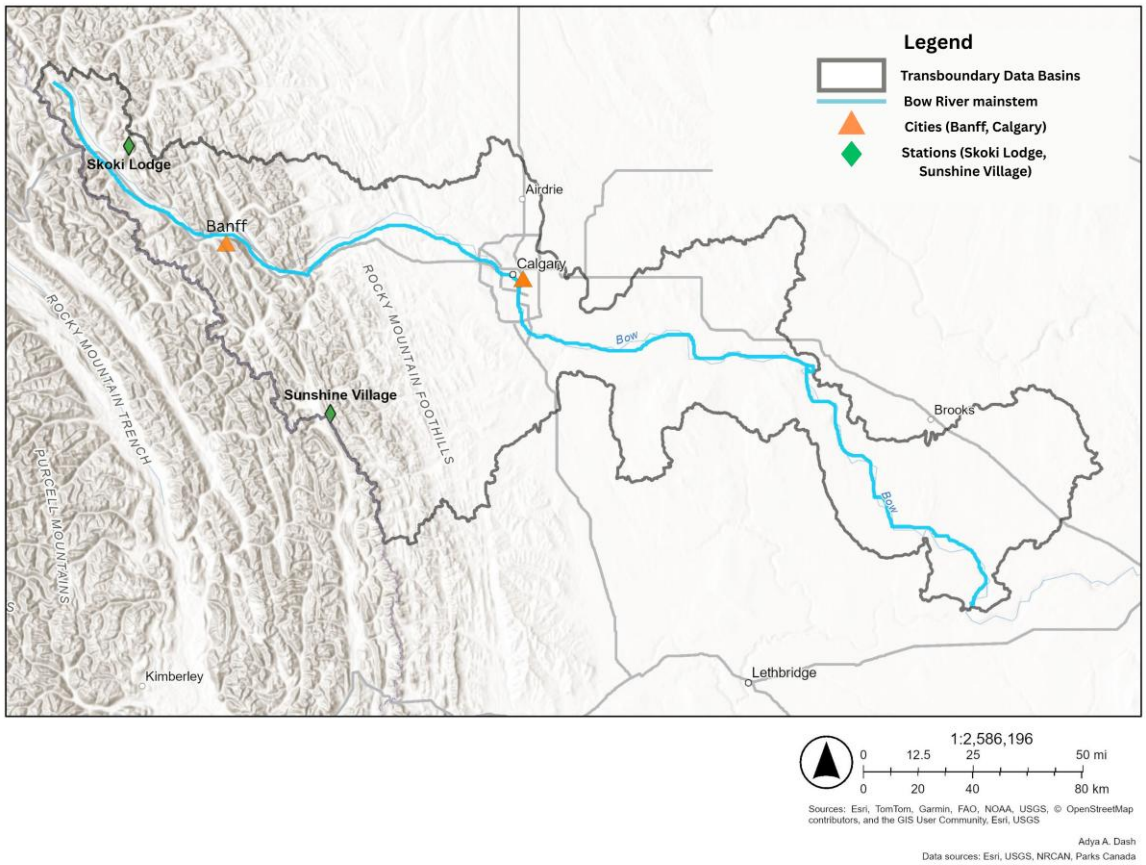

Figure 1: Map of the Bow River Basin, highlighting the study area and the hydrometric station at Banff used for flood forecasting. Adapted from Dash and McBean (2025).

3 METHODOLOGY

This study employs the Prophet time-series forecasting model to predict streamflow in the Bow River at Banff for multiple lead times relevant to flood early warning. Prophet is a decomposable, additive forecasting framework designed to model complex temporal patterns while remaining computationally efficient and interpretable (Taylor and Letham, 2018), making it suitable for operational hydrological applications.

Prophet represents the observed streamflow time series as the sum of trend, seasonal, and external components, expressed as:

$$y(t) = g(t) + s(t) + h(t) + \varepsilon_t \quad (1)$$

where $y(t)$ is the streamflow at time t, $g(t)$ denotes the non-periodic trend component, $s(t)$ represents seasonal variations (e.g., annual and weekly cycles), $h(t)$ captures the effects of external regressors, and ε_t is the residual error term.

The trend component allows for gradual or abrupt changes in river flow behavior, which are common in snowmelt-dominated basins. Seasonal components enable the model to capture strong annual hydrological cycles associated with winter snow accumulation and spring melt. External regressors, including precipitation and temperature, were incorporated to enhance predictive skill during extreme hydrometeorological conditions.

To replicate realistic forecasting conditions, the Prophet model was trained exclusively using historical data available prior to each forecast date. Forecasts were generated for multiple lead times, including 15-day, 10-day, 5-day, and 1-day ahead predictions. Particular emphasis was placed on evaluating model performance during the extreme flood event of June 2013, allowing assessment of the model's ability to capture rapid increases in discharge and peak flood magnitude (Dash and Mcbean, 2025).

Model performance was evaluated using standard statistical indicators, including the coefficient of determination (R^2), root mean square error (RMSE), and mean absolute error (MAE). These metrics were selected to assess both the accuracy and reliability of the forecasts across different lead times, with a focus on their suitability for flood preparedness and early warning applications.

4 RESULTS AND DISCUSSION

4.1 Forecast Performance during the June 2013 Flood Event

The Prophet model was evaluated for its ability to reproduce streamflow dynamics during the extreme flood event of 21 June 2013 at the Bow River, Banff station. Forecasts were generated at multiple lead times, including 15-day, 10-day, 5-day, and 1-day ahead, using only information available prior to each forecast date to replicate realistic early-warning conditions.

Figure 2 presents the 1-day-ahead forecast, demonstrating close agreement between predicted and observed streamflow. The model successfully captured both the timing and magnitude of the peak discharge, indicating strong short-term predictive skill during extreme hydrological conditions.

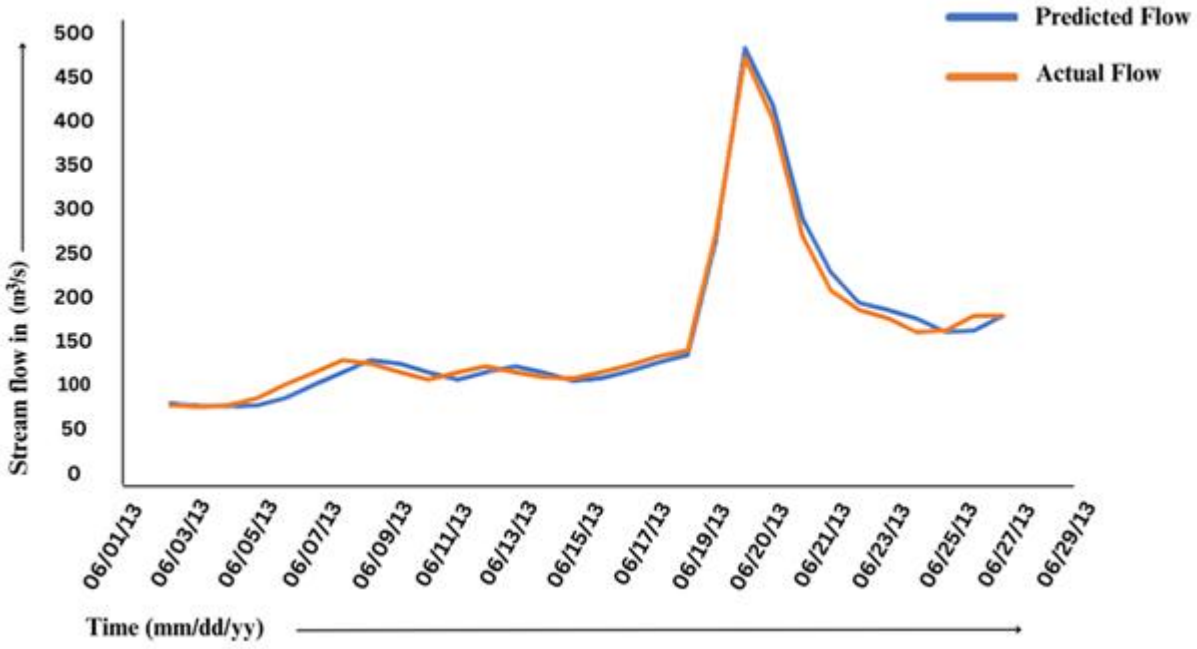

Figure 2: Observed and predicted streamflow for the Bow River at Banff during the June 2013 flood event using a 1-day-ahead Prophet forecast. Adapted from Dash et al. (2024).

4.2 Multi Lead Time Forecast Evaluation

To assess the robustness of Prophet across longer forecasting horizons, predictions were generated for 15-day, 10-day, and 5-day lead times. Figure 3 compares observed streamflow with Prophet forecasts across these horizons for the 2013 flood event.

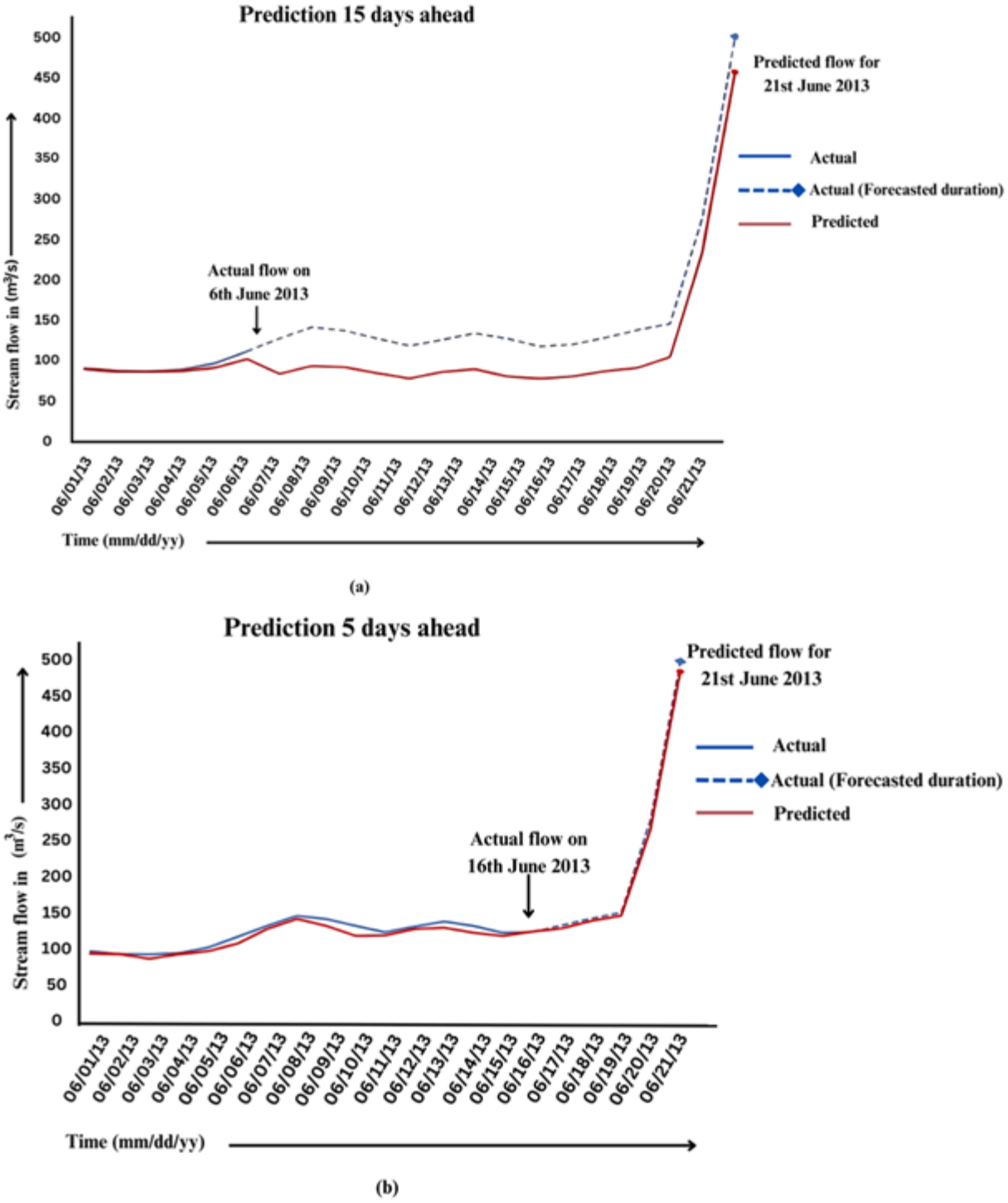

Figure 3: Comparison of observed and Prophet-predicted streamflow for the Bow River at Banff during the 2013 flood event across multiple forecast horizons (15,and 5-day ahead). Adapted from Dash et al. (2024).

The results show a progressive reduction in accuracy with increasing lead time, which is expected given the compounding uncertainty in hydrometeorological drivers. Nevertheless, the Prophet model

retained useful predictive skill at medium lead times, particularly in identifying the onset and general magnitude of flooding, which is critical for preparedness and emergency planning.

4.3 Quantitative Performance Metrics

Model performance was evaluated using standard statistical indicators, including the coefficient of determination (R^2), root mean square error (RMSE), and mean absolute error (MAE), to assess agreement between predicted and observed streamflow during the June 2013 flood event.

The Prophet model demonstrated high predictive accuracy at short forecast horizons, with R^2 values exceeding 0.95, indicating strong correspondence between predicted and observed discharge. Very low error magnitudes further confirmed the model's ability to reproduce rapid increases in streamflow and peak flood conditions. As forecast lead time increased, a gradual reduction in accuracy was observed, consistent with increasing uncertainty in hydrometeorological drivers and basin response.

Despite this decline, the model retained useful predictive skill at longer lead times, successfully capturing the timing and overall magnitude of flooding. This performance is particularly valuable for flood early warning and preparedness, where advance notice despite higher uncertainty supports operational decision-making and risk mitigation.

Overall, the quantitative assessment confirms that Prophet is most effective for short-term flood forecasting, while still providing meaningful information for short to medium term early warning applications in snowmelt-dominated river basins.

4.4 Implications for Flood Early Warning

The results indicate that Prophet is particularly effective for short lead time flood forecasting, where accurate prediction of peak timing and magnitude is essential for evacuation planning and operational decision-making. While longer lead-time forecasts exhibit increased uncertainty, they still provide valuable situational awareness for emergency preparedness in snowmelt-dominated river basins.

Overall, the findings highlight Prophet's potential as a practical and interpretable forecasting tool that balances accuracy, computational efficiency, and operational applicability for flood risk management.

5 CONCLUSION

This study evaluated the applicability of the Prophet time-series forecasting model for flood prediction in the Bow River at Banff, with a particular focus on the extreme June 2013 flood event. Using historical hydrometeorological data, the model was tested across multiple forecast lead times relevant to operational flood early warning.

Results demonstrate that Prophet performs exceptionally well for short lead times, accurately capturing both the timing and magnitude of peak streamflow during the extreme event. While forecast accuracy decreases with increasing lead time, the model retains useful predictive skill at medium horizons, providing valuable situational awareness for flood preparedness and emergency response. These findings are particularly relevant for snowmelt-dominated, cold-region watersheds, where rapid changes in discharge can occur with limited warning.

A key advantage of the proposed approach is its balance between predictive accuracy, interpretability, and computational efficiency, making it suitable for operational deployment. Unlike more complex machine-learning models, Prophet requires limited tuning and can be readily updated as new data become available, which is advantageous for real-time flood forecasting applications.

Overall, the results highlight the potential of Prophet-based forecasting as a practical tool to support early warning systems and flood risk management in mountainous river basins. Future work will explore the integration of additional climate drivers and the application of the framework to other flood-prone regions to further enhance forecasting reliability.

6 ACKNOWLEDGEMENTS

The authors gratefully acknowledge the support provided by the University of Guelph, Canada. Streamflow and meteorological data used in this study were obtained from Environment and Climate Change Canada and Alberta Environment and Parks, whose publicly available datasets made this analysis possible. The authors also thank colleagues and reviewers for their constructive feedback, which helped improve the clarity and presentation of this work.

REFERENCES

Alberta Environment and Parks. Provincial hydrometric and climate datasets. Government of Alberta.

Dash A.A., Castro K., and McBean E. (2024). Modelling for Improved Flood Forecasting in the Bow River Basin Using Prophet. *Journal of Environmental Informatics Letters*, 14(1), 1–13.

Dash A.A. and McBean E. (2025). Prophet-Based Artificial Intelligence Versus Seasonal Auto-Regressive Models for Flood Forecasting with Exogenous Variables. *Water*, 17, 3551.

Environment and Climate Change Canada. Hydrometric and meteorological data for the Bow River Basin. Government of Canada.

Taylor S.J. and Letham B. (2018). Forecasting at scale. *The American Statistician*, 72, 37–45.

Web sites:

Web-1:https://wateroffice.ec.gc.ca, consulted December 2025.

Web-2: https://open.alberta.ca, consulted December 2025.

ICFM 10
Adapting to Global Change:
Innovative Approaches to Flood Management and Resilience
May 20-22, 2026 | Western University, London, Ontario, Canada

An enhanced DP-POA algorithm for reservoir flood control optimization operation

Yawei Ning[1,2*], Minglei Ren[1,2], Junbin Zhang[1,2,3], Rong Tang[1,2], Liping Zhao[1,2], and Gang Wang[1,2]

China Institute of Water Resources and Hydropower Research, Beijing, China[1]
Engineering and Technology Research Center for Flood Control, Drought Mitigation and Disaster Reduction (Flood and Drought Disaster Defense Center), Ministry of Water Resources, Beijing, China[2]
Shenyang Agricultural University, Shenyang, China[3]

* Correspondence: Yawei Ning, ningyw@iwhr.com
Address: A-1, Fuxing Road, Haidian District, Beijing 100038, People's Republic of China

ABSTRACT

The computational efficiency of reservoir optimal operation algorithms is critical for real-time flood control. While traditional DP-POA (Dynamic Programming-Progressive Optimization Algorithm) delivers high-quality solutions, its computational demands are substantial. This study proposes an enhanced DP-POA algorithm that significantly reduces computational load and accelerates computation by simplifying the objective function. Using China's Yuecheng Reservoir as a case study, we conducted comparative analyses of five algorithms: enhanced DP-POA, traditional DP-POA, enhanced POA, traditional POA, and PSO (Particle Swarm Optimization). Results demonstrate that the enhanced DP-POA achieves superior computational efficiency while maintaining solution quality. During the 2021 flood event, it reduced runtime from approximately 30 minutes to less than 5 minutes compared to traditional DP-POA. Moreover, the solutions generated by the enhanced DP-POA either outperformed or matched those of all benchmark methods.

KEYWORDS: Optimal operation algorithm; Flood control; Reservoir operation; Computational efficiency

1 INTRODUCTION

Flood disasters are among the most frequent and destructive natural hazards worldwide, causing losses that include not only casualties and property damage but also long-term socioeconomic impacts(Schaum et al. 2025). Reservoir flood regulation is a critical non-engineering measure for flood mitigation and disaster reduction. Through scientifically and reasonably managing reservoir operations, flood damage both upstream and downstream can be reduced while ensuring the safety of the dam. However, improper regulation may increase flood risks(Ding et al. 2023b). Therefore, reservoir flood regulation has always been a prominent research topic in the field of flood control.

Common regulation methods include conventional operation and optimized operation (Zhou et al. 2018; Xu et al. 2020; Ding et al. 2023a). Conventional operation is simple and easy to implement but often falls short in meeting complex flood control requirements. In contrast, optimized operation can fully utilize the storage capacity of reservoirs, offering significant advantages (Stedinger et al. 1984; Zhou et al. 2018; Zhu et al. 2021; Wu et al. 2024). This technology typically begins with establishing an optimization model and then employs optimization algorithms to search for the optimal solution under multiple constraints,

providing scientific decision support for managers. Due to the substantial computational demands and challenges in finding optimal solutions, exploring efficient and reliable algorithms for solving optimization models is of great importance for enhancing reservoir flood control benefits (Feng et al. 2023; Ning et al. 2024; Wu et al. 2024).

Reservoir optimization solution algorithms can be broadly categorized into linear programming, intelligent optimization algorithms, and dynamic programming (Lai et al. 2022b, a; Feng et al. 2023). Linear programming is relatively mature but limited to linear models. Intelligent optimization methods have gained widespread attention due to their strong capability in handling nonlinear problems and high computational efficiency (Mansouri et al. 2022; Ding et al. 2023a). These mainly include the Particle Swarm Optimization (PSO) algorithm(Wu et al. 2024), Genetic Algorithm (GA) (Zhang et al. 2024), and Simulated Annealing (SA) algorithm (Vasan and Raju 2009). However, intelligent algorithms often face issues such as dependency on initial solutions and premature convergence (Nourani et al. 2020; Ning et al. 2024). Dynamic programming is well-suited for solving reservoir operation problems due to its capability to handle multi-stage decision processes. This includes basic Dynamic Programming (DP) and modified or improved methods based on DP, such as Progressive Optimization Algorithm (POA) and Dynamic Programming Successive Approximation (DPSA) (Stedinger et al. 1984; Zhao et al. 2014). Among the various optimization algorithms, the DP-POA algorithm (Zhu et al. 2021), which combines dynamic programming and progressive optimization, has attracted significant attention for its advantages in handling complex constraints and multi-objective optimization problems. The DP-POA hybrid algorithm integrates the strengths of Dynamic Programming (DP) and Progressive Optimization Algorithm (POA). This algorithm first uses DP to obtain a high-quality initial solution and then introduces POA for further refinement (Zhu et al. 2021). By decomposing multi-stage decision problems into a series of two-stage subproblems, the DP-POA algorithm significantly reduces computational complexity and avoids the "curse of dimensionality" commonly associated with DP. However, the traditional DP-POA algorithm still faces issues such as low computational efficiency and slow convergence in practical applications (Zhou et al. 2018; Zhu et al. 2021; Chen 2021).

To address these limitations, this paper proposes improvements to the traditional DP-POA algorithm by simplifying the objective function during the computational process. This approach aims to reduce the computational load in each iteration and shorten convergence time. Using the Yuecheng Reservoir in northern China as a case study, the performance of the enhanced DP-POA algorithm is compared with four other algorithms to validate its effectiveness.

2 RESEARCH METHODS

2.1 Reservoir optimal operation model

2.1.1 Objective functions and main constraints

Case 1: Minimize the maximum flow at downstream protection section

The objective of this function is to maximize flood retention under the premise of ensuring reservoir safety, thereby reducing the flood peak for the downstream flood control section. By imposing a hard constraint to ensure the reservoir water level does not exceed the allowable value, it minimizes the maximum flow at the downstream control section. Its mathematical expression is:

$$obj1 = \min\{\max[Q_{down}(t)\}, t = 1,2,\ldots T \quad (1)$$

Where: $Q_{\text{down}}(t)$ is the flow at the downstream flood control section at time t; T is the total operation period.

Case 2: Minimize the highest reservoir flood regulation water level

This objective function aims to maximize water release while ensuring the safety of the downstream control section and maintaining dam safety. By imposing a hard constraint that the maximum flow at the downstream section does not exceed the allowable value, the optimization algorithm determines the minimum highest reservoir water level, thereby reducing the reservoir's flood risk. Its mathematical expression is:

$$obj2 = \min\{\max[Z(t)]\}, t = 1, 2, \ldots T \quad (2)$$

Where: Z(t) is the reservoir water level at time t.

2.1.2 Other constraints

(1) Water balance constraint

$$V(t+1) = V(t) + [q_{in}(t) - q_{out}(t)] \times \Delta t \quad (3)$$

Where: V(t) and V(t+1) represent the reservoir storage volume at times t and t+1, respectively; $q_{in}(t)$ is the reservoir inflow at time t; $q_{\text{out}}(t)$ is the reservoir release discharge at time t; and Δt is the time step length.

(2) Reservoir water level constraint

$$Z_{\min} \le Z(t) \le Z_{\max} \quad (4)$$

Where: $Z_{\min}$ and $Z_{\max}$ are the minimum and maximum allowable reservoir water levels, respectively.

(3) Release discharge constraint

$$q_{\min} \le q_{out}(t) \le q_{\max} \quad (5)$$

Where: $q_{\min}$ and $q_{\max}$ are the minimum and maximum allowable reservoir release discharges, respectively.

(4) Release capacity constraint

$$q_{out}(t) \le q_{out}^{\max}(t) \quad (6)$$

Where: $q_{out}^{\max}(t)$ is the maximum release capacity corresponding to the water level at time t.

(5) Flow variation amplitude constraint

$$q_{out}(t) - q_{out}(t-1) \le \varepsilon^* \quad (7)$$

Where: ε* is the maximum allowable flow variation amplitude.

(6) Non-negativity constraint

All variables, including water level, storage volume, and flow, are non-negative.

2.2 River flood routing model

A river flood routing model based on the Muskingum method was used, aiming to accurately simulate the nonlinear propagation process of flood waves along the river channel in the context of reservoir optimal operation. The river reach is divided into n sub-reaches, and the Muskingum method is applied n times for routing. The model parameter system includes characteristic parameters for each sub-reach: storage coefficient K_l, flow weighting factor x_l, and calculation step length Δt.

2.3 Traditional DP-POA algorithm for solving the optimal operation model

The purpose of the Progressive Optimality Algorithm (POA) is to decompose a multi-stage decision problem into a series of two-stage sub-problems, iteratively optimizing decision variables for adjacent time periods to eventually approximate the global optimal solution. However, the traditional POA algorithm also has limitations, the most notable being its high sensitivity to the initial solution. To overcome this limitation, the DP algorithm is used to solve the initial solution for reservoir optimal operation, and then the POA algorithm is applied for further refinement and adjustment. This enhances the quality of the initial solution and improves the overall algorithm's robustness. The procedure of the DP-POA algorithm is as follows:

(1) Initialization: Set an initial solution set $\{H_t^n\}$ for the entire operation period T, where $t \in \{1, 2, ..., T\}$, n denotes the iteration number, initially set to 0.

(2) Iterative Optimization: For time periods t = 2 to T-1, fix H_{t-1}^n and H_{t+1}^n. Find the optimal H_t^n between H_{t-1}^n and H_{t+1}^n that optimizes the objective function. During the search for the optimal H_t^{n+1}, the discrete water level values replace the original operational curve's water levels to form a new operational

curve. Then, the downstream section hydrograph is calculated using the Muskingum segmented flow routing method. The objective function value is computed to obtain the optimal H_t^{n+1}.

(3) Convergence check: Define the newly obtained solution set as $\{H_t^{n+1}\}$. Next, calculate the maximum absolute $\max|H_t^{n+1} - H_t^n| = \varepsilon$. If $\varepsilon \leq \xi$ (where ξ is a predefined precision threshold) or if the maximum number of iterations is reached, terminate the algorithm. Otherwise, set $n = n + 1$ and return to step (2). When the algorithm converges or reaches the maximum iteration count, output the optimized water level sequence $\{H_t^n\}$.

2.4 Enhanced DP-POA algorithm for solving the optimal operation model

The enhanced DP-POA algorithm primarily optimizes the calculation of the hydrograph at the downstream flood control section compared to the traditional DP-POA algorithm. Based on the core characteristic of the POA algorithm, when optimizing the decision variable for time *t*, the decision variables for other times remain unchanged (i.e., maintaining their state from the previous iteration). Traditionally, calculating the hydrograph at the downstream section requires computing the entire flow process. However, this increases the computational load, especially for the downstream peak reduction objective function, which typically involves calculating the sum of squared flow values over the entire hydrograph at the downstream section, making it even more computationally intensive. Since the POA algorithm does not modify decision variables at other times when optimizing the decision variable for the current time step, only the segment of the downstream hydrograph affected by modifying the current decision variable needs to be identified during calculation. The objective function is then calculated based on this modified portion of the flow process. This improvement can significantly shorten the runtime and reduce the algorithm's computational load.

Assume that in the Muskingum method, a change in discharge at the upstream section at a given time causes the length of the range over which the hydrograph at the downstream section varies to be *S*. Therefore, when optimizing the decision variable at time *t*, only the flows within the time interval [*t*-1, *t*+*S*-1] at the downstream section change. Therefore, when the optimization objective is downstream peak shaving, it is only necessary to calculate the sum of squared flow values within this time interval and minimize this sum. For the objective of minimizing the maximum reservoir water level, to calculate the maximum flow at the downstream flood control section, it is only necessary to find the maximum flow within this modified time interval, thereby ensuring it remains below the allowable maximum flow. This method is particularly effective when the inflow sequence is long, significantly reducing the computational load as it focuses only on the portion of the flow process that actually changes, rather than the entire time series.

This improvement approach, based on the stepwise optimization nature of the POA algorithm, is only applicable to POA and its variants. If there is no downstream flood control requirement or other flow routing methods are adopted, the key is still to utilize the stepwise optimization nature of POA or its improvements by separating the changed and unchanged parts of the calculation process and only considering the changed portion. In this way, the computational efficiency of POA and its variants can be greatly improved. This localized calculation method significantly improves the algorithm's runtime efficiency and also offers a reference for the real-time optimal operation of large-scale complex water conservancy systems. The flowchart for the enhanced DP-POA algorithm is shown in **Figure 1**.

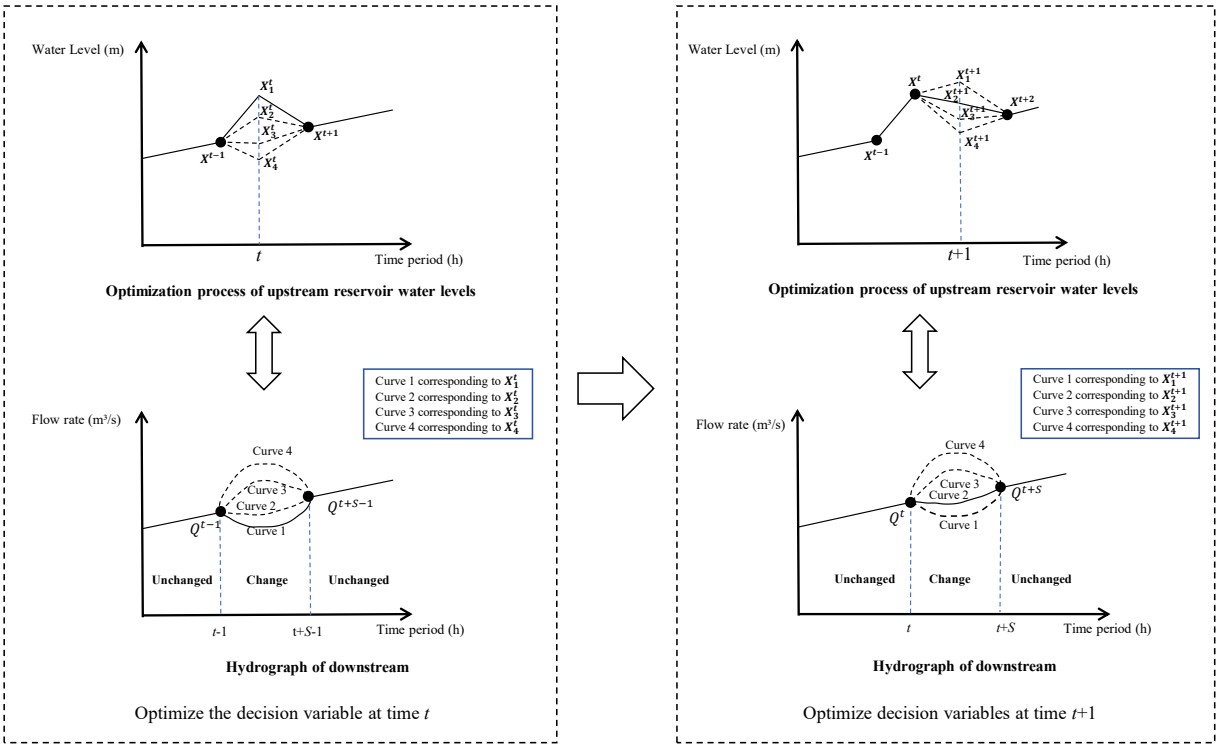

Figure 1 Process diagram of enhanced DP-POA algorithm

3 STUDY AREA

The analysis presented in this paper focuses on the flood control operation of Yuecheng Reservoir, having two main objectives: reservoir safety and the safety of the downstream flood control section. Yuecheng Reservoir, located in Ci County, Handan City, Hebei Province, is a key control project within the Zhang-Wei River system of the Haihe River Basin. It was constructed in 1959, and controls a catchment area of 18,100 km^2. Its total storage capacity is 1.3×10^9 m^3, with design and check flood standards of the 1000-year and 2000-year floods, respectively. It serves multiple functions, including flood control, irrigation, urban water supply, and power generation. By regulating and storing upstream inflows and optimizing downstream releases, the reservoir ensures the safety of the vast downstream plain and several important transportation arteries.

The reservoir's outflow propagates along the Zhang River to the downstream Nantao flood control section, with no significant inflows from surrounding drainage area. The analysed river system is shown in **Figure 2**. Additionally, **Table 1** summarizes the key characteristic parameters of the reservoir, providing an essential basis for subsequent analysis.

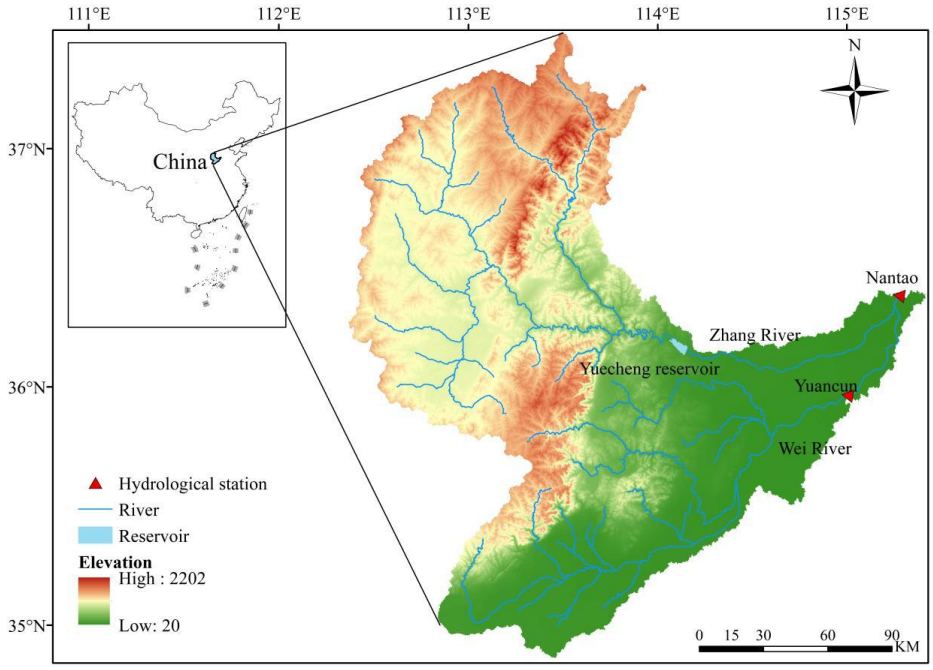

Figure 2: River system of Yuecheng Reservoir.

Table 1 Reservoir characteristic parameters

Minimum operating level (m)	Flood limited water level (m)	Normal storage level (m)	Design flood level (m)	Control flood level (m)
120.00	134.00	148.50	157.45	159.21

4 RESEARCH RESULTS

4.1 Parameter settings

The measured flood hydrograph of Yuecheng Reservoir from July 2021 was used as input for the reservoir operation model. Key parameters such as characteristic water levels, flow rates, and stage-storage-discharge relationships have been collected and systematically organized. To ensure data continuity and completeness, linear interpolation is used to supplement missing data.

To comprehensively evaluate operation performance, five algorithms are employed: traditional DP-POA, enhanced DP-POA, traditional POA, enhanced POA, and PSO. The only differences between these algorithms are calculation process and the type of initial operational curve; all other conditions remained consistent, as shown in **Table 2**.

The convergence criterion for the algorithms is defined as the objective function value remaining unchanged for 30 consecutive iterations. The maximum number of iterations is set to 5000. The initial and final water levels are both set to the flood limited water level of 134 m. In the case of minimizing the peak flow at the Nantao section, the maximum water level constraint for Yuecheng Reservoir is set to the maximum water level under rule-based operation (137.7 m). In the case of minimizing the maximum water level of Yuecheng Reservoir, the maximum flow constraint at the Nantao section is set to the maximum flow at the Nantao section under rule-based operation (2435.4 m^3/s). The particle number for the PSO algorithm is set to 100.

The aim of this analysis is to assess the performance advantages of the enhanced POA and enhanced DP-POA algorithms and explore their application potential in practical reservoir flood control operation by comparing the results of different algorithms.

Table 2 Basic conditions of algorithms

Algorithm	Improved calculation process	Initial operational curve
Traditional DP-POA algorithm	No	DP initial operational curve
Enhanced DP-POA algorithm	Yes	DP initial operational curve
Traditional PSO algorithm	No	Random initial operational curve
Traditional POA algorithm	No	Random initial operational curve
Enhanced POA algorithm	Yes	Standard water level sequence

4.2 Computation results

The objectives of optimal operation models were: minimizing the peak flow at the Nantao section (Case 1) and minimizing the highest water level of Yuecheng Reservoir (Case 2). The calculation results are analyzed in greater detail below, covering: a comparison of computation times between the traditional and improved algorithms, the influence of employing different initial operational curves within the same algorithm, and a detailed analysis of the optimization outcomes produced by the five algorithms.

4.2.1 Computation time comparison

According to the computation time comparison results (**Figure 3**), enhanced POA and enhanced DP-POA require less computation time than their traditional equivalents. Under Case 1 conditions, the computation times of enhanced POA, traditional POA, enhanced DP-POA, traditional DP-POA, and PSO are 984 s, 1573 s, 961 s, 1555 s, and 292 s, respectively. Under Case 2 conditions, the corresponding computation times are 867 s, 1396 s, 943 s, 1386 s, and 189 s. The results indicate that improved algorithms significantly accelerate computation speed compared to traditional ones. PSO is the fastest in terms of computation speed, but in terms of solution effectiveness, its solutions are not optimal.

4.2.2 Impact of initial solution

According to the calculation results (**Table 3**), the initial solution has a significant impact on the performance of POA-based algorithms. The traditional POA algorithm uses rule-based operational scheme as the initial solution, while the DP-POA algorithm uses the solution obtained by the DP algorithm in the initial step. The two algorithms exhibit a significant difference in convergence speed. Under Case 1, the traditional POA algorithm converges and exits after 111 iterations, whereas the traditional DP-POA algorithm converges after only 43 iterations, substantially reducing the computation time.

4.2.3 Comparison of calculation results

Based on the final calculation results, the traditional POA, enhanced POA, traditional DP-POA, and enhanced DP-POA algorithms converge to the same optimal solution. However, there are differences in their computation time and number of iterations: the enhanced DP-POA algorithm converges to this optimum with less iterations and faster than others. The PSO algorithm exhibits some randomness, and its convergence performance is inferior to other algorithms. The figures illustrate that the final calculation results of these four algorithms after convergence are essentially identical, indicating the stability of POA-based algorithms. Details of the calculation results are presented in **Table 3**, **Figures 6** and **7**.

Table 3 Calculation results under different algorithms

Algorithm	Case1				Case2			
	Iterations	Runtime (s)	Nantao Max Flow (m^3/s)	Yuecheng Max Level (m)	Iterations	Runtime (s)	Nantao Maximum Flow (m^3/s)	Yuecheng Max Level (m)
Traditional POA	111	37.3	2083.0	137.70	263	71.5	2435.4	137.03
Traditional DP-POA	43	20.2	2083.0	137.70	87	30.4	2435.3	137.02
Enhanced POA	110	23.0	2083.0	137.70	263	44.3	2435.4	137.03
Enhanced DP-POA	43	15.4	2082.9	137.70	87	23.5	2435.3	137.02
PSO	1080	66.7	2107.0	137.70	1167	50.7	2416.0	137.22

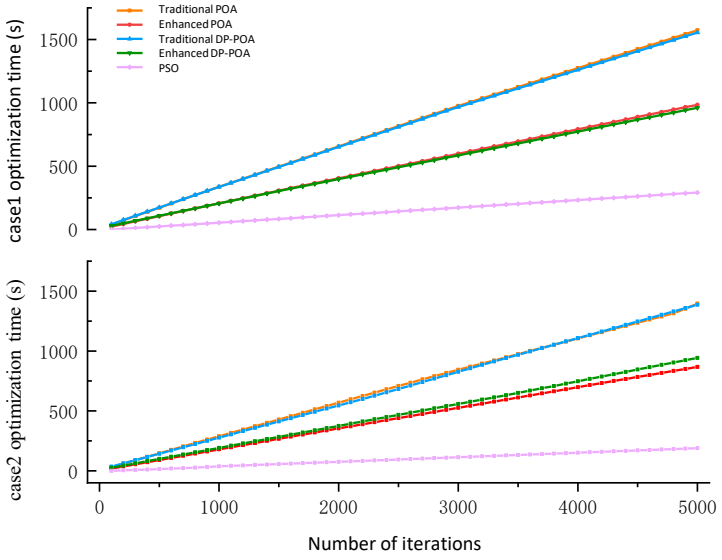

Figure 3: Computation time comparison.

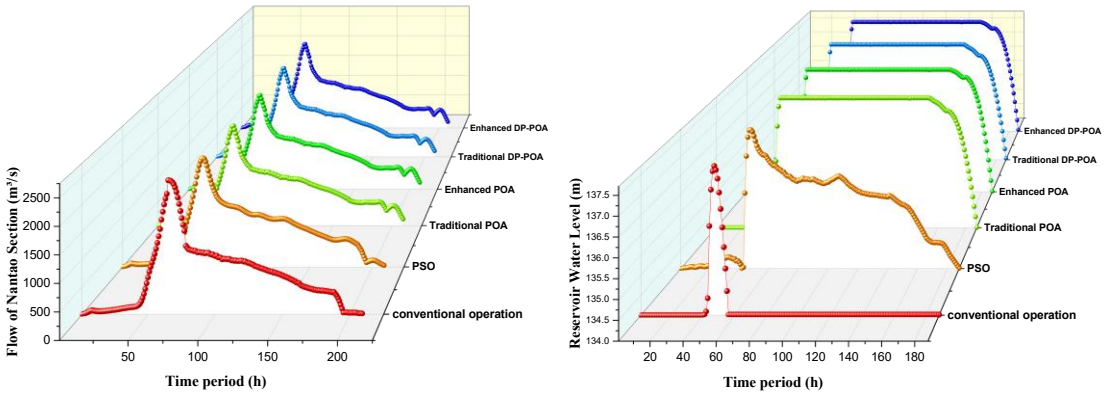

Figure 4: Operation hydrograph for Case 1.

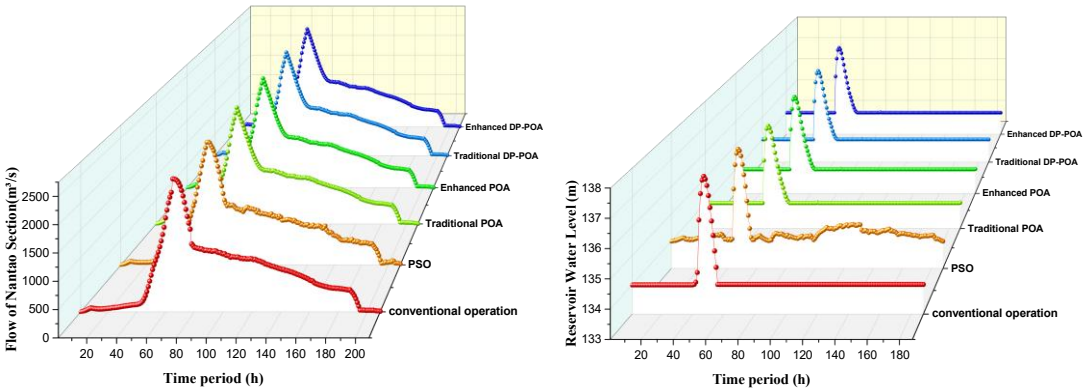

Figure 5: Operation hydrograph for Case 2.

5 CONCLUSIONS

Based on a case study of Yuecheng Reservoir, the following main conclusions on algorithms for optimization of reservoir flood control operation are drawn:

(1) The enhanced DP-POA algorithm demonstrates outstanding performance in computational efficiency. Compared to traditional algorithms, it saves 30-38% of computation time for both objective functions (Case1 and Case2). This significant efficiency improvement makes the algorithm more suitable for practical reservoir flood control operation decision support systems, especially in emergencies requiring rapid response.

(2) The initial solution has a significant impact on the performance of POA algorithms. The DP-POA algorithm, due to its use of a high-quality initial solution, shows markedly better convergence speed and efficiency than the traditional POA algorithm. Under the Case 1 objective function, the DP-POA algorithm reduces the number of iterations by 61% and shortens computation time by nearly 46%. This highlights the importance of selecting an appropriate initial solution in reservoir operation optimization.

(3) Regarding solution quality, traditional POA, enhanced POA, traditional DP-POA, and enhanced DP-POA all converge to the same or very similar optimal solutions. This indicates good stability and reliability of these algorithms. In contrast, the PSO algorithm yields slightly inferior solution quality compared to the other four algorithms.

(4) The results of this study emphasize the need to balance multiple key factors, such as accuracy, computation speed, and result stability, when selecting reservoir optimization operation algorithm. The enhanced DP-POA algorithm performs well in all these aspects, providing an effective solution for reservoir flood control operation optimization.

6 ACKNOWLEDGEMENTS

This study is supported by National key R&D program (No. 2024YFC3212800) and Key Scientific and Technological Programs of the Ministry of Emergency Management (No. 2024EMST050501).

REFERENCES

Chen J (2021) Long-Term Joint Operation of Cascade Reservoirs Using Enhanced Progressive Optimality Algorithm and Dynamic Programming Hybrid Approach. Water Resour Manag 35:2265–2279. https://doi.org/10.1007/s11269-021-02846-y

Ding W, Wei G, Zhou H (2023a) Improving flood resilience through optimal reservoir operation. J Hydrol 620:129494. https://doi.org/10.1016/j.jhydrol.2023.129494

Ding W, Zhang C, Lin J, et al (2023b) Flood Risk Quantification, Transmission, and Propagation Analysis for Flood Water Utilization of Parallel Reservoirs. J Hydrol 618:129202. https://doi.org/10.1016/j.jhydrol.2023.129202

Feng Z, Luo T, Niu W, et al (2023) A LSTM-based approximate dynamic programming method for hydropower reservoir operation optimization. J Hydrol 625:130018. https://doi.org/10.1016/j.jhydrol.2023.130018

Lai V, Essam Y, Huang YF, et al (2022a) Investigating dam reservoir operation optimization using metaheuristic algorithms. Appl Water Sci 12:280. https://doi.org/10.1007/s13201-022-01794-1

Lai V, Huang YF, Koo CH, et al (2022b) A Review of Reservoir Operation Optimisations: from Traditional Models to Metaheuristic Algorithms. Arch Comput Methods Eng 29:3435–3457. https://doi.org/10.1007/s11831-021-09701-8

Mansouri M, Safavi HR, Rezaei F (2022) An improved MOPSO algorithm for multi-objective optimization of reservoir operation under climate change. Environ Monit Assess 194:261. https://doi.org/10.1007/s10661-022-09909-6

Ning Y, Ren M, Guo S, et al (2024) An Advanced Multi-Objective Ant Lion Algorithm for Reservoir Flood Control Optimal Operation. Water 16:852. https://doi.org/10.3390/w16060852

Nourani V, Rouzegari N, Molajou A, Hosseini Baghanam A (2020) An integrated simulation-optimization framework to optimize the reservoir operation adapted to climate change scenarios. J Hydrol 587:125018. https://doi.org/10.1016/j.jhydrol.2020.125018

Schaum S, Stenger-Wolf S, Schüttrumpf H, Jüpner R (2025) An Overview of Long-Term Temporaries After Flood Disasters. J Flood Risk Manag 18:e70109. https://doi.org/10.1111/jfr3.70109

Stedinger JR, Sule BF, Loucks DP (1984) Stochastic dynamic programming models for reservoir operation optimization. Water Resour Res 20:1499–1505. https://doi.org/10.1029/WR020i011p01499

Vasan A, Raju KS (2009) Comparative analysis of Simulated Annealing, Simulated Quenching and Genetic Algorithms for optimal reservoir operation. Appl Soft Comput 9:274–281. https://doi.org/10.1016/j.asoc.2007.09.002

Wu X, Shen X, Wei C, et al (2024) A Hybrid Particle Swarm Optimization-Genetic Algorithm for Multiobjective Reservoir Ecological Dispatching. Water Resour Manag 38:2229–2249. https://doi.org/10.1007/s11269-024-03755-6

Xu C, Xu Z, Yang Z (2020) Reservoir operation optimization for balancing hydropower generation and biodiversity conservation in a downstream wetland. J Clean Prod 245:118885. https://doi.org/10.1016/j.jclepro.2019.118885

Zhang R, Zhang S, Wen X, et al (2024) Optimization of short-term hydropower scheduling with dynamic reservoir capacity based on improved genetic algorithm and parallel computing. J Hydrol 636:131238. https://doi.org/10.1016/j.jhydrol.2024.131238

Zhao T, Zhao J, Yang D (2014) Improved Dynamic Programming for Hydropower Reservoir Operation. J Water Resour Plan Manag 140:365–374. https://doi.org/10.1061/(ASCE)WR.1943-5452.0000343

Zhou C, Sun N, Chen L, et al (2018) Optimal Operation of Cascade Reservoirs for Flood Control of Multiple Areas Downstream: A Case Study in the Upper Yangtze River Basin. Water 10:1250. https://doi.org/10.3390/w10091250

Zhu D, Mei Y, Xu X, et al (2021) Optimal Operation of a Parallel Multireservoir System for Flood Control using a Stagewise Compensation Method. Water Resour Manag 35:1689–1710. https://doi.org/10.1007/s11269-021-02803-9

ICFM 10
Adapting to Global Change:
Innovative Approaches to Flood Management and Resilience
May 20-22, 2026 | Western University, London, Ontario, Canada

A Deep Learning-Enhanced Web Crawling System for Global Water-related Disaster Dataset

Yuexiao Liu[1], Cheng Zhang[1]
Research Center on Flood & Drought Disaster Prevention and Reduction of the Ministry of Water Resources, China Institute of Water Resources and Hydropower Research.[1]
E-mail: yxliu@iwhr.com

ABSTRACT

Global warming intensifies the hydrological cycle and increases the likelihood of extreme precipitation, amplifying flood, flash-flood, and rainfall-triggered landslide risks worldwide. Authoritative disaster inventories (e.g., EM-DAT; NASA Global Landslide Catalog) provide essential baselines, yet they are typically curated post-event and may miss small-to-moderate events or lack physically meaningful attributes such as inundation extent. This paper presents an end-to-end global water-disaster database system that integrates (i) a Chrome-extension web crawler for automatic collection of flood/flash-flood/landslide information from news and social media sources, (ii) real-time dissemination through a WeChat Mini Program, (iii) natural language processing (NLP) for extracting event time, location, hazard type, and triggering factors from structured text, and (iv) Google Earth Engine (GEE) processing of Sentinel-1 SAR imagery to quantify maximum flood inundation area through a change-detection workflow with Otsu thresholding. Processed event records and associated evidence images are stored in an online database and visualized on an interactive map, with a chatbot module supporting query and summary statistics by country and time window. Using pilot-scale deployment statistics (illustrative), the system demonstrates the feasibility of constructing a long-term, continuously updated global water-disaster inventory (2000–2024) with event-level physical quantification and rapid public-facing delivery. The proposed architecture provides a scalable technical basis for disaster risk reduction, emergency response, and climate-risk analytics.

KEYWORDS: Flood inventory, Deep Learning; Convolutional Neural Networks; Web crawling; NLP.

1 INTRODUCTION

Floods and rainfall-triggered landslides are among the most frequent and damaging hydro-meteorological hazards. Building long-term, global-scale disaster inventories is crucial for exposure analysis, early warning validation, and climate risk assessment(Ali et al., 2022). However, traditional global disaster databases rely largely on manual compilation, which introduces delays and biases and often limits attribute completeness(Chen et al., 2025). For example, EM-DAT ("EM-DAT,") provides open-access global records and impacts of “mass disasters” from 1900 onward with systematic recording since 1988, but event inclusion and attribute completeness inevitably depend on reporting channels and thresholds (Cheng et al., 2023). For landslides, the NASA Global Landslide Catalog (GLC) demonstrates the utility of media-based global reporting for rainfall-triggered landslides, yet the broader integration of multi-source signals and physical quantification remains an open challenge, Meanwhile, the global web (news portals, bulletins, and social media) provides near-real-time hazard signals at massive scale. Automated extraction from unstructured text is increasingly feasible using NLP(Duangkhwan et al., 2025; Khatun et al., 2024; Santos et al., 2023). However, web-derived records may be noisy, lack geospatial precision, and can suffer from credibility issues. Remote sensing offers an objective complement: Sentinel-1 SAR provides cloud-penetrating imagery suitable for flood mapping during storms, and GEE enables planetary-scale analysis with consistent workflows (Emberson et al., 2021; Haque et al., 2019).

This study develops a closed-loop system that fuses (i) web crawling, (ii) NLP-based attribute extraction and geocoding, (iii) GEE-based Sentinel-1 flood inundation quantification, and (iv) online database publication and WeChat notification. The main contributions are： (1) an operational architecture spanning collection → extraction → satellite quantification → dissemination; (2) a structured event schema designed for global water-related disasters; (3) an automated Sentinel-1 SAR flood-extent workflow using Otsu thresholding for reproducible inundation-area estimation.

2 DATA SOURCES AND SYSTEM INPUTS

The system ingests three broad categories of data (Table 1).

Web sources. Online news articles, disaster bulletins, and public posts provide narrative descriptions of events (time, place, impacts, triggers). Web pages are retrieved via HTTP requests and parsed through HTML parsing tools (e.g., BeautifulSoup).

Remote sensing. MODIS surface reflectance products offer long-term global coverage; Sentinel-1 SAR provides cloud-penetrating imaging for flood detection.

Reference inventories for validation. EM-DAT and GLC provide authoritative global baselines for floods and landslides, respectively.

Table 1 Core data sources and roles in the framework

Data stream	Examples	Primary role	Typical uncertainties
Web text + metadata	News, bulletins, public posts	Event detection; attribute extraction	Reporting bias; incomplete attributes
Web multimedia	On-site photos, embedded maps	Evidence support; event type confirmation	Mislabeling; reposting
MODIS optical	MOD09 surface reflectance	Broad-scale water mapping and long-term continuity	Clouds; coarse resolution
Sentinel-1 SAR	C-band SAR	Flood extent under clouds; change detection	Speckle;urban backscatter
Validation inventories	EM-DAT; GLC	Benchmarking, cross-checking	Coverage thresholds; reporting delays

3 METHODS

The methodological framework of this study follows an integrated and sequential architecture, as illustrated in Figure 1: in which web-based disaster information, natural language processing, satellite remote sensing analysis, and database dissemination are tightly coupled into a unified system. The framework is designed to transform heterogeneous and structured disaster reports into structured, georeferenced event records enriched with physically meaningful flood inundation metrics at the global scale,while explicitly distinguishing hazard intensity, exposure, and impact and representing associated uncertainties.

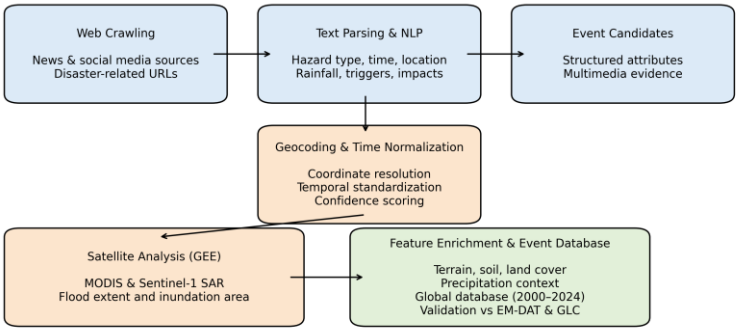

Figure 2: Conceptual framework of the deep learning–enhanced web crawling system for global water-related disaster data construction.

The Figure 1 is developed in this study as a conceptual synthesis of our pipeline; methodological details are provided in the text.

Disaster information acquisition constitutes the first stage of the framework. A deep-learning–enhanced web crawling module automatically collects disaster-related news articles and selected social-media posts from authoritative sources using curated keyword sets for floods, flash floods, and landslides. The retrieved URLs are validated for accessibility and uniqueness, after which the main textual content and embedded multimedia links are extracted. Natural language processing techniques are then applied to parse the unstructured text and identify key disaster attributes, including hazard type, occurrence time, reported location, rainfall characteristics, triggering mechanisms, and impact descriptions. These attributes are organized into structured event candidates and supplemented with multimedia evidence such as on-site photographs and maps(Cheng et al., 2023).

To ensure spatial–temporal consistency, each event candidate undergoes geocoding and time normalization. Extracted place names are converted into geographic coordinates, while temporal expressions are standardized to a unified timestamp format(Hayder et al., 2022). When multiple candidate locations exist, contextual information within the text (administrative levels, river names, referenced infrastructure) is used to resolve ambiguities. A confidence score is assigned to each event based on source reliability and cross-source agreement, providing a preliminary measure of event credibility. Event selection follows explicit criteria designed for representativeness and quality: inclusion requires geocoding precision of $\leqslant$10 km and temporal precision of $\leqslant$3 days, classification into a standard hazard taxonomy (riverine, flash, urban/pluvial, ice-related, typhoon/surge-related), and a minimum confidence threshold. Reports with centroid distance <25 km and temporal overlap >50% are merged into a single event_id, retaining the highest-reliability metadata and reconciling conflicts by weighted majority vote. These choices balance diversity of hazard contexts against the need for reliable downstream quantification.

Satellite-based flood analysis forms the core quantitative component of the framework and is implemented on the Google Earth Engine platform. For each geocoded flood event, a region of interest is defined, and two temporal windows representing pre-event and post-event conditions are specified. All available MODIS and Sentinel-1 C-band synthetic aperture radar (SAR) images intersecting the region of interest are retrieved automatically. Sentinel-1 SAR imagery is employed due to its cloud-penetrating capability and suitability for extreme weather conditions(Hasan et al., 2025). Prior to analysis, SAR images are radiometrically calibrated, terrain-corrected, and filtered using a Refined Lee filter to suppress speckle noise(Hameed et al., 2025).

Flood inundation is identified through SAR backscatter change detection.(Dehghani et al., 2023) Let I_{pre} and I_{post} denote the mean backscatter intensity of the pre-event and post-event image composites, respectively. The backscatter change image ΔI is defined as

$$\Delta I = I_{\mathrm{post}} - I_{\mathrm{pre}}. \tag{1}$$

Flooded areas typically exhibit a decrease in backscatter intensity due to specular reflection from open water surfaces(Windheuser et al., 2023). To objectively separate flooded and non-flooded pixels, Otsu's thresholding method is applied to the histogram of ΔI to determine an optimal threshold τ^* that maximizes the between-class variance:

$$\tau^* = \arg\max_{\tau} \left[\omega_1(\tau)\omega_2(\tau)(\mu_1(\tau) - \mu_2(\tau))^2\right] \tag{2}$$

To further reduce misclassification caused by terrain effects and residual noise, a digital elevation model–derived slope mask is applied to exclude steep terrain areas, and isolated pixel clusters are removed using connectivity analysis(Li et al., 2022). The maximum flood inundation area A_f is calculated as

$$A_f = N_f \times A_p, \tag{3}$$

where N_f is the number of pixels classified as flooded and A_p is the area of a single pixel. The resulting flood extent maps and inundation area estimates provide physically interpretable measures of flood impact.

Intensity is summarized by inundation extent and by the rarity of associated hydrometeorological drivers. Where stream gauges or stage/flow archives exist, we estimate annual-exceedance probability using generalized extreme value or peaks-over-threshold methods and convert to return period; in ungauged basins, we use proxies such as the AEP of event-maximum precipitation from ERA5 (after bias correction) and/or percentile ranks of satellite-derived inundation or depth proxies relative to local histories. Exposure is derived by intersecting flood extents with population, built-up land, land cover, and critical infrastructure layers. Impact is compiled from text (e.g., damage descriptors, displacement) and spatial overlays. For comparability, we report absolute and normalized indicators—affected population per 1,000 residents, exposed built-up area as km² and as a share of local built-up land, and critical-infrastructure intersections as counts and densities—and we stratify summaries by hazard subtype and urban versus rural settings. Event-level aggregates are weighted by confidence and data quality (e.g., higher weights for SAR-mapped events with dense temporal sampling), ensuring that heterogeneous events are not implicitly treated as equivalent.

In the final stage of the framework, disaster events are enriched with environmental variables, including terrain, soil properties, land cover, and precipitation context, and integrated into a global event database covering the period 2000–2024. The database supports interactive visualization, spatiotemporal querying, and real-time dissemination through web interfaces and a WeChat Mini Program(Situ et al., 2024). To enhance reliability, the compiled events are cross-validated against authoritative disaster inventories, including EM-DAT and the Global Landslide Catalogue(Noor et al., 2022).

4 RESULTS

4.1 Global Water-Related Disaster Event Detection and Database Construction

Applying the proposed deep learning–enhanced web crawling framework, a global database of water-related disaster events was successfully constructed for the period 2000–2024. The system continuously collected disaster-related information from online news media and social platforms and transformed heterogeneous, unstructured text into standardized disaster event records through natural language processing and machine-learning-based classification.

The resulting database, as comprises several thousand unique events worldwide, including river floods, flash floods, urban flooding, ice-related floods, and typhoon-related flooding. Each event record contains normalized temporal and spatial information, hazard type, extracted triggering factors, and associated multimedia references. The global coverage of detected events demonstrates the ability of the system to operate across diverse climatic, geographic, and socio-economic contexts, without reliance on manual data entry or region-specific rules.

The spatial distribution of detected events exhibits pronounced regional heterogeneity. Higher event densities are observed in regions frequently affected by extreme precipitation and flooding, such as South and Southeast Asia, parts of Europe, and the Americas. In contrast, lower densities are found in regions with sparse digital reporting. Overall, the observed spatial patterns are consistent with known global hydrometeorological hazard hotspots, indicating that the automated extraction and geocoding procedures recover physically plausible global disaster distributions.

Figure 2: Global distribution of detected water-related disaster events; Each point represents an individual event identified through the proposed framework, with colors indicating major hazard types.

Key statistical characteristics of the constructed global water-related disaster database are summarized in Table 2 and Table 3. The database spans more than two decades, includes multiple hazard types, and integrates both textual and satellite-derived information. A substantial proportion of flood events are associated with quantitative inundation estimates, enhancing the physical interpretability of the dataset.

Table 2. Summary statistics of the global water-related disaster database (2000–2024).

Attribute	Result
Time span	2000–2024
Hazard types	Floods, flash floods, landslides, urban flooding, ice flood, typhoon-related flooding
Spatial coverage	Global
Total events	2300
Events with SAR inundation mapping	Substantial fraction
Event attributes	Time, location, hazard type, triggering factors, multimedia links
Data source	Online news media, social platforms
Validation sources	EM-DAT, GLC

Table 3. Composition of detected water-related disaster events by hazard type

Hazard type	Relative proportion	Typical triggering factors
River flood	Dominant	Prolonged or extreme rainfall
Flash flood	High	Short-duration intense rainfall
Urban flooding	Moderate	Heavy rainfall, drainage failure
Ice flood	Low	Ice jams, snowmelt
Typhoon-related flooding	Low–moderate	Tropical cyclones and storm surge

4.2 Temporal Characteristics and Hazard-Type Composition

The temporal distribution of detected water-related disaster events spans more than two decades, covering both early years with limited digital documentation and recent years characterized by dense online reporting. Events included in Figure 3 were automatically identified using a text-mining and geocoding pipeline applied to global digital reports. A predefined set of flood-related keywords and classification rules was used to extract candidate events, which were subsequently filtered based on confidence scores and duplicate removal procedures. Data prior to the early 2000s are less complete and should be interpreted with caution due to limited observational and reporting coverage. An overall increasing trend in detected events is observed over time. This trend reflects a combination of improved availability of online information sources and increasing exposure to extreme hydrological hazards under climate variability and change.

In terms of hazard-type composition, flood-related hazards dominate the database. River floods and flash floods account for the largest proportion of events, followed by urban flooding, ice-related floods, and typhoon-related flooding. This composition reflects both the global prevalence of flooding and the relatively higher visibility of flood impacts in textual reports and remote sensing observations. The ability to capture multiple hazard types within a unified framework highlights the flexibility of the proposed system and its suitability for comprehensive water-related disaster monitoring.

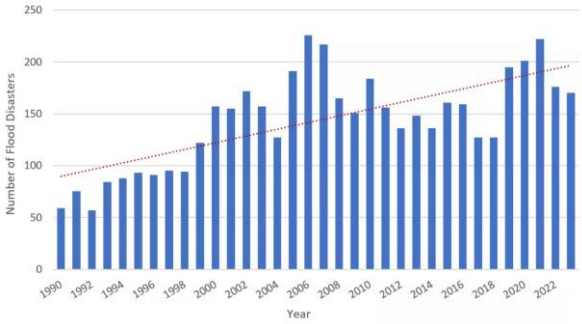

Figure 3: Temporal distribution of detected water-related disaster events

4.3 Satellite-Derived Flood Inundation Mapping Results

For flood events with sufficient spatial precision and temporal information, satellite-based flood inundation mapping was conducted using Sentinel-1 synthetic aperture radar (SAR) imagery on the Google Earth Engine platform. The flood mapping workflow systematically transforms raw SAR backscatter data into physically interpretable flood inundation products through a sequence of processing steps (as shown in Figure 4).

Visual comparison of pre-event and post-event SAR imagery reveals clear backscatter changes associated with flood-induced surface water expansion. Automatic thresholding enables objective separation of water and non-water surfaces, while speckle noise reduction improves the clarity of flood signals. Terrain-based filtering using slope information derived from global digital elevation models effectively reduces misclassification in steep areas where SAR backscatter may resemble open water. Additional spatial filtering removes isolated pixels and enhances the coherence of extracted flood patterns.

The final flood inundation products exhibit spatial continuity and align with expected floodplain morphology. Quantitative inundation areas derived from these products show a highly skewed distribution, with most flood events affecting relatively small spatial extents and a limited number of large-scale floods contributing disproportionately to total inundated area. This size–frequency behavior is consistent with established global flood statistics reported in previous studies and demonstrates the capability of the proposed workflow to generate reliable flood extent estimates suitable for large-scale analysis.

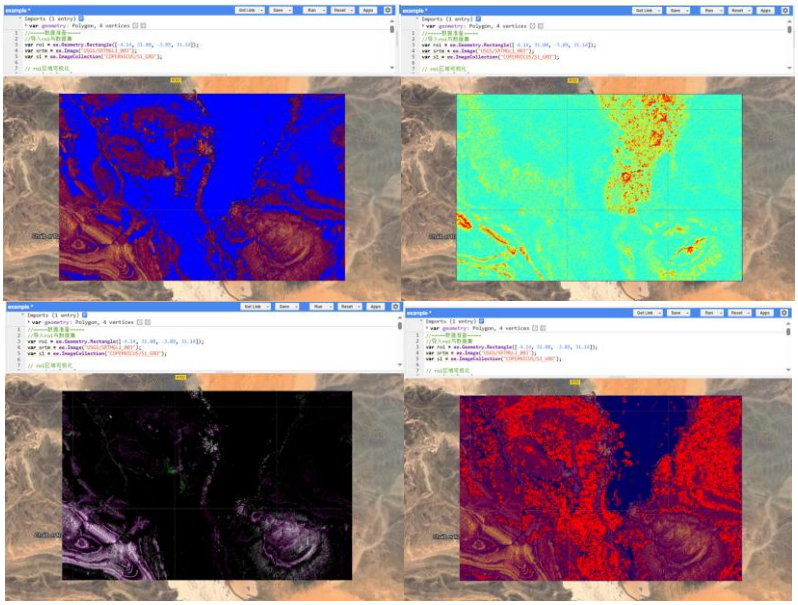

Figure 4: Example of satellite-derived flood inundation mapping using Sentinel-1 SAR imagery, illustrating the transformation from pre- and post-event observations to the final flood inundation extent after thresholding, terrain masking, and spatial filtering.

4.4 Performance of Machine Learning Models for Event Classification

To evaluate the effectiveness of automated disaster event identification from textual sources, four machine learning approaches—Support Vector Machine (SVM), Random Forest, XGBoost, and a BERT-based classifier—were applied to the disaster text classification task. Receiver operating characteristic (ROC) analysis indicates clear performance differences among the models.

As shown in Figure 5, The BERT-based classifier consistently achieves the highest true positive rate across a wide range of false alarm rates, resulting in the largest area under the ROC curve (AUC). XGBoost and Random Forest models also demonstrate strong performance, outperforming the traditional SVM baseline. These results highlight the advantage of deep contextual language representations for extracting disaster-related information from heterogeneous and noisy online texts. The inclusion of robust text classification models contributes to the reliability and scalability of the overall database construction process.

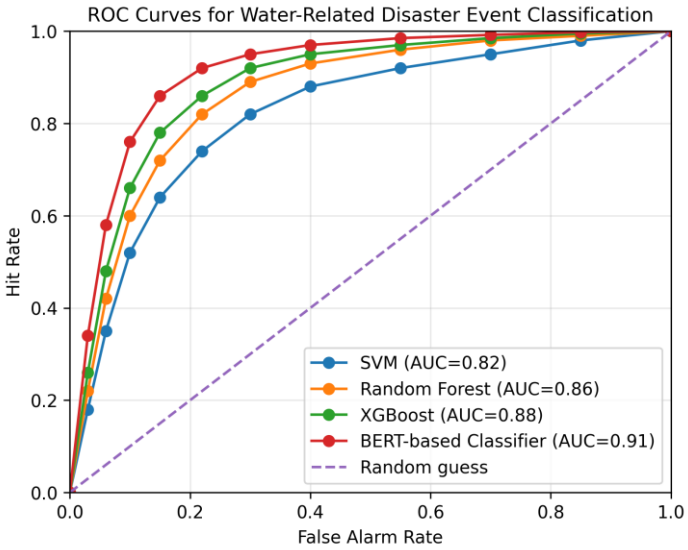

Figure 5: Receiver operating characteristic (ROC) curves of four machine-learning models for automated disaster event identification from textual sources.

5 CONCLUSIONS

This study presents an end-to-end system for constructing a global water-related disaster database by integrating web crawling, natural language processing, machine learning, satellite remote sensing, and online data integration within a unified framework. The system enables automated extraction of disaster information from heterogeneous online sources, standardized spatial–temporal representation of events, and quantitative flood inundation mapping using Sentinel-1 SAR imagery on the Google Earth Engine platform.

The resulting database spans the period 2000–2024 and includes floods, flash floods, and rainfall-triggered landslides at the global scale. By coupling text-derived disaster reports with satellite-based inundation metrics, the proposed approach provides physically meaningful information that is typically absent from text-only disaster inventories. Validation against authoritative databases demonstrates that the system captures most major disaster events while also identifying numerous smaller-scale events that complement existing global records.

The framework offers a scalable and reproducible foundation for global disaster monitoring and analysis. It has the potential to support a wide range of applications, including disaster risk assessment, emergency response, and climate-related hazard analysis. Future work will focus on expanding multilingual information extraction, improving uncertainty characterization, and integrating the database with hydrological and impact models to further enhance its value for disaster risk reduction and climate adaptation.

REFERENCES

Ali, M. H. M., et al. (2022). Flood Prediction using Deep Learning Models. *International Journal of Advanced Computer Science and Applications, 13*(9), 972-981.

Chen, C., et al. (2025). A novel flood forecasting model based on TimeGAN for data-sparse basins. *Stochastic Environmental Research and Risk Assessment, 39*(6), 2267-2280. doi:10.1007/s00477-025-02968-4

Cheng, Q., et al. (2023). DA-Net: Dual Attention Network for Flood Forecasting. *Journal of Signal Processing Systems for Signal Image and Video Technology, 95*(2-3), 351-362. doi:10.1007/s11265-023-01839-x

Dehghani, A., et al. (2023). Comparative evaluation of LSTM, CNN, and ConvLSTM for hourly short-term streamflow forecasting using deep learning approaches. *Ecological Informatics, 75*, 12. doi:10.1016/j.ecoinf.2023.102119

Duangkhwan, W., et al. (2025). DEEP LEARNING-BASED FLOOD INUNDATION PREDICTION IN THE PATTANI RIVER BASIN. *International Journal of Geomate, 28*(125), 133-140. doi:10.21660/2025.125.g14289

EM-DAT. Available from World Health Organization (WHO);Centre for Research on the Epidemiology of Disasters (CRED) The International Disaster Database Retrieved 2025/2/26 https://www.emdat.be/

Emberson, R., et al. (2021). Global connections between El Nino and landslide impacts. *Nature Communications, 12*(1). doi:10.1038/s41467-021-22398-4

Hameed, M. M., et al. (2025). Forecasting monthly runoff in a glacierized catchment: A comparison of extreme gradient boosting (XGBoost) and deep learning models. *Plos One, 20*(5), 29. doi:10.1371/journal.pone.0321008

Haque, U., et al. (2019). The human cost of global warming: Deadly landslides and their triggers (1995–2014). *Science of The Total Environment, 682*, 673-684. doi:10.1016/j.scitotenv.2019.03.415

Hasan, M., et al. (2025). Enhancing flood forecasting performance using effective and transparent explainable hybrid deep learning model. *Earth Science Informatics, 18*(2), 21. doi:10.1007/s12145-025-01930-w

Hayder, G., et al. (2022). Multi-step-ahead prediction of river flow using NARX neural networks and deep learning LSTM. *H2open Journal, 5*(1), 42-59. doi:10.2166/h2oj.2022.134

Khatun, A., et al. (2024). A novel insight on input variable and time lag selection in daily streamflow forecasting using deep learning models. *Environmental Modelling & Software, 179*, 16. doi:10.1016/j.envsoft.2024.106126

Li, P. F., et al. (2022). Prediction of Flow Based on a CNN-LSTM Combined Deep Learning Approach. *Water, 14*(6), 13. doi:10.3390/w14060993

Noor, F., et al. (2022). Water Level Forecasting Using Spatiotemporal Attention-Based Long Short-Term Memory Network. *Water, 14*(4), 21. doi:10.3390/w14040612

Santos, V. O., et al. (2023). A New Graph-Based Deep Learning Model to Predict Flooding with Validation on a Case Study on the Humber River. *Water, 15*(10), 31. doi:10.3390/w15101827

Situ, Z., et al. (2024). Improving urban flood prediction using LSTM-DeepLabv3+and Bayesian optimization with spatiotemporal feature fusion. *Journal of Hydrology, 630*, 17. doi:10.1016/j.jhydrol.2024.130743

Windheuser, L., et al. (2023). An End-To-End Flood Stage Prediction System Using Deep Neural Networks. *Earth and Space Science, 10*(1), 21. doi:10.1029/2022ea002385

ICFM 10
Adapting to Global Change:
Innovative Approaches to Flood Management and
May 20-22, 2026 | Western University, London, Ontario, Ca

Application of Blackbird for large-scale modelling of the Grand River watershed

Robert Chlumsky[1,2] , Roger Niyongira[1], James R. Craig[1,2], Bryan A. Tolson[1,2] , Guénolé Choné[3], and Pascale Biron[3]
Heron Hydrologic Ltd., Baden, ON, Canada[1]
E-mail: robert.chlumsky@heronhydrologic.ca

Department of Civil and Environmental Engineering, University of Waterloo, Waterloo, ON, Canada[2]
Concordia University, Montreal, QC, Canada[3]

ABSTRACT

Flood mapping in Canada has historically focused on engineering scale maps, produced for specific jurisdictions as funding and political will allowed projects to be undertaken. The current system has led to the lack of widely available flood maps, and many maps being years or decades out of date. New approaches as well as ever-improving computational abilities are leading to more efficient and larger scale flood mapping without sacrificing quality, as global flood products often do.

This project presents the Blackbird methodology in recent applications, focusing on the development of a large scale inundation model of the Grand River watershed. The Grand River watershed is approximately 6,800 km2 in size. The model is developed with a cell size of 4m and over 1700 computational streamnodes along the channels, which represents a size and accuracy that would be impractical for 2D models and highly time consuming for other conventional approaches. The flows for each section of the model are generated using the hydrologic modelling framework Raven, which uses gauged information to provide flows directly within the system using assimilation. This allows the estimation of flows for both frequency analysis and real-time throughout the watershed, which are provided to Blackbird as a boundary condition. The comparison of the estimated 100-year inundation maps to the local regulatory maps are shown. The potential of this as a real-time inundation mapping system is demonstrated in a live application for the entire Grand River watershed.

KEYWORDS: Flood mapping, large scale, model, inundation, real-time, regional, Blackbird, Raven

1 INTRODUCTION

Accurate estimation of river discharge in ungauged reaches remains a challenge for large scale flood mapping, and reliable flood extent and depth. This is particularly significant in large systems such as the Grand River, where the streamflow gauges are concentrated in the upstream area. The Grand River watershed presented in this study covers an area of approximately 6,800 km^2 discretized into 1,774 subbasins for hydrologic and hydraulic modelling. The Water Survey of Canada currently operates many active gauges upstream of Brantford within this watershed; however, no active gauges exist on the main channel downstream of the gauge at Brantford (WSC ID 02GB001) to the watershed outlet, near Port Maitland.

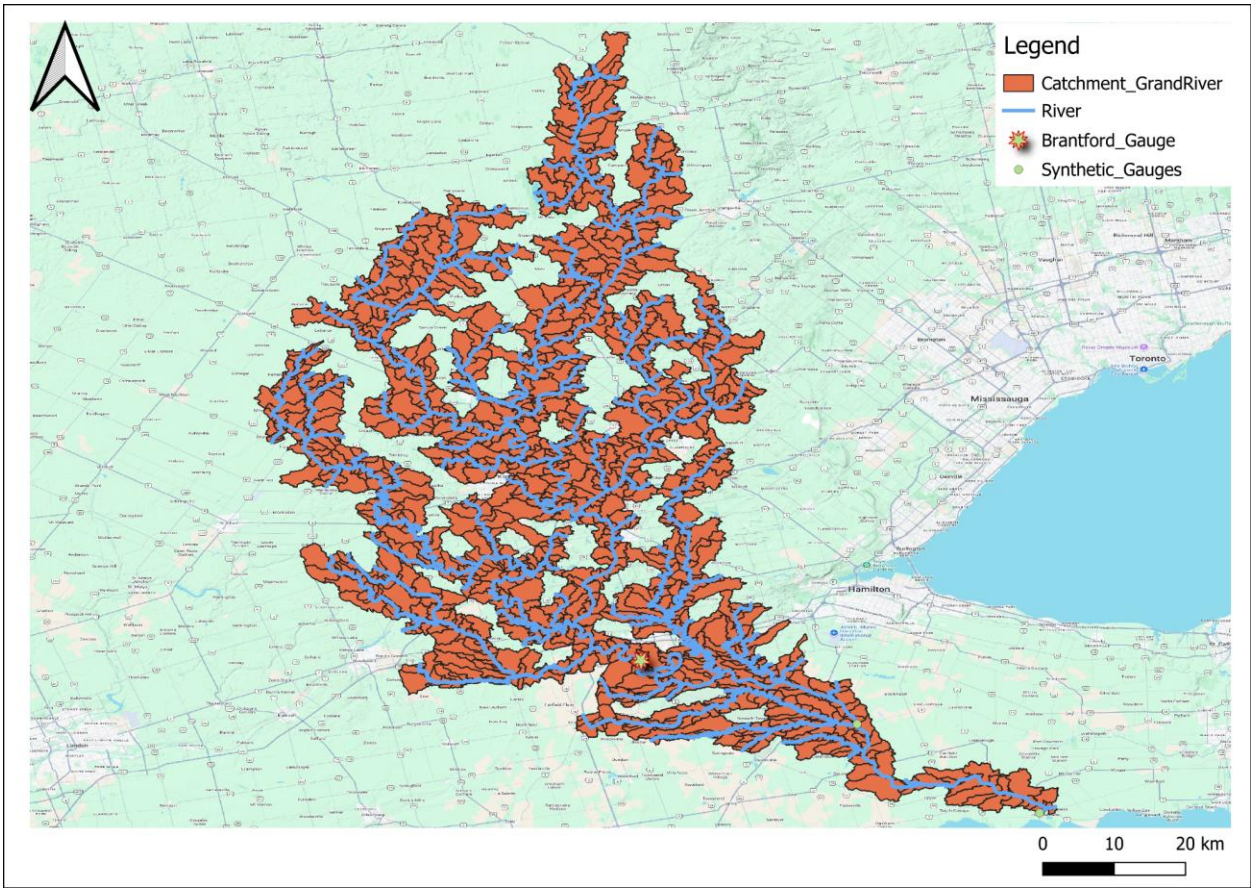

Figure 1: Grand River study area

Hydraulic models are used to translate these flow values into flood extent and depth. Tools such as HEC-RAS (Hydrologic Engineering Center, 2025) simulate river and floodplain hydraulics in both 1D and 2D; however, their application at large spatial scales remains computationally demanding. We look at two problems encountered in these large-scale or regional-scale systems: 1) determining flows in the entire network rather than a small study area, 2) generating inundation mapping for the regional scale in a manner suited to real-time applications. This study applies the Raven (Craig et al., 2020) framework as part of the generation of flows across the large network, and applies the Blackbird hydraulic modelling framework (Chlumsky et al., 2025) for efficient, high resolution flood inundation mapping across the Grand River watershed.

2 METHODOLOGY

This study estimates flow discharges in the Grand River watershed, discretized into 1,744 subbasins, to generate boundary conditions in the Blackbird hydraulic model for large scale flood inundation map. Observed streamflow data were obtained from the Water Survey of Canada hydrometric database via the tidyhydat R package. Flood frequency (FFA) analysis was also conducted at gauged stations with available observations to estimate the discharge values associated with selected return periods. These estimates were then assimilated into Raven to simulate extreme event scenarios within the watershed. The Blackbird model was used to generate flow depths for the Grand River. The results, updated hourly, can be accessed at the Heron Hydrologic - Grand River live page.

To estimate the streamflow at each of the subbasins within the Grand River watershed, synthetic gauges were introduced at specific locations where there are very limited active gauges. One of the synthetic gauges is located at the outlet of the entire watershed and another one between the outlet and Brantford, where a gauged headwater connects to the main channel. These gauges are selected based on their spatial location in the watershed, allowing to estimate discharges at long streams where there are limited observations. Along the main channel, one of the synthetic gauges is located at the watershed outlet, near Port Maitland, allowing to estimate the total discharge for the Grand River watershed. The second synthetic gauge is a discontinued Water Survey of Canada gauge (Station ID: 02GB002), located near York and spatially closer to an active Water Survey of Canada gauge (Station ID: 02GB010).

Using the hydrologic modelling framework Raven, observed streamflow from existing gauges was assimilated at selected locations to generate improved downstream discharge for a given duration. Downstream hydrographs were estimated from the Brantford hydrograph using the drainage area ratio method, a commonly used approach in hydrologic studies for ungauged locations (Archfield and Vogel, 2010), in which discharge is scaled by the ratio of contributing drainage areas.

As Brantford station is the closest gauged station to the Grand River watershed outlet along the main channel, downstream flows were estimated by scaling discharge at Brantford using the ratio of drainage areas.

$$Q_u = Q_g \left(\frac{A_u}{A_g}\right) \tag{1}$$

Q_u is the discharge at ungauged location, Q_g is the gauged discharge, A_u represents the ungauged draining area, while A_g is the drainage area of the gauged location. This approach assumes that meteorological conditions are uniform across the watershed, such that discharges scales proportionally with drainage area.

Discharges under extreme flood conditions were derived using flood frequency analysis (FFA) at the gauged stations for both the 50-year and 100-year return periods. FFA uses historical annual peak flow data to estimate flow values associated with specified return periods. Equation (1) was applied to both the observation data and the FFA quasi steady-state hydrographs. For the observed streamflow, Q_g is the flow at Brantford station while Q_u is the estimated discharge at each of the synthetic gauges. Different statistical approaches can be used to model these extreme events, including the generalized extreme value (GEV) distribution (Jenkinson, 1955) and the Gumbel distribution (Gumbel, 1941). In this study, GEV was adopted. GEV distribution has been widely applied in flood frequency analysis for modelling annual peak discharges and other hydrological extremes (Morrison & Smith, 2002). The resulting flow values were then used to represent extreme flood conditions across the watershed for the hydraulic model. For the flood scenarios, flood frequency analysis was conducted by extracting annual maximum daily discharge series from observed flows and fitting a GEV distribution using the extRemes package in R. Using the maximum

likelihood, model parameters were estimated and return period discharges were derived from the distribution. The 100-year return period discharges were used as quasi steady-state input in Raven for the model duration. Similar to observation data, these flows were assimilated at upstream gauges, and discharges at the synthetic gauges were estimated by scaling flows from the Brantford according to their respective drainage areas.

For the hydraulic model, Blackbird was used due to its efficiency in large scale flood inundation mapping while retaining the accuracy of more computationally expensive hydrodynamic models. In this study, Blackbird applies the Geospatially Augmented Standard Step (GASS) method, which integrates a steady-state model using the standard step method, Height Above Nearest Drainage (HAND) approach to determine cells inundation status based on calculated downstream depth, and the calculation of reach-integrated hydraulic properties within the same framework (Chlumsky et al., 2025). During Blackbird's preprocessing workflow, input datasets including a digital elevation model (DEM), channel geometry, and a Manning's roughness layer are used to derive flow direction, flow accumulation, HAND rasters, and streamnodes. Channel bathymetry was generated using the inverse hydraulic modelling approach of Choné et al. (2021), which uses a combination of flow measurements and timely LiDAR data to estimate the bathymetry of the channel. This bathymetry was incorporated into the DEM to ensure that the channel bathymetry and channel capacity was well-represented.

Flow depths at each streamnode are then computed by Blackbird using the standard step method based on boundary conditions derived from the Raven hydrologic modelling framework for the 100-year return period. The streamnodes used in Blackbird and the subbasins in Raven were one in the same, making the integration of flows into Blackbird straightforward. The post-processing stage consists of interpolating these depths along river reaches and mapping inundation extents, identifying connected areas that are subject to flooding. The resulting flood inundation map is compared to the Grand River Conservation Authority's map as discussed in Section 3.

3 RESULTS AND DISCUSSION

The approach of scaling flows relative to their drainage areas was applied due to the lack of active gauges downstream of Brantford, on the Grand River along the main channel. This approach was first tested on stations where observation data was available, by assimilating observations upstream of the station of interest and evaluating the resulting hydrograph along with the observed hydrograph. From Figure 2 below, the observed hydrographs closely match flows scaled from subbasin 965 at subbasin 819 (located near Cambridge).

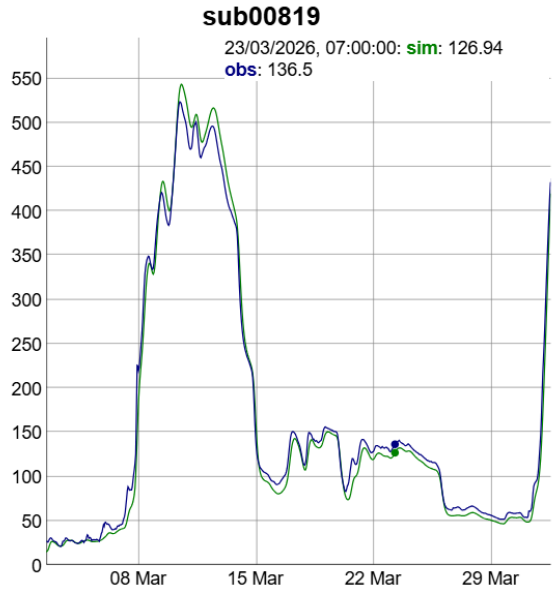

Figure 2 - scaled hydrograph vs observations at subbasin 819

Scaling the synthetic stations' flows at subbasins 229 and 007 (outlet) based on Brantford observed flows resulted in hydrographs presented in Figure 3 and Figure 4, respectively. Peak flows increased downstream, which is expected as the drainage areas are higher, as it was assumed that precipitation is distributed uniformly across the portion of the watershed covered by the synthetic gauges.

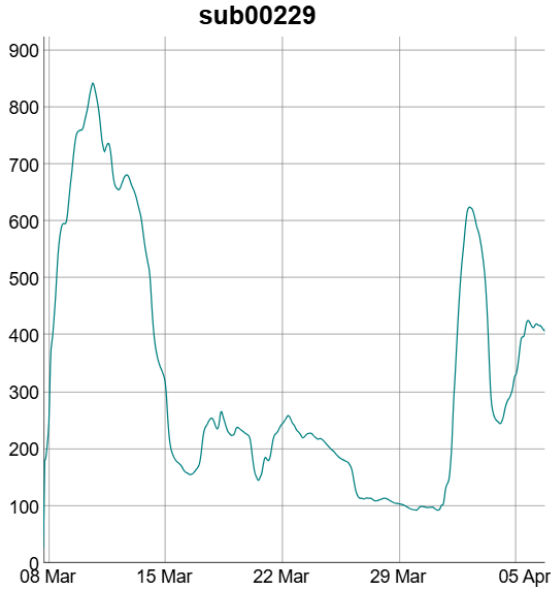

Figure 3 - Hydrograph at the synthetic gauge 2

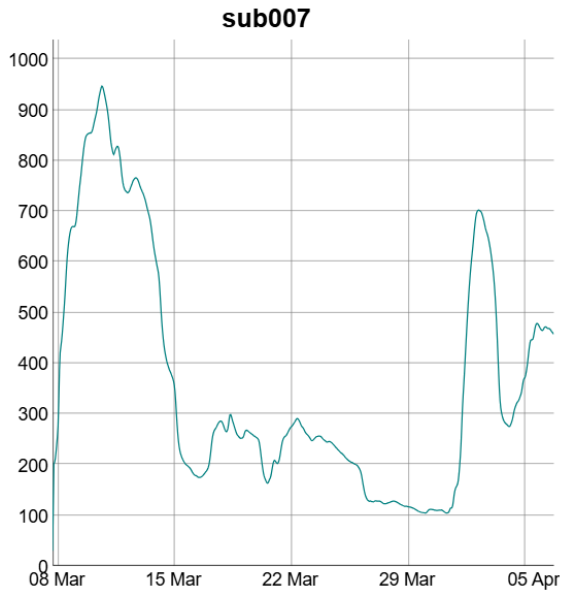

Figure 4 - Hydrograph at the watershed outlet (synthetic gauge 1)

Applying the 100-year flow values as boundary conditions in Blackbird model allowed to compute flow depth at each streamnode, which were then interpolated along the river reaches to generate continuous inundation depths and to create and corresponding flood extents. The Blackbird hydraulic model completed the simulation and map output of the entire watershed in approximately 2 minutes, demonstrating its computational efficiency for regional and large-scale flood mapping. The resulting inundation map was compared to the Grand River Conservation Authority (GRCA) regulatory floodplain for validation in some key areas. GRCA floodplain delineates areas susceptible to flooding based on engineered studies, observations, and mapping analysis to represent regulatory floodplain defined as the greater of 100-year event and the regional storm (Hurricane Hazel rainfall) (Grand River Conservation Authority, 2025). Figure 5 shows the GRCA floodplain map for New Hamburg and the Blackbird model output for comparison, two locations which are know to be susceptible to riverine flooding in the Grand River watershed.

Figure 5 - GRCA regulatory floodplain and Blackbird model output at New Hamburg

Similarly, inundation maps from the GRCA regulatory floodplain maps and the Blackbird model were compared at Brantford, as shown in Figure 6.

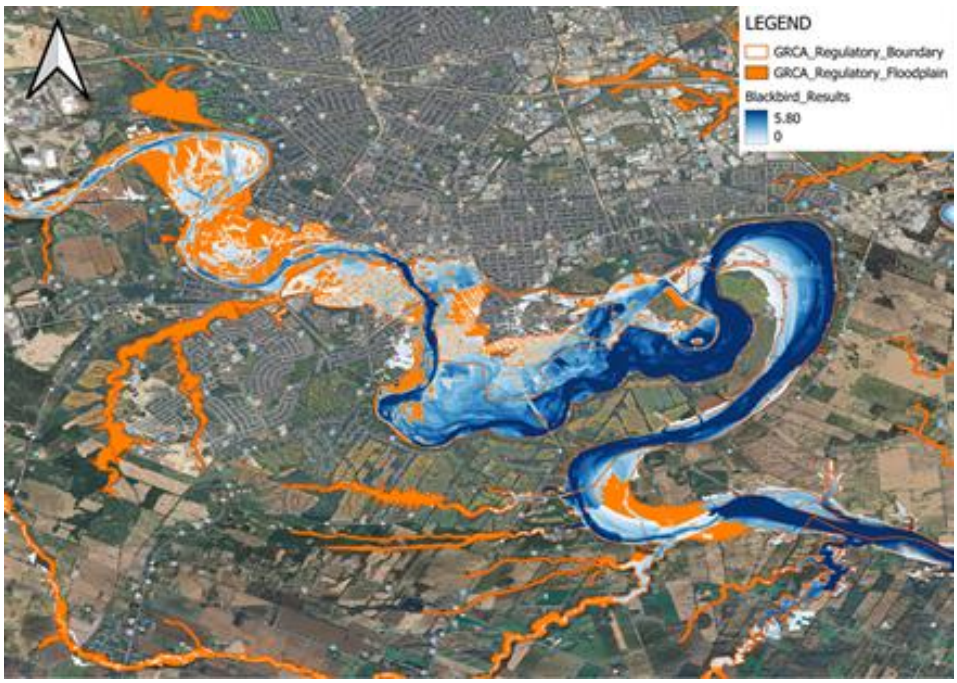

Figure 6 - GRCA regulatory floodplain and Blackbird model output at Brantford

Results from the Blackbird hydraulic model show similarities with the Grand River Conservation Authority (GRCA) regulatory floodplain maps in terms of spatial flooding patterns within the presented watershed. However, the GRCA floodplain maps indicate a greater flood extent compared to the Blackbird model. This difference is expected as the model results relied only on the estimated 100-year flow events, while the regulatory maps included both regional Storm and the 100-year event. Despite differences in flow inputs, results from 100-year estimated flows, used as boundary conditions in Blackbird, remain largely within the regulatory boundary. This indicates the potential alignment of the Blackbird and GRCA regulatory floodplain if consistent flows and conditions were applied. In addition, some differences may be attributed to ongoing refinements in the bathymetry and drainage network, where smaller channels and flow paths may not yet be fully included in the current study.

Blackbird's capacity to efficiently simulate such a large area highlights its potential for not only regional flood mapping, but also near real-time simulations, where the model outputs can be updated dynamically using incoming hydrometric data, with hydrologic model outputs from Raven serving as boundary conditions. This is demonstrated in Figure 7, where the real-time gauge conditions were run through Blackbird for a portion of the model near Waldemar, ON on March 10 during snowmelt-driven high streamflow conditions.

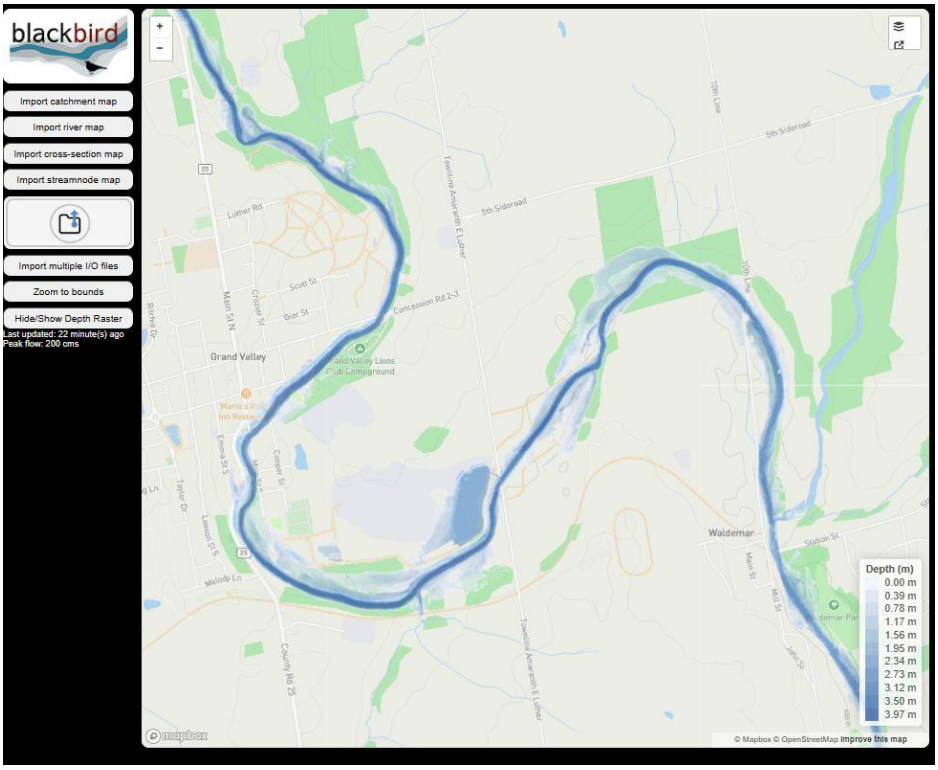

Figure 7 - Real-time simulated flood depths near Waldemar, ON, on Heron's interactive portal

The value and potential of a real-time inundation system is demonstrated, including the possibility of up-to-date spatial information on possible flood depths during flood conditions. This is more actionable information than general warnings of high waters that are often issued, and represents the possibility of more granular information to forecasters and the public alike.

4 CONCLUSION

This project applies the Blackbird hydraulic modelling framework, in combination with hydrologic outputs from Raven, to generate flood large scale inundation maps across the Grand River watershed of approximately 6,800 km^2. Using the 100-year flow estimates as boundary conditions, inundation extents with corresponding depths were produced over the 1,744 subbasins and compared with Grand River Conservation Authority (GRCA) regulatory flood map. The inundation map is calculated and produced in just two minutes, compared to the many days that would be required to run a model with the same computational resources for a 2D hydraulic model at this scale.

The comparison shows consistent spatial patterns, with larger extents observed in the GRCA regulatory maps due to different flow input, where the present model used only estimated 100-year flows while regulatory maps incorporated regional storms in addition to the 100-year event. Ongoing work to improve the model inputs may also reduce these discrepancies. Flood depths results from the discussed framework are presented through a web format, with live updates, demonstrating the potential for such a system to provide up-to-date information on flood depths to both forecasters and the public.

5 REFERENCES

Archfield, S. A., & Vogel, R. M. (2010). Map correlation method: Selection of a reference streamgage to estimate daily streamflow at ungaged catchments. *Water Resources Research*, *46*(10). https://doi.org/10.1029/2009WR008481

Chlumsky, R., Craig, J. R., & Tolson, B. A. (2025). A reach-integrated hydraulic modelling approach for large-scale and real-time inundation mapping. *Geoscientific Model Development*, *18*(11), 3387–3403. https://doi.org/10.5194/gmd-18-3387-2025

Choné, G., Biron, P. M., Buffin-Bélanger, T., Mazgareanu, I., Neal, J. C., & Sampson, C. C. (2021). An assessment of large-scale flood modelling based on LiDAR data. Hydrological Processes, 35(8), e14333. https://doi.org/10.1002/hyp.14333

Craig, J. R., Brown, G., Chlumsky, R., Jenkinson, R. W., Jost, G., Lee, K., Mai, J., Serrer, M., Sgro, N., Shafii, M., Snowdon, A. P., & Tolson, B. A. (2020). Flexible watershed simulation with the Raven hydrological modelling framework. *Environmental Modelling & Software*, *129*, 104728. https://doi.org/10.1016/j.envsoft.2020.104728

Grand River Conservation Authority. (2025). https://data.grandriver.ca/metadata/?id=2394

Gumbel, E. J. (1941). The Return Period of Flood Flows. *The Annals of Mathematical Statistics*, *12*(2), 163–190. https://doi.org/10.1214/aoms/1177731747

Hydrologic Engineering Center. (2025). HEC-RAS Documentation. https://www.hec.usace.army.mil/confluence/rasdocs

Jenkinson, A. F. (1955). The frequency distribution of the annual maximum (or minimum) values of meteorological elements. *Quarterly Journal of the Royal Meteorological Society*, *81*(348), 158–171. https://doi.org/10.1002/qj.49708134804

Morrison, J. E., & Smith, J. A. (2002). Stochastic modeling of flood peaks using the generalized extreme value distribution. *Water Resources Research*, *38*(12), 41-1-41–12. https://doi.org/10.1029/2001WR000502

Chapter 2 - Flood risk assessment, data and modeling

2.3 Use of emerging data sources

ICFM 10
Adapting to Global Change:
Innovative Approaches to Flood Management and Resilience
May 20-22, 2026 | Western University, London, Ontario, Canada

Building large-scale flood defence datasets using open data

Podt, M.[1,2], Bron, C.[1], den Heijer[1], F.[1], Rijke, J.S.[1,2]
HAN University of Applied Sciences, Ruitenberglaan 26, 6826 CC Arnhem, The Netherlands[1]
Delft University of Technology, Mekelweg 5, 2628 CD Delft, The Netherlands [2]
E-mail: maarten.podt@han.nl

ABSTRACT

Reliable technical data are essential for flood defence asset management, yet such data are often fragmented across organisations, technologies, and lifecycle stages. While recent advances in data collection technologies have increased data availability, they have also amplified heterogeneity in data formats, ownership, and resolution, shifting the dominant challenge from data acquisition to data integration. Existing national and international flood defence datasets primarily focus on basic asset location and administrative attributes, while detailed technical information required for engineering analysis remains largely absent.

This paper presents a reproducible workflow for building large-scale technical datasets for earthwork levees using open and publicly available data. The workflow is structured around three core components that together form a technical representation of earthwork levees: (1) geometry, (2) construction, and (3) subsurface. Geometry is reconstructed from high-resolution digital elevation models by extracting kink lines that capture slope transitions along the levee body. Construction is derived from cone penetration test data by interpreting soil behaviour types and mapping material composition onto levee geometries. Subsurface characteristics are integrated by converting volumetric geological models into point-based representations suitable for geospatial analysis. Data preparation and processing are automated using GIS and Python-based workflows to support scalability and future updates.

Although demonstrated using national-scale datasets from the Netherlands, the workflow relies on data sources and processing steps that are widely available. By building technical levee components independently from fragmented organisational data structures, the proposed workflow provides a scalable foundation for improving data availability and consistency in flood defence asset management and supports more data-driven assessment, maintenance, and reinforcement decisions.

KEYWORDS: flood defence, asset management, geotechnics, digital transformation, data management

1 INTRODUCTION

Flood defence data are among the most important assets within flood defence asset management. Technical, performance, and condition data underpin decisions on *if*, *when*, and *how* flood defences require assessment, maintenance or reinforcement. This dependency is widely understood, and flood defence asset managers worldwide invest in digital transformation and data-driven decision making.

Flood defences are often located in public space, fulfil multiple societal functions, and are governed and financed by combinations of national, regional and local governments, and in some cases public-private partnerships. This multi-functional, multi-actor, and multi-financed configuration disperses asset management responsibilities across multiple organisations (den Heijer et al., 2023). Although flood safety as the shared goal, these organisations operate under different mandates, incentives, and financing structures. Consequently, flood defence data are produced by different actors for different purposes and are embedded in different organisational contexts, which limits their alignment in a single asset management logic. Organisational diversification therefore is a structural driver of data fragmentation.

In parallel, the flood defence sector has seen rapid advancements in data collection technologies, including satellite observations (Destefanis et al., 2025), unmanned aerial vehicles (Minh, 2025), and in situ sensor networks (Tao et al., 2024). These developments have led to a significant increase in heterogenous data formats, spatial and temporal resolutions, update frequencies, and ownership (Cohen et al., 2025; Towe et al., 2020). As a result, the dominant challenge has been shifting from data acquisition to data integration (Borowicc & Alves-Souza, 2024). Many technological initiatives remain pilot-based, with limited attention paid to integration across the full data lifecycle (Podt & Rijke, 2024). Technological diversification therefore is a structural driver of data fragmentation.

In this paper, data fragmentation is understood as the unintentional misalignment of flood defence data across organisational, technical, and lifecycle dimensions, resulting in incoherent technical asset representations. This fragmentation makes data less accessible, less consistent, and less accurate. Data fragmentation in flood defence management is widely recognised in practice but rarely explicitly described in literature. Empirical studies report fragmentation in different contexts. Vincke et al. (2019) describe how Flemish levee data are stored in separate, disconnected databases with limited GIS integration and a lack of agreed standards for new monitoring campaigns (Vincke et al., 2019). At a governance level, Mohanty et al. (2020) document how intergovernmental distrust and concerns over data reliability hinder the sharing of flood damage data in India (Mohanty et al., 2020). Similarly, Cohen et al. (2025) show how limited access to flood-related data in Colombia is linked to weak institutional data management practices (Cohen et al., 2025). This grasp of studies illustrate that data fragmentation is a recurring and multifaceted challenge in flood defence management.

Several international initiatives have sought to address data fragmentation through data harmonisation. In the AIMS Spatial Flood Defences project, the UK Environmental Agency runs a daily updated open dataset containing the centreline geometries and metadata of flood defence assets (EA, 2025). Comparable initiatives are the Dutch Basisbestand Primaire Waterkeringen, which provides information on asset location, safety standards, and assessment results (IHW, 2025), and the National Asset Database Wales, which harmonises data on levee type, location, ownership, and maintenance responsibility.

Despite these efforts, existing datasets typically focus on asset location and basic administrative attributes, while the technical characteristics remain largely absent. Although large-scale data harmonisation is feasible, many countries still lack a national, uniform, and publicly accessible technical flood defence dataset. This paper therefore presents a workflow to extract data on the geometry, construction, and subsurface characteristics of earthwork levees from open datasets, providing a technical asset representation that is largely independent of fragmented organisational data structures.

2 METHODS

This section presents a reproducible workflow to reconstruct technical characteristics of earthwork levees from open geospatial datasets. The workflow is structured around three core components that together form a technical representation of earthwork levees: geometry, construction, and subsurface. Although the workflow is demonstrated using national-scale datasets from the Netherlands, all processing steps are transferable to other contexts with comparable data availability, and comparable international datasets are indicated where relevant. The methodology combines geospatial processing of elevation data, cone penetration test data, and lithological subsurface data derived from datasets that are often open, public, and FAIR. Widely available spatial analysis toolboxes within GIS software are used to ensure replicability, with key tools and algorithms indicated in italics (e.g. *Polygon to Line*). Data preparation and processing steps are automated using Python scripts to support scalability and for future updates. Throughout the workflow, a distinction is made between vector data, represented as points, lines, and polygons, and raster data, represented as pixel-based surfaces.

2.1 Component 1: Geometry

Component 1 reconstructs the geometry of earthwork levees by extracting slope transitions from digital elevation models and representing these transitions as kink lines along the levee body. The geometry of a levee can be observed using a digital elevation model (DEM), a digital representation of the surface's topography. In geomatics, such surfaces are often represented as a 'raster'. DEMs are useful for querying specific elevation data, such as extracting cross-sections of a levee. DEMs only contain elevation data and lack zone-specific data, such as crest-width and the presence of berms or ramps. Digital identification of levee zones is important for precise geometry extraction and for enriching inspection data with zone context. For example, communicating that a crack is detected on an inner-berm rather than relying solely on coordinates.

A typical earthwork levee consists of seven zones: the foreland (1), outer-berm (2), crest (3), inner-berm (4), hinterland (5), seepage ditch (6), and the slopes connecting them (7). These zones can be categorised into flat and steep surfaces, where each zone boundary is defined by a kink line formed at a slope transition. That same typical earthwork levee subsequently has six unique kink lines: the outer toe (OT), outer berm (OB), outer crest (OC), inner crest (IC), inner berm (IB), and inner toe (IT). The outer and inner toes and crests each occur once, whereas berm kink lines may occur multiple times depending on the number of berms (e.g. OB_1, OB2, …, OBn).

For the identification of zones and kink lines, the highest resolution DEM available should be used. High-resolution DEMs are typically distributed as tiled raster datasets due to their size. For efficient processing, only tiles intersecting the levee footprint are selected and combined into a *mosaic* raster. To minimise storage requirements and computational load in subsequent analyses, each tile is *clipped* to the spatial extent of the levee prior to mosaicking. In the present implementation, this tile selection and clipping procedure is automated using a Python-script that takes a vector feature of the levee footprint as input, retrieves all intersecting DEM tiles from a selected public elevation database, and *clips* them into efficiently sized levee specific rasters. The input vector feature is an approximate levee footprint created from buffered flood defence centrelines, as described in Component 2.

DEMs often miss pixels due to water surfaces or dense features that the sensor could not penetrate. Before performing geometric extraction, these 'voids' should be corrected using an *elevation void fill* algorithm within a GIS environment. Kink lines can then be extracted by converting the DEM into a slope raster. Using a *Slope* algorithm, each elevation cell in the DEM is converted into a slope value that represents the rate of elevation change in degrees within its neighbourhood, typically a 3x3 cell window. The resulting slope raster can be classified into two categories: flat and steep surfaces. Levee slopes generally range between 1:3 to 1:5. While surfaces with slopes less steep than 1:5, or 11.3°, might not appear entirely flat, this threshold effectively identifies gentle transitions, such as ramps (Figure 1). Because optimal slope thresholds vary with local levee morphology, the classification should be locally

calibrated rather then globally defined. In other words, assign slope thresholds to levee trajectories rather than one slope threshold for the whole dataset.

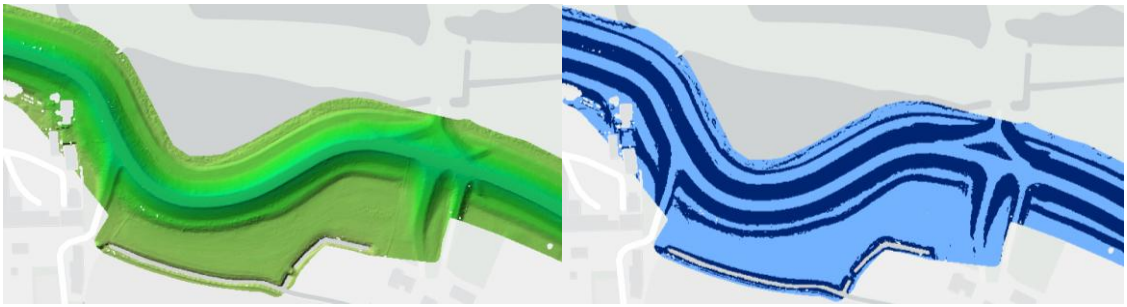

Figure 1 Digital elevation model of an earthwork levee visualised as hillshade (left) and corresponding classified slope raster distinguishing flat and steep surfaces for kink line extraction (right)

After classification of the slope raster, the slope transitions become visible but remain non-interactive. To convert these transitions into useable vector features, the slope raster must be *reclassified* into a binary raster storing integer values. Vector features can only be generated from integer-based raster data within GIS.

Although it might seem logical to extract line features directly from this binary raster, it is advised to first perform a *raster to polygon* conversion with a simplified polygon output. Simplification ensures that the polygons are smoothed rather than constrained by the grid structure of the raster cells, which would otherwise produce blocky edges. Polygon features allow for attribute selection and filtering based on area, unlike line features. To remove noise and minor artifacts that clutter kink lines, polygons smaller than 100m² are selected by attribute and *eliminated* by largest shared area. The results is a smoothed, less-cluttered polygon layer that presents kink-lines already quite well.

The next step in this workflow is to apply a polygon simplification algorithm to reduce feature complexity and eliminate sharp angularities introduced by the raster grid, which do not correspond to real-world geometry. For this purpose, the *bend simplification* (Wang & Müller, 1998) algorithm is particularly well suited, as it preserves geometric characteristics while removing redundant vertices and smoothing non-critical deviations. A simplification tolerance of 8 meters gives clean results. A higher tolerance risks cutting of ramp transitions. During simplification, make sure to resolve topological errors.

The kink lines derived from the DEM now reveal the levee geometry (Figure 3). While these kink lines correspond to features such as crests, berms and toes, the current workflow does not yet assign semantic labels to individual lines. Although humans can reason which line is which, an untrained computer cannot yet make this distinction. Moreover, access ramps cause kink lines associated with different zones to be geometrically connected, for example the crest being connected to the hinterland. This presents challenges for analyses that require computation of distinct features, such as determining crest widths.

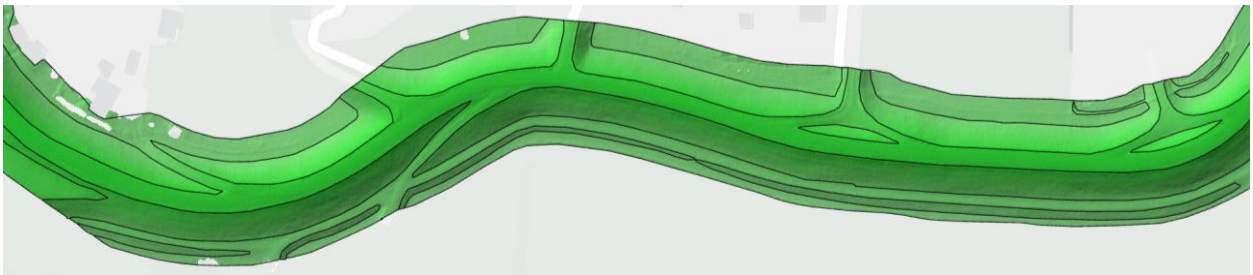

Figure 2 Kink lines extracted from a digital elevation model, representing slope transitions that define the geometry of an earthwork levee

2.2 Component 2: Construction

Component 2 reconstructs the construction of earthwork levees by interpreting material composition from cone penetration tests (CPTs) and mapping interpreted soil types onto levee geometries. The construction of earthwork levees is characterised primarily by its material composition and, where present, additional reinforcement structures such as sheet piles or geotextiles. Data on material composition are generally more extensive and systematically available than data on reinforcement elements, which are often site-specific and inconsistently represented across regional datasets.

Data on material composition are typically obtained from boreholes, which provide lithological descriptions, or CPTs, which record cone tip resistance, sleeve friction, and sometimes pore water pressure. CPTs are generally far more numerous than boreholes due to their practicality and cost-effectiveness and provide high vertical resolution measurements. However, CPTs do not directly indicate soil types and therefore require interpretation. In this workflow, soil types are interpreted using the normalised Soil Behaviour Type (SBTn) chart proposed by Robertson (1990), which provides a widely accepted baseline for translating CPT measurements into material classes. In addition, the authors' soil type interpretation allows for more classification ambiguity in the context of flood defence applications (Figure 3). Distinctions between closely related classes such as 'sand mixtures', 'clean and silty sands', and 'silt mixtures' are of limited practical relevance for large-scale levee characterisation and may introduce unnecessary complexity. It should be noted that the underlying CPT parameters remain unchanged. While artificial neural networks are increasingly applied to capture local soil nuances, these methods typically require extensive training data and site-specific calibration. The SBTn approach therefore offers a robust and reproducible baseline suitable for large-scale and transferable applications.

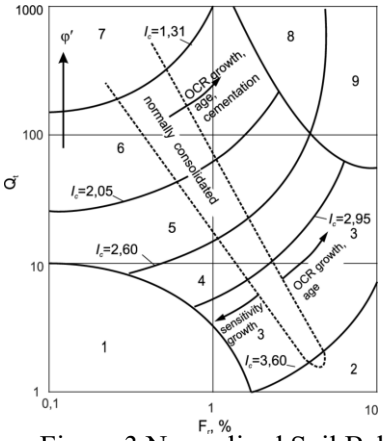

SBTn code	Robertson interpretation	Authors' interpretation	Hex code
-1	No-data	No-data	#E0E0E0
1	Sensitive fine grained	Sensitive clay	#D3956F
2	Clay organic	Peat	#8B4513
3	Clay & silty clay	Clay	#4B9B5E
4	Silt mixtures	Silt/loam	#A9DB7B
5	Sand mixtures	Clayey sand	#E4D449
6	Sand mixtures	Sand	#FFE600
7	Dense to gravelly sand	Gravelly sand	#D4B36D
8	Stiff sand to clay sand	Compact sand	#9E8E75
9	Stiff fine grained	Compact clay	#9E8E75

Figure 3 Normalised Soil Behaviour Type chart (Robertson, 1990) with adapted soil type interpretations for flood defence characterisation

CPT data are collected from national geological survey databases (e.g. BRO, DOV, NADAG, Jupiter GEUS), where they are stored in SQL-readable format. These databases are developed for interdisciplinary research purposes and therefore extend well beyond levee footprints. To associate CPTs with levee bodies, CPT locations are spatially *clipped* using buffered flood defence centrelines, which are available in the national basic flood defence datasets as mentioned in the Introduction. *Buffer* widths are manually selected based on observed footprint, with difference often between levee types (i.e. coastal, fluvial, urban). In the Dutch implementation, buffer widths ranging from approximately 20 to 100 m are applied, depending on levee type and in a satellite map observed footprint. River flood defences typically use buffer widths of around 40 m, while coastal and estuarine flood defences require wider buffers of approximately 80 m. In the current implementation, buffer distances are manually defined, but this buffer step will be replaced by the derived toe lines once available from Component 1.

CPT measurements are typically recorded at high vertical resolution (often at 2 cm intervals), with cone resistance and sleeve friction stored as depth-indexed records in SQL-readable databases. A Python-

based workflow processes these data by (1) computing derived CPT parameters, (2) assigning soil behaviour types using the normalised Soil Behaviour Type (SBTn) chart, and (3) filtering records that are outdated or lie below current levee geometry and therefore indicate CPT before reinforcement. CPT measurements located below the toe elevation derived from Component 1 can be excluded to distinguish levee construction materials from deeper subsurface stratigraphy. The workflow produces a classified, depth-resolved representation of levee material composition and generates scalable vector graphics (SVG) profiles of interpreted soil types for visual integration with the DEM cross section (Figure 4).

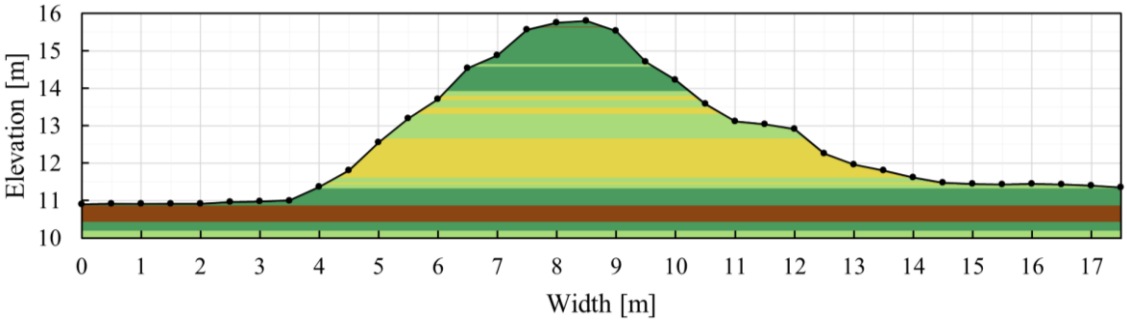

Figure 4 Levee cross-section with soil type interpretation referenced beneath the surface profile extracted from a digital elevation model

2.3 Component 3: Subsurface

Component 3 reconstructs subsurface characteristics beneath earthwork levees by translating volumetric lithological models into point datasets that are suitable for geospatial and geotechnical analysis. Subsurface soil composition is commonly represented in three-dimensional lithological models that integrate borehole and CPT data. These models are often constructed as voxel models (e.g. GeoTOP, DK Model) or volumetric grids (e.g. BGS LithoFrame, USGS Hydrogeological Framework). In many countries, such datasets are provided by national geological surveys and extend to depths of approximately 30 - 50 m below ground level. Although these volumetric datasets store lithological information for each voxel, most GIS environments offer limited support for voxel processing. For spatial integration with levee geometry and construction data from previous components, a volumetric-to-point workflow is therefore applied.

In this workflow, volumetric subsurface models are accessed in NetCDF format via OPeNDAP services are converted into point datasets by extracting the centroid coordinates and lithological attributes of individual voxels. This conversion is performed using a custom Python script (*Compress Voxels*), which compresses the three-dimensional voxel grid into depth-referenced point features. The workflow additionally supports mapping lithological classes from the voxel model to the soil type interpretations used in Component 2, for consistent soil type classes between construction and materialisation. The resulting point datasets (e.g. .csv or .xyz) can be imported into GIS as XY point data, assigned to the appropriate coordinate reference system, and subsequently queried, clipped, and spatially intersected with levee geometries from Component 1.

Figure 5 illustrates a sample of the resulting point dataset, including a visualisation where half of the points are rendered as voxel cells to reflect their volumetric origin (left). The associated attribute table (right) demonstrates the advantage of a point dataset approach: lithological information is stored as depth-referenced records with soil types organised in a single attribute column. This structure enables straightforward identification of aquifer depths, layer thicknesses, and stratigraphic transitions, which can be used in seepage and piping-related risk studies.

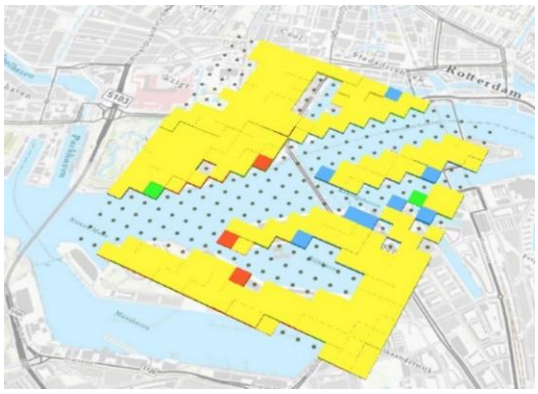

Point_ID: 48815 xy: 170100,435000 (centroid of voxel)	
Depth below surface [m]	**Soil type interpretation**
0	Peat
-0.5	Clay
-1.0	Clay
-1.5	Gravelly sand
-2.0	Sand
…	…
-50.0	Sand

Figure 5 Point dataset representation of the GeoTOP voxel model with selected points rendered as volumetric cells to illustrate voxel origin (left), and corresponding attribute table (right) showing depth-referenced soil types

3 CONCLUDING DISCUSSION

This paper addresses data fragmentation in flood defence asset management by demonstrating how technical characteristics of earthwork levees can be reconstructed at scale from open data. The proposed workflow reduces the impact of fragmented and dispersed data ownership and asset management structures. The workflow complements existing flood defence asset management with technical data that is currently absent in many national contexts.

A key strength of the approach lies in its modular structure. By separating geometry, construction, and subsurface into distinct but interoperable components, the workflow allows heterogeneous data sources to be integrated through shared spatial references rather than through harmonised data governance arrangements. Although not shown explicitly in a single figure, the geometry, construction, and subsurface components are spatially consistent and can be directly combined into integrated levee cross-sections where required. This makes the method particularly suited to contexts where flood defence data are distributed across multiple organisations and collected for different purposes. Although developed and demonstrated using Dutch datasets, digital elevation models, cone penetration tests, and geological models are widely available in many contexts, supporting transferability beyond this study.

At the same time, several limitations should be acknowledged. The geometry component extracts kink lines that capture slope transitions but does not yet assign semantic labels such as crest, berm, or toe. Similarly, construction is reconstructed from CPT-based soil interpretations that remain approximations due to material heterogeneity. These limitations reflects deliberate scope choices and point to opportunities for future refinement, including automated zone identification, improved footprint delineation, and advanced material interpretation that incorporates local nuances.

Overall, this study shows that flood defence data availability does not require complete institutional harmonisation. By using open data and reproducible geospatial workflows, it is possible to build large-scale technical flood defence datasets that are available to all. The proposed workflow is currently being further developed as a web-based application in the Netherlands (visit Dijkatlas.com or Dikeatlas.com), and both the methodology and underlying code are being refined to support application in other national contexts.

4 REFERENCES

Borowicc, S., & Alves-Souza, S. (2024). Heterogeneous Data Integration: A Literature Scope Review: *Proceedings of the 26th International Conference on Enterprise Information Systems*, 189–200. https://doi.org/10.5220/0012551000003690

Cohen, J., Mdee, A., Trigg, M., Singhal, S., Cooper, S., Alemu, A., Seifu, E., Lee, C., Bernhofen, M., Bhave, A., Carr, A., C T, D., Haile, A., Pencue-Fierro, L., Sa'adi, Z., Shukla, P., & Solano Correa, Y. (2025). A Politics of Global Datasets and Models in Flood Risk Management. *Water Alternatives*, *18*, 305–329.

den Heijer, F., Rijke, J., Bosch-Rekveldt, M., de Leeuw, A., & Barciela-Rial, M. (2023). Asset management of flood defences as a co-production—An analysis of cooperation in five situations in the Netherlands. *Journal of Flood Risk Management*, *16*(3), e12909. https://doi.org/10.1111/jfr3.12909

Destefanis, T., Guliyeva, S., Boccardo, P., Fissore, V., Destefanis, T., Guliyeva, S., Boccardo, P., & Fissore, V. (2025). Advancing Flood Detection and Mapping: A Review of Earth Observation Services, 3D Data Integration, and AI-Based Techniques. *Remote Sensing*, *17*(17). https://doi.org/10.3390/rs17172943

EA. (2025). *AIMS Spatial Flood Defences*. https://data.europa.eu/data/datasets/aims-spatial-flood-defences-inc-standardised-attributes?locale=en

IHW. (2025). *Nationale Basisbestanden Primaire Waterkeringen*. https://www.nationaalgeoregister.nl/geonetwork/srv/dut/catalog.search#/metadata/9bc22d59-427f-45c9-9f55-7dbe3985a73c

Minh, D. T. (2025). A comprehensive overview on UAV-based applications for flood management. *Measurement Science and Technology*, *36*(8), 086006. https://doi.org/10.1088/1361-6501/adf871

Mohanty, M. P., Mudgil, S., & Karmakar, S. (2020). Flood management in India: A focussed review on the current status and future challenges. *International Journal of Disaster Risk Reduction*, *49*, 101660. https://doi.org/10.1016/j.ijdrr.2020.101660

Robertson, P. K. (1990). Soil classification using the cone penetration test. *Canadian Geotechnical Journal*, *27*(1), 151–158. https://doi.org/10.1139/t90-014

Tao, Y., Tian, B., Adhikari, B. R., Zuo, Q., Luo, X., & Di, B. (2024). A Review of Cutting-Edge Sensor Technologies for Improved Flood Monitoring and Damage Assessment. *Sensors*, *24*(21), 7090. https://doi.org/10.3390/s24217090

Towe, R., Dean, G., Edwards, L., Nundloll, V., Blair, G., Lamb, R., Hankin, B., & Manson, S. (2020). Rethinking data-driven decision support in flood risk management for a big data age. *Journal of Flood Risk Management*, *13*. https://doi.org/10.1111/jfr3.12652

Vincke, L., Visser, K. P., Peeters, P., & Leus, B. (2019). Dike Data Management in Flanders. *Proceedings of the XVII European Conference on Soil Mechanics and Geotechnical Engineering*, *Geotechnical Engineering, foundation of the future*, 1387–1393. https://doi.org/10.32075/17ECSMGE-2019-0261

Wang, Z., & Müller, J.-C. (1998). Line Generalization Based on Analysis of Shape Characteristics. *Cartography and Geographic Information Systems*, *25*(1), 3–15. https://doi.org/10.1559/152304098782441750

ICFM 10
Adapting to Global Change:
Innovative Approaches to Flood Management and Resilience
May 20-22, 2026 | Western University, London, Ontario, Canada

Urban Flood Prediction Using Products based on Weather Radar Data

Anaí Floriano Vasconcelos[1], Maria Clara Fava[2], Marina Fagundes e Souza[3], Vandoir Bourscheidt[4], Bruno César dos Santos[5], Helber Custódio de Freitas[6], Queren Priscila da Silva[7] and Demerval Soares Moreira[8]

Department of Environmental Sciences, Federal University of São Carlos, Washington Luis Road, km 235, São Carlos, Brazil[1]
E-mail: anai.vasconcelos@ufscar.br

Department of Civil Engineering, Federal University of São Carlos, Washington Luis Road, km 235, São Carlos, Brazil[2]
E-mail: mcfava@ufscar.br

Graduate Program in Urban Engineering, Federal University of São Carlos, Washington Luis Road, km 235, São Carlos, Brazil[3]
E-mail: marina.fagundes@estudante.ufscar.br

Department of Environmental Sciences, Federal University of São Carlos, Washington Luis Road, km 235, São Carlos, Brazil[4]
E-mail: vandoir@ufscar.br

Department of Environmental Sciences, Federal University of São Carlos, Washington Luis Road, km 235, São Carlos, Brazil[5]
E-mail: bcsantos@ufscar.br

Department of Physics and Meteorology, São Paulo State University, Eng. Luiz Edmundo Carrijo Coube Avenue, 14-01, Bauru, Brazil[6]
E-mail: helber.freitas@unesp.br

Department of Physics and Meteorology, São Paulo State University, Eng. Luiz Edmundo Carrijo Coube Avenue, 14-01, Bauru, Brazil[7]
E-mail: queren.silva@unesp.br

Department of Physics and Meteorology, São Paulo State University, Eng. Luiz Edmundo Carrijo Coube Avenue, 14-01, Bauru, Brazil[8]
E-mail: demerval.moreira@unesp.br

ABSTRACT

Urban floods generate economic and social impacts. Due to the characteristics of urban basins, intense rainfall causes flash floods and the spatial variability of rainfall leads to very diverse responses from the basin in terms of flooding. Urban flooding forecasting is usually carried out based on precipitation forecasts and hydrological and hydrodynamic modeling. However, the urban basin specificities mean that common weather forecasts do not meet the temporal and spatial scales required for accurate flash flood prediction. To solve this problem, a more precise precipitation forecast is needed, with higher spatial and temporal resolution. Nowcasting based on radar data can address these issues. In this context, this study aimed to evaluate the accuracy of urban flooding forecasting based on hydrological and hydrodynamic modeling using precipitation estimation from a meteorological radar as the model's input data. Simulations were performed for a calibrated model in the Storm Water Management Model (SWMM) software for the

Monjolinho watershed in São Carlos, São Paulo, Brazil. Precipitation estimates from the meteorological radar operated by the Institute of Meteorological Research at São Paulo State University (IPMet/UNESP), located in Bauru, São Paulo, Brazil, were used. The evaluation was conducted based on the simulation results of the intense rainfall event that occurred on December 28, 2022. The simulation results were compared to the water level data measured by a water level gauge. For the analyzed event, an accurate estimation of the time to peak was observed; however, the peak water level was underestimated when radar-derived data were used as model input. This finding indicates the potential of radar data as input for urban flood forecasting models. Hence, it is recommended that the Z–R relationship is calibrated to better represent precipitation values observed at the ground level.

KEYWORDS: precipitation estimation, urban flood forecasting, hydrological modeling, meteorological radar

1 INTRODUCTION

The global population is still growing and is expected to continue doing so until 2054, likely reaching its maximum by the end of this century (United Nations, 2018). In addition, by 2021, the urban population already accounted for 57% of the world's population, and global urban growth has been projected to reach 68% of the total population by 2050 (UN-Habitat, 2024). In Latin America, the accelerated expansion of urbanized areas, the lack of adequate planning, and the neglect of ecological aspects in public policies intensify the impacts of extreme rainfall events (Coates and Nygren, 2020). In view of future projections, it is therefore critically important to enhance the predictability of extreme flood events, with the greatest possible lead time, in urban centers where the largest populations are and will continue to be concentrated, with the most severe impacts disproportionately affecting populations with fewer financial resources.

In this context, hydrological modeling emerges as an important and robust tool for simulating and forecasting floods resulting from extreme precipitation events, thereby minimizing impacts on property and human life. In general, data used in hydrological process modeling are based on information from rain gauges, general circulation models of the atmosphere, the Weather Research and Forecasting (WRF) model, meteorological radars, and meteorological satellite imagery (Silva et al., 2023). One of the main challenges in hydrological modeling concerns rainfalls' spatial variability assimilation, which is often addressed through interpolation. In many cases, rainfall interpolation using classical methods is the only alternative for estimating precipitation in areas without adequate instrumental coverage or where acceptable-quality measurements are unavailable; however, such approaches often result in low-accuracy information (Hu et al., 2019). In contrast, meteorological radar is generally considered one of the most effective instruments from this perspective.

Sokol et al. (2021) emphasize that rain gauges remain the most widely used instruments for point-scale field measurements of precipitation intensity and duration. However, these devices exhibit limited accuracy in estimating precipitation over complex terrain - such as mountainous regions - due to their sparse spatial distribution. In contrast, weather radars are remote sensing instruments extensively employed in hydrology and meteorology, precisely because they provide precipitation estimates over specific areas with high temporal and spatial resolution. According to Sokol et al. (2021), the use of radar-derived rainfall data in hydrological modeling emerged in response to the need for accurately capturing the spatial structure of precipitation fields and for investigating the potential of such data to generate short-term quantitative forecasts.

The inherent differences between weather radars and rain gauges hinder direct comparisons between data obtained from these two types of instruments (Sokol et al., 2021). Costabile et al. (2026) modeled a rainfall event that occurred in Crotone, Italy, on November 21, 2020, using both rain gauge and radar data, and concluded that simulations based solely on rain gauges often overestimate peak values, whereas radar-based simulations yielded more accurate results. Conversely, Shehu and Haberlandt (2021) underscore the importance of integrating rain gauge and radar data for nowcasting applications in urban hydrology. Their

findings indicate that, among simulations using raw radar data, rain gauge data alone, and a combination of both, only the combined approach exhibited a certain degree of predictability (up to 20 minutes).

Weather radars, however, are not exempt from errors. The main categories of errors affecting weather radars include: (i) hardware-related errors: electronic instability, antenna accuracy, and signal processing quality; (ii) radar beam geometry and scanning strategy: increasing distance from the radar site, beam broadening, and greater spacing between consecutive beams; (iii) data contaminated by echoes from non-meteorological targets, such as tall buildings or electromagnetic interference; (iv) terrain obstructions; (v) signal attenuation due to rainfall; and (vi) anomalous propagation of the radar beam caused by specific atmospheric temperature gradients. Such errors can be mitigated through the application of dedicated quality control techniques (Sokol et al., 2021).

In recent years, substantial progress has been made in the quality control of radar data, driven notably by advancements in programming techniques and image processing - such as Machine Learning (ML), Deep Learning (DL), Neural Networks, and Artificial Intelligence (AI) - as well as by improvements in error and uncertainty correction methods - such as water vapor correction techniques and the assimilation of Doppler radial velocity into Numerical Weather Prediction (NWP) models - and by the evolution of new technologies - including Synthetic Aperture Radar (SAR) and Dual-Polarization (dual-pol) radars (Sokol et al., 2021; Dandekar et al., 2025; Misra et al., 2025). These advances have enabled the application of radar data for diverse purposes, including hydrological modeling, urban flood risk modeling and management, and flood inundation mapping (Sokol et al., 2021; Li et al., 2020; Costabile et al., 2026; Dandekar et al., 2025; Misra et al., 2025). In hydrological modeling, however, it is essential to account for uncertainties arising from initial conditions - such as soil moisture - and from the radar estimates themselves - including incorrect calibration, sample representativeness, non-meteorological echoes, and uncertainties in Z-R relationships (Sokol et al., 2021; Li et al., 2020).

Sokol et al. (2021) assert that, despite all the advancements in rainfall measurement techniques and technologies and the development of urban rain gauge networks, obtaining rainfall data tailored to urban hydrology remains challenging. This is due to the fact that such applications demand greater spatial and temporal precision than is typically required for rural catchments.

Currently, the most widely used meteorological radars are Doppler radars, which operate across different frequency ranges (bands). A meteorological radar functions by emitting electromagnetic pulses that interact with hydrometeors, such as raindrops, snow, or ice. When this interaction occurs, part of the electromagnetic energy is scattered back to the radar as an echo. Based on the characteristics of this echo, it is possible to estimate hydrometeors location and intensity (Doviak and Zrnić, 1993). An S-band radar operates at frequencies between 2 and 4 GHz, which are less susceptible to attenuation compared to radars operating at other bands (such as C or X). This attenuation occurs due to the presence of gases, aerosols, and hydrometeors along the propagation path between the radar and the target. S-band radar is particularly effective for monitoring rainfall over long distances, up to 450 km; however, due to the curvature of the Earth, precipitation volumes are typically estimated within a radius of up to 240 km.

Accordingly, the present study aims to evaluate the response of a previously calibrated hydrological and hydraulic model using both rain gauge data and radar-derived rainfall estimates, in order to assess the spatial and temporal applicability of radar-estimated precipitation for water level estimation in urban rivers. The modeling results are compared with water level gauge data located in the urban area of São Carlos, São Paulo State, Brazil. The analysis had a particular emphasis on extreme events that have occurred in the region.

2 MATERIALS AND METHODS

2.1 Study Area

The Monjolinho watershed is located in the central portion of São Paulo State, Brazil, with its drainage area encompassing the municipalities of Ibaté and São Carlos. A large portion of the urbanized area of São Carlos is drained by the Monjolinho River, as well as by tributaries such as the Mineirinho

Stream, Tijuco Preto Stream, and the Gregório Stream. Owing to the municipality's accelerated urban expansion, an increase in flood events has been observed during periods of high rainfall accumulation, particularly along reaches of the Monjolinho River and the Gregório Stream (Lima and Amorim, 2014), which are located within the urbanized area of the Monjolinho River basin (Figure 1).

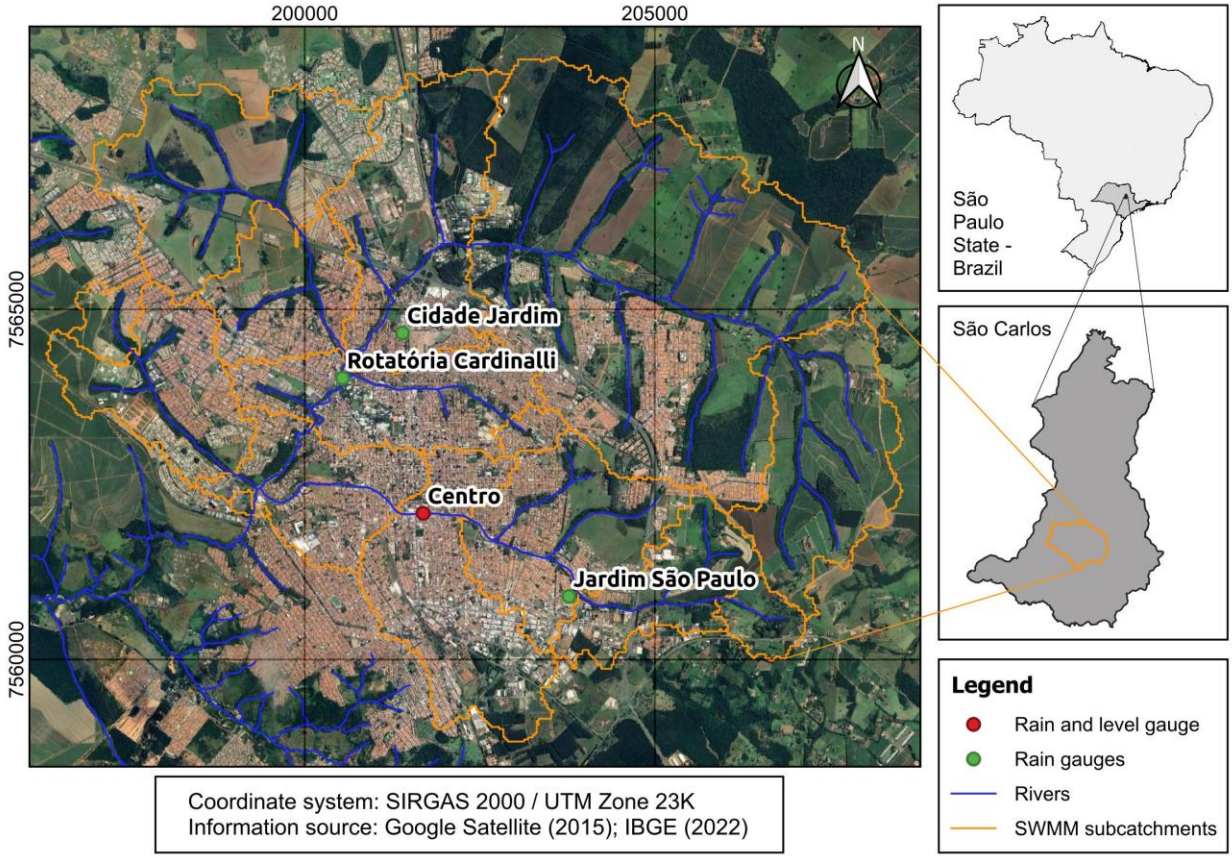

Figure 1: Study area, modeling subcatchments, and level and precipitation gauges' location

2.2 Pluviometric Data

Precipitation estimates from the meteorological radar operated by the Bauru Center for Meteorology, affiliated with the São Paulo State University (IPMet/UNESP), were used in this study. Accumulated rainfall estimates from this radar are generated based on a set of volumetric scanning tasks performed every 7.5 minutes. This set consists of fourteen complete antenna rotations in azimuth, each at a distinct elevation angle, ranging from 0.3° to 45°. Upon completion of the fourteen scans, all volumes are combined to generate the CAPPI (Constant Altitude Plan Position Indicator) product. Due to the beamwidth of the transmitted signal, which for IPMet radars is approximately 2°, spatial resolution decreases with increasing distance from the radar. Nevertheless, the CAPPI product is interpolated onto a regular grid with a spatial resolution of 750 × 750 m.

As reference data, rainfall measurements were collected from two gauges operated by the National Centre for Monitoring and Alerting Natural Disasters (CEMADEN) and from two additional gauges operated by the Municipality of São Carlos (PMSC), in partnership with the Federal University of São Carlos (UFSCar). These gauges provide the only rainfall observations in the region with a 10-minute temporal resolution, which is more suitable for the travel times of flood waves within the study watershed. Data from the four available surrounding gauges were interpolated using the inverse distance weighting (IDW) method to obtain a representative hyetograph for each subcatchment used in the modeling.

The simulations were performed for an intense rainfall event that occurred on December 28, 2022. This event was selected because it is one of the few for which data from both selected precipitation estimation sources are available, as well as water level observations within the study basin, enabling comparison with the modeling results. These water level data were obtained from a water level gauge associated with the aforementioned PMSC rain gauges. The locations of the gauges used in this study are shown in Figure 1.

2.3 Hydrological Model

The Storm Water Management Model (SWMM) is a widely used software for hydrological and hydraulic modeling in urban areas. It enables the simulation of rainfall–runoff transformation in watersheds and can be applied to single-event or long-term simulations, including analyses of both the quantity and quality of surface runoff in micro- and macrodrainage systems. SWMM integrates hydrological and hydraulic components: the surface runoff module is conceptual and concentrated at the subcatchment scale. The hydraulic module adopts a physically distributed approach to model flows and water levels, solving the full one-dimensional (1D) Saint-Venant equations. This integration allows for the assessment of system behavior from runoff generation to its conveyance through drainage networks (James et al., 2010; Perin et al., 2020).

Recognized for its flexibility and robustness, SWMM is widely applied in urban planning and water resources management studies and is considered one of the most commonly used tools for urban stormwater management (Gao et al., 2023; Tamm et al., 2023). Furthermore, its ability to analyze water quality scenarios and to accommodate different watershed configurations makes it an essential tool for environmental impact assessments and for mitigating risks associated with climate change.

For these reasons, SWMM was selected for this study. It was previously calibrated and validated by Fava (2019) based on the subcatchments delineation shown in Figure 1. The calibration followed a multi-event and multi-site approach, developed for a highly urbanized watershed with limited hydrological data. To optimize parameters related to the watershed of interest, an automated tool based on genetic algorithms was employed, considering the absence of discharge measurements and the availability of only water level data. Despite the limitations of using water level data to fully represent the hydrological response of the basin, the model demonstrated consistent performance.

3 RESULTS AND DISCUSSION

Figure 2 illustrates the spatial and temporal distribution of rainfall estimated by the IPMet meteorological radar. Figure 3 presents the hyetograph of the average precipitation within the watershed, obtained through interpolation of rainfall data from CEMADEN and PMSC gauges. The values are similar to those observed in the radar-based estimates, with the identification of three distinct precipitation periods over the analyzed interval, indicating good agreement between the data sources. Nevertheless, it is possible to note that the gauges-based hyetograph showed a greater accumulated precipitation each time step.

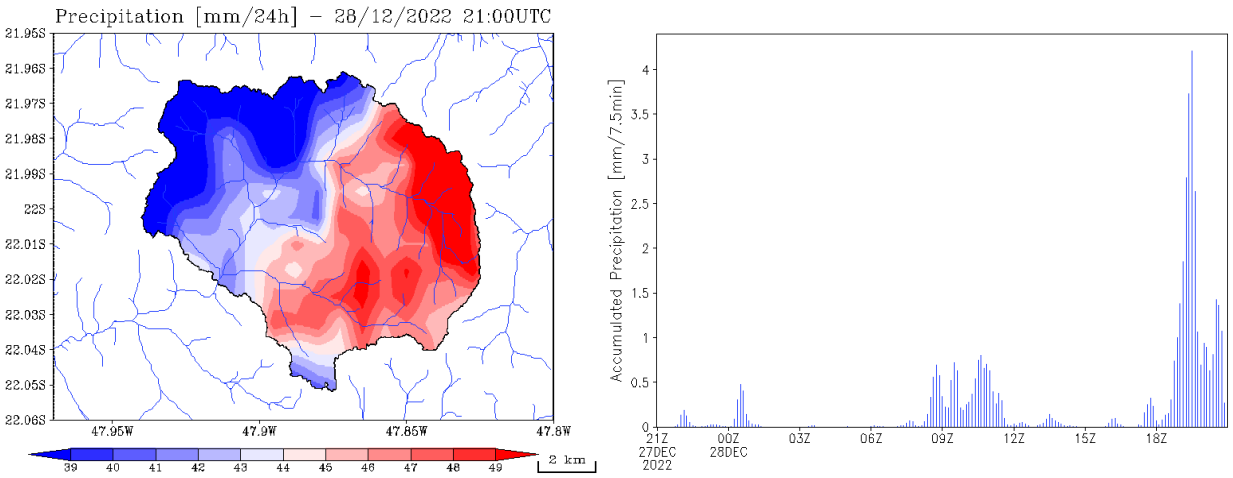

Figure 2: Estimated precipitation based on the meteorological radar for the event of December 28, 2022. The left figure shows the accumulated precipitation in 24 hours, and the right figure shows the average hyetograph for the catchment based on the radar estimates

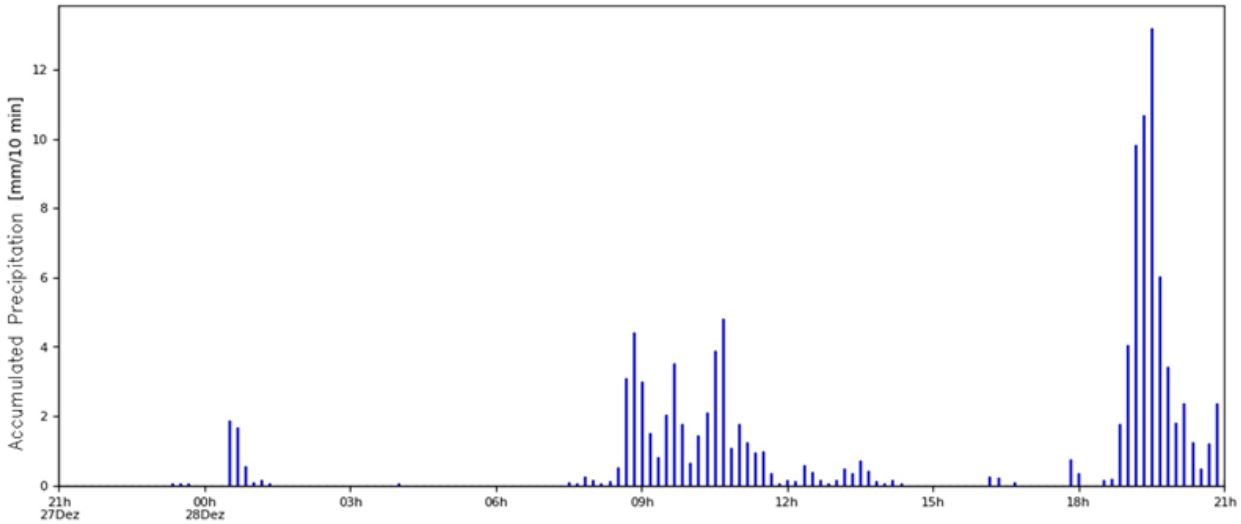

Figure 3: Average hyetograph for the catchment based on the rain gauges for the event of December 28, 2022

Analysis of the results generated by the SWMM model (Figure 4) indicates that both data sources – radar- and rain gauges–based rainfall – produced simulations that could predict the in situ water level observations. The simulation driven by radar products, although underestimating water level values, successfully reproduced the increase in peak stage at the same time it was observed. The simulation based on rainfall interpolated from rain gauges data resulted in the smallest error compared to the observed values, which is consistent with the high sensor density within a relatively small area.

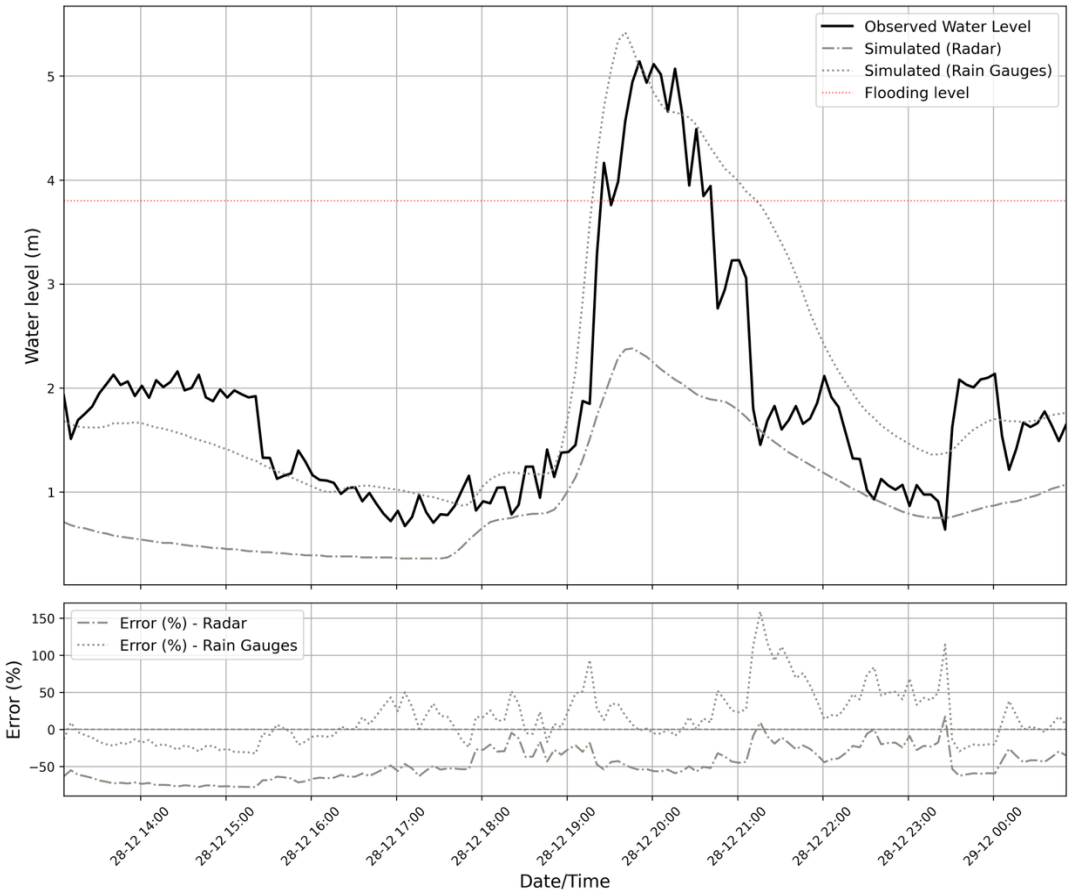

Figure 4: Observed and simulated water levels and respective errors for the event of December 28, 2022

The underestimated water level values generated using radar-derived rainfall, when compared to observations, can be explained by a possible underestimation of rainfall by the radar. This underestimation becomes evident when comparing the hyetographs presented in Figures 2 and 3. Rainfall estimation relies on the relationship between the reflectivity of electromagnetic waves and the effective precipitation rate (the Z–R relationship), which may be inadequate and lead to precipitation underestimation for the analyzed case. Although several Z–R relationships have been proposed in the literature, an accurate estimation of rainfall volume ideally requires that this relationship be locally derived, using reflectivity and observed rainfall at the site of interest. In this study, the Z–R relationship proposed by R. V. Calheiros (Emídio and Landim, 2008), with parameters a = 32 and b = 1.65, was adopted.

The results obtained from rainfall interpolation using data from CEMADEN and PMSC rain gauges showed good performance, adequately reproducing the observed hydrograph in terms of both magnitude and time to peak of the water level. However, the limited spatial distribution of measurement instruments may account for potential discrepancies, which highlights the importance of evaluating alternative sources of precipitation estimates. Radar products, for instance, provide greater spatial representativeness of rainfall distribution and can complement rain gauges data. It is noteworthy that both precipitation estimation approaches could provide suitable inputs for the hydrological model, as they produced water level time series similar to the observed data, indicating their potential applicability under conditions of rain gauge data scarcity or inconsistency. In this context, integrating different precipitation estimation sources may enhance the precision and accuracy of hydrological simulations, particularly in regions with limited rainfall monitoring networks, as is the case in Brazil and many parts of the world. In light of these considerations, future studies are essential to further explore this integration and to develop more robust and reliable approaches for urban floods forecasting.

4 CONCLUSION

Simulations driven by radar-derived rainfall data showed a reasonable agreement with observations, with the timing of the simulated peak water level being consistent with the observed peak. Simulations based on rain gauges data yielded better overall results; however, such data are not always available with adequate spatial distribution and temporal resolution. The scarcity of rain gauges data reinforces radar products' advantage, which provide greater spatial representativeness and can replace or complement local measurements in data-limited contexts. Based on the presented results, future analyses may focus on the integration of the products used to drive the hydrological model, aiming to increase information redundancy. Thus, this study presents a promising scenario for the application of advanced forecasting and disaster management techniques, particularly in regions with insufficient monitoring infrastructure.

The results also highlight the strong capability of SWMM to simulate both the timing and the magnitude of peak water levels using either radar- or rain gauge-based rainfall inputs. This demonstrates the potential for integrating the employed tools by leveraging their complementarity to enhance redundancy and reliability in early warning and nowcasting systems. However, it should be noted that the hydrological model was calibrated using rain gauges data without directly incorporating spatially distributed products such as radar rainfall estimates, which may have influenced the model performance when radar-based estimates were used as inputs.

Given the good performance in reproducing the time to peak of the water level using radar precipitation estimates, despite the underestimation of the peak magnitude, there is a clear need to calibrate radar estimations in order to derive a new, locally representative Z–R relationship for the study area. The Z–R relationship proposed by R. V. Calheiros (Emídio and Landim, 2008), being relatively old, may no longer adequately represent rainfall volumes based on reflectivity, as the radar system may have undergone changes over time, such as variations in transmitted power or attenuation due to residue accumulation on the radome, among other factors. Therefore, in light of the obtained results, the continuation of the research is of fundamental importance.

5 ACKNOWLEDGEMENTS

This research was supported by the Coordination for the Improvement of Higher Education Personnel (CAPES), Finance Code 001, and by the National Council for Scientific and Technological Development (CNPq), through the project "Advances in Nowcasting Tools Applied to Urban Flooding" (grant no. 446043/2023-0) and the project "Multi-scale Forecasting of Extreme Meteorological Events for Hydrological Applications" (grant no. 446029/2023-8).

REFERENCES

Coates R. and Nygren A. (2020). Urban floods, clientelism, and the political ecology of the state in Latin America. Annals of the American Association of Geographers, v. 110, n. 5, p. 1301-1317.

Costabile P., Lombardo M., Chiaravalloti F., Caloiero T., Costanzo C. (2026). Predicting pluvial flood impacts in data-scarce urban environments: Uncertainty and interplay between rainfall inputs and conceptual drainage loss models. Urban Climate, v. 65, 102724.

Dandekar S., Limbashia T., Parab O., Kotecha R., Chakravarty K., Ukarande S., Hosalikar K. (2025). A radar data-driven AI approach for rainfall nowcasting: towards flood preparedness in urban regions. Journal of the Indian Society of Remote Sensing, v. 53, p. 2267-2284.

Doviak R.J. and Zrnić D.S. (1993). Doppler Radar and Weather Observations. Academic Press.

Emídio Z. and Landim P. (2008). Análise de superfície de tendência aplicada à chuva, medida por radar meteorológico, nas regiões de Assis e Piracicaba, SP. Geociências, v. 27, n. 4, p. 439 - 449.

Fava M.C. (2019). Improving flood forecasting using real-time data to update urban models in poorly gauged areas. 2019. 176 p. PhD Thesis (Hydraulic and Sanitation Engineering Graduate Program). São Paulo University, São Carlos.

Gao Z., Zhang Q., Li J., Wang Y., Dzakpasu M., Wang X.C. (2023). First flush stormwater pollution in urban catchments: A review of its characterization and quantification towards optimization of control measures. Journal of Environmental Management, v. 340, p. 117976.

Hu Q., Li Z., Wang L., Huang Y, Wang Y., Li L. (2019). Rainfall Spatial Estimations: A Review from Spatial Interpolation to Multi-Source Data Merging. Water, v. 11, n. 3, p. 579.

James W., Rossman L.A., James W.R.C. User's Guide to SWMM5, 13th ed.; CHI: Guelph, ON, Canada, (2010).

Li Z., Chen M., Gao S., Hong Z., Tang G., Wen Y., Gourley J.J., Hong Y. (2020). Cross-Examination of Similarity, Difference and Deficiency of Gauge, Radar and Satellite Precipitation Measuring Uncertainties for Extreme Events Using Conventional Metrics and Multiplicative Triple Collocation. Remote Sensing, v. 12(8), 1258.

Lima A.P., Amorim M.C.C.T. (2014). Análise de episódios de alagamentos e inundações urbanas na cidade de São Carlos a partir de notícias de jornal. Revista Brasileira de Climatologia, v. 15, p. 182-204.

Misra A., White K., Nsutezo S.F., Straka III W., Lavista J. (2025). Mapping global floods with 10 years of satellite radar data. Nature Communications, v. 16, 5762.

Perin R., Trigatti M., Nicolini M., Campolo M., Goi D. (2020). Automated calibration of the EPA-SWMM model for a small suburban catchment using PEST: a case study. Environmental Monitoring and Assessment, 192, 1-17.

Sokol Z., Szturc J., Orellana-Alvear J., Popová J., Jurczyk A., Célleri R. (2021). The Role of Weather Radar in Rainfall Estimation and Its Application in Meteorological and Hydrological Modelling—A Review. Remote Sensing, v. 13(3). 351.

Shehu B. and Haberlandt U. (2021). Relevance of merging radar and rainfall gauge data for rainfall nowcasting in urban hydrology. Journal of Hydrology, v. 594, 125931.

Silva T.L.V., Lopes Z., Ferreira R., Guedes R., Pereira R., Prestrelo F., Ferreira A., Gomes J., Wanderley C., Santos E., Oliveira P., Gomes V., Dias H. (2023). Previsão de extremos de chuva em Pernambuco: os eventos de maio de 2022. Revista Brasileira de Geografia Física, v. 16, n. 01, p. 646-671.

Tamm O., Kokkonen T., Warsta L., Dubovik M., Koivusalo H. (2023). Modelling urban stormwater management changes using SWMM and convection-permitting climate simulations in cold areas. Journal of Hydrology, v. 622, p. 129656.

UN-Habitat. Cities and climate action - world cities report 2024. (2024). Avaliable at: https://unhabitat.org/sites/default/files/2024/11/wcr2024_-_full_report.pdf

United Nations. World urbanization prospects: The 2018 revision. Population Division-United Nations. (2018). Available at: https://population.un.org/wup/publications/Files/WUP2018-Report.pdf

ICFM 10
Adapting to Global Change:
Innovative Approaches to Flood Management and Resilience
May 20-22, 2026 | Western University, London, Ontario, Canada

Integrating Hydraulic Modeling and Citizen Science for Past Flood Reconstruction in the Upper Paranapanema River Basin

Jaqueline Carolino Santos [1]; Javier Tomasella [2]; Maria Clara Fava [3]; Anai Floriano Vasconcelos [4]; Hélio Rodrigues Bassanelli [5]; Carlos Eugênio Pereira [6]; Pedro Ramos Galvão [7]; Gabriela Gonçalves Cilto [8].

Impacts, Adaptation, and Vulnerabilities Division, National Institute for Space Research, São José dos Campos, SP, Brazil [1]
Email: jaqueline.santos@inpe.br

Impacts, Adaptation, and Vulnerabilities Division, National Institute for Space Research, São José dos Campos, SP, Brazil [2]
Email: javier.tomasella@inpe.br

Civil Engineering Department, Federal University of São Carlos, São Carlos, SP, Brazil [3]
Email: mcfava@ufscar.br

Environmental Sciences Department, Federal University of São Carlos, São Carlos, SP, Brazil [4]
Email: anai.vasconcelos@ufscar.br

Natural Disasters, São Paulo State University "Júlio de Mesquita Filho", São José dos Campos, SP, Brazil [5]
Email: helio.bassanelli@unesp.br

Faculty of Civil Engineering, Federal University of Uberlândia, Uberlândia, MG, Brazil [6]
Email: cepereira@ufu.br

Environmental Sciences Department, Federal University of São Carlos, São Carlos, SP, Brazil [7]
Email:gabrielacilto@estudante.ufscar.br

Environmental Sciences Department, Federal University of São Carlos, São Carlos, SP, Brazil [8]
Email: pedrorg@estudante.ufscar.br

ABSTRACT

The quantification of flood hazards is frequently hindered by the lack of systematized hydrological records, particularly in developing nations. To address this challenge, this study evaluates a methodology that integrates citizen science with hydrodynamic modeling. Focusing on the Upper Paranapanema River Basin in southeastern Brazil, the HEC-RAS model was employed to reconstruct historical flood events. The approach was validated using resident-supplied flood marks and satellite imagery, yielding a Kappa statistic of 0.7 and an NSE of up to 0.79. Additionally, collective memory was instrumental in supplementing peak flow statistics to generate scenarios across multiple return periods. The study further investigated the hydraulic effects of rural earth dikes, revealing that these structures exert negligible influence on flood extent within the urban area. These results highlight the efficacy of combining local knowledge with numerical modeling, validating citizen science as a practical and effective alternative for flood management in data-scarce contexts.

KEYWORDS: flood risk; data scarcity; citizen science; hydrodynamic model; flood scenarios; return period analysis.

1 INTRODUCTION

Floods are among the leading causes of socioeconomic and environmental. Their increasing frequency, linked to global warming (IPCC, 2021), challenges the traditional stationarity assumptions underpinning water resources management. Understanding these events is complicated due to natural and anthropogenic changes in river basins (Berghuijs et al., 2016). Despite advances in modeling, data scarcity remains a critical limitation in developing countries (Krabbenhoft et al., 2022).

In this context of scarcity, evidence from local observations and indirect methods is valuable (Sy et al., 2020). Citizen science emerges as a promising approach to fill data gaps and enrich knowledge about floods, offering a flexible framework for public participation. Beyond data collection, it helps to understand cultural interactions with hydrological systems, relying on collective memory to validate scientific initiatives (Sarmento Buarque et al., 2020).

In Brazil, studies report changes in the magnitude and frequency of floods, with positive trends in the South and Southeast regions (Bartiko et al., 2019), often attributed to extreme precipitation (Chagas et al., 2021), despite recent drought trends in some periods. Flood risk mapping in the country typically relies on limited field observations and coarse extrapolations (Marchezini et al., 2022), highlighting the need for alternative approaches to facilitate knowledge exchange between scientists and communities.

This study focuses on the Upper Paranapanema River Basin in southeastern Brazil, an area frequently affected by major floods and with fragmented hydrological data. The region experienced significant events in 2004, 2010, and 2016, causing substantial losses to agriculture and residents (SISSER, 2016; SEBRAE, 2025). The historical presence of earthen dikes, built in the 1970s and destroyed in 2004, raises questions about flow alteration and the reduction of the natural attenuation capacity of floodplains, which may exacerbate damage in downstream urban areas.

To address these challenges, this study examines whether citizen science can enhance the reliability of hydrodynamic modeling and flood frequency analysis in data-poor regions. The objective is to integrate resident accounts with detailed mapping and hydrological data to calibrate a model that reconstructs the 2004, 2010, and 2016 flood events, as well as to estimate historical peak discharges beyond the instrumental period using citizen-provided information. By combining historical and systematic records, the study assesses flood impacts associated with return periods of up to 500 years. Under these scenarios, the reconstruction of earthen dikes for rural protection is considered, and their effects on the urban area are evaluated, accounting for the reduction in upstream flood attenuation capacity.

2 METHODOLOGY

2.1 Study area

The study site (Figure 1) covers 128.85 km² in the Upper Paranapanema basin, encompassing the confluence of the Paranapanema and Itapetininga rivers. Upstream, the area is dominated by floodplains and a meandering morphology, where the Paranapanema flows north with a low average slope (0.00016 $m.m^{-1}$), while the Itapetininga flows west (0.00020 $m.m^{-1}$). Downstream of the confluence, the river straightens due to topographic constraints; although remnants of old dikes exist along the banks, these anthropogenic structures have been partially destroyed by recurrent flooding.

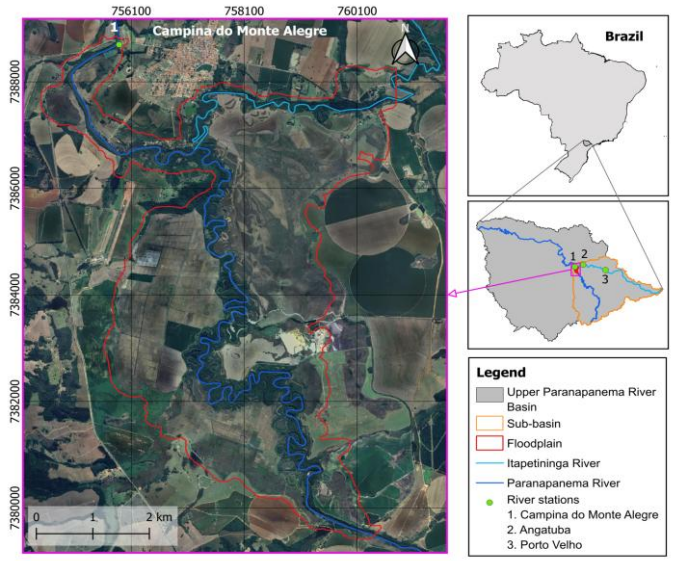

Figure 1: Location of the study site in the Upper Paranapanema River Basin. Projection: SIRGAS 2000, UTM zone 22S. Data sources: Google Satellite (2024), IBGE (2022), ANA (2024).

The main urban center, Campina do Monte Alegre, is located downstream and houses 5,954 inhabitants (IBGE, 2022), with an economy primarily based on agriculture and livestock (SEBRAE, 2025). The region features a Cfa climate with an annual average temperature of 20.2°C and precipitation of 1,324 mm, situated within a geomorphological context dominated by the sedimentary Paraná basin and the Atlantic orogenic belt. Despite economic activities, the area retains significant native vegetation cover from the Atlantic Forest and Cerrado biomes (CBH-ALPA, 2023).

2.2 Citizen science data

To address the absence of systematic records prior to the 2000s, a citizen science approach was applied in Campina do Monte Alegre, combining interviews and physical flood mark documentation. Conducted between January and April 2023 in accordance with ethical standards (CAAE 61253522.3.0000.5504). This method enabled the identification of eight major flood events between 1983 and 2016, with the 2004 flood being the most significant. Local flood-level markings on utility poles supported data validation with rainfall series and satellite imagery, enhancing the reliability of the historical reconstruction in a data-scarce environment, as further detailed in Vasconcelos et al. (2025).

2.3 Topography, river cross-section survey, satellite image, and hydrological data

Topographic data consisted of the ANADEM digital terrain model (ANA, 2025), a 30-m resolution product . This was complemented by a bathymetric survey conducted in May 2023 using a RiverSurveyor M9 ADCP to map cross-sections and longitudinal profiles along the Itapetininga and Paranapanema rivers. Additionally, the precise elevations of historical flood marks on utility poles were acquired using Geomax GNSS RTK receivers, with data post-processed via the IBGE PPP service to ensure high positional accuracy.

For model validation and boundary conditions, a Landsat 8 satellite image (ID: LC08_L2SP_220076_20160120_20200907_02_T1_SR) capturing the 2016 flood was processed in QGIS using spectral indices to isolate open water areas for comparison with simulations. Hydrological data were obtained from the National Water Agency (ANA) platform, Hidroweb (Figure 1). The Angatuba and Campina do Monte Alegre stations defined the boundary conditions, while the Porto Velho station was used to estimate stages at Angatuba for the 2016 event, as direct records at this station were no longer available following its deactivation in 2010.

2.4 Flood Frequency Analysis

Flood frequency analysis was performed using peak flow records from the Angatuba and Campina do Monte Alegre stations. L-Moments were derived through Probability Weighted Moments (Greenwood et al., 1979; Hosking and Wallis, 1997), selected for their reliability with limited datasets (Fischer, 2024). The Angatuba station provided a continuous 76-year series, while the Campina do Monte Alegre dataset required the integration of historical flood events (1983 to 2016) documented by residents. These flood marks were georeferenced and correlated with observed water levels to estimate peak discharges based on the official rating curve.

To address discontinuities in the Campina do Monte Alegre record, partial Probability Weighted Moments were applied (Wang, 1990), splitting the dataset according to a predefined threshold (Fischer, 2024). Twelve probability distributions were evaluated using the methodology developed by Hosking (1985), and the best fit was selected based on the lowest root mean square error and visual inspection. Plotting positions followed the Weibull method for Angatuba and the Hirsch approach (1987) for the historical dataset. Despite potential long-term trends, a stationary assumption was maintained to reduce the high uncertainty typically associated with non-stationary models (Anzolin et al., 2024).

2.5 Hydrodynamic Modeling Setup

Hydrodynamic simulations were performed using the HEC-RAS 6.6 two-dimensional model (USACE, 2024), incorporating geospatial inputs via RAS Mapper and applying a uniform Manning roughness coefficient of 0.07. The model was calibrated under transient conditions with a five-day warm-up period to reconstruct the 2005, 2010, and 2016 flood events. Validation employed NSE, KGE, and RMSE metrics based on observed stages at Campina do Monte Alegre. Boundary conditions included daily discharges from Angatuba, a downstream normal depth slope of 0.00012 metres per metre, and upstream inflow from the Paranapanema River estimated by mass balance, justified by its dominant contribution over the Itapetininga tributary.

In accordance with Brazilian Law 12.608 (Brasil, 2012) and CEMS-Flood guidelines (2025), steady-state scenarios were simulated for return periods of 50, 100, and 500 years. Two configurations were evaluated: one reflecting current condition without flood embankments, and another assuming the reconstruction of dikes lost in 2004 to safeguard agricultural areas. Impacts were assessed by comparing water levels and flow velocities along longitudinal profiles covering three kilometres upstream and six kilometres downstream of the confluence, including urban peripheries.

3 RESULTS

3.1 Reconstruction of Floodplain inundation during the floods of 2004, 2010, and 2016

The hydrodynamic reconstruction of the flood events that occurred in 2004, 2010, and 2016 demonstrated strong model performance in both spatial and temporal dimensions. Spatial validation using Landsat imagery from the 2016 flood resulted in a Kappa coefficient of 0.7 (Cohen, 1960), indicating satisfactory spatial agreement despite minor errors of commission and omission near the riparian boundaries. From a hydrological perspective, the model accurately reproduced discharge magnitude and timing at the gauge located in Campina do Monte Alegre, with Nash-Sutcliffe efficiency values ranging from 0.79 to 0.91, Kling-Gupta efficiency values between 0.74 and 0.84, and root mean square errors below 0.40. In addition, comparison with flood marks identified through citizen science and georeferenced using RTK measurements confirmed the model performance in terms of vertical accuracy, with absolute elevation differences limited to 0.36 meters for the 2004 flood and -0.41 meters for the 2016 flood.

Analysis of inundation patterns reveals that the expansion of the flooded area is topographically constrained by surrounding higher elevations, particularly to the west and near the urban center. Consequently, variations in flood magnitude are primarily reflected in water surface elevations and depths rather than in the lateral extent of the flooded area.

3.2 Statistical Analysis of Peak Flows

The integration of historical flood marks obtained through citizen science with systematic records emphasized the relevance of pre-2000 events, notably the 1983 flood, ranked as the second largest in the 1983–2020 series. By applying a validated elevation offset between utility pole marks (measured with RTK-GPS) and gauge data from the 2004 and 2016 events, peak discharges were estimated for historical floods, four of which ranked among the top seven. For frequency analysis, the Generalized Pareto distribution provided the best fit at both Angatuba and Campina do Monte Alegre. While Angatuba used a continuous series (1935–2010), Campina do Monte Alegre required a partial Probability Weighted Moments approach with a 300 cubic metres per second threshold to incorporate nine events into a censored sample, combining systematic and historical peaks.

The reconstructed flood series revealed significant hydrological differences between the contributing basins. Inclusion of citizen-derived historical events notably altered the frequency curve at Campina do Monte Alegre, underscoring the methodological value of integrating local knowledge to refine flood hazard assessments.

3.3 Scenarios analysis for different return periods and potential impacts of the reconstruction of the earth dike in the floodplain

The comparative analysis of "no dike" and "dike" scenarios for 50, 100, and 500-year return periods reveals that the reconstruction of flood defenses would have negligible impacts on the spatial extent of flooding in the downstream urban area (Figure 2). While the total flooded area and depth increase with return periods, the presence of dikes does not alter the flood limits surrounding the town, as confirmed by the longitudinal profiles downstream of the confluence, where water surface elevations remain virtually identical across scenarios. Instead, the hydraulic impact of the dikes is concentrated upstream of the confluence. On the Paranapanema River, the dikes cause a rise in water levels that intensifies upstream and correlates positively with flood magnitude, whereas on the Itapetininga River, hydraulic differences are more pronounced for lower return periods.

Figure 2: Limits of the flooded area for the 50, 100 e 500-year floods in the vicinity of Campina do Monte Alegre for the “no dike” (a) scenario and for the “dike” scenario (b).

In relation to stream dynamics, velocity profiles confirm that the dikes exert a significant influence on flow energy in the upstream sector, while downstream conditions remain largely unaffected. The topography of the valley limits lateral floodplain expansion, causing flood magnitude to be expressed

primarily through increased depth. Under these constraints, the presence of dikes enables the recovery of agricultural areas in upstream regions without intensifying flood risk in the downstream urban zone. However, this benefit comes with the trade-off of elevated hydraulic energy in rural upstream sections.

4 DISCUSSION

Citizen science played a key role in enhancing flood reconstruction in a data-scarce region, supporting global findings on the reliability of non-expert observations. HEC-RAS simulations compared with citizen-recorded water marks showed vertical errors of 0.3–0.4 m, attributed to DEM and resolution limitations (Patel et al., 2017; Mohanty et al., 2020; Artiglieri et al., 2025). Despite such discrepancies, citizen data extended the flood record to 1983, preventing underestimation of critical flows and improving hydrological accuracy in unmonitored areas (Scheller et al., 2024).

The model demonstrated good performance, with high NSE values, especially for the 2004, 2010, and 2016 events. However, the 2004 peak was slightly underestimated due to uncertainties in friction slopes, mass balance, and rating curve extrapolations. Spatial validation using Landsat imagery confirmed that ANADEM reliably represents floodplain morphology, with differences limited to riparian vegetation zones.

Simulations indicated a limited influence of old earth dikes on downstream flooding because of channelization effects, whereas upstream impacts were more pronounced. Along the Paranapanema River, the presence of dikes reduced the effective flow section, leading to localized increases in flow velocity. In the Itapetininga River, backwater effects became more evident in the vicinity of the confluence. Despite remaining limitations, including uncertainties related to the digital elevation model and Manning roughness assumptions, the results emphasize the spatial heterogeneity of dike effects and underscore the importance of flood management strategies informed by geomorphological controls.

5 CONCLUSION

This study demonstrated the efficacy of integrating remote sensing, hydraulic modeling, and citizen science to reconstruct floodplain dynamics in data-scarce regions. While HEC-RAS simulations showed good agreement with observations, the results highlighted that citizen-derived data is crucial not only for model validation and prioritizing high-resolution topographic surveys in critical areas but, most importantly, for recovering historical peak flows beyond the instrumental period. This methodological integration significantly improves extreme-value statistics and the reliability of flood hazard scenarios, which are imperative given the increasing frequency of extreme events. Ultimately, this approach offers a cost-effective, empowering framework for incorporating disaster resilience into community planning and early warning systems in municipalities across Brazil that lack conventional monitoring networks.

6 ACKNOWLEDGEMENTS

The authors would like to thank the National Council for Scientific and Technological Development (CNPq) for funding the project (Grants No. 409527/2021-1 and 440016/2024-0). We also thank the Postgraduate Program in Natural Disasters at the São Paulo State University "Júlio de Mesquita Filho" (UNESP), as well as the Postgraduate Program in Earth System Science at the National Institute for Space Research (INPE).

REFERENCES

Anzolin G, de Oliveira DY, Vrugt JA, AghaKouchak A, Chaffe PLB (2024) Nonstationary frequency analysis of extreme precipitation: Embracing trends in observations. J Hydrol 637:131300. https://doi.org/10.1016/j.jhydrol.2024.131300

Artiglieri, Pasqualino, et al. Performance of HEC-RAS v6. 5 at basin scale for calculating the flow hydrograph: comparison with TUFLOW. Natural Hazards, 121.8 (2025): 9477-9490. https://doi.org/10.1007/s11069-025-07170-x

Bartiko D, Oliveira D. Y., Bonumá N. B., and Chaffe P. L. B. (2019) Spatial and seasonal patterns of flood change across Brazil, Hydrological Sciences Journal, 64:9, 1071-1079. https://doi.org/10.1080/02626667.2019.1619081

Berghuijs, W.R., et al., 2016. Dominant flood generating mechanisms across the United States. Geophysical Research Letters, 43 (9), 4382–4390. https://doi.org/10.1002/2016GL068070

Chagas, V.B.P., Chaffe, P.L.B. & Blöschl, G. Climate and land management accelerate the Brazilian water cycle. Nat Commun 13, 5136 (2022). https://doi.org/10.1038/s41467-022-32580-x

Cohen, J. (1960). A Coefficient of Agreement for Nominal Scales. Educational and Psychological Measurement, 20(1), 37-46. https://doi.org/10.1177/001316446002000104

Fischer, S (2024) Incorporating historical flood events in type-based statistics. Journal of Hydrology, 636. 131289. https://doi.org/10.1016/j.jhydrol.2024.131289

Greenwood, J.A., Landwehr, J.M., Matalas, N.C., Wallis, J.R., 1979. Probability weighted moments: definition and relation to parameters of several distributions expressable in inverse form. Water Resour. Res. 15 (5), 1049–1054. https://doi.org/10.1029/WR015i005p01049

Hirsch, R.M., 1987. Probability plotting position formulas for flood records with historical information. J. Hydrol. 96 (1), 185–199. https://doi.org/10.1016/0022-1694(87)90152-1

Hosking JRM. 1985. Research Report: Fortran Routines for use with the Method of L-Moments. Version 3.04. IBM Research Division, T. J. Watson Research Center, Yorktown Heights, NY 10598. RC 20525 (90933) 8/5/96, revised 7/25/05. Available from: http://lib.stat.cmu.edu/general/lmoments

Hosking JRM, Wallis JR (1997) Regional frequency analysis: an approach based on L-moments. Cambridge University Press, New York. https://doi.org/10.1017/CBO9780511529443

IPCC. Climate Change 2021: The Physical Science Basis. Contribution of Working Group I to the Sixth Assessment Report of the Intergovernmental Panel on Climate Change. Geneva: IPCC; 2021. https://doi.org/10.1017/9781009157896.001

Krabbenhoft, C. A., Allen, G. H., Lin, P., Godsey, S. E., Allen, D. C., Burrows, R. M., ... & Olden, J. D. (2022). Assessing placement bias of the global river gauge network. Nature Sustainability, 5(7), 586-592. https://doi.org/10.1038/s41893-022-00873-0

Marchezini V, Porto de Albuquerque J, Pitidis V, Rudorff CM, Lima-Silva F, Klonner, C and Martins, MHM (2022) Flood risk governance in Brazil and the UK : facilitating knowledge exchange through research gaps and the potential of citizen-generated data. Disaster Prevention and Management: An International Journal, 31 (6). pp. 30-44. https://doi.org/10.1108/dpm-01-2022-001.

Mohanty, M.P., Indu, J., Ghosh, S., Rao, G., Nithya, S., Karmakar, S., 2020b. Sensitivity of various topographic data in flood management: Implications on inundation mapping over large data-scarce regions. J. Hydrology 590, 125523. https://doi.org/10.1016/j.jhydrol.2020.125523.

Patel, D.P., Ramirez, J.A., Srivastava, P.K. Bray M, Han D. Assessment of flood inundation mapping of Surat city by coupled 1D/2D hydrodynamic modeling: a case application of the new HEC-RAS 5. Nat Hazards 89, 93–130 (2017). https://doi.org/10.1007/s11069-017-2956-6

Sarmento Buarque, A. C., Bhattacharya-Mis, N., Fava, M. C., Souza, F. A. A. D., & Mendiondo, E. M. (2020). Using historical source data to understand urban flood risk: a socio-hydrological modelling application at Gregório

Creek, Brazil. Hydrological Sciences Journal, 65(7), 1075-1083. https://doi.org/10.1080/02626667.2020.1740705

Scheller, Mirjam, Ilja van Meerveld, and Jan Seibert. "How well can people observe the flow state of temporary streams?." Frontiers in Environmental Science 12 (2024): 1352697.

Sy, B., Frischknecht, C., Dao, H., Consuegra, D. and Giuliani, G. (2020) Reconstituting Past Flood Events: The Contribution of Citizen Science. Hydrology and Earth System, 24, 61-74. https://doi.org/10.5194/hess-24-61-2020

Vasconcelos, A. F., Santos, J. C., Cilto, G. G., Galvão, P. R., Fava, M. C., Menezes Filho, F. C. M., Pereira, C. E., Bassanelli, H. R. e Tomasella. Contribuições da ciência cidadã para o gerenciamento de riscos de inundações: o caso de Campina do Monte Alegre – SP, Brasil. In: Souto, Raquel Dezidério (Org.). Estudos de caso em mapeamento colaborativo. Rio de Janeiro: IVIDES.org. p. 303-334. ISBN: 978-65-985676-2-0. doi: 10.5281/zenodo.16808938

Wang, Q.J., 1990. Unbiased estimation of probability weighted moments and partial probability weighted moments from systematic and historical flood information and their application to estimating the GEV distribution. J. Hydrol. 120 (1–4), 115–124. https://doi.org/10.1016/0022-1694(90)90145-N

Web sites:

ANA, (2024): https://www.snirh.gov.br/hidroweb/serieshistoricas, consulted 13 May 2024.

ANA, (2025): https://metadados.snirh.gov.br/geonetwork/srv/api/records/93664c15-1ff8-4e87-bbed-2bb69d321309#:~:text=, consulted 13 Jan 2025.

Brasil. (2012): http://www.planalto.gov.br/ccivil_03/_ato2011-2014/2012/lei/l12608.htm, consulted 07 Ago 2025.

CBH-ALPA. (2023): https://sigrh.sp.gov.br/public/uploads/documents/8124/rs_2014_cbhalpa_vfinal_of.pdf, consulted 5 Jun 2024.

Copernicus Emergency Management Service (2025): https://confluence.ecmwf.int/display/CEMS/CEMS-Flood+flood+inundation+maps, consulted 28 Jul 2025.

IBGE (2022): https://cidades.ibge.gov.br/brasil/sp/campina-do-monte-alegre/panorama, consulted 16 Jun 2024.

SEBRAE (2025): https://datampe.sebrae.com.br/profile/geo/campina-do-monte-alegre, consulted 1 Mar 2025.

SISSER (2022): https://dados.agricultura.gov.br/dataset/sisser3/resource/54e04a6b-15b3-4bda-a330-b8e805deabe4, consulted 11 Aug 2024.

USACE (2024): https://www.hec.usace.army.mil/software/hec-ras/, consulted 17 Jan 2025.

ICFM 10
Adapting to Global Change:
Innovative Approaches to Flood Management and Resilience
May 20-22, 2026 | Western University, London, Ontario, Canada

The Use of Deep Learning to Improve River Channel Detection for Bathymetry Assessment from LiDAR Data in Regional-Scale Flood Modelling

Susan Ly[1], Guénolé Choné[1], Iulia Mazgareanu[1], Pascale Biron[1], Étienne Clabaut[2], Samuel Foucher[2], Thomas Buffin-Bélanger[3]

Department of Geography, Planning & Environment, Concordia University, Montréal, QC, Canada[1]
E-mail: susan.ly@mail.concordia.ca

Département de géomatique appliquée, Université de Sherbrooke, Sherbrooke, QC, Canada[2]

Département de biologie, chimie et géographie, Université de Québec à Rimouski, Rimouski, QC, Canada[2]

ABSTRACT

Accurate representation of river channel geometry remains one of the greatest challenges in regional-scale flood modelling, particularly in regions where bathymetric data and consistent flood mapping practices are limited. Recently, an inverse hydraulic modelling approach based on high-resolution LiDAR digital elevation models was developed to estimate riverbed elevations at the watershed scale, achieving unprecedented accuracy in simulated flood levels in Canadian watersheds. However, creating the wetted (LiDAR) channel polygons required for bathymetry estimation, whether semi-automatically produced by LiDAR vendors or manually digitized by end-users, remains labour-intensive, inconsistent across provinces and difficult to scale nationally. This research presents a deep learning (DL) workflow that automates river-channel detection directly from LiDAR-derived raster products. A convolutional neural network was trained exclusively on 1-m LiDAR derivatives, including DEM, slope, LiDAR point density and intensity. The model predicts continuous channels across diverse geomorphological contexts with strong overall consistency, achieving a mean Intersection-over-Union of 91% when compared with manually digitized ground truths. Performance is highest in large, clearly defined channels with high-quality LiDAR data, and decreases in wetlands, forested zones, and narrow meandering tributaries. The key difficulty lies in managing domain shift, the differences between training conditions and regional-scale production environments, which arises from geomorphological variability between watersheds, differences in LiDAR sensor specifications and spatially heterogeneous point-density distributions. These factors limit model generalization and require careful selection of training sites, extensive input normalization, and targeted data augmentation strategies. Overall, this DL method greatly decreases the resources needed to obtain LiDAR channel polygons. For example, for the Grand River (Ontario), it took approximately 10 seconds per km of river using the DL workflow, compared with roughly 380 seconds per km for manual digitization. This work highlights the potential of scalable DL-based river-geometry extraction to substantially improve the efficiency and consistency of the regional-scale flood modelling process.

KEYWORDS: LiDAR, Deep Learning, River Channel Detection, Semantic Segmentation, Flood Modelling, Bathymetry Estimation

1 INTRODUCTION

Accurate representation of river channel geometry is a key requirement for reliable regional-scale flood modelling, as channel width and depth directly influence water surface elevations and flood extent predictions (Neal et al., 2021; Merz et al., 2010; Trigg et al., 2016). While high-resolution topographic data have improved flood modelling capabilities in recent years, detailed bathymetric information remains largely unavailable over large territories. Field-based surveys are costly and spatially limited, leading many regional flood models to rely on simplified channel representations that introduce uncertainty and reduce model reliability (Wilby & Keenan, 2012; Neal et al., 2021).

To address this limitation, Choné et al. (2021, 2024) developed a LiDAR-derived inverse hydraulic modelling approach that estimates riverbed elevations at the watershed scale using high-resolution digital elevation models, leading to substantial improvements in simulated flood levels (Choné et al., 2021; Neal et al., 2021). The approach requires accurate delineation of wetted river channel widths at the time of LiDAR acquisition. In practice, these channel polygons are typically produced through manual digitization, a process that is labour-intensive, difficult to standardize, and poorly suited for regional or national applications (Choné et al., 2021), particularly given the geomorphological variability of river systems (Biron et al., 2013). Although provincial and federal datasets of river channels exist, they are often limited to large rivers, may be outdated due to geomorphological changes such as meander migration, or reflect river conditions at discharges different from those during LiDAR acquisition. Therefore, they are considered insufficiently reliable for LiDAR-based regional-scale modelling.

This study presents a deep learning workflow that automates river channel detection using LiDAR-derived raster products. A convolutional neural network is trained on 1-m LiDAR derivatives, including digital elevation, slope, point density, and intensity, to perform pixel-wise river channel segmentation across diverse geomorphological contexts. Model performance varies with LiDAR data quality and watershed characteristics, underscoring the need for methods that remain reliable across heterogeneous acquisition conditions. By replacing manual digitization with an automated approach, this method substantially reduces processing time while maintaining high spatial consistency. The workflow is designed to support regional-scale flood-modelling applications, where priority is given to river networks draining areas larger than approximately 50 km², consistent with operational flood hazard mapping practices. The remainder of this paper describes the proposed methodology, evaluates segmentation performance across multiple watersheds, and discusses the implications of automated river channel detection for scalable LiDAR-based bathymetry estimation and flood modelling.

2 METHODS

2.1 Study Areas and LiDAR Datasets

The deep learning workflow was developed and evaluated using airborne LiDAR data from four watersheds in Quebec (Qc) and one in Ontario (On): Gatineau (Qc), Du Nord (Qc), Ristigouche (Qc), Saint-François (Qc) and Grand River (On) (see Training and Validation on Figure 1). These watersheds were selected to represent a range of hydrological and geomorphological conditions, including variations in channel size, planform complexity, and floodplain morphology. Manually digitized wetted river channel polygons at the time of LiDAR acquisition were available for all study areas and served as reference data for model training and validation.

These datasets encompass a range of LiDAR acquisition conditions and point-density configurations, resulting in spatially heterogeneous data quality across watersheds. This heterogeneity provides a realistic and operationally relevant framework for evaluating the robustness of automated river channel detection methods intended for regional-scale flood-modelling applications.

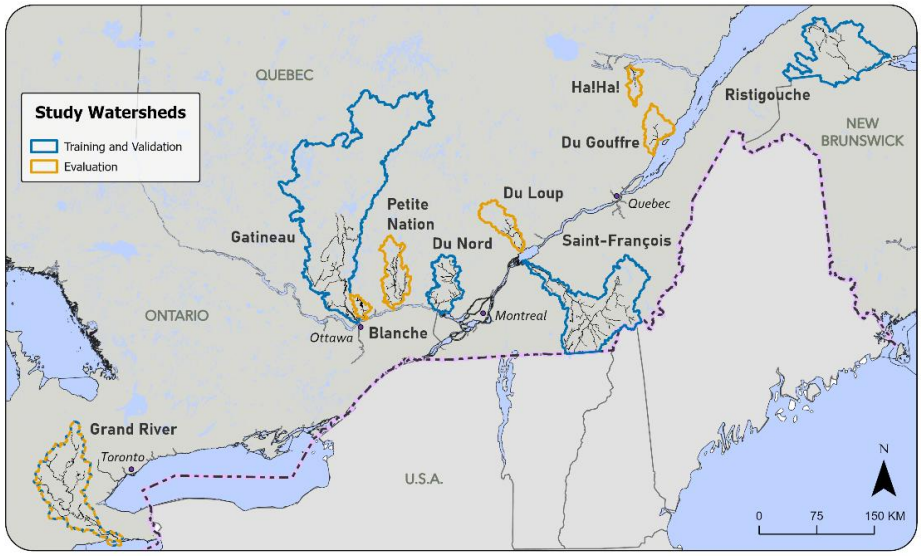

Figure 1: Study areas showing watersheds used for training, validation and evaluation

2.2 Input Data Preparation

Raw LiDAR point clouds filtered by acquisition days were processed into georeferenced raster products at a spatial resolution of 1 m. Only points classified as ground and water were retained in order to minimize the influence of vegetation and built structures and to focus the analysis on terrain and hydrological features relevant to river channel detection. From these filtered point clouds, three primary raster layers were generated: digital elevation model (DEM), LiDAR point density, and intensity. A slope raster was additionally derived from the DEM to provide complementary information on terrain gradients.

All LiDAR-derived raster layers were clipped to the extent of a selected buffer around the river channels. To ensure consistency across watersheds and reduce sensitivity to extreme values, raster inputs were normalized using percentile-based scaling. Both elevation and intensity values were scaled to the range of 0 to 1 using the 1st and 99th percentiles. Elevation values were normalized within each input raster to reduce the influence of large-scale elevation gradients and emphasize channel morphology. Linear interpolation was applied to fill small gaps in the DEM caused by missing LiDAR returns over water surfaces.

2.3 Reference Data and Training Masks

The manually digitized wetted river channel polygons described in Section 2.1 were rasterized at the same spatial resolution and extent as the LiDAR-derived input rasters to generate binary segmentation masks for supervised learning.

In addition to binary channel masks, separate ignore masks were generated to identify pixels excluded from supervision during training. These masks were introduced to account for areas where minor channels, secondary water bodies, or lakes were not consistently annotated in the reference data, thereby preventing ambiguous supervision during training. Ignore masks were implemented as a binary exclusion layer, where pixels marked as ignored were neither assigned to the river nor background class and were excluded from loss computation during supervised training. These masks were generated from the *Gestion des réseaux hydrographiques du Québec* (GRHQ) hydrographic datasets (Web-1). For the Grand River watershed, ignore masks were derived from publicly available hydrographic layers provided by the *Grand River Conservation Authority* (Web-2).

To improve the delineation of riverbanks and narrow channel features, edge maps were derived from the binary masks and incorporated into the training process. These edge maps highlight transition zones between land and water and support more precise learning of channel boundaries.

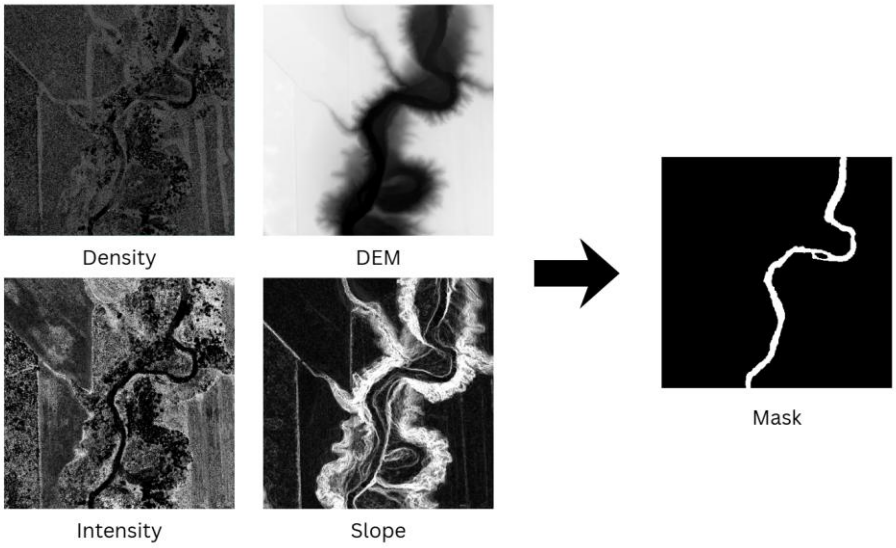

Figure 2: Example of LiDAR-derived input layers and corresponding river channel mask for the Saint-François watershed. Input rasters were scaled to [0, 1] and visualized in grayscale. The mask is binary (1 = channel, 0 = background).

2.4 Deep Learning Architecture

River channel detection was performed using a convolutional neural network (CNN) based on the DeepResUNet architecture, which is well-suited for semantic segmentation tasks requiring pixel-level classification and precise boundary delineation (Zhang et al., 2018; Clabaut et al., 2024).

DeepResUNet follows an encoder–decoder structure similar to U-Net, in which spatial features are progressively extracted from the multi-band LiDAR inputs and then reconstructed into a segmentation map at the original spatial resolution. Skip connections between encoding and decoding layers allow fine spatial details to be preserved during reconstruction, and residual connections enable information from earlier layers to be directly propagated through the network, improving training stability and helping the model retain relevant spatial patterns as depth increases (Zhang et al., 2018). This architecture was therefore selected for automated river channel detection in this study.

2.5 Model Training and Evaluation

The segmentation model was trained using a supervised learning approach with the channel masks described in Section 2.3 serving as reference data. Preprocessed raster layers were stacked into multi-band inputs and subdivided into fixed-size tiles of 512 × 512 pixels (corresponding to 512 m x 512 m at 1 m resolution) for convolutional neural network training (Figure 2). The dataset consisted of 6,375 image tiles extracted from all study watersheds and was randomly split into training (90%) and validation (10%) subsets while preserving representation across different hydrological and geomorphological contexts. The allocation of watersheds between training, validation, and evaluation is summarized in Table 1.

To improve robustness to inter-provincial LiDAR differences, a subset of tiles from the Grand River watershed was incorporated into the training dataset. Approximately 40% of available Grand River tiles, primarily covering continuous river sections in the western portion of the watershed, were included in training, while the remaining 60% were reserved exclusively for inference and evaluation. This strategy exposed the model to LiDAR characteristics specific to Ontario datasets, including differences in point density and intensity distributions, while preserving a spatially independent portion of the watershed for testing.

Table 1. Watersheds used for model training and evaluation (see Figure 1 for watershed locations)

Usage category	Watersheds
Training and validation	Gatineau (Qc) Du Nord (Qc) Ristigouche (Qc) Saint-François (Qc) Grand River (On, partial)
Fully withheld from training (evaluation only)	Petite Nation (Qc) Blanche (Qc) Ha! Ha! (Qc) Du Loup (Qc) Du Gouffre (Qc)

Model performance was evaluated using the mean Intersection-over-Union (mIoU) metric, which quantifies spatial agreement between predicted and reference channel extents by averaging IoU values over the water and background classes. This metric was used for model selection in order to ensure balanced learning and limit false positive predictions. The model achieving the highest validation mIoU was retained for inference. For cross-watershed evaluation, segmentation performance is primarily reported using IoU_{water}, as accurate channel delineation is the main objective of this study.

$$\mathrm{mIoU} = \frac{\mathrm{IoU}_{\mathrm{water}} + \mathrm{IoU}_{\mathrm{background}}}{2} \tag{1}$$

$$\mathrm{IoU}_{\mathrm{water}} = \frac{\mathrm{True\ Positives}}{\mathrm{True\ Positives+False\ Positives+False\ Negatives}} \tag{2}$$

Model optimization was performed using the AdamW optimizer (Loshchilov & Hutter, 2019) with an initial learning rate of 1×10^{-4}, a key hyperparameter that determines how quickly the model updates its internal parameters during training. A learning rate scheduler reduced the rate by a factor of 0.8 after 4 consecutive epochs without improvement in validation mIoU, up to a maximum of 5 changes. This dynamic adjustment helps maintain learning progress and avoid stagnation. Training was conducted using a batch size of 32. During optimization, pixels corresponding to riverbank edges were assigned a multiplicative weight of 3 in the loss computation, encouraging the network to focus on land–water transitions and reduce boundary uncertainty. This edge-aware supervision supports sharper channel boundaries, particularly for narrow channels and complex riverbanks. The final model configuration was selected based on validation performance and training stability.

To improve generalization and reduce overfitting, data augmentation was applied during training. Augmentation strategies included geometric transformations such as rotations, flips, and elastic deformations, as well as photometric adjustments such as brightness and contrast variations, blur, and noise (Buslaev et al., 2020; Minaee et al., 2022). These transformations were designed to expose the model to a broader range of spatial configurations and acquisition conditions while preserving the physical characteristics of river channels.

2.6 Inference

The model producing the highest validation performance was used for inference. During inference, the model produced pixel-level river channel probability scores for each tile. These tile-level predictions were subsequently reassembled to generate continuous river channel maps at the watershed scale. These probability scores provide complementary information for assessing prediction reliability and identifying

areas of increased uncertainty. They also support post-processing and quality control procedures, allowing uncertain predictions to be filtered when required. For channel extraction, probability maps were thresholded using a value of 0.75, such that only pixels with a predicted river probability equal to or greater than 75% were retained. The resulting automated channel delineations are intended for direct integration into LiDAR-based inverse hydraulic modelling workflows for bathymetry estimation.

3 RESULTS

3.1 Model Performance

Figure 4 shows the evolution of training and validation mIoU for the final model used. Both curves show a rapid increase during the early stages of training, indicating that the model is quickly learning to segment river features. The training mIoU increases smoothly throughout optimization and reaches approximately 94.8% towards the end of training.

The validation mIoU follows a similar overall trend but displays greater variability during early training. As training progresses, these fluctuations diminish, and the curve converges. These fluctuations likely reflect differences in the validation dataset, such as variability in LiDAR point density or elevation inconsistencies. The gap between training and validation performance remains limited (below 5%) throughout training, indicating minimal overfitting. By the end of training, the model stabilizes at a validation mIoU of approximately 90.5%, reflecting stable segmentation performance across the evaluated watersheds.

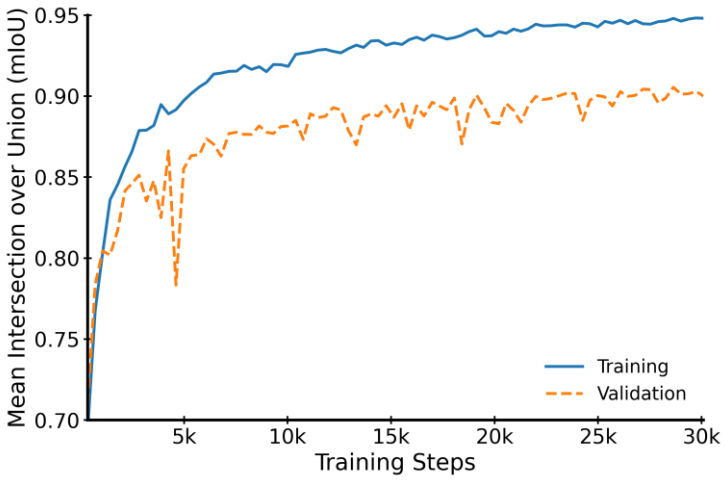

Figure 4: Model performance – Training and validation mIoU curve

3.2 Segmentation Performance Across Watersheds

Large river channels were consistently delineated across all test watersheds, with accurate representation of channel width and riverbank position. All evaluation watersheds except for the Grand River (Figure 1, Table 1) were withheld entirely from training, providing a strict test of model generalization. Despite this, the model produced strong and spatially coherent channel predictions across all sites, consistent with previous applications of deep learning to hydrological feature extraction from remote sensing data (Sun et al., 2018; Ulku & Akagündüz, 2022). From a regional flood-modelling perspective, these results are particularly relevant for river networks associated with a drainage area larger than 50 km^2, which represent the primary targets of operational flood hazard mapping.The Petite Nation and Blanche watersheds both produced consistently high-quality results, with Intersection-over-Union (IoU_water) values approaching 95%, reflecting accurate boundary delineation and strong detection of river features. For the remaining watersheds (Ha! Ha!, du Loup, and Du Gouffre), large river channels were also

well captured, while greater variability was observed in smaller tributaries. In particular, watersheds affected by sparse LiDAR coverage or heterogeneous acquisition conditions, including multi-day surveys, overlapping flight lines, and variable flow conditions, exhibited lower standard IoU values. However, qualitative analysis indicates that these decreases primarily reflect limitations in LiDAR data availability and reference completeness rather than systematic segmentation errors. Importantly, the model consistently detected the primary channels relevant to regional-scale flood-modelling applications.

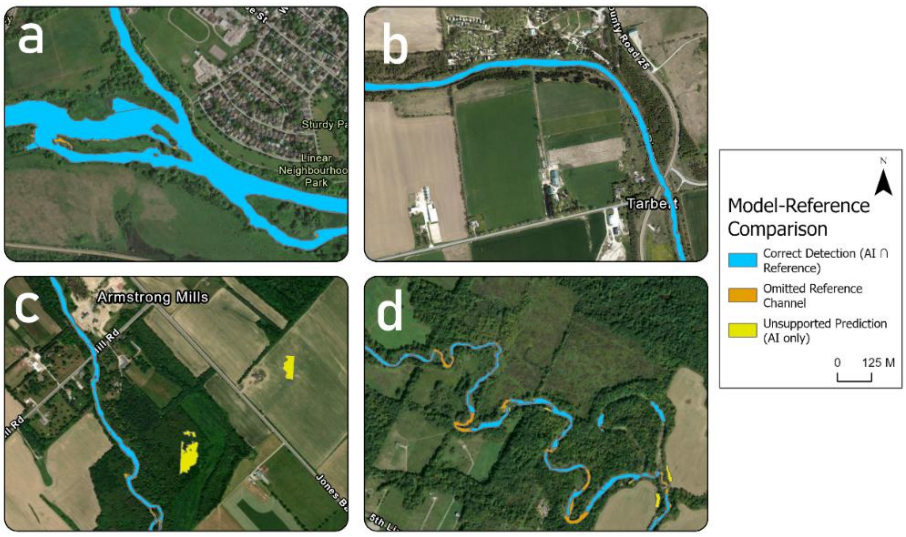

Figure 5: Spatial comparison between model predictions and reference river channels in the Grand River

The differences in omissions across channel sizes are well illustrated in the Grand River watershed (Figure 5). Large and medium-sized channels are accurately delineated, while smaller channels are also detected with good spatial coherence (Figure 5a–b). Here, channel size classes are defined based on approximate bankfull width derived from the LiDAR data: small (≤ 10 m), medium (10–40 m), and large (> 40 m). When the model was trained exclusively on Québec watersheds, inference over the Grand River watershed resulted in a standard IoU of approximately 58.2%, with visible artefacts linked to differences in LiDAR acquisition characteristics, including local edge effects at tile boundaries (Figure 5c). Most omissions occurred in narrow, highly sinuous channels and in reaches affected by dense riparian vegetation, where reduced water-surface visibility limits the quality of LiDAR-derived inputs, and were generally confined to short tributary segments near the operational drainage-area threshold (Figure 5d).

After incorporating a limited, representative subset of Grand River tiles into the training dataset, segmentation performance improved substantially, with IoU increasing to approximately 90.2% and a decrease in edge artefacts. This result highlights the sensitivity of deep learning models to domain shifts in LiDAR characteristics and demonstrates that targeted domain adaptation can significantly improve generalization under heterogeneous acquisition conditions.

The remaining artefacts are spatially limited and do not affect the continuity of the main channel network. In addition, the model frequently detected secondary channels, ponds, and other water bodies not included in the manually digitized reference datasets, but many align with real hydrological features omitted from the reference annotations. Although many were filtered out through provincial hydrographic layers in standard quantitative evaluation, these detections reflect the sensitivity of the model to hydrological signatures in LiDAR-derived inputs and the limitations of incomplete ground truth data (Ulku & Akagündüz, 2022). From an operational perspective, such features can be readily filtered during post-processing when required, while also offering added value for more comprehensive hydrographic analyses beyond the primary flood-modelling objectives.

4 DISCUSSION AND CONCLUSION

The results demonstrate that deep learning–based semantic segmentation can provide accurate and spatially consistent river channel delineation from LiDAR-derived raster products at the watershed scale, as expected for convolutional neural networks trained on spatially coherent data (Sun et al., 2018; Ulku & Akagündüz, 2022). The strong generalization observed across multiple test watersheds that were not used during training confirms the robustness of the proposed workflow and supports its suitability for large-scale use. Model training and inference were performed on a workstation equipped with a single NVIDIA GeForce RTX 4090 GPU (24 GB VRAM). Under this hardware configuration, the trained model processes one 1-km² tile in approximately 10 seconds, allowing rapid inference over large river networks and making the approach computationally practical for regional flood-modelling applications. For example, in the Grand River watershed, automated channel extraction reduced processing time from roughly 380 seconds to about 10 seconds per kilometre of river, making the workflow close to 40 times faster than manual digitization. This directly addresses a major practical limitation in the LiDAR-based inverse hydraulic modelling workflow of Choné et al. (2021, 2024), where manual digitization of wetted channel polygons was highlighted as being time-consuming, subjective, and difficult to scale.

Spatial variability in segmentation performance was strongly linked to LiDAR data quality and acquisition characteristics. Watersheds surveyed with higher point density and more homogeneous acquisition conditions produced sharper channel boundaries, fewer misclassifications, and more continuous channel predictions. In contrast, local decreases in data quality, including weak water-surface returns, variable point density, and acquisition inconsistencies across flight lines and survey days, introduced uncertainty that limited segmentation performance in smaller or more complex channels. This behaviour is illustrated in the Grand River watershed, where both large and smaller channels were generally detected, while differences in acquisition characteristics and inter-tile inconsistencies resulted in localized edge artefacts when the watershed was excluded from the training dataset. Importantly, the affected channel segments were typically short, on the order of a few hundred metres, and did not disrupt the continuity of the primary river network. These results highlight the importance of adopting more standardized LiDAR acquisition protocols to improve data consistency and support reliable automated river channel extraction. These effects reflect fundamental constraints of airborne LiDAR rather than limitations of the deep learning model itself (Legleiter & Harrison, 2019; Canaz et al., 2015; Neal et al., 2021).

The detection of hydrological features absent from the reference datasets further illustrates both the strengths and challenges of automated channel extraction. While these features are penalized as false positives in pixel-based evaluation, many correspond to real secondary channels, wetlands, or floodplain water bodies that are not consistently represented in manually digitized polygons. This highlights the incompleteness of available ground truth data and directly motivated the incorporation of additional hydrographic datasets during evaluation to better account for known water features absent from the reference labels. In parallel, ignore masks were introduced during training to exclude ambiguous regions from loss computation, thereby reducing the impact of annotation inconsistencies on model learning (Clabaut et al., 2024). Together, these steps support a more realistic assessment of segmentation performance and suggest that deep learning models can provide a more comprehensive and objective representation of hydrographic networks when combined with appropriate post-processing and validation.

From an operational flood-modelling perspective, the occasional omissions of short tributary segments near the drainage-area threshold do not compromise the primary objectives of regional-scale applications. Such omissions are typically spatially limited and often involve short channel segments on the order of a few hundred metres. Importantly, the proposed workflow represents a substantial improvement over existing manual digitization practices, where these features are frequently inconsistently represented or omitted entirely. Moreover, when required, these marginal channels can be readily identified and refined during post-processing without affecting the accuracy or continuity of the primary river network targeted by flood-modelling applications.

Overall, the proposed workflow offers a scalable and repeatable alternative to manual channel delineation. It demonstrates strong generalization to independent test watersheds and delivers rapid

inference over large spatial extents. By automating a critical preprocessing step, this approach supports the more rapid updating of physically based flood models over large spatial extents, with direct implications for flood hazard mapping, infrastructure planning, and risk assessment. The proposed workflow could be adopted by LiDAR providers in their classified final products to clients to include LiDAR channel polygons with their product.

Future work will focus on further improving robustness to heterogeneous LiDAR datasets and on evaluating whether more standardized LiDAR acquisition, such as nation-wide specifications, could improve model transferability and comparability across watersheds.

5 ACKNOWLEDGEMENTS

This work is supported by the Flood Hazard Identification and Mapping Program (FHIMP) of Natural Resources Canada (NRCan).

REFERENCES

Biron, P. M., Choné, G., Buffin-Bélanger, T., Demers, S., & Olsen, T. (2013). Improvement of streams hydro-geomorphological assessment using LiDAR DEMs. *Earth Surface Processes and Landforms*, *38*(15), 1808–1821. https://doi.org/10.1002/esp.3425

Buslaev, A., Parinov, A., Khvedchenya, E., Iglovikov, V. I., & Kalinin, A. A. (2020). Albumentations: Fast and flexible image augmentations. Information, 11(2), 125. https://doi.org/10.3390/info11020125

Canaz, S., Karsli, F., Guneroglu, A., & Dihkan, M. (2015). Automatic boundary extraction of inland water bodies using LiDAR data. Ocean & Coastal Management, 118, 158–166. https://doi.org/10.1016/j.ocecoaman.2015.07.024

Choné, G., Biron, P. M., Buffin-Bélanger, T., Mazgareanu, I., Neal, J. C., & Sampson, C. C. (2021). An assessment of large-scale flood modelling based on LiDAR data. *Hydrological Processes*, *35*(8), e14333. https://doi.org/10.1002/hyp.14333

Choné, G., Mazgareanu, I., Biron, P. M., Buffin-Bélanger, T., Larouche-Tremblay, F., Perry, B., & Fortin, M. (2024). Large-scale flood modelling based on LiDAR data: A case study in the Southwest Miramichi watershed, New Brunswick, Canada. *Canadian Water Resources Journal / Revue Canadienne Des Ressources Hydriques*, *49*(4), 460–478. https://doi.org/10.1080/07011784.2024.2430776

Clabaut, É., Foucher, S., Bouroubi, Y., & Germain, M. (2024). Synthetic Data for Sentinel-2 Semantic Segmentation. Remote Sensing, 16(5), 818. https://doi.org/10.3390/rs16050818

Legleiter, C. J., & Harrison, L. R. (2019). Remote Sensing of River Bathymetry: Evaluating a Range of Sensors, Platforms, and Algorithms on the Upper Sacramento River, California, USA. Water Resources Research, 55(3), 2142–2169. https://doi.org/10.1029/2018WR023586

Loshchilov, I., & Hutter, F. (2019). Decoupled weight decay regularization. *Proceedings of the International Conference on Learning Representations (ICLR)*. https://arxiv.org/abs/1711.05101

Minaee, S., Boykov, Y., Porikli, F., Plaza, A., Kehtarnavaz, N., & Terzopoulos, D. (2022). Image Segmentation Using Deep Learning: A Survey. IEEE Transactions on Pattern Analysis and Machine Intelligence, 44(7), 3523–3542. IEEE Transactions on Pattern Analysis and Machine Intelligence. https://doi.org/10.1109/TPAMI.2021.3059968

Neal, J., Hawker, L., Savage, J., Durand, M., Bates, P., & Sampson, C. (2021). Estimating River Channel Bathymetry in Large Scale Flood Inundation Models. Water Resources Research, 57(5), e2020WR028301. https://doi.org/10.1029/2020WR028301

Sun, Y., Zhang, X., Xin, Q., & Huang, J. (2018). Developing a multi-filter convolutional neural network for semantic segmentation using high-resolution aerial imagery and LiDAR data. ISPRS Journal of Photogrammetry and Remote Sensing, 143, 3–14. https://doi.org/10.1016/j.isprsjprs.2018.06.005

Trigg, M. A., Birch, C. E., Neal, J. C., Bates, P. D., Smith, A., Sampson, C. C., Yamazaki, D., Hirabayashi, Y., Pappenberger, F., Dutra, E., Ward, P. J., Winsemius, H. C., Salamon, P., Dottori, F., Rudari, R., Kappes, M. S., Simpson, A. L., Hadzilacos, G., & Fewtrell, T. J. (2016). The credibility challenge for global fluvial flood risk analysis. Environmental Research Letters, 11(9), 094014. https://doi.org/10.1088/1748-9326/11/9/094014

Ulku, I., & Akagündüz, E. (2022). A Survey on Deep Learning-based Architectures for Semantic Segmentation on 2D Images. Applied Artificial Intelligence. https://www.tandfonline.com/doi/abs/10.1080/08839514.2022.2032924

Wilby, R. L., & Keenan, R. (2012). Adapting to flood risk under climate change. Progress in Physical Geography: Earth and Environment, 36(3), 348–378. https://doi.org/10.1177/0309133312438908

Zhang, Z., Liu, Q., & Wang, Y. (2018). Road Extraction by Deep Residual U-Net. IEEE Geoscience and Remote Sensing Letters, 15(5), 749–753. https://doi.org/10.1109/LGRS.2018.2802944

Web sites:

Web-1: https://www.donneesquebec.ca/recherche/dataset/grhq, consulted 22 August 2025.

Web-2: https://data.grandriver.ca/downloads-geospatial.html, consulted 18 January 2026.

ICFM 10
Adapting to Global Change:
Innovative Approaches to Flood Management and Resilience
May 20-22, 2026 | Western University, London, Ontario, Canada

Design Storm Development for Floodplain Mapping and Flood Risk Assessment in Cold Climate Conditions: Credit River Watershed, Ontario

Tim Mereu[1] and Neelam Gupta[2]
Water Analytics Partnership, Toronto, Ontario[1]
E-mail: tmereu@water-analytics.ca

Credit Valley Conservation Authority, Mississauga, Ontario[2]
E-mail: neelam.gupta@cvc.ca

ABSTRACT

In cold-climate watersheds, winter hydrologic processes-including snowfall accumulation, snowmelt, frozen ground conditions, and rain-on-snow events - play a critical role in generating flood peaks. Recognizing these unique dynamics, Credit Valley Conservation (CVC) developed winter-specific design storms to accurately capture the timing, intensity, and runoff response of cold-season events. These storm profiles were derived from historical winter precipitation and temperature records to reflect current winter flood conditions. Incorporating these winter-specific storms provide a more robust basis for assessing peak flows, flood risk, and related hydraulic and erosion impacts under existing and changing winter conditions.

Hydrologic models used for floodplain mapping and flood risk assessment must generate peak flows corresponding to 2- to 100-year return periods, consistent with the availability of monitored streamflow data. Where gauge records exist, modelled peak flows are calibrated to align with observed flood frequency analyses, ensuring realistic representation of local watershed behaviour. Both continuous simulation and event-based modelling approaches are commonly applied, with event-based models relying on design storms as critical inputs. To produce credible runoff estimates, the response from these design storms must reflect observed flood frequency characteristics.

Traditional design storms often emphasize rainfall-driven events, which can overlook the significant contribution of winter hydrology in many rural Canadian watersheds. In regions where winter rainfall, snowmelt, or combined events drive flooding, seasonally tailored design storms are essential for accurate hydrologic modelling. This study presents a methodology for generating winter (and summer) design storms that reproduce observed flood frequencies at site-specific gauged locations.

Results demonstrate that integrating winter-specific hydrologic processes into floodplain mapping and flood risk assessment substantially improves model reliability. By applying these winter-focused design storms, engineers and planners can better evaluate the impacts of land use changes, watershed restoration, and evolving winter conditions on flood risks, supporting more effective and resilient flood management in cold climates.

KEYWORDS: design storm, rainfall–snowmelt, flood risk assessment, flood frequency analysis, hydrologic modelling, cold-climate, urban and rural hydrologic modelling

1 INTRODUCTION

Event-based hydrologic modelling is widely used to estimate return-period peak flows for flood risk assessment and infrastructure design, particularly where continuous simulation is impractical or future land-use and climate scenarios must be evaluated. A key limitation is that generic design storm distributions may

produce peak flows inconsistent with flood frequency analysis (FFA) of observed streamflow records, leading to systematic over- or underestimation of flood risk.

This paper describes the development and calibration of representative design storms for urban and rural subwatersheds in the Credit River watershed, Ontario, Canada. Three dominant flood-generating mechanisms were considered: short-duration convective storms in urban catchments, frontal rainfall in smaller rural catchments, and winter rainfall–snowmelt events in larger rural basins.

For urban subwatersheds, candidate storm distributions were evaluated by applying each to calibrated event-based hydrologic models and comparing peak flows with FFA targets. The 24-hour Chicago distribution provided the closest agreement for fully urbanized catchments smaller than approximately 20 km². For rural subwatersheds, FFA indicated that winter rainfall–snowmelt processes dominate flooding in most basins larger than approximately 30–50 km². A standardized 72-hour rainfall–snowmelt design event was developed and calibrated across multiple gauges spanning a wide range of drainage areas. For smaller rural subwatersheds not dominated by winter runoff, the 12-hour AES storm was selected. The study produced subwatershed-specific design storms that enable CVC to generate peak flows consistent with flood frequency analyses at long-term gauging stations.

2 STUDY AREA

As illustrated in Figure 1, the Credit River watershed in southern Ontario drains to Lake Ontario and includes both urban tributaries in the lower basin and predominantly rural headwater and mid-basin areas. Drainage areas analysed range from less than 20 km² to more than 600 km².

The humid continental climate produces cold winters with seasonal snow accumulation and warm summers with convective rainfall. Flood mechanisms vary spatially: intense short-duration storms dominate urban flooding, while winter rainfall–snowmelt events often control peak flows in larger rural catchments. Multiple long-term streamflow gauges are available across the watershed. The gauges used in this design storm study are noted in Figure 1.

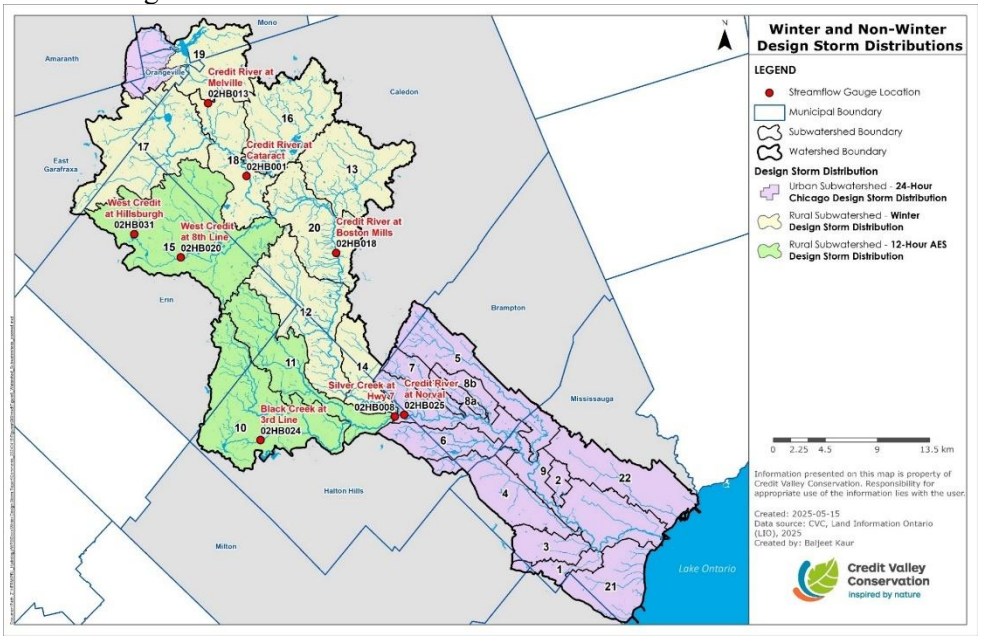

Figure 1: Credit River Subwatersheds and Water Survey Canada (WSC) Gauging Stations

3 DESIGN STORM DEVELOPMENT

3.1 General Considerations

Design storms have long been used for regulatory and design purposes but may produce biased flow estimates if applied without local calibration. Design storm characteristics must therefore reflect watershed-specific hydrologic processes.

In the Credit River watershed, three primary flood mechanisms require distinct design storms:

- Urban watercourses: intense short-duration convective rainfall
- Small rural headwaters: longer-duration frontal rainfall
- Large rural basins: winter rainfall–snowmelt events.

3.2 Design Storms for Urban Watercourses

Urban design storm selection involved calibrating hydrologic models to historical events and identifying storm distributions that reproduce FFA-consistent peak flows.

A generalized continuous simulation model was developed for 19 urban subwatersheds and an additional nearby watershed with a long record (Mimico Creek). Sixty years of precipitation data were used to generate synthetic flow series and derive flood frequency relationships. Candidate design storms were then tested in calibrated models and compared with both measured and simulated FFA results (CVC, 2016).

The 24-hour Chicago distribution provided the best overall agreement and was selected for urban catchments smaller than approximately 20 km². Larger catchments were not evaluated; experience suggests intense Chicago-type storms may overestimate peak flows when applied over larger areas.

Figure 2 presents the FFA results derived from 63 years of continuous simulation together with the 10-year Cooksville Creek record (CVC, 2017). Analyses are shown both including and excluding the July 8, 2013, flood of record, reflecting the sensitivity of short observational records to extreme events. The agreement between observed and simulated flows supports the use of the simulated FFA as representative of conditions at the Cooksville Creek near Cooksville WSC gauging station (02HB030). Peak flows generated by candidate design storms were superimposed, and the 24-hour Chicago distribution was selected for urban watershed applications.

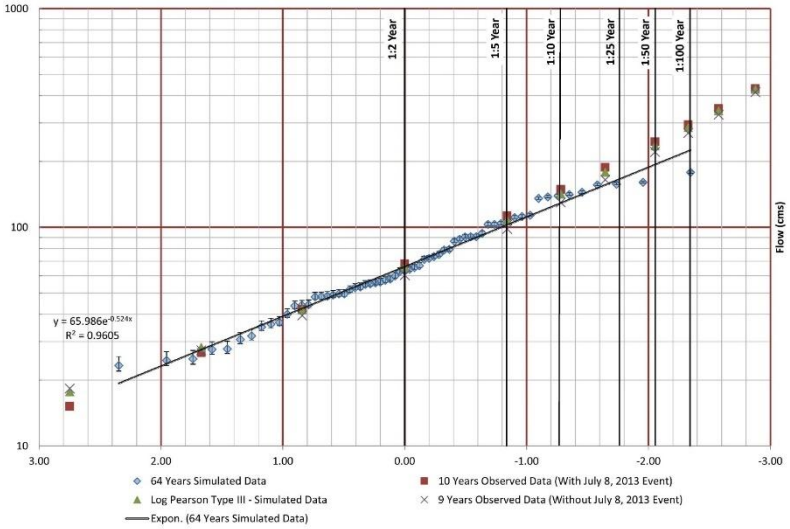

Figure 2: Observed and Simulated Peak Flow FFA at Cooksville Creek at Cooksville- WSC Station (02HB030)

It is important to note that all subwatersheds to which this event is applied have catchment areas smaller than 20 km². Experience elsewhere indicates that as catchment area increases, the Chicago storm and similar high-intensity summer storm distributions tend to overestimate peak flows, as such rainfall intensities are unlikely to occur uniformly across larger watersheds.

3.3 Winter Design Storm Distribution for Rural Subwatersheds

Winter events were developed by:
1. Performing frequency analysis of combined rainfall–snowmelt
2. Selecting representative temperature sequences from major historical events
3. Constructing initial design events from rainfall, snowmelt, and temperature data
4. Applying events to calibrated hydrologic models
5. Iteratively calibrating results to match gauged FFA relationships

3.3.1 Frequency Analysis of Rainfall-Snowmelt

Figure 3 presents the frequency distribution of combined rainfall–snowmelt depths derived from total event runoff volumes recorded at WSC gauging station located near the centre of the watershed (West Credit River at 8th Line (02HB020)). Historical flow records were first used to calculate total event runoff volumes which were subsequently converted to equivalent runoff depths by diving by the contributing catchment area.

An average Curve Number (CN) and Initial Abstraction (IA) value, derived during calibration of the hydrologic model, were applied within the SCS CN equation (USDA, 1986) to estimate corresponding rainfall-snowmelt amounts. The analysis is based on a 20-year period of record, reflecting the availability of hourly data. These data support estimation of total rainfall–snowmelt amounts for return periods of up to 1:100 years.

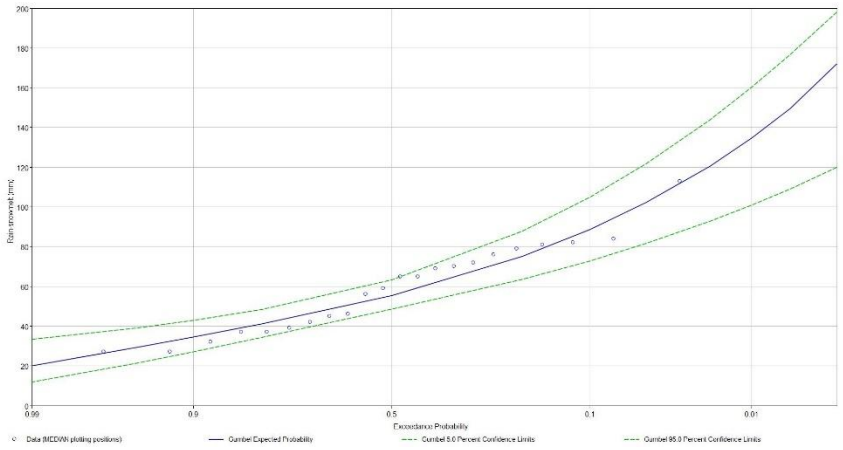

Figure 3: Rainfall-Snowmelt Frequency at West Credit River at 8th Line (WSC Station 02HB020)

3.3.2 Initial Temperature Sequence

A key outcome of the design event calibration was the identification of events lasting at least 48 hours and resulting in complete snowmelt as most representative of major runoff conditions. The February 2018 event, one of the two largest on record, was selected to define the temperature sequence. Figure 4 shows the observed temperature record, in orange and the assumed temperature sequences for the 1:5- and 1:50-year events. These temperature profiles were selected so that the combined rainfall and snowmelt volumes matched the return-period estimates derived from the frequency analysis shown in Figure 3.

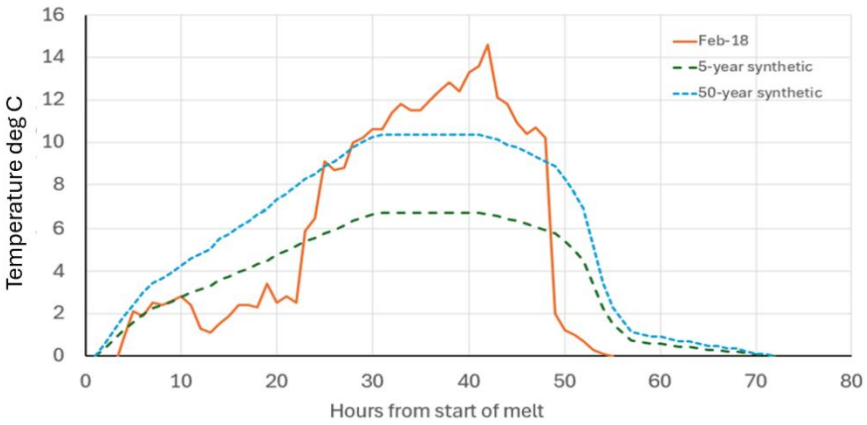

Figure 4: Design Event Temperature Sequence

3.3.3 Initial Series of Design Events

The next step was to develop an initial series of design storms based on the selected temperature sequence, initial snowpack conditions, and total precipitation. Rainfall was assumed to account for 40% of the total, with snowmelt contributing the remaining 60%, consistent with proportions observed during major recorded flood events.

3.3.4 Gauge Locations

As illustrated in Figure 1, the following gauges were identified for comparison and calibration purposes.

1) Credit River at Melville (02HB013; 1967-2024; Drainage area = 61 km^2)
2) Credit River at Cataract (02HB001; 1916-2024; Drainage area = 209 km^2)
3) Credit River at Boston Mills (02HB018; 1982-2024; Drainage area = 415 km^2)
4) Credit River at Norval (02HB024; 1988-2024; Drainage area = 645 km^2)
5) West Credit River at 8th Line (02HB020; 1983-2024; Drainage area = 32 km^2)
6) Silver Creek at Highway 7 (02HB008; 1960-2024; Drainage area = 113 km^2)

3.3.5 Initial Flow Generation

The initial design events were then applied to the calibrated Visual OTTHYMO hydrologic model (CVC, 2025) to generate peak flow rates at the Credit River at Melville (02HB013), Cataract (02HB001) and Boston Mills (02HB018) gauge locations for the 1:2-year to 1:100-year rainfall-snowmelt event. For each of these locations the generated runoff from the design storms was overlayed on the FFA for comparison.

3.3.6 Winter Design Storms Calibration

Initial application of the design events revealed two key trends. First, peak flows generated by the design storms increased more rapidly with return period than indicated by the historical flow record, consistent with the steep curvature observed in the rainfall–snowmelt frequency analysis. Second, results suggested that an aerial reduction factor would be required when applying the design events to larger downstream catchments.

To better align model results with observed conditions, the design events were calibrated through iterative adjustment of the rainfall–snowmelt relationship and application of a modest aerial reduction factor. This process produced a revised return period–rainfall–snowmelt relationship for a standardized 72-hour storm duration. The revised relationship removed the previously observed concave trend while remaining within established confidence limits. Final rainfall–snowmelt volumes for each return period are summarized in Table 1.

Table 1: Final Winter Design Event Volumes

Return Period (Year)	Final Design Event Volume (mm)			
	Credit River at Melville (02HB013)	Credit River at Cataract (02HB001)	Credit River at Boston Mills (02HB018)	Credit River at Norval (02HB025)
2	60	54	51	49
5	77	70	66	64
10	87	79	70	72
25	96	87	82	80
50	104	94	89	86
100	110	100	94	91

Figure 5 illustrates application of the calibrated rainfall–snowmelt volumes within the hydrologic models. In the first three panels, original and calibrated results are shown in yellow and pink, respectively, demonstrating close agreement between modelled peak flows and those derived from FFA. As an additional validation, results were compared at the Credit River at Norval (02HB024) gauge, located farther downstream with an upstream drainage area of 645 km². This location exhibited the strongest overall agreement between modelled and observed frequency relationships.

The design events were subsequently applied to two additional gauges: Silver Creek at Highway 7 (02HB008, drainage area 113 km²) and West Credit at 8th Line (02HB020, drainage area 32 km²). As shown in Figure 6, the design storm tended to overestimate peak flows at both locations, although results generally remained within the 95% confidence limits. These findings suggest that further refinement of the winter design storm for these tributaries may be warranted. Alternatively, the summer design storm described in the following section may provide a suitable option.

3.4 Summer Design Storm Distribution for Rural Subwatersheds

This section describes the development of summer design events for the Credit River watershed. The process involved selecting an appropriate rainfall distribution and conducting a frequency analysis of 12-hour rainfall, followed by application of the design storm to the hydrologic model to generate peak flows for return periods from 1:2 to 1:100 years. The design storms were then adjusted through comparison with flood frequency analyses at gauged locations.

3.4.1 12-hour AES Design Storm Distribution

The 12-hour AES (30%) design storm was selected in accordance with provincial guidance (MNR, 2002). The 12-hour rainfall depths were derived from Pearson Airport records and supplemented with locally refined estimates for Silver Creek and the West Credit River.

Consistent with the methodology applied to the winter design events, these rainfall depths were refined through calibration of peak flows generated by applying the 12-hour AES storm to the calibrated Visual OTTHYMO hydrologic model. Adjustments were constrained within the statistical confidence limits of the available data to ensure that the adopted design storm values remained physically defensible and were not arbitrarily modified to achieve agreement with flood frequency analyses at gauged locations.

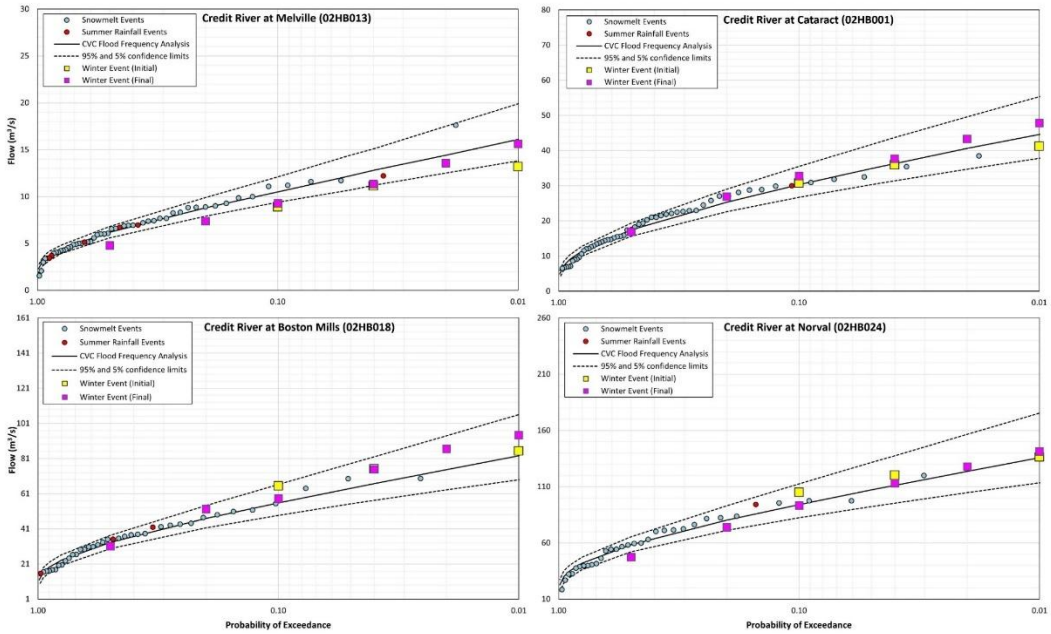

Figure 5: Comparison of Final Winter Design Event and FFAs Flows at Credit River WSC Gauging Stations

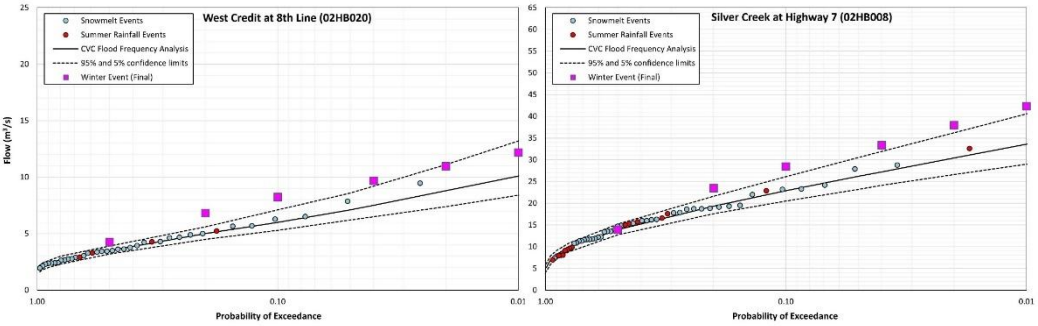

Figure 6: Winter Design Event vs FFA Flows at Silver Creek and West Credit River WSC Gauging Stations

3.4.2 Summer Design Storm Calibration

Figure 7 compares flood frequency estimates with peak flows from the 12-hour AES summer design storm adjusted. As shown, the design storm produces peak flows that are consistent with flood frequency results for events with return periods of 1:10 years and greater. For the 1:2- and 1:5-year events, however, discrepancies are evident, particularly at gauges with the smallest catchment areas (Black Creek at 3rd Line (02HB024) and West Credit near Hillsburgh (02HB031)). These differences likely reflect the small size and unique hydrologic characteristics of these headwater catchments. Although subwatersheds were calibrated at downstream gauges, calibration was not performed at the upper gauges where the largest discrepancies occur. Consequently, the applicability of the rural design storm approach to very small catchments cannot be confirmed without additional calibration at these locations.

For the West Credit River at 8th Line (02HB020) and Silver Creek at Highway 7 (02HB008), both summer design storms and winter rainfall–snowmelt design events were developed. The winter events were applied using the Credit River design storm without further local calibration, whereas the summer design storms were calibrated to local conditions. Figure 8 shows that either may be appropriate depending on the study objectives; thus, for catchments of roughly 30 to 130 km², either approach may be used.

Based on the study findings, the following design storm applications are recommended. For urban catchments smaller than 20 km², apply the 24-hour Chicago design storm distribution using localized Intensity–Duration–Frequency (IDF) data; its applicability to larger urban catchments was not evaluated and requires further study. For rural catchments smaller than 30 km², apply the 12-hour AES (30%) design storm using localized IDF data. For rural catchments between 30 and 130 km², apply either the 12-hour AES (30%) design storm or the winter rainfall–snowmelt design event, depending on watershed characteristics and study objectives. For rural catchments greater than 130 km², apply the rainfall–snowmelt design event. These recommendations provide a consistent framework for flood risk assessment that reflects both regional climate and watershed-specific hydrology. Additional calibration is recommended for smaller catchments and tributaries with higher initial uncertainty.

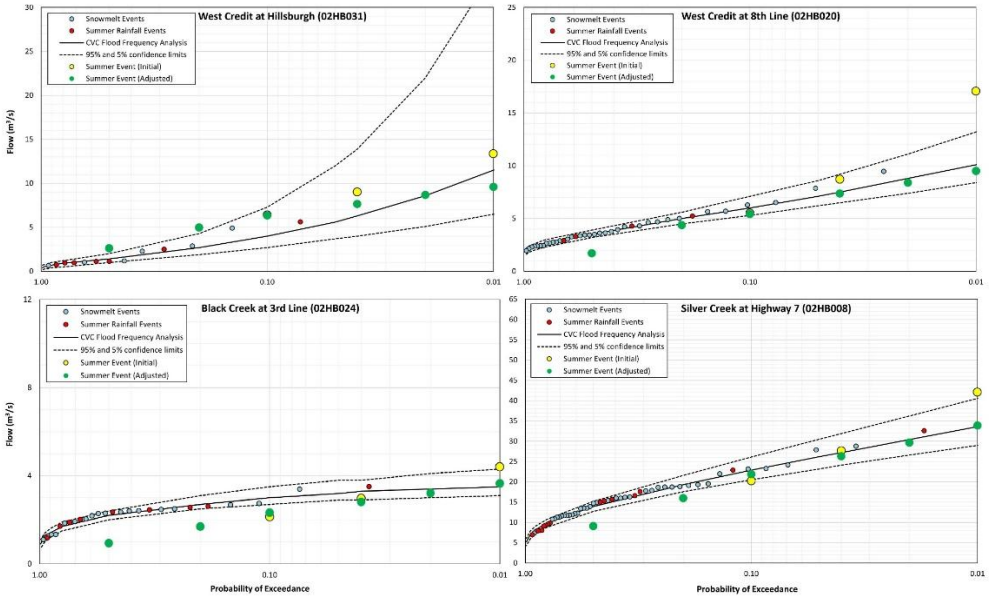

Figure 7: Final Summer Design Event and FFA Flows at Black Creek and West Credit River WSC Stations

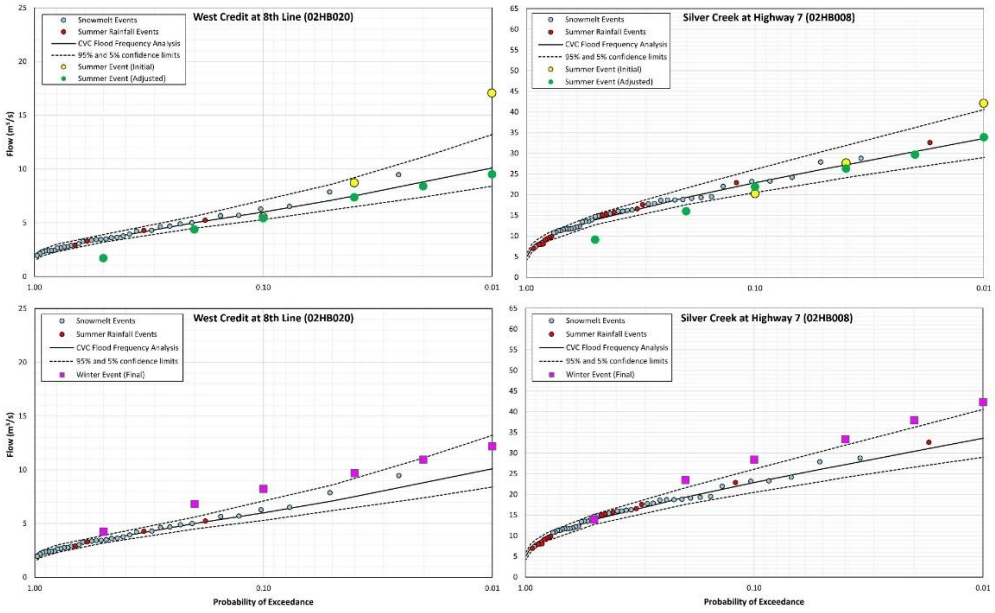

Figure 8: Winter vs. Summer Design Event Flows at Silver Creek and West Credit River for WSC stations

4 ACKNOWLEDGEMENTS

The authors would like to thank their colleagues-Saleh Sebti, Rizwan Ul Haq, Alexandar Pluchik, Andrea Giampuzzi, Graeme McDonald, and Patrcia Cheung at CVC and AECOM for their technical contributions and support throughout this project.

REFERENCES

Credit Valley Conservation (CVC) (2016). Urbanized Flood Flow Analysis for Cooksville Creek watershed and other Lake Ontario Tributaries – Update/Progress Report#3. Schroeter and Associates. November 4, 2016.

Credit Valley Conservation (CVC) (2017). Cooksville Creek & Cawthra Creek Hydrology Update. Aquafor Beech Ltd. August 8th, 2017.

Credit Valley Conservation (CVC) (2025). Hydrologic Model Calibration for Rural Watersheds. CVC Hydrologic Model Calibration. AECOM Canada Ltd. May 30, 2025.

MNR (2002). Technical Guide - River and Stream Systems: Flooding Hazard Limit. Ontario Ministry of Natural Resources, Water Resources Section, Peterborough, Ontario.

United States Department of Agriculture (USDA) (1986). Urban Hydrology for Small Watersheds: Technical Release 55 (TR-55).

ICFM 10
Adapting to Global Change:
Innovative Approaches to Flood Management and Resilience
May 20-22, 2026 | Western University, London, Ontario, Canada

Comparative Analysis of Feature Selection Methods in ML-based Flood Susceptibility Mapping

Heather McGrath[1], Karen E Dunbar[1,2] and Usman Khan[2]
Natural Resources Canada, Ottawa, ON, Canada [1]
E-mail: heather.mcgrath@NRCan-RNCan.gc.ca

Civil Engineering, Lassonde School of Engineering, York University, Toronto, Canada [2]
E-mail: karela@yorku.ca
E-mail: usman.khan@lassonde.yorku.ca

ABSTRACT

Traditional flood susceptibility maps typically rely on static geospatial factors and ignore dynamic meteorological variables, thereby introducing temporal biases. This study addresses these issues by applying different feature selection methods to identify the most influential flood conditioning factors, with a particular focus on including seasonal meteorological data, which is especially important in Canada, where many floods occur during the spring freshet. Three feature selection techniques were used to develop multiple feature sets: Partial Correlation (PC), Partial Mutual Information (PMI), and Combined Neural Pathway Selection (CNPS). In addition to these, two other sets were examined: the full feature set and the base geospatial set (without seasonal meteorological variables). These sets served as inputs for training and evaluating three machine learning models: Extreme Gradient Boosting (XGBoost), an Artificial Neural Network (ANN), and a Convolutional Neural Network (CNN). The PC and PMI feature sets produced results similar to the full feature set, indicating that the feature selection process can reduce model complexity without losing predictive performance. XGBoost performed best, with either the full feature set or the PMI set. Across all models, the highest performance was achieved with the full feature set, highlighting the importance of seasonal meteorological variables for flood susceptibility modelling.

KEYWORDS: Flood susceptibility mapping, feature selection, partial correlation, partial mutual information, combined neural pathway strength

1 INTRODUCTION

Floods are Canada's most expensive hazard, driven by climate change and rapid urbanization (Ajin et al., 2025; Canada, 2025). While Flood Susceptibility Mapping (FSM) is essential for mitigation, traditional methods face challenges regarding data resolution, subjectivity and the exclusion of dynamic variables (El Haou et al., 2025). Most FSM studies rely on static topographic features, overlooking meteorological factors like river gage data, snow accumulation and heavy rain frequency that are crucial for Canadian flood dynamics (Khalid and Khan, 2024; McGrath and Gohl, 2022). Although Machine Learning (ML) methods (e.g., XGBoost, ANN, CNN) excel at modelling non-linear relationships, their performance depends heavily on the quality and quantity of the input data (Bentivoglio et al., 2022; Long et al., 2025). To improve predictive accuracy of ML based FSM, this study focuses on feature selection, which is often overlooked in FSM (Li et al., 2022). By applying Partial Correlation, Partial Mutual Information, and Combined Neural Pathway Strength (Snieder et al., 2020), we aim to integrate seasonal meteorological data in ML models, overcoming the limitations of static susceptibility mapping. To overcome temporal biases in traditional flood modelling, this study focuses on feature selection to integrate

dynamic seasonal meteorological variables. By analyzing multi-year flood data using various feature selection methods, this study aims to produce accurate, seasonally aware flood susceptibility maps. The approach will emphasize the critical role of seasonal dynamics in flood susceptibility, enhancing risk mitigation strategies.

2 METHODS

2.1 Study Area and Data Description

The study area is shown in Figure 1 and was chosen due to the availability of historical flood data from the Canadian Flood Archive (Natural Resources Canada, 2018). It comprises of multiple watersheds that cover distinct areas across Canada. Specifically, the study sites range from the mountainous regions of British Columbia and Alberta to the flatlands of the Canadian Prairies to the maritime environment of the Atlantic provinces. The study areas encompass portions of Canada's Major Drainage Areas (Canada, 2024), including the Yukon River (blue), Pacific (orange), Great Slave Lake (red), Mississippi River (purple), Nelson River (cyan), St. Lawrence (pink), and Maritime (brown). The study areas cover 18 and 28 categories of land use and surficial geology, respectively, and include significant topographical variation, with elevations ranging from 0 to 2082 meters and slopes ranging from 0 to 54 degrees.

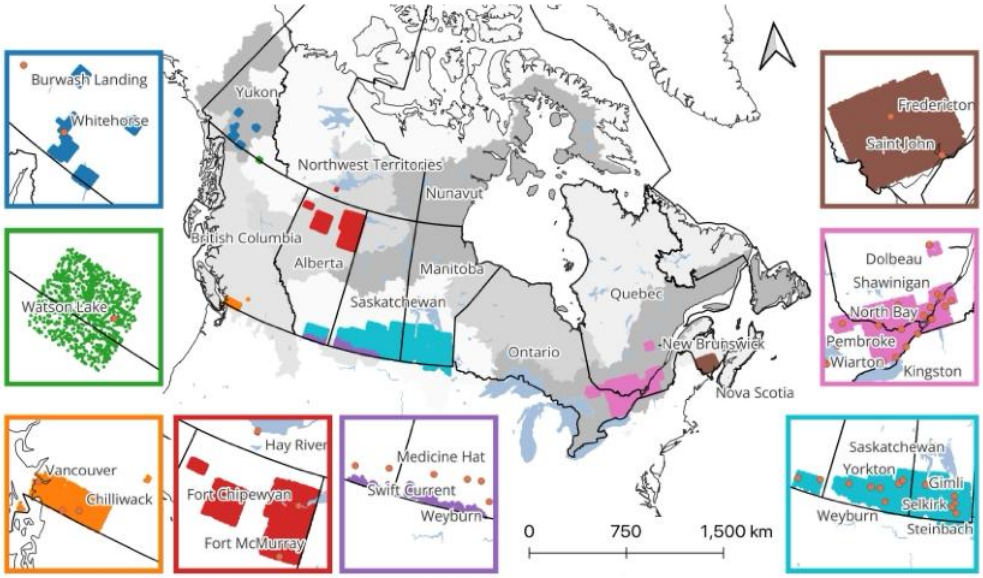

Figure 1: Spatial distribution of the study area, covering multiple zones across Canada. The colours from the inset maps correspond to the specific geographic subsets: Yukon River (blue), Pacific (orange), Great Slave Lake (red), Mississippi River (purple), Nelson River (cyan), St. Lawrence (pink), and Maritime (brown). Shaded areas represent the Major Drainage Areas.

The flood inventory was obtained from the Emergency Geomatics Services (EGS) flood archive, which represents historic flood extents produced using Synthetic Aperture Radar (SAR) and/or optical satellite imagery (Natural Resources Canada, 2018; Natural Resources Canada et al., 2021), with the flood polygon data from 2005 to 2022. There were limited data in Ontario, Northern Quebec and the territories. Overall, 21 data subsets (>200,000 data points) were used in the analysis, distinguished by year, season (Spring, Summer or Fall), and location. One site location can have multiple data points over the study period. An equal number of non-flood points were randomly generated within the study area boundaries to avoid class imbalance, resulting in approximately equal numbers of flood and non-flood points.

FCFs were categorized into geospatial and seasonal climatological groups. Geospatial features included topographical variables (e.g., DTM, slope, aspect, HAND, NDVI, land use), spatial indices (latitude, longitude, Morton/Hilbert indices), and the National Burn Area Composite, reflecting the link between the wildfires and post-fire flood risk (Abogadil and Khan, 2023; Saxe et al., 2018). While often excluded from FSM, meteorological data have recently been shown to improve predictive performance (Khalid and Khan, 2024; McGrath and Gohl, 2022). Consequently, this study integrated seasonal (fall, winter, spring) climatological variables, including total precipitation, temperature extremes, and mean vapour pressure. The full list of FCFs in this study are shown in Figure 2

2.2 Feature Selection Methods

Three feature selection methods were used: Partial Correlation, Partial Mutual Information and Combined Neural Pathway Strength, yielding three ranked feature subsets (in addition to the full set of features and base (only geospatial) to provide insight into the relative strength or influence of each feature on the output. Each feature selection method was use individually for each of the 21 data subsets. The feature subsets were determined using the Natural Breaks optimization (the *jenkspy* algorithm), which calculated intrinsic thresholds for the importance scores.

Partial correlation (PC) measures the direct linear relationship between the target and feature A, while removing the influence of all other features. For instance, the flood label is first predicted using *feature A*, and then using all features other than *A*. The features are ranked by higher linear correlation. This process is repeated for all features until a termination criterion is met. In this case, the process was applied to all features, and the features were selected using Natural Breaks. Partial Mutual Information (PMI) measures the linear or non-linear relationship between the target and feature A, while removing the influence of all other features. The calculation process is similar to PC; however, it uses a non-parametric kernel regression. The residuals from the two models are used to calculate mutual information using the *mutual_info_regression* function from the Sci-Kit (version 1.7.1) package. The features are ranked by higher mutual information. The process is repeated for all features and the final set of features chosen by Natural Breaks. The combined neural pathway strength (CNPS) (Snieder et al., 2020) was used to examine the influence of each feature during model training. In contrast to PC and PMI, CNPS requires a trained ANN model before it can analyze the impact of each feature on the target.

After model training, the weights or strength of pathways for each layer are recorded, and then the input-hidden and hidden-output weight matrices for each fold are multiplied. An alpha variable (Equation 1) measures the consistency of the pathway behaviour. An alpha value of 0.50 means the feature is either excitatory or inhibitory for half of the folds, essentially cancelling its contribution. An alpha value of 1.0 means the feature is either excitatory or inhibitory across all folds and therefore exhibits very consistent pathway behaviour.

$$\alpha_j = \frac{max\left(\sum(CNPS_j > 0), \sum(CNPS_j < 0)\right)}{n} \tag{1}$$

Multiple features may have an alpha value of 1.0, so a score (Equation 2) is calculated to rank the features. The score used in (Snieder et al., 2020) has been modified so that a smaller range between the minimum and maximum CNPS values yields an optimal score of 1.0, which represents more consistent pathway behaviour.

$$score = 1 - \frac{\max\left(CNPS_j\right) - \min\left(CNPS_j\right)}{\left|\max\left(CNPS_j\right)\right| + \left|\min\left(CNPS_j\right)\right|} \tag{2}$$

To balance the CNPS weights with the score, a combined metric (Equation 3) was used to rank the features, assigning equal weight to the score and the CNPS weights (w_1 and w_2).

$$Combined\ Metric = w_1 \cdot Score + w_2 \cdot |Average\ CNPS| \tag{3}$$

2.3 Model Development and Training

Three model algorithms were developed: Extreme Gradient Boosting (XGBoost), Artificial Neural Network (ANN) and Convolutional Neural Network (CNN). All models produced flood probability between 0 and 1, which were subsequently converted to a binary flood/non-flood classification threshold of 0.5. An ensemble of 10 XGBoost models was randomly trained on 70%, validated on 15% and tested on 15% of the dataset. Each tree had a maximum depth of 20, and a maximum of 200 estimators (trees built sequentially). The *subsample* and *colsample_bytree* parameters were 80%; the models were randomly trained on 80% of the rows using 80% of the features (columns). The L1 (*reg_alpha*) and L2 (*reg_lambda*) regularization parameters were set to 0.5 and 5. The model was evaluated using *logloss*.

An ANN is trained using backpropagation, which repeatedly presents the model with data, measures the prediction error, and then adjusts its parameters to reduce the error. An ANN with two hidden layers and 50 neurons was chosen for its higher performance compared to other hidden-layer neuron configurations. The model was trained for 100 epochs with a batch size of 32 and an early stopping patience of 10 epochs. Adam optimizer with a learning rate of 0.0001 and a dropout rate of 50% was used. The activation function was ReLU, and the loss function was binary cross-entropy with logits loss. The ANN model was cross-validated using leave-two-out cross-validation. Since there were 21 data subsets, each was used as a test set at least once, yielding an ensemble of 21 models.

CNNs are trained using a backpropagation process similar to that of ANNs. Two branches processed two different types of input before combining them as input to the dense layers. The CNN branch processed the static geospatial features, while the LSTM branch processed the dynamic temporal features. In each branch, the 1D input was filtered through 1D convolutional filters, where ReLU was applied as the activation function. One-dimensional feature maps were created during max pooling, then further flattened. The flattened feature maps from each branch were then concatenated and fed into a fully dense 128-neuron layer. A 50% dropout layer was applied to create the output, which was activated by the sigmoid function. The CNN model was randomly trained on 70%, validated on 15% and tested on 15%.

Model performance was evaluated using Accuracy, AUC-ROC, and F1 Score. While Accuracy can be biased in imbalanced datasets (El Haou et al., 2025), this was mitigated by the balancing of the training data (~50% flood/ non-flood). AUC-ROC assesses classification capability across the flood thresholds, ranging from 0.5 (random) to 1.0 (perfect classifier) (El Haou et al., 2025; Khalid and Khan, 2024). Finally, the F1 score is the harmonic mean of precision and recall and was used to quantify the trade-off between detecting floods and minimizing false alarms.

3 RESULTS

3.1 Feature Importance

Figure 2 summarizes the feature importance rankings and final selection results across the PC, PMI and CNPS methods. The heatmap indicates the individual rank assigned by each feature selection method; darker blue indicates higher importance (closer to 1). The features are ordered along the x-axis by their average ranking across all three methods. The ranking shows that the seasonal meteorological (labelled in dark blue), particularly the temperature features, consistently rank higher than most geospatial features (labelled in green), indicating that these are less significant predictors. Several features were strongly predicted as high flood drivers (spring maximum temperature, NDVI, and fall minimum temperature). The red border identifies the selected features for each method. The Natural Breaks thresholds yielded varying numbers of features selected by each method (ranging from n = 18 for PC to n = 21 for CNPS).

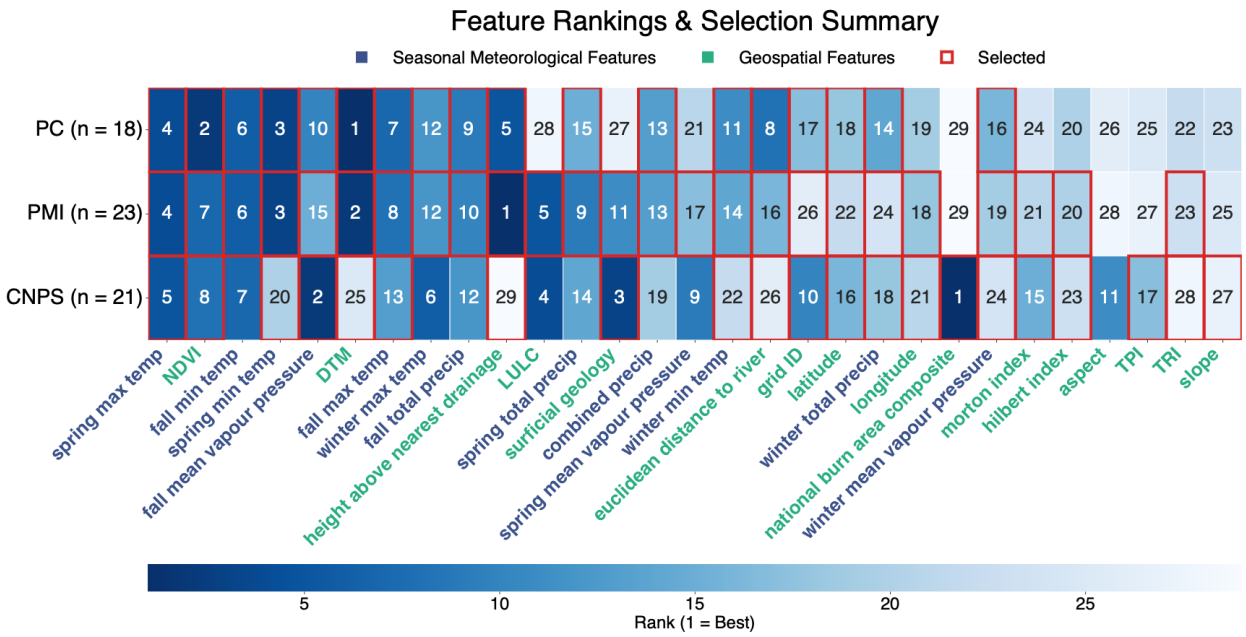

Figure 2: Feature ranking heatmap and selection summary. The rows display the ranks (1-29) assigned to each feature by the PC, PMI, and CNPS methods. The columns are sorted by the average rank across all methods (features on the left had a higher average ranking). The red borders indicate which features are included in each feature subset based on the Natural Jenks thresholds. The count of features per method is represented by n. The text colour distinguishes the seasonal meteorological and geospatial features.

3.2 Model Predictive Performance

Figure 3 displays the AUC-ROC curves for each model across the five feature sets. The top-performing feature set for each model is marked with a star. While the full feature set achieved the highest scores, the performance gap between it and the others is very minimal across all models (< 0.10%); the PMI set had an identical score with the full set with the XGBoost model. Overall, XGBoost was the top classifier (AUC = 0.985), outperforming the top CNN and ANN models by 1.65% and 6.95%, respectively. The top CNN model achieved an AUC of 0.967, while the top ANN model had an AUC of 0.921.

The distribution of performance across the different FS subsets for each model is shown in Figure 4 for the AUC, F1-score and Accuracy metrics. The XGBoost model consistently demonstrated the best performance and stability, achieving the highest mean scores across all three metrics (AUC = 0.981, F1 = 0.932, Accuracy = 0.932), with small variance. The CNN model ranked second-best (mean AUC = 0.962) and demonstrated high stability. In contrast, the ANN model showed the lowest overall performance (mean AUC = 0.847) and high variability in its predictive performance across FS methods.

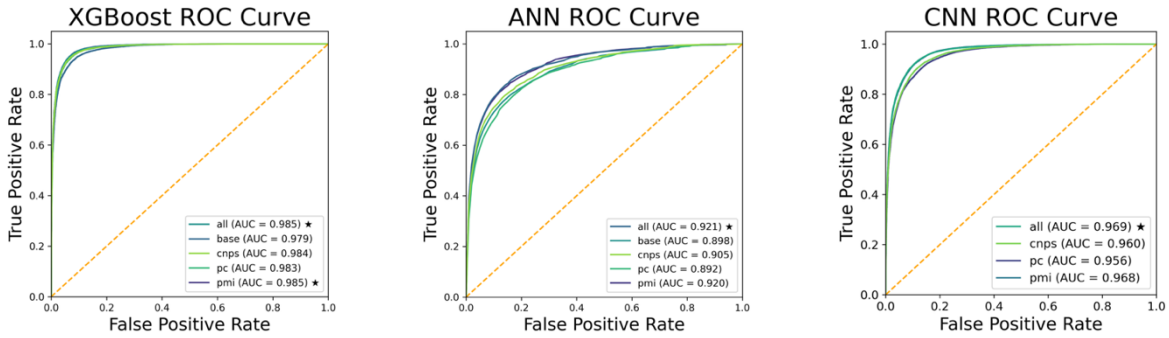

Figure 3: AUC-ROC curves for the three models across the five feature sets

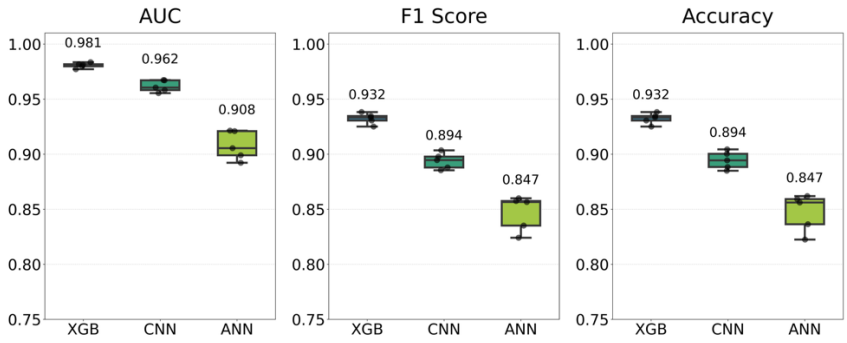

Figure 4: Summary of the model performances for all feature sets across all metrics

3.3 Flood Susceptibility Mapping

The spatial distribution of flood susceptibility for the Spring of 2015 at the New Brunswick study site is shown in Figure 5, generated by the XGBoost model using all features. This area was among the best-predicted of all the study sites. The map shows high susceptibility areas in dark red, strongly correlated with the Saint John River. The near-zero susceptibility areas are transparent.

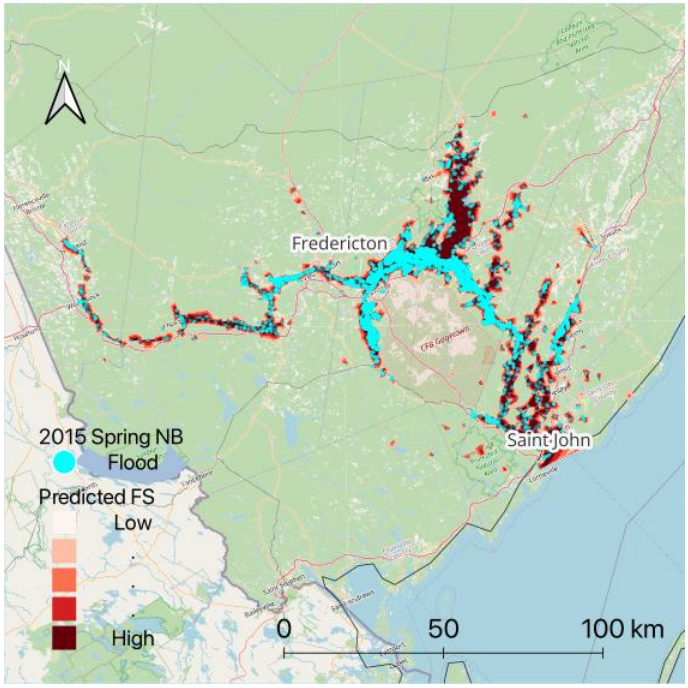

Figure 5: Flood susceptibility output from the XGBoost model using all features.

4 DISCUSSION

Among the feature selection methods, the model trained on the full feature set achieved the highest performance across all model types. However, this came at the cost of greater model complexity, with only a marginal improvement over the models trained on the PC, PMI, and CNPS feature sets. Therefore, these results show that feature selection was highly effective at reducing model complexity without sacrificing predictive power. The PC and PMI feature sets are superior in terms of practicality, requiring less data and achieving faster training and testing times. The feature selection process in this study achieved higher accuracy more efficiently than using the full set of features.

Regarding the specific features selected, it is interesting that not all geospatial features in the baseline set were retained by any of the three feature selection methods; therefore, this baseline set, which is commonly used in FSM studies, is not the optimal feature set. All methods found fewer geospatial indices important (only NDVI, DTM and HAND were included), compared to the higher number of seasonal features. Spatial indices such as latitude, longitude, grid ID, and the Morton and Hilbert Indices were also ranked low, indicating the physical drivers were prioritized over geographic coordinates. This suggests the models prioritized process-based drivers over geographic location which may improve generalizability. All methods excluded aspect. Traditionally important geospatial features such as land use, surficial geology, and derived features such as slope, TPI, and TRI were excluded by either PC or PMI, which could be attributed to existing redundancies with DTM. The importance of seasonal meteorological variables in flood susceptibility is confirmed by its inclusion in all three feature selection methods. There is merit in incorporating seasonal variables that specifically represent local flood characteristics; for instance, this study area may have benefited from temperature and volume variables that capture snowmelt dynamics. PMI and PC selected all (12) except one of the seasonal variables, while CNPS selected seven. The increase in model performance with the inclusion of seasonal variables was the highest for the ANN models, even though the CNPS included the least number of seasonal variables.

When comparing model algorithms, the results of this study show that feature selection methods vary in their rankings, highlighting the different interplay among the features. The predictive power of FCFs varies with the chosen FS method and model, meaning the same variables may contribute differently across models, as observed in other studies (Li et al., 2022; Snieder et al., 2020). On average, the XGBoost models, regardless of the input feature set, performed best (AUC = 0.983, F1 = 0.938, Accuracy = 0.938). However, the best model isn't the one with the highest score, but one that balances performance with simplicity.

Several limitations related to the input data and modelling approach exist for this study. First, the data resolution was 30 meters, which may not be fine enough to capture localized topographical features that contribute to flood patterns; this is highly impactful in areas that have less topographical variability, such as in Manitoba. Further, the absence of urban drainage networks means that the models do not account for infrastructure, which is sufficient for our flood susceptibility focus, but not for hydraulic routing. Regarding the modelling approach, the outputs highlight the flood-susceptible areas; however, they do not provide quantitative measures, such as flood inundation depth, which are important for risk assessment. Since the model outputs were binary, the models were tasked with classification, which makes it easier to achieve a higher performance. Finally, there is inherent difficulty in interpreting the ML models. The feature selection results were complex and, at times, counterintuitive, which could be attributed to the large variability of the study areas in the multiple datasets. This is a common challenge in ML-based FSM studies; employing explainable AI (XAI) methods such as SHAP (SHapley Additive exPlanations) could provide insights into the model's learning process.

Future work can expand on this current study in several ways. Advanced hybrid models, such as CNN combined with Long Short-Term Memory networks (CNN-LSTM), could be tested to capture both the spatial and temporal aspects of flood susceptibility. The generalizability of this model can be examined by training it on a single study area (rather than multiple, as in this study) and evaluating its performance on a second study area. Lastly, incorporating climate change projections would be a valuable next step to help forecast future flood susceptibility, thereby enhancing long-term risk management.

5 CONCLUSIONS

This study developed a data-driven framework for flood susceptibility mapping across diverse Canadian hydroclimatic zones by comparing XGBoost, ANN, and CNN architectures, each combined with three feature selection methods. The results show that, while all models achieved high predictive accuracy, XGBoost consistently outperformed the others. The feature selection analysis demonstrated that the traditional geospatial features and spatial coordinates are often redundant. In contrast, the seasonal meteorological variables are critical for capturing the dynamic nature of flood susceptibility. This research

finds that a simplified XGBoost model, optimized by feature selection, results in the highest performance for a national-level flood susceptibility mapping.

REFERENCES

Abogadil, K., Khan, U., 2023. An analysis of 100 years of post-fire streamflow responses of British Columbia watersheds. https://doi.org/10.5194/egusphere-egu23-8043

Ajin, R.S., Costache, R., Bărbulescu, A., Fanti, R., Segoni, S., 2025. Flood Susceptibility Assessment Using Multi-Tier Feature Selection and Ensemble Boosting Machine Learning Models. Water 17, 2041. https://doi.org/10.3390/w17142041

Bentivoglio, R., Isufi, E., Jonkman, S.N., Taormina, R., 2022. Deep learning methods for flood mapping: a review of existing applications and future research directions. Hydrol. Earth Syst. Sci. 26, 4345–4378. https://doi.org/10.5194/hess-26-4345-2022

Canada, 2024. Atlas of Canada - Canadian Drainage Areas [WWW Document]. URL https://atlas.gc.ca/drainage-areas/Atlas_Drainage_Areas_EN.html?_gl=1*1wbttoy*_ga*MzkzNDA3OTIuMTY4MjcwMjc2MQ..*_ga_C2N57Y7DX5*MTc0MTYzMzMxNy4xMjYuMS4xNzQxNjM0MTM5LjAuMC4w (accessed 12.1.25).

Canada, N.R., 2025. Floods in Canada - Archive - Open Government Portal [WWW Document]. URL https://open.canada.ca/data/en/dataset/74144824-206e-4cea-9fb9-72925a128189 (accessed 9.22.25).

El Haou, M., Ourribane, M., Keshavarzi, A., Ismaili, M., Eloudi, H., Hajji, S., El Bouzkraoui, M., Namous, M., Krimissa, S., 2025. Hybrid machine learning models for urban flood susceptibility assessment in semi-arid Beni Mellal, Morocco: a spatial and comparative analysis. Model. Earth Syst. Environ. 11, 403. https://doi.org/10.1007/s40808-025-02584-9

Khalid, R., Khan, U.T., 2024. Flood susceptibility mapping using ANNs: a case study in model generalization and accuracy from Ontario, Canada. Geocarto Int. 39, 2316653. https://doi.org/10.1080/10106049.2024.2316653

Li, J., Zhang, H., Zhao, J., Guo, X., Rihan, W., Deng, G., 2022. Embedded Feature Selection and Machine Learning Methods for Flash Flood Susceptibility-Mapping in the Mainstream Songhua River Basin, China. Remote Sens. 14, 5523. https://doi.org/10.3390/rs14215523

Long, G., Tantanee, S., Nusit, K., Sooraksa, P., 2025. Flood Susceptibility Mapping Using Machine Learning Models with Novel Flood Inventory Sampling Strategies. Sens. Mater. 37, 3829. https://doi.org/10.18494/SAM5586

McGrath, H., Gohl, P.N., 2022. Accessing the Impact of Meteorological Variables on Machine Learning Flood Susceptibility Mapping. Remote Sens. 14, 1656. https://doi.org/10.3390/rs14071656

Natural Resources Canada, 2018. Floods in Canada - Archive - Open Government Portal [WWW Document]. URL https://open.canada.ca/data/en/dataset/74144824-206e-4cea-9fb9-72925a128189 (accessed 8.13.25).

Natural Resources Canada, Strategic Policy and Innovation, Canada Centre for Earth Observation, Emergency Geomatics Services, 2021. Floods in Canada/ International Floods Product Specifications.

Saxe, S., Hogue, T.S., Hay, L., 2018. Characterization and evaluation of controls on post-fire streamflow response across western US watersheds. Hydrol. Earth Syst. Sci. 22, 1221–1237. https://doi.org/10.5194/hess-22-1221-2018

Snieder, E., Shakir, R., Khan, U.T., 2020. A comprehensive comparison of four input variable selection methods for artificial neural network flow forecasting models. J. Hydrol. 583, 124299. https://doi.org/10.1016/j.jhydrol.2019.124299

Chapter 2 - Flood risk assessment, data and modeling

2.4 Flood forecasting and early warning systems, including ungauged basins

ICFM 10
Adapting to Global Change:
Innovative Approaches to Flood Management and Resilience
May 20-22, 2026 | Western University, London, Ontario, Canada

Response of spring flood to snow cover in Kaidu River Basin, China

Lanhai Li[1,2,*], Farong Huang[2], Chenwei Tu[3]
Zhejiang University of Techology, Hangzhou 310014, China[1]
E-mail: lilanhai@gmail.com

Xinjiang Institute of Ecology and Geography, Chinese Academy of Sciences, Urumqi 830011, China[2]
E-mail: huangfr@ms.xjb.ac.cn

College of Geography and Remote Sensing Sciences, Xinjiang University, Urumqi, 830046, China[3]
E-mail: Tcwruochen@outlook.com

ABSTRACT

Global climate change is projected to transform hydrologic processes, prompting more severe flood risks. Snowpack in mountainous areas is sensitive to climate change, impacting the flood volume. Snowmelt water is an important trigger of spring flood in the Kaidu River Basin (KRB) in the Tianshan Mountains of China. However, research in terms of spring flood (from March to May) response to snow is limited in KRB. Considering the observed snow data are scarce in KRB, the remote sensing snow cover data after cloud removal are used to investigate the response of spring flood to snow variation. Due to the complex topography in KRB, the impact of snow cover in different elevation zones on spring floods is also explored. The results showed that the snow cover area does show an obvious change trend over time and has a significant positive correlation with precipitation and a negative correlation with temperature in winter. The spring flood generally happens in April and May in KRB, and its peak is generally smaller than that in summer. Spring flood in April or May depends on the snow cover area within the elevation of 2000-3000m in April: Flood in April is sensitive to the average snow cover area of 2000-2500m elevation zone in April, while flood in May is sensitive to the maximum snow cover area in April for the whole basin, particularly that in the 2000-3000m elevation zone. These findings can support water resources management and disaster prevention in KRB.

KEYWORDS: Kaidu River Basin, spring flood, snow cover, response mechanism, climate change

1 INTRODUCTION

The world is facing a global changing climate which is projected to transform water cycles and availability, resulting in more severe flooding and water shortage events (Blöschl et al. 2019). The changing climatic conditions alter the hydrological regimes on a local and global scale, impacting the recurrence of flood period (Zafar and Zaidi 2019), especially in the cold and mountainous watersheds where the snowmelt is an important water source (Li and Simonovic, 2001). As an important inland river flowing to the Taklamakan desert in the south of the Tianshan Mountains (TMs), the Kaidu River Basin (KRB) often faces spring floods, which are directly related to downstream water resources management and disaster prevention. Snow situation in spring is one of the key driving factors for the formation of floods. Existing studies have shown that the spatiotemporal changes in snow cover in the TMs directly affect the scale and timing of meltwater runoff (Wu et al., 2023), while the snow melting rate under the background of warming climate may exacerbate flood risks (Zheng et al., 2024). There is still a lack of systematic and in-depth exploration on how snow dynamics specifically affect the formation process, peak flow, and temporal characteristics of spring floods in the KRB, as well as their quantitative

relationships. Understanding the response of spring floods to snow cover has an urgent practical need for predicting the change of flood regimes, optimizing reservoir operation, reducing losses from flood disasters, and ensuring regional ecological security (Zhang et al., 2025).

Existing studies on snow hydrology mainly focus on monitoring snow distribution or simulating snowmelt runoff, but the direct relationship between snow melting processes and flood events lacks (Ni et al., 2023). In the KRB, there have been studies using models such as DHSVM and SDHydro to simulate hydrological processes (Zhang et al., 2016; 2025) or explore the impact of climate change on runoff (Zheng et al., 2024). However, focusing on the response relationship between spring floods and snow cover change, especially in the vertical distribution of snow cover along the elevation in the basin still lacks. Regional studies have shown that vertical changes in snow cover in the Taolai River Basin in the Qilian Mountains (Wu et al., 2023) and other watersheds in the TMs (Ni et al., 2023) have an impact on runoff, providing references for the study. The present study aims to analyze the spatiotemporal variation patterns of snow cover in the KRB and empirically demonstrate its relationship with spring flood processes. The objectives of the study are: (1) to analyze the response of spring floods to snow cover changes in the KRB by integrating remote sensing data and hydro-meteorological observation data, and (2) to explore the impact of climate change. The findings are expected to provide a scientific basis for flood forecasting and early warning, water resource management, and climate change mitigation in the KRB.

2 STUDY AREA AND METHODS

2.1 Study Area

The KRB is located on the south slope of the central TMs in Xinjiang, China. It spans geographic coordinates 82°58′– 85°55′E and 42°19′ –43°21′N, and stretches 525 km with an area of 1,9022 km^2 (Figure 1). With a typical temperate continental climate, the annual average precipitation and temperature are 270 mm and -4.29 °C, respectively. With a range from about 1400 m to 4700 m above sea level, the Kadu River flows from west to east and finally flows into Bosten Lake. The overall terrain of the basin presents the characteristics of high in the west, low in the east, high in the north, and low in the south. This complex terrain pattern profoundly affects the water and heat distribution and snowmelting process within the basin, providing the basic terrain conditions for the formation of spring floods. The snowpack begins to accumulate in November and starts to melt in the next March, leading to flooding in April and May with increasing temperature (Shang et al., 2013). The average annual runoff is 34.21 x 10^8 km^3, in which snowmelt in spring contributes 23.2%. The maximum runoff month is in July, and the minimum runoff month is in February. The runoff from May to August accounts for 56.3% of the annual runoff.

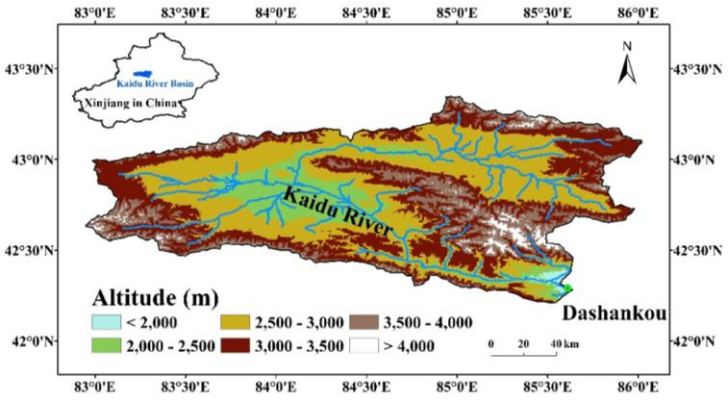

Figure 1 Location of the Kaidu River Basin

2.2 Datasets

(1) Meteorological and hydrological observation data

One meteorological and hydrological observation station with daily recording data is located in Dashankou. Due to the noncontinuous observed data and a dam constructed which inferences the flow, the time scale from 2001 to 2011 was used. Spring peaks occur in April or May from snowmelt contribution, while the annual peak flow generally appears in August, contributing from rainfall mixing with snowmelt in high elevation. The monthly meteorological data, i.e. precipitation and temperature, and streamflow are used in this study to investigate the response of spring flood to snow cover in KRB.

(2) Remote sensing snow cover data

Daily snow cover data during 2001-2011 with a spatial resolution of 500m are from China MODIS Daily Cloudless 500m Snow Area Product Dataset (https://www.ncdc.ac.cn/portal/metadata/be3a4134-2e5c-467f-8a5e-b1c0ed6cc341). This dataset utilizes high-resolution Landsat TM data as ground truth, combined with the MODIS land cover classification product, to train the threshold indicators for snow discrimination in forested and non-forested areas. It employs the MODIS snow retrieval algorithm to obtain the initial product. Invalid values and cloud cover are then removed using a Hidden Markov Model-based cloud removal and snow depth data interpolation method. Finally, a daily cloud-free snow cover area product for the study region is generated (Gao et al., 2019). According to this dataset, snow cover mainly concentrates in the mountainous area during the early snow melt period (Figure 2).

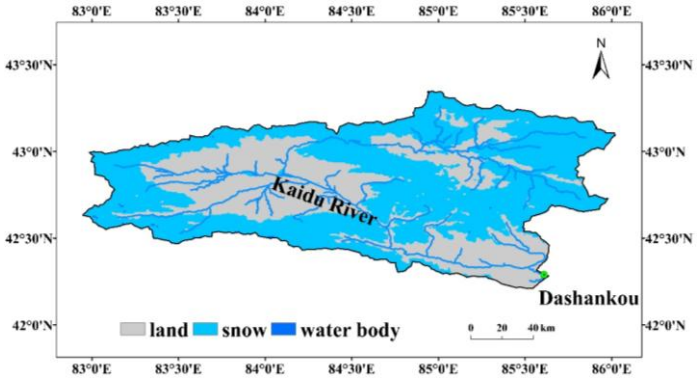

Figure 2 Snow cover on April 1st in 2004

2.3 Method

In order to investigate the spatial heterogeneity of flood sensitivity to snowpack, the study area is divided into six elevation zones, i.e. < 2000m, 2000m-2500m, 2500m-3000m, 3000m-3500m, 3500m-4000m, and >4000m (Figure 1) with one elevation zone of 500m. This study utilizes the correlation coefficient between monthly flood and monthly snow cover area to explore the flood sensitivity to snow cover. Specifically, the maximum daily snow cover area is taken as the monthly snow cover area for the study area in different elevation zones, and the maximum daily streamflow in April and May is taken as the flood volume in the corresponding month, respectively.

3 RESULTS AND DISCUSSION

3.1 Spatiotemporal change of snow cover

3.1.1 Change of snow cover over time

Figure 3a exhibits clear interannual fluctuations cycles of snow cover without obvious change trend over time. This fluctuation is closely related to the winter snowfall and early spring temperature. Snow cover exhibits a typical unimodal variation: snow accumulates from late September, reaches its peak in January and February (with an average snow coverage rate of over 60%), enters a stable melting period in March, and is mostly melted from late April to early May. Average monthly snow cover in Figure 3b further highlights that the growth period of snow cover in the basin starts in September to February of the following year. The snow cover is relatively stable from mid-December to early March of the following year, with the maximum value of 14180 km^2 in January and a minimum snow coverage of about 1000 km^2 in August. This seasonal pattern directly determines the occurrence time and potential scale of spring snowmelt runoff, and is a key background for understanding the formation of spring floods.

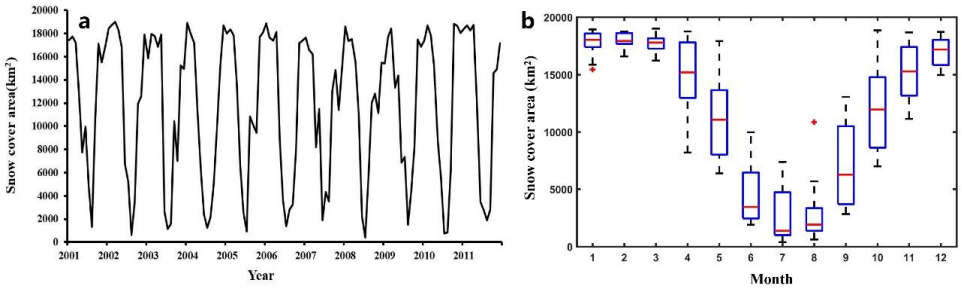

Figure 3 Interannual and monthly variation of snow cover area from 2001-2011. (a) Interannual Snow cover variation. (b) Average monthly snow cover variation

3.1.2 Change of snow cover along different elevation zones

The change pattern of total snow cover area at different elevation zones is shown in Figure 4. The snow cover area is relatively large between elevations of 2000m and 4000m without obvious change trend over time, while relatively small in elevations below 2000m with a slight decreasing trend. The elevation below 2000m shows seasonal snow accumulation, mainly from middle February to middle April with less percentage of cover areas and large fluctuations. The elevation between 2000-3000m is a seasonal snow accumulation zone with a large area and significant fluctuations from February to middle April within a year. The elevation between 3000-4000m is a transitional zone of perennial snow accumulation, with a stable area. The elevation above 4000m is a high-elevation permanent/semi-permanent snow accumulation zone with a high proportion of area and continuous stability.

3.2 Impact of temperature and precipitation on snow cover

Temperature (T) and precipitation (P) presented in Figures 5 and 6 are two important factors affecting snow cover. In order to clarify the impact of changes in T and P on snow cover area, correlation analysis was conducted between T and P data and snow cover data from 2001 to 2011. The results indicate in Table 1 that there is a negative correlation between T and snow cover area in Spring (March-May), summer (June-August), autumn (September-November), and winter (December-February of the following year) at the 1% significance level, indicating that T changes have a significant impact on snow cover. P has the greatest impact on snow cover in winter, showing a significant positive correlation, indicating that winter snowfall is an important accumulation stage of snow; P shows a highly significant negative correlation with snow cover in spring in which T begin to rise and P gradually falls in the form of rain, promoting the melting of snow cover; In summer, there is a positive correlation between P and snow cover, but not at a significant level because the snow cover area mainly exists as permanent snow at high elevation in summer, which is relatively stable. P as the form of rainfall in high-elevation areas replenishes this scattered permanent snow cover; In autumn, there is a low negative correlation between P

and snow cover, because P falls mostly as rainfall, while snow accumulation begins because snowfall starts and T decreases.

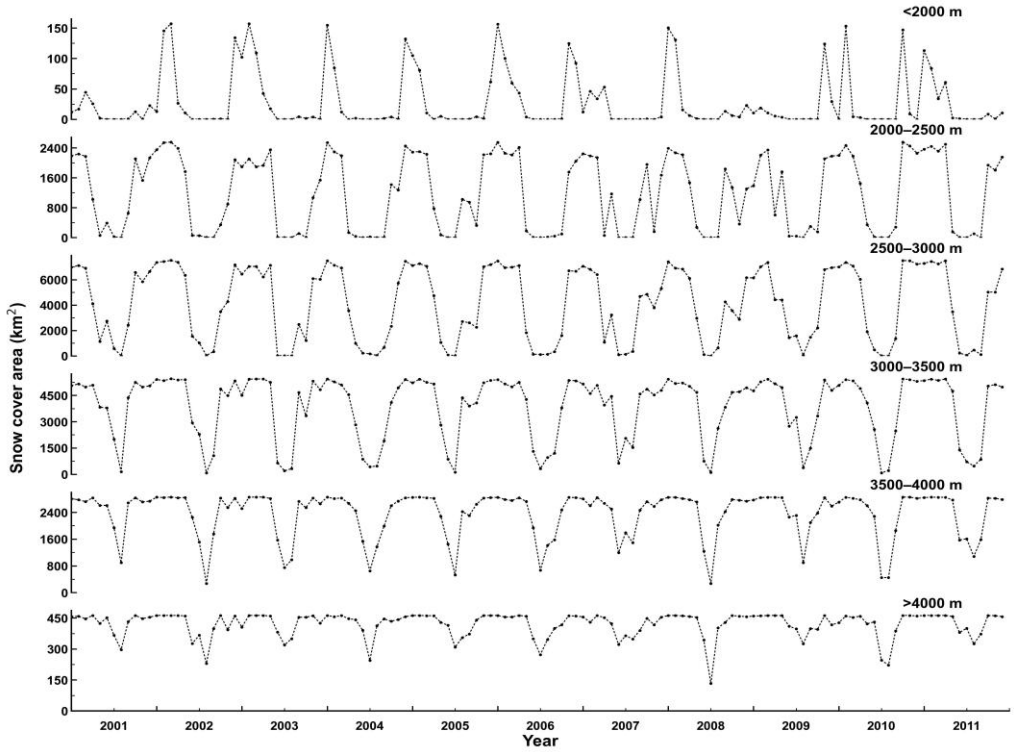

Figure 4 Distribution and variation of Snow cover along the elevation

Table 1. Correlation between snow cover area and precipitation & temperature

	Spring	Summer	Autumn	winter
Precipitation	-0.522**	0.312	-0.230	0.540*
Temperature	-0.807**	-0.480*	-0.806**	-0.831**

** Significant at 0.01, *Significant at 0.05

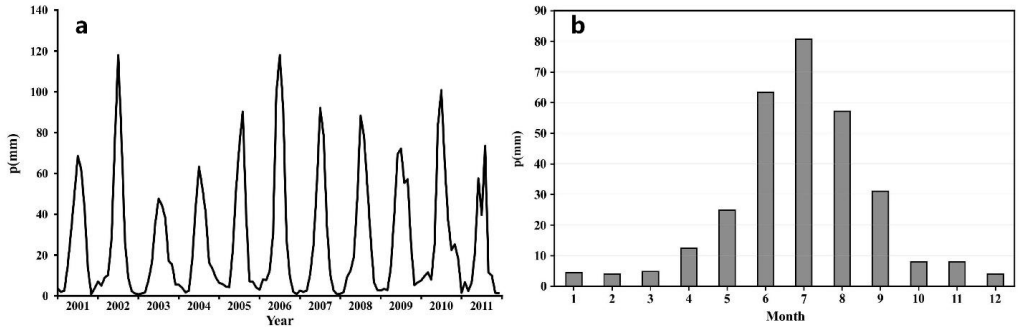

Figure 5 Interannual and monthly precipitation variation from 2001-2011. (a) Interannual precipitation variation. (b) Average monthly precipitation variation

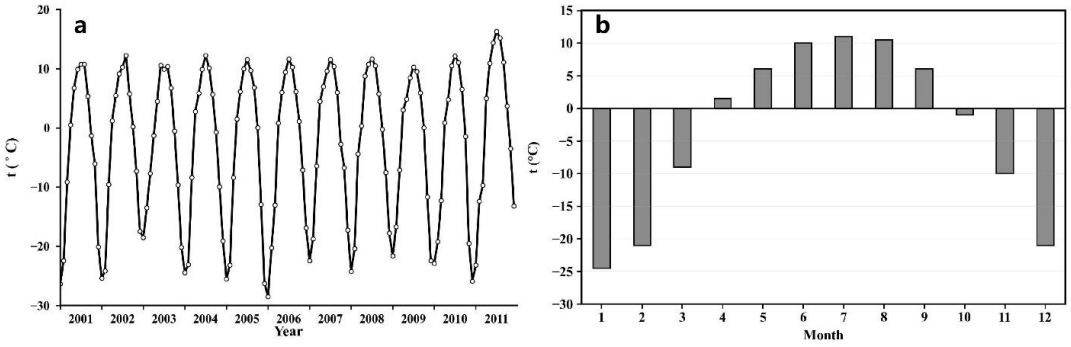

Figure 6 Interannual and monthly temperature variation from 2001-2011. (a) Interannual temperature variation. (b) Average monthly temperature variation

3.3 Streamflow chareateristics

The annual streamflow of the river exhibits certain interannual fluctuations (Figure 7), showing a bimodal characteristic: the first peak occurs in spring (April or May), mainly depending on the melting of seasonal snow in the middle to high mountain range, while the main peak appears in summer (June or August), mainly contributed by the summer P and glacier/snow-melting in high mountains. Streamflow from snowmelt increases in spring, which is closely related to the amount of snowfall in the winter and spring seasons, as well as the rate of T rise in spring (Zhang et al., 2014), but its increase in summer is caused by the amount of rainfall and snow/glacier-melt. The overall streamflow in the KRB showed an increase trend from 2001 to 2011, with a seasonal pattern of "spring increase, summer stability, autumn increase, and winter decrease". Snowmelt runoff accounts for about 30-40%, rainfall runoff accounts for about 45-55% (mainly in summer), and groundwater recharge accounts for about 15% (stable recharge) .

The flood driven by snowmelt generally occurs in April and May, which is generally lower than that in summer, depending on the melting timing and area variation of snow cover at different elevations. The overall trend of spring flood shows a pattern of "early start, stable peak, and prolonged duration" with large interannual fluctuations. The annual snowmelt flood volume in spring increased with a rate of about 16 million m³/a (P<0.05).

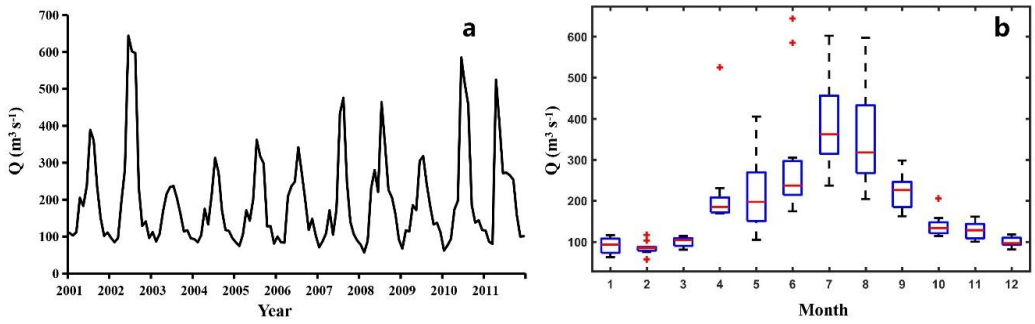

Figure 7 Interannual and monthly streamflow variation from 2001-2011. (a) Interannual streamflow variation. (b) Average monthly streamflow variation

3.4 Response of spring flood to snow cover

Snow cover plays a key role in the spring flood. The peak flow of spring flood has a correlation coefficient of r=0.78 with the spring snow cover area. Spring flood regime depends on snow cover area

and melting at different elevations in spring. Figure 8 shows that flood in April is sensitive to the average snow cover area of 2000-2500m elevation zone in April (R^2 =0.7897), while flood in May is sensitive to the maximum snow cover area in April within the whole basin (Figure 9), particularly that in the 2000-3000m elevation zone (R^2 >0.67). Low elevation snow cover determines the occurrence time and initial intensity of floods, while middle to high elevation snow cover dominates the peak scale and duration of floods. Snowmelt in low elevation below 2000m above sea level starts in March as the T rises rapidly, forming initial runoff and initiating the pre-flood process. With T rise from late March to April, the maximum amount of snowmelting occurs within middle elevations between 2000-3000m above sea level, which significantly increases the streamflow and is the main incremental area of spring floods. A large snowmelt overlapping sudden rainfall in April can easily lead to small-scale excessive floods. After the T rises to the threshold from late April to May, the concentrated snow melting at middle to high elevations (2000-4000m) directly triggers the peak of spring floods. The duration of melting can reach 1.5-2 months, transforming the flood process from a "short-term" to a "gradual and persistent" one.

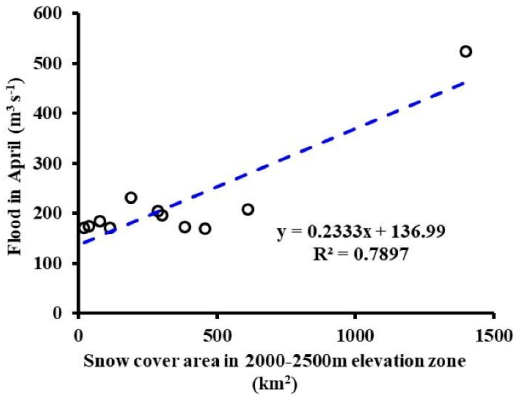

Figure 8 Relation between flood flow in April and snow cover area in the elevation between 2000-2500m

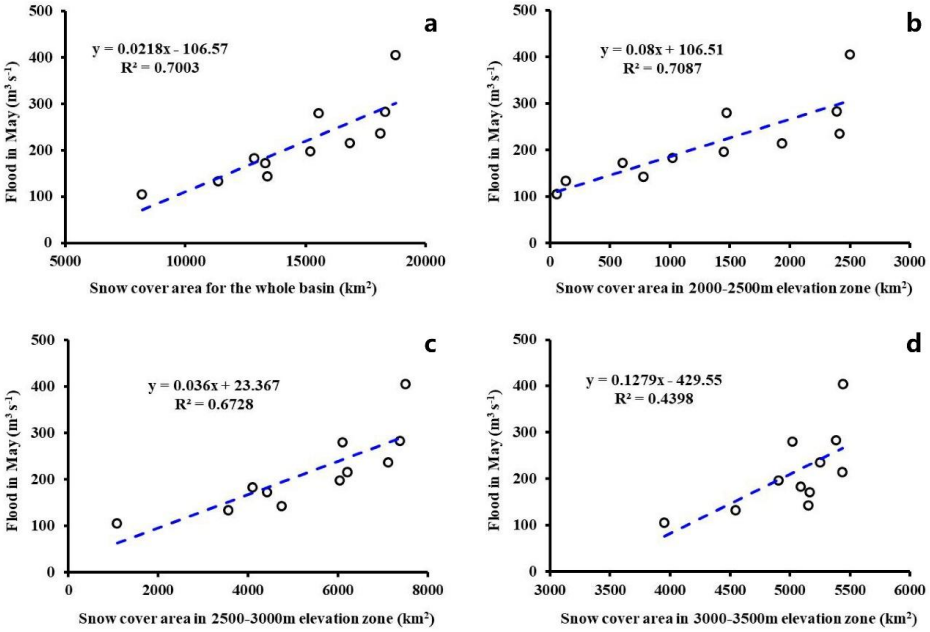

Figure 9 Relation between flood flow in May and snow cover area with different elevations

4 CONCLUSIONS

This study analyzes the spatiotemporal changes of snow cover and its relation with spring floods in the Kaidu River Basin. The results highlight that the snow cover starts accumulation from September, then reaches the maximum in January or February. Snow cover does not show an obvious change trend over 2001-2011. The spring flood generally happens in April and May in the basin, and its volume is generally smaller than that in summer driven by rainfall. Spring flood in April or May depends on the snow cover area in April. Flood in April is sensitive to the average snow cover area of 2000-2500m elevation zone in April, while flood in May is sensitive to the maximum snow cover area in April within the whole basin, particularly that in the 2000-3000m elevation zone. These findings can support water resources management and spring flood disaster prevention in the Kaidu River Basin.

REFERENCES

Blöschl G., Hall J., Viglione A., Perdigão R. A., Parajka J.,Merz B., Lun D., Arheimer B., Aronica G. T. and Bilibashi A. (2019). Changing climate both increases and decreases European river floods. Nature 573(7772): 108-111.

Gao Y., Hao X., He D., et al. (2019). Snow cover mapping algorithm in the Tibetan Plateau based on NDSI threshold optimization of different land cover types [J]. Journal of Glaciology and Geocryology, 41(5): 1162-1172.

Li, L., S. P. Simonovic (2002). System Dynamics Model for Predicting Floods from Snowmelt in North American Prairie Watersheds. Hydrological Processes, 16, 2645-2666.

Ni J., Gao H., Qin Y., Zhang W., He T., Yong L., Feng Z. (2023). The simulation of hydrological elements and climate change impacts in typical basins of Tianshan Mountains[J]. Journal of Glaciology and Geocryology, 45(6): 1875-1886

Shang M., Li L., Yao Y. et al. (2013). Analysis of factors affecting peak flow of the Kaidu river on the southern slope of the Tianshan Mountains [J]. Journal of Arid Land Resources and Environment, 27(9): 85-91.

Wu L., Li F., Li C., LÜ J., Xie X., Zhou X. (2023). Spatiotemporal distribution of snow cover and its variation in the upper reaches of the Taolai River basin， Qilian Mountains, Journal of Glaciology and Geocryology . 2023, (1): 108 -118

Zafar, S. and Zaidi A.(2019). Impact of urbanization on basin hydrology: a case study of the Malir Basin, Karachi, Pakistan. Regional Environmental Change 19(6): 1815-1827.

Zhang F., Li L., AHMAD S., Li X. (2014). Using Path Analysis to Identify the Influence of Climatic Factors on Spring Peak Flow Dominated by Snowmelt in an Alpine Watershed, Journal of Mountain Science, Vol.11 No.4:990-1000

Zhang Q., Xu C., Wang H., Wang Q. Li L., Luo Y. (2025). Simulation and prediction of hydrological processes in Kaidu River Basin based on DHSVM model. Journal of Hydrology: Regional Studies 60 : 102537.

Zhang F., Ahmad S., Zhang H., Zhao X., Feng X., and Li L. (2016). Simulating Low and High Streamflow Driven by Snowmelt in an Insufficiently Gauged Alpine Basin, Stochastic Environmental Research and Risk Assessment, 30:59–75,

Zheng P., Chen Y., Wang H. and Yang Y. (2024). The impact of climate change on extreme runoffs in the Tianshan region:Taking Kaidu River as an example, Journal of Irrigation and Drainage, Vol.4, 4:105-112

ICFM 10
Adapting to Global Change:
Innovative Approaches to Flood Management and Resilience
May 20-22, 2026 | Western University, London, Ontario, Canada

Non-stationary Hydrological Frequency and Uncertainty Analysis of Extreme Tide Levels in the Huangpu River under Changing Environments

Zhihui Liu[1], Shuguang Liu[1,2], Guihui Zhong[1,2]
Department of Hydraulic Engineering, Tongji University, Shanghai 200092, China[1]
E-mail: liuzzh@tongji.edu.cn (Z.L.)
Key Laboratory of Yangtze River Water Environment, Ministry of Education, Tongji University, Shanghai 200092, China[2]
E-mail: liusgliu@tongji.edu.cn (S.L.), 04098@tongji.edu.cn (G.Z.)

ABSTRACT

Increasingly frequent and intense floods driven by climate change and human activities have challenged the assumption of hydrological stationarity. As a result, non-stationary hydrological frequency analysis (NHFA) has become essential for more reliable design estimation of tide levels in tidal rivers under changing conditions. This study focuses on the Huangpu River in China, a tidal river influenced by both upstream inflows from the Taihu Basin and tidal propagation from the Yangtze River Estuary. Using long-term annual maximum tide level records from Wusong Station, trends and abrupt changes were detected through the Mann–Kendall test, Sen's slope estimation, and multiple change-point tests, including the Pettitt and Lee-Heghinian methods. Based on the identified non-stationary characteristics, a conditional probability distribution-based NHFA model was established and compared with traditional stationary and decomposition–composition approaches. Furthermore, a non-stationary Bootstrap uncertainty estimation framework was developed to quantify the parametric and model uncertainties of hydrological design values. Results reveal that both stations exhibit significant non-stationarity, with increased design tide levels and widening confidence intervals as return periods extend. The traditional stationary model fails to capture the uncertainty ranges produced by non-stationary analysis, underscoring the necessity of incorporating non-stationarity into flood design standards. This study provides a scientific basis for resilient flood control planning and adaptive water level management in tidal river systems such as the Huangpu River.

KEYWORDS: Changing environment, Huangpu River, Non-stationary hydrological frequency analysis, Uncertainty analysis, Conditional probability distribution

1 INTRODUCTION

Hydrological frequency analysis is a crucial step in the design and safety assessment of water conservancy and flood control infrastructure. Traditional approaches are established on the assumption of stationarity, which presumes that the statistical characteristics of hydrological processes remain constant over time. In recent years, climate change and human activities have disrupted hydrological systems, leading to more frequent and intense extreme events such as torrential rains, storm surges, and compound floods(IPCC, 2023). This has further resulted in hydrological sequences exhibiting non-stationary characteristics, a phenomenon particularly pronounced in Shanghai, China(Milly, 2008). Incorporating non-stationarity into frequency analysis has become a growing research focus, yet it also introduces more complex sources of uncertainty into design value estimation.

Non-stationary hydrological frequency analysis (NHFA) has evolved from traditional sample reconstruction-based approaches to direct modeling of non-stationary characteristics, including time-varying models, mixture distribution-based approaches, and conditional probability distribution models

(CPDM) (Lu, 2023; Yan et al., 2023). Time-varying models can effectively describe the evolution of hydrological behaviour over time (Anzolin, 2024; Han, 2022; Strupczewski, 2001). However, under the influence of human activities, hydrological series frequently show abrupt changes rather than continuous trends, in which case mixture distributions and conditional probability approaches are more suitable (Liang et al., 2018). Despite differing in their theoretical assumptions, both approaches employ similar computational schemes and have demonstrated robust performance in modeling non-stationary series with abrupt change. The conditional probability distribution model, originally proposed by Singh et al. (2005), assumes that extreme hydrological sequences across different seasons follow distinct distributions and are mutually independent, employing the product rule of probability to conduct frequency analysis on non-stationary hydrological series. Building on this concept, Song et al. (2012) developed a CPDM that explicitly accounts for abrupt changes, and Li et al. (2016) successfully applied it to annual runoff series, obtaining reliable frequency estimates.

As the complexity of NHFA models increases, the sources of uncertainty in hydrological design values also become more diverse. Beyond traditional factors such as sample representativeness, curve selection, and parameter estimation, the model's own handling of non-consistency introduces new uncertainties. Previous research has extended uncertainty analysis to time-varying models through various methodologies. For instance, Hu et al. (2023) combined Bayesian theory with ensemble strategies to quantify parameter uncertainty in NHFA models, and Du Tao et al.(2018) employed a residual Bootstrap method to infer the uncertainty in sample length when calculating design floods using the Generalised Additive Model. Ankush et al. (2024) employed a Bootstrap method based on Markov Chain Monte Carlo algorithms to examine variations in parameter uncertainty within NHFA models under different covariates. Subsequently, they utilised Bayesian theory to explore the uncertainty in covariate selection and assessed the relative importance of covariate uncertainty compared to parameter uncertainty. By contrast, only a handful of scholars have engaged in discussions regarding uncertainty analysis within mixture distribution and conditional probability distribution models. Sen et al.(2020) proposed incorporating particle filtering into mixture distribution models to optimise the estimation of distribution parameters and their uncertainties. Yan et al. (2019) employed the Bootstrap method to analyse parameter uncertainties in mixture distribution models. Regarding conditional probability distribution models, research into parameter uncertainties arising from non-stationary treatments, such as variant point identification, remains a crucial issue that warrants further in-depth exploration.

To address these issues, this study investigates the non-stationary characteristics and associated uncertainty of annual maximum tide levels in the Huangpu River, focusing on the representative hydrological station Wusong. Using tide level records from 1950 to 2024, we first identify the key non-stationary variations in the time series. A conditional probability distribution model is then employed to conduct hydrological frequency analysis under non-stationary conditions. Furthermore, a Bootstrap-based uncertainty quantification framework is proposed to evaluate parameter and model uncertainty under non-stationary conditions. This study provides a methodological basis for improving the reliability of hydrological design values and contributes to the development of adaptive flood control standards in the Yangtze River Delta region.

2 STUDY AREA AND DATA

The Huangpu River, the largest river in Shanghai, is the last major tributary of the Yangtze River before it enters the East China Sea. Originating from Dianshan Lake in the Taihu Basin, the river flows northward through the Shanghai metropolis and joins the Yangtze River at Wusong. It has a total length of about 113 km, with a width ranging from 300 to 770 m and a drainage area of 24,000 km². Although it occupies only 6.6% of Shanghai's river–lake system by area, it stores nearly 28% of the total channel volume, underscoring its strategic importance for urban flood regulation and inland navigation.

As a typical tidal river, the Huangpu River is jointly affected by upstream runoff from the Taihu Basin and downstream tidal forcing from the Yangtze Estuary, producing a distinctive bidirectional flow regime. During the flood season, the combined impacts of wind, precipitation, and storm surges further

intensify hydrodynamic interactions, generating compound flood risks for Shanghai's flood-defence system. Among the hydrological stations along the river, the Wusong Station, located near the estuary, directly reflects tidal–fluvial interactions.

This study focuses on the annual maximum tide levels recorded at these two stations, based on the Hydrological Yearbooks of the People's Republic of China from 1950 to 2024. The dataset provides a continuous and reliable 75-year time series. All water levels are referenced to the Wusong Datum and have been corrected for land subsidence according to data published by the Shanghai Municipal Surveying and Mapping Department.

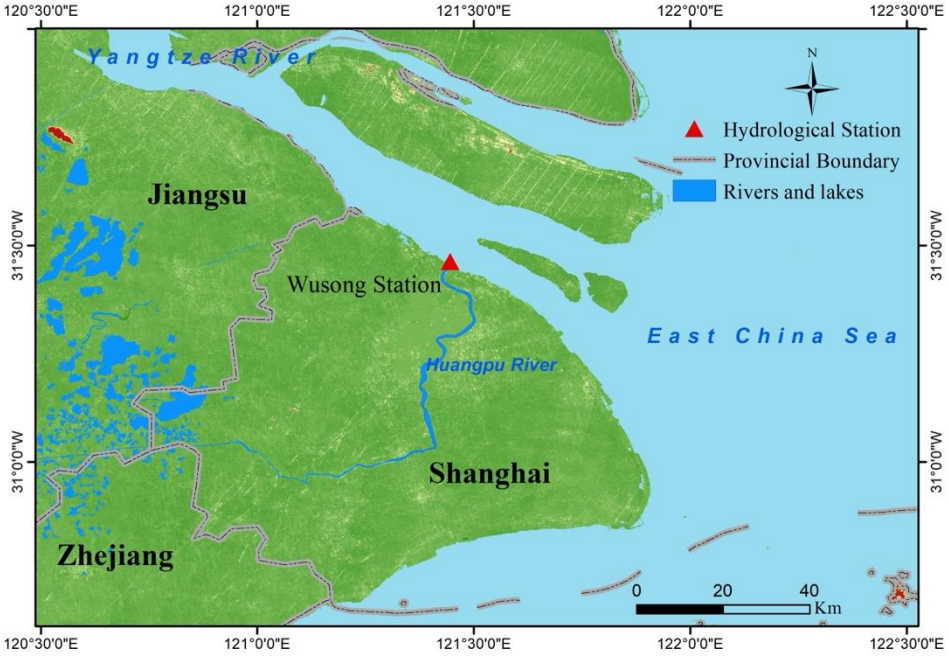

Figure 1: Location of the Huangpu River basin and the distribution of two hydrological stations.

3 METHODOLOGY

The conditional probability approach divides a hydrological sequence with a capacity of N into some periods based on the variance diagnostics. It is generally recommended to divide the sequence into two subsequences $X_1 = \{x_1, x_2, x_3, \ldots, x_\tau\}$, $n_1 = \tau$ and $X_2 = \{x_{\tau+1}, x_{\tau+2}, x_{\tau+3}, \ldots, x_n\}$, $n_2 = N - \tau$ by the mutation point τ, and it is assumed that each subsequence X_i is independent of each other and has its own distribution, then the frequency distribution $F(x)$ of non-sationary distributed hydrological sequences with mutation variances can be expressed as:

$$F(x) = P(X_1)P(x \mid X_1) + P(X_2)P(x \mid X_2) \tag{1}$$

Where $P(X_1) = n_1/N$, $P(X_2) = n_2/N$, n_1 and n_2 are the lengths of the two respective subsequences X_1, X_2, respectively, and N is the sample capacity of the full sequence. $P(x|X_i)$ is in fact the probability of occurrence of the event B in the sequence, which is fitted to determine the corresponding parameter by choosing the appropriate distributional line shape, and then obtaining the frequency distribution of the hydrological text under the conditional probability model. The study adopts P-III type distribution to characterise the distribution of each sub-sequence, and the frequency distribution of the whole sequence is obtained as:

$$F(x) = \frac{n_1}{N}\left(1 - \frac{\beta_1^{\alpha_1}}{\Gamma(\alpha_1)}\int_{a_{01}}^{x}(t-a_{01})^{\alpha_1-1}e^{\beta_1(t-a_{01})}dt\right) + \frac{n_2}{N}\left(1 - \frac{\beta_2^{\alpha_2}}{\Gamma(\alpha_2)}\int_{a_{02}}^{x}(t-a_{02})^{\alpha_2-1}e^{\beta_2(t-a_{02})}dt\right) \tag{2}$$

where α_i, β_i, and a_{0i} represent the shape, scale, and location parameters of the P-III distribution, respectively, relating to the mean $\bar{x}$, coefficient of variation C_v, and skewness coefficient C_s as follows: $\bar{x} = (\alpha/\beta) + a_0$, $Cv = \sqrt{\alpha}/(\alpha + \beta a_0)$ 和 $Cs = 2/\sqrt{\alpha}$ x.

Based on the conditional probability distribution model, the specific procedure for calculating the design tide level uncertainty by the non-consistent Bootstrap method is as follows:

i. Derive the design value H_p of the non-stationary annual maximum tide level series under a certain return period according to Eqs. (2);
ii. Sample the X_1 and X_2 with putback using the Bootstrap method to obtain two new sample sequences X_1* and X_2* of the same length as the corresponding subsequence, respectively;
iii. Based on the new sample sequences X_1* and X_2*, the conditional probabilities $p(x|X_1^*)$, $p(x|X_2^*)$ of each subsequence are calculated, respectively, and the respective distributions of the two sequences before and after the mutation can be obtained. Given the design frequency P, Newton's iterative method is applied to obtain the calculated value of the k+1st iteration of the design value at the corresponding frequency, and finally, the design value H_p* under the corresponding reproduction period T=1/P is obtained;
iv. Repeat (ii) and (iii) N times, i.e., repeat sampling N times to obtain N sampling design values $H_{p,i}$*, i=1,2,..., N;
v. Based on the N sampling design values determined in the above steps, with N ordered from smallest to largest, solve for the confidence interval of H_p at a certain confidence level α.

4 RESULTS AND DISCUSSION

4.1 Detection of non-stationarity

A preliminary diagnosis of the non-stationarity in the observed annual maximum tide level series (H_{max}) at Wusong Station was conducted using the moving average method and cumulative curve slope difference analysis. As illustrated in Figure 2, the five-year moving average and cumulative average of H_{max} at Wusong Station have exhibited an overall trend of fluctuating decline-rise-decline-fluctuating rise since 1950, with distinct inflection points indicating potential non-stationary changes in the sequence. According to the inflection point locations, potential abrupt change points were preliminarily identified as occurring in 1981, 1989, and 2005. Concurrently, the Hurst coefficient method was applied to diagnose the variability of annual maximum tide levels at Wusong Station, with the Hurst coefficient determined to be 0.73, indicating moderate variability in the H_{max}.

Based on the interannual variations and preliminary test results, the trend variation of H_{max} at Wusong Station was examined in detail using the linear trend method, the Mann-Kendall test combined with the Sen slope estimator(Sen+MK), and the Spearman rank test. Using the Pettitt test, the sliding t-test, Lee-Heghinian method, and Mann-Kendall (MK) mutation test, the mutation characteristics of the station are analyzed. The results, as shown in Table 1, indicated that at a significance level of α=5%, the H_{max} at Wusong Station exhibited a significant upward trend and significant mutations. By assigning a score of "1" to the more credible mutation points and accumulating these scores, the years with the highest combined weights for the mutation point of H_{max} at Wusong Station were identified as 1987, indicating that this year was the most probable mutation point for the respective tide level series.

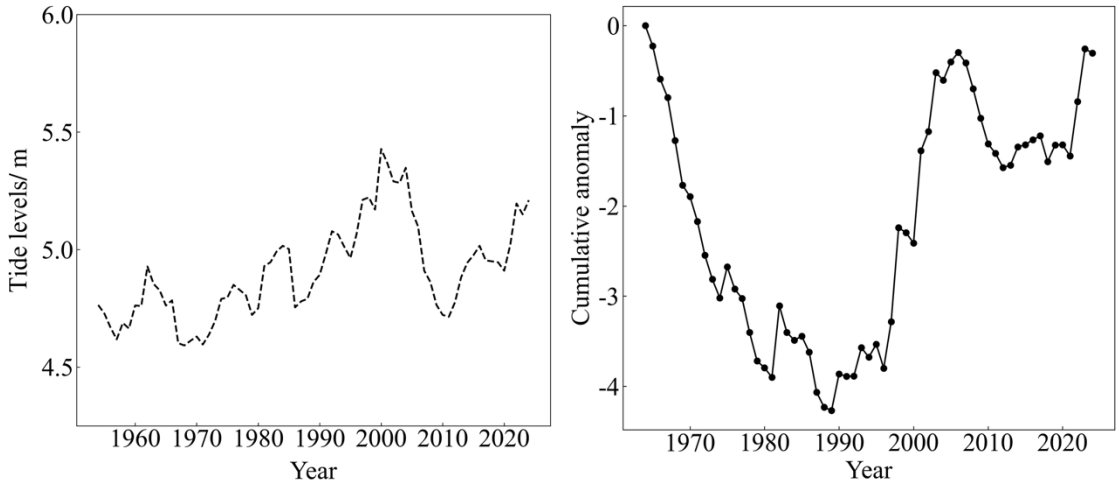

Figure 2: The 5-year sliding average curve and cumulative anomaly of H_{max} at Wusong stations.

Table 1 Detailed hydrological variation analysis of annual maximum tide levels at Stations

Trend test				**Mutation test**			
Diagnostic method	**Statistic**	**Confidence interval threshold**	**Result**	**Diagnostic method**	**Statistic**	**Mutation year**	**Score**
Linear trend	0.0061	> 0	increase	sliding t-test	2.18	2003	1
Sen+MK trend test	β=0.0057, Z=3.99	> 0, 1.960	significant increase	Pettitt	1.24e-4	1987	1
				MK mutation test	-	1987	2
Spearman's rank test	4.44	2.014	significant	Buishand U test	0.1476	1987	3
				Lee-Heghinian	30996.55	1981	1

In view of the fact that both trend and mutation of the tide series at Wusong Station showed significant variations, the study introduced an efficiency coefficient (R^2) to evaluate the degree of fit of the annual maximum tide series to the mutation component and the trend component. The results showed that the efficiency coefficient of the mutability component at this station is greater than that of the trend component, indicating non-stationary changes in the annual maximum tide level series of Wusong Station, with significant variability in mutability. Since the 1970s, Shanghai has implemented integrated management of hydraulic infrastructure, with a particular emphasis on systematic planning and construction around 1987. Gradually, a comprehensive flood control system has been established, dominated by reservoirs, flood detention and retention areas, and major river channels. According to official statistics, by 2019, the total net gate width of sluices along the Huangpu River in Shanghai had reached 826.8 m, and the total installed pumping capacity amounted to 386.82 m³/s. Notably, since 1987, newly constructed sluices along the main stem of the Huangpu River have contributed approximately 518.3 m of net gate width, while pumping stations added an installed capacity of about 382.82 m³/s, accounting for 63% and 99% of the total construction scale from 1967 to 2019, respectively. These substantial hydraulic interventions provide a reasonable and reliable explanation for the statistically identified abrupt change in the annual maximum tide level series at the Wusong station in 1987.

4.2 Parameter calculation and performance evaluation

Based on a comprehensive diagnosis of variability, the annual maximum tide levels at Wusong Station exhibited pronounced non-stationarity, rendering the stationary assumption underlying traditional frequency analysis invalid. Accordingly, this study applied a conditional probability distribution approach (Model 1) to perform non-stationary frequency analysis at Wusong Station and compared the results with those obtained from a time-series decomposition–recomposition method (Model 2) and the traditional stationary hydrological frequency analysis(Model 3).

Table 2 Parameter estimation results for the probability distribution of H_{max} at Wusong Station.

Model	Series	$p(X_i)$	α	ξ	β	S_{AB}	S_{OL}	S_{WL}
Model3	$\boldsymbol{W_0}$	-	1.210	4.910	0.331	2.151	0.128	0.015
Model2	$\boldsymbol{W'_0}$	-	1.209	5.060	0.294	2.174	0.171	0.025
Model1	$\boldsymbol{W_1}$	38	1.326	4.764	0.254	1.236	0.122	0.047
	$\boldsymbol{W_2}$	37	1.531	5.060	0.352	1.227	0.083	0.020

According to the detected change point, the annual maximum tide level series at Wusong Station (n = 75) was divided into two sub-sequences: $\boldsymbol{W_1}$ (1950-1987, n_1 = 38) and $\boldsymbol{W_2}$ (1988-2024, n_2 = 37). Subsequent mutation testing revealed no significant variability, confirming that each sub-series can be regarded as stationary. Using the mutation point of Wusong Station as the boundary, the probability weight $p(X_i)$ of each sub-distribution was determined from the ratio of the sample size of each sub-series to that of the entire dataset. These weights were then incorporated into Eqs. (1) - (2) to derive the non-stationary conditional probability distribution. Under the decomposition–recomposition approach, the mean values of the tide-level series before and after the mutation point were denoted as $\overline{y}_{i1}$ and $\overline{y}_{i2}$, respectively. The deterministic mutation component under current conditions was calculated from the difference between the two means, $\overline{y}_{i2}$ - $\overline{y}_{i1}$. The corrected stochastic component S_t was subsequently obtained by subtracting the mutation component from the original annual maximum tide levels. Accordingly, the corrected sequence S_{t1} for Wusong Station, using the post-mutation state as the baseline, can be written as:

$$S_{t1} = \begin{cases} X_t + 0.378, & 1950 \le t \le 1987 \\ X_t, & 1988 < t \le 2024 \end{cases} \tag{3}$$

The Pettitt test was then reapplied to the corrected series, confirming that no significant mutation remained. This indicated that the corrected series satisfied the stationary assumption required for traditional hydrological frequency analysis. Finally, the maximum likelihood method was used to estimate the parameters of the P-III distribution for the conditional probability model, the decomposition-corrected series ($\boldsymbol{W'_0}$), and the uncorrected measured series ($\boldsymbol{W_0}$) at Wusong Station. As uncorrected observation sequences do not satisfy the stationarity assumption, they are theoretically unsuitable for traditional frequency analysis, with results serving only as comparative tests. As shown in Table 2, we calculated the absolute error sum (S_{AB}), squared error sum (S_{OL}), and weighted squared error sum(S_{WL}) for each model. Results indicated that the conditional probability distribution model yields lower fitting index values than both traditional methods and decomposition-synthesis approaches. Consequently, Model 1 delivers the optimal overall performance for non-stationary frequency analysis at Wusong Station.

4.3 Uncertainty analysis under non-stationary conditions

According to the optimal distribution results of the tide level series, a non-stationary Bootstrap method based on conditional probability was employed to analyse the uncertainty of the distribution results of H_{max} at the Wusong Station. After several rounds of debugging, the number of bootstrap iterations was set to N = 5000, with the resampling sizes n_1 and n_2 taken from the sequence length of H_{max}. For each bootstrap sample, the parameters of the P-III distribution were estimated using the maximum likelihood method, and the iterative trajectories of the parameter estimates were recorded to derive their sample means

and standard deviations. The results showed that when the number of bootstrap samples exceeds approximately 2000, both the mean and standard deviation of the estimated parameters converge to stable values, indicating satisfactory convergence of the resampling process and adequate coverage of the parameter space. To further assess the reliability and uncertainty structure of the estimated distribution parameters, quantile plots and kernel density estimates were constructed, as shown in the Figure. 3. Among them, except for the shape parameters of the pre-mutation series, which show a bimodal distribution, the distribution of each parameter shows a central distribution. The kernel density plot curve is smooth, and the line shape remains good, indicating that the estimated value accuracy of the parameter distribution is good.

Applying the estimated parameters to the conditional probability distribution, the design tide levels and their corresponding 95% confidence intervals were derived for different design frequencies based on N sets of parameter samples. Table 3 summarizes the design tide levels, 95% confidence intervals, and the length of the confidence intervals for Wusong Station under both stationary and non-stationary assumptions. The results indicated that, at all frequencies, the design tide levels obtained under non-stationary conditions are consistently higher than those derived assuming stationarity, and the magnitude of change increases with increasing frequency. Influenced by climate change and intensified human activities, the non-stationary evolution of tide levels at the river estuary leads to elevated hydrological design values. This trend imposes more stringent requirements on flood-protection standards for water conservancy projects in the estuarine region, highlighting the necessity of enhancing flood-defense capacity to mitigate flooding and related hazards.

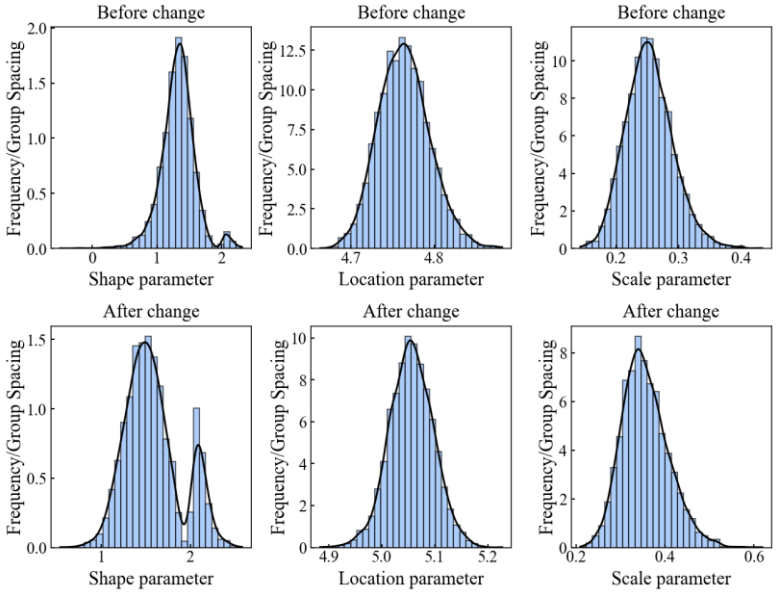

Figure 3: Distribution histogram of the P-III distribution parameters of H_{max} at Wusong Station

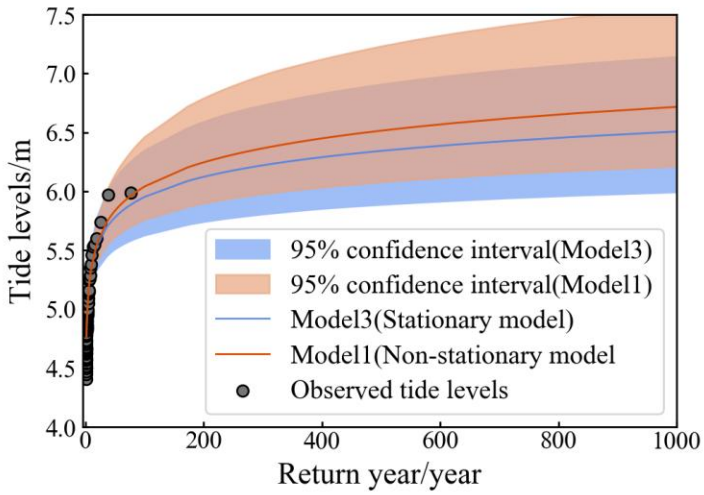

Figure 4: Conditional probability distribution frequency curve (P-III) of H_{max} at Wusong Station

Table 3 Represents the design tide level at Wusong Station under different probabilities.

Frequency	Traditional hydrological frequency calculation (Model 3)			Conditional probability distribution method (Model 1)		
	Design tide level /m	95% confidence interval estimation /m	Interval	Design tide level /m	95% confidence interval estimation /m	Interval
P = 0.1%	6.51	[5.99,7.14]	1.15	6.72	[6.21,7.56]	1.35
P = 0.2%	6.34	[5.89,6.91]	1.02	6.51	[6.08,7.23]	1.15
P = 0.5%	6.12	[5.74,6.59]	0.85	6.25	[5.90,6.79]	0.89
P = 1%	5.95	[5.62,6.35]	0.72	6.04	[5.76,6.46]	0.70
P = 2%	5.78	[5.50,6.10]	0.60	5.84	[5.61,6.14]	0.53

The theoretical frequency distribution curves and uncertainty intervals of H_{max} at Wusong Station were presented in Figure 4. The lengths of the uncertainty intervals for the design tide levels, under both stationary and non-stationary conditions, increased with increasing return period. This behavior occurred because longer return periods were associated with fewer effective samples, resulting in larger estimation errors for extreme values. Moreover, introducing additional variables or distributions, given the limited availability of observed data, often heightens the instability and uncertainty of the model.

However, as shown in Figure 4 and Table 3, the widths of the 95% confidence intervals derived from the non-stationary conditional model were not markedly different from those obtained under the stationary assumption, with only slight increases observed at high return periods (i.e., greater than 100 years). The difference between the two models became more evident as the return period increased. For example, at Wusong Station, the uncertainty intervals for the 500-year and 1000-year return periods increased by 0.13 m and 0.20 m, respectively, compared with those estimated without considering non-stationarity. Under lower return periods, the degree of interval dispersion in uncertain intervals decreases, effectively controlling the uncertainty caused by non-stationarity. This indicates that the non-stationary P-III conditional probability distribution in this study did not significantly increase the uncertainty of the reproducibility level estimation results due to the complexity of model parameters, and effectively reduced the uncertainty interval in the low recurrence period range.

5 CONCLUSION

To address the issue of increasing uncertainty in hydrological frequency analysis caused by non-consistent changes in hydrological series, this paper introduces a non-consistent Bootstrap uncertainty calculation method based on the theory of conditional probability distribution for frequency analysis of variable hydrological series with mutations. Using Wuaong Station as an example, we examine the annual maximum tide level variations at representative hydrological stations in the Huangpu River and further analyze the impact of non-consistency on the uncertainty in design tide level calculations, leading to the following conclusions:

(1) From 1950 to 2024, the annual maximum tide level series at Wusong Station in the Huangpu River exhibited a distinct non-stationary mutation, with the detected change point occurring in 1987.

(2) Under non-stationary conditions, directly estimating the hydrological frequency of annual maximum tide levels using a conditional probability model proved to be more effective than the time-series decomposition–recomposition method. The resulting design tide levels increased across different return periods, indicating that flood control standards should be further enhanced to improve the actual flood defense capacity of the estuarine region.

(3) The proposed non-stationary Bootstrap uncertainty analysis method based on the conditional probability model was well-suited for uncertainty estimation of design tide levels at stations along the Huangpu River. In low return periods (less than 100 years), hydrological non-stationarity increases the uncertainty of design values.

6 ACKNOWLEDGEMENTS

This research was funded by the National Natural Science Foundation of China (42271031). The authors would like to acknowledge the helpful comments of all reviewers, without which the quality of the paper could not be improved.

REFERENCES

Anzolin, G, de Oliveira, DY, Vrugt, JA, AghaKouchak, A, and Chaffe, PLB. (2024). Nonstationary Frequency Analysis of Extreme Precipitation: Embracing Trends in Observations, Journal of Hydrology, 637, 131300.

Ankush, Goel N K, Rajendran V(2024). Modelling climate change-induced nonstationarity in rainfall extremes: a comprehensive approach for hydrological analysis. Technological Forecasting and Social Change, 208:123693.

Du T, Xiong L H, Li S, et al.(2018). Risk-based nonstationary design flood and uncertainty analysis[J]. Journal of Hydraulic Engineering, 49(2):241-25.

Han, X, Mehrotra, R, Sharma, A, and Rahman, A. (2022). Incorporating Nonstationarity in Regional Flood Frequency Analysis Procedures to Account for Climate Change Impact, Journal of Hydrology, 612, 128235.

Hu Y M, Liang Z M, Peng A B, et al.(2023). Nonstationary hydrological frequency analysis in light of model parameters and climate projections uncertainty. Journal of Hydrology, 617:129120.

IPCC. (2023). Ar6 Synthesis Report: Climate Change 2023.

Lu F, Jiang M, Jiang Y Z, et al(2023). Evolution law of wet and dry probability of natural river runoff in Haihe River basin under changing environment. Advances in Water Science,34(1):12-20.

Liang, Z, Yang, J, Hu, Y, Wang, J, Li, B, and Zhao, J (2018). A Sample Reconstruction Method Based on a Modified Reservoir Index for Flood Frequency Analysis of Non-Stationary Hydrological Series, Stochastic Environmental Research and Risk Assessment, 32(6), 1561-1571.

Li L J, Kang Y, Song S B, et al.(2016). Application of conditional probability model in frequency calculation of inconsistent hydrologic series. Journal of Northwest A & F University (Natural Science Edition), 44(8):219-225.

Milly, PCD, Betancourt, J, Falkenmark, M, Hirsch, RM, Kundzewicz, ZW, Lettenmaier, DP, and Stouffer, RJ (2008). Stationarity Is Dead: Whither Water Management?, Science, 319(5863), 573-574.

Strupczewski, WG, Singh, VP, and Feluch, W (2001). Non-Stationary Approach to at-Site Flood Frequency Modelling I. Maximum Likelihood Estimation, Journal of Hydrology, 248(1), 123-142.

Singh V P, Wang S X, Zhang L (2005). Frequency analysis of nonidentically distributed hydrologic flood data[J]. Journal of Hydrology,307:175-195.

Song S B, Li Y, Cai M K (2012). Methods of frequency analysis for hydrologic data with jump up components. Journal of Hydraulic Engineering, 43(6): 734-739,748.

Sen S, He J X, Kasiviswanathan K S (2020). Uncertainty quantification using the particle filter for non-stationary hydrological frequency analysis. Journal of Hydrology, 584:124666.

Yan L, Xiong L H, Ruan G S, et al.(2019). Reducing uncertainty of design floods of two-component mixture distributions by utilizing flood timescale to classify flood types in seasonally snow covered region. Journal of Hydrology,574: 588-608.

Yan L, Zhang L Y, Xiong L, et al. (2023). Flood frequency analysis using mixture distributions in light of prior flood type classification in Norway. Remote Sensing,15(2): 401.

ICFM 10
Adapting to Global Change:
Innovative Approaches to Flood Management and Resilience
May 20-22, 2026 | Western University, London, Ontario, Canada

"Four-pre" application for Flood Control under Matrix Management in Modern Reservoir–A Case Study in Hengshan Reservoir

Lin Wenqing[1,2], Wang Weiqi[1,2], Bi Wuxia[1,2], Wang Fan[1,2*], Zhang Dawei[1,2], Zhang Cheng[1,2], Bao Chunfei[3], Fang Zhanchao[4], Shen Naizheng[3]

1. China Institute of Water Resources and Hydropower Research, Beijing 100038, China; 2. Research Center on Flood & Drought Disaster Prevention and Reduction of the Ministry of Water Resources, Beijing 100038, China; 3. Zhiyang Innovation Technology Co., Ltd., Shandong Zibo 255086, China; 4. Yixing Water Conservancy Bureau, Jiangsu Wuxi 214200, China;

E-mail: First Author linwq@iwhr.com

E-mail: Corresponding Author wangfan@iwhr.com

ABSTRACT

Floods rank among the most severe natural disasters. The development of the "Four Pre" module within the reservoir operation and management matrix provides critical support for flood response operations. Using the flood models embedded in the "Four Pre" module, the research validates reservoir inflow forecasting and simulates reservoir flood routing scenarios. Results show that the distributed hydrological forecasting and regulation model accurately replicates historical flood events, with flood volume relative errors of -8.1% for the representative floods, offering a reliable scientific basis for flood control operations at Hengshan Reservoir. Additionally, the two-dimensional surface water dynamics model enables rapid and precise extraction of key flood parameters—including inundation extent, water depth, flow velocity, and time of arrival—under various scenarios. This study analyzed flood propagation and inundation risks downstream of a reservoir under three dam breach scenarios: design flood level, check flood level, and overtopping flood level The model effectively captures dynamic flood evolution and provides substantial support for flood prevention and mitigation strategies.

KEYWORDS: Reservoir Matrix Management; "Four-pre" for Flood Control; Integration of Hydrological Forecast and Dispatch; Hydrodynamic Model

1 INTRODUCTION

Floods rank among the world's most devastating natural disasters, frequently leading to substantial casualties, economic losses, infrastructure damage, and ecological degradation（UNDRR, 2020）. In response, China has in recent years actively pursued innovation in water conservancy management models to enhance flood control and disaster mitigation capacities and safeguard water resource security. A key initiative in this effort has been the vigorous advancement by China's water resources authorities of a modern reservoir operation and management matrix（MWR, 2023）.

This matrix is structured around four core dimensions: First, realizing "Four Comprehensives" in management—ensuring comprehensive coverage, all-element control, round-the-clock monitoring, and full-cycle supervision. Second, improving the "Four Systems"—namely the institutional, mechanistic, legal, and accountability frameworks. Third, strengthening the "Four Preemptive Measures"—forecasting, early warning, simulation, and contingency planning. Fourth, enhancing the "Four Management Tasks"—risk elimination, inspection, maintenance, and safety oversight. Collectively, these components constitute

a multi-level, systematic management matrix designed to standardize, intellectualize, and coordinate the entire reservoir management process. This matrix has now been implemented in several regions. For instance, Jiangsu Province has preliminarily established matrix management platforms for seven reservoirs, including Hengshan, Laoyaba, and Xiangshan (Cheng, 2024). By integrating functions such as data monitoring, simulation forecasting, and dispatch decision-making, these platforms have significantly improved the precision, informatization, and modernization of reservoir operations, providing crucial support for flood safety and efficient water resource utilization.

As one of Jiangsu's pilot projects in reservoir matrix management, Hengshan Reservoir—supported by digital twin technology—has fully integrated various sensing devices to build a matrix platform that encompasses the four comprehensive aspects, four systems (governance mechanisms), four preemptive measures, and four management dimensions (Lin et al., 2024). In terms of operationalizing the "four preemptive measures," the platform has established a three-tier monitoring and forecasting system for rainfall and water conditions. It incorporates 0–72 hour rainfall forecasts, real-time precipitation data from seven upstream rainfall stations, and flow data from three gauge stations. Using an integrated forecasting and dispatch model, the platform dynamically updates flood forecasts, improving accuracy. It also integrates defenses against rainfall, flood conditions, risks, and disasters, providing real-time warnings for downstream river conditions to enable earlier alerts. Based on a two-dimensional hydrodynamic model, the platform enables dynamic simulation of flood propagation across the entire river basin. It supports forward simulation of forecasted floods and design floods with different return periods (e.g., 10-year, 50-year, 100-year, and 2000-year events) to optimize dispatch strategies, as well as reverse simulation to verify the safety of the dam and downstream protected areas. By incorporating these simulation results, the platform iteratively refines emergency plans, ensuring alignment between online simulations and offline preparedness, thereby enhancing the scientific rigor of contingency planning.

Based on the integrated forecasting and operation model and the two-dimensional hydrodynamic model embedded in the "Four Preemptive Measures" module of the Hengshan Reservoir, this study conducts a backward simulation of historical flood events and performs scenario analyses of dam-break flood propagation downstream of the reservoir. The outcomes provide a reference for enhancing the "Four Preemptive Measures" framework within the reservoir management matrix, thereby effectively supporting flood defense efforts.

2 DATA AND METHOD

Hengshan Reservoir (119.443~119.7°E, 31.1~31.275°N) is located in the mountainous southwest of Yixing City, Jiangsu Province. It is a water retention project in the Zhixi River system, with a catchment area of 154.8 km² and a total storage capacity of 112 million m³. The main dam of Hengshan Reservoir is an earth-rock dam with a length of 4090 m (Cui et al., 2020). The reservoir provides flood protection for an area of approximately 20,000 hectares and a population of 300,000 people.

The upstream basin of Hengshan Reservoir has a multi-year average rainfall of approximately 1225 mm, with water surface evaporation of about 950 mm. The mean annual temperature is around 15 °C, characteristic of a humid subtropical monsoon climate. Between 50% and 60% of the annual precipitation occurs during the flood season from June to September. The period from June to July is prone to continuous rainy plum-weather (Meiyu), while from July to September the area is often affected by typhoons and tropical storms, which can cause intense and rapid-onset heavy rainfall events.

2.1 Data

This study collected geospatial data, rainfall data, and reservoir operation data for the Zhixi River Basin and the downstream area of Hengshan Reservoir. The geospatial data primarily consist of Digital Elevation Model (DEM) data covering the basin and the downstream influence area of the reservoir, with a spatial resolution of 1.8 m × 1.8 m. The rainfall data mainly comprise hourly records from seven rainfall stations—during the flood events of "20240630". The reservoir operation data include hourly records of inflow, outflow, and water level variations throughout these two flood events.

2.2 Method

1. Forecasting and dispatching model

This study employs a watershed forecasting and operation integration model independently developed by the China Institute of Water Resources and Hydropower Research (IWHR) (Lin et al., 2024) to establish a distributed hydrological model of the Zhixi River Basin and to analyze the storm flood processes entering the Hengshan reservoirs. The model enables basin-wide, full-river-segment, and whole-project-system operation pre-simulation and supports parallel computing. The models are managed in a model library format, allowing appropriate processors to be selected based on different computational requirements to enable CPU-GPU heterogeneous parallel acceleration. The supporting model data primarily include watershed topology data, model parameters, reservoir parameters, reservoir operation settings, as well as information such as rainfall and initial reservoir water levels. These data are managed via standardized interfaces and stored in Json files. Based on historical flood event data, parameter tuning for the distributed hydrological model is performed by coupling the SCE-UA algorithm, resulting in a separate set of model parameters for each sub-basin.

2. Hydrodynamic model

This study employs FASFLOOD (Fast Analysis System for Flood) (CDPR., 2021), a domestically developed, general-purpose, high-performance flood analysis software independently created by the China Institute of Water Resources and Hydropower Research. The model engine adopts the shock-capturing Godunov scheme, supports heterogeneous parallel acceleration via GPU, and is capable of rapidly simulating various typical flood scenarios, including dam-break wave propagation, mountainous floods, and urban stormwater inundation.

3. Breaching model

Earth dams typically undergo gradual breaching. The breach dimensions (final breach width and breach development duration) are calculated using the empirical Lu Jikang formula (Lu et al., 2001). To simulate the breach widening process incorporating sediment effects, this study employs the widely applicable and mathematically straightforward de Vries sediment transport rate formula implemented in FASFLOOD to compute sediment transport at the breach.

4. Evaluation index

This study evaluates the hydrological forecast results using the Pearson correlation coefficient (Pearson, 1900), Nash-Sutcliffe efficiency coefficient (Nash, 1950), relative errors in flood volume and peak discharge, peak time error, and runoff depth forecast error.

3 FORECAST FOR THE FLOOD EVENT

During this flood event, rainfall was mainly concentrated from 23:00 on June 29 to 17:00 on June 30. The maximum average hourly rainfall in the basin reached 23.1 mm at 02:00 on the 30th, with the maximum 6-hour cumulative rainfall measuring 75.9 mm and the maximum 24-hour cumulative rainfall reaching 143.6 mm (Lin et al., 2024). The Hengshan Reservoir recorded its peak inflow of 408.2 m^3/s at 15:00 on the 30th. The forecasted flood hydrograph at the cross-section is shown in Figure 1 Verification results indicate a correlation coefficient of 0.97 between the predicted and observed flood hydrographs, with an NSE of 0.92. The relative deviation in flood volume was -8.1%, the forecast error in runoff depth was -8.1%, and the relative deviation in peak flow was -9.5%. No timing error in peak occurrence was observed, and the simulation results were within acceptable error limits.

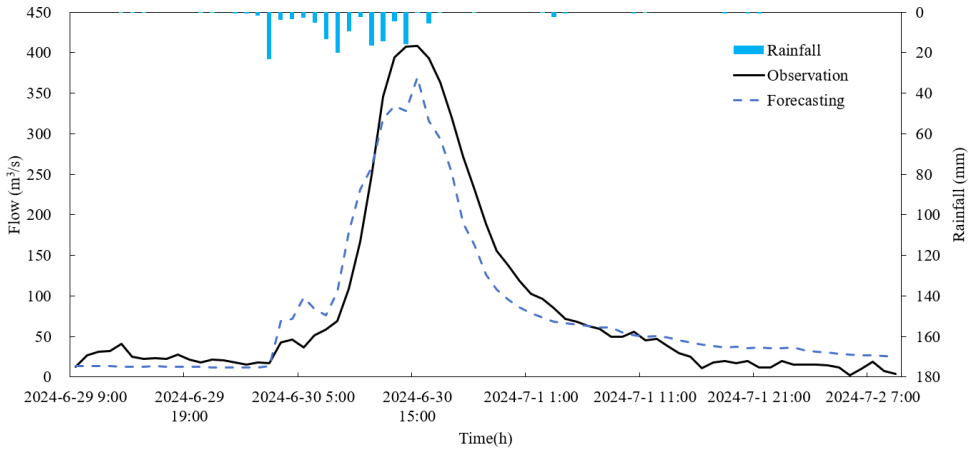

Figure 1: The process of simulated (using observed rainfall) vs. observed flood hydrograph in the Hengshan River Basin (Lin et al., 2024)

4 SCENARIO ANALYSIS OF FLOOD PROPAGATION DOWNSTREAM OF THE RESERVOIR

This study analyzed flood propagation and inundation risks downstream of the reservoir under three dam breach scenarios: the design flood level, the check flood level, and the overtopping flood level.

4.1 The process of outflow from a breach

Based on the calculation results of dam breach parameters under different water level scenarios, the key findings are presented in Table 1 and summarized as follows:

Table 1. Calculated Dam Breach Parameters under Different Water Level Scenarios

Parameter	Design Scenario	Check Scenario	Over-dam Scenario
Initial Invert Elevation (m)	38.75	40.36	42.10
Initial Water Level (m)	38.75	40.36	42.20
Initial Breach Width (m)	10.00	10.00	10.00
Minimum Controlled Water Level (m)	18.00	18.00	18.00
Maximum Breach Width (m)	113.21	122.35	128.31
Breach Development Duration (hr)	2.75	2.85	2.81

The analysis reveals a clear correlation between the initial hydraulic head (represented by the initial water level) and the resulting breach dimensions. As the initial water level increases from the Design (38.75 m) to the Check (40.36 m) and finally to the Over-dam (42.20 m) scenario, the calculated maximum breach width shows a consistent increasing trend, expanding from 113.21 m to 122.35 m and 128.31 m, respectively. This indicates that a higher initial reservoir level leads to the formation of a wider final breach, which is consistent with the expected greater erosive force and energy release during the breach event.

In contrast, the breach development duration remains relatively stable across the three scenarios, with values of 2.75 hours, 2.85 hours, and 2.81 hours. The minor variation suggests that the time required for the breach to develop to its maximum width is less sensitive to the initial water level within this range, potentially reaching a limiting erosion rate governed by the dam material properties or the simplified model assumptions.

The peak discharge exhibits a significant and progressive increase across the escalating scenarios. Compared to the Design scenario (10,931 m^3/s), the peak discharge in the Check scenario rises by approximately 22%, reaching 13,349 m^3/s (Figure 2). Under the most severe Over-dam condition, the peak

discharge escalates to 16,438 m³/s, marking an increase of about 50% relative to the Design scenario baseline.

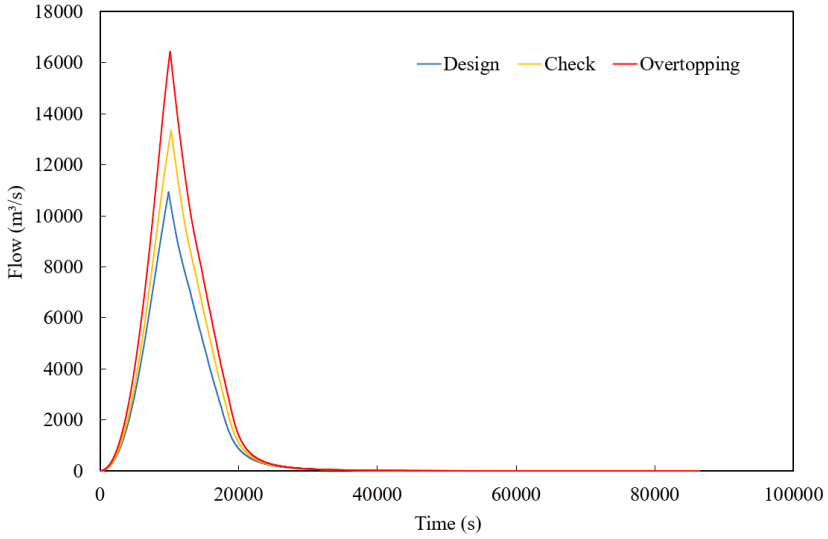

Figure 2: The process of outflow from a breach

4.2 Flood evolution analysis

The upstream boundary was defined as a flow boundary set at the gate of Hengshan Reservoir, while the downstream boundary was set as a free outflow boundary near Xijiu downstream of the reservoir. The simulation assumed dam failure occurring at time T, with the dam-break flood process concluding at T+24 hours, capturing the maximum flood inundation over the 24-hour period. The study area was discretized using an unstructured triangular mesh. To accurately represent the river channels, the channel network was extracted as a control line, with a mesh edge length of 30 meters, resulting in a total of 1,174,938 elements and 588,938 nodes.

The flood routing results indicate a consistent escalation in all key inundation parameters with increasing initial reservoir water levels. For the Design water level breach scenario, the maximum inundation depth, affected area, and flow velocity are 15.6 m, 120.8 km², and 14.3 m/s, respectively (Figure 3). These values increase to 17.0 m, 143.1 km², and 15.9 m/s under the Check water level scenario. The most severe Over-dam water level scenario produces the most extreme conditions, with the maximum inundation depth reaching 18.3 m, the inundated area expanding to 170.1 km², and the flow velocity rising to 17.3 m/s.

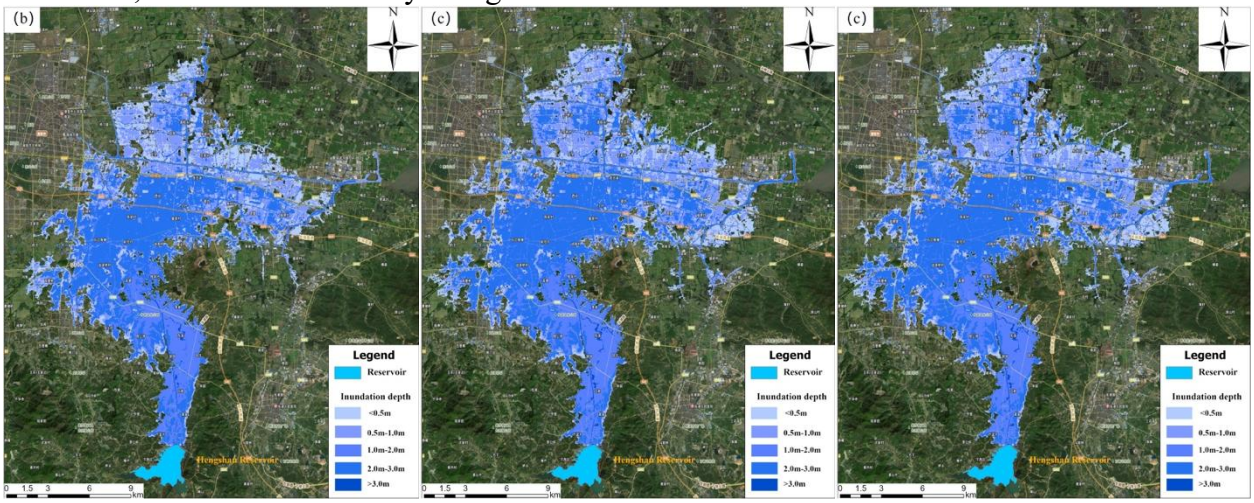

Figure 3: The inundation depth of the downstream flood propagation scenario of Hengshan Reservoir The inundation depth of the downstream flood propagation scenario of Hengshan Reservoir for (a) Design level, (b) Check level and (d) Overtopping level

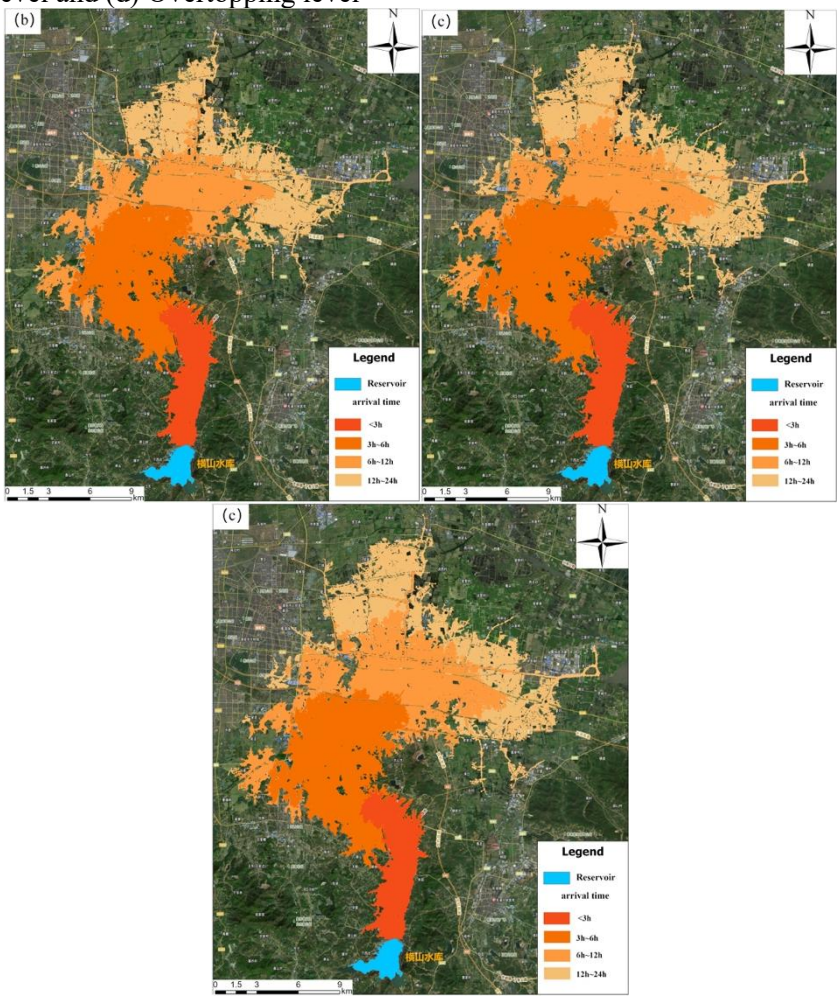

Figure 4: The arrival time of the downstream flood propagation scenario of Hengshan Reservoir The inundation depth of the downstream flood propagation scenario of Hengshan Reservoir for (a) Design level, (b) Check level and (d) Overtopping level

In summary, the "Four Previsions" (forecast, early warning, simulation, and contingency planning) module of the Hengshan Reservoir's comprehensive flood control system can achieve rapid simulation of flood processes under various scenarios based on forecast-based operation results. It provides flood inundation characteristic data for downstream affected areas, thereby offering effective support for flood defense decision-making.

5 CONCLUSION

Based on the developed hydrological and hydraulic models, this study conducted validation of reservoir inflow flood forecasting and scenario-based analysis of reservoir flood routing.

The main findings are as follows:

(1) The integrated watershed forecasting and regulation model demonstrated good performance in simulating the flood hydrograph of the "20240630 flood event." The flood forecasting results were highly accurate, with deviations in peak discharge and flood volume falling within acceptable limits, thus providing a scientific basis for flood control operations at Hengshan Reservoir.

(2) The hydrodynamic model developed in this study can rapidly provide key data—such as flood extent, water depth, flow velocity, and time of arrival downstream of the reservoir under dam breach scenarios—and can accurately and dynamically reflect real-time flood evolution.

6 ACKNOWLEDGEMENTS

This research was jointly supported by the the National Key Research and Development Program of China (Grant No: 2024YFC3214801) and the IWHR Research & Development Support Program (Grant No: JZ110145B0062024).

REFERENCES

Cheng, Y. (2024). Jiangsu builds reservoir operation and management matrix to strengthen flood control and disaster reduction front. China Water Resources News, 007.

Cui, H. F., Chen, S. Y., Yang, C. H., et al. Endogenous pollution and release characteristics of sediment in Hengshan Reservoir, Yixing City [J]. Environmental Science, 2020, 41(12): 5400-5409.

Ministry of Water Resources of the People's Republic of China (MWR). Guidance on Accelerating the Construction of a Modern Reservoir Operation and Management Matrix. Beijing: Ministry of Water Resources, 2023.

LIN Wenqing，WANG Fan，BAO Chunfei，et al. FEDE application for flood management under modern matrix management in reservoirs – A case study in Hengshan Reservoir of Yixing City, Jiangsu Province[J].China Flood & Drought Management，2024，34（12）：73–79. DOI: 10.16867/j.issn.1673-9264.2024431

Lu, J. K., & Nan Linbingnan. (2001). Lin Bingnan collected papers [C]. Beijing: China Water & Power Press, pp. 419-423.

Nash J J F. Equilibrium points in n-person games[J]. Proceedings of the national academy of sciences, 1950, 36(1): 48-49.

Pearson K. I. Mathematical contributions to the theory of evolution.—VII. On the correlation of characters not quantitatively measurable[J]. Philosophical Transactions of the Royal Society of London. Series A, Containing Papers of a Mathematical or Physical Character, 1900, 195(262-273): 1-47.

Research Center on Flood & Drought Disaster Prevention and Reduction of the Ministry of Water Resources (CDPR). Universal high-performance flood analysis and computation software FASFLOOD [Software]. (2021). http://cdr.iwhr.com/fhkhjzzx/shzhzyfxrjxz/webinfo/2022/11/1668157350789555.htm

UNDRR. Human Cost of Disasters. (2020). An Overview of the last 20 years: 2000-2019, https://reliefweb.int/report/world/human-cost-disasters-overview-last-20-years-2000-2019.

ICFM 10
Adapting to Global Change:
Innovative Approaches to Flood Management and Resilience
May 20-22, 2026 | Western University, London, Ontario, Canada

Research on Improving the Accuracy of Flood Prediction Technology Using Satellites, Drones and Digital Testbeds

Tetsuya Takeshita[1], Hisashi Kuronuma[1], Yuki Hamada[1], and Yoshimasa Morooka[1]
National Institute for Land and Infrastructure Management (NILIM),
Ministry of Land, Infrastructure, Transport and Tourism (MLIT),
1, Asahi, Tsukuba, Ibaraki, 305-0804, Japan[1]
E-mail: takeshita-t2hp@mlit.go.jp

ABSTRACT

In response to the frequent occurrence of flood damage, NILIM developed a river-water-level prediction system for Japan. This system has been operational since 2020. The system uses actual and predicted rainfall data as input conditions and predicts river water levels 6 hours ahead at 200-meter intervals. In addition, the accuracy of flood forecasting is improved by assimilating observed water levels from several water level stations in rivers with calculated water levels through data assimilation using particle filters. However, it is difficult to confirm or improve the prediction accuracy of the longitudinal water level of rivers between water level stations because there are no observation data.

Therefore, NILIM has developed 1) a method for grasping the longitudinal water level of the river using satellites with synthetic aperture radar (SAR), 2) a method for correcting observed data by SAR satellites using a water-landing drone equipped with the real-time kinematic global navigation satellite system (RTK-GNSS) and a microwave reflector, and 3) digital testbeds for water level estimation using SAR satellites and flood prediction accuracy evaluation.

The mean absolute errors of the estimated water levels using SAR satellites were 0.35-1.42 m. As a result of a demonstration experiment in the Nikko River, the mean absolute error of water levels was 0.03 m, measured by the water-landing drone and the fixed water-level station, and the trajectory of the drone was confirmed from a SAR satellite image. In addition, NILIM has developed a water-level estimation tool for SAR satellites and an accuracy evaluation tool for flood prediction on digital testbeds, which are experimental sites in a cloud environment.

KEYWORDS: Flood prediction, SAR satellites, drones, digital testbed, accuracy evaluation

1 INTRODUCTION

In response to the recognition of the importance of prediction information in Japan, which was triggered by Hurricane Sandy in the United States in 2012 and torrential rains in the Kanto and Tohoku regions in 2015, NILIM started to develop a flood risk line, a national river water level prediction system, in fiscal 2014. The system has been in operation since 2020 (Web-1) and is currently used for the flood forecasting. Tsuchiya et al. (2023) have described this in detail. The system calculates river water levels 6 hours ahead at 200 m intervals by combining the runoff analysis model and the river channel analysis model with the input conditions of actual rainfall data by radar and predicted rainfall data by the Japan Meteorological Agency. In addition, Tachikawa et al. (2011) attempted to improve flood prediction accuracy by assimilating the observed water level data from several water level observation stations in the target river with the calculated water level using particle filters. The parameters to be filtered by particle

filters are the storage volume of the runoff model and the roughness coefficient of the river channel model.

However, it is difficult to confirm and improve the prediction accuracy of the longitudinal water level of the river between water level observation stations because there are no observation data of the longitudinal water level in the section between the water level observation stations. In addition, the length of Class A rivers managed by the national government is 10,671 km, and it is expensive to install conventional fixed water level observation stations at intervals of 200 m to 1 km to grasp the longitudinal water level.

Therefore, in this study, we first developed an estimation method for river water levels using SAR satellites, which can observe over a wide area at night and under bad weather conditions. Second, to correct the observation error caused by the spatial resolution of SAR satellite data, we examined a correction method for the estimated water level using a joint observation between the SAR satellite and a water-landing drone equipped with a real-time kinematic global navigation satellite system (RTK-GNSS) and a microwave reflector. Third, we developed a water-level estimation tool for SAR satellites and an accuracy evaluation tool for flood prediction on digital testbeds, which are experimental sites in a cloud environment.

2 DEVELOPMENT OF ESTIMATION METHOD OF RIVER WATER LEVELS USING SAR SATELLITES

SAR satellites irradiate L-band or X-band microwaves and measure the intensity of back reflection. It is possible to observe over a wide area at night and under adverse weather conditions. Recently, small SAR satellite constellations have been developed, and observation frequencies have been improved. Regarding the estimation method of river water level using SAR satellites, Biondi et al. (2019) and Chen et al. (2021) estimated the water level near a bridge using the multiple bounce scattering phenomenon of the bridge. However, it is necessary to estimate the water level other than near the bridge to estimate the longitudinal water level of the river.

Therefore, in this study, as shown in Figure 1, we interpreted the position of the waterline from the SAR satellite data and estimated the water level of the water edge line from the point cloud data of the topography. The specific methods, results, and discussion are presented below.

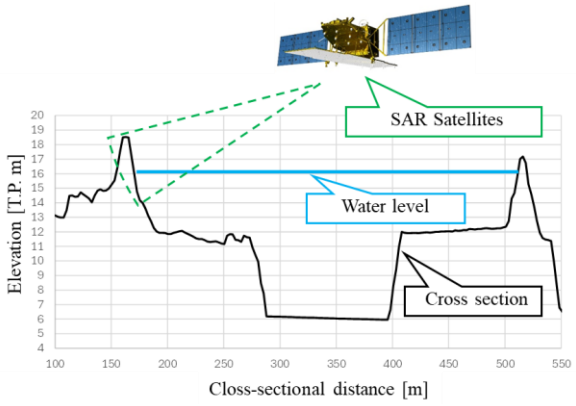

Figure 1: Image of river water level estimation by SAR satellites

2.1 Estimation method of river water level

The procedure for estimating river water levels using SAR satellites is shown below.

1) Preprocessing of SAR satellite images

The SAR satellite images were GEO-TIFF files of product level 2.1, which were converted to orthographic images using ortho-correction. Multiple representative points, such as bridges, were defined as Ground Control Points (GCPs) from the 3D point cloud data of the topography, and the SAR satellite images were geometrically corrected so that the positions of the GCPs in the topography data matched. In addition, filter processing was performed to reduce the speckle noise specific to SAR satellite images. In this study, a Frost filter (Frost et al. (1982)) with a filter window size of 5×5 was used.

2) Creating images near water edge

Because SAR satellites irradiate microwaves in the oblique direction, the backscatter on the water surface is small owing to specular reflection and appears black in SAR satellite images. Therefore, as shown in Figure 2, we extracted digital numbers (integer value with a minimum of 0 and a maximum of $2^{16} = 65536$) of backscatter intensity at several hundred points at the center line of the river, assumed a normal distribution of backscatter intensity in the water area, and binarized the water and land area with a threshold value of $+\sigma$ from the average value. Considering that the water area is underestimated by the average value, we set a threshold value of 84% from the smallest backscatter intensity at the center line of the river.

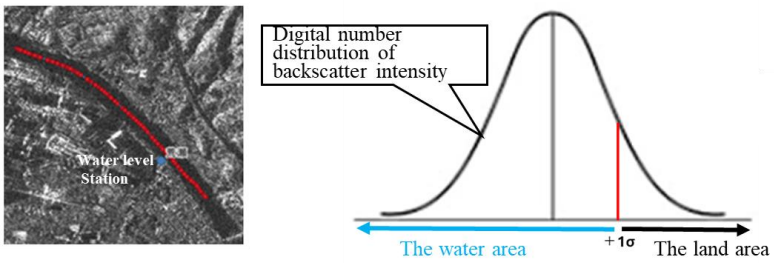

Figure 2: Approach to setting a threshold value for water edge positioning

3) Estimating water levels at water edge lines

As shown in Figure 3, 3D topographic images were displayed on GIS (using Arc GIS) based on topographic point cloud data and aerial photographs, and elevation lines parallel to levee normal lines were displayed at intervals of 2.5 m in the plane width. We then estimated the water levels by overlaying the elevation parallel lines and SAR images near the water edge created in 2) above. For locations where SAR images at two different time points of flood and normal were available, the differences in pixel values between the two time points were also output.

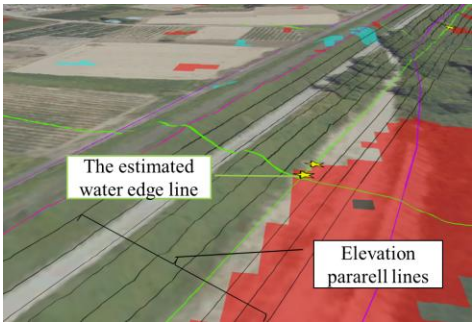

Figure 3: Water level estimation at water edge lines

2.2 Results

Table 1 shows the results of the water level estimation using L-band (ALOS -2, Web-2) and X-band (Strix, Web-3) SAR satellite images.

We calculated the mean absolute error between the estimated water levels using SAR satellites and the longitudinal water levels extrapolated from the observed water levels at water level observation

stations by the longitudinal slopes of the river (slopes of levee normal lines). The mean absolute errors for each type of SAR image and processing condition were between 0.35 and 1.42 m.

Table 1 Results of the estimated water levels using the SAR satellites

Microwaves	Single image or Two images	Mode	Spatial Resolution /Range Azimuth	Number of target points	Mean absolute error (m)
L-band	Two images	Strip map	3m / 3m	6	0.35
L-band	Single image	Strip map	3m / 3m	6	1.42
X-band	Single image	Strip map	3.6m / 2.6m	5	0.51

2.3 Discussion

As shown in Table 1, the estimation method of river water level using only SAR satellites does not have sufficient accuracy to be used as the observation value of the longitudinal river water level. This is due to the limitation of the spatial resolution of satellite data and the use of the mean value and standard deviation of digital numbers of the backscatter intensity of streamlines to set the threshold value for determining the water and land areas.

In the L-band, the mean absolute errors using two images were smaller than those using a single image. This is because it was easier to grasp the position of the waterline by adding the information of the difference using two images. In addition, the mean absolute errors were smaller in the X-band than in the L-band using a single image. This is due to the difference in spatial resolution. In the future, as the number of observation images by SAR satellites increases owing to the development of small SAR satellite constellations, it will be possible to estimate water levels using the X-band difference using two images, and it is expected that the mean absolute errors will be smaller than those obtained using single images. It is also possible to further reduce the mean absolute errors in the L-band by revising the threshold of the water edge position. In particular, the L-band satellite ALOS2 has an observation width of 50 km at a spatial resolution of 3 m, which is wider than the X-band satellite Strix, which has an observation width of 30 km. The advantage is that it is easy to estimate water levels using two images because some images already exist in the dataset.

3 EXAMINATION OF A CORRECTION METHOD FOR ESTIMATED WATER LEVELS BY JOINT OBSERVATION WITH A DRONE AND A SAR SATELLITE

As described in 2., the estimation method of river water levels using only the SAR satellite does not have sufficient accuracy to be used as the observation value of the longitudinal water levels of the river. To improve the estimation accuracy of river water levels, it is necessary to improve the threshold setting of the binarization judgment of the water and land areas using satellite data and the method of water level estimation at the water's edge.

Therefore, in this study, we examined a technology to correct the estimated water level by linking the observation of water levels at the site using a water-landing drone and observation using a SAR satellite. The details are described below.

3.1 Observation method

On February 23, 2025, we conducted water level observations at the mouth of the Nikko River in Aichi Prefecture, Japan (Figure 4), using a landing downstream drone and a SAR satellite. The SAR satellite used Strix to observe an area of approximately 3 km and 10 km, as indicated by the red frame in Fig. 4 in the Staring Spotlight mode. The landing downstream drone (Web-4) is under development by SBIR (Small/Startup Business Innovation Research), a system to promote the R&D of Japanese start-up companies. As shown in Figure 5, it is equipped with a propeller for flight, a self-propelled screw on

water, and an RTK-GNSS positioning function for water-level observation. It is also equipped with a microwave reflector for observations. The river survey method using a SAR satellite and a water-landing drone has been patented by NILIM.

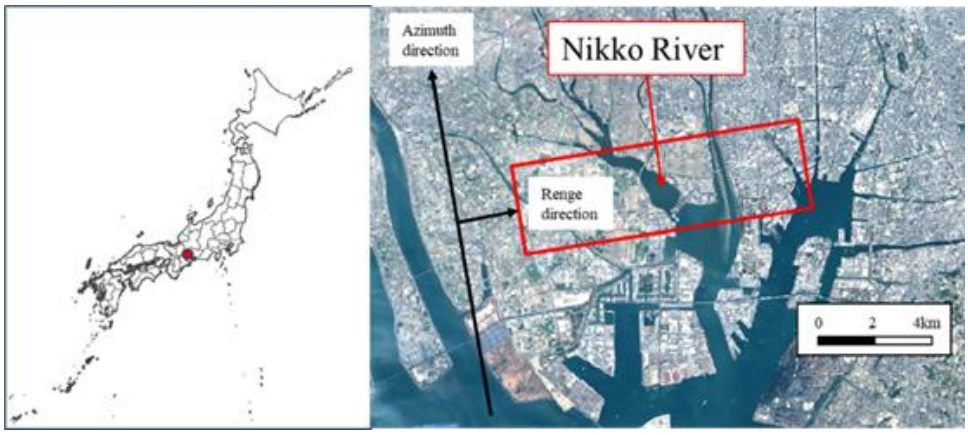

Figure 4: Observation location map (Nikko River)
(Source: partly modified from Geographical Survey Institute map)

Figure 5: Pictures of a water-landing drone (left: before landing, right: after landing)

3.2 Results

The observation results from 15:14 8.8 s to 15.1 s (6.3 s) on February 23, 2025, are shown in Figure 6 and Table 2. As shown in Figure 6, the SAR satellite image confirmed the position of the water-landing drone. In the staring spotlight mode, the SAR satellite fixed the observation range in the red frame in Figure 4 and observed while moving; thus, the movement of the drone under the landing stream was captured as a trajectory. The actual trajectory of the drone and the extension of the trajectory in the SAR satellite image were displayed differently owing to the scattering of microwaves.

Table 2 shows the results of comparing the water level estimated only by the SAR satellite and the water level observed by the water-landing drone with that observed by the fixed water-level observation station at the mouth of the Nikko River.

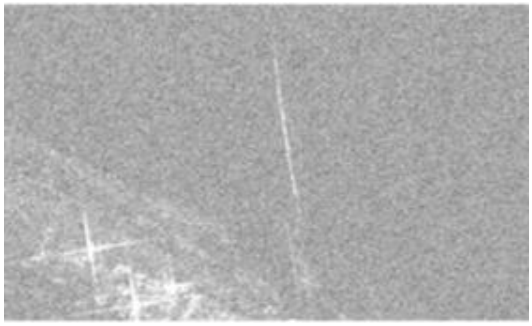

Figure 6: a trajectory of the drone confirmed by the SAR image

Table 2 Comparison results of water level for each observation and estimation method

Observation and estimation method	(a) An observed water level at a fixed water level station	(b) An estimated water level using only a SAR image	(c) An observed water level using a water-landing drone
Water level	T.P. - 0.39 m	T.P. 1.00 m ((b) - (a) = 1.39m)	T.P. -0.43 m (30 second average) ((c) - (a) = - 0.04m) Fluctuation range of instantaneous value T.P.-0.51m ~ -0.35m

T.P. (Tokyo Peil): mean sea level of Tokyo Bay

3.3 Discussion

As shown in Table 2, the water level estimated only by the SAR satellite was 1.39 m higher than that observed by the fixed water level observation station. This is because the wind was slightly strong at the time of the observation (Nagoya observation station: average wind speed 4.4 m/s at 15:10 on February 23, 2025). The fluctuation range of the instantaneous value of the water level observed by the drone below the landing stream also indicated that the water surface fluctuated. Therefore, it is highly probable that the back-reflection intensity was affected by fluctuations in the water surface.

In contrast, the 30 s average water level observed by the drone, as shown in Table 2, had an error of 0.04 m compared with the water level at the fixed water level station, indicating good observation accuracy. It was expected that the drone could observe the water level at any point as a mobile water level gauge and use it as data to correct the water level estimated by the SAR satellite.

In this way, the drone can observe the water level fluctuation and the water level at any point. As shown in Figure 6, the position of the drone can also be identified from SAR satellite images. Therefore, it is expected that the observation data by the drone could be used to set the threshold value of the back reflection intensity (pixel value) and to correct the estimated water level to improve the accuracy of discrimination between water and land areas by SAR images.

4 DEVELOPMENT OF FLOOD FORECASTING ACCURACY EVALUATION TOOL USING DIGITAL TESTBEDS

The Water and Disaster Management Bureau (WDMB) of MLIT is developing a watershed data platform (Hereinafter referred to as DPF), which standardizes the data format and enables automatic updating of watershed data in 109 class A river systems managed by the national government. The DPF is an information infrastructure in a cloud environment, and watershed data, such as 3D topographic point cloud data can be utilized.

Therefore, NILIM, in cooperation with WDMB, developed Digital Testbeds (Hereinafter referred to as DTB) in the DPF as watershed experiment sites in cyberspace that can utilize DPF data (Takeshita et al. (2025)) and started trial use of the DTB in October 2025. As part of the trial use of the DTB, NILIM is using the DTB to visualize rivers in 3D, as shown in Figure 3, and is using it for research on water level estimation by SAR satellites. In addition, an accuracy evaluation tool is under development to verify the prediction accuracy of flood risk lines, in the national flood prediction system.

The display screen of the accuracy evaluation tool is shown in Figure 7, and the main evaluation indices are listed in Table 3. The equations for the Nash-Sutcliffe coefficient and error evaluation index "*E*" are shown in Equations (1), (2) and (3). By utilizing watershed data, visualization tools and accuracy evaluation tools on DTB, we will verify the accuracy of flood risk line prediction in the country and promote R&D to improve the accuracy of flood prediction through public-private collaboration.

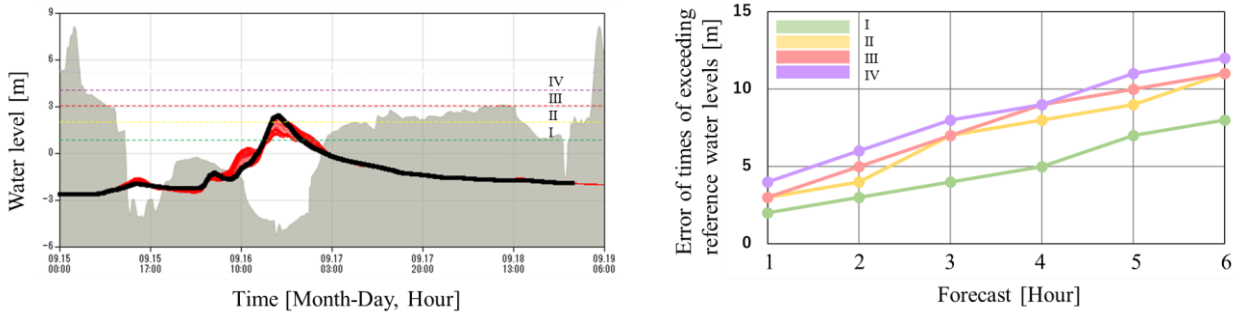

Figure 7: Screen display images of the flood prediction accuracy evaluation tool

Table 3 Evaluation indices of the flood prediction accuracy evaluation tool

Evaluation objects	Evaluation indices
Water levels	Error of peak water level, Error rate (=Error / peak water level)
	Error of reference water levels (I to IV), Error rates (=Errors /reference water levels) I: Reference water levels for flood-fighting corps to begin standby II: Reference water levels for flood-fighting corps to begin activities III: Reference water levels for evacuation of the elderly people, etc. IV: Reference water levels for evacuation instruction
Times	Error of peak water level times
	Error of times of exceeding reference water levels (I to IV)
Water-level hydrographs	RMSE (Root Mean Square Error)
	Nash-Sutcliffe (*NS*) coefficient (Equations (1) and (2))
	Error evaluation index "*E*" (Equation (3))

$$NS = 1 - \frac{\sum_{i=1}^{N}\{h_o(i)-h_c(i)\}^2}{\sum_{i-,}^{N}\{h_o(i)-h_{av}\}^2} \quad (1)$$

$$h_{av} = \frac{1}{N}\sum_{i=1}^{N} h_o(i) \quad (2)$$

$$E = \frac{1}{N}\sum_{i=1}^{N}\left\{\frac{h_o(i)-h_c(i)}{h_{op}}\right\}^2 \quad (3)$$

N: calculation times, $h_o(i)$: measured water levels at time i, $h_c(i)$: calculated water levels at time i, h_{av}: measured average water levels, h_{op}: measured peak water levels

5 CONCLUSIONS

The conclusions of this study are as follows.

1) We developed a river water level estimation method using SAR satellites and compared the measured water level with the estimated water level using SAR satellites. The mean absolute errors were between 0.35 m and 1.42 m for each type of SAR image and processing condition.
2) As a result of carrying out the observation of the Nikko River in cooperation with a SAR satellite and a water-landing drone equipped with an RTK-GNSS positioning function and a microwave reflector, the error of the water level observed by the fixed water level observation station and the water-landing drone was 0.04 m, and the trajectory of the drone was confirmed from the SAR satellite image. This result is expected to be useful for correcting the water level estimated by the SAR satellite based on the water level observed by the drone and for improving the accuracy of discrimination between water and land areas.
3) Using the digital testbed, we conducted research on water-level estimation using SAR satellites and are developing an accuracy evaluation tool for flood forecasting. In the future, we plan to use this tool for research and development to verify and improve the accuracy of the national flood forecasting system.

6 ACKNOWLEDGEMENTS

The authors would like to express their sincere gratitude to WDMB of MLIT, Pacific Consultants Co., Ltd., Remote Sensing Technology Center of Japan, Prodrone Co., Ltd., Synspective Inc., Japan Aerospace Exploration Agency and CTI Engineering Co., Ltd. for their cooperation in this research.

This research was also supported in part by the research budget of BRIDGE (Programs for bridging the gap between R&D and the ideal society (society 5.0) and generating economic and social value). We would like to express our gratitude.

REFERENCES

Biondi, F., Tarpanelli, A., Addabbo, P., Clemente, C. and Orlando, D. (2019). Pixel tracking to estimate rivers water flow elevation using Cosmo SkyMed synthetic aperture radar data, Remote Sensing 11 (21), 2574.

Chen, X., Zheng, Y., Peng, J. and Floris, M. (2021). Monitoring river water level using multiple bounces of bridges in SAR images, Advances in Space Research 68, pp.4016-4023.

Frost, V. S., Stiles, J. A., Shanmugan, K. S. and Holtzman, J. C. (1982). A model for radar images and its application to adaptive digital filtering of multiplicative noise, IEEE Trans. Pattern Analysis and Machine Intelligence, Vol.4, No.2, pp.157-166.

Tachikawa, Y., Sudo, J., Shiiba, M., Yorozu, K. and Kim, S. (2011). Development of A Real-Time River Stage Forecasting Method using a Particle Filter, Journal of JSCE, B1, Vol.67, No.4, pp. I_511-I_516.

Takeshita, T., Morooka, Y., Yamaji, H., Kuronuma, H., Ozawa, K., Hamada, Y. (2025). Development of Digital Testbeds to Support the Policy of River Basin Disaster Resilience and Sustainability by All, Proceedings of the 41st IAHR World Congress, pp.1001-1008, Singapore, June 22-27.

Tsuchiya, S., Morooka, Y. and Takeshita, T. (2023). Development of the river water level prediction method using data assimilation and the display system called Flood Risk Line, Extended Abstracts of the 9th International Conference on Flood Management, No.19-03, Tsukuba, Ibaraki, Japan, February 18-22.

Web sites:

Web-1: https://frl.river.go.jp, consulted 29 November 2025.

Web-2: https://www.eorc.jaxa.jp/ALOS/en/alos-2/datause/a2_format_e.htm, consulted 29 November 2025.

Web-3: https://synspective.com/document/, consulted 29 November 2025.

Web-4: https://sbir.csti-startup-policy.go.jp/phase3fund, consulted 29 November 2025.

(SBIR Demonstration Project Compendium (Ver.2).pdf, p.124)

ICFM 10
Adapting to Global Change:
Innovative Approaches to Flood Management and Resilience
May 20-22, 2026 | Western University, London, Ontario, Canada

Seq2Seq-DDPM: A novel interval flood forecasting model based on Sequence-to-Sequence Denoising Diffusion Probabilistic Model

Chang Chen[1] and Dawei Zhang[2]
State Key Laboratory of Water Cycle and Water Security, China Institute of Water Resources and Hydropower Research, Beijing 100038, China[1]
Research Center on Flood & Drought Disaster Prevention and Reduction, Ministry of Water Resources, Beijing 100038, China[1]
E-mail: 2234104368@qq.com

State Key Laboratory of Water Cycle and Water Security, China Institute of Water Resources and Hydropower Research, Beijing 100038, China[2]
Research Center on Flood & Drought Disaster Prevention and Reduction, Ministry of Water Resources, Beijing 100038, China[2]
E-mail: zhangdw@iwhr.com

ABSTRACT

Accurate flood forecasting performs a vital function in safeguarding basin water security. In recent years, neural network-based hydrological models have shown strong predictive power. However, uncertainties in data, parameters, and structure lead to variability in forecasts. Thus, an innovative flood forecasting model, Seq2Seq-DDPM, is proposed by the integration of the Sequence-to-Sequence (Seq2Seq) framework and the Denoising Diffusion Probabilistic Model (DDPM). It is specifically designed to achieve probabilistic forecasting of streamflow processes, quantifying hydrological uncertainties. It employs the Bidirectional Gate Recurrent Unit (BiGRU) as the Encoder and the Gate Recurrent Unit (GRU) as the Decoder, with the diffusion model serving as the bridge connecting the two. This architecture encapsulates the uncertainty of hydrological processes within the hidden state. Comparative experiments are carried out in the Xiapu River Basin to verify the effectiveness of probabilistic forecasting models. The proposed Seq2Seq-DDPM is compared against various mainstream models, including the Probabilistic Forecasting with Autoregressive Recurrent Networks (DeepAR), the Lower and Upper Bound Estimation (LUBE), and the Quantile Regression (QR) method. The findings confirm that the proposed Seq2Seq-DDPM model achieves the highest Prediction Interval Coverage Probability (PICP) value and the lowest Prediction Interval Normalized Averaged Width (PINAW) value among the compared methods. The forecast intervals reliably encompass most of the observed streamflow values, indicating its superior probabilistic forecasting capability. These outcomes suggest that the model can provide effective risk information for flood control scheduling decisions.

KEYWORDS: Flood probabilistic forecasting; Seq2seq; Diffusion model; Neural networks;

1 INTRODUCTION

Flood forecasting constitutes a crucial non-engineering measure, offering a scientific foundation in basin flood prevention and disaster mitigation, while also offering essential support for the optimal management of water resources. With the rapid advancement of artificial intelligence technology, deep learning has demonstrated great potential in flood forecasting. Among these, recurrent neural networks have captured notable focus in flood forecasting, due to their proven efficacy in sequence prediction. Representative architectures, typified by the Long Short Term Memory (LSTM) and its variants, have

been extensively applied in hydrological modelling. Liu et al., (2023) constructed the LSTM model and applied it to forecast streamflow in the area between the Xiangtan Station and Changsha Station, thereby demonstrating its capability in flood early warning. Yan et al., (2023) proposed a novel flood forecasting model that integrates the simulated annealing (SA) algorithm and the Gate Recurrent Unit (GRU), enabling daily-scale flood forecasting in the central urban area of Hefei. Boughale et al., (2024) utilized the Historical Daily Weather dataset from the Australian Commonwealth Office of Meteorology to test the Bidirectional Long Short Term Memory (BiLSTM). The findings reveal that the BiLSTM model consistently achieved the best forecasts. Fan and Chang, (2024) used the Bidirectional Gate Recurrent Unit (BiGRU) to predict the streamflow and water level in the Xiaoqing River Basin, maintaining a high level of prediction accuracy.

It is important to note that the aforementioned studies are all deterministic forecasts. However, due to the complexity of hydrological processes, flood forecasting inevitably involves uncertainties related to input data, model structures, and model parameters (Matthews et al., 2021). These uncertainties affect the reliability of prediction results, leading to suboptimal robustness in deterministic forecasts. Currently, the deep integration of advanced uncertainty modelling techniques with deep learning frameworks has developed into a vital direction in probabilistic flood forecasting. Chang et al., (2024) created a method based on the Lower and Upper Bound Estimation (LUBE), which illustrated strong performance in reducing forecast uncertainty in the Yalong River Basin. Weng et al., (2023) trained the Quantile Regression (QR) method integrated with LSTM networks (QRLSTM) using both real and synthetic flood sequences in the flood interval prediction field. Xie et al., (2025) designed a modelling framework based on the Probabilistic Forecasting with Autoregressive Recurrent Networks (DeepAR) to better capture the variability of flow uncertainty in two basins.

This study selects the Xiapu River Basin above the Dawuchang hydrological station in Xianning City as the study area and constructs the Seq2Seq-DDPM probabilistic flood forecasting model by integrating the Sequence-to-Sequence (Seq2Seq) framework with the Denoising Diffusion Probabilistic Model (DDPM). The experimental results of Seq2Seq-DDPM are compared and analysed against those of commonly used methods, thereby providing a technical reference for future probabilistic flood forecasting research.

2 METHOD

An innovative flood forecasting model, Seq2Seq-DDPM, is proposed by the integration of the Sequence-to-Sequence (Seq2Seq) framework and the Denoising Diffusion Probabilistic Model (DDPM), as shown in Figure 1. The model combines the Seq2Seq architecture with the DDPM to achieve probabilistic forecasting of streamflow processes. This innovative framework utilizes diffusion processes to encapsulate uncertainty within hidden states, not only providing uncertainty estimates in hydrological models but also significantly reducing computational cost.

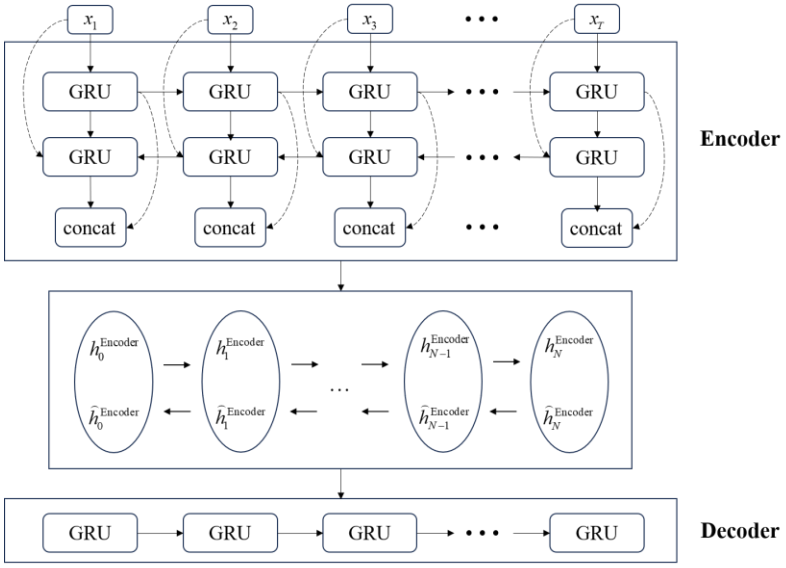

Figure 1: The framework of Seq2Seq-DDPM

The sequence-to-sequence (Seq2Seq, also known as Encoder-Decoder) framework proposed by Sutskever et al., (2014) leverages the information transmission mechanism of the Encoder-Decoder, offering significant advantages in time-series processing and forecasting. Notably, its application in hydrology can effectively capture the dependencies in rainfall-runoff relationships, enhancing the predictive accuracy (Kao et al., 2020; Xiang et al., 2020).

In the Seq2Seq-DDPM model, the Encoder processes input sequences in both forward and backward directions using the BiGRU architecture, enabling the extraction of bidirectional features from flood time series. This bidirectional mechanism enables the retention and more comprehensive exploitation of information during flood peaks. The gating mechanism of the Gate Recurrent Unit (GRU) in the Decoder facilitates the selective retention and updating of information, thereby enhancing the accuracy of the decoding process. The structure of GRU is illustrated in Figure 2, which includes components such as update gates z_t and reset gates r_t to control historical information x_t flow. BiGRU extends the GRU architecture by concatenating the hidden states from both the forward direction $\vec{h}_t$ and the backward direction $\overleftarrow{h}_t$, as defined in Eqs. (1) to (3).

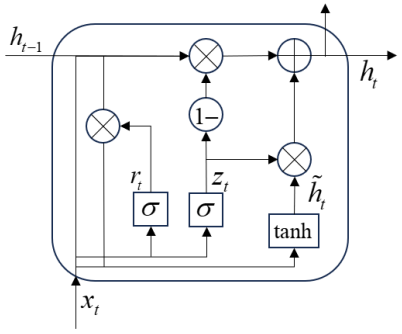

Figure 2: The framework of GRU

$$\vec{h}_t = \begin{cases} \vec{z}_t = \sigma\left(\vec{W}_z \vec{x}_t + \vec{U}_z \vec{h}_{t-1} + \vec{b}_z\right) \\ \vec{r}_t = \sigma\left(\vec{W}_r \vec{x}_t + \vec{U}_r \vec{h}_{t-1} + \vec{b}_r\right) \\ \tilde{h}_t = \tanh\left(\vec{W}\vec{x}_t + \vec{U}\left(\vec{r}_t \odot \vec{h}_{t-1}\right)\right) \\ \vec{h}_t = \left(1 - \vec{z}_t\right) \odot \vec{h}_{t-1} + \vec{z}_t \odot \tilde{h}_t \end{cases} \tag{1}$$

$$\overleftarrow{h}_t = \begin{cases} \overleftarrow{z}_t = \sigma\left(\overleftarrow{W}_z \overleftarrow{x}_t + \overleftarrow{U}_z \overleftarrow{h}_{t-1} + \overleftarrow{b}_z\right) \\ \overleftarrow{r}_t = \sigma\left(\overleftarrow{W}_r \overleftarrow{x}_t + \overleftarrow{U}_r \overleftarrow{h}_{t-1} + \overleftarrow{b}_r\right) \\ \tilde{h}_t = \tanh\left(\overleftarrow{W}\overleftarrow{x}_t + \overleftarrow{U}\left(\overleftarrow{r}_t \odot \overleftarrow{h}_{t-1}\right)\right) \\ \overleftarrow{h}_t = \left(1 - \overleftarrow{z}_t\right) \odot \overleftarrow{h}_{t-1} + \overleftarrow{z}_t \odot \tilde{h}_t \end{cases} \tag{2}$$

$$h_t = \left[\vec{h}_t \oplus \overleftarrow{h}_t\right] \tag{3}$$

where $\rightarrow$ and $\leftarrow$ are the forward and backward processes, respectively. $\tilde{h}_t$ is the hidden input activation vector. b_z and b_r indicate the biases, respectively. W_z, U_z, W_r, U_r and U refer to the weights, respectively. $\sigma(\cdot)$ and $\tanh(\cdot)$ are activation functions, respectively. $\odot$ is an element-wise multiplication. $\oplus$ illustrates an element-wise sum.

Serving as a crucial bridge between the Encoder and the Decoder, the diffusion model provides a probabilistic representation of the latent state space. In hydrological probabilistic forecasting, its core value is to offer a probabilistic modelling framework that generates runoff's conditional probability distributions through the transformation of latent variables using a Markov chain. This approach breaks away from the single-output mode of traditional deterministic forecasting.

Diffusion models consist of forward and reverse processes. The former develops a Markov chain by adding noise $\varepsilon \sim \mathrm{N}\left(0, \mathbf{I}\right)$. The latent variable h_N is shown as Eq. (4), after N steps.

$$h_N = \sqrt{\bar{\alpha}_N} h_0^{\text{Encoder}} + \sqrt{1 - \bar{\alpha}_N}\varepsilon \tag{4}$$

where h_0^{Encoder} is the hidden state output from the Encoder. α_N weights the latent variable and the noise and $\bar{\alpha}_N = \prod_{n=1}^{N} \alpha_n$. The desired distribution of the hidden state is shown in Eq. (5).

$$\begin{cases} q\left(h_1, h_2, \cdots, h_N \middle| h_0\right) = \prod_{n=1}^{N} q\left(h_n \middle| h_{n-1}\right) \\ q\left(h_n \middle| h_{n-1}\right) = \mathrm{N}\left(h_n; \sqrt{1-\beta_n} h_{n-1}, \beta_n \mathbf{I}\right) \end{cases} \tag{5}$$

where $\beta_n = 1 - \alpha_n$. The reverse diffusion process is formulated as Eq. (6).

$$\begin{cases} p_\theta\left(h_0,h_1,\cdots,h_{n-1}\middle|h_N\right)=p\left(h_N\right)\prod_{n=1}^{N}p_\theta\left(h_{n-1}\middle|h_n\right) \\ p_\theta\left(h_{n-1}\middle|h_n\right)=\mathrm{N}\left(h_{n-1};\mu_\theta\left(h_n,n\right),\tilde{\beta}_n\mathbf{I}\right) \\ \tilde{\beta}_n=\left(1-\bar{\alpha}_{n-1}\right)\beta_n/1-\bar{\alpha}_n \end{cases} \tag{6}$$

where $p\left(h_N\right)\square\ \mathrm{N}\left(0,\mathbf{I}\right)$ and $\tilde{\beta}_n=\left(1-\bar{\alpha}_{n-1}\right)\beta_n/1-\bar{\alpha}_n$. $\mu_\theta\left(h_n,n\right)$ denotes the mean value.

3 STUDY CASE

The study area selects for this paper is the Xiapu River Basin above the Dawuchang hydrological station in Xianning City, China, covering an area of 112.5 km^2, as shown in Figure 3. There are three rainfall stations within the catchment: Sanbao Station, Linshang Station, and Huangjin Station. The Dawuchang Hydrological Station is located at the catchment outlet (Zhang et al., 2015).

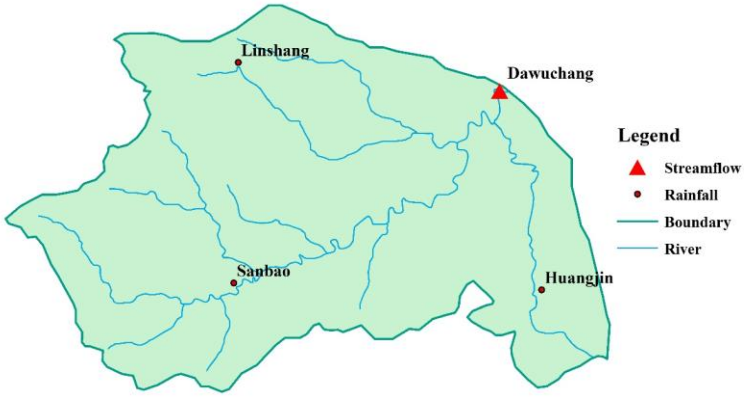

Figure 3: Study area

For probability prediction, two evaluation metrics are used: the Prediction Interval Coverage Probability (PICP), which assesses the percentage of actual values that lie in the forecast interval, and the Prediction Interval Normalized Averaged Width (PINAW), which quantifies the width of the interval relative to the range of observed data. These are defined in Eqs. (7) to (9). The higher the likelihood that the observed value lies in the forecast interval, the greater the PICP value and the better the prediction performance. Conversely, the larger the width of the forecast interval, the bigger the PINAW value and the poorer the predictive capability.

$$c_t=\begin{cases}1 & Q_t^{\mathrm{obs}}\in\left[L_t,U_t\right] \\ 0 & Q_t^{\mathrm{obs}}\notin\left[L_t,U_t\right]\end{cases} \tag{7}$$

$$\mathrm{PICP}=\frac{1}{M}\sum_{t=1}^{M}c_t \tag{8}$$

$$\mathrm{PINAW}=\frac{1}{MR}\sum_{t=1}^{M}\left(U_t-L_t\right) \tag{9}$$

where c_t denotes a Boolean variable. Q_t^{obs} is the observed flows. R indicates the range of the variable. M represents the count of samples. U_t and L_t denote the upper and lower limits.

4 RESULTS

This study reports the evaluation metrics for the 90% confidence interval with different lead times. Figure 4(a) and Figure 4(b) present, respectively, statistical heatmaps of the mean values for the PICP and PINAW evaluation indices in the Xiapu River Basin. These experiments examine the reliability and concentration of probabilistic forecasts from different perspectives.

When the lead time is 1h-3h , the PICP values for Seq2Seq-DDPM are 90.42%-93.68%. The PINAW values for Seq2Seq-DDPM are 0.085-0.098. The PICP values for QR, LUBE, and Seq2Seq-DDPM all exceed or approach the 90% confidence level. However, LUBE has an excessively high PINAW value, suggesting that its interval forecast results are relatively unreliable. Meanwhile, the Seq2Seq-DDPM model exhibits an average PICP value that is 0.7% higher than QR's, while its PINAW value decreases by an average of 0.003. In summary, the Seq2Seq-DDPM model delivers superior probabilistic forecasting performance with narrower intervals while keeping high coverage.

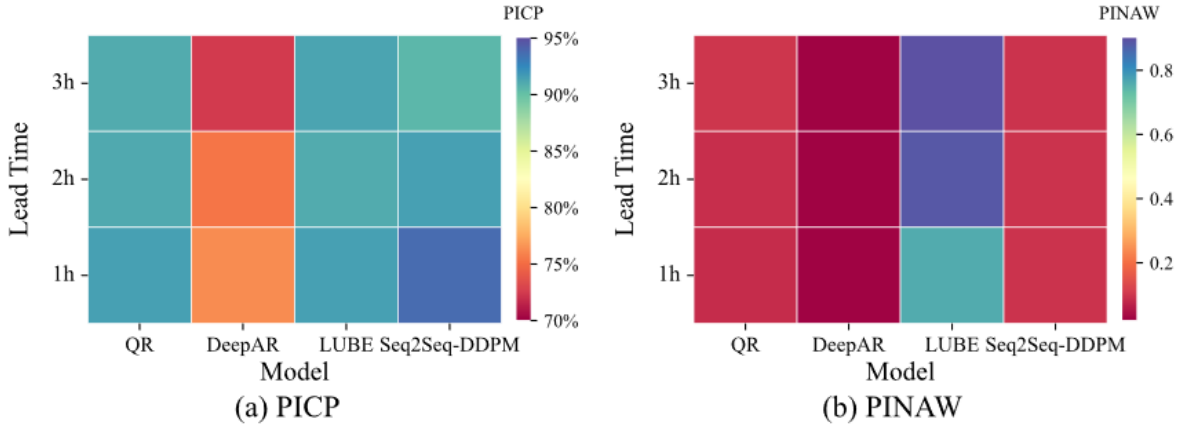

Figure 4: Statistical heatmaps of the average values for probabilistic evaluation metrics

Figure 5 and Figure 6 display the prediction intervals at the 90% confidence interval for Seq2Seq-DDPM, providing a visual analysis of the model's performance in quantifying prediction uncertainty. Using the No. 020513 and No. 040429 flood events at 1h forecast horizon as examples, the Seq2Seq-DDPM model covers most of the observed flow, indicating reasonable reliability of the prediction intervals. However, for the No. 020513 flood event, the Seq2Seq-DDPM model slightly underestimates the peak flows. Enhancing the model's performance in predicting flood peaks is a potential area for future work.

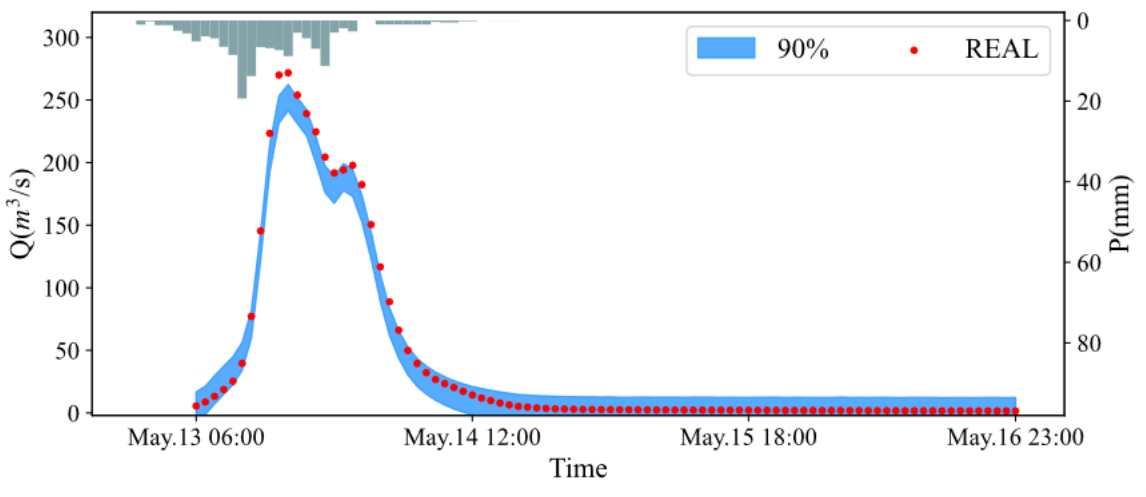

Figure 5: The forecast result of the No. 020513 flood event

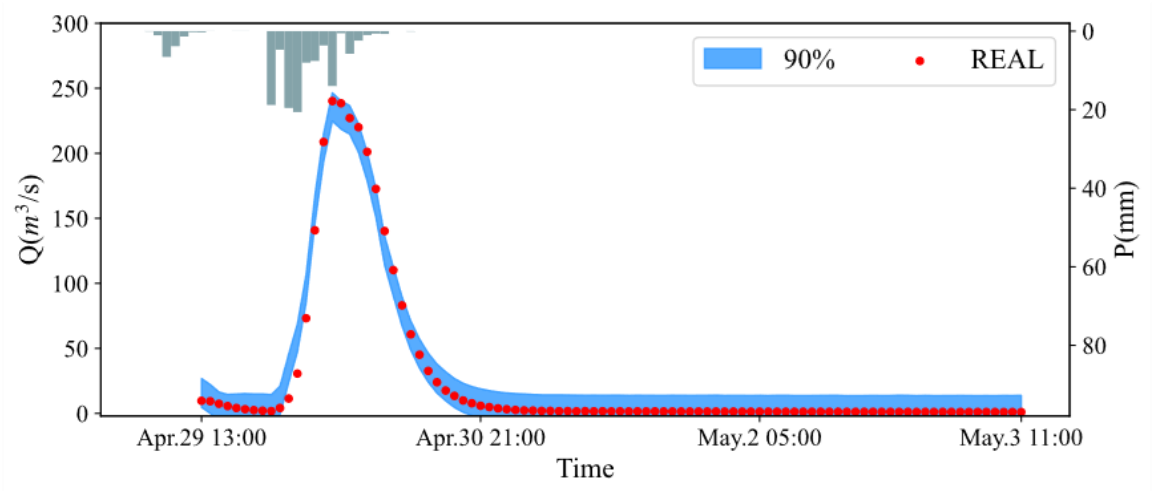

Figure 6: The forecast result of the No. 040429 flood event

5 CONCLUSION

This paper presents a flood probability model based on the diffusion model and the Seq2Seq architecture, termed Seq2Seq-DDPM. It employs the BiGRU as the Encoder and the GRU as the Decoder, with the diffusion model serving as the bridge connecting the two. This architecture encapsulates the uncertainty of hydrological processes within the hidden state, quantifying hydrological uncertainties. The Seq2Seq-DDPM uses observed rainfall and streamflow as inputs to probabilistically forecast future streamflow.

Experimental results demonstrate that the Seq2Seq-DDPM model obtains the highest PICP and the lowest PINAW, which shows that it can create a narrow interval while maintaining high coverage. For model-fitting performance, the Seq2Seq-DDPM model covers most of the observed flow, indicating reasonable reliability of the prediction intervals.

Meanwhile, Seq2Seq-DDPM still presents opportunities for further improvement. The study observes that, in certain scenarios, the model underestimates flood peaks. Consequently, future work may

consider developing a novel loss function that effectively reduces peak errors to further enhance the model's predictive performance.

6 ACKNOWLEDGEMENTS

The study was supported by the National Key Research and Development Program of China (Grant No. 2024YFC3214802) and the IWHR Research & Development Support Program (WH0145B022021).

REFERENCES

Boughale R., Zrelli A. and Ezzedine T. (2024). Enhancing Flood Forecasting with BiLSTM Networks, in "2024 IEEE/ACS 21st International Conference on Computer Systems and Applications (AICCSA),"IEEE, 2024, pp. 1–6.

Chang X., Guo J., Qin H., Huang J., Wang X. and Ren P. (2024). Single-Objective and Multi-Objective Flood Interval Forecasting Considering Interval Fitting Coefficients. Water Resour. Manag., 38, 3953–3972.

Fan W. and Chang C. (2024). Study Of Flood Forecasting Based on Recurrent Neural Network for Urban River in The Piedmont Plain, in "15th International Conference on Hydroinformatics,"2024, p. 289.

Kao I.-F., Zhou Y., Chang L.-C. and Chang F.-J. (2020). Exploring a Long Short-Term Memory based Encoder-Decoder framework for multi-step-ahead flood forecasting. J. Hydrol., 583, 124631.

Liu Y., Yang Y., Chin R.J., Wang Chucai and Wang Changshun (2023). Long Short-Term Memory (LSTM) Based Model for Flood Forecasting in Xiangjiang River. KSCE J. Civ. Eng., 27, 5030–5040.

Matthews G., Barnard C., Cloke H., Dance S.L., Jurlina T., Mazzetti C. and Prudhomme C. (2021). Evaluating the impact of post-processing medium-range ensemble streamflow forecasts from the European Flood Awareness System. Hydrol. Earth Syst. Sci. Discuss., 2021, 1–51.

Sutskever I., Vinyals O. and Le Q.V. (2014). Sequence to sequence learning with neural networks. Adv. Neural Inf. Process. Syst., 27.

Weng P., Tian Y., Liu Y. and Zheng Y. (2023). Time-series generative adversarial networks for flood forecasting. J. Hydrol., 622, 129702.

Xiang Z., Yan J. and Demir I. (2020). A Rainfall-Runoff Model With LSTM-Based Sequence-to-Sequence Learning. Water Resour. Res., 56, e2019WR025326.

Xie S., Wang D., Wang J., Yang C., Shen K., Jia B. and Cao H. (2025). A DeepAR-Based Modeling Framework for Probabilistic Mid-Long Term Streamflow Prediction. Water, 17, 2506.

Yan Y., Zhang W., Liu Y. and Li Z. (2023). Simulated annealing algorithm optimized GRU neural network for urban rainfall-inundation prediction. J. Hydroinformatics, 25, 1358–1379.

Zhang D., Quan J., Zhang H., Wang F., Wang H. and He X. (2015). Flash flood hazard mapping: A pilot case study in Xiapu River Basin, China. Water Sci. Eng., 8, 195–204.

ICFM 10
Adapting to Global Change:
Innovative Approaches to Flood Management and Resilience
May 20-22, 2026 | Western University, London, Ontario, Canada

Regionally Adaptive Assessment of Dams for Forecast-Informed Reservoir Operations Potential

Elissa Yeates,[1] Caitline Barber,[2] Joe Forbis,[1] Rachel Weihs,[3] Eric Shearer,[1] and Cary Talbot[1]
United States Army Corps of Engineers, Coastal and Hydraulics Laboratory, Vicksburg, Mississippi, 39180, United States[1]
E-mail: Elissa.M.Yeates@usace.army.mil

ERG, Concord, MA, 01742, United States[2]
E-mail: Caitline.Barber@erg.com

Center for Western Weather and Water Extremes, Scripps Institution of Oceanography, University of California, San Diego, California, 92093, United States[3]

ABSTRACT

The U.S. Army Corps of Engineers (USACE) research and operations program Forecast-Informed Reservoir Operations (FIRO) seeks to use forecasts to add flexibility to dam release decisions, improving outcomes across objectives including flood risk management, water supply reliability, groundwater recharge, and environmental flows. Pilot sites for the program are on the west coast of the United States and are characterized by short travel times from dams to downstream control points and by relatively high predictability of extreme precipitation events, notably atmospheric rivers. Viability assessment studies of FIRO at several USACE-owned pilot sites are now informing water control plan updates. Deviations in operations using FIRO have demonstrated gains in flood risk management and water storage, leading to expanded demand for FIRO viability assessments and implementation at other reservoirs.

To assess the potential for FIRO implementation across the USACE portfolio of reservoirs, a nationwide screening process was developed. This screening considers the potential for benefits of increased operational flexibility weighed against the level of effort or difficulty to change operations and is underpinned by a multidimensional assessment of the skill of precipitation forecasting in the contributing watershed. FIRO screening is being conducted in stages, with a high-level elimination assessment of ~600 USACE reservoirs recently completed, and more in-depth assessments of site suitability by region underway through 2027. This second stage of the screening process has been applied across the southwest United States and is now being regionally adapted to consider the operational, meteorological, and hydrologic contexts of reservoirs in other parts of the United States. This paper discusses the development and application of this screening process, including results of the national first stage and regional second stage. The goal of the screening effort is to identify FIRO-suitable sites and inform next steps to scale up the modernization of USACE's reservoir operations where possible.

KEYWORDS: Reservoirs, Forecasts, Forecast-Informed Reservoir Operations, Screening Process

1 INTRODUCTION AND BACKGROUND

Dams and reservoirs are critical infrastructure for multiple, sometimes conflicting purposes, including managing flood risk, ensuring reliable streamflow and stored water supply, enabling navigation, and generating hydropower (Ho et al., 2017). Dams in the United States (U.S.) can impound an estimated volume of 1300 km^3 (Graf, 1999). Growing awareness of dams' disturbance to natural flow regimes and riparian ecologies has started to constrain operations and motivates both structure removal and improved operation of existing dams rather than new construction (McKay et al., 2020). Growing populations,

shifting land use and hydrologic regimes, infrastructure aging, and increasing water stress all place demand on these critical infrastructures to be operated efficiently and effectively (Ho et al., 2017).

Forecast-Informed Reservoir Operations (FIRO) has emerged as a strategy to support more efficient management of dams (Dettinger et al., 2023). By allowing reliable forecasts of precipitation to be used in decision-making about when to retain or release water from reservoirs, more flexibility is introduced to operations at participating sites (Forbis and Ly, 2023). Where traditional reservoir guide curves require conservative preservation of a flood control space during flood-prone times of year, implementation of FIRO allows water managers to hold more stored water when forecasts are dry, improving supply reliability, or conversely to prerelease volumes in advance of forecasted precipitation, improving flood risk mitigation (Forbis and Ly, 2023). The FIRO research and operations program, led by the U.S. Army Corps of Engineers in partnership with the Scripps Institution of Oceanography's Center for Western Weather and Water Extremes (CW3E) has piloted the FIRO approach at five sites to date (Web-1). Together with investments in improving the forecast skill for predicting Atmospheric River (AR) events, the dominant driver of flood risk in the U.S. West Coast, FIRO has enabled benefits to water supply, fisheries health, recreation, and flood risk reduction at pilot sites (Forbis and Ly, 2023).

The success of this approach at the pilot sites induced expansion of the research program, including a nationwide screening of the USACE reservoir portfolio to determine where to invest in FIRO studies. At pilot sites, developing alternative forecast-based WCPs and assessing their safety and viability requires a rigorous, multi-agency assessment process that has taken up to five years, followed by a separate process to formally update the site's Water Control Manual for implementation. Pilot sites have so far been selected with reasonable expectation of FIRO viability, and the assessment process has been streamlined as more sites undertake assessment and implementation, but this approach is not efficiently applicable across a wide portfolio. In response to the demand for expansion, a multi-stage FIRO screening process (FIRO-SP) was developed to assess preliminary suitability across the portfolio of ~600 USACE reservoirs. The aim of the FIRO-SP is to efficiently remove from consideration sites with low or no FIRO suitability, and to preliminarily assess the remaining sites to identify where FIRO assessment and implementation would be most beneficial and would face fewer barriers. The resulting assessments and recommendations are meant to inform decisions about where to invest in viability assessments, and to document initial considerations for those more rigorous studies to use in scoping. This paper reports the development of the FIRO-SP, the nationwide results of its first stage, and its full application to 53 projects in the western U.S. Previous large-scale screening efforts for dams have been developed to assess potential for removal (McKay et al., 2020; Naslund et al., 2025) or prioritization for repair and maintenance (Concha Larrauri et al., 2022). The FIRO-SP is novel in attempting to screen for FIRO suitability.

2 METHODOLOGY

2.1 The FIRO-SP Approach

For initial development of the FIRO-SP, expert elicitation was used, taking advantage of the robust community of researchers and practitioners that had been developed through the pilot projects at Lake Mendocino, Prado Dam, and the Yuba-Feather system. Attendees at the CW3E FIRO Workshop in August 2020 provided input for key criteria of FIRO suitability, including precipitation forecast skill at lead times meaningful for operations; willingness of stakeholders to invest in the viability assessment and implementation process; availability of reliable operational models; and capacity of the project to buffer forecast uncertainty (Yeates et al., 2026a). A FIRO-SP steering committee was formed in 2021 consisting of representatives from USACE, the U.S. Bureau of Reclamation, CW3E, Portland State University, and Sonoma and Yuba Water Agencies. This committee determined that screening should take a staged approach and that the process should not be solely algorithmic but must allow for expert judgment. Screening is distinct from the highly rigorous FIRO Viability Assessment process: it does not determine whether or to what extent FIRO can be implemented at a site, but rather that there is potential for the strategy to be possible at and beneficial for operations at the site.

The staged approach is detailed in Table 1. Stage A was envisioned to quickly eliminate broadly unsuitable sites, allowing for more in-depth site assessments in Stage B. Stage C ensures that site-level expertise is reflected in the final scoring and recommendation, and builds a pathway from screening to FIRO viability assessment and implementation.

Table 1. Stages of the FIRO Screening Process

Stage	Description	Components	Products
A	High-level assessment of a large portfolio of reservoirs to eliminate clearly unsuitable sites and to sort the rest into those with standard or significant barriers to FIRO. Applicable to all reservoirs under consideration.	1. Water manager provision of data for lead time estimation 2. Calculation of forecast lead time requirements by site 3. Critical Success Index calculation by site 4. Water manager responses to an 8-question instrument (drop-down responses, optional notes) 5. Data review and scoring	Categorization of all sites into those with prohibitive barriers (eliminated), significant barriers (eligible but not prioritized for Stage B), and standard barriers (prioritized). Technical Report (Yeates et al., 2026a) and ArcGIS Storymap (Web-2)
B	In-depth assessment of the potential for benefit from FIRO, the level of difficulty to assess and implement FIRO, and the supporting forecast skill at each eligible site. Applicable to sites which pass Stage A and are chosen by stakeholders to undergo further screening.	1. Meetings with site stakeholders to review Stage A and decide which sites to progress further 2. Dry Forecast Failure Ratio and Forecast Error Tolerance calculations by site 3. Water manager responses to a questionnaire with 14 data entry items and 22 scored questions (ranked response and text entry) 4. Data review, scoring, and production of site reports	Draft site FIRO suitability reports, including recommendations about whether to pursue FIRO at each site. Technical Report (forthcoming)
C	Dialogues held between water managers, invited stakeholders, and the FIRO-SP team to discuss the results and to finalize scoring and site reports. Applicable for all sites which undergo Stage B.	1. Provision of draft site assessment reports to USACE water managers 2. Regional stakeholder meetings, averaging 30 minutes per site, to discuss results and site context 3. Modify any scoring based on stakeholder review and dialogue 4. Finalize site assessment reports	Site FIRO suitability reports which include scoring, recommendations, and document context. Support for next steps, if applicable, to scope a FIRO study.

Stages were developed by the FIRO-SP working group and tested with a subset of reservoirs in the USACE South Pacific Division (SPD), which includes California, Arizona, New Mexico, Utah, Nevada, and portions of Oregon, Idaho, Wyoming, Colorado, and Texas. SPD was chosen to pilot the FIRO-SP since at the time, all FIRO pilot sites were SPD projects, so there was a high familiarity with the concept among those water managers as well as known potential for FIRO suitability in those regions. Testing was conducted in 2022 for Stage A and in 2023 for Stages B and C. Instruments and methodology were then revised, including the addition of the forecast skill assessment into Stage A. The nationwide Stage A screening was conducted in the fall of 2024 through spring of 2025, and Stages B and C were conducted for 53 eligible reservoirs or reservoir systems in SPD in 2025. Application of Stages B and C is ongoing for USACE reservoirs in the Northwestern and South Atlantic Divisions and planned to be completed for all eligible sites by the end of 2027.

2.2 Stage A Methodology

The first stage was developed with the aim of eliminating from further consideration sites with clear prohibitive barriers to FIRO, and to do so without requiring extensive data elicitation from water managers or computation beyond the precipitation forecast skill assessment. The FIRO expert community was convened to provide input to the Stage A criteria at the FIRO workshops in 2020 and 2021. The USACE Sacramento District's internal Reservoir Modernization Framework and the Lake Mendocino FIRO Final Viability Assessment (Jasperse et al., 2020) were reviewed for criteria. Outcomes of Stage A are described in terms of barriers to FIRO. Prohibitive barriers eliminate a site from further screening, and significant barriers indicate lower priority for screening unless otherwise determined by site stakeholders. "Standard" barriers are so termed because while they were identified as FIRO suitability barriers, they have been successfully addressed in pilot projects. Stage A barriers are listed in Table 2.

Table 2. FIRO Screening Process Stage A barriers and their classifications

Prohibitive barriers	• Dam cannot hold an impoundment • No Water Control Plan • Insufficient forecast skill (both the CSI value is below the 0.33 threshold AND inflow forecasts are deemed insufficient) • Other identified prohibitive barriers
Significant barriers	• Indefinite forecast skill (either inflow forecasts are deemed insufficient OR the CSI value is below the 0.33 threshold) • Low or adverse stakeholder engagement • Legal or technical barriers including low dam safety classification • Other identified significant barriers
Standard barriers	• Part of a system • Section 7 project (i.e., USACE manages the dam for flood risk but does not own the project) • Other identified standard barriers

Forecast skill is assessed in Stage A by means of the Critical Success Index (CSI) for extreme precipitation. CSI describes the ratio of forecasts "hits", "misses", and "false alarms" for precipitation events at a selected percentile in a watershed area (Cordeira et al., 2025). Methodology to calculate CSI for this effort is as described in Cordeira et al. (2025), but for the FIRO-SP CSI was calculated for the precipitation integration period corresponding to an estimated necessary lead time for operational decision-making at each screened site. Lead time estimation assumed that a hypothetical additional stored volume associated with FIRO implementation will need to be evacuated past a downstream flood control point before an incoming flood event, based on reliable forecast information. This required lead time was estimated for each site using Equations 1 and 2, with site gross pool volumes, travel times to downstream control points, release outlet capacities and channel capacities provided by USACE water managers.

$$Release\ Rate = Minimum(Release\ Capacity, Downstream\ Channel\ Capacity) \quad (1)$$

$$Required\ Forecast\ Lead\ Time = \frac{0.05 \times Gross\ Pool\ Volume}{Release\ Rate} + Travel\ Time \quad (2)$$

Volumes were provided in acre-feet, release and channel capacities were provided in cubic feet per second, and travel times to downstream control points were provided in hours or days. Units were converted as necessary to calculate the required lead time in days to the nearest tenth of one day. For the FIRO-SP Stage A, the FIRO volume was assumed to be equal to 5% of the gross pool storage (a conservative estimate based on the 10% flexible FIRO pool assessed for Lake Mendocino (Jasperse et al., 2020)). CSI values for the integration period closest to the required forecast lead time were then calculated for the HUC-6 watershed in which the reservoir was located. A CSI value of 0.33 was chosen as the threshold for indicating

some forecast skill (Weihs et al., 2026). Sites with CSI values below 0.33 were assigned a prohibitive barrier in Stage A if operators of the site also indicated that inflow forecasts were not available or were unreliable, and assigned a significant barrier otherwise. This condition to the interpretation of the CSI metric was intended to reduce the risk of eliminating sites if precipitation forecasts were not reliable enough alone to enable FIRO, but hydrologic response was well understood enough that precipitation forecasts together with inflow forecasts could enable modified operations.

Other Stage A barriers were all determined based on data provided by USACE site water managers via spreadsheets developed for each District's reservoir portfolio. These water managers then reviewed the resulting Stage A classifications, which were also published via an interactive ArcGIS Storymap (Web-2).

2.3 Stages B and C Methodology

Stage B assesses FIRO suitability in terms of the potential for forecast-based flexibility in operations to address water management challenges at that site (benefit), whether there are site factors that significantly inhibit the probability of successfully updating operations using FIRO (level of effort), and whether forecast skill may support operational change. Stage B is conducted by water managers providing quantitative and qualitative project information via an online questionnaire. Potential benefit includes factors such as how frequently operators request to deviate from the water control plan and how interested project stakeholders are in modifying operations to meet different objectives. Effort is assessed via items about stakeholder willingness to engage in the FIRO process, availability of forecast and operational modelling products, complexity of reservoir system operations, and presence of protected species which might be affected by operational change. Water management teams were given the opportunity to suggest additional items and factors based on regional operational conditions and challenges, and a series of workshops is planned to further develop regional methodology adaptative before more USACE divisions are assessed.

Alongside the questionnaire, the FIRO-SP team conducts assessments of a Dry Forecast Failure Ratio (DFFR) metric and a Forecast Error Tolerance (FET) metric in addition to the CSI assessed in Stage A. Benefit, effort, and forecast skill dimensions are all scored and used to calculate a composite FIRO Suitability Index score. These scores are associated with recommendation categories and are intended to inform prioritization of sites for viability assessment and implementation.

DFFR assesses the forecast's complete failure to detect precipitation when observed precipitation exceeds the 90th percentile. Forecast Error Tolerance assesses whether a reservoir's flood storage space can absorb estimated inflow resulting from the mean annual precipitation error over its contributing basin. Both metrics and the CSI are calculated using forecasts from Global Ensemble Forecast System Version 12 Reforecasts, and observational datasets vary by watershed and are reported in site suitability reports. The full instrument and Stage B scoring routines are provided in a forthcoming Technical Report (Yeates et al., 2026b).

Stage C entails the provision of draft scoring and site reports to USACE water managers followed by dialogues, virtual and in-person, to discuss results by site. These meetings have averaged about 30 minutes to an hour per site discussed. Water managers have the option to invite additional stakeholders. Scoring is revised as necessary following these dialogues, and any additional context provided is added to site suitability reports in hopes that it will support development of viability assessments where appropriate.

3 RESULTS

593 reservoirs were screened in Stage A. 184 of these (31%) were eliminated with prohibitive barriers, most commonly having no ability to impound volume (78 sites, such as lock system dams) followed by poor forecast skill. Half of the reservoirs (299 sites) exhibited significant but not prohibitive barriers, most commonly failing either, but not both, the CSI metric or the water manager assessment of inflow forecast sufficiency. 110 sites, 19% of the portfolio of USACE reservoirs, exhibited only standard barriers to FIRO. These sites were primarily in the South Pacific Division (39), Great Lakes and Ohio River Division (32), and Northwestern Division (19). Figure 1 shows the intersection sets of all barriers assessed in Stage A.

Figure 2 shows a histogram of the CSI forecast skill values for all sites assessed. More site-level detail is provided in the Storymap (Web-2).

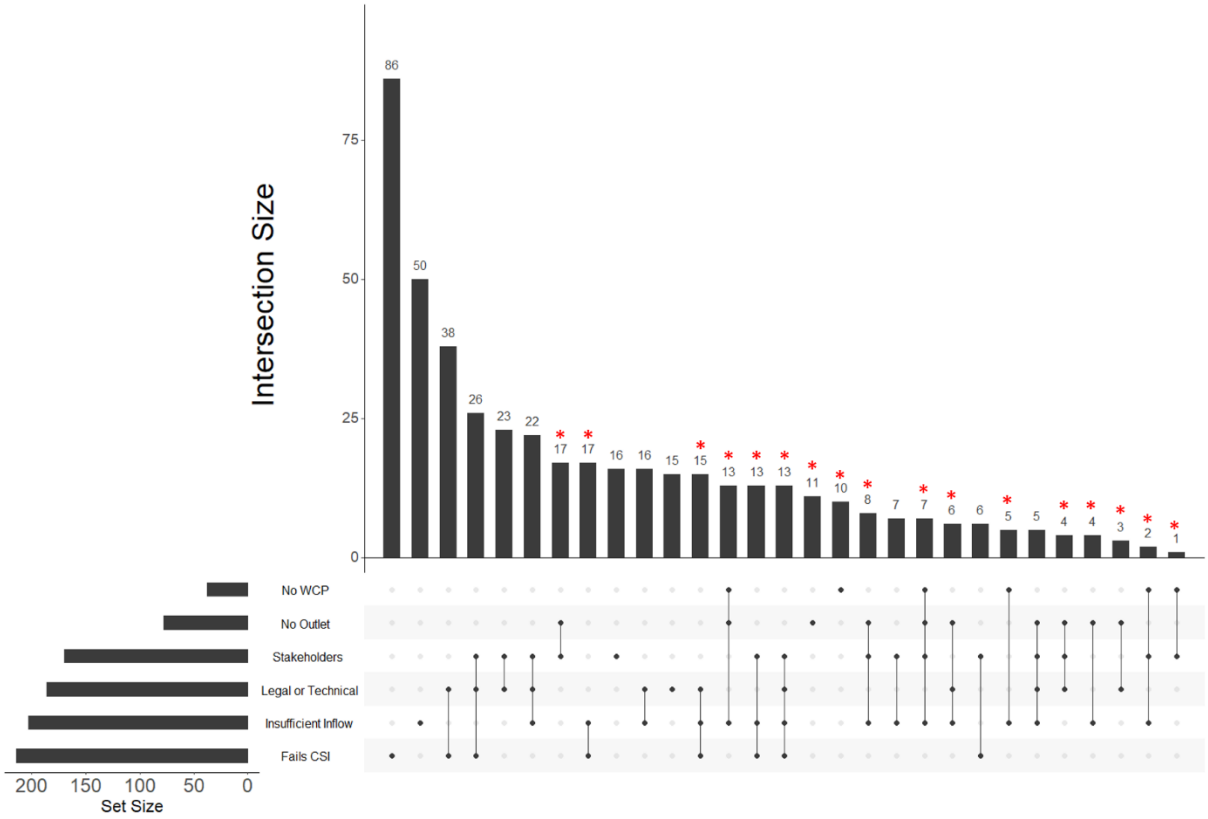

Figure 1: Intersections of barriers across all reservoirs assessed in Stage A. Intersections associated with the "Prohibitive Barrier" classification are denoted with a red asterisk (*).

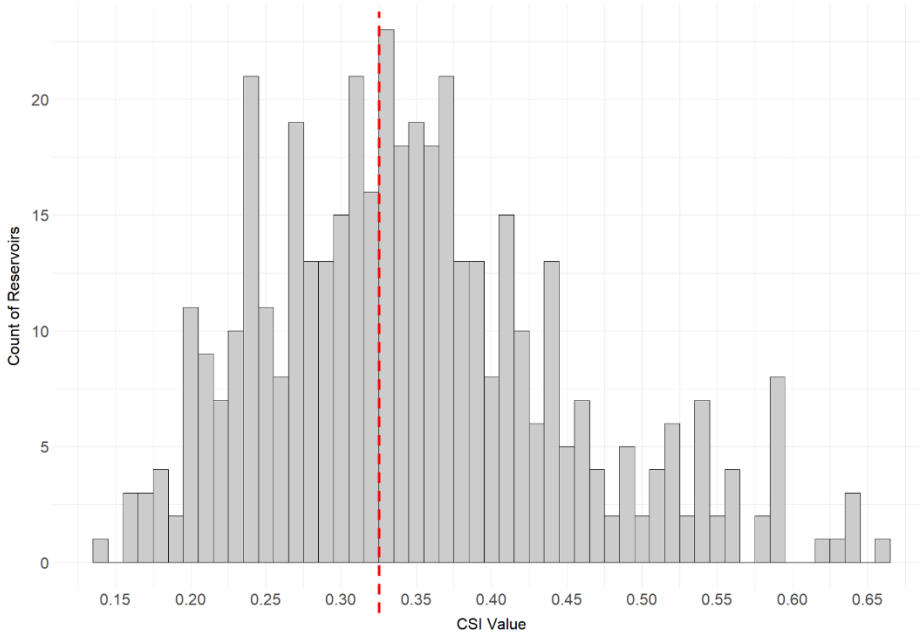

Figure 2: Histogram of CSI values in Stage A. The red dashed line indicates the CSI threshold value of 0.33, below which is considered CSI failure in the screening process.

Stages B and C were applied across 53 sites. The Effort and Benefit scores along with the Forecast Skill scores are plotted in Figure 3. Greener circles further to the right exhibit higher FIRO suitability.

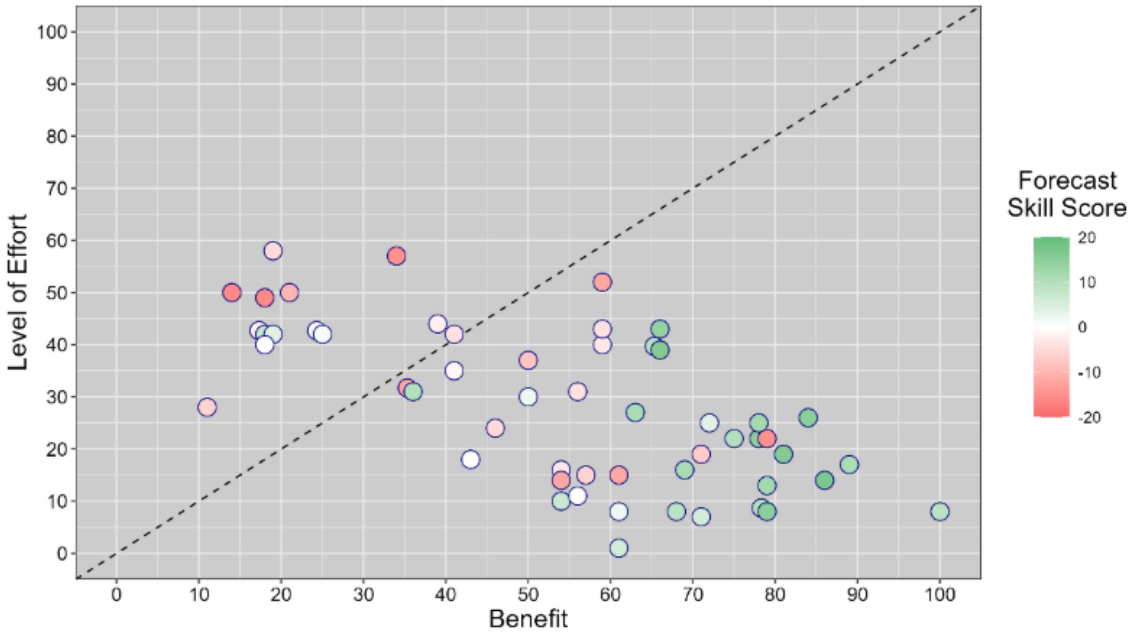

Figure 3: Plot of Stage B results for the South Pacific Division. Scores for the potential benefit from and level of effort to implement FIRO are plotted on the x and y axes, and the circles for each site are shaded by the Forecast Skill Score. The dashed line notes equality between benefit and effort scores, indicating that sites to the right of the line may be more suitable for FIRO.

Site counts associated with each of the four recommendation categories are provided in Table 3. Sites with higher FIRO suitability were further west, along the U.S. Pacific Coast, due to higher forecast skill scores. The current and prior FIRO pilot sites all fell within the highest recommendation category.

Table 3: South Pacific Division Stage B results

Recommendation	Number of Projects
Strongly consider pursuing FIRO	30
Consider pursuing FIRO	6
Make improvements before pursuing FIRO	7
Barriers to FIRO may be prohibitive; do not pursue until significant challenges are addressed	10

4 CONCLUSION

Water managers generally agreed with the initial scoring and recommendations, although most Districts did request minor adjustments to scoring. More substantial revisions were needed when the initial assumptions about forecast lead time requirements were not appropriate, leading to changes in the forecast skill scoring procedure. These are documented in site suitability reports. This upholds the importance of the site-specific dialogues in the FIRO-SP as an opportunity to correct mistaken assumptions and carefully consider the potential of updating operations at each site. Limitations included the exclusion of metrics for hydrologic inflow forecast skill, due to the high variability of inflow forecast models and availability nationwide. The heuristics used for potential benefit and level of effort are also simple, perhaps overly so.

Initial efforts to develop the Stage B methods included more complex value functions for individual scored items, which were later rejected due to the difficulty of communicating these to water management teams. Care was taken to keep the scope of the FIRO-SP simplified rather than veering into viability assessment territory, at the expense of analytical resolution.

The FIRO-SP will continue evolving as more regions are assessed and lessons learned from ongoing FIRO viability assessments are considered. It has served as a "first contact" between site water managers and the research program, providing an opportunity to grow the community of practice and promote two-way learning between researchers and practitioners.

5 ACKNOWLEDGEMENTS

Thank you to Curt Aikens, Chris Frans, Rob Hartman, Jay Jasperse, Andy Martin, Ken Nowak, Arleen O'Donnell, and Marty Ralph for serving on the FIRO-SP Steering Committee. Thank you to all USACE water managers who provided data for this effort, especially those in SPD who helped test the process and improved it drastically. Thank you to Kat Flik, Crystal Painter, Natalie Rodman, and Corey Van Doren for support in this effort. Natalie's impressively efficient administration of the Stage A rollout was key.

REFERENCES

Concha Larrauri, P., Lall, U., & Hariri-Ardebili, M. A. (2023). Needs for Portfolio Risk Assessment of Aging Dams in the United States. *Journal of Water Resources Planning and Management*, *149*(3), 04022083. https://doi.org/10.1061/JWRMD5.WRENG-5673

Cordeira, J. M., Ralph, F. M., Talbot, C., Forbis, J., Novak, D. R., Nelson, J. A., Mahoney, K., Weihs, R., Slinskey, E., & Monache, L. D. (2025). *A Summary of U.S. Watershed Precipitation Forecast Skill and the National Forecast-Informed Reservoir Operations Expansion Pathfinder Effort*. https://doi.org/10.1175/WAF-D-24-0188.1

Dettinger, M., Wilson, A., and McGurk, G. (2023). Keeping Water in Climate-Changed Headwaters Longer. San Francisco Estuary and Watershed Science, 21(4). https://doi.org/10.15447/sfews.2023v21iss4art1

Forbis, J., and C. Ly. (2025). Application of forecast-informed reservoir operations at US Army Corps of Engineers dams in California. *Journal of Flood Risk Management*, *18*(1), e13051. https://doi.org/10.1111/jfr3.13051.

Ho, M., Lall, U., Allaire, M., Devineni, N., Kwon, H. H., Pal, I., Raff, D., & Wegner, D. (2017). The future role of dams in the United States of America. Water Resources Research, 53(2), 982–998. https://doi.org/10.1002/2016WR019905

Jasperse, J., F. M. Ralph, M. Anderson, L. Brekke, N. Malasavage, M. D. Dettinger, J. Forbis, J. Fuller, C. Talbot, R. Webb, R., and A. Haynes. 2020. "Lake Mendocino Forecast Informed Reservoir Operations Final Viability Assessment." https://escholarship.org/uc/item/3b63q04n.

Naslund, L., Buhr, D., Chambers, M., McKay, S. K., Jumani, S., Bledsoe, B., Rosemond, A., & Wenger, S. (2025). Facilitating Dam Removal Decisions With Multiple Objectives. *River Research and Applications*, *41*(3), 745–754. https://doi.org/10.1002/rra.4390

Weihs, R., E. Shearer, E. Yeates, J. Corderia, E. Slinksey, C. Painter, S. Roj, F. M. Ralph, C. Talbot, J. Forbis, N. Rodman, C. Barber, R. Hartman. Designing a robust precipitation forecast skill assessment to screen reservoirs for FIRO. In-prep.

Yeates, E.M., Barber, C.A., Rodman, N. B., Shearer, E., Weihs, R., Forbis, J., Talbot, C. (2026a). FIRO Screening Process: Stage A Development and National Results (Report No. ERDC/CHL TR-26-13). Vicksburg, MS: U.S. Army Engineer Research and Development Center.

Yeates, E.M., Barber, C.A., Shearer, E., Weihs, R., Forbis, J., Flik, K., Van Doren, C., Talbot, C. (2026b). FIRO Screening Process Stages B and C Development and Application in SPD (Report No. ERDC/CHL TR-26-XX). Vicksburg, MS: U.S. Army Engineer Research and Development Center.

Web sites:

Web-1: https://cw3e.ucsd.edu/firo/, consulted 10 January 2026.

Web-2: https://storymaps.arcgis.com/stories/79d51b5579ef4b0493b3c8471443bba4, consulted 10 January 2026.

ICFM 10
Adapting to Global Change:
Innovative Approaches to Flood Management and Resilience
May 20-22, 2026 | Western University, London, Ontario, Canada

Quantifying Flood Risks in New Zealand: A National Scale Assessment

Conrad Zorn[1] and Ryan Paulik[1,2]
Department of Civil and Environmental Engineering, Faculty of Engineering, University of Auckland, Auckland, New Zealand[1]
E-mail: conrad.zorn@auckland.ac.nz

Earth Sciences New Zealand, Wellington, New Zealand[2]
E-mail: ryan.paulik@earthsciences.nz

ABSTRACT

Flooding from fluvial and pluvial sources poses a significant and growing threat to buildings across New Zealand, yet national-scale estimates of direct economic losses have remained scarce. This study fills that gap by implementing the country's first end-to-end, nationwide flood risk workflow that integrates state-of-the-art hydraulic modelling with a flexible risk analysis framework. The approach enables consistent, building-level calculation of expected annual damage (EAD) and scalable reporting across multiple administrative boundaries. We estimate New Zealand's national building EAD to be NZD $190 million per year, with two regions (Canterbury, Waikato) accounting for 35% of total losses. Residential and appurtenant buildings account for 71% of national EAD, demonstrating the high vulnerability of the residential building portfolio, particularly to more frequent flood events. These findings provide the first comprehensive, evidence-based baseline of direct building-related flood risk for the country.

This work establishes a reproducible foundation for strategic, location-based flood mitigation and climate adaptation planning. By advancing the availability of our high-resolution, nationally consistent flood risk models and outputs, it supports more effective investment decisions to reduce flood impacts under both present and future conditions.

KEYWORDS: Flooding, Buildings, Risk, Expected Annual Damage, New Zealand

1 INTRODUCTION

Flooding is among the most frequent and damaging natural hazards globally, with fluvial and pluvial sources causing significant economic and social disruption (Merz et al. 2021). In New Zealand, despite several significant events in the past five years resulting in billions of dollars (NZD) in direct building economic losses (Insurance Council of New Zealand 2025), national-scale building risk assessments have received limited research attention beyond first-order exposure studies (Paulik et al. 2019). Understanding the magnitude and spatial distribution of building economic losses from fluvial and pluvial sources is critical for informing optimal location-based investment in flood mitigation interventions and climate adaptation strategies.

This study addresses a key research gap for New Zealand by presenting the first nationwide evaluation of expected annual damage (EAD) to buildings from fluvial and pluvial flooding under present-day climate conditions. The work applies an end-to-end workflow that integrates state-of-the-art hydraulic modelling with a modular flood risk analysis framework, enabling consistent EAD calculation at the building scale and enumeration at different jurisdictional levels. This paper outlines the model workflow, including the principal hydraulic and risk model components. We then report building EAD at national, regional council, territorial authority and urban-rural area scales, demonstrating the present-day spatial

distribution of fluvial and pluvial flood risk. Finally, we identify current limitations of the model workflow and future enhancements.

2 METHODS AND MATERIALS

The model workflow for simulating nationwide fluvial and pluvial flooding hazards and risks is presented in Figure 1. The framework consists of several core components. First, the *Cylc* engine workflow scheduler (Oliver et al. 2018) orchestrates the sequencing of tasks within three modules for simulating and mapping fluvial and pluvial flooding hazards, including digital elevation, design storm, and flood hazard models. Secondly, the *RiskScape* engine (Paulik et al. 2023) combines output flood inundation maps with building exposure and vulnerability models to calculate and report risk at different spatial scales. The following sections describe these model components.

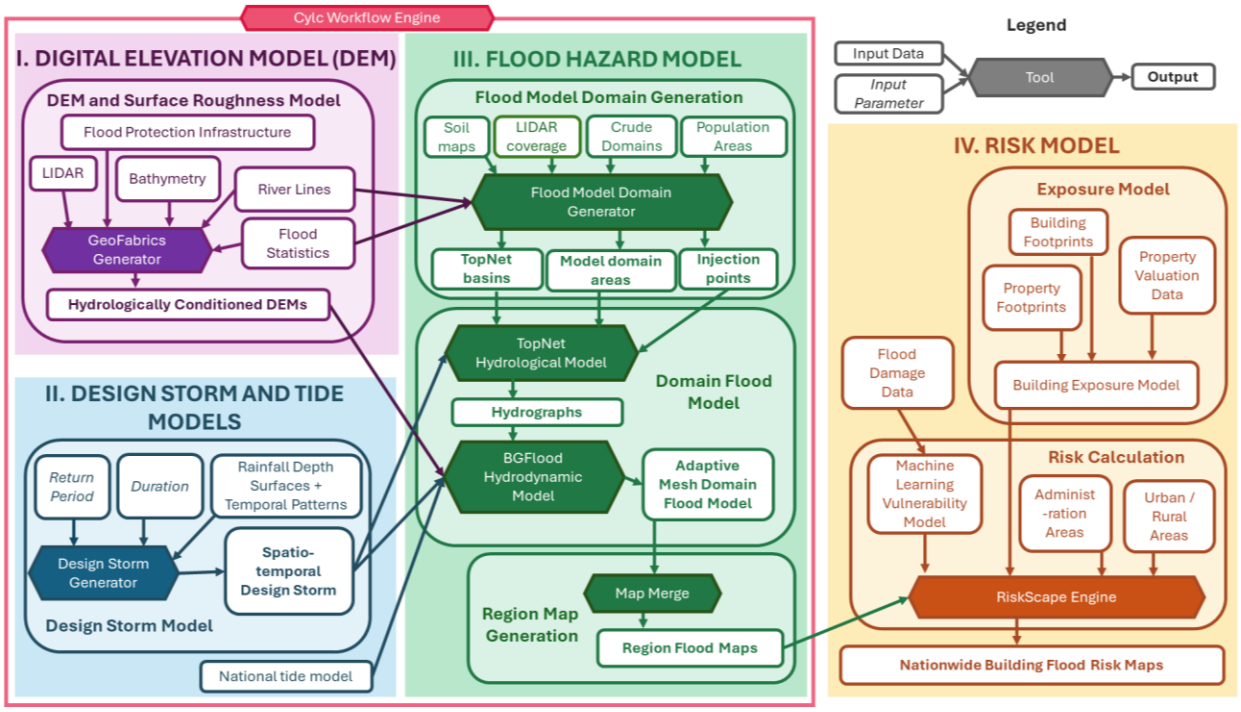

Figure 1: Conceptual diagram of components forming the national fluvial and pluvial flood risk model workflow.

2.1 Flood hazard model

The three modules contributing to fluvial and pluvial flooding hazard map generation several key steps (Figure 1): (I) hydraulically-conditioned digital elevation model (DEM) and surface roughness map generation from LIDAR (Pearson et al. 2023), (II) design storm generation for 10, 20, 50, 100, 200, 500 and 1000-year ARI rainfall events using the high intensity design rainfall system (*HIRDSv4.2*) (Carey-Smith et al. 2018), (IIIa) simulation domain, basin and rain-on-grid mask generation, (IIIb) *TopNet* (McMillan et al. 2016) hydrograph generation at river flow injection points, and (IIIc) inundation modelling incorporating output data from previous steps using the hydrodynamics model *BGFlood* (Bosserelle et al. 2020). Flood hazard intensity maps representing both fluvial and pluvial flood events from ARI rainfall were generated for maximum water depth (m), maximum flow velocity (m/s), and water depth duration (hr) at an 8 m grid resolution.

2.2 Exposure and vulnerability

Building replacement values (B_R) for direct economic loss evaluation were calculated using the general formula:

$$B_R = \sum_{i=1}^{n} C_{RVi} \cdot B_{Ai} \quad (1)$$

where for building i, B_{Ai} is the area (m^2), C_{RVi} is the m^2 unit cost rate (NZD) for structural, external finishes, internal finishes and service components, n is the number of components for B_R calculation. Local unit cost rates were adopted from the first quarter of 2024 (Quotable Value 2024). Buildings mapped from roof outlines represented 3,288,916 structures (Land Information New Zealand 2024). The replacement value calculation utilized physical and non-physical characteristics derived from several nationwide datasets (Paulik et al. 2023a; Scheele et al. 2023). These characteristics include area (m^2), floor level, primary use, number of stories, structural frame, and wall cladding.

Building vulnerability to direct economic loss (L) was calculated using a unit loss approach:

$$L = \sum_{i=1}^{n} R_i \, f_i(d_{ij}, b_i) \quad (2)$$

where for building i, R_i is the replacement value, and f_i the damage function that computes a damage ratio (ranging from 0 to 1). f_i is a function of the maximum water depth (d) sampled at inundation points intersecting building location j and the building's physical and non-physical characteristics (b_i).

In large-scale flood risk models, f_i is typically implemented using univariable 'depth-damage' curves. This study employs an extreme gradient boosting regression algorithm, trained on an empirical dataset comprising 2,320 buildings damaged in seven New Zealand flood events (Paulik et al. 2023b; Paulik et al. 2024; Paulik and Horspool 2024). Model hyperparameter selection involved a grid search to optimize performance over a range of decision trees (100 to 10,000 trees) and learning rates (0.01 to 0.2). Model evaluation employed a leave-one-out cross-validation procedure, with mean absolute error (MAE) and root mean squared error (RMSE) as performance metrics. The optimal model configuration, with 1000 trees and a learning rate of 0.2, achieved an MAE of 0.09 and an RMSE of 0.12 when applied to explanatory variables, including maximum water depth, maximum water depth above floor level, area (m^2), primary use, number of stories, structural frame, and wall cladding.

2.3 Risk analysis

Direct economic loss was enumerated as the expected annual damage (EAD). First, the exceedance probability loss (EPL) for each flood event of probability P was calculated using the formula:

$$EPL(P) = \sum_{i=1}^{N} L(P) \quad (3)$$

where $L(P)$ is the economic loss due to the flood event of probability P, and N represents the total number of buildings impacted by the event. A hypothetical loss curve is formed between EPL and P, representing a positive monotonic trend where EPL increases response to decreasing P. EAD is then calculated using trapezoidal integration to compute the 'area under the curve':

$$EAD = \int_{p_{min}}^{p_{max}} EPL(p) \quad (4)$$

where p_{min} and p_{max} respectively denote the highest and lowest annual probability of occurrence, and $EPL(P)$ is the economic loss for the flood event, given the probability of occurrence P. The integral computes the area under a hypothetical damage-probability curve, representing the monetary loss expected in a single year from flood events simulated within the probability range p_{min} to p_{max}. The EAD computed for each individual building was enumerated at the national level, regional council and territorial authority administration areas, and several urban (major (pop. ≥100,000); large (pop. 30,000–99,999); medium (pop. 10,000–29,999); small (pop. 1,000–9,999) and rural (pop. <1000) land areas on mainland New Zealand.

3 RESULTS AND DISCUSSION

We estimated the EAD for New Zealand buildings to be NZD 190 million. EAD demonstrates significant regional variations (Figure 2), with Canterbury contributing the highest regional EAD at NZD 41.9 million (22% of the national total), mostly occurring in Christchurch City (Figure 3). Waikato and Bay of Plenty follow, contributing NZD 26.2 million (~13%) and NZD 20.3 million (~10%), respectively. Auckland, New Zealand's most populous region, accounts for NZD 17.6 million (~9%). Less populous regions such as Taranaki, Nelson, and Marlborough each contribute less than 3% of the national EAD. EAD as a percentage of the expected annual building replacement value exposure (EAE) exceeds 20% in several territories, including Central Otago District, Clutha District, Opotiki District, Wairoa District and Rotorua District. Despite these territorial authorities making a small contribution to regional EADs, buildings are more likely to sustain economic losses when exposed to flood waters.

The residential building EAD exceeds NZD 78 million, accounting for 41% of the total national EAD. Combined with appurtenant buildings (NZD 57 million), buildings on residential properties account for 71% of the national EAD. The relatively significant contribution of appurtenant buildings signals their vulnerability to damage from relatively frequent flood inundation (i.e., < 50-year ARIs), meaning they contribute more significantly to national EAD than buildings with higher economic value but lower flood exposure. Agriculture has the highest EAD (NZD 23.8 million) for non-residential buildings. Over 50% of national EAD occurs in the Waikato, Bay of Plenty and Canterbury regions, due to the prevalence of high-producing dairy farmland in floodplains (Craig et al. 2021). Commercial and industrial buildings combined account for NZD 15.4 million (8%) of EAD.

EAD reaches NZD 128.6 million (67%) in urban areas (populations >1000), and NZD 62.2 million (33%) in rural areas. While agricultural buildings represent the highest proportion of EAD (37%) for rural land and settlements (pop. <1000), the combined EAD for residential and appurtenant buildings reach NZD 29.9 million (48%). The equivalent EAD for major urban areas (pop. >100,000) exceeds NZD 40 million, accounting for 81% of the total EAD for these areas. Total EAD in rural areas exceeds that in major urban areas by NZD 13 million (23%), and is considerably greater than in small (62%), medium (98%), and large (83%) urban areas. Despite New Zealand's extensive flood protection schemes in rural areas (Walsh et al., 2019), these findings highlight the significant residual risk for buildings in rural communities.

This study employed a state-of-the-art model workflow and datasets, featuring notable advancements in digital elevation model generation, two-dimensional hydraulic flood inundation modelling and mapping, and building risk analysis. Despite these advancements, several limitations and future focus areas for model and data improvement have been noted. Modelled economic losses could not be validated for historic events, as an official economic flood damage database is not currently available for New Zealand. Evaluating model predictive performance then requires flood hazard intensity simulations for historic events, coupled with building exposure inventories and physical damage data, to compare modelled and government-reported economic losses. Flood inundation modelling and mapping also considered ~73% (197,415 km²) of New Zealand's mainland area, where topographical data from LiDAR was available. This

area covers 95% of mapped building structures; however, extending modelling and mapping toward continuous national land coverage requires further LIDAR acquisition from government agencies or the inclusion of lower-resolution, satellite-derived topographical data. Flooding hazards and building risk under present-day climate and socio-economic conditions were evaluated. Escalating flood risk under climate-projected flood regime changes towards the end of this century is well-documented internationally. Incorporating such scenarios in the New Zealand context is required in future modelling and data iterations to inform risk-based flood management. This should be considered in conjunction with anticipated changes in flood mitigation (e.g., levee construction, detention areas), building location, design, and construction materials, as well as the subsequent responses to flood damage vulnerability. The modular model framework is configurable to simulate both spatial and temporal changes in flood risk and associated uncertainty, resulting from model parameters, without requiring significant structural changes.

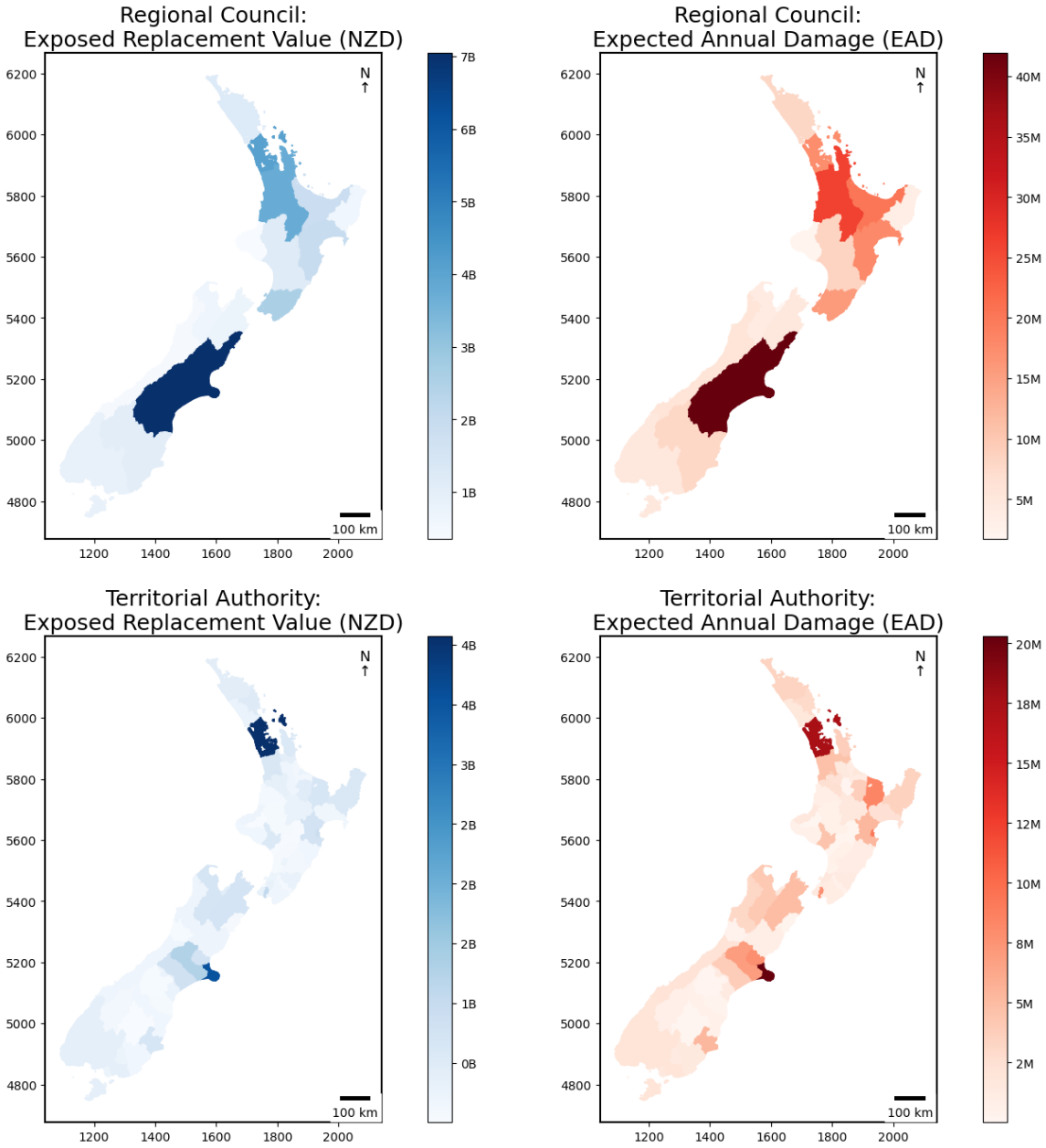

Figure 2: Spatial distribution of exposed building replacement value (NZD) and expected annual damage (EAD) enumerated by regional council and territorial authority area.

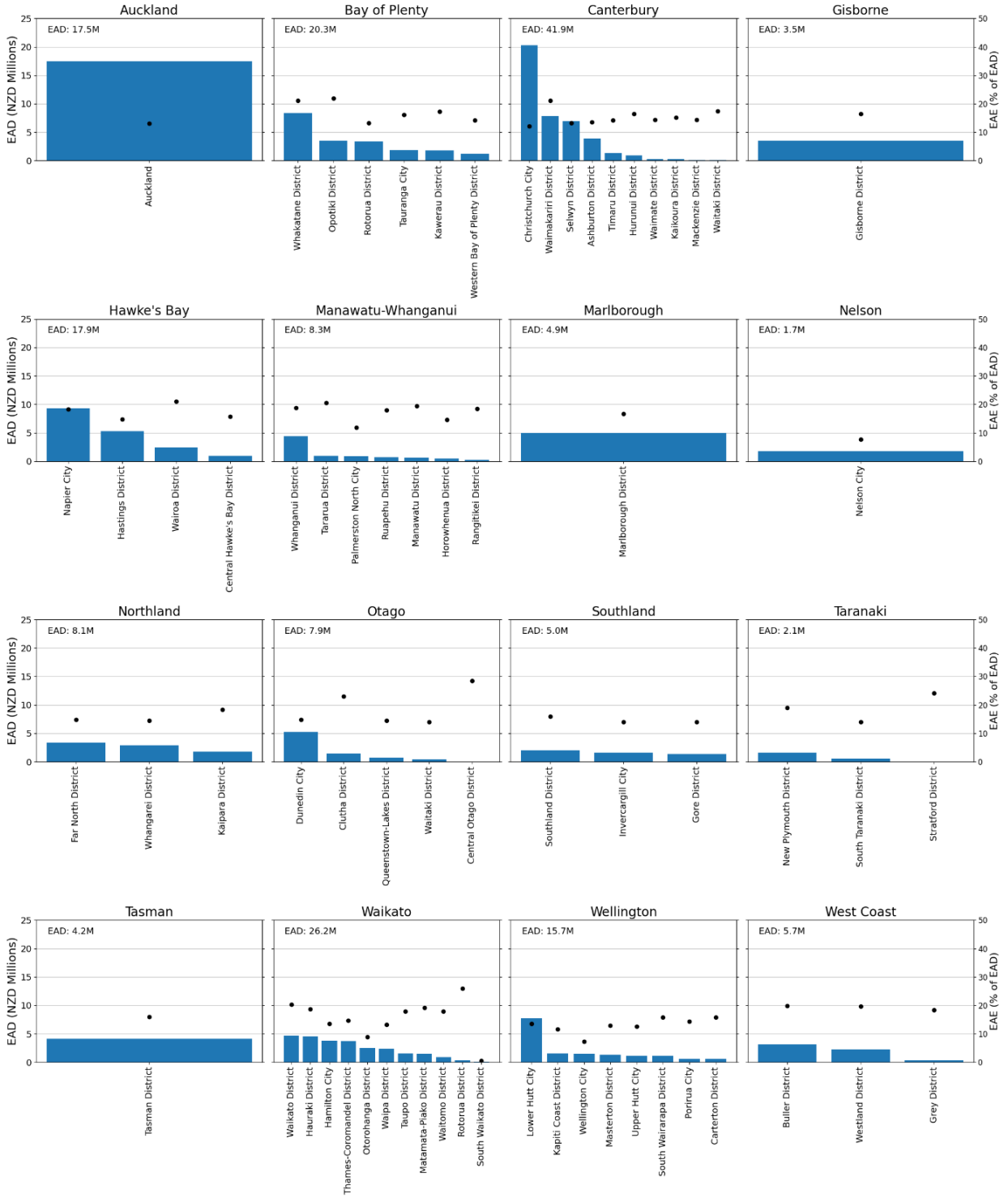

Figure 3: Expected annual damage (EAD) (blue bar) reported as monetary loss (NZD) and as the percentage of the expected annual building replacement value exposure (EAE) (black dot) enumerated by regional council and territorial authority area.

4 CONCLUSION

This study delivers the first nationwide, building-level assessment of expected annual damage (EAD) from fluvial and pluvial flooding in New Zealand, addressing a longstanding gap in the country's flood risk evidence base. By integrating state-of-the-art hydraulic modelling with a modular, end-to-end risk analysis workflow, we compute building-scale losses and consistently aggregate them across national, regional, and local administrative units. The results indicate annualised direct building losses of approximately NZD 190 million, with the greatest concentrations of risk occurring in urban areas and among residential and appurtenant structures, which together account for 71% of national EAD.

While the workflow advances national flood risk modelling capability, several limitations remain. Current inundation modelling covers 73% of mainland New Zealand due to gaps in high-resolution topographic data, highlighting the need for continued LIDAR acquisition or the incorporation of coarser satellite-derived elevation products to achieve full national coverage. Moreover, the present analysis reflects only current climate and socio-economic conditions. Future iterations should integrate climate-change-conditioned flood regimes, evolving patterns of settlement and construction, and the potential influence of mitigation interventions such as new flood defences or changes in building design. Incorporating these dynamics will be essential for characterising future flood risk trajectories and for supporting long-term, risk-informed adaptation planning.

Overall, this work establishes a robust, reproducible framework for national-scale flood risk assessment in New Zealand. By providing the first spatially explicit, evidence-based baseline of direct building flood losses, it supports more targeted and strategic investment in mitigation and adaptation across multiple levels of decision-making.

5 ACKNOWLEDGEMENTS

The work presented was supported with funding from the New Zealand Ministry of Business, Innovation, and Employment (MBIE) Endeavour Fund (CONT-69394-ENDRP-NIW), and Earth Sciences New Zealand Strategic Scientific Interest Fund work programme on "RiskScape" (FPCH2604).

REFERENCES

Bates, P. D., Savage, J., Wing, O., Quinn, N., Sampson, C., Neal, J., & Smith, A. (2023). A climate-conditioned catastrophe risk model for UK flooding. *Natural Hazards and Earth System Sciences*, 23(2), 891-908. https://doi.org/10.5194/nhess-23-891-2023

Bosserelle, C., Williams, S., Cheung, K.F., Lay, T., Yamazaki, Y., Simi, T., Roeber, V., Lane, E., Paulik, R., & Simanu, L. (2020). Effects of source faulting and fringing reefs on the 2009 South Pacific Tsunami Inundation in Southeast Upolu, Samoa. *Journal of Geophysical Research: Oceans*, 125(12), https://doi.org/10.1029/2020JC016537

Carey-Smith, T., Henderson, R., & Singh, S. (2018). High-Intensity Rainfall Design System, Version 4. NIWA Client Report 2018022CH, NIWA, New Zealand.

Craig, H., Paulik, R., Djanibekov, U., Walsh, P., Wild, A., & Popovich, B. (2021). Quantifying national-scale changes in agricultural land exposure to fluvial flooding. *Sustainability*, 13(22), 12495. https://doi.org/10.3390/su132212495

Dottori, F., Mentaschi, L., Bianchi, A., Alfieri, L., & Feyen, L. (2023). Cost-Effective Adaptation Strategies for Rising River Flood Risk in Europe. *Nature Climate Change*, 13(2), 196-202. https://doi.org/10.1038/s41558-022-01540-0

Insurance Council of New Zealand (2025). Cost of Natural Disasters [Data set]. Available at: https://www.icnz.org.nz/industry/cost-of-natural-disasters/.

Land Information New Zealand (2024). NZ building outlines [Data set]. Toitū Te Whenua Land Information New Zealand. Available at: https://data.linz.govt.nz/layer/101290-nz-building-outlines/

McMillan, H. K., Booker, D. J., & Cattoën, C. (2016). Validation of a national hydrological model. *Journal of Hydrology*, 541, 800-815. https://doi.org/10.1016/j.jhydrol.2016.07.043

Merz, B., Blöschl, G., Vorogushyn, S., Dottori, F., Aerts, J.C., Bates, P., Bertola, M., Kemter, M., Kreibich, H., Lall, U. and Macdonald, E. (2021). Causes, Impacts, and Patterns of Disastrous River Floods. *Nature Reviews Earth & Environment*, 2(9), 592-609. https://doi.org/10.1038/s43017-021-00195-3

Oliver, H. J., Shin, M., & Sanders, O. (2018). Cylc: A workflow engine for cycling systems. *Journal of Open Source Software*, 3(27), 737. https://doi.org/10.21105/joss.00737

Paulik, R., Craig, H., & Collins, D. (2019). New Zealand fluvial and pluvial flood exposure. National Science Challenges, The Deep South Te Kōmata o te Tonga and NIWA Taihoro Nukurangi.

Paulik, R., Horspool, N. (2024). Enhanced natural hazard risk assessment for Cyclone Gabrielle recovery: Summary Report. https://doi.org/10.13140/RG.2.2.34855.56488

Paulik, R., Horspool, N., Woods, R., Griffiths, N., Beale, T., Magill, C., Wild, A., Popovich, B., Walbran, G., & Garlick, R. (2023). RiskScape: a flexible multi-hazard risk modelling engine. *Natural Hazards*, 119(2), pp.1073-1090. https://doi.org/10.1007/s11069-022-05593-4

Paulik, R., Zorn, C., Wotherspoon, L., & Sturman, J. (2023a). Modelling national residential building exposure to flooding hazards. I*nternational Journal of Disaster Risk Reduction*, 94, 103826. https://doi.org/10.1016/j.ijdrr.2023.103826

Paulik, R., Zorn, C., & Wotherspoon, L. (2023b). Evaluating the spatial application of multivariable flood damage models. Journal of Flood Risk Management, 16(4), e12934. https://doi.org/10.1111/jfr3.12934

Paulik, R., Zorn, C., Wotherspoon, L. (2024). Residential building and sub-building level flood damage analysis using simple and complex models. *Natural Hazards*, 120(14): 13493-13512. https://doi.org/10.1007/s11069-024-06756-1

Pearson, R.A., Smart, G., Wilkins, M., Lane, E., Harang, A., Bosserelle, C., Cattoën, C., & Measures, R. (2023). GeoFabrics 1.0.0: An open-source Python package for automatic hydrological conditioning of digital elevation models for flood modelling. *Environmental Modelling & Software*, 170, https://doi.org/10.1016/j.envsoft.2023.105842

Quotable Value. (2024). QV CostBuilder [Data set]. QV New Zealand. https://costbuilder.qv.co.nz/

Scheele, F. R., Syed, Y., Hayes, J. L., Paulik, R., & Inglis, S. (2023). Building inventory and vulnerability functions for risk modelling in New Zealand (GNS Science Report 2023/08, 42 p.). GNS Science. https://doi.org/10.21420/G34N-V958

Walsh, P., Robertson, T., & Paulik, R. (2019). Flood mitigation schemes in New Zealand: how is protection distributed. In *24th Annual Conference of the European Association Environmental and Resource Economists*, 26 – 29 June 2019, Manchester, UK.

ICFM 10
Adapting to Global Change:
Innovative Approaches to Flood Management and Resilience
May 20-22, 2026 | Western University, London, Ontario, Canada

Spatial Representation of Wave Run-up in Regional Shoreline Floodplain Mapping

Vanessa McMaster[1], Edwin Wang[1] and Dale Muir[1]
Northwest Hydraulic Consultants, North Vancouver, BC, V7M 3G3, Canada [1]
E-mail: vmcmaster@nhcwater.com, ewang@nhcwater.com,
dmuir@nhcwater.com

ABSTRACT

Flood elevation and extent along coastal and lake shorelines reflect the combined influence of quasi-static water level and wave run-up. Along shoreline margins where waves break and run up the foreshore, development pressures are often greatest, and wave run-up can contribute substantially to flood elevation. Despite this influence, wave run-up is frequently omitted or coarsely approximated in flood mapping, particularly flood mapping at regional scale. This paper examines how wave run-up can be explicitly represented in floodplain mapping at a regional scale, where phase-solving wave modelling is not practical. An applied approach is presented that uses empirical run-up relationships evaluated along densely spaced shoreline transects, allowing spatial variability in wave exposure, nearshore depth, and foreshore characteristics to be represented. The approach is demonstrated through its application to floodplain mapping for Shuswap Lake and associated lakes in southern British Columbia, Canada, with a focus on supporting land use planning.

KEYWORDS: Floodplain mapping, wave run-up, land use planning, shoreline flooding

1 INTRODUCTION

Flood elevation and extent along a shoreline are governed by the combined effects of water level and wave run-up. Shorelines are often preferred locations for development, resulting in infrastructure and communities being located within areas subject to wave-affected flooding. Understanding and representing these combined processes is therefore an important component of floodplain mapping used to inform land use planning.

In many floodplain mapping studies, wave run-up is either omitted or represented indirectly through generalized freeboard allowances. While this approach may be expedient at a regional scale, it can obscure spatial variability in flood elevation along shorelines with differing wave exposure and foreshore characteristics such as slope and surface roughness. As a result, locations subject to elevated wave effects may not be clearly distinguished from more sheltered areas.

This paper addresses how wave run-up can be represented explicitly in regional floodplain mapping, where phase-resolving wave modelling is not practical due to computational and spatial-scale constraints. The objective is to present an applied approach that balances physical representation of wave processes with the constraints of large-area floodplain mapping and produces outputs suitable for supporting land use planning along shorelines and within lakeside communities. This paper focuses on wave run-up and does not describe methods to determine the (quasi-static) design still water level used for floodplain mapping within a lake or coastal environment.

1.1 Background and Motivation

Floodplain mapping in coastal and lake shoreline environments requires consideration of multiple interacting drivers, including water levels, wind forcing, wave generation, and foreshore characteristics.

In contrast to riverine settings, waves can elevate flood levels above design still water conditions through wave run-up, extending flood hazards landward along exposed shorelines.

In many regional floodplain mapping programs, wave effects are either omitted or addressed indirectly through generalized freeboard allowances. While expedient, this approach can mask spatial variability in wave exposure and foreshore conditions along shorelines, particularly where shoreline orientation, fetch, and nearshore geometry vary over short distances. As a result, areas subject to elevated wave influence may not be clearly distinguished from more sheltered locations, limiting the usefulness of floodplain maps for shoreline land use planning.

Wave effects in floodplain mapping are commonly represented through wave run-up, typically quantified using the 2% exceedance level (R_2%). Run-up can be estimated using either phase-resolving wave models or empirical formulations. Although phase-resolving models can provide detailed estimates of run-up for specific sites, their data and computational requirements generally limit their application to small spatial extents, making them impractical for regional floodplain mapping. As a result, empirical formulations are commonly used at regional scales. These formulations relate run-up to incident wave conditions and simplified representations of foreshore slope and surface roughness. By definition, they estimate run-up elevations and do not resolve overtopping, ponding, or inland flow processes; requiring additional interpretation when applied for flood extent delineation.

In British Columbia, areas where wave action influences shoreline flooding are commonly referred to as the wave effect zone, reflecting recognition that waves can extend flooding beyond still water levels. However, despite this recognition, floodplain mapping guidance has not prescribed specific methodologies for explicitly representing wave run-up within this zone. Where wave effects are incorporated, they are typically represented in a coarse manner, using single run-up or freeboard values applied to representative shoreline segments based on generalized wave exposure and foreshore characteristics, rather than through spatially explicit mapping.

In other jurisdictions, such as the United States and Denmark, wave-related processes are considered within coastal flood risk and hazard frameworks. In the United States, wave effects are incorporated within FEMA's coastal flood studies primarily to support regulatory classification and insurance-related risk management, typically through transect-based analyses and zone delineation rather than spatially continuous mapping of wave run-up along shorelines. In Denmark, national and regional flood mapping efforts have focused largely on storm surge and inundation risk under the EU Floods Directive, with wave effects more commonly addressed through coastal protection design and site-specific engineering studies. These approaches serve different objectives and are generally oriented toward open-coast or defended shoreline settings and are therefore not readily transferable to regional floodplain mapping for large lakes or mixed shoreline environments, such as required in British Columbia.

While empirical wave run-up methods suitable for regional analysis are well established, there remains limited guidance on how to apply them in a spatially explicit manner to delineate wave-affected flood extents along long, heterogeneous shorelines for land-use planning. The approach described in this paper addresses this gap at a regional, planning scale.

1.2 Study Area

The approach described in this paper was applied as part of a regional floodplain mapping program for the Shuswap Region in southern interior British Columbia, Canada. The region comprises a system of interconnected lakes and rivers situated within mountainous terrain and includes Adams Lake, Mabel Lake, Mara Lake, Little Shuswap Lake, and Shuswap Lake. The lakes are characterized by long, irregular shorelines with variable orientation and wave exposure, collectively extending over approximately 500 km of shoreline.

Floodplain mapping for the region incorporated explicit estimation and mapping of wave run-up along lake shorelines to support delineation of shoreline flood hazards relevant to land use planning and development in lakeside communities. The Shuswap Region and the lakes included in the floodplain

mapping are shown in Figure 1, with lake extents shown in yellow and shoreline areas mapped as part of this study shown in green.

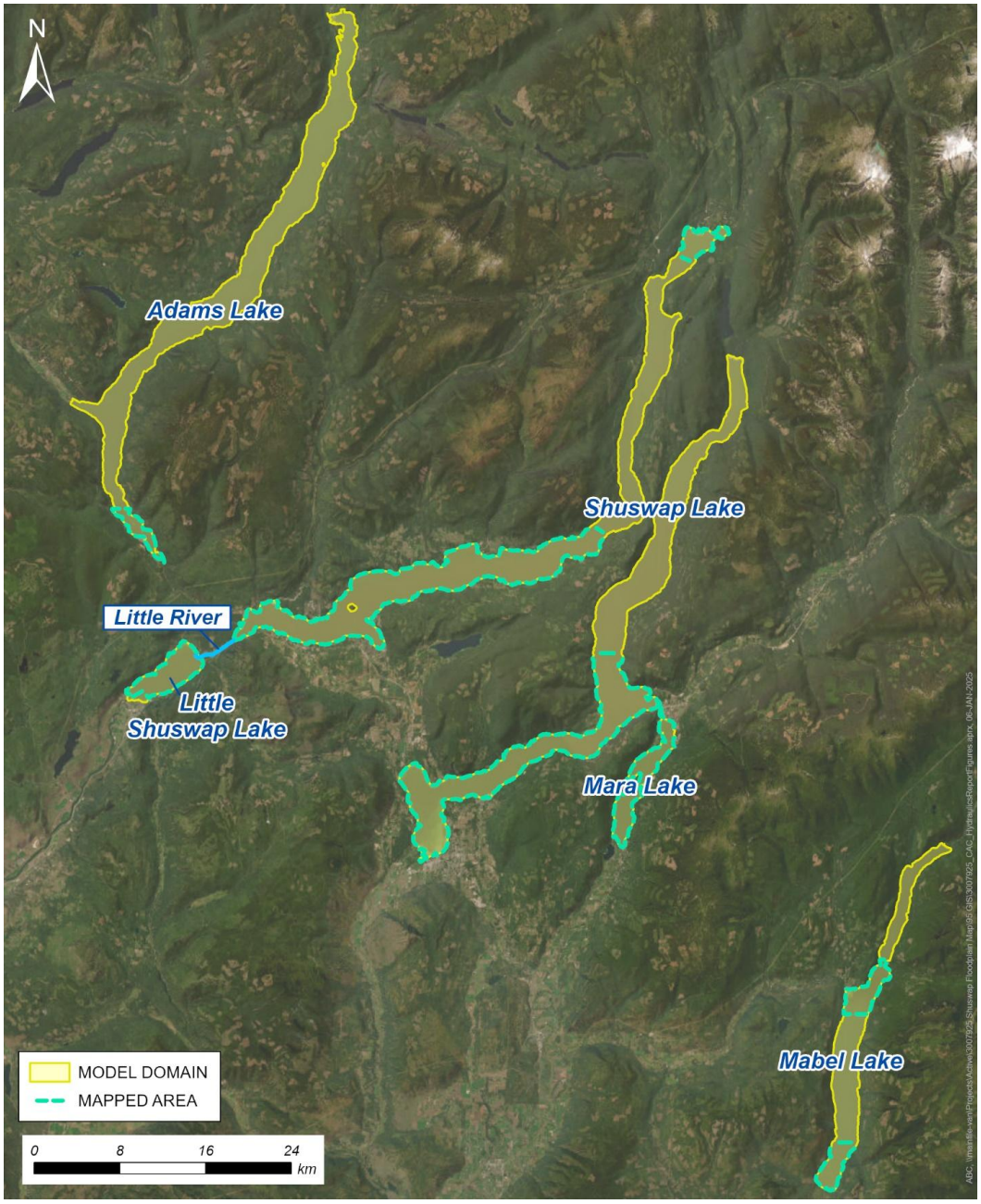

Figure 1: Shuswap Region lakes included in floodplain mapping

2 METHODS

This section describes the sequence of analyses used to estimate and spatially represent wave run-up for regional floodplain mapping. The overall approach consisted of:

(1) determination of design wind conditions and nearshore wave modelling to resolve spatial variability in wave exposure,

(2) generation of shoreline transects at defined spacing
(3) extraction of wave conditions and foreshore characteristics along each transect, and
(4) estimation and spatial mapping of wave run-up using empirical formulations.

2.1 Wind and Wave Analysis

A wind analysis was conducted to define design wind conditions for the study area. These conditions were used as input to a nearshore wave model to simulate the spatial distribution of wave height, period, and direction across the lakes under design water level conditions, accounting for variability in wave generation and propagation associated with lake geometry, fetch, and shoreline orientation.

Because shoreline exposure varies substantially with orientation and fetch, multiple nearshore wave model simulations were undertaken to represent different wind and wave scenarios relevant to the study area. The resulting wave fields provided spatially varying wave conditions along the lake shorelines. These wave conditions formed the basis for subsequent run-up calculations, with the maximum run-up response across applicable wave scenarios retained for floodplain mapping purposes.

2.2 Shoreline Transect Generation

Shoreline transects were generated at regular spaced intervals along the lake shorelines to provide consistent spatial coverage. Transect spacing was selected to balance representation of alongshore variability with practical limits on data processing and analysis effort, with additional transects introduced in locations where shoreline geometry, wave exposure, or development density changed over short distances.

Coastal and lake shorelines exhibit substantial variability in both the alongshore and cross-shore directions, with changes in slope, materials, orientation, and fetch occurring over relatively short distances. Because empirical run-up calculations are inherently local in application, closely spaced transects were used to reduce reliance on interpolation and to better represent localized variations in shoreline conditions. Transects were oriented approximately perpendicular to the local shoreline to represent cross-shore wave transformation and run-up processes.

Shoreline transects were generated at 250 m intervals along lake shorelines across the Shuswap Region, resulting in more than 2,000 transects in total. An example of transect distribution along the Shuswap Arm region of Shuswap Lake is illustrated in **Error! Reference source not found.**.

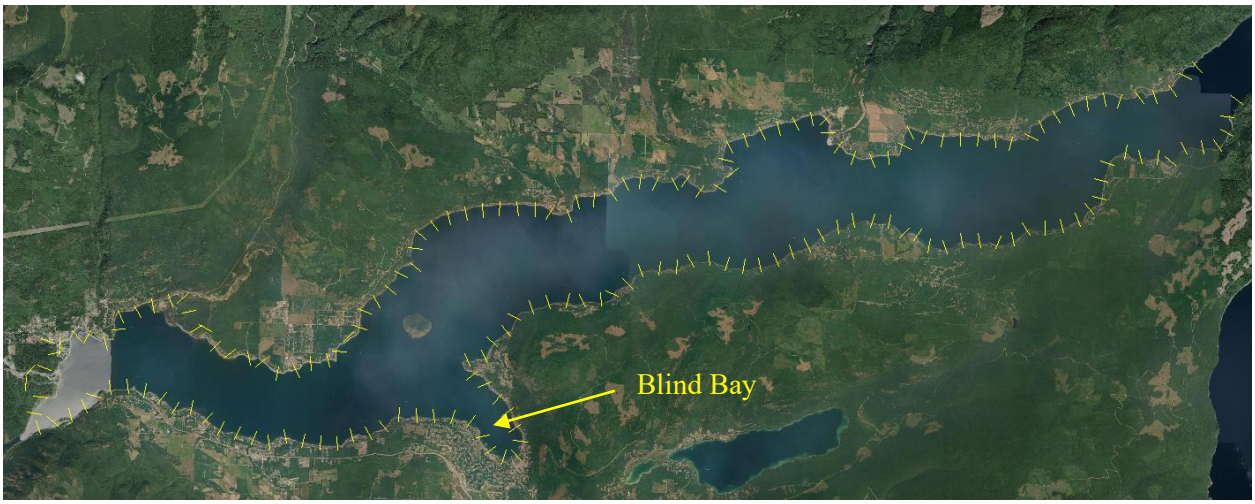

Figure 2: Transects to calculate wave run-up along Shuswap Lake

2.3 Extraction of Foreshore Characteristics and Wave Conditions

For each transect, wave conditions were extracted from the nearshore wave model outputs at the shoreline. Topographic and bathymetric data from a lidar-derived digital elevation model were used to extract shoreline profiles along each transect.

To obtain wave conditions representative of the toe of the shoreline, additional wave transformation was applied within the post-processing workflow. Shoaling and refraction were accounted for using transect-specific shoreline geometry and nearshore bathymetry, translating incident wave conditions from the nearshore model to the toe of shoreline, consistent with the input requirements of the empirical wave run-up formulations.

Foreshore slope was determined algorithmically from the extracted profiles relative to the design still water level, rather than through manual interpretation. This approach reduced subjectivity in slope selection and ensured a consistent and repeatable definition of foreshore slope across all transects. The same procedure can be applied directly to alternative water level scenarios, including design water levels under future conditions (e.g., climate change and subsidence), without requiring re-evaluation of individual shoreline profiles.

Foreshore surface roughness was characterized based on available spatial data, site observations, and interpretation of shoreline materials, consistent with the assumptions required by the selected empirical run-up formulations. Extraction of wave conditions, application of wave transformation, and determination of foreshore characteristics were implemented through a scripted workflow, ensuring consistent and repeatable application across all transects and wave scenarios.

2.4 Wave Run-up Estimation and Mapping

Wave run-up estimates were calculated at each transect using empirical formulations appropriate for the local foreshore characteristics. Empirical equations defined in EurOtop (2018) and the Stockdon (2006) equation for natural beach (slope < 10H:1V) were applied using inputs including significant wave height, wave period, wave direction, nearshore water depth, and foreshore characteristics such as slope and surface roughness. The resulting output at each transect was the 2% exceedance run-up level ($R_2\%$). For floodplain mapping, calculated wave run-up elevations were combined with the design still water level, wind setup, and adopted freeboard (applied in British Columbia along the shoreline to account for uncertainty) to define a flood construction level (FCL) along the shoreline.

Empirical wave run-up equations assume an idealized, continuous foreshore slope extending landward from the shoreline. Where this assumption is reasonably met, such as along uniform – steadily rising slopes, the calculated run-up elevation is typically reached within a short distance landward of the design still water level. However, shorelines that include low-gradient benches, berms, or engineered features, such as dikes or transportation embankments, may violate this assumption, resulting in calculated run-up elevations being projected unrealistically far inland if applied strictly based on elevation alone. In these settings, the empirical equations do not resolve overtopping, ponding, or inland flow processes. This limitation is illustrated conceptually in Figure 3, which contrasts wave run-up on a continuous sloping foreshore with conditions where a low-gradient bench or dike causes the infinite-slope assumption to break down.

Calculated FCL elevations were projected landward to the corresponding terrain elevation on a lidar-derived digital elevation model to delineate flood extent. To limit unrealistically large inland extends where the infinite-slope assumption is not met, the landward projection of wave influence was constrained to a maximum horizontal distance of 30 m from the intersection of the design still water level and the foreshore. This distance represents a planning-scale wave effects zone, consistent with emerging provincial floodplain mapping practice, and is intended to bound the zone of direct wave influence rather than to represent overtopping behaviour or inland flood hydraulics.

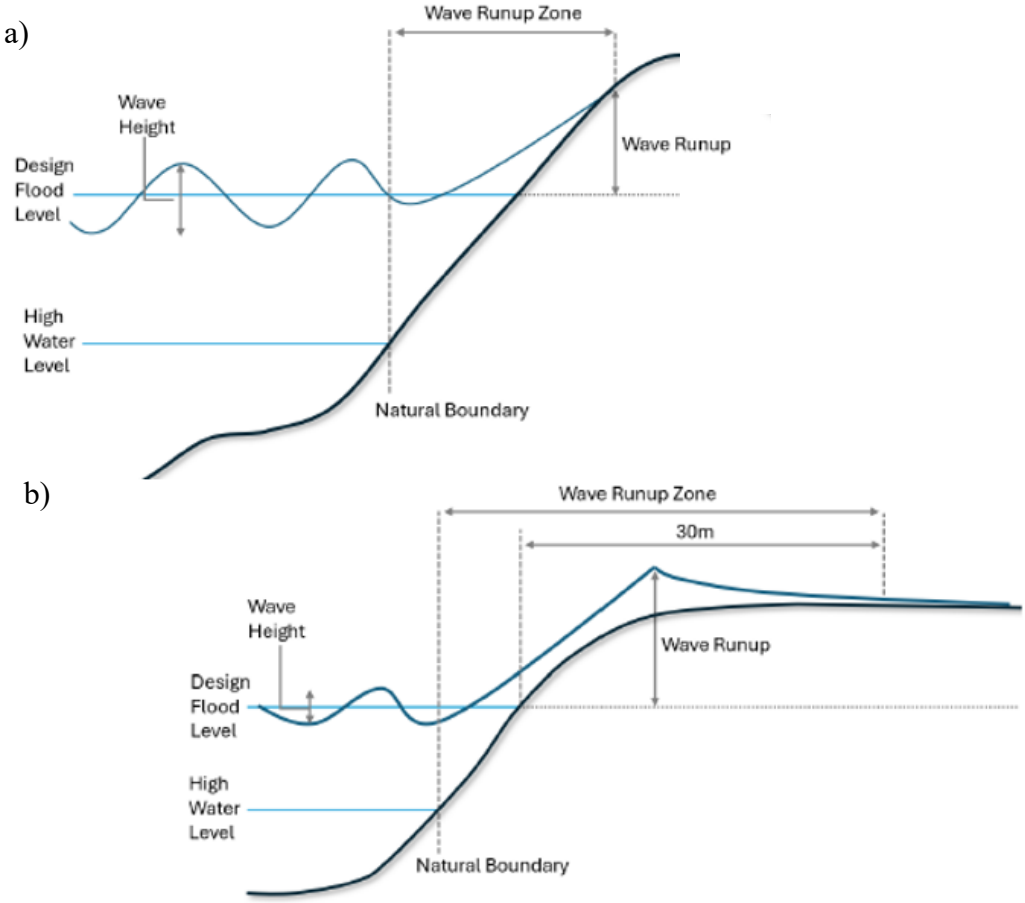

Figure 3: Illustrations of shoreline profiles showing a) continuous sloping foreshore (top panel) and 2) low-gradient bench (bottom panel)

3 MAPPED RESULTS

An example of mapped wave run-up along a section of the Shuswap Lake shoreline is shown in Figure 4. The example focuses on Blind Bay, a recessed embayment located along the mid-lake shoreline, the location of which is shown in Figure 2. The mapped output is presented as a series of shoreline segments corresponding to individual transects. For each segment, the landward extent of the shaded polygon represents the mapped flood extent, while the polygon colour indicates the calculated vertical wave run-up value (R_2%). The values labelled along each transect line represent the corresponding FCL calculated at that location based on local wave and foreshore conditions.

The figure illustrates pronounced spatial variability in wave run-up along the Blind Bay shoreline. Shoreline segments located within the recessed portion of the bay exhibit relatively low run-up values (shown in lighter colours), reflecting limited effective fetch and reduced wave growth despite exposure to prevailing winds. In these areas, the orientation of the shoreline and the sheltered setting constrain wave development, resulting in lower wave run-up elevations.

In contrast, shoreline segments toward the outer margins of Blind Bay exhibit higher run-up values (shown in medium to darker colours). These locations are exposed to a broader range of wind directions, including westerly and northeasterly winds, and are associated with longer effective fetch lengths across the lake. As a result, larger waves are generated and propagate toward these shoreline segments, producing higher wave run-up elevations relative to more sheltered areas within the bay. Variation in run-

up along similarly exposed shoreline results from the variability in shoreline slope and surface roughness. Adjacent transects subject to similar wave conditions can yield substantially different run-up elevations. Steeper foreshore slopes were generally associated with higher run-up, with the largest values occurring where slopes approached approximately 2H:1V.

Variability in wave exposure and shoreline results in irregular patterns of run-up and shoreline FCL. This differs from the consistent, linear increase in FCL typically observed progressing up a riverine flood map; and hence challenges the suitability of interpolation between adjacent FCL when applying floodplain maps to shoreline locations between two FCL isolines. Instead, it has been recommended that the higher of the two adjacent FCL values is applied for locations between shoreline FCL isolines.

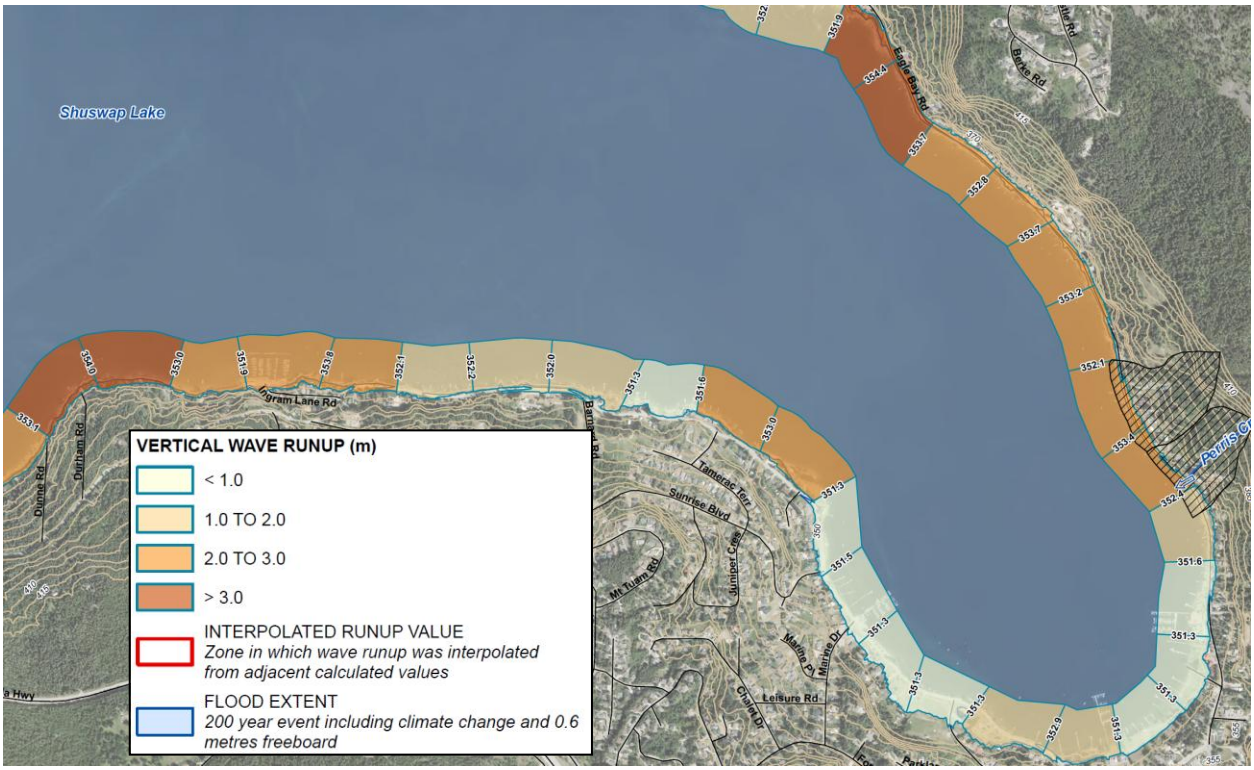

Figure 4: Example of mapped wave run-up on Shuswap Lake

4 CONCLUSION

This paper presented an applied approach for incorporating wave run-up into regional floodplain mapping of shoreline environments, demonstrated using lakes within the Shuswap Region. Wave run-up was estimated along regularly spaced shoreline transects using empirical formulations and combined with design still water levels, wind setup, and adopted freeboard to define flood construction level (FCL) elevations. The resulting wave-affected flood extents were mapped as spatially explicit polygons along the shoreline, supporting interpretation of wave-related flood hazards for land use planning.

The approach is efficient, repeatable, and suitable for application at a regional scale relative to phase-resolving wave models. Spatial resolution can be increased, where warranted due to complex shoreline geometry or development pressure, by reducing transect spacing. By explicitly representing spatial variability in wave exposure and run-up, the method provides increased value and greater transparency for property owners and land use planners than floodplain mapping approaches based on uniform run-up or freeboard allowances.

Several limitations and residual risks remain inherent to the approach. Empirical run-up equations rely on simplified representations of shoreline conditions and may overpredict run-up where the infinite-slope assumption is not realized, particularly in areas with low-gradient benches, berms, or engineered shoreline features. The method does not resolve overtopping, ponding, or dynamic inland flow processes, sub-transect spaced variability, or future changes in shoreline geometry or materials.

Accordingly, while the approach provides a consistent and defensible basis for regional floodplain mapping and planning-scale decision-making, residual risk remains at specific sites. Site-specific assessments may be warranted in locations where shoreline conditions substantially deviate from those represented by the transects, where development sensitivity is high, or where more detailed evaluation of wave processes is required to support design or risk management decisions.

5 ACKNOWLEDGEMENTS

We respectfully acknowledge that the study area for the Shuswap Region Floodplain Maps project lies within the traditional territories of the Secwepemcúl'ecw (Secwépemc), Ĩyãhé Nakón mąkóce (Stoney), Syilx (Okanagan), Ktunaxa ʔamakʔis, snʕickstx tmxʷúlaʔxʷ (Sinixt), and the Confederated Tribes of the Colville Reservation.

Northwest Hydraulic Consultants Ltd. (NHC) would like to thank Fraser Basin Council (FBC) for initiating and supporting this study. We also thank Environment and Climate Change Canada (ECCC), Natural Resources Canada (NRCan), and the British Columbia Ministry of Water, Land and Resource Stewardship (WLRS) for providing additional support during the project. This project is funded by the Government of Canada and the Government of British Columbia. through the Flood Hazard Identification and Mapping Program (FHIMP).

REFERENCES

EurOtop (2018). Manual on wave overtopping of sea defences and related structures. An overtopping manual largely based on European research, but for worldwide application. Van der Meer, J.W., Allsop, N.W.H., Bruce, T., De Rouck, J., Kortenhaus, A., Pullen, T., Schüttrumpf, H., Troch, P. and Zanuttigh, B.

Stockdon, H. F., Holman, R. A., Howd, P. A., & Sallenger, A. H. (2006). Empirical parameterization of setup, swash, and runup. Coastal Engineering, 53(7), 573–588.

ICFM 10
Adapting to Global Change:
Innovative Approaches to Flood Management and Resilience
May 20-22, 2026 | Western University, London, Ontario, Canada

Workflow Insights for Operationalizing a Hydrological Forecasting Model in Brazil

Anne Caroline Negrão[1]; Roberto Ferreira dos Santos Junior[2]; Karine Cristine Teixeira Xavier; Henrique von Linsingen Pereira and Julia Cristine Lucion Lima

Tractebel Engineering LTDA., Av. Rio Branco, Florianópolis, SC, Brazil[1]
E-mail: annecnegrao@gmail.com

Exiti Soluções Digitais LTDA., Rua Oswald de Andrade, Ilha Solteira, SP, Brazil[2]
E-mail: roberto@exiti.com.br

ABSTRACT

In a scenario of adaptation to global climate change, integrating multiple sources of information to support decision-making becomes essential, especially in the face of extreme events, which are expected to become more intense and frequent. However, implementing an effective monitoring system requires creativity and innovation, particularly when it involves meteorological and hydrological forecast models, which depend on the continuous updating of heterogeneous data. This study presents the operationalization of the Distributed Hydrological Model developed by the National Institute for Space Research of Brazil (MHD-INPE) to produce daily short- and medium-range streamflow forecasts. The model requires a significant amount of input data, some of which do not need frequent updates, such as topographic information, land use and land cover data, and pre-calibrated parameters. However, daily data input goes beyond streamflow and precipitation, including other meteorological variables. Furthermore, both observed data, for model spin-up, and meteorological forecasts are necessary. To meet these demands, daily assimilation of nationally available information from INPE was performed, including the WRF meteorological forecasts and the MERGE satellite and station-based precipitation estimates. Additionally, international data were incorporated, such as the ERA5 reanalysis (ECMWF). The dependence on the availability of all these datasets makes the operationalization of the model complex, as it requires designing a logical workflow that considers the release schedule of each dataset, processing time, and the possibility of delays, gaps, or inconsistencies. This paper details how these diverse data sources were organized and how the logical workflow was structured to make operational streamflow forecasting feasible. The results provide practical insights into data integration strategies, demonstrating the importance of innovation and careful planning for the effectiveness of monitoring systems.

KEYWORDS: hydrological forecasting; operational workflow; data assimilation; data integration.

1 INTRODUCTION

Implementing a hydrological forecasting system is a challenging task that requires designing and structuring multiple procedures to manage heterogeneous data from various sources and release schedules, while accounting for potential failures, inconsistencies, computational performance, and the integration of different development platforms. Although many studies discuss the challenges of translating scientific advances – such as physical representation, calibration, and uncertainty analysis of hydrological models – into operational systems (Emerton et al., 2022; Almeida et al., 2019; Siqueira et al., 2018), few publications detail the practical aspects of implementation, data integration, and workflow maintenance in operational environments (Ayzel, 2021; De Filippis et al., 2022; Ahmad and Hossain,

2019). In this context, this study presents a practical experience in the operational implementation of the Distributed Hydrological Model developed by the National Institute for Space Research of Brazil (MHD-INPE) (Rodriguez e Tomasella, 2016), aiming to foster knowledge exchange and collaboration.

2 DATABASE

The database was structured to receive data from multiple sources and formats and to feed the hydrological model. To facilitate data management and processing, two categories were considered: Structured Data, referring to point data at specific locations, and Unstructured Data, referring to distributed data across the study area and other types of files (Figure 1).

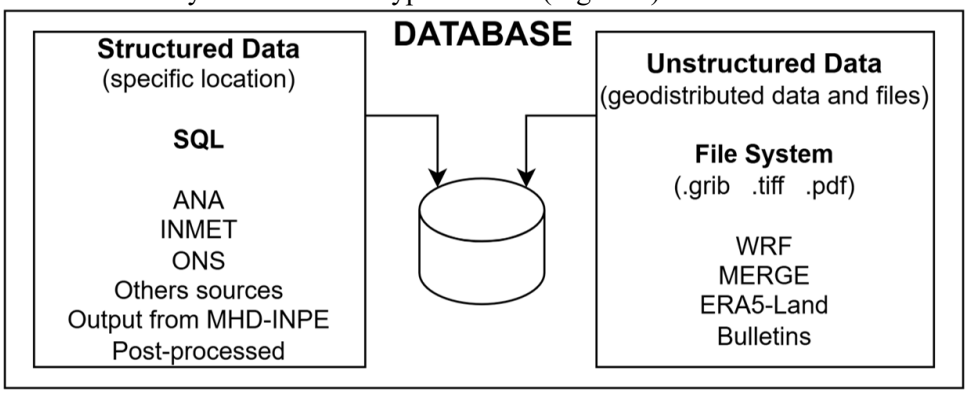

Figure 1: Database

Point data were stored as Structured Data in a relational PostgreSQL database, accessible via an API (Application Programming Interface). These data mainly consist of time series from hydrometeorological stations, managed by Brazilian National Water and Sanitation Agency (ANA) and Brazilian National Institute of Meteorology (INMET), as well as information from hydropower plants, managed by Brazilian National System Operator (ONS). Private data sources are also accessed. These data are accessed via API or web services. Given the heterogeneity of these sources, a unified structure was designed so that all time series - including observed and forecasted - follow a standardized table schema linked to reference tables that define each data source and type. This standardization facilitated API development and integration with web platforms.

Spatially distributed data, such as satellite products and meteorological model outputs, require specific handling due to their complexity, leading to the use of Unstructured Data storage. Most of these datasets are provided in the GRIdded Binary (GRIB) format, widely adopted for meteorological information because of its high compression efficiency and international standardization (WMO, 2019). To preserve data integrity, the files are kept in their original format and organized within a traditional file system following a logical structure like that used by INPE: /{product}/{year}/{month}/{day}/. After download, the data go through preprocessing steps – including geographic subsetting, variable selection, unit conversion, and temporal adjustments. The processed outputs are stored in GeoTIFF format, facilitating visualization in Geographic Information System (GIS) and representation on web platforms. Additionally, accuracy reports and monitoring bulletins, generated in PDF format, are also stored in the same file system.

The main distributed data sources used include national and international meteorological and reanalysis products. Table 1 summarizes their main characteristics and access methods. These datasets provide both observed and forecasted variables required by the MHD-INPE model.

The WRF is the main forecast model used. Since the CPTEC/INPE repository only provides full-domain files for Brazil, the downloading and processing are computationally intensive and time-consuming. Whenever possible, smaller subsets (“prec” and “singleLevel”) are preferred, but when unavailable, the complete raw files containing multiple atmospheric layers and variables must be

downloaded. Managing this assimilation step is the most demanding part of the workflow, as it requires verifying product availability and initiating downloads and preprocessing as early as possible.

Table 1: Characteristics of Meteorological Data Sources

Source / Institution	Model / Product	Description	Resolution	Coverage	Access Method
CPTEC/INPE	WRF (Weather Research & Forecast Model)	Daily meteorological forecast	7 km, hourly, 7.5-day forecast	Brazil	FTP
CPTEC/INPE	MERGE	Daily rainfall estimates combining satellite and ground station data	10 km, daily	Brazil	FTP
ECMWF	ERA5-Land	Reanalysis datatset near-surface meteorological variables	9 km, hourly	Global (subset by basin area)	Python API library

3 MODEL IMPLEMATATION

The MHD-INPE is a conceptual rainfall-runoff-routing model implemented on a regular grid using a fully distributed approach. The model structure allows straightforward coupling with meteorological models and the representation of land-use changes over time (Rodriguez & Tomasella, 2016; CEMADEN, 2022).

Figure 2 illustrates the two stages of model implementation: Customization and Operational. The Customization stage is a pre-operational phase in which the target basin is analysed to define its representation in the model and to calibrate and validate its parameters. This stage is based on the processing of geospatial information, including topography (INPE's Topodata), land-use (MapBiomas), and soil type (IBGE-EMBRAPA). In addition, it uses at least five years of historical data from hydrometeorological stations (ANA and INMET) and dam operation information (ONS), when reservoirs were present upstream.

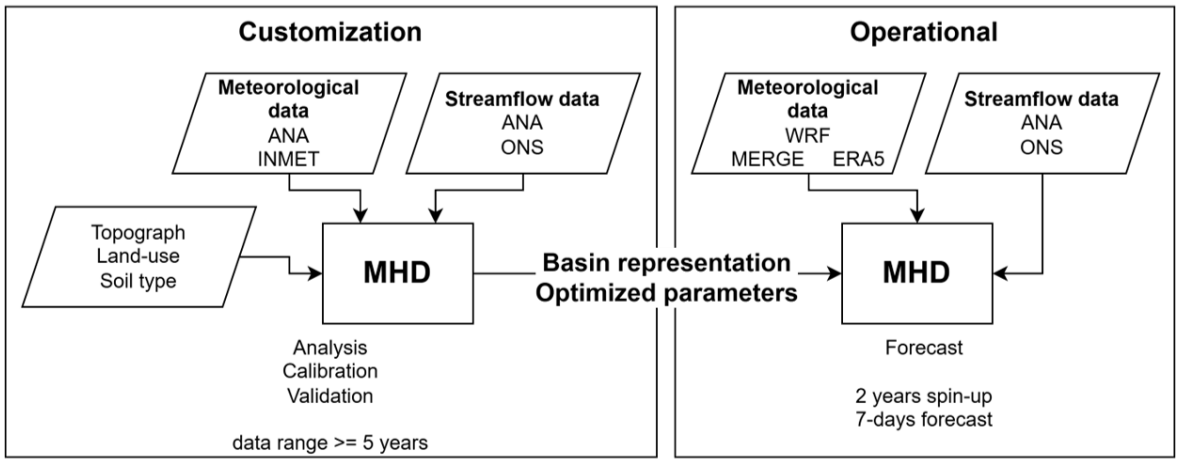

Figure 2: Stages of Hydrological Model Implementation

In the Operational stage, the basin configuration and optimized parameters are used to generate streamflow forecasts. To address the limited availability of recent data from telemetric stations and to reduce inconsistencies, satellite-based products (MERGE) and reanalysis data (ERA5-Land) were adopted. These datasets offer more stable availability and have undergone prior quality control by the source institutions.

To illustrate the implementation, the model was applied to the Araguari River basin, located in the state of Amapá, Brazil, with an approximate drainage area of 31,000 km². Figure 3 shows the basin location and its spatial representation within the model.

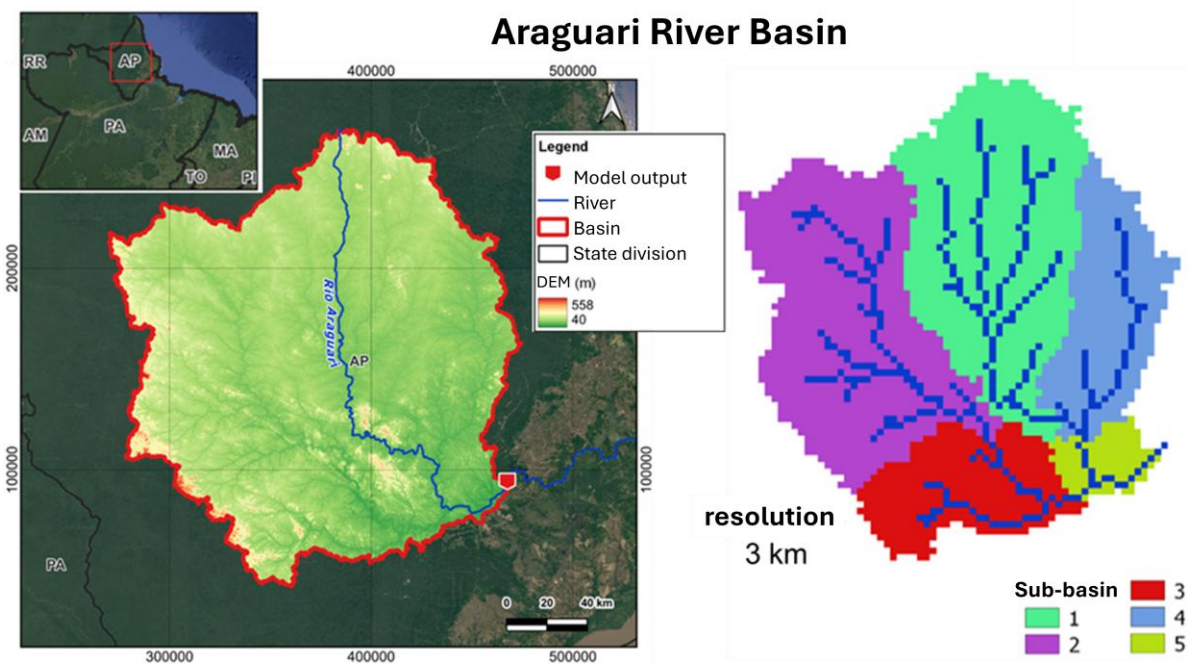

Figure 3: Araguari River Basin Representation

4 COMPUTATIONAL RESOURCES

The original version of MHD-INPE was maintained in FORTRAN due to its computational efficiency in performing the numerous calculations required by the model. The preprocessing stage, which involves database access via API, extraction of GRIB files, variable conversion, temporal adjustment, and input formatting, is implemented in Python, using several well-established open-source libraries such as: cdsapi, pygrib, xarray, scipy, pandas, numpy, matplotlib, rasterio, requests, and subprocess.

The API (backend) was developed in Spring (Java) and deployed in a Kubernetes cluster, following a microservices architecture. Python routines are executed as processes triggered by the API whenever required. The entire system runs in a Linux environment, ensuring compatibility with the libraries used and stable performance.

5 OPERATIONAL WORKFLOW

The operational routine begins daily at 04:00 (UTC-3) with data assimilation; after downloading, the data are preprocessed (spatial clipping, unit conversion and daily aggregation). Figure 4 illustrates the routines and file-system organization.

The system tries automatic assimilation between 04:00 and 07:00 (UTC-3); if data are not available by 07:00, assimilation is stopped and the model run proceeds using whatever data are available, including retrospective forecasts. This logic ensures that a forecast is generated daily despite the occasional unavailability of external sources.

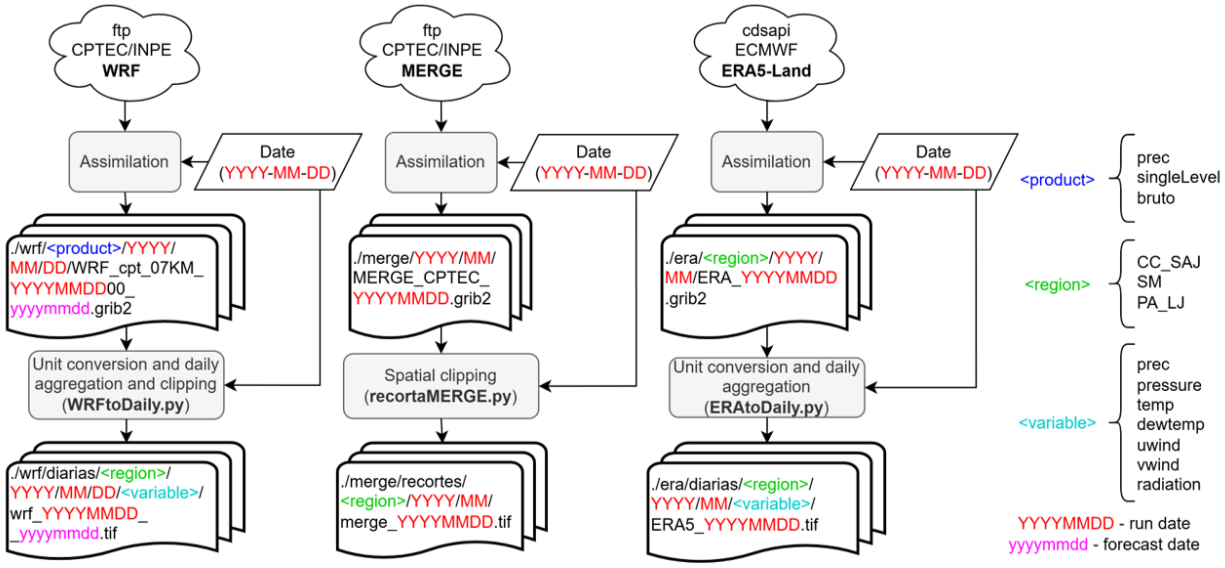

Figure 4: Data Assimilation and Storage Process

The MHD-INPE requires at least two years of data for model spin-up. In the operational application, the simulation starts 720 days before the run date (D-720), using observed meteorological data up to one day before the run date (D-1). The following days are driven by forecast data up to a seven-day horizon (D+7). A schematic representation of the meteorological input assembly is shown in Figure 5.

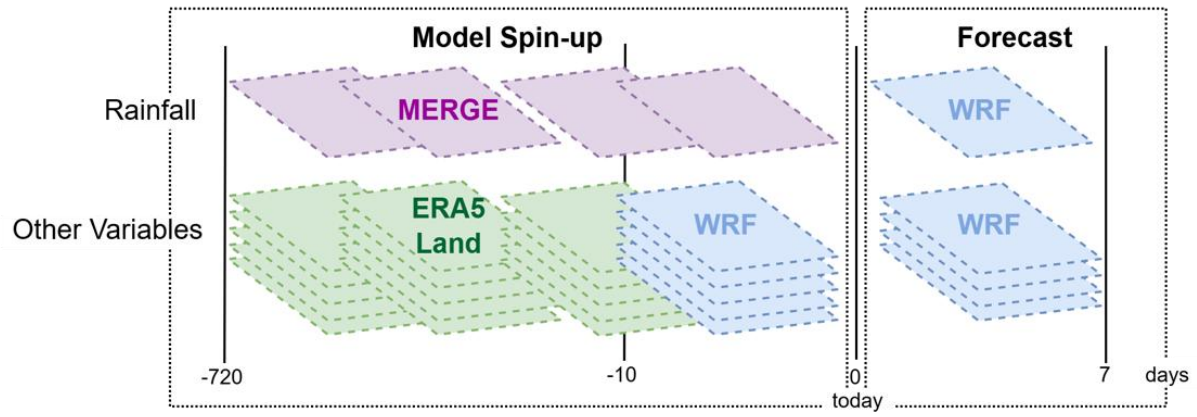

Figure 5: Meteorological Input Assembly

MERGE is used to represent observed rainfall, while other meteorological variables are from ERA5-Land. Although ERA5-Land is updated daily, it has a temporal lag of approximately five days. To fill this gap, the first day of WRF hindcasts is used. The input data are stored in binary format: one file for observed rainfall (*Prec.bin*) and another for the remaining variables (*Met.bin*) (CEMADEN, 2022). To optimize processing time, these files are updated daily through data appending. When necessary, missing data are filled using WRF hindcasts.

Figure 6 presents a summary of the procedures and routines used to prepare the model inputs, run the MHD, post-process the results, and publish them to the system API. Execution control is handled by a main routine (*inputMHD.py*), which identifies the run date and time, checks data availability, and triggers all subsequent routines.

The first and most critical step of the operational workflow is the construction of the meteorological input files for observations (*Prec.bin* and *Met.bin*). This step is executed by the routines *WRFupdateMHD.py*, *ERA5updateMHD.py*, and *MERGEupdateMHD.py*, depending on data availability. Next, the meteorological forecast inputs are formatted through WRFtoMHD.py, which generates the binary files *preprev.bin* and *metprev.bin*. The Qobs.prn file is also updated with the latest observed discharge, and the fixed parameter file is updated with the simulation and forecast periods and input files required by the model. With all inputs configured, the MHD-INPE is executed, and the outputs are posted to the API (postMHD.py). Finally, post-processing procedures are applied, including converting the daily forecast to 30-minute intervals using a cubic spline technique (PostSpline.py) and computing observed and forecast average rainfall for each sub-basin (*ChuvaMediaWRF.py* and *ChuvaMediaMERGE.py*). All post-processed results are stored in the API and subsequently used to generate bulletins and feed the web platform.

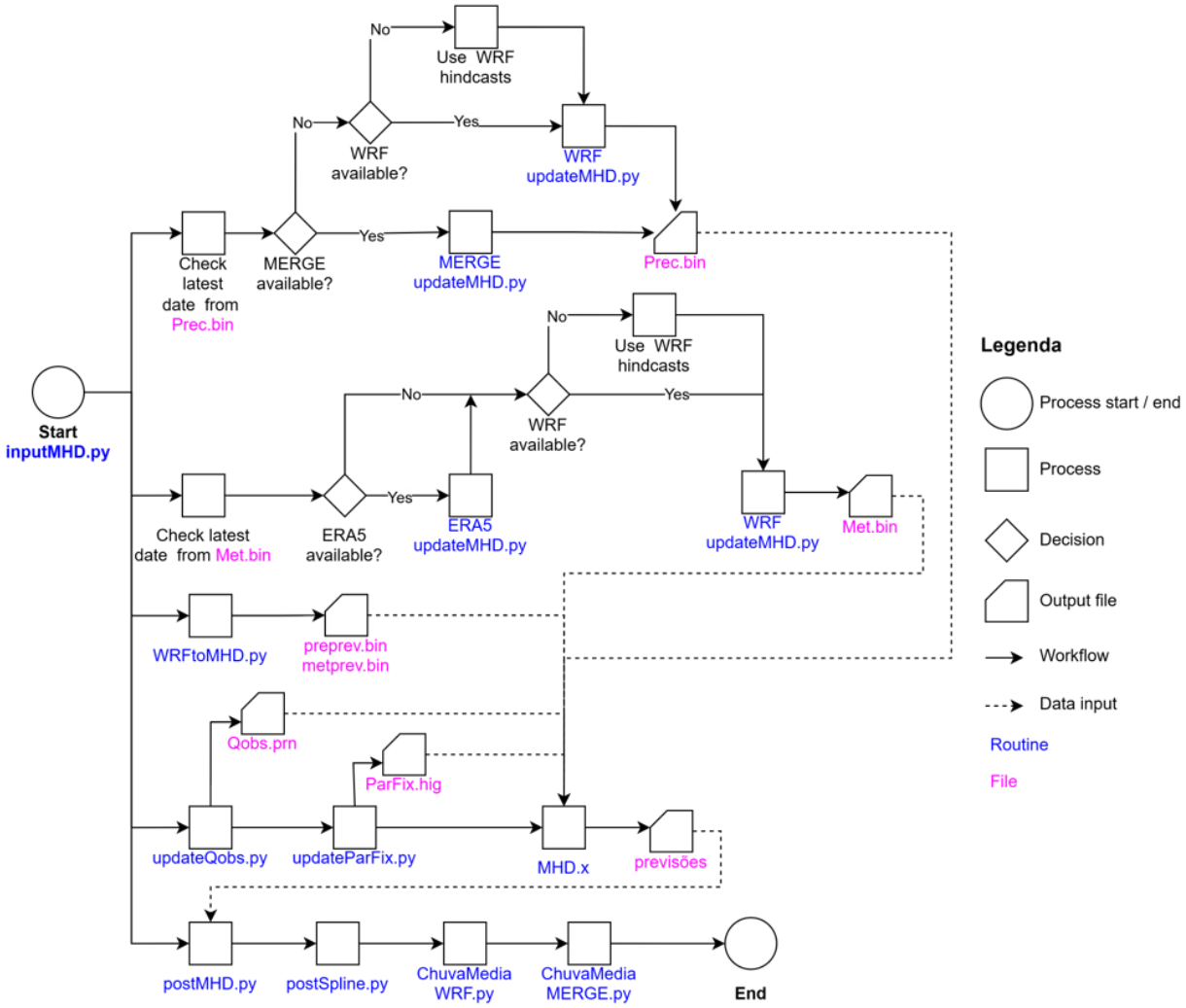

Figure 6: Operational Worflow Logic

6 CONCLUSION

This work presents the practical experience of implementing and maintaining an operational hydrological forecast system based on the MHD-INPE, highlighting the integration of heterogeneous

hydrometeorological data, the selection of computational resources, and the design of a logical operational workflow. The database – combining structured and unstructured data – enabled robust storage and standardized access to time series and geospatial files, while Python-based automation ensured a logical process capable of handling data availability failures and ensuring continuous system operation.

Although the system can incorporate private datasets, it operates entirely using open data and open-source software. The proposed solution is also adaptable to different river basins, extended forecast horizons – such as long-term forecasts and climate projections – and diverse water resources management contexts.

Developing an operational forecasting system requires a multidisciplinary approach. This intersection of fields, combined with the dependence on external systems, results in high implementation complexity. Moreover, working with large environmental datasets demands robust computational infrastructure. In the initial implementation, storing GRIB data in a traditional file system was a simple and practical solution. However, as data volumes increase and applications expand, a transition to more specialized technologies – such as geospatial database systems – will be necessary to ensure scalability.

Despite these challenges, the strategies adopted enabled the operational implementation of a conceptual, distributed, and complex hydrological model. System maturity has increased over time, as continuous operation provides opportunities to identify bottlenecks, adjust routines, and refine workflows. This growing maturity is essential for strengthening the reliability of the forecasts.

REFERENCES

Ahmad, S. K. and Hossain, F. (2019). A web-based decision support system for smart dam operations using weather forecasts. Journal of Hydroinformatics, 21.5, pp. 687-707.

Almeida, A. S.; Sorribas, M. V.; Gonçalves, J. E. and Leite, E.A. (2019). Estimativas da Precipitação Média na Bacia e a Calibração de Modelos Hidrológicos para fins de Previsão Operacional. XXIII Simpósio Brasileiro de Recursos Hídricos, Foz do Iguaçu, PR.

Ayzel, G. (2021). OpenForecast v2: Development and Benchmarking of the First National-Scale Operational Runoff Forecasting System in Russia. Hydrology, 8, 3.

CEMADEN (2022). Modelo Hidrológico Distribuído MHD-INPE: Manual de Implementação. Version 2.0. Cachoeira Paulista, SP.

Cuartas, L.A.; Tomasella, J.; Nobre, A.D.; Nobre, C.A.; Hodnett, M.G.; Waterloo, M.J.; Oliveira, S.M.de; Randow, R.C.von; Trancoso, R.; Ferreira, M. (2012). Distributed hydrological modeling of a micro-scale rainforest watershed in Amazonia: Model evaluation and advances in calibration using the new HAND terrain model. Journal of Hydrology, Volumes 462–463, Pages 15-27, ISSN 0022-1694.

De Filippis, T.; Rocchi, L.; Massazza, G.; Pezzoli, A.; Rosso, M.; Housseini Ibrahim, M.; Tarchiani, V. (2022). Hydrological Web Services for Operational Flood Risk Monitoring and Forecasting at Local Scale in Niger. ISPRS - International Journal of Geo-Information, 11, 236.

Georgakakos, K. P. (2022). Effective Transfer of Science to Operations in Hydrometeorology Considering Uncertainty. Hydrology, 9, 55.

Rodriguez, D. A. and Tomasella, J. (2016). On the ability of large-scale hydrological models to simulate land use and land cover change impacts in Amazonian basins. Hydrological Sciences Journal, 61(10), 1831-1846.

Siqueira, V.A. ; Paiva, R.C.D. ; Fleischmann, A.S. ; Fan, F.M. ; Ruhoff, A.L. ; Pontes, P.R.M.; Paris, A.; Calmant, S.; Collischonn, W. (2018). "Toward continental hydrologic–hydrodynamic modeling in South America. Hydrology Earth System Sciences", 22, 4815–4842.

WMO. (2019). Manual on Codes, Volume I.1 – International Codes. Annex II to the WMO Technical Regulations. Part A – Alphanumeric Codes. WMO-No. 306.

Chapter 2 - Flood risk assessment, data and modeling

2.5 Uncertainty, causality, and confidence in flood risk information

ICFM 10
Adapting to Global Change:
Innovative Approaches to Flood Management and Resilience
May 20-22, 2026 | Western University, London, Ontario, Canada

Hazard Risk Communication: A Canadian Case Study

Jennifer Spinney[1] and Nirupama Agrawal[1]
Disaster and Emergency Management, York University, 4700 Keele St., Toronto M3J 1P3, Canada
E-mail: jspinney@yorku.ca
E-mail: nirupama@yorku.ca

ABSTRACT

This study examines Canada's extreme weather warning system by analyzing the experiences and perspectives of broadcast meteorologists (BMs) from across the country. In addition, a review of risk communication principles and theories underscores the importance of these components. Through this dual lens, the paper identifies similarities and differences between established theoretical frameworks and the realities of the current weather communication practice. The qualitative analysis highlights opportunities to strengthen the design and delivery of hazard-related risk messaging. The findings contribute to a better understanding of the warning system's limitations and inform evidence-based strategies to enhance its effectiveness, bolster public trust, and increase the public uptake of extreme weather warnings.

KEYWORDS: Extreme weather warning, Broadcast meteorologist, Risk communication, Canada.

1 INTRODUCTION

Risk communication and early warning systems are central to reducing the impacts of hazards across sectors and contexts. Canadian Broadcast Meteorologists (BMs) are an essential part of the extreme weather forecast system, providing timely risk communication to socially, economically, and geographically diverse communities (Agrawal & Spinney, 2025). In public health, for example, timely communication about outbreaks of infectious diseases (biological hazards) is key to mitigating the spread of pathogens with pandemic potential. For other types of natural hazards, such as floods, severe storms, or extreme weather, timely information is critical for the public and authorities alike, as these events can have the potential to disrupt critical infrastructure and services, such as power outages due to a winter storm, water contamination due to a flood, or disruptions to fuel supply so that protective action can be taken.

This paper explores extreme weather warning systems in Canada and discusses a range of risk communication frameworks that have guided understanding and analysis of the transmission and uptake of information over decades. We draw on perspectives gleaned from interviews with a small group of Canadian Broadcast Meteorologists (BMs), thematically organized here as a coupling of operational challenges and ways for managing them, to highlight risk communication as a social process, and to show the importance of BM expertise and public trust as key contributors to effective alert distribution and uptake in severe and extreme weather contexts.

Early warning systems (EWS) form a core component of disaster mitigation strategies. The degree to which EWS are established varies across hazard types. In North America, hurricane and typhoon activity is monitored extensively by the U.S. National Hurricane Center and the Canadian Hurricane Centre, both of which are relied upon in Canada. Earthquake activity with the potential to generate tsunamis is monitored by the U.S. Geological Survey and Natural Resources Canada, which recently expanded earthquake monitoring and early warning beyond the west coast provinces to include eastern Ontario and Quebec. Likewise, weather forecasting and warning is the mandate of the U.S. National Weather Service and Environment and Climate Change Canada (ECCC). These agencies employ networks of monitoring stations and instruments, radar and satellite platforms, and numerical forecast

models to detect, track, and anticipate a range of meteorological and hydrological hazards, such as extreme wind, rainfall, heat and cold.

A substantial body of literature offers diverse frameworks for understanding risk communication applicable to natural hazards. These include the Transmission Model (Shannon, 1948); the Theory of Reasoned Action and its extensions (Fishbein, 1979; Sheppard et al., 1988; Trofimov, 2009); Grounded Theory (Mileti & Sorensen, 1990a); Trust-Determination Theory (Peters et al., 1997); the Elaboration Likelihood Model (Petty & Wegener, 1999); Mental Noise Theory (Lundgren & McMakin, 2008); the Protective Action Decision Model (Lindell & Perry, 2012); and the three-point guidance for effective communication proposed by Janoske et al. (2012). The three points are: (a) understanding the characteristics of an audience is essential to developing effective risk communication efforts; (b) how, when, and by whom a message is delivered impacts its effectiveness; and (c) communicators must continually adapt to changing situations.

The 'transmission model' is a linear process in which thoughts or information are transmitted from a sender through a medium to a receiver (Fig. 1). The 'grounded theory' (Fig. 2) proposes that an integrated warning system should have factors such as monitoring, detecting, and interpreting, as well as a warning method, content, and channel or medium. Furthermore, it suggested that message attributes should include content and style, and the source attributes must demonstrate credibility and familiarity. Mileti and Sorensen's (1990b) Information Processing Model shifts the focus in risk communication to the receiver and suggests that people's response to warning information follows a sequential process of six steps: hear, understand, believe, personalize, decide and confirm. The sequence may not be the same for every person, and each stage isn't necessary for a response to occur. The 'Predictive Theory of Reasoned Action' is based on individual risk perceptions and perceived control of decisions. Their behaviour is more likely to be acted when there is both personal and societal acceptance (Fig. 3). The 'Trust Determination Theory' is rooted in the audience's trust in the messenger, a vital determinant in message acceptance, risk perception, and subsequent behaviour. The 'Elaboration Likelihood Model' is a dual process where people may engage in scrutiny and analysis of the evidence in a message, or they may rely on simple heuristic rules of thumb. 'Mental Noise Theory' accounts for the decreased ability of individuals to receive and process information when they perceive themselves at risk due to mental noise during sudden-onset events. To rectify this, communication should avoid repeated messaging, jargon, acronyms, and technical terms. Lastly, the 'Protective Action Decision Model' accounts for how individuals integrate information from social and environmental cues and conform to the three pre-decision processes — reception, attention, and comprehension of warnings or threats. Although these frameworks differ in scope and complexity, they share an emphasis on understanding the intended audience of a risk message.

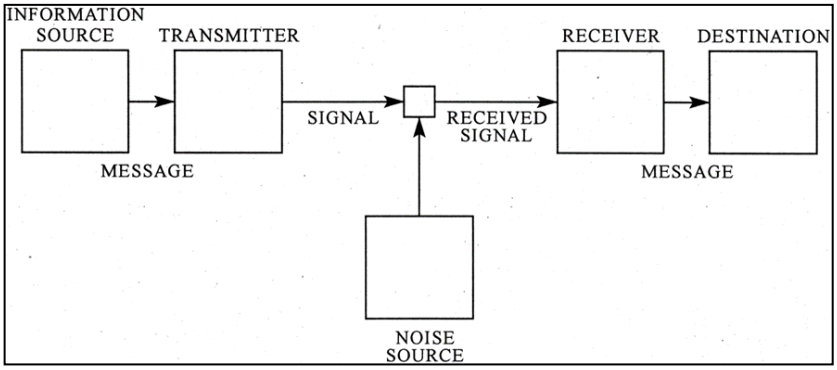

Figure 1: The Transmission Model of Communication (Shannon, 1949).

Expertise in broadcast meteorology is a temporal and socially mediated achievement, continually negotiated between scientific authority, institutional protocols, and audience expectations (Daston & Galison, 2007; Collins, 2018). BMs understand that knowing their audience is critical for designing and delivering extreme weather messaging. They note, "*If they [meteorologists] are new to the place, the lack of local knowledge may hinder their ability to convey the weather risk effectively and accurately*." In this context, the concept of intersubjectivity as a way to explain how individuals experience and constitute a shared world through mutual understanding becomes crucial (Duranti, 2010). This common ground cannot be assumed; it must be created across differing backgrounds, varying levels of trust, and diverse weather experiences. In essence, meteorologists across multiple domains and audiences must repeatedly build enough shared understanding of risk, what it is, why it matters, and what to do about it.

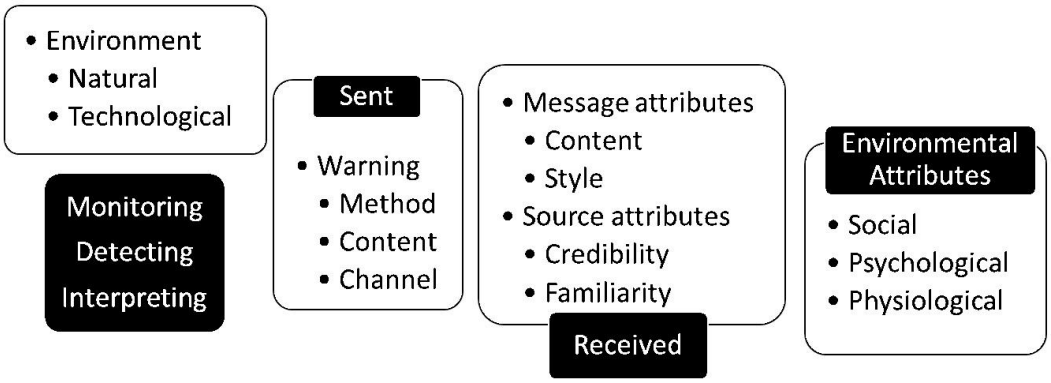

Figure 2: Grounded Theory: Risk Messaging Component Benchmarking (Mileti & Sorensen, 1990a)

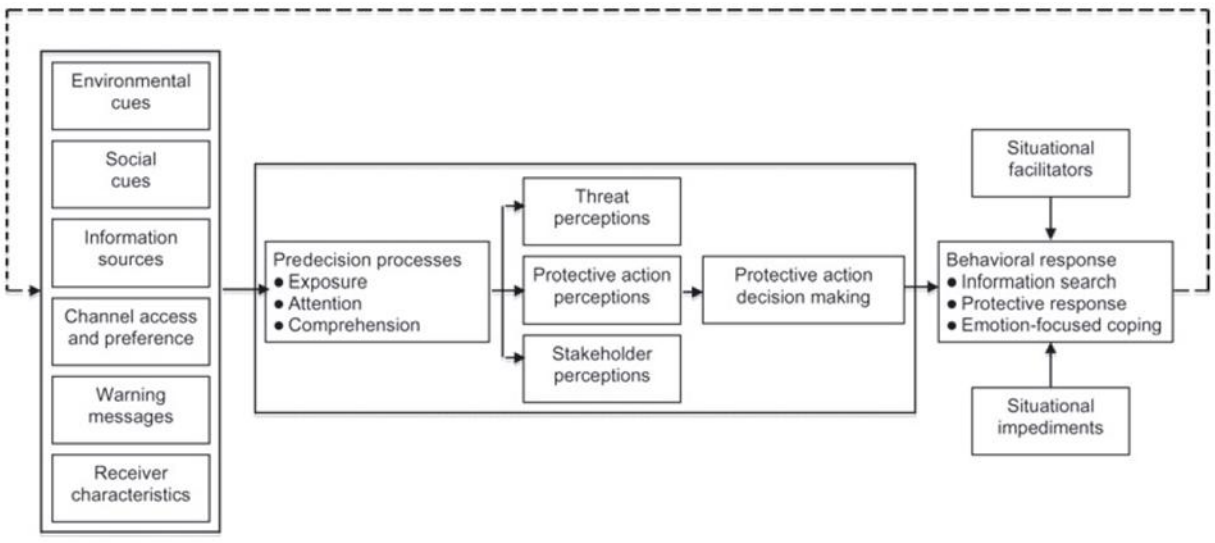

Figure 3: Protective Action Decision Model (Lindell & Perry, 2012)

2 METHOD

This study draws on 11 interviews with Canadian BMs conducted as part of a larger research project titled "A community-based approach to improve weather-related warnings in Ontario," undertaken in collaboration with the Meteorological Service of Canada. A purposeful sampling strategy was used to

select participants, and interviews were conducted by the principal investigator and co-investigator. The sample included professionals employed by major national TV networks who provide weather information to the public through both daytime and evening broadcasts. Participants were based in various Canadian cities, including urban centres on the West Coast, the western prairies, southwestern Ontario, and Atlantic Canada. Interviewees' professional experience ranged from 10 to 40 years, and their educational backgrounds included degrees in meteorology, atmospheric science, broadcast journalism, or communications.

The research team employed a semi-structured interview approach and conducted virtual interviews with 11 participants via Zoom between December 2022 and April 2023. Interviews followed a consistent protocol that included a list of 20 questions while allowing space to pursue emergent themes with each participant. This balance of consistency with flexibility generated a comparable and reliable data set (Bernard, 2002) that also included perspectives deemed important to each participant. Each interview lasted between 40 minutes and just under two hours and was audio-recorded and then transcribed using AI-assisted tools (Otter.ai). Transcripts were subsequently cleaned by student research assistants, and interview data were thematically analyzed within an interpretivist framework (Upadhyay, 2012), a common anthropological approach that understands reality as subjective and socially constructed.

3 RESULTS

3.1 BM Experiences

A typical day for a BM begins with integrating model outputs, observational data, and official forecasts obtained from Environment and Climate Change Canada (ECCC) with their real-time interpretation of atmospheric patterns and local conditions. The myriad tasks include accessing and interpreting weather data, producing graphics, developing forecasts, and sharing them across TV, radio, online, and social media platforms (Facebook/ Instagram/ TikTok/ X) in both recorded and live formats. Each shift requires coordinating short-, medium-, and long-term predictions to ensure consistency across time, space, and the larger work cycle. Their reliance on triangulation and cross-referencing functions as a system of stability within the instability of weather. Through these acts, BMs navigate the boundary between what they can know and what remains uncertain, adjusting forecasts for local conditions through their embodied attentiveness to both data and the environment. BMs' interpretive work takes place within a wider media environment marked by misinformation, accusations of exaggeration, and significant public scrutiny, including gendered and racialized responses directed especially at women broadcasters and women of colour (Hallows, 2020; Perryman & Theiss, 2014). These dynamics underscore that BMs are not only interpreters of data but also managers of public perception and trust.

3.2 BM Challenges

Inter-institutional procedural suspension: A closer look at broadcast meteorological work reveals a dense bureaucratic infrastructure and a set of practices that organize not only what is communicated but also when, where, and to whom, thereby imposing significant communication challenges. The Canadian early warning system for severe and extreme weather is made up of a range of stakeholders, including alert issuers (ECCC), alert distributors and aggregators, as well as various publics who use information and make decisions to protect themselves. BMs serve as an alert distributor in this system but rely on official alerts to generate weather warnings. ECCC meteorologists, organized by their own temporal regimes made up of centralized processes of data processing, interpretations of the atmosphere, and adherence to criteria-based warning rules, to name only a few, are at times themselves waiting to ensure the necessary pieces of the atmospheric puzzle are in place before issuing an official alert for an emerging weather hazard. Once the official warning is issued, alert distributors and aggregators, such as BMs and Pelmorex's Alert Ready[1] system, respectively, spread the message in ways to promote maximum public

[1] Alert Ready is Canada's emergency alerting system. The Alert Ready system was developed with many partners, including federal, provincial and territorial emergency management officials, Environment and Climate Change Canada, Pelmorex, the broadcasting industry and wireless service providers. https://www.alertready.ca/

uptake. BMs are thus embedded within a dense web of governmental agencies and media institutions, where they aim to condense complex meteorological alerts into meaningful segments of a few minutes or a couple of hundred characters, while maintaining fidelity to ECCC's authoritative language. For example, Participant #4's experience highlights the intersection of atmospheric and media temporalities with bureaucratic structures:

> *"I know I see a tornado happening. You know, ..., like, it's absolutely a critical moment that we are out, you know, that we need to get that information back. And [my colleague] is getting that information back to Environment Canada to get that warning out. It happens all the time. And it's terrible. I hate it. But it's sometimes really difficult to get that two-way flow of information or that information flowing back to them fast enough."*

3.3 Network-Specific Structures

The work routines of broadcast meteorologists are shaped as much by the criteria set by ECCC for issuing warnings as by network-specific systems, including temporal pressures intensified by shrinking budgets and staffing cutbacks. It results in tight deadlines and heavy workflows. As Participant #6 mentioned, they are "*covering multiple provinces' worth of weather, […]. A thunderstorm warning in Alberta may coincide with a heat advisory in Manitoba or an overnight frost risk in Saskatchewan.*" BMs must synchronize their reports with these shifting temporal layers while adhering to network schedules that demand consistent delivery across regions. This can be challenging for networks that cover topics beyond weather, as the participant above described: "*I am covering three provinces' worth of weather. We are not The Weather Network that has unlimited, you know, weather content time*."

BMs also need to communicate across multiple media platforms, including television, radio, websites, and social media; each demanding a distinct temporal harmony and communicative tone. Participant #3 mentions that they use YouTube, Twitter (now X), and Instagram as the main social media channels, and that it is a challenging process:

> *"…think of Twitter, for example, it has limited character spaces, you're on air, I've given a minute and a half on the radio, I'm given 45 seconds, you try and give a detailed forecast in 45 seconds. So yeah, that is my biggest challenge every day, but I feel like I'm learning. I really feel like it's over time, like I've been doing this for more than 20 years now. But over time, I've been able to hone in on really what it is that people need to know now. And as I said, try and fill in the details and other platforms."*

3.4 Navigating Challenges

The practices in place in weather forecasting are not merely technical strategies; they are deeply entangled with questions of authorship and accountability. Participants articulated that contextualization through familiar references, a sense of humour, or links to local community events enhances message retention and fosters trust. Several participants acknowledged that while at times they may disagree with official ECCC warnings, they are careful not to express such divergences on-air, instead layering the official warning with their own professional judgment and expertise of the local environment, which frames the threat in meaningful ways. Participant #5 gives an example of how they navigate the official warnings with their expertise:

> *"In the accountability factor, like what if your message you just sent out is not accurate? For whatever reason, right? Well, so I will only treat our warnings, obviously, once Environment Canada issues them. There have been times when they've issued a watch or warning, and I don't agree with it. And I will say that now we have a snowfall warning issued for [X location]. From what I can see on the models, I don't see us reaching that 15-centimetre threshold; I see it closer to 10. But here's the warning with the highest amounts through the West End, you know, so I'll kind of add a little bit of that human factor in there and experience."*

4 DISCUSSION

The discussion of BM experiences, the operational challenges they operate under, and the different strategies they employ to manage reveals important features of conventional risk communication frameworks (Fig. 1-3). First, the frameworks show that the '*source of information*' to be communicated is an integral component of every risk communication model. BMs in Canada obtain weather information from Environment and Climate Change Canada (ECCC), the federal agency authorized to disseminate weather information to interested parties, including issuing extreme weather warnings. BMs use supplementary resources, such as commercial weather models, to customize local weather for their region. While they do not initiate official warnings themselves, they simplify complex information to enhance clarity and accessibility for the public. It is reasonable to say that BMs conform to the theoretical communication principle of having a robust information source.

BMs acknowledge that "*Forecasts are never perfect*," but sought better tools to improve the accuracy of the timing and spatial extent of impending hazards. BMs noted a lack of a 'community' of weather forecasters for periodic dialogue on various aspects of the job. They wished to have opportunities to exchange ideas and experiences with other professionals, as their counterparts do in the U.S.: "*The National Weather Service holds its annual meteorological convention in the US; we do not have anything like that in Canada."*

Second, risk models emphasize '*the message*.' BMs across the country use the same template to convey extreme weather to the public in simple language. The main challenge involved in their job is how best to simplify the message for public comprehension without losing critical details. Some risk communication models (Petty & Wegener, 1999) suggest that the public may either prefer to use heuristic cues (source identity, colour, or visuals) or, in rare cases, engage in scrutiny and analysis of the evidence in a message. The Grounded Theory model (Mileti & Sorensen, 1990a, Fig. 2) and the Protective Action Decision Model (Lindell & Perry, 2012, Fig. 3) also account for message interpretation and comprehension as critical components of message design. Message attributes, including content, style, and familiarity, are equally important, according to both theoretical frameworks and BMs. In line with these theoretical concepts, broadcasters cultivate confidence while acknowledging uncertainty, using linguistic strategies to make the warnings more memorable, strategically adjusting tone when necessary to calibrate urgency. In doing so, they transform data outputs into social meaning, turning centimetres of snow or kilometres per hour windspeeds or millimetres of rainfall into behavioural guidance about whether to delay a commute, cancel an event, or prepare for power outages, to name a few. BMs' ability to synchronize, anticipate, and improvise ECCC warning information enables them to help audiences hear, understand, believe, and act upon the warning (Mileti & Sorensen, 1990b; Lindell & Perry, 2012).

Third, '*transmission'* of the message is critical. BMs, as alert distributors in the warning system, play a role akin to "transmitter" in the Transmission Model of Communication (Shannon, 1948, Fig. 1). This helps extend our thinking of "transmitter" in risk communication beyond equipment, cabling, and other physical tools to include social and human dimensions. For example, people and businesses living and operating in hazard-prone areas, such as floods, tornadoes, winter storms, avalanches, hurricanes, and wildfires, can use weather information to take measures to mitigate risk. BMs recognize the importance of transmitting complete weather risk information to their constituents and of building trust in that information so people heed advisories to stay safe. However, they identified several challenges to achieving this goal. The weather hazard information typically covers a large area and an approximate time of arrival for the event, with varying degrees of risk, creating uncertainty, and leading people to ignore the warning altogether. Therefore, BMs believe that high-resolution spatial weather forecast maps will improve situational awareness, thereby building trust in the information over the long term.

Fourth, the '*receiver of the message*' is a key factor in this process, as they must interpret the message and use the information to reduce hazard risk. BMs primarily broadcast weather to the public; therefore, they sometimes find it challenging to perform their duties with limited financial, technical, or personnel resources, under tight timelines, and across multiple platforms. Furthermore, the conceptual frameworks underscore the need to include social, psychological, physiological, and behavioural

attributes to help recipients of the message use their context and interpret the risk information accordingly. Analysis of interview data showed that the challenges BMs experience can both hinder their ability to communicate in a timely fashion and cause confusion, limiting information processing, public uptake, and protective action. A closer look at BM expertise also helps us to see this group of alert distributors as uniquely suited, given they are familiar sources and are often deemed credible in the eyes of the public, to create parcels of information with a particular style and content to promote effective receipt, in keeping with Grounded Theory (Fig. 2). The Protective Action Decision Model (Fig. 3) recommends similar considerations, such as environmental and social cues and receiver characteristics.

Evident from the interviews is the fact that BMs shared significant common elements, such as describing communication as a process of balancing scientific accuracy with strategies that sustain audience attention and comprehension. Furthermore, across the board, BMs reveal how they transform constraint into a workable rhythm by synchronizing, improvising, and adding their informed input to the communication, while ensuring that weather information remains both scientifically reliable and socially intelligible, thereby sustaining the social pulse of a system otherwise defined by institutional time and atmospheric uncertainty. Another key common dimension was the need to navigate the dynamic nature of channels (TV, radio, online, and social media platforms (Facebook/ Instagram/ TikTok/ X) through which risk information must be communicated. Among many individual issues that came to light, gender disparities, unequal access to resources, and differences between large-urban and small-rural jurisdictions stood out. Indeed, BM expertise extends beyond interpreting data, and they bring in their personal element, including education, training, personalities, and backgrounds.

5 CONCLUSION

Risk communication and early warning systems are central to reducing the impacts of hazards across multiple sectors and contexts, including severe and extreme weather in Canada. Our analysis confirmed the contemporary relevance of traditional risk communication frameworks in weather hazard communication and showcased the importance of BMs in the Canadian early warning system, especially the value of their expertise in effectively communicating threats. The discussion has been productive not simply for illuminating BM operational challenges and how they are managed, but also for the potential the exploration creates for understanding the merit of shared comprehension, or intersubjectivity, across domains of meteorological expertise. Our efforts to highlight broadcast meteorological work in Canada enable other meteorological experts involved in the Canadian weather forecast and warning system to understand the time pressures and challenges they face, such as delivering warnings quickly or condensing complex information. In that sense, we have enhanced conceptual bridging between the ECCC and broadcast meteorology worlds, enabling increased intersubjectivity across the fields. When meteorologists across different agencies understand each other's workflows and time pressures, they may be more willing to collaborate, making forecasting and warning practices more efficient and effective. While time has long been a means of disciplining labour (Thompson, 1967), in meteorological contexts, it also becomes a medium of collaboration, and through that medium, greater shared understanding has the potential to produce more effective communication with the public, and ultimately, safer outcomes for Canadian society, especially in times of severe weather with consequences such as floods.

6 ACKNOWLEDGEMENTS

An SSHRC Explore grant supported the study. We are thankful to the exceptional research assistants of York University's Disaster & Emergency Management: Elif Birbiri, Cecilia Parras, Trevor Doak, Jennifer Sze, Jacob Ploszaj, and Iana Shatilova. We are also grateful for the valuable advice from experts at Meteorological Services Canada: Lisa Vitols, Gabor Fricska, and Brittany Murphy.

REFERENCES

Agrawal, N, Spinney, J (2025). Extreme Weather Warnings: Perspectives on the Role of Broadcast Meteorologists, J Extreme Events https://doi.org/10.1142/S2345737625400019

Bernard, H. (2002). *Research methods in anthropology: Qualitative and quantitative approaches*. 3rd Alta Mira Press; Walnut Creek, CA.

Collins, H. (2018). *Tacit and Explicit Knowledge*. University of Chicago Press.

Daston, L., & Peter Galison. (2007). *Objectivity*. Zone Books.

Duranti, A. (2010). Husserl, Intersubjectivity and Anthropology. Anthropological Theory, 10(1), 1–20.

Fishbein, M (1979). A theory of reasoned action: Some applications and implications. Nebraska Symposium on Motivation, 27: 65–116.

Hallows, D. W. (2020). "The Full Forecast: A Gender and Racial Analysis of Broadcast TV Weathercasters." Undergraduate Honours Theses. Brigham Young University. Department of Communications. 117.

Janoske, M, Liu, B., & Sheppard, B. (2012). Understanding Risk Communication Best Practices: A Guide for Emergency Managers and Communicators, Report to US Department of Homeland Security.

Lindell, M. & Perry, R. (2012). The protective action decision model: theoretical modifications and additional evidence. Risk Analysis: An Official Publication of the Society for Risk Analysis, 32(4): 616–632. https://doi.org/10.1111/j.1539-6924.2011.01647.x.

Lundgren, R. E., & McMakin, A. H. (2008). Approaches to Communicating Risk, In Risk Communication: A Handbook for Communicating Environmental, Safety, and Health Risks, 4th Edition, Wiley-IEEE Press, https://doi.org/10.1002/9780470480120.ch2

Mileti, D.S., & Sorensen, J.H. (1990b). *Communication of Emergency Public Warnings: A Social Science Perspective and State-of-the-Art Assessment*. No. Report ORNL-6609, Federal Emergency Management Agency. DOI: 10.2172/6137387

Mileti, D.S. & Sorensen, J.H. (1990a). Communication of Emergency Public Warnings: A Social Science Perspective and State-of-the-Art Assessment. Technical Report. doi:https://doi.org/10.2172/6137387.

Perryman, N., & Sandra Theiss. (2014). "Weather Girls" on the Big Screen: Stereotypes, Sex Appeal, and Science. *Bulletin of the American Meteorological Society*, 95(3): 347–356 https://doi.org/10.1175/BAMS-D-12-00079.1.

Peters, R.G., Covello, V.T. & McCallum, D. (1997). The determinants of trust and credibility in environmental risk communication: An empirical study. Risk Analysis: An Official Publication of the Society for Risk Analysis, 17(1): 43–54.

Petty, R.E. & Wegener, D.T. (1999). The elaboration likelihood model: Current status and controversies. In: Chaiken, S., and Trope, Y. (eds.) Dual-Process Theories in Social Psychology. The Guilford Press, pp. 37–72.

Shannon, C.E. (1948). A mathematical theory of communication, Bell System Technical Journal, 27(3): 379–423.

Sheppard, B., Hartwick, J., & Warshaw PR (1988). The theory of reasoned action: A meta-analysis of past research with recommendations for modifications and future research. Journal of Consumer Research, 15(3): 325–343.

Thompson, E. P. (1967). "Time, Work-Discipline, and Industrial Capitalism." *Past & Present,* 38 (1): 56–97. https://doi.org/10.1093/past/38.1.56

Trofimov, D. (2009). The Theory of Reasoned Action. Theory & Psychology, 19: 501–518;doi: 10.1177/0959354309336319.

Upadhyay, P. (2012). "Interpretivist Tradition in Qualitative Anthropological Research Writings". *Himalayan Journal of Sociology and Anthropology* 5 (November):123–37. https://doi.org/10.3126/hjsa.v5i0.7044

ICFM 10
Adapting to Global Change:
Innovative Approaches to Flood Management and Resilience
May 20-22, 2026 | Western University, London, Ontario, Canada

Flood hazard identification and mapping program (FHIMP): Technical Bulletins and Uncertainty in Flood Mapping

Shawn Tse[1] and Serges Zango[2]
Environment and Climate Change Canada, 7400 – 64 Street SE, Calgary AB, Canada[1]
E-mail: shawn.tse@ec.gc.ca

Environment and Climate Change Canada, 351 Boulevard Saint-Joseph, Gatineau QC, Canada[2]
E-mail: serges.zango@ec.gc.ca

ABSTRACT

Flood mapping is a critical tool for risk and emergency management, yet it is unavoidably subject to uncertainty arising from natural variability, data scarcity, analytical limitations, and natural variability. This paper examines uncertainty in flood mapping and its implications for decision-making. It outlines the sources of uncertainty and quantification methods, such as probabilistic approaches and sensitivity analyses. A case study of sensitivity demonstrates how parameter variability and calibration data validity influence peak flows, and flood hazard delineations. Best practices for communicating uncertainty to technical and non-technical audiences emphasize clarity, transparency, and the use of visual tools to convey confidence levels. Finally, strategies for managing uncertainty include a method to assess uncertainty and periodic map updates to account for climate change and evolving land use. By identifying the sources of uncertainty, quantifying this uncertainty, and communicating it via into flood mapping products, practitioners can create an appropriate degree of confidence in results and guide informed decision-making.

KEYWORDS: flood hazard, flood mapping, hydrometrics, hydrometeorology, uncertainty, sensitivity analysis, probability, communication

1 INTRODUCTION

As part of the federally funded Flood Hazard Identification and Mapping Program (FHIMP), Environment and Climate Change Canada (ECCC) acts as technical advisors on provincial and territorial flood mapping projects, advances the science of flood mapping, and provides guidance on best practices. This guidance is offered in the Federal Flood Mapping Guidelines Series and the Federal Flood Mapping Technical Bulletins Series (the Technical Bulletins). These Technical Bulletins complement the Federal Flood Mapping Guidelines Series by addressing specific flood mapping topics in more detail.

Currently a single Technical Bulletin is available: Geomorphic Considerations in Flood Mapping. Work is currently underway on a few more, including:

1. Flood Data Collection
2. A Framework for Review and Update Cycle of Flood Maps
3. Pluvial Flood Mapping Guidance
4. Uncertainty in Flood Mapping
5. Wave Hazards

This paper explores the Technical Bulletin on Uncertainty in Flood Mapping in more detail. Generally, the development of a flood hazard map involves three sequential steps (Figure 1):

1. Selection of the design flood flow,
2. Hydraulic modelling of floodwater elevation calculations from these design flood flows, and
3. Mapping and estimation of spatial flood extent from the hydraulic model results.

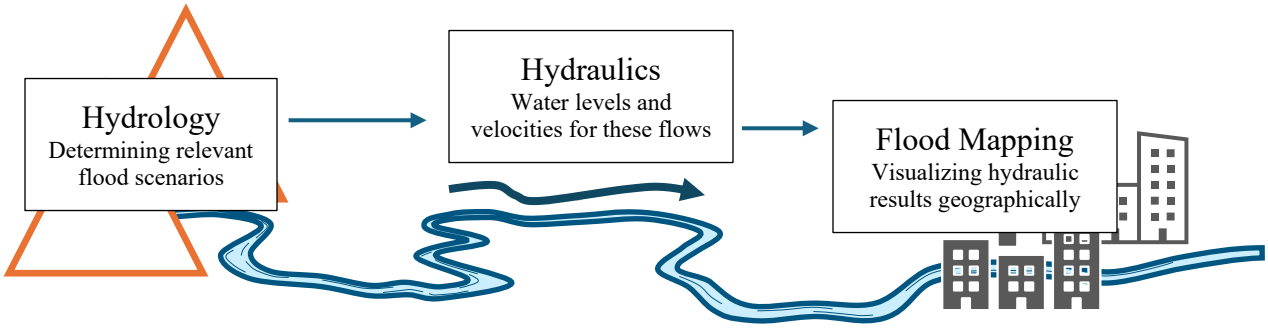

Figure 1: Potential Framework for Uncertainty by Workflow Step. Adapted from KWL (2024)

Each step relies on data, analysis, and assumptions, each with its own uncertainty. It is impossible to precisely measure all these processes in detail, to measure the quantity of every fluctuation. Therefore, flood maps are unavoidably subject to uncertainty. This uncertainty accumulates as calculations and decisions from the previous step are used, as shown below in Figure 2.

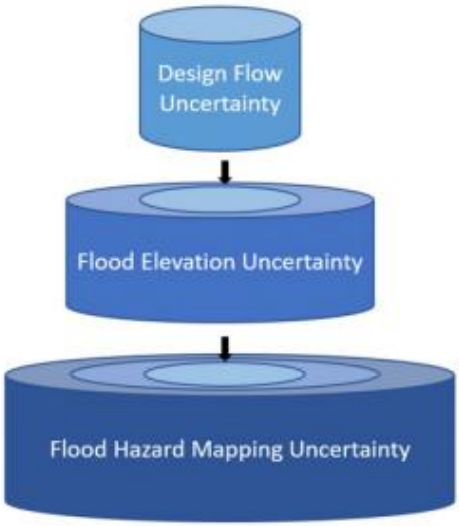

Figure 2: How uncertainty can propagate through the flood mapping process and potentially have additive impacts, increasing the potential uncertainty of the final flood hazard map. (MacHydro, 2023)

To address this uncertainty, it must first be understood and characterized. Then this uncertainty must be effectively communicated, as flood mapping is in-and-of-itself a communication tool. Finally, the uncertainty can be managed, limited, and accounted for.

2 UNDERSTANDING UNCERTAINTY

Uncertainty refers to limitations both in the accuracy and the confidence of results due to incomplete, imperfect, and unknown information, measurements, and analysis. It has several common characteristics:

- Uncertainty may be *quantifiable* or *unquantifiable*. Quantifiable uncertainty can be measured and expressed as a relative or absolute measure. Unquantifiable uncertainty may stem from elements that may change in the future or where there is insufficient information or understanding to adequately account or characterize the uncertainty.
- Uncertainties may be *reducible* (e.g. through more or better data collection or study) or *irreducible* (e.g. cannot be reduced by any means available at the time the knowledge is required).
- There may also be unknowable uncertainties, which cannot reasonably be anticipated or quantified.

Uncertainty is an unavoidable component of flood mapping. It must therefore be understood and managed, which requires an appreciation of both where it stems from (sources of uncertainty) and the relative impact of that uncertainty on the final output (quantifying uncertainty and sensitivity analysis).

The first step to understanding uncertainty in a study is to set an optimization goal (i.e. an objective function) for the analytical technique used (e.g. flood frequency analyses, synthesized data records, hydrologic, and/or hydraulic modelling). This defines the acceptable tolerance between the simulated and observed series. Then determine if a bias correction is required to meet this tolerance, then run the model again until no further correction is necessary.

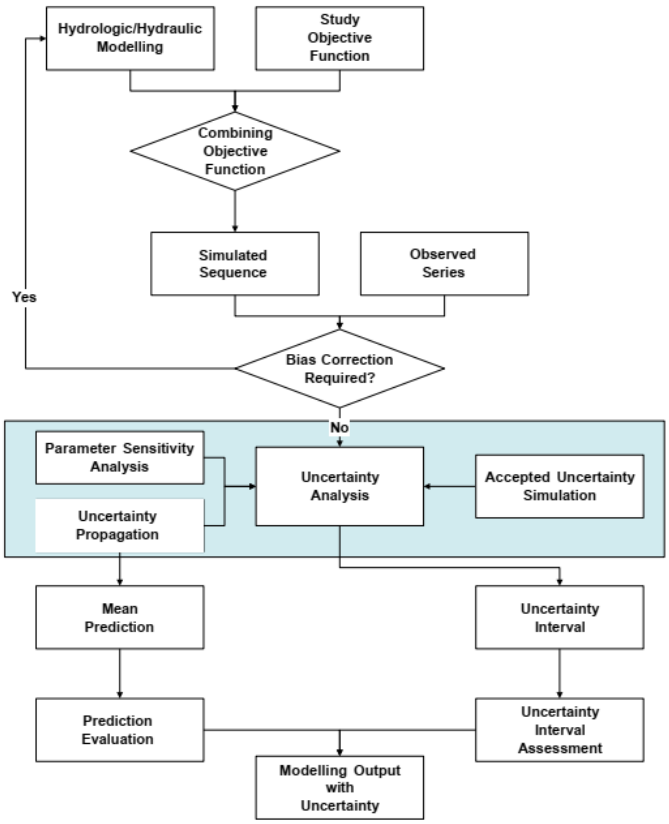

Figure 3: Uncertainty workflow of hydrologic and hydraulic modelling (NRCan and ECCC, 2023)

Then perform a sensitivity analysis or Monte Carlo simulation of the model's output for each non-constant parameter. Adjust each parameter and compare the results to determine each parameter's relative impact. These analyses/simulations will produce a mean prediction with an uncertainty interval (e.g. the average value of design flood events with confidence limits or min/max differences of different analyses).

2.1 Sources of Uncertainty

The *Federal Hydrologic and Hydraulic Procedures for Flood Hazard Delineation* (NRCan and ECCC, 2023) classifies uncertainty into four characteristics categories based on the origin of that uncertainty:

1. **Natural or intrinsic uncertainty** from the inherent randomness of natural processes, which varies over time and space. This natural uncertainty is difficult to reduce and quantify as the data is irreproducible. Examples include changes to bathymetry/topography (e.g. due to erosion), and/or natural physical processes (e.g. weather patterns, heterogeneity in soil hydraulic conductivity).

2. **Data uncertainty** from measurement errors, instrumentation errors, inconsistencies and non-homogeneity of the data, data handling, and inadequate representativeness of data over time and space. This data uncertainty is reducible with better or increased measurements. Examples include spatial/temporal data availability (e.g. proximity of monitoring stations, data gaps), data quality, accuracy and precision (e.g. measurement/instrument error, data handling), and/or climate change projections (e.g. availability of projections for key parameters, reliance on interpretation/analysis, changing flood mechanisms).
3. **Calculation uncertainty** from the inability of a mathematical technique or model to accurately represent the true physical behaviour of the natural world. The technique or model may be poorly or incompletely specified, or the phenomena modelled has instabilities and non-linearities which are not reflected in the modelling approaches. For example, historic flood event classification (e.g. rainfall, snowmelt, or rain-on-snow), choice of statistical distributions within a frequency analysis, model choices and associated limitations (e.g. 1D vs. 2D hydraulic models), and/or processing hydraulic models to develop flood maps (e.g. interpolation of a river flood profile)
4. **Parameter uncertainties** from inaccurately assessed parameter values in the test or calibration data, due to limited numbers of observations, and statistical imprecision. Examples include the selection of most-fitting frequency distribution parameters, the abstraction of physical properties such as sediment grain size, or hydraulic roughness, and/or assumptions made due to limited availability of data.

These categories of uncertainties are interdependent and overlap. The overlap of these interdependencies reduces the overall uncertainty. An example of the interdependence is how natural uncertainty impacts the measurement of water levels, which in turn reduces the certainty of the parameter valuation. Having uncertain values for the parameters inherently makes the model uncertain.

2.2 Quantifying Uncertainty

A wide range of possible methods and approaches for uncertainty quantification exist, requiring a different amount of effort. Therefore, the practitioner should select the uncertainty quantification method that is appropriate for their level of required precision, the resources available, and the requirements of the end users and decision makers. Quantification methods are discussed in greater detail in *Federal Hydrologic and Hydraulic Procedures for Flood Hazard Delineation (NRCan and ECCC, 2023)*, *Guidelines for Communication of Uncertainty in Flood Maps (KWL, 2024)*, and *ECCC Uncertainty in Floodplain Mapping (MacHydro, 2023)*. Some methods include the following:

- Uncertainty allowances and/or relative magnitudes based on subjective judgement.
- Uncertainty estimates based on multiple measurements and/or reported data accuracies for inputs.
- Uncertainty estimates based on multiple analysis approaches for a given item (for example, by determining river flood design flows using two different methods and comparing the results).
- Best estimates and upper and lower bounds developed for all uncertainty components and propagated through the analysis to determine corresponding flood mapping results for the best estimate and reasonable upper and lower bounds (i.e. three sets of results for a given event).
- Analytical techniques, which involve a derivation of the exact probability density function and/or statistical moments of a model as a function of several stochastic variables. (Yung, 2011)
- Approximate techniques involve probabilistic assessment based on a broad spanning sensitivity analysis, such as a Monte Carlo simulation. These approach assigns probability distributions for the range of values considered in the sensitivity analysis and then runs multiple simulations where the values for each of the parameters being varied is selected randomly based on their probability distributions. (Yung, 2011) Sensitivity analyses are discussed in more detail below.

Ideally, uncertainty assessments should also state items which cannot be quantified.

2.3 Sensitivity Analysis and Case Studies

A sensitivity analysis involves changing the model input parameters by a set amount, then examining how those changes affect the model's output. The parameters that are selected to be varied are sources of uncertainty. Once these parameters have been selected, the model is run repeatedly, increasing or decreasing a parameter each time, and the subsequent changes to the results (i.e. water levels, velocities, flooding extents, and depths) are recorded while holding all other parameters constant. Once all parameters have been run, a list is prepared with the parameter causing the largest response of the results first. This technique highlights the input parameters that will most significantly change the results, and therefore the input parameters to pay particular attention to during model calibration.

In 2024, CBCL and Associated Engineering conducted a sensitivity analysis on the flood mapping process completed for one flood study in Nova Scotia, and another in British Columbia (CBCL, 2025). The focus of this analysis was to examine the impact of the variability of parameter selection on the resulting flows, water levels and flood maps.

The study concluded that the most sensitive parameters affecting the estimated peak flows included, in order: the source calibration event, the maximum overland flow parameter, IDF data source, discretization level of sub-catchments, soil hydraulic conductivity, and hyetograph distribution (Figure 5 below). It is noted that these findings may be limited to watersheds with rainfall-dominated runoff responses.

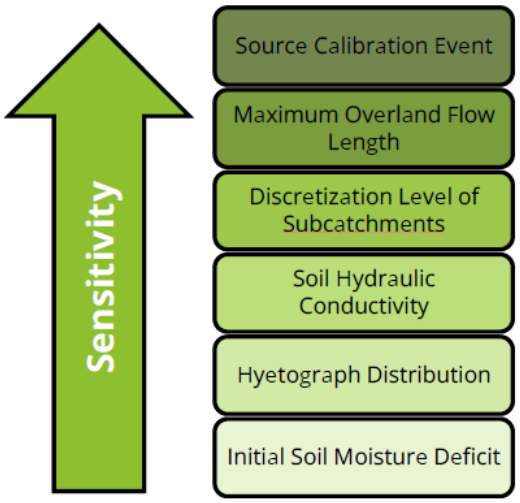

Figure 4: The Most Sensitive Hydrologic Input Model Parameters (CBCL, 2024)

This study also revealed that the highest sensitivity of flood extents was less focused on how calibration parameters were selected, but rather more focused on the validity of the calibration data in the first place. The study therefore recommended prioritizing the identification of a representative flow gauging station, the selection of a suitable flow calibration event and in turn, the identification of a suitable climate station that recorded the rainfall that generated the peak flow used for calibration, and then the selection of a suitable design rainfall event data source and distribution. These aspects, admittedly, are highly dependent on the availability, quality and suitability of flow gauging and climate station data to represent of the local hydrologic processes.

Model calibration based on alternate hydrologic parameters values did not greatly change the estimates of peak flow, reinforcing the finding that the most significant source of uncertainty is the precipitation and flow data that is used for model calibration and design hyetograph generation.

Similar to peak flow, for a given measured rainfall, and gauged flow to calibrate to, using different sets of parameter adjustments in the calibration process had minor impacts to the resulting flood extents, so long as the modelled hydrograph closely represented the measured hydrograph, notably the peak flow.

3 COMMUNICATING UNCERTAINTY

The goal of communicating uncertainty in flood mapping is to help end users appreciate how results and conclusions might vary in different circumstances, enabling them to interpret results with an appropriate level of confidence. Clear communication of the limitations and uncertainties in flood mapping is critically important because these maps may result in planning, regulatory and legal ramifications, but can also be used by the larger public to help understand the personal risk to them.

Communication approaches range from limited information/quantification (acknowledgement and qualitative commentary) to very detailed analysis and quantification, including mapping specific uncertainty outcomes.

Communicating uncertainty in a way that is accurate, scientifically defensible, and broadly accessible involves balancing objectives that sometimes conflict. Flood maps should be communicated in a way that best serves both their ultimate purpose and intended audience, where appropriate communication may look different depending on both.

The most important piece of information communicated within flood hazard maps is flood inundation extent (and potentially depth). A major limitation of current flood maps is that flood inundation levels are usually binary (i.e., they show a single inundation stage). While this creates the impression that a high degree of certainty is imbued within that single line, significant uncertainty exists within this precise inundation level: adjacent areas on either side of the inundation line may share a similar flood hazard and a single line may give a false sense of precision that does not exist. Specifically, flood hazard exists as a gradient around the presented inundation extent, even though very few flood hazard maps present it as such. This gap could undermine public trust in flood hazard maps, especially if the design flood flow occurs and inundates beyond the single flood line contained within the flood hazard map. This highlights the importance of clearly communicating key assumptions within the analysis to the public (for example, which design flow was selected to calculate the inundation level).

Effective communication of uncertainty should strive first and foremost to convey the desired information in a way that is easily understandable by the intended audience. For instance, public communication and other non-technical products (such as a public flood map) should prioritize clarity and key messages over more technical details (which could be provided in an accompanying technical document). Communication should be done using clear and simple language and information regarding the analysis should also be presented in a 'tiered' format that accounts for the level of detail needed by a specific audience.

Uncertainty should be presented in a way that highlights which limitations exist as well as what conclusions can still be made despite this uncertainty. Visual communication, such as the presentation of a 'gradient' around the flood inundation level, should be clearly defined. Including this information in the final mapping product communicates that inundation levels are not binary but rather contain a range of probable values due to uncertainties in the methodology that decision makers and other members of the public must consider. By comparison, technical documents require comprehensive information detailing study assumptions and methods used to determine uncertainty. Details regarding methods used to define flood maps, as well as major assumptions made, should be readily available. At a minimum, study results and interpretation should be accompanied by a statement of sources of uncertainty, and the limitations in the final product.

4 MANAGING UNCERTAINTY

The effort required to assess uncertainty in flood mapping depends on the type of assessment, and to efficiently use limited resources, the uncertainty assessment process should be defined at the project outset. The aspects of uncertainty of most concern to the map users should be targeted.

Generally, an uncertainty assessment process includes the following steps:

1. Identify and list anticipated sources of uncertainty (including data, parameters, assumptions, analysis, modelling) for all stages of the project. Include acknowledgement that there may be unknown uncertainties that are not identified.
2. Qualitatively rate all sources of uncertainty on two scales:
    a. the degree to which they are expected to affect the end results (i.e. sensitivity), and
    b. how well they can currently be addressed or accounted for.
3. Categorize these uncertainties into appropriate functional groups for analysis and communication, taking into account their relative sensitivity.
4. In collaboration with users and decision-makers, rank sources of uncertainty and assumptions in terms of how they affect their specific decisions, then collaboratively decide which uncertainties and assumptions to prioritize and the uncertainty quantification methods to be used. This should be completed before the data analysis and modelling step.
5. For the prioritized uncertainties, quantify, propagate, and analyze uncertainties in the process of producing the required flood maps.
6. Review the initial decisions taken under Steps 1-4 to confirm that the decisions remain appropriate in the context of the results.
7. Communicate uncertainty in project deliverables.
8. Evaluate the communication for efficacy and audience needs and adapt as appropriate for future communications.

Flood maps are useful to understand and mitigate flood risk, despite (and because of) the uncertainty. To improving this usefulness, explicitly state the required level of certainty, and understand that the data, models, and methods used do not have to be perfect to be useful.

4.1 Planning for Potential Change and Aging Flood Maps

As part of each flood mapping study, practitioners should review the intended scope and use of the flood maps in the context of ongoing and expected changes within the watershed and along the floodplain. Studies should identify an appropriate planning horizon for flood risk management that considers climate and land use changes expected (e.g., sea-level rise, changes in precipitation, and/or urbanization of natural areas). Precautionary factors of safety may be appropriate in situations where uncertainty is high.

Climate change is one of the largest considerations of future uncertainty in the flood mapping process. Climate change uncertainty is the combination of a cascade of uncertainties from various sources: emissions scenarios, climate models, downscaling and bias-correction methods, natural variability, statistical parameter estimation, and the applications methods that are being used to incorporate climate information as inputs. Because the approaches to incorporate climate change in flood mapping differ from jurisdiction to jurisdiction and analysis to analysis, a consistent approach should be considered to standardize and characterize uncertainty.

A major event like a major flood, ice jam, or storm surge event larger than the historical record used in any FFA (flood frequency analysis) for a flood hazard delineation could warrant a re-examination of the FFA. In addition, if the channel or infrastructure changes from the initial study, a new hydraulic analysis will indicate whether risks of inundation have increased, even if the hydrology remains essentially the same.

4.2 Technical Bulletin on Flood Map Updating

Many jurisdictions legislate a periodic re-assessment of flood hazard. The United Kingdom (UK Environmental Agency, 2019) requires a review every six years, and FEMA must assess the need to revise flood mapping every five years (Department of Homeland Security, 2017). ECCC is currently drafting guidance on the recommended time interval between flood map updates, based on academic and non-academic publications, articles, flood mapping reports, guidelines from other countries, and subject matter experts.

The recommended baseline for review and update of flood maps is 5 years. However, there are several circumstances that would trigger an unscheduled review, such as: new planning guidance that creates a substantial change in flood mapping methodology; identification of an error or inaccuracy in the existing flood map or study; or major terrain and structural alterations that would affect the results.

5 CONCLUSION

The following is a summary of notable considerations for uncertainty with flood mapping:

- **Uncertainty is unavoidable and should therefore be acknowledged and quantified**: While it may not be possible to completely identify, quantify, or remove all sources of uncertainty, there is still value in understanding, quantifying, and addressing uncertainty.
- **Maintain confidence in flood mapping through clear communication**: Communication of uncertainty is important for informed decision making and public awareness, but it must be carefully balanced against the need to maintain a reasonable level of confidence in the mapping results. Methods of communicating uncertainty therefore needs to create the appropriate level of confidence in results while acknowledging limitations.
- **Uncertainty increases over time, therefore managing uncertainty includes planning for change**: Updating flood maps reduces the uncertainty caused by gradual changes in the environmental factors, as well as those factors that increase uncertainty by the passage of time, or analytical techniques that are shown to increase certainty. Planning for future changes is therefore critical, and periodic reviews (typically every five years) and unscheduled updates triggered by major events can help maintain map reliability.

6 ACKNOWLEDGEMENTS

We gratefully acknowledge the contributions of CBCL, Associated Engineering, Kerr Wood Leidal, and MacDonald Hydrology for their technical expertise and support, without which this paper could not be written. We also extend our appreciation to Natural Resources Canada, and Public Safety Canada for their guidance, collaboration, and commitment to advancing flood mapping and risk management.

REFERENCES

CBCL Ltd. (CBCL) (2025). Flood Hazard Modelling Sensitivity Pilot Study. 140 pp. Internal report.

Department of Homeland Security (2017). FEMA Needs to Improve Management of its Mapping Programs Office of Inspector General p.2.

Kerr Wood Leidal Associates Ltd. (KWL) (2024). Guidelines for Communication of Uncertainty in Flood Maps. 72 pp. Internal report.

MacDonald Hydrology Consultants Ltd. (MacHydro) (2023). ECCC Uncertainty in Floodplain Mapping. Internal report.

Natural Resources Canada and Environment and Climate Change Canada (NRC and ECCC). (2023). Federal Hydrologic and Hydraulic Procedures for Flood Hazard Delineation. Version 2.0. General Information Product, 113e, 177 pp. Available online: https://natural-resources.canada.ca/science-data/science-research/natural-hazards/flood-mapping/federal-hydrologic-hydraulic-procedures-flood-hazard-delineation.

UK Environmental Agency (2019). 2009 No. 3042 Environmental protection: The flood risk regulations 2009. Available online: Guidance - Flood risk management plans (FRMPs): responsibilities.

Yung, Yeou-Koung Tung. (2011). Uncertainty and Reliability Analysis in Water Resources Engineering. In Journal of Contemporary Water Research and Education, 103(1)4, 10 pp. Available online: https://opensiuc.lib.siu.edu/jcwre/vol103/iss1/4/.

ICFM 10
Adapting to Global Change:
Innovative Approaches to Flood Management and Resilience
May 20-22, 2026 | Western University, London, Ontario, Canada

A novel and efficient approach to estimate lifetime exposure risk with changing flood probabilities

Mark Babister[1], Harrison Babister[1], Behzad Jamali[1], Nathan Dunning[1], and Monique Retallick[1]
WMAwater Pty Ltd, Sydney NSW Australia [1]
E-mail: babister@wmawater.com.au

ABSTRACT

The widely adopted 1% AEP design flood level has been the backbone of flooding and stormwater design standards for over 50 years. The choice of the 1% AEP design flood was often justified by its equivalent "lifetime flood exposure risk" which is equal to (approximately) a 50% chance of experiencing one or more floods over a typical 70-year life. Lifetime exposure risk is simply calculated using the binomial distribution with the core assumption that flood probabilities do not change over the design life. The impact of climate change on flood producing rainfall has been a concern in Australia since 1987 with adjustment factors being introduced in 2016. The design rainfall increases in the future, in most of climate change scenarios. Therefore, assessing lifetime flood exposure risk using the binomial theorem is no longer valid. As the probability of design rainfalls and flood levels are changing every year, estimation of lifetime exposure risk presents additional computational complexity. This paper presents a novel and practical method for evaluating lifetime flood exposure risk using a full solution to the Poisson binomial formula. The solution is complete and computationally viable using a discrete Fourier transform. The technique also allows a better understanding of the mean exceedance chance over an exposure risk period rather than a fixed chance. The approach has also been adapted for use outside Australia and can be applied to any situation where the change in flood probability can be defined over time.

KEYWORDS: flood, lifetime exposure, risk, changing climate

1 INTRODUCTION

Design standards like the 1% AEP flood level have been the backbone of flooding and stormwater design for over 50 years and was widely adopted in Australia in the 1970s (Cardno, 2015). Similar 1% AEP design standards have found wide use in the United States of America, United Kingdom, New Zealand and Canada. Drainage standards around Australia were widely adopted at that time but with design standards varying between states and local government areas. Australian Rainfall and Runoff (ARR) 1987 (Pilgrim Ed.(1987) lists some typical drainage standard values of 20%-10% AEP for residential areas.

Standards based approaches for floodplain management assume the consequences of flooding and the overall risk can be managed by a 1% likelihood (NSW Government, 2005) and 1% is considered a reliable balance between acceptable and unacceptable flood risk (NSW Government, 2005). For stormwater systems this is less of a problem, as pipe capacity based on likelihood is really a measure of how frequent a major inconvenience will occur as events exceed the pipe drainage capacity (Ball Et al., 2019). Australian stormwater design standards tend to vary with the intensity of design rainfall, with locations of higher design rainfalls generally having a lower standard, as it is difficult to fit the higher design flows that occur as a result of the higher rainfall into a stormwater pipe system (Pilgrim Ed. 1986). Ironically, locations with lower pipe standards tend to have better regulated overland flow paths for when the stormwater system capacity is exceeded (QLD Department of Energy and Water Supply, 2013).

The impact of climate change on flood producing rainfall has been a concern in practice since ARR 1987 (Pilgrim Ed., 1987). ARR1987 (Pilgrim Ed. (1987) stated:

"*It should be noted that no consideration has been given to the long term effects of climatic change, a topic which is receiving increasing attention in the scientific literature.*"

ARR1987 (Pilgrim Ed.(1987) then quotes the conference statement from the 1985 Villach WMO conference (International Conference on the Assessment of the Role of Carbon Dioxide and of Other Greenhouse Gases in Climate Variations and Associated Impacts, (1985 : Villach, Austria), 1986):.

"*Many important economic and social decisions are being made today on long term projects based on the assumption that past climatic data, without modification, are a reliable guide to the future. This is no longer a good assumption since the increasing concentrations of greenhouse gases are expected to cause a significant warming of the global climate in the next century. It is a matter of urgency to refine estimates of future climate conditions to improve these decisions.*"

ARR1987 (Pilgrim Ed., 1987) continues:

"As no reliable estimates of climatic change are available, it has been assumed that the statistical characteristics of heavy rainfall and floods remain constant throughout the design life of projects. This is implied in the use of all of the probability terms in ARR"

Approaches to estimate the impact of climate change on rainfall only became available in Australian Rainfall and Runoff (Australian flood design standard) in 2016 (Ball Et al. (2016) and for Probable Maximum Precipitation (PMP) in 2024 (Ball Et al, 2019). The 2024 update provides additional advice on adjusting antecedent conditions and incorporating these changes into design event modelling.

The choice of the 1% AEP design flood was often justified by its equivalent "lifetime flood exposure risk" which is equal to (approximately) 50% chance of experiencing one or more floods over a typical 70-year life (Pilgrim Ed.(1987), SCARM (2000), Commonwealth of Australia, (2018)). With an assumption of stationarity, lifetime exposure risk is simply calculated using the binomial distribution.

2 BACKGROUND

Lifetime exposure risk is presented in many Australian flood and floodplain management guidelines., including ARR 1987 (Pilgrim Ed. (1987) and SCARM (2000). This includes all versions of the NSW Floodplain Management Manual (NSW Government, 1986, 2001, 2005), and the national guideline (Handbook 7 Managing the Floodplain; Commonwealth of Australia, 2018). Table 1 provides the lifetime exposure risk from NSW Floodplain Development Manual (NSW Government, 2005) which uses a 70-year design life, and Table 2 is based on an 80-year design life in the Handbook 7: Managing the Floodplain (Commonwealth of Australia, 2018). Lifetime exposure to flood risk is considered a better measure than annual risk because it accurately reflects the cumulative probability of experiencing a flood over the duration of home ownership or a lifetime.

The Commonwealth of Australia (2018) updated the design life from 70 to 80 years to accommodate changes in Australian life expectancy (Australian Bureau of Statistics (ABS), 2024). Similar increases in life expectancy have occurred in many western countries (Leon et al, 2019). The examples in this paper are restricted to 70 years as most IPCC and Australian climate change predictions either do not extend past 2099 or are considered too uncertain that their use is discouraged (Ball Et al, 2019).

Under stationary conditions, exposure risk is simple to calculate using the binomial formula; where the probability of n exceedances over y years is for an annual Probability p is:

$$\text{Exposure probability} = p^n * (1-p)^{(y-n)} * \frac{y!}{n!*(y-n)!} \quad (1)$$

For the case of one or more floods this can be reduced to:

$$\text{Exposure probability} = 1 - (1-p)^y \quad (2)$$

Table 1: Lifetime risk exposure table adapted from Floodplain Development Manual (NSW Government, 2005)

Chance of occurrence in any year (ARI/AEP)	Probability of experiencing the given flood in a period of 70 years	
	At least once (%)	At least twice (%)
1 in 10 (10%)	99.9	99.3
1 in 20 (5%)	97.0	86.4
1 in 50 (2%)	75.3	40.8
1 in 100 (1%)	50.3	15.6
1 in 200 (0.5)	29.5	4.9

Table 2: Flood Risk recurrences table adapted from Handbook 7 Managing the Floodplain Best Practice (Commonwealth of Australia, 2018)

Annual Exceedance probability (%)	Approximate Average recurrence interval (years)	Probability of experiencing a given sized flood in an 80 year period	
		At least once (%)	At least twice (%)
20	5	100	100
10	10	99.9	99.8
5	20	98.4	91.4
2	50	80.1	47.7
1	100	55.3	19.1
0.5	200	33.0	6.11
0.2	500	14.8	1.14
0.1	1000	7.69	0.30
0.01	10000	0.80	0.003

The binomial formula (Eq. 1) is simple to calculate with the combinational part of the formula calculating the unique number of ways a fixed number of floods can occur. This can be explained with the example of 10 floods in 70 years when assessing a 1 in 5 AEP level bridge performance over a 70-year design life. There are $3.96*10^{11}$ = (70!/(10!×(70-10)!)) combinations where 10 floods exceeding a specific threshold can occur in 70 years. With fixed probabilities in a stationary climate there is no need to calculate each separately. With climate change, each of the $3.96*10^{11}$ combinations has a unique probability and must be calculated separately to address non stationarity. That is not trivial, as 70 unique probabilities need to be multiplied for each case and summed. To calculate the probability of 10 or more floods one would also need to work out the probabilities for 0 to 9 exceedances. In a stationary climate with fixed probabilities there are 70 unique combinations but with changing probabilities there are 2^{70} ($1.181*10^{21}$) unique combinations.

The Poisson binomial distribution formula is written below:

$$P(Y \leq y) = \sum_{s=0}^{y} \sum_{A \in F_s} \prod_{i \in A} P_i \prod_{i \in A^c} (1-P_i) \quad (3)$$

Where F_s is defined as the set of all subsets of size s that can be chosen from the set $\{1,2 \ldots n\}$, P_i is the probability of failure or exceedance in year i and Y is the number of failures in y years. Where the first sum operator sums the probability of 1 to Y failures, the 2nd sums all the combination of a fixed number of failures, that were identical in the simple binomial case. The two product operators multiply the probability of failures and non failures over y years. This case can be calculated by the Poisson binomial distribution formula. As the direct calculation is numerically intractable, various approximations have been proposed as well as recursive approaches tested to reduce the number of calculations required. For small number of failures the numerical overhead can be improved by multiplying the no failure case in equation 4:

$$\prod_{i=1}^{y}(1-p_i) \tag{4}$$

by the sum of the n cases of the product of the ratio of the failure over the non failure. The formula for the simple case of 2 failures (n=2), where the first failure is i and the second is j becomes:

$$\sum_{i=1}^{y-1}\sum_{j=i+1}^{y}(p_i)*\frac{p_j}{(1-p_i)*(1-p_j)} \tag{5}$$

This reduces the numerical load from 2415 combinations of multiplying 70 probabilities to multiplying 70 probabilities once and multiplying this by the sum of 2415 combinations of 2 probability ratios. This increases speed for small values of n but is still too computationally complex for an online calculator where multiple future scenarios are considered. The numerical overhead can also be reduced by working in log space. The problem is further complicated by the need to sum a very large number of small probabilities together, which if not done carefully can lead to numerical rounding errors.

There are approximation formulas (Hong, 2013), that include very simple approaches based on the mean failure probability, but using an accurate formula was too slow and approximation methods too inaccurate, for a successful online calculator. Hong (2013) and Biscarri et al. (2017) presented accurate, computationally efficient methods based on a Fourier transformation. Hong's approach is available as Python functions (Straka, 2016) and provides exact solutions.

Some Australian design standards require performance over a design life without providing advice on how this should be carried out (for example Ball et al, 2019). Common approaches include design for adequate performance on the last day of the design life or designing for adequate performance at the midpoint of the design life. The geometric mean of the failure probabilities over a given design life can also be used as a more realistic design input if average performance over the design life is required. For the example of a 70 year design life equation 6 gives the geometric mean of the failure probabilities.

$$p = \sqrt[70]{\prod_{i=1}^{70} p_i} \tag{6}$$

Where p is the average risk that will occur across the design life.

3 RISK EXPOSURE TOOL

A lifetime exposure tool was original developed for the Australian climate change calculator (Babister et al. 2024), and has now been generalised for broader application where the user defines the change in probability of failure over time. The tool is available at exposure.wmawater.com.au. Once the

change in future flood risk has been uploaded the user can explore how lifetime exposure changes and compare this to the traditional stationary climate case.

This tool can calculate the change in probability over time from three or more points by fitting a curve through these points. The tool then applies the Poisson binomial formula to the selected design life. Testing found that the change in flood risk under Shared Socioeconomic Pathway (SSP) is well described by a simple 2nd order polynomial (Figure 1). This example is for the 11,500km^2 Hawkesbury Nepean catchment to Penrith in Western Sydney, Australia. Figure 1 shows how smooth probability change curves can be fitted to climate change results for different SSPs. The 2nd order polynomial through data for 2025, 2030, 2050 and 2090 for each SSP is a good approximation of the intermediate decadal values.

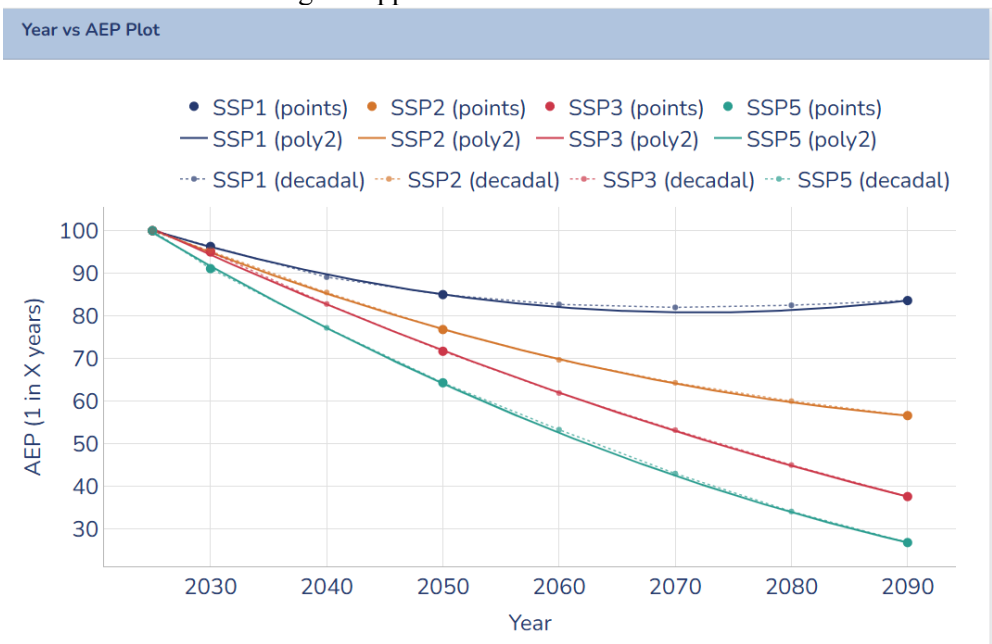

Figure 1: Change in probability of a 2025 1% AEP flow estimate for various SSP – decadal data fitted with 2nd order polynomial

The tool also allows the uses of a piecewise spline or simple linear segment interpolation (Figure 2) for cases where mitigation measures or other works cause more abrupt changes in probability over time. Figure 2 shows the landing page, how future flood risk is uploaded, and fitting method selected along with exposure period.

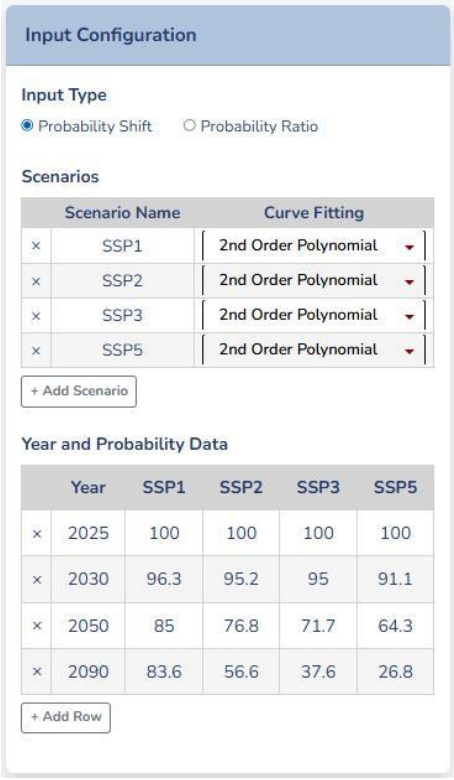

Figure 2: Tool input configuration.

The steps in the tool are:

1. Upload the change in failure risk at discrete intervals (such as SSP2 2030,2050 2090). Up to 4 scenarios can be included. Changes in future flood risk can be uploaded as either probabilities or ratios
2. Fit a smooth relationship so annualised change in risk can be calculated. While a 2nd order polynomial is recommended other options include a piecewise spline or simple linear segment.
3. Fit statistics and graphs are produced to aid in the selection final section of fitting method.
4. Selected the start and finish year for exposure risk calculation.
5. After submitting tabulated and graphic exposure risk is calculated

4 RESULTS

Results are presented for two examples using the current Australian climate change guidance (Ball et al., 2019) for SSP1, SSP2, SSP3 and SSP5. The examples use a 70-year design life. For each example the change in flood probability is shown graphically along with graphs and tables of exposure risk. The two examples are:

1. A development at the 1% AEP level in a catchment with a 24-hour critical storm duration
2. A development at the 1% AEP level in a catchment with a 1-hour critical storm duration

These examples have been selected to show how the exposure risk under current guidance changes more dramatically on catchments with a shorter response time.

Example 1 - For a development built at the 1% AEP level in a catchment with a 24-hour critical storm duration the chance of 1 or more exceedances in the 70-year design life goes from around 50% under historic conditions to approximately 82% in SSP5 (Figure 3 and Table 3).

Example 2 - For a similar development built in a catchment with a 1-hour critical duration at the 1% AEP level the chance of 1 or more exceedances in the 70-year design life goes from around 50% under historic conditions to approximately 99% in SSP5 (Figure 4 and

Table **4**).

When undertaking risk or design life assessment in a non-stationary climate it is common to undertake an assessment at a representative point in the project's life, with the midpoint often being used. The midpoint works well when the rate of change is relatively linear. However, as SSP1 peaks and drops off and SSP5 shows an increasing rate of change in rainfall, a midpoint can be a poor choice. For a 70-year design life on a catchment with a 24-hour critical duration the use of the midpoint produces the following errors, SSP1 and SSP2 overestimate the frequency of events by 5.6% and 3.2%, respectively and SSP3 and SSP5 underestimate the frequency by 2.7% and 2.8% respectively.

5 CONCLUSIONS

Before now, it has not been practical to accurately calculate the exposure risk for reasonable values of n exceedances in non-stationary conditions. Previous solutions to calculating the probability mass function of a Poisson binomial distribution were largely intractable for large values of n. Accurate methods were computationally intensive and approximation methods inaccurate. With new approaches (Hong 2013) it is now practical to calculate exposure risk under climate change. This approach has been built into the Australian Climate Change Calculator (ccc.wmawater.com.au). This allows the tool to calculate the expected number of exceedances in a changing climate and is increasingly important to flood planning in a changing climate.

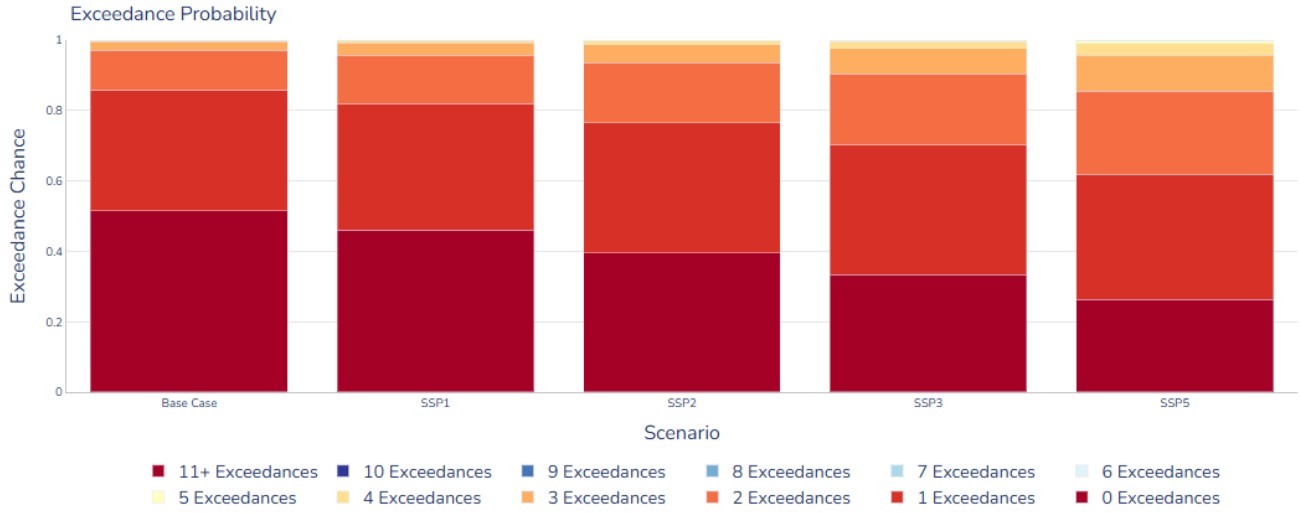

Figure 3: Number of exceedances in a 24-hour catchment over a 70-year design life

Table 3: Exceedance Probability (%) for 24-hour catchment over a 70-year design life

Number of Exceedances	Historic	SSP1	SSP2	SSP3	SSP5
0 Exceedances	49.48	46	40	33	26
1 Exceedance	34.99	36	37	37	36
2 Exceedances	12.19	14	17	20	24
3 Exceedances	2.79	3.5	5.1	7.2	10

4 Exceedances	0.47	0.65	1.1	1.9	3.3
5 Exceedances	0.06	0.096	0.2	0.39	0.82
6 Exceedances	0.01	0.012	0.029	0.066	0.17
7 Exceedances	0.00	0.0012	0.0035	0.0094	0.029
8 Exceedances	0.00	0.0001	0.00036	0.0011	0.0043
9 Exceedances	0.00	7.8E-06	0.000033	0.00012	0.00055
Ten or More	0.00	5.2E-07	2.6E-06	0.000012	0.000063

Figure 4: Number of exceedances in a 1-hour catchment over a 70-year design life

Table 4: Exceedance probability (%) for 1-hour catchment over a 70-year design life

Number of Exceedances	Historic	SSP1	SSP2	SSP3	SSP5
0 Exceedances	49.48	43	32	22	12
1 Exceedances	34.99	37	37	34	26
2 Exceedances	12.19	15	21	26	28
3 Exceedances	2.79	4.2	7.8	13	19
4 Exceedances	0.47	0.85	2.1	4.6	9.5
5 Exceedances	0.06	0.13	0.46	1.3	3.8
6 Exceedances	0.01	0.018	0.082	0.31	1.2
7 Exceedances	0	0.0019	0.012	0.061	0.33
8 Exceedances	0	0.00018	0.0016	0.01	0.075
9 Exceedances	0	0.000015	0.00017	0.0015	0.015
Ten or More	0	0.0000011	0.000017	0.0002	0.0026

REFERENCES

Australian Bureau of Statistics (ABS), (2024) https://www.abs.gov.au/statistics/people/population/life-expectancy/latest-release, [accessed 21 October 2024]

Babister, M., Retallick M, Jamali B, Babister H, Dunning N, Bodenlenz F, (2024) “Impacts of the new ARR climate change factors on flood planning levels”, Floodplain Management Australia Conference Brisbane

Babister, M., Trim, A., Testoni, I. & Retallick, M, (2016) “The Australian Rainfall & Runoff Datahub”, 37th Hydrology and Water Resources Symposium Queenstown NZ

Babister, M., & Barton, C. (Editors), (2012) “Australian Rainfall and Runoff Revision Project 15: Two Dimensional Modelling in Urban and Rural Floodplains- Stage 1&2 Report P15/S1/009”, Engineers Australia

Ball J, Babister M, Nathan R, Weeks W, Weinmann E, Retallick M, Testoni I, (Editors), (2016) “Australian Rainfall and Runoff: A Guide to Flood Estimation Version 4.0”, Commonwealth of Australia, Australia

Ball J, Babister M, Nathan R, Weeks W, Weinmann E, Retallick M, Testoni I, (Editors), (2019) “Australian Rainfall and Runoff: A Guide to Flood Estimation Version 4.2”, Commonwealth of Australia, Australia

Biscarri, W., Zhao, S.D., Brunner R. J., (2018) “A simple and fast method for computing the Poisson binomial distribution function”, Computational Statistics & Data Analysis, Volume 122 pp 92-100.

Cardno (2015), “Australian Rainfall and Runoff Revision Project 20: Risk Assessment and Design life – Stage 3 Report, P20/S3/022”, Commonwealth of Australia

Commonwealth of Australia, (2018) “Australian Disaster Resilience Handbook 7 Managing the Floodplain: A Guide to Best Practice in Flood Risk Management in Australia”, AIDR

Hong, Y., (2013) “On computing the distribution function for the Poisson binomial distribution”, Computational Statistics & Data Analysis, Volume 59, pp 41-51.

International Conference on the Assessment of the Role of Carbon Dioxide and of Other Greenhouse Gases in Climate Variations and Associated Impacts, (1985: Villach, Austria), (1986) “Report of the International Conference on the Assessment of the Role of Carbon Dioxide and of Other Greenhouse Gases in Climate Variations and Associated Impacts, Villach, Austria, 9-15 October 1985” World Meteorological Organisation

Leon, D., Jdanov D., Shkolnikov V, (2019) “Trends in life expectancy and age-specific mortality in England and Wales, 1970–2016, in comparison with a set of 22 high-income countries: an analysis of vital statistics data” The Lancet Public Health Volume 4, Issue 11, November 2019, Pages e575-e582

NSW Government, (1986) “Floodplain Development Manual”

NSW Government (2005) “Floodplain Development Manual: The management of flood liable land”

NSW Government (2001) “Floodplain Management Manual: The management of flood liable land”

Pilgrim, D. H. (Editor in Chief), (1987) “Australian Rainfall and Runoff – A Guide to Flood Estimation”, Institution of Engineers, Australia, Barton, ACT

QLD Department of Energy and Water Supply (2013) “Queensland Urban Drainage Manual” - Third edition

SCARM (2000) “Floodplain Management in Australia: Best Practice Principles and Guidelines.” Agriculture and Resource Management Council of Australia and New Zealand, Standing Committee on Agriculture and Re-source Management (SCARM). Report No 73. CSIRO Publishing

Straka, M., (2016) “Poisson Binomial Distribution for Python”, (https://github.com/tsakim/poibin)

ICFM 10
Adapting to Global Change:
Innovative Approaches to Flood Management and Resilience
May 20-22, 2026 | Western University, London, Ontario, Canada

Uncertainty in Climate Projection Indicators for Flood Risk Assessment of Dam Infrastructure

Jack W. Warden[1], M. Reza Najafi[2] and Hamidreza Shirkhani[3]
Department of Civil and Environmental Engineering, Faculty of Engineering, Western University, London, Ontario, Canada N6A 5B9[1,2]
E-mail: jwarden6@uwo.ca[1]
E-mail: mnajafi7@uwo.ca[2]

National Research Council of Canada, Ottawa, Canada[3]
E-mail: hamidreza.shirkhani@nrc-cnrc.gc.ca[3]

ABSTRACT

Projected changes in extreme precipitation are increasingly considered in dam safety and flood risk assessments, yet substantial uncertainty limits their direct application in engineering practice. This study evaluates climate model uncertainty in precipitation-based indicators relevant to flood impact assessment for dams. Using a multi-model ensemble of dynamically downscaled climate projections under a single emissions scenario, flood-relevant indicators describing extreme magnitude, frequency, and accumulation are derived and analyzed. Uncertainty is quantified as inter-model variability, enabling assessment of confidence in projected changes. Results emphasize the importance of uncertainty-aware interpretation of climate indicators to support robust, climate-informed dam safety evaluations.

KEYWORDS: Climate Change, Flooding, Dam Safety, Infrastructure,

1 INTRODUCTION

Design and safety assessment of dam infrastructure increasingly require consideration of projected changes in extreme precipitation under a changing climate. Climate projections provide critical information for evaluating future flood hazards; however, their direct application in impact assessments is complicated by substantial uncertainty, particularly in metrics relevant to dam safety such as extreme rainfall magnitude and frequency (Fluixá-Sanmartín et al., 2018; IPCC, 2021; Myhre et al., 2019).

For engineering applications, it is not sufficient to identify projected changes alone. Understanding how uncertainty propagates into flood-relevant indicators is essential for interpreting projection reliability and for supporting robust, climate-informed dam design and management decisions (Fluixá-Sanmartín et al., 2018; Ozkan et al., 2023). This research focuses on evaluating climate model uncertainty in precipitation-based indicators used for flood impact assessment, with an emphasis on their relevance to dam safety.

2 CLIMATE DATA AND PROJECTION FRAMEWORK

This study employs a multi-model ensemble of dynamically downscaled regional climate projections evaluated under a single emissions scenario. All simulations are analyzed on a common spatial grid and within a consistent modelling framework to isolate uncertainty arising from climate model structure rather than from scenario differences or internal variability.

Projected changes are assessed across historical and future periods, allowing comparison of baseline and future climate conditions relevant to flood risk. Future periods are based on the use of a Global Warming Levels approach. This approach reflects the structure of many climate datasets commonly used in applied engineering studies and supports direct interpretation of model-driven uncertainty (Bush & Lemmen, 2019; Seneviratne et al., 2016).

3 FLOOD RELEVANT CLIMATE INDICATORS

A suite of precipitation-based climate indicators relevant to dam safety and flood impact assessment is derived from the climate projections. These indicators are selected to reflect key hydrological stressors influencing dam performance, including:

- Magnitude of extreme precipitation events,
- Frequency of threshold exceedance,
- Accumulation-based metrics associated with flood generation.

Indicator selection and formulation are informed by established climate-impact frameworks and dam safety literature, including CLIMDEX-based indices and extreme-event metrics commonly used in infrastructure assessments (ETCCDI, n.d.; Fluixá-Sanmartín et al., 2018; Myhre et al., 2019). Indicators are computed consistently across all models to ensure comparability of projected changes and associated uncertainty.

4 QUANTIFICATION OF MODEL UNCERTAINTY

Uncertainty in projected changes is quantified as inter-model variability across the ensemble of climate projections. For each indicator, uncertainty is evaluated using variance-based metrics that characterize the spread of model responses relative to the ensemble mean, providing a direct measure of confidence in the projected signal (Ozkan et al., 2023; Schwarzwald & Lenssen, 2022).

By focusing exclusively on climate model structural uncertainty, this analysis provides a clear assessment of how differences in model formulation and physical representation influence projected changes in flood-relevant indicators. This targeted focus avoids conflating uncertainty sources and enables transparent interpretation of projection confidence for impact assessment purposes, consistent with current engineering-facing climate analyses (Fluixá-Sanmartín et al., 2018; Seneviratne et al., 2016).

5 APPLICATION TO DAM SAFETY AND FLOOD RISK DECISION MAKING

The quantified uncertainty in climate indicators is evaluated in the context of dam safety and flood impact assessment. Results highlight how model uncertainty varies across indicators and spatial domains, influencing confidence in projected changes relevant to design thresholds and operational decision-making (Bush & Lemmen, 2019; Ozkan et al., 2023).

Rather than prescribing deterministic future values, this work emphasizes uncertainty-aware interpretation of climate projections. By identifying indicators with relatively robust signals versus those dominated by model spread, the analysis supports more defensible use of climate information in dam safety evaluations.

To facilitate exploration and interpretation of results, the indicator calculations and uncertainty metrics are implemented within a web-based interface, which is currently in development. The tool

functions as a visualization and analysis platform, allowing users to interactively examine projected changes and associated uncertainty across indicators and locations. The scientific analysis, however, remains independent of the delivery mechanism.

6 CONCLUSIONS AND FUTURE WORK

This research presents a structured assessment of climate model uncertainty in flood-relevant precipitation indicators used for dam impact assessment. By centering on indicators, projections, and uncertainty quantification, the work advances scientific understanding of how climate projection uncertainty affects flood resilience evaluations for dam infrastructure. This work has let to the development of a comprehensive dataset of indicator projections, along with their associated uncertainties. This data will provide a valuable resource to practitioners working with dams, allowing them to assess potential risks through the interface currently under development.

Future work will extend this framework to additional indicators and uncertainty sources, including emissions scenario uncertainty and internal climate variability, to support more comprehensive climate-informed dam safety assessments.

7 ACKNOWLEDGEMENTS

The authors acknowledge the support from the Climate Resilient Built Environment initiative of the National Research Council Canada for this study

REFERENCES

Bush, E., & Lemmen, D. S. (2019). *Canada's Changing Climate Report*. Government of Canada.

ETCCDI. (n.d.). *Climdex*. Retrieved March 10, 2025, from https://www.climdex.org/

Fluixá-Sanmartín, J., Altarejos-García, L., Morales-Torres, A., & Escuder-Bueno, I. (2018). Review article: Climate change impacts on dam safety. *Natural Hazards and Earth System Sciences*, *18*(9), 2471–2488. https://doi.org/10.5194/nhess-18-2471-2018

Intergovernmental Panel On Climate Change. (2021). *Climate Change 2021 – The Physical Science Basis: Working Group I Contribution to the Sixth Assessment Report of the Intergovernmental Panel on Climate Change* (1st ed.). Cambridge University Press. https://doi.org/10.1017/9781009157896

Myhre, G., Alterskjær, K., Stjern, C. W., Hodnebrog, Ø., Marelle, L., Samset, B. H., Sillmann, J., Schaller, N., Fischer, E., Schulz, M., & Stohl, A. (2019). Frequency of extreme precipitation increases extensively with event rareness under global warming. *Scientific Reports*, *9*(1), 16063. https://doi.org/10.1038/s41598-019-52277-4

Ozkan, I., Kadhom, B., Roshani, E., Shirkhani, H., Hiedra-Cobo, J., Cusson, D., & Nkinamubanzi, P.-C. (2023). *Adaptation of dams to climate change: Gap analysis* (p. 194 p.). National Research Council of Canada. Construction Research Centre. https://doi.org/10.4224/40002994

Schwarzwald, K., & Lenssen, N. (2022). The importance of internal climate variability in climate impact projections. *Proceedings of the National Academy of Sciences*, *119*(42), e2208095119. https://doi.org/10.1073/pnas.2208095119

Seneviratne, S. I., Donat, M. G., Pitman, A. J., Knutti, R., & Wilby, R. L. (2016). Allowable CO2 emissions based on regional and impact-related climate targets. *Nature*, *529*(7587), Article 7587. https://doi.org/10.1038/nature16542

ICFM 10
Adapting to Global Change:
Innovative Approaches to Flood Management and Resilience
May 20-22, 2026 | Western University, London, Ontario, Canada

Enhancing Flood Management in Canada: Leveraging SAR and AI for Improved Emergency Flood Mapping

Nicolas Desrochers[1], Fatemeh Esfahani[2], Mathieu Turgeon-Pelchat[3], Hospice Houngbo[4], Nicolas Svacina[1], Zarrin Langari[4], Simon Tolszczuk-Leclerc[1]

Canadian Center for Remote Sensing, Natural Resources Canada, Ottawa, Canada[1]
E-mail: Nicolas.desrochers@nrcan-rncan.gc.ca; nicolas.svacina@nrcan-rncan.gc.ca; simon.tolszczuk-leclerc@nrcan-rncan.gc.ca.

Canadian Forest Service, Natural Resources Canada, Victoria, Canada[2]
E-mail: fatemeh.esfahani@nrcan-rncan.gc.ca

Geobase, Natural Resources Canada, Sherbrooke, Canada[3]
E-mail: mathieu.turgeon-pelchat@nrcan-rncan.gc.ca

Digital Accelerator, Natural Resources Canada, Ottawa, Canada[4]
E-mail: hospice.houngbo@nrcan-rncan.gc.ca; zarrin.langari@nrcan-rncan.gc.ca

ABSTRACT

Floods are among Canada's most frequent natural disasters, leading to significant infrastructure damage and economic loss. This paper presents a proof of concept that convolutional neural networks (CNNs) can be effectively trained using historical flood product data from Natural Resources Canada's Emergency Geomatics Service (EGS) to enhance flood mapping accuracy and reduce processing time. Utilizing a subset of RADARSAT Constellation Mission (RCM) imagery, combined with auxiliary data such as Local Incidence Angle, land cover, and historical surface water occurrence, we conduct experiments to assess their impact on the model's performance. The baseline CNN model, using only the RCM backscatter bands, showed strong detection capabilities for open water with precision and recall values reaching 0.97 and 0.98, respectively. In contrast, incorporation of the Local Incidence Angle and land cover data improved recall and overall classification performance for flooded vegetation while demonstrating the limitations of water frequency data. Based on the obtained results, the model that included Local Incidence Angle was selected as the best-performing model for training on the entire dataset, as it achieved a better F1-score for flooded vegetation while maintaining strong performance for open water. A comparison between the CNN model trained on the entire dataset and EGS's unedited flood product reveals similar F1-scores, with the CNN model achieving higher precision and requiring less manual editing. This study outlines the potential for automated flood mapping systems that enable efficient flood product generation for emergency response efforts in Canada. Future work will focus on expanding the dataset to include diverse landscapes and exploring the use of Compact Polarimetry SAR data for improved classification accuracy.

KEYWORDS: SAR, Floods, Mapping, CNN, RCM, Near-Real Time, Emergency

1 INTRODUCTION

Floods represent one of Canada's most frequent and costly natural disasters, causing substantial damage to infrastructure and disruption to supply chains across Canada (Public Safety Canada, 2023). The Bank of Canada has identified flood risk as a growing concern, noting that flooding is expected to cause approximately $2 billion in structural damages to residential properties per year on average (Johnston et al., 2024). Rapidly rising waters, flash floods, and ice-jam flooding can wash out roads and bridges, isolate communities, disrupt essential services, and threaten public safety. In the initial hours to days of a flood event, emergency responders require current, map-based situational awareness to prioritize evacuations, maintain access to hospitals and supply routes, protect critical infrastructure (such as water and wastewater treatment plants or electrical substations), and coordinate road closures and rescue operations (Oddo & Bolten, 2019). However, timely field information is often lacking, as on-the-ground reports are sparse, and flood conditions evolve swiftly. Near-real-time mapping of flood extent mapping is therefore critical to support effective decision-making.

Earth observation satellites, particularly those equipped with synthetic aperture radar (SAR), have enabled near-real-time flood mapping for decades (Huang et al., 2018; Martinis et al., 2009; Mason et al., 2012; Matgen et al., 2007; Mohamadiazar et al., 2024). SAR technology is especially valued for its ability to collect imagery day or night and through clouds and precipitation. Furthermore, the SAR signal exhibits characteristically low backscatter over smooth surfaces with high dielectric constants, such as open water, due to specular reflection away from the sensor (Henderson & Lewis, 2008). This enhances contrast with the surrounding land making it efficient at delineating open water floods. In contrast, flooded vegetation often produces elevated backscatter due to double-bounce scattering between the water surface and vertical vegetation structure, increasing contrast relative to non-flooded vegetation (Hess et al., 2003). However, automatic and semi-automatic approaches to detect flooded vegetation can misclassify other high intensity backscattering landcover types, such as urban area, for flooded vegetation (Pierdicca et al., 2018).

For over twenty years, Natural Resources Canada's Emergency Geomatics Service (EGS) has delivered SAR-based flood mapping anywhere in Canada, building a substantial archive of historic flood maps using semi-automated classification approaches. While current EGS workflows can delineate open water and flooded vegetation, extensive manual quality control and editing are often required before publication, limiting the speed of response during large or concurrent flood events. Convolutional neural networks (CNNs) have emerged as a promising approach to fully automating flood mapping (Bentivoglio et al., 2022). CNNs can learn contextual patterns across polarimetric SAR channels and have shown great capability at delineating open water floods. Multiple studies have reported F1-scores of approximately 0.9 for open water delineation using CNN-based flood mapping models trained on SAR data (e.g., Andrew et al., 2023; Nemni et al., 2020). Flooded vegetation has also been mapped successfully with a CNN model trained on Sentinel-1 data achieving strong performance(F1-Score of 0.85; Tavus et al., 2022).

The present study evaluates a proof of concept that using CNN models trained on RADARSAT Constellation Mission (RCM) imagery and archived EGS flood products would increase accuracy and reduce processing time of flood mapping at a national scale. The impact of incorporating auxiliary data on improving the detection of flooded vegetation is also evaluated for CNN-based flood mapping. Multiple training scenarios were constructed using archived EGS-labelled events from floods across Canada, with auxiliary inputs designed to mitigate common

mapping errors: local incidence angle from RCM, 2020 NALCMS land cover data, and the JRC Global Surface Water dataset (Pekel et al., 2016). The contributions of this work are twofold: (i) evaluate the use of auxiliary data to increase delineation accuracy of open water and flooded vegetation from a CNN model; and (ii) to demonstrate that a CNN trained on RCM and EGS inputs can maintain or improve mapping accuracy for open water and flooded vegetation while reducing operator intervention.

2 DATA AND METHODOLOGY

This study utilized multiple geospatial datasets for model training with RCM as the primary remote sensing data source. The dataset consists of 61 Analysis Ready Data (ARD; Charbonneau et al., 2024) images of HH and HV polarisation (figures 1-a and 1-b), along with the corresponding EGS flood product used as labels for model training and testing (figure 1-c), distributed across three areas of interest. The ARD format ensures that the imagery has undergone standardized radiometric and geometric preprocessing, allowing for consistent comparison across dates and locations. Local incidence (figure 1-d), which is a byproduct of the ARD processing, angle information from RCM was also used to correct for backscatter variations due to topography and sensor geometry. Land cover (figure 1-e) information was derived from the North American Continuous Landcover Map (CEC, 2025), providing detailed classification of surface types such as forest, urban, agriculture, and wetlands. This dataset enabled the identification of areas susceptible to flooding and improved the interpretation of SAR backscatter signals. In addition, the Pekel global water frequency dataset (figure 1-f) (Pekel et al., 2016) was employed to account for historical surface water dynamics. This dataset provides the long-term occurrence of surface water at high spatial resolution and was used to distinguish permanent water bodies from transient flood events.

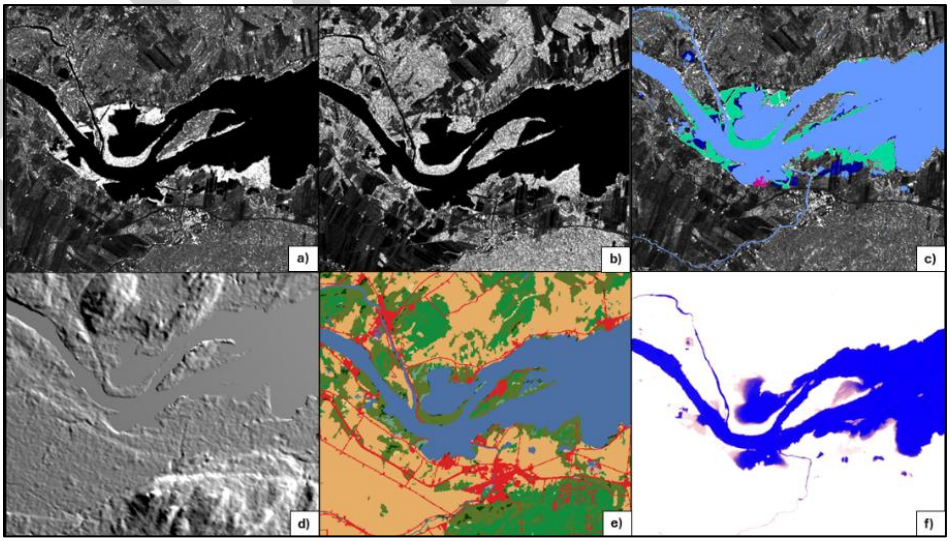

Figure 1: Examples of the six datasets used in this study, shown over the town of Rigaud along the Ottawa River: a) RCM-ARD HH, b) RCM-ARD HV, c) EGS flood labels, d) Local incidence angle, e) NACLM 2020, f) Pekel's global water frequency.

A preprocessing workflow was implemented prior to training to ensure correct matching between RCM ARD imagery and flood labels, as well as to harmonize all auxiliary datasets with the RCM data in terms of projection, spatial resolution, and spatial alignment. The workflow

involved several key preprocessing steps. First, the RCM ARD data was matched with the corresponding EGS flood files, and the boundaries of the RCM ARD products were aligned with those of the EGS datasets. Issues identified in the edited EGS labels were corrected to ensure consistency and accuracy. Next, the auxiliary datasets—including land cover and water frequency—were clipped and reprojected to match the spatial extent and projection of the RCM ARD rasters. The HH and HV backscatter values were then converted to decibels (dB), after which the HH/HV polarisations were stacked together with the user-defined selection of auxiliary layers. Finally, a new geopackage (GPKG) file was created for each flood shapefile to structure and organize the outputs.

As for the EGS flood products, the methodology involves a semi-automated thresholding classification approach using Random Forest. This technique automatically identifies threshold pixel values for open water and subsequently employs region growing to detect flooded vegetation, using a manually specified value for flooded vegetation. After this step, a manual editing process is required, which can take between 1 and 2.5 hours, to enhance the product's accuracy to a level suitable for publication. Two versions of this dataset are used in the study. First, the publish version (manually edited) is used as training and testing labels. Second, an unedited version, generated by the semi-automated EGS workflow prior to the time-consuming manual editing step, is used for comparison with the CNN model trained on the full dataset, allowing for unbiased comparison of the two approaches.

Model development was conducted using the NRCan Geo-Deep Learning (GDL) repository, with minor adjustments applied as required (Natural Resources Canada, 2025). GDL provides a unified framework for applying deep learning to multi-sensor Earth observation data. Using PyTorch Lightning as its foundation, it combines a modular model architecture with flexible data ingestion tools to support tasks such as segmentation, detection, and regression. GDL incorporates established and emerging model families, scalable WebDataset-based training, and comprehensive experiment tracking, offering researchers a practical platform for building and evaluating geospatial deep learning workflows. Its ability to integrate heterogeneous auxiliary inputs—such as SAR polarimetry, landcover, DEM derivatives, or hydrological layers—makes it particularly well suited for flood mapping, where combining complementary sensor modalities is critical for capturing inundation under cloud cover, variable surface conditions, and rapidly evolving hydrological dynamics.

As shown on **Error! Reference source not found.** and Figure 3, the model is organized into three main components: Tiling, Training, and Inference. GDL uses a reference file to organize the input data for each workflow. This file lists all imagery and labels and assigns each item to a specific split—training (*trn*), testing (*tst*), validation (*val*) or inference. Because satellite images are typically very large, GDL's Tiling module divides them into smaller, uniformly sized tiles. These tiles are automatically grouped into *trn*, *val*, and *tst* sets, which are then passed directly to the Training module.

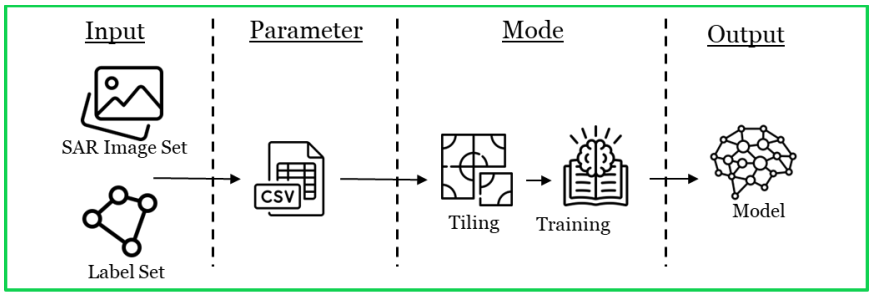

Figure 2: Diagram of GDL training Pipeline

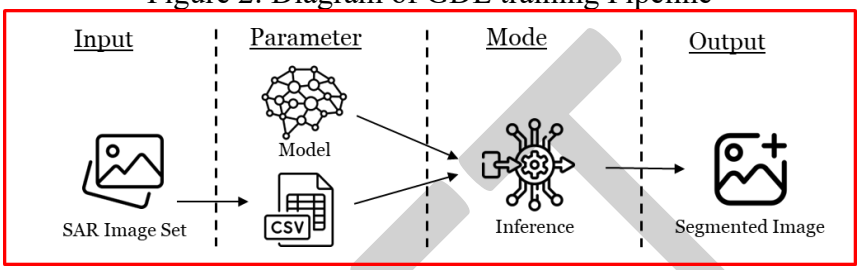

Figure 3: Diagram of GDL inference pipeline

The Training module allows segmentation models to learn from the tiled data under user-defined hyperparameters. After each epoch, validation loss is computed, and the model with the lowest validation loss is retained. Upon completion of training, this model is evaluated on the independent *tst* tiles. The final trained model is then applied to new imagery to generate pixel-level class predictions, such as Open Water and Flooded Vegetation.

GDL provides multiple options for tailoring the training process. Several loss functions are implemented, including Cross-Entropy, Lovász, Focal, and Dice losses. We additionally implemented a Tversky loss function in PyTorch and verified its compatibility with GDL. To mitigate class imbalance, GDL supports class weighting, enabling higher penalties for misclassification of minority classes. The framework also supports various optimizers and learning-rate schedulers (e.g., SGD, Adam, Adabound), which may be tuned via learning rate, weight decay, step size, and gamma. Standard data-augmentation operations (e.g., random flipping and rotation) are applied to RCM ARD tiles during training.

GDL also computes standard performance metrics for image segmentation, including precision, recall, F1-score, and Intersection over Union (IoU), which are evaluated on test tiles and inference results. In addition, it calculates non-background IoU for all water-related classes, providing a measure of how accurately the model reproduces flood inundation maps relative to the EGS products (Zhang et al., 2015).

To evaluate the contribution of each auxiliary dataset, first experiment was conducted, using a subset of the available data, in which models were trained by adding each auxiliary variable individually. In all cases, the RCM HH and HV data were used along with the corresponding EGS edited labels. A baseline scenario was first established using only the RCM data, providing a reference against which the impact of each auxiliary dataset could be assessed. Subsequent scenarios incorporated a single auxiliary variable at a time to isolate its individual effect. Testing was done on a single image from the Upper Saint Lawrence River where each model ran 5 times and metrics were compiled. A model was then trained with the whole dataset using the best performing auxiliary data and testing images metrics were compared with the corresponding unedited EGS flood product.

3 RESULTS AND DISCUSSION

The results of this study demonstrate that the inclusion of auxiliary datasets—local incidence angle, land cover, and historical surface water occurrence—consistently improved the performance of CNN-based flood mapping over the baseline model which uses RCM ARD imagery only. The first experiment was designed to quantify the performance differences associated with each auxiliary dataset.

As shown on Figure 4, the baseline model, utilizing only RCM HH and HV polarisations, showed robust performance in detecting open water areas. Precision and recall for the open water class averaged 0.97 and 0.98 respectively, with F1-scores above 0.97 and IoU of over 0.95. Furthermore, adding auxiliary data did improve the classification of open water but not significantly. The variation in precision between all models does not exceed 0.01 on average. Slight increase (0.01-0.06) in recall can be observed with the addition of any of the auxiliary data separately, with Local Incidence Angle being most notable. This could be attributed to false positives being removed from dark pixels in shadow areas of various terrain features.

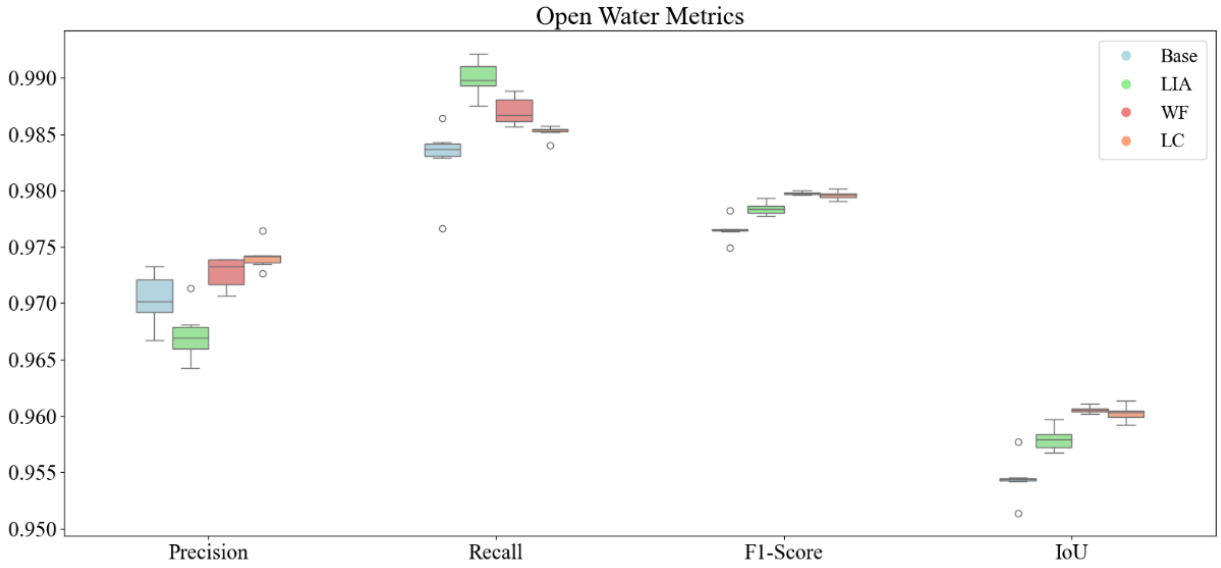

Figure 4: Precision, Recall, F1-Score and IoU metric results from open water classification.

As for flooded vegetation (Figure 5), results are more variable. Precision improves slightly on average when incorporating the local incidence angle and landcover layers, whereas water frequency degrades performance. Recall increases by approximately 0.2 on average with both local incidence angle and land cover. Overall, local incidence angle and landcover show improve F1-score and IoU, with the former showing the best performance.

Incorporating NALCMS land cover provided contextual cues, allowing the model to better differentiate vegetated areas from urban, agricultural, and wetland surfaces. Adding local incidence angle data allowed the model to account for backscatter variation due to topography and sensor geometry, which reduced confusion between terrain-induced brightness and actual flood signals, particularly on slopes or heterogeneous terrain.

Water frequency shows recall comparable to the baseline model and does not improve overall performance. This could be explained by the fact that water frequency is highly correlated with permanent water boundaries and does not capture the dynamic extent of flood events.

Consequently, it provides little additional information for identifying flooded areas and does not reflect the transient vegetation changes associated with floods. In other words, its similarity to existing permanent water masks limits its effectiveness as an auxiliary input for flood detection or flood-vegetation analysis.

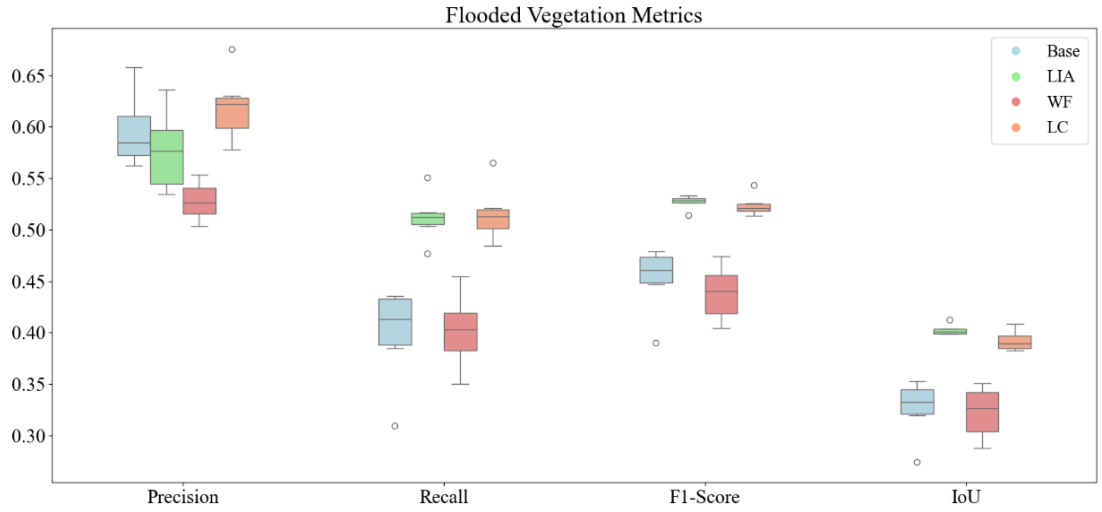

Figure 5: Precision, Recall, F1-Score and IoU metric results from flooded vegetation classifications.

Based on the results of the first experiment, the local incidence angle was selected as the best performing auxiliary data, since it resulted in the highest F1-Score for flooded vegetation class while maintaining reasonable performance for open water. The final CNN model was then trained on the full dataset. Figure 6 and Figure 7 shows the metrics comparison between the CNN model's predictions and the unedited labels obtained by the EGS model for open water and flooded vegetation, respectively. For each comparison, the metrics were calculated on the 10 testing scenes for which unedited EGS flood data were available, as such data were obtainable for only 10 of the 17 test images due to lost data.. The edited EGS products were used as ground truth labels.

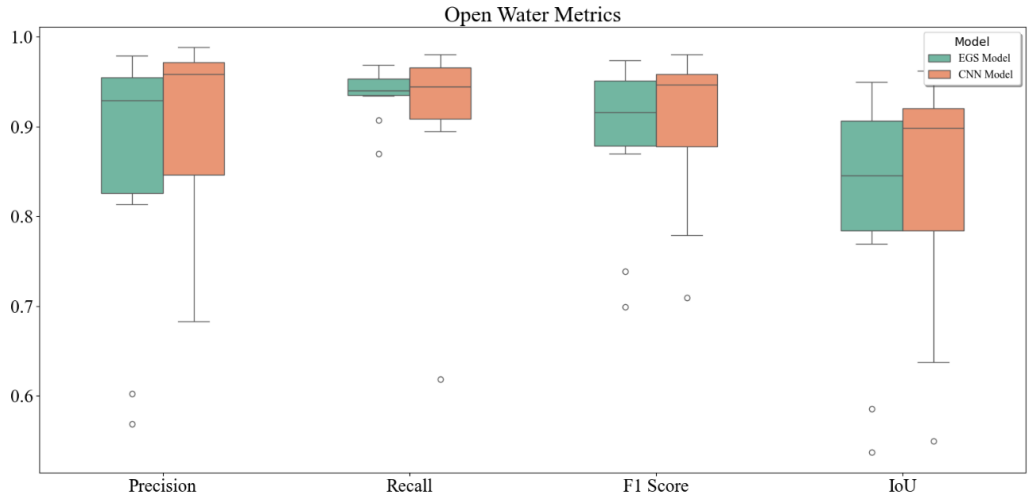

Figure 6: Comparison of open water detection performance between the CNN and EGS models across 10 test scenes.

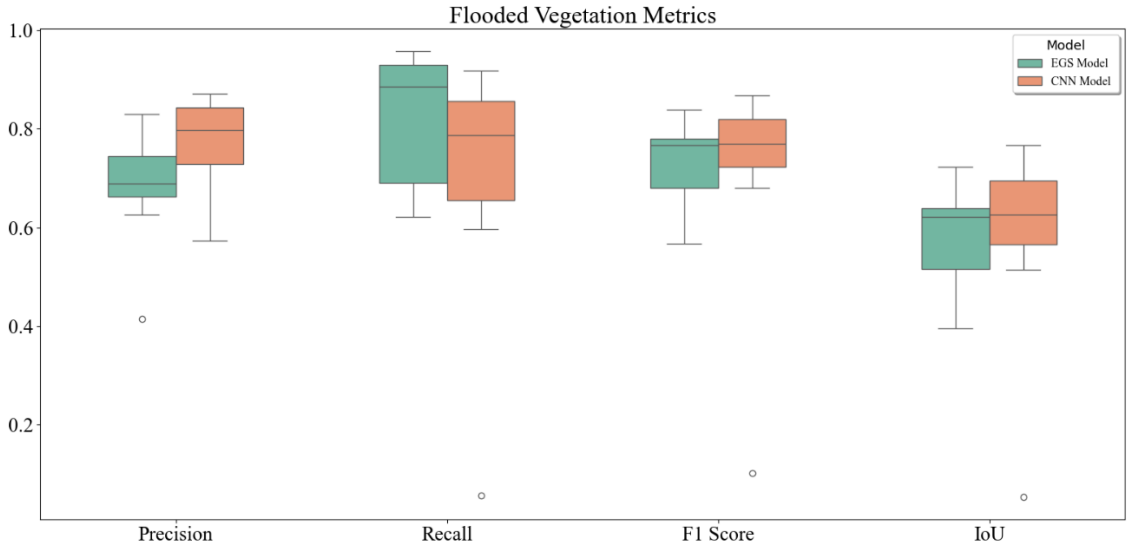

Figure 7: Comparison of flooded vegetation detection performance between the CNN and EGS models across 10 test scenes.

The metrics for open water detection are comparable for both models, with the CNN model demonstrating a slight advantage evidenced by higher precision, F1-score, and IoU values. Visual inspection indicates that the increased precision of the CNN model is due to its reduced classification of cropland as open water compared to the EGS method. This distinction contributes to the CNN's slightly improved F1-score and IoU. Overall, these results suggest that the fully trained CNN model effectively replicates the initial accuracy of the EGS workflow.

As for flooded vegetation, the CNN model shows a significant increase in Precision while the EGS model shows better recall values. The high recall of the EGS unedited layer is unsurprising since most of the manual editing is about removing false positives and not adding area that appeared as false negatives. A visual inspection reveals that most false negatives occur

from reduced extent of existing flooded vegetation areas rather than complete omissions of said areas. As such, the current CNN model appears to be more conservative than the current EGS workflow although with a higher degree of precision. Both these metrics contributed to an overall similar F1-Score and IoU which, once again, indicate that the CNN model is in line with the initial accuracy of the EGS workflow.

It is worth noting that the model was trained with only a relatively small portion of EGS products. Since the launch of RCM, EGS has mapped floods over 198 scenes in 13 different regions across Canada. Of that total, only 61 over three regions were used to train this specific model. As with most CNN models, adding more data from different regions to the model could lead to a more accurate classification and also reduce the risk of overfitting. Furthermore, although EGS is confident in the accuracy of its product, some classification errors still occur and may affect training and inference performance metrics. Moreover, classification performance across the incidence angle range of an RCM acquisition (near- to far-range) has not been explicitly assessed and may affect flood detection accuracy within a scene. However, once trained, the CNN model requires significantly fewer inputs than the current EGS pipeline, which requires manual selection of open water and flooded vegetation threshold values. This represents a major advantage for programming a fully automated flood mapping sequence, particularly in a cloud environment. The elimination of these input requirements positions EGS towards achieving a completely automated system, enabling any user to seamlessly order flood products for any RCM scene as a value-added offering in relatively near future.

4 CONCLUSION

The study aimed to explore the proof of concept that a CNN flood mapping model can be trained using EGS flood product data to achieve a comparable level of accuracy. To do so, a first experiment tested the use of various auxiliary data using a subset of the dataset. Then a model was trained using all the dataset and the predictions were compared with EGS unedited flood product.

In the first experiment. the baseline model, using only RCM HH and HV polarisations, achieved strong detection of open water areas with precision and recall values of 0.97 and 0.98, respectively. While auxiliary data improved classification slightly, the Local Incidence Angle significantly enhanced recall by reducing false positives in shadowed terrain. For flooded vegetation, the Local Incidence Angle and land cover layers improved both precision and recall, resulting in better F1-scores and IoU. The NALCMS land cover provided essential context for distinguishing vegetation types, while the Local Incidence Angle allowed the model to account for backscatter variation driven by local geometry. In contrast, water frequency data showed limited effectiveness due to its strong correlation with permanent water boundaries, restricting its ability to capture dynamic flood events. A comparison between the fully trained CNN model's predictions and the EGS unedited flood product reveals similar F1-scores; however, the CNN model demonstrates a higher overall precision and a lower recall. This indicates that the CNN model is currently more conservative than the EGS flood product but potentially requires less editing to achieve publishing accuracy.

Following this initial experiment, the next step of the project is to build and test the concept of operations as it relates to the use of the CNN model during an emergency flood mapping activation. At this stage, a time comparison between the EGS workflow and the CNN model will be conducted. Further model development is also under way to test other model architecture, such as diffusion models, and train the model with a bigger dataset that covers other types of landscapes in Canada in order to improve the accuracy before starting testing in an actual emergency flood

mapping situation. It is still uncertain whether these improvements will be operational for the upcoming 2026 flood season. Other areas of further development include the use of RCM Compact Polarimetry data, where additional information on the SAR signal could help discriminate the different classes.

REFERENCES

Andrew, O., Apan, A., Paudyal, D. R., & Perera, K. (2023). Convolutional Neural Network-Based Deep Learning Approach for Automatic Flood Mapping Using NovaSAR-1 and Sentinel-1 Data. *ISPRS International Journal of Geo-Information*, *12*(5), 194. https://doi.org/10.3390/ijgi12050194

Bentivoglio, R., Isufi, E., Jonkman, S. N., & Taormina, R. (2022). Deep learning methods for flood mapping: A review of existing applications and future research directions. *Hydrology and Earth System Sciences*, *26*(16), 4345–4378. https://doi.org/10.5194/hess-26-4345-2022

Canada, P. S. (2023, May 11). *Backgrounder: Floods*. https://www.publicsafety.gc.ca/cnt/mrgnc-mngmnt/ntnl-rsk-prfl/bckgrndr-flds-en.aspx

Charbonneau, F., Rosenqvist, A., Truckenbrodt, J., Albinet, C., Small, D., Chapman, B., Zebker, H., Zhou, Z.-S., Brancato, V., Dadamia, D., Deschamps, B., Hajduch, G., Kellndorfer, J., Lavalle, M., Lewis, A., Logan, T., Meyer, F., Miranda, N., Pinheiro, M., … Yuan, F. (2024, July 23). *CEOS Analysis Ready Data Product Family Specification: Synthetic Aperture Radar. Version 1.1* [Other]. Committee on Earth Observation Satellites (CEOS). https://ceos.org/ard/files/PFS/SAR/v1.1/CEOS-ARD_PFS_Synthetic_Aperture_Radar_v1.1.pdf

Commission For Environmental Cooperation. (2025). *NALCMS: The North American Land Change Monitoring System—A trinational collaboration of more than 21 million square kilometers* (p. 50). Commission for Environmental Cooperation. https://www.cec.org/files/pulications/cec_nalcms-en_final.pdf

Henderson, F. M., & Lewis, A. J. (2008). Radar detection of wetland ecosystems: A review. *International Journal of Remote Sensing*, *29*(20), 5809–5835. https://doi.org/10.1080/01431160801958405

Hess, L. L., Melack, J. M., Novo, E. M. L. M., Barbosa, C. C. F., & Gastil, M. (2003). Dual-season mapping of wetland inundation and vegetation for the central Amazon basin. *Remote Sensing of*

Environment, Large Scale Biosphere Atmosphere Experiment in Amazonia, *87*(4), 404–428. https://doi.org/10.1016/j.rse.2003.04.001

Huang, X., Wang, C., & Li, Z. (2018). A near real-time flood-mapping approach by integrating social media and post-event satellite imagery. *Annals of GIS*, *24*(2), 113–123. https://doi.org/10.1080/19475683.2018.1450787

Johnston, C., Vallée, G., Hosseini Jebeli, H., Molico, M., Tremblay, M.-C., & Witts, A. (2024, January 15). *Flood risk and residential lending*. Bankofcanada.Ca. https://www.bankofcanada.ca/2024/01/flood-risk-and-residential-lending/

Martinis, S., Twele, A., & Voigt, S. (2009). Towards operational near real-time flood detection using a split-based automatic thresholding procedure on high resolution TerraSAR-X data. *Natural Hazards and Earth System Sciences*, *9*(2), 303–314. https://doi.org/10.5194/nhess-9-303-2009

Mason, D. C., Davenport, I. J., Neal, J. C., Schumann, G. J.-P., & Bates, P. D. (2012). Near Real-Time Flood Detection in Urban and Rural Areas Using High-Resolution Synthetic Aperture Radar Images. *IEEE Transactions on Geoscience and Remote Sensing*, *50*(8), 3041–3052. https://doi.org/10.1109/TGRS.2011.2178030

Matgen, P., Schumann, G., Henry, J.-B., Hoffmann, L., & Pfister, L. (2007). Integration of SAR-derived river inundation areas, high-precision topographic data and a river flow model toward near real-time flood management. *International Journal of Applied Earth Observation and Geoinformation*, *9*(3), 247–263. https://doi.org/10.1016/j.jag.2006.03.003

Mohamadiazar, N., Ebrahimian, A., & Hosseiny, H. (2024). *Near Real-Time Flood Inundation Prediction Using Sentinel-1 Imagery and Deep Learning*. 824–834. https://doi.org/10.1061/9780784485477.073

Natural Resources Canada. (2025). *Geo Deep Learning* (Version 1.1.0) [Computer software]. https://github.com/NRCan/geo-deep-learning

Nemni, E., Bullock, J., Belabbes, S., & Bromley, L. (2020). Fully Convolutional Neural Network for Rapid Flood Segmentation in Synthetic Aperture Radar Imagery. *Remote Sensing*, *12*(16), 2532. https://doi.org/10.3390/rs12162532

Oddo, P. C., & Bolten, J. D. (2019). The Value of Near Real-Time Earth Observations for Improved Flood Disaster Response. *Frontiers in Environmental Science*, *7*. https://doi.org/10.3389/fenvs.2019.00127

Pekel, J.-F., Cottam, A., Gorelick, N., & Belward, A. S. (2016). High-resolution mapping of global surface water and its long-term changes. *Nature*, *540*(7633), 418–422. https://doi.org/10.1038/nature20584

Pierdicca, N., Pulvirenti, L., & Chini, M. (2018). Flood Mapping in Vegetated and Urban Areas and Other Challenges: Models and Methods. In A. Refice, A. D'Addabbo, & D. Capolongo (Eds.), *Flood*

Monitoring through Remote Sensing (pp. 135–179). Springer International Publishing. https://doi.org/10.1007/978-3-319-63959-8_7

Tavus, B., Can, R., & Kocaman, S. (2022). A Cnn-based flood mapping approach using sentinel-1 data. *ISPRS Annals of the Photogrammetry, Remote Sensing and Spatial Information Sciences*, *V-3–2022*, 549–556. https://doi.org/10.5194/isprs-Annals-V-3-2022-549-2022

Zhang, X., Feng, X., Xiao, P., He, G., & Zhu, L. (2015). Segmentation quality evaluation using region-based precision and recall measures for remote sensing images. *ISPRS Journal of Photogrammetry and Remote Sensing*, *102*, 73–84. https://doi.org/10.1016/j.isprsjprs.2015.01.009

ICFM 10
Adapting to Global Change:
Innovative Approaches to Flood Management and Resilience
May 20-22, 2026 | Western University, London, Ontario, Canada

Assessing Flood Risk in the Lower Reaches of the Red-Assiniboine River under a Changing Climate

Yongbo Liu[1,4], Yonas Dibike[2], Rajesh Shrestha[3], Prasad Daggupati[4]
Climate Modelling Division, Environment and Climate Change Canada, Burlington, ON, Canada[1]
E-mail: Yongbo.Liu@ec.gc.ca
Watershed Hydrology and Ecology Research Division, Environment and Climate Change Canada, Victoria, BC, Canada[2]
Email: Yonas.Dibike@ec.gc.ca
Climate Research Division, Environment and Climate Change Canada, Victoria, BC, Canada[3]
E-mail: Shrestha.Rajesh@ec.gc.ca
School of Engineering, University of Guelph, Guelph, ON, Canada[4]
E-mail: Pdaggupa@uoguelph.ca

ABSTRACT

The impacts of projected climate change on flood risk in the lower reaches of the Red River in Manitoba, Canada, were investigated using the Soil and Water Assessment Tool (SWAT) with the current land management practices. Climate change scenarios were constructed based on seven global climate models (GCMs) and two shared socioeconomic pathways (SSP-245 and SSP-585). The impact of climate change at four global warming levels (GWLs) of 1.5 °C, 2 °C, 2.5 °C, and 3 °C above the pre-industrial level on flow and flood risk at three control stations was assessed. Compared with the 1980–2010 reference period, the ensemble means of the fourteen climate change scenarios indicate increases in annual flow and flood peaks at the 1.5 °C, 2 °C, and 2.5 °C GWLs, followed by a decrease at the 3 °C GWL. Relatively higher increases in the simulated flow were projected during the winter and spring snowmelt periods. This underscores the need to update flood management strategies to address combined snowmelt–rainfall flooding under a warming climate.

KEYWORDS: Flood risk, Climate change, SWAT model, Red and Assiniboine Rivers

1 INTRODUCTION

Flooding is a severe natural hazard in the Red and Assiniboine Rivers due to flat terrain, snowmelt, and extreme precipitation. Major floods in the Red River Basin (RRB) occurred in 1826, 1950, 1997, and 2009-2011, driven primarily by spring snowmelt and ice jams, while major floods in the Assiniboine River Basin (ARB) occurred in 1882, 1976, and an unprecedented event in 2011 dominated by prolonged rainfall and basin-wide runoff (Web-1). The RARB basin has experienced substantial hydroclimatic changes driven by land-use changes and climate warming. Observations showed significant winter and spring warming, earlier snowmelt, and a shift from snowfall to rainfall, while total precipitation trends remain weak (Dumanski et al., 2015; Grenier et al., 2024). These changes have contributed to nonstationary flow regimes, such as increased runoff, higher peak discharges, and a transition from snowmelt-dominated to mixed and rainfall-dominated flood events in recent decades (Ehsanzadeh et al., 2012; Dumanski et al., 2015). Process-based and statistical modelling studies projected a shortening of snow cover duration, reduced snow water equivalent, earlier freshet, and increasing importance of rainfall and rain-on-snow processes under future climate warming (Musselman et al., 2018; Shrestha et al., 2021). Flood-generating mechanisms are expected to shift toward rainfall dominance, particularly under high-emission scenarios, while mitigation measures consistent with 2 °C warming could limit these changes

(Teufel and Sushama, 2021). However, the potential impact of climate change on flow regimes and flood frequencies in the lower Red River has not been addressed.

The objective of this study is to quantify the potential impacts of climate change on future flow regimes and flood frequencies in the lower Red River that passes through the city of Winnipeg based on the calibrated Soil and Water Assessment Tool (SWAT) and precipitation and temperature projections of eight Global Climate Models (GCMs) from the CMIP6 database. Four Global Warming Levels (GWLs) (1.5 °C, 2.0 °C, 2.5 °C, and 3.0 °C), each under two Shared Socioeconomic Pathways (SSPs) (SSP245 and SSP585), were analysed to assess potential changes in climate, flow regimes, and flood frequencies relative to the reference period (1980–2010). These results provide a useful reference for planning and managing water resources and maintaining water-related infrastructure while accounting for changing climate conditions.

2 MATERIALS AND METHODS

2.1 Study Area

The Red River drains an area of approximately 287,500 km^2 (Figure 1), with its mouth near Selkirk downstream of Winnipeg, contributing significantly to Lake Winnipeg's inflow and nutrient loadings. The Red River originates in southern North Dakota (ND) and Minnesota (MN) of the U.S., flows northward, and crosses into Canada at Emerson, Manitoba (Figure 2b). The Red River Floodway is a 47 km artificial flood-control waterway with its inlet near St. Norbert, designed to divert floodwaters from the Red River around the city of Winnipeg. A significant expansion of the channel was completed in 2014 with a discharge rate up to 4,000 m^3/s (Haque et al., 2023). The Assiniboine River is the largest tributary covering a drainage area of 162,000 km^2 encompassing diverse prairie landscapes across Saskatchewan and Manitoba, and joining the Red River at the Forks in downtown Winnipeg. The Portage Diversion, a 29 km flood-control channel located at Portage la Prairie downstream of Holland, was constructed in the 1960s to divert excess water from the Assiniboine River north to Lake Manitoba, designed to protect the city of Winnipeg and surrounding areas from devastating floods.

The RARB has extremely flat topography with very small elevation changes, particularly along the Red River valley, where rivers flow slowly due to low gradients and broad floodplains. Clay and silty clay are the dominant soils in the river basin, with relatively poor natural drainage conditions. Cropland (cereals, oilseeds, corn, and soybeans) is the dominant land use in the Red River Basin (RRB) (approximately 62%), followed by forest and wetland (20%), grass and pasture (10%), open water (4%), and built-up areas (4%) (Figure 2a). In the Assiniboine River Basin (ARB), the dominant land use is cropland (approximately 59%), followed by grass and pasture (22%), forest and wetland (12%), open water (3%), built-up areas (3%), and barren land (1%), based on US Geological Survey (USGS) and Agriculture and Agri-Food Canada (AAFC) 2016 crop inventory data. Wetlands are common in the river basin, but have been extensively drained in many areas.

The RARB has a continental climate characterized by long, cold winters and short, cool to warm summers. Annual precipitation ranges from 350 mm in the Northwest of ARB to 700 mm in the South of RRB over the 1990-2018 period. Most precipitation falls during late spring and summer, while winters are relatively dry. Flooding in the region is typically caused by snowmelt over frozen soils, which is shaped by a cold-season water cycle, very flat terrain, and depressions in numerous pothole wetlands. Rain-on-snow events and heavy summer rainstorms can intensify floods (Buttle et al., 2016). Because of the dry weather in the ARB, the annual mean discharge at its lower reaches is several times less than that of the Red River upstream of the confluence based on flow monitoring data.

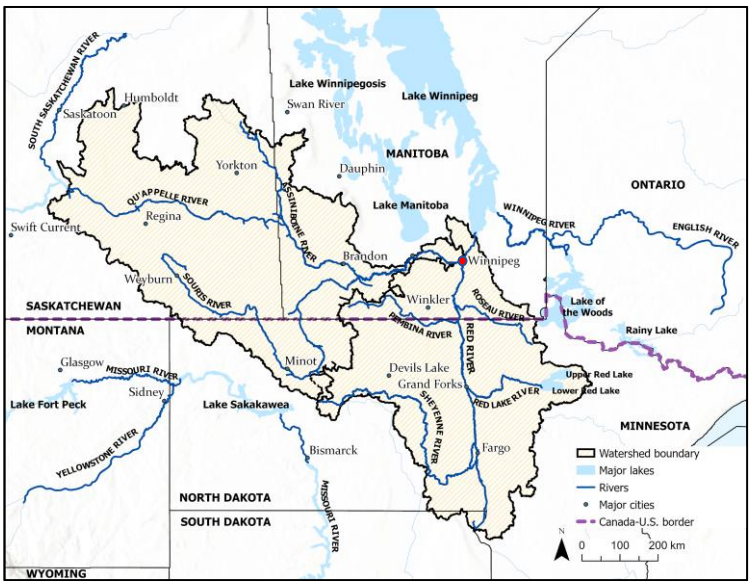

Figure 1: Location and stream network of the Red-Assiniboine River Basin

2.2 Data Availability

In this study, DEM (30-m) data were obtained from USGS for the U.S. side and Natural Resources Canada (NRC) for the Canadian side. Streams from the USGS National Hydrography Dataset (NHD) were hydro-enforced onto the DEM to ensure streamlines are accurately delineated. Land-use data were obtained from USGS National Land Cover Database (NLCD) and AAFC Annual Crop Inventory (ACI). These land uses were combined and processed with the same land-use classification (Figure 2a). Soil data were obtained from USDA State Soil Geographic Dataset (STATSGO) and AAFC Soil Landscapes of Canada (SLC), both with a 30-m resolution.

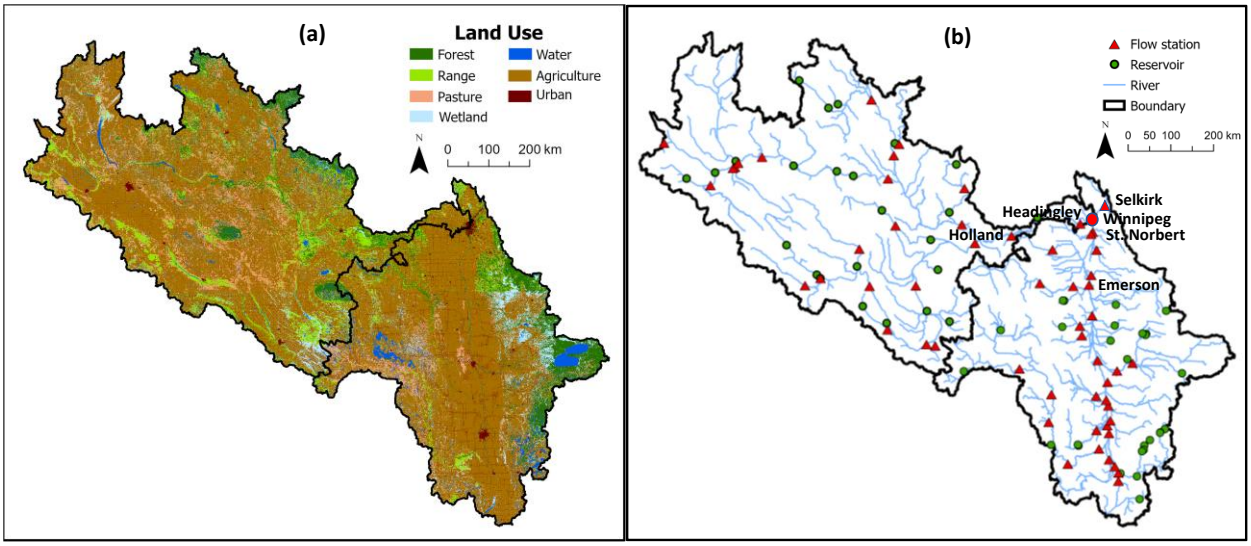

Figure 2: (a) Land use and (b) location of major reservoirs/lakes and flow monitoring stations in the Red-Assiniboine River Basin

The extended observation-based gridded meteorological data (Livneh et al., 2015), consisting of daily precipitation, maximum, and minimum temperature for the 1950-2018 period, were used as climate inputs in this study. The dataset has a 6-km resolution, providing a consistent representation of climatic variables and reduced transboundary discontinuity, and has been used in several hydro-climate studies in

the region (e.g., Shrestha et al., 2021; Dibike et al., 2021). Daily flow data at 30 stations in RRB and 19 stations in ARB were collected from the USGS and Water Survey Canada (WSC) historical hydrometric database (Figure 2b). 22 large reservoirs/lakes in RRB and 23 in ARB (Figure 2b) were identified as flow-controlling structures in the model. The location and associated reservoir/lake data were collected from the U.S. Army Corps of Engineers (USACE), U.S. National Inventory of Dams (NID), Manitoba, Sustainable Development (MSD), and other literature sources. In addition, tile-drain licence data in the upper RRB were obtained from ND and MN documents and were used in the model setup and simulation.

2.3 Watershed Hydrologic Modelling

Two SWAT models were developed, one for RRB and one for ARB. The simulated flow at the ARB outlet joined the simulated flow at the City of Winnipeg, and the total flow was then routed to the mouth of the Red River with the RRB SWAT model. Watershed delineation was conducted by placing subbasin outlets at the confluence of major tributaries and sub-tributaries, monitoring stations, and outlets of major reservoirs and lakes. Threshold values of 15/15/15% for land-use/soil/slope were used to create Hydrologic Response Unit (HRUs) within each subbasin. A total of 283 subbasins and 10,003 HRUs were derived for the RRB SWAT modelling, while 284 subbasins and 6,357 HRUs were derived for the ARB SWAT modelling.

Non-contributing areas play a critical role in runoff dynamics in the RARB. Runoff can be retained in potholes, and only large storm or snowmelt events can create hydrologic connectivity, allowing these areas to contribute flow. To account for this specific hydrologic characteristic in the RARB, the GIS approach developed by Liu et al. (2018) was employed to delineate non-contributing areas in the basin, which were incorporated in the wetland and pond management inputs to the RARB SWAT models. Crop rotation also influences the water balance and runoff generation. In this study, Canadian agriculture was simulated using a canola-spring wheat rotation, and U.S. agriculture using a corn-soybean rotation based on analyses of available crop inventory and literature data. Surface runoff was estimated using the SCS-CN method, while tile flow was simulated using SWAT tile-flow algorithms with default parameter values in the SWAT parameter database. In the absence of reservoir operation data, the target storage method (Neitsch et al., 2011) was used for reservoir routing based on the difference between actual and target storage, subject to specified minimum and maximum release constraints. The outflow from the reservoir joined the streamflow and was then routed through channel reaches to the watershed outlet using the variable storage method (Neitsch et al., 2011).

The RRB and ARB SWAT models used Livneh's gridded climate data as weather inputs and daily flow data at monitoring stations (Figure 2b) for model calibration and validation. Three statistical criteria, the percentage of bias (PBIAS), the Nash-Sutcliffe Efficiency (NSE) (Nash and Sutcliffe, 1970), and the coefficient of determination (R^2), were employed to evaluate the model's performance in simulating daily streamflow. In addition, visual comparisons between observed and simulated hydrographs were performed, and model performance was deemed satisfactory when the timing and magnitude of peaks, as well as baseflow patterns, were closely aligned.

2.4 Climate Change Projections

An ensemble of eight GCMs, including CanESM5, INM-CM5-0, IPSL-CM6A-LR, MIROC6, FGOALS-G3, GFDL-ESM4, UKESM1-0-LL, and CNRM-CM6-1, from the Coupled Model Intercomparison Project Phase 6 (CMIP6) (Eyring et al., 2016) was selected in this study with climate variables of precipitation, maximum temperature, and minimum temperature. For each GCM, we considered two SSP scenarios, SSP585 and SSP245. The GCMs were selected based on the previous study by Mahony et al. (2022), which identified the best-performing GCMs for different IPCC reference regions in North America. Following the methodology described in Shrestha et al. (2021; 2025), we used annual and seasonal changes in temperature and precipitation under 1.5 °C, 2.0 °C, 3.0 °C, and 4.0 °C global mean temperature (GMT) changes above the pre-industrial (PI) period of 1850–1900 by considering 31-year periods for each GCM.

2.5 Flood Risk Analysis

Flood risk was quantified using a frequency analysis of annual maximum daily discharge simulated by the calibrated SWAT models under the reference period (1980–2010) and future climate scenarios. The Pearson Type III (P-III) distribution was adopted to estimate flood quantiles for selected return periods (e.g., 2-, 5-, 10-, 25-, 50-, and 100-year events). In this study, flood frequency curves were derived separately at three control sites (Red River at Floodway Inlet, Assiniboine River near Holland, and Red River Mouth) for the reference period (1980–2010), each GWL (1.5 °C, 2.0 °C, 2.5 °C, 3.0 °C), and each SSP (SSP245 and SSP585). Flood frequency analysis was conducted using the annual maximum flow series derived from SWAT simulations driven by multiple GCM projections. The analysis was performed separately for each climate model simulation, and the resulting flood quantiles were combined to derive ensemble statistics. Changes in flood risk were quantified by combining projected flood peaks from individual model simulations and comparing them with those from the reference period. Based on these results, shifts in return periods relative to historical frequency analysis were evaluated. This approach preserves the variability among climate projections and avoids smoothing of extreme events that can occur when peak flows are averaged before frequency analysis (Giuntoli et al., 2015).

3 RESULTS AND DISCUSSION

3.1 Model Calibration and Validation

The SWAT models for the RRB and ARB were calibrated and validated using observed daily streamflow data at 49 stations (30 in the RRB and 19 in the ARB). These stations have relatively long-term historical flow records and are primarily located along the main rivers and their major tributaries (Figure 2b). A global optimization algorithm, Sequential Uncertainty Fitting 2 (SUFI-2), was used to generate 1000 runs and find the optimal parameter set that satisfied the performance criteria for all calibration stations in the RRB and ARB SWAT models. Model parameters were further adjusted separately for each river network using the optimized parameters as initial values and then fine-tuned to achieve improved results. In general, the model performed very well at mainstream stations and less satisfactorily at stations with smaller drainage areas. Table 1 presents model performance statistics at the four control stations in the lower RARB for the calibration and validation periods. During calibration, NSE values ranged from 0.63 to 0.81, R^2 values ranged from 0.66 to 0.85, and Bias ranged from –6.50% to –2.21%. During validation, NSE values ranged from 0.52 to 0.72, R^2 values ranged from 0.57 to 0.74, and Bias ranged from –4.70% to 4.18%. These model performance results can be considered satisfactory for daily streamflow simulations according to the criteria of Moriasi et al. (2007).

Table 1 Model performance in simulating daily streamflow at Emerson, Holland, Headingley, and Selkirk stations in the Red-Assiniboine River Basin

River	Station	Area (km^2)	Period	Bias (%)	NSE	R^2
Red	Emerson	104,120	Calibration (2000-2018)	-3.15	0.73	0.76
			Validation (1990-1999)	-4.70	0.72	0.73
Assiniboine	Holland	160,000	Calibration (2000-2018)	-2.21	0.75	0.77
			Validation (1990-1999)	3.25	0.71	0.74
Assiniboine	Headingley	162,000	Calibration (2000-2018)	-5.80	0.63	0.66
			Validation (1990-1999)	4.18	0.52	0.57
Red	Selkirk	287,000	Calibration (2008-2018)	-6.50	0.81	0.85

Although performance at Headingley during validation (NSE = 0.52) falls at the lower bound of the satisfactory range, it remains acceptable given the complex hydrologic regulation in

the lower Assiniboine River, including reservoir operations and the Portage Diversion. Visual inspection of hydrographs (Figure 3) confirms that the model reasonably reproduces seasonal flow variability, snowmelt-driven spring peaks, and baseflow conditions, with minor underestimation during extreme flood years. Overall, the calibrated SWAT models meet established hydrologic performance standards and provide a robust foundation for evaluating projected changes in flow regimes and flood risk under future climate scenarios.

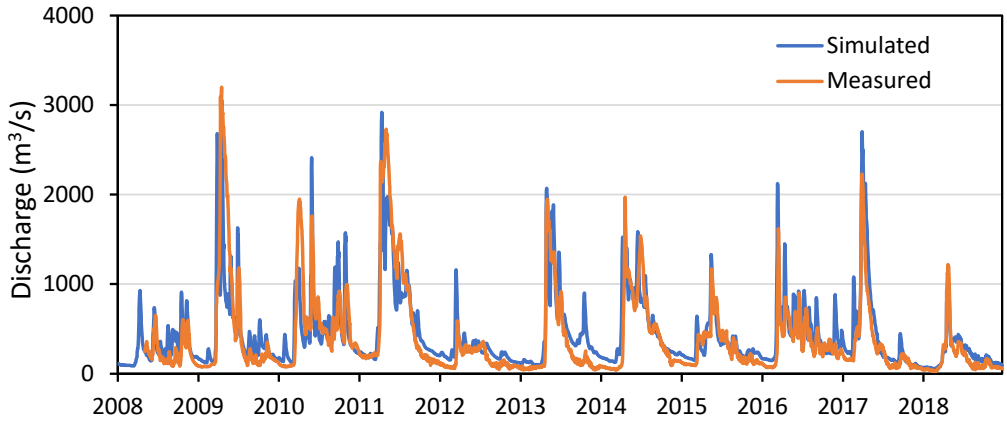

Figure 3. Comparison of measured and SWAT-simulated daily flow at the Selkirk station

3.2 Climate Change under SSP Emission Scenarios

Projected seasonal changes in temperature and precipitation for the RRB and ARB were analysed using the ensemble mean of eight CMIP6 GCMs under the SSP245 and SSP585 scenarios for four GWLs relative to the 1980–2010 reference period. Figure 4 shows the projected seasonal mean changes and inter-model standard deviations under SSP585, with similar patterns observed under SSP245 but with smaller magnitudes. Temperature is projected to increase across all seasons and GWLs in both basins, with the largest warming occurring in winter due to strong cold-season amplification in high-latitude continental regions. Spring warming in the ARB is slightly higher than in the RRB, while summer and autumn warming in both basins are comparatively smaller but still significant. In contrast, precipitation projections exhibit greater seasonal and inter-model variability. In both basins, precipitation generally increases in winter and spring, while summer changes are more uncertain, with some models projecting slight increases and others decreases, resulting in a small overall decrease in ensemble mean values. The larger inter-model standard deviations for precipitation indicate greater uncertainty compared with temperature projections. Overall, the ensemble projections suggest warmer and wetter winters and springs across the RARB under future climate conditions.

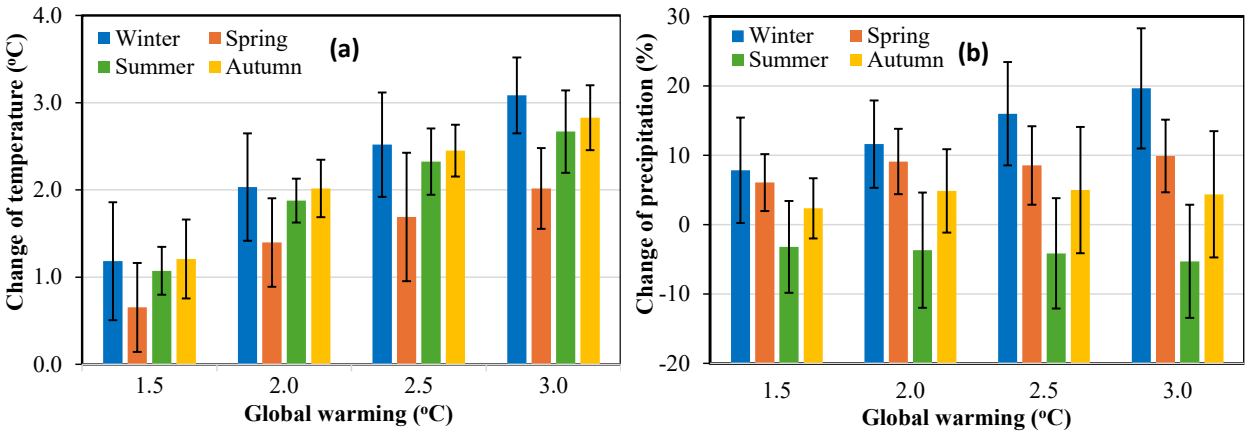

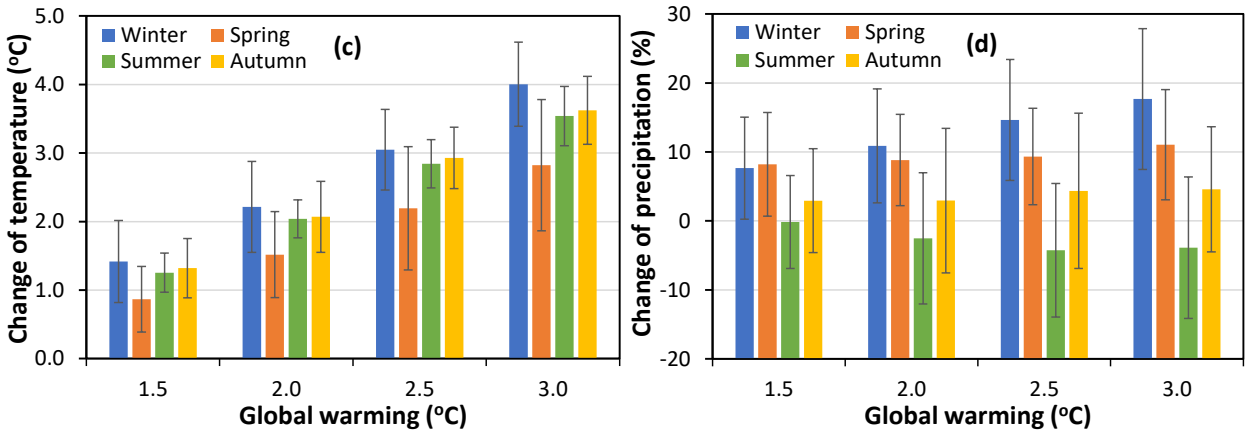

Figure 4: Changes in ensemble seasonal mean of (a) RRB temperature, (b) RRB precipitation, (c) ARB temperature, and (d) ARB precipitation and their standard deviations under SSP585 for the four GWLs compared to the reference period 1980-2010

3.3 Flow Regimes under Climate Change Projections

Projected changes in seasonal streamflow were analysed at two control stations: Emerson on the Red River and Holland on the Assiniboine River (Figure 2b), representing the main hydrologic contributions from RRB and ARB. Figure 5 illustrates the ensemble mean seasonal flow changes simulated by the SWAT model driven by eight GCM projections under the SSP585 scenario for different GWLs, relative to the reference period of 1980–2010. Scenario SSP245 exhibited similar patterns with smaller changes than SSP585.

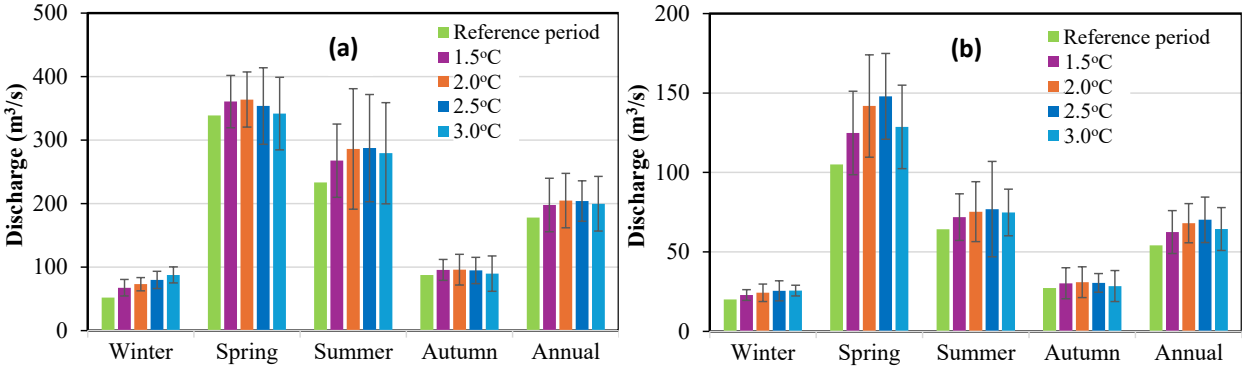

Figure 5. Projected ensemble seasonal mean flow and standard deviation at (a) Emerson station of RRB and (b) Holland station of ARB under SSP585 compared to the 1980-2010 reference period

The projected flow regimes indicate noticeable seasonal shifts in response to climate warming. In RRB, winter flows are projected to increase consistently across all warming levels. The increase in winter discharge is primarily associated with warmer temperatures, which reduce snow accumulation despite increased winter precipitation and promote more frequent mid-winter melt and rainfall events. Similar increases are projected during the early spring period, reflecting earlier snowmelt and enhanced runoff generation. Spring flows, which historically dominate the annual hydrograph due to snowmelt, exhibit a more complex response. At lower warming levels (1.5 °C and 2.0 °C), spring peak flows generally increase compared with the reference period. These increases are mainly driven by enhanced snowmelt runoff combined with higher cold-season precipitation. However, at higher warming levels (2.5 °C and 3.0 °C), further increases in spring flows tend to stabilize or decrease slightly as a result of reduced snow accumulation and

earlier melt timing, which shifts part of the runoff toward the winter season. Summer flows exhibit relatively smaller changes compared with winter and spring. In some projections, summer discharge increases slightly due to higher rainfall intensity, while in others it remains close to the reference level. Autumn flows generally show modest increases, mainly related to increased precipitation and soil moisture carryover from preceding seasons.

A similar seasonal pattern is observed in ARB at the Holland station, although the magnitude of changes differs from those in RRB. Winter and early spring flows increase noticeably across most warming levels, reflecting similar hydroclimatic drivers such as warmer temperatures and increased winter precipitation. Overall, the projected changes suggest a gradual shift from a strongly snowmelt-dominated flow regime toward a more mixed rainfall–snowmelt regime in RARB. These changes in seasonal flow distribution have important implications for flood risk management and water resources planning in the basin.

3.4 Flood Risk under Climate Change Projections

Flood quantiles were estimated at three key control locations: the Red River at the Floodway Inlet, the Assiniboine River near Holland, and the Red River mouth. The approach proposed by Giuntoli et al. (2021) was adopted to evaluate changes in flood risk under future climate conditions. The calibrated SWAT model was forced with each GCM projection, from which annual maximum flows were extracted. The P-III flood frequency analysis was then performed separately for each model simulation, and the resulting flood quantiles were combined using ensemble statistics.

Table 2 Simulated 100-year peak flood under different GWLs and SSPs (m^3/s)

Station	Reference period	SSP	Global warming level			
			1.5°C	2.0°C	2.5°C	3.0°C
Red River at Floodway Inlet	4100	245	4252	4804	4396	3659
		585	4579	4988	4818	4413
Assiniboine River near Holland	1220	245	1329	1421	1635	1210
		585	1384	1541	1732	1264
Red River Mouth	4650	245	4913	5620	5145	4180
		585	5208	5945	5430	4902

Table 2 summarizes the projected 100-year flood discharges at the three control locations. Compared with the reference period (1980–2010), flood magnitudes generally increase under lower and mid-warming levels (1.5 °C and 2.0 °C) for both SSP scenarios. For example, the projected 100-year flood at the Red River Floodway Inlet increases from 4,100 m^3/s during the reference period to approximately 4,252–4,579 m^3/s at 1.5 °C warming and up to 4,804–4,988 m^3/s at 2.0 °C warming. Similar increases are observed at the Assiniboine River near Holland and the Red River Mouth, indicating a basin-wide intensification of flood peaks under moderate warming conditions. At higher warming levels, however, the projected flood response becomes more complex. Under the 2.5 °C and 3.0 °C warming scenarios, the simulated 100-year flood magnitudes tend to stabilize or decrease. For example, at the Red River mouth, the projected 100-year flood decreases from 5,620 m^3/s at the 2.0 °C warming level to approximately 5,145 m^3/s at 2.5 °C and 4,180 m^3/s at 3.0 °C under SSP245. A similar pattern is observed under SSP585, although flood magnitudes remain slightly higher than under SSP245 due to stronger warming and changes in precipitation.

The flood frequency curves at the Red River mouth (Figure 6) further illustrate these shifts in flood risk. Under both emission scenarios, flood peaks increase under the lower warming levels, indicating an elevated likelihood of extreme flow events. However, at higher warming levels, the curves shift downward, reflecting reduced peak flows associated with declining snowpack and earlier snowmelt timing. These results suggest that moderate climate warming may intensify flood risk in the lower RARB, particularly due to enhanced snowmelt and increased cold-season precipitation. Under the higher

warming levels, however, reductions in snow accumulation and shifts toward earlier runoff generation may partially offset these increases. Consequently, flood-generating mechanisms in the basin may transition from snowmelt-dominated events toward mixed rainfall and snowmelt processes. These projected changes highlight the importance of adaptive flood management strategies that consider evolving hydrologic conditions under future climate scenarios.

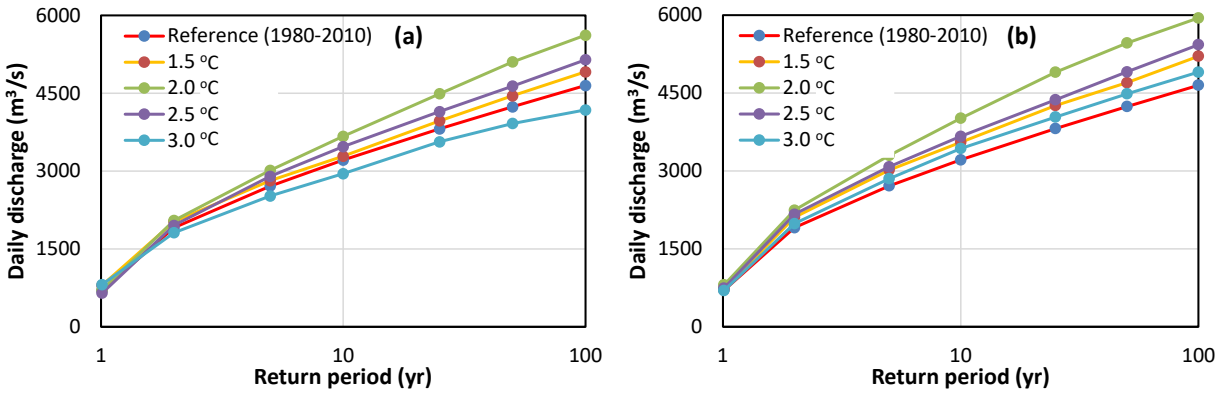

Figure 6: Flood frequency curves of daily discharge at the Red River mouth based on the ensemble mean of eight selected GCMs under (a) SSP245 and (b) SSP585 compared to the reference period 1980-2010

3.5 Discussion

The projected changes in flow regimes and flood risk reflect the complex interactions among temperature increases, precipitation variability, and basin hydrologic processes in RARB. Warmer winters and increased cold-season precipitation contribute to higher winter and early spring runoff. These findings are consistent with previous studies suggesting that climate warming in prairie river basins is likely to reduce snowpack, accelerate snowmelt, and increase the contribution of rainfall and rain-on-snow events to flood generation (Dumanski et al., 2015; Grenier et al., 20240).

Differences among GCMs in climate sensitivity and precipitation patterns can lead to varying hydrologic responses when used as inputs to the SWAT model. To address this uncertainty, flood frequency analysis was conducted separately for each model simulation, and the resulting flood quantiles were then combined for the risk assessment. This approach preserves the variability among models and avoids smoothing extreme events. Despite these uncertainties, the ensemble analysis of model simulations consistently indicates increasing flood risk under moderate warming levels, followed by stabilization or decline in extreme floods under higher warming levels due to reduced snowpack and much higher evapotranspiration losses.

Another important consideration is the assumption of stationarity in the flood frequency analysis. The P-III distribution assumes that the statistical properties of flood peaks remain constant over time. However, climate change introduces nonstationary hydroclimatic conditions that may violate this assumption. In this study, the GWL framework was adopted to partially address this issue by grouping climate projections around specific temperature thresholds. Nevertheless, residual trends in precipitation intensity, snowmelt timing, and antecedent soil moisture conditions may still influence the distribution of extreme flows. In addition, the expansion of tile drainage in the basin may contribute to higher winter and early spring flows, particularly when combined with warmer temperatures and more frequent rain-on-snow events. However, the current study assumed existing land management practices and did not explicitly simulate future changes in tile drainage extent, which may introduce additional uncertainty in projected hydrologic responses.

Overall, the results highlight the importance of considering both hydroclimatic changes and basin characteristics when assessing future flood risk in RARB. Adaptive flood management strategies that account for earlier snowmelt, increased winter runoff, and evolving flood-generating mechanisms will be essential to mitigate potential impacts under future climate conditions. These findings provide valuable

insights for long-term planning of flood control infrastructure, including the Red River Floodway and the Portage Diversion.

4 CONCLUSION

This study assessed the potential impacts of climate change on future flow regimes and flood risk in the lower RARB using the SWAT hydrologic model driven by eight CMIP6 GCM projections under two SSPs and four GWLs. Climate projections indicate consistent warming across all seasons in both RRB and ARB, with the largest increases occurring during winter. Seasonal precipitation generally increases in winter and spring, and changes in summer and autumn precipitation show larger variability among climate models. Projected hydrologic responses indicate significant seasonal shifts in flow regimes. Winter and early spring flows increase across most warming levels due to warmer temperatures and increased cold-season precipitation. At lower warming levels (1.5 °C and 2.0 °C), spring peak flows generally increase, reflecting enhanced snowmelt runoff. However, at higher warming levels (2.5 °C and 3.0 °C), reductions in snow accumulation and earlier snowmelt tend to redistribute runoff toward winter, resulting in stabilization or slight decreases in spring peak flows. Flood frequency analysis indicates that extreme floods in the lower RARB are likely to intensify under moderate warming levels. The simulated 100-year flood magnitudes at key control locations increase under the 1.5 °C and 2.0 °C warming levels for both SSP scenarios. However, under the 2.5 °C and 3.0 °C warming levels, flood peaks tend to stabilize or slightly decline due to increased evapotranspiration, reduced snowpack, and shifts in the timing of snowmelt-driven runoff.

Overall, the results suggest that moderate climate warming may increase flood risk in RARB, particularly due to enhanced snowmelt and increased winter precipitation, while higher warming levels may alter flood-generating mechanisms and reduce the magnitude of traditional spring floods. These findings highlight the importance of considering changing hydroclimatic conditions in future flood risk assessments and infrastructure planning. Flood management strategies that address joint snowmelt–rainfall events and increasing winter runoff will be essential for mitigating potential climate change impacts in the basin.

ACKNOWLEDGEMENTS

This study was funded by the Lake Winnipeg Basin Initiative of Environment and Climate Change Canada (ECCC). We gratefully acknowledge Curtis Struyk and Courtney Shaw (University of Guelph), as well as Shreya Tanguturi, Phil Fong, and Nigel Van Nieuwenhuizen (ECCC), for their data provision and technical support. We also thank Ram Yerubandi (ECCC) and Lieserl Woods and Arthur Friesen (Canadian Water Agency) for their project management.

REFERENCES

Buttle, J.M., Allen, D.M., Caissie, D. et al. (2016). Flood processes in Canada: Regional and special aspects. Can. Water Resour. J., 41(1-2), 7-30.

Dibike, Y., Muhammad, A., Shrestha, R.R. et al. (2021). Application of dynamic contributing area for modelling the hydrologic response of the Assiniboine River Basin to a changing climate. J. Great Lakes Res., 47(3), 663–676.

Dumanski, S., Pomeroy, J.W., and Westbrook, C.J. (2015). Hydrological regime changes in a Canadian Prairie basin. Hydrol. Process. 29(18), 3893-3904.

Ehsanzadeh, E., Van Der Kamp, G., and Spence, C. (2012). The impact of climatic variability and change on the hydroclimatology of the Lake Winnipeg watershed. Hydrol. Process, 26(18), 2802-2813.

Eyring, V., Bony, S., Meehl, G. A. et al. (2016). Overview of the Coupled Model Intercomparison Project Phase 6 (CMIP6) experimental design and organization. Geosci. Model Dev. 9(5), 1937-1958.

Giuntoli, I., Prosdocimi, I. and Hannah, D.M., 2021. Going beyond the ensemble mean: Assessment of future floods from global multi-models. Water Resour. Res. 57(3), e2020WR027897.

Giuntoli, I., Vidal, J.P., Prudhomme, C., and Hannah, D.M. (2015). Future hydrological extremes: The uncertainty from multiple global climate and global hydrological models. Earth Syst. Dyn. 6(1), 267–285.

Grenier, M., Boudreault, J., Raymond, S. and Boudreault, M. (2024). Projected seasonal flooding in Canada under climate change with statistical and machine learning. J. Hydrol. Reg. Stud., 53, 101754.

Haque, C.E., Zaman, J.R., and Walker, D. (2023). Risk-reduction, coping, and adaptation to flood hazards in Manitoba, Canada: Evidence from communities in the Red River Valley. Geosciences, 13(3), 88.

Liu, Y., Yang, W., Shao, H., Yu, Z., and Lindsay, J. (2018). Development of an integrated modelling system for evaluating water quantity and quality effects of individual wetlands in an agricultural watershed. Water, 10(6), 774.

Livneh, B., Bohn, T.J., Pierce, D.W. et al. (2015). A spatially comprehensive, hydrometeorological data set for Mexico, the U.S., and Southern Canada 1950–2013. Sci. Data, 2, 150042.

Mahony, C.R., Wang, T., Hamann, A. and Cannon, A.J., 2022. A global climate model ensemble for downscaled monthly climate normals over North America. Int. J. Climatol., 42(11), 5871-5891.

Moriasi, D.N., Gitau, M.W., Pai, N., and Daggupati, P., 2015. Hydrologic and water quality models: Performance measures and evaluation criteria. Trans. ASABE 58(6), 1763-1785.

Musselman, K.N., Lehner, F., Ikeda, K. et al. (2018). Projected increases and shifts in rain-on-snow flood risk over western North America. Nat. Clim. Chang, 8(9), 808-812.

Nash, J.E. and Sutcliffe, J.V. (1970). River flow forecasting through conceptual models. Part 1: A discussion of principles, J. Hydrol. 10, 282–290.

Neitsch, S.L., Arnold, J.G., Kiniry, J.R., Williams, J.R. (2011). Soil and Water Assessment Tool Theoretical Documentation Version 2009. Tech. Rep. TR-406. Texas A&M University, USA.

Shrestha, R. R., Cannon, A. J., Hoffman, S., Whibley, M., and Lima, A. (2024). Benchmarking historical performance and future projections from a global hydrologic model with a basin-scale model. EGUsphere, 2024, 1-26.

Shrestha, R.R., Bonsal, B.R., Kayastha, A., Dibike, Y.B., and Spence, C. (2021). Snowpack response in the Assiniboine-Red River basin associated with projected global warming of 1.0 °C to 3.0 °C. J. Great Lakes Res., 47(3), 677–689.

Teufel, B. and Sushama, L. (2021). 2 °C vs. high warming: Transitions to flood-generating mechanisms across Canada. Water, 13(11), 1494.

Web-1: Flooding events in Canada: prairie provinces. https://www.canada.ca/en/environment-climate-change/services/water-overview/quantity/floods/events-prairie-provinces.html, consulted 5 Oct. 2025.

Chapter 3 - Urban flooding and infrastructure systems

3.1 Drivers of urban flooding and interactions with the urban water cycle

ICFM 10
Adapting to Global Change:
Innovative Approaches to Flood Management and Resilience
May 20-22, 2026 | Western University, London, Ontario, Canada

The Resilience Assessment Study Based on Urban Flooding Model：A Case Study of Suqian City

ZHANG Cheng[1] and WANG Kaifeng[2]
China Institute of Water Resources and Hydropower Research, Beijing 100038, China[1]; Beijing Municipal Engineering Design & Research Institute Co., Ltd., Beijing 100082, China[2]
E-mail: zhch16_1981@126.com

ABSTRACT

In recent years, urban water security issues have become increasingly prominent due to multiple factors such as climate change, accelerated urbanization, and intensified human activities. Flooding disasters have become a global issue, and the concept of resilience has provided new insights for urban flood control research. To quantitatively assess the resilience of cities in responding to flooding disasters, this study is based on the theories of resilient cities and disaster chain. It selects indicators from three dimensions—urban space, lifeline infrastructure, and rapid recovery capacity—to establish an evaluation system. By combining a one-dimensional and two-dimensional coupled urban flooding model, a method for quantifying urban flood resilience levels is proposed. This method is used to investigate the spatial distribution of urban resilience and explore the driving factors of flood resilience. The study focuses on the southwest area of Suqian City, which is frequently affected by flooding disasters. Using the proposed method, the resilience level of Suqian City in 2022 is evaluated. The results show that: (1) The level of urban waterlogging risk is positively correlated with the resilience level—higher waterlogging risk corresponds to lower resilience; (2) Indicators such as green coverage rate, distance to river networks, distance to waterlogging-prone areas, and drainage network density have a significant impact on resilience levels; (3) The distribution of resilience levels in the study area is not completely random but exhibits spatial clustering, with 38.7% of the area showing significant clustering. The proposed method for quantifying resilience levels has important significance for urban flood control and disaster reduction.

KEY WORDS: urban flooding; resilience assessment; flood simulation; assessment framework; Quantitative evaluation indicators

1 INTRODUCTION

Against the backdrop of climate change, the frequency, duration, and spatial impact of extreme disaster events are continuously increasing. Among these, flood disasters, as one of the most prevalent natural hazards globally, inflict the most severe damage and losses. A report issued by the United Nations Office for Disaster Risk Reduction (UNDRR) indicates a trend of increased occurrence and frequency of global flood disasters. Compared to the previous 20-year period, the number of flood events from 2000 to 2019 increased by approximately 2.3 times. Globally, 3,254 flood-related disaster events were recorded, accounting for 44% of all disaster events, resulting in 104,614 fatalities and economic losses totaling USD 651 billion, and affecting nearly 1.65 billion people[1]. CHENG et al.[2] found that under the influence of climate change, the global water cycle has intensified by 2.6% to 4.4% since 1960, posing challenges to urban water security. Some

studies estimate that nearly 23% of the global population is currently directly exposed to the threat of a 1-in-100-year flood[3].

Currently, the flood risk management paradigm reliant solely on urban flood control and drainage engineering systems is insufficient to address the challenges posed by the changing environment. While flood risk may be unavoidable, it can be substantially mitigated through the adoption of resilience-based flood management concepts[4]. The concept of "resilience" moves beyond a purely defensive approach, viewing the enhancement of urban capacity as a dynamic process. This provides a new perspective for urban development. Building resilient cities is a key strategy for addressing urban flood issues and achieving sustainable urban development, making related research urgently needed.

Internationally, the conceptual approach to flood management has undergone several shifts, evolving through three distinct phases: the initial flood defense stage, followed by the flood risk management stage, and currently progressing towards the flood resilience management stage. Numerous scholars have conducted extensive research on urban flood resilience. For instance, Cutter et al.[5] developed the Baseline Resilience Indicators for Communities (BRIC) model, which assesses resilience across five dimensions—economic, social, ecological, institutional, and infrastructural—to measure changes in resilience over time. Joerin et al.[6] constructed the Climate Disaster Resilience Index (CDRI) based on economic, institutional, natural, physical, and social aspects, with results reflecting the capacity of people and institutions in Chennai, India, to cope with potential climate-related disasters. Bruneau et al.[7] introduced a quantitative framework for disaster resilience, using system performance curves to depict urban resilience levels and defining resilience as the system's ability to reduce disaster probability, absorb shocks, and recover rapidly.

Building upon domestic and international research on urban flood resilience, this paper selects Suqian City—a plain river-network city—as the study area. Based on an established urban flood model, an urban flood resilience assessment framework is constructed to conduct research on urban flood resilience.

2 MATERIALS AND METHODS

2.1 Study Area

This study selects Suqian City, located in Jiangsu Province, China, as the research subject. Situated in northern Jiangsu, Suqian features convenient transportation with an extensive network of land and water transportation routes. Characterized by relatively flat terrain, it is a typical plain river-network city.

Precipitation in Suqian is spatially uneven, generally increasing from north to south. The multi-year average annual precipitation is 915 mm, with approximately 70% of the annual total concentrated during the flood season from June to September. This precipitation pattern makes the area highly prone to floods and droughts. The topography of the SW District is generally higher in the north and lower in the south, as well as higher in the west and lower in the east. The overview of the SW District is shown in Fig. 1. The land use pattern is presented in Fig. 2.

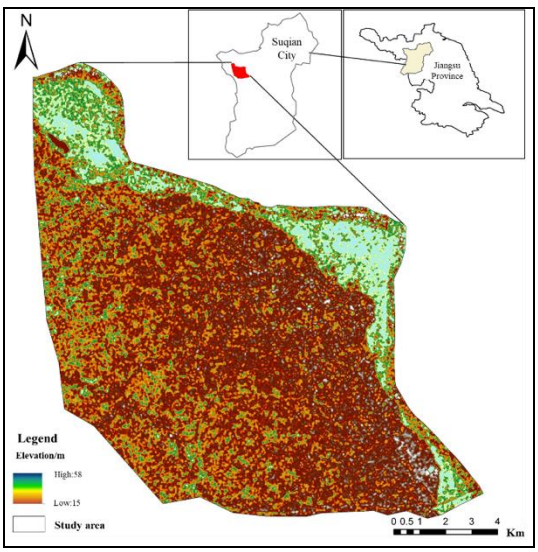

Fig. 1: Study Area

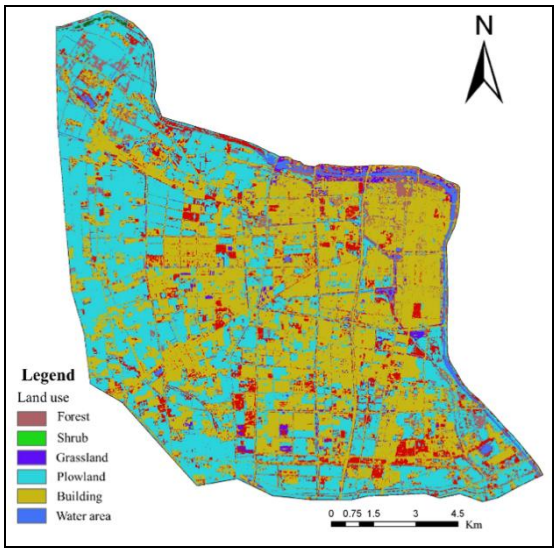

Fig. 2: Land Use Map of the Study Area

2.2 Research Framework

Based on literature review, analysis of typical urban flood disaster cases, historical disaster records, and urban drainage system data, and in conjunction with the city's spatial layout, topography, and infrastructure development, this study classifies urban flood risk zones of different levels for storms of various recurrence intervals. This model identifies high-risk locations with significant water depth and flow velocity, thereby clarifying the baseline conditions of urban flood disasters.

The framework assesses urban flood risk points based on the hazard level of disaster-inducing factors, the risk of hazard-formative environments, and the vulnerability of hazard-affected bodies. It defines key evaluation objectives for urban flood resilience. Considering dimensions such as urban space, society, economy, and infrastructure, and accounting for characteristics of different city types, the framework identifies key urban protection targets.

The framework establishes tailored resilience enhancement strategies for different cities, focusing on multiple phases: adaptation, resistance, and recovery. In the adaptation phase, measures include deploying green sponge facilities to improve urban surface runoff control, and implementing retrofitting measures in high-risk buildings, and integrates technologies such as various infrastructure sensors and big data to enhance urban situational awareness. This enables refined forecasting and early warning, thereby strengthening the city's ability to withstand disasters. In the recovery phase, rapid response capability is paramount. Furthermore, establishing a disaster insurance system can effectively disperse losses and plays a crucial role in post-disaster urban recovery, enabling the city to return swiftly, either fully or partially, to its pre-disaster state.

Resilience enhancement measures aligned with waterlogging prevention and control goals are integrated into the urban landscape. Combined with refined modeling and simulation methods, the layout of these resilience measures is optimized through simulation analysis. Through exercises and drills, the city's disaster response capability and flood resilience level are continuously improved.

The research framework is illustrated in Figure 3.

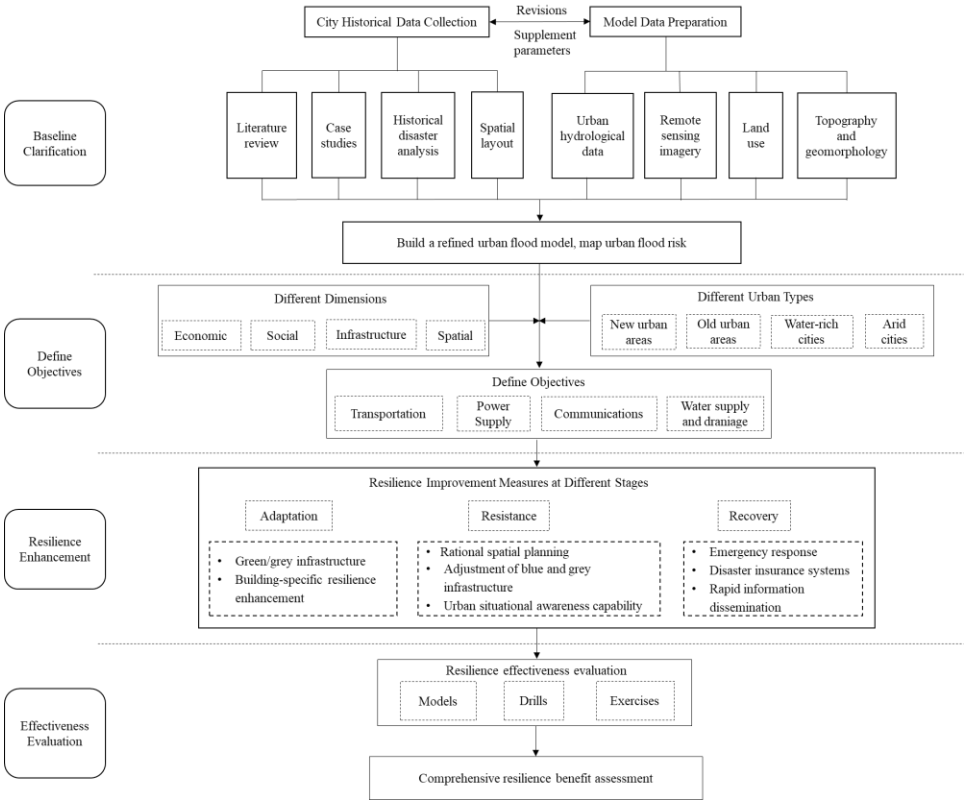

Fig. 3: Research Framework

3 RESEARCH METHODS

3.1 IFMS Model

This study utilizes the Integrated Flood Modeling System for Urban areas (IFMS/Urban) software platform. This platform integrates modules for urban drainage networks, one-dimensional river networks, and two-dimensional overland flow, enabling coupled 1D-2D modeling. The software is broadly applicable to various scenarios, including river flood control assessment, urban stormwater and flood risk analysis, drainage network evaluation, and the design of stormwater storage facilities. Its practicality and reliability have been effectively validated through application in multiple practical engineering projects[8]. The modeling domain for the southwestern district of Suqian City is shown in Fig. 4.

Fig. 4: 1D-2D Coupled Model

3.2 Calculation of Indicator Weights

3.2.1 Methods for Calculating Indicator Weights

To enhance the scientific rigor and reliability of the indicator weight assignment and to mitigate the limitations inherent in using a single assignment method, this study adopts a combined subjective-objective approach to calculate indicator weights. The subjective method employs the Analytic Hierarchy Process (AHP), while the objective method utilizes the entropy weight method. The final comprehensive weight for each indicator is derived by combining the weights obtained from both methods.

3.2.2 Analytic Hierarchy Process (AHP)

The Analytic Hierarchy Process (AHP) is a multi-criteria decision-making method that facilitates quantitative analysis of qualitative problems. Its characteristic lies in classifying and synthesizing the various factors of a complex problem, typically structuring them into a hierarchy comprising the goal layer, criterion layer, and indicator layer. The operational procedure involves constructing a judgment matrix to compare the relative importance of indicators within the same hierarchical level. The relative priorities of these indicators are then calculated. Finally, these priorities are used to compute the weights for each indicator at every level of the hierarchy. Based on the main influencing factors of urban flood resilience and their interrelationships, a hierarchical structure model was constructed, consisting of the goal layer, the criterion layer, and the indicator layer.

3.3 Urban Flood Resilience Level

The Technique for Order Preference by Similarity to Ideal Solution (TOPSIS) evaluation method is employed to classify the resilience levels of urban areas. TOPSIS is a widely used

comprehensive evaluation method that fully utilizes the information from raw data, and its results can accurately reflect the differences among various evaluation alternatives[9].

Urban flood resilience can be represented by this relative closeness S_i, with a value range of 0 to 1. A value closer to 1 indicates a higher level of urban flood resilience, while a value closer to 0 indicates a lower level.

4 CASE STUDY

4.1 Selection of Evaluation Indicators

As a complex social-ecological system, cities have prompted some scholars to propose resilience assessment frameworks encompassing four dimensions: social, economic, ecological, and infrastructural[10~12]. Other researchers have categorized the influencing factors of urban systems into three dimensions—Pressure, State, and Response—for resilience level evaluation[13]. Additionally, frameworks have been established based on the three dimensions of resilience building: resistance capacity, recovery capacity, and adaptive capacity[14]. While resilience is a dynamic process, most existing frameworks often treat it as a static concept for easier quantification[15]. Drawing upon the concept of urban flood resilience achieved through "transformation," and considering the disaster chain propagation of urban flood hazards, this study references domestic and international scholarly frameworks. It views resilience as a dynamically evolving process, establishing an urban flood resilience assessment framework based on three dimensions: pre-disaster urban spatial layout, protection of lifelines during disasters, and post-disaster rapid recovery, as illustrated in Figure 5.

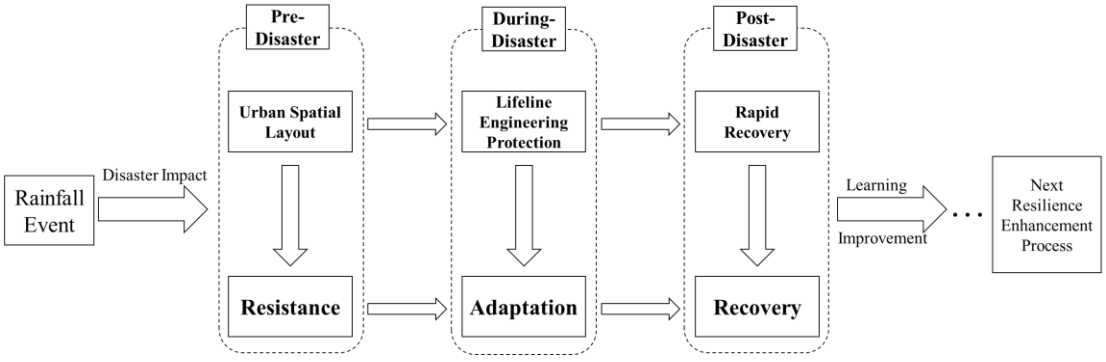

Fig. 5: Dimensions of Urban Flood Resilience

These three dimensions collectively constitute the full-process framework of urban flood resilience. Emphasizing comprehensive measures across the pre-disaster planning, in-disaster protection, and post-disaster recovery stages helps cities better cope with natural disasters such as floods. This paper selects indicators from the three dimensions of urban space, lifeline systems, and rapid recovery to establish an evaluation system. The assessment indicators are shown in Table 1.

Table 1 Urban Flood Resilience Evaluation Indicator System

Dimension	Indicator	Description	Representation Data
Urban Space (A)	Land Use (A_1)	The proportion of the total area of blue space and green space to the	Green coverage rate (A_{11})

		total area of the city; **positive indicator**	Water body coverage rate (A_{12})
	Topography & Landscape (A_2)	Terrain slope and ground elevation are important factors affecting urban waterlogging; **positive indicator**	Terrain slope (A_{21}) Ground elevation (A_{22})
	Urban River Network (A_3)	The ratio of natural rivers to artificial ditches, accounting for the total length of the river network in the area; **positive indicator**	Distance to river channel (A_{31})
	Urban Waterlogging (A_4)	Ground water accumulation during flood disasters; areas with a water depth > 0.15m are defined as waterlogging points; **negative indicator**	Distance to waterlogging point (A_{41}) Ground water depth (A_{42})
Lifeline Engineering (B)	Medical Resources (B_1)	Ability to provide medical assistance during flood disasters (including hospitals, medical institutions); **negative indicator**	Distance to medical institutions (B_{11})
	Transportation Network (B_2)	The proportion of road network length to the area of the district; **positive indicator**	Road network density (B_{21}) Distance to transportation stations (B_{22})
	Pipeline Facilities (B_3)	The proportion of drainage pipeline length to the area of the district; **positive indicator**	Drainage pipeline network density (B_{31})
	Communication Facilities (B_4)	Information transmission during disasters; **negative indicator**	Distance to communication maintenance stations (B_{41})
	Water Supply Facilities (B_5)	Water supply guarantee for residents during disasters; **positive indicator**	Water supply pipeline network density (B_{51})
	Power Facilities (B_6)	Power supply guarantee during disasters; **negative indicator**	Distance to power maintenance stations (B_{61})
	Population Density (B_7)	Population density; **negative indicator**	Population density (B_{71})
Rapid Recovery (C)	Regional Economic Situation (C_1)	Night lighting is positively correlated with social economy; used to characterize economic conditions; **positive indicator**	Night lighting (C_{11})
	Emergency Drainage &	Represented by the total hourly drainage capacity of emergency	Distance to drainage pump stations (C_{21})

	Rescue Capacity (C_2)	drainage and rescue equipment; **positive indicator**	Distance to sluice gates (C_{22})
	Emergency Rescue (C_3)	Preparedness for emergency management, command and rescue during disasters; the more timely the rescue, the more the indicator is reduced; **negative indicator**	Distance to emergency rescue stations (C_{31})
	Shelter (C_4)	Including civil engineering, schools, gymnasiums, hotels, squares, parks, etc.; **negative indicator**	Distance to shelter (C_{41})

4.2 Resilience Assessment Framework

Based on an analysis of the concept of urban flood resilience, the process by which a city copes with flood disasters can be divided into three stages: pre-disaster, in-disaster, and post-disaster. Initially, a city demonstrates its capacity to resist disasters before they occur. Once the disaster intensity exceeds the system threshold, the city enters an unpredictable state during the disaster, testing its adaptive capacity. Finally, the city undergoes a recovery process after the disaster. The level of urban resilience is reflected in the system's resistance, adaptation, and recovery capabilities. Ideally, a city will also undergo a process of learning and enhancement, leading to a continuous improvement in its resilience level.

To assess flood resilience, this study selects 20 indicators from three dimensions: pre-disaster urban spatial layout, in-disaster protection of lifeline systems, and post-disaster rapid recovery, thereby constructing an urban flood resilience evaluation indicator system. An improved entropy weight method combining subjective and objective approaches is used to describe the causal relationships among indicators and quantify their contribution rates to the resilience level. Furthermore, reasonableness analysis and correlation analysis are employed to evaluate the research results. Finally, based on simulation results from the urban stormwater model and combined with the evaluation indicator system, the city's resilience level and its spatial distribution characteristics are quantitatively analyzed.

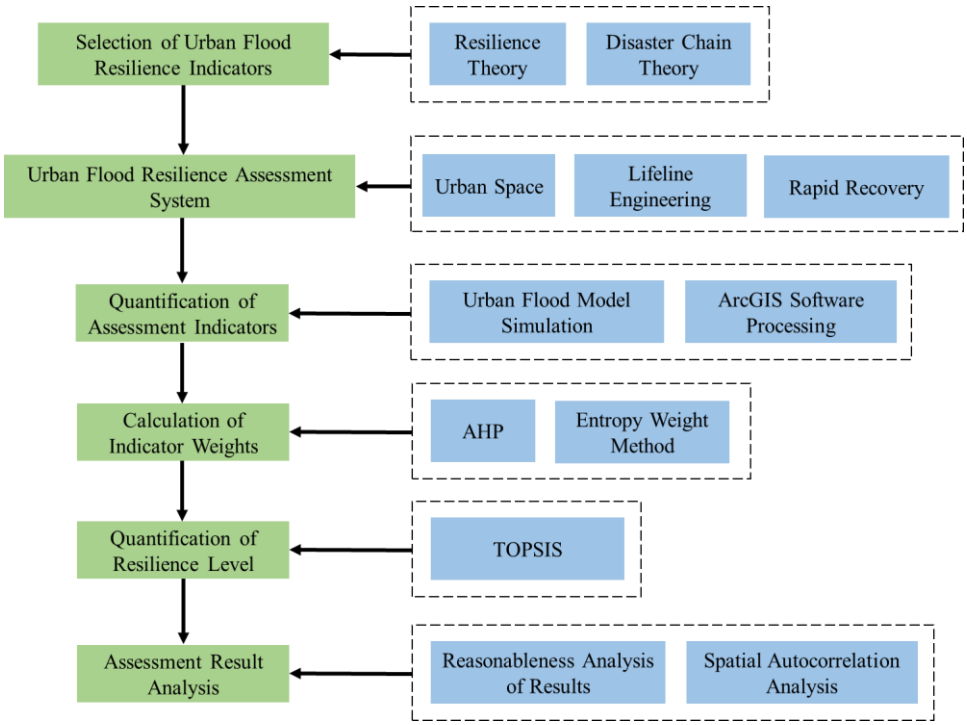

Fig. 6: Technical Workflow of the Urban Flood Resilience Assessment Framework

Based on scenario simulations using the IFMS/Urban model, the water depth and inundation duration within the study area under different scenarios were determined. The validation of urban waterlogging results was primarily conducted through the following methods: comparing waterlogging points and water depths, and assessing whether the simulated maximum water depth aligned with actual conditions. This study employed two approaches for model validation: comparing observed waterlogging-prone points and maximum inundation depths. Rainfall events from May 29, 2023, and July 13, 2023, were selected for validation. The maximum hourly rainfall intensities for these two events were 33 mm and 27.5 mm, respectively, both causing urban waterlogging and inundation. Using the rainfall data and corresponding urban river stage-discharge relationships from these two events as model inputs, the simulated inundation distribution and results were largely consistent with the actual situation, verifying the reliability of the waterlogging model simulation. The model-simulated distribution of waterlogging-prone points was used for quantitative resilience assessment, supporting urban flood resilience evaluation research, as shown in Figure 7.

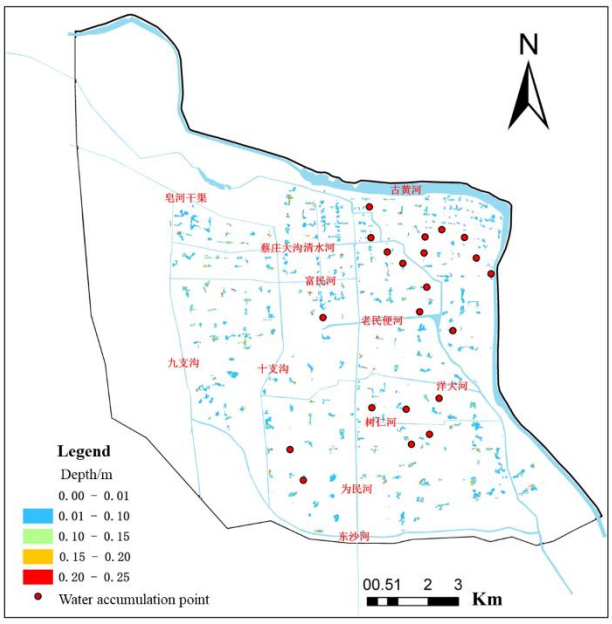

Fig. 7: Simulation Results of Waterlogging Points

5 RESULTS AND DISCUSSION

5.1 Urban Flood Resilience

This study utilized the indicator values from each grid cell and the indicator weights calculated using the improved entropy weight method. The Technique for Order Preference by Similarity to Ideal Solution (TOPSIS) method was then employed to calculate the resilience level of the southwestern district of Suqian City, resulting in a resilience score between 0 and 1 for each grid cell. The natural breaks classification method (Jenks) was applied to categorize the urban flood resilience levels in the southwestern district of Suqian into five grades: high resilience, relatively high resilience, medium resilience, relatively low resilience, and low resilience.

By synthesizing the spatial distribution of resilience levels across the three dimensions—urban space, lifeline systems, and rapid recovery—a comprehensive resilience level distribution map for the southwestern district of Suqian City was generated, as shown in Figure 8. The resilience levels were classified into the aforementioned five grades using the natural breaks method. Among the sub-districts, the Jiuzhigou sub-district, the Ximinbian River sub-district 1, and the ancient Yellow River sub-district 1 scored relatively high in the urban space and lifeline system dimensions but lower in the rapid recovery dimension. Overall, their comprehensive resilience levels were the highest. In contrast, the ancient Yellow River sub-district 2, the Weimin River sub-district, and the old Minbian River sub-district scored lower in the urban space and lifeline system dimensions, resulting in the lowest overall comprehensive resilience levels.

Overall, the central urban area, compared to the peripheral suburban and village areas, exhibits advantages primarily in relatively well-developed infrastructure and higher economic levels. However, excessive urban development and irrational urban planning can increase flood risk, exposing the city to higher hazards and lower resilience. Furthermore, as central urban areas concentrate a large number of infrastructure and lifeline systems (e.g., power, water supply, transportation), the impact of flooding on these critical facilities may lead to widespread consequences, thereby reducing the overall urban resilience. Suburban and village areas, despite

facing challenges such as lagging infrastructure construction and lower economic levels (which can hinder post-disaster rescue and recovery), generally face lower flood risks. Consequently, when confronting extreme disaster events, the impacts are often less severe, contributing to their relatively higher resilience levels.

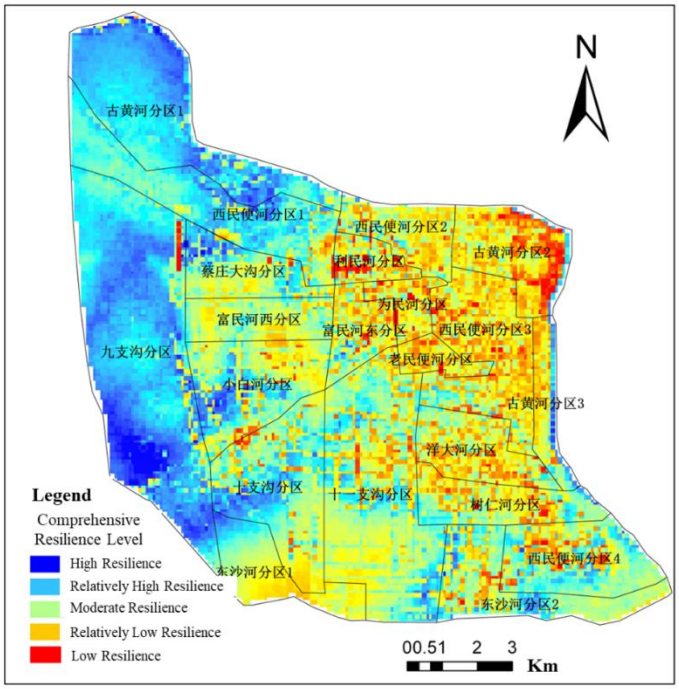

Fig. 8: Comprehensive Resilience Level Distribution

5.2 Reasonableness Analysis of Results

Based on the resilience assessment results obtained from the improved entropy weight-TOPSIS method, the reasonableness of these results was analyzed. Radar charts were constructed using the average values of indicators for different resilience grades, as shown in Figure 9. Indicators such as green coverage rate, distance to the river network, distance to waterlogging-prone points, sluice-gate regulation capacity, and drainage network density have a significant impact on the resilience assessment results.

As indicated in Figure 9, areas with high resilience levels are generally located farther from the river network and waterlogging-prone points, exhibit higher green coverage rates, denser water supply and drainage networks, lower population densities, and stronger sluice-gate regulation capacities. When flood disasters occur, these areas, being farther from hazard sources (river network, waterlogging-prone points), face lower risks of waterlogging and inundation. Factors such as low population density, high green coverage, and strong sluice-gate regulation capacity contribute to their higher resilience levels. Conversely, areas with low resilience levels are often located near waterlogging-prone points, characterized by lower densities of water supply and drainage networks, poorer sluice-gate regulation and pumping station drainage capacities, and greater distances from hospitals and emergency shelters. Furthermore, the spatial distribution of these low-resilience areas largely aligns with the high-risk waterlogging points identified in the "Systematic Implementation Plan for Urban Waterlogging Control in Suqian Central City." Therefore, the resilience level assessment results for the southwestern district of Suqian City presented in this study can be considered fundamentally reasonable.

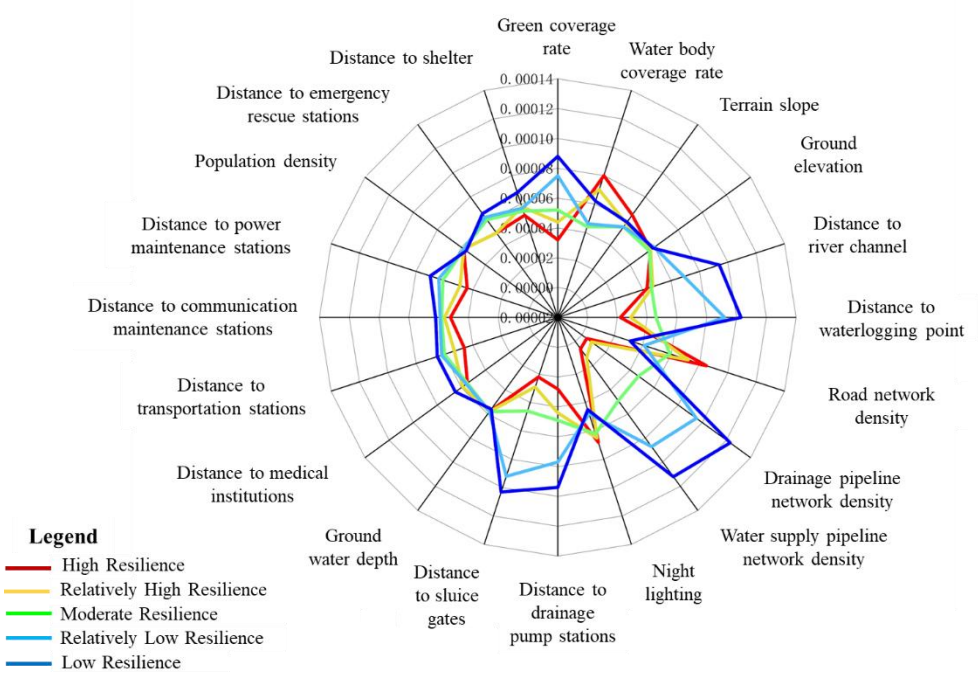

Fig. 9: Average Indicator Values for Different Resilience Grades

5.3 Spatial Autocorrelation Analysis

Spatial autocorrelation refers to the correlation of the same variable across different spatial distributions. It is a method used to measure the degree of clustering of attributes across spatial units and can reveal patterns and trends in the spatial distribution of a given attribute. This study employed the spatial autocorrelation index (Moran's I) to conduct a correlation analysis of the resilience results. The obtained Moran's I score was 0.708, with a p-value less than 0.05, passing the significance test. This indicates a global spatial clustering pattern in the distribution of resilience levels across the southwestern district. Furthermore, using the LISA (Local Indicators of Spatial Association) cluster analysis method in ArcGIS, a local clustering analysis of the resilience levels in the southwestern district was performed, as shown in Figure 10.

The results indicate that areas with non-significant clustering account for 61.23% of the region, while areas with significant clustering account for 38.77%. This suggests that the distribution of resilience levels within the study area is not completely random; rather, there is spatial clustering of similar values. Specifically, the proportions of High-Low and Low-High cluster areas are 0.31% and 0.25%, respectively. High-High cluster areas account for 19.93%, indicating that areas with high resilience levels are concentrated, primarily located in the western part of the study area. Low-Low cluster areas account for 18.29%, showing that areas with low resilience levels are also concentrated, mainly distributed in the central urban area on the eastern side of the study area.

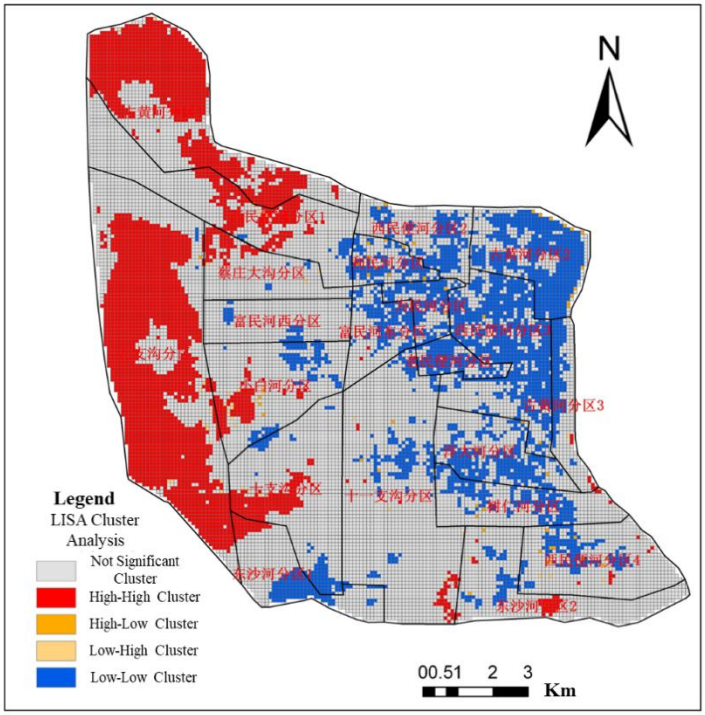

Fig. 10: LISA Cluster Analysis

6 CONCLUSIONS

This study focuses on the issue of urban flood disasters. Integrating the current resilience concept in flood management and the theory of urban flood disaster chains, and based on a systematic review of the fundamental concepts and influencing factors of urban flood resilience, an urban flood resilience assessment framework was proposed using the IFMS/Urban urban flood simulation model. Taking the southwestern district of Suqian City as a case study, factors affecting the urban resilience level were analyzed. Addressing the practical needs of urban disaster prevention and mitigation, the overall strategy and technical system for enhancing urban flood resilience were proposed. Based on the resilience assessment results for the southwestern district of Suqian City, specific resilience improvement strategies were suggested, and their potential effects were analyzed.

The research findings indicate that indicators such as green coverage rate, distance to the river network, distance to waterlogging-prone points, sluice-gate regulation capacity, and drainage network density significantly influence the resilience assessment results. The resilience assessment results largely align with the locations of high-risk urban waterlogging points published by Suqian City, demonstrating the fundamental reasonableness of the assessment. The results also reveal that the flood resilience index for most areas exhibits a clear local spatial clustering effect. Within the study area, there are High-High clusters and Low-Low clusters. High-resilience cluster areas account for 19.93%, while low-resilience cluster areas account for 18.29%.

As an interdisciplinary and comprehensive subject, research on urban flood resilience will, with deepening theories and advancing technologies, increasingly emphasize the integration and synergy in urban resilience building in the future. This will promote the translation of theory into practice, providing sustainable solutions for cities worldwide to cope with flood disasters.

7 REFERENCES

[1] United Nations Office for Disaster Risk Reduction. Human cost of disasters 2000-2019 report - un office for disaster risk reduction[R]. Geneva, Switzerland: UNDRR, 2021.

[2] CHENG L, TRENBERTH K E, GRUBER N, et al. Improved estimates of changes in upper ocean salinity and the hydrological cycle[J]. Journal of Climate, 2020, 33(23): 10357~10381.

[3] RENTSCHLER J, SALHAB M, JAFINO B A. Flood exposure and poverty in 188 countries[J]. Nature Communications, 2022, 13(1): 3527.

[4] VITALE C, MEIJERINK S, MOCCIA F D. Urban flood resilience, a multi-level institutional analysis of planning practices in the metropolitan city of naples[J]. Journal of Environmental Planning and Management, 2023, 66(4): 813~835.

[5] CUTTER S L, BURTON C G, EMRICH C T. Disaster resilience indicators for benchmarking baseline conditions[J]. Journal of Homeland Security and Emergency Management, 2010, 7.1.

[6] JOERIN J, SHAW R, TAKEUCHI Y, et al. The adoption of a climate disaster resilience index in chennai, india[J]. Disasters, 2014, 38.3: 540~561.

[7] BRUNEAU M, CHANG S E, EGUCHI R T, et al. A framework to quantitatively assess and enhance the seismic resilience of communities[J]. Earthquake Spectra, 2003, 19(4): 733~752.

[8] MA Jianming, YU Haijun. ZHANG Dawei, et al. Adoption of evaluation software in flood risk map drawing [J]. China Water Resources,2017,(05):17-20.

[9] MOGHADAS M, ASADZADEH A, VAFEIDIS A, et al. A multi-criteria approach for assessing urban flood resilience in tehran, iran [J]. International Journal of Disaster Risk Reduction, 2019, 35: 101069.

[10] CHEN Y, ZHU M, ZHOU Q, et al. Research on spatiotemporal differentiation and influence mechanism of urban resilience in china based on mgwr model: 3[J]. International Journal of Environmental Research and Public Health, 2021, 18(3): 1056.

[11] XUN X, YUAN Y. Research on the urban resilience evaluation with hybrid multiple attribute topsis method: an example in china[J]. Natural Hazards, 2020, 103(1): 557~577.

[12] DONG X, SHI T, ZHANG W, et al. Temporal and spatial differences in the resilience of smart cities and their influencing factors: evidence from non-provincial cities in china: 4[J]. Sustainability, 2020, 12(4): 1321.

[13] HUANG Jing, SHE Jing-wen, YUAN Xiao-mei, et al. Simulation of Urban Flood Resilience Based on A System Dynamic Model: A Case Study in Nanjing [J]. RESOURCES AND ENVIRONMENT IN THE YANGTZE BASIN, 2020(11 vo 29): 2519~2529.

[14] ZHU S, LI D, FENG H, et al. The influencing factors and mechanisms for urban flood resilience in china: from the perspective of social-economic-natural complex ecosystem[J]. Ecological Indicators, 2023, 147: 109959.

[15] CUTTER S L, BARNES L, BERRY M, et al. A place-based model for understanding community resilience to natural disasters[J]. Global Environmental Change, 2008, 18(4): 598~606.

ICFM 10
Adapting to Global Change:
Innovative Approaches to Flood Management and Resilience
May 20-22, 2026 | Western University, London, Ontario, Canada

Cost Effective Hydraulic Modelling to enable Resilient Urban Regeneration within Reservoir Inundation Areas

Dr Philip Hull PhD Beng CEng MCIWEM C.WEM MICE MIEI
Flood Risk Consulting Ltd, 93 Hillsborough Road, Lisburn, Co Antrim, Northern Ireland, BT281JN
E-mail: phil@floodriskconsulting.com

ABSTRACT

Within Northern Ireland (NI), planning policy severely restricts development within the predicted inundation area of dams that are not considered to have responsible reservoir manager status. This paper aims to present a cost-effective method to allow these brownfield sites to be regenerated by applying appropriate flood resilience measures at hydraulic modelling stage. DfI Rivers, who are the flood defence and drainage authority for NI, are in possession of detailed hydraulic modelling of dam failures, but they will only release limited information from those models due to national security reasons. To develop a site within an inundation area, a developer would therefore have to create their own hydraulic model from the reservoir to their site and then demonstrate the above restrictions regarding risk to life and third-party land can be overcome. With reservoirs often being several miles from the site and the bathymetry of the reservoir being unknown, most small-scale developers cannot afford the substantial surveying costs for the land between the reservoir and their site, as well as acquiring details for the dam and reservoir itself, in order to build an appropriate hydraulic model. In order to address the growing number of brownfield sites that cannot be regenerated because of the above restrictions, the author has developed an Infoworks ICM hydraulic model method that uses basic reservoir measurements and free Digital Terrain Model (DTM) data to mimic DfI Rivers' predicted inundation area from the reservoir to the site in question and then applies parameters to the hydraulic model based on DEFRAs "Hazard to People Classification using Hazard Rating" to determine flood risk to various people groups using the developed site, including vulnerable people, the general public and the emergency services.

1 INTRODUCTION

Proposed regeneration of brownfield sites in NI often encounters planning issues whenever the dams and reservoirs that sit above the towns and cities within which the regeneration is being proposed are not considered to be in an appropriate state of repair. The majority of these proposed regeneration schemes are relatively small in nature and so the developer does not have adequate funds to fully hydraulically model potential reservoir failures from reservoirs potentially miles from their sites in order to propose mitigation measures that would allow the proposal to proceed beyond planning stage. This paper will present a case study that made use of cost-effective hydraulic modelling that used basic reservoir measurements and free topographical survey information between the reservoir and the site and then proposed reconfiguration of the topography of the site itself in order to address future reservoir flood risk to people using the regenerated site without increasing risk to third party land beyond the site.

2 RESERVOIR MODELLING IN THE UK

2.1 Historical context for reservoir modelling

There has been no loss of life from reservoir failure in the UK since reservoir safety legislation was introduced in 1930. Nevertheless, a risk was identified that should the potential collapse of a reservoir be considered imminent, the emergency services would not have easily accessible information on which areas to evacuate first. In 2007, Sir Michael Pitt therefore recommended creating national flood maps for reservoir failure to enable Local Resilience Forums to assess risks and plan for contingency, warning and evacuation. The Reservoir Inundation Mapping (RIM) Specification, now known as Reservoir Flood Mapping (RFM) Specification, was first established in 2009 (EA, 2009) and used to produce a total of 2,232 reservoir flood maps in England and Wales.

Dam breach flooding happens when a dam impounding a reservoir breaches, causing water stored in the reservoir to be released through the breach and flooding areas downstream of the dam. The dam breach scenario simulated on the reservoir flood maps is a "credible worst case" scenario that represents a generic dam failure that could be adopted across the country. The procedure for the development of the flood maps included the prediction of the dam breach outflow hydrograph and routing of the hydrograph downstream of the reservoir, where the approach for the modelled breach scenario for an impounding reservoir assumed that the reservoir water level has risen to dam crest level plus 0.5, leading to overtopping over the entire height of the dam. These breach assumptions were intended to produce a single, simplified dam breach hydrograph that reflected a credible worst-case scenario for a hypothetical dam breach. In addition to the above addition to crest level, the calculation method of the outflow hydrographs used for the flood mapping for earthfill embankments identifies that a factor of safety of 1.5 is applied to the peak discharge (according to Froehlich (1995)). Therefore, the modelling of an impounding reservoir generally assumes a crest level plus 0.5m, that the full extent of the dam structure itself effectively disappears, causing flooding that occurs along the full length of the reservoir rather than at an isolated breach location, and that a safety factor of 1.5 is applied to the discharge flow.

The topography downstream of the reservoirs is presented in the hydraulic model by a digital terrain model (DTM), constructed using either LiDAR or IFSAR data. Flood plain features such as road and railway embankments are represented in the hydraulic model, but buildings, bridges and culverts are not represented. Finally, a Manning's friction *n* value of 0.10 is set globally for the reservoir flood modelling.

2.2 Flood Risk to People Methodology

In order to quantify risk to life from various forms of flooding, such as from rivers, estuaries and the sea, the Risks to People Methodology was created as a multi-criteria assessment based on the concepts of flood hazard, area vulnerability and people vulnerability. As such, the methodology does not consider a specific threshold for tolerable risk such as flood hazard, but instead combines the hazard with both area and people vulnerabilities to determine risk. Phase 1 of the above methodology then used the above criteria to calculate whether the annual risk of fatality from a potential flood source was deemed 'acceptable' if it was less than a 'tolerable' value (HR Wallingford, 2005a).

Phase 1 methodology is outlined by the following equation, applied to a particular flood risk:

$$Ninj = NZ \times HR \times AAV \times PV \quad (1)$$

Where Ninj = number of injuries

NZ = population at risk of flooding
HR = Hazard Rating, a function of flood depth and velocity and debris factor
AV = Area Vulnerability, a function of effectiveness of flood warning, speed of onset of flooding and nature of area (including types of buildings)
PV = People vulnerability, a function of presence of people who are very old and/or infirm/disabled/long term sick

2.3 Flood Hazard (HR)

There is a broad consensus that the degree of hazard that floodwaters present to people (and to vehicles and property) is a function of both velocity and depth. In addition, other factors may affect the stability of people during flooding, where a debris factor is included in the flood hazard equation. The equation for Flood Hazard HR is as follows:

$$HR = d(v + 0.5) + DF \quad (2)$$

Where HR = flood hazard rating
d = depth of flooding (m)
v = velocity of floodwaters (m/s)
DF = debris factor (+0, 0.5 or 1 depending on the probability that debris will lead to a significantly greater hazard)

The supplementary note on flood hazard ratings and thresholds by Surendran et al. (2008) was produced to reconcile the above information with planning policy in England and Wales, which requires that people should be appropriately safe around new development. This document emphasised that rather than concentrating on Phase 1 of the Risks to People methodology, which also allows consideration of factors such as the population at risk of flooding and the Area Vulnerability factor, Flood Risk Assessment (FRA) reports that are produced as part of a planning application for an individual site should take a simplified approach by concentrating on the flood hazard rating (HR) and the people vulnerability (PV).

2.4 Planning Policy in NI for Development in Proximity to Reservoirs

Policy FLD 5 of PPS 15 (DOE, 2014) states that new development in NI will only permitted within the potential flood inundation area of a controlled reservoir (i.e. reservoirs with an individual or combined capacity greater than 10,000 cubic metres above the natural level of any part of the surrounding land) if the applicant can demonstrate that the condition, management and maintenance regime of the reservoir is appropriate to provide sufficient assurance regarding reservoir safety, so as to enable the development to proceed. Where a reservoir has been conferred 'Responsible reservoir management status' the above criteria is assumed to have been met. However, where this status has not been conferred, DFI (2020) have stated that the Flood Risk to People Methodology proposed by HR Wallingford (2005a) & HR Wallingford (2005b) should be used in conjunction with Surendran et al.'s (2008) simplified approach of considering flood hazard ratings for various people groups when applying Policy FLD 5 of PPS 15 to proposed development that lies within the predicted inundation path of a controlled reservoir.

DfI Rivers, who are the NI government body responsible for flood defence, watercourse maintenance and managing river and sea defences, are in possession of reservoir inundation mapping for

all the controlled reservoirs across NI. However, they will only release limited information from those models due to national security reasons. Instead, DfI Rivers will advise the Planning Authority when an FRA would be required to assess the Flood Hazard Rating (HR) for an individual planning application that lies within the predicted inundation area of a controlled reservoir that is not in possession of Responsible reservoir management status. However, the majority of proposed regeneration schemes are relatively small in nature and so the developer does not have adequate funds to fully hydraulically model potential reservoir failures from reservoirs potentially miles from their sites in order to propose mitigation measures that would allow the proposal to proceed beyond planning stage. The author therefore developed cost-effective hydraulic modelling that uses basic reservoir measurements and free topographical survey information between the reservoir and the site and then proposes reconfiguration of the topography of the site itself in order to address future reservoir flood risk to people using the regenerated site without increasing risk to third party land beyond the site. The remainder of this paper will present a case study of this approach.

3 CASE STUDY OF COST-EFFECTIVE HYDRAULIC RESERVOIR MODELLING

3.1 Dam breach hydrograph calculation

EA (2016) presents guidance on dam breach modelling, including the determination of a dam breach hydrograph which can be calculated based on the dimensions and nature of the embankment structure and the impounded waters. The peak discharge from the reservoir and the time to peak discharge are calculated using the Froehlich (1995) equation (Equation 3) and the Brown and Gosden (2004) equation (Equation 4). Finally, the time of end discharge can be calculated based on the consideration that the volume under the hydrograph represents the volume of water within the reservoir above the adjacent ground level.

$$Q_P = FOS\ [0.607(V_W^{0.295} \times H_W^{1.24})] \quad (3)$$

where Q_P = Peak discharge (m3/s)
FOS = Factor of safety: 1.5
V_W = Volume of reservoir above adjacent ground levels (m^3)
H_W = Dam height (m)

$$T_P = 120\ H_W \quad (4)$$

Where T_P = Time to peak discharge (s)
H_W = Dam height (m)

Therefore, by recording basis measurements for both the dam height and adjacent ground level and then calculating the footprint area of the reservoir using available mapping, it is possible to estimate both a peak discharge and hydrograph shape for the design flow from the failed reservoir. In NI, free DTM data is available at 10m resolution across the country, with some areas of the country also providing free 1m LiDAR information. Based on the best information that can be freely sourced, a ground model is therefore created using Infoworks ICM (Integrated Catchment Modelling) software. A 2D line source can be created along the boundary of the reservoir and the design flow hydrograph applied to order to create

the appropriate inundation area for the failed reservoir. Figure 1 presents the case study's inundation area 6 minutes and 18 minutes after the commencement of the flood event.

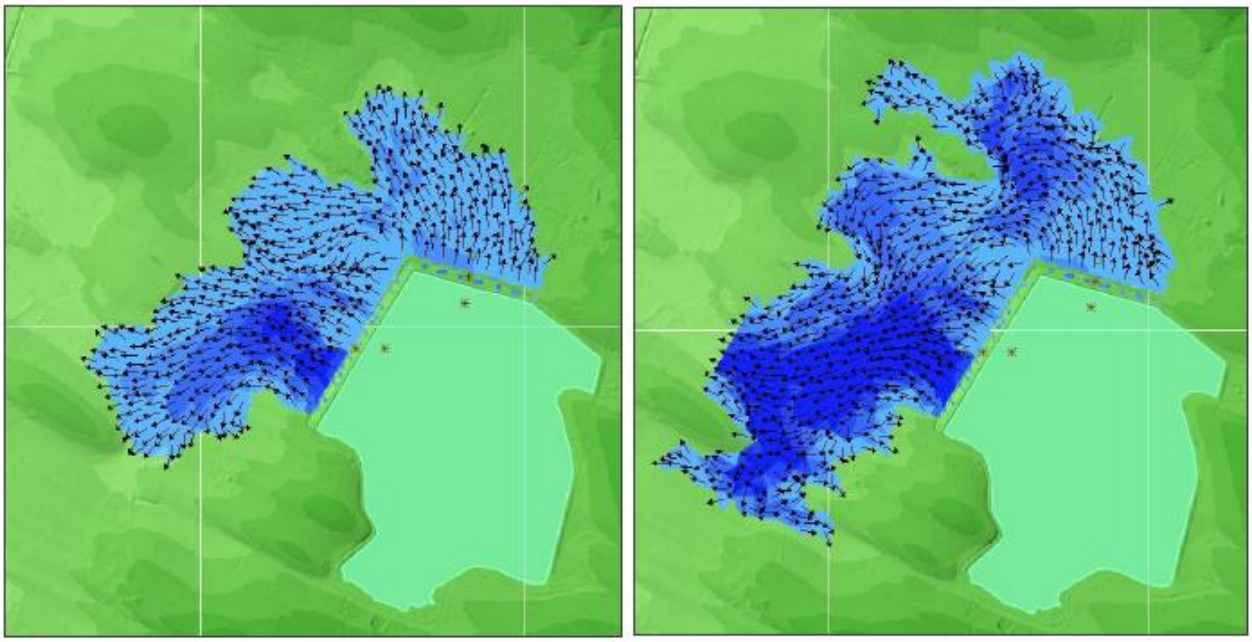

Figure 1: Time series of inundation area from failed reservoir

Figure 2 presents the maximum flood extent and depths from the hydraulic model, as focused on the proposed site (red line). Inundation is predicted across the majority of the site, with the main route and therefore deeper flooding (darker bands of blue hatching) predicted immediately south of the site.

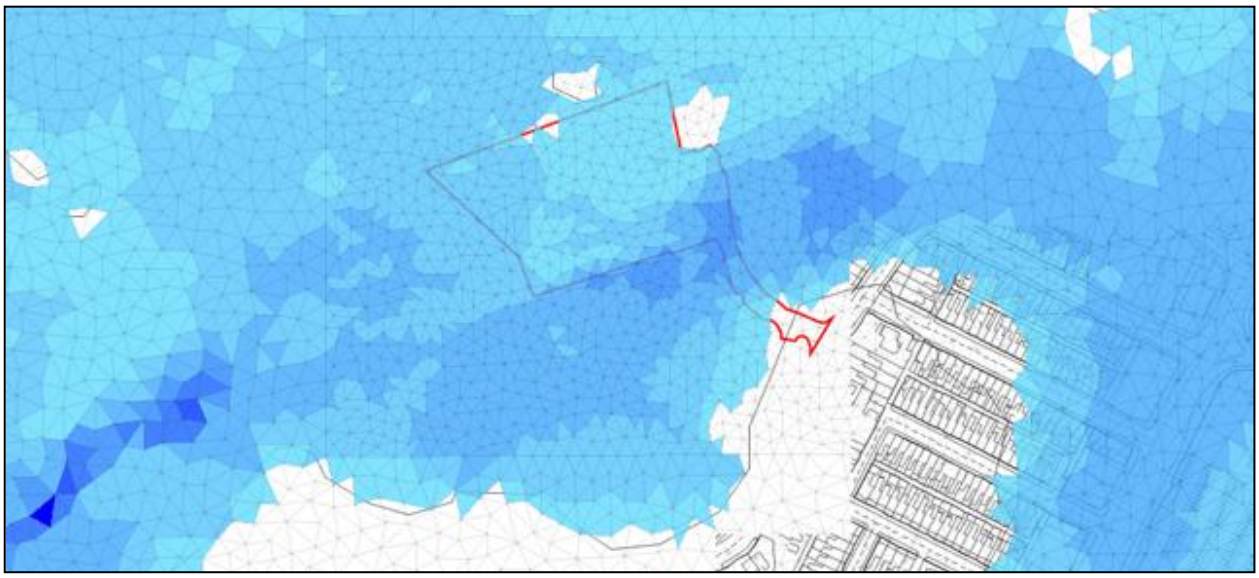

Figure 2: Maximum flood extents and depths at the site

A 'theme' is then applied to the results of the Infoworks ICM hydraulic model that is defined by both the predicted depth and velocity and each individual element within the hydraulic model mesh, as

based on the parameters set out by Surendran et al. (2008). Figure 3 presents the predicted flood 'hazard to people' results, which reflect the parameters used by Defra/EA. These results show that the red banding, categorised as 'Danger to all – includes the emergency services' extends along the western and southern sides of the site. Orange banding, categorised as dangerous to the general public, extends across the majority of the western half of the site, while yellow (danger for some – includes children, the elderly and the infirm) and blue hatching (very low hazard) extends across the remainder of the eastern half of the site. The planning application proposed constructing 18 dwellings within the eastern part of the site (red rectangles), but 3 of the 18 dwellings were located within areas of land that were considered either dangerous to the general public or to the emergency services and therefore the planning application in its present state was not deemed viable.

Figure 3: Hazard to people (HR) results

A trial-and-error process was therefore undertaken to reprofile the site by applying various 'mesh level zones' to the footprint of the site within the hydraulic model. The goal of the trial and error process was to allow reservoir inundation to continue passing through the site, so as not to increase flood risk beyond the site. However, by some minor reprofiling of the site, it was possible to reduce the orange and red hatched areas in the eastern part of the site and so allow all 18 dwellings to fall into the low hazard rating categories. Figure 4 presents a 3D image of the reprofiled site, with vehicle access provided from the south to a slightly elevated residential area. Figure 5 presents the hazard to people (HR) results for the reprofiled residential development, where flooding continues to pass through the residential area at a low risk combination of depth and velocity without increasing the predicted hazard rating beyond the site.

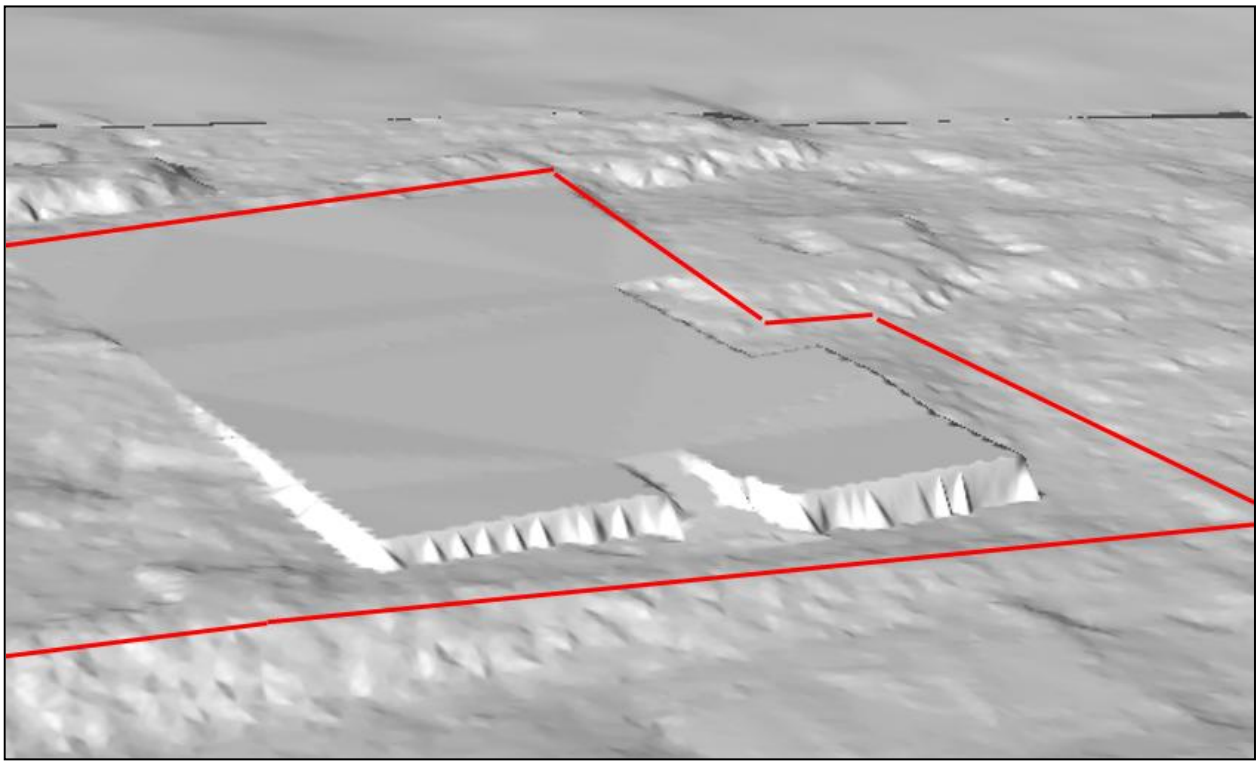

Figure 4: 3D image of reprofiled site

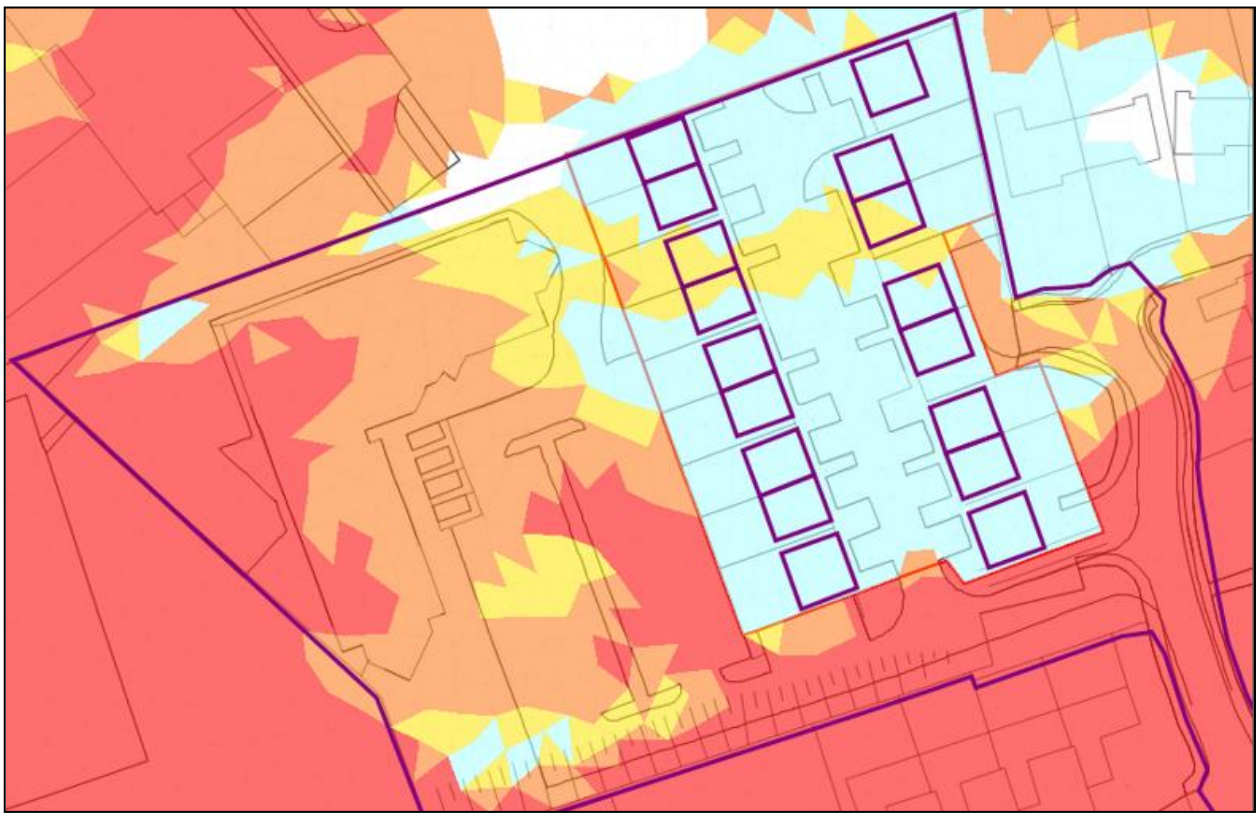

Figure 5: Hazard to people (HR) results for reprofiled site

4 CONCLUSION

Planning policy in NI is restricting development within the predicted inundation area of dams that are not considered to have responsible reservoir manager status. With the drainage authority for NI only allowed to release limited information on potential reservoir inundation areas for national security reasons, developers of small sites cannot afford to have detailed hydraulic models constructed from reservoirs that could be several miles from their site. This paper has therefore presented a case study to demonstrate how an Infoworks ICM hydraulic model can be constructed using basic reservoir measurements and free Digital Terrain Model (DTM) data to mimic DfI Rivers' predicted inundation area from the reservoir to the site in question. DEFRAs "Hazard to People Classification using Hazard Rating" method can then be examined within the hydraulic model and where feasible, the site can be topographically reconfigured within the hydraulic model to maximise the area of land that is considered to have an acceptable hazard rating for future development, while ensuring that flood risk is not increased to adjacent third-party land.

REFERENCES

BROWN, AJ & GOSDEN JD (2004). Interim guide to quantitative risk assessment for UK reservoirs, Thomas Telford Ltd, London, UK

DFI (2020). TGN 25 Revised: The practical application of Strategic Planning Policy for 'Development in Proximity to Reservoirs', Belfast, UK.

DOE (2014). Revised Planning Policy Statement 15 'Planning and Flood Risk', Belfast, UK.

EA (2009). Reservoir Inundation Mapping Specification. Environment Agency, Bristol, UK.

EA (2016). Reservoir Flood Maps (RFM) Guide: Explanatory Note on Reservoir Flood Maps for local resilience Forums, Version 4. Environment Agency, Bristol, UK.

Froehlich D C (1995). Peak outflow from breached embankment dam. ASCE Journal of water resources planning and management 121(1) 90-97.

HR Wallingford, 2005a, FDR2321/PR. Flood Risks to People Phase 2. Project Record.

HR Wallingford, 2005b. FD2321/TR1. Flood Risks to People Phase 2. Technical REPORT 1: The Risks to People Methodology.

SURENDRAN S, GIBBS G, WADE S & UDALE-CLARKE H (2008). Supplementary note on flood hazard ratings and thresholds for development planning and control purpose – Clarification of the Table 13.1 of FD2320/TR2 and Figure 3.2 of FD2321/TR1. Environment Agency, Bristol, UK

ICFM 10
Adapting to Global Change:
Innovative Approaches to Flood Management and Resilience
May 20-22, 2026 | Western University, London, Ontario, Canada

A Data-Driven SPC Framework for Flood Prevention Using SNIRH Time Series in R and Python

André L. Teixeira[1], João Victor S. Maia[1] and Nicolly de Lima Barbosa[1]
Business Administration, Faculdade Engenheiro Salvador Arena, São Bernardo do Campo, 09850-550, Brazil[1]
E-mail: pro21002391@cefsa.edu.br

ABSTRACT

Statistical Process Control (SPC) is a widely adopted methodology for monitoring production systems and has recently gained attention in water resource management. This study explores the application of SPC in flood prevention, focusing on the detection of anomalies in hydrological time series. Using 25 years of historical data from the Brazilian National Water Resources Information System (SNIRH) and open-source tools (R/Python), we developed an automated framework integrating Multivariate SPC (Hotelling's T^2) and Process Capability (C_{pk}) analysis.

The results demonstrate the effectiveness of the T^2 chart in identifying the 50 most critical hydrological events between 2000 and 2025, decomposing the contribution of precipitation and river discharge to each alert. A process capability study revealed a C_{pk} of 2.45 for the basin's operational limits, providing a quantitative metric for resilience. Furthermore, Cross-Correlation Analysis (CCF) successfully identified the hydrological lag time, essential for early warning precision. The integration of SPC with residual analysis from regression models proved capable of detecting "model ruptures" caused by soil saturation. These findings confirm that SPC is a powerful complementary tool for flood forecasting, providing scalable, real-time situational awareness for public authorities and contributing to data-driven, resilient disaster risk management strategies.

KEYWORDS: Statistical Process Control (SPC), Flood Forecasting and Prevention, Hydrological Time Series Analysis, Statistical Modeling (R, Python), Anomaly Detection, Real-time Monitoring and Early Warning Systems

1 INTRODUCTION

Floods are among the most recurrent and devastating natural disasters in Brazil, leading to significant economic, social, and environmental losses. Efficient forecasting and management of these events require robust methodologies for the continuous monitoring of hydrological and meteorological variables. In this context, Statistical Process Control (SPC) has emerged as a promising approach for the early detection of anomalies and trends in hydrological time series, contributing to more effective mitigation and response strategies.

The integration of computational tools such as R and Python enables the implementation of advanced statistical techniques and predictive modeling. These languages are widely utilized for data acquisition, manipulation, and interpretation, facilitating the understanding of patterns in complex time series (Reis Jr. et al., 2023). Furthermore, accessing high-resolution data from the Brazilian National Water Resources Information System (SNIRH) ensures a reliable foundation for monitoring variables such as precipitation, river discharge, and water levels (ANA, 2023). Therefore, applying SPC alongside these tools represents a significant advancement in water risk management, enabling more assertive decision-making.

1.1 Problem Statement and Rationale

The urgency of this research is grounded in the increasing need for effective flood prevention methods, as extreme events become more frequent and severe due to climate change and disordered urban expansion. Adapting SPC—traditionally used in industrial quality control—to hydrological monitoring allows for the identification of critical patterns and anomalous trends before extreme events occur. By exploring the intersection of quality engineering, statistics, and environmental science, this study seeks to modernize water disaster management. The proposed framework is designed to be scalable across different geographic contexts, supporting data-driven public policies.

1.2 Research Objectives

The primary objective of this study is to evaluate the application of Statistical Process Control (SPC) in flood prevention by utilizing SNIRH data processed through R and Python. To achieve this, the research initially focuses on the collection and harmonization of hydrological data, specifically precipitation and river discharge, to ensure a robust foundation for statistical analysis. Building upon this dataset, the study implements Multivariate SPC techniques—centered on Hotelling's T^2 charts—to monitor hydrological variables and identify critical shifts in the process. Furthermore, the research involves developing statistical models and residual analysis to detect 'model ruptures' within the rainfall-runoff relationship, thereby enhancing the precision of anomaly detection. The effectiveness of this methodology is assessed by benchmarking statistical alerts against historical flood records. Finally, the study provides strategic guidelines for integrating SPC into existing Early Warning Systems (EWS), aiming to enhance the resilience of vulnerable watersheds through proactive, data-driven monitoring.

2 THEORETICAL FRAMEWORK

2.1 Statistical Process Control (SPC) Foundations

The theoretical basis of Statistical Process Control (SPC) lies in the distinction between common and special causes of variation, as established by Shewhart (1931) and further developed for modern engineering by Montgomery (2020). SPC employs control charts to monitor process stability and detect anomalies before they reach critical levels. For hydrological monitoring, the choice of charts depends on data nature: variables (continuous data) or attributes (discrete counts). While traditionally industrial, recent studies by Schreiber et al. (2022) demonstrate that SPC charts are robust tools for identifying non-random patterns in environmental time series.

2.2 Hydrological Context and Flood Monitoring

Inland flooding is a complex phenomenon driven by intense rainfall and drainage failures (Alves et al., 2024). In Brazil, the intensity of these events has increased significantly—up to 32% per decade in some regions (Chagas et al., 2022). The 2024 catastrophe in Rio Grande do Sul, which impacted 80% of the state's territory, highlights the urgency of non-structural mitigation strategies like Early Warning Systems (RS, 2024). According to Lima et al. (2019), extreme precipitation events can be modeled using SPC to provide advanced alerts, bridging the gap between quality management tools and disaster prevention.

2.3 Data Sources and Computational Tools

The Brazilian National Water Resources Information System (SNIRH), managed by the National Water Agency (ANA, 2023), provides a robust database for this study, monitoring over 23,000 stations with data on river stage, discharge, and rainfall. The integration of this big data with computational languages like R and Python allows for automated statistical modeling. Libraries such as hydroTSM (R) and Pandas/SciPy (Python) facilitate the handling of complex time-series, increasing the reliability of flood forecasting models while reducing manual intervention (Marengo et al., 2025).

To address the challenge of data longevity over a 25-year horizon, this study prioritized stations with at least 95% data completeness. This ensures that the 'multivariate space' remains populated throughout the longitudinal analysis, avoiding the risks associated with sparse data in the training of the SPC model.

3 MATERIALS AND METHODS

3.1 Study Design and Data Acquisition

This research employs an applied quantitative approach, utilizing a 25-year historical dataset (2000–2025) obtained from the Brazilian National Water Resources Information System (SNIRH) via the Hidroweb platform. The study area focuses on watersheds with a history of recurrent flooding. Data selection criteria included stations with over 20 years of records and a minimum of 95% completeness to ensure statistical robustness (Table 1).

Table 1: Statistical Summary of the SNIRH Hydrological Dataset

Data Category	Total Stations	Median (Years)	Mean (Years)	Min. (Years)	Max. (Years)
Pluviometry (Rainfall)	12,188	26.5	31.6	0.0	80.0
River Stage (Level/Cota)	6,020	12.9	23.3	0.0	80.0
Discharge (Flow/Vazão)	4,604	11.6	23.8	0.0	80.0
Climatological Data	691	49.5	53.2	0.2	80.0
Water Quality	5,456	9.8	13.4	0.0	80.0
Sedimentometry	2,052	5.6	10.8	0.0	54.1
Telemetry (Digital)	10,849	4.1	6.5	0.0	25.1

Note: The minimum values in Table 1 for Discharge and Sedimentometry represent raw metadata artifacts from the SNIRH database, often indicating stations in initial testing phases. For this study, a strict filtering process was applied to select only monitoring stations with a continuous and positive 25-year history (2000–2025) to ensure the longevity and consistency required for the SPC baseline.

Source: SNIRH (2025)

The primary variables analyzed are:

- River Stage (m) and Discharge (m^3/s): Indicators of the physical state and volume of the watercourse.
- Accumulated Precipitation (mm): The primary input variable driving flood events.

3.2 Data Processing and Standardization

Data processing was performed using an integrated environment of R (v4.4) and Python (v3.11). Given the high frequency of hydrological data, pre-processing involved linear interpolation for minor gaps and synchronization of time series.

To enable multivariate analysis, variables were standardized using the Z-score method:

$$Z = \frac{x - \mu}{\sigma}$$

where x is the measured value, μ the historical mean, and σ the standard deviation of the "in-control" period (defined as periods without extreme flood events).

3.3 Multivariate Statistical Process Control (MSPC) Framework

The core methodology transitions from univariate to multivariate monitoring to capture the interaction between rainfall and river response. The framework follows four stages:

I. Hotelling's T^2 Chart: Used to monitor the combined variability of precipitation and river stage. This multivariate approach detects system-wide anomalies that univariate charts might miss.

II. Contribution Analysis: For points exceeding the Upper Control Limit (UCL), a contribution analysis was performed to determine whether the "out-of-control" state was primarily driven by extreme rainfall (blue signature) or pre-existing high river levels (orange signature).

III. Residual Analysis: A linear regression model (River Stage \ Precipitation) was established. The residuals (errors) were monitored using an X-bar and S chart to identify "model ruptures," which occur when the physical rainfall-runoff relationship shifts due to soil saturation.

IV. Process Capability (C_{pk}): The basin's "safety margin" was quantified by treating the flood overflow level as the Upper Specification Limit (USL). A C_{pk} index was calculated to measure how far the operational "process" (river flow) is from its physical failure point (flooding).

Regarding the visual characteristics of the resulting monitoring charts, the perceived smoothness of the T^2 series is a deliberate outcome of the Z-score standardization and the multivariate aggregation of variance. From an SPC perspective, this is highly defensible as it filters out high-frequency 'common cause' noise, allowing the model to highlight only the 'special cause' signals (extreme hydrological events). This ensures that the detection of the 50 critical points remains robust and free from false-positive fluctuations inherent in raw hydrological data.

A key advantage of this SPC-based approach is its computational efficiency and scalability across SNIRH's Big Data network (12,000+ stations) without requiring the site-specific physical parameters (e.g., bathymetry, soil hydraulic conductivity) needed for hydrodynamic models. However, a limitation for flood management is that the framework is strictly empirical; it detects statistical 'out-of-control' states but does not simulate the physical propagation path or water velocity. Thus, it is proposed as a high-speed, complementary monitoring layer rather than a replacement for localized physical modeling.

3.4 Validation and Performance Metrics

The framework was validated by comparing statistical alerts with historical flood records. Performance was measured by the system's ability to identify "True Positives" (actual floods detected as out-of-control points) and the analysis of "Lag Time" through Cross-Correlation Functions (CCF), determining the lead time provided by the SPC alerts for early warning purposes.

4 RESULTS AND DISCUSSION

This section presents the empirical findings derived from the application of the SPC-based framework to the SNIRH big data. The results are structured to demonstrate the progression from raw data characterization to advanced multivariate anomaly detection. By integrating statistical control charts with process capability indices, the analysis provides a quantitative assessment of the watershed's behavioral patterns and its resilience against extreme events. The following subsections discuss the implications of these findings for modernizing early warning systems and disaster risk management.

4.1 Multivariate Anomaly Detection and Joint Variability Analysis

The core of the proposed monitoring framework is the Hotelling's T^2 control chart (Figure 1), as presented in Figure 1. Unlike traditional univariate charts that monitor precipitation and river stage in

isolation, the T^2 statistic accounts for the covariance between these variables, allowing for the detection of "out-of-control" states that signify a rupture in the standard rainfall-runoff relationship.

As observed in the analysis of the 2000–2025 series (comprising 722 sub-groups), the system identified a calculated Upper Control Limit (UCL) of 10.38. A total of 25 major groups were identified as being significantly beyond these limits, with a peak T^2 value reaching approximately 60.0.

From a technical standpoint, these peaks do not merely represent "heavy rain" but rather systemic anomalies where the joint behavior of the variables deviates from historical stability. The Contribution Analysis (integrated into the multivariate logic) reveals that during the most critical phases, the "Precipitation" variable acted as the primary driver of the T^2 inflation. This indicates a high sensitivity of the watershed to intense meteorological events, where the rapid increase in the T^2 statistics provides a "statistical alert" before the river stage reaches the physical bankfull level. This methodology successfully captures the non-stationary nature of the hydrological series, providing a more robust signal for Early Warning Systems (EWS) than simple linear thresholds.

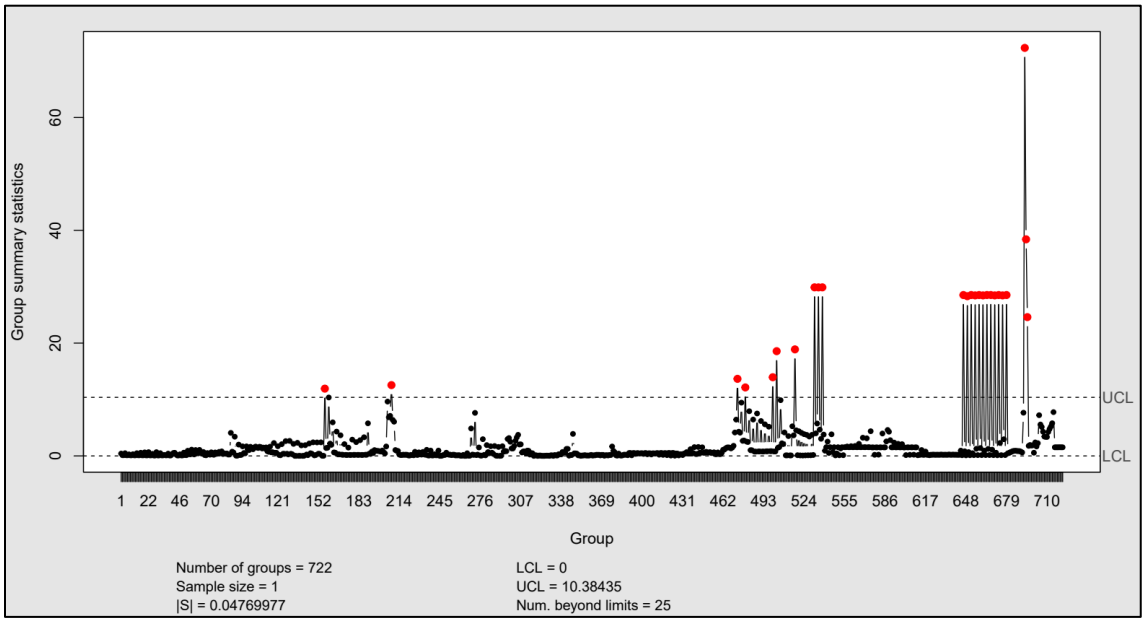

Figure 1: T^2 Control Charts for precipitation and river stage

4.2 Decomposition of Anomalies: Variable Contribution Analysis

While the T^2 statistic effectively identifies the timing of a multivariate deviation, the Variable Contribution Analysis presented in Figure 2 is essential for interpreting the underlying hydrological drivers. This chart decomposes the 50 most significant T^2 peaks recorded between 2000 and 2025, revealing the relative influence of precipitation (blue) versus river stage (orange) for each "out-of-control" state.

The empirical results show a dominant "precipitation-driven" signature in over 80% of the recorded alerts. This indicates that the watershed's response is highly sensitive to intense meteorological inputs, characteristic of flash-flood dynamics where the T^2 index reacts to rainfall intensity before the river stage reaches a critical overflow point. Conversely, events with a higher "stage contribution" (orange) signify periods of sustained high-water levels, often associated with soil saturation or downstream backwater effects. As emphasized in the project's final technical report, this decomposition allows decision-makers to distinguish between sudden rainfall-induced spikes and gradual hydrological "model ruptures," enabling more targeted emergency response protocols. This capability transforms the SPC framework from a simple alarm system into a diagnostic tool for real-time watershed situational awareness.

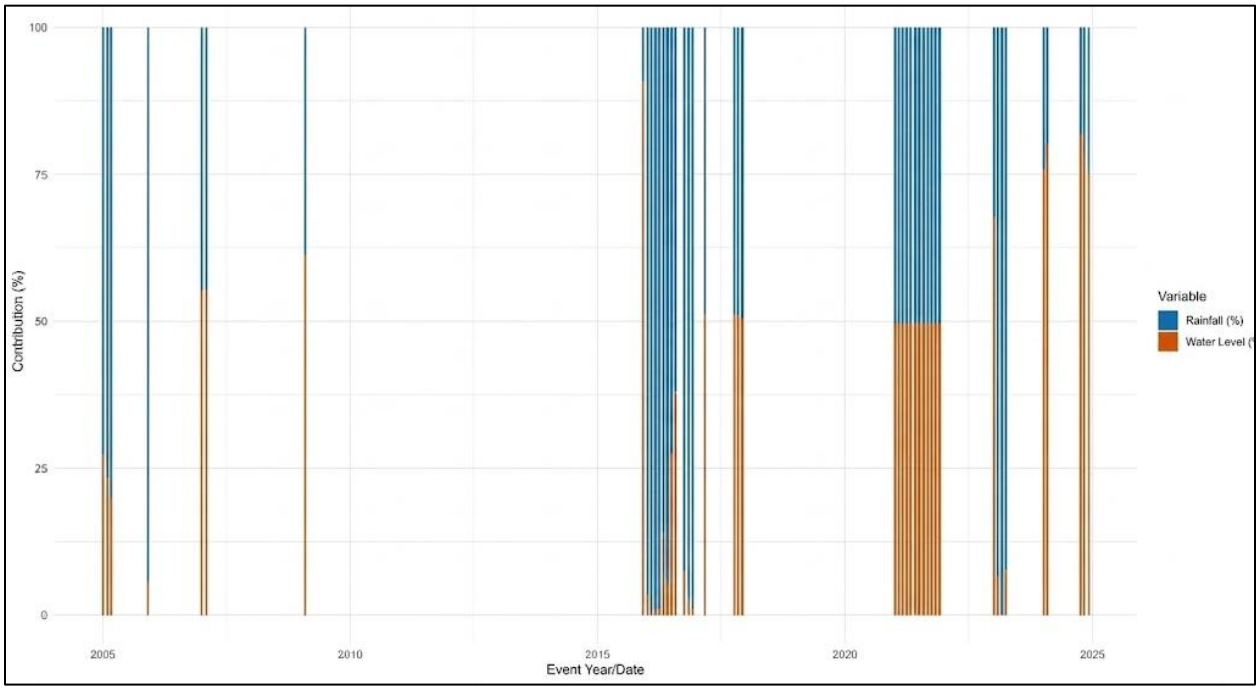

Note: Each bar represents the relative weight of the variables when the T^2 threshold was breached. Blue segments (Rainfall) indicate anomalies driven by precipitation intensity, while orange segments (River Stage) highlight events where the water level was already critical, often due to soil saturation or upstream discharge.

Figure 2: Decomposed contribution analysis for the 50 most critical alerts.

4.3 Quantitative Assessment of Basin Resilience via Process Capability (C_{pk})

The integration of Process Capability analysis into hydrological monitoring provides a standardized, quantitative metric for basin resilience. As illustrated in Figure 3, the river stage data (standardized via Z-scores) was evaluated against an Upper Specification Limit (USL) of 3.0, which serves as a statistical proxy for the bankfull discharge or physical overflow threshold.

The analysis of 722 observations yielded a C_{pk} specifically C_{pk} of 2.45. In an industrial context, a C_{pk} > 1.33 denotes a highly capable and stable process; applied here, it demonstrates that the watershed possesses a significant natural capacity to attenuate standard hydrological variability. However, the empirical data reveals that 2.2% of the observations (Obs > USL) fell beyond the safety margin. These points correlate precisely with historical extreme events where the basin's "process" failed to contain the volume within the standardized limits. By utilizing the C_{pk} index, water resource managers can move beyond qualitative descriptions of risk and adopt a numerical benchmark to compare the flood-containment efficiency of different urban watersheds, facilitating prioritized interventions in regions with lower capability indices.

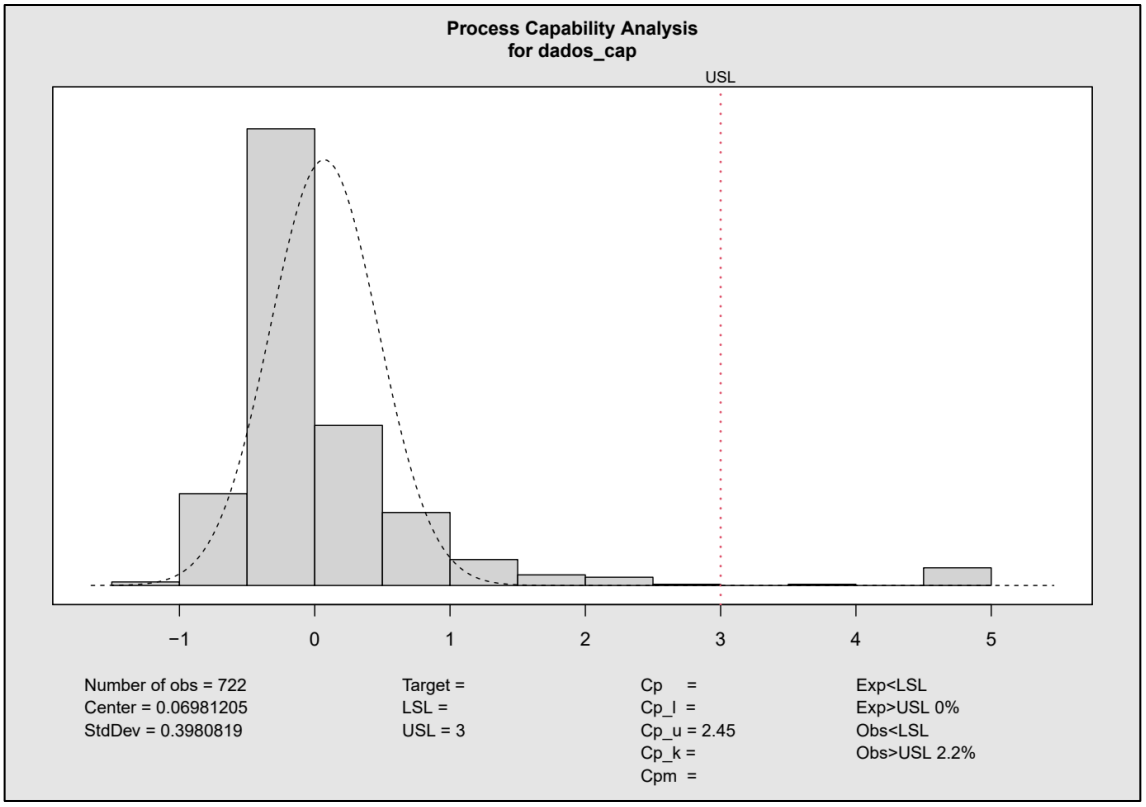

Figure 3: Process Capability Histogram

4.4 Residual Analysis and Monitoring of Model Rupture

While the T^2 chart monitors joint variability, the Residual Control Chart (Figure 4) is employed to detect "model ruptures" - instances where the established relationship between precipitation and river stage breaks down. This analysis utilizes the residuals from a linear regression model, where river stage is predicted by rainfall; any point exceeding the control limits indicates that an external factor, other than immediate precipitation, is driving the hydraulic response.

The chart, comprising 722 groups, establishes a stable center at approximately zero with Upper and Lower Control Limits (UCL/LCL) of ±0.491. The 44 identified model ruptures are particularly relevant for flood experts as they capture the transition from standard infiltration to total soil saturation. By signaling when the river level rises disproportionately to rainfall (the residual peak), the framework identifies the 'tipping point' of the watershed's absorption capacity purely through statistical breakdown, bypassing the need for expensive, high-maintenance soil moisture sensor networks."

The detection of 270 violating runs further suggests a non-random, persistent shift in the basin's behavior during specific climatic windows. By monitoring these residuals in real-time, the SPC framework can signal when a watershed has reached a "tipping point" of saturation, providing a sophisticated layer of intelligence that goes beyond simple threshold monitoring and captures the complex, non-linear nature of hydrological systems.

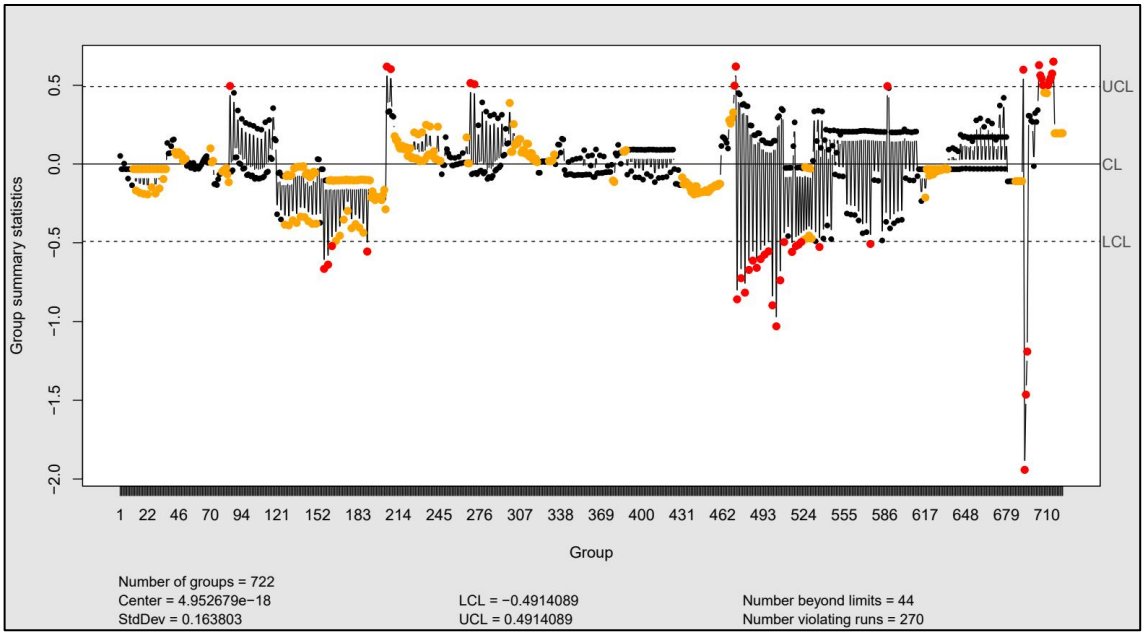

Figure 4: Bar Residual Control Chart

4.5 Hydrological Lag-Time and Early Warning Window

The final component of the framework involves quantifying the temporal displacement between meteorological input and hydrological response. Figure 5 presents the Cross-Correlation Function (CCF) between standardized Z-scores for precipitation (X) and river stage (Y). This analysis is fundamental to validating the predictive lead time of the SPC alerts.

The results reveal a significant correlation peak occurring at a positive lag of 6 to 12 hours (where $r > 0.6$). This peak indicates the typical hydrodynamic response window for the studied watershed—the duration required for surface runoff to propagate through the drainage network and register as a stage increase. From an operational standpoint, this statistical lag serves as a "Lead Time Benchmark." By identifying "out-of-control" multivariate states in the T^2 chart (Figure 1) during the initial rainfall phase, the system effectively provides a half-day window for civil defense agencies to activate emergency protocols before the physical water levels reach critical inundation thresholds. This high-resolution temporal analysis confirms that the integration of SPC with SNIRH Big Data is not only descriptive but serves as a viable engine for real-time early warning systems.

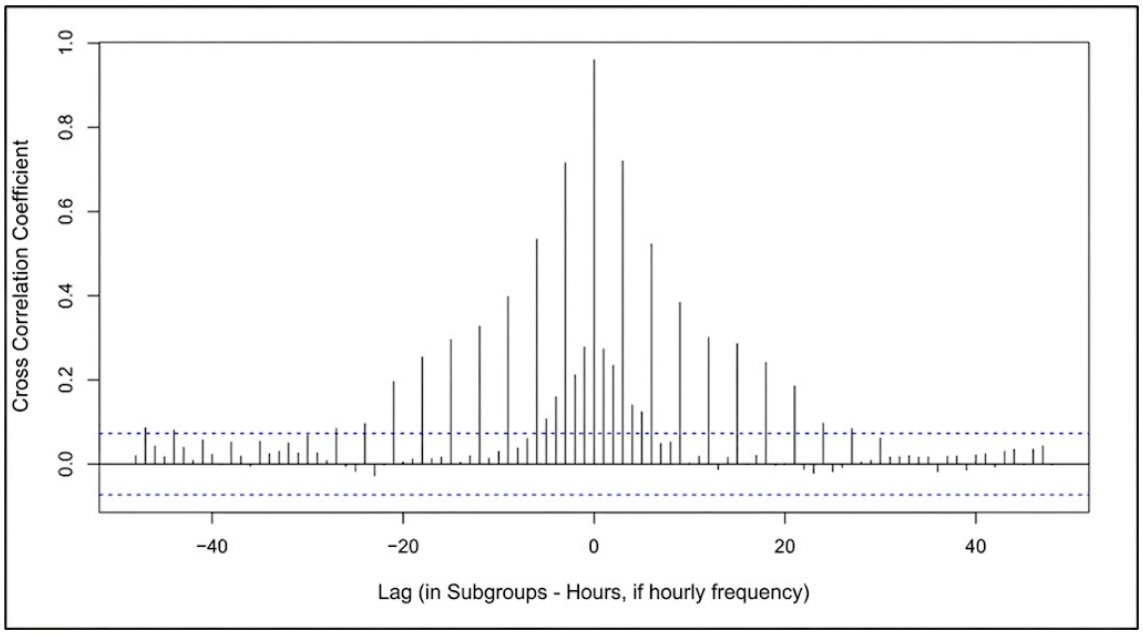

Figure 5: - Cross-Correlation Analysis (Rainfall vs. River Level)

The practical application of this framework is designed to support Decision Support Systems (DSS) within Civil Defense and Watershed Management agencies. By transitioning from the monitoring of raw hydrological levels to an SPC-based threshold-crossing alert system, operators can identify 'special cause' variations before physical overflow occurs. Regarding the visual characteristics of the T^2 charts, the perceived smoothness of the plotted data is statistically defensible as a result of the Z-score standardization and the multivariate aggregation of variance. Rather than representing raw sensor noise, the smoothed T^2 statistic effectively filters 'common cause' fluctuations, thereby emphasizing high-magnitude anomalies. This approach reduces false-positive alerts and provides a robust, high-level diagnostic for emergency mobilization, where the priority is the detection of significant process shifts rather than high-frequency hydrological oscillations. To bridge the gap between statistical modeling and operational practice, these findings suggest specific guidelines for EWS integration. It is recommended that the T^2 statistics be embedded as a dynamic trigger within agency dashboards, where the 6-to-12-hour lead time identified via CCF serves as the primary window for the proactive deployment of emergency resources. By transitioning from static univariate thresholds to these multivariate 'process-shift' alerts, authorities can achieve a higher degree of predictive resilience before physical operational limits are violated.

5 CONCLUSION

This study successfully established a scalable framework for flood risk management by adapting Statistical Process Control (SPC) to the Big Data infrastructure of the Brazilian National Water Resources Information System (SNIRH). The transition from conventional univariate monitoring to a Multivariate SPC (MSPC) framework—specifically utilizing Hotelling's T^2 charts—enabled the identification of 50 critical anomalies between 2000 and 2025 that signify systemic hydrological risks.

The application of Process Capability (C_{pk}) analysis provided a novel, quantitative metric for basin resilience; the calculated index of 2.45 serves as a standardized "safety margin" benchmark, allowing for objective comparisons between different urban watersheds. Furthermore, the integration of residual control charts and Cross-Correlation Functions (CCF) confirmed that statistical deviations precede physical flood stages by a 6 to 12-hour predictive window. This lead time is vital for detecting "model ruptures" triggered by soil saturation and antecedent moisture, which traditional linear thresholds often fail to capture.

The development and empirical validation of the RStudio-based prototype establish a robust foundation for modernizing Early Warning Systems (EWS). This framework provides a proven "research avenue" for real-time data ingestion and large-scale automated monitoring. By shifting the paradigm from reactive threshold monitoring to proactive statistical process control, this research offers public authorities a high-precision, data-driven strategy for enhancing disaster mitigation and climate resilience in vulnerable urban environments.

This study addresses the research gap by providing a 6 to 12-hour 'predictive buffer' (Figure 5). By shifting the paradigm from reactive 'threshold-crossing' alerts to proactive 'statistical-process-deviation' alerts, the framework offers a superior 'first-line of defense' for large-scale urban monitoring, effectively bridging the gap between Big Data science and practical disaster mitigation.

Finally, beyond its statistical robustness, the practical value of this framework lies in its ability to support real-time disaster management. By implementing the automated R/Python engine, environmental agencies can move from traditional reactive monitoring to a proactive-based governance. This system enables the establishment of dynamic 'early-warning' thresholds that account for multivariate interactions—such as the synergy between soil saturation and peak rainfall—providing a more reliable safety buffer for civil defense mobilization compared to univariate methods. Thus, the model serves as a scalable decision-support tool for increasing the resilience of vulnerable watersheds in the face of global climate change.

6 ACKNOWLEDGEMENTS

The authors would like to express their gratitude to the Faculdade Engenheiro Salvador Arena (FESA) and the Salvador Arena Foundation (FSA) for the financial support and the research scholarships provided. This support was fundamental for the development of computational models and the processing of the SNIRH big data. We also thank the Brazilian National Water Agency (ANA) for providing the historical datasets essential for this study.

REFERENCES

Agência Nacional de Águas e Saneamento Básico - ANA (2023). *Relatório de Conjuntura dos Recursos Hídricos no Brasil 2023*. Brasília: ANA.

Alves J., Amanguah E., McNally A. and Espinoza V. (2024). Global monitoring of urban flooding: Challenges and opportunities in data-scarce regions. *Journal of Flood Risk Management*, 17(1), e12940.

Chagas V.B.P., Chaffe P.L.B. and Blöschl G. (2022). Effects of land use and climate change on Brazilian river flows. *Journal of Hydrology*, 608, 127621.

Creswell J.W. and Creswell J.D. (2021). *Research Design: Qualitative, Quantitative, and Mixed Methods Approaches*. 6th Edition, SAGE Publications.

Emad A., Naimi S., Altaie A. and Abdul Hameed H. (2023). Hybrid AI-SPC models for real-time water quality monitoring. *Environmental Science and Pollution Research*, 30, 4512–4528.

Hipel K.W. and McLeod A.I. (1994). *Time Series Modelling of Water Resources and Environmental Systems*. Elsevier.

Lima J.P., Fernandes L. and Nascimento R. (2019). Statistical process control applied to the management of water resources: A case study in Southern Brazil. *Brazilian Journal of Water Resources (RBRH)*, 24, e32.

Marengo J.A., Alcantara E. and Moraes M. (2025). Intelligent early warning systems (iFAST) for flash flood monitoring in Brazil. *Climate Resilience and Sustainability*, 4(1), 112–125.

McKinney W. (2010). Data Structures for Statistical Computing in Python. in "Proc. 9th Python in Science Conf. (SciPy 2010)," S. van der Walt and J. Millman, Eds., Austin, TX, June 28–July 3, 2010, pp. 51–56.

Montgomery D.C. (2020). *Introduction to Statistical Quality Control*. 9th Edition, Wiley, New York.

Reis Jr. D.S., et al. (2023). Computational tools for hydrological time series analysis: Applications in R and Python. *Hydrological Sciences Journal*, 68(4), 589–604.
Schreiber R., Schreiber T., Tanna S. and Roberts J. (2022). Using statistical process control for monitoring environmental systems. *Water Research*, 215, 118231.
Shewhart W.A. (1931). *Economic Control of Quality of Manufactured Product*. D. Van Nostrand Company, Inc., New York.
Van Loenhout J.A., Below R. and McClean D. (2020). *The Human Cost of Disasters: An overview of the last 20 years (2000–2019)*. CRED and UNDRR.

Web sites:
Web-1: http://www.snirh.gov.br, consulted 20 January 2025.
Web-2: http://www.ana.gov.br, consulted 20 January 2025.

ICFM 10
Adapting to Global Change:
Innovative Approaches to Flood Management and Resilience
May 20-22, 2026 | Western University, London, Ontario, Canada

Flood defense technology of "July 23" catastrophic floods in the Haihe River based on hydrodynamic model and remote sensing data

Jie Mu[1,2], Fan Wang[1,2,*], Cheng Zhang[1,2], Binbin Wu[1,2], Huimin Xu[1,2], Fuxin Chai[1,2], Wenlong Song[1,2]

State Key Laboratory of Water Cycl and Water Security, China Institute of Water Resources and Hydropower Research, Beijing 100038, China[1]

Technology Innovation Center for Flood and Drought Prevention and Disaster Reduction, Ministry of Water Resources, PRC, Beijing 100038, PR China[2]

E-mail: mujie@iwhr.com

ABSTRACT

In 2023, the Haihe River Basin experienced catastrophic flooding triggered by the heavy rainfall of Typhoon Doksuri. To support real-time forecasting and the strategic operation of flood control infrastructure, the China Institute of Water Resources and Hydropower Research (IWHR) independently developed a 1D-2D coupled hydrodynamic model leveraging the high-performance IFMS/Urban platform, alongside an emergency monitoring system integrated with remote sensing. Taking the Dongdian Flood Storage and Detention Area (FSDA) as a case study, this paper evaluates the entire spatio-temporal evolution of inundation through numerical simulation and satellite observations. Furthermore, a comprehensive technical framework for basin-wide flood defense is proposed. The findings provided critical scientific support for the regulation of detention areas and governmental decision-making during the flood, offering a reproducible framework for modern flood management strategies.

KEYWORDS: flood evolution; hydrodynamic model; remote sensing ; flood storage and detention areas; the Haihe River Basin

1 INTRODUCTION

Flood storage and detention areas (FSDAs), which serve as crucial zones for diverting and detaining floodwater during major river floods, are an essential component of flood control engineering systems. The coordinated operation of FSDAs, river channels, and reservoirs effectively attenuates flood peaks, stores excess volume, and enhances the overall flood defense capability of a river basin (Wang, 1998; Hou and Shen, 2010). Chinese researchers have conducted extensive studies on the rational operation of these areas. In particular, two-dimensional (2D) hydrodynamic numerical models, as well as coupled 1D-2D models, are widely utilized to simulate flood propagation within FSDAs.

Two-dimensional (2D) hydrodynamic models are well-suited for simulating flows in wide and shallow water bodies. However, when a significant scale disparity exists between river channels and detention areas, relying solely on 2D models becomes computationally prohibitive and inefficient (Li et al., 2017; Li et al., 2018). To address this, coupled 1D-2D hydrodynamic models have been developed to represent the complex flow interactions and water exchange between rivers and FSDAs. This coupled approach effectively balances computational efficiency with simulation accuracy (Liu et al., 2020; Chen et al., 2017). Previous studies have demonstrated the robust performance of 1D-2D models in simulating flood propagation across various regions, including the Daming Floodplain (Wu et al., 2019), the five FSDAs in the Daqinghe River (Li et al., 2009–2016), and the Guduiwei area (Fu et al., 2013). Furthermore, satellite remote sensing has increasingly been integrated into flood monitoring due to its broad spatial coverage and near-real-time data acquisition capabilities.

Remote sensing imagery enables rapid, large-scale monitoring of flood disasters. It facilitates the delineation of inundated areas and associated hydrological features, which is critical for effective emergency response and damage assessment(Liu et al., 2023; Sui et al., 2021).

As climate change drives the northward shift of rain belts, Northern China is experiencing more frequent flooding and an increased frequency of FSDAs utilization. Consequently, high-fidelity flood propagation modeling and remote sensing are paramount for informed decision-making in flood dispatching (Feng et al., 2002; Song et al., 2022).

2 OVERVIEW OF THE "JULY 23" CATASTROPHIC FLOODS IN THE HAIHE RIVER BASIN

Driven by the interaction between the northward-moving Typhoon Doksuri and cold air masses, the Haihe River Basin experienced extreme rainfall from July 28 to August 1, yielding a basin-wide average precipitation of 155.3 mm.

This triggered floods surpassing warning levels in 22 rivers, with the Daqing and Yongding Rivers experiencing catastrophic inundation. Formally designated by the Ministry of Water Resources as the "23·7" Haihe River Basin Flood, it represents the region's most severe hydrological event since 1963.

2.1 Natural Overview of the Haihe River Basin

The Haihe River Basin comprises three primary water systems: the Haihe, Luanhe, and Tuhai-Majia Rivers. Within the Haihe system itself, the network is further divided into several key tributaries, including the Jiyun, Chaobai, Beiyun, Yongding, Daqing, Ziya, and Zhangwei Rivers, as well as the drainage systems of the Heilonggang and Yundong regions. The basin boasts a dense hydrological network, with 59 rivers each possessing a drainage area exceeding 1,000 km^2.

Covering a vast expanse of 320,600 km^2, the basin encompasses Beijing, Tianjin, and parts of six provinces, including Hebei and Shanxi. It supports a population of approximately 150 million (11% of the national total) and generates roughly 13% of China's GDP. With 9.33 million hectares of arable land, the region functions as the center of nation's political and cultural, a powerhouse of economic development, and a strategic hub for grain and energy production.

2.2 Characteristics of Rainfall

The rainfall event exhibited pronounced spatial extensiveness, substantial volumetric magnitude, spatiotemporal concentration, and elevated intensity. Spatial analysis indicated that precipitation exceeding 50 mm and 100 mm enveloped approximately 77.4 % and 52.8 %, respectively, of the entire catchment area. The preliminary estimation of total rainfall volume amounted to 49.4 billion m^3. Notably, accumulated areal precipitation attained 155.3 mm, equivalent to roughly 30.5 % of the multi-year mean annual precipitation for the region.

The heavy rainfall was primarily concentrated in the following regions: the Juma River within the Daqing River basin; the Hutuo and Fuyang Rivers of the Ziya River basin; and the Guanting Gorge section of the Yongding River basin. Within a 83-hour window (from 20:00 on July 29 to 07:00 on August 2), Beijing recorded precipitation equivalent to 60% of its long-term annual average. The maximum hourly intensity reached 111.8 mm at the Qianlingshan station in Fengtai District, surpassing the peak intensity recorded during the "7·21" extraordinary rainstorm of 2012. Comparative rainfall data for historical flood events are summarized in Table 1.

Table 1: Rainfall Comparison in the Haihe River of historical flood events

Rainfall Event	Duration	Storm Center	Cumulative Area Precipitation (mm)	Total Rainfall Volume（$10^8 m^3$）

"23·7" Rainfall	July 28 – Aug 1	Juma River, Fuyang River, Guanting Canyon (Yongding River)	155.3	494
"63·8" Rainfall	Aug 1 – Aug 11	Zhangmo Station (Ziya River)	139.9	624
"96·8" Rainfall	Aug 2 – Aug 7	Windward slopes of the Taihang Mountains	97.6	310
"21·7" Rainfall	July 17 – July 22	Xinxiang, Jiaozuo, Hebi (Henan) and Handan (Hebei)	79.9	253

2.3 Hydrological Characteristics

The catastrophic flooding in the Haihe River basin was characterized by synchronous flooding across both mainstreams and tributaries, marked by extreme magnitudes and massive runoff volumes. The event triggered water levels exceeding warning stages in 22 rivers, eight of which experienced unprecedented floods since records began. Notably, the Yongding and Daqing Rivers experienced catastrophic floods (highest classification), while the Ziya River experienced a major flood. Figure 2 illustrates the flood hydrographs at key hydrological stations. The total runoff is preliminarily estimated at 20 billion m^3, significantly surpassing the scale of the "96·8" major basin-wide flood.

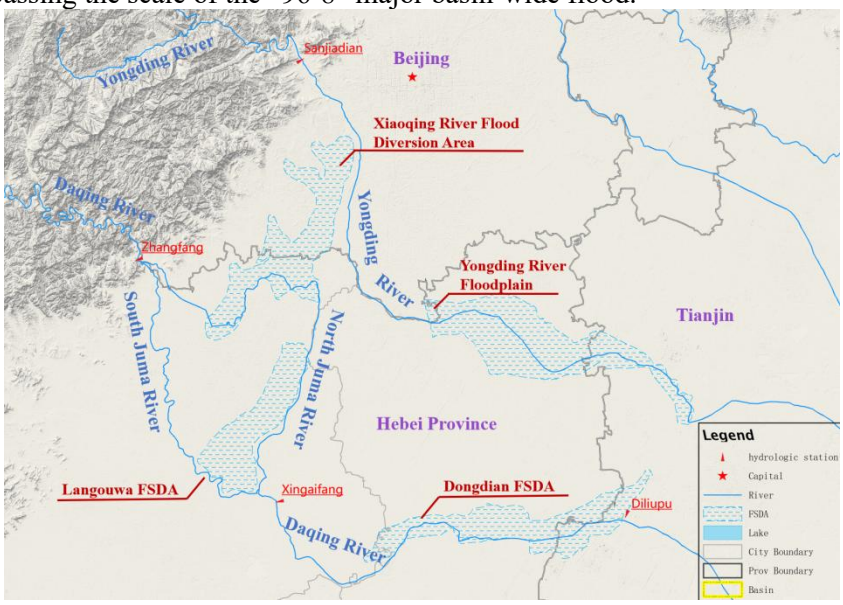

Figure 1:Distribution of hydrological control stations

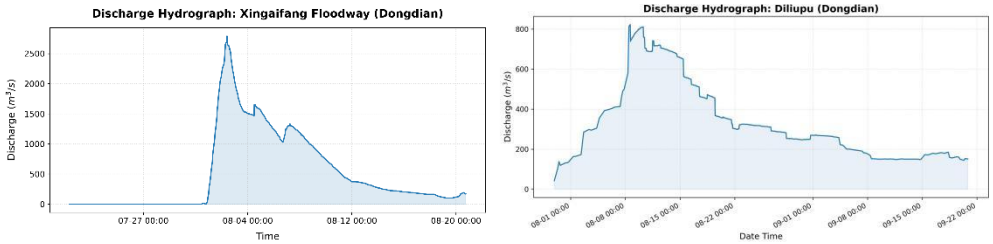

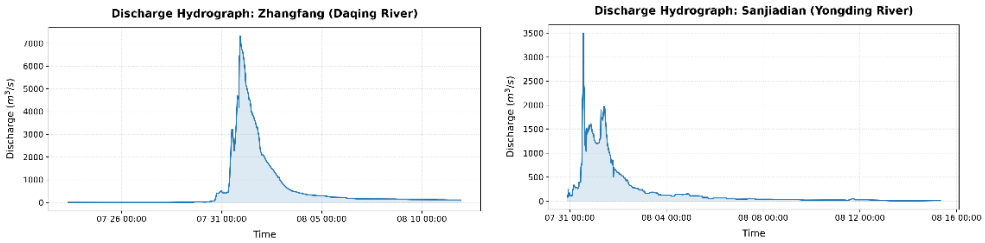

Figure 2:Flood hydrographs at key hydrological control sections

1.1 3 UTILIZATION AND TECHNICAL SUPPORT OF FLOOD STORAGE AND DETENTION AREAS IN THE HAIHE RIVER BASIN

3.1 Utilization of Flood Storage and Detention Areas

In response to heavy rainfall and flood warnings, eight Flood Storage and Detention Areas (FSDAs) within the Haihe River Basin were promptly activated. These included the Gongquxi FSDA; the Daluze and Ningjinbo FSDA, and Xianxian flood plain zoning; the Xiaoqing River FSDA , Langouwa FSDA, and Dongdian FSDA ; and the Yongding River flood plain zoning. The cumulative peak storage volume reached 2.53 billion m³. The spatial distribution of these FSDAs is illustrated in Figure 3.

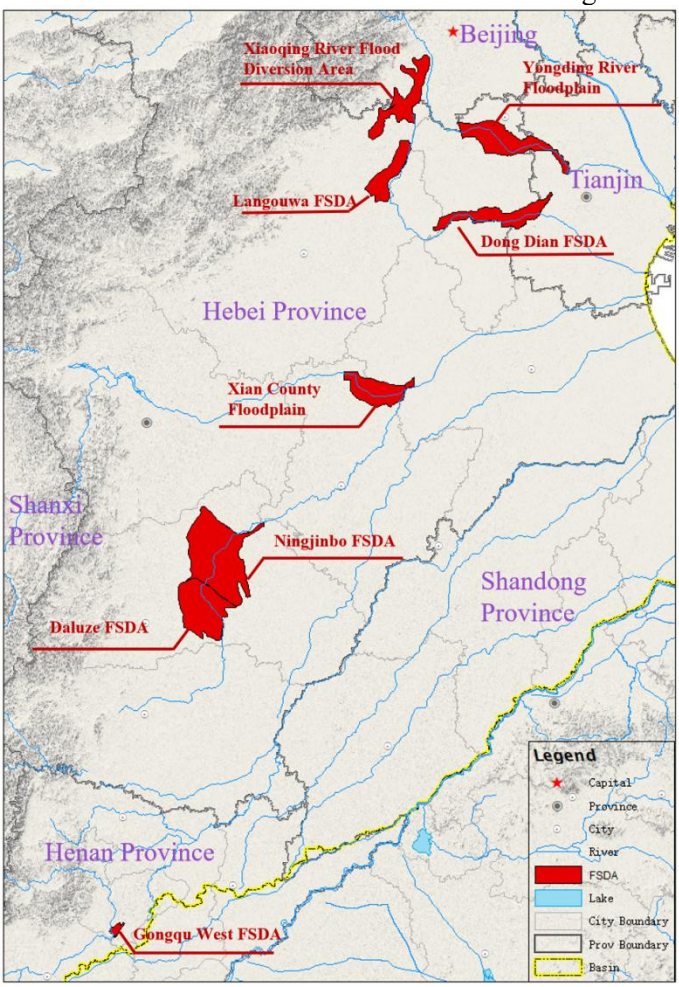

Figure 3: Utilization of FSDAs in the “July 23” catastrophic floods in the Haihe River Basin

3.2 Hydrodynamic flood models

In the course of the flood defense, 1D and 2D coupled hydrodynamic flood models were constructed for the eight FSDAs(Wang et al., 2023). Analysis was conducted based on the outputs of the flood risk maps and the "Four-Pre" flood defense system (forecast, early warning, simulation, and emergency planning). By integrating on-site surveys, satellite remote sensing, and UAV imagery, the hydrodynamic parameters were dynamically calibrated in real-time. This approach significantly refined the accuracy of flood simulations, providing essential technical support for the scientific operation of FSDAs, levee patrolling, and the strategic management of post-flood recession and resident repatriation.

(1) Model Principles

A 1D and 2D coupled hydrodynamic model was employed to simulate flood routing within the FSDAs. The model implements a Godunov-type scheme discretized via the Finite Volume Method (FVM).. Specifically, the Riemann problem is addressed using Roe's approximate Riemann solver, while the bottom slope source terms are treated using characteristic decomposition. The river channels and FSDAs are linked via hydraulic structures—including weirs, sluice gates, inlets, and levee breaches. The exchange of flow at the 1D-2D coupling interfaces is quantified using the weir flow formulation.

(2) Model Construction

In the development of the 1D riverine model, the modeling extent was defined to encapsulate the dynamic interaction between flood detention basin storage and mainstem water levels, while also incorporating the spatial distribution of hydrological stations. Correspondingly, the 2D model domain was delineated to match the geographical boundaries of the flood storage and detention areas (FSDAs). Within the 2D grid discretization, linear features such as highways, railways, internal embankments, and minor drainage channels were treated as internal constraint boundaries. Grid refinement was implemented at critical locations, such as flood diversion gates, with cell elevations interpolated from either preliminary risk map datasets or high-resolution field survey data.

The model's upstream and downstream boundary conditions were prescribed based on observed and forecasted discharge and water levels from hydrological stations. Roughness coefficients were initially assigned according to standard ranges provided in the Hydraulic Calculation Manual and further informed by regional planning reports and historical studies within the basin.

(3) Activation and Evolution Simulation of Flood Storage and Detention Areas

Based on hydrological forecasts, flood routing simulations are conducted for main channels prior to the deployment of Flood Storage and Detention Areas (FSDAs). Activation timing is determined in strict accordance with the basin's flood control scheduling protocols. Through multi-scenario simulations, optimized schemes are developed for gate operations and zonal flooding sequences.

Upon FSDA activation, multi-source remote sensing data are integrated with water distribution forecasts to predict critical hydrodynamic metrics, including flood-front progression (water head locations), inundation depths, and flow velocities. These results are used to assess the vulnerability of key infrastructure, such as village foundations and safety zones.

Following peak regulation, a coordinated water release plan is formulated based on forecasted river levels and simulated hydrographs. This plan defines the optimal timing, aperture (degree of gate opening), and duration of discharge to ensure a safe and efficient recession process.

3.3 Remote sensing monitoring

As a rapidly evolving geospatial technology, remote sensing offers unparalleled capabilities for wide-area, high-frequency, and all-weather surface observation. Following decades of specialized research and practical application, our center has established a comprehensive remote sensing framework for flood disaster monitoring, providing end-to-end analysis across the entire pre-disaster, during-disaster, and post-disaster spectrum.

In response to the Haihe River "23· 7" basin-wide catastrophic floods, wwe quickly formed an air-space-ground integrated remote sensing monitoring and analysis team, coordinating more than 20 domestic and international optical and radar remote sensing satellite resources.

By integrating emergency response with routine operations and leveraging our self-developed Water Conservancy Remote Sensing Emergency Monitoring System Platform, we designed a multi-satellite synergistic observation strategy. This approach combined optical and synthetic aperture radar (SAR) assets to achieve 1 to 3 daily remote sensing observations of the eight FSDAs in the Haihe River Basin. It effectively mitigated the limitations of optical sensors in acquiring reliable data under persistent cloud cover and rainfall−common during flood seasons, thereby significantly enhancing the satellite-based emergency monitoring capabilities for flood disasters.

Based on the platform, we automated the end-to-end workflow for multi-source satellite imagery, encompassing querying, downloading, ingestion, radiometric calibration, geometric correction, and noise filtering. By integrating expert knowledge, the system achieved precise identification of the extent of inundated water bodies. Furthermore, it dynamically extracted critical flood parameters−including inundated area and duration−for the eight detention basins. This continuous monitoring spanned the entire flood lifecycle from July 31, 2023, covering the phases of “flood warning activated - flood invasion - peak flow occurrence - floodwaters began to recede - floodwaters fully receded”.

Aerial remote sensing proved indispensable for this emergency monitoring mission. Low-altitude UAVs, characterized by sub-cloud operation, high maneuverability, and rapid deployment cycles, effectively mitigated the limitations of satellite imagery−namely cloud interference, latency, and high tasking costs. By integrating both platforms through data fusion and cross-verification, we achieved comprehensive multi-source information acquisition. Specifically, we deployed the Kodiak 100 aircraft equipped with the Optech Galaxy T2000 LiDAR to conduct high-precision surveys over activated flood detention zones. This yielded critical LiDAR point clouds and orthophotos, providing essential “ground truth” for flood analysis. Additionally, portable UAVs, powered by our self-developed YC-mapper rapid processing system, were utilized for real-time monitoring of breach sites along the dike of Langgouwa FSDA and Baigou Rivers, enabling the swift measurement of key metrics such as breach dimensions.

Remote sensing monitoring technology provides robust scientific support for the safe operation of flood storage and detention areas. It provides a comprehensive perspective on current flood dynamics within the FSDAs, offering critical datasets for hydrodynamic simulation, flood forecasting, and disaster impact assessment.

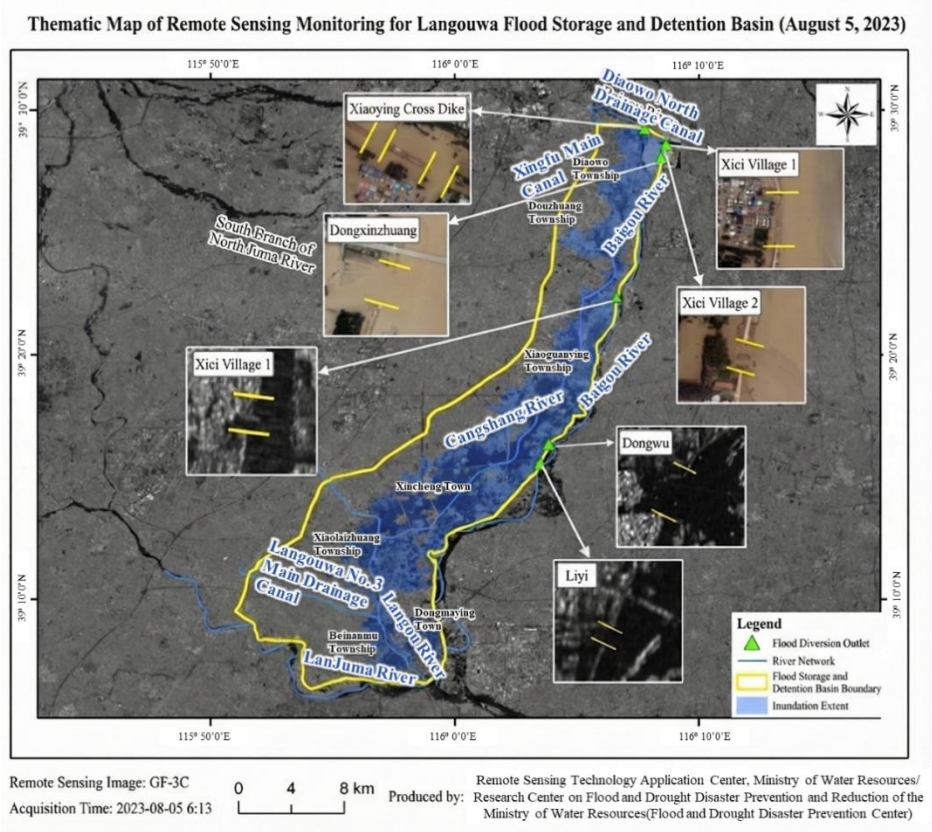

Figure 4: Satellite and Aerial Remote Sensing Map of Flood Inundation in Langgouwa FSDA

3.4 Supporting case — Flood evolution analysis of the dongdian FSDA

The Dongdian FSDA is located in the downstream reaches of the Daqing River basin. Covering a total area of 377 km^2, the Dongdian FSDA acts as the ultimate convergence point for floodwaters from the northern and southern branches of the Daqing River basin, as well as the regional runoff from the Qingnan and Qingbei areas.. A 1D-2D coupled hydrodynamic model, integrated within the IFMS (Integrated Flood Management System) software developed by the China Institute of Water Resources and Hydropower Research (IWHR), was employed to simulate flood propagation across the primary river networks-including the Daqing, Zhaowangxin, and Ziya Rivers-as well as the Dongdian FSDA. The model architecture comprises 359 river cross-sections with an average spacing of 400 m, integrated with 114,000 2D grid cells at a spatial resolution of approximately 60 m. Leveraging the full GPU heterogeneous parallel acceleration of IFMS v4.0, the system significantly enhances computational efficiency. A 30-day flood inundation simulation for the Dongdian FSDA (from August 1 to August 31) can now be completed within 20 minutes. This high-performance capability ensures the platform meets the rigorous demands of real-time operational forecasting.

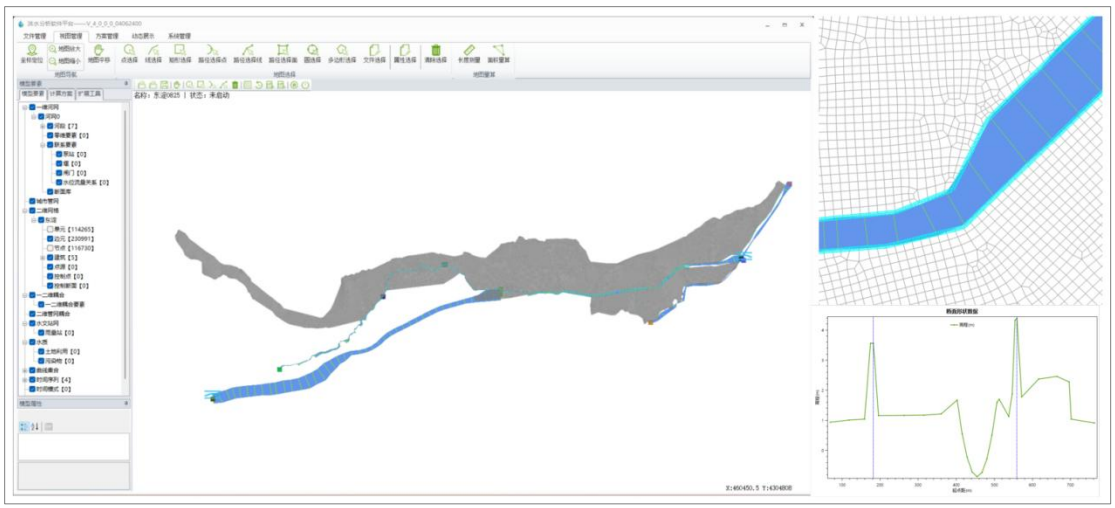

Figure 5: Construction diagram of the 1D-2D coupled model of Dongdian FSDA

The model's upstream boundary conditions are driven by real-time monitoring and forecast discharge data from the Xingaifang Diversion Hub and the Baiyangdian outflow. For the downstream boundary, a stage-discharge rating curve at the Duliu Jianhe Floodgate is applied to ensure hydraulic consistency.

This framework enables the simulation and predictive analysis of flood propagation within the Dongdian FSDA. The model undergoes daily calibration and validation using inundation extents derived from remote sensing imagery and field surveys. For over a month, continuous rolling forecasts have been maintained, with results demonstrating a high degree of consistency between the simulated inundation patterns and the actual satellite-observed data.

Based on monitoring and forecast data as of 12:00 on August 4, the peak flood originating from the Xingaifang Diversion was projected to reach Tianjin by 08:00 on August 5. Field validation confirmed the actual peak arrived at Taitou Town between 09:00 and 10:00 on August 5. These results demonstrate the high precision of the Dongdian flood evolution model developed in this study, which successfully achieved a 20-hour lead time with a temporal error of less than one hour. These forecasts were promptly submitted to the Ministry of Water Resources, the Haihe River Water Conservancy Commission, and the Hebei Provincial Department of Water Resources, providing critical lead time for strategic flood diversion and emergency response.

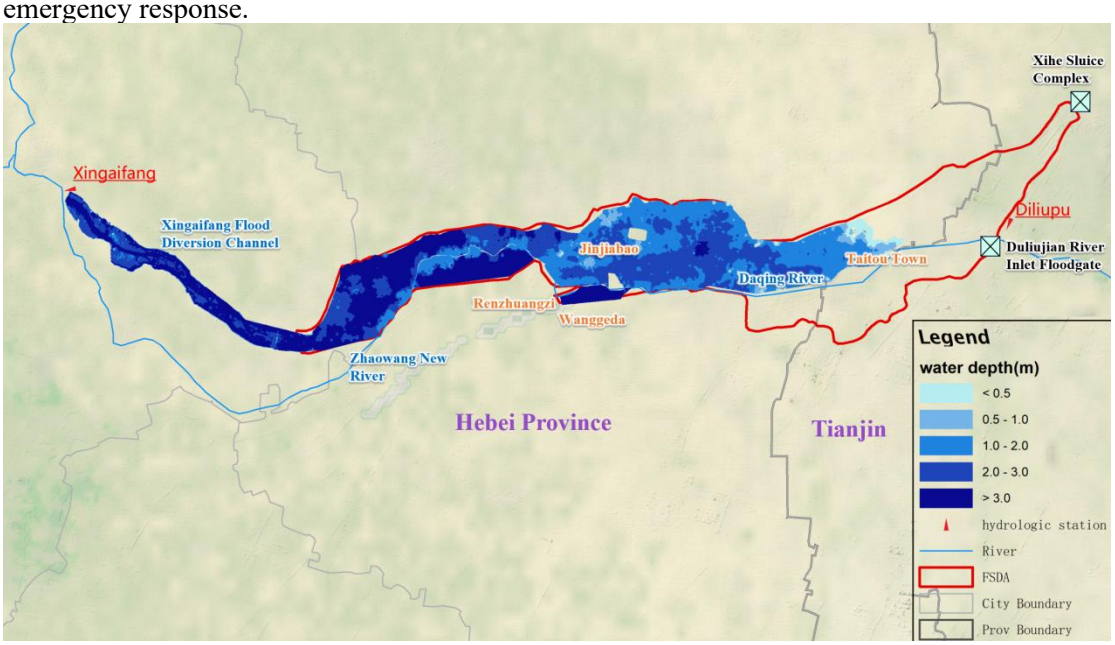

a) 08:00 on August 5

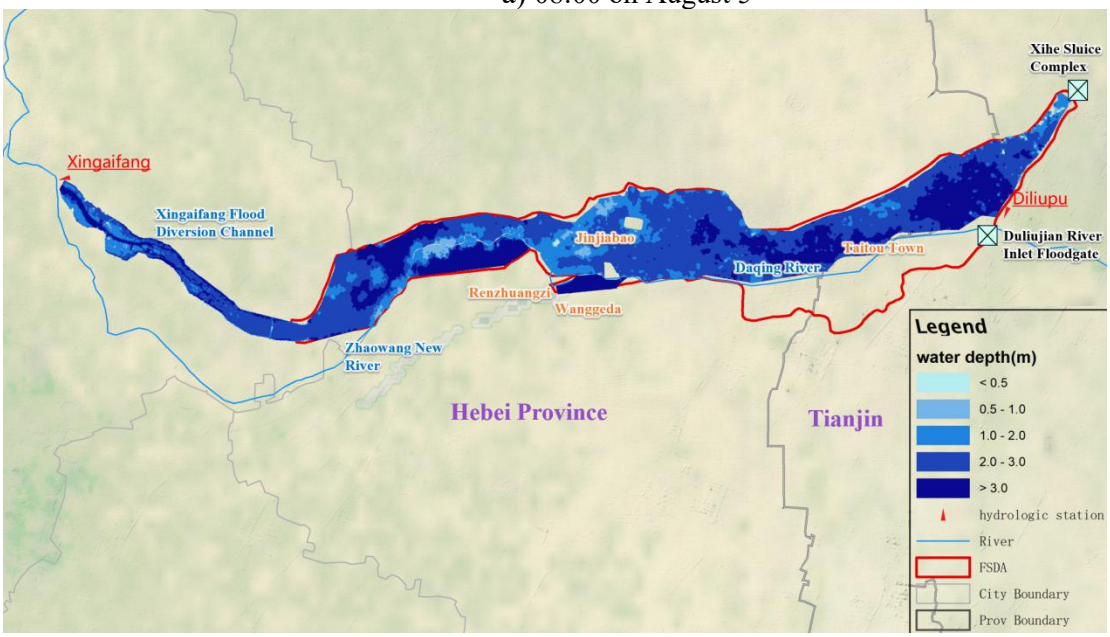

b) 11:10 on August 9

Figure 6: Model predicted flood water in the FSDA

1.2 4 SUMMARY AND RECOMMENDATIONS

4.1 Conclusion

The “July 23” catastrophic floods in the Haihe River Basin, the FSDAs played an irreplaceable and important role. To address critical challenges-including optimized activation timing for FSDAs, embankment integrity, flood propagation dynamics, and precise water diversion schedulin-the Flood and Drought Disaster Prevention and Reduction Engineering Technology Research Center(CDPR) provided strategic technical support in the following areas:

(1) Space-Ground Integration: Leveraging a multi-source remote sensing network, the CDPR achieved high-precision, real-time observation of flood storage and detention areas. During the flood periods, inundation analyses were performed 1 to 3 times daily to track flood-front progression (water head), assess the status of safe zones, and monitor village-level flooding with high frequency.

(2) Hydraulic Modeling and Forecast Operations. Leveraging coupled 1D-2D hydrodynamic models, flood evolution simulations were developed for eight FSDAs. The model’s reliability was cross-validated against remote sensing data, ensuring high fidelity. Integrating these with hydrological forecasts, the CDPR formulated optimized dispatching strategies and delivered daily rolling evolution forecasts, providing critical early warnings for key downstream regions.

(3) Drawing on defense experience from the “23· 7” catastrophic flood in the Haihe River Basin, this paper proposes an integrated technical support framework for flood storage and detention areas. This system leverages the synergy between remote sensing (RS) monitoring and hydrodynamic modeling: while 1D-2D coupled models enable rapid forecasting and early warning, RS-derived data provides critical empirical calibration, ensuring the high fidelity of simulation outcomes.

4.2 Limitations of the Current Defense System

(1) Engineering System

The flood defense infrastructure in the Haihe River Basin remains relatively fragmented, with critical river sections lacking essential control reservoirs. Much like the “63· 8” catastrophic flood event, the “23·

7” extreme rainfall was concentrated downstream of existing reservoirs-specifically along the windward slopes and piedmont plains of the Taihang Mountains-rendering upstream reservoir regulation largely ineffective. This hydrological pattern bypassed primary defenses and struck the system’s most vulnerable points. Consequently, The flood storage and detention areas, the final line of defense, were forced into operation to compensate for key dikes and channels that significantly underperform their design standards.

Besides, the construction of flood storage and detention areas lags behind-the control facilities are inadequate. Among the 28 flood storage and detention areas in the Haihe River Basin, only three have completed construction to design standards. Critically, none of the eight activated flood storage areas had fully completed their safety-standardized construction.

(2) Non-Engineering System

The digital twin watershed construction and the "four-prevention" system are not well-developed. In terms of forecasting, factors such as special complex terrain and typhoon impacts causing uncertainties, along with the damage to some hydrological stations, have led to large adjustments in heavy rainfall and flood forecasting; in terms of early warning, the limitations of hydrological forecast accuracy and changes in the underlying surface leading to variations in flood risk distribution have affected precise early warning capability, which needs improvement; in terms of simulation exercises, the conditions of the underlying surfaces of flood storage areas are unclear, and the data foundation cannot be quickly obtained, making real-time dynamic simulation based on gate conditions impossible; in terms of emergency plans, the dynamic adjustment of dispatching plans still needs improvement; emergency monitoring capabilities are greatly affected by floods and traffic conditions.

(3) Technical Support Enhancement

Several flood dispatching schemes require urgent revision. Significant shifts in land surface characteristics, driven by crustal subsidence and rapid socio-economic development, have altered local hydraulic responses. Currently, when independent discharge-reduction rivers reach their design flow, actual water levels remain below the benchmarks set in existing flood control plans. Furthermore, the “Four Preventions” digital system for flood storage and detention areas remains incomplete, limiting the capacity for precision decision-making. Given the substantial changes in the physical and socio-economic landscape of these areas, a comprehensive update of flood risk mapping is now imperative.

4.3 Proposed Countermeasures and Recommendations

(1) Optimization of Watershed Flood Control Infrastructure

Future efforts should align with the upcoming round of watershed flood control planning revisions to further optimize the spatial layout of flood control projects. This includes a systematic enhancement of the regional defense system and the rigorous demonstration and advancement of pre-feasibility studies for key projects, such as the Zhangfang Reservoir in the Daqing River Basin. Priority must also be given to the standardized construction of river embankments and the strengthened management of flood storage and detention areas (FSDAs).

(2) Digital Twin Integration and Intelligent Decision Support

Based on current hydraulic conditions and recent flood events, the revision of flood dispatching protocols should be expedited. Leveraging the “Four Preventions” framework alongside Digital Twin Watershed initiatives, it is essential to develop intelligent monitoring and rapid fusion technologies for underlying surface data. Furthermore, research should focus on high-fidelity flood modeling, dynamic simulation, and real-time risk assessment to generate dynamic flood risk maps. These advancements will facilitate iterative plan updates and enable the integrated forecasting and scheduling of reservoirs, rivers, embankments, and FSDAs, ultimately providing robust decision support for scientific flood defense.

Funding: This work was supported by the National Major Science and Technology Projects for Integrated Environmental Governance of the Beijing-Tianjin-Hebei Region (Grant No. 2025ZD1208304); the National Natural Science Foundation of China (Grant No. U2340225); and the Construction Project of Tianjin Flood Control Dispatching and Emergency Command Platform (Grant No. JZ120205A0042024).

REFERENCES

Chen P., Fu C.F., Yu J.Y., et al. (2017). Research on the Numerical Simulation of Flood Routing for the Flood Detention Basin Based on Mike 21. China Rural Water and Hydropower, (8), 113–116.

Feng M.Q., Zhou X.D. and Wang K.P. (2002). A Review of Flood Simulation Studies in Flood Detention Areas. Power System and Clean Energy, 18(1), 5–8, 23.

Fu C.W., Yuan X.M. and Yang M. (2013). A real-time dynamic coupling model for flood routing and its application to flood risk charting. Hydro-Science and Engineering, (5), 32–38.

Hou C.H. and Shen F.X. (2010). Ideas on the Planning and Construction of Flood Storage and Detention Areas in China. China Water Resources, 20(6), 40–44, 64.

Li C.H., Xu G.B., Yuan X.M., et al. (2017). Research progress on numerical simulation of joint flood control in river and flood detention area. Journal of Water Resources and Water Engineering, 28(6), 139–144.

Li D.M., Guan Y.K., Li L.L., et al. (2011). Flood routing mathematical model for flood detention basin. Hydro-Science and Engineering, (3), 27–35.

Li D.M., Lin Y., Xu Y.N., et al. (2009). Numerical Model of Flood Propagation of Rivers and Flood Detention Basin. Strategic Study of CAE, 42(1), 47–55.

Li D.M., Lin Y. and Zhou Z.H. (2010). Research on 1D and 2D numerical simulation of flood routing and its application of combined-regulation in detention basin. Strategic Study of CAE, 12(03), 82–89.

Li D.M., Wang Z.C., Li Y.Y., et al. (2016). Research on Steering Flood Routing Model and Its Application in Flood Combined-Regulation in Detention Basin. Journal of Tianjin University (Science and Technology), 49(10), 1084–1092.

Li Y.J., Xu Q., Zhou Y.B., et al. (2018). Application of 2-D hydrodynamic model on flood routing simulation analysis in flood storage and detention area. Jiangsu Water Resources, 12(5), 68–72.

Liu H.J., Song W.L., Yang K., et al. (2023). Emergency remote sensing monitoring of "2022.6" flood disaster of the Pearl River basin. China Flood & Drought Management, 33(2), 20–25.

Liu X.Q., Liu G.L. and Wang Z. (2020). The Study and Application of Flood Simulation at Detention Basin Based on Mike Series Model. China Rural Water and Hydropower, (6), 10–15, 20.

Song W.L., Lü J., Liu C.J., et al. (2022). Research progress and prospects of water conservancy remote sensing technology and application. China Flood & Drought Management, 32(1), 34–40.

Sui H.G., Zhao B.F., Xu C., et al. (2021). Rapid Extraction of Flood Disaster Emergency Information with Multi-modal Sequence Remote Sensing Images. Geomatics and Information Science of Wuhan University, 46(10), 1441–1449.

Wang W.Q., Lin W.Q., Wang F., Bi W.X., Zhang D.W. and Chai F.X. (2023). Numerical simulation study on the evolution of floods in the Gongquxi Storage and Retention Area—A case study in the Haihe "23·7" basin-wide extreme flood. China Flood & Drought Management, 33(09), 45–49.

Wang Z.L. (1998). A Brief Discussion on the Role of Flood Detention Areas in Flood Prevention and Disaster Reduction. Water Conservancy Construction and Management, 18(4), 13–16.

Wu B.B., Yu H.J., Mu J., et al. (2019). Flood simulation in river and flood storage-detention area considering infiltration. Water Resources Protection, 35(6), 68–75.

Chapter 3 - Urban flooding and infrastructure systems

3.2 Urban flood mitigation and stormwater management strategies

ICFM 10
Adapting to Global Change:
Innovative Approaches to Flood Management and Resilience
May 20-22, 2026 | Western University, London, Ontario, Canada

Identifying and Prioritizing Mitigation Options to Address Climate-Related Flooding in an Established Urban Area: A Case Study of Sophia Creek Subcatchment, Barrie, Ontario

Mohammad Hajiseyedjavadi[1], Khashayar Saniei[1], Bill Thompson[1], Kenneth Cheney[1]
[1]Lake Simcoe Region Conservation Authority, 120 Bayview Parkway, Newmarket, Ontario, L3Y 3W3, Canada
E-mail: M.Hajiseyedjavadi@lsrca.on.ca
E-mail: K.Saniei@lsrca.on.ca
E-mail: B.Thompson@lsrca.on.ca
E-mail: K.Cheney@lsrca.on.ca

ABSTRACT

Climate change is increasing urban flooding frequency and intensity across eastern Canada, with flood damages representing Ontario's largest climate-related financial impact. The City of Barrie experienced major floods in 2017, 2019, and 2022, with climate projections indicating increasing frequency of high-intensity storms that will overwhelm aging infrastructure. However, infrastructure upgrades are costly, requiring systematic prioritization to maximize flood risk reduction with limited capital budgets.

Lake Simcoe Region Conservation Authority partnered with the City of Barrie to undertake a pilot study in the highly urbanized Sophia Creek catchment, evaluating how climate change could influence flood risks in the subwatershed. The study developed flood depth and inundation models under climate projections from four global circulation models for 5-, 10-, 50-, and 100-year events using an integrated 1D-2D PCSWMM modeling framework.

The Risk and Return on Investment Tool (RROIT) integrates hydrologic and hydraulic modelling outputs with GIS data to quantify flood damages and evaluate the cost-effectiveness of mitigation options under both historical and future climate conditions. RROIT reports financial metrics to identify areas of greatest risk and prioritize investments that deliver the highest return on flood resilience spending. Model outputs informed a facilitated process to identify downstream areas experiencing increased flooding under climate change and their upstream contributing areas. Conservation Authority and City staff identified potential mitigation options including structural measures (trunk sewer upgrades, stormwater management facilities), distributed approaches (low impact development), and watercourse modifications (daylighting).

Results revealed that climate change increases damages by 48-204% depending on storm frequency, with most severe impacts on frequent events. Constructing a stormwater management pond emerged as the highest-priority investment with the greatest annual damage reduction of 31%, lowest capital cost ($7.3M), highest annual savings ($7.16M/yr), shortest payback period (3.0 years), and highest return on investment (98% Internal Rate of Return (IRR), $211M Net Present Value (NPV)). Expansion of a trunk sewer, currently under construction, provides complementary benefits with 4.7-year payback and 47% IRR. This methodology provides a replicable framework for evidence-based prioritization of cost-effective flood resilience investments.

KEYWORDS: Climate change adaptation, Urban flooding, Flood risk mitigation, Cost-benefit analysis, Infrastructure planning, PCSWMM, RROIT, Average annual damage

1 INTRODUCTION

Climate change is fundamentally altering precipitation patterns globally, with profound implications for urban flood management (IPCC, 2021). In Ontario, Canada, flood damages to homes and infrastructure represent the largest financial impacts associated with climate change, surpassing all other climate-related damages combined (Warren & Lemmen, 2014). Historical climate data and future projections consistently indicate that high-intensity rainfall events are becoming more frequent, more severe, and longer in duration , placing increasing stress on aging urban stormwater infrastructure that was designed using historical climate norms rather than future conditions (Bush & Lemmen, 2019).

The City of Barrie, located in central Ontario approximately 90 km north of Toronto on the western shore of Lake Simcoe, exemplifies these challenges. Historically developed along the shores of Kempenfelt Bay, Barrie transitioned from a military outpost in the early 19th century into a transportation hub and, eventually, a commuter city within the Greater Golden Horseshoe. Much of its older urban fabric was constructed in the post-war period, before contemporary floodplain management or stormwater regulations were in place. Today, Barrie is one of Ontario's fastest-growing cities (City of Barrie, n.d.), with a population nearing 150,000, experiencing increasing pressure on its natural and built drainage systems due to urban infill and intensification.

The city experienced significant flood events in 2017, 2019, and 2022, causing extensive property damage and infrastructure strain. Media reports following the July 2022 event documented extensive road closures and damage in the city's core, reinforcing the need for anticipatory planning and investment in both grey and nature-based solutions. As climate projections indicate these intense storms will become more frequent, the city faces difficult decisions about where to invest limited capital budgets for maximum flood risk reduction.

The Sophia Creek catchment, a highly urbanized subwatershed in northern Barrie, presents a particularly complex challenge. Originally a natural creek that meandered across a glacial till plain, much of the watercourse has since been altered: sections have been buried in culverts, channelized, or straightened to accommodate development and road construction. These interventions have reduced floodplain connectivity and increased the speed and concentration of surface runoff during storm events. Combined with aging infrastructure and increasing imperviousness, this has made the area highly susceptible to pluvial and fluvial flooding. This paper presents a systematic methodology for identifying, evaluating, and prioritizing flood mitigation investments under climate change uncertainty using the Risk and Return on Investment Tool.

2 METHODOLOGY

The methodology for this study followed a structured approach to identify, evaluate, and prioritize flood mitigation investments under climate change uncertainty in the Sophia Creek subwatershed. Lake Simcoe Region Conservation Authority (LSRCA), in partnership with the

City of Barrie, developed climate-informed flood models, identified vulnerable areas and contributing sources, generated mitigation alternatives through a facilitated stakeholder process, and evaluated options using the Risk and Return on Investment Tool (RROIT). The primary objective was to assess climate change impacts on flood risk and establish a replicable framework for prioritizing cost-effective urban flood resilience investments.

The project involved several key stages: data acquisition and preprocessing; development of future climate scenarios and intensity–duration–frequency (IDF) curves; mitigation scenario identification; hydrologic and hydraulic model construction and scenario-specific modifications; flood inundation analysis; RROIT input preparation and damage assessment; and mitigation scenario evaluation. All steps were guided by municipal and conservation authority technical standards and informed by current hydrologic science.

2.1 Study Area

The Sophia Creek subwatershed drains approximately 470 hectares in northern Barrie, Ontario, and is characterized by dense urban development with a mix of residential, commercial, institutional, and transportation land uses and extensive impervious cover. The watercourse flows southwest toward Lake Simcoe through a combination of straightened open channels and enclosed storm sewer infrastructure, resulting in frequent system overtopping and overland flooding during intense rainfall events.

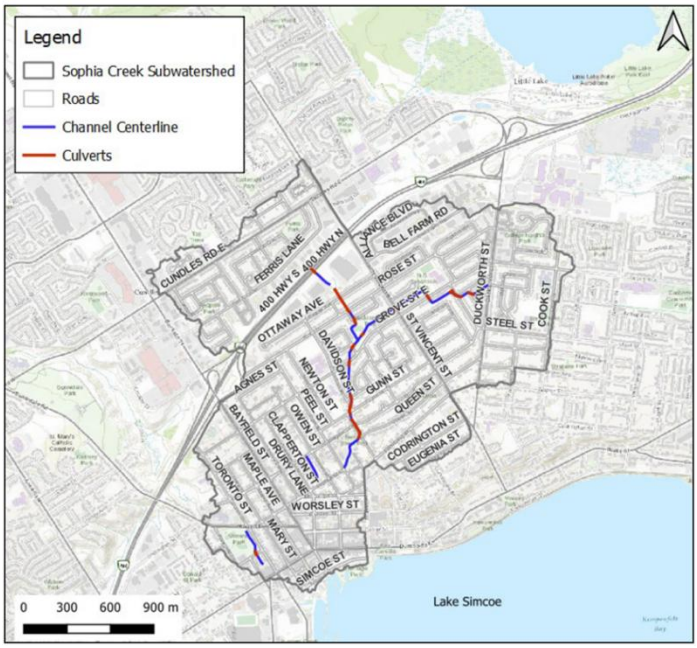

Figure 1. Sophia Creek Subwatershed

2.2 Climate Change Scenarios and Design Storms

Climate change scenarios were developed using downscaled global climate model projections from the Government of Canada's Climate Scenarios portal (CMIP6, BCCAQv2). The analysis focused on the SSP5-8.5 high-emission scenario to assess flood risk under a severe future climate pathway.

Projected changes in mean annual temperature between a historical baseline (1979–2014) and a future period (2021–2050) were calculated for available global climate models. Models were grouped into quartiles representing increasing levels of warming, and one representative model from each quartile was selected to capture a plausible range of climate futures.

Changes in extreme precipitation were estimated using temperature-based scaling consistent with the Clausius–Clapeyron relationship and national guidance (Environment and Climate Change Canada, 2023). These scaling factors were applied to regional Intensity–Duration–Frequency (IDF) relationships obtained from the Western University IDF_CC tool to generate climate-adjusted design storms for 5-, 10-, 50-, and 100-year return periods. These climate-informed design storms were used as inputs for all hydrologic and hydraulic simulations.

The scaling relationship is expressed as follows (Resilient Consulting Corporation, 2025):

$$Rp = Rc \times 1.07\Delta T \qquad (1)$$

where Rp represents future precipitation intensity for a given duration and return period, Rc represents historical precipitation intensity for the same duration and return period, and ΔT represents the projected change in mean annual temperature (in °C).

2.3 Mitigation Scenario Development

Mitigation scenarios evaluated in this study were derived from preferred alternatives identified in the Sophia Creek Watershed & Mulcaster Drainage Area Environmental Assessment Update (C.C. Tatham & Associates Ltd., 2017), completed under the Schedule 'B' Municipal Class Environmental Assessment process. That assessment identified flooding under both minor and major storm events and evaluated a range of flow reduction, conveyance, and restoration-based solutions through a multi-criteria framework.

A facilitated workshop involving Lake Simcoe Region Conservation Authority staff, City of Barrie engineers, and technical specialists was used to select a subset of Environmental Assessment-recommended alternatives for evaluation under climate change conditions. Preliminary flood mapping from the baseline storm sewer model was used to identify downstream flood-prone areas and their upstream contributing sources, enabling targeted selection of mitigation measures.

Seven scenarios were evaluated:

- **Scenario 1:** Existing infrastructure under historical climate conditions.
- **Scenario 2:** Climate change baseline representing the most severe warming scenario (Q4).
- **Scenario 3:** Stormwater management pond providing upstream storage (Q4).
- **Scenario 4:** Trunk storm sewer upgrade addressing downstream conveyance constraints (Q4).
- **Scenario 5:** Distributed Low Impact Development implementation (10% coverage) (Q4).
- **Scenario 6:** Watercourse daylighting along a constrained urban reach (Q4).

- **Scenario 7:** Combined trunk sewer upgrades (Q4).

Together, these scenarios represent a range of storage-based, conveyance-based, distributed, and restoration-oriented flood mitigation strategies.

2.4 Hydrologic and Hydraulic Modelling

Flood hazard modelling was conducted using an integrated one-dimensional–two-dimensional (1D–2D) PCSWMM framework, building on the City of Barrie's existing storm sewer model. The 1D component represents subsurface storm sewer conveyance, while the coupled 2D domain simulates overland flow and surface flooding, enabling representation of both piped and surface flow processes within a partially enclosed urban system. Model development followed standard municipal practice and PCSWMM guidance (CHI Water, 2021).

Design storm simulations were conducted for return periods ranging from 5 to 100 years. The model incorporated updated storm sewer, culvert, and channel data and LiDAR-derived surface elevations, with boundary conditions established at Lake Simcoe using a fixed water level. Model performance was evaluated through comparison with an independent HEC-RAS hydraulic model for the 100-year design event, and quality assurance procedures confirmed numerical stability, network connectivity, and acceptable mass balance prior to analysis.

2.5 Flood Damage and Economic Assessment

Flood damages and cost–benefit analyses were conducted using the Risk and Return on Investment Tool (RROIT), which integrates hydraulic model outputs with GIS-based exposure data to quantify flood damages and evaluate mitigation effectiveness. In this study, the RROIT was applied using flood mapping outputs from the integrated 1D–2D PCSWMM model to assess climate-driven flood risk and compare mitigation scenarios.

2.5.1 Building Damage Estimation

The RROIT relies on depth–damage curves derived from the Provincial Flood Damage Assessment Study for Alberta (IBI Group and Golder Associates, 2015), subsequently adapted for Ontario conditions. These depth–damage relationships were applied to buildings within the modeled floodplain by intersecting flood extents and water surface elevations with building footprints.

Buildings were classified using LSRCA land-use data, and appropriate depth–damage curves were assigned based on building type. Flood damages were calculated conservatively using standardized elevation offsets and depth–damage relationships, reflecting typical residential and non-residential construction in Ontario.

Residential damage values were adjusted to 2025 dollars using an 85% inflation factor based on Statistics Canada construction price indices (Statistics Canada, 2025).

2.5.2 Economic Performance Metrics

Economic performance was evaluated using Average Annual Damage (AAD), calculated as probability-weighted damages across return periods. Investment performance metrics included internal rate of return (IRR), representing the discount rate at which net benefits equal costs, and

net present value (NPV), representing the discounted value of benefits minus costs over the asset life.

Capital costs were based on inflation-adjusted Environmental Assessment estimates, with infrastructure service lives consistent with municipal practice.

3 RESULTS

3.1 Climate Change Impacts on Flood Damages

Climate change dramatically increases flood damages across all return periods, with particularly severe impacts on more frequent storm events. Under the most severe climate scenario (Q4), 5-year storm damages increase by 204% (from $20.8M to $63.1M), while 100-year storm damages increase by 48% (from $157.0M to $232.4M). This pattern reflects the compounding effect of increased rainfall intensity on infrastructure that is already stressed during design events.

The results demonstrate that climate change does not simply shift the probability distribution of storms; it fundamentally alters the damage-frequency relationship in ways that disproportionately affect more frequent events that drive long-term expected annual damages. Climate change (Q4) will expose 69-281% more buildings to flooding, with the 5-year event seeing the number of buildings affected increase from approximately 41 to 157.

Table 1. Climate change impact on flood damages (Q4 Scenario vs Existing Conditions)

Return Period	Existing Damages ($M)	Q4 Climate Damages ($M)	Buildings Affected (Existing)	% Increase
5-year	$20.8	$63.1	41	+204%
10-year	$47.3	$102.5	121	+117%
50-year	$124.7	$197.1	303	+58%
100-year	$157.0	$232.4	392	+48%

3.2 Mitigation Scenario Performance

Table 2 presents the physical and economic performance of each mitigation scenario under the most severe climate scenario (Q4). The SWM pond at MacMorrison Park (Scenario 3) provides the greatest overall benefit with the lowest AAD of $16.0M, representing a 31% reduction from the climate baseline. This scenario performed best in four of five return periods (5-, 10-, and 100-year events), with damage reductions ranging from 15.1% to 47.4%.

The Owen Street trunk sewer upgrade (Scenario 4, currently in construction) provides the best performance for the 50-year event with 17.5% damage reduction. Scenarios 4 and 7 show nearly identical results, confirming that the Clapperton Street trunk adds minimal benefit beyond Owen Street alone. Notably, the daylighting scenario (Scenario 6) increases damages across all return periods, with AAD increasing by $903,024 compared to the climate baseline. This finding indicates that removing the culvert increases flood depths in some areas despite improved conveyance.

Table 2. Mitigation scenario performance under Q4 climate scenario

Scenario	Current AAD ($/year)	AAD Reduction vs Baseline	100-yr Damage ($M)	Ranking
Scenario 1 (Existing)	$8.4M	Reference	$157.0	N/A
Scenario 2 (Climate Q4)	$23.2M	Baseline	$232.4	Baseline

Scenario	Current AAD ($/year)	AAD Reduction vs Baseline	100-yr Damage ($M)	Ranking
Scenario 3 (SWM Pond)	$16.0M	-$7.16M	$197.3	1
Scenario 4 (Owen Trunk)	$18.1M	-$5.13M	$201.5	2
Scenario 5 (LID 10%)	$18.7M	-$4.52M	$213.1	4
Scenario 6 (Daylighting)	$24.1M	+$0.90M	$244.7	Not Recommended
Scenario 7 (Both Trunks)	$18.1M	-$5.14M	$201.5	3

3.3 Spatial Damage Analysis

Aggregation plots from RROIT reveal where damage concentrations spatially occur across the subwatershed, representing the cumulative effect of upstream subcatchment contributions. Under the Q4 climate scenario, damage concentrations are highest in the downstream portions of the watershed near Bayfield Street and along the main Sophia Creek corridor, where flooding from surcharging storm sewers affects adjacent properties.

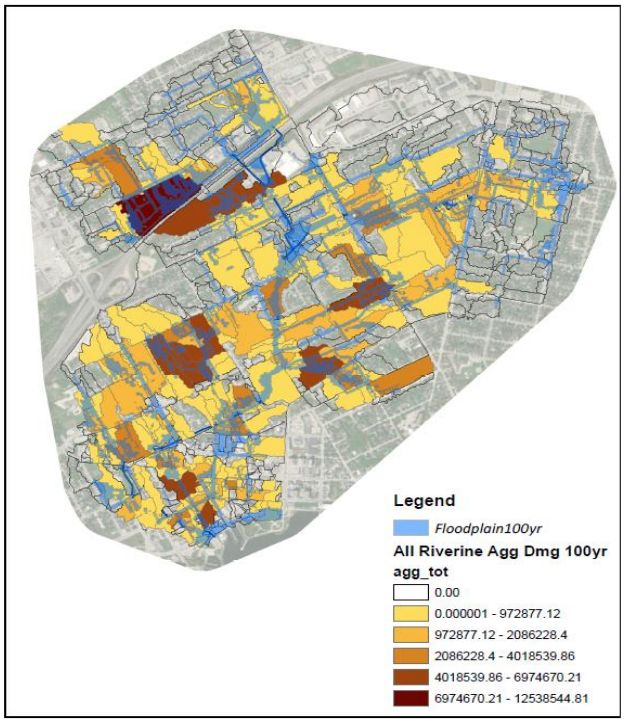

Figure 2. Damage Aggregation Plot for Scenario 3 (SWM Pond) under 100-Year Q4 Climate Event

Re-aggregation plots identify which individual subcatchments contribute to downstream flooding, providing insight into retrofit opportunities beyond where flooding occurs. For Scenario 3 (SWM Pond), the re-aggregation analysis shows significant damage reduction in subcatchments downstream of MacMorrison Park, demonstrating the pond's effectiveness in attenuating peak flows that would otherwise cause downstream property damage.

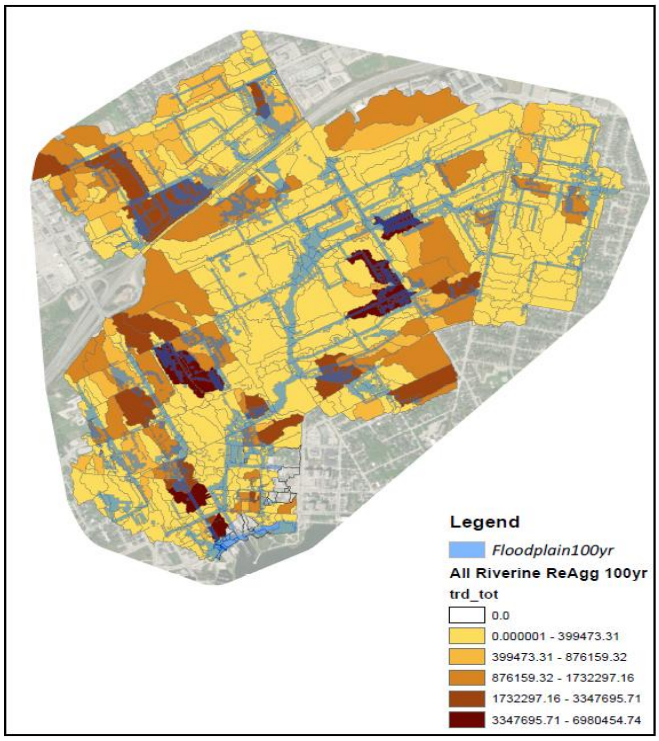

Figure 3. Damage Re-Aggregation Plot for Scenario 3 (SWM Pond) showing Contributing Subcatchments

Building-level riverine damage results for Scenario 3 (Stormwater Management Pond) indicate that the facility protects 69 buildings and reduces damages by $35.10M compared to the Q4 baseline. The spatial distribution of protected buildings is shown below:

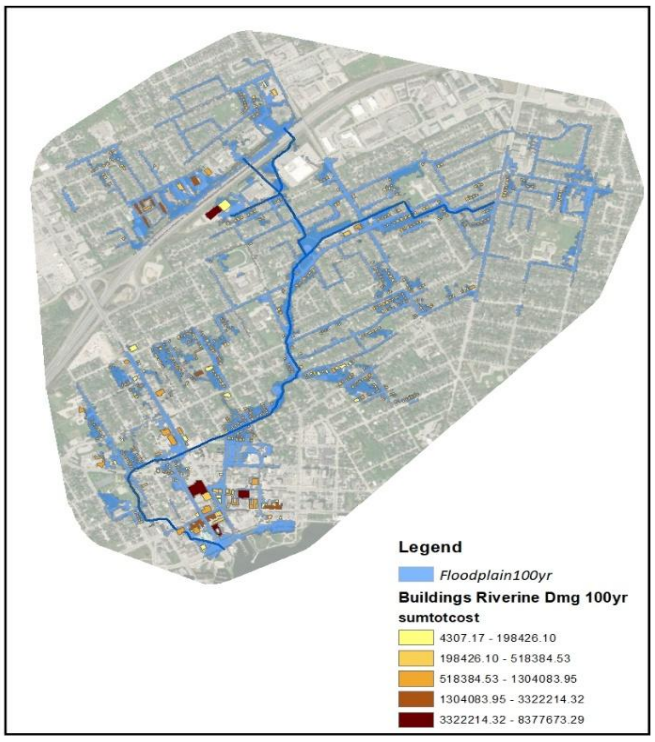

Figure 4. Building Riverine Damage for Scenario 3 (SWM Pond)

3.4 Average Annual Damage Analysis

Average Annual Damage (AAD) provides a probability-weighted measure of expected flood damages that accounts for the full range of storm frequencies. Under existing conditions, AAD is $8.4M per year. Climate change (Q4) increases this to $23.2M per year—a 176% increase that reflects the combined effect of more intense storms across all return periods.

While no mitigation scenario fully restores damages to pre-climate change levels, Scenarios 3, 4, 5, and 7 all substantially reduce impacts compared to the climate baseline. Scenario 3 (SWM Pond) achieves the greatest AAD reduction of $7.16M per year, followed by Scenario 7 (Both Trunks) at $5.14M and Scenario 4 (Owen Trunk) at $5.13M. The LID scenario provides a more modest $4.52M reduction. Industrial/Warehouse buildings emerged as the most vulnerable building type, with the highest damage per building across all return periods.

3.5 3.5 Cost-Benefit Analysis

Return on investment metrics were calculated using RROIT's cost-benefit module, comparing AAS against capital costs over each scenario's service life (Table 3). From an economic perspective, Scenario 3 (SWM Pond) emerges as the clear winner with the lowest capital cost ($7.31M), highest annual savings ($7.16M/yr), shortest payback period (3.0 years), and highest internal rate of return (97.86%). The NPV of $211M over the 75-year service life represents exceptional value for this investment.

Table 3. Cost-benefit analysis of mitigation scenarios

Scenario	Capital Cost ($M)	Annual Savings ($/yr)	Payback (yrs)	IRR (%)	NPV ($M)
Sc 3 (SWM Pond)	$7.31	$7.16M	3.0	97.86	$211
Sc 4 (Owen Trunk)	$10.89	$5.13M	4.7	47.13	$144
Sc 7 (Both Trunks)	$21.79	$5.14M	8.6	23.60	$128
Sc 5 (LID 10%)	$62.40	$4.52M	32.5	7.21	$50
Sc 6 (Daylighting)	$7.63	-$0.90M	Never	N/A	-$39

The next best economic option is Scenario 4 (Owen Street Trunk Sewer), which is already under construction. With a capital cost of $10.9M, annual savings of $5.13M, payback period of 4.7 years, IRR of 47.13%, and NPV of $144M, this scenario provides strong return on investment. Scenario 7 (Both Trunks) has a capital cost of $21.8M with nearly identical annual savings ($5.14M) and a very similar spatial pattern of flood damage reduction compared to Scenario 4, resulting in a longer payback period (8.6 years), lower IRR (23.60%), and lower NPV ($128M)—confirming that the Clapperton Street trunk provides minimal incremental benefit beyond Owen Street alone.

Scenario 5 (LID) requires the highest capital investment ($62.4M) with modest annual savings ($4.52M), resulting in a 32.5-year payback period and NPV of $50M. While still providing positive returns, the extended payback period reflects the distributed nature and higher implementation costs of watershed-wide LID retrofits. Scenario 6 (Daylighting) produces negative annual savings (-0.9M/ yr) and negative NPV (-$39M), making it economically unviable as a standalone flood mitigation measure. This scenario actually increases flood damages rather than reducing them.

4 DISCUSSION

This study demonstrates a systematic approach for prioritizing flood mitigation investments under climate change uncertainty and highlights several implications for municipal adaptation planning.

Integrating climate projections into flood risk assessment substantially alters the economics of flood management. Projected increases in damages across return periods indicate that reliance on historical climate data can significantly underestimate future risk and lead to underinvestment in adaptive infrastructure.

Mitigation performance varied widely across intervention types, underscoring the importance of rigorous quantitative evaluation. The superior performance of the stormwater management pond reflects its upstream location, available storage capacity, and ability to attenuate peak flows affecting multiple downstream areas. In contrast, other interventions provided more limited or localized benefits, reinforcing the need for evidence-based prioritization rather than qualitative preference.

The daylighting scenario evaluated in this study illustrates that flood risk reduction should not be assumed as an inherent outcome of restoration projects. Under the specific site conditions and conceptual design assessed, daylighting increased flood depths in some areas due to constrained urban geometry and limited floodplain capacity. This finding is site- and design-specific and emphasizes the importance of context-sensitive, hydraulically informed evaluation of nature-based solutions.

Finally, the integration of PCSWMM with the Risk and Return on Investment Tool represents a practical methodological advancement for urban flood risk assessment in partially enclosed catchments. By capturing both storm sewer surcharging and overland flooding processes, this approach supports more reliable damage estimation and investment prioritization under climate change.

5 CONCLUSIONS

This study developed and applied a systematic framework for prioritizing flood mitigation investments under climate change uncertainty in the Sophia Creek catchment, Barrie, Ontario. Climate-informed flood modeling indicates that damages could increase by 48–204% across return periods under a high-emission scenario, highlighting the growing long-term liability associated with more frequent flood events.

Five mitigation scenarios were evaluated using integrated 1D–2D PCSWMM modeling and the Risk and Return on Investment Tool. Among these, the stormwater management pond emerged as the highest-priority investment, achieving a 31% reduction in Average Annual Damage and performing best across most return periods. While combined mitigation strategies produced greater absolute damage reductions, they offered diminished marginal returns relative to the pond's standalone performance.

Overall, the results underscore the importance of rigorous, quantitative evaluation in climate adaptation planning. The integrated PCSWMM–RROIT framework provides municipalities with a replicable, evidence-based approach for prioritizing cost-effective flood resilience investments and avoiding reliance on qualitative or ad hoc decision-making. As climate change continues to intensify flood risk, such systematic frameworks will be increasingly critical for effective municipal infrastructure planning.

6 ACKNOWLEDGEMENTS

This project was undertaken with financial support from the Ontario Ministry of Environment, Conservation and Parks. The authors gratefully acknowledge Kenneth Cheney and Bill Thompson for their guidance throughout the project, Emma Haug-Kindellan and Kristopher Robinson from Credit Valley Conservation for RROIT technical support and training, Lauren Moretto for her review contributions and advice on climate change considerations, Indraneel Bhattacharjee for his assistance in preparing RROIT input datasets, the City of Barrie Public Works Department for providing technical data and engineering expertise, Resilient Consulting Corporation for hydraulic modeling support and quality assurance, CHI for guidance on PCSWMM, and LSRCA modeling and planning staff for their contributions to scenario development and technical review.

7 REFERENCES

Bush, E. and Lemmen, D.S. (Eds.) (2019). Canada's Changing Climate Report. Government of Canada, Ottawa, ON. 444 pp.

C.C. Tatham & Associates Ltd. (2017). Sophia Creek Watershed & Mulcaster Drainage Area Environmental Assessment Update. Prepared for City of Barrie.

CHI Water (2021). PCSWMM User's Guide. Computational Hydraulics International, Guelph, Ontario, Canada.

City of Barrie. (n.d.). Growth management. https://www.barrie.ca/planning-building infrastructure/development-planning/growth-management

Credit Valley Conservation (2020). Guidance for Lowest Opening Elevation Assignment in Flood Risk Assessment.

Environment and Climate Change Canada. Primer on Climate Change and Extreme Precipitation. ClimateData.ca. [Online resource]. Available: https://climatedata.ca/resource/primer-on-climate-change-and-extreme-precipitation/ (accessed Jan 2026).

IBI Group and Golder Associates (2015). Provincial Flood Damage Assessment Study. Prepared for Alberta Environment and Sustainable Resource Development, Edmonton, Alberta.

IPCC (2021). Climate Change 2021: The Physical Science Basis. Contribution of Working Group I to the Sixth Assessment Report of the Intergovernmental Panel on Climate Change. Cambridge University Press, Cambridge, UK.

Lake Simcoe Region Conservation Authority (2022). Landcover 2018. Available from https://lsrca-open-data-camaps.opendata.arcgis.com, accessed 01 September 2025

Resilient Consulting Corporation (2025). Sophia Creek Climate Change & Urban Flood Inundation Assessment – Final Report. Prepared for Lake Simcoe Region Conservation Authority, Project 2024-036, January 2025.

Tatham Engineering Limited (2019). Drainage Master Plan Municipal Class Environmental Assessment Phases 1 & 2. Prepared for City of Barrie.

Toronto and Region Conservation Authority & Credit Valley Conservation (2010). Low Impact Development Stormwater Management Planning and Design Guide.

US Army Corps of Engineers (2020). HEC-RAS River Analysis System User's Manual, Version 6.0. Hydrologic Engineering Center, Davis, CA.

Warren, F.J. and Lemmen, D.S. (Eds.) (2014). Canada in a Changing Climate: Sector Perspectives on Impacts and Adaptation. Government of Canada, Ottawa, ON. 286 pp.

ICFM 10
Adapting to Global Change:
Innovative Approaches to Flood Management and Resilience
May 20-22, 2026 | Western University, London, Ontario, Canada

Reducing flood risk by improving the hydraulic capacity of box culverts through inlet modifications

Thea M.D. Giliomee[1], Ione Loots[1] and Marco van Dijk[1]
Department of Civil Engineering, University of Pretoria, Lynnwood Road, 0002, Pretoria, South Africa[1]
E-mail: u20424028@tuks.co.za

ABSTRACT

Culverts are an important part of a stormwater drainage system. When culverts can discharge the required flows during flood events, they ensure sufficient drainage from roads, preventing flood risks, infrastructure damage, and safety hazards. However, culverts can become insufficient over time due to increasing flood peaks caused by climate change and urbanisation. Culvert capacity can be increased by retrofitting inlet modifications, which may help with adaptation to higher flows. These modifications create a more gradual flow transition at the inlet, reducing the impact of the contraction after the inlet and increasing discharge capacity. In many instances, this can negate the need to rebuild an insufficient culvert, offering a cost-effective upgrade with minimal traffic disruption.

This study used physical modelling to evaluate different inlet modifications for box culverts under inlet control, and the performance of the best inlet was then theoretically evaluated for an existing culvert as a case study. The tested modifications included adjustments to wingwall and headwall angles, as well as a rounded inlet edge. For box culverts, a 15º headwall with a 30º wingwall increased flow capacity by up to 15% at a headwater depth equal to the culvert height (1D) and up to 34% at a headwater depth equal to twice the culvert height (2D). A flow-improvement coefficient, C_{TG}, was used to quantify the increase in performance for each inlet configuration. This coefficient can be applied to existing equations for standard square-edge inlets to calculate the improved discharge capacity when inlet modifications are implemented.

Inlet modifications are a practical way to enhance culvert performance and reduce flood risks, particularly given the increasing hydrological pressures of climate change and urbanisation. Implementing such improvements can support the development of more resilient and sustainable drainage infrastructure.

KEYWORDS: risk reduction, inlet modification, wingwall, headwall, climate change, urbanisation, box culvert

1 INTRODUCTION AND BACKGROUND

Culverts are hydraulic structures that transport water from one side of a road, highway, or railway embankment to the other. Their design focuses on identifying the most economical configuration capable of conveying the required discharge without allowing upstream water levels to exceed acceptable limits (Houghtalen et al., 2010). However, higher peak floods are placing additional stress on stormwater drainage systems, which can result in culverts becoming insufficient and headwater levels exceeding acceptable limits. Extreme storm events are expected to occur more frequently due to climate change. The effect of ongoing urbanisation is evident, as reduced infiltration in urban areas means that heavy rainfall can rapidly increase runoff (Agonafir et al., 2023). When drainage capacity is insufficient, the risk of infrastructure damage, traffic disruption, and safety hazards increases.

Culverts are designed to convey a specific capacity, but the barrels often do not achieve full-flow conditions (Straub et al., 1953). The momentum of water entering a square-edge inlet culvert creates a flow contraction, or vena contracta, just after the inlet (West, 1956). At the vena contracta, the cross-

sectional flow area is at a minimum, which reduces the culvert capacity (Jaeger, 2019). The contraction is more pronounced for a square-edge inlet than for a rounded-edge inlet or one with wingwalls, as shown in Figure 1. Improving the culvert inlet can either increase its capacity for a specific headwater depth or pass the design discharge at a lower headwater depth.

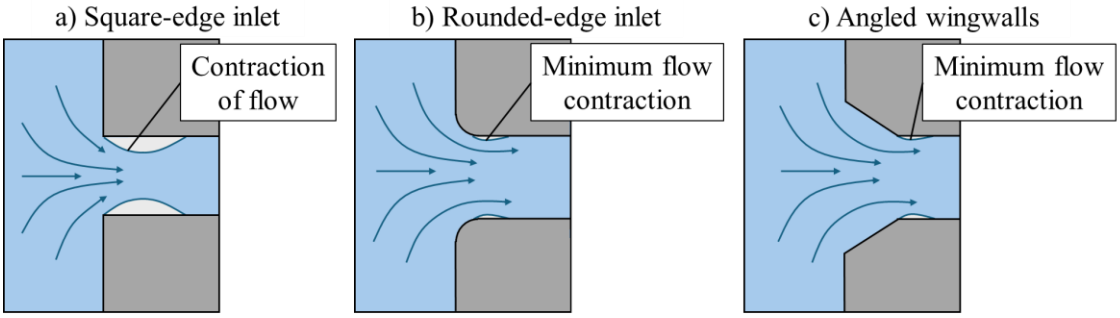

Figure 1: Plan view of flow contraction at a) a square edge inlet, b) a rounded edge inlet, and c) wingwalls

Some of the most promising inlet configurations include tapered inlets (Schall et al., 2012), 15º headwalls (Ashour et al., 2014), 45º wingwalls (West, 1956), and rounded inlets (at least 0.15D or 0.15B) (Jaeger, 2019). Headwalls and wingwalls are already widely used as retaining structures. Limited research has examined combinations of different wingwall and headwall angles, typically using the same angle when combined or testing wingwalls and headwalls separately. Therefore, different wingwall and headwall angles were tested and compared to a rounded-edge inlet. A new coefficient to quantify capacity improvements was developed to assist in designing or upgrading culverts, and it was then used to theoretically upgrade an existing culvert as a case study using inlet modifications.

2 METHODOLOGY

Physical modelling was conducted in a hydraulic flume to evaluate culvert inlet performance under inlet-control conditions. Each tested model culvert was positioned in the hydraulic flume, as shown in Figure 2. The flume is 450 mm wide, 500 mm high and 10 m long. A depth gauge (①) was placed 4D upstream of the model culvert, where D is the culvert height. A measurement ruler (②) was placed 0.75D upstream of the culvert inlet, which measured the headwater, H_I, and another depth gauge (④) was positioned 4D downstream of the culvert outlet. The slope was set to 1%, as recommended by SANRAL (2013), as the minimum slope to prevent silt deposition. The steep slope also ensured inlet control conditions for all the tests performed. Under inlet control conditions, the inlet geometry has a greater influence on the flow through the barrel than under outlet control (West, 1956).

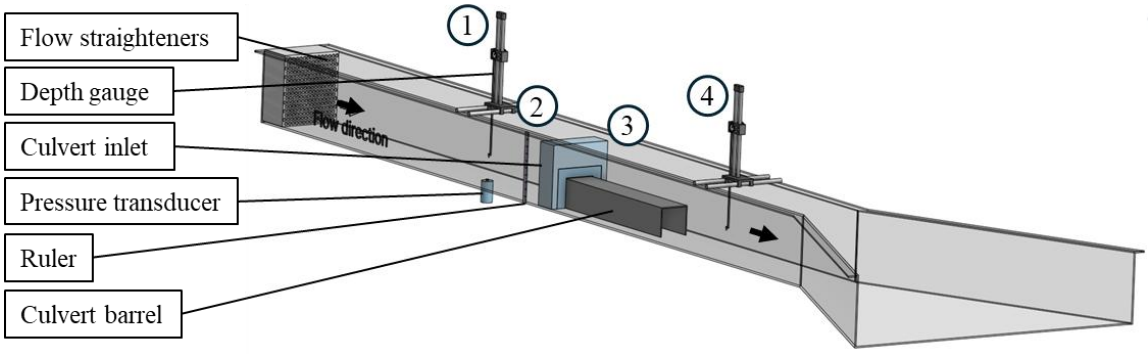

Figure 2: Physical model setup in the hydraulic flume

The physical models consisted of various inlet configurations for a 200 x 200 mm square box culvert. 0º, 45º and 90º wingwalls as well as 15º, 30º, 45º and 90º headwalls were combined and tested.

The 90º wingwall and 90º headwall represent the standard square edge inlet. The wingwalls and headwalls were compared to a 0.25D rounded-edge inlet. The model culvert dimensions and the physical model, constructed from acrylic plastic with a 3D-printed inlet sealed in place with silicone, are shown in Figure 3. The wingwalls extended 0.4D to the sides of the barrel, and the headwall extended 0.4D upward to ensure the enlarged inlet cross-sectional area of 360 x 280 mm was kept the same for all the tests, providing a consistent inflow area.

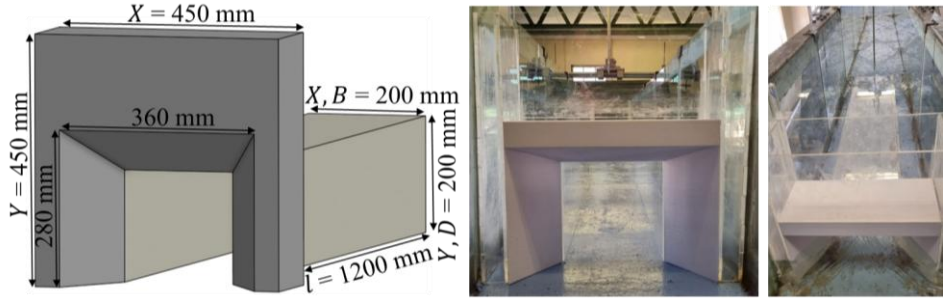

Figure 3: Model culvert dimensions and model culvert installed in the hydraulic flume

Water was pumped into the flume, and different flow rates were achieved by adjusting three control valves. Approximately 20 flow rates, ranging from 4 l/s to 82 l/s, were tested for each inlet modification. The flow rates were recorded using an ultrasonic flow meter. Furthermore, the flow depths corresponding to each flow were measured just upstream (H_1) and at 4D upstream and downstream of the culvert.

3 RESULTS

3.1 Physical modelling testing

Figure 4 illustrates the difference in upstream ① and downstream ④ water levels between a) a standard square-edge inlet and b) a modified inlet. The flow through the culvert in Figure 4a) and Figure 4b) is the same. Therefore, as water flows through a square-edged inlet culvert, the cross-sectional area decreases ③ while the velocity increases, in accordance with the continuity equation. For the same flow rate, inlet improvements allow for a larger cross-sectional area to be utilised inside the culvert barrel ③ with a smaller increase in velocity compared to the square edge inlets. This reduces the upstream headwater level, (H_1) or ②, which lowers the risk of upstream flooding and road overtopping.

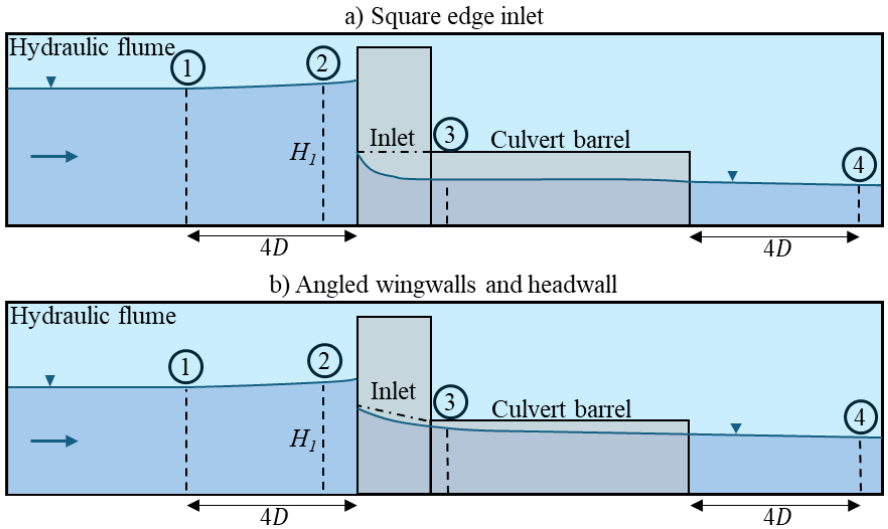

Figure 4: Side view of hydraulic flume illustrating the flow through a culvert with a) a square edge inlet and b) an angled wingwalls and headwall for the same flow rate

During the tests, the water level upstream of the culvert inlet ② was higher than downstream ④, indicating a damming effect. Subcritical flow upstream of the culvert went through critical flow after the inlet and then to supercritical flow in the barrel due to the steep slope (West, 1956). Figure 5 verifies this behaviour for the 90º wingwall and 90º headwall box culvert by plotting the Froude numbers at the three depth-measurement locations defined in Figure 4. All other inlet modifications showed similar behaviour.

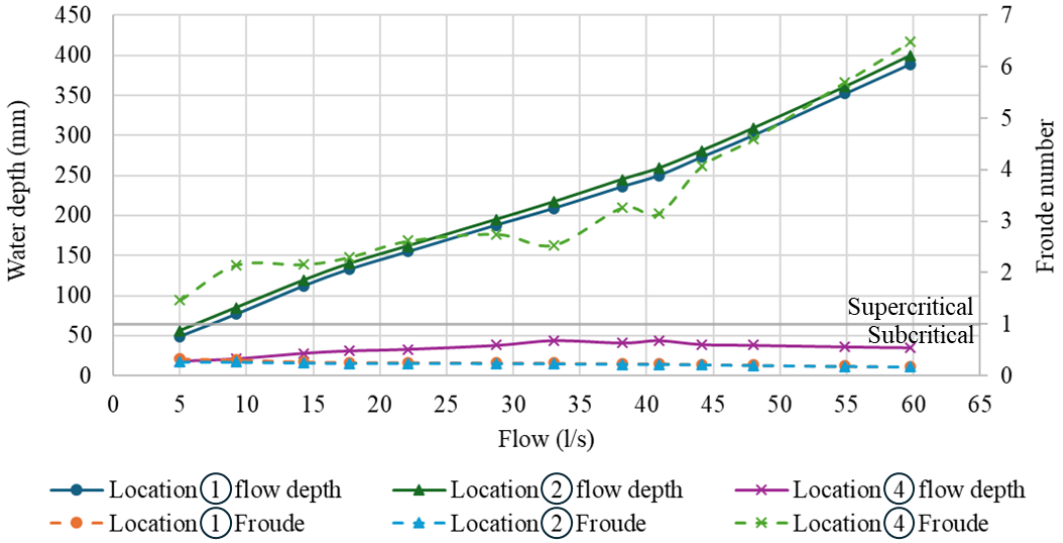

Figure 5: Water depth and Froude numbers for the 90º wingwall and 90º headwall box culvert at i, ii and iv in the hydraulic flume

Figure 6 shows the performance curves for each inlet modification, generated using third-degree polynomial fits to the flow versus headwater data. A 1*D* line marks the point of inlet submergence, and a 2*D* line represents the maximum allowable headwater for a given design recurrence interval defined in the South African design guideline (SANRAL, 2013). Once submerged, the influence of the modifications became significant (>15%). The 30º wingwall with a 15º headwall performed best, increasing flow by 34% at $H_1/D = 2$. It was followed by a rounded-edge inlet and a 45º wingwall with a 15º headwall.

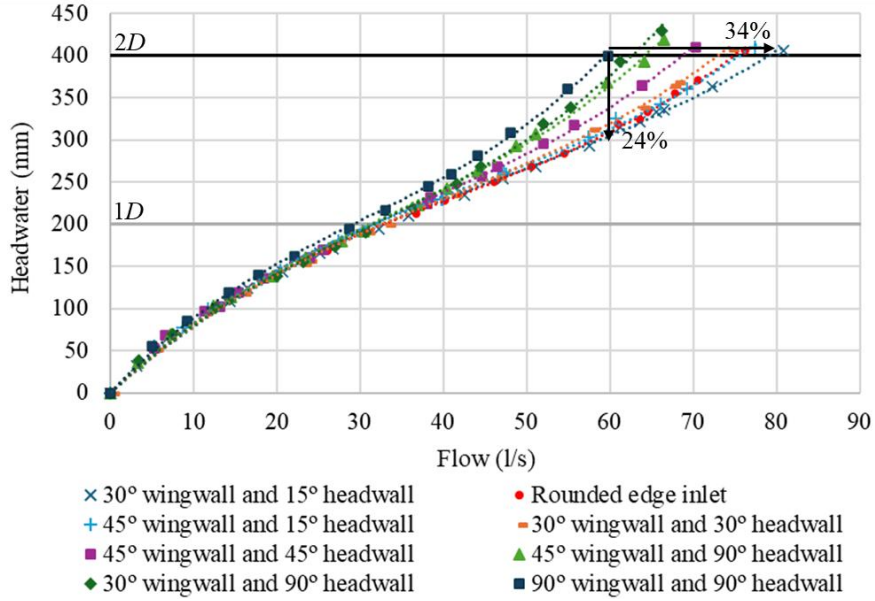

Figure 6: Headwater to discharge relationship for improved square box culvert inlets tested, ranked from most to least effective, after Giliomee et al. (2025)

Figure 7 shows the percentage improvement for different wingwall and headwall angle combinations at different levels of submergence. When the inlet is unsubmerged, only the wingwalls influence the flow, but once submerged, the headwall angle has a much greater effect. At H_1/D = 1.5, the wingwall and headwall contribute almost equally, while at H_1/D = 2 the headwall governs. The 15º headwall reduces contraction losses notably, with the 30º wingwall and 15º headwall conveying 28% more flow than the same wingwall angle with a 90º headwall. Overall, the optimal wingwall angle lies between 0º and 30º, and the optimal headwall angle between 0º and 15º. Among the configurations tested from the literature, the 30º wingwall and 15º headwall provided the greatest increase in discharge.

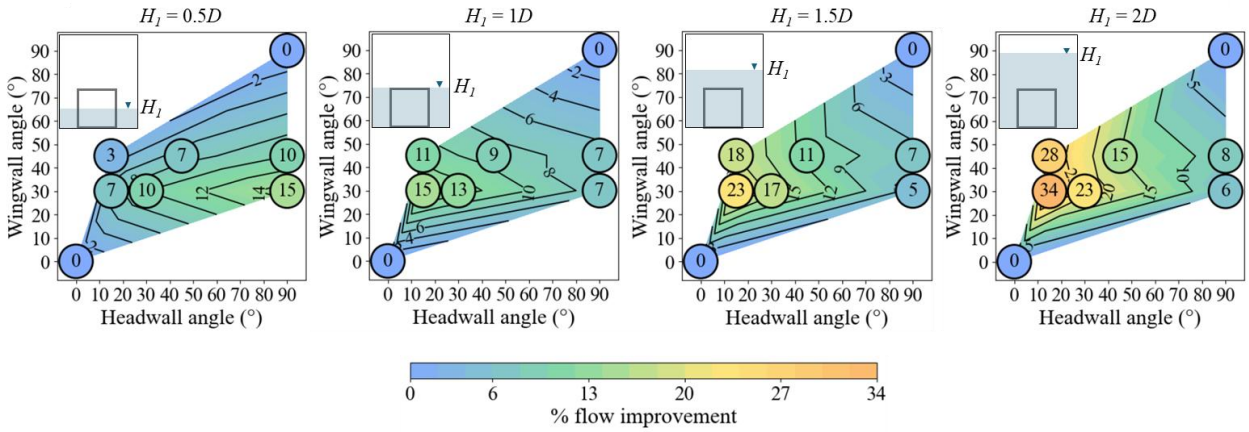

Figure 7: Percentage flow improvement at headwater levels of 0.5*D*, 1*D*, 1.5*D* and 2*D*

3.2 Flow improvement coefficient

The capacity improvement results were used in Giliomee et al. (2025) to develop a coefficient for flow improvement, C_{TG}, which quantifies the increase in discharge provided by each inlet modification. It can be applied as an adjustment factor to the standard square-edge culvert discharge calculated using existing guidelines, as shown in Eq. (1). A higher C_{TG} indicates better performance; for example, a C_{TG} of 1.34 corresponds to a 34% increase in flow at that headwater depth. For any specific headwater level larger than H_1/D = 0.5, the coefficient was calculated with Eq. (2).

$$Q_{Improved} = Q_{Square\ edge\ inlet\ culvert} \times C_{TG} \quad (1)$$

$$C_{TG} = \frac{Flow\ improvement\ (\%)}{100} + 1 = \frac{(Q_{Improved\ inlet} - Q_{Square\ edge\ inlet})}{Q_{Square\ edge\ inlet}} + 1 \quad (2)$$

The flow improvement provided by each inlet modification varies with headwater depth. Therefore, C_{TG} coefficients were linked to ranges of H_1/D using separate equations for unsubmerged conditions ($0.5 \leq H_1/D \leq 1.2$) and submerged conditions ($1.2 < H_1/D \leq 2$). Table 1 presents the C_{TG} equations for the 30º wingwall with a 15º headwall and the 45º wingwall with a 15º headwall, allowing the coefficient to be calculated for any headwater depth. Table 1 also lists the percentage flow improvement at H_1/D = 1.2 and H_1/D = 2, along with the standard square-edge inlet equations from SANRAL (2013) as an example of existing guidelines to which the C_{TG} values can be applied.

Table 1: Inlet-controlled square box culvert improvement coefficient equations and their percentage improvement in discharge capacity after Giliomee et al. (2025)

SANRAL (2013)	**C_{TG} coefficient equations**
For: $0 < H_1/D \leq 1.2$	Equations only apply for $0.5 \leq H_1/D \leq 1.2$
$Q = \frac{2}{3} C_B B H_1 \sqrt{\frac{2}{3} g H_1}$	30º wingwall and 15º headwall (18% at 1.2D)
	$C_{TG} = 0.1532(H_1/D) + 0.9953$
Where: $C_B = 0.9$	45º wingwall and 15º headwall (14% at 1.2D)
	$C_{TG} = 0.1477(H_1/D) + 0.9645$
For: $H_1/D > 1.2$	Equations only apply for $1.2 < H_1/D \leq 2$
$Q = C_h B D \sqrt{2g(H_1 - C_h D)}$	30º wingwall and 15º headwall (34% at 2D)
	$C_{TG} = 0.0897(H_1/D)^2 - 0.0836(H_1/D) + 1.1517$
Where: $C_h = 0.6$	45º wingwall and 15º headwall (28% at 2D)
	$C_{TG} = 0.0632(H_1/D)^2 - 0.0346(H_1/D) + 1.0919$

4 CASE STUDY

The physical modelling results were theoretically applied to an existing culvert as a case study to demonstrate how discharge capacity can be increased and flood risks reduced through inlet modifications. The culvert is a single-barrel box culvert with a width of 1.2 m and a height of 0.6 m, installed on a 0.069 m/m slope and a total length of 17.55 m. This culvert functions under inlet control.

Table 2 shows the culvert analysis comparing the design flood with the culvert capacity, both without and with inlet modifications, at different levels of submergence. The South African design criteria specifies that inlet submergence should be limited to H_1=1.2D for the design flow Q_T, while for the higher flow Q_{2T}, the upstream level should be limited to the minimum of 2D or the shoulder break point (SBP) level (SANRAL, 2013). The C_{TG} coefficient for the 30º wingwall with a 15º headwall was used to calculate the increased discharge capacity. Before the inlet modifications, the culvert was insufficient for its design floods, but calculations show that the improvements now allow the culvert to convey the 1:20 return-period flood under the South African performance criteria. This is important because it is critical to prevent roadway overtopping during high flood conditions. The culvert with inlet modifications would not convey the desired flow at 1.2D for the 1:10 design flood, but it would do so at approximately 1.3D, which remains acceptable for design purposes.

Table 2: Case study culvert analysis comparing the design flood to the culvert capacity without and with inlet modifications at headwater depths of 1.2D, 2D, and the shoulder breakpoint (SBP)

Headwater data			**Design return period**	**Before inlet modifications**		**After inlet modifications**	
H_1 (m)		**H_1/D**	**Q_T=Q_{10} (m^3/s)**	**Q (m^3/s)**	**Sufficient (Y/N)**	**$Q_{improved}$ (m^3/s)**	**Sufficient (Y/N)**
1.2D	0.720	1.20	1.624	1.125	No	1.326	No
H_1 (m)		**H_1/D**	**Q_{2T}=Q_{20} (m^3/s)**	**Q (m^3/s)**	**Sufficient (Y/N)**	**$Q_{improved}$ (m^3/s)**	**Sufficient (Y/N)**
2D	1.200	2.00	2.025	1.754	No	2.356	Yes
SBP	1.392	2.32	2.025	1.944	Almost	2.605	Yes

Figure 8 presents the performance curve for the current culvert and when a 30º wingwall with a 15º headwall is retrofitted. For the 1:20-year flood, a 30% (0.44 m) reduction in headwater is observed, or alternatively, a 34% (0.66 m^3/s) increase in discharge is observed at a headwater depth equal to the height from the invert to the SBP. At a headwater depth up to the road level (SBP), the culvert could convey

only a 1:15-year return-period flood without an inlet modification, but with the inlet modification, it is able to convey a 1:49-year return-period design flood.

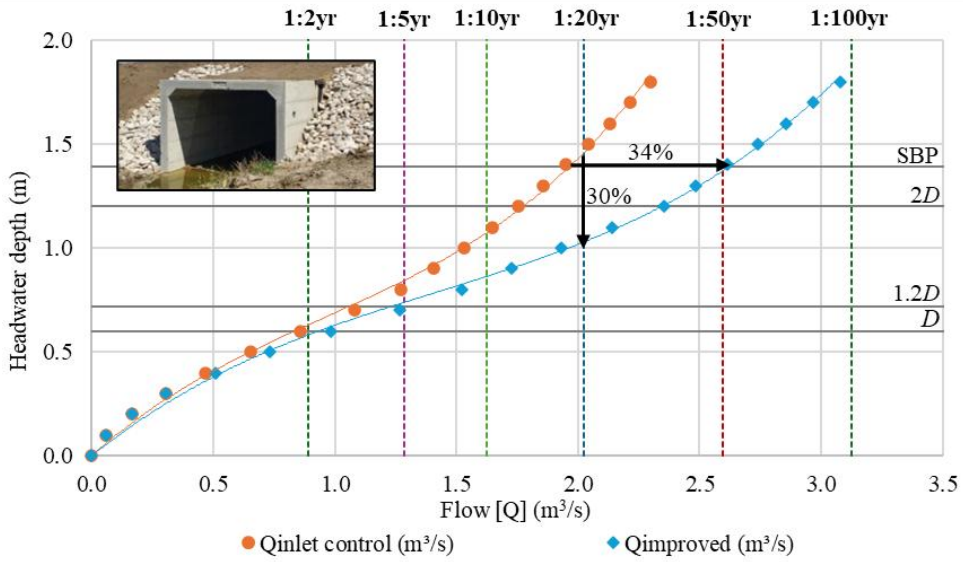

Figure 8: Case study box culvert performance curve analysis under inlet control, without, and with a modified inlet

Figure 9 indicates the percentage reduction in headwater levels when the inlet modification is theoretically applied to the case study culvert under different return-period design floods. Reducing the upstream headwater depth lowers the risk of culvert overtopping. This is expected to improve road safety and protect infrastructure.

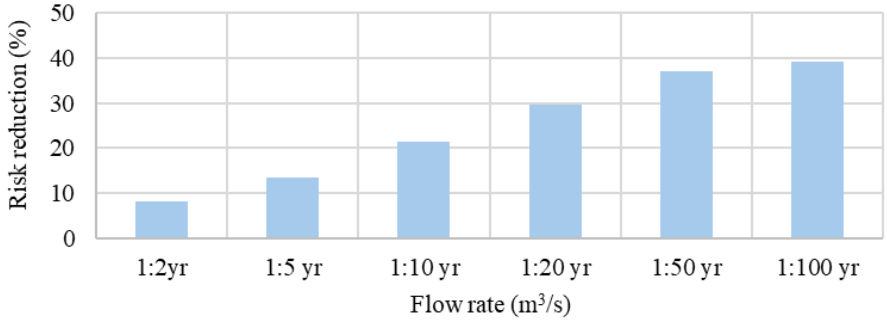

Figure 9: Percentage reduction in headwater levels when the inlet modification is applied to the case study culvert, analysed under different return-period design floods

5 CONCLUSION

A modified inlet reduces flow contraction at the entrance, lowers headwater levels for a given flow, or increases discharge capacity for a similar headwater depth. The results showed that a box culvert's capacity can improve by up to 15% at 1*D* and up to 34% at 2*D* when an inlet modification is applied, providing a cost-effective alternative to adding barrels or rebuilding an inadequate structure. The combination of a 30º wingwall with a 15º headwall performed the best, even better than the rounded-edge inlet. Once the inlet was submerged, the headwall had a greater influence on flow than the wingwalls.

Flow improvements were quantified using the C_{TG} coefficient and theoretically applied to a case study culvert. The inlet modification enabled the insufficient case study culvert to convey its required design flood, reducing headwater levels enough to prevent road overtopping; for the 1:20-year event, the headwater depth decreased by about 30%. The reduction in headwater depth was more pronounced at

higher flows, lowering flood risk during extreme events and supporting more sustainable drainage infrastructure.

6 ACKNOWLEDGEMENTS

Special thanks to Mr. Jan Ngwenya for assisting with lab testing, to Mr. Jordan Mostert for installing instrumentation and managing the 3D printing. This work was supported by the South African National Roads Agency SOC Limited (SANRAL) (Project number: 1002-58600-2018-P7a.10) and the Water Research Commission (WRC) (Project number: C2023/2024-01295).

7 DATA DISCLOSURE

The dataset used in this study was originally generated by the authors and first reported in Giliomee et al. (2025). The present paper builds on that work through additional analyses and new interpretations that extend the original findings.

REFERENCES

Agonafir C., Lakhankar T., Khanbilvardi R., Krakauer N., Radell D. and Devineni N. (2023). A review of recent advances in urban flood research. Water Security, 19, 100141. https://doi.org/10.1016/j.wasec.2023.100141.

Ashour M.A., Aly T.E. and Abdou A.A. (2014). Inclined headwall is an efficient tool for maximizing the discharge efficiency through culverts in 3rd International conference (Water resources and wetlands), Tulcea, Romania, September 8-10, 2016, pp. 184-193. https://www.researchgate.net/publication/355209300.

Giliomee T. M. D., Loots I. and van Dijk M. (2025) Increasing culvert hydraulic capacity for improved climate resilience: a physical modelling analysis. Water and Climate Change, 16, 8, 2503-2518. https://doi.org/10.2166/wcc.2025.033.

Houghtalen R.J., Akan A.O. and Hwang N.H.C. (2010). Fundamentals of Hydraulic Engineering Systems. 4th ed. Upper Saddle River, NJ: Pearson Education.

Jaeger R. (2019). Hydraulic improvements in culverts for climate change adaptation. Unpublished Doctor of Philosophy thesis, University of the Sunshine Coast, University of the Sunshine Coast's Research Repository (UniSC Research Bank).

South African National Roads Agency SOC Limited (SANRAL). (2013). Drainage Manual. 6th Edition, Pretoria, Available from: https://www.nra.co.za/uploads/27/Drainage-Manual-6th-Edition-Sept-2013.pdf.

Schall J.D., Thompson P.L., Zerges S.M., Kilgore R.T. and Morris J.L. (2012). Hydraulic Design of Highway Culverts Third Edition, Hydraulic Design Series Number 5. FHWA-HIF-12-026, Colorado, United States of America.

Straub L.G., Anderson A.G. and Bowers C.E. (1953). Importance of Inlet Design on Culvert Capacity. University of Minnesota, Minneapolis, Minnesota, United States of America, http://purl.umn.edu/108023, consulted 11 November 2025.

West E.M. (1956). Hydraulic Model Studies of Culvert Operation. Commonwealth of Kentucky Department of Highways. Lexington, Kentucky, United States of America, Report No.1, http://dx.doi.org/10.13023/KTC.RR.1956.118.

ICFM 10
Adapting to Global Change:
Innovative Approaches to Flood Management and Resilience
May 20-22, 2026 | Western University, London, Ontario, Canada

Debris Retention Upstream of Culverts: Pier Structure Optimization Through Physical Modelling

Kayuri Govender[1], Maria Dorothea Giliomee[2] and Ione Loots[3]
University of Pretoria, Lynnwood Road, Hatfield, Pretoria, 0002, South Africa[1]
E-mail: u2145538@tuks.co.za

University of Pretoria, Lynnwood Road, Hatfield, Pretoria, 0002, South Africa[2]
E-mail: u20424028@tuks.co.za

University of Pretoria, Lynnwood Road, Hatfield, Pretoria, 0002, South Africa[3]
E-mail: ione.loots@up.ac.za

ABSTRACT

Debris accumulation at culvert inlets during flash floods can cause severe hydraulic blockage and overtopping. This study investigated non-mechanised debris piers as a cost-effective alternative for South African stormwater management infrastructure. Froude-scaled physical modelling in a hydraulic flume was used to assess the effects of pier layout angle (30°, 60°, 90°), pier shape (circular, square, downward teardrop and upward teardrop) and V-apex orientation on debris retention, backwater rise, and hydraulic blockage. Debris retention and backwater significantly decreased as pier angle widened. Pier shape had an overall weak influence and was not found to significantly affect the pier performance. The upstream-facing V-apex resulted in lower backwater accumulation by diverting debris toward the sides of the channel, rather than retaining it in the center. Hydraulic blockage was lowest at 90° due to improved debris alignment allowing for more debris to cleanly pass through the culvert. Higher pier-side retention did not correspond to lower culvert blockage. Trade-off and sensitivity analyses identified 90° upward teardrop piers with an upstream-facing V-apex as optimal and robust. This preliminary debris testing provides a foundation for future debris pier testing with the aim of developing technical design guidelines for debris piers in South Africa and similar developing countries, where the use of mechanised structures is not practical.

KEYWORDS: Debris, culvert, blockage, hydraulic model, debris retention, backwater

1 INTRODUCTION AND BACKGROUND

Urban flooding is exacerbated by debris accumulation at culvert inlets, which reduces hydraulic capacity and increases the likelihood of upstream inundation, erosion, and structural failure (Diehl and Bryan 1993; Bradley et al. 2005; Balkham et al. 2010; Schmocker and Hager 2013; Blanc et al. 2014; Panici and De Almeida 2018; Miranzadeh et al., 2023). Flow through these culverts partially blocked by debris is governed by the culvert geometry, channel flow characteristics, and debris properties (Miranzadeh et al., 2023). Debris characteristics vary with catchment conditions (Diehl and Bryan 1993), and blockage formation depends on debris orientation relative to flow and pier structures (De Cicco et al., 2020).

A range of debris retention structures is used internationally with mixed success (Blanc et al., 2014). Mechanised debris control structures have shown to be highly effective, however, developing countries like South Africa face poor infrastructure management through lack of planning, limited funding, corruption and vandalism or theft (Mazele and Amoah, 2022). Therefore, non-mechanised debris control structures present an ideal solution for mitigating culvert blockage in South Africa and other developing countries. Piers placed upstream of culverts can retain debris effectively while reducing inlet maintenance compared to deflectors or racks (Wallerstein et al., 1997). The efficiency of such systems depends on providing adequate retention volume (Blanc et al., 2014), with pier spacing small enough to trap debris, yet wide enough to maintain flow and allow machinery access (Wallerstein et al., 1997; Schmocker and Hager, 2013; Lange and Bezzola, 2006). Spacing becomes less important once initial accumulation occurs (Lange and Bezzola, 2006). Debris volume and Froude number strongly influence backwater rise, whereas pier diameter has limited effect. Pier shape controls water surface profiles and blockage probability, with flat shapes most prone to blockage and ogival shapes least (Schmocker and Hager, 2013; Panici and De Almeida, 2020). Wallerstein et al. (1997) found a V-shaped configuration with the apex pointing downstream provided optimal retention with minimal backwater rise, although only circular piers at a 60° orientation were assessed.

The present study therefore investigates the pier shape and orientation with a V-shaped configuration that maximizes debris retention at the piers while minimizing backwater and culvert hydraulic blockage. It further examines whether orienting the V apex upstream could redirect debris toward channel margins, reducing trapping between piers. Identifying the most effective pier arrangement can significantly reduce culvert blockage, thereby mitigating flood risk and infrastructure damage.

2 METHODOLOGY

The study modified the V-shaped pier retention structure, identified as the most effective debris-retention system in previous research, and tested scaled physical models of a culvert–pier system in a hydraulic channel. A constant, subcritical flow of 12.8 l/s (Fr = 0.45) was used for the model to ensure deep flow, minimize meniscus effects, and maximize blockage probability under uncongested conditions (De Cicco et al., 2020). Flow was measured using an ultrasonic flow meter. Froude similarity (Fr_{model} = $Fr_{prototype}$ = 0.45) governed scaling, with model dimensions based on standard portal culverts (Web-1) and pier configurations from Lange and Bezzola (2006). A scale ratio of n = 12.5 was applied, based on the restricted flume width of 450 mm and a 1500 x 1500 mm rectangular portal culvert with three barrels as the prototype. Figure 1 shows the dimensions (mm) of the model culvert used in the experiments.

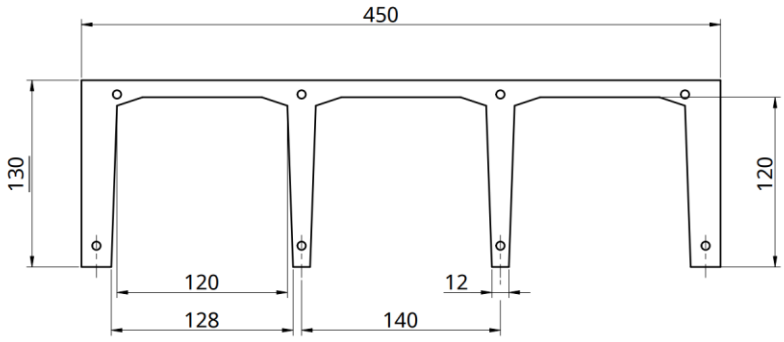

Figure 1 : Dimensions of the model culvert

Piers of circular, square and teardrop shapes were constructed from dowels and medium density fiberboard each with a constant 32 mm cross-section. Pier diameters were chosen to be consistent with an existing structure at Faerie Glen Nature Reserve, South Africa, since pier diameter has minimal influence on debris accumulation or backwater rise (Schmocker & Hager, 2013; Panici & De Almeida, 2020). The pier rig was positioned 1.2 m upstream of the culvert in the model, maintaining proportional field spacing

to that of the Faerie Glen Nature Reserve debris pier system. Clear pier spacing *s* was set at 100 mm, satisfying L ≥ 1.5s (Lange and Bezzola, 2006), where L is the minimum length of debris that will initially get caught. This ensures debris ≥ 150 mm would be retained at the piers rather than at the culvert ($L_{culvert}$ ≥ 192 mm; Web-1). The pier rig dimensions (mm) for the model are shown in the side and front-view schematic in Figure 2.

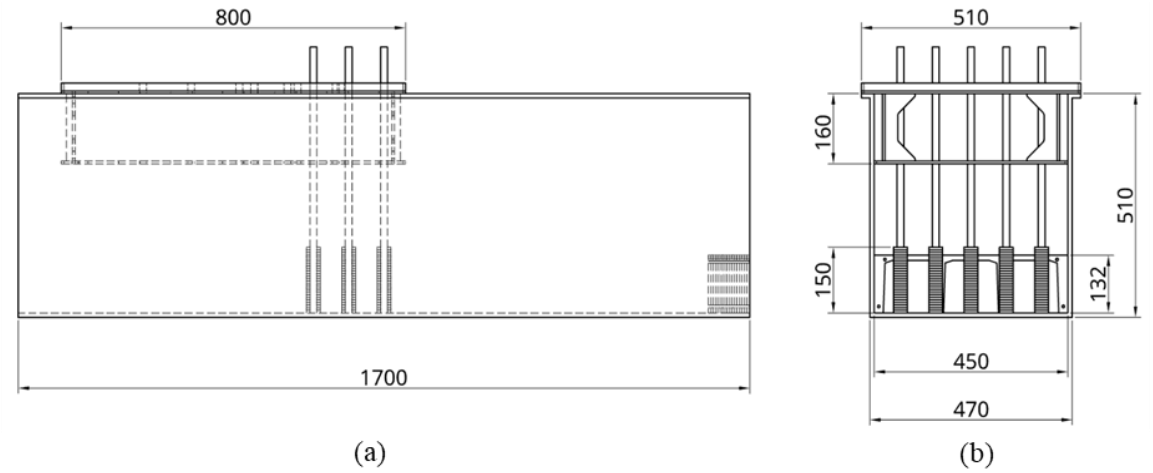

Figure 2: Dimensions of the (a) side view and (b) front view of the model pier rig

To avoid overestimating accumulation associated with using uniform debris material in testing (Panici and De Almeida, 2018), a non-uniform debris mixture of various shapes and lengths, including plastic bags to reflect debris common in developing regions, was used in line with Lyn et al. (2003). A total of 200 pieces of mixed debris was used in the experiments. Water levels were recorded at four locations before and after debris release. A baseline test without piers established culvert behaviour under uncontrolled accumulation. For all other tests, debris was released over two minutes from 4.15 m upstream of the culvert and the water level was measured at specified locations upstream of the culvert. Figure 3 shows the positioning of the four water level measuring points used in the tests, with the pier rig being placed 1.2 m upstream of the culvert. After each run, debris retained at the piers, retained at the culvert, and passing downstream were counted.

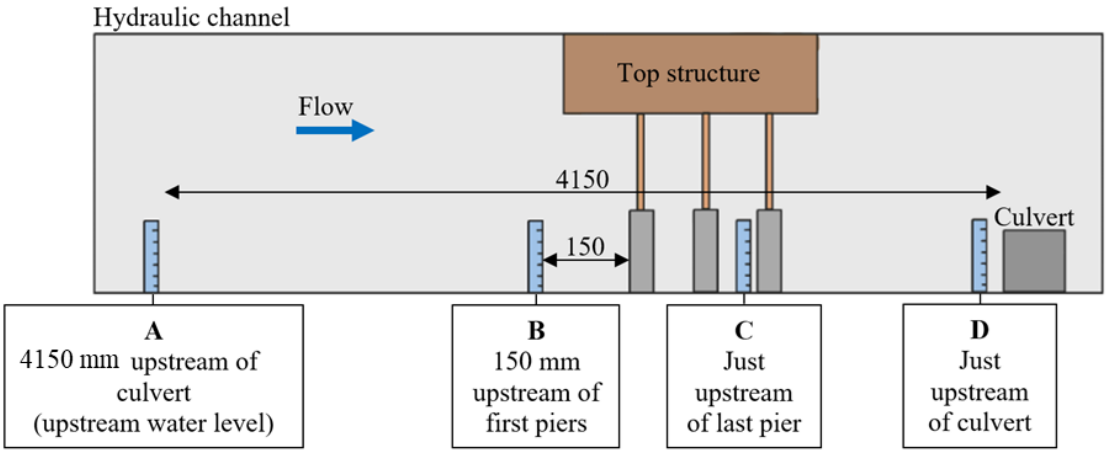

Figure 3: Position of water-level measuring points in the model

Three V-shape angles (30°, 60°, 90°) were tested with apex directions both upstream and downstream, across four pier shapes: circular, square, upward (apex facing upstream) teardrop, and

downward (apex facing downstream) teardrop. Each configuration was tested in triplicate. The most effective configuration was defined as retaining the most debris at the piers, for the lowest backwater accumulation with minimal culvert blockage. The debris retention was calculated as a percentage of the total amount of debris fed during a single test that was caught at the piers. The backwater rise was measured as the change in backwater height after debris is added into the flume. Hydraulic blockage was calculated as a percentage using Eq. (1):

$$Hydraulic\ blockage\ (\%) = \frac{H_{blocked} - H_{unblocked}}{H_{blocked}}\ x\ 100 \quad (1)$$

The debris retention, backwater accumulation and hydraulic blockage result data were plotted and visually analyzed to determine trends in the data. Multiple linear regression (MLR) analyses were then conducted in RStudio, to determine the significance of the influence of the predictors (pier angle, pier shape, V-apex direction) on the responses (debris retention, backwater rise, hydraulic blockage). All predictors were considered to be categorical, and a 95 % confidence interval was used in the MLR, therefore any predictor with a p-value ≤ 0.05 was deemed as significant. Lastly, a multi-objective trade-off analysis was also done in RStudio to determine the optimal pier structure based on the main objectives of minimizing hydraulic blockage and reducing backwater rise, with the secondary objective of maximizing debris retention at the piers. The data for each objective was normalized (since the units of each objective were not the same) according to Eq. (2). A weighted sum approach was then used to calculate a trade-off score for the tests done (see Eq. (3)), and the configurations with the highest trade-off score were chosen to have optimal performance. H_{norm}, B_{norm} and D_{norm} represent the normalized hydraulic blockage (%), backwater rise (mm) and debris retention (%) respectively. A sensitivity analysis was done on weightings w_1, w_2 and w_3 using 500 iterations with randomly generated weightings in RStudio, to ensure that the chosen optimal configuration performed consistently well.

$$Data_{norm} = \frac{Data - Data_{min}}{Data_{max} - Data_{min}} \quad (2)$$

$$Trade - off\ Score = w_1(1 - H_{norm}) + w_2(1 - B_{norm}) + w_3(D_{norm}) \quad (3)$$

3 RESULTS AND DISCUSSION

3.1 Debris retention

The average results of the percentage of debris retained at the piers for each layout angle and pier shape are shown in the bar charts of Figure 4. The bar charts generally exhibit a slight decrease in the debris retention at the piers as the pier layout angle becomes wider. The MLR showed that debris retention decreased slightly (but not significantly) from 30° to 60° ($p = 0.20 > 0.05$) and decreased significantly at 90° ($p = 0.00045$). The pier shape demonstrated a very slight decrease in the debris retention as the shaped changed from circular and square to teardrop shaped for the V-apex facing downstream. The pier shape did not exhibit consistent trends in the debris retention at the piers for the V-apex facing upstream, however the circular pier shape resulted in the least debris retention at the piers compared to the other shapes. From the MLR, square piers significantly increased debris retention ($p = 0.015$), however the upward ($p = 0.12$) and downward teardrop ($p = 0.062$) showed weak, non-significant increases in the debris retention, compared to the circular piers. There was also no distinct trend observed in debris retention when changing the V-apex from upstream to downstream-facing. The MLR showed that changing the V-apex direction had no significant effect ($p = 0.46$).

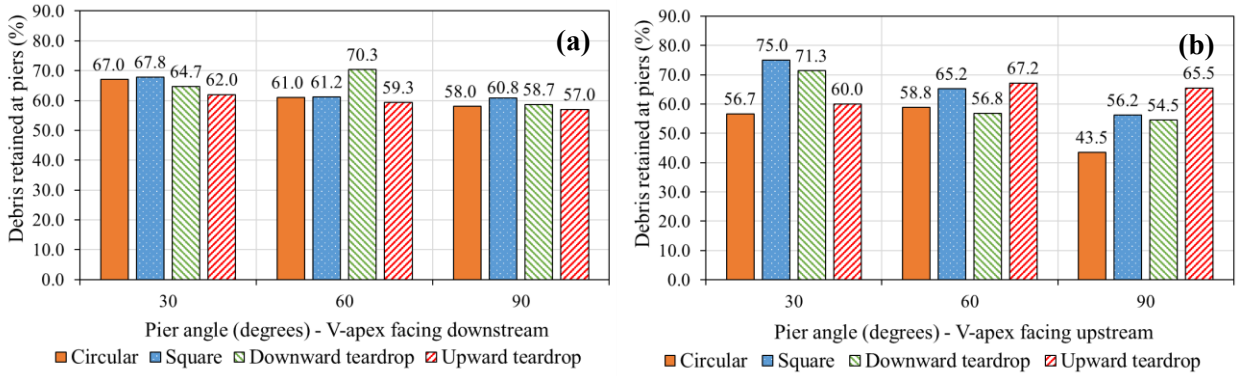

Figure 4: Bar charts of average debris retention for V-apex (a) downstream and (b) downstream

3.2 Backwater accumulation

The average results of the backwater rise at the piers for each layout angle and pier shape are shown in the bar charts of Figure 5. From the charts, there is a distinct decrease in the backwater rise across all pier shapes as the pier layout angle becomes wider. Therefore, the narrower the pier angle layout, the higher the backwater accumulation at the piers. This is directly related to the debris accumulation at the piers, as it was determined previously that the narrow pier angles allow for greater debris accumulation at the piers, therefore resulting is more blockage at the piers and higher backwater. The MLR showed that the backwater accumulation decreased significantly with increasing pier angle, with both 60° and 90° having $p < 0.001$, and 90° producing the largest decrease. Pier shape did not seem to consistently influence the backwater rise, seen by the fluctuating trends in the backwater rise between the pier shapes.

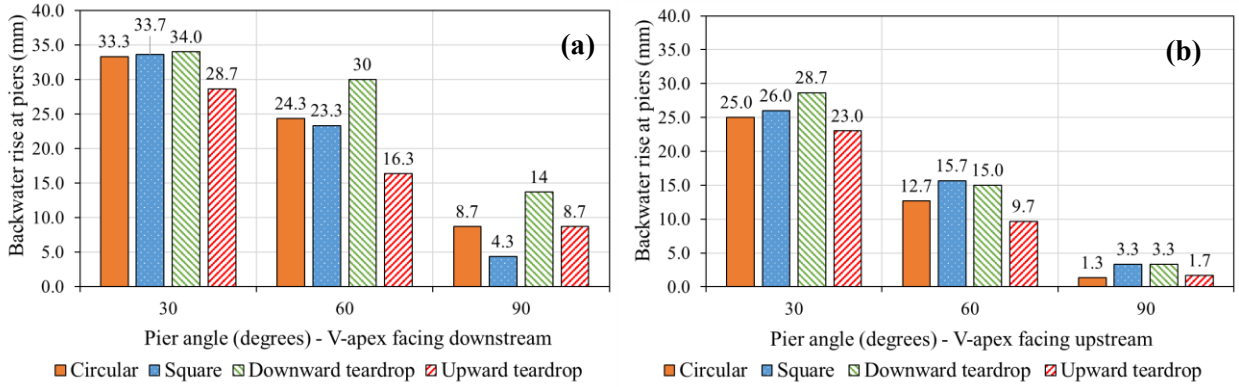

Figure 5: Bar charts of average backwater for V-apex (a) downstream and (b) downstream

The upward teardrop pier shape was generally seen to have the lowest backwater accumulation, and the downward teardrop the highest backwater accumulation. From the MLR, square piers showed no significant effect ($p = 0.92$), while the upward teardrop ($p = 0.088$) and downward teardrop ($p = 0.058$) showed weak, non-significant decrease and increase to the backwater accumulation respectively, compared to the circular piers. The backwater accumulations for the pier configurations with the V-apex facing downstream were higher than those with the V-apex facing upstream. From the MLR, the V-apex facing downstream significantly increases backwater accumulation ($p < 0.001$) compared to the V-apex facing upstream. Although changing the V-apex direction had no significant effect on the amount of debris accumulated at the piers, the placement of where the debris was caught in-channel influenced the backwater accumulation. When the apex faced downstream, it allowed the debris to get caught in the

middle of the channel between the arms of the V, causing significantly more backwater rise opposed to when the apex faced downstream and more debris tended to be retained on the sides of the channel.

3.3 Hydraulic Blockage

The averaged results of the percentage hydraulic blockage at the culvert for each layout angle and pier shape are shown in the bar charts of Figure 6. Baseline tests resulted in an average of 18.4% hydraulic blockage at the culvert. Compared to the baseline, the average hydraulic blockage with the inclusion of pier structures ranged from 0% - 10.3% across all tests done. This demonstrates that even the worst performing pier configuration (upward teardrop, 30° pier angle with V-apex facing upstream) allowed for a 44% decrease in the hydraulic blockage, showing the effectiveness of these pier structures placed upstream of culvert. Across the pier angle, it can be seen that the hydraulic blockage decreases as the angle becomes wider. The MLR showed a slight (non-significant) decrease in hydraulic blockage from 30° to 60° ($p = 0.20$) and a significant decrease at 90° ($p = 0.0082$). Wallerstein et al. (1997) based the optimal pier structure on its ability to retain the most debris for minimal backwater. Therefore, it was intuitively assumed better debris retention at the piers results in less culvert blockage. In this case, although more debris was retained at the piers for narrower pier layout angles, the wider angles resulted in better orientation of debris to pass through the culvert openings and flow further downstream, therefore resulting in lower hydraulic blockage at the culvert.

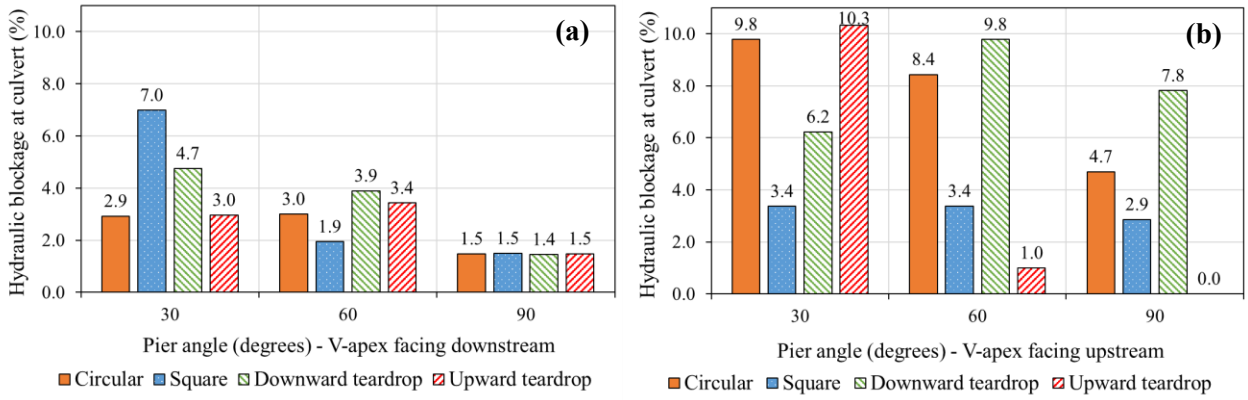

Figure 6: Bar charts of average hydraulic blockage for V-apex (a) downstream and (b) downstream

The circular and downward teardrop piers had greater hydraulic blockage compared to the square piers, however the pier shape generally did not exhibit any distinct trends in the hydraulic blockage. The MLR confirmed that all pier shapes showed small, non-significant reductions in blockage ($p > 0.1$). The configurations with the V-apex facing downstream tended to have smaller hydraulic blockages at the culvert compared to the upstream-facing V-apex, confirmed by the MLR which showed the V-apex facing downstream to significantly reduce hydraulic blockage ($p = 0.0083$), compared to the upstream V-apex.

3.4 Multi-Objective trade-off analysis

Although optimal pier structures were recommended based on their ability to retain the most debris for minimal backwater (Wallerstein et al., 1997), it has been shown in this study that increasing the debris retention at the piers does not necessarily decrease the debris accumulations at the culvert. Therefore, a three-way trade-off between the hydraulic blockage, backwater rise, and debris retention at the piers was done instead to determine the optimal pier configuration. Hydraulic blockage was prioritized and given a weighting $w_1 = 0.5$, while backwater rise had $w_2 = 0.3$ and debris retention a weighting of $w_3 = 0.2$.

Table 1 gives the results of the trade-off score and weighting sensitivity analysis done in RStudio. Based on the chosen weightings, the upward teardrop pier shape with the V-apex facing upstream for 90º and 60º pier angles performed the best, with trade-off scores of 0.937 and 0.826 respectively. Additionally, 90º angles with the V-apex facing downstream also performed well, demonstrating that the 90º angle offers the best trade-off between hydraulic blockage, backwater rise and debris retention. The sensitivity analysis revealed that the top three performing pier configurations for the chosen weighting remain in the top 5 for nearly 100 % of the 500 iterations run with varying weightings. Therefore, 90º and 60º pier angles with upward teardrop pier shapes and the V-apex facing upward are recommended as the optimal pier structures, due to their superior trade-off performance, as well as their stability across weighting scenarios. Additionally, since the change in pier shape showed weak influence on the pier performance, a general pier angle recommendation of 90º pier angles, with any pier shape, and the V-apex facing upstream or downstream is considered optimal.

Table 1: Results of trade-off analysis and sensitivity analysis of the top 5 pier configurations

Pier angle (º)	Pier shape	V-apex	Trade-off score	Top 5 frequency (%)
90	Upward teardrop	Upstream	0.937	100
60	Upward teardrop	Upstream	0.826	99.8
90	Square	Downstream	0.810	97.2
90	Circle	Downstream	0.753	80.0
90	Upward teardrop	Downstream	0.747	25.2

4 CONCLUSIONS

This study investigated how pier angle, shape, and V-apex orientation influenced the debris retention at piers, backwater accumulation at piers, and culvert hydraulic blockage at culverts. Visual data analyses and multiple linear regression were used to determine the type of influence and significance level.

Debris retention decreased as pier angle became wider, with 90° pier angle showing a significant reduction in debris retention. Square piers increased the debris retention, however other shapes showed generally weak effects, and the V-apex orientation showed no significant influence on retention. Backwater rise also decreased with wider pier angles, with 60° and 90° producing significant reductions compared to 30º. The V-apex facing upstream demonstrated significantly lowered backwater accumulations by diverting debris toward the sides of the channel rather than trapping it in the center. This provides cause for the expansion of the use of debris piers not just for in-channel retention, but potentially diversion of the debris to the sides of the channel and onto sloped channel banks, which would majorly benefit the reduction of backwater accumulation in-channel. Hydraulic blockage at the culvert was substantially reduced by widening the pier angle, with 90° providing the lowest blockage due to improved debris alignment, allowing for clear passage through the culvert. Pier shape had a weak influence on hydraulic blockage, and the downstream-facing V-apex reduced blockage significantly. Notably, higher debris retention at piers did not guarantee lower hydraulic blockage at the culvert, with wider angles (particularly 90°) resulting in lower culvert hydraulic blockage, even while exhibiting lower debris retention at the piers. Further testing with angles wider than 90° is recommended to determine whether favorable debris alignment continues toward 180°.

A multi-objective trade-off analysis minimizing hydraulic blockage and backwater and maximizing debris retention found that 90° and 60° pier angles with upward teardrop piers and the apex facing upstream were optimal, with 90° pier angles consistently offering the best combined performance. Sensitivity analyses confirmed these configurations were robust across variations in the weightings used. Overall, 90° pier angles with either V-apex orientation are recommended as the optimal pier arrangement, since pier shape generally had non-significant effects.

The results of this study provide a starting point for formalized debris pier testing in South Africa and similarly developing countries. Like all debris testing, there is an inherent degree of randomness associated in its hydraulic behaviour. However, further experimental testing by expanding the range of currently tested variables, considering other influencing factors (such as flow rate, channel dimensions, culvert dimensions, debris transport mechanism, sediment etc.,) and increasing the scale of the model will allow for the development of technical design guidelines for the implementation of debris piers upstream of culverts in developing countries and other parts of the world where non-mechanised solutions are the most practical.

5 ACKNOWLEDGEMENTS

Gratitude is expressed to Mr. Jan Ngwenya and Mr. Jordan Mostert from the University of Pretoria for their assistance in the construction of the flume model and instrumentation calibration and repairs.

REFERENCES

Balkham M., Fosbeary C., Kitchen A. and Rickard C. (2010). *Culvert design and operation guide*. CIRIA, Classic house. London.

Blanc J., Wallerstein N.P., Arthur S. and Wright G.B. (2014), April. Analysis of the performance of debris screens at culverts. In *Proceedings of the Institution of Civil Engineers-Water Management* (Vol. 167, No. 4, pp. 219-229). Thomas Telford Ltd.

Bradley J., Richards D. and Bahner, C. (2005). *Debris Control Structures Evaluation and Countermeasures.* U.S. Department of Transportation, Federal Highway Administration. Oregon.

De Cicco P. N., Paris E., Solari L. and Ruiz-Villanueva V. (2020). Bridge pier shape influence on wood accumulation: Outcomes from flume experiments and numerical modelling. *Journal of Flood Risk Management*, *13*(2), p.e12599.

Diehl T. H. and Bryan B. A. (1993). Supply of large woody debris in a stream channel. In *Proceedings of the 1993 National Conference on Hydraulic Engineering. Part 1 (of 2)* (No. pt 1, pp. 1055-1060).

Lange D. and Bezzola G. R. (2006). *Schwemmholz Probleme und Lösungsansätze* (Driftwood problems and solutions). VAW Bulletin 188, Technical University of Zürich. Zürich.

Lyn D. A., Cooper T., Yi Y., Sinha R, and Rao A. R. (2003). *Debris Accumulation at Bridge Crossings: Laboratory and Field Studies.* Indiana Department of Transportation and Federal Highway Administration. West Lafayette.

Mazele O. and Amoah C., (2022). The causes of poor infrastructure management and maintenance in South African municipalities. *Property Management*, *40*(2), pp.192-206.

Miranzadeh A., Keshavarzi A. and Hamidifar H., (2023). Blockage of box-shaped and circular culverts under flood event conditions: a laboratory investigation. *International Journal of River Basin Management*, *21*(4), pp.607-616.

Panici D. and De Almeida G. A. M., (2018). Formation, Growth, and Failure of Debris Jams at Bridge Piers. *Water Resources Research*, *54*(9), pp.6226-6241.

Panici D. and De Almeida G. A. M. (2020). Influence of pier geometry and debris characteristics on wood debris accumulations at bridge piers. *Journal of Hydraulic Engineering*, *146*(6), p.04020041.

Schmocker L. and Hager W.H. (2013). Scale modeling of wooden debris accumulation at a debris rack. *Journal of Hydraulic Engineering*, *139*(8), pp.827-836.

Wallerstein N., Thorne C. R. and Abt S. R. (1997). *Debris Control at Hydraulic Structures*. U.S. Army Research Development & Standardization Group. London.

Web sites:

Web-1: http://www.rocla.co.za/products/rectangular-portal-culverts, consulted April 2025

ICFM 10
Adapting to Global Change:
Innovative Approaches to Flood Management and Resilience
May 20-22, 2026 | Western University, London, Ontario, Canada

Beyond Room for the River: Towards a Multifunctional, Climate-Robust, and Resilient Management Strategy in the Netherlands

Ralph M.J. Schielen[1] , Saskia van Vuren[2] and Marco Taal[3]
DG for Public Works and Water Management, Utrecht, The Netherlands, and Delft University of Technology, Delft, The Netherlands[1]
E-mail: ralph.schielen@rws.nl

Staff Deltacommissioner, The Hague, The Netherlands[2]
E-mail: saskia.van.vuren@deltacommissaris.nl

Ministry of Infrastructure and Water Management, The Hague, The Netherlands[3]
E-mail: marco.taal@minienw.nl

ABSTRACT

The Room for the River programme (2007–2018) transformed the Dutch river landscape by increasing flood safety while improving spatial quality, ecology, and landscape value. In a low-lying and densely populated country such as the Netherlands, however, river management is a continuous task rather than a one-off effort. Ongoing investments are required to maintain embankments, floodplains, and navigation channels, while adapting to long-term challenges including climate change, population growth, and land-use change. For this reason, river management is not considered complete, and the follow-up programme Room for the River 2.0 (RftR 2.0) has been initiated.

Compared to its predecessor, RftR 2.0 addresses both persistent and emerging challenges. Flood safety and spatial quality remain central, but increasing riverbed erosion, freshwater scarcity, and tensions between navigation, nature development, and climate adaptation have become more prominent. These challenges are intensified by the bifurcating layout of the Rhine, where water and sediment are distributed across multiple branches during both low and high discharges.

This paper examines how these growing and sometimes competing demands can be addressed from a long-term, system-level perspective. Focusing on the Rhine and its branches, we explore pathways towards a multifunctional river system that supports navigation, freshwater supply, and nature development while remaining safe under climate change towards 2100. Also, potential spatial reservations for future river widening are identified.

Recent studies indicate that historical interventions—such as channel straightening, embankment reconstruction, and flow regulation—have pushed the river system out of morphological and hydraulic balance. The delayed system response, combined with climate-driven shifts towards higher winter discharges and prolonged summer low flows, increases risks of floodplain desiccation, freshwater shortages, and navigation problems. Against this background, measures such as side channels and more natural floodplains are explored as promising strategies to restore system balance, enhance ecosystem services, and strengthen climate robustness.

KEYWORDS: flood risk management, climate resilience, river morphology, multifunctional river systems

1 INTRODUCTION

1.1 From High-Water Events to Room for the River

In December 1993 and January 1995, exceptionally high discharges occurred in both the Rhine and Meuse rivers, resulting in some of the highest water levels recorded in the Netherlands in the twentieth century. Although no major dike breaches occurred, these events brought the river system close to its physical limits and exposed the vulnerability of a densely populated, low-lying country that relies heavily on flood protection infrastructure.

The high-water events caused major social disruption. As a precautionary measure, approximately 250,000 people were evacuated from riverine areas along the Rhine and Meuse. The evacuations, extensive media attention, and visible stress on embankments acted as a national wake-up call. They demonstrated that the prevailing strategy of continually raising dikes to accommodate higher design discharges was reaching its societal, spatial, and technical limits.

In the immediate aftermath, emergency reinforcement measures were implemented to restore confidence in the flood protection system. More importantly, however, the events triggered a fundamental rethinking of Dutch river management. Rather than continuing a strategy focused solely on dike reinforcement, a new approach emerged that aimed to increase the discharge capacity of the river system itself. This marked the conceptual starting point of the Room for the River programme.

The core idea of Room for the River was to reduce flood levels by giving rivers more space instead of further confining them. Measures such as floodplain lowering, dike relocation, side-channel construction, and the removal of hydraulic obstacles were combined to increase conveyance capacity during high flows. At the same time, the programme explicitly introduced spatial quality as an objective, aiming to enhance landscape values, ecological conditions, and the integration of river areas with their surroundings. This approach was often described as reconnecting with the river's 'DNA'.

Parallel to the implementation of Room for the River (2007–2018), Dutch flood risk management evolved towards a more risk-based approach, influenced by international events such as Hurricane Katrina. This shift placed greater emphasis on consequences, system robustness, and societal resilience. The process culminated in the Dutch Delta Programme, which provides a long-term framework to keep the Netherlands safe and liveable towards 2050 and beyond.

From the outset, Room for the River was not intended as a final endpoint. Long-term visions already acknowledged that ongoing climate change and increasing spatial claims—such as for nature development, navigation, recreation, cultural heritage, and urban growth—would eventually exhaust the available space within the river system. This insight necessitated an integrated, system-level analysis of future river management.

This analysis was elaborated within the Integrated River Management programme (Ministry of Infrastructure and Water Management, 2025).

1.2 New challenges ahead

Spatial pressure in river areas has increased rapidly over recent decades. Whereas development around 1900 was limited, many former floodplains have since been transformed into residential areas, business parks, and infrastructure corridors. Large investments in roads, railways, and bridges have locally narrowed the winter bed, creating hydraulic bottlenecks at various locations.

In the future, housing, economic activity, and mobility demands in river areas are expected to continue to grow, particularly around large and medium-sized cities. These urban centres are also the locations where major infrastructure corridors intersect the river system. Together, these developments intensify land use and reduce the space available for river widening or other system improvements. Bottlenecks that limit the safe conveyance of high discharges are already apparent near urban areas. In historic city centres and villages, further dike raising will often be infeasible without major impacts on existing buildings. Cultural-historical values, such as characteristic riverfronts, visual relationships

between inner and outer dikes, and flood defences as landscape elements—further constrain adaptation options. Three developments negatively affect the functioning of the river system:

1. More frequent occurrence of high discharges;
2. More frequent occurrence of low discharges;
3. Continued erosion of the main channel bed, largely resulting from interventions carried out up to 150 years ago.

(1): The increasing frequency of high water levels intensifies the challenge of safely conveying river discharges to the sea. Higher and more frequent floods also affect the river system itself: hydraulic bottlenecks cause additional backwater effects and increased flow velocities, which can locally accelerate erosion. This increases the demands on flood risk management and may generate new challenges beyond the current Flood Protection Programme (HWBP, Web-1). Measures to accommodate higher discharges invariably require additional space, which is becoming increasingly scarce.

(2): Projections indicate that low-flow periods may occur more frequently and become more extreme, leading to increased problems related to low groundwater tables. It also leads to an increased disconnection between main channel and floodplains, which reduces the inundation of the floodplains. This is necessary for a natural dynamical situation, with creating opportunities for nature and a rich biodiversity. Economic losses in agriculture and inland navigation during low-flow periods are substantial.

(3): Riverbed erosion in free-flowing rivers is a growing concern because of its wide-ranging impacts on river functions and ecological values (Ylla Arbos et al. 2020). The effects are most severe during droughts, affecting not only the river and its floodplains but also surrounding regions far beyond the river corridor (figure 1). Inland navigation becomes problematic during low flow conditions, due to limited navigational depth. The fact that at certain locations there are non-erodible (man-made or natural) sections in the riverbed exacerbates the problems for navigation, as these protrude with respect to the erodible river bed and become an obstacle for ships.

Figure 1: Schematic of the river's main channel and flood plains. In red, the challenges are denoted: river bed erosion, disconnection of main channel and flood plains, and lowering ground water tables.

In addition, the partitioning of river discharges across the Netherlands plays a crucial role under both high- and low-flow conditions (Chowdhury et al., 2023). Ongoing erosion in the Waal branch gradually alters this distribution: at low discharges, an increasing share of water remains in the Waal, reducing flows towards Lake IJssel, the Netherlands' primary freshwater reservoir. During extreme high discharges, changes in the distribution increase hydraulic loads on some river branches at the expense of others. Restoring a balanced discharge distribution therefore requires careful consideration of costs and benefits at the national scale.

In section 2, we describe the ambition and working method of Room for the River 2.0 (Web-2), the follow-up of Room for the River. Section 3 presents the underlying concepts and solution directions, while Section 4 discusses the first results and their implications and we conclude in section 5.

2 AMBITION AND WORKING METHOD OF ROOM FOR THE RIVER 2.0 (RFTR2.0)

The ambition of RftR 2.0 is "a future-proof river system that functions well as an integrated system and can be used in multiple ways." This refers to a river system that, as far as possible, is self-regulating through natural processes and possesses the system characteristics required to support its various functions effectively. RftR 2.0 focuses on the following five river functions:

1. Water conveyance (flood protection);
2. Freshwater availability and drinking water supply;
3. Nature and ecological water quality;
4. Navigability;
5. Regional economic development and spatial quality, including agriculture, recreation, and mineral extraction.

In a preliminary study (Ministry of Infrastructure and Water Management, April 2025), two overarching policy goals were formulated for the river area. Within the RftR 2.0 programme, these goals are elaborated into policy choices along two main lines, one on the riverbed, and one the discharge capacity and room for the river.

Riverbed and sediment management: A sufficiently stable and manageable summer-bed level that contributes to the restoration of natural river dynamics and ensures good navigability and an adequate distribution of water across the Netherlands during low discharges.

Discharge capacity and room for the river: Sufficient capacity to safely accommodate the higher river discharges expected over the course of this century, while also enabling spatial developments, nature development, subsurface considerations, and other societal tasks.

The challenges associated with the different river functions cannot be addressed in isolation. The river area is therefore approached as a coherent system, and the tasks related to the various functions are addressed in conjunction. The two policy choices act as the main system controls for designing a river system that optimally supports all five river functions (figure 2).

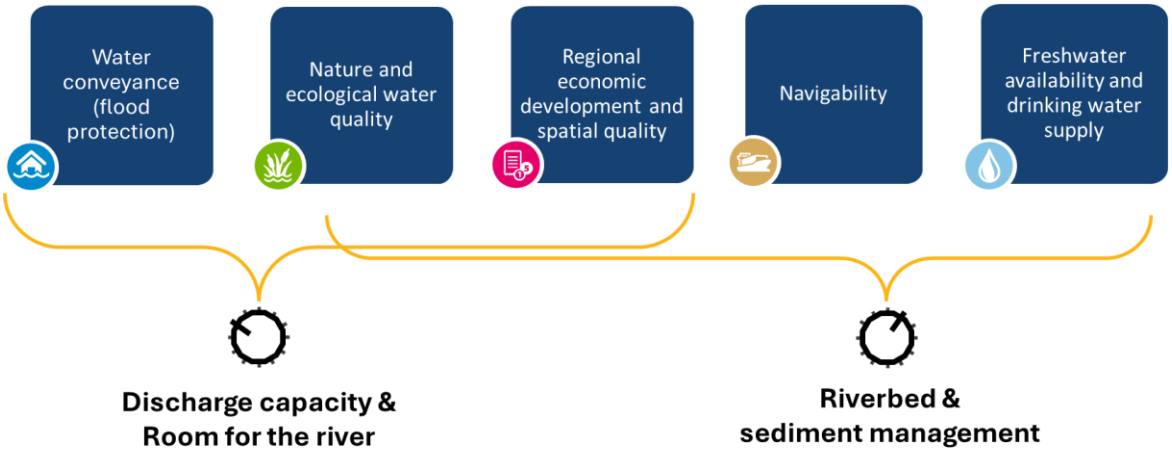

Figure 2: The two policy choices in relation to the five river functions

To keep this integrated approach manageable, RftR 2.0 adopts a clear division of roles with other programmes. Parties work within RftR 2.0 on system-level design questions, while sectoral objectives—such as freshwater supply, nature restoration, navigation, and flood protection—remain the responsibility of dedicated sectoral programmes. There is no transfer of tasks or decision-making powers.

Decisions on sectoral objectives are taken within the administrative platforms of the relevant programmes, while impacts on other river functions are explicitly considered by addressing these

interactions early in the RftR 2.0 context. Where necessary, RftR 2.0 may place on the agenda the need to reconsider sectoral objectives if they prove mutually incompatible or cannot be achieved in a timely manner.

3 UNDERLYING CONCEPTS AND SOLUTIONS

3.1 Coherence of policy choices in the main water system of the Netherlands

The policy choices prepared within RftR 2.0 also affect other, interrelated choices in the main water system of the Netherlands. Coherence among these decisions is achieved through the process leading to a national Delta Decision on Large Rivers and Deltas which will be taken in the context of the national Delta Programme.

The Delta Decision addresses strategic choices for the design of the major rivers and deltas in the Rhine–Meuse system, including the Meuse, the Rhine branches, Lake IJssel, the lower river area up to the river mouths at sea, and the Southwest Delta. The Decision is periodically reassessed based on updated climate and Delta Scenarios, drawing on input from multiple national and regional programmes.

Increasing system degradation and the accumulation of water-related challenges mean that tasks in different regions are becoming more interdependent. This requires coherent decision-making.

Four sequential steps structure the preparation of the Delta Decision:

1. **Towards a low-water-resilient delta**
   Preparing the main water system for periods of low and insufficient water availability, in parallel with initial adaptations in land use.

2. **More space for water in a busy delta**
   Creating additional room in and along rivers in a timely manner to anticipate higher water levels in rivers and tributaries.

3. **Sea in sight!**
   Aligning the design of the main water system and land use with the long-term impacts of sea level rise.

4. **Leap in scale along the chosen pathway**
   Implementing further measures that build on and scale up previously made strategic choices

Each step consists of interrelated components that must be addressed jointly.

3.2 Sequence of policy choices

Chapter 2 describes how RftR 2.0 relates to the five river functions and how the two policy choices **'Riverbed and sediment management'** and **'Discharge capacity and room for the river'**—act as two key system controls for designing a river system that optimally supports these functions. These two choices are strongly interrelated, and their effects influence one another.

It is therefore essential to consider alternatives and measures for both policy choices in conjunction, while at the same time keeping the process manageable. To avoid an excessive number of combinations—many of which would be neither logical nor relevant—the **RftR 2.0** programme applies a deliberate sequencing of policy choices to reduce complexity. This sequencing also reflects the urgency of the underlying problems and the alignment with the recalibration of the Delta Decision on Large Rivers and Deltas.

The RftR 2.0 programme follows the sequence below:

1. **Discharge distribution at low flows**, which is essential for elaborating riverbed solutions (see points 2).

2. **Stabilisation and, where feasible, elevation of the riverbed** to a level that effectively addresses existing problems.
3. **Discharge distribution at high flows**, which informs the elaboration of branch-specific solutions (see point 4).
4. **Dimensions of the floodplains (discharge capacity)**, including the combination of functions and the preferred order of measures.

This order is crucial, as the choices made in steps 1 to 3 largely determine the scope and scale of the task in step 4, concerning discharge capacity.

In practical terms, this means that the policy choice **'Riverbed and sediment management'** (steps 1 and 2) is guiding for the policy choice **'Discharge capacity and room for the river'** (steps 3 and 4). Interactions and synergies between both solution pathways are explicitly taken into account when substantiating the overall solution strategies.

3.3 Policy choice Riverbed

To prevent continued erosion of the summer bed, the balance between sediment supply and sediment removal must be restored. When sediment input and output are in equilibrium, the riverbed remains stable and there is no net aggradation or degradation.

Two principal solution directions have therefore been explored to restore this balance:

1. **Sediment nourishment**
   Increasing sediment supply by adding sediment to the river system, with the aim of annually compensating for the volume lost through erosion.
2. **Widening**
   Addressing the root cause of riverbed erosion by widening the riverbed. Increased cross-sectional width reduces flow velocities, thereby decreasing sediment transport capacity and limiting erosion.

3.4 Policy choice Discharge capacity and room for the river

To ensure that measures for safe discharge remain feasible in the long term, additional space must be reserved along rivers, both between the main embankments and at the land-side of the embankments. These spatial reservations provide planning certainty and contribute to a safe and robust river system under future conditions. At the same time, they create opportunities to restore natural river dynamics. A river system with sufficient space and connectivity is essential for resilient and climate-adaptive riverine ecosystems.

Within RftR 2.0, the areas required at the land-side of the embankments to guarantee long-term flood risk management have been identified. This assessment is complex, as future discharge projections span a wide range due to uncertainties in climate change trajectories and spatial developments in upstream river basins. Furthermore, strategic choices regarding discharge distribution across the Rhine branches and the selection of an open or closed delta system to address sea level rise also influence outcomes.

To account for these uncertainties, both a high and a moderate climate scenario were considered, in combination with two alternative discharge distributions across the Rhine branches. For each scenario, bottlenecks were identified where flood safety cannot be ensured through dike reinforcement or river widening outside the dikes alone. For these locations, scenario-specific packages of measures were developed, comprising combinations of dike reinforcement and river widening both between the embankments and at the land-side of then embankments. The concept of river widening is explored through the implementation of a system of multiple side channels located within the floodplains, combined with a narrowing of the main channel. The side channels are equipped with a weir, leading to increased water levels during low discharges. During high discharges, the side channels increase the

discharge capacity, leading not only to lower flood water levels, but also to less erosion of the main channel.

For each package, impacts and indicative costs were assessed, allowing for comparison across scenarios. Potential synergies with nature development and other spatial objectives were also examined. On this basis, the implications of different discharge distribution choices across the Rhine branches were mapped.

At this stage, the administrative choices prepared within RftR 2.0 are limited to spatial reservations at the land-side of the embankments for potential future river widening. These choices are informed by considerations such as the time horizon for which flood safety must be guaranteed, the degree of uncertainty to be accommodated, and the distribution of impacts across regions.

4 FIRST RESULTS

The overall picture emerging from the studies confirms earlier conclusions: by the end of this century, opportunities to further increase the resilience of the river system will be limited, although negative climate impacts can still be mitigated. It will no longer be possible to fully accommodate all river functions simultaneously, making difficult trade-offs unavoidable. These trade-offs concern both the degree to which future climate developments are anticipated and the extent to which hydraulic, morphological, and ecological bottlenecks—including the declining possibilities for dike reinforcement—are addressed.

Not all of these choices fall within the scope of the RftR 2.0 programme. Responsibilities for freshwater availability, navigation, and nature (restoration) remain with the relevant sectoral programmes. Within this framework, RftR 2.0 focuses on assessing how adaptations to the geometry and layout of the Meuse and Rhine branches can continue to support sectoral objectives. The analyses show that under continued climate change, freshwater availability limits will be exceeded: in all scenarios, water demand cannot always be met. Similar constraints apply to navigability. Measures to counteract riverbed erosion cannot fully resolve these issues but can substantially reduce their severity.

After 2050, the current strategy of meeting flood protection standards mainly through dike reinforcement reaches its limits in terms of both discharge capacity and space. River widening outside the dikes will therefore be required in all scenarios to compensate for limited dike-raising options and existing bottlenecks, ensuring safe conveyance of river discharges to the sea.

Under a high climate scenario towards 2100, river widening inside the dikes also becomes unavoidable. Part of this task results from the assumption that Germany will likewise reinforce its dikes. Selecting a multi-channel system on the Waal as a riverbed erosion measure would also significantly increase discharge capacity there and relieve pressure on the IJssel.

For nature development, two minimum conditions were applied: system conditions must not deteriorate, and remaining statutory obligations under existing nature restoration programmes must be met. In addition, opportunities to contribute to UN and EU Biodiversity Strategy ambitions were explored, focusing not only on increasing natural areas but particularly on enhancing hydro-morphodynamics and floodplain connectivity.

The results show that many measures aimed at increasing discharge capacity can simultaneously contribute to nature objectives, revealing substantial synergy potential outside the dikes. Similar opportunities exist inside the dikes, where it was assumed that at least 25% of river widening would be nature-based.

Finally, solutions to riverbed erosion are partly determined by their ability to reduce navigation bottlenecks and improve low-flow water distribution, supporting freshwater availability and limiting salinisation. For the Waal, sediment replenishment and a multi-channel system were assessed. While both can halt further erosion, only the multi-channel system contributes to improving freshwater distribution and reducing navigation bottlenecks. Even so, it cannot fully eliminate these challenges.

Overall, the analyses confirm that under continued climate change, structural limits will be reached: freshwater demand and navigability cannot always be guaranteed. System-level interventions can mitigate these impacts, but they cannot remove them entirely.

5 CONCLUSION

The analyses presented in this paper show that Dutch river management is entering a phase in which structural limits become increasingly apparent. Under continued climate change, not all river functions can be fully accommodated simultaneously, making explicit and timely trade-offs unavoidable. The Room for the River 2.0 (RftR 2.0) programme provides a system-level framework to address these trade-offs by linking riverbed management and discharge capacity to multiple societal and ecological functions. Results indicate that river widening outside the dikes is unavoidable after mid-century, while widening inside the dikes becomes necessary under high climate scenarios. Measures targeting riverbed erosion, particularly multi-channel systems, can substantially reduce impacts on freshwater availability and navigation, although they cannot fully eliminate constraints. Importantly, many safety-driven measures offer strong synergies with nature development, especially through enhanced hydro-morphodynamics and floodplain connectivity. Overall, RftR 2.0 demonstrates that a coherent, long-term, and multifunctional system approach is essential to maintain a safe, resilient, and usable river system under future climate conditions.

REFERENCES

Chowdhury, M.K., Blom, A., Ylla Arbós, C., Verbeek, M.C., Schropp, M.H.I., and Schielen, R.M.J. (2023) Semicentennial Response of a Bifurcation Region in an Engineered River to Peak Flows and Human Interventions, Water Resources Research 59 (4), https://doi.org/10.1029/2022WR032741

Ministry of Infrastructure and Water Management (2025). Towards a future-proof river zone, Integrated River Management Programme, Start of the Programme, Room for the River 2.0, retrieved from https://www.platformparticipatie.nl/irm/documenten-programma-irm/handlerdownloadfiles.ashx?idnv=3032216

Ylla Arbós, C., Blom, A., Viparelli, E., Reneerkens, M., Frings, R.M. and Schielen, R.M.J. (2020), River Response to Anthropogenic Modification: Channel Steepening and Gravel Front Fading in an Incising River, Geoph. Res. Letters 48 (4), https://doi.org/10.1029/2020GL091338

Web-sites:
Web-1: https://www.hwbp.nl/
Web-2: https://www.ruimtevoorderivier.nl/

Chapter 3 - Urban flooding and infrastructure systems

3.3 Flood impacts on infrastructure and critical services, including cascading failures

ICFM 10
Adapting to Global Change:
Innovative Approaches to Flood Management and Resilience
May 20-22, 2026 | Western University, London, Ontario, Canada

Navigating Tracks of Resilience: Integrating Climate Change Flood Risks into Rail Transit Infrastructure Design, Asset Management, and Operations & Maintenance

Quentin Chiotti
Department of Environmental Science, University of Toronto Scarborough, Toronto, ON, Canada
E-mail: drq.chiotti@utoronto.ca

ABSTRACT

This paper describes how to navigate through the application of a climate risk assessment throughout the lifecycle of rail and transit infrastructure, addressing design standards, asset management, and operations and maintenance practices. With increasing climate change, a proactive, inclusive, transparent, and evidence-based approach towards managing flood-related risks can help safeguard infrastructure assets, ensure reliability, and meet expectations for performance, revenue, and service delivery. The approach addresses vulnerabilities, takes into account current and planned measures that shape adaptive capacity, and considers various resilience options and strategies that are aimed to reduce risk to projected changes in acute and chronic climate conditions. By embedding climate risk considerations in procurement and throughout asset lifecycle, this approach supports sustainable transit development and enhances the sector's ability to withstand future physical climate hazards.

Drawing from select examples in Canada and Australia, this paper illustrates how to navigate through an assessment using the PIEVC Protocol, in relation to managing flood risk for legacy assets and new infrastructure projects for rail and transit. The discussion further outlines four key challenges for effective flood risk management that are often encountered in the climate risk assessment process: (i) using the right climate data, that is informed by historical experience and accepts the wide range of uncertainty in climate change projections; (ii) understanding the complexities of impacts, including interactions between natural and built systems; (iii) consideration of costs and benefits associated with adaptation options; and (iv) the adoption of adaptation expenditure pathways that cut across design, asset management, and operations and maintenance activities. The discussion highlights that managing future fluvial/riverine and pluvial/overland flood risks with climate change is a complex process, potentially involving cumulative, compounding, and cascading impacts; that it requires consideration of interdependencies with ancillary systems; and requires the engagement of internal and external multistakeholders from across disciplines.

KEYWORDS: climate change, flood risk management, adaptation pathways

1 INTRODUCTION

Extreme weather and the direct impacts of climate change continue to be cited among the top global risks (Elsner et al., 2025). Flooding is widely considered to be the most damaging of climate hazards to the condition of public infrastructure assets, and the services dependent upon them. This also applies to rail and transit infrastructure across Canada, and by extension will become an even bigger and more costly concern as the climate changes and heavy rainfall, sea level rise, and flood risk increases (Ness et al., 2021). Builders, owners and operators of rail and transit systems and the infrastructure that supports the delivery of freight and passenger services face a daunting challenge of designing and constructing new infrastructure and/or managing legacy assets to be climate resilient to flood risk due to acute and chronic changes in climate, such as heavy rainfall events and slow changes in watersheds and sea level, respectively.

Operations and maintenance functions must also be enhanced in response to increasing flood risks, as well as emergency management and business continuity planning.

Managing future flood risks can be supported by the application of climate change risk assessment tools, in order to identify medium and high risks to climate hazards, followed by the identification and implementation of measures that reduce vulnerability and enhance resilience and adaptive capacity. While various frameworks exist to undertake such an analysis (e.g., ISO 31000 and the suite of ISO 1409X standards), the Public Infrastructure Engineering Vulnerability Committee (PIEVC) Protocol (ICLR, 2016a and 2016b) is the tool that is widely used in Canada and has been required through Climate Lens in order to receive Federal funding for new public infrastructure projects since 2018 (Infrastructure Canada, 2023). The PIEVC Protocol provides a useful framework for assessing climate-related risks, and it may be helpful to users and practitioners to understand the process based on real world examples, appreciate some of the potential challenges that they may encounter, and consider important lessons learned that will help maximize the outcomes of their efforts. At minimum, a climate risk assessment is a "check the box" exercise that identifies medium and high risks in order to meet regulatory requirements, but at maximum it presents an opportunity and a mechanism to educate, inform, and push decision makers to consider how climate risk and adaptation cuts across the entire procurement process, and implement a pathway to enhance adaptive capacity and resilience in infrastructure assets and the services that they provide.

A climate risk assessment approach has the potential to provide useful insights into flood risks for the design, management and operations of rail and transit infrastructure, and as such needs to be viewed as just one step along the long journey ahead to take actions that reduce the vulnerability of assets, enhance adaptive capacity, and ensures more reliable service delivery in face of climate change. Given the extent of legacy assets, the challenges for the design of new infrastructure projects, and the uncertainty and complexities of climate change, risk management must be seen as a process that faces an uphill battle managing assets and delivering safe and reliable service as the climate changes and more frequent and intense rainfall and flood events occur. This paper emphasizes the urgency to take action on adaptation – the process of adjustment to actual or expected climate and its effects, in order to moderate or avoid harm or exploit beneficial opportunities, and resilience – the capacity of interconnected social, economic and ecological systems to cope with a hazardous event, trend or disturbance, responding or reorganizing in ways that maintain their essential function, identity and structure (IPCC, 2014).

The discussion begins by providing a brief background and science-based context regarding the urgency and necessity of adaptation. This is followed by an outline of the six steps that are typically taken during a climate risk assessment process using the PIEVC Protocol that includes adaptation measures, through the lens of transit and rail infrastructure. The discussion then highlights four challenges that are typically encountered during the climate risk process that warrants close attention pertaining to managing flood risk: (i) the importance of using the right climate data; (ii) understanding the complexities of impacts; (iii) the emergence of cost and benefit considerations associated with the selection and implementation of adaptation options; and (iv) the adoption of adaptation expenditure pathways that cut across design, asset management, and operations and maintenance functions.

2 BACKGROUND AND CONTEXT

In 2024 the annual global surface mean temperature momentarily exceeded 1.5°C above the pre-industrial baseline period (1850-1900), driven by a continuing increase in CO_2 concentration levels in the atmosphere. Recent measurements indicate that levels at the Mauna Loa Observatory in Hawaii have reached 427.49 ppm (as of December, 2025), up from 315.71 ppm when records began in March 1958 (Web-1). Global emissions of greenhouse gases due to fossil fuel combustion and land use changes have increased steadily since the 1950s, and while they reached a new high in 2024, in recent years the rate of growth has been slowing, thanks in part to commitments and actions made by signatories to the Paris Climate Agreement in 2015. These emission reduction commitments, however, will not be sufficient to prevent global mean temperatures from reaching a level that is 2°C above pre-industrial levels by 2050, let alone by the end of this century. Emerging from the recent Conference of the Parties (COP) 30 meetings

held in Belém, Brazil, was the harsh reality that global average temperatures could rise anywhere from an extremely optimistic scenario of +1.5°C to a more likely scenario based on existing policies and actions of +3.3°C by 2100. It has been argued that global efforts to meet Article 2 of the United Nations Framework Convention on Climate Change (UNFCCC) should be given a failing grade, and as a result an urgent call for action on adaptation is needed for public infrastructure assets (Chiotti and Van Vliet, 2024).

In Canada annual mean temperatures have been increasing at twice the global average and are projected to continue to rise faster under future high emissions scenarios. While there are reports that Canada's public infrastructure, transportation included, is at risk to extreme weather and climate change (Ness et al., 2021), insured Catastrophic Losses over the past 40 year have increased substantially, exceeding $9 Billion in 2024 (Web-2). Uninsured losses have been even greater, and this does not take into account the costs associated with service disruptions and reputation incurred by rail and transit providers. Many of the extreme weather events affecting transportation infrastructure have involved heavy rainfall and flooding. However, the actual impacts and associated costs for rail and transit across Canada is not well documented, perhaps reflecting a low level of awareness of climate-related risks, but also due to the scarcity of published studies that assessed these hazards (e.g., see Haghighi et al., 2025). A review of published PIEVC reports indicates an absence of transit related assessments (Web-3), perhaps reflecting issues around confidentiality, liability, political bias, and other factors.

Nonetheless, in recent years there has been a rapid emergence of activities across rail and transit systems and projects towards managing climate change risks, including Metrolinx, Canada's largest regional transit provider (e.g., Metrolinx, 2018). A record heavy rainfall and flood event on July 8th, 2013, followed by a freezing rain/ice storm event in December of that year, prompted senior management at Metrolinx to create a senior advisor position in climate risk and resilience, and publicly commit to develop a corporate climate change adaptation strategy by 2018 (Metrolinx, 2015). This resulted in a climate change risk assessment using the PIEVC Protocol that was applied to a selection of legacy infrastructure assets (AECOM et.al., 2016), of which heavy rainfall and flooding was a prominent hazard of concern. In addition, climate risks via the application of the PIEVC Protocol was included as a requirement outlined in the Project Agreements for multiple new transit projects and was incorporated into both the Metrolinx Sustainability Design Standard DS-05 (Metrolinx, 2021a) and the Climate Change Informed Data Standard (Metrolinx, 2021b). Many of their new Light Rail Transit Lines, Subways, and Rail Expansion Projects are subject to these standards. Similarly, recent record flooding in Australia, especially in New South Wales in 2021 and 2022, elevated concerns over flood risk and damages to freight and passenger rail infrastructure assets and service delivery, resulting in the procurement of a high-level flood risk assessment based on historical conditions and future climate change projections. Drawing selectively from these examples provides important lessons learned when managing flood risks under climate change.

3 CLIMATE CHANGE RISK ASSESSMENT

In 2005 the Public Infrastructure Engineering Vulnerability Committee was created by Engineers Canada to develop the PIEVC Protocol to provide a framework/process to conduct a vulnerability assessment of climate change impacts on Canada's public infrastructure. Since its release in 2011, the assessment tool has been applied to over 100 different infrastructure assets, initially to legacy assets, and more recently to new infrastructure projects (MacMillan et al., 2024). For this paper it is important to note that to date, no studies on transit and rail have been publicly released, even through PIEVC-based assessments have been conducted in this sector and in some cases are being used to inform the design, construction, and operations and maintenance of new infrastructure projects (e.g., AECOM et al., 2016).

In 2020 the PIEVC Protocol and Program were assumed by the PIEVC Program Alliance, consisting of the Institute for Catastrophic Loss Reduction ("ICLR"), the Climate Risk Institute ("CRI") and Deutsche Gesellschaft für Internationale Zusammenarbeit ("GIZ") GmbH. Since then a number of new complementary protocols have been developed, referred to as the PIEVC family of protocols, and these are compliant with ISO 31000 Risk Management - Guidelines, ISO 31010 Risk Management – Risk Assessment Techniques, and ISO 14090/14091/14092 Adaptation to Climate Change Standards (Nodelman

et.al, 2022). The PIEVC Protocol provides a qualitative step-by-step framework/process for assessing the risk, vulnerability, and adaptive capacity of the interactions between infrastructure assets and climate parameters, with both current conditions and future projections as illustrated in ISO 31000:2018 (Figure 1).

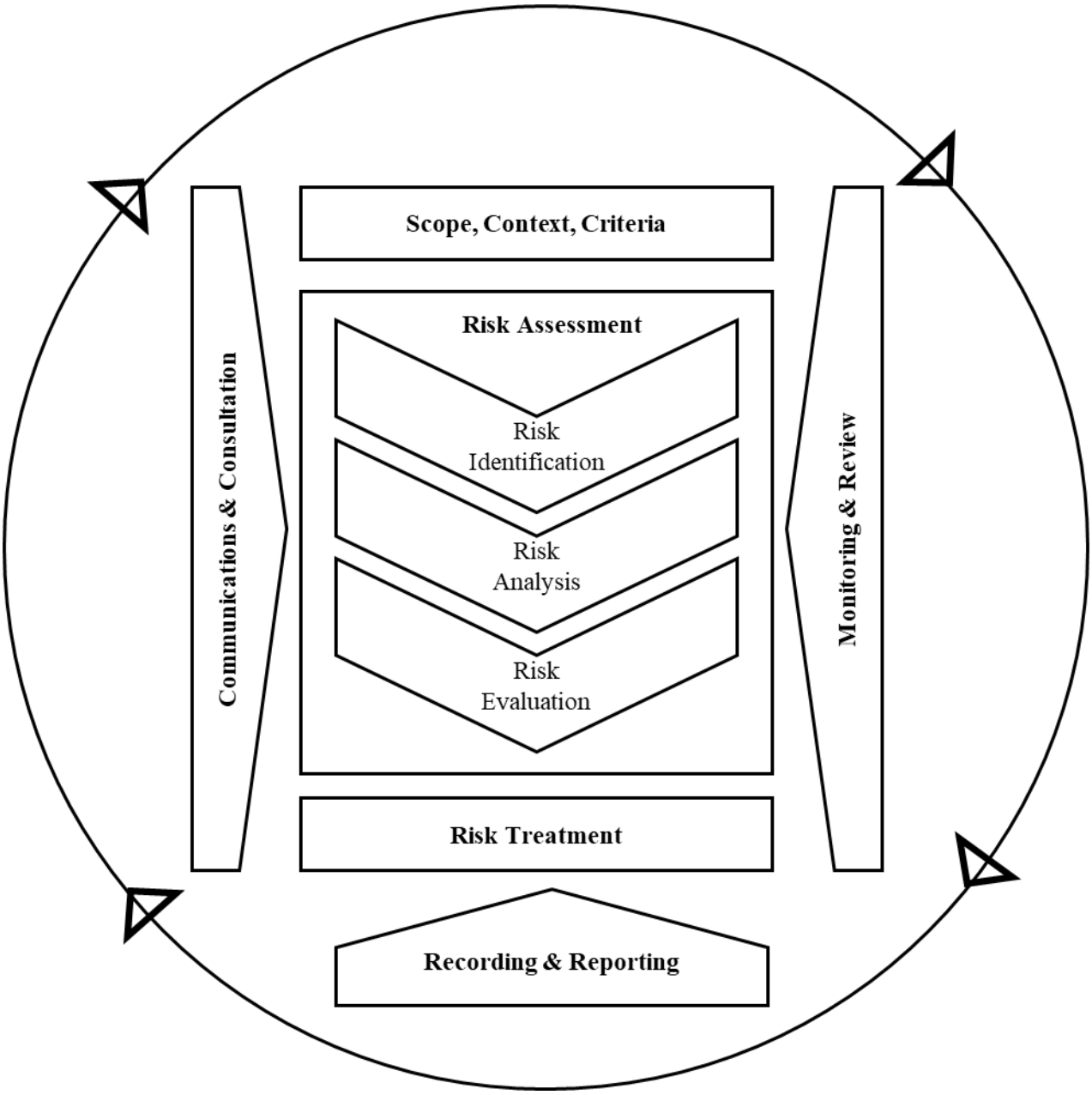

Figure 1: Risk Assessment Process (from ISO 31000:2018)

Detailed explanations of the steps involved and the potential output from each is outlined elsewhere (e.g., Web-4), but for the purposes of this paper they are worth reviewing through a flood mitigation lens that illustrates the importance of applying the PIEVC Protocol to legacy assets and new infrastructure projects. From a scoping and engagement perspective, the PIEVC process represents an opportunity to bring together internal and external subject matter experts and other stakeholders in a structured and focused manner to evaluate climate risk to legacy assets and/or new infrastructure projects. Managing flood risk

effectively is rarely the responsibility of a single agency, and more often than not requires a coordinated, multistakeholder solution. Responsibility for climate risk and adaptation cuts across business units and stakeholders, and the PIEVC process can help break through silos that tend to exist in agencies, companies and government.

The PIEVC process provides a structured and transparent framework to assess flood risk that can be applied to legacy assets and/or new infrastructure projects and can consider risks from both pluvial and fluvial flooding at various spatial and temporal scales, including cascading, compounding, and cumulative effects. In terms of rail and transit infrastructure, whether it is assets covered in the asset management plan for legacy infrastructure, or the infrastructure outlined in the Project Agreement for new projects, the number of assets captured in a climate risk assessment can be substantial. It is important to have widespread consensus on the assets to be included in the assessment, and consistency across projects where multiple consortia may be responsible for discrete segments of a subway or corridor. In either case the selection of assets should be guided by ASTM classification standards for buildings and railroads (e.g., Charette et.al., 1999). In the case of transit and rail, this could include subway/LRT lines, tunnels and corridors, stations and facilities, and fleet vehicles, categorized by asset class, asset groups, and asset elements. For example, a Rail Corridor may include track, bridges, abutments and piers, retaining walls and embankments, signal bridges, etc. that may be exposed to flooding.

The PIEVC process can push stakeholders to confront what they know and what they don't know about flood risk, especially from a historical perspective in face of a changing climate. This involves addressing what Donald Rumsfeld would describe as Known Knowns, Known Unknowns, Unknown Unknowns, and the less recognized Unknown Knowns. Uneven documentation of washouts, differential flood exposure across watercourses, and the variable conditions of legacy assets (especially bridges, crossings and culverts) are just some of the data and knowledge gaps that can apply to individual assets as well as linear systems or networks. Not all flood risks are alike or equal, and one can expect that there will be different levels of consequences that could occur, depending upon the degree of flooding and the impacts on assets and service delivery. Consequences can be evaluated based on an agency's enterprise risk matrix and their level of risk tolerance, and in its place the PIEVC process provides multiple infrastructure response considerations such as functionality, environmental effects, and even watershed and surface water conditions. In practice, consequences have been assessed for transit and rail infrastructure in terms of asset performance, level of service delivery, and safety for employees, contractors, and customers.

The calculation of risk is a function of frequency of a critical threshold for a specific climate parameter being met or exceeded multiplied by the likelihood of its occurrence during a future time period (e.g. typically 2050s and 2080s) relative to the historical baseline (e.g. 1981-2010) (Figure 2). A high emissions scenario is also typically used, such as the SSP5-8.5 scenario, which assumes fossil-fuelled development, high consumption, and high economic growth, that generates the greatest changes in climate that are consistent with a "worst case" risk approach. There is the opportunity here to consider vulnerability and adaptive capacity specifically, as existing or planned actions may affect the likelihood of a flood event damaging infrastructure assets and disrupting service. Along a rail corridor well known for its risk of flooding (located adjacent to a watercourse below the 2-year flood level), for example, a severe storm event on July 8, 2013, led to a combination of record overland and riverine flows, causing water levels to overtop tracks and submerge a commuter train, stranding 1,400 customers (Chiotti et al., 2017). Improvements in operational protocols, weather forecasting, direct stream level monitoring, track level monitoring, and rail corridor monitoring by close circuit camera, have reduced the risk of another flooded train to virtually zero. Tracks would continue to be at risk to overtopping and flooding, but the likelihood of a train being exposed and trapped in a flood was reduced considerably. Nonetheless, plans to electrify this rail corridor and/or increase rail service (two-way, all-day service) would increase flood risk exposure considerably by increasing the frequency of trips, perhaps requiring a transformative design and construction of an adaptation response in the form of an elevated corridor, costing billions of dollars in order to reduce risk to a more tolerant level.

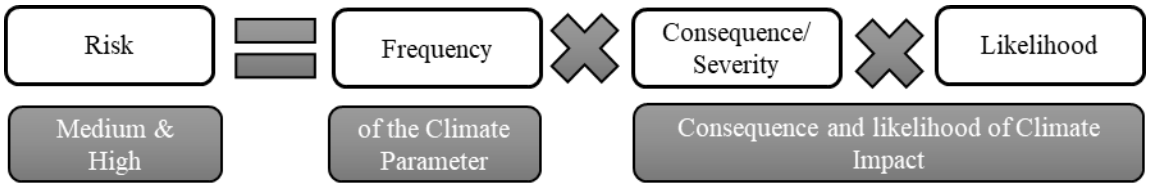

Figure 2: Risk Equation

For special cases where an initial assessment is inconclusive, an engineering analysis may be required, especially for key infrastructure assets. If a deeper dive engineering analysis is not possible, it is not surprising to discover during the PIEVC process that equivalent studies have already been undertaken. For example, in the case of managing potential flood risk to an operations, maintenance and storage facility that was to be located within a regional storm floodplain, the proposed site was subject to a stormwater management report where the application of a sustainable/climate design standard of increased precipitation and/or peak flows were to be applied, that are consistent with climate change projections of Intensity-Duration-Frequency (IDF) statistics (Metrolinx, 2021a). Adaptation measures being considered include improvements in culvert size, the addition of a green roof, and the strategic implementation of low impact development measures on site such as permeable paving and bioswales, among others.

Risk treatment involves the identification, selection and implementation of adaption measures to reduce vulnerability and risk, and it is important to recognize that there is likely to be some degree of residual risk that will occur, despite whatever actions are taken. In the case of new infrastructure projects, for example, one can anticipate that when designing track, stations, or maintenance facilities, and their respective asset components, some transfer of residual risks across procurement to other business functions will be inevitable (Figure 3). These residual risks, from limitations in design standards, will then need to be managed through asset management plans and capital planning over the service life of the assets, while maintenance and operations departments will be responsible for the remaining residual risks through their annual, seasonal and daily activities. Operation activities will be enhanced and supported through (i) water level monitoring of watercourses vis-à-vis track, crossings and bridges; (ii) the installation of ballast sensors; (iii) monitoring of key infrastructure assets through the use of closed circuit camera; and (iv) the installation of weather station instruments along bridges or other key infrastructure assets that provide real time data for precipitation, temperature, high wind gusts, and other climate hazards. When in rare cases infrastructure assets fail and disasters happen, those responsible for emergency management and business continuity planning will need to be engaged.

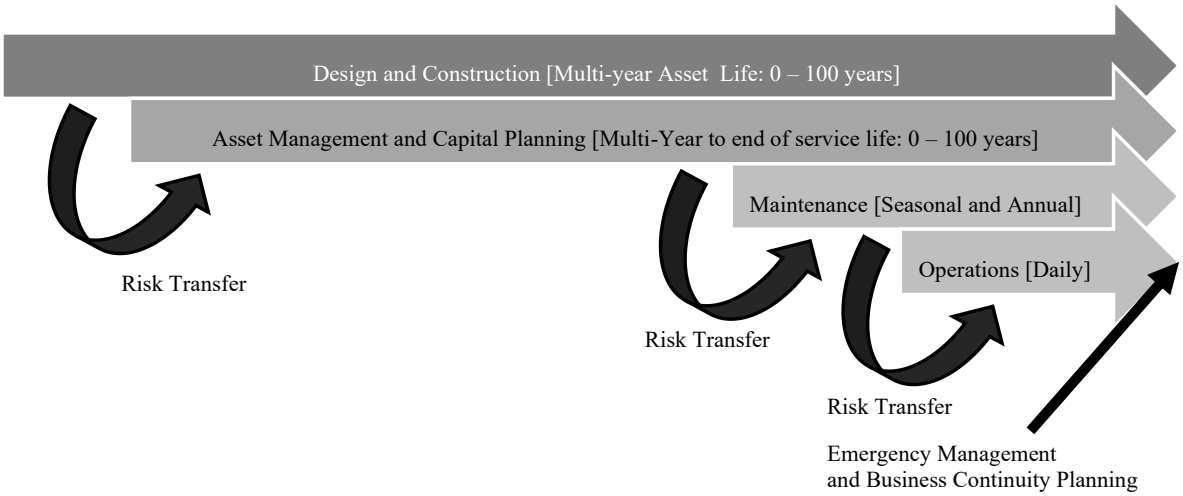

Figure 3: Risk Transfer Across Procurement and Business Functions (from Metrolinx, 2021b)

4 KEY CHALLENGES

Whether it is applying the PIEVC process to legacy assets or new infrastructure projects, a number of challenges are likely to be encountered. Based on experience with assessing flood risk for legacy assets and new infrastructure projects for transit and rail systems in Canada and Australia, the following four challenges are worth noting, in particular how asset owners and designers can pursue four different adaptation expenditure pathways, or a combination of them, to ameliorate flood risk over the lifecycle of infrastructure.

4.1 Using the Right Climate Data

Using the right climate data for climate risk assessment is fundamentally important, noting that it should be informed by historical experience and accepts the wide range of uncertainty in climate change projections. While it is widely accepted that climate is no longer stationary and that historical trends are no longer a good indicator of future climate conditions, in recent years many locales have been experiencing record heavy rainfall and flood events, which shape perceptions of current and future flood risk. It is important then to situate assets that are being assessed within the recent historical context (e.g., past 30 years), especially recent extreme events that are more reflective of the changing climate and then consider how the rainfall contributing to these flood events are projected to change even moreso in the future. The City of Toronto, for example, has experienced record rainfall and flood events in 2005, 2013 and 2024, with each exceeding the historical 1-100 year storm amounts, and are comparable to future projections under high emission scenarios for median values, if not also upper percentiles.

Since there is more confidence in climate change projections of temperature than precipitation, it has been recommended that precipitation projections should be used for the purposes of risk assessment rather than to inform design standards (Cannon et al., 2020). IDF projections are based on existing weather stations and are somewhat dependent upon the length and accuracy of the historical record. In Canada, there has been a long and slow deterioration of the weather station network across the country and many large gaps exist which then requires extrapolation to determine IDF statistics for many locations. Fortunately, in Canada we have data portals that provide credible and defensible projections of IDF statistics, notably the Western IDF CC Tool portal (Web-5) and the Federally supported climatedata.ca portal (Web-6). Future projections of IDF statistics are calculated using different methods, such as the Equidistant Quantile Matching Algorithm, which is precipitation based, and the Clausius-Clapeyron relationship, which is based on temperature scaling, and are spatially extrapolated to areas where there is limited historical data.

Regardless of the data source and method selected, it is important to recognize how this data can support a climate risk assessment. Total precipitation amounts for multiple types of storms for convection events can be helpful (e.g., short term events such as 15-minute, 1-in-10-year storms; slightly longer term events such as a 2-hour, 1-in-100-year storm), but some decision-makers and practitioners may find it more important to have changes in IDF Statistics translated into changes in return periods, typically examining how historical storms will become more frequent in the future. In conjunction with the IDF data portals noted above, this information can be coupled with NOAA's National Weather Service flood return period calculator to illustrate how specific storms will become more frequent in the future (Web-7). For example, different decision-makers for design, asset management, or operations and maintenance may find that knowing that a 2-hour, 100-year storm could become a 1-20 year storm by the 2050s is more important than knowing that the total precipitation for such an event could be 20 mm above the historical baseline.

In the case of Australia, a climate risk assessment focusing on flooding was applied to a large, state-wide rail network, where the scope was greatly influenced by the availability of data for asset condition, landscape elevations, and climate. A large geographical area known for multiple floods over this past century (including 10 since 2012), recent back-to-back mega-floods during 2021 and 2022 had elevated the need for a climate risk assessment that was a desk top exercise, which was followed by an unofficial site visit in 2024. Noting that the rail network traversed highly differentiated landscapes, ranging from corridors crossing multiple rivers in a regulated watershed dominated by dams and reservoirs, suburban/commuter

communities with concrete stormwater channels constructed in the 1970s, and predominantly agricultural tablelands surrounded by mountains, the assessment required making major assumptions regarding geography and topography. While the weather station network and historical climate dataset were many times greater than what exists in Canada (e.g., over 17,000 weather stations were in the Australian Government Bureau of Meteorology database, from which about 400 were selected for the historical weather assessment), future climate projections were limited to daily precipitation amounts, requiring creativity in the translation of heavy rainfall events into flooding. Based on expert judgement, rainfall and flood conditions were differentiated between site specific flooding (24-hour rainfall event for flash flooding), flooding within a catchment area (72-hour rainfall event for slow flooding), and watershed-wide flooding (168-hour rainfall event for prolonged riverine flooding) (Chiotti et al., 2022).

4.2 Complexity of Impacts

The pathway from heavy rainfall to flooding, resulting in damage to infrastructure assets, disruptions in service delivery, and potential injuries and death is not always linear or simple, and can be quite complicated if not complex. Understanding the complexities of impacts, especially in terms of ecosystem conditions and hydrology that can shape flooding is critically important, noting that compounding, cascading and cumulative effects can greatly influence the degree of flooding and other disasters (UNDRR, 2022). Broader watershed issues where a combination of soil saturation levels, drought, wildfires, and removal of vegetative cover has the potential to exacerbate water flows after periods of heavy rainfall that can unfold over weeks, if not months, and in some cases even longer. Similarly, snowpack, glacial melt, spring rainfall and freshet, and even ice jams can be compounding factors not easily projected by climate models or through the application of a climate risk assessment, thereby likely requiring expert judgement and acceptance of more uncertainty when determining potential impacts and the level of risk. On an urban basis the interplay between fluvial and pluvial flooding, and where the age and capacity of adjoining stormwater management systems can limit the conveyance of water flows is another example of complexity that challenges our ability to estimate risk.

From an adaptation perspective complex outcomes also highlight the importance of nature-based solutions, especially at the watershed level, not just when applied in situ at specific asset locations. While this generally applies to issues around water quality (e.g., when preserving upper watershed ecosystems and forests reduces the need for downstream end of pipe water treatment solutions), the same may also apply to water quantity and flood risk. Hardened and impervious surfaces will exacerbate runoff during heavy rainfall events, potentially maxing out stormwater management system capacity, causing backflows, or preventing outflows from occurring. In contrast, the enhancement of natural infrastructure will help reduce and slow the total amount and rate of runoff, in addition to generating multiple co-benefits such as carbon sequestration, biodiversity, and recreation, among others.

4.3 Costs and Benefits of Adaptation Measures

Risk treatment and the consideration of adaptation measures inevitably involve consideration of costs and benefits, both in terms of embedding resiliency into the design standards of new infrastructure, and in the repair, refurbishment and rebuilding of legacy infrastructure assets. The financial benefits of implementing adaptation measures in face of climate change and increased flood risks are compelling, as is the business case for adaptation. Generally, for every dollar invested in adaptation and resilient infrastructure, the return on investment is between $13-$15 from a combination of direct and indirect savings (Sawyer et al., 2022). A report from the Financial Accountability Office of Ontario (FAO) that examined changes in extreme rainfall, extreme heat, and freeze-thaw cycles on transportation infrastructure under a high emissions scenario, builds the business case even further (Afroz et al., 2022). The FAO compared cumulative climate-related infrastructure spending through asset management and capital improvements until the end of this century, comparing no adaptation with reactive and proactive adaptation responses. The report found that proactive adaptation will cost about 33% less than a no adaptation response, and slightly less than reactive adaptation, and that the residual risk will be highest with no

adaptation, and progressively lower with reactive and proactive adaptation. A recent national assessment report builds upon these findings and makes the case to apply proactive adaptation to public infrastructure across the country (Ness et al., 2026).

Through the PIEVC process the costs and benefits for adaptation options can be evaluated qualitatively (e.g., Low, Medium and High), and applied to multiple criteria, including costs, effectiveness of adaptation, barriers to action, and difficulty of implementation, in addition to designating responsibility to design or operations and maintenance, and identifying whether the measure involves monitoring and evaluation (Tonto et al, 2024). For legacy rail infrastructure assets in Australia, a number of financial metrics were considered, and the results overwhelmingly supported the view that by implementing a strategic approach to climate change resilience, the future likely costs of flooding can be reduced substantially (Partners in Performance et al., 2022). The assessment found that the value of risk (e.g., magnitude of repair costs, immediate revenue losses, emergency response costs, and long-term reputational costs) from flooding could increase significantly by mid-century, the annual risk value (e.g., expected annual damages or losses) could be reduced substantially, and that capital investments in infrastructure resilience could yield a much larger net present value whereby the avoided losses over decades would far exceed upfront capital costs of adaptation and resilience measures.

4.4 Adaptation Expenditure Pathways

In terms of developing and implementing an adaptation strategy to reduce flood risks for legacy and new infrastructure assets under a changing climate, it is important to recognize that responsibility will fall upon multiple business units, each with their own business cycle, and each with their own time horizons and planning schedules (e.g., see Viner et al., 2015). It is possible to imagine multiple approaches to design, manage, maintain and operate rail and transit infrastructure assets and service delivery into the future, but four are presented here (Figure 4) as representative examples, with each pathway considering cumulative expenditures and residual risk by the end of this century (Maclellan and Chiotti, 2016). Companies or agencies may follow one or a combination of adaptation expenditure pathways for their legacy and new infrastructure assets, depending upon their risk tolerance and other considerations.

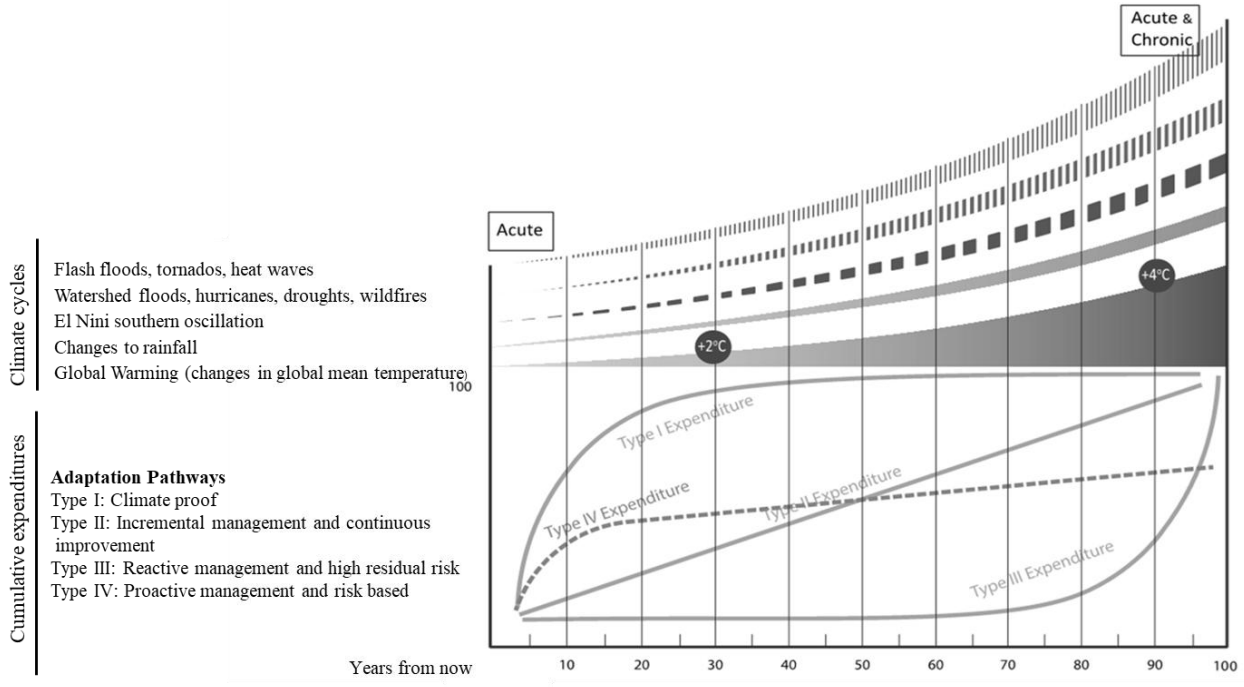

Figure 4: Managing Climate Change Risks Through Adaptation Pathways (adapted from Viner et al., 2015)

The Type I adaptation expenditure pathway aims to be climate proof, that typically involves designing new infrastructure to the highest possible climate standard, with the expectation that asset management and operations and maintenance functions will be minimized throughout the lifetime of the asset. In this case residual risks will also be minimized upon commission, but at the cost of substantial upfront expenditures. The Type II adaptation expenditure pathway tends to apply to the management of legacy assets and is most effective when the improvement is incremental and there is a corporate commitment to continuous improvement. Residual risks tend to be manageable during normal or slightly abnormal conditions, but this approach remains vulnerable to extreme weather conditions. The degree of improvement must be agile and able to respond quickly to any unexpected changes in climate, otherwise risk losing ground and incurring an increasing adaptation deficit.

The Type III adaptation expenditure pathway applies to managing an expansive array of legacy assets, especially for systems and networks that are old, designed to outdated standards, where the state of good repair is poor, and where finances are limited. Capital expenditures, asset management, and operations and maintenance functions are kept to a minimum, and following a "hope for the best" approach tends to leave the owners and operators of these assets continuously exposed to maximum risk, and where a reactive and costly response is the likely, if not inevitable, outcome. The most prudent and cost-effective approach that seeks an illusive "sweet spot" for balancing expenditures with risk is the Type IV adaptation expenditure pathway that is characterized by a proactive management approach which is risk based. This pathway lends itself to the application of a climate risk assessment using the PIEVC process. Design standards of new infrastructure assets and capital improvements for deteriorating legacy assets are given priority but expenditures are less than what is needed to achieve a climate proof standard. The level of standard achieved is very much related to the level of risk tolerance in face of potential future floods. This results in initial expenditures relative to the other pathways being medium to high, followed by minimal, and more manageable expenditures applied for asset management and ongoing operations and maintenance functions.

5 CONCLUSIONS

There is growing acceptance that adaptation to climate change is no longer a "nice to have" option but is necessary to reduce vulnerability and enhance adaptive capacity for legacy assets and new public infrastructure projects. This applies to transit and rail, and particularly in response to future changes in heavy rainfall and increased flood risk. Many agencies and companies are already taking steps to address climate change and flood risks, but overall they need to do more in face of a rapidly changing climate. Managing future risks will benefit from being informed by science and should be evidence-based, and a good starting point is to apply a climate risk assessment to legacy and new infrastructure assets. In this regard the PIEVC Protocol is a useful tool, and the process is a constructive multi-step approach to assess climate change flood-related risks and develop/implement appropriate design and management practices that reduces vulnerability and leads to more adaptive and resilient infrastructure. Using the right climate data, including projections of future IDF statistics, consideration of cumulative impacts, and demonstrating the financial costs and benefits of implementing adaptation measures, are just some of the key elements of the climate risk assessment process.

Managing climate-related risks is complex and challenging, but there is a strong business case to support adaptation and flood mitigation for transit and rail infrastructure. Whether it is the design of new infrastructure or the management of legacy assets, improvements can be made that are cost effective, will prolong the lifecycle of infrastructure assets, and deliver safety benefits. It is important to recognize that some risk transfer can be expected, which will ultimately be left in the hands of those responsible for operations and maintenance activities. Multiple adaptation expenditure pathways are possible, but applying a risk approach will help decision makers make more informed choices in face of climate change.

REFERENCES

AECOM, RSI and TRCA (2016) Metrolinx PIEVC Climate Change Vulnerability Assessment – Final Report , Metrolinx RQQ-2015-IN-021, AECOM, Markham, ON, Canada, 196 p.

Afroz, S., Rhodes, N. and Park, J. (2022) Costing Climate Change Impacts to Public Infrastructure: Transportation – Assessing the financial impacts of extreme rainfall, extreme heat and freeze-thaw cycles on public transportation infrastructure in Ontario, Financial Accountability Office of Ontario, Toronto, ON, Canada, 52 p.

Cannon, A., Jeong, D., Zhang, X. and Zwiers, F. (2020) 2020 Climate-Resilient Buildings and Core Public Infrastructure: An Assessment of the Impact of Climate Change on Climatic Design Data in Canada . Environment and Climate Change Canada, Gatineau, QC, Canada, 106 p.

Charette, R. and Marshall, H. (1999) UNIFORMAT II Elemental Classification for Building Specifications, Cost Estimating, and Cost Analysis, U.S. Department of Commerce, Technology Administration, National Institute of Standards and Technology NISTIR 6389, 93 p.

Chiotti, Q. and Van Vliet, D. (2024) "A call to action: the emergence of climate change adaptation in infrastructure planning", ReNew Magazine, April/May, pp. 10-12.

Chiotti, Q., Chan, K., Gulecoglu, E., Belaieff, A. and Noxon, G. (2017) Planning for Resiliency: Toward a Corporate Climate Adaptation Plan, Metrolinx, Toronto, ON, Canada, 86 p.

Chiotti, Q., Moreno, N. and Manas, M. (2022) Climate Hazards Report, Matrix-Solutions, Calgary, AB, Canada, for the Australian Rail Track Corporation, 73 p.

Elsner, M., Atkinson, G. and Sahidi, S. (2025) The Global Risks Report 2025, 20th Edition Insight Report, World Economic Forum, Geneva, Switzerland, 104 p.

Haghighi, E., Kasreai, A., Famurewa, S., Strandberg, G., Sas, G. and Garmabaki, A.H.S. (2025) "Climate change risks on railway infrastructure: A systematic review and analysis", Sustainable Cities and Society, 129, pp. 1-20.

Infrastructure Canada (2023) The Climate Lens – Investing in Canada Infrastructure Program, General Guidance v 2.1, Infrastructure Canada, Ottawa, ON, Canada, 25 p.

Institute for Catastrophic Loss Reduction (2016a) PIEVC Engineering Protocol for Infrastructure Vulnerability Assessment and Adaptation to a Changing Climate: Principles and Guidelines. Version PG-10.11 (June), Institute for Catastrophic Loss Reduction, Toronto, ON, Canada, 184 p.

Institute for Catastrophic Loss Reduction (2016b) PIEVC Engineering Protocol for Infrastructure Vulnerability Assessment and Adaptation to a Changing Climate: Vulnerability Assessment Module, Version VA-10.11 (June), Institute for Catastrophic Loss Reduction, Toronto, ON, Canada, 79 p.

International Organization for Standardization (2018) ISO 31000:2018 Risk Management – Guidelines, Second edition. 22 p.

IPCC, 2014: Summary for policymakers. In: Climate Change 2014: Impacts, Adaptation, and Vulnerability. Part A: Global and Sectoral Aspects. Contribution of Working Group II to the Fifth Assessment Report of the Intergovernmental Panel on Climate Change [Field, C.B., Barros, V.R., Dokken, D.J., Mach, K.J., Mastrandrea, M.D., Bilir, T.E., Chatterjee, M., Ebi, K.L., Estrada, Y.O., Genova, R.C., Girma, B., Kissel, E.S., Levy, A.N., MacCracken, S., Mastrandrea, P.R., and White, L.L. (eds.)]. Cambridge University Press, Cambridge, United Kingdom and New York, NY, USA, pp. 1-32.

MacLellan, J. and Chiotti, Q. (2016) 'Climate Decision Timelines' *Presented at:* The Forest Climate Workshop, Association of Registered Professional Foresters of New Brunswick, New Brunswick Climate Change Research Collaborative, March 7th to 9th Fredericton, NB, Canada.

MacMillan, K., Symonds, M, and Sparling, E. (2024) PIEVC Meta-Analysis Summary Report. A publication of the PIEVC Program. Institute for Catastrophic Loss Reduction and Climate Risk Institute, Toronto and Sudbury, ON, Canada, 56 p.

Metrolinx (2014) Metrolinx Five Year Strategy, 2015-2020, Metrolinx, Toronto, ON, Canada, 30 p.

Metrolinx (2018) Metrolinx Climate Adaptation Strategy, Metrolinx, Toronto, ON, Canada, 36 p.

Metrolinx (2021a) DS-05 Sustainable Design Standard, Version 1.0, Metrolinx, Toronto, ON, Canada, 108 p.

Metrolinx (2021b) DS-25 Climate Change Informed Data Standard, Version 1.0, Metrolinx, Toronto, ON, Canada, 17 p.
Ness, R., Clark, D.G., Bourque, J., Coffman, D., and Beugin, D. (2022) Under Water: The Costs of Climate Change for Canada's Infrastructure. Canadian Institute for Climate Choices, Ottawa, ON, Canada, 81 p.
Ness, R., Carriere, A. and Gauer, V. (2026) Prepare or Repair: How climate-proofing public infrastructure pays off. Canadian Climate Institute, Ottawa, ON, Canada, 46 p.
Nodelman, J., Nodelman, J., Shippee, N., O'Driscoll, J., and Sparling, E. (2022) PIEVC© Family of Resources Catalogue: A Guide for Selecting Climate Risk Assessment Methods, Data, and Supporting Materials, published by the PIEVC Global Partnership, 56 p.
Partners in Performance, VIRIDI Global and Matrix-Solutions (2022) Australian Rail Track Corporation Climate Resilience Final Report, VIRIDI Global, Ottawa, ON, Canada, 62 p.
Sawyer, D., Ness, R., Lee, C. and Miller, S. (2022) Damage Control: Reducing the costs of climate impacts in Canada. Canadian Climate Institute, Ottawa, ON, Canada, 86 p.
Tonto, F., Iwanicki, A., Chiotti, Q. and Felio, G. (2024) Ontario Line – Southern Civil, Stations and Tunnel Project: Vulnerability Assessment Report, prepared by Matrix-Solutions, Guelph, ON, Canada, for the Ontario Transit Group, 115 p.
UNDRR (2022), Scoping Study On Compound, Cascading And Systemic Risks In The Asia Pacific 2021, United Nations Office for Disaster Risk Reduction (UNDRR), Geneva, Switzerland, 60 p.
Viner, D., Rawlins, M., Allison, I., Howarth, C. and Jones, A. (2015) Climate change and business survival: The need for innovation in delivering climate resilience. Mott MacDonald, p. 10-11.

Websites:
Web 1: https://gml.noaa.gov/ccgg/trends/ consulted December 31st, 2025.
Web 2: https://bac-quebec.qc.ca/en/insurance-issues/disaster/ consulted December 20th, 2025.
Web 3: https://www.pievcanalysis.ca/ consulted December 21st, 2025
Web 4: https://pievc.ca/ consulted December 21st, 2025
Web 5: https://www.idf-cc-uwo.ca/ consulted December 28th, 2025
Web 6: https://climatedata.ca/ consulted December 28th, 2025
Web 7: https://www.weather.gov/epz/wxcalc_floodperiod consulted December 29th, 2025

ICFM 10
Adapting to Global Change:
Innovative Approaches to Flood Management and Resilience
May 20-22, 2026 | Western University, London, Ontario, Canada

Surrogate Modelling for Uncertainty Analysis of Dike Breach Floods

Leon S. Besseling[1], Anouk Bomers[1], Jord J. Warmink[1], Suzanne J.M.H. Hulscher[1]
University of Twente, Enschede, The Netherlands[1]
E-mail: l.s.besseling@utwente.nl

ABSTRACT

Dike breaches are sudden and severe events that need to be predicted and managed for public safety. Important flood characteristics such as flood arrival times are required for effective decision making. Current tools, such as hydrodynamic models, offer this information at long simulation times to be used during an emergency situation. Surrogate models leave out complex physical descriptions of the system in favour of simplified hydraulic principles. In this study, we couple a conceptual breach outflow hydrograph model with a fast flood arrival time model. The low computation times of the coupled framework allow for 10.000 simulations to be conducted in around 5 minutes. We investigate the effect of two sources of uncertainty on the breach outflow and on the flood arrival times: the uncertain moment of dike failure due to wave overtopping, and the uncertain river water level forecast with a number of days lead-time. The results illustrate that the models effectively compute the breach outflow and flood arrival times, and that the river water level causes greater uncertainty than the wave overtopping failure mechanism. We further conclude that the method shows the potential of surrogate modelling frameworks for flood emergency decision making thanks to the low data demand and computational cost.

KEYWORDS: Levee breach, conceptual modelling, real-time flood forecasting

1 INTRODUCTION

Dike breach floods are disastrous events that threaten the lives and livelihoods of many people worldwide. Before a breach occurs, it is essential that the public is informed in time about flood consequences and is possibly evacuated. Decision makers require indicators such as water depths, flow velocities and flood arrival times (Leskens et al., 2014). The most common tool to obtain this information is a hydrodynamic model of the area at risk. These models capture the physics of flowing water through solving the shallow water equations, and accurately model the flood event as it might unfold (Teng et al., 2017). However, hydrodynamic models are computationally expensive, especially at the large scales of dike breach flood events. The computation times can be in the order of hours to days, which is not in line with the fast response time required by decision makers during an emergency. During such an event, decision makers can benefit from a fast model that can simulate the flood event with the most up-to-date information, and take into account uncertainties that are present in the system (Leskens et al., 2014). The fastest hydrodynamic model simulations might be able to deliver output of a single model run, but an ensemble of runs for uncertainty estimates is not yet possible.

Alternative modelling techniques for fast flood modelling after dike breaches have focused on two main research directions. First, machine learning techniques have been explored by Bentivoglio et al. (2023) and Besseling et al. (2024), for example. These models are able to accurately capture breach flood dynamics after being trained on large datasets of pre-generated breach flood scenarios. The input of the machine learning model is a breach outflow hydrograph, while the output is water depths in the hinterland through time. Research into flood modelling using machine learning is currently focused on the ability of the models to generalise to unseen locations and events that were not present in the training data, and to lower the amount of data required for a model that is applicable in many scenarios.

The other main research direction for fast flood modelling concerns conceptual modelling, which relies on simplified hydraulic concepts instead of detailed physical processes (Teng et al., 2017). Compared to machine learning models, these techniques require less data to operate as they do not need to be trained on large datasets. In order to develop these models, calibrating and validating hydrodynamic simulations may be necessary, but the data requirements for the models themselves are low. Similar to machine learning models, the computation times of conceptual models are sufficiently low to enable uncertainty analysis during emergency flood situations. Currently, the main focus of research in the field of conceptual modelling is on integrating more dynamics in the simulations. For example, a main criticism of these kinds of models is that their use of level-pool flooding can lead to very inaccurate water depths (Sanders et al., 2024). Additionally, these flood models have been able to predict only maximum inundation extents, and not the flood arrival times due to flood propagation that occurs in the hours after a breach. This makes these models largely unsuitable for use in dike breach modelling in flat delta regions. Therefore, there is a need to develop a conceptual modelling framework for dike breaching studies that is able to deliver dynamic flood information on flood arrival times to decision makers fast.

In this study, we evaluate the use of a conceptual modelling framework for uncertainty analysis during a dike breach. It combines the model that generates a breach outflow hydrograph by Besseling et al. (2025) and a fast arrival time model by Besseling et al. (submitted). These models have a low run time, enabling analysis of the effects of uncertainties on the arrival times of the flood after a breach. The novel method is presented in Section 2, with model descriptions for the outflow hydrograph model and arrival time model. The results of the coupled framework are shown in Section 3, with a discussion and conclusion in Section 4 and Section 5, respectively.

2 METHODOLOGY

2.1 Case study

The study area of the research is near the Dutch-German border, where the river Rhine bifurcates into the Waal river and the Pannerdensch Canal (Figure 1). This canal bifurcates again into the Nederrijn river and IJssel river. Between the Rhine, the canal and the IJssel is an area ringed by dikes that is the case study of the research. A dike breach is modelled in the far south-east of the area, and the flood spreads in north-westerly direction (Figure 1).

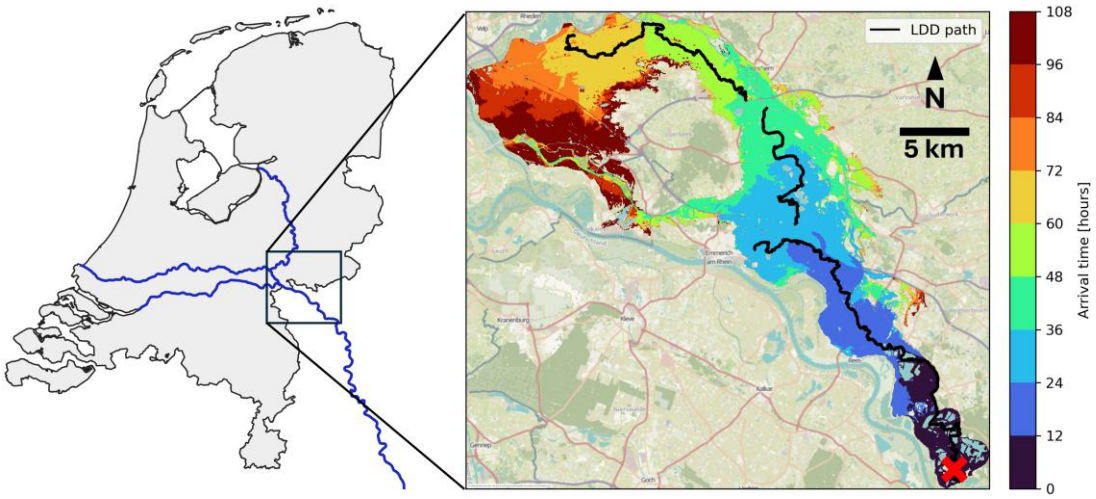

Figure 1: Study area along the Dutch-German Rhine with arrival times of a 10,000 year return period dike breach flood event (breach at red X)

2.2 Breach outflow model

The breach outflow is modelled using the conceptual model proposed by Besseling et al. (2025). A short description of the model is provided here. The model contains three modules: (1) the river water level module, (2) the breach growth and outflow module, and (3) the hinterland water level module.

First, the river water level has to be computed for every time step. The required input is a forecast of the river discharge, which are often available by water authorities through the use of hydrological models and weather forecasts. The forecasted river discharge is converted to a river water level at the dike breach location through the use of stage-discharge relationships that are available for the study area.

Second, the breach growth and breach outflow are computed. For the breach growth, two-stage breach growth equation by Verheij-Van der Knaap (Verheij, 2003) is used. The breach first deepens to the level of the hinterland behind the breach in a pre-defined amount of time. Then, it widens based on the water level difference between the river and the hinterland, with steeper water level gradients resulting in faster growing breaches. The breach outflow is computed using the broad-crested weir equation, first as unsubmerged and later as submerged based on the water level in the hinterland.

Third, the hinterland module uses a 0D approach to simulate the hinterland water level. The water level is computed by dividing the total flood volume up to that time step by the surface area of the hinterland. This eventually leads to the drowning of the breach and the breach outflow being computed by the submerged broad-crested weir equation. However, for larger study areas the water level in the hinterland rises slowly, thereby overestimating the water level gradient and leading to unrealistically large breach growth. Therefore, the model assumes near-critical flow in the breach opening by setting the water level in the hinterland as 2/3 of the river water level. This ratio may be calibrated due to local terrain effects such as elevation differences and friction. The water level using this near-critical flow assumption is maintained until the water level using the volume/area computation exceeds it.

For a more detailed description on the model, we refer to Besseling et al. (2025). The output of the breach outflow model is a breach discharge hydrograph that is used as input for the flood arrival time model.

2.3 Flood arrival time model

The flood arrival times behind the dike breach is modelled using a fast model developed by Besseling et al. (submitted). It is based on the Digital Elevation Model (DEM) of the study area. From the breach location, the steepest downstream path into the hinterland is identified according to the D8-algorithm (Local Drainage Direction, or LDD path). Following an analysis of idealized breach simulations (varying uniform downstream slopes, varying uniform peak breach discharges, varying uniform Manning's roughness), a linear regression model was created relating the flood front's propagation velocity to these idealized parameters.

This linear regression model was applied to the case study scenario (Figure 1). The required input is a peak breach outflow and the DEM of the study area. For each of the grid cells along the steepest downstream LDD path, a propagation velocity and corresponding traversal time is computed. The arrival times of the flood along this steepest downstream path are now known. Besseling et al. (submitted) found that this technique results in accurate arrival time estimates when applied to the case study dike breach of two different return periods: a 100-year return period and a 10,000 year return period. The model predicted near-identical flood arrival times for the critical first 48 hours after the dike breach compared to a process-based hydrodynamic model of the same events (the flood propagates 25–30 kilometres in this time period).

2.4 Uncertainty analysis

Both the breach outflow model and arrival time model are deterministic in nature. Through their fast computation times, the effect of uncertainties on the model output can quickly be analysed. This allows the use of the combined models during a flood emergency.

The dike breach location for the case study is along the German section of the Rhine, so to illustrate the working of the method we extrapolate the Dutch fragility curve for overtopping to a German dike section most upstream in the study area (Figure 1). A breach here significantly affects the Netherlands as well, since the flood propagates downstream parallel to the Rhine river and into the Netherlands. Because of the distance of flood propagation (~50 km for the entire flood event), this breach location can show interesting insight in the effect of uncertainties on the flood arrival times.

In this uncertainty analysis, we analyse the effects of two uncertainties on the breach outflow and subsequent flood arrival times: (1) breach initiation uncertainty due to failure mechanisms and (2) river water level uncertainty due to discharge forecasting lead-times. First, the breach initiation depends on the failure mechanism of the breach, but it is highly uncertain when and how a breach will form. That is why for many dike sections, fragility curves are set up for a number of failure mechanisms. These fragility curves define the probability that a dike will fail at a given water level due to that failure mechanism. We obtained fragility curves for the Dutch dike sections along the Rhine river. Second, the river water level needs to be forecasted, because possible flood risk reduction measures need to be taken ahead of time. For example, evacuating a large area that is possibly affected by the flood requires a considerate amount of time. Therefore, authorities rely on discharge forecasts that have increasing uncertainty for longer lead times. To illustrate the method, we add a fixed uncertainty in the river water level that is normally distributed (mean of 0, standard deviation of 0.1 m). This standard deviation roughly corresponds with the 10-90% confidence interval of a 5-day lead time water level forecast that the Dutch authorities make for the Rhine during normal discharge ranges (see for example Rijkswaterstaat, n.d.). However, this uncertainty could increase even further when forecasting for extreme river discharges.

We conducted three uncertainty analyses. First, we sample 9500 scenarios with different critical water levels from the fragility curve (i.e. the river water level at which the dike breaches) and run the model using a fixed river discharge wave. The discharge wave of interest reflects the design discharge for Dutch dikes along the Rhine under climate change, which has a peak discharge of 18,000 m^3/s. For the second analysis, we sample 9500 river water level uncertainties from the normal distribution described above. The river water level of the design discharge wave is increased or decreased with the sampled amount. These scenarios have a fixed critical water level for all 9500 simulations. The third uncertainty analysis combines both uncertainty sources, generating 9500 scenarios by sampling a critical river water level from the fragility curve and by sampling a water level difference from the water level uncertainty.

Each of the three analyses will result in 9500 breach outflow hydrographs that contain a spread of possible peak breach outflows. The arrival time model then uses these peak breach outflow hydrographs to compute the flood propagation velocity along the steepest downstream path through the hinterland. This results in varying arrival times throughout the flooded area, and an insight in how the fragility curve of overtopping and the river water level forecast affects the flood arrival times.

3 RESULTS

The breach outflow model computes a spread of possible breach outflows for the design river discharge scenario, based on the fragility curve for overtopping and on the river water level uncertainty (Figure 2). The uncertainty in the breaching moment is about 2 days, meaning that the river water level can cause dike breaches from day 13 to about day 15 (peak river water level reached) in this discharge wave scenario. The resulting breach outflow hydrographs vary only slightly in their peak discharge for the wave overtopping uncertainty (Figure 2a). Larger variations are seen for the river water level uncertainty (Figure 2b), and the largest spread in breach outflows is visible for the combined runs (Figure 2c). Earlier breaches have a higher peak breach discharge, because the breach has time to widen before the peak river water level occurs. The total flood volume entering the hinterland also increases for earlier breaches, as there is more time for flood water to enter the hinterland (Figure 2b-d-f).

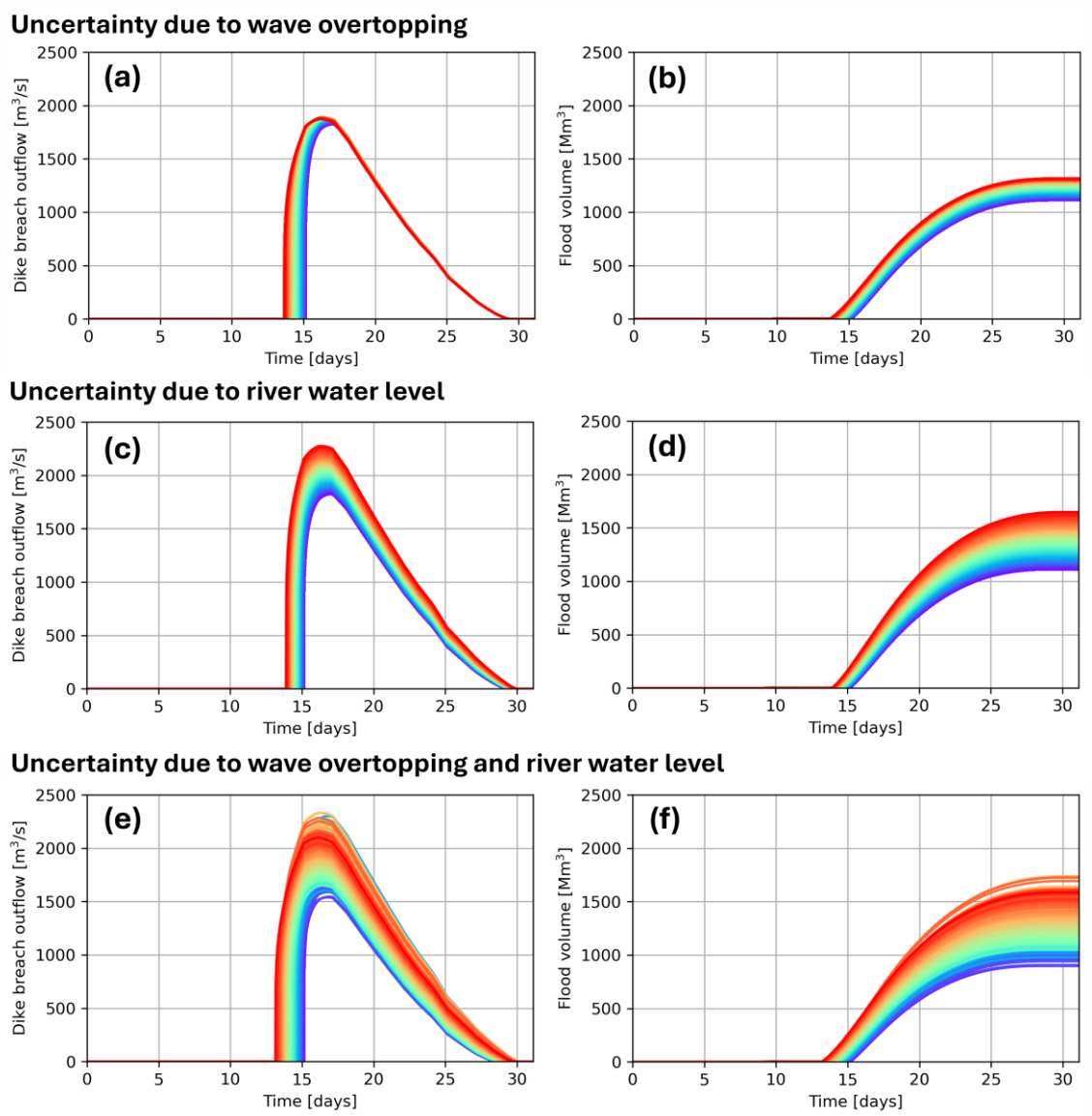

Figure 2: Uncertainty in breach discharge and cumulative flood volume due to **(a-b)** wave overtopping fragility curve, **(c-d)** river water level forecast, **(e-f)** combined wave overtopping fragility curve and river water level forecast. Colors reflect the breach time, with a gradient between early breaches in red towards late breaches in purple.

The resulting spread in peak breach outflow forms the input for the arrival time model. The combined models run the 9500 scenarios in around 5 minutes. The arrival time model output shows the boundary for flood arrival time zones using a thin line (Figure 3). Each line is color-coded to reflect the location of the flood front after a particular time period. Because of the difference in peak breach outflows, different flood propagation velocities are computed for the 9500 simulations. Therefore, the thin lines marking the flood arrival time zones slightly differ per simulation, and a band-width is obtained (Figure 3). This band-width shows the uncertainty in arrival time zone boundaries, indicating how strongly the arrival time is affected by the fragility curve for overtopping and by the river water level uncertainty.

The figure shows that nearest to the breach, the bandwidth for the arrival time zone up to 6 hours after the breach is quite narrow. This means that in the short distance from the breach to here, the difference in propagation velocity caused by the different breaching moments and river water levels is not very significant. Further away from the breach location, the band-widths of arrival time zone uncertainty gradually increase. For the wave overtopping uncertainty, even at the furthest location from the breach, it seems that the uncertainty only amounts to a difference of about 4 kilometers between the slowest and the fastest propagating floods (Figure 3a). However, the spread in arrival times due to the river water level uncertainty is much larger, as the locations of the expected arrival time zone boundaries become quite spread out and even overlap (Figure 3b).

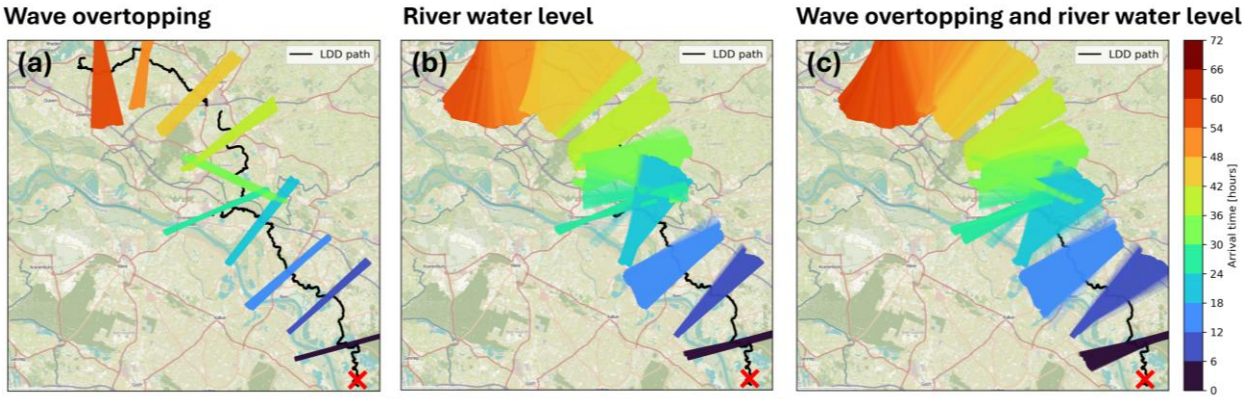

Figure 3: Uncertainty in the location of the flood front for various time periods after the dike breach. **(a)** Uncertainty due to wave overtopping fragility curve. **(b)** Uncertainty due to river water level forecast. **(c)** Uncertainty due to wave overtopping fragility curve and river water level forecast.

4 DISCUSSION

In this study, we present a combination of two conceptual models that model the breach outflow and subsequent flood arrival times for a large-scale dike breach flood. The framework is applied to study the effect of uncertainties like the wave overtopping failure mechanism and the water level forecasts. As a result of the low computational demand, such analyses are now possible during an emergency situation. Decision makers can model the situation as it is unfolding, and obtain a first indication of the flood consequences.

This work illustrates the methodology of the framework, and can be extended to more accurately reflect local conditions and relevant uncertainties. For example, the fragility curve for wave overtopping at the breach location along the German Rhine was derived from available data along the Dutch Rhine. More accurate analysis can include additional fragility curves for dike failure mechanisms of piping and slope instability, if they are available and relevant. Furthermore, the uncertainty in the river water level was included here based on a 5-day lead-time during normal discharge regimes, which was fixed for the entire flood event. However, uncertainty in river water level forecasts generally increases for longer lead-times, so the method can be improved by introducing a lead-time-dependent water level uncertainty. Lastly, we are visually comparing here the effects of the introduced uncertainties (e.g. Figure 2), but the method also allows for a more advanced approach using Sobol' indices (Saltelli et al., 2010), for example. This could illustrate the most important sources of uncertainty in the dike breaching system, and provide directions on which streams of information are most important to focus on clarifying during an emergency situation.

A challenge of the method lies in the coupling of the two models. The arrival time model relies on the assumption that the peak breach outflow forces its way through the hinterland and is the main driver

of the flood propagation. The regression model for front propagation velocity was therefore derived using the peak breach outflow that occurs quickly after the breach develops. However, Besseling et al. (2025) showed that the breach outflow hydrograph model can make accurate predictions of the flood volumes and breach outflows, but that the peak breach outflows are underestimated and occur later than in hydrodynamic model simulations of the same event. This limitation causes the arrival time zones to be shifted compared to the actual peak breach outflow values, but the general effect of the uncertainties on the arrival times remains the same.

Future work can extend the arrival time model by including the volumes from the breach outflow hydrographs. The arrival time model defines the extent of the flood along the Local Drainage Direction (LDD) path, but does not yet compute the water depths. Imposing the volume that has entered the hinterland per time step onto the section of the LDD that has flooded, water depths can be computed using the Height Above Nearest Drainage principle (HAND; Nobre et al. 2011). This would make the model applicable in different cases, ranging from flat and open areas to areas which contain flood defences or local terrain that slows down or blocks the flood from propagating until a water level is reached to overtop this structure or terrain feature. The fast method would then allow insights into the flood extent and water depths in addition to the predicted arrival time zones. Authorities can benefit from this additional data for the decision making during an emergency flood situation.

5 CONCLUSION

We propose a framework of coupled conceptual models for flooding after dike breaches, that simulates the breach outflow hydrograph and subsequent flood arrival times. As a result of the low computation times, the coupled models can be used to simulate thousands of flood scenarios in a few minutes. Using the framework, this study presents an analysis of the effects of two uncertainties on the breach outflow and flood arrival times: the uncertainty in dike failure due to wave overtopping, and the uncertainty in river water levels due to lead-times of forecasting. The framework successfully illustrates the effect of these uncertainties, showing that water level uncertainty has a large impact on breach outflow and subsequent flood arrival time. The framework can be used to identify important sources of uncertainty and allow decision makers to make more informed decisions regarding data requirements and evacuation strategies, among other things.

6 ACKNOWLEDGEMENTS

This research was funded by the Dutch Research Council's (NWO) Simon Stevin Mastery grant received by prof.dr. Suzanne Hulscher. The authors would like to thank the executive agency of the Dutch ministry of infrastructure and water management, Rijkswaterstaat, for providing input data for the breach outflow model.

REFERENCES

Bentivoglio, R., Isufi, E., Jonkman, S. N., and Taormina, R. (2023). Rapid spatio-temporal flood modelling via hydraulics-based graph neural networks, Hydrol. Earth Syst. Sci., 27, pp. 4227–4246.

Besseling, L. S., Bomers, A., and Hulscher, S. J. M. H. (2024). Predicting Flood Inundation after a Dike Breach Using a Long Short-Term Memory (LSTM) Neural Network. Hydrology, 11(9), 152.

Besseling, L. S., Bomers, A., Warmink, J. J., and Hulscher, S. J. M. H. (2025). A conceptual model to quantify probabilistic dike breach outflow. Natural Hazards 121, pp. 17935–17963.

Besseling, L. S., Bomers, A., Warmink, J. J., and Hulscher, S. J. M. H. (submitted). Fast arrival time modelling for dike breach floods.

Leskens, J. G., Brugnach, M., Hoekstra, A. Y., Schuurmans, W. (2014). Why are decisions in flood disaster management so poorly supported by information from flood models? Environ Model Softw 53, pp. 53–61.

Nobre, A. D., Cuartas, L. A., Hodnett, M., Rennó, C. D., Rodrigues, G., Silveira, A., Waterloo, M., and Saleska, S. (2011). Height Above the Nearest Drainage – a hydrologically relevant new terrain model. Journal of Hydrology 404.1-2, pp. 13–29.

Rijkswaterstaat. (n.d.) Lobith: waterstanden en afvoeren. Last accessed on 02-12-2025. https://www.rijkswaterstaat.nl/water/waterdata-en-waterberichtgeving/waterdata/lobith-waterstanden-en-afvoeren.

Saltelli, A., Annoni, P., Azzini, I., Campolongo, F., Ratto,M., and Tarantola, S. (2010). Variance based sensitivity analysis of model output. Design and estimator for the total sensitivity index. Computer Physics Communications 181.2, pp. 259–270

Sanders, B. F., Wing, O. E., and Bates, P. D. (2024). Flooding is Not Like Filling a Bath. Earth's Future 12.12, e2024EF005164

Teng, J., Jakeman, A. J., Vaze, J., Croke, B. F. W., Dutta, D. and Kim, S. (2017). Flood inundation modelling: A review of methods, recent advances and uncertainty analysis. Environ. Model. Softw. , *90*, pp. 201–216.

Verheij, H. J. (2003) Aanpassen van het bresgroeimodel in HIS-OM.

ICFM 10
Adapting to Global Change:
Innovative Approaches to Flood Management and Resilience
May 20-22, 2026 | Western University, London, Ontario, Canada

Healthcare Facilities And Flood Risk Management: The July 2021 Flood In The Netherlands, Germany And Belgium

Yared A. Abebe[1] , M. Pregnolato[2] and Sebastiaan N. Jonkman[3]

Delft University of Technology, Dept. of Hydraulic Engineering, Delft, 2628 CN, Netherlands[1]
E-mail: Y.A.Abebe@tudelft.nl

Delft University of Technology, Dept. of Hydraulic Engineering, Delft, 2628 CN, Netherlands[2]
E-mail: m.pregnolato@tudelft.nl

Delft University of Technology, Dept. of Hydraulic Engineering, Delft, 2628 CN, Netherlands
Institute for Disaster Resilient Texas, Houston, TX, USA
Texas A&M Galveston, Galveston, TX, 77554, USA[3]
E-mail: S.N.Jonkman@tudelft.nl

ABSTRACT

Flooding is an escalating global challenge, causing loss of life and severe economic and infrastructure damage. Climate change is intensifying this risk by increasing the frequency and severity of extreme events such as heavy rainfall, flash floods, and storm surges. The July 2021 floods in the Netherlands, Germany, and Belgium were among the most devastating in recent European history, significantly affecting healthcare facilities (HCFs).

This study systematically reviews scientific literature on flood impacts on HCFs and related risk management measures. Following PRISMA guidelines, four databases (MEDLINE, Embase, Web of Science, and Scopus) were searched for English-language studies addressing flood and cyclone hazards, various HCF types, and disaster risk management strategies. From 7,500 initial records, 74 studies met the inclusion criteria. Most focused on cyclone-induced flooding in the United States, with hospitals as the primary facility type examined, followed by long-term care facilities. Basement flooding was identified as a critical vulnerability, as essential infrastructure (such as power systems, medical equipment, and supplies) is often located there. Disruptions to electricity and water services were also frequently reported, severely affecting healthcare delivery.

The study further analyses the impacts of the July 2021 floods on HCFs in the Netherlands–Germany–Belgium border region, examining risk management activities across preparedness, response, and recovery phases. Focusing on patient logistics and flood risk governance, the findings identify key impacts, response strategies, and governance approaches. Lessons learned aim to inform policy and strengthen flood preparedness and resilience in healthcare systems.

KEYWORDS: healthcare, hospital, flooding, preparedness, impact

1 INTRODUCTION

Floods are the most common natural hazard worldwide and pose severe risks to human health, infrastructure, and economic stability. In 2023 alone, 164 flood events were recorded globally, resulting in over 7,700 fatalities, affecting approximately 32 million people, and causing economic losses exceeding US$20 billion (CRED, 2003). Flooding has both direct health consequences, such as injuries, infectious disease outbreaks, and mental health impacts, and indirect effects including food insecurity and

disrupted access to medical care due to damaged or inaccessible healthcare facilities (HCFs) (Bloomer et al., 2019).

The July 2021 floods in Western Europe were among the most extreme hydrometeorological events recorded, both in terms of rainfall intensity and impacts. Between 13 and 15 July, parts of Germany and Belgium experienced exceptional precipitation, exceeding 150 mm and 210 mm in 48 hours, which led to unprecedented water levels in the Rhine, Meuse, and their tributaries. Flood severity was intensified by emergency dam releases and debris blocking bridges, causing backwater effects. Downstream in the Netherlands, peak discharges along the Meuse reached record levels, with estimated return periods of up to 1 in 200 years on the main river and up to 1 in 1000 years on some tributaries (Dietze et al., 2022).

The floods caused widespread loss of life and severe socioeconomic damage. Germany recorded 190 fatalities and hundreds of serious injuries, while Belgium reported 39 deaths and extensive population impacts; no fatalities were reported in the Netherlands. Significant damage occurred across housing, agriculture, and critical infrastructure, including transport networks, utilities, and public services such as education and healthcare.

Beyond immediate casualties, the floods had substantial health impacts. Studies documented increased psychosocial distress, including anxiety and stress, in affected populations in both the Netherlands and Germany. Damage to and inaccessibility of healthcare facilities further worsened outcomes by disrupting routine care, contributing to more severe health conditions. These impacts highlight the vulnerability of healthcare infrastructure to extreme flooding and underline the importance of systematically documenting flood effects on healthcare facilities and associated disaster management responses.

Healthcare facilities are expected to remain operational during disasters to provide essential services such as emergency care, dialysis, laboratory services, and access to medicines (WHO, 2010). However, recent flood events have demonstrated that HCFs themselves can be highly vulnerable, as illustrated by the evacuation of a flooded hospital in the United States (Hammond et al., 2024). Ensuring continuity of care requires HCFs to reduce flood risk and recover rapidly through hazard and vulnerability assessments, preparedness planning, coordination with authorities and other facilities, and implementation of structural and non-structural risk reduction measures in line with safety guidelines and building standards (WHO, 2010).

Previous reviews have examined disaster impacts on healthcare systems across multiple hazards, with a strong focus on hospitals (Waddell et al., 2021). While all-hazard approaches to risk management are widely recommended (WHO, 2015), the increasing frequency of floods and their specific operational challenges justify a focused examination of flood-related impacts on HCFs. Moreover, non-hospital facilities such as nursing homes and outpatient centres also play a critical role during emergencies and warrant greater attention.

This systematic review therefore aims to synthesise existing evidence on the impacts of flooding on healthcare facilities and the strategies adopted to manage flood risk. The article also analyses the effects of the floods on healthcare facilities in the Netherlands, Germany and Belgium, with a particular focus on the disaster management measures adopted, especially evacuation practices.

2 METHODS

This systematic review was conducted using four major electronic databases: MEDLINE ALL, Embase, Web of Science Core Collection, and Scopus (Abebe et al., 2025). The search strategy was developed in collaboration with a biomedical information specialist and executed on 20 November 2023, covering all records available up to that date. Search terms were organised into three thematic groups addressing: *(i)* flood-related hazards, *(ii)* HCFs, including hospitals, long-term care facilities, dialysis centres, and pharmacies, and *(iii)* disaster risk management across all phases. These groups were combined using Boolean operators to ensure comprehensive coverage. Only English-language journal articles were included, and non-relevant document types such as reviews, book chapters, and data papers were excluded.

Following duplicate removal, study screening was conducted independently by two reviewers using the Rayyan platform, with disagreements resolved through discussion. Eligibility criteria required studies to address flood or cyclone hazards affecting healthcare facilities and to report disaster risk management measures implemented before, during, or after events. Records focusing on other hazards, public health outcomes, staff or patient perspectives alone, governance issues, modelling studies, animal research, or lacking abstracts were excluded. Full-text screening further removed studies that did not provide sufficient detail on flood impacts or risk management practices, or that focused on non-hydrometeorological flooding.

Data extraction was undertaken for all eligible studies, capturing information on publication characteristics, hazard type, healthcare facility type, reported impacts (including physical damage, service disruption, and financial losses), and flood risk management strategies such as evacuation, structural and non-structural measures, preparedness planning, and insurance. Data were tabulated and analysed using descriptive statistics where possible, with narrative synthesis applied otherwise. The entire review process followed the PRISMA 2020 guidelines to ensure transparency and methodological rigour (Page et al., 2021). Our assessment of how the 2021 floods affected health system governance in the three countries mainly draws from grey literature sources.

3 RESULTS

The literature search across four databases yielded 7,500 records, which were reduced to 3,719 after removing duplicates. Following screening and eligibility checks, 74 studies were included in the review. Of these, 51 were case reports on HCFs, while 23 used qualitative, quantitative, or mixed methods involving a broader range of HCFs, such as 217 long-term care facilities (LTCFs) and 64 hospitals with 186 healthcare centers (Castro et al., 2008). Most studies focused on cyclone-related floods (n = 56), particularly hurricanes like Katrina (n = 13), Sandy (n = 9), and Rita (n = 7), with some comparing multiple events (Espiritu et al., 2014). Other studies examined riverine, pluvial, or unspecified floods. Geographically, the majority were conducted in the United States (n = 57), with limited representation from Australia, Canada, Thailand, and other countries. Hospitals were the most studied HCFs (n = 54), followed by LTCFs (n = 11), with a few studies covering pharmacies, dialysis centers, primary health centers, and post-acute rehabilitation facilities.

Floods directly damaged HCFs, particularly basements housing vital services such as laboratories, morgues, and electrical systems. Above-ground floors, parking areas, and equipment rooms were also affected (Khan et al., 2018). Flooding led to patient deaths in a few instances, notably 72 hospital patients during Hurricane Katrina (Gray et al., 2007) and 35 LTCF residents (Stall, 2010), along with physical injuries and mental distress (Claver et al., 2013). Floods caused interruptions to utilities: power outages affected medical equipment, elevators, air conditioning, and refrigeration, directly influencing evacuation and reopening decisions. Water supply disruptions compromised hygiene, surgeries, and overall care, while telecommunication failures hindered coordination (Irvin-Barnwell et al., 2020). Fig. 1 offers a visual summary.

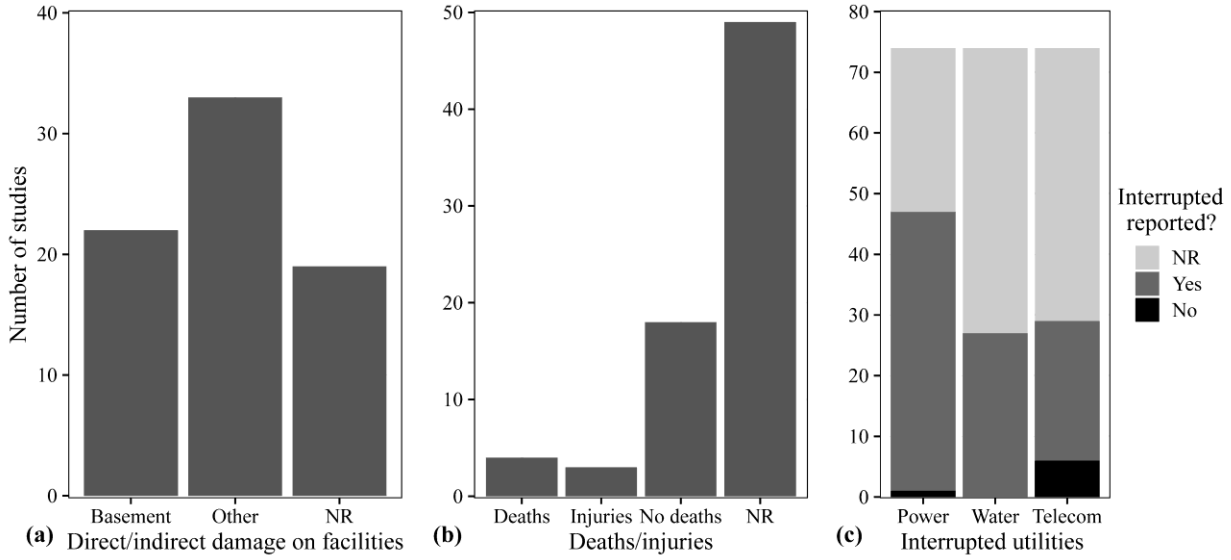

Figure 1: Result from the literature review about flood impact on HFCs: (a) direct/indirect damage on facilities; (b) people deaths/injuries; (c) interrupted utilities

Healthcare services were significantly disrupted. Hospitals and other HCFs often canceled surgeries, discharged patients, or temporarily closed for days to months, with some facilities permanently ceasing operations (Irvin-Barnwell et al., 2020). Additional impacts included blocked access due to flooded streets, staff shortages, logistical difficulties, and substantial financial losses from closures, evacuations, and repair costs (Castro et al., 2008).

Flood risk management strategies were classified into evacuation, shelter in place, structural and temporary measures, and preparedness plans with insurance. Approximately two-thirds of studies reported patient evacuations, which could occur before or after flooding. Evacuation decisions varied based on patient severity, available transport, and receiving facilities, with ambulances, buses, helicopters, boats, and even military vehicles employed (Espiritu et al., 2014). Challenges included road congestion, delayed transportation, medical record management, equipment relocation, and communication with families (Espiritu et al., 2014).

Sheltering in place was less common but practiced in some hospitals and LTCFs, sometimes due to mandatory government orders or risk assessments of evacuation hazards (Jarrett et al., 2018). Structural flood mitigation measures were implemented in a few facilities, notably at the Texas Medical Center, including floodwalls, watertight doors, elevated utilities, improved drainage, and relocation of critical equipment (Brands et al., 2013). Temporary measures included sandbags, pumping water, relocating equipment to higher floors, sealing pharmacies, and storing data off-site. The integration of structural, temporary, and procedural strategies highlights the importance of multi-layered flood risk management in HCFs.

3.1 The 2021 flood in Netherlands, Belgium and Germany

The July 2021 floods demonstrated that healthcare facilities across the Netherlands, Germany, and Belgium remain highly vulnerable to flooding, particularly due to critical functions located in basements, limited structural flood protection, and cascading disruptions to utilities and access. The events underscore the urgent need for flood-resilient design, coordinated emergency planning, and long-term adaptation strategies tailored to different types of healthcare facilities (Table 1).

In the Netherlands, the July 2021 floods primarily affected HCFs in Limburg, particularly in and around Valkenburg along the River Geul. Long-term care and residential facilities were the most severely impacted. Several Sevagram-managed facilities experienced direct inundation, with flood depths reaching

up to 80 cm. Valkenheim nursing home suffered irreparable damage and was ultimately demolished, while the Geerlings hospice and Oosterbeemd nursing home required extensive repairs, leading to long service interruptions. The total damage across these facilities exceeded €40 million. Other facilities, such as the Adelante child and youth rehabilitation center and the Rothemermolen residential care complex, also experienced flooding, mainly affecting basements and technical installations, resulting in prolonged closures.

Major hospitals in the Netherlands largely avoided direct flood damage but implemented precautionary evacuations due to forecasted risks. VieCuri Medical Center and Maastricht University Medical Center (UMC+) were protected by dikes and emergency measures, including sandbags, temporary flood defenses, and power shutdowns. Although these hospitals were not flooded, hundreds of patients were evacuated as a preventive measure, highlighting the vulnerability of critical hospital functions located in basements and the reliance on accurate flood forecasting and emergency preparedness.

Germany experienced the most severe impacts among the three countries, particularly in North Rhine-Westphalia (NRW) and Rhineland-Palatinate (RLP). Numerous hospitals were directly flooded, leading to catastrophic damage to buildings, technical infrastructure, and high-value medical equipment. Basements housing emergency generators, laboratories, imaging equipment, pharmacies, and IT systems proved especially vulnerable. Facilities such as Leverkusen Hospital, St. Antonius Hospital in Eschweiler, and Marien-Hospital in Erftstadt suffered damages ranging from tens to over one hundred million euros. Several hospitals required years to resume normal operations, and at least one hospital (Klinikum Mutterhaus der Borromäerinnen in Trier-Ehrang) was permanently closed due to reconstruction costs and time constraints. Beyond hospitals, a wide range of other HCFs were affected, including rehabilitation clinics, radiology practices, nursing homes, and facilities for people with disabilities. Nursing homes faced particularly severe consequences, including prolonged closures and, in the case of the Lebenshilfehaus in Sinzig, tragic loss of life. Many facilities required complete reconstruction, often taking more than two years. The floods exposed systemic vulnerabilities related to the placement of critical systems in basements, dependency on digital patient data, and limited flood-proofing of healthcare infrastructure.

In Belgium, the floods had a major impact across Wallonia, disrupting hospitals, nursing homes, and pharmacies. Several hospital sites activated emergency plans, suspended non-essential services, and cancelled COVID-19 vaccinations. At CHR de Huy, flooding of underground levels disabled critical electrical infrastructure, while multiple sites of CHU de Liège were either flooded or rendered inaccessible due to damaged bridges and roads. Some facilities, such as the Chaudfontaine polyclinic, were heavily damaged and permanently closed, while others experienced temporary service interruptions and patient evacuations. Long-term care facilities were also significantly affected. Residence Wégimont required the evacuation of 70 residents and underwent a complete redevelopment lasting three years. Pharmacies were particularly vulnerable, with widespread damage across multiple municipalities. In some cases, relatively shallow flooding caused long-term closures due to contamination from flooded hydrocarbon storage. Overall, the Belgian case highlights how indirect impacts (such as inaccessibility, supply chain disruption, and contamination) can severely impair healthcare delivery even when buildings are not structurally destroyed.

Table 1: Comparison of the three countries: the Netherlands, Germany and Belgium.

	no. HFCs	**tot patients (across all HFCs)**	**no. evacuated HFCs**
the Netherlands	18	439	17
Germany	16	1908	14
Belgium	12	N/A	2

4 DISCUSSION AND FUTURE RESEARCH

This review highlights clear geographic and thematic imbalances in the literature on flood impacts and preparedness of HCFs. More than three quarters of the reviewed studies were conducted in the United States, a pattern consistent with earlier disaster health reviews (Sweileh, 2019). In contrast, regions that experience frequent and severe flooding (such as parts of Asia including China, India, the Philippines and Indonesia) remain underrepresented, despite their high exposure to flood risk. Expanding research beyond the US context is therefore essential to capture a wider range of experiences and lessons. The literature also focuses predominantly on hospitals, while other critical facilities, particularly LTCFs, receive far less attention, despite serving highly vulnerable populations (McCann, 2011).

Evacuation emerged as the most frequently reported flood risk management strategy, mentioned in around two thirds of studies. However, the review shows that evacuation is complex and highly variable, involving difficult decisions about timing, prioritisation of patients, transport, destinations and return procedures. Practices differ even between facilities exposed to the same flood event, echoing earlier findings on the lack of consistency in hospital evacuation planning (Khorram-Manesh et al., 2002). Similar variability was observed in decisions to shelter in place. These inconsistencies point to the need for clearer regional or national guidance on evacuation and sheltering, such as state-level frameworks already developed in some contexts (HSPH, 2014). Effective coordination with other HCFs, emergency services and authorities (through mechanisms such as healthcare coalitions) is also critical to support evacuation and traffic management during emergencies (ASPR, 2016).

Preparedness planning showed comparable shortcomings. Although many HCFs reported having disaster plans, their scope, quality and implementation varied widely. Plans are most effective when they go beyond regulatory compliance and are regularly exercised through drills and staff training (Richter, 1997). Standardised emergency management requirements, such as those set by The Joint Commission in the United States (The Joint Commission, 2021), can support more consistent preparedness, but plans must be actively used and periodically updated to reflect lessons learned from past floods (Zork, 2014).

The review also identified recurring failures in critical infrastructure. While most facilities experiencing power outages had backup generators, these often malfunctioned due to flooding of basements or fuel shortages. Locating generators above flood levels and ensuring adequate fuel supplies are therefore key resilience measures (Toner et al., 2017). Water supply strategies were similarly diverse, ranging from bottled water to storage tanks and wells, reinforcing the need for advance planning rather than ad hoc responses (van der Heijden et al., 2022). Permanent structural flood protection measures were rarely reported, largely due to cost barriers, particularly for smaller hospitals (Hines and Reid, 2023), underscoring the value of international guidance on assessing and addressing structural vulnerabilities, such as the WHO safe hospital framework (WHO, 2010).

5 CONCLUSION

Given the essential function of healthcare facilities (HCFs) during emergencies and the increasing frequency of flood events, this systematic review examined how floods affect HCFs and the measures adopted to manage flood risk. The findings show that flooding of basements is among the most damaging impacts, often leading to direct harm to buildings, medical equipment, and critical infrastructure. Disruptions to essential utilities (particularly electricity and water) were also common and had serious consequences for the continuity of healthcare services. Patient evacuation emerged as the most frequently reported response strategy, despite the significant logistical and clinical challenges it presents. In contrast, relatively few facilities reported the use of permanent or temporary structural flood protection measures. Although many HCFs had disaster preparedness plans, their scope, quality, and level of implementation varied considerably.

The review highlights several priorities for future research and practice. From a research perspective, existing studies predominantly focus on hospitals, while non-hospital facilities (such as outpatient centres, nursing homes, and long-term care facilities) remain underexplored, despite their critical role during emergencies. Disruptions to these facilities can increase pressure on hospitals,

underscoring the need for more comprehensive investigation. Further research is also required in flood-prone and underrepresented regions, including parts of Asia, Africa, South America, and Europe. Scenario-based studies could support awareness-raising and help evaluate the effectiveness of adaptation measures. In addition, incorporating grey literature in future reviews would provide a more complete picture of flood impacts and preparedness.

From a practical standpoint, the findings indicate that flood preparedness is complex and unevenly implemented across HCFs. Public authorities should take a leading role in developing standards and guidance to support flood risk assessment and preparedness planning. Healthcare facilities would benefit from clearer direction on maintaining, updating, and rehearsing preparedness plans to ensure staff and patients are familiar with procedures. Coordinated emergency exercises involving multiple HCFs and response agencies are also essential. Finally, flood-resilient building codes should be promoted, including requirements for elevating critical systems and equipment, and ensuring that any necessary basements are flood-resistant and limited to non-essential uses.

The findings of this study strongly reflect the vulnerabilities observed during the July 2021 floods in the Netherlands, Germany, and Belgium. As illustrated in the cross-border cases, critical functions located in basements, limited structural protection, and cascading disruptions to utilities and accessibility significantly amplified impacts on healthcare facilities. These lessons reinforce the need for flood-resilient design, strategic relocation of essential infrastructure, and coordinated governance approaches to strengthen the long-term resilience of healthcare systems.

6 ACKNOWLEDGEMENTS

This work was carried out within the Frontrunner 3 project “Pandemic lessons for flood disaster preparedness,” and funded by the Pandemic and Disaster Preparedness Center (PDPC) [grant number 2022.003]. The authors thank Wichor Bramer for developing and updating the search strategies. The authors also thank the other PDPC Frontrunner 3 project members for their valuable feedback during the literature search and selection process. This work is partly published in Abebe et al. (2025).

REFERENCES

Abebe, Y. A., Pregnolato, M., & Jonkman, S. N. (2025). Flood impacts on healthcare facilities and disaster preparedness–A systematic review. International Journal of Disaster Risk Reduction, 119(10534). https://doi.org/10.1016/j.ijdrr.2025.105340

ASPR (2016). 2017–2022 health care preparedness and response capabilities. U.S. Department of Health and Human Services, Assistant Secretary for Preparedness and Response. Available at: https://aspr.hhs.gov/HealthCareReadiness/guidance/Documents/Health-Care-Preparedness-and-Response-Capabilities-for-Health-Care-Coalitions.pdf (Accessed 21 November 2025)

Bloomer, E., Landeg, O. and le Polain de Waroux (2019) Floods as human health risks, in: J. Nriagu (Ed.), Encyclopedia of Environmental Health, second ed., Elsevier, Oxford, 8–18, https://doi.org/10.1016/B978-0-12-409548-9.11462-9

Brands, C. K., Hernandez, R. G., Stenberg, A., Carnes, G., Ellen, J., Epstein, M. and Strouse, T. (2013). Complete self-sufficiency planning: designing and building disaster-ready hospitals. Southern Medical Journal, 106(1), 63-68. https://doi.org/10.1097/SMJ.0b013e31827cb1b2

Castro, C., Persson, D., Bergstrom, N. and Cron, S. (2008).Surviving the storms: emergency preparedness in Texas nursing facilities and assisted living facilities. Journal of Gerontological Nursing, 34(8), 9–16. https://doi.org/10.3928/00989134-20080801-01](https://doi.org/10.3928/00989134-20080801-01

Claver, M., Dobalian, A., Fickel, J.J., Ricci, K.A. and Mallers, M.H. (2013). Comprehensive care for vulnerable elderly veterans during disasters. Archives of Gerontology and Geriatrics, 56(1), 205–213. https://doi.org/10.1016/j.archger.2012.07.010](https://doi.org/10.1016/j.archger.2012.07.010

CRED (2024). 2023 Disasters in Numbers: A Significant Year of Disaster Impact. Centre for Research on the Epidemiology of Disasters (CRED)[Online]. Available: https://files.emdat.be/reports/2023_EMDAT_report.pdf. (Accessed 25 November 2024)

CRED and UNDRR (2020). Human cost of disasters: an overview of the last 20 years (2000–2019). Centre for Research on the Epidemiology of Disasters and United Nations Office for Disaster Risk Reduction. Available at: https://www.cred.be/sites/default/files/CRED-Disaster-Report-Human-Cost2000-2019.pdf (Accessed 20 November 2025).

Dietze, M., Bell, R., Ozturk, U., Cook, K. L., Andermann, C., Beer, A. R., Damm, B., Lucia, A., Fauer, F. S., Nissen, K. M., Sieg, T. and Thieken, A. H. (2022). More than heavy rain turning into fast-flowing water – a landscape perspective on the 2021 Eifel floods. Natural Hazards and Earth System Sciences, 22(6), 1845–1856. https://doi.org/10.5194/nhess-22-1845-2022

Espiritu, M., Patil, U., Cruz, H., Gupta, A., Matterson, H., Kim, Y., Caprio, M. and Mally, P. (2014). Evacuation of a neonatal intensive care unit in a disaster: lessons from Hurricane Sandy. Pediatrics, 134(6), e1662-e1669. https://doi.org/10.1542/peds.2014-0936

Gray, B.H. and Hebert, K. (2007). Hospitals in Hurricane Katrina: challenges facing custodial institutions in a disaster. Journal of Health Care for the Poor and Underserved, 18(2), 283–298. https://doi.org/10.1353/hpu.2007.0031](https://doi.org/10.1353/hpu.2007.0031

Hammond, E., Chavez, N., Sottile, Z. and Smart, S. (2024). Dozens rescued from roof of Tennessee hospital during flooding from Helene. CNN, 27. Available at: https://edition.cnn.com/2024/09/27/us/unicoi-county-hospital-tennessee-flooding-helene/index.html (Accessed 26 November 2025)

Hines, E. and Reid, C.E. (2023). Hospital preparedness, mitigation, and response to Hurricane Harvey in Harris County, Texas. Disaster Medicine and Public Health Preparedness, 17, e18. https://doi.org/10.1017/dmp.2021.146

Irvin-Barnwell, E.A., Cruz, M., Maniglier-Poulet, C., Cabrera, J., Diaz, J.R., Perez, R.D.L.C., Forrester, C., Shumate, A., Mutter, J., Graziano, L. and Gonzalez, L.R. (2020). Evaluating disaster damages and operational status of health-care facilities during the emergency response phase of Hurricane Maria in Puerto Rico. Disaster Medicine And Public Health Preparedness, 14(1), 80-88. https://doi.org/10.1017/dmp.2019.85](https://doi.org/10.1017/dmp.2019.85

Jarrett, M.P., Schwartz, Z., Solazzo, M. and Tangney, E. (2018). Evacuate or shelter in place: a view from the water's edge. Journal of Emergency Management, 16(2), 95–106. https://doi.org/10.5055/jem.2018.0358](https://doi.org/10.5055/jem.2018.0358

Khan, Z.A., Bhatti, A.M. and Akhtar, F. (2018). Safety of electro-medical equipment in floods in austere environment. Disaster Medicine and Public Health Preparedness, 12(6), 803–805. https://doi.org/10.1017/dmp.2017.145

Khorram-Manesh, A., Phattharapornjaroen, P., Mortelmans, L.J., Goniewicz, K., Verheul, M., Sörensen, J.L., Pereira, I., Ricklin, M.E., Faccincani, R., Dark, P.M. and Carlström, E. (2022). Current perspectives and concerns facing hospital evacuation: the results of a pilot study and literature review. Disaster Medicine and Public Health Preparedness, 16(2), 650–658. https://doi.org/10.1017/dmp.2020.391

McCann, D.G. (2011). A review of hurricane disaster planning for the elderly. World Medical and Health Policy, 3(1), 1–26. https://doi.org/10.2202/1948-4682.1144

MDPH (2014). Hospital evacuation planning guide. MDPH (Massachusetts Department of Public Health) Hospital Evacuation Toolkit. Available at: https://www.mass.gov/lists/hospital-evacuation-toolkit (Accessed 21 November 2025)

Page, M.J., McKenzie, J.E., Bossuyt, P.M., Boutron, I., Hoffmann, T.C., Mulrow, C.D., Shamseer, L., Tetzlaff, J.M., Akl, E.A., Brennan, S.E. and Chou, R. (2021). The PRISMA 2020 statement: an updated guideline for reporting systematic reviews. BMJ, 372(71). https://doi.org/10.1136/bmj.n71

Richter, P.V. (1997). Hospital disaster preparedness: meeting a requirement or preparing for the worst? Healthcare Facilities Management Series, August, 1–11

Stall, R.S. (2010). Hurricane Katrina: more lessons learned. Journal of the American Medical Directors Association, 11(9), 677–679. https://doi.org/10.1016/j.jamda.2010.03.009](https://doi.org/10.1016/j.jamda.2010.03.009
Sweileh, W.M. (2019). A bibliometric analysis of health-related literature on natural disasters from 1900 to 2017. Health Research Policy and Systems, 17(1), 18. https://doi.org/10.1186/s12961-019-0418-1
The Joint Commission (2021). R3 report: new and revised standards in emergency management. R3 Report, Issue 34. Available at: https://www.jointcommission.org/standards/r3-report/r3-report-issue-34-new-and-revised-standards-in-emergency-management/ (Accessed 21 November 2024)
Toner, E.S., McGinty, M., Schoch-Spana, M., Rose, D.A., Watson, M., Echols, E. and Carbone, E.G. (2017). A community checklist for health sector resilience informed by Hurricane Sandy. Health Security, 15(1), 53–69. https://doi.org/10.1089/hs.2016.0079
van der Heijden, S., Cassivi, A., Mayer, A. and Sandholz, S. (2022). Water supply emergency preparedness and response in health care facilities: a systematic review on international evidence. Frontiers in Public Health, 10, 1035212. https://doi.org/10.3389/fpubh.2022.1035212
Waddell, S.L., Jayaweera, D.T., Mirsaeidi, M., Beier, J.C. and Kumar, N. (2021).Perspectives on the health effects of hurricanes: a review and challenges. International Journal of Environmental Research and Public Health, 18(5), 2756. https://doi.org/10.3390/ijerph18052756](https://doi.org/10.3390/ijerph18052756
WHO (2010). Safe Hospitals in Emergencies and Disasters: Structural, Non-structural and Functional Indicators. World Health Organization [Online]. Available: https://iris.who.int/bitstream/handle/10665/207689/9789290614784_eng.pdf. (Accessed 24 November 2025)
WHO (2015). Western Pacific regional framework for action for disaster risk management for health. WHO Regional Office for the Western Pacific. Geneva, Switzerland. Available at: https://iris.who.int/bitstream/handle/10665/208200/9789290617082_eng.pdf (Accessed 25 November 2025)
Zork, F. (2014). Nursing home disaster planning and response: a policy perspective. Journal of Gerontological Nursing, 40(12), 16–24. https://doi.org/10.3928/00989134-20141111-02

ICFM 10
Adapting to Global Change:
Innovative Approaches to Flood Management and Resilience
May 20-22, 2026 | Western University, London, Ontario, Canada

Flash Flood Disaster Risk Simulation Technology Based on Classified Recursive Feature Elimination-Random Forest Optimization Algorithm

Xiaolei Zhang[1*], Ruihua Qin[2], Changqi Dong[3], Xuecheng Xing[1], Cheng Zhang[1], Jing Xiao[4], Ronghua Liu[1]

Research Center on Flood & Drought Disaster Prevention and Reduction of the Ministry of Water Resources, China Institute of Water Resources and Hydropower Research, Beijing, 100038, China[1,*]
Email: zhangxl@iwhr.com

Xi'an University of Architecture and Technology, Xi'an, 710311, China[2]
Email: 1106236218@qq.com

Sun Yat-sen University, Guangzhou, 510275, China[3]
Email: dongchq5@mail2.sysu.edu.cn

China Institute of Water Resources and Hydropower Research, Beijing, 100038, China[1]
Email: xingxch@iwhr.com

Research Center on Flood & Drought Disaster Prevention and Reduction of the Ministry of Water Resources, China Institute of Water Resources and Hydropower Research, Beijing, 100038, China[1]
Email: zhangc@iwhr.com

Hydrology and Water Resources Survey Bureau of Hainan Province, Haikou, 570100, China[4]
Email: xiaojing2012tju@163.com

State Key Laboratory of Water Cycle and Water Security, China Institute of Water Resources and Hydropower Research, Beijing, 100038, Research Center on Flood & Drought Disaster Prevention and Reduction of the Ministry of Water Resources, Beijing, 100038, China[1]
Email: liurh@iwhr.com

ABSTRACT

Flash flood disasters inflict severe economic losses and casualties on human society, making the scientific identification and assessment of these risks an urgent priority in disaster management research. This study aims to improve the accuracy of flash flood risk prediction by coupling feature selection and the Random Forest algorithm, thereby establishing a scientific basis for disaster early warning. Seventeen features influencing flash flood occurrence were initially identified, and a feature selection technique coupling Recursive Feature Elimination (RFE) with the Random Forest-based optimization algorithm was developed, which effectively determines the optimal feature combination for flash flood risk simulation. The research results indicate that the optimal feature combination obtained using classification-based RFE significantly improves the predictive performance of the Random Forest model, achieving an ROC value of 0.947. High-risk areas for flash flood disasters in Fujian Province are mainly distributed in the Wuyi Mountains, Daiyun Mountain, and Damao Mountain regions. These areas cover 49,000 km² and affect 27 million people.

KEYWORDS: Random forest; Recursive feature selection; Flash flood disaster risk; Small watershed scale

1 INTRODUCTION

With continuous socio-economic development and worsening climate change, flood disasters have gradually increased, causing heavy casualties and economic losses. Flash floods are particularly prominent due to their characteristics of intense short-duration rainfall, rapid outbursts, and high risk to human safety and property (Fu et al., 2024). Flash floods account for approximately 70% of flood-related fatalities. Therefore, Strengthening prevention measures and accurately identifying high-risk areas is vital for reducing casualties and property losses. To achieve this goal, scientific and systematic risk assessment and prediction of flash flood are essential.

Current flash flood risk assessment primarily include mathematical models, physical models, and hybrid approaches that integrate machine learning with statistical models. The first category comprises deterministic mathematical models, which use coefficient of determination method to evaluate the sensitivity of various influencing factors across different intervals and classify flash flood risks using the relative entropy index (Yang et al., 2023). Raillani et al. employed the Dirac delta function approximation to estimate the probability density function, describing disaster occurrence rates in different regions to identify high-risk areas (Rayllani et al., 2023). Nugraheni et al. integrated 15 primary indicators (e.g., social, economic, policy, and land use factors) with 65 secondary indicators (e.g., working-age population, land-use change trends, and policy objectives) in combination with the CLEAR model, CLUE-S model, and DROP model to identify flash flood risk areas (Nugraheni et al., 2018). Chen et al. established a flash flood risk assessment system for Qingyuan City based on GIS and the Analytic Hierarchy Process (AHP), delineating risk zones into different levels. Their results delineated the spatial distribution of flash flood risks in Qingyuan City and provided technical support for flood risk management planning (Chen et al., 2017). Zhang et al. investigated flash floods in Chongqing, identifying key influencing factors and calculating risk indices to support decision-making in risk management (Zhang et al., 2019). Zhang et al. employed GIS, geographic detectors, and AHP, using nine indicators such as snow water equivalent, slope, and the maximum 1-hour precipitation to identify key drivers of flash flood risk in Xinjiang. Their study comprehensively assessed the risks based on disaster-causing factors, environmental conditions, and vulnerability (Zhang et al., 2024). Wibowo et al. used a composite flood disaster index to assess flash flood risk (Wibowo et al., 2020).

The second category comprises physically based models solving shallow water equations. One-dimensional and two-dimensional hydraulic models have been employed to simulate flood dynamics in developing mountainous areas, which supports precise risk zoning and hazard mapping. (Zhang et al., 2020;Hu et al., 2018). Liu et al. established a bidirectional coupled hydrological-hydrodynamic model (CNFF-IFMS) to simulate flash floods in the Zhaigang River Basin, validating the performance of the coupled model in mountainous flood simulations (Liu et al., 2025). Waleed et al. integrated ArcGIS, ERDAS, and WMS with HEC hydrological model and HEC-RAS two-dimensional hydraulic modeling software to assess the impact of flash floods on the holy sites and eastern urban areas of Mecca (Waleed et al., 2022).. Salih et al. applied the HEC-HMS model and IMERG data to evaluate flood risks in the Wadi Hail basin in southwestern Saudi Arabia, providing valuable insights for flood management strategies (Salih et al., 2024). Li et al. simulated flash flood processes by integrating hydrological and hydrodynamic models and developed flood risk maps (Li et al., 2019). Al-Kuisi et al. applied a hydrological model coupled with GIS-based AHP analysis to generate flash flood risk zoning maps for Petra and Wadi Musa, Jordan, supporting the local early warning system(Al-Kuisi et al., 2023).

Furthermore, studies demonstrate that single-model approaches (e.g., hydrological and hydrodynamic) are inherently limited in quantifying cumulative effects of riverine structures (e.g., bridges, weirs, and dams) on flood propagation dynamics, particularly their backwater interactions. This can lead to an underestimation of flash flood susceptibility and potential hazards. Therefore, the

development of coupled hydrological-hydrodynamic models (such as CNFF-IFMS) enables more accurate and refined flash flood simulation studies (Liu et al., 2025).

The third category comprises hybrid statistical-physical models that integrate machine learning and physical mechanisms. In particular, machine learning techniques are increasingly applied in flash flood risk assessment and management. Fan et al. employed Light Gradient Boosting Machine (LightGBM) and Extreme Gradient Boosting (XGBoost) algorithms to construct flash flood risk maps, providing more accurate data support for disaster early warning systems (Fan et al., 2023). Chu et al. used the Bayesian Model Averaging (BMA) approach combined with three classical machine learning algorithms—Gradient Boosting Decision Trees (GBDT), Backpropagation Neural Networks (BP), and Random Forest (RF)—to simulate flash flood risk (Chu et al., 2023). Ma et al. applied Least Squares Support Vector Machines (LS-SVM) and other artificial intelligence techniques to assess flash flood risk in Yunnan, generating risk maps of flash flood occurrences (Ma et al., 2019). Jing et al. adopted a combination of Fuzzy Comprehensive Evaluation, Analytical Hierarchy Process (AHP), and GIS to evaluate flash flood risk in Datong City (Jing et al., 2018). Ruidas et al. proposed a bivariate logistic regression method to map flash flood risk in the Gandheswari River Basin, India (Ruidas et al., 2022). Ju et al. employed five different machine learning regression models, including Random Forest, Support Vector Regression (SVR), XGBoost, and LightGBM, to assess the risk of four types of natural disasters in Changzhou, demonstrating the advantages of machine learning algorithms in risk assessment(Ju et al., 2024). These studies establish physical principles and quantitative tools (e.g., risk assessment matrices) for flash flood management, directly informing the development of mitigation strategies in operational contexts.

Flash flood risk simulation is requires multi-physics coupling due to the nonlinear interactions of multi-factor, including meteorological conditions, topography, and land-use changes, making it difficult to predict. Previous studies have shown that: (i) deterministic mathematical models and traditional physical models have played a significant role in simulating and predicting flash floods. However they have many limitations—they require specific types of data and lack flexibility, while mathematical models may be influenced by the designer's experience and biases, potentially introducing additional errors. Flash floods often involve multiple nonlinear interactions; (ii) compared to physical models, machine learning models are data-driven and effectively capture complex nonlinear relationships, resulting in more accurate predictions. Furthermore, they leverage historical historical data and identify complex nonlinear patterns; and (iii) Compared to Deterministic mathematical models, machine learning algorithms reduce subjective errors. However, they may be prone to overfitting in certain scenarios, where the model performs well on training data but lacks generalization ability when applied to new data, preventing it from achieving the expected outcomes (Bu et al,, 2020).

To improve flash flood risk risk simulations and support flood forecasting and early warning, this study proposes a coupling technique based on Recursive Feature Elimination and Random Forest (RFE-RF). A classification-based RFE method is applied to remove insignificant features, which reduces data dimensionality, mitigates overfitting, and simplifies the model requirements. Historical flash flood data are then used for risk analysis and prediction. The results show that compared to using all features, reducing dimensionality not only lowers the degree of overfitting but also improves prediction accuracy to 0.88 and increases the ROC value to 0.947.

2 METHODOLOGY

This study establishes a flash flood disaster risk identification methodology combining the categorical feature elimination method and a random forest coupling algorithm to identify flash flood disaster risk areas and summarize their risk characteristics. The specific process includes eigenvalue classification, feature combination screening, model training, and risk simulation.

a. Eigenvalue Classification: In this study, to analyze the causes of flash flood disasters, the influencing factors are categorized into three main groups: rainfall datasets, underlying surface datasets, and socio-economic datasets.

b. Feature Combination Screening: In this study, to optimize the feature selection process and accurately identify the most significant factors influencing flash flood disasters, Recursive Feature Elimination (RFE) is used to process each category of data (i.e., rainfall datasets, underlying surface datasets, and socio-economic datasets) separately. At least one factor from each category is retained to reflect the causes of flash flood disasters.

c. Model Training: The optimal feature combinations obtained from the RFE process are used to train a random forest model. 80% of the historical flash flood disaster dataset is allocated for model training, while the remaining 20% reserved for testing the model's accuracy.

d. Risk Simulation: Using the trained random forest model, the likelihood of flash flood disasters is predicted and categorized into five distinct groups: extremely high, high, medium, low, and extremely low.

Recursive Feature Elimination (RFE) iteratively removes the least important features, gradually refining the feature set. Initially, all available features are used to train the model, after which the model is repeatedly retrained while eliminating insignificant features until the feature count meets a predetermined condition. Through RFE, redundancy in the feature space can be effectively reduced, improving both the efficiency and performance of the model (Han et al., 2021). On large datasets, selecting an optimal subset of features is essential for machine learning algorithms, such as Random Forest. Too many features can degrade algorithm performance and increase the risk of overfitting (Jeon et al., 2020).

Random Forest is a classifier that that constructs multiple decision trees to predict sample outcomes. Introduced by Breiman in 2001, this algorithm has been widely adopted for both classification and regression tasks, particularly when the number of variables far exceeds the number of observations (Blau-G et al., 2016). It improves predictive performance by averaging the outcomes of individual trees for regression tasks or by applying majority voting for classification tasks. Its advantages include high accuracy, the capability to handle large datasets and high-dimensional features, and the capability to assess feature importance.

This study employs a coupled RFE-Machine Learning algorithm, leveraging RFE to reduce excessive feature dimensionality and mitigate overfitting, thereby enhancing the performance of the Random Forest model. This methodology is used to identify key features influencing flash flood disasters and simulate flash flood disaster risks in Fujian Province.

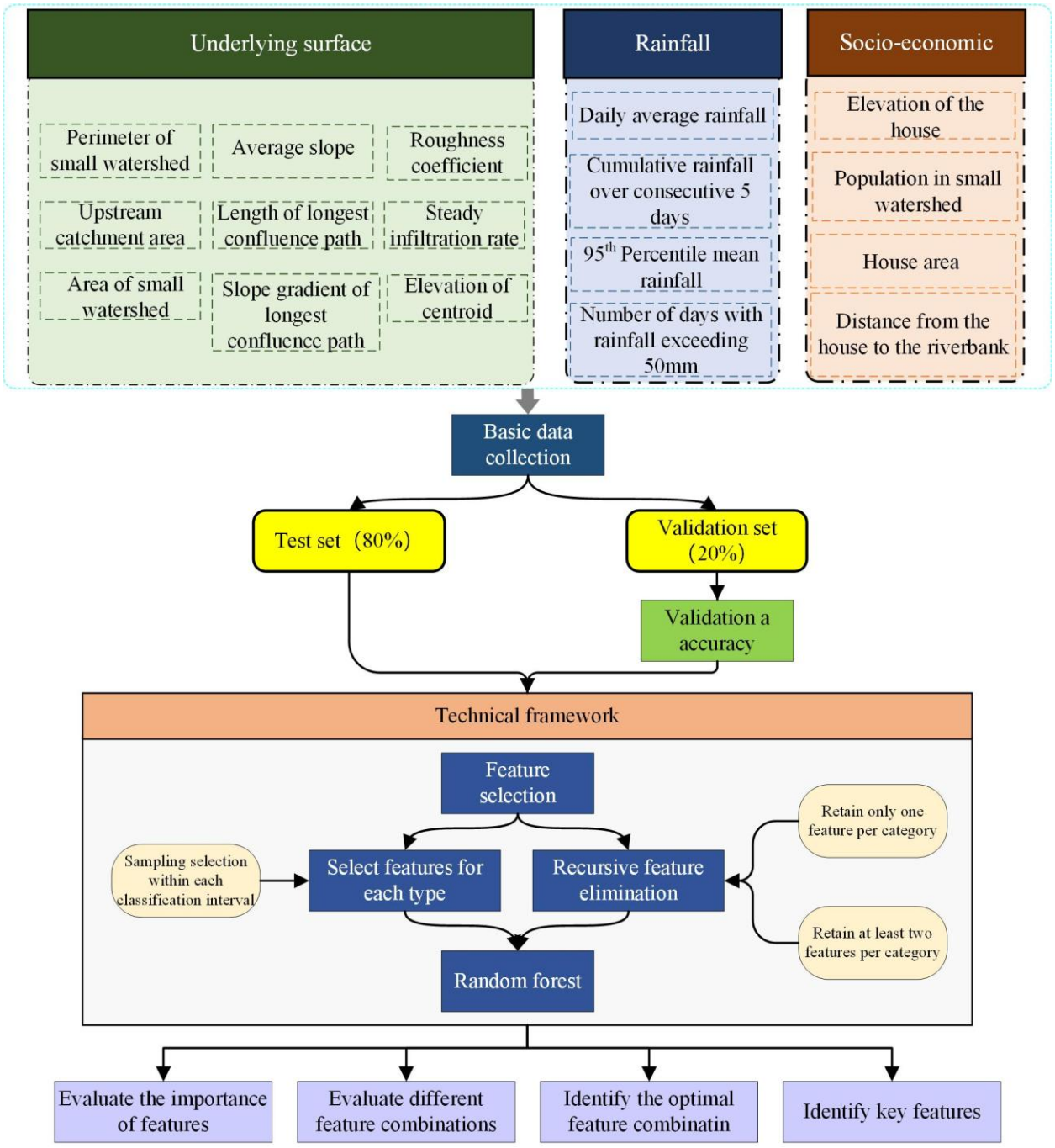

Figure 1: Technical Framework

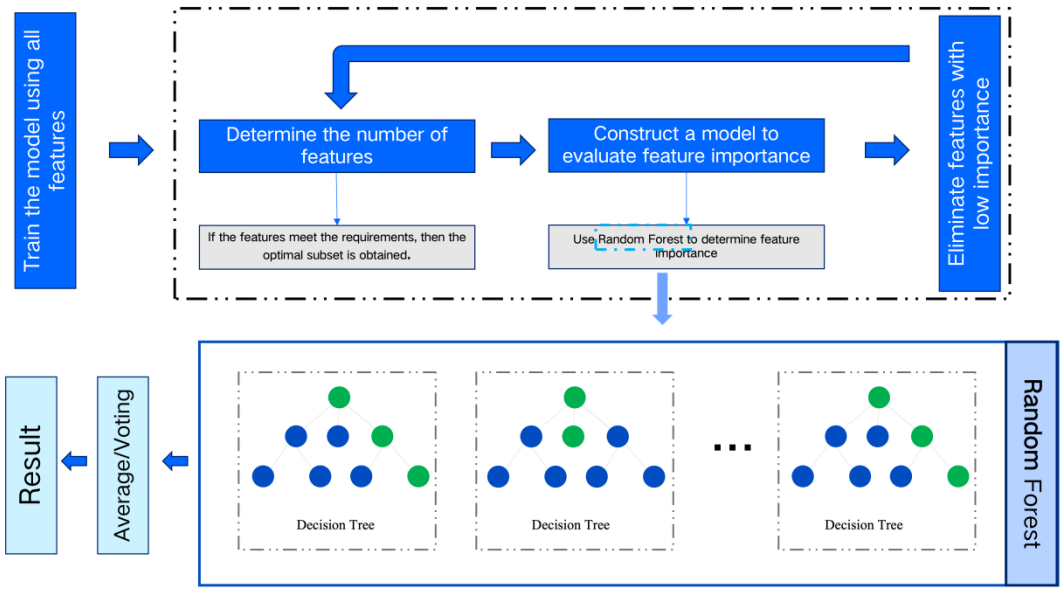

Figure 2: Classification based recursive feature selection method

3 CASE STUDY

3.1 Study Area

Using Fujian Province as a case study, this paper aims to identify key contributing factors to flash flood disasters, assess high-risk zones across the province, visualize risk distribution patterns, and investigate the underlying mechanisms of hazard concentration areas. Fujian Province, situated along China's southeastern coast, is dominated by mountainous terrain where 90% of its land exhibits undulating topography, 1.35 times the national average. Notably, 66 counties (77.7% of provincial municipalities) fall within these geologically active mountain zones. The unique landform and climate change result in frequent occurrences of flash flood disasters, causing significant casualties and posing a severe challenge to flood control and disaster mitigation (Liang et al., 2020). According to the database of the National flash flood Disaster Survey and Evaluation Results from the China Institute of Water Resources and Hydropower Research, there have been 2,306 recorded historical flash flood disaster events in Fujian Province since the founding of the People's Republic of China, causing severe economic damage and casualties. Notably, the number of flash flood disasters has increased sharply since 1988 (Xiong et al., 2020; Li et al., 2022; Zhang et al., 2019).

3.2 Data

Based on data availability, this study identified 17 impact factors in Fujian Province, categorized into four types of rainfall factors, nine underlying surface factors, and four socio-economic factors. Departing from grid-scale methodologies, this study uses small watersheds as research unit (ranging from 15 to 50 km^2) as research units and fully considers the topological relationships between upstream and downstream watersheds. The impact factors of flash flood disasters are processed and analyzed at the watershed scale. Historical data on these disasters—encompassing casualties and property losses from various watersheds in Fujian Province—serve as the sample. In this study, data from 2,306 historical disaster sites in Fujian Province were employed. Using a random sampling method, the small watersheds containing these historical disaster sites were divided into a training set (80%) and a validation set (20%).A binary classification method is adopted to quantify the casualties and economic losses from flash flood disasters at the small watershed scale. Small watersheds with casualties and economic losses due to

flash flood disasters are labeled as 1, while those without losses are labeled as 0. Twenty percent of the sample is used as the test set, while the remaining eighty percent is used for training.

Table 1: Flash flood influencing features of Fujian province

Data type	Characteristic factor	Data source	Abbreviation in English
Rainfall indicators (4 indicators)	a.Daily average rainfall(1951-2013)	China Meteorological Data Network Rainfall Dataset	ADP
	b. Days with rainfall exceeding 50mm (1951-2013)		RF>50mm
	c. Cumulative rainfall over five consecutive days (1951-2013)		CAVD
	d. 95th percentile rainfall (1951-2013)		P95R
	e. Perimeter of a small watershed		SWP
	f. Outlet drainage area		UCA
	g. Small watershed area		SAW
Underlying surface type indicators (9 items)	h. Average slope	National Flash Flood Disaster Prevention Project Team National Flash Flood Disaster Investigation and Assessment Database	AvSl
	i. Longest flow path length		LCP
	j. Longitudinal slope of the longest flow path		LSPG
	k. Roughness coefficient		N
	l. Steady infiltration rate		SIR
	m. Centroid elevation		CE
	n. Building elevation		BE
Socio-economic indicators (4 items)	o. Distance of the building from the riverbank	National Flash Flood Disaster Prevention Project Team National Flash Flood Disaster Investigation and Assessment Database	NH50SW
	p. Building area		BA
	q. Population of the small watershed		PSW
Sample data	r. Historical flash flood disaster data	National Flash Flood Disaster Prevention Project Team National Flash Flood Disaster Investigation and Assessment Database	HFFD

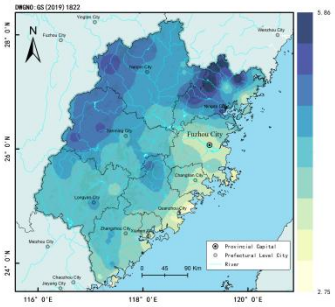

(a) Daily average rainfall

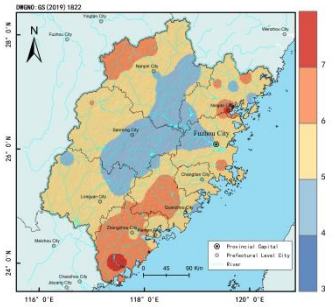

(b) Days with rainfall exceeding 50mm

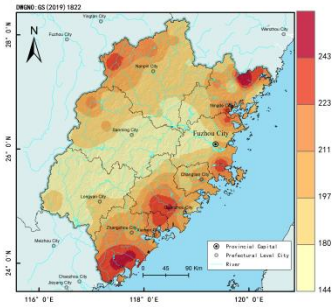

(c) Cumulative rainfall over five consecutive days

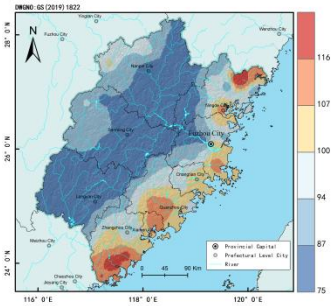

(d) 95th percentile rainfall

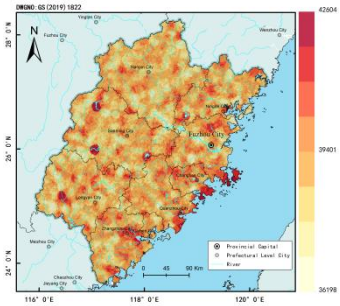

(e) Perimeter of small watershed

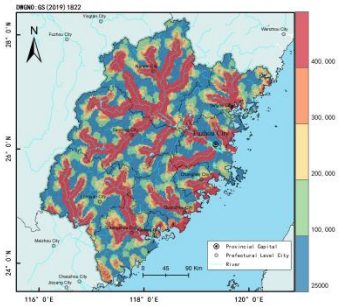

(f) Outlet drainage area

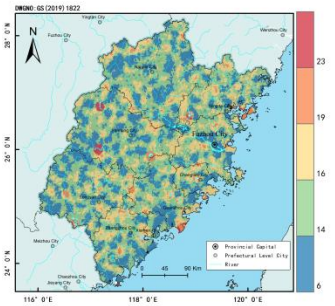

(g) Small watershed area

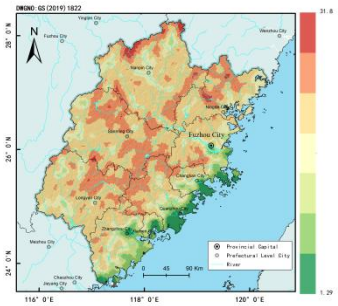

(h) Average slope

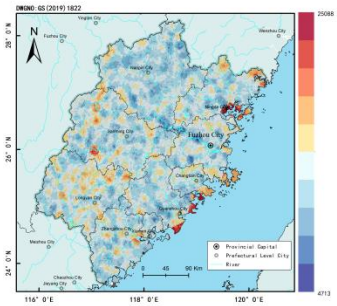

(i) Longest flow path length

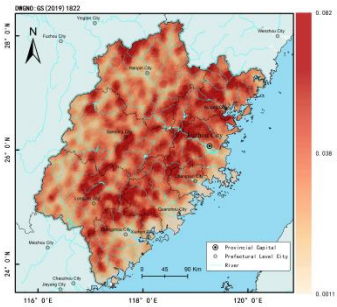

(j) Longitudinal slope of the longest flow path

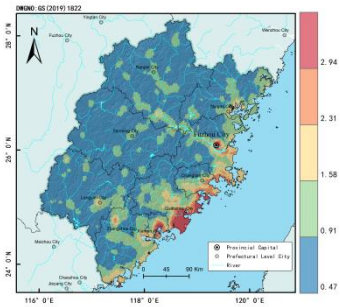

(k) Roughness coefficient

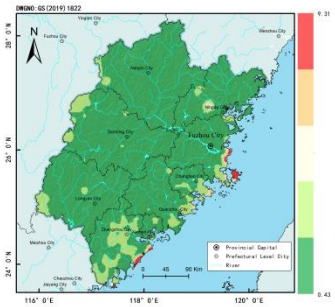

(l) Steady infiltration rate

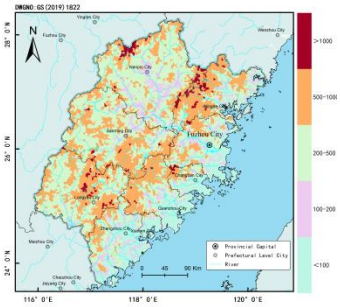

(m) Centroid elevation

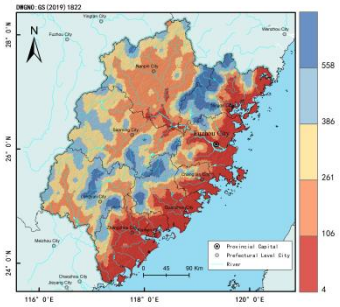

(n) Building elevation

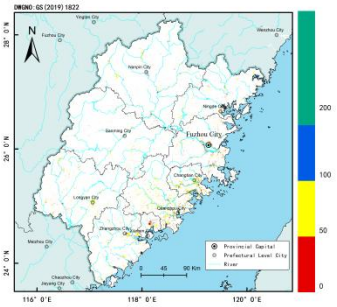

(o) Distance of the building from riverbank

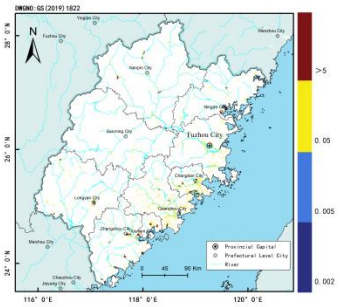

(p) Building area

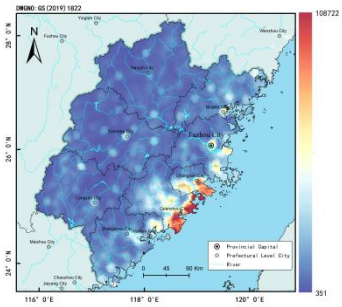

(i) Population of the small watershed

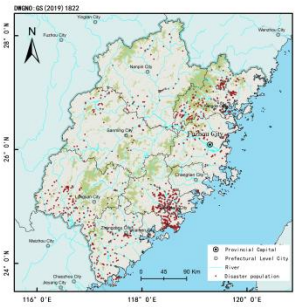

(r) Historical flash flood disaster data

Figure 3: Feature section datasets and historical flash flood disaster data

4 RESULT ANALYSIS

4.1 Results

After 14 rounds of iterative training, the optimal feature combination was determined and used to simulate flash flood risk levels in Fujian Province. The results indicate that high-risk areas encompass a population of approximately 27 million, and the total area of small watersheds in the medium-high risk zones reaches 49,000 km^2. The extremely high-risk and high-risk areas for flash floods are mainly concentrated in mountainous regions, particularly in the Wuyi Mountains, Daiyun Mountains, and Daimai Mountains. These regions are characterized by steep slopes and highly variable terrain, with complex topographical conditions and sharp elevation changes. Combined with the abundant daily rainfall of the subtropical monsoon climate, these factors markedly increase the likelihood of flash floods.

As shown in Fig. 4, high-risk areas in Fujian Province are primarily distributed in regions closely connected to mountain ranges. This distribution pattern is closely related to the province’s complex topography, particularly in mountainous areas where the risk is most pronounced. Notably, the spatial distribution of these high-risk areas does not strictly follow watershed boundaries but is more significantly influenced by the orientation of the mountain ranges. Due to the unique topographical features of these areas, flash floods are more likely to occur during heavy rainfall events. Additionally, the study indicates that the risk of flash floods is relatively low in coastal regions and low-altitude areas in the southwest. This phenomenon further validates the significant influence of high-altitude regions on the probability and severity of flood disasters.

The study’s findings not only provide critical support for disaster prevention and mitigation in Fujian Province but also offer a scientific basis for developing future flash flood early warning and prevention strategies.

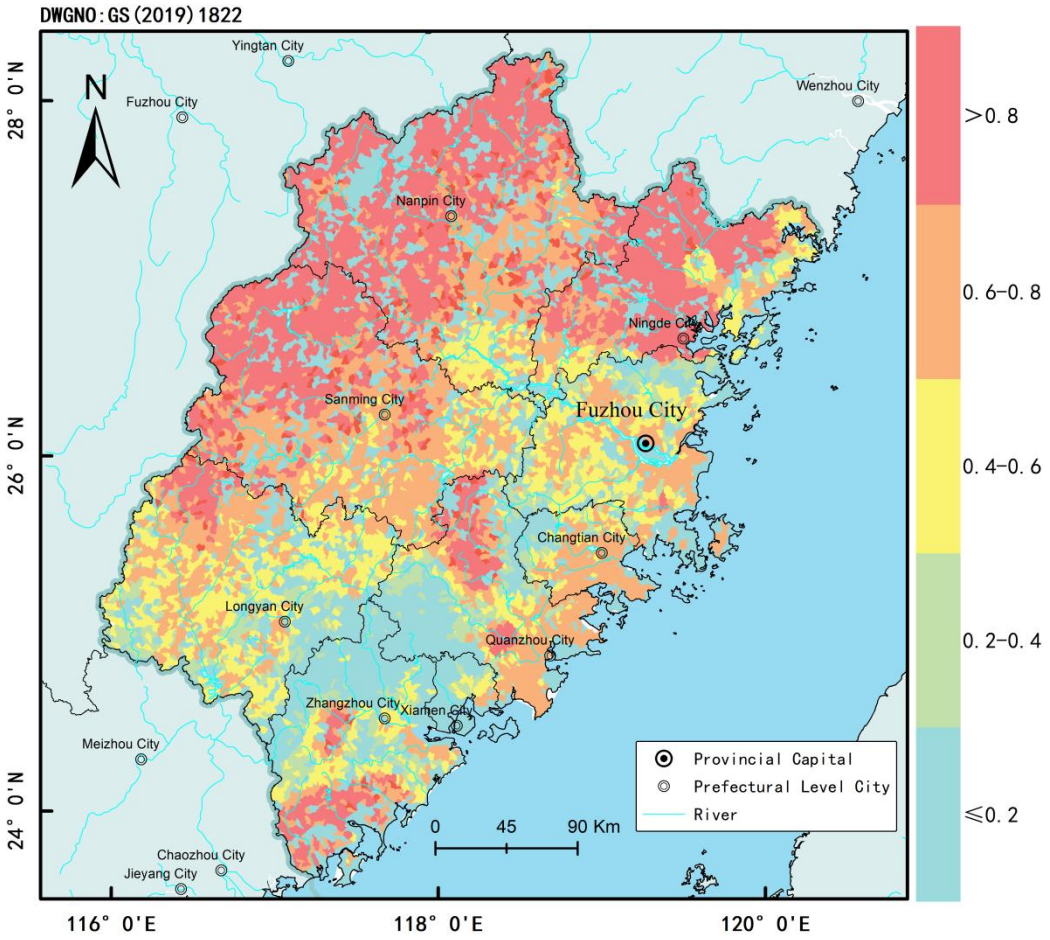

Figure 4: Risk Distribution Map of Flash Flood Disasters

4.2 Discussions

4.2.1 Accuracy Analysis Using Classification RFE

This study employed the classification recursive feature elimination (RFE) method, which progressively removes factors with low correlation to flash flood occurrences while retaining key features that contribute significantly to flash flood events (Table 2). The Receiver Operating Characteristic (ROC) value initially increased as insignificant features were eliminated; however, when the number of selected features became too small, the ROC value began to decline. After multiple iterations, optimal model performance was achieved with eight selected features. The eight key features identified were: Number of days with rainfall exceeding 50mm, Daily average rainfall, Five-day cumulative rainfall, 95th percentile rainfall, Slope, Longitudinal slope of the longest flow path, Building elevation, Population of the small watershed. The model achieved an ROC value of 0.947. The model comprehensively considered three major categories of key features: rainfall, underlying surface conditions, and socio-economic factors. The optimized feature combination not only improved the predictive performance of the model but also more accurately reflected the primary influencing factors of flash flood occurrences in Fujian Province. This approach provides a reliable and comprehensive basis for subsequent flood prevention and mitigation decision-making.

Table 2: Risk indicators of flash floods in mountainous areas

Indicator combination	Remaining indicators after feature selection	ROC value	Indicator number	Eliminated features
(4，4，2)	Number of days with rainfall exceeding 50mm, Daily average rainfall, Five-day cumulative rainfall, 95th percentile rainfall, Slope, Longitudinal slope of the longest flow path, Roughness coefficient, Centroid elevation, Building elevation, Population of the small watershed	0.946	10	Steady infiltration rate, Perimeter, Outlet drainage area, Area, Longest flow path length, Centroid elevation, Number of buildings, Distance of buildings from the riverbank
(4，3，2)	Number of days with rainfall exceeding 50mm, Daily average rainfall, Five-day cumulative rainfall, 95th percentile rainfall, Slope, Longitudinal slope of the longest flow path, Roughness coefficient, Building elevation, Population of the small watershed	0.945	9	Steady infiltration rate, Perimeter, Outlet drainage area, Area, Longest flow path length, Centroid elevation, Number of buildings, Distance of buildings from the riverbank, Centroid elevation
(4，2，2) Optimal combination	**Number of days with rainfall exceeding 50mm, Daily average rainfall, Five-day cumulative rainfall, 95th percentile rainfall, Slope, Longitudinal slope of the longest flow path, Building elevation, Population of the small watershed**	**0.947**	**8**	**Steady infiltration rate, Perimeter,Outlet drainage area, Area, Longest flow path length, Centroid elevation, Number of buildings, Distance of buildings from the riverbank, Centroid elevation**
(3，2，2)	Number of days with rainfall exceeding 50mm, Daily average rainfall, Five-day cumulative rainfall, Slope, Longitudinal slope of the longest flow path, Building elevation, Population of the small watershed	0.937	7	Steady infiltration rate, Perimeter,Outlet drainage area, Area, Longest flow path length, Centroid elevation, Number of buildings, Distance of buildings from the riverbank, Centroid elevation, Roughness coefficient, 95th percentile rainfall

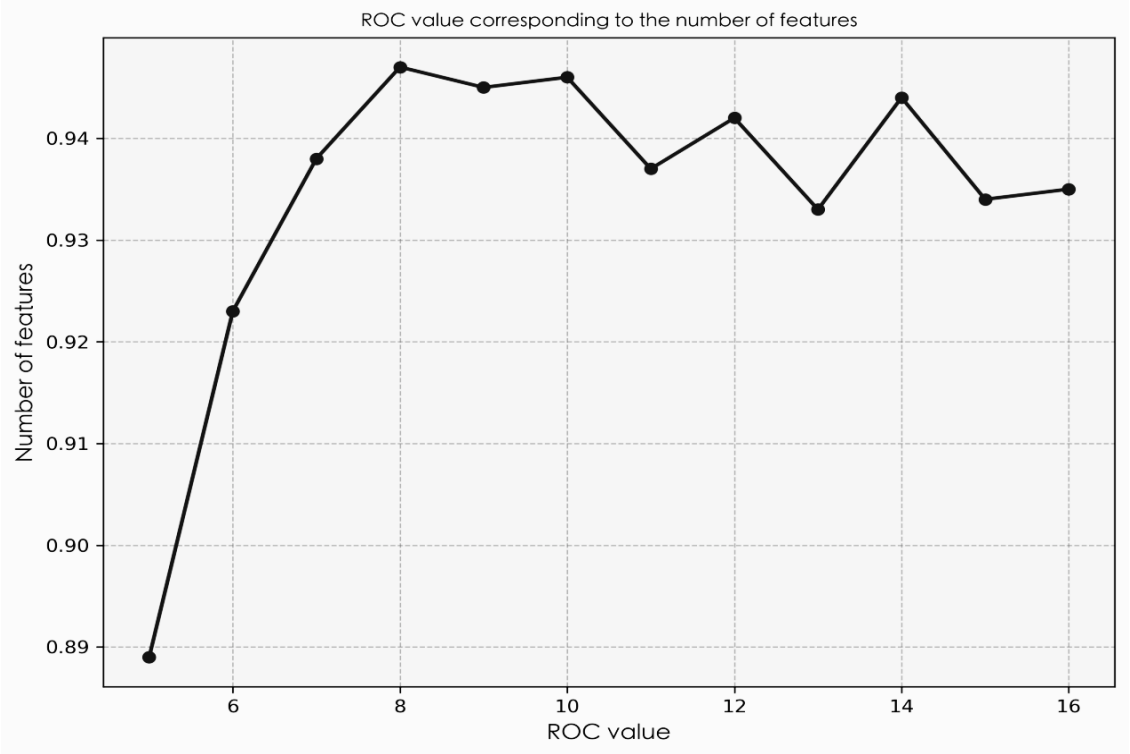

Figure 5: The corresponding ROC values for different numbers of features

4.2.2 Analysis of Flash Flood Disaster Leading Factors

Fig. 6 presents the importance assessment results of various factors. Daily average rainfall is identified as the most critical, followed by the number of days with rainfall exceeding 50 mm, indicating that rainfall-related indicators predominantly influence the final outcome. Among the three indicator categories, underlying surface factors rank second, with the longitudinal slope of the longest flow path exerting the most significant effect within this group. Among socio-economic factors, the small watershed population is the most influential. Overall, the analysis in Fig. 7 underscores the central role of rainfall indicators in prediction and analysis, while also emphasizing the significance of underlying surface characteristics and socio-economic factors. This findings provides scientific basis for further optimizing disaster risk assessments.

The study results further demonstrate that rainfall factors, socio-economic factors, and terrain factors all play key roles in the model. Validation using the classification feature elimination method reveals that the predictive accuracy decreases when only one type of indicator is retained thus substantiating the necessity of a multi-factor joint analysis to enhance model performance. This conclusion highlights the interdependence of different indicator types and offers theoretical support for optimizing future disaster risk assessment and prediction models.

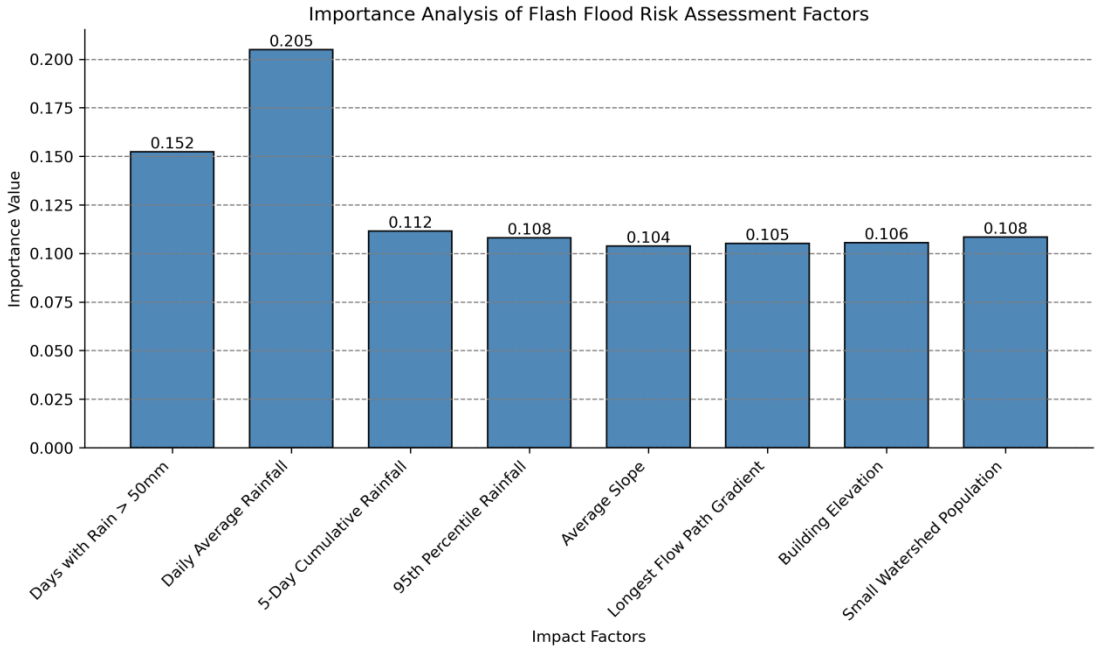

Figure 6: The importance of each feature in the optimal feature combination

Figure captions and table headings should be sufficient to explain the figure or table without needing to refer to the text. Figures and tables not cited in the text should not be presented. The following is an example for Table 1.

Table 2 Title of the Table

Type of nanoparticles	**Average size (nm)**	**Variance (nm)**
CuO	47	4.2
NiO	35	6.4
Al_2O_3	42	2.1
SnO_2	27	3.9

Tables and figures should be placed close after their first reference in the text. All figures and tables should be numbered with Arabic numerals. Table headings should be centred above the tables. Figure captions should be centred below the figures as shown in Figure 1.

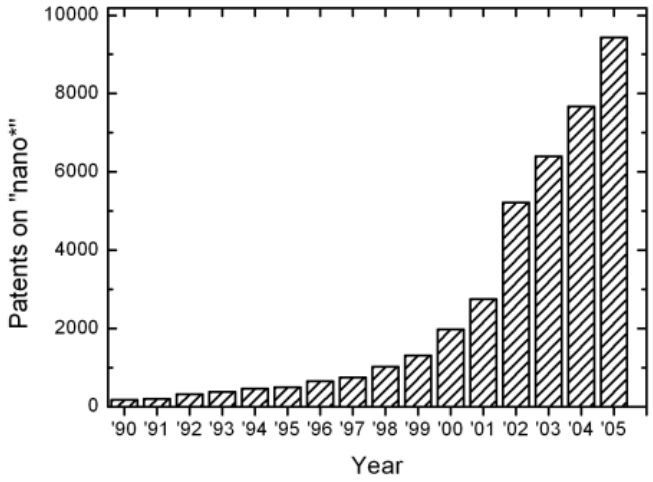

Figure 1: Number of patents on nanotechnology with time

5 CONCLUSIONS

This study developed a flash flood disaster risk prediction model by coupling Random Forest (RF) with Recursive Feature Elimination (RFE), systematically revealing the spatial distribution patterns of flash flood disaster risk levels and providing a scientific basis for disaster prevention. The study focuses on the southeastern coastal region of China, Fujian Province, and uses a classification recursive feature elimination method to optimize feature selection, identify key influencing factors, and build a high-precision risk assessment model, thereby improving the accuracy of risk prediction. The main conclusions are as follows:

(i)A flash flood risk assessment model based on the RFE-RF optimization algorithm was developed, achieving an ROC value exceeding 0.947, which demonstrates its high predictive capability.

(ii)Dominant predictive factors were identified, including the number of days with rainfall exceeding 50mm, daily average rainfall, cumulative rainfall over five consecutive days, 95th percentile rainfall, slope, longest flow path gradient, building elevation, and population in small watersheds.

(iii)Spatial analysis revealed that high-risk flash flood areas in Fujian Province are primarily concentrated in the Wuyi Mountains, Daiyun Mountains, and Hainan Mountains, where steep terrain and abundant rainfall increase the likelihood of flash floods.

The study provides technical support for the precise identification of high-risk flash flood areas and offers a scientific foundation for local governments and relevant agencies to develop disaster prevention and mitigation policies. The findings can guide the enhancement of flash flood monitoring, forecasting, and early warning systems, particularly in formulating detailed emergency response plans and raising public awareness of disaster prevention measures to minimize human and economic losses.

6 ACKNOWLEDGEMENTS

This work was supported by the Jing-Jin-Ji Regional Integrated Environmental Improvement-National Science and Technology Major Project (2025ZD1208302) and National Natural Science Foundation of China (NSFC) [Grant number: 52239006, 42201093].

REFERENCES

Al Kuisi, M., Al Azzam, N., Hyarat, T., Al-Qudah, K., Al-Mughaid, H., & Alshawamreh, B. (2023). Flood hazard and risk assessment of flash floods for Petra catchment area using hydrological and analytical hierarchy (AHP) modeling. Water, 15(16), 2910. https://doi.org/10.3390/w15162910

Biau, G., & Scornet, E. (2016). A random forest guided tour. TEST, 25(2), 197–227. https://doi.org/10.1007/s11749-016-0481-7

Bu, C., & Zhang, Z. (2020). Research on overfitting problem and correction in machine learning. Journal of Physics: Conference Series, 1693(1), 012100. https://doi.org/10.1088/1742-6596/1693/1/012100

Chen, G., Li, W., & Lin, K. (2017). GIS-based risk assessment of flash flood disasters in Qingyuan City. Pearl River, 38(10), 55–59.

Chu, Y., Song, W., & Chen, D. (2023). Risk identification of flash flood hazard using machine learning and Bayesian model averaging techniques. Water, 15(11), 1890–1897. https://doi.org/10.3390/w15111890

El-Saoud, W. A., & Othman, A. (2022). An integrated hydrological and hydraulic modelling approach for flash flood hazard assessment in eastern Makkah city, Saudi Arabia. Journal of Hydrology, 33(4), 102045. https://doi.org/10.1016/j.jhydrol.2022.102045

Fan, G., Tang, J., Gao, X., Wang, R., & Li, X. (2023). Risk assessment of flash flood disasters in the Western Region of Nanyang City based on LightGBM. China Rural Water and Hydropower, 8, 135–141.

Fu, X., Wang, Z., Qi, S., Song, L., & Han, X. (2024). Review and response process analysis of flash flood disasters from an emergency perspective: A case study of six typical events in 2022. Water Resources and Hydropower Engineering (in Chinese and English), 55(11), 15–25.

Han, Y., Lan, H., & Zhang, F. (2021). A dynamic recursive feature elimination framework (dRFE) to further refine a set of omic biomarkers. Bioinformatics, 37(18), 2845–2852. https://doi.org/10.1093/bioinformatics/btab151

Hu, X., & Song, L. (2018). Hydrodynamic modeling of flash flood in mountain watersheds based on high-performance GPU computing. Natural Hazards, 91(3), 1265–1284. https://doi.org/10.1007/s11069-018-3185-3

Jeon, H., & Oh, S. (2020). Hybrid-recursive feature elimination for efficient feature selection. Applied Sciences, 10(9), 3211. https://doi.org/10.3390/app10093211

Ju, W., Xing, Z., & Wu, J. (2024). Comprehensive risk assessment of natural disasters based on machine learning in Changzhou City, China. Environment, Development and Sustainability. Advance online publication. https://doi.org/10.1007/s10668-024-04485-w

Li, W., Cao, W., Wang, Y., & Zhao, J. (2019). Risk assessment and sensitivity analysis for flash floods in ungauged basins using coupled hydrological and hydrodynamic models. Journal of Hydrology, 574, 884–896. https://doi.org/10.1016/j.jhydrol.2019.04.093

Liang, L., & Bi, Q. (2020). Fujian Province innovates defense means to enhance the level of flash flood disaster prevention. China Flood Control & Drought Relief, 30(Z1), 105–108.

Liu, Z., Wang, H., & Zou, Y. (2025). Multi-scenario simulation study of flash flood disasters in the Zhaigang River Basin under the influence of water-related engineering. Water Resources and Hydropower Engineering (in Chinese and English), 56(1), 1–21.

Ma, M., Liu, C., Zhao, G., Li, J., & Wang, H. (2019). Flash flood risk analysis based on machine learning techniques in the Yunnan Province, China. Remote Sensing, 11(2), 197–203. https://doi.org/10.3390/rs11020197

Nugraheni, I. L., Widayati, A., Supriharyono, S., Suman, A., & Mahmudah, I. (2018). Flood disaster mitigation modeling using participation community based on land conversion and disaster resilience. International Journal of Environmental Science and Development, 9(4), 98–102.

Raillani, H., Chen, W., Ye, Z., & Zhang, Q. (2023). Uncertainty quantification for disaster modelling: Flooding as a case study. Stochastic Environmental Research and Risk Assessment, 5(1), 1–7. https://doi.org/10.1007/s00477-023-02448-7

Ruida, S., Saha, A., Islam, A. R. M. T., Kundu, B., & Matin, A. (2022). Development of geo-environmental factors controlled flash flood hazard map for emergency relief operation in complex hydro-geomorphic environment of tropical river, India. Environmental Science and Pollution Research, 29, 1–16. https://doi.org/10.1007/s11356-022-19220-3

Salih, A., & Hassablla, A. (2024). Flash flood risk assessment in the Asir region, southwestern Saudi Arabia, using a physically-based distributed hydrological model and GPM IMERG satellite rainfall data. Atmosphere, 15(6), 624. https://doi.org/10.3390/atmos15060624

Shuang, Y., Xin, M., & Yu, L. (2018). Risk assessment of flash flood disasters in Datong City based on fuzzy comprehensive evaluation method. China Water Resources and Hydropower Engineering, 49(5), 84–89.

Sun, L., Renberth, K. E., Ren, Z., & Li, C. (2022). Development of an ensemble Bayesian inference-based copula approach for bivariate risk evaluation of extreme precipitation under climate change. International Journal of Climatology, 42(14), 7417–7436. https://doi.org/10.1002/joc.7668

Wibowo, R. C., Sarkowi, M., Setiawan, A. F., & Prasetyo, Y. (2020). Flash flood hazard areas assessment in Bandar Negeri Suoh (BNS) region using an index-based approach and analytical hierarchy process. Journal of Physics: Conference Series, 1434(1), 012006. https://doi.org/10.1088/1742-6596/1434/1/012006

Xiong, J., Lu, D., Tian, F., & Liu, H. (2020). Spatiotemporal characteristics and driving force analysis of flash floods in Fujian Province. International Journal of Geo-Information, 9(2), 133–137. https://doi.org/10.3390/ijgi9020133

Yang, L., Fang, X., Yuan, L., & Wang, X. (2023). Sensitivity analysis of flash flood factors and disaster risk assessment in small watersheds of Jiangxi Province. Science Technology and Engineering, 23(10), 4448–4456.

Zhang, J., Dong, L., Zhang, N., & Li, Y. (2024). GIS-based risk assessment of flash flood disasters in Xinjiang Uyghur Autonomous Region. Yangtze River, 55(11), 81–88, 95.

Zhang, Q., Zhang, H., Li, Y., & Wang, S. (2019). Research on Chongqing flash flood disaster risk assessment system based on AHP-GIS. In IOP Conference Series: Earth and Environmental Science (Vol. 330, No. 3, p. 032028). IOP Publishing. https://doi.org/10.1088/1755-1315/330/3/032028

Zhang, W., Ma, G., Wu, J., & Li, X. (2020). Assessment of flood inundation by coupled 1D/2D hydrodynamic modeling: A case study in mountainous watersheds along the coast of Southeast China. Water, 12(9), 2550. https://doi.org/10.3390/w12092550

Zhang, X., Liu, R., Liu, Q., Li, C., & Guo, L. (2019). Risk identification and quantitative analysis of flash flood disasters in Fujian Province. Journal of China Institute of Water Resources and Hydropower Research, 17(4), 6–12.

ICFM 10
Adapting to Global Change:
Innovative Approaches to Flood Management and Resilience
May 20-22, 2026 | Western University, London, Ontario, Canada

Vulnerability Analysis of China's Integrated Transportation Network Under Flooding: A Case Study of the July 20 Heavy Rain in Zhengzhou

Jingjing Kong[1], Shuhe Lian[1], Chao Zhang[2]
School of Civil Engineering, Shanghai Normal University, Shanghai, China[1]
E-mail: kongjingjing@shnu.edu.cn

School of Finance, Shanghai University of Finance and Economics, Shanghai, China [2]
E-mail: zhang.chao@sufe.edu.cn

ABSTRACT

Frequent extreme rainfall and flooding increasingly threaten transportation system performance. This study constructs a China-wide integrated transportation network of expressways, railways, and aviation and develops a post-disaster passenger mode-switching model to assess network vulnerability based on passenger flow, travel delay, and on-time arrival rate. Using the July 20, 2021 Zhengzhou heavy rain as a case study, results show that modal complementarity limits functional degradation at the national scale, yielding relatively low overall vulnerability, with railways being the most vulnerable, followed by expressways and aviation. In flood-affected regions, however, vulnerability increases substantially, with aviation most affected, followed by expressways and railways. The findings provide quantitative support for flood risk management and resilience enhancement of integrated transportation systems.

KEYWORDS: comprehensive transportation system, vulnerability analysis, passenger flow, passenger delay time, passenger punctuality

1 INTRODUCTION

Transportation infrastructure, including highways, railways, and aviation systems, plays a critical role in supporting large-scale intercity passenger and freight mobility. In recent years, however, the increasing frequency and intensity of extreme weather events—particularly extreme rainfall and flooding—have posed growing threats to the functional safety and service continuity of transportation systems, leading to widespread disruptions and substantial economic and social losses. China has experienced multiple large-scale transportation disruptions caused by extreme weather, such as the 2008 southern China snow and ice disaster, the 2012 Beijing rainstorm, Typhoon Lekima in 2019, and the July 2021 extreme rainstorm in Zhengzhou, all of which resulted in expressway closures, railway suspensions, and large-scale flight cancellations.

Transportation system vulnerability is commonly defined as the sensitivity of a system to events that may cause a substantial reduction in service capacity (Berdica, 2002). Existing studies have extensively examined the vulnerability of individual transportation systems using network-based models, in which structural vulnerability is evaluated through topological indicators such as connectivity, centrality, clustering coefficient, and accessibility (Zhang et al., 2016; Kasturi and Amy, 2020; Yin and Wang, 2020; Sen et al., 2021). To better reflect real-world disruptions, a growing body of literature incorporates traffic flows and performance indicators—such as passenger volume, travel delay, and service disruption—into vulnerability analysis (Fang et al., 2016; Hong et al., 2015; Hong et al., 2019; Voltes-Dorta et al., 2017).

With increasing modal integration, transportation systems are interconnected through travelers' mode choice behavior, making integrated transportation networks more complex. Recent studies have examined complementary transportation systems, particularly coupled high-speed rail and aviation

networks, and shown that modal complementarity can partially mitigate vulnerability by providing alternative travel options (Ouyang et al., 2015; Li et al., 2019; Feng et al., 2021; Li and Rong, 2022). Nevertheless, existing research still pays limited attention to large-scale infrastructure failures caused by extreme weather and the resulting cascading disruptions across multiple transportation modes. Moreover, passenger behavioral responses—especially post-disaster mode switching—are often simplified or neglected.

To address these gaps, this study constructs a national integrated transportation network comprising expressway, railway, and aviation systems and develops a post-disaster passenger mode-switching model to capture interactions among transportation modes. Using the July 20, 2021 Zhengzhou extreme rainstorm as a case study, the proposed framework simulates the dynamic evolution of passenger flow, travel delay, and on-time arrival rate, thereby assessing the vulnerability of the national integrated transportation network from a functional perspective.

2 MODEL FORMULATION

2.1 Construction of the Integrated Transportation Infrastructure Network

To represent China's integrated transportation system, a three-layer network is constructed based on expressways, railways, and aviation. The integrated transportation infrastructure network is defined as $G=\{G_H, G_R, G_A\}$, as illustrated in Figure 1, where nodes correspond to prefecture-level cities.

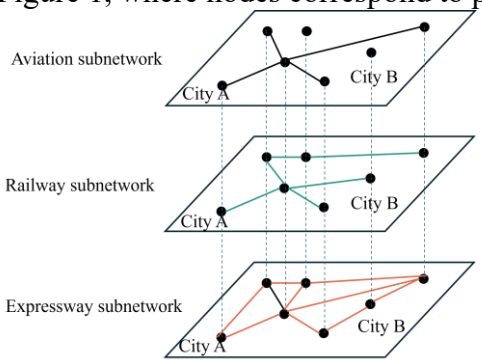

Figure 1: Schematic diagram of integrated transportation network

In the expressway subnetwork G_H, edges represent direct expressway connections between cities. The network is defined as $G_H=\{N_H, E_H, L_H\}$, where N_H denotes the set of cities connected by expressways, E_H the set of expressway links, and L_H the corresponding link lengths. Similarly, the railway subnetwork is defined as $G_R=\{N_R, E_R, L_R\}$, and the aviation subnetwork is defined as $G_A=\{N_A, E_A, L_A\}$.

To construct the national integrated transportation network, 293 prefecture-level cities with at least one of the three transportation modes are selected as nodes. City coordinate data and expressway and railway network data are obtained from the Amap (AMAP) open platform, while aviation network data are sourced from the OAG Analytics global aviation database. Owing to differences in infrastructure availability across cities, the expressway network contains 293 nodes and 625 edges, the railway network contains 275 nodes and 1,362 edges, and the aviation network contains 137 nodes and 1,949 edges.

2.2 Traffic Flow Modelling in Single-Layer Transportation Networks

To assess the impact of extreme weather on transportation service capacity, baseline passenger flows of expressway, railway, and aviation systems under normal conditions are first estimated.

For the expressway network, intercity coach schedules from the Checi platform (October 16, 2019) are used to identify direct services between city pairs. Passenger flows are allocated using an all-or-

nothing assignment along shortest paths, with vehicle type proportions determined based on national statistics.

For the railway network, train timetables released by the China Railway Customer Service Center (October 16, 2019) are used to construct intercity origin–destination pairs. For each pair, the train service with the fewest intermediate stops is selected as the representative flow. Given the short ticket inspection time, railway waiting time is not explicitly considered.

For the aviation network, only domestic prefecture-level flights are included. Flight schedules and passenger data are obtained from OAG Analytics (October 16, 2019), and a minimum pre-departure waiting time of 30 minutes is assumed in accordance with civil aviation regulations.

To ensure comparability across transportation modes, expressway vehicle flows, railway train capacities, and aircraft seating capacities are converted into passenger volumes using mode-specific assumptions. A standard passenger car is assumed to carry one passenger, train capacity corresponds to a conventional 16-car train set, and flight capacity equals the maximum seating capacity of the aircraft type. City-level origin–destination data are filtered and verified using Python. Due to data limitations, Hong Kong, Macao, and Taiwan are excluded from the analysis.

2.3 Passenger Mode Switching Model

Extreme weather may disrupt transportation services through expressway closures, railway station shutdowns, or airport closures, resulting in congestion and large numbers of stranded passengers. Assuming that passengers do not cancel their trips, they may switch travel modes to reach their destinations, thereby creating interactions among expressway, railway, and aviation networks. Under severe disruptions, travel time is assumed to be the primary criterion guiding passengers' mode choice.

Because railway and aviation services operate on fixed timetables, travel time after switching modes includes both waiting time for the next available service and in-vehicle travel time. Urban access time associated with mode switching is not considered, and waiting time is ignored when switching to expressways. The remaining travel time after switching modes is defined as the minimum sum of waiting time and in-vehicle travel time across all available modes:

$$\boldsymbol{T}_{iD}^{change} = \min_{v \in \Omega^{-}} \{\boldsymbol{T}_{iD}^{wait_v} + \boldsymbol{T}_{iD}^{trval_v}\} \tag{1}$$

where v denotes an alternative travel mode, and Ω is the set of available modes, including expressway, railway, and aviation. $\boldsymbol{T}_{iD}^{wait_v}$ represents the required waiting time before boarding mode v, and $\boldsymbol{T}_{iD}^{trval_v}$ denotes the corresponding in-vehicle travel time to destination D.

When disruptions occur, passengers stranded at a network node (city i) evaluate alternative modes based on the remaining travel time and switch only if sufficient capacity is available. If the selected mode exceeds its capacity constraint, another mode is considered. If all alternatives are capacity-constrained, the passenger remains stranded until service is restored. Passengers stranded on network links (e.g., expressway or railway segments) are assumed unable to switch modes and continue along the original route until infrastructure recovery. This process represents a flow reallocation mechanism across complementary transportation networks under capacity constraints.

2.4 Vulnerability Metrics for the National Integrated Transportation Network

From the perspective of transportation service performance, network vulnerability is evaluated using three key indicators: passenger flow, average travel delay, and on-time arrival rate. Vulnerability is quantified by the magnitude of changes in these indicators after extreme weather events, with larger deviations indicating higher vulnerability.

(1) Passenger Flow

Passenger flow at time t is defined as the total flow across expressway, railway, and aviation networks. Under normal conditions, flows follow shortest paths and published schedules. After extreme events, infrastructure disruptions such as road closures, train cancellations, and flight suspensions lead to congestion and flow redistribution across modes. Expressway flows are constrained by roadway capacity, while railway and aviation flows are limited by train and aircraft capacities. Passengers stranded on

network links remain on the original route until recovery, whereas those stranded at nodes may switch modes subject to capacity constraints, resulting in dynamic flow reallocation.

(2) Average Travel Delay

Average travel delay captures the extent to which passengers fail to reach their destinations as planned. It is defined as the passenger-flow-weighted average delay across transportation modes. For expressways, delays arise from congestion and closures; for railways and aviation, delays result from disrupted or cancelled services. When mode switching is allowed, delays also include waiting time and remaining travel time after switching, capturing both direct disruption effects and indirect impacts of passenger reallocation.

(3) On-Time Arrival Rate

The on-time arrival rate measures system reliability under extreme conditions. It is defined as the passenger-flow-weighted proportion of travelers who arrive within their planned travel time across all modes, accounting for both original and mode-switched trips. Lower on-time arrival rates indicate more severe disruptions and higher network vulnerability.

3 SIMULATION ANALYSIS

3.1 Scenario Construction: The July 20, 2021 Zhengzhou Rainstorm

From July 17 to July 23, 2021, Henan Province experienced an unprecedented extreme rainstorm, with Zhengzhou being the most severely affected city. The spatial distribution of cumulative precipitation in Henan province from July 17 to 21 is shown in Figure 2.

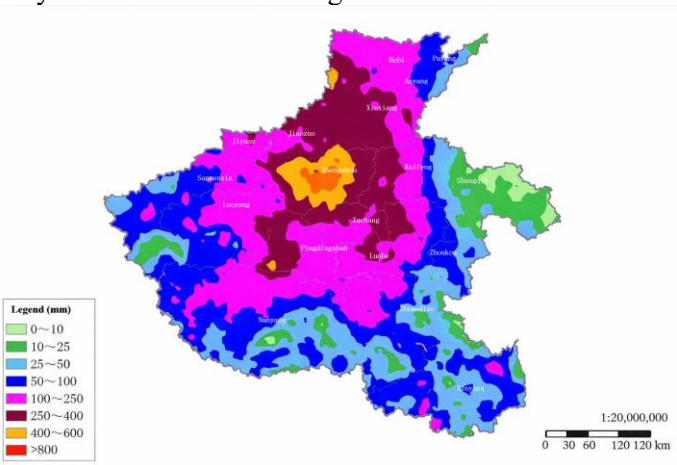

Figure 2: The spatial distribution of cumulative precipitation in Henan province from July 17 to 21

Record-breaking cumulative and hourly rainfall occurred during this period, causing widespread disruptions to transportation infrastructure, including expressway closures, railway service suspensions due to flooded tracks and damaged facilities, and large-scale flight cancellations at Zhengzhou Airport. Based on the observed impacts, a disaster scenario is constructed in which all expressway links, railway stations, and airports within the affected area are assumed to be closed, resulting in the suspension of corresponding services. Transportation facilities are assumed to operate in either a normal or failed state. The disaster onset time is set to 17:00 on July 20, corresponding to the peak hourly rainfall. Passenger flows are updated dynamically according to the proposed passenger flow and mode-switching models.

3.2 Vulnerability Analysis of the National Integrated Transportation Network

The simulation adopts a time step of 0.5 hours, yielding 48 time steps per day. Network performance is evaluated using three indicators—passenger flow, average travel delay, and on-time arrival rate—under both scenarios with and without passenger mode switching. To better demonstrate the post-disaster changes, the curve under normal conditions is also presented as a baseline for comparison. The normal or baseline state is defined as the routine operating condition of the integrated transport

system in the absence of extreme rainfall and flooding impacts. Under this condition, all relevant transport links and nodes are assumed to remain fully functional and accessible.

(1) Passenger Flow

Figure 3 illustrates the temporal evolution of passenger flow in the national integrated transportation network. Under normal conditions, passenger flow exhibits a clear 24-hour periodic pattern. After the disaster, total passenger flow increases slightly regardless of whether passenger mode switching is considered, as some passengers are unable to reach their destinations and remain within the network.

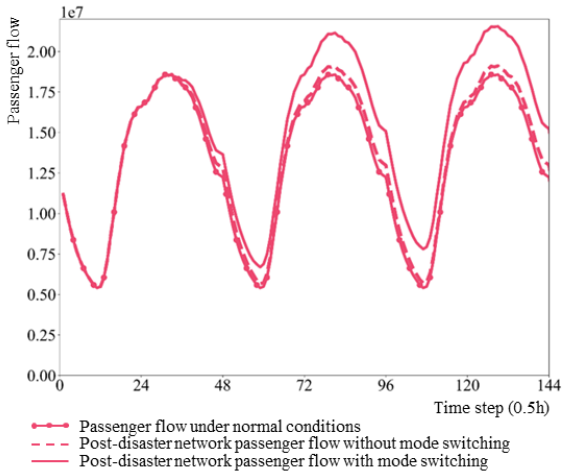

Figure 3: Passenger flow of China's integrated transportation network

To further examine the contribution of different transportation modes, Figure 4 presents passenger flow variations in expressway, railway, and aviation networks. After the disaster, expressway passenger flow increases, while railway and aviation passenger flows decline. When passenger mode switching is allowed, the increase in expressway flow becomes more pronounced, whereas the reductions in railway and aviation flows are larger. This indicates that passengers tend to switch from rail and air transport to expressways under prolonged service disruptions. In terms of flow variation, the expressway network exhibits the highest vulnerability, followed by the railway network, while the aviation network is the least affected.

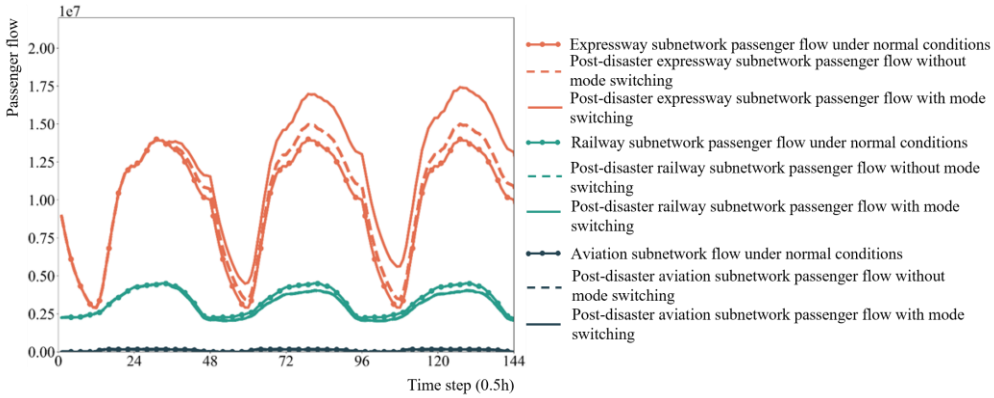

Figure 4: Passenger flow of subnetworks

(2) Average Travel Delay

Figure 4 shows the average travel delay of the national integrated transportation network. After the disaster, average delay increases continuously, with a progressively rising growth rate. When passenger mode switching is allowed, average delay is consistently lower than in the no-switching scenario, indicating that mode switching can partially mitigate delay accumulation. Nevertheless, delays can still reach several times the normal average travel time, suggesting high vulnerability from a delay perspective.

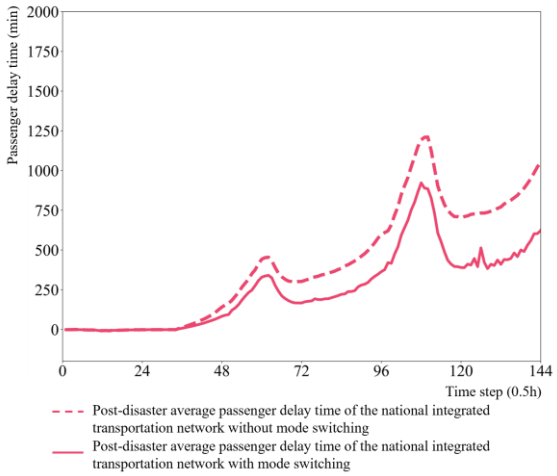

Figure 5: Average travel delay of China's integrated transportation network

Figure 6 further reports average travel delays by transportation mode. Without mode switching, railway delays are the largest, followed by aviation, while expressways experience the smallest delays. Allowing passenger mode switching substantially reduces delays in railway and aviation networks, but has limited impact on expressway delays due to capacity constraints. The two rapid growth phases of network-wide average delay are mainly driven by sharp increases in expressway and aviation delays.

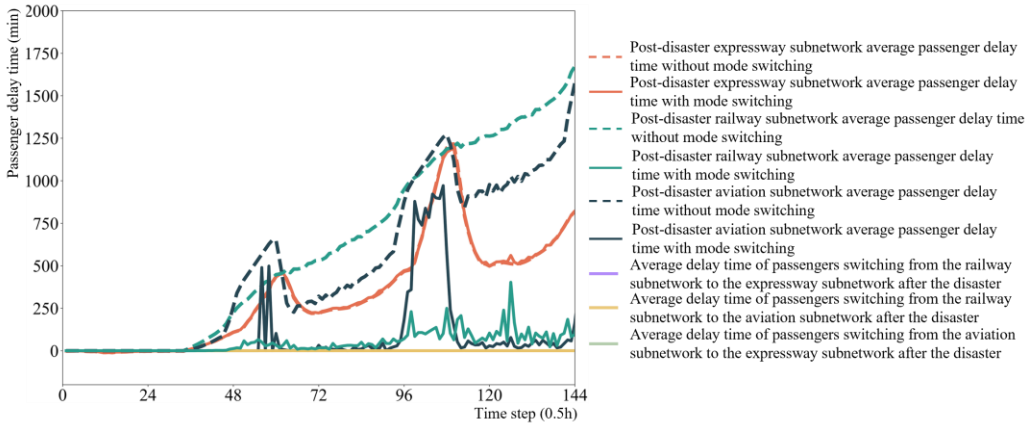

Figure 6: Average travel delay of subnetworks

(3) On-Time Arrival Rate

Figure 7 presents the on-time arrival rate of the national integrated transportation network. After the disaster, the on-time arrival rate experiences several sharp declines, corresponding to the disaster onset and periods of rapidly increasing delays. When passenger mode switching is considered, the on-time arrival rate is lower than in the no-switching scenario, as most switching involves longer expressway travel times.

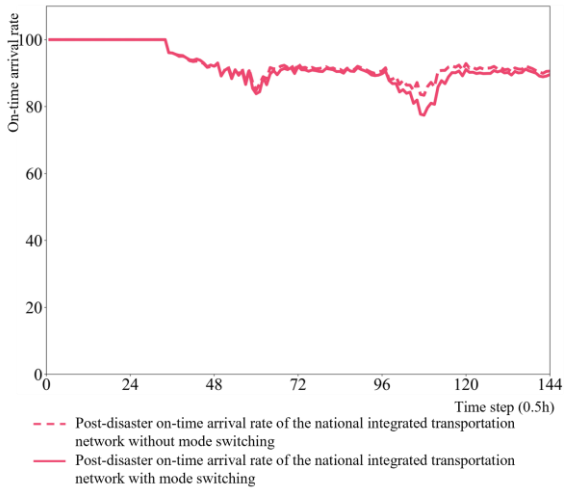

Figure 7: On-time arrival rate of China's integrated transportation network

Figure 8 reports on-time arrival rates for expressway, railway, and aviation networks. Aviation experiences the smallest decline, followed by expressways, while railways exhibit the largest reduction. These differences reflect the fixed schedules of rail and air services and the longer travel times associated with expressway substitution. The on-time arrival rates of railway and aviation networks are largely unaffected by whether mode switching is considered, as passengers originally using these modes cannot arrive on time once switching occurs.

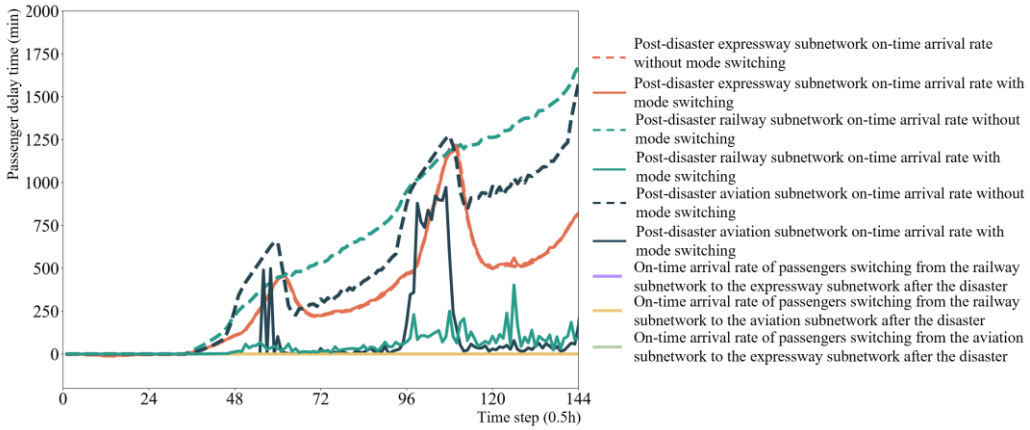

Figure 8: On-time arrival rate of subnetworks

Overall, the July 20 Zhengzhou rainstorm causes moderate disruptions to passenger flow and on-time arrival rates, but leads to substantial increases in travel delays. This indicates that the national integrated transportation network is more vulnerable from a delay perspective than from a flow or punctuality perspective. Allowing passenger mode switching reduces average travel delays but may further lower on-time arrival rates. From a mode-specific perspective, the expressway network exhibits the lowest vulnerability in terms of accessibility, followed by aviation, while the railway network shows the highest vulnerability when passenger flow, travel delay, and on-time arrival rate are jointly considered.

4 CONCLUSION

This study proposes a post-disaster passenger mode-switching framework for a national integrated transportation network and evaluates functional vulnerability using the July 20, 2021 Zhengzhou rainstorm. Results indicate that China's transportation system exhibits low system-

level vulnerability due to strong modal complementarity, with railways being the most vulnerable, followed by expressways and aviation. The framework is extensible to other integrated transportation systems, while future work should incorporate behavioral responses, transfer times, and extreme congestion effects.

REFERENCES

Berdica K. (2002). An introduction to road vulnerability: What has been done, is done and should be done. *Transport Policy*, 9, 117–127.

Fang S., Bian K. and Xie K. (2016). Vulnerability analysis of highway traffic networks using origin–destination tollgate data. *Proc. IEEE Int. Conf. Intell. Transp. Syst.*, 1–6.

Feng X., He S., Chen X. et al. (2021). Mitigating the vulnerability of an air–high-speed railway transportation network: From the perspective of predisruption response. *Proc. Inst. Mech. Eng. Part O*, 235, 474–490.

Hong L., Ouyang M., Peeta S. et al. (2015). Vulnerability assessment and mitigation for the Chinese railway system under floods. *Reliab. Eng. Syst. Saf.*, 137, 58–68.

Hong L., Ye B., Yan H. et al. (2019). Spatiotemporal vulnerability analysis of railway systems with heterogeneous train flows. *Transp. Res. Part A*, 130, 725–744.

Kasturi M. and Amy M.K. (2020). Vulnerability assessment of Alberta's provincial highway network. *Transp. Res. Interdiscip. Perspect.*, 6, 100071.

Li T., Rong L. and Yan K. (2019). Vulnerability analysis and critical area identification of public transport systems: A case of high-speed rail and air transport coupling in China. *Transp. Res. Part A*, 127, 55–70.

Li T. and Rong L. (2022). Spatiotemporally complementary effect of high-speed rail network on robustness of aviation network. *Transp. Res. Part A*, 155, 95–114.

Ouyang M., Pan Z. and He Y. (2015). Vulnerability analysis of complementary transportation systems with applications to railway and airline systems in China. *Reliab. Eng. Syst. Saf.*, 142, 248–257.

Sen P., Dasgupta S., Chatterjee A. et al. (2021). Impacts of service features on vulnerability analysis of high-speed rail networks. *Transport Policy*, 110, 238–253.

Voltes-Dorta A., Rodríguez-Déniz H. and Suau-Sánchez P. (2017). Vulnerability of the European air transport network to major airport closures from the perspective of passenger delays: Ranking the most critical airports. *Transp. Res. Part A*, 96, 119–145.

Yin L. and Wang Y. (2020). Network characteristics and vulnerability analysis of Chinese railway networks under earthquake disasters. *Int. J. Geo-Inf.*, 9, 697.

Zhang J., Hu F., Wang S. et al. (2016). Structural vulnerability and intervention of high-speed railway networks. *Physica A*, 462, 743–751.

ICFM 10
Adapting to Global Change:
Innovative Approaches to Flood Management and Resilience
May 20-22, 2026 | Western University, London, Ontario, Canada

Fuzzy logic control implementation for flow regulation in stormwater urban reservoirs

Mateo Hernández Sánchez[1] and Eduardo Mario Mediondo[2]

University of São Paulo, Department of Hydraulic Engineering and Sanitation- São Carlos School of Engineering, São Carlos, Brazil[1,2]
E-mail [1]: mathernandezsan@usp.br / mateohs23@gmail.com
E-mail [2]: emm@sc.usp.br

ABSTRACT

The uncertainty surrounding climate change and urban expansion adds pressure to urban drainage systems by increasing rainfall frequency and elevating peak runoff rates. To reduce urban flooding, stormwater infrastructure can be managed in real-time by retrofitting it with sensors and controllable gates, facilitating dynamic adjustments across entire watersheds during rainfall events and enhancing the resilience of these structures. In this study, we introduce a Fuzzy Logic Control (FLC) implementation for five online stormwater reservoirs located in the Aricanduva basin (São Paulo, Brazil), using experience-based rules aimed at promoting intelligent flood mitigation decision-making, as the first steps to implementing real-time control systems. A 2D hydrodynamic model was employed to apply FLC in the five reservoirs, and their effectiveness in reducing flood effects was evaluated using a 25-year design storm hydrograph. The findings indicate that the FLC implementation decreases peak flow by 38.15%, 20.60%, 14.40%, and 12.04% in the Aricanduva I, Limoeiro, Caguaçu, and Aricanduva III reservoirs, respectively. However, for the Aricanduva II reservoir, the peak flow increases by 2.11%. In contrast, the accumulated volume flooding reduction values were 1.20%, 0.60%, and 0.58% in the Aricanduva I, Limoeiro, and Aricanduva III reservoirs, respectively, while the values were -5.83% and -2.11% for the Caguaçu and Aricanduva II reservoirs, respectively. This approach allows for the assessment of which reservoirs with FLC implementation could effectively assist flood risk managers in reducing urban flooding, particularly in data-scarce watersheds. This research aligns with the Sustainable Development Goals (SDGs) 6, 9, 11, and 13 by improving resilient urban drainage systems, alleviating climate-related flood risks, safeguarding water ecosystems, and integrating smart technologies for adaptive infrastructure.

KEYWORDS: Fuzzy Logic Control (FLC); Flood control; Stormwater management reservoirs; Urban flooding.

1 INTRODUCTION

The rapid growth of megacities with an intense densification and verticalization, the aging infrastructure and along with the increasing frequency and intensity of extreme weather events, presents significant challenges to become cities resilient to urban floods. Urban flood risk management focuses on developing strategies to mitigate the impacts of climate change, particularly the damages resulting from flooding caused by the overflow of urban rivers or canals. Building a resilient city entails the capacity to adapt to such hazards, thereby reducing human and economic losses while leveraging natural advantages for sustainable urban development (Nkwunonwo et al., 2020).

There are modeling approaches to simulate the complex non-linear dynamics of urban floods and assess their impacts or the effectiveness of the measures against them. Some of them are focus on the

optimal operation of the detention or retention urban reservoirs by implementing Real-time control (RTC) strategies on outlet devices (e.g., pump systems, orifices, gates) (Qi et al., 2021; Li, 2020).

Despite its significant potential benefits, the implementation of RTC strategies in urban drainage systems remains limited to only a few cities worldwide (Lund et al., 2018). Additionally, existing studies have largely been conducted in catchments with high-quality and detailed data on urban drainage networks, including high-resolution flow and water level time series (Mounce et al., 2020; Li, 2020), or with a suitable sensor distribution (Bartos and Kerkez, 2021). Such data availability is relatively rare in urban basins of less developed countries, highlighting a critical gap in knowledge and practice (Sánchez, 2025).

This study aims to reduce a crucial knowledge gap by providing the first steps of the implementation of Fuzzy Logic Control (FLC) as a RTC flood risk reduction measure. Specifically, it investigates that manually configuration of a Fuzzy Interference System (FIS) for each outlet device of multiple urban reservoirs can reduce peak flow and the accumulated flooding volume. The configuration of each FIS was done by a rule-based method that take into account the constructive characteristics of the reservoir. After that, it was compared the flow rates of a rainfall-runoff simulation with a design precipitation of 25-year return period of the baseline and FLC implementation scenario by using two indexes.

This control approach is planned to be applied in an urban basin with poorly gauged characteristics, serving as a proof of concept for the practical application of a fuzzy real-time control in outlet devices of reservoirs with monitoring limitations. Overall, this analysis represents the initial steps toward evaluating the potential of the FLC control implementation as a reactive control strategy and contributes to the broader discussion on urban flood risk management in less developed countries.

2 MATERIALS AND METHODS

This study implemented a reproducible framework to address the implementation of a flow control strategy with data scarcity conditions in an urban watershed, by using the open source hydrodynamic-hydrological model HydroPol2D (Gomes Jr et al., 2023) with a FAIR data principles approach (Wilkinson et al., 2016).

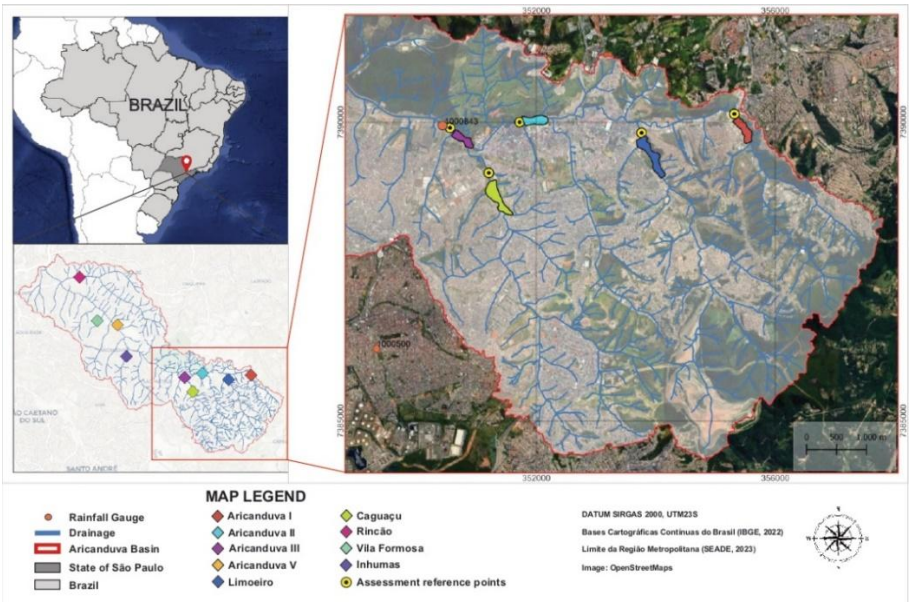

Figure 1: Location of the analysed reservoirs in the study. Taken from Sánchez (2025).

We chose the upstream online reservoirs of the Aricanduva watershed to implement the controllers. This watershed is one of the largest within the São Paulo Metropolitan Area (SPMA), located in the eastern

part of the city and encompasses approximately 100 km^2, where multiple studies had assessed its vulnerability to floods (Sanchez, 2025). The online reservoirs where the FLC is implemented are Limoeiro, Caguaçu, and Aricanduva I, Aricanduva II, and Acricanduva III (Figure 1).

To evaluate FLC performance for each stormwater reservoir, we simulated hydrographs generated by the SCS Unit Hydrographs Runoff Method based on each reservoir's drainage area characteristics. Then, we compared the baseline scenario (without FLC implementation) with the control scenario (with FLC implementation) by using the Accumulated Flooding Volume Reduction (AFVR) (Li, 2020) and the Peak Flow Reduction (PFR) indexes.

2.1 Fuzzy Logic Control implementation

The stormwater reservoirs analysed have culverts and spillways as outlet devices. These structures were modeled through rating curves as a function of the water level (Gomes Jr et al., 2024). However, if the culvert and the spillway are retrofitted with a vertically controllable device that modifies the cross-sectional area, the sluice fate equation with discharge to the atmosphere, can be applied (Sánchez, 2025). Thus, these devices have the dual functionality of culvert /spillway or gated culvert/gated spillway (Sánchez, 2025).

The development of a fuzzy controller involves the building of a Fuzzy Interference System. The FIS is established with two components: the controller membership function parameters (CMFPs) and the fuzzy control rules (FCRs) (Li, 2020). The CMPs implemented for controlling the gated culvert and the gated spillway of the reservoirs are defined for two input variables and one output variable. The first input variable is the water level (WL) at the current time and the second input variable is the water level variation (WLV) between the control intervals.

The WL has three membership functions (MFs) in the gated culvert case and four in the gated spillway case. On the other hand, The WLV has five MFs in the gated culvert and two in the gated spillway case. Lastly the output variable is the Gate Opening (GO), selected to characterize gate openness, defined with five MFs ranging from 0% to 100% in increments of 25%. This output variable is the same for both outlet devices.

The FCRs are based on CMFP values and establish an effective IF-THEN statement by defining the degree of relationship between the input and output MFs. Table 1 shows the inputs MFs and summarizes a total of fifteen FCRs for each reservoir in the gated culvert case. Table 2 shows the input MFs and summarizes eight FCRs for each reservoir in gated spillway case. The defuzzification method chose was Mean of Maxima (MOM), that is the commonly used in the creation of FISs. Taking into account the established rules and the method of defuzzification can be generated an output surface, which describes all possible combinations of WL and WLV across the range, as well as their relation with GO.

Table 1 Title of the Table

Reservoirs	Water Level (WL)	Water Level Variation (WLV)				
		N. High (NH)	N. Low (NL)	Zero (Z)	P. Low (PL)	P. High (PH)
Aricanduva I	Low (L)	Open 25	Open 25	Open 100	Open 50	Open 50
	Medium (M)	Open 25	Open 25	Open 100	Open 50	Open 75
	High (H)	Open 75	Open 75	Open 100	Open 100	Open 100
Limoeiro	Low (L)	Open 25	Open 25	Open 25	Open 50	Open 50
	Medium (M)	Open 25	Open 25	Open 50	Open 75	Open 75
	High (H)	Open 50	Open 50	Open 75	Open 100	Open 100
Caguaçu	Low (L)	Open 25	Open 25	Open 25	Open 50	Open 50
	Medium (M)	Open 25	Open 25	Open 25	Open 75	Open 75
	High (H)	Open 25	Open 50	Open 50	Open 100	Open 100
Aricanduva II	Low (L)	Open 25	Open 25	Open 25	Open 50	Open 50
	Medium (M)	Open 25	Open 25	Open 25	Open 75	Open 75

	High (H)	Open 50	Open 50	Open 50	Open 100	Open 100
Aricanduva III	Low (L)	Open 25	Open 25	Open 25	Open 50	Open 50
	Medium (M)	Open 25	Open 25	Open 25	Open 75	Open 75
	High (H)	Open 25	Open 50	Open 50	Open 100	Open 100

Table 2 Title of the Table

Reservoirs	Water Level Variation (WLV)	Water Level (WL)			
		Low (L)	M. Low (ML)	M. High (MH)	High (H)
Aricanduva I	Negative (N)	Open 0	Open 0	Open 25	Open 25
	High (H)	Open 0	Open 0	Open 25	Open 50
Limoeiro	Negative (N)	Open 0	Open 0	Open 25	Open 25
	High (H)	Open 0	Open 25	Open 25	Open 50
Caguaçu	Negative (N)	Open 0	Open 25	Open 25	Open 25
	High (H)	Open 0	Open 25	Open 25	Open 50
Aricanduva II	Negative (N)	Open 0	Open 0	Open 0	Open 25
	High (H)	Open 0	Open 25	Open 25	Open 50
Aricanduva III	Negative (N)	Open 0	Open 0	Open 25	Open 25
	High (H)	Open 0	Open 25	Open 25	Open 50

This study used a coupled hydrological-hydrodynamic model, called HydroPol2D (Gomes Jr et al., 2023), of the Aricanduva river Basin previously calibrated (Sánchez, 2025) for the implementation of this controller. The model is an open code source based on MATLAB programming language, providing the possibility to modify their modules and the implementation of the FLC by creating ".fis files". Therefore, for our approach the process begins with HydroPol2D's hydrological-hydraulic solver. Then, as we established a control interval of five minutes, during the simulation time every five minutes is done the FIS evaluation using the current state conditions of WL and WLV. Later, the output generated by the FIS is defuzzified into gate openness and will adjust the boundary internal conditions of the gated culvert and spillway. This looping mechanism is to represent the conditions of an RTC simulation.

2.2 Simulated hydrographs

The inflow hydrographs for each reservoir were determined by using the SCS Unit Hydrograph Method. The curve number were calculated by weighting the land use land cover areas form Brown et al. (2022) and considering references to the curve number from HEC-HMS within each drainage area. The time of concentration was estimated by using both the California (USBR) and Kiprich methods. The duration of the event between reservoirs varies and a time step of 10 minutes was determined.

Storm events were modeled by using an alternating block method derived from the equation of the intensity-duration-frequency (IDF) curve (Equation 1) obtained from the Aricanduva River Watershed Notebook (FCTH, 2022). The rain was characterized by a duration of 2 hours and a 25-year return period.

$$I_{t_d,t_r} = 32.77(t_d + 20)^{-0.878} + 16.1(t_d + 30)^{-0.9306}\left\{-0.4692 - 0.8474\, ln\left[ln\left(\frac{Tr}{Tr-1}\right)\right]\right\} \quad (1)$$

Where I_{t_d,t_r} is the intensity of the rain [mm / min] for a duration of the rain t_d [minutes] in the return period Tr [years].

2.3 Indexes for flooding severity assessment

We considered the Accumulated Flooding Volume Reduction (Li, 2020) and the Peak Flow Reduction as indexes to describe the changes in severity of the flooding approximately 100 meters

downstream of the reservoir. The equation for calculating AFVR under the 25-year hydrograph scenario is formulated in Equation 2. PFR index shows the reduction in the maximum flow downstream of the reservoir under the 25-year hydrograph scenario. This index is determined by the Equation 3.

$$AFVR = \int_{t_0}^{t_n} \frac{Q_{b,i} - Q_{o,i}}{Q_{b,i}} \, d_t \quad (2)$$

$$PFR = \frac{Q_{b,max} - Q_{o,max}}{Q_{b,max}} . 100\% \quad (3)$$

Where $Q_{o,i}$ is the downstream flow rate in the control scenario, $Q_{b,i}$is the downstream flow rate in the base scenario, t_o is the start time of the simulation, $t_n$is the end time of the simulation, $Q_{o,max}$ is the maximum downstream flow rate during the control scenario, and $Q_{b,max}$ is the downstream flow rate during the base scenario.

3 RESULTS

This study developed individual simulations for each reservoir to establish control rules to reduce peak flows. Figure 2 compared the hydrographs for the Aricanduva I reservoir between the baseline and the FLC implementation scenario, using the outflow hydrographs generated with a 25-yeat design storm as inflow (dark blue line). The baseline scenario (red line) shows the performance of the outlet devices without FLC implementation. The reservoir delayed and reduced the inflow peak, and both outlet devices generate a peak flow with a rapid recession limb.

In contrast, the FLC implementation scenario (teal line) demonstrated how controllers further reduce the peak flow with gradual discharge. This behavior resulted from control rules for the gated spillway that increase the reservoir storage capacity, using the orifice condition in the gated culvert and its discharge capacity to increase the upstream energy head at the outlet device. This condition is verified in the right subplot, which shows the opening states of the gated culvert (green line) and gated spillway (purple line); the latter remains closed throughout the event.

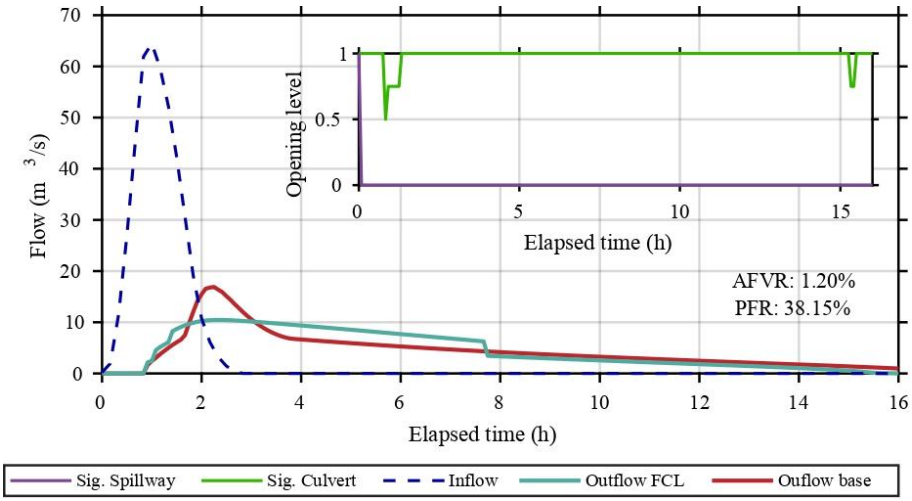

Figure 2: Hydrographs comparison between the baseline scenario (red line) and FLC application scenario (teal line) of the Aricanduva I reservoir at 100 meters downstream from the weir produced by the inflow (dark blue line). Taken from Sánchez (2025).

The PFR values in this study were 38.15%, 20.60%, 14.40% and 8.30% for the Aricanduva I, Limoeiro, Caguaçu, and Aricanduva III reservoirs, respectively. These values indicated a reduction in peak

flow discharge in all reservoirs except Aricanduva II (Figure 3), which shows a 2.11% inverse in peak flow, due to aspects of the FLC configuration in this reservoir. First, we established rules for the gated spillway to increase reservoir storage capacity up to a specified level, utilizing the gated culvert condition to maximize discharge capacity during the hydrograph's rising limb. Consequently, the increased upstream energy head and adaptable cross-section culvert size enhanced the discharge in this structure.

Second, we implemented gate openings with steps of 25% to establish minimal rules in FISs, then for Aricanduva II's gated spillway, once discharge begins, sufficiently high upstream energy head accumulates to increase the discharge through this structure. Consequently, the flow was raising at the assessment point. After testing various MF configurations, the Aricanduva II reservoir did not show any improvement with the controller application.

The AFVR values were 1.20%, 0.60%, 8.30%, and 0.58% for the Aricanduva I, Limoeiro, Aricanduva II, and Aricanduva III reservoirs, respectively. These results indicated that the implementation of FLC slightly outperforms the baseline scenario in reducing flood volume. In contrast, the Caguaçu reservoir showed an AFVR value of -5.83%, indicating poor performance in reducing flood volume.

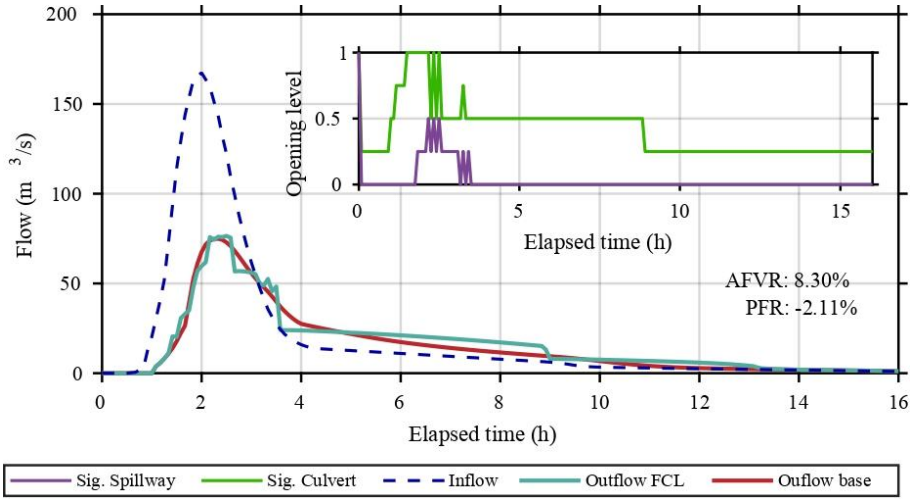

Figure 2: Hydrographs comparison between the baseline scenario (red line) and FLC application scenario (teal line) of the Aricanduva II reservoir at 100 meters downstream from the weir produced by the inflow (dark blue line). Taken from Sánchez (2025).

4 DISCUSSION

In this study, we assessed a fuzzy logic control strategy with rule-based membership functions for online stormwater reservoirs located in the watershed upstream area to reduce flooding flow. For that purpose, we evaluated each FLC's performance using AFVR and PFR metrics. This is a decentralized analysis for each reservoir that helps to determine whether FLC implementation can reduce the watershed flood impacts. Moreover, this framework was adopted due to the insufficient records of precipitation, water level, and discharge near the online reservoirs analysed.

Consequently, we found that FLC implementation in the outlet devices of the Aricanduva II reservoir (Figure 3), with established membership functions and rules, was ineffective in reducing the flood impacts. Furthermore, AFVR values were lower than those reported in previous studies using data-driven strategies with genetic algorithms (GA) (Li, 2020; Talei et al., 2010). This discrepancy may be due to some predetermined control rules that do not match optimal measurements and limited sluice gate opening ranges that cause significant flow variation.

Nevertheless, FLC can be tuned in various ways, with different and multiple membership functions or rules that could be explored to enhance the reservoir operation. Several studies have focused on

developing accurate and optimal fuzzy interference systems using appropriate tuning methods (Li, 2020; Mounce et al.,2020; Ostojin et al., 2011; Talei et al., 2010). Future research could apply these tuning methods to improve FLC in stormwater reservoirs by using these individual hydrodynamic models for and employing data-driven, stochastic, and heuristic algorithms under various precipitation regimes (e.g., multiple design storms with return periods using non-stationary IDF curves or climate change scenarios).

4.1 Uncertainties and limitations

Although the effectiveness of the implementation of FLC as a flood control strategy is implemented individually in each reservoir, it is important to recognize that certain uncertainties and limitations inherent to the hydrodynamic model and the used approach also influence this analysis. The precision of the modelling results remains dependent on the quality of the input data, the methodologies used, and the assumptions made throughout the process.

In this study, only the outlet devices that regulate the outflow of the reservoir was explicitly modeled, with limited data available on the structures, constraining comprehensive representation. For example, some reservoirs present energy dissipators or culverts in some of their entrance that could not be represented in the model due to lack of information. These data limitations, along with uncertainties in the DEM generated form LiDAR processing and the assumption of static initial conditions prior to flood events contribute to the overall uncertainty in the simulation outcomes.

Other limitation is that FLC performance heavily depends on the quality of fuzzy control rules and membership functions, which are often designed empirically or based on limited data. Although subjective rule definition may capture complex hydrological dynamics, as observed in four of the face addressed reservoirs, this approach may also result in suboptimal gate operations. Future studies could incorporate metaheuristic optimization algorithms to automate rule tuning and MFs parameterization, thus reducing subjectively and improving adaptability.

Furthermore, the practical effectiveness of this controller in real-world scenarios warrants further validation, potentially through predictive fuzzy logic controllers that incorporate probabilistic rainfall forecasts and ensemble modelling to quantify uncertainty (Sun et al., 2024; Amitaba et al., 2024).

5 CONCLUSION

This study proposes the first steps to apply a fuzzy logic control tool based on fuzzy logic theory on outlet devices of stormwater reservoirs to reduce downstream flooding volume in poorly gauged urban watershed. The results demonstrate that upstream stormwater reservoirs can be controlled by using FLC to leverage their hydraulic characteristics and reduce the peak flow and the accumulated flooding volume for lowering flood impacts in downstream. Additionally, this framework of control simulation tool opens the possibility to integrate various metaheuristic and stochastic algorithms to enhance the FLC performance.

The main contributions of this study are: (i) The simulation of a RTC strategy incorporating FLC into rainfall-runoff model to increase the resilience of the reservoirs. (ii) The development of a framework to establish a FISs using a manually rule based method for each reservoir. (iii) The implementation of the AFVR and the PFR indexes can assess the effectiveness of FLC implementation in the outlet devices and assist in the assessment of the membership functions and the fuzzy control rules.

This study demonstrates the potential benefits of implementing FLC into urban flood control structures, especially in stormwater reservoirs with data scarcity. However, several uncertainties and limitations remain, including model assumptions, the data limitations, and the sensitivity of FLC input inaccuracies. Future research should focus on integrating advanced optimization algorithms and robust filtering methods into the established framework to enhance system reliability and performance. Finally, the implemented approach allows the assessment of which reservoirs with FLC implementation could effectively reduce urban flooding impacts, particularly in data-scarce watersheds.

6 ACKNOWLEDGEMENTS

The authors appreciate the backing of the WadiLab collegues. This work was supported by CNPq Scholarship, FAPESP and the PPG-SHS PROEX Graduate Program.

REFERENCES

AMITABA, I.W., JUWONO, P.T., LIMANTARA, L.M., ASMARANTO, R. (2024). Real time operation simulation model with early release reservoir storage. Journal of Human, Earth, and Future 5, 574–590

BARTOS, M., KERKEZ, B. (2021). Pipedream: An interactive digital twin model for natural and urban drainage systems. Environmental Modelling & Software 144, 105120.

BROWN, C.F., BRUMBY, S.P., GUZDER-WILLIAMS, B., BIRCH, T., HYDE, S.B., MAZZARIELLO, J., CZERWINSKI, W., PASQUARELLA, V.J., HAERTEL, R., ILYUSHCHENKO, S., ET AL. (2022). Dynamic world, near real-time global 10 m land use land cover mapping. Scientific Data 9, 251

FCTH, (2022). Caderno de bacio hidrogr´agica - Bacia do Rio Aricanduva. 2 ed., Prefeitura do Munic´ıpio de São Paulo Secretaria Municipal de Infraestrutura Urbana e Obra. Web-1

GOMES, M. N. et al. (2023) HydroPol2D — Distributed hydrodynamic and water quality model: Challenges and opportunities in poorly-gauged catchments. Journal of Hydrology, v. 625, p. 129982.

GOMES, M. N., Jr et al. (2024) Spatio-Temporal performance of 2D local inertial hydrodynamic models for urban drainage and Dam-Break applications. SSRN.

LI, J. (2020). A data-driven improved fuzzy logic control optimization-simulation tool for reducing flooding volume at downstream urban drainage systems. The Science of the Total Environment, v. 732, p. 138931.

LUND, N.S.V., FALK, A.K.V., BORUP, M., MADSEN, H., STEEN MIKKELSEN, P. (2018). Model predictive control of urban drainage systems: A review and perspective towards smart real-time water management. Critical reviews in environmental science and technology 48, 279–339.

MOUNCE, S. R. et al. (2019) Optimisation of a fuzzy logic-based local real-time control system for mitigation of sewer flooding using genetic algorithms. Journal of Hydroinformatics, v. 22, n. 2, p. 281–295.

NKWUNONWO, U. C.; WHITWORTH, M.; BAILY, B. (2020) A review of the current status of flood modelling for urban flood risk management in the developing countries. Scientific African, v. 7, p. e00269.

OSTOJIN, S., MOUNCE, S., BOXALL, J. (2011). An artificial intelligence approach for optimizing pumping in sewer systems. Journal of hydroinformatics 13, 295–306

QI, W. et al. (2021) A review on applications of urban flood models in flood mitigation strategies. Natural Hazards, v. 108, n. 1, p. 31–62.

SÁNCHEZ, M. H. (2025) A novel framework for flood Vulnerability Assessment and FuzzyControlled Reservoir Optimization in Data-Scarce Urban Watersheds. Dissertation (Master of Science)—[s.l.] São Carlos School of Engineering, University of São Paulo. Web-2.

SUN, L., XIA, J., SHE, D., DING, W., JIANG, J., LIU, B., ZHAO, F. (2024). A predictive fuzzy logic and rule-based control approach for practical real-time operation of urban stormwater storage system. Water Research 266, 122437.850

TALEI, A., CHUA, L.H.C., QUEK, C. (2010). A novel application of a neuro-fuzzy computational technique in event-based rainfall–runoff modeling. Expert Systems with Applications 37, 7456–7468

Web sites:

Web-1:

https://www.prefeitura.sp.gov.br/cidade/secretarias/upload/obras/cadernos_de_drenagem/CBH_2022_Aricanduva_ed2.pdf.

Web-2: https://teses.usp.br/index.php?option=com_jumi&fileid=38&Itemid=183&id=77AD002BD8E7

ICFM 10
Adapting to Global Change:
Innovative Approaches to Flood Management and Resilience
May 20-22, 2026 | Western University, London, Ontario, Canada

Empirical Insights from Post-Event Coastal Flood Damage Surveys after Hurricanes Helene and Milton in Florida

Ahmed U. Abdelhady* **and Raulina Wojtkiewicz**
Catastrophe and Risk Solutions, Verisk, Boston, MA, 02111, USA
*E-mail: ahmed.abdelhady@verisk.com

ABSTRACT

Post-event damage surveys provide critical empirical evidence for understanding how buildings perform after a natural catastrophe. This paper presents findings from a post-event damage survey conducted after Hurricanes Helene and Milton, which impacted Florida's Gulf Coast in October 2024. The survey focused on six coastal counties: Lee, Charlotte, Sarasota, Manatee, Hillsborough, and Pinellas. It documents flood damage in buildings exposed to storm surge.

Field observations were collected through rapid, street-level assessments conducted within days of landfall, capturing perishable indicators such as flood depths, sediment deposition, debris accumulation, and damage to structural and non-structural components. The surveyed building stock included single-family homes, multi-family residential buildings, low-rise commercial structures, and mobile or manufactured housing spanning multiple construction eras and flood mitigation regimes. Observed damage patterns highlight strong spatial variability in flood impacts, particularly within the first few blocks from the shoreline, where several buildings experienced extensive interior damage accompanied by deep silt and mud deposition.

Survey findings demonstrate the significant influence of building elevation and mitigation measures on damage outcomes. Elevated structures generally limit damage to sacrificial lower levels, while non-elevated buildings exposed to similar surge depths sustained substantial interior and exterior damage. These observations provide clear, field-based evidence of the effectiveness of elevation and modern coastal construction practices in reducing flood impacts.

By centering on empirical survey data, this study underscores the essential role of post-event damage surveys in advancing coastal flood risk understanding. The findings offer practical insights for flood vulnerability assessment, mitigation planning, and the interpretation of hurricane flood impacts in coastal communities.

KEYWORDS: Damage Surveys; Coastal Flooding; Flood Risk; Catastrophe Modelling

1 INTRODUCTION

Coastal flooding from hurricanes remains one of the most damaging natural hazards affecting the built environment, particularly along low-lying coastlines where storm surge, wave action, and coastal rainfall interact to produce complex damage patterns. In the United States, hurricane-driven flooding accounts for a substantial portion of disaster-related economic losses, with damage mechanisms varying significantly over short spatial scales due to elevation, building characteristics, and mitigation practices (Merz et al., 2010; Wing et al., 2020). These complexities pose persistent challenges for flood risk assessment and loss modelling in coastal environments.

Advances in flood catastrophe modelling have improved the representation of coastal storm surge hazard. However, the reliability of modelled loss estimates remains strongly dependent on exposure data and assumptions used to represent building vulnerability (Merz et al., 2010). Vulnerability functions embedded in catastrophe models are often developed using limited empirical datasets, increasing epistemic uncertainty, particularly for extreme events where observational data are scarce. As a result,

post-event validation is essential to ensure that modelled losses reflect real-world building performance under flood conditions.

Post-event damage surveys play a critical role in addressing this gap by providing direct empirical observations of how buildings perform during extreme flooding. Unlike modelled outputs or insurance claims alone, damage surveys capture physical evidence of flood depths, damage mechanisms, construction details, and mitigation features that help explain why damage occurred (Do et al., 2025; Webb et al., 2024). These surveys are especially valuable in coastal settings, where surge-driven flooding can vary sharply within neighbourhoods due to small changes in elevation and local site conditions. From both academic and industry perspectives, systematic post-event surveys are a foundational component of catastrophe model development, enabling the identification of model biases and supporting iterative refinement of vulnerability assumptions (Johnson et al., 2019).

Hurricanes Helene and Milton, which impacted Florida's Gulf Coast in 2024, provide an opportunity to examine coastal flood damage through post-event reconnaissance. Both events produced significant storm surge along the coast, with additional contributions from rainfall and local drainage effects within coastal communities. Rapid reconnaissance efforts following Hurricane Milton documented widespread coastal flooding and building damage across southwest Florida, highlighting the importance of timely post-event surveys for capturing perishable damage evidence (Do et al., 2025; Webb et al., 2024). Building on these efforts, targeted damage surveys were conducted in six heavily impacted coastal counties: Lee, Charlotte, Sarasota, Manatee, Hillsborough, and Pinellas. These counties encompass a diverse coastal building stock, including single-family homes, condominiums, low-rise commercial buildings, and mobile or manufactured housing, constructed across multiple code eras and mitigation regimes.

The results of the survey presented below focused exclusively on coastal areas, with emphasis on surge-dominated flooding and compound coastal flood effects. Inland regions outside the coastal zone were not surveyed; therefore, this study does not attempt to characterize inland riverine flooding or rainfall driven flooding away from the coast. Inland flooding is considered only where it manifested within coastal communities, such as back-bay flooding, canal overflow, and drainage related failures occurring behind surge affected shorelines. This explicit focus allows for clearer interpretation of observed damage mechanisms and avoids overgeneralization beyond the surveyed regions.

The objective of this paper is to demonstrate the value of post-event coastal damage surveys in improving flood risk understanding and catastrophe model performance. Specifically, the paper (1) describes the design and execution of coastal damage surveys conducted after Hurricanes Helene and Milton in Florida coastal counties; (2) provides observed damage patterns and mitigation features across different coastal buildings; and (3) discusses how these observations serve to inform and validate flood catastrophe modelling. By centring empirical survey evidence, this work highlights the essential role of field reconnaissance in advancing coastal flood risk assessment and supporting the development of more resilient coastal communities.

2 POST-EVENT DAMAGE RECONNAISSANCE SURVEYS

2.1 Survey Scope and Study Area

Hurricane Helene made landfall on September 26th, 2024, as a Category four hurricane near the mouth of the Aucilla River in the Big Bend area, Florida. Followed by Hurricane Milton, which made landfall near Siesta Key, Florida, on the evening of October 9, 2024, as a Category three hurricane. Both producing widespread coastal flooding across west Florida. In response to these events, the survey team mobilized rapidly to capture perishable damage evidence before cleanup and repair activities significantly altered site conditions.

The survey team arrived in Tampa, Florida, early on Wednesday, 23 October 2024, and conducted field surveys over three consecutive days. This deployment window allowed for systematic coverage of multiple coastal communities across six counties: Lee, Charlotte, Sarasota, Manatee, Hillsborough, and

Pinellas as shown in fig. 1. Surveys were conducted while visible flood indicators, such as waterlines, debris accumulation, and sediment deposition, were still present, enabling more reliable interpretation of flood intensity and associated damage mechanisms.

Survey teams conducted street-level assessments using a rapid reconnaissance approach, documenting damage at the individual building level. Observations were collected across a range of building occupancies and construction types, including single-family residences, multi-family residential buildings, low-rise commercial structures, and mobile or manufactured housing.

Figure 1: Damage survey study area

2.2 Data Collection and Damage Classification

The surveys relied primarily on exterior visual assessments, supplemented by limited interior observations where access was available. For each surveyed structure, the following information was documented: Building occupancy and general construction type; Apparent construction era and elevation characteristics; Presence of mitigation features, such as elevated foundations, breakaway walls, or impact-resistant openings; Observable flood damage to structural and non-structural components.

Flood intensity was inferred using physical indicators including visible waterlines, debris accumulation, sediment deposition, and damage to lower-level components such as doors, wall finishes, and mechanical or electrical equipment. Damage was classified qualitatively based on the extent and severity of observed impacts, with particular emphasis on distinguishing flood-related damage from wind-driven effects where possible.

2.3 Survey Limitations and Sources of Uncertainty

The following limitations inherent to post-event damage surveys should be noted. Access to building interiors was often restricted, limiting the ability to fully assess interior damage and contents losses. In some locations, debris removal and early repairs may have obscured flood indicators prior to survey arrival. Additionally, distinguishing flood damage from wind-related damage was challenging in areas where both hazards were present.

Despite these constraints, the survey provide a robust empirical dataset capturing spatial patterns of coastal flood damage across multiple building types and mitigation measures. The consistency of observed damage mechanisms across surveyed counties supports the use of these findings to inform coastal flood vulnerability assessment and interpretation of hurricane flood impacts.

3 OBSERVED COASTAL FLOOD DAMAGE AND BUILDING PERFORMANCE

Post-event damage surveys conducted across the six coastal counties revealed consistent spatial patterns of flood damage driven primarily by storm surge. Damage severity was strongly correlated with proximity to the shoreline, local elevation, construction material, and building age. In many surveyed communities, the most severe impacts were observed within the first two to three blocks inland from the coastline, where surge depths and sediment transport were greatest.

3.1 Residential Building Damage

Single-family residential buildings constituted a significant portion, around 65%, of the surveyed structures. As shown in fig. 2-4, for non-elevated homes, floodwaters frequently entered living spaces, resulting in extensive damage to interior finishes, wall assemblies, flooring, and household contents. Exterior damage was typically limited to lower wall finishes, doors, and garage components, though prolonged exposure led to staining, material deterioration, and contamination.

In contrast, fig. 5 and 6, elevated residential buildings often exhibited minimal damage to primary living spaces, even when evidence of surge inundation was present at ground level. For these structures, observed damage was largely confined to garages, storage areas, or unoccupied lower levels. These contrasting performance outcomes were frequently observed between neighbouring homes subjected to similar flood depths, underscoring the influence of building elevation and configuration on damage severity.

Figure 2: Interior damage of residential buildings in Punta Gorda.

Figure 3: Widespread damage to interiors and content was found in most of the surveyed residential neighbourhoods

3.2 Commercial Building Damage

Low-rise commercial buildings in coastal areas experienced damage patterns similar to residential structures but often at larger scales. Ground-floor commercial spaces showed widespread interior damage, including failure of drywall systems, damage to electrical and mechanical equipment, and loss of inventory as shown in figure 7. In several cases, thick sediment deposits covered entire ground-floor areas, complicating cleanup efforts and extending business interruption periods.

Commercial buildings located within the immediate coastal zone were particularly susceptible to flood damage due to slab-on-grade construction and limited elevation above surrounding grade. As shown in figure 8, exterior walls, exterior signage, storefront glazing, and service equipment were commonly damaged or displaced, although structural frame damage was generally limited.

Figure 4: A coastal house that is covered in 3-4 ft of silt and mud in Manasota Key.

Figure 5: Elevated buildings, on the coast in Manasota Key, suffered minimal damage.

3.3 Wind–Flood Damage Interaction

Although the focus of this study is flood damage, evidence of wind-related impacts was observed in several surveyed communities, figure 9. This included roof covering damage, loss of exterior attachments, and damage to carports and screened enclosures, particularly in mobile and manufactured housing. In some cases, wind damage may have increased flood vulnerability by creating additional pathways for water entry. Distinguishing between wind and flood damage was not always possible using exterior observations alone and represents a source of uncertainty in damage interpretation.

Figure 6: Two single-family houses across the street from each other, affected by around 4 feet of storm surge, in Punta Gorda.

Figure 7: Interior and content damage of commercial buildings in Punta Gorda.

Figure 8: Low-rise commercial buildings, near the coastline, suffered damage to exterior walls and windows due to storm surge in Manasota Key.

4 MITIGATION PERFORMANCE AND KEY LESSONS FROM FIELD OBSERVATIONS

Post-event damage surveys conducted after Hurricanes Helene and Milton provided clear empirical evidence of the influence of mitigation measures on coastal flood damage outcomes. Across the surveyed coastal communities, mitigation performance varied substantially depending on building elevation, construction era, and the treatment of lower building levels. Field observations consistently demonstrated that relatively simple mitigation measures, particularly elevation above anticipated surge levels, were highly effective in reducing damage severity.

Figure 6 shows a representative example observed during the surveys involved two single-family homes located directly across the street from one another, both exposed to approximately 3–4 ft of storm surge inundation. The non-elevated home experienced substantial interior damage, including impacts to wall finishes, flooring, and building services, along with minor exterior damage. In contrast, the adjacent elevated home showed almost no observable damage, with floodwaters restricted to the lower, non-habitable level. This side-by-side comparison highlights the effectiveness of elevation in mitigating flood damage under similar hazard intensity and exposure conditions.

Figure 9: Widespread roof damages for mobile/manufactured homes in Hillsborough County.

5 CONCLUSION

This study demonstrates the critical value of post-event damage surveys in advancing the understanding of coastal flood impacts and building performance during hurricane events. Through targeted field surveys conducted after Hurricanes Helene and Milton in six coastal counties along Florida's Gulf Coast, empirical observations were collected that document flood damage mechanisms, mitigation effectiveness, and spatial variability in surge-driven impacts.

Survey findings highlight the dominant role of storm surge in driving damage within the first several blocks from the shoreline, where inundation depths and sediment deposition were often severe. Extensive interior damage, accumulation of silt and mud, and impacts to mechanical and electrical systems were commonly observed in non-elevated residential and commercial buildings. In contrast, elevated structures generally performed significantly better, with floodwaters confined to lower levels and limited or no damage to primary living spaces. These observations provide clear, field-based evidence of the effectiveness of elevation as a flood mitigation measure in coastal environments.

By centring on direct field observations, this work reinforces the essential role of post-event damage surveys in capturing perishable evidence that cannot be fully inferred from hazard models or remote data alone. The findings from Hurricanes Helene and Milton contribute to a growing body of empirical knowledge that supports improved coastal flood vulnerability assessment, more informed mitigation strategies, and enhanced interpretation of hurricane flood impacts. Continued investment in systematic post-event damage surveys will remain vital for strengthening flood risk understanding and promoting resilience in coastal communities.

6 ACKNOWLEDGEMENTS

We would like to acknowledge all the research engineers from Verisk that participated in this survey: Dr. Xinzhe Yuan, Dr. Ameyu Tolera, and Dr. Aman Karamlou. We would also like to thank to Rebecca Keiver her valuable insights of building inventory and flood damage performance of properties as Siesta Key.

REFERENCES

Merz, B., Kreibich, H., Schwarze, R. and Thieken, A. (2010). Assessment of economic flood damage. Natural Hazards and Earth System Sciences, 10, 1697–1724.

Wing, O.E.J., Pinter, N., Bates, P.D. and Kousky, C. (2020). New insights into U.S. flood vulnerability revealed from flood insurance data. Nature Climate Change, 10, 1–6.

Do, T., W. Wang, M. Amini, A. U. Abdelhady, S. Xu, R. NEGRI, S. Kameshwar, C. Wang, H. Dang, A. Jana, E. Carter, M. Alam, T. Kijewski-Correa, D. Prevatt, D. Roueche, K. Wolohan (2025). "StEER: Hurricane Milton Preliminary Virtual Reconnaissance Report (PVRR)", in StEER - Hurricane Milton. DesignSafe-CI. https://doi.org/10.17603/ds2-resg-ah65

Webb, B., D. Prevatt, T. Kijewski-Correa, M. Amini, R. Ramponi, T. Tomiczek, S. Pilkington, H. Pham, K. Mostafa, D. Kalliontzis, S. Kameshwar, H. Dang, A. Kyprioti, J. Capa Salinas, S. Xu, T. Do, M. Gutierrez Soto, A. Diekmann, A. Jana, T. Lin, T. Lahna, S. Ray, M. Alam, D. Roueche, K. Wolohan (2024). "StEER: Hurricane Helene Preliminary Virtual Reconnaissance Report (PVRR)", in *StEER - Hurricane Helene* [Version 2]. DesignSafe-CI. https://doi.org/10.17603/ds2-rgnq-e383

Johnson, T., Bobby, S., and Ramanathan, K. (2019). Modeling Fundamentals: Why Does Verisk Conduct Post-Event Damage Surveys?. Verisk. Retrieved December 22, 2024 from https://www.verisk.com/blog/modeling-fundamentals-why-does-verisk-conduct-post-event-damage-surveys/

ICFM 10
Adapting to Global Change:
Innovative Approaches to Flood Management and Resilience
May 20-22, 2026 | Western University, London, Ontario, Canada

Assessment of Urban Flood Risk and River Network Regulation Capacity Under Extreme Rainfall Conditions

Jingxiu Wu[1,2], Bin Luan[1,2], Ziwu Fan[1,2], Liansheng Li[3], Wei Wang[1,2], Jianhao Sun[3]
Hydraulic Engineering Department, Nanjing Hydraulic Research Institute, Nanjing, 210029, China[1]

Key Laboratory of Taihu Basin Water Resources Management, Ministry of Water Resources, Wuxi, 214125, China[2]

Nanjing Ruidi Water Resources Information Technology Co., Ltd., Nanjing, 210029, China[3]
E-mail: jxwu@nhri.cn

ABSTRACT

Global climate change has led to frequent extreme rainfall events, increasing the probability and intensity of urban flood disasters. This study employs a hydrological-hydrodynamic coupled method for urban flood risk assessment. The extreme "Zhengzhou 7·20" rainstorm event that occurred in China was transposed to Lianyungang City. An analysis of urban inundation and flood risk for 34 types of urban spatial objects across 3 categories was conducted, resulting in a compiled list of hidden hazards. With the objective of preventing overflow in main urban drainage channels while allowing overflow in most secondary channels, an analysis of the urban river network's regulation and storage capacity was performed. This study proposes the ultimate rainfall intensity bearing capacity of the urban engineering system, clarifies the distribution of urban flood risk hazards, and provides technical support for enhancing the city's ability to respond to extreme rainstorms.

KEYWORDS: Urban flood risk assessment; Extreme rainfall; Hydrological-Hydrodynamic coupled model; River storage capacity; Urban resilience

1 INTRODUCTION

Global climate change leads to frequent extreme rainfall events, increasing the probability and intensity of urban flood disasters (Rentschler et al.,1985; Zhang et al., 2016), while also highlighting the limitations of traditional flood disaster response models. Urban flood disasters caused by extreme rainstorms are often characterized by sudden onset, numerous hidden hazard points, significant impact, intertwined flood and waterlogging, multiple types of secondary disasters, and substantial losses. The catastrophic 2021 Zhengzhou "7·20" extreme rainstorm and the 2023 Zhuozhou "7·30" rainstorm in China resulted in significant casualties and property damage, providing painful lessons. Relevant management authorities can utilize the risk levels and distribution to implement early risk warnings, allocate resources, and organize evacuations in advance, thereby minimizing losses caused by flood disasters. Addressing the question posed by managers—"What magnitude of rainfall can the city's current flood control, drainage, and sewerage engineering system withstand?"—this study provides an answer by analyzing urban flood risk under different rainfall intensities and assessing the urban river network's regulation and storage capacity.

Existing risk assessments for extreme rainstorm flood disasters are mostly based on numerical simulation schemes. Domestic and international experts and scholars have conducted in-depth research on urban rainstorm and waterlogging risk assessment, which can be categorized according to their principles into hydrological methods, hydrodynamic methods, and hydrological-hydrodynamic coupled methods

(Huang et al., 2020;Xu et al., 2021;Qi et al., 2021). Hydrodynamic methods (including 1D hydrodynamic models, 2D hydrodynamic models, and 1D-2D coupled hydrodynamic models) offer significant advantages in the refined simulation of water flow dynamics. The hydrological-hydrodynamic coupled method combines the strengths of both hydrological and hydrodynamic approaches, yielding more accurate assessment results and broader applicability, and has been widely adopted in recent years. Commonly used rainstorm and flood models include SWMM (Storm Water Management Model), MIKE, InfoWorks ICM (Integrated Catchment Modelling), IFMS (Integrated (IWHR) Flood Modeling System), etc. (Li et al., 2022). Overall, the computational principles of these urban rainstorm and flood models are similar. However, due to the complexity of urban rainstorm and flood processes and data conditions, as well as insufficient understanding of model principles and simulation objects by modelers, significant discrepancies often exist between model construction aspects—such as delineation of the modeling area, runoff generation and concentration simulation, structure generalization, and engineering operation simulation—and actual conditions.

In light of this, this study takes the central urban area of Lianyungang City, where rainstorms and floods occur relatively frequently, as the research area. Based on an approach combining the physical mechanisms of surface drainage following the "surface ponding-pipe network-river network" concept with generalization methods, a refined model for the entire process of urban rainstorm and flood is constructed. This model is used to assess urban flood risk under extreme rainfall conditions and to analyze the urban river network's regulation and storage capacity, providing technical support for urban flood risk management under extreme conditions and for measures such as "prevention-evacuation-emergency response-rescue."

2 STUDY AREA

Lianyungang City is located in Jiangsu Province on the eastern coast of China, situated on the shores of the Yellow Sea, boasting a unique geographical location. Climatically, it belongs to the northern subtropical monsoon climate zone, characterized by four distinct seasons, mild temperatures, and humidity, but it also faces threats from summer typhoons and winter cold waves (Wang et al., 2024). The maximum annual precipitation was 1308.0 mm (2005), and the minimum was 504.9 mm (1978), with a ratio of maximum to minimum annual precipitation of 2.7. Spatial distribution of precipitation is also uneven, decreasing from south to north.

Figure 1: Distribution of water conservancy projects in Lianyungang city

3 RESEARCH METHODOLOGY

To systematically simulate the runoff generation, concentration, and inundation processes in Lianyungang's urban area under extreme rainfall conditions, this study employs InfoWorks ICM software to establish a hydrological-hydrodynamic coupled model. This model integrates watershed hydrological runoff generation, hydraulic transport in pipe networks and channels, and 2D surface inundation processes, enabling the reflection of interactions among watershed-pipe network-surface elements within a unified framework. The model encompasses 843 km of 1D river channels and pipe networks and 201,325 grid cells. Model validation was performed using measured water level data from a rainfall event on October 2, 2025. The average Nash-Sutcliffe Efficiency (NSE) was 0.93, indicating a good fit.

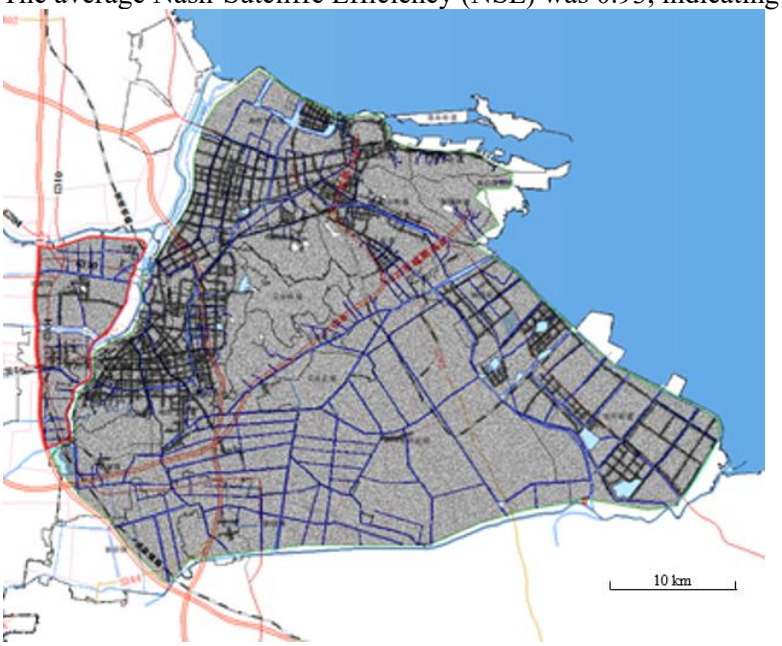

Figure 2: Model building

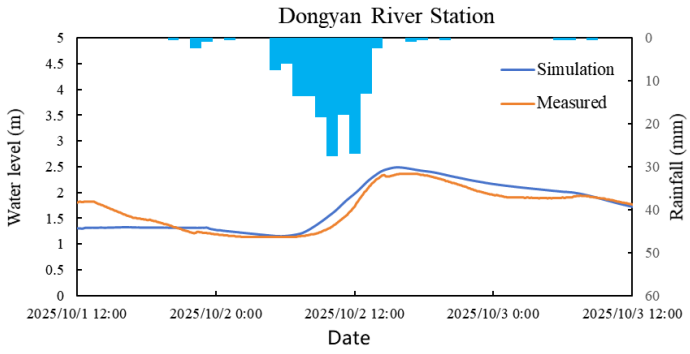

Figure 3: Modelling verification

4 ANALYSIS OF FLOOD RISK

Fully referencing the threat level of inundation depth to pedestrian safety and the mapping standards of the water resources industry, the inundation risk for extreme rainstorm events was divided into four levels: low risk (inundation depth 0.15m-0.3m), medium risk (inundation depth 0.3m-0.6m), high risk (inundation depth 0.6m-1.0m), and extremely high risk (inundation depth 1.0m and above). A flood risk map was generated based on the model calculation results. According to the risk map

distribution, if the entire 1162.9 km² area of Lianyungang urban district were subjected to the Zhengzhou station rainstorm process (maximum 1-hour: 201.9 mm, maximum 24-hour: 645.6 mm, maximum 3-day: 789.1 mm), widespread flooding would occur. The total inundation area would be 526.23 km², accounting for 45.25% of the total area. The area with inundation depth exceeding 0.6 m would be 152.9 km², accounting for 29.06% of the total inundated area. The current engineering system would be unable to cope, making it crucial to prepare defense measures and emergency plans in advance. Compared to Lianyungang's current 20-year drainage standard (maximum 1-hour rainfall: 89.9 mm), the calculated 1-hour rainfall is 2.2 times higher; compared to the 20-year standard 24-hour rainfall (242.9 mm), the calculated 24-hour rainfall is 3.2 times higher. The proportions of different risk levels for each administrative district are shown in Table 1 and Table 2.

Based on fundamental data and model results, inundation risk maps were created. The flood disaster risk to urban spatial objects was analyzed, and thematic risk maps for these objects were produced. These involve 2 types of hydraulic structures (sluices, pumping stations), 7 types of lifeline projects (underground spaces, power supply facilities in low-lying areas, power supply facilities for underground spaces, water supply projects, underpass transportation works, transportation hubs, communication facilities, oil and gas stations), and 15 types of key protected objects (water-reactive hazardous chemical enterprises, highly toxic chemical enterprises, government service centers, hospitals, schools, nursing homes, welfare institutions, kindergartens, underground shopping malls, dilapidated buildings/houses/grain depots, geological hazard risk points, evacuation and resettlement sites/communities, and flood control material warehouses). A risk and hidden hazard checklist covering 24 types of key objects across 3 categories was compiled. The list includes risk elements such as the object's latitude/longitude, surrounding average ground elevation, ground water level during flooding, inundation depth, risk level, and risk point description. Based on this checklist, urban spatial objects at risk can be further identified.

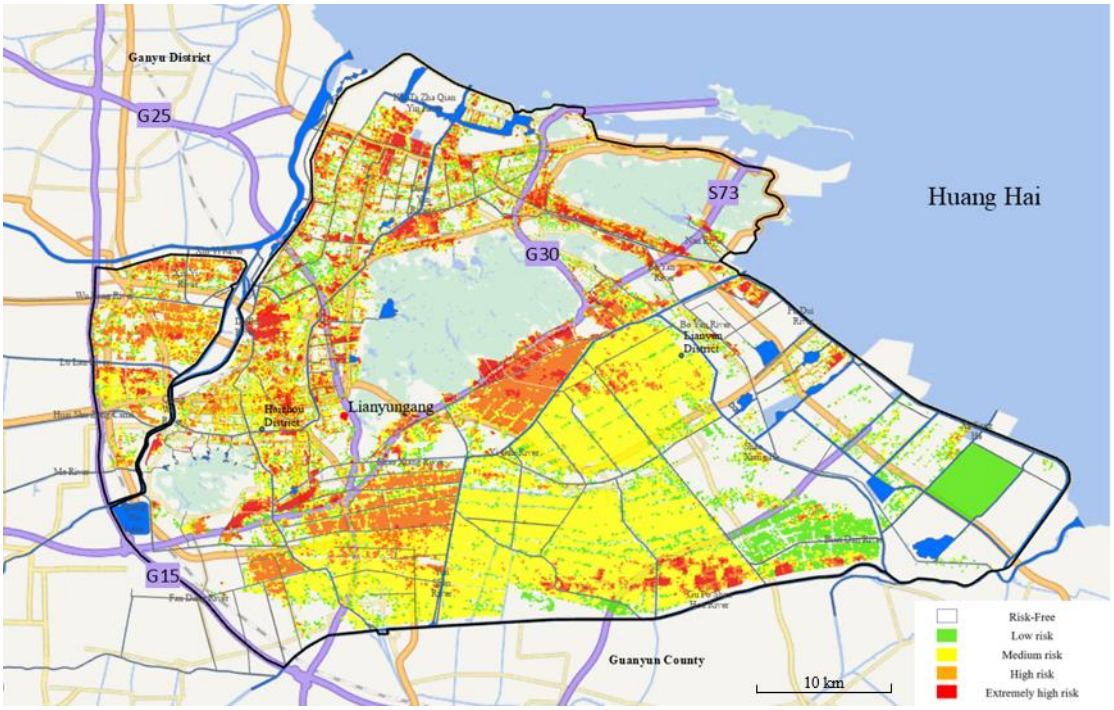

Figure 4: Urban Flood Risk Submersion Map under Extreme Heavy Rainfall Conditions

Table 1 Statistical table of submerged area and proportion of built-up area and non-built-up area in Haizhou District of Lianyungang City under the boundary scenario of '7·20' rainstorm combination in Zhengzhou

Risk level / Flooded area (km^2)	Haizhou (243.59km^2)							
	Haizhou (excluding Yuntai Mountain Scenic Area)				Yuntai Mountain Scenic Area (0.06)			
	built up area	percentage	unbuilt area	percentage	built up area	percentage	unbuilt area	percentage
Extremely high risk	8.31	2.88%	11.84	1.30%	/	/	/	/
High risk	12.58	4.36%	63.15	6.95%	/	/	0.02	0.00%
Medium risk	23.08	8.00%	93.48	10.28%	0.01	0.00%	/	/
Low risk	8.74	3.03%	22.35	2.46%	0.03	0.01%	/	/
Aggregate	52.70	18.28%	190.83	20.99%	0.04	0.01%	0.02	0.00%

Table 2 Statistical table of submerged area and proportion of built-up area and non-built-up area in lianyun district, lianyungang city, zhengzhou '7·20' heavy rain combination live boundary scenario

Risk level / Flooded area (km^2)	Lianyun (282.64)															
	Lianyun (excluding the development zone and Xuxu New Area) (31.91)				Economic and technological development zone (56.17)				Yuntai Mountain Scenic Area (0.04)				Xuwei New District (194.52)			
	built up area	percentage	unbuilt area	percentage	built up area	percentage	unbuilt area	percentage	built up area	percentage	unbuilt area	percentage	built up area	percentage	unbuilt area	percentage
Extremely high risk	2.90	1.01%	4.17	0.46%	8.12	2.82%	1.85	0.20%	/	/	0.01	0.00%	0.39	0.13%	3.97	0.44%
High risk	2.98	1.03%	5.98	0.66%	12.21	4.23%	2.46	0.27%	/	/	/	/	0.62	0.22%	11.35	1.25%
Medium risk	3.04	1.05%	7.40	0.81%	15.85	5.50%	2.18	0.24%	/	/	0.01	0.00%	0.97	0.34%	123.58	13.60%
Low risk	1.75	0.61%	3.70	0.41%	12.53	4.35%	1.00	0.11%	/	/	/	/	14.19	4.92%	39.44	4.34%
Aggregate	10.66	3.70%	21.25	2.34%	48.71	16.89%	7.48	0.82%	/	/	0.02	0.00%	16.17	5.61%	178.34	19.62%

5 RIVER NETWORK REGULATION AND STORAGE CAPACITY

River network regulation and storage capacity refers to the ability of a region's river channel system to temporarily store (regulate) and safely discharge (store + drain) rainwater during a rainstorm. The stronger this capacity, the greater the ability to resist flooding and prevent waterlogging.

This study evaluates the overflow risk of main channels and secondary drainage channels in key urban areas of Lianyungang City under designed 24-hour rainfall amounts of 300 mm, 350 mm, 400 mm, 500 mm, and 800 mm. The results are shown in the table below.

The results indicate that Lianyungang's urban river network regulation and storage capacity exhibits four main characteristics. First, the drainage method significantly impacts the capacity. For example, in the West Tongyu River area and the secondary channels of the Dapu River area, gate-controlled drainage generally enhances the channel's anti-overflow capability compared to pump-controlled drainage. This is because drainage capacity is a key component of the overall bearing capacity. Gate-controlled drainage allows for utilizing tidal conditions or low external river water levels for natural discharge, dynamically enhancing the river network's drainage capacity and thus increasing the overall bearing capacity. Pump-controlled drainage is limited by fixed power and becomes a bottleneck during extreme rainstorms. This highlights the importance of optimized operation for unlocking potential capacity.

Second, secondary channels are more prone to overflow than main channels. The main channels in the Dapu River area (Dapu River and Dongyan River) did not overflow under both pump and gate drainage scenarios for 24-hour rainfalls of 300 mm, 350 mm, 400 mm, and 500 mm. However, under pump drainage, secondary channels basically all overflowed even under the 24-hour 300 mm rainstorm. This indicates weaknesses exist within the river network system. Even if main channel capacity is strong, insufficient capacity or poor drainage in secondary channels can lead to local overflows, constraining the effective bearing capacity of the entire area.

Third, the Shaoxiang River overflowed in all scenarios. This area's river network has an inherently insufficient base regulation and storage capacity. The main reasons are its location at the southern foothills of Yuntaishan Mountain and the coastal plain, with higher terrain in the west and lower in the east. Upstream mountain floods and regional stormwater converge rapidly, while the downstream terrain is flat. The estuary is affected by tides, and drainage is hindered during high tide, leading to limited outlet capacity. Even with gates open (gate drainage), water levels cannot be effectively lowered.

Furthermore, extreme rainfall (800 mm) poses severe challenges to all areas, with water levels in most channels approaching or exceeding safety limits. This indicates an upper limit to the current river network system's bearing capacity. Almost all areas were near or beyond their limits under the 800 mm scenario. Therefore, facing super-standard rainstorms requires reliance on emergency management or stronger engineering measures.

Considering the above issues, several governance approaches are proposed. First, for areas with weak regulation and storage capacity like the Shaoxiang River area, it is necessary to expand storage volume (through dredging, channel widening) or construct powerful pumping stations. For areas like the West Tongyu River area, priority should be given to optimizing drainage operations and considering upgrading pumping station capacity. For secondary channel bottlenecks, it is essential to improve the pipe network and enhance channel connectivity and flow capacity. Emergency management measures need to be formulated for different areas when rainfall exceeds the river network's regulation and storage capacity.

Table 3 Elevation of main waterways in each drainage zone and water levels under different heavy rainfall scenarios (yellow shading indicates water levels exceeding ground elevation, bold lines represent major waterways)

Drainage area	**River name**	**Ground elevation (m)**	**Water level (m)**									
			300 mm in 24 h		**350mm in 24 h**		**400mm in 24 h**		**500mm in 24 h**		**800mm in 24 h**	
			pump	**Sluice**	**pump**	**Sluice**	**pump**	**Sluice**	**pump**	**Sluice**	**pump**	**Sluice**
Dapu River area	Dapu River	4.58	4.14	2.71	4.15	2.90	4.16	3.07	4.44	3.36	4.82	4.08
	Dongyan River	4.80	4.17	3.71	4.21	3.89	4.31	4.06	4.51	4.32	4.88	4.77
	Longwei River	3.83	4.17	3.58	4.20	3.78	4.30	3.98	4.49	4.27	4.83	4.69
	Yudai River	4.23	4.18	3.75	4.29	3.95	4.36	4.12	4.63	4.46	5.15	5.12
	Dapufu River	3.97	4.14	3.17	4.23	3.59	4.24	3.76	4.39	4.05	4.71	4.51
West Tongyu River area	Yan River	4.03	4.10	3.40	4.20	3.88	4.25	4.03	4.41	4.26	4.72	4.65
	Bayi River	4.23	4.06	3.11	4.19	3.49	4.28	3.62	4.40	3.90	4.66	4.51
Shaoxiang River area	Shaoxiang River	3.23	3.51	3.71	3.55	3.43	3.59	3.49	3.67	3.57	3.90	3.81
	Yunshan River	3.73	3.52	3.34	3.57	3.37	3.61	3.43	3.68	3.57	3.94	3.81
	Shaoxiangnan River	3.63	3.53	3.10	3.58	3.42	3.62	3.49	3.69	3.59	3.86	3.80
Lingang area	Caowei River	4.23	3.51	3.36	3.57	3.42	3.93	3.87	4.16	4.03	4.35	4.33
Paidan River area	Paidan River	4.29	3.74	3.28	3.84	3.67	3.94	3.80	4.13	4.04	4.56	4.52
	Beipaidan River	4.23	3.90	3.32	4.03	3.37	4.17	3.46	4.34	3.61	4.66	3.95
Xuwei area	Xuwei River	4.03	2.81	2.05	2.80	2.38	2.80	2.48	2.93	2.71	3.71	3.44

6 CONCLUSION

This study focused on Lianyungang City as the research area, collecting data on urban hydrology, river networks, hydraulic engineering, stormwater and municipal drainage networks, and high-resolution terrain. A refined, hydrological-hydrodynamic coupled model for the entire urban rainstorm and flood process was constructed and calibrated/validated using historical typical rainstorms. A flood risk simulation was conducted by transposing the "Zhengzhou 7·20" rainstorm to Lianyungang. The simulation indicates that Lianyungang's current flood control and drainage system would be unable to cope with a "Zhengzhou 7·20" type rainstorm, making advance preparation of defense measures and emergency plans crucial. Regarding the adjustable storage capacity of the urban river network, under pump drainage conditions, the existing main channels (except Shaoxiang River) can generally regulate and store rainfall up to 400 mm in 24 hours, during which most secondary channels would overflow. Under gate drainage conditions, the existing main channels (except Shaoxiang River) can generally regulate and store rainfall up to 500 mm in 24 hours, during which most secondary drainage channels would overflow.

In the research on urban resilience for coping with flood disasters, there is an urgent need to establish urban resilience assessment methods suitable for responding to extreme rainstorm and flood disasters. Based on evaluation results, vulnerable links in flood disaster prevention and control can be identified, providing technical support for enhancing urban resilience.

7 ACKNOWLEDGEMENTS

This work was supported by the Water Conservancy Science and Technology Project of Jiangsu Province (Grant No. 2025018).

REFERENCES

Rentschler J., Avner P, Marconcini M., et al. (1985). Global evidence of rapid urban growth in flood zones since. Nature, 2023, 622(7981): 87-92.

Zhang J., Wang Y., He R., et al. (2016). Discussion on the urban flood and waterlogging and causes analysis in China. Advances in Water Science, 27(4): 485-491. (in Chinese))

Huang G.,Luo H.,Lu X,,et al. (2020) Study on risk analysis and zoning method of urban flood disaster. Water Resources Protection, 36: 1-6,17.(in Chinese))

Xu Z., Ye C. (2021).Simulation of urban flooding/waterlogging processes: Principle, models and prospects. SHUILI XUEBAO, 52: 381-92.(in Chinese))

Qi W., Ma C., Xu H., et al. (2021). A review on applications of urban flood models in flood mitigation strategies . Natural Hazards, 108(1): 31-62.

Li C., Sun N., Lu Y., et al. (2022). Review on urban flood risk assessment. Sustainability, 15(1): 765.

Wang D., Ji C., Zhang L., et al. (2024). Multi-methods combination assessment and application of urban flood risk. Science of Disaster， 39(1): 96-103.

Chapter 4 - Flood resilience, adaptation, and recovery

4.1 Community, infrastructure, and system resilience to flooding

ICFM 10
Adapting to Global Change:
Innovative Approaches to Flood Management and Resilience
May 20-22, 2026 | Western University, London, Ontario, Canada

Trust, Distrust, and Individuals' Flood Mitigation Decisions

Luke H. Briccetti[1,2], Kimberly J. Coleman[1], Lakelyn E. Taylor[1]
Rubenstein School of the Environment and Natural Resources, University of Vermont, Burlington, VT 05405, USA[1]
Gund Institute for Environment, University of Vermont, Burlington, VT 05405, USA[2]

Email: luke.briccetti@uvm.edu
Email: Kimberly.coleman@uvm.edu
Email: lakelyn.taylor@uvm.edu

ABSTRACT

Extreme weather intensification due to climate change will necessitate significant human adaptation, either by implementing flood mitigation measures, or by vacating flood zones altogether. Although household-level decision-making strategies for flood mitigation have been studied, little attention has been given to how these decisions are made when repeated floods occur. To address this gap, we interviewed 13 flood-impacted residents of Waterbury, VT – a community that has experienced recent reoccurring flooding – to explore the factors influencing their flood mitigation decisions. Using *Trust Ecology* as a theoretical framework to guide our analysis, we uncovered key themes relevant to the adoption of mitigation behaviours. Specifically, our results suggest that two forms of distrust – rational and procedural – played important roles in determining behaviour following repeated flooding. These findings are relevant for practitioners who assist with localized flood mitigation efforts, and advance an understanding of how (dis)trust impacts mitigation efforts broadly.

KEYWORDS: *Flood mitigation, individual decision-making, trust, distrust*

1 INTRODUCTION

Flooding has an immense impact on human life at a global scale, and as climate change and associated extreme weather events increase in frequency and severity, the size and duration of floods are expected to intensify (Caretta et al., 2022; Rainey et al., 2021). As such, there is an increasing need for the adoption of mitigation actions on the global scale, as well as at regional and local scales (Brody & Atoba, 2017; Rainey et al., 2021). A robust body of research exists that seeks to understand individual decision-making in the aftermath of a single flood (Billman et al., 2023; Bubeck et al., 2020; Mondino et al., 2020; Weyrich et al., 2020), including for flood mitigation decisions. However, limited research exists exploring these dynamics for recurrent and compound flooding events in the United States (e.g., Cass et al., 2022; Mukherji et al., 2024; Perls, 2020; Sebastian, 2022; Sun et al., 2024).

In particular, trust and distrust play important roles as drivers of household-level flood mitigation decisions (Babcicky & Seebauer, 2019; Dias et al., 2020), but work exploring these roles remains scarce and fragmented (Voogd et al., 2022). Accordingly, this work uses the *Trust Ecology* framework to explore the role of (dis)trust on the willingness of flood-vulnerable residents and business owners to take flood mitigation actions on their property. This study analyses interviews from a single community (Waterbury, VT) aiming to encourage the adoption of mitigation behaviours, and to understand the factors that drive individuals' mitigation decision-making in the face of intensifying extreme weather.

2 BACKGROUND

2.1. Trust

Trust has been consistently shown to be a critical component of natural resource management because it allows for more effective information sharing and cooperative relationships (Ostrom, 1990; Wondolleck & Yaffee, 2000). Previous research has demonstrated that trust is an important factor in successful flood management work (Babcicky & Seebauer, 2019; Dias et al., 2020) yet trust is underexplored in the context of water governance such as flood management (Voogd et al., 2022). A

2022 systematic literature review (Voogd et al., 2022) found only 24 papers that explore the role of trust in flood management; the authors concluded that studies about trust are fragmented geographically and that trust is often poorly conceptualized and operationalized within the papers that do exist, as few define trust explicitly, and even fewer conceptualize it as multi-dimensional or context-specific.

2.3. Conceptualizing Trust

To fill this conceptual gap, we studied trust within the context of a river floodplain community in Vermont, United States, using the *Trust Ecology* framework. Trust is typically conceptualized as a three-part relationship, where a "trustor" accepts some level of risk and believes in a "trustee" to do some specific action (Hardin, 2002). Additionally, *Trust Ecology* theory asserts that trust is a multidimensional concept, with four distinct forms: dispositional, rational, affinitive, and procedural trust (Stern & Coleman, 2015; Coleman & Stern 2018a; Coleman & Stern 2018b). *Dispositional trust* describes trust resulting from a general predisposition of an individual to trust others (Mayer et al., 1995; Mollering, 2006; Spector & Jones, 2004). *Rational trust* is based primarily upon expectations of reciprocity or perceived utility in strategic interaction (Coleman, 1990; Hardin, 2002; Mollering, 2006). *Affinitive trust* focuses more on the qualities of the potential trustee (Stern & Coleman, 2018b), and may arise through feelings of social connectedness, positive shared experiences, perceptions of shared identities, or assumptions of similar salient values (Braithwaite, 1998; Cvetkovich & Winter, 2003; Stern, 2008). *Procedural trust* is based on the presence of effective control systems (the context and structure in which trust-related decisions are made) (Mayer et al., 1995; Schoorman et al., 2007). These systems might include official rules or procedures that make behaviours more predictable and thus reduce the risk of a trust violation. The trustor then responds to the assessment (see Figure 1). For example, an individual (trustor) may believe that a municipal official (trustee) is providing accurate information about a predicted weather event because they have provided accurate information in the past (rational trust). As a result, the trustor heeds the official's warning and prepares for the upcoming storm (response).

Figure 1. Conceptual Trust Model. A visual representation of trust, including the multiple dimensions of trust and how these dimensions inform trustor actions. Figure made using XMind.

Distrust, on the other hand, involves an explicit negative expectation about the potential trustee (Lewicki & Stevenson, 1997; Ullmann-Margalit, 2004). Distrust occurs as the result of a trust violation, when the trustor receives information about the trustee that does not meet the trustor's expectations (Lewicki & Wiethoff, 2000).

Given that flood mitigation efforts take place through a complex network of organizations requiring collaboration to function, we posit that the concept of *trust ecology* is highly relevant to individual decision-making in the context of flooding, given that trust in town officials, state and federal agencies, and neighbours are likely to influence the decisions that people make around mitigation behaviours.

2.4. The Vermont Context

This paper focuses on one community that has experienced recurring flood events to examine the role of (dis)trust in the adoption of household-level mitigation actions. In Vermont, heavy rains on July 10-11, 2023 resulted in destructive flooding that inundated floodplain communities throughout the state, including many of those along the Winooski River, which rose over 16 feet in 24 hours (Poniz, 2023). The flooding resulted in multiple fatalities (Banacos, 2023), millions of dollars in damage to property and infrastructure (Giles & Dockser, 2023), and a reduced sense of security for residents (Poniz, 2023).

For many Vermonters, this was not their first "generational" flood. In 2011, heavy rainfall from Tropical Storm (TS) Irene led to a 500-year flood event in many of the same places that were flooded in

2023. Vermonters living in the Winooski River watershed endured additional localized severe flooding events in December of 2023 and July of 2024 (Goff, 2023; Goff et al., 2024). Thus, many Vermont residents have experienced three floods within two years (and four within 13 years) that approach or exceed the previously accepted 100-year flood level (FEMA, 2013). The result has been a major increase in attention and funding from government agencies, non-profits (Cutler, 2023), and universities (Defibaugh, 2023) across the state. However, it remains unknown what the cumulative impact of these floods has been on the willingness of Vermonters to adapt and to mitigate in the face of future hazards.

Waterbury, VT – a small community of approximately 5,500 people (depicted in Figure 2) – was severely impacted by each of the four flood events described above. During the 2023 floods, damage was particularly concentrated along the properties adjacent to the Winooski River (Van Dine, 2023; Waterbury Roundabout, 2023). TS Irene and the 2024 flooding were the result of storms with greater local rainfall, resulting in additional impacts to homes adjacent to smaller tributaries.

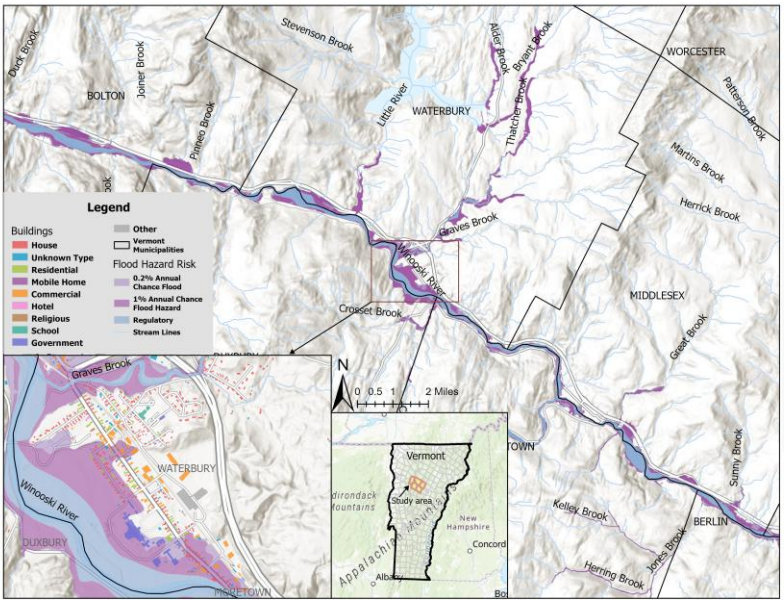

Figure 2*. Map of the greater Waterbury area (including the towns of Middlesex, Moretown, Duxbury, and Bolton), as well as the more densely populated Waterbury Village (inset).* Purple shaded areas represent FEMA-assessed 100 and 500-year flood zones. Data sources: ESRI, FEMA, VCGI.

After TS Irene in 2011, large-scale floodplain restoration projects were proposed in three locations in Waterbury (Milone & MacBroom, Inc., 2013), and detailed cost-benefit analyses revealed significant benefit to the impacted municipalities (Schiff et al., 2015). One component of the project was designed to protect a state office complex and was successfully completed by the state. Two other components were designed to protect the village (floodplain restoration at a cornfield in Waterbury and a racehorse training field in Duxbury) but ran into complications and were not completed despite urging from some impacted community members to do so (Elder-Conners, 2023; Kravitz, 2024). Carmichael and colleagues (2020) conducted a study in Waterbury and discussed some residents' interest in dredging the river as a mitigation tactic. They termed this mitigation option a regional "heritage narrative"—a story that appeals to a subsection of a community and reveals information about the community's social underpinnings and development.

Following the 2023 flooding, a local nonprofit formed a group called Community Resilience for the Waterbury Area (CReW) to focus specifically on flood recovery and mitigation. CReW became an important community partner that helped to facilitate this research.

3 METHODS

We conducted semi-structured interviews with 13 individuals from Waterbury, VT who experienced flooding in either their home or business. Initial interview participants were recruited from a pool of respondents to a flood mitigation survey distributed in the Spring of 2024 by CReW and via snowball sampling from this initial pool of participants (Noy, 2008; Weech, 2023). These data collection methods were appropriate given our study population was relatively homogeneous (individuals in

Waterbury, VT who experienced flooding). Work by Hennink & Kaiser (2022) demonstrates that, in empirical studies of relatively homogenous populations, a narrow range of interviews (9–17) is sufficient for reaching thematic saturation.

3.1. Data Collection

Semi-structured interviews took place during September and October of 2024. The interviews ranged from 40 to 80 minutes in length and took place in-person (n = 10) and virtually (n = 3). Interview questions focused on participants' experiences during the four major flood events that occurred in Waterbury between 2011 and 2024, as well as their decisions about flood mitigation actions. Interviewees were asked to describe how they were impacted by these flood events. They were also asked questions about the specific mitigation actions they adopted, the actions they did not adopt, and the factors that impacted those adoption decisions. These questions allowed the interviewers to learn about trusting relationships without directly asking about trust, which may have risked biasing the remainder of the interview. Finally, a set of questions explicitly focused on trust were asked at the end of each interview.

3.2. Data Analysis

We created a codebook using *Trust Ecology* as our theoretical lens with *a priori* codes that described trust and distrust, including dispositional, rational, affinitive, and procedural antecedents. Our coding took an iterative approach, with multiple rounds of coding to develop themes related to trust and flood mitigation behaviours. Specifically, we followed Glesne's (2016) process for analysis by first reviewing relevant literature on *Trust Ecology*, then examining our data to add nuance to existing knowledge, and finally referring to relevant literature to contextualize our findings. To validate our coding interpretation, we had two members of the research team independently code four of the same interview transcripts (O'Connor & Joffe, 2020). We then ran a query in NVivo 14 to compare coding. The average intercoder agreement was very high (99.38%).

4 RESULTS

Across all our interviews, both trust and distrust emerged as consistent factors that impacted interviewees' willingness to implement mitigation actions. Interviewees had positive and negative experiences from past floods, which in turn impacted how those interviewees placed trust in different entities (i.e. people, organizations, and information sources). Rational distrust, procedural distrust, and affinitive trust emerged as particularly relevant in relation to repeat flooding. We discuss each of these forms of trust and distrust below. We did not find consistent themes related to the other forms of trust and distrust.

4.1. Rational Distrust

Interviewees developed rational distrust for individuals who were perceived to have done an inadequate job, as well as for information sources that were consistently inaccurate. This rational distrust discouraged interviewees from working with these individuals or groups on mitigation action. Interviewees described rational distrust in state officials because of their perceived lack of progress on landscape-level flood mitigation projects. One interviewee told us: "*Knowing that there was that study that was done... like with the cornfield that could be lowered. These reports came out 10 years ago, and this could have had an impact if somebody acted in the past 10 years… and so knowing that there are options out there that could have been acted on at this point and haven't been has definitely increased my weariness of bureaucracy and made me question the effectiveness of some local politics."*

In another example, an interviewee described mitigation projects that were never completed when they stated, "And I understand there was supposed to be two other phases of similar work where they did that for the rest of the town. That never happened." They went on to say how this lack of follow-through was discouraging for them. This sentiment – that more could have been done to accomplish large-scale mitigation projects – was pervasive across interviews, despite not always being about the same project or mitigation strategy. Ultimately, this sentiment facilitated reluctance to implement individual mitigation strategies. One interviewee explained how the lack of follow-through with planned landscape-level

mitigation projects made them question the effectiveness of individual mitigation efforts. The interviewee stated, “But I think it would have to be higher scale mitigation, like cornfields, the river itself, et cetera, to really make a difference. I don't perceive most of these [household-level mitigation practices] really helping when it comes to these catastrophic level floods that we've experienced.”

Another interviewee expressed frustration that the river wasn’t being dredged to reduce flood impacts, and then connected this larger frustration to pushback they received from conservation professionals about a planned individual mitigation strategy: *“At least clean the beds so the water can flow through like it used to… I got some riverbank that's eroding there, and* [conservation professionals] *came along and said, ‘Well, if you rip-rap that, it's going to make it erode down the river.’… And I said, ‘That ain't how it works.’* In short, when individuals expressed doubt about the response efficacy of household-level mitigation practices, these doubts were often expressed in the context of distrust in the competency and lack of follow-through on the part of officials to adequately address flooding.

Rational distrust also impacted individuals’ flood response. For example, one interviewee shared how a police officer advised her to evacuate during the July 2023 flood, leading to her car getting caught in a flash flood. This interviewee told us: “*I was on the road, almost got swept out into the river… I do not trust 211 because they're the ones that initially sent me down a flooded road, and then the state police did the same thing…if they tell me to evacuate again, I won’t.”*

We heard consistently from interviewees that they had rational distrust in the river’s flood gauge system because it frequently failed to provide timely and accurate information about water levels. One interviewee told us, “I don't know who is responsible for updating the Winooski projections and water levels, but it's pretty garbage, because every single flood, it said it's going to be feet lower.” A second interviewee echoed that sentiment when they described their experience: “*I used to check the Waterbury Winooski River gauge estimation. Recently what I noticed is that anytime they give 420, it goes to 425. So, I say five feet more than what they forecast actually… if they say 420 and you get 425, how are you able to sleep? And this is the problem… I do not know if it's the federal government, or the state, or the national water prediction service. They give all this prediction, and everything is wrong.”*

As a result, individuals plan their actions based on the perceived inaccuracy of the flood gauge. One interviewee said, “I trust that when it says it's going to be bad, to just assume it's going to be way worse than what they think it's going to be.” In this way, rational distrust impacted people’s responses to the flooding because it directly impacted who they were willing to work with or accept information from.

4.2. Procedural Distrust

Interviewees also told us about procedural distrust in federal, state, and local systems and programs that lacked transparency. For example, one interviewee whose business was flooded told us the following story about a local fundraising effort: “*Speaking of trust, and I can't remember the name of this, but the funds that they set up last year where every restaurant would have, "Add 2% for the flood economic relief," or whatever it was. I really don't know where that money went… that felt really shady… It didn't feel like it trickled down to any of us.*

A second interviewee shared similar feelings of procedural distrust when it came to applying for FEMA mitigation funding. They described how they would put in hours of time applying for financial assistance to implement mitigation actions only to be informed after they submitted their application that they did not meet income requirements. They then explained how this scenario played out for them repeatedly when they told us, *“They never say that there is a salary limit, actually. Then I go and spend time with them, email them and they explain everything and they will say, ‘Oh, your annual cap is this.’ And I always go beyond this cap… there is always a catch. That's what I notice.”*

We heard from interviewees who had similar experiences with the Small Business Administration (SBA). One interviewee stated, “SBA are pretty quick to pull the rug out from under you.” The interviewee went on to tell us that their neighbour put a new foundation in to raise their building, only to be told after that, “[SBA] had made a mathematical mistake and overqualified him for $90,000”. As a

result, the neighbour had to apply for another loan to cover the difference for the repair/mitigation action and was unsure if they would be able to keep the building because of the expense.

The procedural distrust that was engendered from these experiences led people to adopt mitigative actions on their own, without the aid of official programming. For example, one interviewee told us, "*We were very proactive and did what we needed to do. I don't think I waited for any communication from anyone. I'm sure with all the paperwork and all that stuff that came out, I'm sure there was some information there, but I feel like that would've been months after we needed it."* In short, people described being wary of official programming aimed at relief and resilience. As a result, people did work on their own or relied on friends and neighbours for advice, as described in the section below.

4.3. Affinitive Trust

While we heard about distrust in official entities like the state police, FEMA, the flood alert system, and other entities described above, we heard consistently that interviewees had affinitive trust in friends, neighbours, and locally-run volunteer efforts, such as CReW. In the absence of trusted official sources of information about both flood response and mitigation, members of the community created their own networks to support each other. One interviewee told us, "I trust myself and I trust the few people that I've connected with who are in the same situation as me. So we are very connected during storms. Before the storm hits, we get in touch with each other and say, 'Who's going to be around? Who's going to let us know?'" A second interviewee echoed this experience when they said, "I now have a system with friends on social media and all of us that have gotten flooded, we let each other know what's going on. So, we've kind of developed our own, because I don't know what else is out there." A third interviewee told us a story of how this network of friends and neighbours not only influenced her decision-making ahead of a flood event, but how the mitigation actions she took were so impactful because the official information about the flooding turned out to be an underestimation of the severity of the flood: "*Well, for the first flood, people were saying it might flood and I was like, 'Oh, I'll get things off the floor before I go.'... And then my landlord showed up and all my staff showed up and they're like, "No, no, this is going to be bad." So without them telling me how bad it was going to be, I would've lost a lot more.*

Similarly, interviewees described trusting those who were perceived to have been helpful in past floods. Even though they did not have direct evidence of specific high-quality work performed by these individuals, their positive relationships led to trust. That affinitive trust, in turn, led them to implement mitigation actions. For example, one interviewee implemented a sewer backflow valve at the behest of a local plumber. Yet another interviewee shared an anecdote about how a positive relationship and affinitive trust with CReW volunteers revealed to their son-in-law that he needed help to implement certain mitigation actions, even though doing so went against his initial instincts. The interviewee stated, "They were very helpful with telling [him] exactly what he needed to do. He's kind of like, 'I know what I have to do and I'll just go do it,' which wasn't really in his best interest." Thus, in the absence of rational and procedural trust in official entities, people in Waterbury relied on affinitive trusting relationships to inform their decisions about mitigation actions.

5 DISCUSSION

5.1. The Role of Trust and Distrust

We heard consistently that rational distrust and procedural distrust were both important factors influencing an individuals' decision-making around both flood response and flood mitigation behaviours. These forms of distrust drove individuals' decision-making because they influenced who people were willing to work with, as well as who they accepted information from. We consistently heard from interviewees that a lack of large-scale mitigative action—like floodplain restoration—on the part of the state or municipality led to fatalism and apathy toward household-level mitigation, as well as feelings of rational distrust. A connection between fatalism around flooding and reduced individual mitigation intent is supported by previous research (Bubeck et al., 2018; Vishwanath Harish et al., 2023; Weyrich et al., 2020), which found that high perceptions of future flood severity spark apathy in household-level damage mitigation efforts. However, the co-occurrence of apathy and distrust within our interviews conflicts with

previous work on public planning efforts, which suggests that individuals who are distrusting of agency personnel are more likely to become engaged (Smith et al. 2013). We suggest more work is needed to explore the connections between apathy and trust in the context of flooding.

We also suggest that the perception of a lack of progress in this community (and subsequently, distrust) are closely tied with knowledge of the proposed but incomplete floodplain restoration projects outlined in the post-Irene flood studies (Schiff et al., 2015). These perceptions may also arise from any of the longstanding traditional ideas about how to reduce flooding, which have been termed "heritage narratives" in previous research conducted in this area of Vermont (Carmichael et al., 2020). A pertinent example of a heritage narrative from this study would be dredging the river in selective locations to protect the village, an action which came up occasionally in our interviews and is an important historical idea for how to prevent flooding in the community. This action would likely increase damage downstream of the dredged location (Olson, 2000) and is a practice that flood practitioners are seeking to discourage in the area (Blair, 2024). However, the public is unlikely to ever be in universal agreement on the details of these dynamics, and indeed, several interviewees expressed exasperation at the state for not pursuing these actions. As such, ignoring this heritage narrative (especially without other meaningful mitigation action) may have served to undermine rational trust, and subsequently impact individual responses.

Previous work in the context of wildland fire demonstrates that procedural and rational distrust can lead individuals to disengage from formal planning processes (Coleman & Stern, 2018a). We observed such disengagement in this study as interviewees described their wariness of official sources of information and recovery programming. As such, our findings corroborate earlier studies about distrust and disengagement. These studies suggest that, even when individuals are vulnerable to disasters like flooding, procedural and rational distrust in official communications and programs are likely to lead individuals to shy away from mitigation actions – impeding broader, community-level resilience. Our results also suggest that rational distrust can erode predictability in the decisions that individuals make in response to flooding. For example, individuals made decisions in response to river flood gauge information because they rationally did not trust it. These potential impacts to resilience work are consistent with *Trust Ecology*, which suggests that all four forms of trust play critical roles in supporting the resilience of a system (Stern & Baird, 2015; Stern & Coleman, 2019).

As extreme weather increases under climate change, it is critical to understand how trust and distrust can support or impede communities' resilience goals. We suggest that, in communities where distrust drives individuals' decision-making about mitigation behaviour, community resilience will suffer. Conversely, we suggest that communities with multidimensional trusting relationships between officials, friends, and neighbours will be well positioned to implement mitigation work and build resilience.

5.2. Building and Repairing Trust

Our results point to the importance of building and repairing trust. Given the potential impact of distrust on community-level resilience, we suggest that officials across governance levels may be well served to take specific steps to engender and preserve rational and procedural trust. Doing so will promote the adoption of mitigation behaviours, ideally ahead of emergency response and with careful attention during a response effort. Prior research demonstrates that procedural trust can be engendered through using clear and consistent centralized communication and hosting meetings, field days, or other media opportunities. These events are designed to clarify decision-making processes around state and federal projects, such as buy-outs (Coleman & Stern 2018a; Coleman et al. 2017). Similarly, rational trust can be built by federal and state agency staff, state emergency response crews, and town planners hosting presentations to demonstrate professional competence and the timely completion of high-quality work (Coleman & Stern 2018a; Coleman et al. 2017). For example, as described earlier, one interviewee in our study community shared uncertainty about how money from a local relief fund had been used due to a perceived lack of follow-up communication. Through another conversation, we verified that this money was used to help individuals who were severely flooded, and to purchase materials for future mitigation (sewer backflow valves and basement drains). Therefore, effective follow-up communication from the organization responsible for the fund may have helped to build procedural trust.

Across our interviews, affinitive trust in friends, neighbours, and volunteers influenced decision-making around both flood mitigation and response behaviours. These results are notable and point to the power of social ties for building resilience under climate change and the importance of proactively building affinitive trust. Work by Coleman and colleagues (2017; 2018a; 2018b) suggests affinitive trust can be engendered when people demonstrate qualities associated with core values like fair-mindedness, empathy, and willingness to listen. We did not hear about affinitive trust with federal, state, or municipal officials in our interviews, but we did hear about affinitive trust in volunteers from the local non-profit organization, CReW. We assert that individuals in government roles may also be able to build affinitive trust with individuals by spending time within communities and demonstrating the qualities listed above.

We recognize that trust repair and trust development take substantial time and resources and that these actions may be viewed as less urgent in times of crisis, such as extreme flood events. However, our results demonstrate that the work of trust building and trust repair are critical steps in accomplishing the goal of building climate-resilient communities. Simultaneously, perceived value dissimilarity between government agencies and individuals have driven affinitive distrust in other natural resource management (Stern, 2008). Federal/state agencies have power through their ability to fund flood response and recovery that may contribute to distrustful dynamics, irrespective of efforts by individual representatives of these agencies to cultivate affinitive trust. Future work could further explore the conditions under which affinitive trust can be built in situations where there is a power imbalance.

Finally, given that all forms of trust often reside within personal relationships (i.e. between two individuals), we also suggest officials pay careful attention to the issue of high personnel turnover. High turnover rates can threaten trust, especially on longer projects, such as flood recovery and resilience efforts that takes place over multiple years (Coleman et al., 2021). As such, organizations should consider strategies to manage turnover, including recruiting replacements, developing leadership pipelines, and implementing onboarding practices when resources allow (Coleman et al., 2021). By taking specific steps to build / repair trust, officials across governance levels can promote adoption of mitigation behaviours.

5.3. Limitations

In this study, we took a qualitative, case study approach, focusing on only one community. Our results highlight themes related to different forms of trust and distrust, but similar studies in other communities may reveal different themes about the function of (dis)trust in flood mitigation decision-making, depending on the context within those communities. Thus, more research is required in other communities to test the transferability of our results, and we encourage scholars to build on our work by replicating, testing, refining, and validating our findings on a broader scale. Nevertheless, this study provides a valuable example of the important role that trust plays in decision-making for flood mitigation action in a context where residents have experienced repeated flood events. This study also contributes to an integrated knowledge about trust in water governance by using a trust framework that accounts for the multidimensionality of trust, as called for by Voogd et al. (2022). Further, case studies like ours provide a foundation for future research that may contribute to the development of theory, such as metanalyses and Systematic Literature Reviews that look across case studies to establish common findings.

6 CONCLUSIONS

Extreme weather events are increasingly common under climate change and communities around the globe are faced with the urgent need to adopt mitigation action and increase resilience. Our findings help to improve our understanding of the role that trust plays in building resilience to these extreme events. Although our work focused on flooding, our findings are relevant to communities grappling with other extreme events such as wildland fire, drought, and other climate-induced disasters. Given that our interviewees experienced a high level of vulnerability due to reoccurring flooding in their community, our results highlight the need for federal and state agency staff, state emergency response crews, town planners, and others in official positions to invest in trust building within communities as a strategy for supporting resilience efforts. Finally, our findings are pertinent to scholars researching trust as it provides fruitful avenues for future research, particularly work that seeks to understand how trust and distrust can support or impede communities' climate resilience goals.

7 ACKNOWLEDGMENTS

Thank you to the Natural Hazards Center at the University of Colorado Boulder for funding this work. Special thanks to the volunteers at CReW for their assistance within the community of Waterbury, and to the Gund Institute for Environment at the University of Vermont for supporting this project.

8 PRIOR PUBLICATION DISCLOSURE

Material from this paper has been previously published in the Journal of Environmental Planning and Management. Citation: Briccetti, L. H., Coleman, K. J., & Taylor, L. E. (2025). "They're the ones that sent me down a flooded road": trust, distrust, and individuals' flood mitigation decisions. *Journal of Environmental Planning and Management*, 1–23. https://doi.org/10.1080/09640568.2025.2524444

9 REFERENCES

Andráško, I. (2021). Why People (Do Not) Adopt the Private Precautionary and Mitigation Measures: A Review of the Issue from the Perspective of Recent Flood Risk Research. *Water*, *13*(2). https://doi.org/10.3390/w13020140

Babcicky, P., & Seebauer, S. (2019). Unpacking Protection Motivation Theory: Evidence for a separate protective and non-protective route in private flood mitigation behaviour. *Journal of Risk Research*, *22*(12), 1503–1521. https://doi.org/10.1080/13669877.2018.1485175

Banacos, P. (2023). *The Great Vermont Flood of 10-11 July 2023: Preliminary Meteorological Summary*. NOAA; NOAA's National Weather Service. https://www.weather.gov/btv/The-Great-Vermont-Flood-of-10-11-July-2023-Preliminary-Meteorological-Summary

Billman, M., Atoba, K., Thompson, C., & Brody, S. (2023). How about Now? Changes in Risk Perception before and after Hurricane Irma. *Sustainability*, *15*(9), Article 9. https://doi.org/10.3390/su15097680

Blair, J. (2024, April 16). Understanding Dredging. *Friends of the Winooski River*. https://winooskiriver.blog/2024/04/16/understanding-dredging/

Bockarjova, M., Veen, A. van der, & Geurts, P. A. T. M. (2009). *A PMT-TTM model of protective motivation for flood danger in the Netherlands*. ITC.

Braithwaite, V. (1998). Communal and exchange trust norms, their value base and relevance to institutional trust. In V. A. B. null Margaret Levi (Ed.), *Trust and governance* (Vol. 1, pp. 46–74). Russell Sage Foundation.

Brody, S. D., & Atoba, K. (2017). Flood resiliency in the United States: Setting a framework for reducing losses. In *Vulnerability and resilience to natural hazards* (pp. 237–256). Cambridge University Press.

Bubeck, P., Berghäuser, L., Hudson, P., & Thieken, A. H. (2020). Using Panel Data to Understand the Dynamics of Human Behaviour in Response to Flooding. *Risk Analysis*, *40*(11), 2340–2359. https://doi.org/10.1111/risa.13548

Bubeck, P., Wouter Botzen, W. J., Laudan, J., Aerts, J. C. J. H., & Thieken, A. H. (2018). Insights into Flood-Coping Appraisals of Protection Motivation Theory: Empirical Evidence from Germany and France. *Risk Analysis*, *38*(6), 1239–1257. https://doi.org/10.1111/risa.12938

Caretta, M. A., Mukherji, A., Arfanuzzaman, M., Betts, R. A., Gelfan, A., Hirabayashi, Y., Lissner, T. K., Liu, J., Morgan, R., Mwanga, S., & Supratid, S. (2022). *Climate change 2022: Impacts, adaptation and vulnerability. Contribution of Working Group II to the Sixth Assessment Report of the Intergovernmental Panel on Climate Change* (pp. 551–712). Cambridge University Press.

Carmichael, C., Danks, C., & Vatovec, C. (2020). Assigning Blame: How Local Narratives Shape Community Responses to Extreme Flooding Events in Detroit, Michigan and Waterbury, Vermont. *Environmental Communication*, *14*(3), 300–315. https://doi.org/10.1080/17524032.2019.1659840

Coleman, J. (1990). *Foundations of Social Theory*. The Belknap Press. https://www.hup.harvard.edu/books/9780674312265

Coleman, K. J., Butler, W. H., Stern, M. J., & Beck, S. L. (2021). "They're Constantly Cycling Through": Lessons about Turnover and Collaborative Forest Planning. *Journal of Forestry*, *119*(1), 1–12. https://doi.org/10.1093/jofore/fvaa041

Coleman, K., & Stern, M. J. (2018a). Boundary spanners as trust ambassadors in collaborative natural resource management. *Journal of Environmental Planning and Management*, *61*(2), 291–308. https://doi.org/10.1080/09640568.2017.1303462

Coleman, K., & Stern, M. J. (2018b). Exploring the Functions of Different Forms of Trust in Collaborative Natural Resource Management. *Society & Natural Resources*, *31*(1), 21–38. https://doi.org/10.1080/08941920.2017.1364452

Coleman, K., Stern, M. J., & Widmer, J. (2017). Facilitation, Coordination, and Trust in Landscape-Level Forest Restoration. *Journal of Forestry*. https://doi.org/10.5849/jof.2016-061

Cutler, C. (2023, November 21). State aims to raise more money to help Vermont flood victims. *Https://Www.Wcax.Com*. https://www.wcax.com/2023/11/21/state-aims-raise-more-money-help-vermont-flood-victims/

Cvetkovich, G., & Winter, P. L. (2003). Trust And Social Representations Of The Management Of Threatened And Endangered Species. *Environment and Behaviour*, *35*(2), 286–307. https://doi.org/10.1177/0013916502250139

De Koning, K., Filatova, T., Need, A., & Bin, O. (2019). Avoiding or mitigating flooding: Bottom-up drivers of urban resilience to climate change in the USA. *Global Environmental Change*, *59*, 101981. https://doi.org/10.1016/j.gloenvcha.2019.101981

De Moel, H., Van Alphen, J., & Aerts, J. C. J. H. (2009). Flood maps in Europe – methods, availability and use. *Natural Hazards and Earth System Sciences*, *9*(2), 289–301. https://doi.org/10.5194/nhess-9-289-2009

Defibaugh, J. (2023). *UVM Launches Six Innovative Flood Research Projects*. The University of Vermont. https://www.uvm.edu/news/ovpr/uvm-launches-six-innovative-flood-research-projects

Dias, P., Bertoldo, R., Guignard, S., & Schleyer-Lindenmann, A. (2020). Trust in Public Risk Management and Social Dynamics in the Case of Flood Risk. *CES Psicología*, *14*(1), 49–63. https://doi.org/10.21615/cesp.14.1.5

Elder-Conners, L. (2023, December 11). *A proposed floodplain could have spared Waterbury from severe flooding. It was never built*. Vermont Public. https://www.vermontpublic.org/local-news/2023-12-11/waterbury-vermont-flooding-mitigation-duxbury-floodplain

Erickson, B. D., & Biedenweg, K. (2025). The Shared Antecedents of Trust and Distrust. *Society & Natural Resources*, *0*(0), 1–28. https://doi.org/10.1080/08941920.2025.2509306

Federal Emergency Management Agency. (2013). *National Flood Hazard Layer* (0209E) [..Tif]. https://www.arcgis.com/apps/webappviewer/index.html?id=8b0adb51996444d4879338b5529aa9cd

Federal Emergency Management Agency. (2024, January 22). *Flood Maps*. FEMA.Gov. https://www.fema.gov/flood-maps

Federal Emergency Management Agency. (2025, January 21). *Mitigation for Homeowners*. FEMA.Gov. https://www.fema.gov/fact-sheet/mitigation-homeowners

Federal Emergency Management Agency, & Risk Mapping, Assessment and Planning. (2020). *Protect Your Home from Flooding: Low-cost Projects You Can Do Yourself*. FEMA.Gov.

Giles, A., & Dockser, C. (2023, August 24). July flooding pulled nutrients, waste into Vermont's waters—And climate change is making it worse. *Vermont Public*. https://www.vermontpublic.org/local-news/2023-08-24/july-flooding-pulled-nutrients-waste-into-vermonts-waters-and-climate-change-is-making-it-worse

Gillespie, N., & Dietz, G. (2009). Trust repair after an organization-level failure. *The Academy of Management Review*, *34*(1), 127–145. https://doi.org/10.5465/AMR.2009.35713319

Glesne, C. (2016). Becoming Qualitative Researchers: An Introduction. In *Pearson* (5th ed.). Pearson.

Godschalk, D. R., Rose, A., Mittler, E., Porter, K., & West, C. T. (2009). Estimating the value of foresight: Aggregate analysis of natural hazard mitigation benefits and costs. *Journal of Environmental Planning and Management*, *52*(6), 739–756. https://doi.org/10.1080/09640560903083715

Goff, J. (2023). *The Major Snowmelt and Flooding Event of December 18-19, 2023*. National Weather Service.

Goff, J., Taber, B., & Banacos, P. (2024, August). *The Significant Flooding and Severe Weather Event of 10-11 July 2024*. National Weather Service. https://www.weather.gov/btv/The-Significant-Flooding-and-Severe-Weather-Event-of-10-11-July-2024

Hardin, R. (2002). *Trust and Trustworthiness*. Russell Sage Foundation.

Hennink, M., & Kaiser, B. N. (2022). Sample sizes for saturation in qualitative research: A systematic review of empirical tests. *Social Science & Medicine*, *292*, 114523. https://doi.org/10.1016/j.socscimed.2021.114523

Kravitz, B. (2024, July). *LETTER: Look to cornfield for flood mitigation*. Waterbury Roundabout. https://www.waterburyroundabout.org/opinion-archive/8tht8np2xdu4bwbagdf1s9gos8s665

Lewicki, R. J., & Stevenson, M. A. (1997). Trust Development in Negotiation: Proposed Actions and a Research Agenda. *Business and Professional Ethics Journal*, *16*(1), 99–132. https://doi.org/10.5840/bpej1997161/2/311

Lewicki, R. J., & Wiethoff, C. (2000). Trust, trust development, and trust repair. In *The handbook of conflict resolution: Theory and practice* (pp. 86–107). Jossey-Bass/Wiley.

Mayer, R. C., Davis, J. H., & Schoorman, F. D. (1995). An Integrative Model of Organizational Trust. *The Academy of Management Review*, *20*(3), 709–734. https://doi.org/10.2307/258792

Milone & MacBroom, Inc. (2013). *Winooski Street Bridge Restriction Study Phases II and III Summary* (4942–01).

Mollering, G. (2006). *Trust: Reason, Routine, Reflexivity*. Elsevier.

Mondino, E., Scolobig, A., Borga, M., & Di Baldassarre, G. (2020). The Role of Experience and Different Sources of Knowledge in Shaping Flood Risk Awareness. *Water*, *12*(8), Article 8. https://doi.org/10.3390/w12082130

Morris, S. A., & Tippett, J. (2024). Perceptions and practice in Natural Flood Management: Unpacking differences in community and practitioner perspectives. *Journal of Environmental Planning and Management*, *67*(11), 2528–2552. https://doi.org/10.1080/09640568.2023.2192861

National Conference of State Legislators. (2019). *Flood Mitigation*. Ncsl.Org. https://www.ncsl.org/environment-and-natural-resources/flood-mitigation

NOAA National Severe Storms Laboratory. (n.d.). *Severe Weather 101—Flood Basics* [Text]. Nssl.Noaa.Gov. Retrieved February 11, 2025, from https://www.nssl.noaa.gov/education/svrwx101/floods/

Noy, C. (2008). Sampling Knowledge: The Hermeneutics of Snowball Sampling in Qualitative Research. *International Journal of Social Research Methodology*, *11*(4), 327–344. https://doi.org/10.1080/13645570701401305

O'Connor, C., & Joffe, H. (2020). Intercoder Reliability in Qualitative Research: Debates and Practical Guidelines. *International Journal of Qualitative Methods*, *19*, 1609406919899220. https://doi.org/10.1177/1609406919899220

O'Connor, K. (2021, August 22). What Tropical Storm Irene can teach Vermont 10 years later. *VTDigger*. http://vtdigger.org/2021/08/22/tropical-storm-irene-vermont/

Olson, S. A. (2000). *Simulation of the Effects of Streambed-management Practices on Flood Levels in Vermont*. U.S. Geological Survey.

Ostrom, E. (1990). *Governing the Commons: The Evolution of Institutions for Collective Action* (7th ed.). Cambridge University Press.

Poniz, A. (2023). *Community resilience in Vermont after the 2023 flooding event*.

Rainey, J. L., Brody, S. D., Galloway, G. E., & Highfield, W. E. (2021). Assessment of the growing threat of urban flooding: A case study of a national survey. *Urban Water Journal*, *18*(5), 375–381. https://doi.org/10.1080/1573062X.2021.1893356

Sadoff, K., & Barton, A. (2023). Flooded fields leave Vermont farmers with major crop loss. *Burlington Free Press*. https://www.burlingtonfreepress.com/story/news/2023/07/18/vermont-flooding-farms-intervale-burlington-damage-loss-irene-winooski-river/70415891007/

Schiff, R., Bighinatti, S., Fitzgerald, E., Wahlund, N., Carlton, D., Church, A., Lousios, J., & Cote, B. (2015). *Evaluating the Costs and Benefits of Floodplain Protection Activities in Waterbury, Vermont and Willsboro, New York, Lake Champlain Basin, U.S.A.* (78). Lake Champlain Basin Program.

Schoorman, F. D., Mayer, R. C., & Davis, J. H. (2007). An Integrative Model of Organizational Trust: Past, Present, and Future. *The Academy of Management Review*, *32*(2), 344–354.

Spector, M. D., & Jones, G. E. (2004). Trust in the Workplace: Factors Affecting Trust Formation Between Team Members. *The Journal of Social Psychology*, *144*(3), 311–321. https://doi.org/10.3200/SOCP.144.3.311-321

Stern, M. J. (2008). The Power of Trust: Toward a Theory of Local Opposition to Neighboring Protected Areas. *Society & Natural Resources*, *21*(10), 859–875. https://doi.org/10.1080/08941920801973763

Stern, M. J., & Baird, T. D. (2015). Trust ecology and the resilience of natural resource management institutions. *Ecology and Society*, *20*(2). https://www.jstor.org/stable/26270214

Stern, M. J., & Coleman, K. J. (2019). Trust ecology and collaborative natural resource management. In *A New Era for Collaborative Forest Management*. Routledge.

Tomlinson, E. C., & Mryer, R. C. (2009). The Role Of Causal Attribution Dimensions In Trust Repair. *Academy of Management Review*, *34*(1), 85–104. https://doi.org/10.5465/amr.2009.35713291

Ullmann-Margalit, E. (2004). Trust, Distrust, and In Between. In *Distrust* (Vol. 8, pp. 60–82). Russell Sage Foundation.

Van Dine, A. (2023, July 21). How Waterbury residents are recovering after 100-year floods happened twice in 12 years. *Vermont Public*. https://www.vermontpublic.org/local-news/2023-07-21/how-waterbury-residents-are-recovering-after-100-year-floods-happened-twice-in-12-years

Verlynde, N., Voltaire, L., & Chagnon, P. (2019). Exploring the link between flood risk perception and public support for funding on flood mitigation policies. *Journal of Environmental Planning and Management*, *62*(13), 2330–2351. https://doi.org/10.1080/09640568.2018.1546676

Vishwanath Harish, T., Sairam, N., Yang, L. E., Garschagen, M., & Kreibich, H. (2023). Identifying the drivers of private flood precautionary measures in Ho Chi Minh City, Vietnam. *Natural Hazards and Earth System Sciences*, *23*(3), 1125–1138. https://doi.org/10.5194/nhess-23-1125-2023

Vitale, C., Meijerink, S., & Moccia, F. D. (2023). Urban flood resilience, a multi-level institutional analysis of planning practices in the Metropolitan City of Naples. *Journal of Environmental Planning and Management*, *66*(4), 813–835. https://doi.org/10.1080/09640568.2021.2006156

Voogd, R., Rudberg, P. M., de Vries, J. R., Beunen, R., Espiritu, A. A., Methner, N., Larsen, R. K., Fedreheim, G. E., Goes, S., & Kruger, E. (2022). A systematic review on the role of trust in the water governance literature. *Water Research X*, *16*, 100147. https://doi.org/10.1016/j.wroa.2022.100147

Wang, L., Cui, S., Li, Y., Huang, H., Manandhar, B., Nitivattananon, V., Fang, X., & Huang, W. (2022). A review of the flood management: From flood control to flood resilience. *Heliyon*, *8*(11), e11763. https://doi.org/10.1016/j.heliyon.2022.e11763

Waterbury Roundabout. (2023, July 12). Flood update: Weds., July 12. *Waterbury Roundabout*. https://www.waterburyroundabout.org/news-archive/flood-response-update-weds-july-12

Weech, S. (2023). Climate Change, Snowball Sampling, and Discourse-based Interviews: A Mixed Method for Studying Networked Rhetorics. *Proceedings of the 41st ACM International Conference on Design of Communication*, 32–38. https://doi.org/10.1145/3615335.3623007

Weyrich, P., Mondino, E., Borga, M., Di Baldassarre, G., Patt, A., & Scolobig, A. (2020). A flood-risk-oriented, dynamic protection motivation framework to explain risk reduction behaviours. *Natural Hazards and Earth System Sciences*, *20*(1), 287–298. https://doi.org/10.5194/nhess-20-287-2020

Wondolleck, J., & Yaffee, S. (2000). *Making Collaboration Work: Lessons from Innovation in Natural Resource Management*. Island Press.

ICFM 10
Adapting to Global Change:
Innovative Approaches to Flood Management and Resilience
May 20-22, 2026 | Western University, London, Ontario, Canada

Flood resilient landscapes: application of a design approach for future-proof landscapes

De Leeuw, A.M.[1] , de Boer, F.M.[2] , de Vries, M.C.J.[4], Koppel, S.[3] , Rooze, D.[1], Vinke-de Kruijf, J[4].
Deltares, Delft, 2600 MH, The Netherlands[1]
E-mail:Annemargreet.deleeuw@deltares.nl and Daan.Rooze@deltares.nl
Reframing Studio, Amsterdam, 1053 VN, The Netherlands[2]
E-mail: femke@reframingstudio.com
MUST stedebouw BV, Ridderspoorweg 140, 1032 LL Amsterdam[3]
Email: saide@must.nl
University of Twente, Drienerlolaan 5, Enschede[4]
Email: joanne.vinke@utwente.nl and m.c.j.devries@utwente.nl

ABSTRACT

Society faces a wide range of societal and climatic challenges that impact various sectors, including agriculture, energy, and ecosystem restoring. Additionally, these complex challenges are highly interdependent with the need to develop housing, industry, and infrastructure. Meanwhile, the Netherlands is starting to experience the effects of climate change-induced weather extremes, calling for renewed strategies for flood risk management and freshwater supply. At first sight, societal development and response to climate change seem conflicting as implementation of water measures requires space. How to make the right decisions in spatial planning which will not be regretted in 100 years?

At ICFM9, we presented a new approach that offers the prospect of keeping the Netherlands safe beyond 2100 at a socially acceptable cost and with public support (De Leeuw et al., 2024). This paper presents a further elaborated version of this approach including how it has been applied to Zwolle region, the Netherlands, and lessons learned. The six-step approach comprises of: 1) preparation: setting process rules, mutual agreement on process rules and a shared understanding of the system; 2) area analysis with a focus on values and historical developments; 3) exploration of the future for various themes and the water system; 4) exploration of possible futures using narratives and visuals, including the development of a value framework; 5) alternative landscapes and building blocks; and 6) transformation pathways that reason backwards using tipping-points and building blocks. For the Zwolle case, the approach resulted in illustrative products that allow stakeholders to experience different futures, as well as a qualitative comparison of a "business as usual development" with three value-oriented, but very different future perspectives. In future projects, we aim to test the approach with more stakeholders, in other areas and to extend the scope to water resilience in general.

KEYWORDS: Flood resilience, design methodology; landscape planning; cross-sectoral collaboration; governance.

1 INTRODUCTION

The Netherlands, a low-lying and densely populated country, is situated at the delta of rivers Rhine, Meuse and Scheldt. To protect residential and rural areas from flooding, an extensive flood defence system has been implemented over the last decades (de Leeuw et al., 2024 and Tromp et al., 2022). This system requires regular maintenance, e.g., due to increasing river discharges and expected sea level rise. Dealing with this challenge, the Dutch Flood Protection Programme (DFPP) primarily focuses on effectiveness (production rate) and efficiency (reduction of cost per kilometre) (de Leeuw et al., 2024). The DFPP is an alliance of the Ministry of Infrastructure and Water management and regional water authorities, and is responsible for keeping the flood defence system up to date, while considering societal developments and new insights (Jorissen et al., 2016). However, the challenge associated with achieving set flood defence

targets is especially wicked due to a high level of complexity, uncertainty and conflicting interests (Tromp et al, 2022). Flood risk issues are for example highly interdependent with other societal and spatial challenges related to agriculture, housing or energy, which all require the involvement of diverse stakeholders. Furthermore, governance of Dutch flood risk management is institutionally fragmented: Coastal and fluvial floods are managed by a national agency and regional water authorities, while the responsibility for managing pluvial flood issues is delegated to municipalities. Responsibility for spatial planning lies with national government, provinces and municipalities – the water authorities only have an advisory role.

Meanwhile, consequences of climate change are becoming increasingly evident in water management in the Netherlands, and urbanisation further increases pressure on available space. Consequently, its margins to cope with extreme weather—such as heavy rainfall and drought—are narrow, calling for more integrated flood risk management approaches. To preserve perspective for future generations, long-term climate risks must be considered in short-term spatial projects and decisions (Pot et al. 2022), which requires diversification of flood risk management strategies (Hegger et al. 2016). However, integrating water management with other spatial challenges appears to be challenging. New residential areas are still being built in low-lying, flood-prone areas and floodplains, and agriculture and natural areas continue to dry out because economic decisions often ignore soil and water system characteristics. How can we ensure robust spatial choices so that future generations also enjoy a prosperous and attractive future?

To answer this question, this paper presents how the novel '*Flood Resilient Landscapes*' (FRL) approach, which was presented at ICFM9 (De Leeuw et al., 2024), can be practically applied. To illustrate this, we use the application in Zwolle region, the Netherlands, as a case. This case was selected given the urgent need to find new ways to achieve socio-economic development and climate resilience in an area where space is limited and also needed for other transitions. In this case, the approach was translated into six steps that guided diverse stakeholders in designing future landscapes that can address both climatic and societal challenges and identifying transformation pathways. After showing how each of the steps were applied in this case, we conclude with lessons learned and an outlook towards the future.

2 APPLICATION OF THE STEP-WISE APPROACH

The FRL approach was developed as context-driven and human-centred design approach (Hekkert and Van Dijk, 2017). Through application in Zwolle region, we were able to further develop and test the approach. In this case, an interdisciplinary team of area partners and experts active in water management and spatial planning followed six steps (see figure 1) to collaboratively design future-oriented perspectives for a landscape where flood resilience goes hand-in-hand with other developments (De Leeuw et al., 2025a and 2025b, www.waterveiligheidslandschappen.nl). Each step involved at least one workshop. The steps are elaborated below.

2.1 Preparation

Implementation of design-based approaches like the FRL approach demands collaboration between diverse actors. In the case of Zwolle, we paid specific attention to developing a shared understanding of the area and making process rules and values explicit. In developing a shared understanding of the area, we prepared a comprehensive systems analysis and also organized a field trip. We learned that approaches like this necessitate flexibility and a different mindset, regarding existing information and its application. Hence, we really invited participants to take time and space for internalising and reinterpreting existing data collaboratively.

As previous research into integrative approaches (Warbroek et al., 2023; Bakhanova et al. 2025) shows that collaboration between diverse sectors benefits from designing process rules that can guide cross-sectoral collaboration, we paid explicit attention to drafting process rules. Inspired by the rules as presented in the Institutional Analysis and Development framework of Elinor Ostrom (2011), we made specific agreements about scope, participation, positions, information, expectations of way of involvement, decision-making and results.

Another key element of the preparation phase was making professional values explicit. Using value cards that were developed as part of a research project, we asked experts to identify and reflect on values that guide their work. This exercise showed that professional values of experts in water management differ significantly from experts in spatial planning (De Vries et al., under review). In later steps, we built on these insights to develop an integrated value framework.

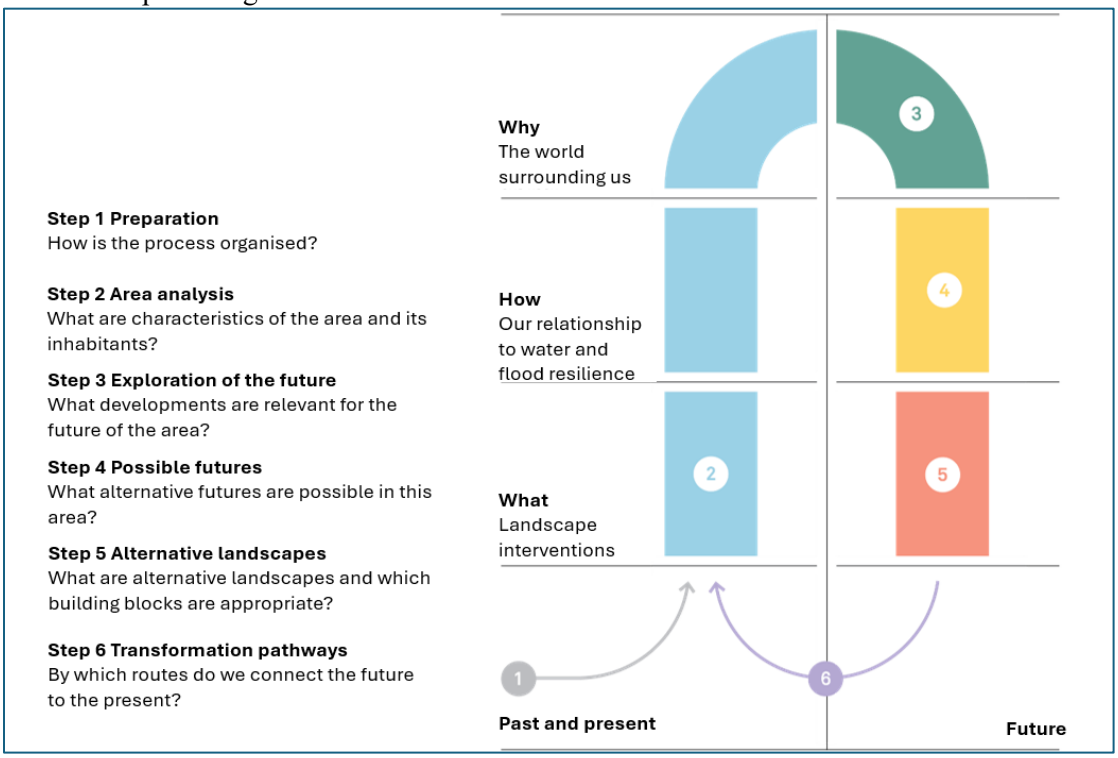

Figure 1: Central approach to the Joint exploration of flood resilient landscapes

2.2 Area analysis

Central in the second step is the analysis of the study area, with a focus on developing an in-depth, shared understanding of the region and its historical development. The analysis addresses not only the physical evolution of the area, but also the extent to which human decisions have influenced that evolution. By jointly engaging in this process, stakeholders gain insight into the values that are important to the local population and how these values have shaped the current spatial configuration. Such an analysis gives insight into how, in the study area, tipping points lead to changing views or strategies. To support the area analysis and apply different perspectives, the framework of narratives for flood resilient landscapes (Reframing Studio & Deltares, 2022, de Leeuw et al., 2024) inspires a holistic analysis. This framework distinguishes future oriented narratives along three perspectives and was used to construct a historic timeline to analyse developments at three interrelated levels: the physical water and spatial system (matterscape), institutional arrangements and power relations (powerscape), and societal values and practices (mindscape) (De Leeuw et al, 2025a and 2025b). By jointly reconstructing these developments in the Zwolle case, participants built a shared understanding of how past choices have shaped the current landscape and water management practices.

2.3 Exploration of futures

The analysis of the past is followed by a forward-looking exploration that systematically examines future trends and changes within the area. In the Zwolle case, we considered a broad set of themes: demography, social developments, spatial developments and developments in technology, economy, culture, and (geo)political situation. Additionally, we conducted an in-depth analysis of the capacity of

the current water system to cope with climate change impacts, including flood management in response to increasing precipitation and sea level rise, as well as drought management.

During the process, it appeared essential to spatially represent the urgency of emerging challenges. In the case of Zwolle, we therefore performed a stress-test that was inspired by cloud bursts that occurred in 2021 in the Eiffel and caused flooding in Germany, Belgium and the south of the Netherlands (figure 2). This stress-testing exercise provided critical insight into the necessity of making informed strategic choices. Additionally, there appeared to be a need to visually represent consequences of continuation of the traditional Dutch spatial development and water and flood management practices; this led to a "Business as usual" exploration of spatial development and served as reference scenario for comparing alternative futures in step 5.

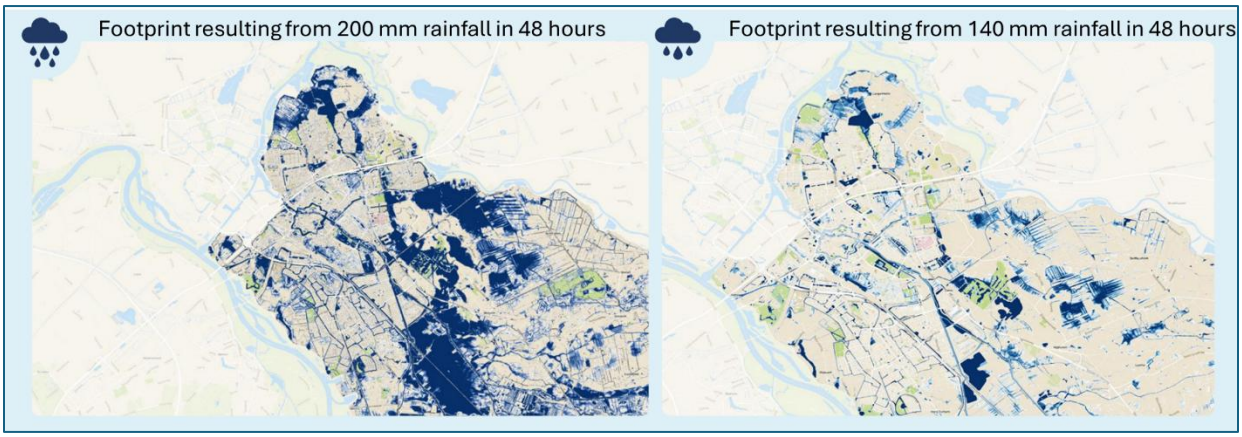

Figure 2: Stress-tests to generate a joint sense of urgency

2.4 Possible futures

Conventional approaches to regional development processes tend to reason from current challenges. The FRL approach differs in this regard; it reasons from societal values associated with diverse future user groups and their relationship to managing flood risks. Following up on the exploration of the past in step 2, the exploration of possible futures is inspired by the national framework of narratives for flood resilient landscapes (Reframing Studio & Deltares, 2022; de Leeuw et al., 2024). This framework distinguishes future-oriented narratives along three perspectives (mattercape, powerscape and mindscape) which articulate alternative ways of understanding and organizing the relationship between society, water and space. The narratives are used as a design and dialogue tool to move beyond current problem definitions and to explore fundamentally different long-term approaches to deal with water-related challenges. Since it is important to *temporarily* let go of current (organizational) challenges and objectives, this step starts with a role play in which participants are asked to step into the role of a future inhabitant of the area. Through dialogic engagement, supported by narratives and visualizations, multiple future perspectives are collectively explored and prioritized. Prioritized perspectives are elaborated in suitable and plausible future narratives informed by the local context. To refine the narratives that were generated and making them immersive, visuals were created. Table 1 gives an overview of three future perspectives of the Zwolle case.

Table 1: Future perspectives for the Zwolle case

Selected and applied narrative	Description	Example of visual	Agriculture visual
Protectionistic	*Business as usual* The story of continuing traditional spatial planning, creating housing, and technology-driven water management (protection by levees)	Not available	Not available

Collectivist and protectionstic	*New Neighborship* The story of traditional view on flood risk management, protecting cultural heritage, traditions and sense of community, e.g. through neighbourhoods.		
Ecocentric and amphibious	*Big Marshes* The story of adaptation to nature and a society that puts ecosystem thinking central.		
Ecomodern and global	*Hanze Deltalab* The story of a strong belief in technology as means to cope with global challenges. Functions are separated leading to strong contrast between urban and nature areas.		

In parallel to creating future visions, a shared value framework was established, enabling joint decision-making and bridging the identified gap between the water management and spatial planning domains (see step 1, De Vries et al., under review). In mixed groups, participants were able to develop an integrated, and shared value framework. The framework that was developed for comparing long-term landscape variants (100 years) contains the following values:

- **Ecological sustainability**: The landscape variant contributes to biodiversity, improved water and soil quality, and an ecologically sustainable design that supports climate resilience;
- **Economic sustainability**: The landscape variant creates opportunities for the economy and ensures the continuous functioning of the landscape without pursuing economic depletion;
- **Socio-cultural sustainability**: The landscape variant leverages cultural heritage, strengthens social cohesion, and avoids passing burdens onto future generations;
- **Adaptivity**: The landscape variant is adjustable, flexible, and capable of responding to changing conditions;
- **Safety**: The landscape variant guarantees safety and health for residents.

2.5 Alternative landscapes

In the fifth step, future perspectives are elaborated and concretised. In the Zwolle case, this was done through the development of three landscape variants, following the narratives of step 4, which were called: New Neighborship, Big Marches and Hanze Deltalab. Spatial representations make these future perspectives tangible and reveal spatial interconnections. For each future perspective, a set of building blocks is selected and further defined in terms of spatial scale, and level of integration. Building blocks refer to interventions in the water system, spatial design, legislation and regulation, as well as education and knowledge development, all of which are necessary to realize a future perspective. Therefore, these building blocks often serve multiple functions. Figure 3 shows the results of the Zwolle case, with a focus on water and spatial design at a system scale and a local scale.

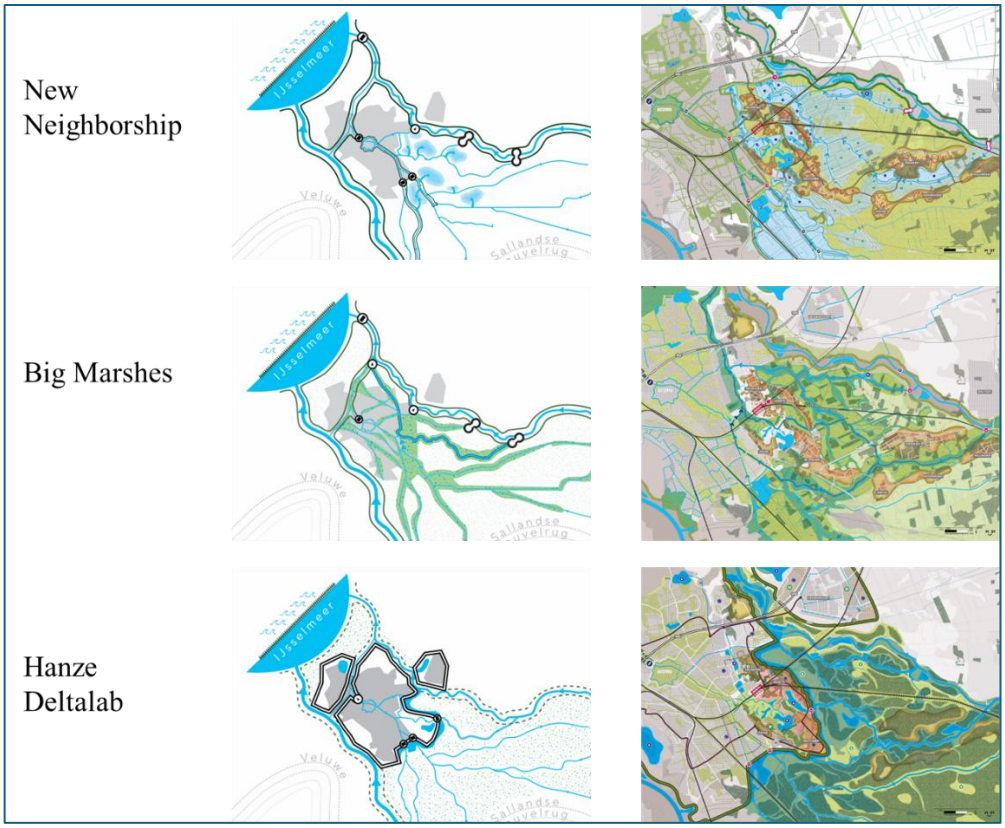

Figure 3: Landscape variants of Zwolle case

2.6 Transformation pathways

The final step in the FRL approach is to develop transformation pathways using a back-casting procedure for each future perspective. In this process, future tipping points (derived from step 3, Exploration of the future) play a key role since building blocks should be implemented before reaching a tipping point. In the Zwolle case, we emphasized that implementation requires not only construction activities but also preparation: e.g., securing funding, acquiring societal support in participation processes and setting up legal and governmental settings. Drafting timelines created urgency, as implementing building blocks in a few decades often requires preparation in the immediate future. In estimating the potential societal transitions required, attention is given to conditions across social, technical, spatial, economic, legal, ecological, and knowledge domains.

3 REFLECTIONS & CONCLUSIONS

When we started application of the FRL approach to Zwolle, many experts involved and participants were not or only familiar with part of the approach. Given the openness of the process and the need to learn we decided to adopt a 'reflection-in-action' methodology (c.f. Hartmann et al., 2023) throughout the process. This method has been developed for large construction projects but was used here to support continuous reflection, keeping track of lessons learned and, where possible, apply them directly in the project. At different points in time, we organized reflection and learning moments (three in total). Each moment was organized as follows. First, participants individually completed a questionnaire, which addressed the process and content of the organized activities, as well as the relevance of the project and the insights gained for the national programme that funded the project, water authorities, provinces, and municipalities. After processing the individual responses, we collectively reflected on them and drew conclusions. Some of the key insights that emerged from these reflections are:

- By exploring different values of spatial planners, designers and flood risk managers followed by discussing the results, mutual understanding, a shared vision, and a common narrative were fostered.
- The approach facilitates meaningful discussions about what matters for the area's development and which qualities should be preserved or enhanced. By confronting future transition challenges, the approach generates insights into smart combinations.
- A shared understanding of the area's history is essential for exploring an uncertain future together.
- Eight national narratives (Reframing Studio & Deltares, 2022) provided a strong foundation for discussing future storylines.
- The design-based research approach and intermediate reflections led to the integration of useful tools like timelines, a serious game based on role-playing, and transformation path-building tools.
- Stress tests and extrapolations of the current discourse ("business as usual") help identify problematic future choices.
- More, integrative and multi-use building blocks are desired.
- The Zwolle case showed that current practices are not fostering resilience in the long term. Each of the future perspectives reacted in its own character to enhance the robustness and flexibility of the water system, to enable it to cope with the effects of climate change. To the municipality, the case was another sign that future water management issues needed to be addressed in their new spatial perspective on housing and other transitions, which was adopted by the Council on July 7, 2025.

In the Zwolle case, the approach was applied in a rather 'informal' setting, giving space to participants to share opinions and views without the fear of being compromised for their views and opinion. Inhabitants or interest groups were not included. Also, decisions were not an intended outcome. As such, participants could freely explore the diversity of possible futures for an area. Future steps include supporting the implementation of area-specific choices in the short and medium term, while also considering long-term scenarios. This includes calculating the effectiveness of measures and socio-economic welfare impacts across timeframes, and providing governance advice for realizing attractive, future-proof, productive, water-robust landscapes. In this next phase, the project team advances on the main project insights, moving away from the term 'flood resilience', as water issues are not only bound to flood risks, but also to droughts and water quality.

An important reason for selecting Zwolle region as a case was that many issues are at play. Each (economic) sector tends to look for space from its own objectives, whereas from a water system point of view, the robustness and flexibility are too low to be able to cope with future challenges in which different sectors take space, and where climate change stresses the system. We expect that the case is quite representative for the Dutch institutional context, which is characterised by the tradition of creating a man-made environment optimised for economic use. International perspectives on the approach and its underlying cultural assumptions would be needed to evaluate applicability in other international delta areas.

4 ACKNOWLEDGEMENTS

This text is based on the development of the Flood Resilient Landscapes approach, leading to area visions and associated transition paths in the DFDP Innovation project Flood Resilient Landscape Zwolle and the TKI project www.waterveiligheidslandschappen.nl. Contributors include: Deltares, Wageningen Environmental Research, Wageningen University, University of Twente, Reframing Studio, MUST Urban Landscape Architects, LAOS Landscape Architects, SWECO, and RHDHV. The Zwolle case was successfully carried out thanks to the support and active involvement of the municipalities of Zwolle, water authority Drents Overijsselse Delta, the province of Overijssel, DFDP, and the Ministry of Infrastructure and Water Management.

REFERENCES

Bakhanova, E., Vinke-de Kruijf, J. Wöhler, L, Warbroek, B. Arentsen, M. (2025). Integrative Approaches to Interconnected Environmental Challenges: How Institutional Factors Influence Cross-Sector Integration in Dutch Rural Areas . Environmental Management 75:1308–1321. https://doi.org/10.1007/s00267-025-02140-2

De Leeuw, A.M., Tromp, E. and de Boer, F: Flood resilient landscapes: area-based solutions combine added value for society with flood risk management, Proc. IAHS, 386, 173–179, https://doi.org/10.5194/piahs-386-173-2024, 2024.

De Leeuw, A.M., de Boer, F.M., Koppel, S, Mateman, E., Vinke de Kruif, J. (2025a): Aanpak waterveiligheidslandschappen: Een methodiek om in zes stappen te komen tot een toekomstbestendig landschap. https://publications.deltares.nl/WeL3280.pdf.

De Leeuw, A.M., de Boer, De Vries, M.C.J., F.M., Dijkstra, M.J., Köppel, S., Mateman, E, Niesten, M., Oenema, A.J., Rooze, D., van den Berg, F., Vinke de Kruif, J: (2025b): Toekomstbestendig landschap Zwolle : een toepassing van de methodiek Waterveiligheidslandschappen. https://publications.deltares.nl/11209756_000_0005.pdf.

De Vries, M.C.J., Vinke-de Kruijf, J., Volker, L., Augustijn, D.C.M., Mind the gap: the role of values in integrated flood risk management. Under review in Environmental Science and Policy.

Hartmann, A., Vinke-de Kruijf, J., & Van Weesep, R. (2023). Asking the right questions: The role of reflection for learning in and between projects. International Journal of Project Management, 41(5), 102494. https://doi.org/10.1016/j.ijproman.2023.102494

Hegger, D. L. T., P. P. J. Driessen, M. Wiering, H. F. M. W. Van Rijswick, Z. W. Kundzewicz, P. Matczak, A. Crabbé, G. T. Raadgever, M. H. N. Bakker, S. J. Priest, C. Larrue, and K. Ek. 2016. Toward more flood resilience: Is a diversification of flood risk management strategies the way forward? *Ecology and Society* 21(4):52. https://doi.org/10.5751/ES-08854-210452

Hekkert, P. and Dijk, M. van: Vision in design, a guidebook for innovators. ISBN 978-90-6369-371-8, 2nd printing 2017Tromp, E., te Nijenhuis, A. and Knoeff, H.: The Dutch Flood Protection Programma: Taking innovations to the next level, Water 2022, 14(9), 1460; https://doi.org/10.3390/w14091460.

Jorissen, R.; Kraaij, E.; Tromp, E. Dutch flood protection policy and measures based on risk assessment. In Proceedings of the 3rd European Conference on Flood Risk Management (FLOODrisk 2016), Lyon, France, 17–21 October 2016.

Ostrom, E. (2011). Background on the institutional analysis and development framework. Policy Studies Journal, 39(1), 7-27 https://doi.org/10.1111/j.1541-0072.2010.00394.x

Pot, W.D., De Vaan, K., Dewulf, A. (2022), Institutions for long-term problems: the influence of the Dutch Delta Programme on forward-looking climate adaptation responses at the local level, https://doi.org/10.1080/09640568.2022.2153331

Reframing Studio & Deltares (2022) – in Dutch. Toekomstige narratieven rondom waterveiligheid: Als onder deel van het Raamwerk Waterveiligheidslandschappen. https://cms.deltares.nl/assets/common/downloads/221208_WVL2100_Eindrapportage-gecomprimeerd-1.pdf

Tromp, E., te Nijenhuis, A. and Knoeff, H.: The Dutch 50 Flood Protection Programma: Taking innovations to the next level, Water 2022, 14(9), 1460; https://doi.org/10.3390/w14091460

Warbroek, B., Holmatov, B., Vinke-de Kruijf, J., Arentsen, M., Shakeri, M., de Boer, C., Flacke, J., & Dorée, A. (2023). From sectoral to integrative action situations: an institutional perspective on the energy transition implementation in the Netherlands. Sustainability Science, 18, 97-114 https://doi.org/10.1007/s11625-022-01272-2

Web sites:

www.waterveiligheidslandschappen.nl, consulted 30 November 2025

ICFM 10
Adapting to Global Change:
Innovative Approaches to Flood Management and Resilience
May 20-22, 2026 | Western University, London, Ontario, Canada

A Flood Risk Analytics and Visualisation Platform for Socio-Economic Scenarios

Isha Dev[1], Sabirul Sk[2], Nirul Ranjan Patra[1] and Subhankar Karmakar[1,3]

Environmental Science and Engineering Department, Indian Institute of Technology Bombay, Mumbai 400076, India [1]

E-mail: ishadev.iitb@gmail.com; sabirul@iitb.ac.in; nirul23@iitb.ac.in

Centre for Climate Studies, Indian Institute of Technology Bombay, Mumbai 400076, India[2]

E-mail of corresponding author: skarmakar@iitb.ac.in

ABSTRACT

Flood risk assessments increasingly require integration of hazard impacts with socioeconomic vulnerability (SEV) to support equitable resilience planning, as emphasised by the Intergovernmental Panel on Climate Change (IPCC) in their last two cycles of Assessment Reports (AR5 and AR6). This study presents a Flood Risk Analytics and Visualisation Platform, an interactive tool that links flood hazard information with diverse socioeconomic scenarios to support decision-making. Developed using PowerBI, an interactive data visualisation tool that enables rapid exploration of flood-prone areas, associated socioeconomic conditions, and localised vulnerability drivers, providing actionable insights for policymakers and practitioners. Maharashtra, India's second-most populous state and a region experiencing recurrent floods every two to three years, is used as a case study to demonstrate the platform's applicability. While previous national and regional assessments have evaluated vulnerability, they often lack sub-district (talukas/tehsils) level resolution with limited SEV indicators. To address these gaps, the study quantifies SEV for 357 sub-districts using demographic and census-based indicators, with indicator weighting optimised through a non-parametric Data Envelopment Analysis (DEA) approach to minimise subjective bias. The results reveal high vulnerability clusters in the Central and Eastern Vidarbha Zone, moderate vulnerability across the Central Maharashtra Plateau, and relatively lower vulnerability in the North Konkan Coastal and Western Maharashtra zones. By integrating these analytical outputs into an interactive visual platform, the study provides a scalable and adaptable decision-support tool capable of informing targeted vulnerability reduction and resilience strategies. The platform's capacity to evaluate fine-resolution SEV alongside flood hazard information strengthens its utility for locally grounded adaptation planning and policy formulation.

KEYWORDS: Adaptation planning, decision-support platform, disaster risk reduction, flood risk, Socioeconomic vulnerability, vulnerability indicators

1 INTRODUCTION

Natural catastrophes have become both more frequent and more financially devastating since the 1970s (Yamamura, 2015), a trajectory expected to intensify as greenhouse gas concentrations continue to rise (IPCC, 2018). The uneven spatial and social distribution of disaster impacts underscores the interplay between climate change, hazard recurrence, and socioeconomic vulnerability (Groeschl & Noy, 2020). Marginalised and resource-constrained populations consistently bear a disproportionate share of losses (Benson et al., 2001; Sakai et al., 2017), highlighting the critical need for inclusive risk-reduction policies that prioritise vulnerability reduction and resilience building. In developing nations such as India, where more than 95% of global disaster-related deaths between 1970 and 2008 were recorded (IPCC, 2012), the growing recurrence of floods, droughts, and heatwaves continues to threaten sustainable development trajectories.

Floods are among the most recurrent natural hazards worldwide, primarily driven by extreme rainfall events that disrupt livelihoods and cause substantial socio-economic losses (IFRC, 2011; Dottori et al., 2018).

While accurate flood forecasting and preparedness are essential for risk reduction, they remain challenging due to the complexity of atmospheric and land–surface interactions (Fritsch et al., 1988). The IPCC AR6 (2023) conceptualises disaster risk as a function of hazard, exposure, and vulnerability, with hazards escalating into disasters when they intersect with populations lacking adaptive capacity (Birkmann, 2006). In Maharashtra, existing vulnerability assessments are commonly aggregated at the district level, obscuring intra-district heterogeneity that is crucial for targeted interventions. To address this limitation, the present study develops a high-resolution socioeconomic vulnerability (SEV) assessment at the sub-district (tehsil) scale using 23 indicators derived from the 2011 Census of India. Indicator weighting subjectivity is reduced via a non-parametric Data Envelopment Analysis (DEA) optimisation approach. Complementarily, a probabilistic rainfall hazard model combining IMD observations with GEFSv12 forecasts captures event-specific hydroclimatic extremes, validated using two intense rainfall events in Raigad during 2015 and 2016.

Building on these analytical outputs, the study operationalises high-resolution SEV and hazard results through a Flood Risk Visualisation Platform developed in PowerBI (Bhargava et al., 2018). Integrating both components within an interactive dashboard environment enables users to explore spatial patterns of flood susceptibility, interrogate the socioeconomic drivers of vulnerability, and compare risk profiles across sub-districts. By combining analytical rigour with intuitive geo-visualisation, the platform strengthens the accessibility and usability of spatial risk evidence for policymakers, disaster managers, and development practitioners supporting informed prioritisation, early-warning preparedness, and locally grounded adaptation planning.

2 DATA AND METHODOLOGY

2.1 Study Area

Maharashtra, located in western–central India, is the country's second-most populous and third-largest state, spanning ~0.31 million km² and hosting 112.4 million people (Census of India, 2011). It is highly urbanised, with major metropolitan centres such as Mumbai, Pune, Nagpur, and Nashik, and serves as India's leading state economy with a GSDP of ~USD 435 billion in 2022–23 (Maharashtra State Disaster Management Plan, 2023).

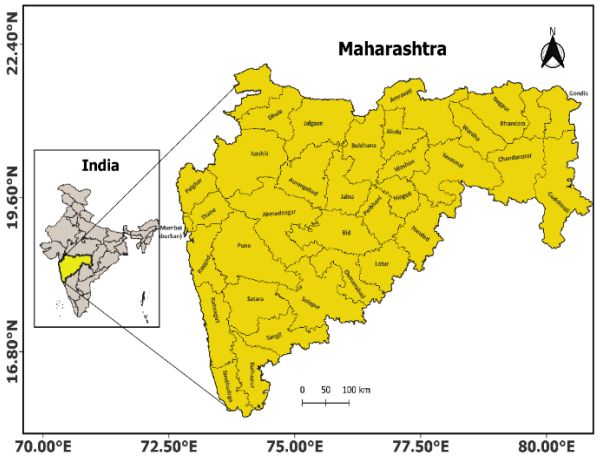

Figure 1. A map developed in QGIS showing the study area with a subdistrict-level map of Maharashtra showing the area.

2.2 Socioeconomic Vulnerability

The methodology comprises two core components: (i) high-resolution socioeconomic vulnerability (SEV) assessment at the sub-district scale, and (ii) probabilistic rainfall-based hazard estimation. The integrated

workflow adopted in this study is summarised in Figures 2 and 3. First, SEV indicators derived from demographic and census datasets were pre-processed, normalised, dimension-reduced using Principal Component Analysis (PCA), and weighted through a Data Envelopment Analysis (DEA) framework to produce sub-district-level vulnerability scores (Figure 2). Second, observed IMD rainfall records and GEFSv12 forecasts (2000–2019) were jointly modelled using kernel-based bivariate functions to estimate conditional exceedance probabilities representing rainfall-induced hazard values (Figure 3). The resulting SEV and hazard layers form the basis for spatial flood risk estimation and visualisation.

2.2.1. Normalisation of Indicators

The socioeconomic data for the 357 sub-districts in Maharashtra were extracted from the recent Indian Census of 2011 from the Census of India (CoI) official website. Indicator selection was based on a comprehensive review of relevant literature. The selected indicators should be relevant, highly feasible, better representative, and justifiable with respect to the particular study (Bogardi & Birkmann, 2004; Sherly et al., 2015). Initially, 35 indicators were chosen for their relevance and availability at the sub-district level. These indicators were classified as sensitive and adaptive, depending on whether they increase or decrease SEV. The selected indicators were then merged into 23 composite indicators. The indicators were then normalised to make them dimensionless (Wu et al., 2002; Karmakar et al., 2010). The normalisation process followed the equations mentioned in the study –

$$V_{ij}^{std} = \frac{V_{ij} - V_i^{min}}{V_i^{max} - V_i^{min}} \qquad (\forall i \subseteq S) \qquad (1)$$

$$V_{ij}^{std} = \frac{V_i^{max} - V_{ij}}{V_i^{max} - V_i^{min}} \qquad (\forall i \subseteq S^C) \qquad (2)$$

where, V_{ij}^{std} represents the standardised indicator value and V_{ij} is the actual value of the i^{th} indicator for the jth decision-making unit (DMU). The DMUs are the sub-districts selected in the study domain, i.e., the entire Maharashtra state. The S and S^C represent the set of sensitive and adaptive indicators for all the DMUs. In the above equation, the V_i^{max} and V_i^{min} are the maximum and minimum values of the indicator for the ith indicator, considering all sub-districts.

2.2.2 Principal Component Analysis and Data Envelopment Analysis

Principal Component Analysis (PCA) was used to identify the key components and to decorrelate and reduce the indicators' dimensions after normalisation. The Kaiser criterion was used to select the number of significant PCs. According to the Kaiser criterion, six components (i.e., the first 6 PCs) were identified as significant. The Kaiser rule suggests discarding any components with eigenvalues less than 1.0, as an eigenvalue of 1.0 represents the amount of information explained by an average individual item. PCA was performed using MATLAB Software. Six significant PCs were selected as per the analysis, which explains 84.86% of the total variance, and the resulting components were then input into the Data Envelopment Analysis (DEA) model in R Software. This model was used to determine the efficiency of the decision-making units (DMUs), the sub-districts in this case. This technique is a non-parametric approach, which optimises each sub-district to calculate a discrete piecewise frontier, as per the estimation by the complete set of Pareto-efficient DMUs (Vittal et al., 2020).

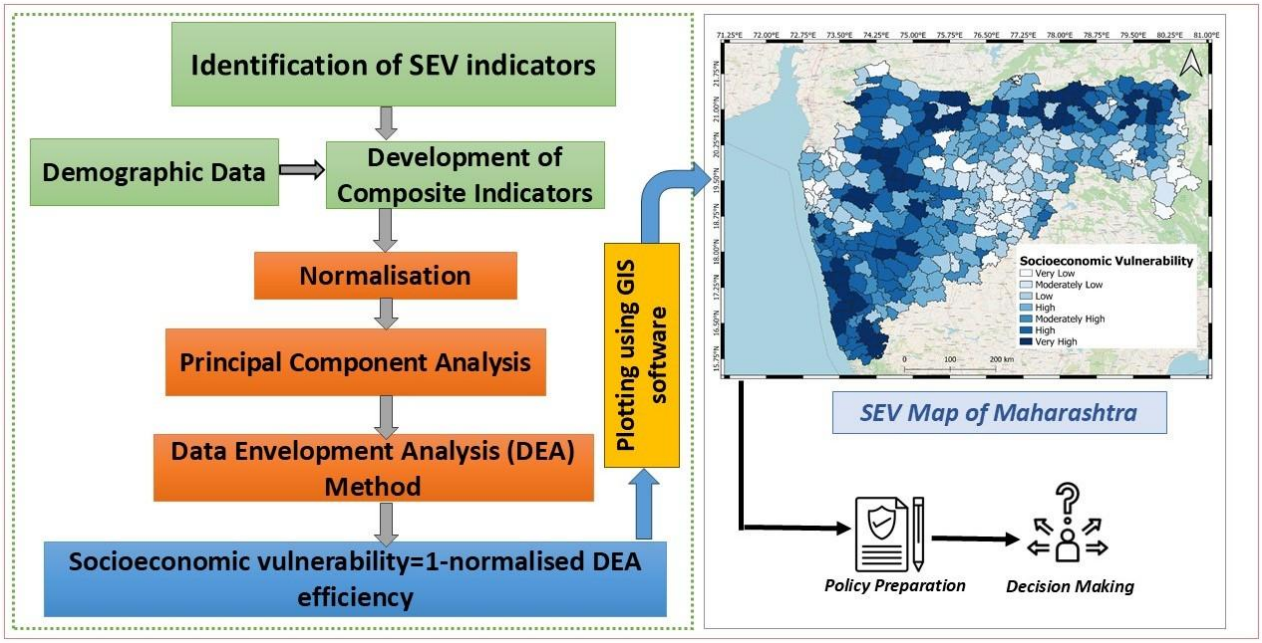

Figure 2. Methodological framework for constructing the Socio-Economic Vulnerability (SEV) map using a hybrid approach integrating Principal Component Analysis (PCA) and Data Envelopment Analysis (DEA). It also represents the sequential workflow from indicator selection and data normalisation to dimensionality reduction via PCA and efficiency score estimation using DEA

2.2.3 Finding major drivers of vulnerability

To identify the major drivers of socioeconomic vulnerability, the variance-based factor analysis was done to find the contribution of the important indicators in the significant PCs. The significance of an observation for a component is determined by the ratio of the observation's squared factor score to the eigenvalue corresponding to that component. This ratio is referred to as the observation's contribution to the component (Abdi & Williams, 2010; Dhakal et al., 2020; Shlens, 2014; Uddin et al., 2019). This method is based on variance; the variance of individual indicators is evaluated only on the significant PCs (here, 6 PCs).

2.3 Hazard Calculation

For this study, year-wise precipitation forecasts during the Indian summer monsoon months—June to September (122 days/year) were utilised. The final dataset has dimensions of 122 × 11 × 40 × 33 × 26, representing days, ensemble members, 6-hourly forecast steps across 10 days, and spatial grids (latitude × longitude). GEFSv12 provides 5 ensemble members per day (c00, p01–p04) and 11 members on Wednesdays (c00, p01–p10). From these files, only the 6-hourly forecast steps were retained. Time series models were applied separately to observed and forecasted datasets to capture temporal dependencies. A bivariate kernel density estimation method was used to construct a joint distribution, enabling the computation of conditional probabilities of extreme rainfall events. The methodology was applied to two heavy rainfall events—3rd August 2016 and 22nd June 2015—in the Raigad district of Maharashtra.

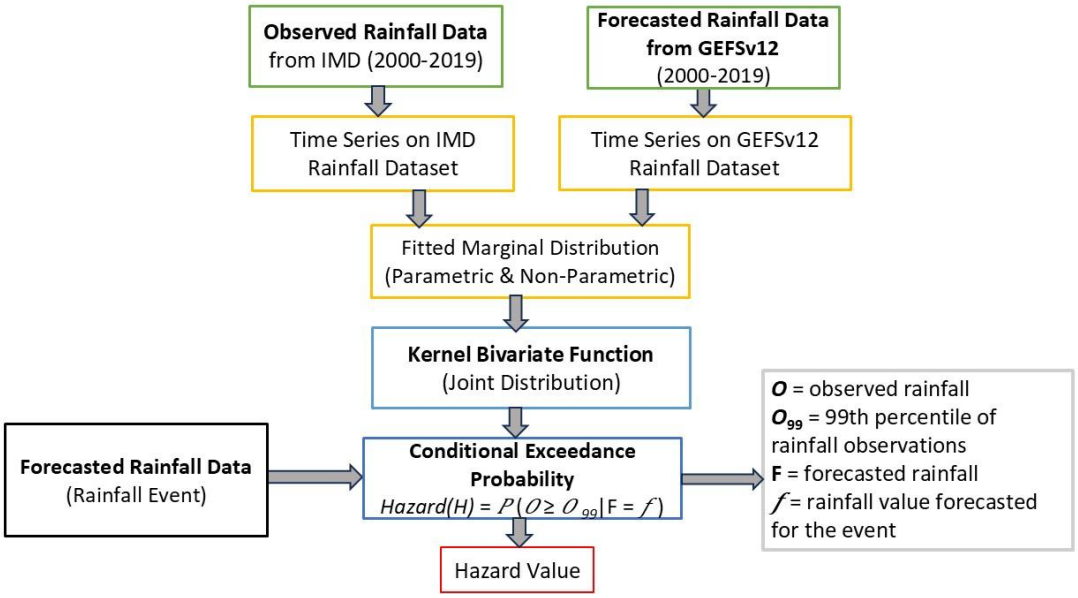

Figure 3. Methodological framework for deriving hazard values using bivariate modelling of observed and forecasted rainfall. The observed (IMD) and forecasted (GEFSv12) rainfall datasets for the period 2020–2019 are individually fitted with marginal distributions and time series models. These are then combined using a Kernel Bivariate Function to estimate the joint distribution. This joint probability is used as the hazard value.

2.3.1 Extreme Precipitation Risk Mapping

Conventionally, risk associated with extreme events is conceptualised as the product of hazard, vulnerability, and exposure, a framework widely adopted in disaster risk science (Chen et al., 2015; Gusain et al., 2020; IPCC, 2012; Karmakar et al., 2010; Kron, 2005; Sahani et al., 2019). This formulation emphasises that the overall risk is not solely dependent on the likelihood of an extreme event (hazard), but also on how exposed a system or population is, and how susceptible they are to harm.

$$\text{Risk} = \text{Vulnerability} \times \text{Hazard} \tag{3}$$

3 RESULTS

3.1 Socioeconomic Vulnerability Assessment

Figure 4 illustrates the spatial distribution of socioeconomic vulnerability at the sub-district level across Maharashtra, derived using a composite index developed through Data Envelopment Analysis (DEA). DEA, a non-parametric linear programming technique, was employed to assess the relative vulnerability of sub-districts by benchmarking multiple Census of India (2011) indicators representing demographic pressure, housing conditions, access to basic services (drinking water, electricity, sanitation), employment characteristics, and social marginalisation. Vulnerability is quantified as deviation from an efficiency frontier, enabling the identification of sub-districts performing poorly relative to comparable administrative units under similar constraints. The resulting vulnerability scores were classified into seven ordinal categories—Very Low (VL), Low (L), Moderately Low (ML), Medium (M), Moderately High (MH), High (H), and Very High (VH)—using the Jenks natural breaks algorithm. This approach minimises within-class variance while maximising inter-class differences, thereby enhancing the representation of spatial heterogeneity.

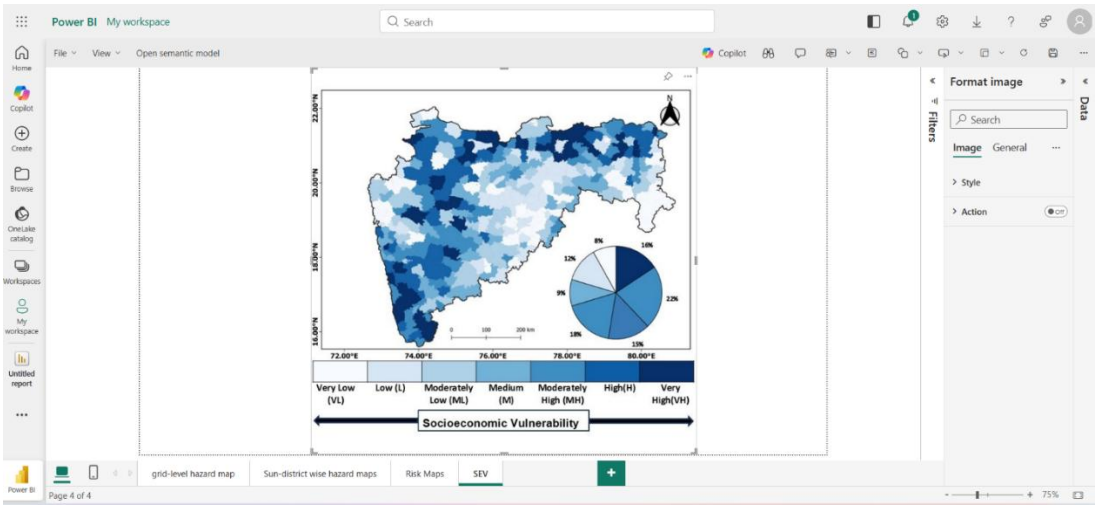

Figure 4. A PowerBI snippet showing the spatial distribution of the Socio-Economic Vulnerability (SEV) Index across sub-districts in Maharashtra, India. The SEV scores are classified into seven ordinal categories, ranging from "Very Low" to "Very High," with progressively darker shades indicating higher vulnerability levels. An inset pie chart displays the proportion of the total geographic area falling within each SEV class across the state.

The map reveals pronounced clustering of higher vulnerability classes (H and VH) in the southern, southeastern, and northeastern regions of Maharashtra. These areas are predominantly characterised by rural settlements, greater dependence on climate-sensitive livelihoods such as agriculture, and relatively limited access to public infrastructure, increasing their susceptibility to hazard-induced disruptions.

3.2 Hazard

To demonstrate and validate the proposed hydroclimatic hazard assessment framework, two major extreme rainfall events in Maharashtra were selected as case studies. The first occurred in June 2015 during the early monsoon, with a maximum daily rainfall of 292.21 mm centred near Poladpur. The second event took place in August 2016 in the Konkan region and recorded one of the highest single-day rainfall intensities in the dataset (338.52 mm), again focused around Poladpur in Raigad district (Fig.5). These events were chosen due to their high spatial rainfall variability, severe impacts on infrastructure and livelihoods, and their representativeness of monsoon-driven hazards along the Western Ghats.

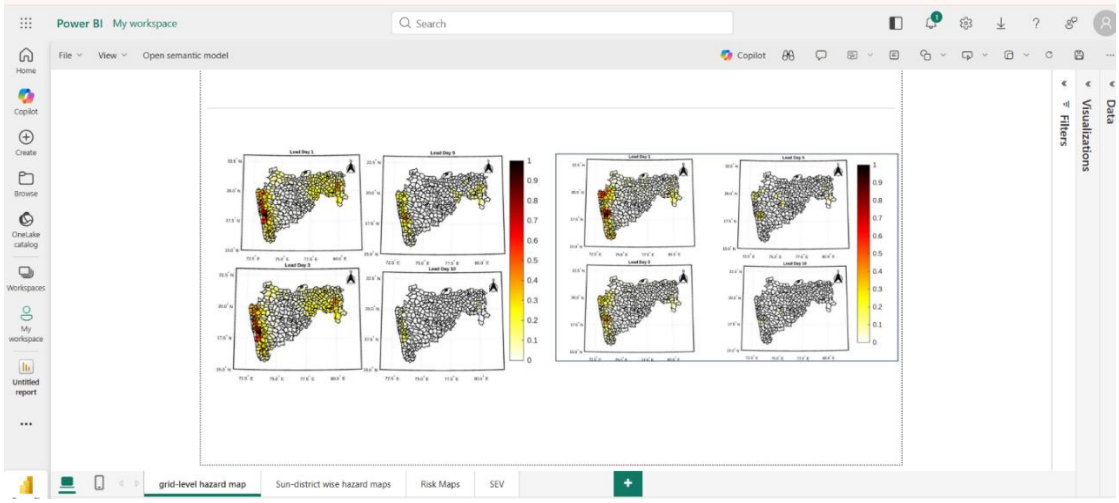

Figure 5. A PowerBI snippet showing Grid-level hazard probability maps for 19 June 2015 and 3rd August 2016 across increasing lead times

For both events, grid-wise hazard values were computed for forecast lead times of 1, 3, 5, and 10 days, representing the joint probability of observed rainfall exceeding the 99th percentile given forecasted rainfall. For the June 19, 2015 event, lead day 1 exhibits high hazard values (>0.9) concentrated along the Konkan coast, particularly in southern Raigad, indicating strong forecast–observation agreement (Fig.6). The hazard zone expands modestly at lead day 3, while probabilities weaken at lead day 5 and become spatially diffuse by lead day 10. A similar pattern is observed for the August 3, 2016 event, with sharply localised high hazard at short lead times and rapid degradation of predictability at longer leads. Overall, the Konkan coast, especially Raigad, consistently emerges as a high-risk zone, with maximum predictive skill at shorter forecast horizons.

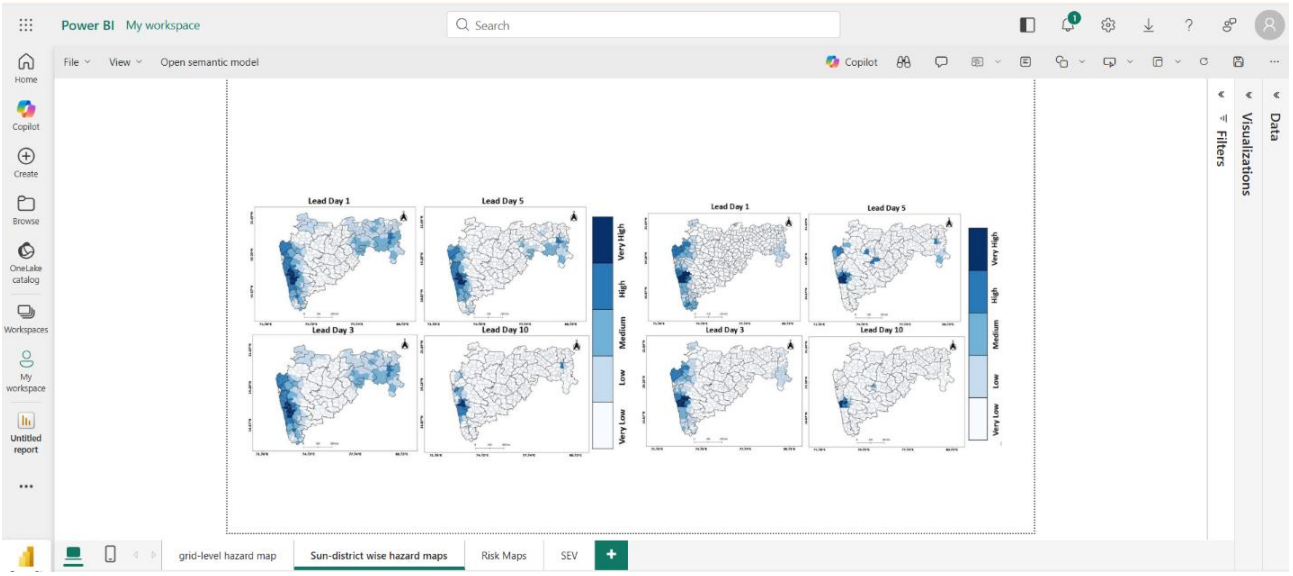

Figure 6. A PowerBI snippet showing the sub-district level hazard classification maps for 19 June 2015 and 3rd August for lead times

3.3 Risks Mapping

The spatial distribution of flood risk for the June 2015 event was analysed across forecast lead times of 1, 3, 5, and 10 days. The risk maps indicate that sub-districts in the Konkan region, particularly Raigad, Ratnagiri, and Sindhudurg, consistently exhibit High to Very High-risk levels at shorter lead times (Lead Days 1 and 3) (Fig.7). This pronounced clustering reflects the convergence of elevated hazard probabilities with high socioeconomic vulnerability. At Lead Day 1, risk is most intense, forming large contiguous Very High-risk zones along the western coast, where extreme rainfall coincided with vulnerable populations and infrastructure. With increasing lead time, particularly by Lead Day 10, both the spatial extent and intensity of risk decline markedly, indicating reduced forecast reliability and weaker alignment between hazard and vulnerability patterns. Notably, parts of the Vidarbha region display Moderate to High risk despite lower hazard levels, underscoring the amplifying role of vulnerability in shaping overall risk outcomes. For the August 2016 event, risk patterns show both similarities and contrasts. At Lead Day 1, the Konkan coast again emerges as the dominant high-risk zone, especially in southern districts such as Ratnagiri and Sindhudurg. By Lead Day 3, although Very High-risk areas contract, much of the western belt remains in High to Medium risk categories. At Lead Day 5, the focus of elevated risk shifts inland towards the Western Ghats and central Maharashtra, notably parts of Satara and Pune. By Lead Day 10, risk becomes sparse and spatially fragmented, reaffirming the importance of short-lead forecasts for effective flood risk preparedness.

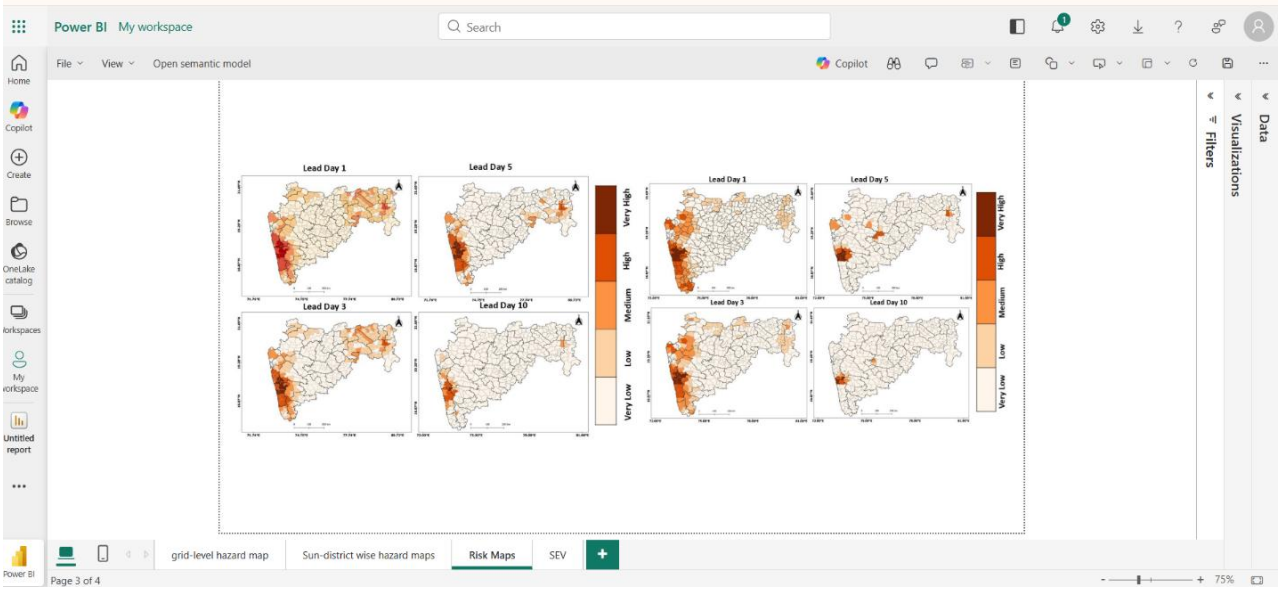

Figure 7. A PowerBI snippet showing sub-district level risk classification maps for 19 June 2015 and 3rd August

4 CONCLUSION

This study develops a high-resolution flood risk assessment framework for Maharashtra by combining sub-district-scale socioeconomic vulnerability (SEV) mapping with probabilistic rainfall hazard modelling, and translating these outputs into an interactive geospatial visualisation and decision-support platform. The resulting SEV surface highlights pronounced vulnerability in Central and Eastern Vidarbha and comparatively lower levels in Konkan and Western Maharashtra. Rainfall-induced hazard was estimated using a bivariate kernel density model of IMD observations and GEFSv12 forecasts (2000–2019), enabling robust characterisation of extreme rainfall probabilities.

Integrating SEV and hazard fields produced spatially explicit flood risk maps that were operationalised through a PowerBI dashboard to improve accessibility, interpretation, and scenario exploration, which are important prerequisites to sustainable adaptation planning. The platform enables policymakers and practitioners to interactively compare regions, analyse risk drivers, and evaluate targeted adaptation options, thereby strengthening evidence-based decision-making.The proposed framework is scalable, adaptable to additional hazard types, and demonstrates how modern visual analytics platforms can bridge the gap between research-oriented risk assessment and operational disaster risk management.

5 ACKNOWLEDGEMENTS

This research was supported by the Department of Science and Technology (DST), Government of India, through the SPLICE–Climate Change Programme (Sponsored Project: DST/CCP/CoE/140/2018), and by the Green Energy and Sustainability Research Hub (GESH) at the Indian Institute of Technology Bombay (Sponsored Project: DO/2024-RHUB004-003; Grant Number: 00000000000050004495). IIT Bombay has provided support with computational resources. The corresponding author gratefully acknowledges the generous support of the donors, Dr Vinaya Kapoor and Dr Samir Kapoor, for endowing the Vinaya & Samir Kapoor Chair Professorship in Climate Studies at the Centre for Climate Studies. The authors also gratefully acknowledge Dr Sohom Mondal for his valuable guidance and insights provided through telephonic and virtual discussions. The authors extend their gratitude to the Census of India and the Government of India for providing the detailed demographic dataset.

REFERENCES

Abdi, H. and Williams, L.J. (2010) Principal Component Analysis. Wiley Interdisciplinary Reviews: Computational Statistics, 2, 433-459.

Benson, C., Twigg, J., & Myers, M. (2001). NGO initiatives in risk reduction: an overview. *Disasters*, *25*(3), 199-215.

Bhargava, M. G., Kiran, K. T. P. S., & Rao, D. R. (2018). Analysis and design of the visualisation of the educational institution database using PowerBI tool. *Global Journal of Computer Science and Technology*, *18*(C4), 1-8.

Birkmann, J. (2006) Measuring Vulnerability to Promote Disaster-Resilient Societies: Conceptual Frameworks and Definitions. In: Birkmann, J., Ed., Measuring Vulnerability to Natural Hazards: Towards Disaster Resilient Societies, United Nations University Press, Tokyo, 9-54.

Dottori, F., Szewczyk, W., Ciscar, JC. *et al.* Increased human and economic losses from river flooding with anthropogenic warming. *Nature Clim Change* **8**, 781–786 (2018).

Fritsch, J. M., Houze, R. A., Adler, R., et al. (1998). Quantitative Precipitation Forecasting. *Bulletin of the American Meteorological Society, 79*(2), 285–299.

Groeschl, J., & Noy, I. (2020). *Poverty, Inequality, and Disasters – An Introduction to the Special Issue*. Economics of Disasters and Climate Change, Springer.

IFRC. (2018). *World Disasters Report 2018: Leaving no one behind.*

IPCC. (2012). *Managing the risks of extreme events and disasters to advance climate change adaptation: A special report of Working Groups I and II of the Intergovernmental Panel on Climate Change* (C. B. Field, V. Barros, T. F. Stocker, D. Qin, D. J. Dokken, K. L. Ebi, ... P. M. Midgley, Eds.). Cambridge University Press.

Sakai, Y., Estudillo, J. P., Fuwa, N., Higuchi, Y., & Sawada, Y. (2017). Do natural disasters affect the poor disproportionately? Price change and welfare impact in the aftermath of Typhoon Milenyo in the rural Philippines. *World Development*, *94*, 16-26.

Vittal, H., Karmakar, S., Ghosh, S., & Murtugudde, R. (2020). A comprehensive India-wide social vulnerability analysis: highlighting its influence on hydro-climatic risk. *Environmental Research Letters*, *15*(1), 014005.

Yamamura. (2015). *The impact of natural disasters on income inequality: Analysis using panel data from 1970 to 2004*. International Economic Journal, 29(3), 359–374.

Web References

Asian Development Bank < https://www.adb.org/what-we-do/topics/climate-change/overview#disaster-resilience> (accessed on 28.09.2024)

Census of India (CoI) <https://censusindia.gov.in/census.website/data/census-tables> (accessed on 5.08.2023)

Organisation for Economic Co-operation and Development (OECD) < https://web-archive.oecd.org/temp/201708/374943approachtowardsdisasterriskreductionandresilience.htm> (accessed on 2.08.2023)

United Nations Disaster Risk Reduction (UNDRR) <https://www.undrr.org/gar> (accessed on 15.09.2024)

ICFM 10
Adapting to Global Change:
Innovative Approaches to Flood Management and Resilience
May 20-22, 2026 | Western University, London, Ontario, Canada

Flood-Resilience Priorities for Infrastructure Through Multi-Stakeholder Causal Mapping

Maria Pregnolato[1,2]
Delft University of Technology, Dept. of Hydraulic Engineering, Delft, 2628, CN, Netherlands[1]
E-mail: m.pregnolato@tudelft.nl

University of Bristol, Dept. of Civil Engineering, Bristol, BS8 1TR, UK[2]

ABSTRACT

Urban resilience to natural hazards could make our cities less vulnerable to adverse weather events. However, the implementation of resilience actions is currently not effective, as mechanisms to facilitate collaboration among involved stakeholders are missing. This paper for the first time explores causal mapping as a method to disassemble major issues of urban resilience into a more manageable understanding, and thus identify key objectives, barriers and opportunities in thinking "resilient cities". In this study, a cognitive-mapping-based workshop was held to elicit information from stakeholders in the remit of urban resilience to flooding. The statements and connections identified during the workshop led a consolidated map, analysed using the StrategyFinder software. This analysis highlighted barriers related to data availability, silo-based approaches and lack of funding; it also evidenced shared goals, such as the need to protect the built environment and minimise impact from flooding. Overall, causal mapping resulted a powerful analytical tool for improving understanding of the complex dynamics of urban resilience, identifying key variables and relationships, as well as eliciting information from stakeholders. Furthermore, this approach facilitated systems thinking, communication and collaboration in view of policy-making. This enhanced understanding is fundamental for advancing strategies for future planning, contributing to urban sustainability and liveability.

KEYWORDS: flood, risk, resilience, stakeholder, workshop, causal mapping, infrastructure

1 INTRODUCTION

Urban areas are becoming increasingly vulnerable to natural hazards, particularly flooding, as a result of climate change and rapid urbanisation. Flooding imposes significant economic burdens, including direct damage to infrastructure, housing, and agriculture, alongside indirect impacts such as business disruption, health consequences, and population displacement. In 2019 alone, floods accounted for over 45% of climate-related disasters globally, contributed to more than 40% of disaster-related deaths, and caused average annual losses of approximately US$40 billion. As centres of economic activity, innovation, social interaction, and infrastructure connectivity, cities play a critical role in societal functioning and sustainability (Pregnolato et al., 2021). Their importance is expected to intensify, with around 68% of the global population projected to reside in urban areas by 2050. Urban resilience has therefore become a central policy concern, reflected in the United Nations Sustainable Development Goal 11, which aims to make cities inclusive, safe, resilient, and sustainable (UN, 2015). Urban resilience refers to a city's capacity to withstand, adapt to, and recover from shocks and stresses while maintaining essential services and safeguarding residents' well-being (Bruneau, 2003). This concept extends beyond recovery to include proactive actions that address long-term vulnerabilities and support sustainable development. Despite growing recognition, the practical implementation of resilience strategies in urban planning remains limited and often ineffective.

One key challenge lies in the inherent complexity of cities, which consist of interconnected infrastructures, institutions, and communities (Cimellaro, 2010). Addressing urban resilience therefore requires clear identification of priorities and barriers, as well as collaboration among diverse stakeholders such as

planners, policymakers, engineers, and analysts. However, resilience initiatives are frequently led by single institutions, limiting their transformative potential and reducing coordination across sectors (Elmqvist et al., 2019). This gap highlights the need for more integrated and participatory approaches to understanding and strengthening urban resilience. Understanding stakeholder perspectives is a crucial first step in developing effective resilience tools. Stakeholders often differ in their definitions, objectives, priorities, access to data, and available resources, and these differences are compounded by limited cross-organisational knowledge sharing (Cantelmi et al., 2021). A variety of methods have been used to elicit stakeholder input, including surveys, interviews, workshops, focus groups, and mixed approaches (Pacheco et al., 2018), as well as more innovative techniques such as serious games and diagnostic tools (Wehrle et al., 2022). Additional approaches include Delphi studies, storylines, and other participatory methods (de Bruijn et al., 2016).

Problem Structuring Methods (PSMs) provide a useful framework for addressing such complexity by helping groups explore and structure ill-defined problems (Ahmad et al., 2021). Within this family, Strategic Options Development and Analysis (SODA) employs cognitive or causal mapping to capture and analyse stakeholders' perceptions, objectives, and perceived causal relationships (Eden, 1989). These maps support negotiation, strategic thinking, and collective learning by making interdependencies and assumptions explicit. Cognitive and causal mapping have been widely applied across domains such as project management, health systems, supply chains, policy analysis, energy transitions, and risk perception (Ackermann et al., 2014). However, there is limited evidence of their application to urban resilience, particularly in the context of flooding (Pregnolato and Pyrko, 2022; Pregnolato et al., 2024). This study addresses this gap by applying multi-stakeholder causal mapping to explore objectives, barriers, and opportunities related to urban flood resilience in UK cities. The research investigates how causal mapping can enhance understanding, collaboration, and decision-making among stakeholders, with the aim of bridging gaps between policy intentions and practical implementation. The findings contribute to broader efforts in disaster risk reduction and urban resilience planning.

2 METHODOLOGY

This study applies cognitive (causal) mapping, to examine how multiple stakeholder groups perceive urban infrastructure resilience to flooding (Eden, 1989). A structured workshop was used to elicit stakeholders' views on key objectives, barriers, opportunities, and the causal relationships between them. Participants worked in separate groups to develop individual causal maps, which were later consolidated into a single composite map and analysed using StrategyFinder software (Web-1).

Causal mapping is a participatory, co-creation method that supports collaboration, shared understanding, and capacity building among diverse stakeholders (Marana et al., 2019). It has been successfully applied in complex sectors such as aviation (Ahmad et al., 2021) and was selected here for its ability to explicitly represent causal relationships and support emergent strategy development through an active process of collective sense-making (Pyrko et al., 2019). A causal map represents a system as a network of statements (nodes) connected by directed links that indicate "may-lead-to" relationships. This graphical representation enables the exploration of problem complexity, interdependencies, and patterns that are often difficult to capture through linear methods (Eden, 2004).

In this study, cognitive mapping was conducted in two stages (Fig. 1). First, four separate causal maps were developed by different stakeholder groups during the workshop. Second, these maps were merged into a single composite map following a structured four-step procedure adapted from previous studies (Ahmad and Xu, 2021): identifying overlapping concepts, integrating additional causal links, preserving the internal structure of each group's map, and interpreting the final consolidated map. Interpretation focused on identifying macro-themes, goals, feedback loops, and isolated concepts that could inform actionable strategies (Marana et al., 2019). The analysis of the composite map relied on established structural properties of causal maps (Eden, 2004)], including causal links, central or "potent" nodes, clusters of related concepts, reinforcing or undermining feedback loops, and directional features such as "tails" (triggers) and "heads" (end goals). StrategyFinder supported this process by providing both graphical visualisation and quantitative analytics, such as link density and identification of critical nodes and cycles.

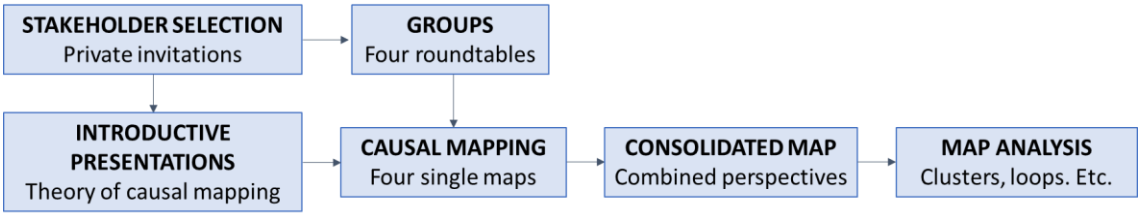

Figure 1: Graphical summary of the methodology

Primary data were collected during a one-day workshop held on 30 November 2021 in Bristol, UK. The overarching question guiding the exercise was: "How can infrastructure resilience to flooding be improved in urban environments?", grounded in participants' professional experience. Twenty-three stakeholders took part, representing policymakers, researchers, practitioners, and private-sector actors. The workshop combined introductory sessions with a facilitated causal mapping exercise, in which participants worked in diverse groups to reflect on challenges and goals related to urban flood resilience. The resulting causal maps provided a structured representation of stakeholder knowledge and perceptions, forming the basis for subsequent analysis and discussion.

3 RESULTS

During the workshop, four stakeholder groups independently developed causal maps that captured key objectives, gaps, and causal relationships related to urban infrastructure resilience (Fig. 2).

(a) (b)

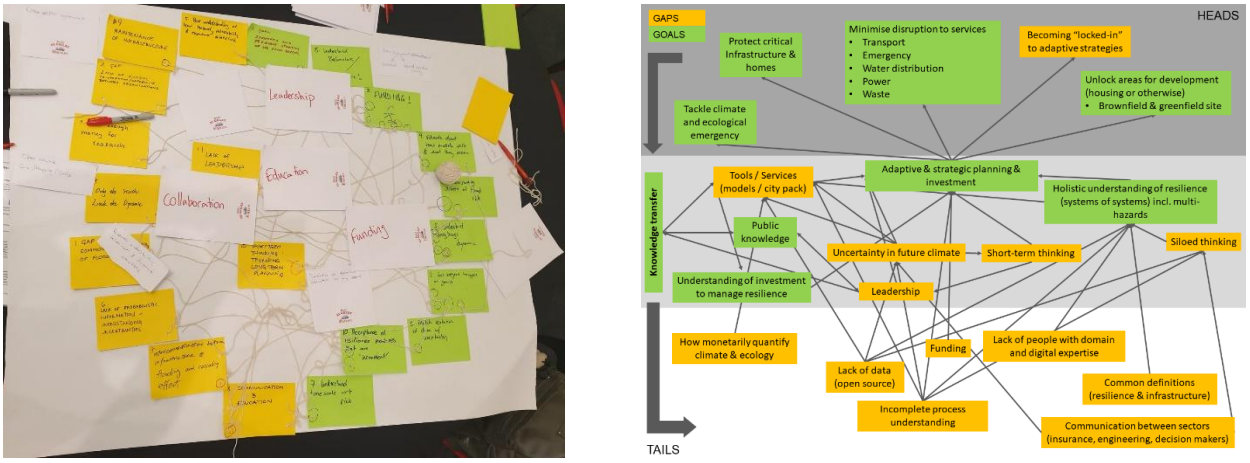

Figure 2: Example of (a) hard copy map produced during the workshop in one of the roundtables; (b) elaborated map, obtained from the hard copy.

In total, 88 statements were elicited, almost evenly split between goals and gaps (see Table A1 in Appendix A). These group-level maps were subsequently integrated into a single consolidated causal map following a structured harmonisation process, in which similar statements were merged and all causal links retained. The consolidated statements were categorised into four thematic clusters: Data; Technical and Technological Knowledge; Leadership and Relationships; and Modelling and Tools. They were further classified according to structural properties such as: heads, tails, and central nodes.

The largest proportion of statements related to Modelling and Tools (34.5%), followed by Leadership and Relationships (28%), Technical and Technological Knowledge (25%), and Data (12.5%). This distribution

reflects the areas that stakeholders considered most salient when discussing urban resilience. The consolidated map was implemented and analysed using StrategyFinder, allowing a system-level interpretation of the complex interdependencies among issues, goals, and enabling factors.

Analysis of the consolidated map began with the identification of central nodes (statements with the highest number of incoming and outgoing connections) highlighting priority areas for stakeholders. Five central priorities emerged: developing adaptive and strategic planning and investment, producing tools and services, maintaining clear communication with citizens, assessing future flood risk using high-resolution climate data, and training staff to use models and interpret outputs. These priorities were distributed across all four thematic clusters, underscoring the multi-dimensional nature of urban resilience.

Further examination revealed that staff training and flood risk assessment function primarily as enabling actions (tails), while strategic planning and public communication represent end goals (heads). The development of tools and services plays a pivotal intermediary role, translating staff capability and data into actionable adaptation strategies. Sub-map analyses showed that staff skills are essential for producing and communicating information, while tools and risk assessments underpin effective strategic planning. Notably, none of the central nodes appeared exclusively as heads or tails, indicating that the core of resilience lies in the processes and interactions between elements rather than isolated starting points or endpoints.

Head statements represented the desired outcomes of resilience efforts, including protecting critical infrastructure and homes, minimising disruptions to essential services, unlocking safe areas for future development, and developing a shared vision of resilience. These outcomes collectively reflect stakeholders' overarching aim of safeguarding the built environment and supporting safer, more robust urban systems. Conversely, tail statements captured the drivers and constraints shaping resilience pathways, such as data scarcity, limited funding, short-term thinking, lack of shared definitions, community engagement challenges, and uncertainty in returns on resilience investments. Addressing these drivers was identified as a necessary first step in any effective resilience strategy.

Thematic cluster analysis provided further insight. The Modelling and Tools cluster emerged as the most complex and influential, containing two central nodes and closely aligning with final resilience goals. This cluster highlighted the importance of impact modelling, real-time warning systems, climate information, and policy tools for reducing disruptions and enhancing asset protection. It also revealed how modelling activities can help address data gaps by generating new, decision-relevant information. The Data cluster emphasised challenges related to data availability, resolution, accessibility, and management, reinforcing the need for improved data practices to support risk assessment.

The Technical and Technological Knowledge cluster underscored the dominance of knowledge-related issues, particularly the need to understand physical processes, risk components, and modelling outputs. Staff capacity and skills were identified as critical enablers, highlighting training as a priority intervention. The Leadership and Relationships cluster focused on communication with citizens, community engagement, cooperation across institutions, funding, and leadership. Together, these elements point to the importance of trust, shared understanding, and coordinated governance in delivering resilience.

Overall, the analysis shows that urban resilience emerges from interconnected processes involving data, knowledge, tools, leadership, and community engagement, rather than from isolated actions.

4 DISCUSSION

This study investigated how causal mapping can support improved decision-making and collaboration among multiple stakeholders to strengthen resilient infrastructure in UK cities. By applying causal mapping in a multi-stakeholder workshop, the research captured and analysed the mental models of participants from different professional backgrounds involved in urban resilience. The approach enabled the identification of key objectives, barriers, and opportunities related to urban resilience to flooding, while recognising that results are context-specific and influenced by participant composition and facilitation dynamics (Lami and Todella, 2019).

The study highlights both methodological considerations and practical insights. While the workshop format is flexible and adaptable to different contexts, the authors note the importance of careful

stakeholder selection, facilitation, and post-workshop validation to improve reliability and learning outcomes (Ahmad and Xu, 2021). Disseminating findings to participants for feedback was identified as particularly valuable for enhancing ownership, reflection, and cross-disciplinary learning (Tavella and Papadopoulos, 2017). Feedback from participants confirmed that causal mapping was engaging, accessible, and effective in supporting systems thinking, networking, and shared understanding, reinforcing evidence from earlier studies (Ackermann and Eden, 2005).

From an urban resilience perspective, the study demonstrates the value of causal mapping as a novel method for engaging stakeholders in a field characterised by complexity and multi-disciplinarity. The resulting composite map revealed four operational thematic clusters (data, technical and technological knowledge, leadership and relationships, and modelling and tools) which are not explicitly identified in existing resilience frameworks. Key challenges included data limitations, siloed working practices, and insufficient funding, while shared goals focused on protecting the built environment and minimising flood impacts, consistent with prior research (Godschalk, 2003).

Importantly, the analysis highlighted staff skills, capacity building, and knowledge transfer as central drivers of urban resilience, alongside community engagement and leadership. These findings suggest that resilience strategies should prioritise training, institutional collaboration, and public involvement, complementing policy-focused approaches in the literature (Ahmad and Xu, 2021). Overall, the study shows that causal mapping effectively supports visualisation, systems thinking, communication, and collaboration, offering a practical foundation for developing holistic and integrated urban resilience strategies (Sharifi and Yamagata, 2016).

5 CONCLUSION

The limited implementation of resilience measures in urban planning highlights the need for platforms that foster stakeholder collaboration. Problem Structuring Methods (PSMs), particularly causal (cognitive) mapping, offer a way to structure complex challenges into manageable components. This study identifies three gaps: limited effectiveness of current resilience measures, lack of applications of cognitive mapping in urban resilience, and underuse of multi-level cognitive mapping. It investigates how causal mapping can improve understanding of barriers and opportunities for collaborative decision-making. A stakeholder workshop was conducted to develop group cognitive maps, later integrated into a consolidated multi-level map and analysed using established indicators. Key barriers included limited data availability, siloed practices, and insufficient funding, while shared goals focused on protecting the built environment and reducing flood impacts. The findings demonstrate that causal mapping supports systems thinking, communication, and collaborative strategy development, offering practical guidance for strengthening urban resilience planning.

6 ACKNOWLEDGEMENTS

This study was supported by the GW4 Building Communities Generator Fund; MP was supported by the Engineering and Physical Sciences Research Council (ESPRC) LWEC (Living With Environmental Change) Fellowship (EP/R00742X/2).

APPENDIX A

Table A1. List of statements, and relative assigned theme. Colour legend: Data - yellow; Technical and technological knowledge - green; Leadership and relationships - blue; Modelling and tools - orange.

Statement	Theme	Note
1 to work with lack of data	Data	Tail
2 to quantify climate and ecology	Technical and technological knowledge	Tail
3 to gather funding	Leadership and relationships	-

4 to work in a condition of incomplete process understanding	Technical and technological knowledge	Loop B
5 to keep data open-source	Data	-
6 to cope with little funding	Leadership and relationships	Tail
7 to have staff with domain and digital expertise	Technical and technological knowledge	-
8 to lack of common definitions on resilience and infrastructure	Technical and technological knowledge	Tail
12 to communicate among sector (insurance, engineering, policy, etc.)	Leadership and relationships	-
13 to understand investments in resilience management	Technical and technological knowledge	-
14 to possess public knowledge	Technical and technological knowledge	Loop A
15 to produce tools/services (e.g., models, city pack)	Modelling and tools	Central node
16 to develop adaptive and strategic planning and investments	Modelling and tools	Central node
17 to account for uncertainty in future climate	Modelling and tools	-
18 to provide leadership among all players	Leadership and relationships	Loop A
19 to think in short terms	Leadership and relationships	Tail
20 to think in longer-terms	Leadership and relationships	-
21 to overcome siloed-thinking	Leadership and relationships	-
22 to account for a holistic understanding or resilience, e.g., system of systems and multi-hazards	Technical and technological knowledge	-
23 to tackle climate and ecological emergency	Modelling and tools	Head
24 to protect critical infrastructures and homes	Modelling and tools	Head
25 to minimise disruptions to services (transport, water, power, waste)	Modelling and tools	Head
26 to develop adaptive strategies	Modelling and tools	Head
27 to unlock "safe" areas for development (housing or otherwise), also in the future	Modelling and tools	Head
28 to transfer knowledge across sectors and institutions	Technical and technological knowledge	Loop A
29 lack of data integration across different systems	Data	-
30 to increase accuracy while limiting computing resources	Modelling and tools	-
31 to develop real-time warning system	Modelling and tools	Loop B
33 to manage inter-dependency of infrastructure	Modelling and tools	-
35 to work with lack of real-time dynamic data (e.g. flood outputs)	Data	-
36 to use technology to optimise transport system during flooding	Technical and technological knowledge	-
37 to define a business case for adaptation (e.g., blue-green infrastructure)	Modelling and tools	-
38 to include climate information into planning process	Modelling and tools	-
40 to model different parts of the network	Modelling and tools	-
41 to assess future flood risk using high resolution climate data	Data	Central node
42 to improve public awareness to flood risk	Leadership and relationships	-

43 to deliver risk information to cities	Leadership and relationships	-
44 to maintain clear communication with citizens	Leadership and relationships	Central node
45 to map safe zones of the city	Modelling and tools	-
46 to develop methods based on limited data	Data	-
47 to improve protection of assets	Modelling and tools	-
48 to deliver best-value plans for flood risk management authorities	Modelling and tools	Head
49 to use appropriate databases for data of ecosystem services	Data	Tail
50 to develop a societal mindset on infrastructure issues	Leadership and relationships	-
51 to engage the wider community	Leadership and relationships	Tail
52 to develop and share a consistent common language	Modelling and tools	-
53 to develop standards and rules	Modelling and tools	-
54 to understand the interlink among hazard, vulnerability and exposure	Technical and technological knowledge	Loop B
55 to improve/optimise infrastructure maintenance	Modelling and tools	-
57 to improve cooperation among organisations	Leadership and relationships	-
58 to consider the interaction among infrastructure, flooding and casualty effects	Technical and technological knowledge	-
59 to gather funding for research	Leadership and relationships	-
60 to deal with lack of leadership	Leadership and relationships	-
61 to train staff to use models and understand outputs	Technical and technological knowledge	Central node
62 to pair data resolution and uncertainty	Data	-
63 to develop a shared vision	Leadership and relationships	Head
64 to understand the drivers of flood risk	Technical and technological knowledge	-
65 to understand the risk timescale	Technical and technological knowledge	Head
66 to educate the general public	Leadership and relationships	-
67 to update/keep records of flood happenings	Technical and technological knowledge	Head
68 to accept resilience measure whose return is uncertain	Technical and technological knowledge	Tail
69 to conduct research	Technical and technological knowledge	-

REFERENCES

Ackermann, F. and Eden, C. (2005). Using causal mapping with group support systems to elicit an understanding of failure in complex projects: some implications for organizational research. Group Decis. Negot., 14, 5, 355–376. https://doi.org/10.1007/s10726-005-8917-6

Ackermann, F., Howick, S., Quigley, J., Walls, L. and Houghton, T. (2014). Systemic risk elicitation: using causal maps to engage stakeholders and build a comprehensive view of risks. Eur. J. Oper. Res., 238, 1, 290–299. https://doi.org/10.1016/j.ejor.2014.03.035

Ahmad, S. and Xu, B. (2021). A cognitive mapping approach to analyse stakeholders' perspectives on sustainable aviation fuels. Transp. Res. Part D: Transp. and Env., 100, 103076.

Bruneau, M., Chang, S.,. Eguchi, R., Lee, G., O'Rourke, T., Reinhorn, A., Shinozuka, M., Tierney, K., Wallace, W. and von Winterfelt, D. (2003). A framework to quantitatively assess and enhance the seismic resilience of communities. EERI Spectra Journal, 19, 4, 733–752. https://doi.org/10.1193/1.162.

Cantelmi, R., Di Gravio, G. and Patriarca, R. (2021). Reviewing qualitative research approaches in the context of critical infrastructure resilience. Environ. Syst. Decis., 41, 341–376.
Cimellaro, G.P., Reinhorn, A.M. and Bruneau, M. (2010). Framework for analytical quantification of disaster resilience. Eng. Struct., 32, 11, 3639–3649. https://doi. org/10.1016/j.engstruct.2010.08.008.
de Bruijn, K.M., Lips, N., Gersonius, B. and Middelkoop, H. (2016). The storyline approach: a new way to analyze and improve flood event management. Nat. Hazards, 81, 99–121.
Eden, C. (1989). Using cognitive mapping for strategic options development and analysis, in: J. Rosenhead (Ed.), Rational Analysis for a Problematic World. Wiley, Chichester
Eden, C. (2004). Analyzing cognitive maps to help structure issues or problems, Eur. J. Oper. Res., 159, 3, 673–686. https://doi.org/10.1016/S0377-2217(03)00431-4
Elmqvist, T., Andersson, E., Frantzeskaki, N., McPhearson, T., Olsson, P., Gaffney, O., Takeuchi, K. and Folke C. (2019). Sustainability and resilience for transformation in the urban century. Nat. Sustain, 267–273. https://doi.org/10.1038/s41893-019-0250-1
Godschalk, D. (2003). Urban hazard mitigation: creating resilient cities, Nat. Hazards Rev., 4, 3, 136–143. https://doi.org/10.1061/(asce)1527-6988(2003)4:3(136)
Lami, I.M. and Todella, E. (2019). Facing urban uncertainty with the strategic choice approach: the introduction of disruptive events. Riv. Estet., 71, 2, 222–240. https://doi.org/10.4000/estetica.5769
Marana, P., Eden, C., Eriksson, H., Grimes, C., Hernantes, J., Howick, S., Labaka, L., Latinos, V., Lindner, R., Majchrzak, T., Pyrko, I., Radianti, J., Rankin, A., Sakurai, M., Sarriegi, J.M. and Serrano, N. (2019). Towards a resilience management guideline - cities as a starting point for societal resilience. Sustain. Cities Soc., 48,101531. https://doi.org/10.1016/j.scs.2019.101531
Pacheco, C., García, I. and Reyes, M. (2018). Requirements elicitation techniques: a systematic literature review based on the maturity of the techniques. IET Softw., 12, 365–378.
Pregnolato, M., Lo Jacomo, A., De Risi, R., Haung, J.S., Agarwal, J. and Han, D. (2021). Resilient infrastructures for reducing urban flooding risks, in: G. Fu, X. Wang (Eds.), Water-Wise Cities and Sustainable Water Systems - Concepts, Technologies, and Applications, Chapter 7, IWA Publishing, London. https://doi.org/10.2166/ 9781789060768
Pregnolato, M. and Pyrko, I. (2022). Using Multi-Stakeholder Causal Mapping to Explore Priorities for Urban Resilience: Unpacking Barriers, Opportunities, and Pathways for Improvement. MSc thesis, University of Bristol, School of Management, 2022
Pregnolato, M., West, C., Evans, B., Lam, M. Y., Chen, A. S., Ahmadian, R. and Djordjević, S. (2024). Using multi-stakeholder causal mapping to explore priorities for infrastructure resilience to flooding. International Journal of Disaster Risk Reduc., 101, 104189.
Pyrko, I., Dorfler, V. and Eden, C. (2019). Communities of practice in landscapes of practice, Manag. Learn. 50, 4, 482–499. https://doi.org/10.1177/1350507619860854
Sharifi, A. and Yamagata, Y. (2016). On the suitability of assessment tools for guiding communities towards disaster resilience. Int. J. Disaster Risk Reduc., 18, 115–124. https://doi.org/10.1016/j.ijdrr.2016.06.006.
Tavella, E. and Papadopoulos, T. (2017). Applying OR to problem situations within community organisations: a case in a Danish non-profit, member-driven food cooperative. Eur. J. Oper. Res., 258, 2, 726–742.
UN (2015). Transforming Our World: the 2030 Agenda for Sustainable Development. A/RES/70/1. https://www.refworld.org/docid/57b6e3e44.html.
Web-1: https://www.strategyfinder.com/ consulted 22 December 2025
Wehrle, R., Wiens, M. and Schultmann, F. (2022). Application of collaborative serious gaming for the elicitation of expert knowledge and towards creating Situation Awareness in the field of infrastructure resilience. Int. J. Dis. Risk Reduc., 67, 102665. https://doi.org/10.1016/j.ijdrr.2021.102665

ICFM 10
Adapting to Global Change:
Innovative Approaches to Flood Management and Resilience
May 20-22, 2026 | Western University, London, Ontario, Canada

FLOOD RISK MANAGEMENT IN THE UPPER NEPEAN RIVER CATCHMENT, AUSTRALIA

Maria Pinto[1], Warick Honour[2] and Yasitha Bopetta[1]
Camden Council, New South Wales, Australia[1]
email: maria.pinto@camden.nsw.gov.au
Worley Consulting, Sydney, Australia[2]
email: warick.honour@worley.com
email: Yasitha.bopetta@camden.nsw.gov.au

ABSTRACT

Flooding is a natural disaster that causes significant damage globally. Australia is prone to devastating floods. La Nina and climate change are considered to have contributed to the rise in wet weather events that occurred in Australia during 2022 (BoM, 2022). Floods across eastern Australia in February/March 2022 damaged thousands of houses, caused widespread evacuations, power outages and restricted mobility.

A scoping study for Voluntary House Raising (VHR) was conducted for a section of the Upper Nepean River floodplain that is vulnerable to mainstream riverine flooding, local catchment tributary flooding and overland flows. The scoping study was recommended by the Flood Risk Management Plan prepared for the study area, which involved the use of detailed computer flood models of catchment hydrology and floodplain hydraulics to test a range of flood mitigation measures (Camden Council, 2023).

The objective of a VHR scheme is to reduce flood damages and increase the flood resilience of the community in the study area. Eligibility criteria contained in flood risk management guidelines published by the New South Wales (NSW) Department of Planning and Environment (NSW DPE, 2023a and 2023b) were used to identify houses for inclusion in the VHR scheme. This included consideration of the location of the houses relative to floodway or high flood hazard areas, the age of the dwellings and the cost-effectiveness of raising the houses. Community consultation was also a major component of the study, which was addressed via community consultation sessions.

KEYWORDS: voluntary house raising; flood damage; floodway; flood hazard; benefit-cost.

1 INTRODUCTION

Flooding is one of the common natural disasters that causes the most damage globally. In 2022 La Nina and climate change contributed to the rise in wet weather events in Australia (BoM, 2022). In NSW alone, during flood events in February/March 2022 over 8,000 properties were inundated, over 10,000 were damaged, and over 4,000 properties were deemed uninhabitable. The cost of the floods reached $5.28 billion in insured losses from more than 233,000 claims (ICA, 2022). The direct economic cost of extreme weather events is expected to grow by 5.13 per cent each year and reach a total of about $35 billion in annual costs by 2050 (TMI, 2022).

Climate change has the potential to worsen flooding problems in some regions, while continued urbanisation of floodplains will increase potential flood damages and vulnerability (Schreider et al., 2000; Milly et al., 2002). An important challenge in sustainable floodplain management is balancing the long-term risk of increasing flood damage with the ongoing benefits that floodplains provide to both human and natural systems (Zhu et al., 2007). The severity of flood events is expected to increase significantly in the future, and if flood protection measures remain at current standards, the resulting impacts could become

unbearable for Australia, as it will be for west (web- 1). Given the complex and evolving nature of climate change, an adaptive approach is essential for managing the uncertainties surrounding flood hazards, their impacts, and associated risks.

A scoping study for a Voluntary House Raising (VHR) scheme was completed for the lower section of the Upper Nepean River Catchment, which is an area known to be vulnerable to flooding. Figure 1 shows the study area and the Upper Nepean River catchment. The Nepean River enters the study area at its southern boundary, just south-east of the township of Camden, and meanders approximately 30 km northwest before exiting the study area. The study area spans 140 km² within the Camden Local Government Area (LGA) in Western Sydney, located about 65 km from the Sydney Central Business District (CBD). It is a semi-rural area facing increasing development pressures and intensifying consequences of climate change.

Multiple flooding mechanisms affect the area, including mainstream riverine flooding, local tributary flooding, and overland flow. In 2022, the catchment experienced three significant flood events in March and July, with the July event being the most severe, corresponding to an estimated Annual Exceedance Probability (AEP) of 10% to 20%. Evacuations were required during all three events. There was a clear expression of community interest in implementing a VHR scheme following these events.

House raising has been a suitable flood resilient design strategy adopted for many homes in Queensland, Australia (QRA, 2019). The technique of constructing houses on stilts prevalent in south-east Asia and South America has been adopted in the Netherlands as well (Naga, 2021).

VHR is a flood risk management tool that involves elevating a dwelling above the minimum flood design level or relocating it to higher ground within the same lot (NSW DPE, 2023b). It is effective in reducing the frequency of flood-related property damage and associated social and psychological impacts on residents. However, VHR should be implemented as part of a broader floodplain risk management strategy for an area, as it does not address all hazards, such as risk to life. Following the development of a Scoping Study, the implementation of a VHR scheme is partially funded by the NSW Government, which currently covers up to two-thirds of the cost through local councils (NSW DPE, 2023b).

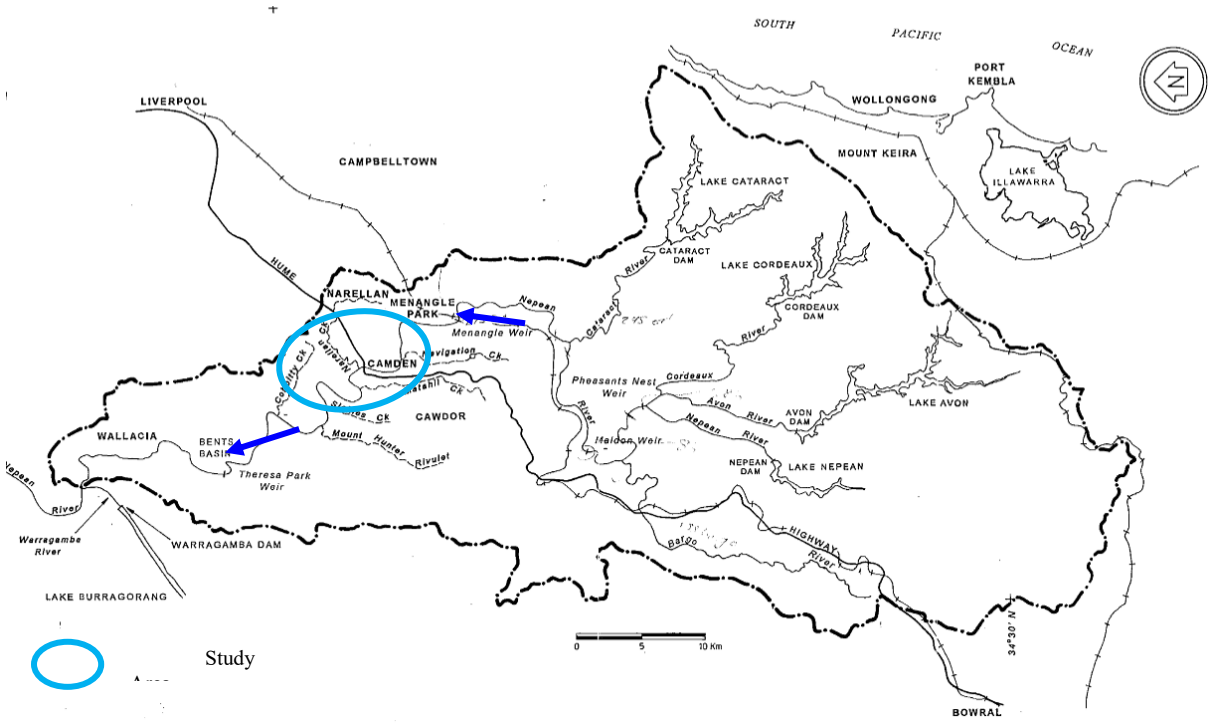

Figure 1: Study area relative to the Upper Nepean River Catchment

2 BACKGROUND

Historic flood data indicates that flood events between the 0.5 EY (Exceedances per Year) / 39.35% Annual Exceedance Probability (AEP) and 20% AEP have occurred in the study area during the past two decades. The most significant flood on record was a 0.5% AEP (1-in-200-year) event that occurred in 1873. Inundation of the Camden CBD starts to occur from the 0.5 EY event, with full inundation occurring during the 20% AEP and larger events.

Figure 2 illustrates the extent of flooding in the Camden CBD during the July 2022 flood, which was estimated to be between a 20% and 10% AEP event. Several other locations within the study area exhibit similar flood behaviour.

During mainstream 1% AEP flooding and the Probable Maximum Flood (PMF), the maximum flood depths at properties in Camden reach up to 9 and 11 meters, respectively (Camden Council, 2023). Most roads get cut in frequent flood events and hence emergency management and evacuation are difficult (Camden Council, 2023). Due to the combination of high flood depths and velocities, most of the floodplain within the study area is classified as high hazard (Camden Council, 2023). The extent of nominated high-risk areas is even larger, as many regions become inaccessible during floods, further complicating emergency response. Additionally, land situated outside the Flood Planning Area (defined as the 1% AEP flood level plus freeboard) but within the PMF extent is considered to carry residual risk, which also requires targeted emergency management planning (Camden Council, 2023).

The study area is considered highly sensitive to climate change impacts. For Representative Concentration Pathway (RCP) 4.5, which is approximately equivalent to 10% increase in 1% AEP rainfall intensity, the flood level increases in the study area would vary from 0.5m to 1.5m (Camden Council, 2023).

Figure 2: Camden CBD during the July 2022 flood

3 STUDY OBJECTIVES

The primary objective of this study was to assess the implementation of Voluntary House Raising (VHR) as a suitable flood risk mitigation measure for the study area. A scoping study was initiated to

evaluate the feasibility of VHR and to develop a VHR Scheme aimed at reducing flood damages and enhancing community resilience, thereby contributing to broader flood risk management efforts across New South Wales (NSW DPE, 2023b). This work was partially funded by the NSW Government.

Residential properties with over floor flooding in the 5% AEP event were identified for VHR as a high-priority property modification measure in the Nepean River Floodplain Risk Management Study and Plan (Plan). The assessment was based on a Multi Criteria Assessment, with the scoring based on a triple bottom line approach, incorporating economic, social and environmental criteria (Camden Council, 2023). The scoping study is required to define the scheme's scope, estimated costs, and prioritise properties before seeking funding for implementation (NSW DPE, 2023b).

4 METHODOLOGY

The following criteria were adopted in the identification and eligibility assessment of houses for VHR, as outlined in the NSW Guidelines for Voluntary House Raising Schemes (NSW DPE, 2023b)

1. The full range of flood events are to be considered in the damages assessment of each property.
2. Floodway areas in the 1% AEP event are to be excluded, which denote areas of high flood conveyance as part of hydraulic category (flood function) mapping.
3. VHR is to be limited to low hazard areas, which means that dwellings are not to be in high hazard areas (H5 to H6 classification as per Australian Rainfall & Runoff 2019).
4. The effectiveness as an ongoing maintenance requirement to address risk to life, such as those based around supporting self-evacuation in response to directions from the State Emergency Service. The Local Flood Plan must be communicated to the residents and complied with.
5. Assessment of the suitability of individual houses for raising, including building age, whether houses are of slab-on-ground or brick construction.
6. Cost-effectiveness of the VHR Scheme (benefit-cost ratio) measured across the full range of floods with the aim to generate positive financial returns from reduced damage relative to costs.
7. Viability of the scope and scale of the VHR Scheme and how the Scheme will be prioritized.

Support of the affected community for VHR as determined through consultation with affected property owners. All above criteria were considered. The benefit-cost ratio (BCR) for each dwelling was calculated and used to prioritise properties for raising. Consultation with landowners was completed during the study. A VHR implementation plan was prepared, comprising information on the number of properties targeted, the estimated cost of house raising, and the priority ranking based on the benefit-cost ratio for each property.

1.1 4.1 Assessment of Flood Behaviour

Flood model results from the Nepean River FRMSP (2023) were used to describe the flood behaviour at the study area, including flood extents, hydraulic category and hazard mapping to address the criteria listed in the NSW Guidelines (NSW DPE, 2023b). An XP-RAFTS hydrologic model and 1D/2D TUFLOW hydraulic model were developed for the study area and calibrated to four historical flood events. The models were used to define flood behaviour for the 0.5 EY (Exceedances per Year), 20% AEP, 5% AEP, 2% AEP, 1% AEP, 0.5% AEP and 0.2% AEP events and PMF.

Table 1 identifies the number of properties within the study area that are affected by flooding for the full range of events. In the 5% AEP event, 190 properties will be flooded, including 147 inundated above floor level, of which 108 are residential properties (Camden Council, 2023).

Table 1: Flood affectation for full range of design flood events (Camden Council, 2023)

Flood event	Properties with over floor flooding	Properties with over floor flooding (residential only)	Properties with over ground flooding
0.5 EY (Exceedances	6	5	10

per Year) or 39.35% AEP			
20% AEP	13	11	18
5% AEP	147	**108**	190
1% AEP	271	**200**	347
0.5% AEP	361	283	454
0.2% AEP	519	431	629
PMF	2306	2071	2505

The flood model results were used for hydraulic category and hazard mapping and the calculation of Average Annual Damages (AAD) (Camden Council, 2023, 2025).

1.2 4.2 Stage 1 - Dwelling Eligibility Assessment

The first stage of investigations involved a desktop assessment of the 108 dwellings affected by over floor flooding in the 5% AEP flood against the VHR eligibility criteria. The following information was considered.

- Hydraulic category (flood function) mapping for the 1% AEP event to identify floodway, flood storage and flood fringe areas (NSW DPE, 2023a).
- Flood hazard mapping for the 1% AEP event to classify the hazard at each property from H1 to H6. The Australian Rainfall and Runoff flood hazard curves provided in Figure 3 were used for hazard mapping (Camden Council, 2023).
- Construction age to confirm whether houses were built before or after 1986. The NSW State Flood Prone Land Policy came in to force in 1986 and the dwellings built after 1986 are not eligible for VHR funding (NSW DPE, 2023b).
- Dwelling construction type: whether slab-on-ground, weatherboard, fibro, brick, etc.

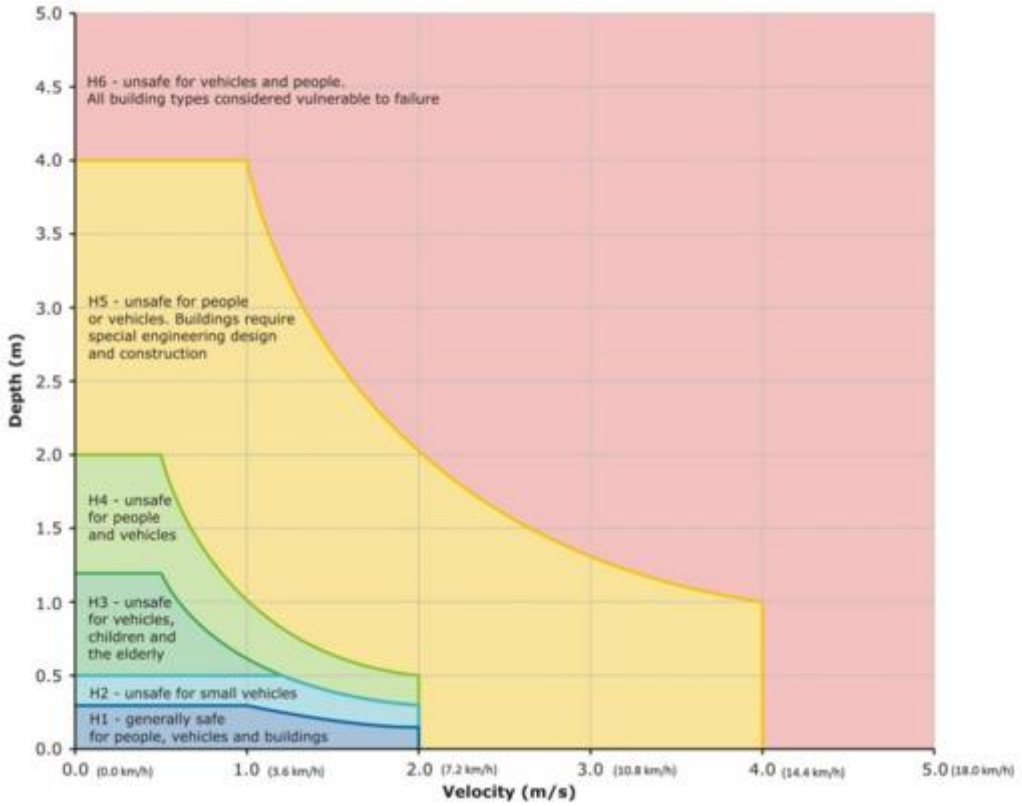

Figure 3: Flood Hazard Vulnerability Curves (Source: AEMI 2013)

1.3 4.3 Stage 2 - Benefit-Cost Assessment

After identifying the dwellings eligible for the VHR scheme, the next step was to calculate the BCR for voluntary house raising by comparing the Net Present Value (NPV) of the flood damage reduction over the lifespan of the works against the cost of the house raising works.

The proposed house raising of eligible dwellings would involve raising the existing floor level to the Flood Planning Level (FPL), which aligns with Councils Flood Risk Management Policy for habitable floor levels and the requirements listed in the Flood Risk Management Measures, MM01 (DPE, 2023a). The FPL is the 1% AEP flood level plus a freeboard of 500mm. An Average Annual Damages (AAD) calculation was completed for each dwelling under both scenarios; existing conditions and raised conditions. The cost of house raising works was estimated according to information provided by local builders specialising in house raising (Camden Council, 2025).

The NPV of the costs and benefits accounts for the value of all future costs and benefits over the entire life (50 years) of an investment discounted (7%) to the present. The BCR for house raising works at each property was calculated as the NPV of the AAD reduction divided by the NPV of the house raising costs. The BCR results were used to rank properties in the VHR scheme.

1.4 4.4Community Consultation

The Nepean River FRMSP, incorporating the recommended Voluntary House Raising (VHR), was publicly exhibited in 2023.

After completion of the Stage 1 investigations, a drop-in session was held to inform homeowners of eligible dwellings, address questions, and gather feedback. Key concerns included exclusion of high-risk properties, construction-related issues such as asbestos removal, services relocation, temporary accommodation, builders' reliability, and potential impacts on neighbouring properties due to overland flow. One-on-one follow-ups were conducted with the affected homeowners expressing the most support or interest in the VHR scheme. Ongoing updates were provided to the Camden Flood Risk Management Committee. A VHR Implementation Plan was subsequently developed and publicly exhibited as part of the draft Scoping Study, accompanied by general and property-specific information sheets for residents (Camden Council, 2025).

5 RESULTS AND DISCUSSION

Of the 108 properties inundated in the 5% AEP flood, only 16 were determined to be outside of both the 1% AEP high flood hazard areas (H5 or H6 classification) and the 1% AEP floodway. However, none of those 16 properties met the construction type and/or construction date eligibility criteria. Accordingly, the Scoping Study was extended to include investigation of properties inundated with over floor flooding in the 1% AEP flood.

There are an additional 92 dwellings inundated in the 1% AEP event (Table 1, Figure 4), which were assessed according to the same eligibility criteria outlined in Section 4 above.

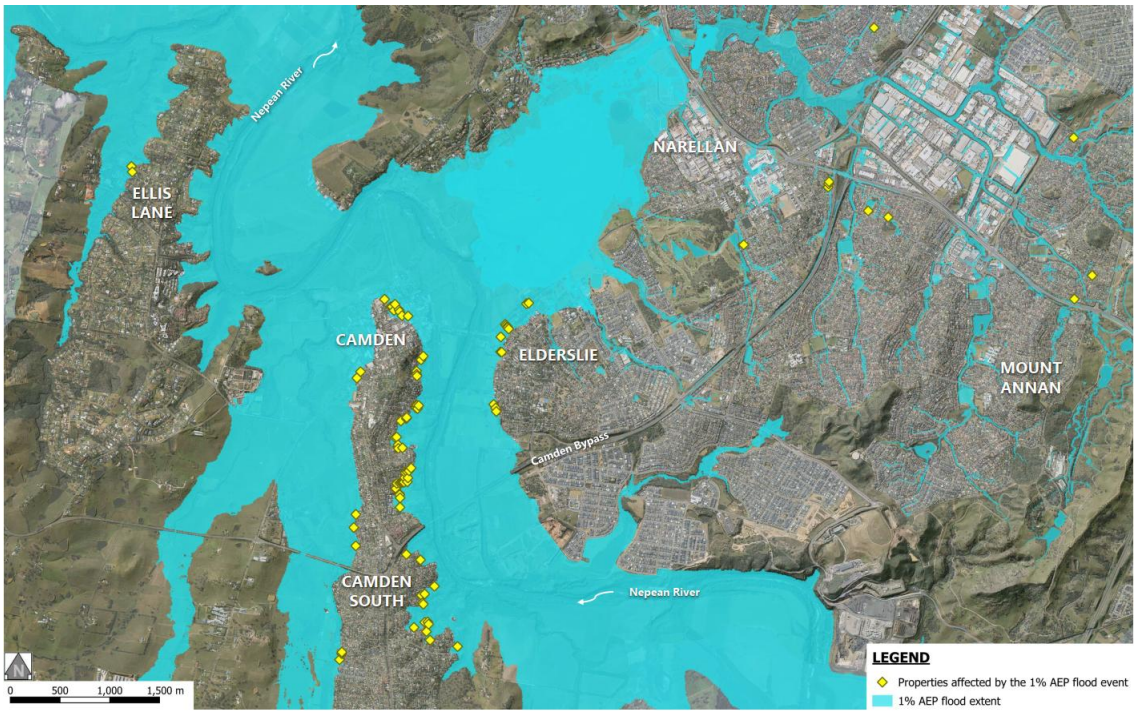

Figure 4: Additional dwellings inundated in the 1% AEP event considered for voluntary house raising

Of the 92 dwellings, an initial assessment showed that 28 dwellings met the flood hazard and floodway eligibility criteria. Based on construction type and the date of construction, a residual of 19 eligible dwellings were taken through to the Stage 2 benefit-cost investigations (Figure 5).

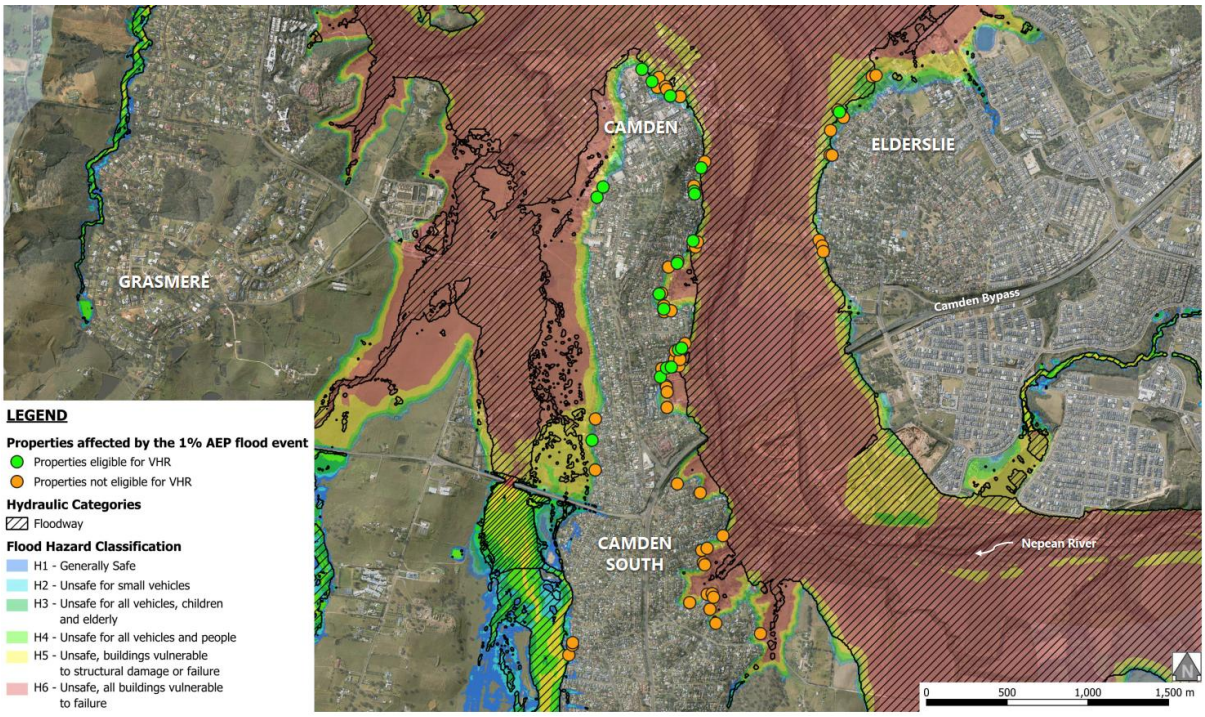

Figure 5: Final set of 19 dwellings assessed as part of Stage 2 investigations

The house raising required for the 19 dwellings would range between 0.7 and 2.0 metres. The assessment showed that dwelling floor areas ranged from 126 m² to 305 m², with the median house size being about 150 m². The reduction in AAD at each house (i.e., the benefit) was estimated to be between $2,700 to $9,400, with the average reduction being about $4,300. The total AAD reduction afforded by raising all 19 dwellings was estimated to be about $81,500.

The adopted cost rates for house raising were applied to each dwelling based on the estimated house floor area, which yielded total raising costs between $128,000 and $275,000 per dwelling. The total cost for all 19 dwellings was estimated to be $3.3M.

The NPV of the reduction in AAD due to house raising was calculated to range between $40,000 and $139,000 per property. The NPV of the total AAD reduction across all 19 properties was estimated to be about $1.2M.

The Benefit-Cost Ratio (BCR) for house raising works at each property was calculated as the NPV of the AAD reduction divided by the NPV of the house raising costs. The BCRs for individual dwellings range from 0.3 to 0.5, with the overall BCR for all dwellings in the scheme estimated to be about 0.4.

6 CONCLUSION

The VHR Scoping Study for Camden determined that 19 dwellings affected in the 1% AEP flood meet the VHR eligibility criteria, are of appropriate construction type, and are therefore recommended for inclusion in the proposed VHR Scheme. Dwellings were prioritised according to the benefit-cost ratio of the raising works at each property, which ranged between 0.3 and 05. Community consultation played a vital role in the study, providing valuable insights into local concerns and practical considerations essential for the successful completion of future VHR activities.

It was determined that dwellings affected in the 5% AEP flood would not be eligible for house raising, primarily due to being located in floodway and/or high flood hazard areas, or otherwise not being of suitable construction age or type. These properties were therefore recommended for consideration under a future Voluntary House Purchase (VHP) Scheme. A VHP Scheme would operate under a different set of eligibility criteria and may be more appropriate for addressing the flood risk in these high hazard areas. VHP is a risk management strategy involving the voluntary purchase of flood-prone properties to permanently remove people from high-risk areas, with the land typically cleared and rezoned for flood-compatible use (DCCEEW, 2024).

7 ACKNOWLEDGEMENTS

Wasif W, Department of Climate Change, Energy, the Environment and Water, Australia acknowledged for their contribution.

REFERENCES

[1] BoM (2022). Special Climate Statement 76 – Extreme rainfall and flooding in south-eastern Queensland and eastern New South Wales, Bureau of Meteorology, Australian Government.
[2] Camden Council (2023). Nepean River Floodplain Risk Management Study and Plan prepared by Stantec for Camden Council.
[3] Camden Council (2025). Nepean River Voluntary House Raising Scoping Study. Report prepared by Worley Consulting.
[4] DCCEEW (2024). Guidelines for the voluntary house purchase scheme, Department of Climate Change, Energy, the Environment and Water.
[5] ICA (2022). Insurance Catastrophe Resilience Report, Insurance Council of Australia.
[6] Milly et al. (2002). Increasing risk of great floods in a changing climate, Nature, 415(31), 514 – 517.

[7] Naga. (2021). Flood Resistant Construction Techniques used around the world – RTF, Rethinking the Future.
[8] NSW DPE (2023a). Flood Risk Management Measures MM01- Flood Risk Management Manual, NSW Department of Planning and Environment.
[9] NSW DPE (2023b). Guidelines for the Voluntary House Raising Scheme - Floodplain Management Program, NSW Department of Planning and Environment.
[10] Schreider et al. (2000). Climate change impacts on urban flooding, Climate Change, 47, 91 – 115.
[11] QRA. (2019). Flood Resilient Building Guidance for Queensland Homes. Queensland Reconstruction Authority, The State of Queensland.
[12] TMI (2022) The Cost of Extreme Weather, Building Resilience in the Face of Disaster, The McKell Institute.
[13] Zhu et al. (2007). Climate change, urbanization, and optimal long-term floodplain protection. Water Resources Research 43, no. 6 (2007).

Web sites:
Web- 1: Climate change supercharged Europe's floods, scientists warn

ICFM 10
Adapting to Global Change:
Innovative Approaches to Flood Management and Resilience
May 20-22, 2026 | Western University, London, Ontario, Canada

A Decade after Bodil: Assessing Coastal Flood Adaptation in Roskilde, Denmark

Tatiana Ferrari[1] and Heiko Apel[2] and Kaija J. Andersen[1] and Martin Drews[1]
Department of Technology, Management and Economics, Technical University of Denmark (DTU), Produktionstorvet B.424, 2800, Denmark[1]
E-mail: tatikol@dtu.dk, kjuan@dtu.dk, mard@dtu.dk

Section Hydrology, GFZ Helmholtz Centre for Geosciences, Potsdam, Germany[2]
E-mail: heiko.apel@gfz.de

ABSTRACT

The 2013 Bodil storm caused severe coastal flooding in Roskilde city. This paper evaluates to which degree adaptation measures implemented or planned since Bodil reduce the flood risk under present and future conditions. Municipal climate plans are analysed, and the Bodil event is forensically reconstructed and re-simulated using hydrodynamic modelling under present and future scenarios. Results show that implemented measures, particularly the Inner Harbour Dike, effectively reduce inundation under Bodil-scale conditions, while their protective capacity is exceeded under more extreme water levels, with flooding occurring through indirect pathways. The study highlights the need for continuous reassessment of adaptation strategies using process-based flood modelling to support climate-resilient urban planning.

KEYWORDS: Flood adaptation; Storm surge flooding; Flood risk; Climate change.

1 INTRODUCTION

Coastal cities are increasingly exposed to flood risk as climate change intensifies storm surges and raises mean sea level, challenging existing protection standards and urban planning practices. In low-lying historic waterfronts, even moderate increases in sea level can lead to rapid inundation, prolonged flooding, and disproportionate damage to cultural heritage, infrastructure, and urban functions. Understanding whether current adaptation strategies remain sufficient to manage these evolving risks requires not only forward-looking projections, but also systematic evaluation against past extreme events and improved knowledge.

The 2013 storm surge event Bodil represents a critical reference point for coastal flood risk in Denmark. The event produced the highest recorded water levels in parts of the Roskilde Fjord in more than a century, resulting in extensive flooding in Roskilde city, particularly in the harbor area. In the aftermath of Storm Bodil, Roskilde Municipality developed and implemented climate adaptation measures, ranging from structural flood protection and hybrid defenses to spatial transformation and risk avoidance. More than a decade later, Bodil provides a narrative for assessing whether these measures have meaningfully reduced flood risk and whether they are robust under future climatic conditions.

The main objective of this paper is twofold. First, it evaluates whether the adaptation measures implemented or currently planned in Roskilde city are sufficient to prevent flooding during a recurrence of the 2013 Bodil event**.** Second, it assesses how these strategies perform under more extreme conditions associated with future sea-level rise, representing plausible high-end storm surge scenarios. To address these objectives, the study combines an analysis of municipal climate planning documents with a set of hydrodynamic simulations using the RIM2D model. The Bodil event is forensically reconstructed using observed water levels and pre-event topography, and then re-simulated under present-day conditions and future extreme water levels, incorporating implemented and planned adaptation measures.

By focusing on a single, well-documented city and a historically extreme event, the paper contributes to a growing body of research that seeks to bridge climate adaptation planning and process-based flood modelling using a storyline approach. The results provide empirical insight into how urban adaptation

strategies perform in practice, highlight remaining vulnerabilities, and underscore the importance of continuous reassessment of coastal protection standards in the face of rising sea levels.

2 METHODOLOGY

2.1 Study Area

The Roskilde Fjord area in Denmark faces a growing set of climate-related hazards, with storm surges and coastal flooding posing as the most significant threat. The fjord's long, narrow, and funnel-shaped geography amplifies water levels when strong winds push water inland, highly exposing nearby towns and infrastructure. Roskilde Fjord extends approximately 42 km from its connection to the Kattegat to its southern inner reaches and hosts several urban settlements and critical infrastructures along its shoreline. In this study, the analysis focuses on the harbor area of Roskilde municipality (Figure 1).

The Roskilde harbor area is characterized by its low-lying waterfront directly adjacent to the historic city center. Large parts of the harbor and surrounding urban fabric are located only slightly above mean sea level, making them highly sensitive to even moderate storm surges. The area contains valuable cultural heritage assets, including a national museum featuring a unique collection of Viking ships, historic buildings, public spaces, and archaeological sites, which constrain the implementation of large-scale structural protection measures. Flooding in Roskilde therefore not only carries high economic risks but also irreversible cultural and social losses.

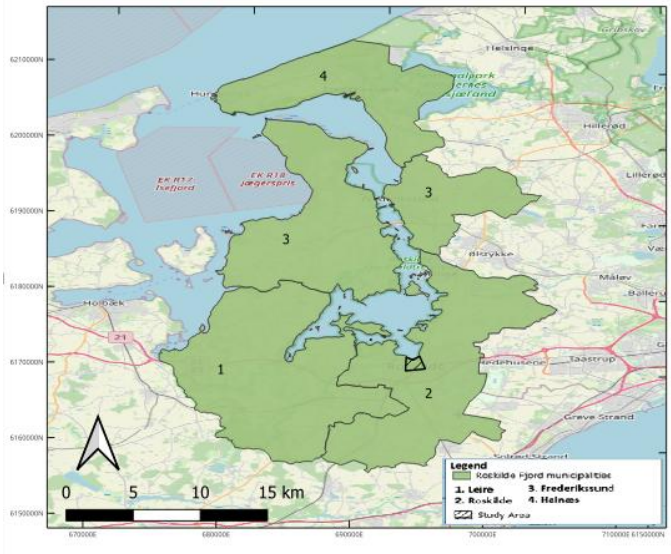

Figure 1 - Roskilde Fjord and selected study area at Roskilde municipality.

2.2 Flood Modelling

Flood simulations were carried out using the raster-based hydrodynamic model RIM2D, which solves an inertial formulation of the shallow water equations and is suitable for simulating fluvial, pluvial, and coastal flooding processes (de Almeida et al., 2013). The model has been widely applied in previous studies and is described in detail elsewhere (e.g. Apel et al., 2016; 2022; 2024). In this study, coastal inundation is driven by elevated water levels recorded at tidal gauges; wind and wave effects are not explicitly modelled due to limited data availability.

The model domain covers the Roskilde Fjord and adjacent land areas (approximately 1,379 km²) at a spatial resolution of 2 m. Land-surface roughness was derived from land-use data using standard Manning coefficients associated to land-use classes from literature, while buildings were represented using a building-hole approach based on OpenStreetMap footprints. Spatially distributed saturated infiltration rates were assigned using soil substrate maps. Urban drainage by the sewer system was accounted for using a capacity-based approach, assuming a drainage capacity of 20 mm/h. Simulations were performed on a high-

performance computing system on Graphical Processor units (GPUs), allowing efficient execution of high-resolution scenarios.

To evaluate flood risk evolution and the effectiveness of adaptation measures in Roskilde Harbor, a set of progressively structured scenarios was developed. First, the 2013 Bodil event was forensically reconstructed using observed hourly water levels from the Roskilde Harbor gauge (DMI station 30407) and a 2007 digital elevation model (DEM) representing pre-event conditions. Second, the Bodil event was re-simulated using its maximum observed water level (2.06 m) under present-day topography, incorporating implemented adaptation measures. A further scenario includes both implemented and planned measures. Finally, a future extreme scenario was simulated using a water level of 2.50 m, representative of a potential 100-year event under sea-level rise. Together, these simulations allow systematic comparison of baseline flooding, current protection performance, and robustness under more extreme future conditions.

2.3 Event Description

Storm surges are created by wind that pushes water towards coasts, which causes the water level to rise (Needham et al., 2015). Denmark has a long history of storm surges with the Bodil event of December 2013 representing the most severe storm surge event affecting the Roskilde Fjord area in recent decades. The event developed from a rapidly deepening low-pressure system over the North Atlantic and, upon reaching Denmark, strong northwesterly winds pushed large volumes of seawater into the narrow Roskilde Fjord, producing extreme storm surge conditions (Andrée et al., 2021). This wind-driven set-up led to sustained elevated water levels during 6–7 December 2013.

Observed water levels at Roskilde Harbour reached just more than 2 m above mean sea level, the highest levels recorded in more than a century. The event was characterized not only by a high peak but also by several hours of elevated water levels, substantially increasing flood exposure and damage potential (Figure 2a). The forensic reconstruction of Bodil shows a rapid and non-linear flooding response in the harbor area. Flooding began in the western harbor around 02:00 on 6 December, and a small additional rise in water level (approximately 0.10 m) was sufficient to trigger inundation of the inner harbor by 04:00. By 08:00, the entire harbor area is flooded, despite peak water levels occurring later, indicating that critical flooding thresholds are exceeded well before the event maximum (Figure 3).

The Bodil storm caused significant impacts in Roskilde city. The flooding primarily affected the harbor area and the adjacent historic city center, where the storm surge inundated waterfront quays, public spaces, and basements of historic buildings. Damage to cultural heritage assets, commercial properties, and waterfront facilities was reported, and access to central areas was temporarily disrupted during the peak of the event (Roskilde Municipality, 2014; *Politiken*, 2013).

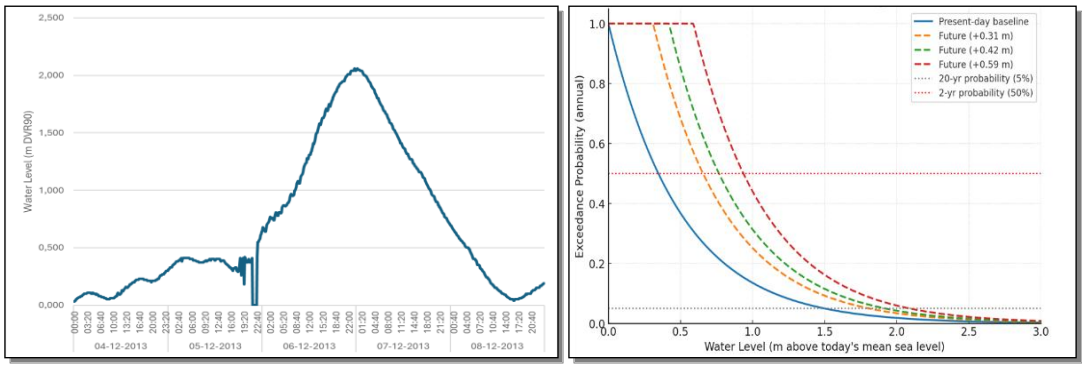

a **b**

Figure 2a. Observed water level at Roskilde Harbour (DMI gauge 30407) during Storm Bodil, from 4 to 8 December 2013. Figure 2b. Projected mean sea-level rise under different emission scenarios translates into increased water levels in Denmark based on DMI (Klimataatlas, 2025).

Figure 3. Simulated temporal evolution of flooding in the Roskilde Harbour area during the Bodil storm. Snapshots at 02:00, 04:00, and 08:00 on 6 December 2013.

According to the Danish Meteorological Institute (DMI), the frequency of storm surges of comparable or greater magnitude is expected to increase significantly in the future. Events that currently have a statistical return period of once every 20 years are projected to occur on average every second year. This shift is driven primarily by mean sea-level rise, which elevates the baseline water level from which storm surges develop, thereby increasing the probability that extreme thresholds are exceeded (DMI, Climate Atlas).

This mechanism is often described as a nonlinear frequency shift, whereby relatively small increases in mean sea level lead to disproportionate increases in the frequency of extreme coastal flooding events (Figure 2b). Consequently, events that are considered rare under present-day conditions may become commonplace within a few decades.

According to IPCC, by 2050, global mean sea level is expected to rise by additional 10-25cm, regardless of reductions in greenhouse gas emissions. Even under scenarios where net-zero emissions are achieved, thermal expansion of seawater and ongoing ice-sheet contributions ensure that sea-level rise will persist well beyond this century. For Denmark, regional projections provided by DMI's Climate Atlas indicate that under climate change scenario SSP3-7.0, mean sea level in Roskilde Fjord could rise by approximately 47 cm by 2071-2100. While this increase may appear moderate in absolute terms, it has disproportionate consequences for the potential impact of storm surges (Figure 2b). Such changes expose low-lying coastal regions, including areas around Roskilde Fjord, to recurrent flooding, undermining existing protection standards and challenging long-term adaptation strategies.

3 ADAPTATION MEASURES

Climate change adaptation has become a central concern in urban and spatial planning, as climate impacts are primarily experienced at the local level. Planning frameworks translate long-term climate risks into spatial strategies, land-use regulations, and infrastructure investments tailored to local conditions and capacities. Local governments play a key role in this process, as they are responsible for implementing national and international objectives through concrete planning decisions. As a result, municipal climate plans serve as a critical link between climate science, policy goals, and practical risk reduction.

In Denmark, the DK2020 initiative has for the first time introduced a common structure to municipal climate plans. DK2020 originally targeted a selection of Danish municipalities but has developed into a national platform designed to support local governments in developing comprehensive climate action plans aligned with the Paris Agreement. Based on the C40 Climate Action Planning Framework, DK2020 requires municipalities to combine climate mitigation targets with systematic assessments of climate risks and vulnerabilities, and to define adaptation measures across sectors. The framework emphasizes implementation pathways, monitoring, and periodic revision, thereby enabling an evaluation of both planned and realized adaptation actions.

Between 2013 and 2024, Roskilde Municipality developed and implemented a series of climate adaptation and urban planning documents in response to increasing flood risk and long-term climate change (Table 1). In the harbor area, adaptation is guided by a layered planning framework, in which strategic

climate objectives are progressively translated into operational measures and spatial interventions. These documents range from high-level climate action plans aligned with national and international targets to detailed adaptation action plans and site-specific urban redevelopment projects. Together, they establish a coherent pathway from policy intent to physical implementation, with storm surge, sea-level rise, and compound flooding in Roskilde Harbor forming a central and recurring focus.

At the strategic level, Roskilde Municipality's Climate Plan (Klimaplan) 2024 (DK2020) defines the overarching climate objectives and identifies coastal flooding and sea-level rise as key long-term risks for low-lying waterfront areas. While primarily a strategic framework, the plan explicitly acknowledges that protection efforts in Roskilde Harbor are largely implemented yet emphasizes the need for continuous reassessment of protection levels in response to future sea-level rise and extreme events. This positions the harbor as an area where adaptation is ongoing rather than complete.

These strategic objectives are operationalized through the Climate Action Plan (Klimahandleplan) 2024, which specifies concrete adaptation actions relevant to the harbor area. A central measure is the protection of Roskilde Inner Harbor, where a new harbor promenade functions as an integrated coastal defense. The project combines permanent structural protection - a raised promenade with cast concrete paving and a continuous half-wall - with deployable flood barriers, allowing detachable aluminum boards to be installed during extreme events. This hybrid system raises the effective protection level for direct flooding, i.e. dike overtopping, to approximately +2.75 m, directly addressing storm surge impacts comparable to the 2013 Bodil event, while balancing flood protection with urban accessibility and heritage considerations.

Complementing these defenses, the climate plan also addresses compound flooding through targeted interventions such as the Tømmergrunden adaptation project, in the west part of Roskilde Inner Harbor. This project introduces a dike designed to protect against elevated fjord water levels while enabling controlled discharge of cloudburst runoff via a longitudinal depression and a closable opening. The measure explicitly recognizes the interaction between storm surge and extreme precipitation. However, this dike is still in the planning and design phase.

Table 1- Key climate and urban planning documents guiding flood adaptation in Roskilde Harbour

Document	Year	Type	Main focus	Relevance
Klimatilpasningsplan for Roskilde Kommune [1]	2014	Climate adaptation plan	Identification of flood risks (storm surge, cloudbursts, groundwater) and priority areas	Establishes Bodil as reference event and identifies Roskilde Harbour as a high-risk zone
Klimaplan 2024 – DK2020 [2]	2024	Climate action plan	Integrated mitigation and adaptation aligned with the Paris Agreement	Frames long-term adaptation objectives and acknowledges need for reassessment under sea-level rise
Klimahandleplan 2024 [3]	2024	Adaptation action plan	Concrete adaptation actions, timelines, and responsibilities	Specifies implemented and planned flood protection measures in Roskilde Harbour (e.g. Inner Harbour West, Tømmergrunden)
Kyststrategi – Administrationsgrundlag for kystbeskyttelse [4]	2023	Coastal strategy / regulatory framework	Principles, design guidelines, and decision criteria for coastal protection under sea-level rise	Defines protection standards, adaptable design requirements, and retreat logic applied in Roskilde Harbour projects
Kommuneplan (Municipal Plan) [5]	2016; 2019: 2009; 2026	Urban / spatial plan	Land-use regulation and urban development	Integrates flood risk into land use and constrains development in exposed harbour areas
Handleplan for klimatilpasning 2026–2029 [6]	2025	Adaptation implementation plan	Monitoring, model updates, and continuation of adaptation projects	Confirms harbour area as a priority and supports scenario-based evaluation
Harbour redevelopment & Viking Ship Museum relocation plans [7]	2017–ongoing	Urban project plans	Waterfront transformation, cultural heritage protection	Introduce accommodation and retreat strategies central to the harbour adaptation concept

[*] the numbers in brackets indicate the references

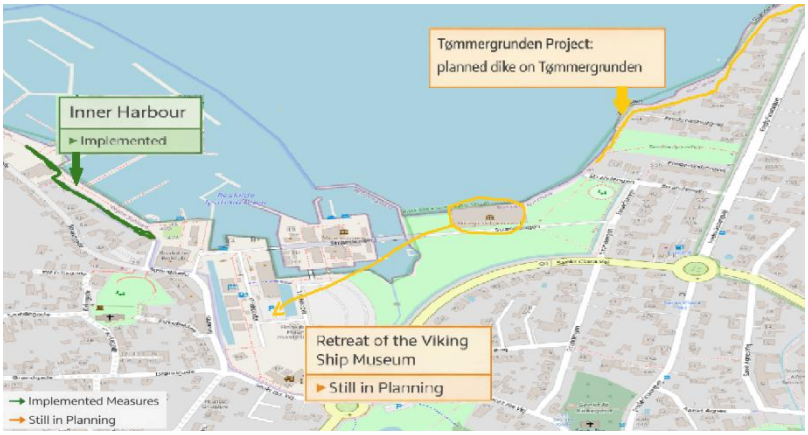

Figure 4 – Adaptation measures implemented and planned in the Roskilde's Climate Plan.

Beyond structural protection, Roskilde's adaptation strategy also incorporates elements of spatial transformation and risk avoidance. A prominent example is the decision to relocate the Viking Ship Museum to a safer location, reducing exposure of irreplaceable cultural heritage assets to future flooding. The redevelopment of the former museum area and adjacent harbor zones into Havneparken, a multifunctional public park, reflects an adaptive approach that accommodates periodic flooding while enhancing recreational and urban qualities. By transforming highly exposed waterfront areas into flexible public spaces rather than intensively used buildings, the municipality reduces potential damage while maintaining public access to the fjord.

The implementation and coordination of these measures are supported by the Action plan for Climate Change Adaptation (Handleplan for Klimatilpasning) (2026–2029), which consolidates adaptation projects and emphasizes the importance of maintaining and updating hydrodynamic and drainage models to evaluate local climate adaptation scenarios. This commitment to model-based assessment underlines the municipality's recognition that protection levels and spatial strategies must be revisited as sea levels continue to rise.

In addition, Roskilde's Coastal Strategy (2023) provides the regulatory and design framework for coastal protection, specifying protection heights, adaptability requirements, and the balance between hard protection, retreat, and public access, thereby shaping the form and limits of the harbor adaptation measures analyzed in this study.

The structural interventions described above form the basis for the modified topographic representation used in the hydrodynamic simulations presented in the following section.

4 RESULTS – ADAPTATION EFFECTIVENESS AND FUTURE SCENARIOS

The numerical simulations presented in this section are designed to evaluate how the implemented and planned adaptation measures for the Roskilde harbor perform under extreme coastal flooding conditions. Building on the preceding assessment, the simulations address two central questions: first, whether the adaptation measures implemented or currently planned are sufficient to prevent flooding during a recurrence of the 2013 Bodil event; and second, how these strategies respond to more extreme conditions associated with future sea-level rise (Figure 5).

The simulation results indicate that the Inner Harbor dike provides effective protection under a Bodil-scale maximum water level of 2.06 m, preventing direct inundation of the urban areas located behind the harbor promenade. Under this scenario, the dike blocks the primary flood pathways observed during the 2013 event, resulting in a substantial reduction in flood extent and water depths landward of the harbor front. However, when the maximum water level is increased to 2.50 m, representing a more extreme future event, the Inner Harbor dike cannot prevent flooding of the protected area behind it. The dike continues to prevent direct overtopping along the harbor edge, but flooding occurs indirectly via the area surrounding the Viking Ship Museum from where floodwaters propagate inland and inundate the protected area from

the land side. This suggests that under higher water levels, secondary flood pathways bypass the main line of defense, indicating either the presence of additional protection measures not captured in the digital elevation model or an inherent limitation of the current protection system under extreme conditions. It also illustrates that system performance is controlled not only by the crest height of individual protection structures but also by the connectivity of surrounding low-lying areas.

In contrast, the Tømmergrunden dike exhibits limited influence on flooding patterns in the simulations. The area is inundated already under the 2.06 m scenario, primarily due to inflow from the harbor and museum area behind the dike, rather than from direct fjord overtopping at the Tømmergrunden frontage. Increasing the water level to 2.50 m leads to earlier and more extensive flooding, reinforcing the conclusion that the planned dike, as represented in the model, does not significantly alter the dominant flood pathways. This outcome may reflect missing design details in the model representation, such as crest height, continuity, or the operation of closable openings; alternatively, it may indicate that the planned measure is insufficient when considered in isolation. Overall, the results show that while current adaptation measures in Roskilde Harbour reduce flood impacts under Bodil-scale conditions, their effectiveness diminishes under more extreme water levels, highlighting the importance of addressing indirect inundation pathways and system-wide connectivity in future adaptation planning.

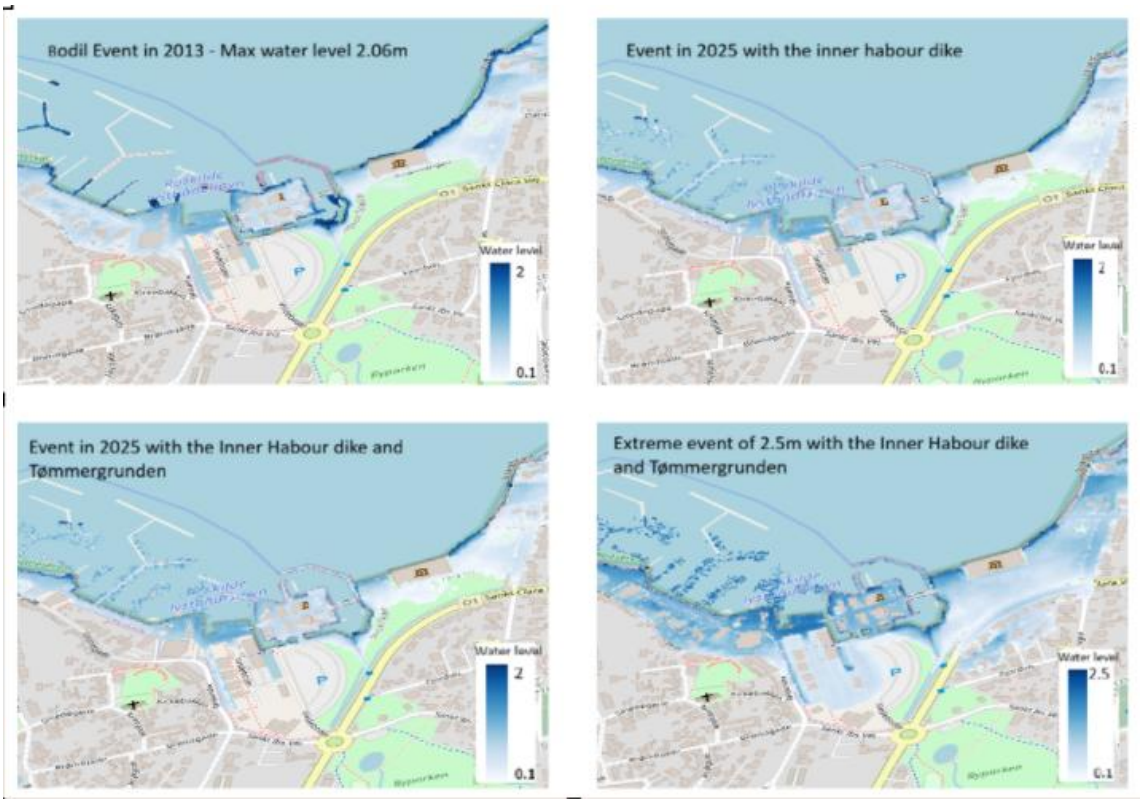

Figure 5 - Simulated flooding scenarios in the Roskilde Harbor area. *(a)* Forensic reconstruction of the 2013 Bodil event at its maximum observed water level (2.06 m). *(b)* Replication of the Bodil event under present-day conditions, including the implemented Inner Harbor Dike. *(c)* Replication of the Bodil event incorporating both implemented and planned adaptation measures - Inner Harbor Dike and Tømmergrunden dike. *(d)* Extreme future scenario with a water level of 2.50 m, simulated with both implemented and planned dikes.

5 CONCLUSION

This study evaluated the effectiveness of climate adaptation measures in Roskilde Harbor by reconstructing the 2013 Bodil storm and re-simulating it under present-day and future extreme water-level scenarios. The results show that adaptation measures implemented since Bodil, particularly the Inner Harbor Dike, substantially reduce flooding under Bodil-scale conditions. However, under more extreme water levels representative of future scenarios, the protective capacity of the system is strongly reduced, mainly by inundation occurring through indirect pathways rather than direct overtopping.

The planned Tømmergrunden dike shows limited additional benefit in the simulations, suggesting that either key design elements are not yet fully defined or that the measure alone is insufficient to address dominant flood pathways. Overall, the findings highlight that while current strategies improve resilience to present-day extremes, they do not fully prevent flooding under high-end future scenarios.

This underscores the importance of continuous, model-based reassessment of adaptation measures and of addressing system-wide connectivity and residual risk in coastal urban planning. Following the Bodil event, Roskilde Municipality developed a comprehensive set of climate adaptation and urban planning documents, reflecting a systematic effort to translate scientific knowledge into local planning and infrastructure measures. While these strategies uses Bodil as a benchmark, are grounded in current climate projections and aligned with frameworks such as DK2020, the simulation results indicate that protection measures implemented and planned may still be exceeded under higher water levels. Importantly, the findings show that system performance depends not only on the crest height of individual protection structures but also on the connectivity of surrounding low-lying areas, which may allow floodwaters to propagate through indirect pathways. Although hydrodynamic simulations inevitably involve uncertainty, the forensic reconstruction and re-simulation of past extreme events provide a practical methodological approach for municipalities to reassess existing protection systems and support iterative adaptation planning under changing climate conditions. These findings are generic and can be translated to other coastal communes facing the same problem of increasing flood risk.

REFERENCES

Andrée, E. and Su, J. and Larsen, M. A. D. and Madsen, K. S. and Drews, M. (2021). Simulating major storm surge events in a complex coastal region. "Ocean Modelling", 162, Doi: 10.1016/j.ocemod.2021.101802.

Apel, H., Vorogushyn, S., and Merz, B. (2022). Brief communication: Impact forecasting could substantially improve the emergency management of deadly floods: case study July 2021 floods in Germany. Nat. Hazards Earth Syst. Sci. 22(9), 3005-3014. doi: 10.5194/nhess-22-3005-2022.

Apel, H., Benisch, J., Helm, B., Vorogushyn, S., and Merz, B. (2024). Fast urban inundation simulation with RIM2D for flood risk assessment and forecasting. Frontiers in Water 6. doi: 10.3389/frwa.2024.1310182.

Apel, H., Martínez Trepat, O., Hung, N.N., Chinh, D.T., Merz, B., and Dung, N.V. (2016). Combined fluvial and pluvial urban flood hazard analysis: concept development and application to Can Tho city, Mekong Delta, Vietnam. Nat. Hazards Earth Syst. Sci. 16(4), 941-961. doi: 10.5194/nhess-16-941-2016.

de Almeida, G.A.M., and Bates, P. (2013). Applicability of the local inertial approximation of the shallow water equations to flood modeling. Water Resources Research 49(8), 4833-4844. doi: 10.1002/wrcr.20366.

Intergovernmental Panel on Climate Change (IPCC). (2021). "Climate Change 2021: The Physical Science Basis. Contribution of Working Group I to the Sixth Assessment Report of the Intergovernmental Panel on Climate Change" (eds. V. Masson-Delmotte, P. Zhai, A. Pirani, et al.). Cambridge University Press. https://doi.org/10.1017/9781009157896

Klimaatlas, 2025. Denmark's national climate atlas. Available at: https://www.dmi.dk/klimaatlas. (Accessed 05 December 2025).

Needham, H. F. and Keim, B. D. and Sathiaraj, D. (2015). A review of tropical cyclone-generated storm surges: Global data sources, observations, and impacts. "Reviews of Geophysics, " *53*(2), pp. 545-591.
[1]Roskilde Municipality. (2014). *Klimatilpasningsplan for Roskilde Kommune*. Roskilde Kommune.
[2]Roskilde Municipality. (2024). *Klimaplan 2024 – DK2020*. Roskilde Kommune. Available at: https://www.roskilde.dk/media/sadjl4dc/klimaplan-2024.pdf
[3]Roskilde Municipality. (2024). *Klimahandleplan 2024*. Roskilde Kommune. Available at: https://www.roskilde.dk/media/5qxnylgh/handleplan-2024-2028_161224_vedtaget.pdf
[4]Roskilde Municipality. (2023). *Kyststrategi: Administrationsgrundlag for kystbeskyttelse i Roskilde Kommune*.
[5]Roskilde Municipality. (2016). *Kommuneplan*. Roskilde Kommune. Available at: https://www.plandata.dk/
[6]Roskilde Municipality. (2026). *Handleplan for klimatilpasning 2026–2029*. Roskilde Kommune. Available at: https://www.roskilde.dk/media/vnxdu1aq/handleplan_klimatilpasning_2026-29.pdf
Web-1: https://www.dmi.dk/nyheder/havet-truer-men-hvor-hvor-meget-og-hvornaar, consulted 17 August 2025.
Web-2: Roskilde Municipality (2014). *Stormflod Bodil – Erfaringer og opfølgning*.
Web-3: *Politiken*, *DR Nyheder*, *Berlingske* articles from December 2013–January 2014.
Web-4: [7] https://www.cfmoller.com/p/Viking-Ship-Museum-in-Roskilde-i3938.html#

ICFM 10
Adapting to Global Change:
Innovative Approaches to Flood Management and Resilience
May 20-22, 2026 | Western University, London, Ontario, Canada

How to keep the Netherlands safe and liveable for future generations as sea levels rise? Current approach, a solid basis!

Annemiek Roeling[1], Saskia van Vuren[2], Quirijn Lodder[1], Saskia van Gool[1] and Menno van Manen[1].
Ministry of Infrastructure and Water Management, The Hague, The Netherlands[1]
E-mail: Annemiek.Roeling@minienw.nl
Staff of the Delta Commissioner, The Hague, The Netherlands[2]
E-mail: Saskia.van.Vuren@deltacommissaris.nl

ABSTRACT

The Netherlands is one of many densely populated deltas in the world. In areas such as these the availability of fresh water and the proximity to the sea are simultaneously a blessing and a threat. Over centuries, the Dutch delta has developed into a safe and prospering area, relying on a comprehensive system of flood defences and an intricate water system. Due to global climate change and socio-economic developments both the system of flood defences and the water system will be under increased pressure in the future. The Netherlands in particular needs to find ways to cope with sea level rise (SLR) to keep the delta safe and liveable for generations to come.

Through the Knowledge Programme on Sea Level Rise, a coherent series of studies has been performed in order to understand the consequences of a SLR of up to 5m for the water system and the options for action. Model based studies have shown that the current approach for flood risk management technically could be prolonged up to a SLR of 3 to 5m. While consequences for the economy, nature and society increase with the sea level over time, other perspectives may become attractive. Four alternative conceptual perspectives have been explored by multidisciplinary teams, leading to useful building blocks. However, up to 5m of SLR, levees and beach nourishments remain basic elements in all different perspectives.

The current approach provides a solid basis for the future and from a flood protection perspective there is no necessity to make major changes now. However, as transition processes will take decades, it is advisable to prepare in a timely manner. Foreseeable future adaptation should be taken into account in today's spatial planning and decision-making processes. The adopted structured, policy driven knowledge development may be a valuable approach for other regions and subjects.

KEYWORDS: Netherlands, climate adaptation, sea level rise, Knowledge Programme, flood protection

1 INTRODUCTION

Because of its geographical location, with around 50% of the surface of the country being flood prone, flood risk and water management are key to the safety and prosperity of the Netherlands. Flood protection and water management systems are never 'finished', but after the Delta works and the Room for the River programme, recent efforts seem to have mainly been aimed at the optimization of the existing system. However, adaptation to climate change in general and SLR in particular may implicate larger changes in the future. The publication of a paper (De Conto and Pollard, 2016) on possible extreme SLR through accelerated mass loss of Antarctic ice and a subsequent report on possible consequences for the Netherlands (Haasnoot et al. 2018), led to a range of articles and opinions in the media on the (possible

absence of a) future for the Netherlands. Although several studies in the past addressed the subject of SLR in the Netherlands (PBL, 2007) no detailed studies of the consequences had been performed so far.

Therefore in 2019, a national research programme was developed by the Ministry of Infrastructure and Water Management and the Delta Commissioner in order to create a sound knowledge basis as a starting point for policy development.

1.1 Scope of the Knowledge Programme on Sea level Rise

The knowledge programme consisted of several 'tracks' each with a different focus. Main objectives and budget of the programme were determined before the programme started. Throughout the duration of the programme however, a certain amount of flexibility was permitted to make changes in method or focus. As the programme aimed to develop information for flood risk and water management, it was policy oriented. Resulting in a programme considered very technical within the policy environment, and at the same time very policy focussed within a scientific environment. In order to create the most objective value possible, the developed knowledge has consciously been reported separately from the associated policy discussion, that is taking place within the ministry and the delta programme.

Because of the importance of flood risk and water management for the perdurance of the Netherlands and the huge potential impact, a SLR of up to 5 m was taken into account. Such is in line with the recommendation in the sixth assessment report of the IPPC (IPCC, 2023) for exposed countries to take extreme scenarios into account. Because of the large uncertainty of the speed and amount of SLR in the future, studies were performed scenario independent whenever possible, in order to be able to translate results to different (future) scenarios. In case this was not possible, several different working scenarios were taken into account in order to obtain as much information as possible. The most extreme working scenario consisted of 2 metres (m) of SLR in 2100 and 5.4m of SLR in 2200, which would be well above the 17th to 83rd percentile range of SPS5-8.5 and in the order of the *low likelihood high impact* storylines of the SLR scenarios for the Netherlands (KNMI, 2023). This most extreme scenario is considered to be a 'stress-test-scenario', and has also been used to develop the alternative conceptual perspectives.

The different tracks consisted of:

a) Research on SLR itself: contributing to the development of different scenarios for SLR to be expected on the Dutch coast in the future, and the interpretation of sea level measurements/SLR measured at present. An important goal of this track was to participate in international knowledge development. It is the most academic part of the knowledge programme.
b) A series of **system oriented studies** on effects of SLR on 1) flood risk management of the main water system (sea, main rivers and big lakes), and 2) on salination, both within the water system and through salty seepage. These studies involved modelling and took several years.
c) Development of several **alternative conceptual perspectives** to keep the Netherlands safe and liveable in the future. These studies had a more explorative character, although more or less information from the system oriented studies could be used, depending on the nature of the conceptual perspective.
d) Communication, participation and decision-making; Special effort has been put into communication of current findings to inform politicians and the general public. A group of representatives of different NGOs (e.g. on nature conservation) and sectors (e.g. on agriculture, sand extraction, recreation) has been kept up to date of developments and results, leading to a grown consciousness on difficulty of future choices in water management and the necessity of adaptation (of sectors)to SLR. Additionally, conceptual reflection has been organised on public decision-making under high uncertainty (van der Steen et al., 2025).

This publication focusses mainly on flood risk management aspects of b) the system oriented studies (under 2) and c) the alternative conceptual perspectives (under 3). General aspects of a) and d) are part of the discussion (under 5).

2 SYSTEM ORIENTED STUDIES

The main aspect of the current Dutch approach for flood risk management consists of statutory standards for flood protection infrastructure, stipulated in law. Standards have been deducted using risk assessments. Standards provide at least a *base level of flood protection*, the probability of an individual drowning in a flood will not exceed 1/100,000 per year. Standards provide a higher protection whenever appropriate, following the outcomes of local cost-benefit analyses and group risk assessments. The resulting standards are expressed as 'a maximum permissible probability of failure per year' and prior to exceeding this maximum, infrastructure should be upgraded. This means that higher expected river discharges and rising sea levels will over time require stronger levees, dunes, dams etc.. The current set of standards has been introduced in 2017 and is planned to be completely met in 2050. Counter-intuitively this is leading to a progressive risk reduction towards 2050, in spite of climate change.

On top of the standards there are regional strategies defining how national and regional authorities, together with other regional and local parties, want to achieve the required safety level. An example is the 'closable-open' strategy in the highly urbanised and industrialized region of Rotterdam. In this region the Maeslant barrier ensures easy access to the port and the hinterland from the sea on a daily basis, while protecting the area from extreme water levels during storm surge, thus reducing the necessary dimension of levees behind the barrier as well as the amount of water nuisance in unprotected areas.

Both the standards for flood protection infrastructure and the regional strategies are taken as a premise for the system oriented studies. The effects of SLR combined with expected development of (extreme) river discharges are taken into account to calculate hydraulic loads for 0.5, 1, 2 and 3 m of SLR. These hydraulic loads have been extrapolated to 5 m of SLR to extend the range of the assessments. Under different climate scenarios different combinations of sea level and river discharges are expected, hence different hydraulic loads have been determined.

2.1 Sandy coast

Part of the system studies focused on the impact of accelerated SLR on the sustainability and adaptability of the coastal management strategy. This strategy aims to maintain the coastline dynamically through sand nourishments, ensuring safety and preserving functions and uses of dune areas while allowing the coast to gradually rise with sea level (Lodder and Slinger, 2022; Brand et al. 2023).

Currently, about 11 million m^3 of sand is added annually via beach, shoreface, and channel nourishments. Estimates of future nourishment demand have been made based on assessment of the current sediment budgets, conceptual and numerical modelling. These assessments indicate that the long-term goals can likely be met by allowing the most active parts of the coast (between approx. –8 m MSL and the first dune row) to rise with sea level. Sand nourishments spread within this zone.

The sand demand will increase significantly in the future: under the extreme scenario of 2 m SLR in 2100 and 5.4 m in 2200, the annual nourishment demand is estimated to be 4× current levels by 2100 and 5× by 2200. However, there are significant regional differences. The Northern part of the coast (Wadden Coast) requires up to 7× more sand, while the middle part (Holland Coast) and Southern part (Delta Coast) are estimated at 3.5× and 2.5× respectively.

To supply these nourishment volumes, innovations in nourishment techniques are likely to be needed. In addition to the current nourishment types, larger scale nourishments are needed. These

innovations include nourishment forms but also should address aspects like emission reduction and reduction of environmental disturbance.

Overall it is concluded that the coastal management strategy is sustainable and adaptable.

2.2 Flood protection structures

In order to assess the necessary adaptation of the (system of) primary flood defences, a standardized method based on models has been used. It consists of combining hydraulic loads (forces from water), with failure models of the flood defence, which includes the dike profile, foreshore, revetments, dike materials, soil properties, and water pressure effects. Hydraulic loads were deducted using hydrodynamic and wave models for thousands of combinations of surge water level, river discharge (River Rhine and Meuse) and wind properties. The study focused on three main failure mechanisms: *dike height* (overtopping and overflow), *slope stability* and *piping*. All failure processes were modelled using fragility curves.

The flood safety assessment used a probabilistic approach, with water level and wave load as key stochastic variables. Hydraulic loads were computed with models such as **SOBEK3** for rivers (Rhine and Meuse), **IMPLIC** for the Eastern Scheldt and **WAQUA** for the Western Scheldt and Wadden Sea. Waves were modelled using a fetch approach for the rivers and **SWAN** (coastal areas). Inputs were based on statistical analyses of historical seawater levels, wind, and river discharge, covering return periods from years up to 100,000 years. The spatial and financial impacts of reinforcement were assessed with a dedicated cost model (OKADER). Where plan view space was limited, hard vertical structures or demolition of buildings were assumed for the necessary flood defence upgrades, with costs including depreciation of existing houses.

- **Variation in dike heightening**
  Simulations show large regional differences. For 3 m SLR, required dike heightening exceeds 5 m in the northern part of the country (up to 7 m in some Wadden Sea areas), decreasing to 1–4 m in central and southern regions and further inland along the Rhine and Meuse. Extra height beyond SLR is mainly due to wave run-up and depth-limited wave growth.
- **Wave dynamics and foreshore effects**
  Higher water levels allow larger waves to reach flood defences, increasing wave setup and reducing bottom friction. Seabed growth (sedimentation) slightly reduces required heightening (≈1 m less), while foreshore vegetation improves stability but does not affect dike height.
- **Storm surge barriers**
  Rising SLR drastically increases closure frequency if closure levels remain fixed. For example, the Maeslant barrier would close every tidal cycle at 3 m of SLR. Raising closure levels reduces closure frequency but makes outer embankments more flood-prone. For areas protected by both barriers and dikes, required dike heightening is roughly equal to SLR.
- **Land Use**
  Dike reinforcement requires significant space: when there is 3m of SLR an extra width of 50-150m is needed, in extreme cases up to 200m. This is especially challenging in urban areas. Built-up floodplain areas will face more frequent flooding.

2.3 Findings on current approach

The results have shown that it is *technically possible* to protect the Netherlands against flooding using the current approach, up to 3 m of SLR, possibly 5 m (Friocourt et al. 2025). However, this requires major ongoing efforts and spatial adjustments. With continued SLR, larger sand nourishments, stronger

dikes and more frequent barrier closures will be needed, as well as increased pumping capacity to drain low lying areas. Furthermore, areas without flood protection will experience frequent or even permanent inundation. This includes some urban areas.

"Technically possible" means designs can withstand the studied SLR, but societal impacts are not yet (well) assessed. The availability of clay and sand and space for e.g. wider dikes is crucial. Logistics could become a major challenge if SLR accelerates, requiring simultaneous action in many places. Furthermore, the actual societal challenge is larger than here presented since SLR also effects the fresh water supply and other aspects of society such as space for nature and recreation, risk perception etc. These factors will co-determine how long the current approach remains viable in practice. This raises the question what other strategies for adaptation could look like. To address this question alternative conceptual future perspectives have been developed.

3 CONCEPTUAL FUTURE PERSPECTIVES

Based on an inventory of existing 'plans' for the future of the Netherlands, different conceptual perspectives were determined: Protect (2x), Advance (seaward) and Accommodate (Haasnoot et al. 2020). The existing plans were deconstructed into 'building blocks'; measures that can be combined in order to find new possible strategies (Haasnoot and Diermanse 2022). Government authorities, knowledge institutes, and stakeholder organizations explored how these building blocks could be used to address the long-term consequences of SLR, leading to regional drafts of designs for each of the conceptual perspectives. In order to get a better idea of their feasibility and of the resulting alternative solution space at hand, a more detailed and technical description and design was needed. These were elaborated for the three above perspectives, as well as for a fourth perspective that was introduced in 2024: Grow.

To obtain the best possible results in a short period of time, a co-creation process was chosen. For each of the perspectives a multidisciplinary team was formed, consisting of e.g. hydraulic engineers, landscape architects, morphologists, ecologists, cost experts, etc., from various types of organizations: consultancy firms, designers from architects' firms, scientists from knowledge institutions and universities, government authorities, project contractors and NGOs and stakeholder organizations. A so-called 'core team' was responsible for designs and descriptions, analyses and calculations for the specific conceptual perspective of their attention. While a wider group was used to reflect upon results and to collect knowledge and input for the next step. In less than ten months, in a series of working meetings of the core teams and hackathons with the wider group, each team finalized a more detailed elaboration of its specific perspective: a landscape design including a more detailed and technical description of measures (Web-1). This formed the basis for an assessment of its effectiveness and feasibility. The conceptual perspectives have been developed for a SLR of 2 and 5.4 m in resp. 2100 and 2200 by means of a stress test; as alternatives are expected to be especially useful, and maybe sooner necessary, under extreme conditions. A short description of the perspectives is given below.

3.1 Protect

In the perspective Protect, the Netherlands is being kept safe and liveable by building upon the current approach to water management using hydraulic engineering works to direct, divert, and control water. This means upgrading dikes, storm surge barriers, locks, dams and pumping stations. In this way, the delta is protected against flooding, and the water system for both freshwater usage and excess water drainage can be optimised. With sand nourishments, the coastline is kept in place, and rises with the sea

level. Different decisions are to be made concerning the configuration of the delta, in this study leading to four different alternatives:

1. Sea fronts closable with storm surge barriers, with two options;
   a) maintaining the current discharge distribution over the river branches
   b) adapting the current discharge distribution over the river branches during high river flows; and
2. Sea fronts closed by dams, with again two options;
   a) maintaining the current inland water level using pumping stations
   b) increasing the inland water level with SLR enabling discharging of river water by using gravity forces as much and as long as possible.

3.2 Advance

In the perspective Advance the Dutch delta is extended in seaward direction by building a large 'lake' in front of the coast of the southwestern part of the delta. This constructed lake creates extra storage capacity for peak discharges of the Rhine and Meuse, such that less pumping capacity is required to discharge flood peaks from the river.

The perspective can be considered as an extension of the protect-closed perspective in the previous paragraph. Like the protect-closed perspective, it may reduce salinization problems in this part of the delta. The construction of the lake requires technical measures: dams, nourishments, break waters, pumping stations and ship locks. A new coastal lake would have a major impact on nature and ecology as the dynamics (water, waves, sediment) would be drastically altered.

3.3 Grow

The perspective Grow is based on the principles of nature based solutions (NBS). In this perspective, the Netherlands remains safe and liveable by making use of the natural processes that built the delta. This can be achieved by on the one hand stimulating the natural dynamics of water, sand and silt, and at the same time creating space to capture sand and silt, leading to transition zones between sea and land that grow along with SLR. These growing transition zones contribute to flood protection and provide a robust ecosystem. This could provide a flexible, climate-resilient alternative to the current approach, comparable to the current coastal management strategy for the sandy coast (see 2.1). However, in some places where this perspective could be applied existing traditional infrastructure impedes or limits both the exchange of sediment necessary for optimal siltation processes and a gradual freshwater-saltwater transition important for ecology. In these cases, dams and storm surge barriers would need to be removed or adapted in order to create the right conditions. On the long run annual SLR many exceed sedimentation speed and reduction of intertidal flats will occur, or additional nourishments will be necessary.

Although natural processes are heartily welcomed in the delta in this perspective, to preserve protection against flooding, this is only possible in combination with traditional dikes. And in order to optimise availability of fresh water, one of the two developed strategies combines open estuaries in the southern part of the with a closed off Rotterdam area (Protect). Hence, building blocks in this perspective are: nature-friendly storm surge barriers, transition zones between sea and land that grow along with SLR; either between dikes or as vegetated foreshores in front of dikes, (restored) tidal basins (former inlets along the coast), and nourishments and measures to accelerate or supplement natural accretion.

3.4 Accommodate

In the perspective Accommodate, land use and society is adapted as much as possible to the effects of SLR. The assumption is that existing water infrastructure and engineering works will not be further

upgraded after 2050 (but neither will they be removed). Everyone will retain the base level of flood protection (see under 2).

Special attention has been given to the Randstad urban agglomeration, the low-lying economic heart of the Netherlands, including the Port of Rotterdam. It is important for the Netherlands to maintain its earning capacity in order to adapt to climate change. After extensive exploration of alternative ways to keep this area fully functioning, it was concluded that the only cost-effective way to do so, is by continuing a 'protect-perspective' with hydraulic engineering infrastructure for as long as possible.

Other parts of the country may use building blocks that mitigate the consequences of flooding, for example raised or floating housing, evacuation plans, and water-robust vital networks (electricity, drinking water). To cope with more saline conditions, one can think of salt-tolerant agriculture, or 'footloose' agriculture. Encouraging investments in higher situated parts of the country, is also part of this perspective. It was not possible within the available timeframe to obtain a fully developed landscape plan.

3.5 Findings on alternative perspectives

The programme shows different options to design a realistic and liveable future for the Dutch Delta, and delivers a vast amount of useful building blocks. However, it seems unlikely that one of the conceptual perspectives will suffice to obtain a future-proof country. Most probably a combination of elements from all four conceptual perspectives is required (van Alphen et al., 2025). The performed research can serve as a knowledge basis and a source of inspiration.

4 IMPACTS, COSTS

Current land use and functions are highly optimised. Multiple developments, such as housing, industry and the energy transition, need more space. The impact of SLR on all of these socio-economic functions will in any case be negative compared to *the current situation*. Adaptation measures always ask space and construction materials and a serious increase of salinization is unavoidable in the end. It is possible to estimate the amount of space needed for adaptation to SLR on the long run, for different perspectives or using a combination of building blocks. It is difficult however, to determine impact in general, as land use and functions develop over time as well. Future SLR in itself may stimulate transformation of sectors, due to foreseeable effects, such as the reduction of the availability of fresh water. The impact in the end will be specific for a certain area and will depend on the amount of SLR, on water management and on the adaptability of future land use and functions.

To continue the *current strategy,* upgrading and replacing existing water management infrastructure such as levees, dams and storm surge barriers is necessary, as well as continuing beach nourishments to maintain the coastline. This will result in costs of approximately EUR 200 billion in 2200, with a SLR of 5.4 m, meaning an increase by 1.5 to 2 times the current cost of the strategy. In the *Protect perspective*, investment costs are comparable, amounting to EUR 100 billion in 2100 to 200 billion in 2200, for resp. 2 and 5.4 m of SLR. Different water management infrastructure will be realised and upgrading of levees and beach nourishments are still necessary. For the *Advance perspective* an extra EUR 30-35 billion should be added for the construction of the artificial lake. For the *Grow perspective* two different strategies have been assembled, leading to an extra estimated EUR 21-40 billion.

Costs of the Accommodate perspective could not be estimated based on the outcome of the co-creation study. In a case study (outside the programme) for the province of North-Holland, costs were estimated for several possible interpretations of an Accommodate perspective. The costs of the variant yielding the lowest total costs were around 60 times higher than those of the Protect perspective (Kolen, 2025). A more detailed overview of comparable costs of alle alternatives is yet to be concluded.

Costs have a large, but not calculated bandwidth. Costs for areas that are not protected by dikes and will be more sensitive to flooding in the future, costs for the regional water systems, or benefits that may occur are not included.

5 CONCLUSIONS AND DISCUSSION

5.1 The current approach for now most attractive.

The current flood risk management approach has been shown to be technically effective up to 3-5 m of SLR. However, its actual feasibility depends on multiple factors, like the availability of resources such as sand an clay. Different alternative conceptual perspectives provide useful building blocks for the future and these also need resources and space. Besides, the larger **i**nterventions are, the more impact they will have on land use and 'functions'. As land use and water management co-developed over time, continuing the same approach has the least impact for at least the decennia to come. Over time, SLR will have increasing impact and other configurations of the water system might become more attractive.

5.2 Major decisions will be complicated decisions

Both the coherence within the water system, and the coherence between the water system and land use and functions, ask for a comprehensive approach to future decisions. Strategies for flood risk management can't be seen separately from those for fresh water management, and both should serve a safe, pleasant and sustainable environment and a thriving economy. Certain decisions do not only have large regional consequences for land use and functions, but influence large parts of the main water system, and therefore (land use and functions in) other regions or even the country as a whole. As positive and negative effects vary between regions and functions, obtaining sufficient political and societal support will be complex.

A first reflection on the difficulty of decision-making in regard to SLR pointed out the importance of 'unknown unknowns'. If decisions are only taken when there is certainty, they will never be taken. Moreover, if a specific choice or development is presented as a true 'solution', this reduces the flexibility to keep on adapting in the future. An alternative approach could be *enlarging* the scope of decisions, this may lead to a larger solution space and a different balance of positive and negative effects (van der Steen et al., 2025). Still, coherence within the water system should always been taken into account.

5.3 There seems to be time, but..

Renovation and replacement of 'dominant' flood risk infrastructure, such as storm surge barriers, will lead to natural decision moments for future strategies. As these aren't expected the next decades, there seems to be sufficient time for a step-by-step approach. However, should 'sedimentation' be used as a building block in order to raise land in the estuaries, then this strategy should be implemented in time to be effective. Moreover, the availability of fresh water will become an issue earlier than flood protection. Any measures that could be implemented in the main water system should be seen in a broader perspective. In the end other developments, like the energy transition and housing, may lead to earlier decision-making. This could either accelerate decision-making for flood protection or limit future possibilities.

Adaptation itself takes time, too. Necessary knowledge should be collected, difficult decisions taken and measures implemented (Haasnoot and Diermanse, 2022). Moreover, changes in the water system may require additional adaptation or mitigation measures. Replacing a storm surge barrier by a dam for example, will heavily impact shipping and harbour activities. Therefore additional time or early decisions may be needed. In any case, timely preparation is essential. At the same time, it is economically costly to replace either structure or strategy much earlier than necessary. Balance is needed.

5.4 Structured knowledge development

In order to address the subject of SLR, a 'knowledge programme' in a policy context has been organised; a new approach for the Netherlands. Although a formal evaluation hasn't been performed yet, we would like to point out some specific aspects.

First of all, the comprehensive approach, with different tracks focussing on different aspects, worked well in itself. However, the flexibility to adapt the programme when necessary was just as important. During the programme, it appeared to be easier to attend to certain parts of the initial plan in a later phase, such as the operationalisation of 'early warning signals'. The co-creating process around different conceptual perspectives developed during the programme, and the extra perspective Grow was added because information on the potential of nature based measures was lacking.

Reporting the developed knowledge separately from the associated policy discussion, keeping the reports as objective as possible, seems to work well. In general results are being embraced. At the same time, the orientation of the studies towards policy issues is very useful. The results provide important information for the (regular) updating of the current strategies for water management in the Netherlands. Although time span addressed is beyond the lifetime of the waterworks, the results also provide a certain comfort to continue investing in the current system and endorse its importance for the future.

SLR in the order of two to five metres will have a major impact and adapting to it will in any case require enormous efforts. There are no easy solutions. The developed knowledge provides a good start for discussions about the future, but it isn't fit for decision-making yet. More insights are needed, but uncertainty will remain and decisions should be taken in time. In any case, the current approach is viable and can be used as a solid basis for future choices.

6 ACKNOWLEDGEMENTS AND STATEMENT ON THE USE OF ARTIFICIAL INTELLIGENCE

A special thanks to all the people and parties that contributed to regional and co-creating meetings.

Artificial Intelligence has been applied to summarize and translate pre-existing (internal) documents. The resulting parts of the manuscript have been reviewed and proof edited by the authors.

REFERENCES

Brand, E., Ramaekers, G., & Lodder, Q. (2022). *Dutch experience with sand nourishments for dynamic coastline conservation – An operational overview. Ocean & Coastal Management, 217*, Article 106008. https://doi.org/10.1016/j.ocecoaman.2021.106008 [research.tudelft.nl]

Brand, E., Lodder, Q. J., Quataert, E., & Slinger, J. (2025). Sustainable coastline management – the cumulative effects of 30 years of nourishments in the Netherlands. Ocean & Coastal Management, 270, Article 107895. https://doi.org/10.1016/j.ocecoaman.2025.107895

DeConto, R.M. and D. Pollard, 2016: Contribution of Antarctica to past and future sea-level rise. Nature, 531(7596), 591–597, doi: 10.1038/nature17145.

Friocourt, Y., Blaas, M., Bonte, M., Vos, R., Slomp, R., Wilmink, R., Lodder, Q., Brakenhoff, L., & van Gool, S. (2025). The Impact of Extreme Sea Level Rise on the National Strategies for Flood Protection and Freshwater in the Netherlands. *Water*, *17*(7), 919. https://doi.org/10.3390/w17070919

Haasnoot, M., Bouwer, L., Diermanse, F., Kwadijk, J., van der Spek, A., Oude Essink, G., Delsman, J., Weiler, O., Mens, M., ter Maat, J., Huismans, Y., Sloff, K., Mosselman, E. (2018). Mogelijke gevolgen van versnelde zeespiegelstijging voor het Deltaprogramma. Een verkenning. Deltares rapport 11202230-005-0002.

Haasnoot, M, Diermanse, F., Kwadijk, J., de Winter R., Winter, G. (2019). Strategieën voor adaptatie aan hoge en versnelde zeespiegelstijging. Een verkenning. Deltares rapport 11203724-004

Haasnoot, M, Diermanse F. (ed.) (2022) Analyse van bouwstenen en adaptatiepaden voor aanpassen aan zeespiegelstijging in Nederland. Deltares 11208062-005-BGS-0001

IPCC (2023). Climate Change 2023: Synthesis Report. Contribution of Working Groups I, II and III to the Sixth Assessment Report of the Intergovernmental Panel on Climate Change [Core Writing Team, H. Lee and J. Romero (eds.)]. IPCC, Geneva, Switzerland, pp. 35-115, doi: 10.59327/IPCC/AR6-9789291691647.

KNMI (2023). National Climate Scenarios 2023 for the Netherlands, scientific report. KNMI WR-23-02

Kolen, B. (2025). Economic Implications for Accommodate, Retreat, Protect and More in Case of Sea Level Rise for the Dutch Delta. *Water*, *17*(24), 3486. https://doi.org/10.3390/w17243486

Lodder, Q., & Slinger, J. (2022). The 'Research for Policy' cycle in Dutch coastal flood risk management: The Coastal Genesis 2 research programme. Ocean and Coastal Management, 219, Article 106066. https://doi.org/10.1016/j.ocecoaman.2022.106066

Ministry of Infrastructure and Water Management (2023, translation 2024) How Can The Netherlands Cope with Sea-Level Rise? Interim Report of the Knowledge Programme on Sea-Level Rise. Available online: **https://www.deltaprogramma.nl/documenten/publicaties/2024/08/06/interim-report-for-the-sea-level-rise-knowledge-programme.**

Ministry of Infrastructure and Water Management (2024): Room for sea level rise; An exploration of conceptual perspectives to keep the Netherlands safe and liveable in the long term as sea levels rise Available online: https://english.deltaprogramma.nl/documents/2024/06/13/room-for-sea-level-rise

Planbureau voor de Leefomgeving (2007). Zeespiegelstijging in IPCC rapport - Betekenis voor Nederland, productnummer 91941

van Alphen, J., van der Biezen, S., Bouw, M., Hekman, A., Kolen, B., Steijn, R., & Zanting, H. A. (2025). Room for Sea-Level Rise: Conceptual Perspectives to Keep The Netherlands Safe and Livable in the Long Term as Sea Level Rises. *Water*, *17*(3), 437. https://doi.org/10.3390/w17030437

van der Steen, M., Toonen, T., Hill, R., Scherpenisse, J. (2025). Volgens het boekje; een bestuurskundige verkenning van langetermijnstrategie voor zeespiegelstijging. ISBN 978-90-83475-49-3

Websites:

Web1: Aanpak van het Kennisprogramma Zeespiegelstijging | Deltaprogramma , under 3

Chapter 4 - Flood resilience, adaptation, and recovery

4.2 Adaptation strategies under increasing flood risk

ICFM 10
Adapting to Global Change:
Innovative Approaches to Flood Management and Resilience
May 20-22, 2026 | Western University, London, Ontario, Canada

Flood Management Strategies in Hong Kong: Addressing Climate Change through Progressive Adaptive Approach combining with Adaptation, Resilience, and Management (ARM)

K. W. Yuen[1], C. M. Lee[1], M. Y. Ng[1], Y. F. Wu[2], J. Lai Ng[2] and T. H. Chiu[2]
Land Drainage Division, Drainage Services Department, HKSAR, China[1]
E-mail: cmlee@dsd.gov.hk

AECOM Asia Co. Ltd, 9/F, Tower 2, Grand Central Plaza
138 Shatin Rural Committee Road
Shatin, HKSAR, China[2]
E-mail: alex.yf.wu@aecom.com

ABSTRACT

This paper presents a case study on development of a comprehensive flood management strategy for Hong Kong, a highly urbanized and densely populated megacity. It examines the challenges, investigations, and outcomes associated with establishing strategy to improve flood resilience of the city under climate change.

Hong Kong, located in a subtropical climate with an average annual rainfall of 2,400 mm, faces increasing flood risks due to extreme rainfall, rising sea levels, and storm surges exacerbated by climate change. To address these issues, Drainage Services Department of the Government of the Hong Kong Special Administrative Region of the People's Republic of China commissioned AECOM Asia Co. Ltd to conduct the Strategic Planning Study on Flood Management against Sea Level Rise and Extreme Rainfall (the Study).

Hong Kong has made significant investments in drainage infrastructure. However, under threat of climate change, it might no longer be practical to invest unlimited resources in providing massive drainage infrastructure to withstand very extreme event. Drawing references from international practices, a paradigm shift from focusing on structural measures to striving for a balance mix of structural and non-structural measures is promoted. An Integrated Flood Management Strategy that incorporates Adaptation, Resilience, and Management (ARM) is recommended to address the flood risks associated with climate change.

To address the uncertainties for development of climate change in future, the Study also promotes a Progressive Adaptive Approach which involves progressively enhancing drainage infrastructure with continuous monitoring of the climate change trend for long term planning. This approach helps avoid premature implementation of extensive infrastructure, thus preventing unnecessary construction and operation cost, while ensuring that decision-makers can respond effectively to evolving climate conditions. Together with ARM, the government is committed to protecting public safety while ensuring long-term sustainability.

KEYWORDS: Hong Kong, Climate change, Integrated Flood Management Strategy, Progressive Adaptive Approach, Extreme rainfall, Sea level rise.

1 INTRODUCTION

Hong Kong is one of the most densely populated coastal cities in the world, with over 7.5 million inhabitants occupying about 25 % of its 1,115 km² land area. Urban areas are highly concentrated along coastal areas or close to the steep hillsides. Hong Kong's subtropical climate delivers an average annual rainfall of approximate 2,400 mm, one of the highest in East and Southeast Asia. Rainfall distribution is uneven, with about 80 % concentrated between May and September (Web-1). The city also lies in the regular path of tropical cyclones, making it vulnerable to both intense rainstorms and storm surges brought by tropical cyclones. In recent years, Hong Kong experienced extreme weather events including series of extreme rainstorms necessitated issue of 4 Black Rainstorm Warnings in August 2025, record-breaking rainstorm on 7–8 September 2023 (with hourly rainfall of 158 mm registered at the Hong Kong Observatory Headquarters), Super Typhoons Ragasa (2025) and Mangkhut (2018) resulting significant storm surge along Victoria Harbour.

Global climate is expected to continue changing in the future. The Intergovernmental Panel on Climate Change (IPCC) has identified several critical impacts of climate change that directly affect urban drainage systems worldwide. According to the IPCC (2021), rising global temperatures intensify the hydrological cycle, which results in more frequent and intense precipitation events. This increase in rainfall can overwhelm existing drainage infrastructure, especially in densely populated, low-lying urban areas and coastal cities. Drainage systems, traditionally designed based on historical weather patterns, may be insufficient in coping with these new extremes. Consequently, cities are facing increased flooding risks and infrastructure strain.

2 CHALLENGES

Hong Kong's steep terrain, high urban density (as shown in Figure 1), and extensive impervious surfaces cause rapid runoff convergence into downstream drainage system, resulting in frequent flash floods. Low-lying coastal areas are simultaneously threatened by storm surges during passage of tropical cyclones and potential high astronomical tides. Sea level exceeding drainage outlets, can create backwater effects, which may result in inland flooding. Climate change exacerbates both threats through higher rainfall intensity and accelerating sea-level rise.

Figure 1: Steep terrain and dense urban setting of Hong Kong (DSD and AECOM, 2025)

Traditional urban flood management in Hong Kong has long relied on constructing large-scale drainage infrastructure to mitigate flood risks. However, with the increasing frequency and intensity of extreme weather events driven by climate change, the adequacy of this approach has come under scrutiny. A central debate has emerged over whether it is justifiable—or even feasible—to continuously invest

unlimited resources to reinforce infrastructural capacity against increasingly extreme yet relatively rare events. Moreover, even the most robust designs have inherent limitations and may be exceeded by unforeseen events such as blockages of drains caused by leaves, debris, or waste, which can severely compromise system performance during critical moments.

Furthermore, the construction of large-scale drainage infrastructure is constrained by factors such as limited land availability and complex site conditions common in dense urban environments. In a compact city like Hong Kong, the public is cautious about allocating valuable space primarily for infrastructure intended to address future climate risks that may not yet be imminent. Instead, there is growing preference to use such land for purposes that deliver immediate social or economic benefits. These challenges highlight the need to move beyond purely structural measures toward an adaptive, resilient, and space-efficient approach to flood risk management.

3 INTEGRATED FLOOD MANAGEMENT STRATEGY

With reference to the Integrated Flood Management Concept Paper (the Concept Paper) by World Meteorological Organization and Associated Programme on Flood Management, it highlighted that *"flood management policy had already shifted in various places towards an approach beyond the myth of "absolute safety from flooding" towards a more flexible and adaptive approach of "living with flood risk". Such an approach recognizes the value of flood protection measures, yet also recognizes such residual risks as levee failure. Flood management needs to provide strategies for such eventualities, further strengthening the need for a balanced combination of structural and non-structural approaches."* (World Meteorological Organization. 2009)

A desktop review of global practices in tackling flood risks was conducted under the Study. It revealed that most cities adopt a combination of engineering infrastructure, sustainable drainage systems, floodproofing barriers, emergency preparedness, land use planning, etc, to handle flood risks. Although the extent and implementation details vary across locations, these measures share similar objectives and underlying principles in flood risk management. Drawing references from the Concept Paper and international practices, a paradigm shift from focusing on structural measures to striving for a balance mix of structural and non-structural measures in Hong Kong is promoted. An Integrated Flood Management Strategy that incorporates ARM is recommended to address the flood risks associated with climate change.

3.1 Adaptation

"Adaptation" was defined to suit the local context in Hong Kong. It refers to implementing various drainage improvement works such as constructing drainage tunnels, stormwater storage schemes, widening rivers, etc to enhance the drainage capacity of the drainage systems and hence reduce the flood risks. Given the high rainfall intensity experienced in Hong Kong, continued implementation of drainage infrastructure remains crucial, as extreme rain events are likely to exceed the capacity of other measures such as sustainable drainage systems. Tailored to the steep terrain of Hong Kong, a three-pronged flood prevention approach as illustrated in Figure 2 has been adopted in implementing drainage improvement works to reduce flood risks in various districts:

- Upstream - Interception
  Building drainage tunnels to intercept stormwater from the mid-levels and discharge it directly into the sea or to other channels.
- Midstream - Storage
  Building stormwater storage tanks in the mid-stream for temporary stormwater storage to attenuate the peak runoff and relieve the discharge load of the downstream drainage system.
- Downstream – Drainage Improvement

Carrying out river training works or build new drainage channels and drains to upgrade the capacity of drainage system.

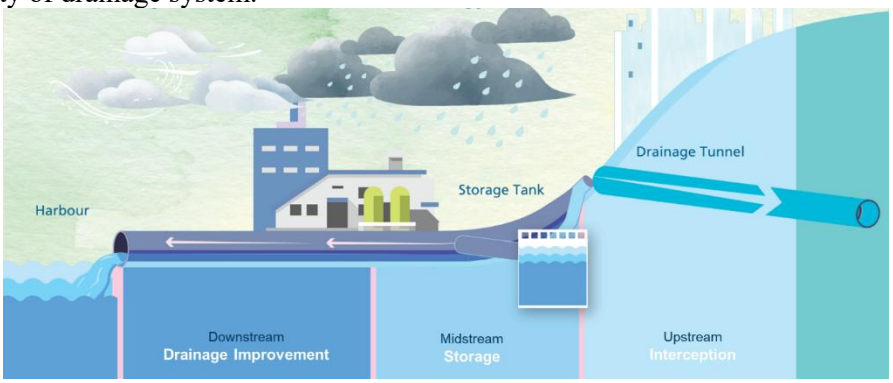

Figure 2: Three-pronged flood prevention approach (DSD and AECOM, 2025)

To effectively adapt to rising sea levels, measures such as smart penstocks/flap valves at drainage outlets to protect low-lying areas against backflow of seawater, barrage schemes at river channels to prevent seawater inundation due to high sea level and pumping systems for floodwater displacement would also be considered depending on the size and characteristic of the catchment to be protected. These measures are essential for safeguarding urban areas against the long-term threats of sea-level rise.

So far, as shown by DSD and AECOM (2025) key drainage infrastructures including four drainage tunnels with a total length of more than 20 km, five underground stormwater storage tanks with a combined capacity of approximately 250,000 m³, equivalent to 100 standard swimming pools, over 2,400 km stormwater drains and over 370 km engineered channels were built to protect the city from flooding. Meanwhile, 15 drainage improvement projects including 9 stormwater storage schemes (with a total capacity of 320,000 m³) and a barrage scheme are under construction in Hong Kong (Development Bureau et al., 2025).

3.1.1 Progressive Adaptive Approach

To address the uncertainties surrounding future climate change development and to align with the public expectations for more efficient use of resources in infrastructure implementation amid the evolving challenges, the Study advocates a Progressive Adaptive Approach. This approach, similar to the 'adaptive pathways' adopted in the United Kingdom, involves progressively enhancing drainage infrastructure with continuous monitoring of the climate change trend for long term planning as shown in Figure 3.

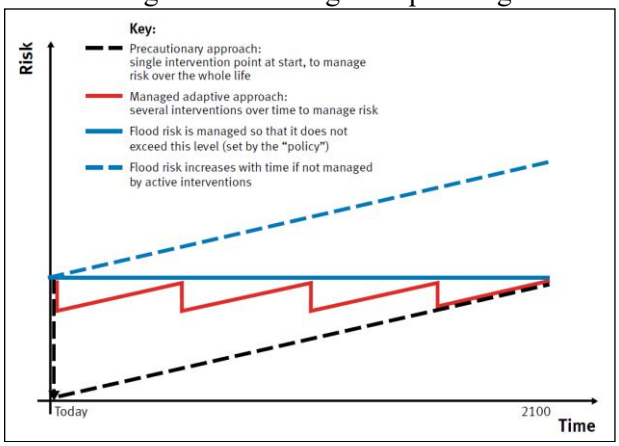

Figure 3: Managing flood risk through the century using the TE2100 managed adaptive approach (Environments Agency, 2012)

With reference to the Figure 3 from Thames Estuary 2100 (TE2100) Plan by the Environment Agency (2012), when compared to the precautionary approach, which relies on a single intervention at the start to manage risk throughout the entire life cycle, the managed adaptive approach—similar to the Progressive Adaptive Approach—involves multiple interventions implemented over time to continuously manage and adjust to evolving risks.

As the pathway of climate change development depends on global commitments toward carbon neutrality, Progressive Adaptive Approach provides flexibility to accommodate evolving needs over time. It enables drainage system to be designed, implemented, and adjusted progressively in response to changing climatic, technological, and societal conditions. At the same time, it would help avoiding the premature implementation of extensive drainage infrastructure, thus preventing unnecessary construction, operation and maintenance costs. Meanwhile, it would ensure the decision maker to plan ahead following the latest climate change development.

According to the climate change projections in various time horizons and greenhouse gas emissions scenarios for Hong Kong based on the "Sixth Assessment Report" (AR6) published by the IPCC (2021) and other related studies, the difference in the climate change impacts for Hong Kong between the intermediate and very high greenhouse gas emissions scenarios at mid-century is insignificant. Depending on the effectiveness of decarbonisation efforts by various nations, there are considerable uncertainties in the climate change impacts at the end of the century. The difference between intermediate and very high greenhouse gas emissions scenarios is more prominent. Table 1 (Web-2 and Web-3) below refers.

Table 1 Climate Change Projections in Hong Kong

	Rainfall Increase		**Mean Sea Level Rise (m)**	
	Intermediate Greenhouse Gas Emissions Scenario (SSP2-4.5)	Very High Greenhouse Gas Emissions Scenario (SSP5-8.5)	Intermediate Greenhouse Gas Emissions Scenario (SSP2-4.5)	Very High Greenhouse Gas Emissions Scenario (SSP5-8.5)
Mid 21st century	11.1%	10.6%	0.20	0.23
End of 21st century	16.0%	28.1%	0.47	0.64

Notes: The projections are relative to the average of 1995-2014. Median projection values are adopted for mean sea level rise and mean projection values are adopted for rainfall increase. Mid 21st century refers to years 2041 – 2060 and end of 21st century refers to years 2081 – 2100.

According to the Emissions Gap Report 2025 (United Nations Environment Programme, 2025), the latest trend of climate change is more likely to follow the intermediate greenhouse gas emissions scenario. For the scenario of Unconditional Nationally Determined Contributions, global temperature will increase below 2.5 ℃ with about a 66% chance and below 2.9℃ with about a 90% chance by 2100, which falls within the intermediate greenhouse gas emissions scenario (SSP2-4.5) with best estimate of 2.7℃ and very likely range from 2.1℃ - 3.5℃ by end of 21st century from IPCC AR6 (IPCC, 2021). Intermediate greenhouse gas emissions scenario at mid-century was taken as the design basis, where practically feasible, design provisions shall be included to enable timely upgrade of infrastructure in the future as needed, up to the climate change effects under the very high greenhouse gas emissions scenarios at the end of the century. As there exist considerable uncertainties in the impacts of climate change near the end of the century, the Progress Adaptive Approach provides sufficient flexibility and adaptability so that we can have sufficient time to develop effective and cost-efficient measures according to the actual situation.

An illustrative example of the application of Progressive Adaptive Approach is shown in Figure 4 below. For an area prone to potential flood risk under the current situation, the underground space beneath the recreational area can facilitate the "Single Site, Multiple Use" initiative to implement measures to

mitigate possible flood risks up to mid-century. In the short and medium-term (up to mid-century), a stormwater storage scheme can be constructed underneath the recreational area, with space reserved for future expansion of the stormwater storage tank where practically feasible based on the anticipated climate scenario by the end of the century.

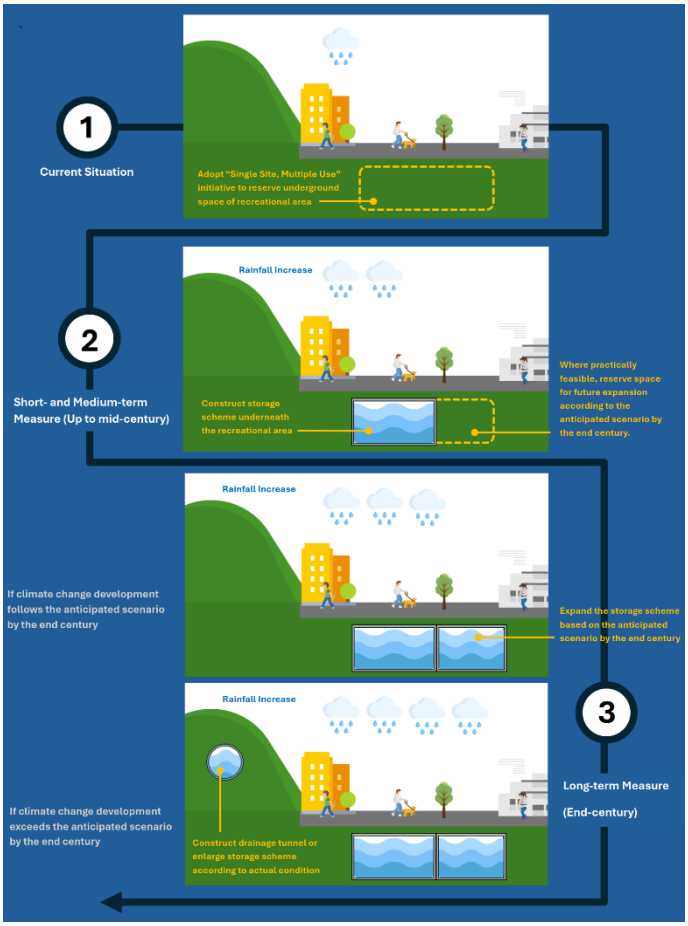

Figure 4: Illustrative Example of Progressive Adaptive Approach (DSD and AECOM, 2025)

The development of climate change will be under close monitoring. If the climate change trend aligns with the anticipated scenario, the remaining reserved space can be utilized to expand the stormwater storage scheme, accommodating the additional flood risk from climate change at the end of the century. If the climate change trend exceeds the anticipated scenario, additional measures such as constructing a drainage tunnel or further enlarging the stormwater storage scheme may be required based on the actual conditions.

3.2 Resilience

"Resilience" was defined to suit the local context in Hong Kong. It refers to adopting temporary or non-structural measures to control flood risks or reduce flooding impact for speedy society recovery. It creates a line of defence to form a buffer zone or limit the extent of flooding. It mainly includes blue-green drainage infrastructure and floodproofing measures.

Blue-green drainage infrastructure resembles other similar concepts, such as the "Sponge City", the "Active, Beautiful, Clean Waters", the "Sustainable Drainage System" and the "Low Impact Development" being adopted in the Mainland China, Singapore, the United Kingdom and the United States respectively. Blue-green drainage infrastructure emphasizes the importance of ecosystems and improvement of water

resources such as water quality, climate regulation and habitat provision, as well as enhancing the city's flood adaptive capacity through promoting infiltration, storage, purification, reuse and discharge. Although blue-green drainage infrastructure alone cannot fully manage extreme rainfall events in Hong Kong, it can effectively handle a portion of the rain load and help reduce pressure on the conventional drainage system. Beyond its hydraulic benefits, it provides multiple co-benefits, including enhanced urban greening, improved environmental quality, and opportunities for land co-use. These features contribute to creating a more liveable cityscape and are widely appreciated and supported by the public.

Blue-green elements including revitalised river channel, bioretention system, green roof, porous paving system and water harvesting are commonly utilized to reduce surface runoff entering into the drainage system under normal rainfall events, hence improving the tolerability of the drainage system and reducing the risk of flooding. Another key blue-green element - floodable area, is used as recreational facility such as basketball courts, sports fields, and green parks during normal days and can be transformed into temporary flood storage facility under extreme rainfall events for benefits of land co-use.

As mentioned previously, even the most robust drainage designs have inherent limitations and may be exceeded under unforeseen extreme events, potentially resulting in flooding. In such cases, floodproofing measures, such as various types of flood barriers, can effectively minimize flood impacts by preventing floodwater intrusion into properties and enabling swift post-event recovery. In addition, when social impacts limit the full adoption of adaptation measures, resilience measures can serve as effective supplements. For instance, high flood walls may obstruct scenic views or reduce public interaction with water bodies. Therefore, a balanced approach integrating adaptation and resilience measures—such as constructing permanent flood walls at balustrade height with demountable barriers installed during extreme weather—may offer effective flood protection while preserving social and aesthetic values.

3.3 Management

"Management" refers to enhancements aimed at improving emergency response/preparedness for flooding through Just-in-time Clearance, adoption of innovative technologies, and effective information dissemination. It also covers updating standards and guidelines for flood management.

The Just-in-time Clearance focuses on addressing blockages in drainage systems caused by leaves, debris, or waste. Upon the issuance of rainstorm warnings by the Hong Kong Observatory, maintenance staff are immediately deployed to inspect drainage spots known to be prone to blockage, ensuring timely clearance and minimizing the risk of localized flooding.

The adoption of innovative technologies is essential for strengthening emergency response against flooding. For instance, installing Flood Monitoring Device along road kerbs at locations prone to blockages enables the collection of real-time water level data, supporting timely clearance operations. The application of artificial intelligence (AI) for real-time flood monitoring further enhances response efficiency by enabling automated detection and continuous assessment of flood severity. The use of "Mosaic Model Map" (M^3), a platform that integrates short-term precipitation and tidal forecasts with hydraulic model simulation results for prediction of flood risk across districts, facilitates advance planning for emergency preparedness. The deployment of powerful pumping robots can significantly strengthen emergency response by efficiently removing floodwater, thereby shortening flood duration and expediting society recovery.

Effective information dissemination on potential flood risk to the public is essential for enhancing preparedness, enabling timely protective actions and minimizing potential losses for the society. With the disclosure of the list of flood-prone areas, which includes Locations Prone to Blockage, Locations with Drainage Improvement Works in Progress and Coastal Low-lying or Windy Areas, the public are informed with areas with potential flood risks. In addition, water level sensors have been deployed along major rivers

in Hong Kong to support digital transformation. Allowing public access to real-time water level information via a dedicated website can alert the community on potential flooding areas and make informed preparations, thereby facilitating safer travel and enhancing overall transparency of information.

Updating standards and guidelines for flood management is essential to adapt to climate change, incorporate new technologies, and reflect current best practices. As flooding events become more frequent and severe, revised standards ensure that flood management strategies remain effective and efficient. They enhance community resilience by integrating flood preparedness into urban planning, promote regulatory compliance, and improve coordination among stakeholders.

4 STRATEGIC APPLICATION OF ADAPTATION, RESILIENCE AND MANAGEMENT MEASURES FOR FLOOD EVENTS

In flood management, determining when to adopt structural (adaptation) measures versus non-structural (resilience and management) strategies depends largely on the predictability and characteristics of the flooding event. In Hong Kong, flooding can result from either extreme rainfall or during passage of tropical cyclones. Extreme rainfall events are highly unpredictable under current technology, offering very limited lead time for preparation. Consequently, structural measures are crucial to mitigate flooding impacts, particularly under normal societal operations when daily activities continue. In contrast, tropical cyclones related flooding is generally more predictable, with higher forecasting confidence and longer lead times for advance preparation. In addition, Hong Kong's established emergency mechanism—where the hoisting of Typhoon Signal No. 8 or above suspends schools and most work activities—ensures the majority of the population remains safely at home. Under such conditions, non-structural measures have greater room for effective implementation, as advance planning is essential to maximize their operational efficiency. Therefore, while adaptation measures play a vital role in responding to sudden extreme rainfall, resilience and management approaches are better suited to manage typhoon-induced flooding, where early warnings and organized societal responses can be leveraged to minimize risks and enhance overall preparedness.

5 CONCLUSION

Hong Kong faces intensifying flood risks from climate-driven extreme rainfall and sea-level rise. The Study provides a robust response through two interconnected frameworks: the Progressive Adaptive Approach, which phases investment according to evolving climate projections, and an Integrated Flood Management Strategy built on ARM pillars.

By combining flexible structural upgrades with enhanced resilience and management measures, Hong Kong can protect lives, critical infrastructure, and economic activity while optimising public resources. Continuous monitoring, periodic review aligned with IPCC assessment cycles, and active stakeholder collaboration will ensure the strategy remains effective against an uncertain climate future.

REFERENCES

Development Bureau, Civil Engineering and Development Department and Drainage Services Department (2025). Legislative Council Panel on Development, Long-term Flood and Shoreline Management Integrated Strategies to Cope with Climate Change, pp. 2

DSD and AECOM (2025). Executive Summary. Strategic Planning Study on Flood Management Against Sea Level Rise and Extreme Rainfall – Feasibility Study, pp. 4-8, 13-16

Environment Agency (2012). Thames Estuary 2100 Plan. Managing flood risk through London and the Thames estuary. Environment Agency, London, UK, pp.34-35

IPCC (2021). Climate Change 2021: The Physical Science Basis. Contribution of Working Group I to the Sixth Assessment Report of the Intergovernmental Panel on Climate Change, pp. 14, 233, 1557-1567

United Nations Environment Programme (2025). Emissions Gap Report 2025: Off Target – Continued collective inaction, Nairobi, Kenya, pp. 38

World Meteorological Organization (2009). Integrated Flood Management Concept Paper. WMO-No. 1047, World Meteorological Organization, Geneva, Switzerland, pp. 13

Web sites:

Web-1: https://worldweather.wmo.int/en/city.html?cityId=1, consulted 19 November 2025.

Web-2: https://www.hko.gov.hk/en/climate_change/proj_hk_msl_med_conf_info.htm, consulted 29 December 2025.

Web-3: https://www.hko.gov.hk/en/climate_change/proj_hk_rainfall_rx1day_info.htm, consulted 29 December 2025.

ICFM 10
Adapting to Global Change:
Innovative Approaches to Flood Management and Resilience
May 20-22, 2026 | Western University, London, Ontario, Canada

Resilient City-Oriented Flood Control and Waterlogging Prevention Planning for the Beijing Municipal Administrative Center

Zhengyao Fu[1]
Beijing Municipal Institute of City Planning and Design, Beijing, 101117, China[1]
E-mail: Fuzhengyao@foxmail.com

ABSTRACT

Against the backdrop of the Beijing Municipal Administrative Center (BMAC) undertaking the historic mission of relieving non-capital functions and advancing high-quality development, this study addresses the prominent challenges of flood control and waterlogging prevention in the BMAC, including the natural vulnerability of "the lower reaches of nine rivers", the mismatch between low-standard existing drainage systems and high-standard construction requirements in the new era, and the transition from human-water alienation to city-water integration. Based on the goal of building a millennium city with integrated water and city, resilient safety, and sponge city features, this paper proposes five core strategies: establishing the "Tongzhou Weir" flood control system with the concept of "upper storage, middle diversion, and lower drainage", creating ecological and water-friendly riverside spaces, implementing zone-specific waterlogging prevention measures, integrating green and gray infrastructure to upgrade pipe and river networks, and advancing sponge city construction to enhance rainwater control and utilization. Furthermore, four recommendations for overall coordination are put forward: improving the coordination of flood and waterlogging encounter scenarios, strengthening urban space planning coordination, enhancing the connection between new and existing infrastructure, and improving emergency management coordination. This research provides a systematic planning framework for the BMAC to achieve the 100-year flood control standard and high-standard waterlogging prevention capacity, and offers a valuable reference for the construction of flood safety patterns in other similar cities under the new development philosophy. Keywords: Beijing Municipal Administrative Center (BMAC); flood control and waterlogging prevention; planning strategy; resilient city; sponge city; water-city integration

KEYWORDS: Beijing Municipal Administrative Center (BMAC); flood control and waterlogging prevention; water-city integration; resilient city; sponge city

1 INTRODUCTION

As one of the two core pillars of Beijing's planning and development in the new era, the Beijing Municipal Administrative Center (BMAC) is a landmark project of historic significance. It is tasked with relieving Beijing of non-capital functions and advancing the coordinated development of the Beijing-Tianjin-Hebei (BTH) region, representing a century-long endeavor and a millennium-scale initiative. In recent years, the BMAC has undergone rapid construction and development in line with the overall urban layout of "one core, one sub-center, two axes, and multiple nodes" outlined in the Beijing Master Plan (2016–2035). Since the relocation of municipal organs and enterprises kicked off in 2019, the center is projected to accommodate 400,000 to 500,000 permanent residents relocating from the central urban area by 2035 (People's Government of Beijing Municipality, 2017). However, the original Tongzhou New Town, which undertakes this historic mission, is endowed with unfavorable natural conditions. Its hydrological and geographical setting renders it highly susceptible to both external flooding and internal waterlogging. Meanwhile, the existing urban municipal infrastructure, though still inadequate, must be upgraded expeditiously to meet world-class standards. Therefore, adhering to the strategic orientation of

high-quality development, establishing a benchmark for people-centered projects in the capital in the new era, and safeguarding flood safety in the BMAC are critical initiatives pivotal to national welfare and people's livelihood.

This paper elaborates on the problems and challenges encountered in constructing the flood control and waterlogging prevention framework of the BMAC, summarizes key planning strategies and priorities, and puts forward insights and recommendations. It aims to fully leverage the exemplary role of the BMAC's planning and construction, thereby providing a reference for gradually shaping a new paradigm of high-quality urban development under the new era and new development philosophy.

2 CURRENT SITUATION AND CHALLENGES

The BMAC is situated in the northern part of Tongzhou District, Beijing, covering an administrative area of roughly 155 square kilometers. It lies in the alluvial plain of the Yongding and Chaobai Rivers, boasting a warm temperate continental semi-humid monsoon climate. The multi-year average rainfall stands at 541.3 mm (1956 – 2015), with precipitation hitting 775.6 mm in 2021 (Compilation Committee of Tongzhou District Local Chronicles, 2023). Pursuant to the Beijing Master Plan (2016 – 2035), the original Tongzhou New Town was redesignated as the BMAC, which mandates high-standard planning and construction to exemplify and facilitate the alleviation of non-capital functions. By 2035, it is anticipated to initially evolve into an internationally renowned, harmonious, livable, and modern urban area. In December 2018, the CPC Central Committee and the State Council, in their approval of the Regulatory Detailed Plan for the Beijing Municipal Administrative Center (2016 – 2035), required the construction of a green, forested, sponge, smart, humanistic, and livable city, positioning the BMAC as a new landmark of the capital. To further implement urban planning arrangements, constructing a robust flood control and waterlogging prevention safety framework for the BMAC confronts three major challenges.

2.1 The Natural Context of "the Lower Reaches of Nine Rivers" and the Assurance of 100-Year Flood Control Safety

The BMAC is a confluence of numerous rivers, historically known as "the lower reaches of nine rivers". It encompasses 24 rivers, including the North Canal, Wenyu River, Xiaozhong River, Yunchao Flood Diversion River, Tonghui River, Liangshui River, and Yudai River, with a total length of around 106 kilometers and a total water area of approximately 1,850 hectares. All these water bodies fall under the Chaobai River and North Canal systems within the Haihe River Basin. The BMAC has a long history of frequent flood disasters, which have inflicted heavy losses on people's lives and property. Statistical data on flood disasters over 255 years (from 1736, the first year of the Qianlong reign, to 1990) indicate that years with moderate to severe waterlogging account for roughly 20%. After the founding of the People's Republic of China, flood disasters were mainly concentrated in the 1950s. Since 1958, the construction of water conservancy projects in the upper reaches, such as the Huairou Reservoir and Miyun Reservoir, coupled with the reinforcement of dikes, dredging of rivers, and excavation of artificial flood diversion channels, has significantly enhanced flood detention and discharge capacity, thus minimizing the occurrence of major flood disasters in recent decades.

The BMAC is located in the lower reaches of the main streams of the Wenyu River and North Canal. The main stream of the North Canal assumes the responsibility of draining rainwater from Beijing's central urban area and multiple districts along its course. In recent years, rapid urbanization has brought about significant changes in the basin's underlying surface and an increase in the surface runoff coefficient, leading to greater runoff generation and accelerated confluence. This has intensified the flood control pressure on the main streams of the Wenyu River and North Canal. Rough calculations reveal that the peak flood discharge of different frequencies in the current Lingoukou – Beiguan Barrage section of the Wenyu River main stream has increased by 25% to 48% compared with the original design (Beijing

Municipal Institute of City Planning and Design, 2018). Meanwhile, the accelerated construction of the BMAC has driven the continuous expansion of urban planned construction land (according to the Tongzhou New Town Plan (2005–2020), the planned urban construction land area was 86 square kilometers; according to the Regulatory Detailed Plan for the Beijing Municipal Administrative Center (2016–2035), the construction land scale of the center is controlled at approximately 110 square kilometers) (People's Government of Beijing Municipality, 2018). Some original farmland drainage ditches have been converted into urban drainage rivers or rainwater pipelines, reducing natural water storage and infiltration space. Consequently, this has caused regional drainage difficulties and underscored the risks of external flooding and internal waterlogging.

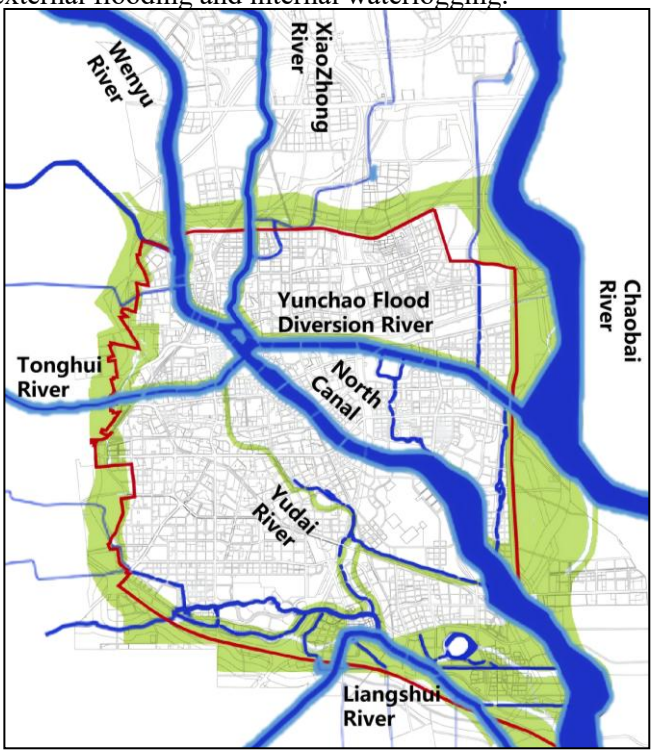

Figure 1: River system of Beijing Municipal Administrative Center

2.2 The Existing Low-Standard Drainage System and the Construction of a High-Standard Waterlogging Prevention System in the New Era

According to statistics as of 2016, the BMAC houses approximately 58 existing rainwater pipeline systems, with a total length of about 173 kilometers and pipe diameters ranging from Φ300 mm to □ 4000×2600 mm. A dynamic coupled model integrating pipelines, river networks, and two-dimensional ground surfaces was established using Mike software for evaluation, and InfoWorks software was employed for simulation comparison and verification. The results indicate that roughly 113 kilometers (67%) of the existing rainwater pipelines in the BMAC have a design standard lower than a 1-year recurrence interval, and about 37 kilometers (22%) have a standard lower than a 2-year recurrence interval. Analysis of pipe network survey data reveals that most existing rainwater pipelines and canals were constructed decades ago, and their design standards are no longer compatible with current requirements.

In addition to its dense river network, the BMAC has constructed numerous large-scale transportation facilities in tandem with urban development, which have altered the natural rainwater drainage basins. These facilities mainly include the Beijing-Qinhuangdao Railway, Beijing-Chengde

Railway, and Tongsan Railway, as well as the Beijing-Tianjin Expressway, Tongyan Expressway, East Sixth Ring Road, and Beijing-Harbin Expressway. Their intersections with other urban roads have formed concave overpasses. As of 2016, there were 20 existing rainwater pumping stations at these concave bridges, most of which have a low design standard of 5 to 10-year recurrence intervals. In the event of heavy rainfall, these stations are prone to malfunction, resulting in road traffic disruptions.

2.3 The Past of Human-Water Alienation and the Future of City-Water Integration

The BMAC is characterized by a low-lying and flat natural terrain, slightly higher in the northwest and lower in the southeast, with a ground elevation ranging from 28.5 meters to 14.3 meters and an average terrain slope of approximately 0.955%. The North Canal runs through the BMAC from northwest to southeast and assumes the primary responsibility for flood control and waterlogging prevention. Its planned water level for a 50-year recurrence interval is roughly 21.8 meters to 18.57 meters, and for a 100-year recurrence interval, it is about 21.9 meters to 18.90 meters. Therefore, under the dual impacts of backwater from high external flood levels and the low-lying, waterlogging-prone terrain, rational vertical zoning and control of the BMAC are of utmost importance. Due to insufficient attention to urban vertical planning in the early construction stages, the ground elevation and slope direction of some existing roads and residential communities are improperly designed, leading to water accumulation and internal waterlogging during heavy rainfall events. For instance, during the "8.8" heavy rainfall event in 2018 (with a maximum hourly rainfall of 78.2 mm), among the 74 waterlogging points, 29 were low-lying communities and 36 were low-lying roads.

There are still 78 kilometers of substandard dikes along the main rivers in the BMAC, such as the North Canal, Chaobai River, and Wenyu River. The most prominent issue is the absence of dikes on the left bank of the North Canal. The 100-year flood level of this section is higher than the elevation of surrounding roads and ground. Currently, the riverbank and beach in this section are occupied by the Canal Square and Olympic Sports Park, making it challenging to implement the original dike construction plan and posing significant flood control safety hazards. Therefore, on the basis of respecting the natural context, current conditions, and the demands of urban residents, it is an important challenge to gradually address the insufficient attention to water safety in the development process, systematically enhance urban flood safety, and transition from human-water alienation to city-water integration.

3 STRATEGIES FOR CONSTRUCTING A FLOOD SAFETY PATTERN

To further implement General Secretary Xi Jinping's important instructions on the planning and construction of the Beijing Municipal Administrative Center (BMAC), comprehensively improve the flood control and waterlogging prevention capacity of the BMAC, ensure the safety of people's lives and property as well as urban operation, and build the BMAC into a millennium city that carries Chinese wisdom, integrates water and city, and is safe and livable, the BMAC has proposed three main strategies and five key points: constructing a flood control pattern integrating water and city, building a resilient and safe waterlogging prevention system, and systematically advancing sponge city construction.

3.1 Intelligent Water Management and Establishment of the "Tongzhou Weir" Series of Flood Control System

In accordance with the concepts of water regulation, water governance, and water-friendly development, and drawing on the ancient wisdom of using "weirs" to divert water, a series of flood control system featuring "upper storage, middle diversion, and lower drainage" has been constructed to reduce flood pressure in the BMAC, effectively detain and store rainwater and floods, and achieve the 100-year flood control standard. Specifically, upper storage involves building 2 new reservoirs and 48 flood storage and detention areas in the upper reaches to store and control mountain floods; middle diversion includes digging the new Wenchao Flood Diversion River and dredging the Yunchao Flood

Diversion River to divert floods to the Chaobai River; lower drainage focuses on renovating key rivers such as the Wenyu River and North Canal to ensure unimpeded drainage; a circular green recreational belt is reserved on the periphery of the BMAC, serving both flood regulation and storage and optimizing the spatial ecological pattern. These measures together form the overall flood control water system pattern of Tongzhou District, characterized by "three horizontal and two vertical lines for external flood defense, multiple points for rainwater and flood storage and detention, one circular belt around the city, and nine rivers integrating harmoniously".

3.2 Creating Dynamic Water-Nurturing and Attractive Water-Friendly Riverside Spaces

Through micro-topography treatment and optimization of construction design, and by adopting a mode of integrating green spaces, buildings and dikes, the 3-kilometer dike-less section of the North Canal, which was previously difficult to construct, will be built into an ecological dike shoreline. This will comprehensively meet the needs of flood control, landscape, and water-friendly activities, forming a demonstration riverside space. The Wenchao Flood Diversion River and its adjacent riverside spaces will be planned and constructed to divert 440 cubic meters per second of floodwater from the Wenyu River under the 100-year flood scenario, ensuring the flood control safety of the BMAC without raising the existing dikes. An open green space at the junction of Shunyi and Tongzhou Districts will be constructed to connect the Wenyu River-Chaobai River ecological corridor, forming a shared, safe, and pleasant riverside space.

3.3 Zone-Specific Measures, Customized Waterlogging Prevention Zoning and Refined Governance Strategies

In line with the high-standard waterlogging prevention requirements of the 50-year to 100-year flood recurrence interval, the BMAC coordinates rivers, lakes, rainwater pipelines, and pumping station system, and delineates hierarchical waterlogging prevention zones integrating storage, drainage, and elevation raising based on local conditions. Under the comprehensive consideration of safety, ecology, water-friendly features, and landscape conditions, zone-specific waterlogging prevention strategies are formulated ("one zone, one policy"), with a focus on ensuring the safety of high-risk areas such as depressed overpasses, existing low-lying communities, and built-up low-lying areas. For urban construction areas with favorable topographical conditions, gravity flow self-drainage or elevation drainage is prioritized; for local low-lying areas, measures such as local external water interception and high-lift pumping stations are appropriately adopted to meet waterlogging prevention requirements; for regional low-lying areas, the final plan is determined by comparing and selecting between the flood storage and drainage scheme using rivers or flood storage areas and the high-lift drainage scheme by constructing regional pumping stations. In accordance with the planning idea of integrating "self-drainage, high-lift drainage, storage-drainage, and elevation drainage", the BMAC plans to construct and reconstruct more than 60 various rainwater storage and drainage facilities, including depressed overpass pumping stations, community rainwater pumping stations, and flood drainage pumping stations.

3.4 Integration of Green and Gray Infrastructure, High-Standard Construction of Pipe Network and River Network Systems, and Scientific Support for Vertical Planning Compilation

It is planned to construct, renovate, and expand 282 kilometers of main rainwater pipelines, raising the recurrence interval to 3 to 10 years. Ecological treatment will be carried out on 17 flood drainage rivers with a total length of approximately 117 kilometers to ensure unimpeded drainage in the lower reaches. Six dual-purpose flood storage and detention areas (for both normal and emergency use) will be built, with a total storage capacity of 2.67 million cubic meters for storing and detaining floodwater in the rainy season and serving as urban public recreational spaces for residents in the dry season. In addition, based on the simulation results of hydrological numerical models, the risk of waterlogging within 50 to 100 years is evaluated, and vertical adjustments are optimized for 23 road sections to mitigate

waterlogging risks. A total of 46 rainwater regulation and storage areas with a total capacity of 26,000 cubic meters will be set up by comprehensively utilizing green spaces, squares, and stadiums.

Figure 2: Jing River of Beijing Municipal Administrative Center

3.5 Implementing Sponge City Construction Requirements and Proposing Planning and Design Key Points for Rainwater Control and Utilization

Adhering to the core concept of sponge cities of "natural storage and natural infiltration", technical guidelines for planning and design are provided for permeable building communities, self-purifying road squares, and rainwater-harvesting green spaces and parks to implement the sponge city concept and promote the planned construction of sponge cities in the BMAC in an orderly manner. Taking the Urban Green Heart as an example, the surface runoff storage mode is widely adopted to replace the traditional rapid drainage mode of rainwater pipelines, giving full play to the role of ecosystems such as buildings, roads, green spaces, and water systems in absorbing, retaining, infiltrating, and slowly releasing rainwater (Fu, Zhang, et al. 2022). Overall, a large storage-type sponge dominated by old canal courses and flood storage areas is constructed, and small permeable sponges dominated by rain gardens, grass swales, and bioretention facilities are created in detail. This will enable 91.7% of rainwater to be absorbed and utilized on-site, with the annual total runoff control rate reaching over 90%.

Figure 3: The Urban Green Heart of Beijing Municipal Administrative Center

4 CONCLUSION AND RECOMMENDATION

Urban flood control and waterlogging prevention systems are important components of municipal infrastructure. With the frequent occurrence of extreme climates, the demand for urban development and construction, and the further upgrading of the resilient city concept in recent years, the importance of urban flood safety has become increasingly prominent. Under the new era and new development philosophy, constructing an urban flood control and waterlogging prevention pattern that ensures the safety of people's lives and property, maintains stable urban operation, improves the water ecological environment, and promotes the improvement of the whole-basin flood control system is of great significance. Drawing on the experience of constructing the flood control and waterlogging prevention pattern in the BMAC, the following four aspects of overall coordination work are recommended:

4.1 Improve Coordination of Flood and Waterlogging Encounter Scenarios

Flood and waterlogging disaster risks often occur simultaneously. The "23 • 7" catastrophic basin-wide flood in the Haihe River Basin caused severe losses in Fangshan, Mentougou and other districts of Beijing, and one of the important reasons was the concurrent occurrence of floods and the superposition of flood peaks. Taking the BMAC as an example, due to the large drainage area of the North Canal and the 50-year flood process that can last for about 3 days, the calculated waterlogging area in the urban area differs by twice under two working conditions: simultaneous rainfall in the entire North Canal basin, and local rainfall superimposed with external flood peaks. Therefore, in areas with low-lying natural terrain and prominent external flood and internal waterlogging problems, special attention should be paid to coordinating the risks brought by the superposition of floods and waterlogging. Special research should be carried out, and refined drainage and waterlogging prevention models should be used to simulate multiple encounter scenarios and operating conditions, so as to scientifically and reasonably determine the encounter conditions of external floods and internal waterlogging, pipeline flow processes, the operating conditions of waterlogging prevention pumping stations and gates, and the relationship with the scale of waterlogging prevention pumping stations.

4.2 Strengthen Coordination of Urban Public Space Planning

With urban development and construction, changes in underlying surface conditions have led to a gradual increase in urban runoff, while the original flood storage space has been continuously reduced. Relying solely on source sponge measures and small rainwater pumping stations is inevitably insufficient to cope with the risks posed by flood and waterlogging. To align urban flood safety with urban development positioning, in the planning stage, it is necessary to reserve "leeway" in urban public space, coordinate the relationship between water area land and construction land, and focus on the reservation and management of flood storage and detention areas; at the design stage, on the premise of ensuring safety, flexible technical means should be adopted to coordinate the landscape effects on and off the banks, creating riverside spaces integrating blue and green areas and combining water and forests; in the construction stage, along with urban construction and renewal, synchronous progress should be made in river dredging and renovation as well as the construction of supporting drainage and waterlogging prevention facilities, proactively plan the construction of major flood control and waterlogging prevention facilities, and dynamically eliminate annual flood season waterlogging points.

4.3 Enhance Coordination of New and Existing Infrastructure Connection

To meet the needs of urban development, the planning and design standards for flood control and waterlogging prevention have been gradually improved. However, the existing built-up areas have low drainage and waterlogging prevention standards, and the construction of new surrounding projects may further exacerbate the waterlogging risk in the existing built-up areas. Therefore, in the process of new project construction and renewal and reconstruction, the regional waterlogging prevention safety should be systematically improved from the perspective of basin-wide comprehensive coordination. Taking the BMAC Comprehensive Transportation Hub as an example, the project plan comprehensively coordinates the drainage and waterlogging prevention planning and design conditions of key projects such as the transportation hub, the Sixth Ring Road High Line Park, and the undergrounding of the Sixth Ring Road Expressway. It has carried out research and impact analysis on multiple system schemes such as pumping station drainage, linear project regulation and storage, and park green space regulation and storage. While meeting the requirements of the above key projects, it has simultaneously solved the historical waterlogging problems of surrounding existing low-lying communities such as Ziyunnanli Community, greatly improving the drainage and waterlogging prevention level of the basin.

4.4 Improve Coordination of Emergency Management

In recent years, disasters caused by extreme climates have become increasingly frequent worldwide. Relying solely on gray infrastructure construction to resist excessive flood threats can no longer meet the city's safety guarantee requirements. Promoting the in-depth integration of resilient city construction with modern urban operation and management has become a key task under the new development philosophy. In July 2022, Beijing took the lead in organizing the compilation and release of the Beijing Urban Waterlogging Risk Distribution Map, which shows the distribution of potential waterlogging risk points to the public and provides corresponding evacuation measures and prevention guidelines. To further refine the support for scientific decision-making by government departments, urban planning units have superimposed important urban elements such as key infrastructure, buildings, transportation, and population on this basis, and compiled the Beijing Central Urban Area and Municipal Administrative Center Waterlogging Risk Impact Analysis Map with "one point, one map". This map is used to quantitatively analyze not only the direct impact of waterlogging but also the indirect impacts on social functions, crowd activities, and transportation. The analysis results will be incorporated into the annual physical examination and evaluation of territorial space planning, providing technical support for implementing the deployment of resilient city construction, promoting the orderly development of urban waterlogging control work, and improving the level of emergency management.

REFERENCES

People's Government of Beijing Municipality. Beijing Master Plan (2016–2035) [Z]. Beijing: People's Government of Beijing Municipality, 2017.

Compilation Committee of Tongzhou District Local Chronicles. Beijing Tongzhou Yearbook 2022 [M]. Beijing: People's Government of Tongzhou District, 2023.

Beijing Municipal Institute of City Planning and Design. Flood Control and Waterlogging Prevention Plan for the Beijing Municipal Administrative Center [R]. Beijing: Beijing Municipal Commission of Planning and Natural Resources, 2019.

People's Government of Beijing Municipality. Regulatory Detailed Plan for the Beijing Municipal Administrative Center (2016–2035) [Z]. Beijing: People's Government of Beijing Municipality, 2018.

Zhengyao Fu, Wenyong Zhang, et al. Practicing the Concept of Ecological Civilization and Creating a Model of Harmonious Coexistence — Exploration and Practice of Municipal Infrastructure Planning for the Urban Green Heart in the Municipal Administrative Center [J]. Beijing: Beijing City Planning & Construction Review, 2022.

ICFM 10
Adapting to Global Change:
Innovative Approaches to Flood Management and Resilience
May 20-22, 2026 | Western University, London, Ontario, Canada

Flood protection based on the concept of differentiated design levels in Hungary

Örs Antal[1] and Anita Mária Süveggyártó[2]
Department of Flood Protection, General Directorate of Water Management, Budapest, 1012, Hungary[1]
E-mail: antal.ors@ovf.hu

Department of Flood Protection, General Directorate of Water Management, Budapest, 1012, Hungary[2]
E-mail: suveggyarto.anita@ovf.hu

ABSTRACT

Hungary is located in Central Europe, within the territory of the Carpathian Basin. Due to its hydrographic and basin-like, lowland characteristics, the country is highly exposed to fluvial flood phenomena.

Extreme meteorological conditions and the continuous deterioration of the water-carrying capacity of riverbeds necessitate the constant increase of design flood levels and the elevation of dikes. However, it is evident that continuously raising the height of dikes is an irrational and unsustainable solution due to infrastructural constraints and financial considerations.

With regard to this paradigm, the concept of differentiated flood protection was elaborated. This approach considers not only hydrological factors when determining the design level of dikes but also takes into account quantifiable factors related to the protected side and flood control response possibilities.

The consequence of risk-based, necessary development of dikes is the efficient use of resources, focusing on the necessary and sufficient reduction of risks, avoiding unjustified developments based on risk, and formulating a strategy that is feasible in medium and long term and whose effectiveness can be verified through risk calculations.

The current design regulations can be considered as rigid, determining the construction level of flood protection dikes based on determined height levels and safety levels derived from hydrological statistics. The developed differentiated methodology and concept aim to change this overly rigid and unviable practice. In summary, this new approach based on the principle of differentiation allows financial resources allocated for dike development to be directed to sections where technical considerations and risk assessments indicate a genuine need. By reallocating these funds, we can achieve a reduction in risk for areas that are truly high risk.

This paper presents the methodological background and practical results of this principle, highlighting the technical aspects applied during the differentiation process.

KEYWORDS: design level, differentiated method, flood risk mitigation, risk analysis, freeboard, dike

1 INTRODUCTION

Flood protection in Hungary is primarily ensured by approximately 4.400 km of flood protection dikes across the country. The current regulation of design framework for the construction of flood protection lines is overly rigid. It is based on hydrological statistical methods that no longer adequately address several factors of growing importance, such as the impacts of climate change, the dynamic

evolution of risk levels or the constraints imposed by cross-river structures (e.g. utilities, bridges, etc.). In the existing design system, the most critical issue is that, as a result of both natural processes and human interventions, design flood levels have increased to such an extent compared to earlier levels that upgrading the flood protection system to the prescribed standard is neither economically nor technically feasible within a foreseeable timeframe.

A potential solution is the introduction of flood protection based on differentiated design levels, which emerged as a national flood risk management alternative during the preparation of the Hungarian Flood Risk Management Plan. In addition, this approach offers an effective means of optimizing the use of available financial development resources, thereby enabling faster and more sustainable improvements in flood safety. The development of the hydrological, mathematical, and risk assessment foundations of the differentiated methodology took place over several years as part of a complex planning process. Its development is closely linked to the implementation of the EU Floods Directive; during the first review cycle of Hungary's Flood Risk Management Plans, the methodological development of differentiation was identified as a priority measure. The work aimed at defining the principles and levels of differentiated flood protection was being carried out under the coordination of the General Directorate of Water Management, which organisation is responsible for the operational management of water resources in Hungary. This comprehensive task was implemented by experts of the Hungarian water management planning company, called VIZITERV Environ Non-profit Ltd., with the involvement of the territorial water management directorates.

The new concept in Hungary treats construction levels in a differentiated manner depending on the design flood levels. The main flood protection lines must be constructed to an optimal level everywhere, ensuring the prescribed height safety (freeboard), which is determined solely based on technical criteria.

This manuscript presents the developed methodological aspects of this approach and discusses the concept within the context of international practice.

2 FLOOD PROTECTION SYSTEM OF HUNGARY: DESIGN PRINCIPLES AND ORIGINS OF FLOOD DEFENCE LINES

2.1 Characteristics of flood hazard in Hungary (in international comparison)

The flood hazard in Hungary is fundamentally determined by the country's hydrological and topographical conditions. Hungary is located in the Carpathian Basin, which is the largest intermontane basin in Europe; consequently, the discharges of its watercourses are predominantly influenced by the surrounding mountain ranges forming the upstream catchment areas. In addition, the high level of flood and inland excess water hazard is further reinforced by the fact that approximately 68 % of the country's territory lies below 200 m above sea level. Depending on precipitation conditions, about 95 % of the annual discharge of Hungarian rivers originates outside the national borders. This flow rate enters the country through a transit river network with an uneven spatial distribution, concentrated towards the central lowland areas, and subsequently leaves Hungary in a southward direction. Altogether, 22 rivers flow through the territory of Hungary, with a total length of approximately 2.800 km *(Antal, 2017)*, which is considered significant relative to the size of the country.

Flood waves and flood events along Hungarian rivers are primarily generated and controlled by precipitation amounts measured within the upstream catchments, as well as by the magnitude and rate of snowmelt associated with rising temperatures. Due to the characteristic ecosystems of lowland areas, favourable loess-based soils for agricultural production, and a specific vegetation structure with relatively limited forest cover, conditions are particularly conducive to the formation of inland excess water and floods. Approximately 30 % of Hungary's agricultural land is affected by flood hazard *(Tasnádi, 2020).* These findings are further supported by studies examining the impacts of climate change on the vulnerability and economic performance of European countries. In the case of Hungary, research has demonstrated that large river floods, along with impacts on agricultural production and broader

hydrological risks – including changes in precipitation patterns – represent a significant economic exposure both at present and in the future *(Boitier et al., 2024)*.

Based on the above mentioned factors, it can be concluded that the flood hazard in Hungary is primarily governed by fluvial flooding. These phenomena are caused by large rivers and flood waves originating from upstream catchments located outside the country. Owing to the country's topography and the dominance of a temperate continental climate, local precipitation events and flash floods are of lesser importance in terms of overall flood hazard and risk.

The flood protection system in Hungary has been developed in accordance with these characteristics. As a result, the backbone of the flood protection system consists mainly of long, continuous embankment sections, behind which substantial assets are concentrated. Defence capacities, intervention capabilities, as well as strategic and technical design principles and developments, are therefore largely aligned with these linear flood protection structures. The severe Central European flood events of 2024 further confirmed that, compared to neighbouring countries, Hungary generally benefits from longer lead times, which – beyond civil protection tasks – allow for a strong focus on the proper operation and application of flood protection infrastructure, as well as on the high level of technical expertise required for flood control operations.

2.2 Methodology of design flood level determination in Hungary: an international comparison

The fundamental design unit of Hungary's flood protection system is the design flood level calculated using a standardized hydrological-hydraulic statistical methodology. Based on the analysis of discharge time series observed along a given river, the corresponding water level is determined for a flood wave with a specified return period (e.g. 100–1.000 years). Earlier practice defined the design level on the basis of the historically observed maximum water levels, however, as this approach did not account for morphological changes of the river channel, human interventions affecting the channel, or land-use changes, the derivation of water levels from discharge statistics proved to be a more appropriate methodology. Consequently, since the 1970s, the design flood level determining the crest elevation of flood defence lines has been uniformly defined as the statistically derived value of the annual maximum ice-free floods corresponding to a given probability of occurrence (return period). The impacts of climate change, together with successional and sedimentation processes taking place within floodplains, have demonstrated scenarios in which the repeatedly revised calculated design flood levels remain economically viable only if appropriate interventions are implemented within the floodplains and riverbeds. For this reason, Hungarian water management bodies prepared Floodplain Management Plans for the country's major watercourses in 2015 *(General overview of floodplain management plans, 2015).*

The above mentioned considerations demonstrate that, throughout the country's history, the vertical upgrading of the flood protection line system has consistently been a fundamental element of Hungary's flood protection strategy. This strategy has evolved over time in response to changing water management demands and climate change scenarios, while its design basis in Hungarian practice has remained the design flood level corresponding to the 100-year return period flood event (Q_{100}).

Directive 2007/60/EC of the European Parliament and of the Council (the EU Floods Directive) prescribes only one specific return period ($\geq Q_{100}$) as direct design parameters for the Member States, rather defines probability-based categories. This provides Member States with the flexibility to develop their flood hazard and flood risk management plans, as well as their design and dimensioning criteria, in accordance with scenarios relevant to their own territories. As a result, regional heterogeneities and economic considerations can be more effectively taken into account. The latter plays a particularly important role in Hungary in the methodology applied for the differentiation of flood defence design levels.

The "FLOPROS" database developed by *Scussolini et al. (2016)* analyses national and regional differences in flood return periods associated with flood protection measures across Europe and worldwide. This provides a solid basis for comparing the degree of flexibility applied in neighbouring

countries' design standards, as well as for examining how climate change and other influencing factors are incorporated into design calculations. Based on FLOPROS data, the characteristic return periods used as typical design bases in several countries have been compiled (Table 1):

Table 1 Design flood return periods applies in different countries *(Scussolini et al., 2016)*

Country	Typical Design Basis (Return Period)	Other scenarios
Hungary	Q_{100}	Additional freeboard above the design flood level depending on the built-up intensity (1.0-1.5 metres)
Germany	Q_{100}	Higher standards (Q_{200}-Q_{500}) for critical areas depending on regional regulation
Austria	Q_{100}	Additional freeboard depending on the importance of the protected area (typically 0.5–1.0 metres)
Switzerland	Q_{30}-Q_{200}	Differentiated per land use, Q_{30} in rural areas
Slovak Republic	Q_{100}	Additional freeboard
France	Q_{100}	
Italy	Q_{100}	Q_{200}-Q_{500} for densely populated areas, critical infrastructures and high-value assets
United Kingdom	Q_{10}- Q_{1000}	Q_{200}-Q_{1000} in urban areas. Tidal flooding also considered
Netherlands (Jorissen et al., 2016)	Q_{250}–Q_{10000}	Highest protection standards based on dike ring areas
Poland	Q_{100}-Q_{500}	
Czech Republic	Q_{20}-Q_{200}	
Canada	Q_{100}-Q_{700}	Mainly Q_{200}. Provincial regulation, values vary by regions and municipalities.
United States	Q_{100}	Q_{200}-Q_{500} for major cities and critical infrastructure

For the countries listed, the regulation of the design reference levels is typically established at the national level (with the exception of Canada, where regulation is defined at the provincial level). In the practice of several countries, however, differentiation at the local (municipal) level is also applied, primarily driven by the risk characteristics of major urban areas. In Hungary, such local-level differentiation is prescribed specifically with respect to the required freeboard above the design flood level.

The data presented in the table clearly indicate that in most European countries, as well as in Canada and the United States, return periods of approximately 100–200 years are predominantly adopted as design bases. However, beyond coastal flooding considerations, local flood protection levels may be significantly influenced by the spatial distribution and magnitude of flood risk. Consequently, the observed differences do not arise from hydrological conditions, but rather from risk-related considerations, typically associated with densely populated areas or the presence of critical infrastructure.

2.3 Technical and economic performance of developments based on the current design standards

To provide budgetary support for the differentiated methodology underpinning a sustainable development strategy, the height-deficient sections of flood protection lines and the costs required to upgrade them to comply with current standards can be straightforwardly presented based on the national registry of the General Directorate of Water Management *(Table 2).*

Table 2 Length of state-managed flood protection lines with height deficiencies relative to current standards *(Off. register, 2025)*

Total length of flood protection lines:	**4.414 km**
Earthen embankments:	4.099 km
High banks:	219 km
Flood protection walls:	22 km
Other (railway, road, wall):	74 km
Sections with height deficiency:	**3.055 km**
Degree of height deficiency:	**69 %**

Based on the above data, it can be stated that currently only approximately 30 % of the primary flood protection lines in Hungary comply with the applied design standards. In addition, around 250 km of flood protection sections under municipal management must also be considered, where this proportion is even lower.

According to embankment development projects implemented during the 2014–2020 European Union funding period *(Government Resolution 1084/2014),* the total cost of upgrading 1 kilometre of flood embankment - including land acquisition and other project-related costs - amounted to approximately HUF 600 million gross (≈1.6 million EUR). Taking into account changes in the construction producer price index *(Hungarian Central Statistical Office, 2025),* this corresponds to an estimated compound price increase of approximately +75 % by the end of 2025, meaning that the current unit cost now exceeds 1 billion HUF per kilometre (≈ 2.6 million EUR).

This clearly demonstrates that achieving full compliance with the current design standards does not represent a rational solution for either the state or local governments, even over several decades, particularly given that ongoing morphological changes and the increasing extremes associated with climate change are expected to further raise design flood levels in the future.

All of these factors necessitate a revision of the current rigid regulatory framework in Hungary and support the introduction of a differentiated approach. Cost rationalisation is further enhanced by the fact that differentiation enables the integration of the risk reduction effects of existing flood retention reservoirs, as well as the quantification of flood control and emergency response capacities.

3 PRINCIPLES AND CALCULATION METHODOLOGY FOR DIFFERENTIATED FLOOD PROTECTION DESIGN LEVELS

3.1 Principle of differentiation of flood protection design levels

Based on the discussion above, it can be concluded that the nationally prescribed design requirement in Hungary – based on a 100-year return period flood event and a uniform freeboard – constitutes an excessively rigid system that is neither technically nor economically sustainable. Taking international practice into account, this has prompted efforts to establish the foundations of a more flexible design regulation as an addition to the current provisions. As part of this process, a new calculation methodology has been developed which, in addition to hydrological considerations, also forward-lookingly incorporates territorial characteristics, risk levels and defendability. In the long term,

this represents a section-by-section differentiated approach that facilitates the efficient and targeted use of financial resources allocated to flood protection.

In Hungarian professional practice, the strategic approach to differentiated design levels is defined by water management experts as follows: *"The fundamental objective of differentiated development – based on the risk values on the protected side of flood defence embankments – is to establish a sustainable flood protection system that, in addition to ensuring flood safety, demonstrates clear social acceptance and effectiveness" (Dobó, 2023).*

According to the nationally developed calculation methodology, the differentiated level represents an optimal, defensible protection level, which incorporates technical freeboard, the effects of flood retention storage and linear flood control measures. Furthermore, in parallel, compared to the examined parameters it identifies the optimal level of embankment development at which the invested costs remain rational relative to the residual risk values achieved through the intervention.

The minimum development level was defined as [current design flood level-60 cm]. This threshold was introduced to avoid significant inequalities in flood defence capacities at the national scale. Accordingly, all flood defence lines are required to be upgraded at least to the level of the current design flood level minus 60 cm. Any protection level above this threshold is determined on a risk basis within the framework of differentiated flood protection, in accordance with the EU Floods Directive.

Under the differentiated approach, the extent of development for a given flood protection cross-section is determined as the sum of the differentiated level – defined relative to the currently prescribed design flood level – and the required freeboard, as outlined below:

Differentiated design level = Differentiated level + freeboard

3.2 Methodology for calculating differentiated levels

The differentiated level represents a "maximum defensible level," corresponding to a flood peak at which the given floodplain compartment can still be effectively protected.

The basis of differentiation is the flood risk calculated for the protected floodplain compartment as a whole and the relevance of the required investments. The assessment accounts for the risk-reducing effects of existing flood retention reservoirs and linear flood defence operations. According to the methodology, embankment upgrades to the differentiated levels are justified where the combined effects of retention and operational flood defence do not achieve the defined optimal level, or where the cost of embankment development to the current design levels is disproportionate relative to the risk reduction attained. All of these relationships are summarised schematically in the figure below *(Figure 1)*.

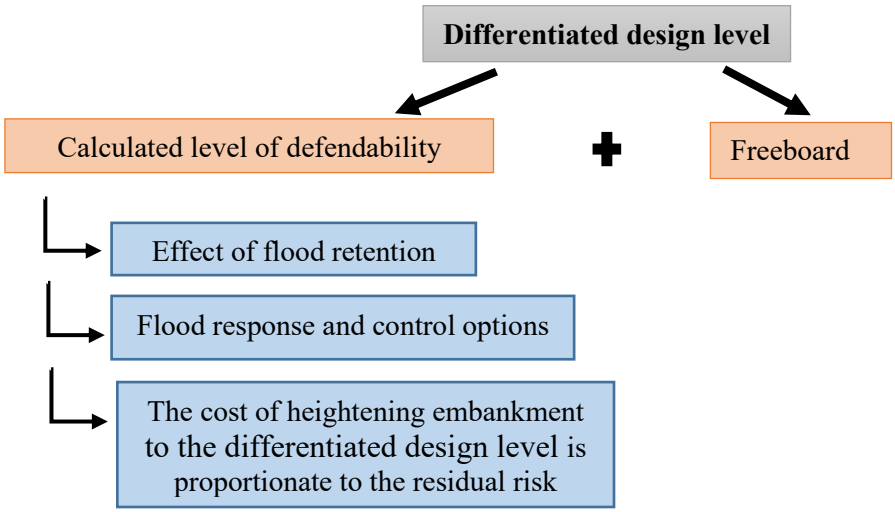

Figure 1: Methodology for calculating the differentiated design level *(edited by the authors)*

In Hungary, the methodological basis of flood risk calculation is provided by the risk assessment framework developed within the Flood Risk Management Planning (FRMP) project, prepared as part of the implementation of the EU Floods Directive. The differentiated calculation method does not modify the fundamental FRMP risk calculation formula, however, it treats protected floodplain compartments separately and assigns different acceptable risk levels to them. The spatial calculation of flood risk within the FRMP is based on flood hazard (inundation) maps produced through hydrodynamic modelling. Risk is calculated for each spatial unit of the exposed area using a raster resolution of 20×20 m. Based on the inundation simulations, the expected damages associated with individual flood events are determined and weighted by the probability of occurrence of the respective inundation events. The resulting risk is expressed as the expected annual average damage.

According to the risk assessment, the determination of acceptable risk levels was based on the ALARP (As Low As Reasonably Practicable) risk tolerance principle, applying evaluations grounded in cost-benefit analysis and affordability considerations. An optimal level of risk can be considered achieved when the risk assessment confirms that, in accordance with the ALARP principle, no residual risk remains within the unacceptable region, and that, as a result of risk reduction measures, the remaining risk is reduced to an acceptable level *(Ganszky, 2023).*

3.3 Calculation of freeboard

Under the current design regulations, a uniform freeboard of 1.0 m is prescribed for all rivers in the case of primary flood defence lines. Higher values – typically between 1.2 and 1.5 m – are required for major urban areas and for flood protection lines forming state borders. The application of lower freeboard values is permitted by regulation only in a limited number of cases, mainly for embankments along channels affecting only agricultural areas. This simplified, largely analogue calculation approach therefore fails to account for several factors that could allow for the determination of more realistic freeboard values based on defendability and technical parameters. In the case of differentiated design levels, the calculation methodology weights the following technical factors when determining the required freeboard for a given flood protection section:

1. Average embankment height (**$\bar{H}$**)

Criterion (m)	**Freeboard (m)**
$\bar{H} < 2$	0.5
$2 \leq \bar{H} < 5$	1
$5 \leq \bar{H}$	1.2

2. Extent of available lead time **(D)**

Criterion (day)	**Freeboard (m)**
$3 \leq D$	0.5
$1 \leq D < 3$	1
$D < 1$	1.2

3. Total floodplain width **(W)**

Criterion (m)	**Freeboard (m)**
$W < 200$	0.5
$200 \leq W < 1000$	1
$1000 < W$	1.2

4. Distance from river mouth (**D**)

Criterion (km)	Freeboard (m)
$15 \leq D$	0.5
$5 \leq D < 15$	1
$D < 5$ km	1.2

5. Type of flood defence structure

Criterion	Freeboard (m)
wall	1
earthen embankment	1.2

The value of the freeboard is calculated as a weighted average of the factors listed above, with priority given to embankment height and the structural type of the flood defence.

3.4 Social conflicts and their management

One of the primary objectives of differentiation is to allocate proportionally greater development efforts within the differentiated approach to high-risk protected floodplain compartments (and river reaches) than to medium- and low-risk areas, thereby focusing interventions on the most problematic locations. As a consequence, social conflicts may arise. The essence of the methodology is differentiation rather than discrimination. Nevertheless, these issues must be addressed through engagement with local stakeholders. Within a research project, the General Directorate of Water Management examined the management of socially related conflicts, leading to the following key findings *(Revision of flood safety concepts, 2023):*

- the development of a national-scale socio-economic evaluation model is required, including the assessment of risk threshold values based on the economic performance capacity of the economy and the affordability of the population, as well as for productive sectors, considering both the current situation and the differentiated flood protection alternatives;
- for those river sections or protected proteted floodplain compartments that are assigned lower development priority due to limited defence capacities and possibilities, it is essential to ensure the maintenance of flood defence resources and operational capabilities;
- in the case of opposing flood protection lines, the differences resulting from differentiated developments must be addressed through national-level coordination combined with local-level social consultation. For this purpose, focus-group stakeholder forums were organised within the framework of the National Laboratory for Water Science and Water Security, based on designated pilot areas*;*
- and the population and local governments must be adequately informed about the rationale of investments and strategic decisions, as sociological research has shown that they often lack information regarding the challenges faced by water management authorities and the organisation's long-term plans.

4 EXPECTED OUTCOMES OF THE METHODOLOGY

4.1 Advantages of applying the differentiated methodology

Given that differentiated embankment development seeks an optimal solution, it approaches – though does not fully attain – the flood protection effectiveness of full-scale development, while requiring substantially fewer resources, thereby representing a more sustainable alternative. Quantitatively, this implies that, at the national level, the differentiated approach achieves a lower residual risk at

approximately one-third of the cost, meaning that financial resources can be utilised far more efficiently while delivering benefits (risk reduction) of a comparable magnitude. During the first review cycle of the Flood Risk Management Plans, VIZITERV Environ Non-profit Ltd., commissioned by the General Directorate of Water Management, carried out calculations to compare the risk reduction effects of the currently prescribed standards with those of the differentiated alternative. The results of this comparison are presented in the table below.

Table 3 Cost-benefit indicators of the currently applied design level and the differentiated design level *(FRMP, 2021)*

Indicator	Currently applied design level	Differentiated design level
Cumulative initial asset risk [thousand HUF/year]	152 151 470	152 151 470
Residual risk [thousand HUF/year]	50 073 346	11 501 516
Residual risk ratio [%]	33	8
Risk reduction [thousand HUF/year]	96 544 740	124 901 984
Risk reduction ratio [%]	63	82
Risk reduction over 30 years [thousand HUF/30 years]	1 892 276 904	2 448 078 887
Investment cost (2022 price level) [thousand HUF]	866 884 457	166 848 141
Benefit-cost ratio	2,18	14,67
Expected annual flood defence cost [thousand HUF]	618 538	680 540
Expected flood defence cost over 30 years [thousand HUF]	12 123 351	13 338 591
Expected total cost [thousand HUF]	879 007 808	180 186 732
Expected benefit [thousand HUF]	1 892 276 904	2 448 078 887
Overall benefit–cost ratio	2,15	13,59

Based on the above indicators, it is evident that implementing the differentiated alternative results in substantially greater risk reduction while requiring only a fraction of the investment cost. It should be noted that the values presented in the table above do not include the examination of all protected floodplain areas in Hungary, they only cover areas with high and extremely high risk from the FRMP review. In the current implementation cycle of the Floods Directive, a partial modification of the differentiated levels is underway prior to the legislative process of the new design units.

4.2 Priorisation of developments

During the first review cycle of the Flood Risk Management Plans – within which the development of the differentiated alternative was identified as a priority measure – experts selected, based on flood risk calculations, those protected floodplain comaprtments where high and extremely high risk could be identified and the embankment developments should be prioritised from among the 145 protected floodplain compartments designated in Hungary. As part of the development of the differentiated alternative, a phasing proposal was also prepared, which is illustrated in the figure below. It can be clearly

observed that the primary development areas are located in the Tisza River basin, particularly along the Middle-Tisza and the Körös regions.

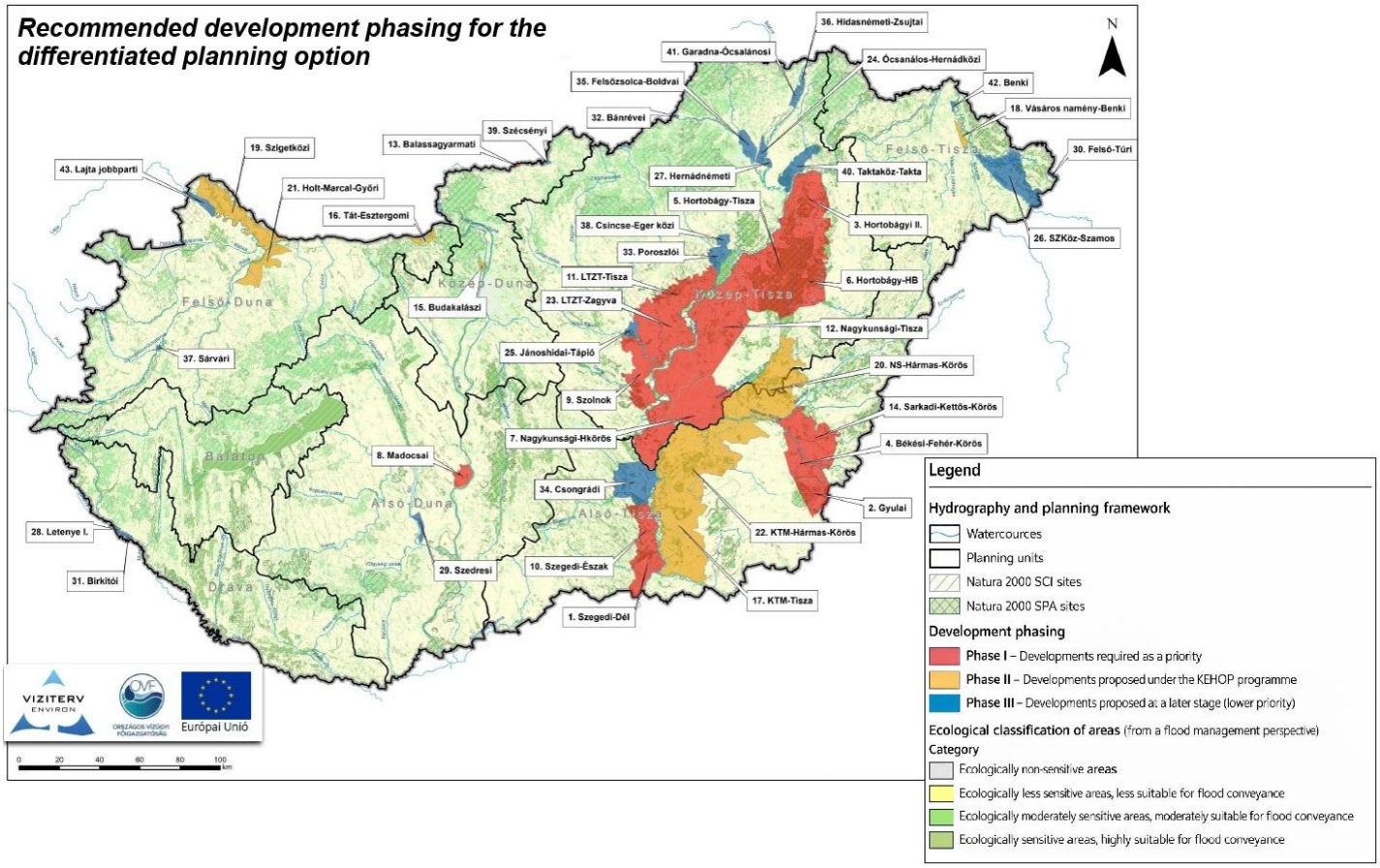

Figure 2: Recommended implementation phasing for the differentiated design option *(FRMP, 2021)*

5 CONCLUSIONS

In Hungary, the regulation governing the vertical development of flood protection lines defines the prescribed design levels based on a hydrological statistical approach. By now, it has become evident that this methodology requires further development. This necessity arises partly from economic feasibility considerations, and partly from the need to methodologically incorporate additional factors which – by explicitly addressing defendability – can provide a far more efficient and sustainable alternative in terms of both risk reduction and costs.

Compared to international practice, flood safety standards in Hungary are generally more moderate rather than more stringent, and further easing of these standards would not be appropriate. However, achieving and constructing the prescribed level of full protection would impose a substantial burden on the Hungarian economy or would require an excessively long implementation period, particularly in view of the continuous increase in design flood levels and the exceptionally long extent of flood protection lines by European standards.

The application and implementation of differentiated development levels as a governing design standard can bring the most significant improvements especially in locations where the risk is high or extremely high and the height of flood embankments does not even reach the currently prescribed design flood level. By exploiting this approach – namely, upgrading critically low sections to a defensible level –

critical deficiencies can be eliminated more rapidly, as defendability can be achieved over longer sections at lower cost than full protection. The reduced costs associated with the proposed alternative result from incorporating the risk-reducing effects of flood control operations and flood retention storage, which can be realised at more favourable costs, while embankment upgrades are carried out only to the extent required on a risk basis.

A key methodological element of the differentiated design levels planned to be introduced in the near future is that the prioritisation and extent of proposed developments are determined based on the level of risk on the protected side of the flood protection facilities. This, in turn, necessitates continuous updating through Flood Risk Management Plans in order to adequately capture the dynamic evolution of flood risk. It is also important to note that the sustainability of the design levels underpinning embankment developments can only be ensured through the implementation of floodplain management interventions and construction regulations given the adverse changes occurring on the floodplains of Hungary's typically low-gradient rivers.

6 ACKNOWLEDGEMENTS

The presentation of this study at ICMF10 is supported by the General Directorate of Water Management. The authors would like to express their special thanks to Director General István Láng and Head of Department Dr. Kristóf Dobó, who personally supported the presentation of the topic.

A decisive contribution to the preparation of the manuscript was provided by Anita Mária Süveggyártó, who also serves as the project leader. The methodological development of differentiated flood protection was significantly supported and implemented by the experts of VIZITERV Environ Non-profit Ltd., with particular acknowledgment of the work of Márton Ganszky, András Horkai and Márton Bálint.

REFERENCES

Antal Ö. The theoretical and technical issues of effective protection in the period of prevention against the harmful effects of disasters caused by floods and earthquakes (2017). Doctoral (PhD) thesis. National University of Public Service, Doctoral School of Military Engineering p. 43.

Boitier B., Mekki H., Le Mouël P. and Zagam P. (2024). Projected climate impacts and impact-specific damage functions for EU countries: A review and estimation. Climatic Change, Volume 178, article number 189, 2025, pp. 1-25.

Dobó K. Differentiated flood protection in Hungary (2023). Doctoral (PhD) thesis. National University of Public Service, Doctoral School of Military Engineering pp. 9-10.

Flood Risk Management Plan of Hungary (2021). General Directorate of Water Management. Prepared by: VIZITERV Environ Non-profit Ltd. Web: https://vizeink.hu/wp-content/uploads/2022/10/akk/Arvizkockazat-kezelesi_terv.pdf, consulted 29 December 2025

Ganszky M. Presentation of flood risk management results for protected floodplain compartments (2023). Published by the Hungarian Hydrological Society, November 2023. Web: https://www.hidrologia.hu/wp-content/uploads/2023/11/0110_ganszky_marton_bence.pdf, consulted 29 December 2025

General overview of floodplain management plans. General Directorate of Water Management (2015). Web: https://www.vizugy.hu/vizstrategia/documents/8F5D53BE-F66B-47F3-81A5-787C68417B52/Nagyvizi%20mederkezelesi%20mintatervek.pdf, consulted 22 December 2025

Government Resolution No. 1084/2016 (II. 29.) on the establishment of the annual development framework of the Environmental and Energy Efficiency Operational Programme. Annex 2 - lists the priority flood embankment development projects.

Hungarian Central Statistical Office, Quarterly construction producer price indices, cumulative since the beginning of the year 2020-2025. Web: https://www.ksh.hu/stadat_files/ara/hu/ara0061.html, consulted 27 December 2025

Jorissen R., Kraaij E. and Tromp E. Dutch flood protection policy and measures based on risk assessment (2016). FLOODrisk 2016 - 3rd European Conference on Flood Risk Management. p. 2.

Official register of state-managed flood protection lines based on the data provided by the regional water management directorates (2025). General Directorate of Water Management

Revision of flood safety concepts and prevention-focused flood protection. 1st book - Comprehensive assessment of the social, economic and ecological impacts of the differentiated strategic plan, including analyses in two pilot areas (2023). General Directorate of Water Management. pp. 97-100.

Scussolini P., Aerts J., Jongman B., Bouwer L., Winsemius H., de Moel H. and Ward P. FLOPROS: an evolving global database of flood protection standards (2016). Natural Hazards and Earth System Sciences, 16, 1049–1061, 2016.

Tasnádi G. The interrelationships between flood hazard and agricultural land use. National Chamber of Agriculture (2020). Web: https://www.nak.hu/tajekoztatasi-szolgaltatas/mezogazdasagi-termeles/101154-az-arvizi-veszelyeztetettseg-es-az-agrargazdalkodas-osszefuggesei, consulted 20 December 2025

Chapter 5- Governance, policy, and societal engagement

5.1 Flood risk governance, policy frameworks, and institutional coordination

ICFM 10
Adapting to Global Change:
Innovative Approaches to Flood Management and Resilience
May 20-22, 2026 | Western University, London, Ontario, Canada

Flood-Related Land Use Control in Japan: Reverse Zoning, Location Optimization Plan and Basin Flood Control

Kuniyoshi Takeuchi
Interdisciplinary Centre for River Basin Environment, University of Yamanashi, Kofu, 400-0016, Japan
E-mail: takeuchi@yamanashi.ac.jp

ABSTRACT

In response to ever increasing hydro-meteorological risks, land use control has become indispensable for flood-related disaster risk reduction in urbanized parts of Japan. This study examines three major policy instruments: Reverse Zoning, Location Optimization Plans (LOP), and Basin Flood Control, and analyses the conditions under which they can function in synergy. Employing comparative case analysis, this research investigates reverse zoning in Kitakyushu City and Hiroshima Prefecture, LOP implementation in Toyama City and Hanamaki City, and the institutional framework of the 2021 Basin Flood Control-related Act. The findings reveal that while each policy addresses a distinct aspect of exposure control, spatial efficiency, and systemic coordination, their effectiveness is limited when implemented in isolation. The study underscores the importance of transdisciplinary approach (TDA), formalized through the River Basin Flood Risk Reduction Councils mandated by the Basin Flood Control-related Act, which enables collaboration among diverse stakeholders in developing and implementing flood risk management strategies. Especially, the integration of land use control for exposure reduction with infrastructure development and enhancing societal resilience is important for a comprehensive approach to disaster resilience. In conclusion, the coordinated implementation of reverse zoning, LOPs, and basin flood control under TDA is vital for building a resilient and sustainable urban environment. Ongoing collaboration and community engagement will be crucial for the success of these reforms in the face of increasing hydro-meteorological risks.

KEYWORDS: flood-related disasters, reverse zoning, location optimization plan, basin flood control, transdisciplinary approach (TDA)

1 INTRODUCTION

Since around the turn of the millennium, the impacts of climate change have become increasingly severe, with flood-related disasters occurring almost annually in Japan. Notable events include the 2004 season with over ten typhoons making landfall (Web-1), the 2014 August linear rain band (Web-2), the 2018 July Heavy Rains (Web-3), and the 2019 Super Typhoon Hagibis (Web-4). These events have highlighted the urgent need for proactive disaster risk reduction strategies, particularly in the realm of land use control.

A striking observation is that in many prefectures the population growth continues in flood-prone areas while their overall population declines. According to Nozawa et al. (2023), in urban planning area designated by prefectural governors by City Planning Act of 1968, the total population decreased by 719,000 in between 2010-2020 which was after Japanese total population peak out in 2008, while the total population in over 3m inundation risk areas designated by 2022 hazard maps increased by 289,000. According to Ministry of Finance material (Web-5), in 36 prefectures out of 47 prefectures in total, the total population decreased in between 1995 and 2015, among which 22 prefectures experienced an increase in residents living within flood inundation risk areas designated by 2012 hazard maps. Even in prefectures where both the total population and the population in risk areas decrease, the decline is less in

risk areas in percentage wise. Likewise, even where both increase, the increase is more in risk areas in percentage wise. These paradoxes are driven by two main factors: land price is lower in high-risk areas, and more people want to buy. The other is that local governments are reluctant to restrict development in risk areas due to concerns over depopulation and economic decline.

This situation exemplifies the difficulty of implementing effective land use regulation in democratic societies. While earlier efforts, such as the City Planning Act and compact city initiatives, aimed to guide urban development, their impact on disaster risk reduction has been limited. In response, Japan introduced a new policy framework in 2021: River Basin Disaster Resilience and Sustainability by All, commonly known as the Basin Flood Control policy.

This paper examines three key land use policies: reverse zoning, location optimization plans (LOPs), and basin flood control, and analyses the conditions under which they can function synergistically. The central hypothesis is that a Transdisciplinary Approach (TDA), involving collaboration across sectors and disciplines, is essential for the successful integration and implementation of these policies (Takeuchi et al., 2024).

2 METHOD

To identify the key factors for successful land use control in flood-prone areas, this study employs a comparative case analysis of three major policy instruments: reverse zoning, LOPs, and basin flood control. Case studies were selected based on differences in policy approach and the transferability of their experiences to other cities.

First, two cases of reverse zoning are examined: Kitakyushu City and Hiroshima Prefecture. These cases provide insights into the political, social, and administrative approaches of rezoning inhabited areas especially with respect to residents at sites.

Second, the study analyses LOP implementation in Toyama and Hanamaki Cities. These cases are selected for their contrasting approaches to compact city development and stakeholder engagement. The analysis focuses on their transit corridors as essential necessity, effectiveness of designating Residential Induction Areas (RIAs) and Urban Function Induction Areas (UFIAs), and the role of intersectoral collaboration.

Finally, the Basin Flood Control policy is assessed in terms of its institutional design and capacity to integrate the lessons learned from reverse zoning and LOPs. Particular attention is given to the role of River Basin Flood Risk Reduction Councils in facilitating TDA.

The findings from these cases are synthesized to evaluate the extent to which the three policies align with the principles of TDA and contribute to a coherent, resilient land use strategy.

3 REVERSE ZONING

"Reverse Zoning (gyaku senbiki)" is a land use policy based on City Planning Act of 1968 (Act no. 100 of 1968) and Ministry of Construction Ordinance in 1980 (Ministry of Construction, 1980) that allows previously designated urbanization promotion areas into urbanization control areas. Originally introduced in the 1980s to prevent inefficient urban sprawl, reverse zoning has gained renewed attention as a tool for disaster risk reduction in the context of climate change and depopulation (Nagasue et al., 2023; Asano and Yamaguchi, 2015).

3.1 Kitakyushu City

Kitakyushu City, located in Fukuoka Prefecture, has a long history of flood-related disasters, including the 1953 West Japan Flood and the 2018 July Heavy Rain, the latter caused 407 slope failures and 2 fatalities in the city (Web-6). In response, the city proposed a reverse zoning plan in 2018 to

reclassify approximately 1,157 hectares, which are home to around 35,200 residents and about 18,000 houses and buildings, as urbanization control areas (Web-7).

During around 280 extensive public briefings, however, the plan faced strong opposition. Residents expressed concerns over declining land price, lack of compensation, and even potential violations of property rights. As a result, the final plan, approved in 2024, was significantly scaled down to cover only 263 hectares, affecting 165 residents and 215 buildings (Web-8). This was despite the fact that the city adopted a gradual implementation strategy over 30 years, allowing current residents to remain while restricting new development.

This case illustrates the political and social sensitivity of reverse zoning. While the city's initiative was forward-looking and aligned with disaster risk reduction goals, the lack of financial support and limited public consensus hindered its full realization. At the same time, it demonstrated the importance of discussion with residents from the planning stage.

3.2 Hiroshima Prefecture

Hiroshima Prefecture experienced severe sedimentary disasters in 2014 and 2018. In August 2014, heavy rain caused by linear rain bands led to 77 deaths including 3 associated deaths, mainly due to landslides and debris flows in Hiroshima City's Asaminami and Asakita areas (JSCE Hydraulic Eng. Committee, 2015; CO Bousai, 2018). In response, the prefecture accelerated the designation of sediment disaster warning zones. As of September 2025, 47,879 zones, including 45,092 red zones were designated which was the highest number of sites in Japan (Web-9). About 10,000 of these are in urbanized areas (Web-10).

In July 2018, the West Japan Heavy Rain caused 231 deaths and missing persons nationwide (Web-11). Hiroshima Prefecture alone recorded 114 death and missing, including 87 from sedimentary disasters where 79 due to debris flows (MLIT, 2019). These events prompted the prefecture to consider reverse zoning.

In 2020, Hiroshima launched its "Safety, Pride, Challenges: Hiroshima Vision," aiming for a disaster-resilient urban structure. In 2021, it introduced a three-step reverse zoning concept: (1) immediate zoning in 800 uninhabited sites; (2) within 20 years, restrict new settlements in 5,000 fringe zones; (3) within 50 years, relocate all residents from 10,000 red zones (Web-12). A detailed plan was proposed in FY2024, followed by public hearings and approval in 2025.

Implementation begins with uninhabited areas. For populated zones, the focus is on early warning systems and voluntary relocation through support programs. While the approach may appear cautious, it is wise to prevent new settlements in undeveloped land and allow residents in red zones time to understand the risks and move voluntarily. Prefecture's follow-up reports are awaited.

3.3 Lessons Learned

These cases highlight the challenges of implementing reverse zoning in democratic societies. Key barriers include property rights concerns, economic disincentives, and limited public trust. Successful implementation requires long-term vision, transparent communication from the initiation stage, and supportive measures such as relocation assistance and land value compensation. Also, it suggests the importance of a rare opportunity window after experiencing sever disasters as people become acceptive to displacement.

Moreover, reverse zoning cannot function in isolation. Its effectiveness depends on integration with broader spatial planning frameworks, such as location optimization plans and basin flood control strategies. The next sections explore how such integration can enhance policy coherence and resilience outcomes.

4 LOCATION OPTIMIZATION PLAN (LOP)

The "Location Optimization Plan (LOP)" was introduced through the 2014 Amendment to the Act on Special Measures concerning Urban Renaissance (Act no. 36 of 2014). It aims to promote compact city development by designating RIAs and UFIAs, thereby concentrating population and services in safe, efficient zones while discouraging development in disaster-prone or low-density areas. As of July 2025, the number of cities tackling their LOPs was 935 among which 634 cities made their plans open to the public (Web-13).

For this enactment, studies of Tohoku Regional Bureau of Ministry of Land Infrastructure, Transport and Tourism (MLIT) and good practice of Toyama City must have played a considerable role as forerunners of the compact city concept. Toyama City's Light Rail Transit (LRT) was highlighted by OECD comparative assessment study (OECD, 2012) as a leading case of compact city and network under shrinking population by revitalizing public transportation, promoting residential concentration along transit corridors, and regenerating the city center.

4.1 Toyama City

Toyama City is widely recognized as a pioneering case of compact city development in Japan. Facing rapid population decline and urban sprawl, the city initiated its compact city strategy in 2002, centered around the introduction of a Light Rail Transit (LRT) system. The LRT served as a backbone for urban regeneration, connecting dispersed neighboring towns and encouraging residential concentration along transit corridors (Toyama City, 2024).

The city implemented a suite of supportive measures, including housing subsidies for relocation into RIAs, land-use incentives for developers, and the revitalization of public spaces in the city center. These efforts were coordinated by municipal departments such as urban planning, transportation and welfare that were supported by private sector partners as well as active participation of citizen groups by promoting LRT use. Here the leadership of Mayor Masashi Mori was important in aligning these actors under a shared vision (Fukayama et al., 2007).

Empirical studies (Fujioka & Sakakibara, 2023) show a modest recovery in population and service density within targeted areas since the LOP's implementation. Toyama's experience demonstrates that policy integration, strong leadership, and stakeholder collaboration are critical to the success of compact city strategies.

4.2 Hanamaki City

Hanamaki City in Iwate Prefecture stands out as the first municipality in the Tohoku region to launch a compact city initiative under the national LOP. Its role as an early model dates back to 2008, when it was selected as a focus area in the Tohoku-initiated Compact City Study Committee, established by the MLIT's Tohoku Regional Bureau to explore sustainable urban forms in shrinking regions (Tohoku-initiated Compact City Study Committee, 2024).

As a regional hub facing population decline and spatial dispersion, Hanamaki has taken structured steps to concentrate on urban functions and housing. It has designated RIA to guide new housing toward existing centers and UFIA to cluster services such as healthcare, education and commerce.

Although development outside the designated areas continues, empirical studies show some success in directing new construction within the target zones (Yamanashi & Ubaura, 2020). What makes Hanamaki notable is its effort to align spatial planning with long-standing practices of shared responsibility between local government and community groups. These include disaster response and infrastructure maintenance, such as snow removal and road upkeep in peripheral settlements (Yakushige & Hirota, 2014). While public participation in the initial planning phase was limited, this tradition of collaboration offers a foundation for more integrated governance.

Hanamaki's experience highlights the importance of combining formal planning tools with informal local capacities. As many regional cities struggle to implement compact city policies, Hanamaki provides insight into how spatial strategies can be grounded in existing social frameworks.

4.3 Comparative Insights

The contrasting experiences of Toyama and Hanamaki underscore the importance of implementation over policy design. Toyama's progress reflects strong mayor's leadership, cross-departmental coordination, private sector involvement and sustained civic support. In contrast, Hanamaki's efforts were shaped by early foresight and community cooperation, rooted in its participation in the 2008 Tohoku-initiated Compact City Study Committee.

Although institutional integration was limited and outcomes modest, these efforts represent a significant departure from inaction. Hanamaki's case suggests that even incremental steps, when grounded in local collaboration and long-term vision, can lay the foundation for more resilient urban futures. These findings reinforce the need for context-sensitive, participatory approaches in land use planning, especially in regions facing demographic and fiscal stress.

5 BASIN FLOOD CONTROL

"Basin Flood Control (Ryūiki Chisui)" is a basin-wide flood risk management policy that directs river and sewerage managers of Specified Urban Rivers and Basins designated by the Minister of MLIT to develop a river basin flood damage countermeasures plan and implement it in collaboration with all relevant stakeholders. This policy was introduced by "Act Partially Amending the Act on Special Urban River Inundation Damage Countermeasures, etc." (Act No. 31 of 2021), often referred to as the Basin Flood Control-related Act, which simultaneously amended nine related Acts concerning comprehensive flood-related disaster risk management, thereby making the policy jointly actionable.

The nine acts are on special urban rivers, rivers, sewerage, flood control, sediment disasters, city planning, finance to relocation, urban green space, and building standards. Thus, the Basin Flood Control-related Act seeks not only engineering approaches but also sociological measures, ensuring that diverse stakeholders work together to efficiently manage floods across entire river basins. Briefly, the Act directs river and sewerage managers of specified river basins:

(1) development of river basin flood damage countermeasures plan,
(2) establishment of River Basin Flood Risk Reduction Council,
(3) installation of infiltration and storage facilities,
(4) introduction of licensing regulation for actions interfering infiltration and storage functions in the basin,
(5) designation of retardation and storage ponds to be conserved,
(6) instruction of displacement of houses under high potential damage,
(7) designation of inundation prevention areas where any actions interfering inundation prevention are restricted, and
(8) provision of financial support for such works with subsidies from the central government.

Among these mandated actions, two stand out for their significance in land use and governance. That is, (2) establishment of *river basin flood risk reduction council* is particularly important as it institutionalizes multi-stakeholder collaboration, ensuring that river and sewerage administrators, local governments, academic experts, and community representatives jointly formulate and implement flood damage countermeasures plans. It is indeed pivotal to TDA. On the other hand, (7) designation of *inundation prevention areas* plays a connector to the LOP policy. Namely, areas designated as inundation prevention areas must not be included in RIA ensuring consistency between flood risk management and urban planning.

6 DISCUSSIONS

The comparative analysis of reverse zoning, LOPs, and basin flood control revealed both the potential and limitations of Japan's evolving land use policies for disaster risk reduction. While each policy addresses a distinct dimension, reverse zoning focuses on exposure control, LOPs on spatial efficiency and service provision, and basin flood control on systemic coordination of all control means, their effectiveness hinges on the degree to which they are implemented in concert.

Key Insights from Case Studies may be:

(1) Policy Design Alone is Insufficient:
- Kitakyushu and Hiroshima show that even well-intentioned reverse zoning plans can fail without public support based on collaborative engagement from the early stages.
- Toyama and Hanamaki demonstrate that the success of LOPs depends less on formal designation of zones and more on the quality of stakeholder collaboration, including citizen participation and interdepartmental coordination.

(2) Central Role of the Basin Flood Control-related Act
- Legal framework for land use regulation: The Act now serves as the central legal framework for land use regulation in flood-prone areas.
- Institutionalization of TDA: The compulsory establishment of *river basin flood risk reduction councils* mandates collaboration among diverse actors. These councils are empowered to coordinate flood risk management and regulate land use, integrating engineering, sociological, and urban planning measures across disciplines and sectors.
- Explicit linkage with urban planning: The designation of inundation prevention areas and their exclusion from RIAs under LOPs demonstrates how the Act places land use control at the heart of flood risk management.

This legal and institutional integration operationalizes TDA, transforming land use decisions from siloed, sectoral processes into inclusive, multi-stakeholder governance.

(3) Challenges and Future Directions
- Governance and implementation: The effectiveness of *river basin flood risk reduction councils* varies depending on local administrative capacity, political will, and the maturity of civil society engagement.
- Temporal mismatch: There is often a mismatch between policy cycles and the long-term nature of land use change, requiring adaptive governance frameworks.
- Cultural and institutional transformation: Achieving disaster-resilient, compact urban development requires not only legal alignment but also cultural and institutional transformation.
- Importance of leadership: Leaders' capacity is so important in political level, administerial level and communities' level. Without any of these, TDA for efficient and resilient land use is unachievable. Of course, it is only possible by people's awareness of risk.

Building trust, fostering dialogue, and empowering local actors are as critical as technical planning in achieving sustainable outcomes.

7 CONCLUSIONS

This study has examined the evolution and integration of Japan's land use policies for flood risk reduction, focusing on reverse zoning, LOPs, and the 2021 Basin Flood Control-related Act. Through comparative case analysis, several key conclusions emerge:

(1) Synergy through Integration:

While each of these policies addresses disaster risk reduction from distinct aspects, their true effectiveness is realized only when implemented in a coordinated and mutually reinforcing manner. Fragmented or isolated efforts are insufficient to address the complex, systemic nature of flood risk in contemporary Japan.

(2) Centrality of the Basin Flood Control-related Act:

The 2021 Act has become the cornerstone of land use regulation in flood-prone areas, uniquely institutionalizing the TDA. By mandating the establishment of *river basin flood risk reduction councils*, the Act ensures that diverse stakeholders collaborate in both planning and implementation, bridging the gap between engineering, sociological, and urban planning measures.

(3) Land Use Regulation as a Core Strategy:

The explicit linkage between the designation of inundation prevention areas and their exclusion from RIA under LOPs demonstrates a paradigm shift: land use control is now at the heart of Japan's flood risk management strategy. This legal and institutional integration is essential for preventing new development in high-risk zones and promoting resilient urban forms.

(4) Challenges Remain:

Despite these advances, significant challenges persist. Effective implementation depends on local administrative capacity, sustained political will, and the maturity of civil society engagement. Enlightened leadership supported by enlightened public is a common difficulty in democratic nations. The temporal mismatch between policy cycles and the long-term nature of land use change further complicates progress. Building public trust, fostering dialogue, and empowering local actors remain critical tasks.

(5) Lessons for Broader Application:

Japan's experience offers valuable lessons for other countries facing similar hydro-meteorological risks. The shift from siloed, top-down planning to collaborative, place-based governance, anchored in legal frameworks that prioritize not only infrastructure development and societal resilience building but also exposure control by land use regulation and stakeholders' collaboration, represents a promising direction for building resilient and sustainable urban futures.

In conclusion, the integration of reverse zoning, LOPs, and basin flood control under a shared vision of disaster-resilient, compact urban development marks a significant step forward. The institutionalization of TDA through the Basin Flood Control-related Act provides a robust platform for aligning diverse policies and actors. Continued efforts to strengthen collaboration, adapt governance frameworks, and sustain community engagement will be essential for realizing the full potential of these reforms in the face of escalating flood-related disaster risks.

8 ACKNOWLEGEMENT

The author is indebted to Professor Toshio Koike, Director of ICHARM/PWRI, Tsukuba, Japan for his precious suggestions on the Basin Flood Control-related Act and related literature.

9 REFERENCES

Takeuchi K., Mangada L., Inoue M. et al. (2024) Challenges of transdisciplinary approach in disaster recovery management. Natural Hazards 120, 12471–12489. https://doi.org/10.1007/s11069-024-06693-z

Nozawa C., Ueda S. and Kakinuma D. (2023) A study on population change and residence induction by land use regulation in flood inundation hazard areas in case of maximum expected rainfall. Reports of the City Planning Institute in Japan, 21(4), 452-459. https://doi.org/10.11361/reportscpij.21.4_452

Ministry of Constrution (1980) City Planning Bureau Ordinance 100, 1980.9.16

Nagasue K., Yamasaki J. et al. (2023) Reality and Issues of Reverse Area Division in Response to Depopulation and Disaster Risk. Journal of the City Planning Institute of Japan, 58(3), 1203-1210.

Asano J. and Yamaguchi K. (2015) A Study on Application and Problem of Reverse Area Division in Local Cities. Journal of the City Planning Institute of Japan, 50(2), 246-251

JSCE Hydraulic Eng. Committee (2015) Aug 2014 Hiroshima Heavy Rain Disaster Investigation Report, https://committees.jsce.or.jp/hydraulic05/system/files/%E5%B9%B3%E6%88%9026%E5%B9%B48

%E6%9C%88%20%20%E5%BA%83%E5%B3%B6%E8%B1%AA%E9%9B%A8%E7%81%BD%E5%AE%B3%E8%AA%BF%E6%9F%BB%E5%9B%A3.pdf
CO Bousai (2018) Heavy Rain Disaster Since August 19, 2014. https://www.bousai.go.jp/kaigirep/houkokusho/hukkousesaku/saigaitaiou/pdf/02jirei5.pdf
MLIT (2019) July 2018 Heavy Rain. MLIT Chugoku Regional Bureau. https://www.cgr.mlit.go.jp/photo/h3007gouu_kiroku/pdf/h3007gouu_kiroku_all.pdf
OECD (2012) Compact City Policies: a comparative assessment. OECD Green Growth Studies. https://www.oecd.org/content/dam/oecd/en/publications/reports/2012/05/compact-city-policies_g1g191f1/9789264167865-en.pdf
Fukayama T., Kato H. and Shiroyama H. (2007) Why did LRT success in Toyama City? Transport Policy Study 10(1), 22-37. https://www.jstage.jst.go.jp/article/tpsr/10/1/10_TPSR_10R_03/_pdf/-char/ja
Fujioka, T. and Sakakibara, K. (2023). Compact City and Transit-Oriented Development in Shrinking Cities: A Case Study of Toyama. Journal of Urban Planning Studies, 59(2), 201–215.
MLIT (2025) Compact City Policies in Japan. Transport System Study, https://www.jstage.jst.go.jp/article/tpsr/10/1/10_TPSR_10R_03/_pdf/-char/ja
Tohoku-initiated Compact City Study Committee (2024) LRT networks in Japan https://www.thr.mlit.go.jp/compact-city/contents/susume2/data/zentaiban.pdf
MLIT (2025). Compact City Policies in Japan. Ministry of Land, Infrastructure, Transport and Tourism. Web-9.
Toyama City (2024.8) Outline of Project for LRT Networks. https://www.city.toyama.lg.jp/_res/projects/default_project/_page_/001/011/334/2024gaiyou.pdf
Yakushige, M. and Hirota, J. (2022). Regional Characteristics of Territorial Management in the Division of Roles between Local Governments and Communities: A Case Study of Hanamaki City, Iwate Prefecture. Regional Policy Studies, 35(Special Issue), 321–330.
Yamanashi, Y. and Ubaura, M. (2020). A Study on the Actual Conditions of Building Activities in Municipalities with Location Optimization Plans: Focusing on the Changes Before and After the Publication of the Plan. Journal of the City Planning Institute of Japan, 55(3), 1165–1172. https://doi.org/10.11361/journalcpij.55.1165

Web sites:
Web-1: https://www.mlit.go.jp/river/pamphlet_jirei/bousai/saigai/kiroku/suigai/suigai_1-3-1.html
Web-2: https://www.bousai.go.jp/kaigirep/houkokusho/hukkousesaku/saigaitaiou/output_html_1/pdf/201402.pdf
Web-3: https://www.fdma.go.jp/relocation/e-college/e-college/03H30saigaijireisyu.pdf
Web-4: https://www.fdma.go.jp/publication/hakusho/r1/topics1/47534.html
Web-5: https://www.mof.go.jp/about_mof/councils/fiscal_system_council/sub-of_fiscal_system/proceedings/material/zaiseia20231019/01.pdf
Web-6: https://www.city.kitakyushu.lg.jp/files/000957824.pdf
Web-7: https://www.city.kitakyushu.lg.jp/files/001124556.pdf
Web-8: deleted by Kitakyushu City around summer 2025
Web-9: https://www.sabo.or.jp/topics/0005-0508/shitei-jyoukyou.htm
Web-10: https://www.pref.hiroshima.lg.jp/uploaded/attachment/624275.pdf
Web-11: https://www.mlit.go.jp/river/shinngikai_blog/hazard_risk/dai01kai/dai01kai_siryou2-1.pdf
Web-12: https://www.pref.hiroshima.lg.jp/uploaded/attachment/635061.pdf
Web-13: https://www.mlit.go.jp/en/toshi/city_plan/content/001893723.pdf

ICFM 10
Adapting to Global Change:
Innovative Approaches to Flood Management and Resilience
May 20-22, 2026 | Western University, London, Ontario, Canada

Flood Hazard Identification and Mapping Program (FHIMP): Research Update

Baba Serges Zango[1], Shawn Tse[2], Christie Cho[1]
Environment and Climate change Canada (ECCC), 351 Boul. St-Joseph, Gatineau, Canada[1]
E-mail: Serges.Zango@eccc.gc.ca

Environment and Climate Change Canada, 7400 – 64 Street SE, Calgary AB, Canada[2]
E-mail: shawn.tse@ec.gc.ca

ABSTRACT

The Government of Canada's Flood Hazard Identification and Mapping Program was established in 2021 to help Canadians better plan and prepare for future flood risks. A key activity of the program is to support the advancement of flood hazard studies through research and developing technical guidance to promote best practices for flood mapping in Canada. In this presentation, Environment and Climate Change Canada will provide updates on the ongoing research activities that were initiated since 2024, including work completed internally as well as by external academic and research institutions. These initiatives aid in decision-making for land use planning, emergency management, and the protection of communities and infrastructure from potential flood damage

KEYWORDS: Hydrological & hydraulic modelling, flood mapping, climate change, machine learning

1 INTRODUCTION

Through the Flood Hazard Identification and Mapping Program (FHIMP), Environment and Climate Change Canada (ECCC) is investing in Canadian universities and research organizations to foster new knowledge and train the next generation of flood experts in Canada. Within the first three years of the program (Phase 1), eleven (11) academics and research organizations were recipients of the Grant and Contribution (G&C) funding program, with fifteen (15) research projects completed. In the second phase (2024-28), which is the focus of this paper, nine (9) projects were funded. The key themes of these projects included hydrological modelling and data, exploring different methodologies for flood estimation, investigating the impacts of bathymetric data on flood mapping, understanding flood mechanisms, and analysing climate change impacts, and estimating future hydrology.

With the various research topics assessed and currently on-going, the objective of this paper is to provide an overview of the activities being completed; the paper does not focus on detailed technical aspects of each individual project.

The sections below present the nine (9) different projects funded by the FHIMP during the second phase of the program.

2 MACHINE LEARNING FOR ENHANCED HYDRODYNAMIC AND FLOOD IMPACT MODELLING IN COLD-REGION RIVERS

2.1 Summary

Flood modeling in cold-region rivers is challenging due to ice processes and the computational cost of high-resolution simulations. This project addresses these issues by developing a hybrid framework that combines physics-based models with machine learning (ML) to deliver accurate, efficient predictions for real-time forecasting and climate scenario analysis. Case studies include the St. Lawrence and Athabasca Rivers.

2.2 Objectives

The project is guided by three main objectives:

- Develop and validate models: Build high- and low-resolution hydrodynamic models with ice processes and create a comprehensive simulation dataset.
- Advance ML techniques: Design physics-informed ML models for surrogate prediction and super-resolution downscaling.
- Operational integration: Embed ML-enhanced models into an automated flood forecasting system linked to hydrologic and climate data.

2.3 Progress to Date

Significant progress has been achieved in model development and machine learning integration. Hydrodynamic modelling has advanced with Delft3D models for both synthetic and real rivers, and high- and low-resolution datasets are being assembled. For ML-based downscaling, initial architectures such as U-Net and encoder–decoder have been tested, while work continues on dynamic, physics-consistent models using graph neural networks (GNN) and Fourier neural operators (FNO). In surrogate modelling, POD–DNN and hybrid RF–ANN models have been developed, and physics-informed neural network (PINN) approaches are currently under development.

2.4 Next Steps

The next phase of the research will focus on completing model development and enabling operational deployment. In the short term, the priority would be to finalize machine learning models, expand datasets, and benchmark hybrid approaches. Over the longer term, efforts will focus on integrating these models into forecasting systems, validating them against real flood events, and adapting the framework for application to other rivers, including data-scarce northern regions.

3 HYDROLOGIC-HYDRAULIC MODELLING FRAMEWORK FOR IMPROVING DYNAMIC ICE JAM FLOOD MAPPING UNDER A CHANGING CLIMATE

3.1 Summary and objective

River ice jams cause significant flood risks in many areas of Canada, but assessing this risk is challenging since the peak water levels during river breakup depend on many factors such as ice jam location, ice strength, river discharge, and dynamic ice jam releases. Existing ice jam flood maps rely on historical records, yet in many regions the data needed for accurate ice jam flood frequency analyses are lacking.

This research project aims to address this challenge by developing an "operations-ready" framework that integrates hydrological, hydraulic, and ice modelling to enhance the characterization of

breakup hydrographs. This comprehensive modelling framework will improve both "current generation" and "next generation" ice jam flood maps, especially where historical data is limited. It will also make it possible to consider the effects of climate change, addressing an important source of uncertainty in “current generation” flood maps.

3.2 Progress to date

At this stage of the project, several activities have been completed with others are ongoing. These activities include:

- Compilation and analysis of historical records of ice jam occurrence in the study reach (historical flight records, historical oblique air photos, all remote sensing data).
- Monitoring of the Smoky River 2025 breakup.
- Bank and overbank survey of 6 sites.
- Development of ice consolidation modelling capability in River1D (in progress), and implementation of a quasi-dynamic ice consolidation algorithm to determine where the ice is unstable and where the ice should move to. The algorithm is currently being tested.
- Compilation of climate data.

3.3 Next steps

The next steps in the project have been divided into 4 components:

- Component 1: Gain understanding of breakup on the Smoky River and prepare information for the modelling framework
- Component 2: Improve the River1D ice process model to enhance its ability to simulate ice jam formation locations and ice movements
- Component 3: Integrate the Raven hydrological model and the River1D hydraulic and ice process model
- Component 4: Utilize the modelling framework to generate results

4 INTEGRATING HYDROLOGICAL MODELLING UNCERTAINTY INTO FLOOD CHARACTERIZATION FOR FUTURE CLIMATE

4.1 Summary

The project connects ECCC's Surface Prediction System (SPS) to outputs of the Canadian Regional Climate Model (CRCM). It allows different land-surface models to be run offline at different resolutions from the regional atmospheric model. Land-surface models simulate water runoff and infiltration, which are then routed onto a river network to assess the influence of climate change on hydrologic regimes and floods.

4.2 Objectives

The main goal of the project is to build a physically-based hydrological modelling platform that facilitates the evaluation of the hydroclimatologic impacts of climate change, and in particular flood mechanisms.

4.3 Progress to date

To date, the following modelling tasks have been completed:

- Implemented SPS at Ouranos and ran the land surface model SVS from CRCM's outputs;
- Implemented the CLASS land-surface model within SPS;
- Routed SPS outputs on the southern Québec river network using Raven;
- Identified and implemented hydrological signatures to be used in the evaluation of the performance of the model framework.

4.4 Next steps

Although the modelling work is currently being completed, the research team will also be evaluating the calibration options as well as performance of the models. The datasets produced will be published and accessible to the public.

5 ASSESSMENT OF EMERGING TECHNOLOGIES TO OPTIMIZE ICE-JAM FLOOD RISK ASSESSMENT AND MAPPING

5.1 Summary

This project investigates the dynamics of open-water and ice-jam flooding, which pose serious socio-economic and environmental risks. It leverages advanced remote sensing technologies—the SWOT mission and GNSS-IR—to improve flood hazard mapping and forecasting. SWOT provides high-resolution two-dimensional water surface maps, while GNSS-IR offers non-contact water level measurements. The research applies these tools to rivers in Québec and Alberta, analyzing sensor signals under ice-covered and open-water conditions to retrieve critical hydrological parameters. By integrating these observations into geospatial models, the project aims to enhance flood prediction accuracy and develop next-generation dynamic mapping capabilities, advancing hydrology, hydraulics, and remote sensing.

5.2 Objectives

The main goal in this project is to evaluate the added value of combining GNSS-IR and SWOT and other altimetry data to achieve improved retrieval of hydrological parameters during the ice-on season for supporting ice-related flood monitoring.

5.3 Progress to date

To date, the project team has deployed GNSS-IR sensors and cameras along the Chaudière River, supported by winter-ready power systems, and conducted field campaigns to collect water level and ice data. A processing codebase and machine learning modules were developed for surface-type classification, later enhanced with deep learning and GPU acceleration. Ground truth masks were generated using Sentinel-2 imagery and DEMs, enabling automated river ice detection with SWOT data, though further refinement is needed for complex melt conditions. Preliminary results and methods have been shared at major conferences, generating valuable feedback for improvement.

5.4 Next steps

The remaining tasks to achieve the project objective include:

- Refining and validating performance of the classification methods of GNSS signals.
- Sensor leveling and integration of satellite altimetry.
- Field work to capture a broader range of hydrological and ice-cover conditions.
- Deep learning river ice classification of SWOT data.

6 ESTIMATION OF INTENSITY–DURATION–FREQUENCY (IDF) CURVES FOR PRECIPITATION UNDER CURRENT AND FUTURE CLIMATE CONDITIONS ACROSS CANADA

6.1 Summary and objectives

This project aims to improve the estimation of intensity–duration–frequency (IDF) curves for precipitation across the entire Canadian territory, both under current and future climate conditions. It seeks to make better use of available information by incorporating the Canadian Surface Reanalysis

(CaSR) as well as the dependence between accumulation durations, spatial dependence, and the influence of climate change. Ultimately, the project will produce a unified statistical framework capable of delivering IDF curves at any location in Canada while providing a robust quantification of uncertainty.

More specifically, the project involves:

- Modelling the dependence between accumulation durations to produce more coherent and physically consistent IDF relationships.
- Modelling the spatial dependence using a Bayesian hierarchical model informed by the CaSR reanalysis, ensuring spatial consistency of IDF estimates across Canada.
- Integrating climate change effects into the estimation of IDF curves to reflect both current and future climate conditions.
- Developing a unified statistical model combining duration dependence, spatial dependence, and climate change effects to generate IDF curves with appropriate uncertainty estimates at any location.

6.2 Progress to date

- The dependence between accumulation durations has been successfully modelled, achieving the first objective.
- Climate change effects have been incorporated into the IDF curve estimation framework, completing the third objective.
- Work on the second objective—modeling spatial dependence using a Bayesian hierarchical model and CaSR—is underway.

Early results demonstrate that incorporating duration dependence and climate change effects leads to improved consistency and realism in IDF curve estimates.

6.3 Next steps

The remaining work on the project is as follow:

- Complete the spatial dependence modelling using the Bayesian hierarchical framework and CaSR data.
- Begin development of the overarching integrated statistical model that will bring together all components—duration dependence, spatial dependence, and climate change effects.
- Ensure that the final framework can produce IDF curves at any location in Canada while providing reliable uncertainty quantification.

7 INTEGRATED FRAMEWORK FOR ASSESSING COMPOUND COASTAL AND INLAND FLOODING UNDER CLIMATE CHANGE ACROSS CANADA

7.1 Summary and objectives

The project develops an integrated statistical, hydrologic, and numerical modelling framework to assess compound coastal and inland flooding across Canada under climate change. Objectives include characterizing multivariate flood drivers, projecting changes in compound pluvial, riverine, and coastal events, and generating flood maps for key regions using advanced models and machine-learning tools.

7.2 Progress to date

- Completed projected analyses of compound pluvial-coastal events over the Pacific, including future storm surge-wave interdependencies.
- Completed numerical modelling for Tofino, including hydrodynamic setup and development of a machine-learning surrogate model for pluvial-surge-tide conditions.

- Analyzed rain-on-snow, saturation-excess, and successive rainfall flooding across North America and regionally over the Great Lakes under climate change.
- Started initial multivariate dependence analyses for key atmospheric, marine, and hydrologic drivers.

7.3 Next steps

- Finalize Raven model calibration for the Atlantic.
- Assess compound riverine-pluvial-coastal flooding for the Atlantic region.
- Evaluate future compound pluvial-coastal events across the Atlantic, Pacific, and Great Lakes.
- Extend numerical and hydrologic modelling to additional coastal sites.
- Finalize and apply the machine-learning surrogate model for large-ensemble compound flood simulations.

8 DEVELOPING A CONSOLIDATED FLOOD FREQUENCY ANALYSIS SYSTEM FOR CANADA IN A CHANGING CLIMATE

8.1 Summary

Researchers will implement comprehensive hydrometeorological and statistical modelling processes required for modelling the hydrologic impacts of climate change throughout Canada. The modelling framework will help increase the understanding of future flood hazards for the purpose of improving floodplain mapping methods and standards. The purpose of the framework is to support more informed decision-making and policy development, while also serving as an essential tool for sharing knowledge between researchers and flood mapping practitioners.

8.2 Objectives

The primary objective of the work is to develop a consistent hydrometeorological and statistical modelling chain to span Canada. Specifically, the two goals are:

- To develop hydrological models to predict how flooding will be affected by climate change across Canada.
- To create a method for flood frequency analysis that accounts for changes in flood magnitudes and types on rivers in Canada between the present day and the end of the century (2100).

8.3 Progress to date

In part 1 of the project, the research team is currently conducting hydrologic modelling for gauged and ungauged areas across Canada. They are developing a national hydrological prediction system using downscaled climate scenarios to estimate flows at all floodplain endpoints. This system is being built on the model-agnostic framework from the Global Water Futures (GWF) program. Researchers are running ensembles of models (HYPE, MESH, SUMMA) across selected basins under current climate conditions to evaluate parameterization, model accuracy, and suitability for climate change impact studies.

The second part of the project is applying climate scenarios for floodplain mapping and uncertainty analysis. A key focus is identifying the best methods for determining streamflow values for floodplain delineation that accounts for climate change. Traditional flood frequency analysis (FFA) assumes floods follow a single distribution, which may not hold when multiple mechanisms (snowmelt, rainfall, rain-on-snow) drive flooding. Mixed distributions can address this but require splitting flood records by type, increasing uncertainty. Peaks-over-threshold (POT) methods improve estimates but involve subjective choices and assumptions. Flood type identification often relies on seasonality or conditions during the event. This work intends to improve FFA realism by using novel Metastatistical approaches that incorporate both extreme and ordinary events to better represent physical flood-generating processes.

9 CLIMATE CHANGE AND HURRICANE IMPACTS TO ATLANTIC COASTS

9.1 Summary

This project applies a suite of coastal numerical models to assess storm-driven inundation in vulnerable Atlantic Canada sites. The approach combines a regional Delft3D–SWAN hydrodynamic-wave model for Nova Scotia's coast, high-resolution site modelling, and XBeach morphodynamic simulations for overwash and flooding. Martinique Beach serves as the key study site, where field observations include waves, water levels, groundwater, and beach topography. Validated models will be used to evaluate future climate scenarios, including sea-level rise and changing storm characteristics, producing detailed coastal floodplain maps and a transferable methodology for hazard assessment across Canada.

9.2 Objectives

The goal of the proposed research is to strengthen floodplain modelling and mapping science and practice through the development and application of coastal numerical models for extreme storm events. Validated by field observations collected at an exposed ocean beach to measure model performance, the models will be used to simulate the inundation of shorelines on ocean coasts caused by the interaction of surface waves, storm surges, and tides that drive flooding and erosion

9.3 Progress to date

The Scotian Shelf model has been completed and applied to simulate hurricane-driven waves. Field sensors were deployed at Martinique Beach in 2025, with data collected on waves, groundwater, and beach topography. Two major storms caused significant erosion and morphological changes, and all data is now archived and under analysis. Preliminary results have been obtained and presented at a national conference in June 2025.

9.4 Next steps

The reserach team will finalize the fine-scale XBeach model for Martinique Beach using field data for validation and apply it to simulate wave runup and inundation. After analyzing the 2025 data, a second field season will be planned for 2026 to continue monitoring hurricane impacts, with possible adjustments to instrument locations. The first journal manuscript on regional wave modeling will be submitted in 2026, and additional theses and publications are scheduled through 2028.

10 PROBABILISTIC PREDICTIONS OF HYDROLOGICAL EXTREMES ACROSS TIMESCALES AND THEIR INFORMATION-THEORETICAL EVALUATION

10.1 Summary and objective

This project is investigating methods to advance probabilistic extreme flood predictions across timescales for both gauged and ungauged basins, using machine-learning models. A framework for Information-theoretical evaluation of such forecasts will be developed to properly measure forecast quality of the predictive distributions. The expected results are prediction models producing probabilistic flow predictions for approximately 100 locations located mainly in British Columbia and Yukon, which, on average, will show increased reliability of forecasted tail probabilities of extremes compared to benchmark models.

The reliability will be demonstrated through an information-theoretical evaluation framework that will be developed alongside the modeling. This evaluation framework will, for example, use metrics that directly work on forecast distributions, such as Entropy and Kullback-Leibler divergence.

More specifically, the project aims at applying machine-learning (ML) methods to improve the estimation of probabilities of extreme flows in BC and the YT. It will also assess the ability of these ML

methods to accurately estimate the probabilities of extreme flow occurrences, both at gauged and ungauged sites, and for different timescales (from short lead-time forecasts up to long-term exceedance probabilities).

10.2 Progress to date

Progress so far has focused on laying the groundwork for probabilistic flood prediction using machine-learning models. Most of the key predictors and evaluation metrics for estimating flow probabilities have been identified. Three major families of methods for estimating daily flow probability density functions (PDFs) at ungauged sites have been tested across more than 700 basins in the Pacific Northwest, showing comparable performance individually but notable improvements when combined. Preliminary experiments have explored training LSTM-based models using information-theoretical metrics, and the Kullback–Leibler divergence has proven to be a robust measure for assessing PDF accuracy, even under varying flow units and intermittent conditions, provided measurement uncertainty is explicitly accounted for.

10.3 Next steps

- Continue to assess different methods to directly output encodings of full distributions.
- Adapt the previous methodologies to fully ungauged sites.
- Adapt the methodology for large-scale, longer timescales, non-stationary flood frequency analysis.
- Compare previous methods to conventional static methods based on observed flows.
- Adapt the previous methodology to ungauged sites.
- Perform the predictions and estimated non-stationary flood-frequency analyses for ungauged sites and present them in an experimental system.

11 CONCLUSION

Investment in research by the Government of Canada through the Flood Hazard Identification and Mapping Program continues to advance the science of flood mapping in Canada. Outcomes of the research will help practitioners better assess flood hazard under a changing climate.

ICFM 10
Adapting to Global Change:
Innovative Approaches to Flood Management and Resilience
May 20-22, 2026 | Western University, London, Ontario, Canada

Gaming Good Governance: Co-Design of a Serious Game about Overcoming the Barriers of Natural Flood Management

Andrew David Tabas,[1] Ian Pattison,[1] Leo Peskett,[1] and Lindsay Beevers[2]
[1]School of Energy, Geoscience, Infrastructure and Society, Heriot-Watt University, EH14 4AS, Scotland, United Kingdom
E-mail: adt2001@hw.ac.uk

[2]Institute of Infrastructure and Environment, School of Engineering, University of Edinburgh, EH9 3FG, Scotland, United Kingdom

ABSTRACT

Natural Flood Management (NFM) implementation faces many barriers, notably governance and collaboration challenges, at catchment scales. During an embedded research project on NFM implementation in the Allan Water and River Esk catchments in Scotland, United Kingdom, we suggested that serious game co-creation would be an effective tool to improve cooperation. We conducted five 2.5-hour game co-creation workshops aimed at understanding the reality of NFM implementation, the potential purpose of a game, and the elements that could be included in gameplay. We found that the game co-design process led to an improved understanding of NFM implementation. The workshops led to a defined game purpose: players experience the barriers to NFM implementation and try to find ways to overcome these barriers by collaborating at catchment scales. The workshops also led to ideas for elements to be included in the game, such as uncertainty and trade-offs. The game could be a useful resource for catchment stakeholders to increase cooperation.

KEYWORDS: Natural Flood Management; Serious Games; Game Design; Stakeholder Engagement; Decision-Making

1 INTRODUCTION AND LITERATURE REVIEW

Natural Flood Management (NFM) implementation is a complex challenge because it involves coordinating decisions between diverse stakeholders at large spatial scales in the face of uncertainty. Uncertainty exists in two forms, both physical uncertainty about flood risk, and social uncertainty about the decisions that people make (Thorne et al., 2018). For these reasons, NFM has been described as a "wicked problem" (Blackett et al., 2022; Rittel & Webber, 1973; Wingfield et al., 2021).

NFM has been used in pilot projects around the world but has not yet been implemented at a large scale due to various "barriers" (Holstead et al., 2014; Tabas et al., 2025; Wingfield et al., 2021). Catchment organisations often face "complexity" (Waylen et al., 2023). Furthermore, governance challenges, especially constraints at the local government level, make it difficult to upscale NFM (Tabas et al., 2026). Innovative approaches are needed to encourage collaboration to increase NFM implementation.

This paper argues that Serious Game (SG) co-creation is a useful stakeholder engagement tool to enable a deeper understanding of NFM implementation. It presents evidence from a SG co-developed in Scotland with stakeholders from two river catchments, the Allan Water and the River Esk. As explained by Lankford & Craven (2020), "the game design process is valuable in itself." This paper describes the co-

development process for a new game which is focused specifically on understanding and overcoming the barriers to NFM upscaling.

1.1 Serious Games and Flood Risk Management

A game is "a system in which players engage in artificial conflict, defined by rules, that results in a quantifiable outcome" (Salen & Zimmerman, 2003). SGs are a subset of games with a purpose beyond the game such as education, negotiation, and decision-making (Abt, 1987; Djaouti et al., 2011; Uskov & Sekar, 2014). SGs have the potential to build enthusiasm and investment among players (Harteveld & Suarez, 2015; Mendler de Suarez et al., 2012) and can have real-world impact, such as encouraging new types of thinking and "paradigm shifts" (Garcia et al., 2022; Kuhn, 1962).

SGs are uniquely suited to solve wicked problems like the challenge of NFM upscaling because they allow a simulation of different perspectives and decision-making in the face of uncertainty (Mendler de Suarez et al., 2012; Powell et al., 2021). A review of flood-related SGs found diverse types of games: board games and computer games, real and imaginary settings, and emphases on different phases of the disaster cycle (Forrest et al., 2022). Examples of existing SGs related to flooding include a computer game on flood risk management in Millbrook, UK (Khoury et al., 2018), the "Upstream, Downstream" board game simulating farming decisions in Nicaragua and Guatemala (Mendler de Suarez et al., 2012), and a land use-focused game in Scotland (Novotny et al., 2025).

1.2 Designing and Evaluating Serious Games

Triadic Game Design (TGD) conceptualizes SGs as having three key components: a realistic game represents a problem well; a meaningful game achieves a clear purpose; and a fun game keeps players involved (Harteveld, 2011). "Iteration" is an important part of game design (Baaden et al., 2018; Craven et al., 2017; Kellerhals et al., 2021; Salen & Zimmerman, 2003). Co-design can improve how well the game represents the real world (Ball et al., 2021) and give agency to the communities involved in the research (Blackett et al., 2022). Three methods for measuring how well SGs achieve their purpose are before/after questionnaires, in-game observations, and debrief discussions (Forrest et al., 2022).

2 METHODS

The SG co-creation described in this paper emerged from an extensive, four-year embedded research project on NFM implementation in the Allan Water and River Esk catchments in Scotland, UK. This paper aims to answer the following research questions:

1. In what ways can the process of co-creating a SG improve understanding of NFM implementation?
2. What are the central ideas that should be included in a game about NFM implementation?

The Allan Water and River Esk have catchment areas of approximately 200 km^2 and 300 km^2, respectively (Figure 1). The catchments include upstream farms and small towns, and downstream urban areas with significant flood risk. The authors learned that governance-related challenges make NFM upscaling challenging to achieve in practice: it is difficult for catchment stakeholders at various levels (local, national, etc.) to collaborate with each other to implement NFM (Tabas et al., 2026). Based on research by Garcia et al. (2022), Harteveld (2011), and Mendler de Suarez et al. (2012), the researchers recommended that a SG would be an effective method to increase cooperation between upstream and downstream communities. When asked about this idea, catchment stakeholders expressed keen interest in participating in the game design process.

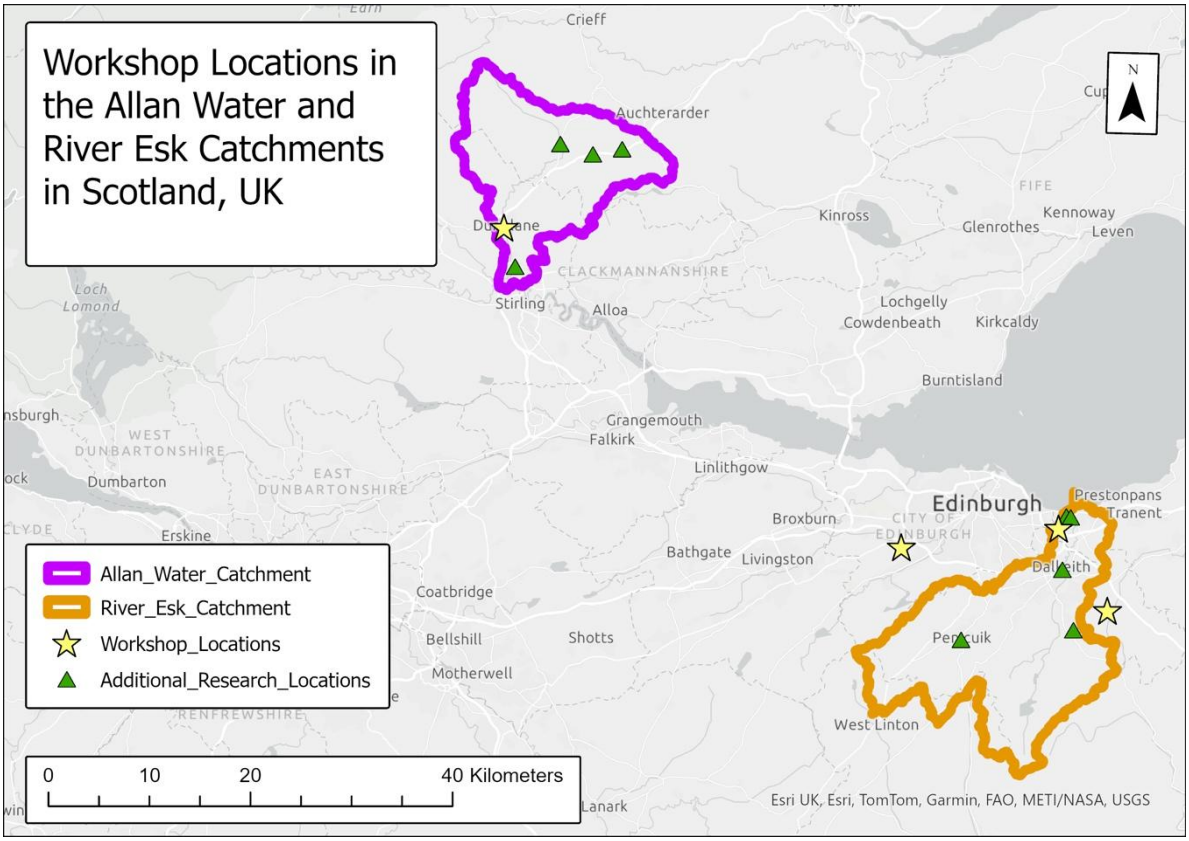

Figure 1: Map showing the workshop locations within the Allan Water and River Esk catchments in Scotland, United Kingdom.

The research team chose the triadic game design (TGD) approach because it provides a clear structure for conceptualizing SGs (Harteveld, 2011). We note that others have used TGD for SG design such as Kellerhals et al. (2021) and Holstead et al. (2026). The fact that TGD's three areas of Reality, Meaning, and Play correspond roughly with Salen & Zimmerman (2003)'s three areas of Rules, Play, and Culture was an added reason for selecting this method. Furthermore, because the research team has experience using TGD to teach undergraduate classes about catchment flood risk management, the team has a familiarity with TGD that made it easier to implement and to explain to the stakeholder co-creation team. The research team also considered advice from Douven et al. (2014) regarding game design to include "imaginary, but realistic" catchments in water management games.

This paper reports on five game co-design workshops with catchment stakeholders and additional data gathering conducted from January – July 2025 in the Allan Water and River Esk catchments. The workshops each had a theme from TGD, as shown in Table 1. Each workshop was 2.5 hours in length, and researchers took handwritten notes and audio recorded discussions. The workshop content is treated like a focus group (Bryman, 2004) for data analysis purposes. Quotes include a participant code which indicates where the workshop was conducted (A1-A12 represents Allan Water participants; E1-E14 represents River Esk participants). Data also includes land managers' responses to questionnaires conducted in-person at a community event in July 2025 to provide additional context.

Table 1: Description of Game Co-Design Workshops and Research, January – July 2025

Workshop Number	Stakeholder Group	Number of Participants (not including facilitators)	TGD Focus Area
1a	Allan Water	10	Reality
1b	River Esk	11	
2a	Allan Water	5	Meaning
2b	River Esk	7	
Additional data	Land managers	15	Reality
3	Combined	3	Play

This research was conducted as part of the project "Making Natural Flood Management at the Catchment Scale a Reality." Phase 1 ethics approval (2023-4979-7567) and Phase 2 ethics approval (2024-9018-12600) were provided by Heriot-Watt University (Edinburgh, Scotland).

3 RESULTS

The game co-design process led to an improved understanding of NFM implementation (section 3.1); a consensus around the reason for developing the game (section 3.2); and initial ideas of elements to include in the game (section 3.3).

3.1 How does Natural Flood Management implementation work?

In workshops 1a and 1b, participants described NFM implementation and its role in flood risk management. First, they listed the key decision-makers: national government and public-sector organisations, local government, landowners, NGOs, communities, and consultants. These organisations have a variety of interests, resources, and priorities, and one of the key governance-related challenges is finding ways for them to cooperate effectively (Tabas et al., 2026). Second, they discussed potential flood resilience measures, including engineered defenses and NFM techniques such as ponds, wetlands, and leaky dams. Third, participants described the various types of land use that exist in Scottish catchments. Initial land uses highlighted in workshops 1a and 1b were urban, agriculture, forestry, peatland, and wetland.

3.2 Why play a game?

Participants were enthusiastic about the potential of a game to inspire change. As stated by one participant, "*I think one benefit of using the gaming approach would be being able to demonstrate the benefits of working together*" (A7). Collaboration therefore emerged as a key theme of the game. Similarly, another participant emphasized the potential of the game to be a tool to increase empathy: "*I think it's a really powerful opportunity for people to potentially role-play and try to understand other peoples' perspectives*" (E14). Based on these and other insights, the following purpose for the game was established: Players experience the barriers to NFM implementation and try to find ways to overcome these barriers by collaborating at catchment scales. This purpose emphasises that the goal of the game is to inspire paradigm shifts (Kuhn, 1962) among the people who play it.

Participants also explained the importance of including NFM's co-benefits beyond flooding-related impacts in the game. As one participant stated, "*Could you also have it show all the different outcomes? You could get rewards for the co-benefits*" (E11). A consideration of NFM's flooding-related benefits would only tell part of the story, missing the implications of these practices for biodiversity, recreation, carbon sequestration, and other ecosystem services.

3.3 What experience will the players have?

The researchers suggested that a multi-player board game would be an effective platform to highlight the social dynamics at play in flood risk management and achieve the purpose stated above. Participants highlighted the importance of including trade-offs in the game: "*Tradeoffs would be, I would think, an interesting part. Priorities, impact, and cost*" (E7). Participants also suggested that the game include uncertainty: "*Include a random element though in it. Because life's random*" (E5). Based on these discussions, balancing trade-offs and managing uncertainty became central features to include in the game. Workshop 2a and 2b participants were invited to sketch what the game could look like. Initial ideas from the workshops (Figure 2) included a variety of designs, with common themes including rivers, catchments, and water drops.

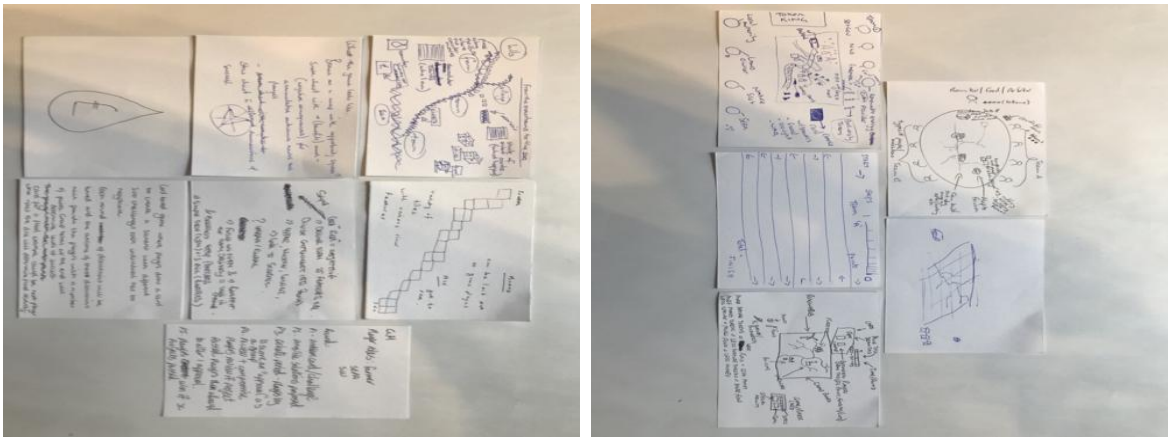

Figure 2: Catchment stakeholders' illustrations of the potential look of the game.

4 CONCLUDING DISCUSSION

Researchers co-designed a SG about NFM implementation with catchment stakeholders in the Allan Water and River Esk catchments in Scotland, United Kingdom. During five workshops and one stakeholder outreach session, the researchers gathered data about views on NFM to inform game design.

This project has resulted in an improved understanding of NFM implementation, a clear purpose for the game, and a list of elements for inclusion in the final game such as uncertainty and trade-offs. These insights will be central to continued game development.

A limitation of this research is that both case studies are located in the same country. Researching this topic in an international context could lead to new insights. However, researchers feel that the lessons learned during game design are of global relevance, as stakeholder cooperation in the face of wicked problems is a universal challenge.

Future research will involve the continuation of game development workshops: the researchers intend to iterate the game and to hold one additional "Balancing" (Harteveld, 2011) workshop in each catchment to ensure that the final game design is effective. Once the game is completed, it will be played with NFM stakeholders in Scotland. Researchers will use questionnaires, observations, and discussions to evaluate whether it is effective (Forrest et al., 2022). The intention is that the game will be an effective tool for changing minds about NFM implementation.

5 ACKNOWLEDGEMENTS

This research is supported by The Hydro Nation Scholars Programme funded by the Scottish Government and managed by the Hydro Nation International Centre (Scottish Funding Council Project

Code: H14002). Many thanks to the game development workshop participants who contributed their time and ideas to this project: without your insight and deep knowledge about NFM in the Allan Water and River Esk catchments, this research would not have been possible. Thank you to Forth Rivers Trust for enabling these catchment connections.

Thank you to the many game experts who shared ideas about how to design games, notably Dr. Pablo Suarez, Dr. Kate Sullivan, and Yvris Burke; as well as Professor Kate Withy for the introduction to the concept of paradigm shifts. Finally, thank you to the many game testers: Dorothy Heinrich; undergraduate and graduate students at Heriot-Watt University; and the Hydro Nation Scholars.

REFERENCES

Abt, C. C. (1987). *Serious Games*. University Press of America.

Baaden, M., Delalande, O., Ferey, N., Pasquali, S., Waldispühl, J., & Taly, A. (2018). Ten simple rules to create a serious game, illustrated with examples from structural biology. *PLoS Computational Biology*, *14*(3), e1005955. https://doi.org/10.1371/journal.pcbi.1005955

Ball, K., Jalbert, K., & Test, L. (2021). Making the board: Participatory game design for environmental action. *Journal of Environmental Studies and Sciences*, *11*(1), 12–22. https://doi.org/10.1007/s13412-020-00645-2

Blackett, P., FitzHerbert, S., Luttrell, J., Hopmans, T., Lawrence, H., & Colliar, J. (2022). Marae-opoly: Supporting localised Māori climate adaptation decisions with serious games in Aotearoa New Zealand. *Sustainability Science*, *17*(2), 415–431. https://doi.org/10.1007/s11625-021-00998-9

Bryman, A. (2004). *Social Research Methods* (Second Edition). Oxford University Press.

Craven, J., Angarita, H., Corzo Perez, G. A., & Vasquez, D. (2017). Development and testing of a river basin management simulation game for integrated management of the Magdalena-Cauca river basin. *Environmental Modelling & Software*, *90*, 78–88. https://doi.org/10.1016/j.envsoft.2017.01.002

Djaouti, D., Alvarez, J., Jessel, J.-P., & Rampnoux, O. (2011). Origins of Serious Games. In M. Ma, A. Oikonomou, & L. C. Jain (Eds.), *Serious Games and Edutainment Applications* (pp. 25–43). Springer. https://doi.org/10.1007/978-1-4471-2161-9_3

Douven, W., Mul, M. L., Son, L., Bakker, N., Radosevich, G., & Hendriks, A. (2014). Games to Create Awareness and Design Policies for Transboundary Cooperation in River Basins: Lessons from the Shariva Game of the Mekong River Commission. *Water Resources Management*, *28*(5), 1431–1447. https://doi.org/10.1007/s11269-014-0562-x

Forrest, S. A., Kubiková, M., & Macháč, J. (2022). Serious Gaming in Flood Risk Management. *WIREs Water*. https://doi.org/10.1002/wat2.1589

Garcia, C. A., Savilaakso, S., Verburg, R. W., Stoudmann, N., Fernbach, P., Sloman, S. A., Peterson, G. D., Araújo, M. B., Bastin, J.-F., Blaser, J., Boutinot, L., Crowther, T. W., Dessard, H., Dray, A., Francisco, S., Ghazoul, J., Feintrenie, L., Hainzelin, E., Kleinschroth, F., … Waeber, P. O. (2022). Strategy games to improve environmental policymaking. *Nature Sustainability*, *5*(6), Article 6. https://doi.org/10.1038/s41893-022-00881-0

Harteveld, C. (2011). *Triadic Game Design*. Springer. https://doi.org/10.1007/978-1-84996-157-8

Harteveld, C., & Suarez, P. (2015). Guest Editorial: Games for Learning and Dialogue on Humanitarian Work. *Journal of Humanitarian Logistics and Supply Chain Management*, *5*(1), 61–72. https://doi.org/10.1108/JHLSCM-01-2015-0005

Holstead, K., Ellen, G. J., Van Doorn-Hoekveld, W. J., & Van den Bergh, L. E. (2026). Balancing reality, meaning, and play for water governance transformation: A triadic game design perspective on the Aquaconnect serious game. *Journal of Cleaner Production*, *538*, 147252. https://doi.org/10.1016/j.jclepro.2025.147252

Holstead, K. l., Kenyon, W., Rouillard, J. j., Hopkins, J., & Galán-Díaz, C. (2014). Natural flood management from the farmer's perspective: Criteria that affect uptake. *Journal of Flood Risk Management*, *10*(2), 205–218. https://doi.org/10.1111/jfr3.12129

Kellerhals, U., Burgess, N., & Wetzel, R. (2021). *Let it Bee: A Case Study of Applying Triadic Game Design for Designing Virtual Reality Training Games for Beekeepers*. (world). Proceedings of the 16th International Conference on the Foundations of Digital Games. https://doi.org/10.1145/3472538.3472558

Khoury, M., Gibson, M. J., Savic, D., Chen, A. S., Vamvakeridou-Lyroudia, L., Langford, H., & Wigley, S. (2018). A serious game designed to explore and understand the complexities of flood mitigation options in Urban-Rural Catchments. *Water (Switzerland)*, *10*(12). Scopus. https://doi.org/10.3390/w10121885

Kuhn, T. (1962). *The Structure of Scientific Revolutions*. University of Chicago Press.

Lankford, B. A., & Craven, J. (2020). Rapid Games Designing; Constructing a Dynamic Metaphor to Explore Complex Systems and Abstract Concepts. *Sustainability*, *12*(17), 7200. https://doi.org/10.3390/su12177200

Mendler de Suarez, J., Suarez, P., Bachofen, C., Fortugno, N., Goentzel, J., Gonçalves, P., Grist, N., Macklin, C., Pfeifer, K., Schweizer, S., van Aalst, M., & Virji, H. (2012). *Games for a New Climate: Experiencing the Complexity of Future Risks*. Pardee Center Task Force Report.

Novotny, I., Ghazoul, J., Dray, A., Wierer, J., & Golling, H. (2025). *ScotScape: Negotiating Landscape Transition in Scotland*. https://negotiating-landscape-scotland.com

Powell, N., Do, T., Bachelder, S., Tattari, S., Koskiaho, J., Hjerppe, T., Väisänen, S., Giełczewski, M., Piniewski, M., & Księżniak, M. (2021). Rethinking Decision Support Under Conditions of Irreducible Uncertainty: Co-Designing a Serious Game to Navigate Baltic Sea Nutrient Enrichment. *Society & Natural Resources*. (world). https://www.tandfonline.com/doi/abs/10.1080/08941920.2021.1934930

Rittel, W., & Webber, M. (1973). Dilemmas in a General Theory of Planning. *Policy Sciences*, *4*(2).

Salen, K., & Zimmerman, E. (2003). *Rules of Play: Game Design Fundamentals*. MIT Press.

Tabas, A. D., Pattison, I., Peskett, L., & Beevers, L. (2025). Spatial relationships matter: How a spatial lens can illuminate barriers and motivators of natural flood management. *Environmental Science & Policy*, *174*, 104259. https://doi.org/10.1016/j.envsci.2025.104259

Tabas, A. D., Pattison, I., Peskett, L., & Beevers, L. (2026). Multi-level governance for effective natural flood management: Different roles at different scales. *International Journal of Water Governance, 13.* https://doi.org/10.59490/ijwg.13.2026.8005

Thorne, C. r., Lawson, E. c., Ozawa, C., Hamlin, S. l., & Smith, L. a. (2018). Overcoming uncertainty and barriers to adoption of Blue-Green Infrastructure for urban flood risk management. *Journal of Flood Risk Management*, *11*(S2), S960–S972. https://doi.org/10.1111/jfr3.12218

Uskov, A., & Sekar, B. (2014). Serious games, gamification and game engines to support framework activities in engineering: Case studies, analysis, classifications and outcomes. *IEEE International Conference on Electro/Information Technology*, 618–623. https://doi.org/10.1109/EIT.2014.6871836

Waylen, K. A., Blackstock, K. L., Marshall, K., & Juarez-Bourke, A. (2023). Navigating or adding to complexity? Exploring the role of catchment partnerships in collaborative governance. *Sustainability Science*, *18*(6), 2533–2548. Scopus. https://doi.org/10.1007/s11625-023-01387-0

Wingfield, T., Macdonald, N., Peters, K., & Spees, J. (2021). Barriers to mainstream adoption of catchment-wide natural flood management: A transdisciplinary problem-framing study of delivery practice. *Hydrology and Earth System Sciences*, *25*(12), 6239–6259. Scopus. https://doi.org/10.5194/hess-25-6239-2021

ICFM 10
Adapting to Global Change:
Innovative Approaches to Flood Management and Resilience
May 20-22, 2026 | Western University, London, Ontario, Canada

When Creeks Spill into Cities: Flood Forecasting and Warning, and Interagency Coordination

Rita Lucero[1] and Nick Lorrain[2]
Toronto and Region Conservation Authority - Flood Risk Management, Toronto, Ontario, Canada[1]
E-mail: Rita.Lucero@trca.ca

TRCA, 5 Shoreham Drive, Toronto, Ontario, Canada[2]
E-mail: Nick.Lorrain@trca.ca

ABSTRACT

In July and August 2024, the Dixie-Dundas neighbourhood in the City of Mississauga, Ontario experienced two severe storm events that exceeded the 100-year storm threshold in parts of the Little Etobicoke Creek subwatershed. The neighbourhood is located within a floodplain spill area where flows from Little Etobicoke Creek overtopped its banks and spilled into the urban environment travelling along roadways and private properties creating a combination of riverine and urban flooding, resulting in significant impacts to people, infrastructure, and property.

Flood risk management in Ontario operates through a shared responsibility framework involving municipalities, conservation authorities, and the Province of Ontario. This paper presents a case study of how this framework functioned during the 2024 storm events, drawing on the experience of Toronto and Region Conservation Authority and its municipal partners. The paper describes flood conditions in the Little Etobicoke Creek subwatershed, flood and monitoring systems, flood forecasting and warning actions that were taken during the events, and post event documentation and risk reduction efforts.

The 2024 storms tested flood forecasting and warning systems, and interagency coordination under extreme rainfall conditions. Lessons from this case highlight the importance of detailed floodplain mapping, real time monitoring, clear and timely flood communications, site specific emergency planning, and sustained collaboration between conservation authorities and municipalities. The findings offer practical insights for flood management agencies managing compound flooding risks in highly urbanized watersheds.

KEYWORDS: flood forecasting and warning, shared responsibility, urban flooding, floodplain mapping, emergency response, watershed management

1 INTRODUCTION

Insured losses from weather events have been climbing for years (Web-1), and climate related infrastructure costs are expected to increase significantly without increased investment in risk reduction (Web-2). This is placing growing pressure on flood forecasting, warning, and emergency response systems, and infrastructure to achieve long term risk reduction. These challenges are particularly acute in highly urbanized watersheds (Konrad, 2003, p. 3), where intense rainfall can overwhelm the capacity of both river systems and municipal drainage infrastructure, producing both overland and basement flooding that requires rapid coordination among multiple agencies.

In Ontario, Canada, flood risk management operates through a shared responsibility framework involving municipalities, conservation authorities (CA's), the Province of Ontario, and the public. This framework, known as Ontario's flooding strategy, builds on the four core components of emergency management, namely mitigation, preparedness, response, and recovery (Ontario Ministry of Natural Resources and Forestry, 2020, p. 5). Two of the key responsibilities in this framework are to manage urban drainage infrastructure and undertake emergency response. Conservation authority responsibilities differ from that of municipalities with regards to flood risk management. CA's focus on anticipating flooding risks through riverine floodplain modelling and mapping, real-time monitoring of weather and watershed conditions, forecasting and warning of increasing flood risks, providing technical support to emergency response providers during flood events, and documenting conditions following events. Floodplain modelling and mapping services also support land development regulations, whereby land development restrictions limit the creation of additional riverine flood risk exposure. Keeping the public safe during severe storms depends on strong interagency coordination before, during, and after flood events, and this framework reinforces interagency coordination.

Toronto and Region Conservation Authority (TRCA) is one of 36 conservation authorities in Ontario (Web-3) and supports municipal partners across nine watersheds draining into Lake Ontario (Web-4). This paper presents a case study of collaborative flood risk management in the Little Etobicoke Creek subwatershed, with a focus on the Dixie Dundas neighbourhood in the City of Mississauga, one of the highest ranked riverine flood vulnerable clusters within the TRCA jurisdiction. The neighbourhood is located within a floodplain spill area of Little Etobicoke Creek and has experienced significant flooding during major summer storm events, including July 8, 2013, and two severe events in July and August 2024.

Using the 2024 storm events as a focal point, this paper describes existing flood risk conditions, floodplain mapping and watershed monitoring systems, flood forecasting and warning actions, and post event collaboration with municipal and regional partners. The objective is to illustrate how Ontario's shared responsibility model functions during extreme rainfall and highlights practical lessons for flood communications, emergency preparedness, and long-term flood mitigation planning in highly urbanized watersheds.

2 EXISTING FLOOD RISK IN LITTLE ETOBICOKE CREEK SUBWATERSHED

2.1 Dixie-Dundas Flood Vulnerable Cluster

TRCA's 2018 Flood Risk Assessment and Ranking Project identified and ranked clusters of roads and structures at risk of riverine and overland flooding across its jurisdiction (IBI Group, 2019). This study undertook detailed flood damage analysis considering expected flood depths across a spectrum of storm events allowing a consistent approach for quantifying and prioritizing flood risks between vulnerable clusters. Being able to quantify potential damages is critical for risk mitigation and remediation planning as well as emergency and disaster response planning.

Two Flood Vulnerable Clusters were identified along Little Etobicoke Creek in the City of Mississauga, between Eglinton Avenue and south of Dundas Street East. Flooding within this highly urbanized subwatershed typically occurs during the 100-year event or larger regional storms as a result of the majority of the watershed not having stormwater management controls (<22% of the urbanized area employs modern stormwater management controls (Toronto and Region Conservation Authority, 2021, p. 42). Within TRCA's jurisdiction, the 100-year event refers to the storm event with a 1% chance of occurring each year in a specific location, while the regional storm is a historical storm that is derived from the Hurricane Hazel storm that impacted Ontario in 1954. TRCA's jurisdiction encounters and has experienced both short duration intense storm events (e.g., thunderstorms), and longer large volume storm events (e.g., hurricane events).

The Dixie Dundas Flood Vulnerable Cluster is located near the intersection of Dixie Road and Dundas Street East and includes areas designated as a provincial Special Policy Area (Web-5). A Special Policy Area is a land use policy planning tool that allows a historically developed area within a floodplain to continue to exist while limiting intensification. The cluster is ranked first in flood risk within the Region of Peel and third overall across the TRCA jurisdiction. It is fully urbanized, consisting primarily of commercial and industrial land uses with adjacent high density residential areas. The combination of dense development, floodplain spill behaviour, and limited attenuation capacity makes this cluster particularly susceptible to short duration, high intensity summer storms, as demonstrated during flood events in 2013 and 2024.

2.2 Floodplain mapping

In 2015, TRCA completed an updated floodplain mapping study for the Dixie Dundas and Applewood Special Policy Area to improve characterization of flood risk within and adjacent to the SPA. The study used high resolution topographic data and two dimensional (2D) hydraulic modelling, using MIKE Flood modelling software, to assess flood behaviour under extreme storm conditions.

The analysis identified a significant floodplain spill area along Little Etobicoke Creek upstream of the Dixie Road crossing, where creek flows overtop the channel and spread laterally into surrounding urban areas. This spill mechanism increases flood exposure beyond the SPA boundaries and contributes to downstream impacts during major storm events.

Subsequent studies by the City of Mississauga extended floodplain coverage downstream into the Credit Valley Conservation Authority jurisdiction, confirming that flood impacts extend across conservation authority boundaries. The mapping results have directly informed flood forecasting and warning operations, site specific flood risk packages, land use decisions, and the development of long term flood mitigation strategies for the Dixie Dundas area (McKay & Hofbauer, 2024).

2.3 Existing flood mitigation measures and studies

Following the July 8, 2013, storm event, the City of Mississauga and TRCA initiated a series of technical studies to better understand flood mechanisms and evaluate mitigation options within the Little Etobicoke Creek subwatershed. These studies focused on areas with the highest flood risk, including the Dixie Dundas Flood Vulnerable Cluster.

TRCA developed a detailed 2D hydraulic model of Little Etobicoke Creek, and the City of Mississauga completed two Municipal Class Environmental Assessment studies examining riverine flooding associated with floodplain spill and pluvial flooding resulting from capacity exceedance of the storm sewer system. Together, these studies assessed a range of structural and non-structural mitigation options in a fully urbanized environment with limited space for large scale infrastructure.

The outcomes of these studies have informed both long term flood mitigation planning and short-term preparedness measures, including emergency response planning and enhancements to flood forecasting and warning. As of 2024, the City of Mississauga had completed an Environmental Assessment focused on reducing flood risk in the Dixie Dundas area, providing the basis for advancing future infrastructure solutions.

2.4 TRCA Monitoring and Flood Infrastructure

TRCA operates a network of precipitation and water level monitoring stations within the Little Etobicoke Creek subwatershed to support its Flood Forecasting and Warning Program. Near real time data from these stations are used to assess watershed response during storm events and to inform flood

messaging and coordination with municipal emergency response agencies. The data from this system is available to emergency management personnel and the public in real-time at 5-minute intervals (Web-6).

The monitoring network includes a stream gauge located upstream of the Dixie Dundas area and a precipitation station within the subwatershed. While these stations do not provide direct discharge measurements, they offer critical information on rainfall intensity, water level trends, and rates of rise during extreme events. This information supports situational awareness and decision making under rapidly changing conditions.

In addition to monitoring, flood control infrastructure exists along portions of Little Etobicoke Creek, including flood walls, channels, and dike systems constructed to reduce flood risk from higher frequency storm events. While these structures provided localized protection, the 2024 storm events exceeded their design capacity, reminding us that structural flood protection solutions can provide a false sense of security, and reinforcing the need for flood forecasting, emergency planning, and long term removal of risks rather than defense against risks.

2.5 Emergency planning

Conservation authority flood forecasting and warning data along with mapping supports municipal emergency response during riverine flood events. Little Etobicoke Creek responds rapidly to rainfall leading to very small flood warning lead times. Site specific planning is critical to minimizing emergency response actions once flooding is expected.

In response to the high risk ranking of the Dixie Dundas Flood Vulnerable Cluster, TRCA worked with the City of Mississauga and the Region of Peel to develop a Site Specific Flood Risk Package for this area. The package provides location specific flood hazard information, identifies vulnerable infrastructure and properties, and supports municipal decision making during flood events, including road closures, evacuations, and resource deployment.

This site specific approach strengthened coordination between TRCA and municipal emergency management agencies and played an important role in informing response actions during the 2024 storm events. It also provided a foundation for post event updates to emergency planning and preparedness within the subwatershed.

3 SUMMARY OF 2024 FLOODING EVENTS

The summer of 2024 presented exceptionally challenging hydrometeorological conditions across the Toronto and Region Conservation Authority jurisdiction, culminating in two severe rainfall events that stress-tested flood forecasting, warning, and municipal emergency response systems. Antecedent wet conditions amplified the impacts of the first storm event, which occurred on July 16.

Rainfall totals in June and July far exceeded long term averages, resulting in saturated soils across southern Ontario prior to the July 16 event. Over 100 mm of rain in June and 215 mm in July were recorded at Environment Canada's Toronto Pearson Airport weather station —well above the monthly average of approximately 75 mm for each month (Web-7). The July total exceeded the previous monthly record set in October 1954 during Hurricane Hazel (Web-7). Rainfall from the remnants of Hurricane Beryl on July 10–11, and multiple thunderstorms between July 12–15 saturated soils across southern Ontario and the GTA, which reduced infiltration capacity and increased runoff potential prior to the July 16 event.

On July 16, sustained heavy rainfall occurred for 3–4 hours, with the most intense precipitation affecting Mississauga and Toronto. Rainfall totals across TRCA watersheds ranged from 8 mm to 102 mm,

with intensities between 5 mm/hr and 58 mm/hr, highest in the western and southern areas. Storm return period analysis showed significant variation, with the largest return period recorded in the Little Etobicoke Creek sub-watershed, slightly exceeding the 100-year storm threshold.

3.1 Flood forecasting and warning actions during the July 16, 2024, event

During the July 16 storm, TRCA actively monitored watershed and weather conditions in accordance with internal procedures and Provincial guidelines for flood event messaging (Toronto and Region Conservation Authority, 2025, pp. 11-13). Flood messaging was escalated as conditions and weather forecasts deteriorated. A Flood Watch was issued at 9:30 AM, followed by a Flood Warning at 11:30 AM as rainfall intensities increased and water levels rose rapidly across multiple watersheds. A Flood Watch is issued when flooding is possible and is intended to advise municipalities, emergency services, and individuals in flood vulnerable areas to prepare for possible flooding impacts, while a Flood Warning indicates that flooding is imminent or already occurring, and is the highest level of messaging. Flood messages were distributed through established channels to municipal partners, emergency response agencies, media, and the public.

The escalation to Flood Warning coincided with TRCA activating its emergency storm event procedures. These procedures were guided by Emergency Management Ontario's Incident Management System (IMS), a standardized framework used by TRCA to support municipal coordination of emergency response actions (Web-8). In addition, TRCA engaged in direct communications with affected municipalities and agencies. These direct phone communications with municipal emergency management and transportation agencies supported real time coordination of response actions during the rapidly developing event.

3.2 Flood impacts during the July 16, 2024, event

Flood impacts during the July 16 event reflected the combined effects of riverine flooding and exceedance of urban drainage systems. Within the City of Mississauga, water levels along Little Etobicoke Creek rose rapidly and overtopped channel banks within one and a half hours of the onset of rain, resulting in a major floodplain spill near the Dixie Road and Dundas Street East intersection. Floodwater extended beyond the regulated floodplain, impacting roads, commercial and industrial properties, and adjacent residential areas within the Dixie Dundas Flood Vulnerable Cluster.

Impacts included significant flooding at the Tyndall Seniors Residence, where emergency evacuations were required (Web-9). Flooding patterns observed during the event were consistent with previous floodplain mapping and hydraulic modelling, validating existing risk assessments. Additional impacts occurred across the City of Toronto, including flooding of major transportation corridors such as the Don Valley Parkway (web-10), further demonstrating the vulnerability of highly urbanized systems under extreme rainfall conditions.

3.3 August 17, 2024, storm event and comparative impacts

A second severe rainfall event occurred on August 17, 2024, approximately one month after the July storm. Slow moving thunderstorms produced intense short duration rainfall, with peak totals exceeding those observed on July 16, 2024, with 136 mm of rainfall. Flooding again affected the Dixie Dundas Flood Vulnerable Cluster, with floodplain spill behaviour similar to that observed during the earlier event.

The close succession of the July and August storms reduced recovery capacity and amplified cumulative impacts. Together, the events highlighted the vulnerability of highly urbanized watersheds to both sustained wet periods and intense convective storms and provided an opportunity to evaluate the consistency of flood response actions and communication strategies under repeated extreme conditions.

4 POST EVENT ACTIVITIES AND MULTI-AGENCY COLLABORATION

4.1 TRCA Flood Communications

Flood messaging is a core component of TRCA's Flood Forecasting and Warning Program and a primary mechanism for communicating flood risk to municipalities, emergency response providers, media, and the public. Following the July and August 2024 storm events, post event discussions with municipal partners and elected officials identified opportunities to improve the accessibility and immediacy of flood message communications, particularly for residents in high risk areas.

In response, TRCA expanded its public flood message distribution to include text message notifications in addition to emails, and then promoted the new notification option using a combination of social media advertising and messaging during public meetings. This enhancement was added to better align with how residents access time sensitive information and to complement existing communication channels. By the end of 2025, public subscription to flood messages had increased, by approximately 130%, indicating improved reach and uptake of flood warning information. TRCA also worked with municipal partners to display flood messages directly on municipal websites to reinforce consistent messaging across jurisdictions.

4.2 Municipal collaboration

The 2024 storm events required close coordination between TRCA and municipal partners across the response phase of emergency management. Following the events, TRCA staff coordinated post event data collection, including documentation of high water marks and verification of monitoring records, to support flood analysis and validation of existing flood models.

TRCA also engaged with municipal staff through technical meetings, site visits, and debriefing sessions to review flood response actions, identify priority impact locations, and discuss opportunities for improvement. These collaborative efforts supported a shared understanding of flood mechanisms and response challenges and informed future mitigation and preparedness priorities.

4.3 Preparedness and updates to emergency planning

Post event reviews emphasized the importance of preparedness and continuous improvement in emergency planning. TRCA supported municipal emergency management activities, including training exercises and debriefing sessions, to evaluate communication pathways and interagency coordination during fast developing flood events.

A key outcome of these efforts was the updating of the Dixie Dundas Site Specific Flood Risk Package to incorporate lessons learned from the 2024 flood events. Flood risk mapping and emergency planning were also expanded to include a second Flood Vulnerable Cluster within the Little Etobicoke Creek subwatershed that experienced significant impacts during the storms. These updates strengthen the ability to respond quickly during future events in the communities.

4.4 Future flood mitigation projects

Advancing long term flood mitigation projects remains a priority following the 2024 storm events. TRCA continues to work with municipal, provincial, and federal partners to support flood mitigation planning and to pursue external funding opportunities. While federal and provincial programs have enabled progress on floodplain mapping and infrastructure projects, competition for funding and complex implementation timelines remain ongoing challenges.

Within the Dixie Dundas area, collaboration with the City of Mississauga and the Region of Peel is focused on identifying phased mitigation solutions that provide the greatest flood risk reduction within feasible timeframes. These efforts highlight the importance of sustained interagency collaboration and long term investment in flood mitigation to address increasing risks associated with extreme rainfall and urbanization.

5 CONCLUSION

The July and August 2024 storm events in the Little Etobicoke Creek subwatershed illustrate the increasing complexity of flood risk management in highly urbanized watersheds under extreme rainfall conditions. Flooding in the Dixie Dundas neighbourhood resulted from the combined effects of riverine overflow and the exceedance of urban drainage systems, reinforcing the need for coordinated approaches that extend beyond individual jurisdictions and infrastructure systems.

This case study demonstrates how Ontario's shared responsibility framework for flood risk management functions in practice during severe events. Conservation authorities contribute impartial science based expertise through floodplain mapping, monitoring, and flood forecasting and warning, while municipalities lead emergency response and recovery activities. The 2024 events highlighted the importance of timely escalation of flood messaging, established communication pathways, and strong interagency relationships developed in advance of extreme events.

Post event learning and adaptation following the 2024 storms strengthened preparedness through updated emergency planning, improved flood communications, and continued collaboration on flood mitigation planning. At the same time, the events underscored ongoing challenges related to the pace of and complexity of implementing large scale mitigation projects in built up environments.

As extreme rainfall events become more frequent and intense, the experience from the Dixie Dundas neighbourhood highlights the value of detailed floodplain mapping, real time monitoring, and sustained collaboration as foundational elements of flood resilience. While the institutional context in Ontario is specific, the lessons from this case study are broadly applicable to other jurisdictions managing compound flooding risks in urban watersheds.

6 ACKNOWLEDGEMENTS

The authors thank David Kellershohn for his valuable input and review of this paper, and the efforts of TRCA staff, municipal staff, members of the public, and public officials that were involved with the emergency response and post-storm actions, discussions, and collaborative activities.

7 REFERENCES

IBI Group. (2019). *Toronto Flood Risk Ranking.* Toronto: Toronto and Region Conservation Authority. Retrieved from https://trcaca.s3.ca-central-1.amazonaws.com/app/uploads/2021/04/13132621/TRCA-FloodRiskAssessment_forweb-updated04_13_2021.pdf

Konrad, C. P. (2003). *Effects of Urban Development on Floods.* Tacoma, WA: U.S. Geological Survey - Water Resources.

McKay, A., & Hofbauer, K. (2024). *Dixie-Dundas Flood Mitigatoin Project, Municipal Class Environmental Assessment, Environmental Study Report, Little Etobicoke Creek.* Guelph: Matrix Solutions Inc. Retrieved from https://www.mississauga.ca/wp-content/uploads/2024/06/19152312/dixie-dundas-flood-mitigation-environmental-assessment-study.pdf

Ontario Ministry of Natural Resources and Forestry. (2020). *Protecting People and Property: Ontario's Flooding Strategy.* Government of Ontario. Retrieved from https://files.ontario.ca/mnrf-2020-flood-strategy-en-2020-03-07.pdf

Toronto and Region Conservation Authority. (2021). *Etobicoke Creek Watershed Characterization Report.* Toronto: Toronto and Region Conservation Authority.

Toronto and Region Conservation Authority. (2025). *2025 Flood Contingency Manual.* Toronto: Toronto and Region Conservation Authority.

WEB SITES:

Web-1: https://www.ibc.ca/news-insights/news/august-flooding-in-gta-and-parts-of-southern-ontario-caused-over-100-million-in-insured-damage, consulted 20 October 2025.

Web-2: https://fao-on.org/en/report/cipi-summary/, consulted 20 November 2025.

Web-3: https://conservationontario.ca/conservation-authorities/find-a-conservation-authority, consulted, 11 December 2025.

Web-4: https://trca.ca/about/, consulted 30 September 2025.

Web-5: https://www.mississauga.ca/projects-and-strategies/city-projects/dundas-street-special-policy-area-review/#heading-resources, consulted 9 October 2025.

Web-6: https://trcagauging.ca/gauge/little-etobicoke-dixie-wl, consulted 21 December 2025.

Web-7: https://www.theweathernetwork.com/en/news/weather/forecasts/current-toronto-officially-records-its-rainiest-month-ever, consulted 20 October 2025.

Web-8: https://www.ontario.ca/document/incident-management-system-ims-guidance-version-2/section-1-introduction, consulted 22 December 2025.

Web-9: https://thepointer.com/article/2024-07-29/11-years-2-destructive-floods-millions-in-damages-why-hasn-t-mississauga-moved-quicker-to-protect-residents, consulted 23 September 2025.

Web-10: https://www.thestar.com/news/gta/why-the-massive-don-river-redesign-won-t-stop-flooding-on-the-dvp-but-what/article_e5262da2-439a-11ef-84fd-03a972f5db59.html, consulted 13 October 2025.

ICFM 10
Adapting to Global Change:
Innovative Approaches to Flood Management and Resilience
May 20-22, 2026 | Western University, London, Ontario, Canada

Hazard zone planning in Austria – a tool to link flood risk management and settlement development

Clemens Neuhold
Flood Risk Management Directorate, Federal Ministry of Agriculture and Forestry, Climate and Environmental Protection, Regions and Water Management, Vienna, Austria
clemens.neuhold@bmluk.gv.at

ABSTRACT

The focus of flood risk management in Austria is on retaining water where possible and constructing protecting infrastructure where needed. During recent decades, the approach of managing flood risk changed significantly, driven by lessons learnt from severe flood events. Flood protection nowadays is complemented with ecological and hydro-morphological goals as well as tools to reduce - and even avoid - new risks in potentially inundated areas. Spatial planning and building regulation obligations and permits proved to be particularly efficient when it comes to risk avoidance. In a federal state like Austria, this is a challenging task, as the water legislation is being taken care of on federal level and the legislation for spatial planning, building regulation, emergency management and nature conservation is being defined on provincial level. Furthermore, municipalities generally regulate zoning and issuing of building permits. Therefore, there was a clear need to link the administrative levels and sectors to ensure a flood-aware settlement development.

Decisions for zoning and construction permits, however, have to be made upon reliable basis which is provided by an advisory opinion of flood risk managers derived from two dimensional hydrodynamic models. The decision criteria are related to flood intensities with recurrence intervals of 100 and 300 years. This ensures that risk and residual risk is considered, as the strived design level of dykes and retention basins in Austria is a 100-year flood event. In a first step, the hazard is calculated based on flood intensities for the 100-year flood event and subdivided in yellow and red zones. These zones are referenced in the spatial planning regulations and building codes accordingly, as red zones have to be kept free of development and for yellow zones there are at least some obligations to fulfil when building inside these zones. Based on the 300-year flood recurrence interval, zones with specific hydrological function are defined. These zones need to be kept free as they serve for retaining water, providing conveyance routes for extreme events and avoid the increase of flood risk further downstream. The delineation of zones as well as respective exposures are, in a first step, consulted with the public and interested parties. Based on feedback from public participation, the final version is elaborated and approved by the minister for water management. If significant hydrological changes are observed in the catchment area or flood related parameters change due to occurred flood events or climate change, the hazard zone plan has to be reviewed and revised accordingly.

The findings of a decade of implementing this coordination approach to close the gap between flood risk management, spatial planning and building regulation show that advisory opinions with a plot scale resolution provide reliable information for decision making on local level. However, they also require significant resources especially for the active involvement of potentially affected citizens.

KEYWORDS: Flood Risk Management, Austria, Hazard Zone Plan, Spatial Planning, Building Regulation, Settlement development, Risk avoidance

1 INTRODUCTION

The total number of approximately 9 million inhabitants in Austria whereof 1,4 million people live or work in areas prone to floods combined with a limited area suitable for permanent settlement due to topographical boundary conditions makes a sound approach in managing flood risk inevitable. In post-World War II decades, food security was of utmost priority. However, priorities changed significantly over time, essentially driven by flood events. Until the 1960s, flood protection by embankments and river straightening as well as land drainage were state of the art, reflecting the strong confidence in the ability to control rivers. In the middle of the 1960s, in two consecutive years 1965 and 1966, this concept proved wrong in large parts of southern Austria. Rivers overtopped dykes and inundated whole valley plains mainly used as arable land.

These catastrophes were the starting point to rethink the approach of dealing with floods in Austria by incorporating environmental goals such as retaining water in floodplains. An ecologically oriented flood management was established, prioritizing water retention over embanking rivers.

After some decades without severe flood events in Austria, the event in 2002 along the Danube and 2005 in Alpine areas stressed the need for an intersectoral, forward looking approach of flood risk management. Not only first signs of climate induced changes in frequency and severity of flood events led to casualties and significant damages, but especially human behaviour in terms of settlement development highlighted the need for an anticipatory approach to reduce and, where possible, avoid flood risk.

Therefore, two comprehensive research projects in close cooperation with administration were set up including all relevant sectors with the potential of contributing to risk reduction. The need for intensified cooperation with spatial planning, building regulation and emergency management in all phases of the risk cyle was one of the key conclusions in terms of setting up a new understanding on how to manage flood risk. Key conclusions related to the 2002 and 2005 flood events also triggered the negotiations of the EU Floods Directive under Austrian Presidency in 2006. After only one and a halfyears of negotiation, the Directive for the Assessment and Management of Flood Risk (2007/60/EC) was set into force in 2007. This was the starting point of a holistic management approach accompanied by an institutionalised inter-sectoral cooperation (Web-1).

After the implementation of the EU Floods Directive, two more large-scale flood events – comparable to the event in 2002 – hit Austria in 2013 and 2024. Measures for flood retention and flood protection, implemented in cooperation with river basin management, nature conservation, recreation, agriculture and forestry, spatial planning, building regualtion and emergency management, proved to be efficient, as overall monetary damages decreased.

One of the lessons learnt will be discussed in the paper, as reliable information from flood risk management is the key foundation for making robust decisions in spatial planning and building regulation. This link is being ensured by the hazard zone planning process which is a participative and, therefore, awareness raising and well accepted approach including the potentially affected population (Web-2).

2 THE HAZARD ZONE PLAN

As a local planning tool on plot scale, the hazard zone plan aims at achieving multiple goals: The overarching one is to avoid the generation of new flood risk, further ones are to reduce existing risks and at the same time raise awareness. These multiple benefits are achieved through an institutionalised inter-sectoral cooperation amongst flood risk management, spatial planning and building regulation authorities. The hazard zones are based on the results of a 100-year flood event referring to the current situation of settlement development and hydrologic boundary conditions, whereas, the areas with a specific function are used as a tool for future decisions and are based on a 300-year flood event. They are based on the same model, however, with different decision spheres.

A hazard zone plan, which generally corresponds to a map scale of 1:2000, is based on 2D hydrodynamic model results. The models are based on an 1x1 m elevation model which is available for the whole territory of Austria. Relevant topographic characteristics are complemented by terrestrial survey. Hydrologic boundary conditions are based on gauge data or precipitation-runoff models.

Calibration and validation are done by reference measurements or documented historic events. The main outputs of these models are maps of inundation areas, water depths, and flow velocities for each hydrologic scenario.

Based on the hydrodynamic model results, a flood risk manager distinguishes and identifies relevant hazard zones and areas with a specific function or indication as an advisory opinion. In this process the model results are revised to identify potential conveyance routes, areas to retain water, spillway options and the smoothing of model results by delineating the inundation area considering calculated low value water depth and the deletion of islands resulting out of e.g. houses, installations, etc. in the digital terrain models.

2.1 Hazard Zones

Hazard zones are identified based on the flood intensity (Figure 1). A function of water depth and flow velocity distinguishes between yellow and red hazard zones within the inundation area of 100-year flood scenarios. This indicates yellow zones - areas where building obligations or adaptation of buildings and infrastructure might enable development if absolutely necessary - and red zones, where development and settlement have to be avoided by any means.

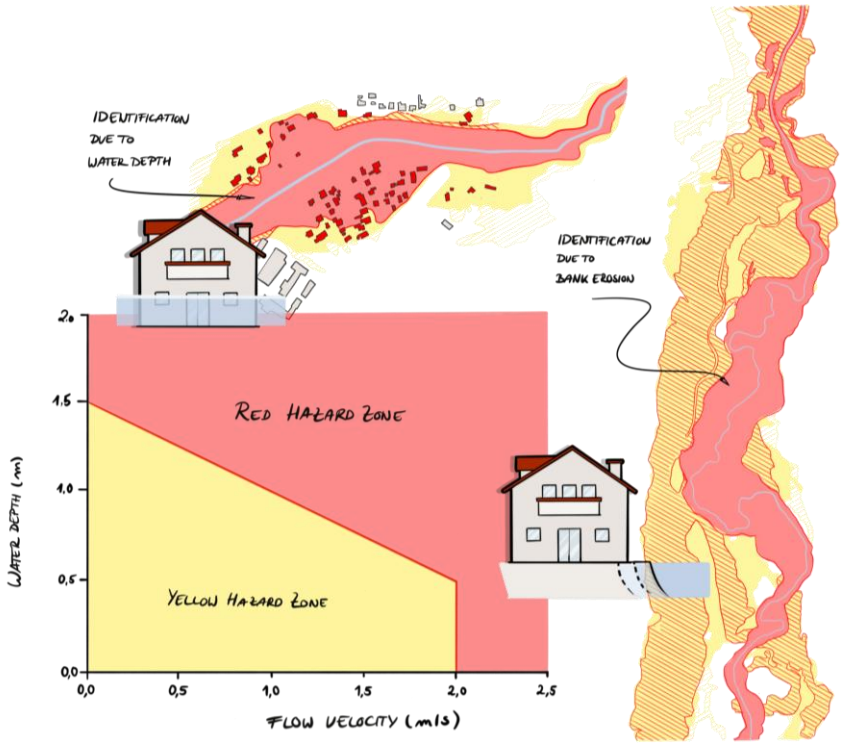

Figure 1: Hazard zones based on 100-year flood scenarios

2.2 Areas with a specific function or indication

In addition to the hazard zones based on 100-year flood scenarios, areas with a specific function or indication are definitions based on 300-year flood scenarios. The primary goal of these area definitions is to avoid risk and increase awareness of residual risk. The areas are indicated as yellow, red and red/yellow shaded areas, accordingly (Figure 2):

Yellow shaded areas indicate areas with no flood protection which are inundated by a 300-year flood scenario, red shaded areas indicate areas with flood protection which are inundated by a 300-year flood, therefor focussing on overtopping and failure scenarios. In terms of awareness raising these areas focus on indicating that total safety is not possible and there is always residual risk.

Figure 2: Areas with a specific function or indication based on a 300-years flood event

Red/yellow shaded areas delineate areas within a 300-year flood scenario with a specific function for the flood process and resulting risk itself. These areas are related to flood conveyance, flood retention and avoidance of increasing the damage potential. To avoid additional risk, these areas shall be kept free of development.

The red/yellow shaded areas are also calculated based on flood intensity and are, therefore, based on the same method like the red and yellow zones. The intensity diagram to calculate the areas with a specific function is pictured in Figure 2.

2.3 Legal context

Austria as a federal state has two levels of jurisdiction – the federal level and the level of nine provinces. The water law as a federal law has, therefore, to be implemented by all federal provinces. At the same time flood risk management as part of the water law can only provide recommendations for provincial laws such as spatial planning, building regulation and emergency management.

Generally, in all nine provincial legal frameworks it is intended to keep the 100-year flood area free of settlement development and infrastructure. However, due to restricted availability of land especially in alpine areas there are some exemptions. For this reason, the differentiation in yellow and red zones is of hight relevance. As an advisory opinion by flood risk managers the hazard zone plan can be seen as a reliable recommendation to spatial planning and building regulation.

However, in the end these plans can be overruled in the frame of the weighing of different, and sometimes contradicting, interests. For such cases, at least red zones shall be avoided by any means.

In terms of funding flood retention and protection measures the hazard zone plans are a prerequisite. If areas with a specific function are defined to be kept free by the municipality their funding share - which in average is 20 % of the overall investment - is reduced significantly by 5 percentage points.

Depending on the provincial legal framework, there is a strong commitment that red hazard zones are to be kept free from spatial dedication as building area. Some exemptions for the expansion of buildings and settled areas with high land-use pressure e.g. in touristic areas or areas for industry and trade are defined. For yellow zones based on 100-year flood events, the commitment is broad to at least restrict settlement development or oblige for flood adapted construction of new buildings.

For areas with a specific function, spatial planning starts to consider keeping free these areas to secure retention and conveyance areas based on 300-year flood events. These areas also prove as a valuable tool to communicate residual risk. Nevertheless, a stronger incorporation of the advisory opinion on areas with a specific function are of high interest as efficient risk reduction is associated to the planning principle.

In building regulations there is also a strong commitment that red hazard zones, independent from their spatial dedication, do not receive a building permit. For exemptions in yellow zones, conditionality is defined by means of having the ground floor elevated in reference to the 100-year flood level. Filling to elevate the terrain are prohibited, as it can cause deterioration in up- or downstream areas.

2.4 Public participation

To achieve active participation and, at the same time, raise flood awareness, hazard zone plans have to be submitted to the mayor of the respective municipality for four weeks of public consultation. All flood prone inhabitants are invited to review the plan and, if needed, suggest changes. These suggestions are then discussed and, if reasonable, taken care of in the frame of the endorsement of the hazard zone plan.

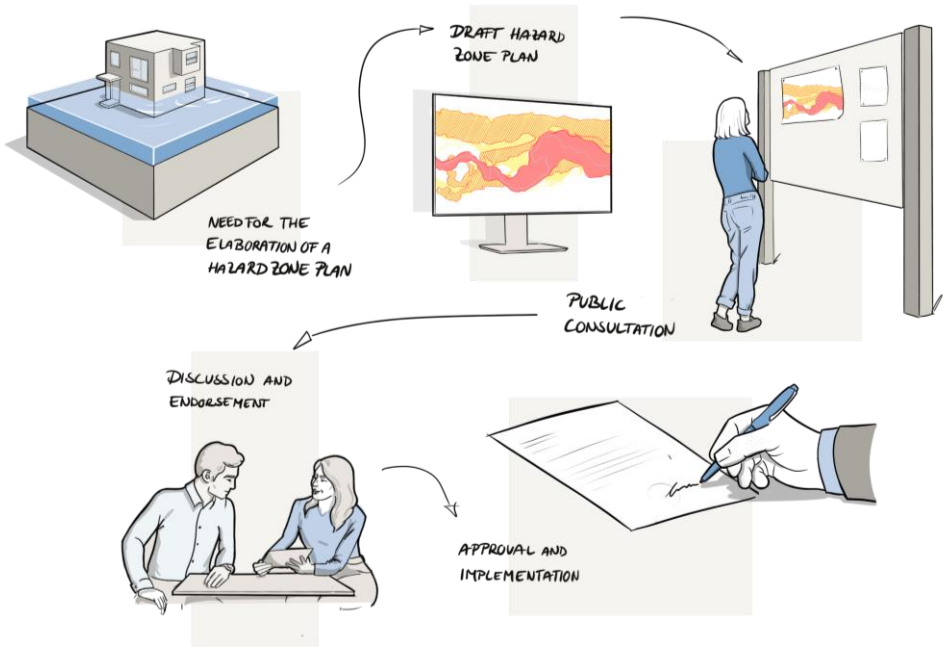

Figure 3: The process of active public participation in the frame of elaborating a hazard zone plan

If significant hydrological changes are observed in the catchment area or flood related parameters change due to occurred flood events or climate change, the hazard zone plan has to be reviewed and revised within the same setup, accordingly.

3 DISCUSSION AND CONCLUSION

Due to the federal administration in Austria, there are different time periods of experience with hazard zone planning in Austria. For torrent and avalanche control in Alpine areas hazard zone plans have been implemented for 50 years, however, applied criteria are differing from those presented in the paper (Web-3). The tool in these areas is widely accepted and well understood by people and the administration. For the water management sector - for rivers and streams - in Austria, hazard zone planning has been systematically applied since 2011. Nevertheless, the tool already proved its applicability in several occasions. Since the hazard zone plan is a funding prerequisite for flood protection and retention measures, the areal coverage of these plans is constantly and significantly increasing. Flood protection and retention measures are generally funded by three entities in Austria: the municipality, the federal province and the federal state. If municipalities commit to keeping areas with a specific function (retention, conveyance, damage potential) free of new settlement development the funding rate by the federal state is higher than without this commitment. This clearly highlights the link provided by flood risk management to spatial planning and building regulation.

This approach institutionalises the effort to avoid new flood risk by keeping potentially inundated areas free from settlement and infrastructure development. At the same time, the designation of hazard zones and areas with a specific function or indication raises awareness and highlights the need (i) for other relevant sectors to take action respectively (ii) for people potentially affected to set measures at their own property, such as demountable barriers or waterproof installations.

For zones with hazard of low probability, the implementation of emergency plans is an effective tool to reduce flood risk through better preparedness for the case of emergency. At the same time, property owners are encouraged to consider object-oriented measures in order to be better prepared for floods.

In terms of flood preparedness and awareness raising, the hazard zone planning approach proofs to be an efficient tool (Web-4). Its incorporation into to the Austrian funding scheme supports the implementation substantially. Achieving key goals – such as the avoidance or risk by keeping free hazard zones, the reduction of risk by adapting buildings in hazard zones or even resettlement and the raising of flood awareness and inherent uncertainties such as overtopping and failure - is therefore a realistic perspective.

The main lessons learned, despite having set up a participatory approach, refer to the permanent need to inform potentially affected people and to keep their level of flood awareness high. One key is to convey and highlight facts and figures on residual risk, uncertainty and the efficiency of self-responsibility for different target groups.

REFERENCES

Web sites:
Web-1: https://www.bmluk.gv.at/themen/wasser/wisa/hochwasserrisiko.html
Web-2: https://www.bmluk.gv.at/themen/wasser/schutz-vor-hochwasser/richtlinien-leitfaeden/technische-richtlinien-fuer-gefahrenzonenplanung.html
Web-3: https://www.bmluk.gv.at/themen/wald/wald-und-naturgefahren/leben-mit-naturgefahren.html
Web-4: https://gefahrenzonenplan.at/

ICFM 10
Adapting to Global Change:
Innovative Approaches to Flood Management and Resilience
May 20-22, 2026 | Western University, London, Ontario, Canada

FROM STATUES TO SYSTEMS: EVALUATING LEGAL AND POLICY COHERENCE FOR BLUE GREEN INFRASTRUCTURE IN ENGLAND AND CANADA

Ruth Awara
Birmingham City University, Birmingham, United Kingdom
Ruth.awara@mail.bcu.ac.uk

Claudia Carter
Birmingham City University, Birmingham, United Kingdom
Claudia.Carter2@mail.bcu.ac.uk

Hong Xiao
Birmingham City University, Birmingham, United Kingdom
Hong.Xiao@bcu.ac.uk

David Proverbs
De Montfort University, United Kingdom
David.proverbs@dmu.ac.uk

ABSTRACT

Flood risk management is increasingly challenged by climate change and continued development in flood-prone areas, exposing the limitations of traditional grey infrastructure such as levees, dikes and flood walls. Blue green infrastructure (BGI) has emerged as a nature-based approach that can support flood mitigation while delivering wider ecological and social benefits. Despite growing policy support, the adoption of BGI remains uneven across jurisdictions. This paper examines how legal and policy frameworks shape the conditions under which BGI is implemented in flood risk management. It compares two common law jurisdictions facing rising flood risk England and Canada each operating under different governance arrangements: a more centralised system in England and a polycentric, multi-level governance structure in Canada. The study analyses legislation and policy across flood risk management, planning and environmental governance using four analytical dimensions: legal and policy mandates, governance allocation, resources, and enforcement and monitoring. The findings highlight how institutional design influences the implementation of BGI and provide insights for strengthening governance frameworks supporting nature-based flood management.

KEYWORDS: Blue Green Infrastructure; Flood risk management; Legal frameworks; Adaptive governance; England; Canada.

1 INTRODUCTION

Flooding is occurring more frequently across many developed countries as climate change, urbanisation and changing rainfall patterns intensify hydrological pressures (IPCC, 2022). In England, one in six properties is at risk of flooding which is likely to increase under future scenarios (Sayers et al., 2020; Environment Agency, 2022). These tendencies suggest that traditional grey flood infrastructure, designed for more stable hydrological conditions, is becoming increasingly strained

by more variable flood risks (Dong et al., 2017) Blue–green infrastructure (BGI) offers an alternative approach that works with natural processes through networks of wetlands, bioswales, floodable parks and green corridors that slow runoff while delivering wider environmental and social benefits (O'Donnell et al., 2017). Although policy support for BGI has strengthened, the integration of BGI measures into flood risk management remains patchy. This is largely due to legal, institutional and governance barriers that still favour hard engineering solutions (Matthews et al., 2015).

This paper examines how law and policy influence the uptake of BGI in flood risk management through a comparison of England and Canada. Both are predominantly common-law countries facing increasing flood risk but operating under different governance arrangements. England depends on a more centralised, statute-driven system, while Canada operates through a polycentric, multi-level governance regime involving the federal, provincial and municipal government. The analysis reviews flood, planning and environmental legislation and policy documents through four analytical lenses statutory duties; policy integration; governance arrangements; and enforcement and funding. Using this framework, the paper traces how responsibilities are distributed among key actors, including the Environment Agency, lead local flood authorities and planning bodies in England, and federal departments, provinces, municipalities and conservation authorities in Canada. The aim is to illustrate how legal and policy decisions may either enhance or restrict the systematic implementation of BGI in flood risk management, as well as to bring to light lessons that may assist in the design or reform of flood governance systems in different contexts.

2 METHODS

This paper employs a qualitative research design based on the systematic analysis of documents. This study aims to explore the way in which England and Canada are using BGI in law and policy to support flood resilience. Laws, policies and strategies are not just treated as technical rules, but as dynamic statements of how a society understands risk, distributes responsibility and what kinds of interven-tion are considered acceptable. Consequently, the approach is interpretative rather than doctrinal in nature. No interviews or questionnaires were conducted; all findings are derived from existing legal and policy documents. The analysis focuses on laws, statutes, strategies and guidance documents that were in force, or under active revision, between 2010 and 2024. This period was selected because climate adaptation and nature-based solutions gained prominence quickly on policy agendas during these years (IPCC, 2022). The aim is not to evaluate implementation in a concrete project but to investigate the formal opportunities and constraints created by the legal and policy framework for BGI in flood risk management. England and Canada were selected as case studies because they are both common law jurisdictions facing growing flood risk, yet they differ significantly in territorial scale, governance structure and planning traditions (Golnaraghi et al., 2020; Mehryar and Surminski, 2020). In comparative policy analysis, this type of pairing is often described as a most different systems design, where cases share a similar core problem but differ in important institutional features (De Wee, 2022). This design allows the analysis to investigate how different territorial/country governance arrangements shape the legal and policy terrain for BGI and to identify enabling and constraining conditions that are associated with national and sub national contexts, rather than the common law tradition or the general reality of rising flood risk. In each country, the first step was to identify core documents focusing on instruments which clearly govern the four mandated domains: flood risk management, spatial planning, water management and climate adaptation. These domains were selected as they constitute the principal mechanisms through which BGI is planned, funded and delivered (Awara, 2025). The initial list of instruments was then expanded in an iterative manner. Initial documents were identified through targeted searches of official government and agency websites, including national legislative databases, departmental policy portals, and environmental and planning authority websites in England and Canada. The search was guided by keywords such as flood risk management, blue-

green infrastructure, nature-based solutions, spatial planning, water governance, climate adaptation, policy, strategy, Act, and guidance.

The selection process was iterative. Core documents were read in full and examined for references to additional relevant legislation, policy instruments, and technical guidance. In-depth and systematic cross-checking of the documents was undertaken, alongside a review of Scopus-indexed academic literature, to identify frequently cited and policy-significant laws and policy instruments. Official government portals were also searched to identify relevant Acts, strategies, and technical guidance. Both keyword searching and full-text reading were used to ensure relevance. Documents were included where they established statutory responsibilities, informed planning or implementation practices, or were consistently referenced in policy or academic sources. All selected documents were analysed against four analytical dimensions: legal and policy mandates, governance arrangements, enforcement and monitoring, and resources. This approach resulted in a coherent yet wide-ranging corpus of legal and policy documents shaping the planning, funding, and delivery of BGI in the flood risk management context. In total, the study analysed 15 documents for England and 26 documents for Canada (10 federal and 16 provincial/municipal).

The analysis of the document was guided by adaptive governance theory, which highlights uncertainty, cross-scale coordination and learning-oriented institutional arrangements (Allen et al., 2023; Awara, 2025). Building on this literature, the study examines legal and policy frameworks across four analytical dimensions relevant to BGI for flood risk management: legal and policy mandates which refers to how laws and policies acknowledge and prioritise BGI; governance which in this context refer to the distribution of roles and decision-making power across institutions; enforcement and monitoring which refer to the mechanisms for implementation, oversight and policy learning; and resources which refer to financial capacity, technical expertise and institutional support. These dimensions serve as the analytical framework for the qualitative content analysis. Policy and legislative documents were examined to assess whether provisions enable, constrain or have mixed implications for BGI implementation. The framework structures the comparative analysis of England and Canada presented in Figure 1.

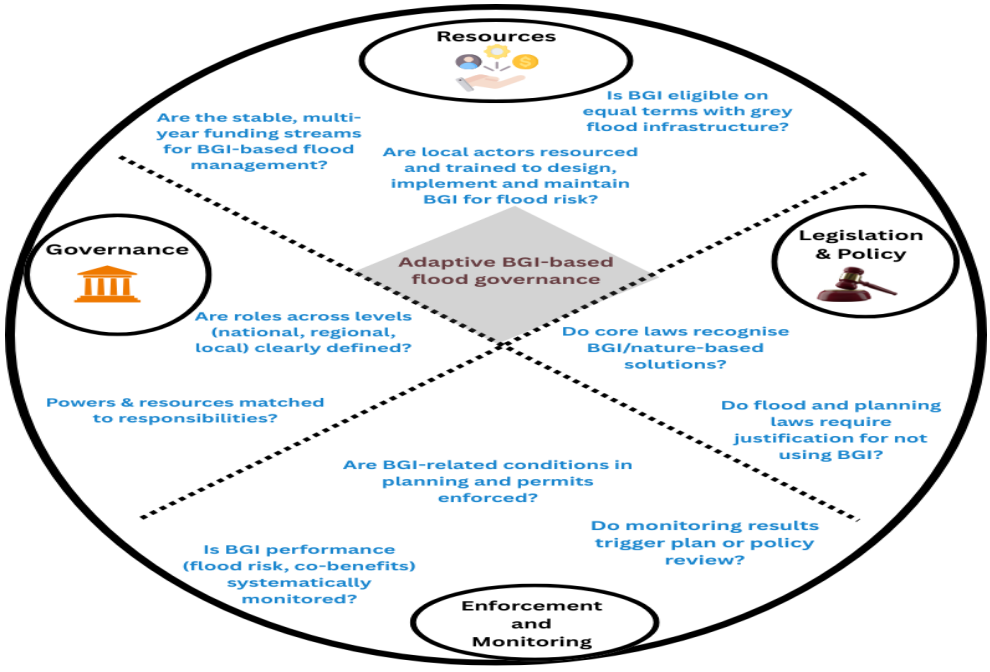

Figure 1: framework for adaptive, BGI-centred flood governance (Allen et al., 2023, Awara, 2025)

3 LEGISLATIVE FRAMEWORK: ENGLAND

Flood governance in England operates within a relatively centralised legislative system in which statutory responsibilities and policy direction are largely defined at the national level, with implementation carried out by local authorities and agencies (Awara, 2025). However, the institutional integration of BGI into the institutional processes of flood management agencies and actors at the national and local levels remains partial (O'Donnell et al., 2017). Within the legal and policy instruments, BGI is referenced as a mechanism for climate adaptation in the Flood and Water Management Act 2010, Environment Act 2021 and National Planning Policy Framework (Pitt, 2008; Defra, 2010; MHCLG, 2024; Grace et al., 2025). However, these provisions mainly operate through policy guidance rather than legal obligations. From a governance perspective, responsibilities for flood risk management, spatial planning and environmental regulation remain distributed across the Environment Agency, Lead Local Flood Authorities and planning authorities, creating coordination challenges (O'Donnell et al., 2017). The level of resource capacity varies significantly across local governments which influences the uneven implementation of BGI (Thorne et al., 2015). Finally, enforcement and monitoring remain fragmented, with limited systematic assessment of BGI performance. As a result, while there are strong legal and policy signals for using nature-based flood risk management approaches in England, institutional mechanisms which embed BGI into routine flood governance are limited (Scott and Hislop, 2024).

4 LEGISLATIVE FRAMEWORK: CANADA

Canada's flood governance architecture is shaped by a polycentric constitutional arrangement in which control of water management, land use and environmental regulation is divided among federal, provincial and municipal governments (Bakker and Cook, 2011; Renzetti and Dupont, 2017; GLC and CVC, 2018). Within this framework, support for BGI varies across the dimensions of legal and policy, governance, resources, and enforcement and monitoring. On legal and policy levels, Canada Water Act, and Fisheries Act implement principles of co-operative and ecological governance. However, federal instruments such as the Canada Water Act and the Fisheries Act do not contain explicit statutory requirements for BGI, with only limited indirect support at the provincial level (e.g. Ontario and British Columbia), and more explicit policy-driven implementation emerging at the municipal level in cities such as Toronto and Vancouver (Venton, 2016; GLC and CVC, 2018).

Most governance responsibilities in flood management are exercised at the provincial and municipal levels and there is considerable variation in actual flood management approaches and institutional capacity (Bakker and Cook, 2011; Renzetti and Dupont, 2017; Curran, 2019). Resource capacity similarly differs across jurisdictions, with larger municipalities generally better positioned to finance and implement BGI initiatives (Maloney et al., 2024; Jandrevska, 2025). The mechanisms for enforcement and monitoring remain fragmented and often sit within broader environmental reporting systems rather than dedicated flood governance systems (Zoghi et al., 2025). As a result, Canada's polycentric governance structure allows for local experimentation, but creates unequal institutional support for BGI across different provinces and territories.

5 COMPARATIVE SYNTHESIS: ENGLAND AND CANADA

The comparison highlights two contrasting institutional pathways through which BGI is incorporated into flood risk governance. Flood management in England operates within a relatively centralised statutory framework, in which legislation such as the Flood and Water Management Act 2010, the Environment Act 2021 and the National Planning Policy Framework sets a strong formal policy framework for environmental objectives (Awara, 2025). However, regulatory density has not yet led to coherence of cross-sectoral practices on the ground. BGI implementation is predominantly

promoted through policy guidance, non-statutory standards, and discretionary planning decisions rather than binding legal instruments. As a result, this can create uneven implementation across local authorities (Thorne et al., 2015; O'Donnell et al., 2017; Scott and Hislop, 2024). In contrast, Canada's flood governance involves an institutional structure with polycentric features in which responsibilities are distributed among all three levels of government (federal, provincial and municipal government) (GLC and CVC, 2018). The flexibility of this arrangement supports the implementation of locally driven BGI initiatives, which are often designed through a watershed-based planning and conservation authority (GLC and CVC, 2018). Yet the lack of coherent national standards results in diverging practices in BGI interpretation and implementation across jurisdictions, reflecting differences in statutory tools, fiscal capacity and technical expertise (Maloney et al., 2024).

Viewed through the analytical framework adopted in this study legal and policy, governance, resources, and enforcement and monitoring these cases illustrate the institutional trade-offs associated with centralised and polycentric governance systems. England gives clearer indications in terms of policy but is weak regarding coordination monitoring and enforcement. Alternatively, Canada supports experimentation and locally adapted solutions, but the regulatory consistency for widespread diffusion of BGI is lacking. To further illustrate this contrast, Table 1 presents the key features of the legislative and policy environment for BGI in flood risk management in both countries across the four analytical dimensions.

Table 1 Comparative assessment of legislative and policy conditions for blue–green infrastructure in flood risk governance

Dimension	England	Canada
Legal mandate	Strong statutes but no binding BGI duty	Environmental laws exist; BGI mostly discretionary
Policy integration	Flood, planning and biodiversity policies weakly integrated	Integration varies across provinces
Governance	Central guidance with local implementation	Polycentric federal–provincial–municipal system
Enforcement & monitoring	Limited monitoring of BGI delivery	Enforcement varies by province
Resources	Short-term funding; uneven local capacity	Capacity depends on provincial and municipal resources

Source: (Thorne et al., 2015; O'Donnell et al., 2017; GLC and CVC, 2018, Mell and Scott, 2023; Scott and Hislop, 2024, Maloney et al., 2024; Jandrevska, 2025, Awara, 2025)

Table 1 illustrates that the effectiveness of BGI governance is shaped less by the degree of centralisation than by the institutional alignment of legal mandates, governance responsibilities, resourcing arrangements and monitoring mechanisms. In both countries, the main constraint lies, not in a lack of policy commitment, but rather in governance systems that do not foster BGI as part of standard flood risk management practice.

6 DISCUSSION: FROM LAW TO LEARNING SYSTEMS

The comparison reveals a persistent tension within contemporary flood risk/management governance. Institutional frameworks in England and Canada continue to privilege regulatory

stability and hard engineering control over soft engineered / nature-based solutions and adaptive solutions/learning despite increasing climate risks and negative impacts. According to Mehryar and Surminski (2020), many flood management regimes were created under conditions of predictable hydrological risk in which governance was defined by clearly delineated responsibilities and top-down regulatory controls. With climate change introducing greater extent, frequency and uncertainty into flood risk, these institutional arrangements are turning out to be ill-suited compared to more extensive, flexible, ecosystem-based approaches such as BGI (O'Donnell et al. 2017). Despite widespread referencing of BGI in policy discourse, implementation is restricted as regulatory systems and investment practices are still favouring traditional grey infrastructure with more easily calculable flood mitigation performances (GLC and CVC, 2018; Mell and Scott, 2023; Scott and Hislop, 2024). BGI currently faces these institutional constraints needing a systemic change that considers long-term ecological processes, cross-sectoral coordination and distributed governance responsibilities (Mell and Scott 2023). As a result, stronger coordination between flood risk management, spatial planning and environmental governance is required for its implementation (Awara, 2025). Where statutory frameworks, funding mechanisms, and performance metrics remain oriented towards engineered solutions, BGI is often regarded as an add-on instead of a core solution for flood resilience (Scott and Hislop, 2024).

Such dynamics reflect deeper variants of institutional path dependency. Historical patterns of authority allocation, technical standard-setting and financial resource dispersal continue to support established infrastructure approaches limiting the change capacity of governance systems towards integrated nature-based approaches (Wiering et al., 2017). Viewed through the analytical framework developed by Awara (2025) regarding legal and policy mandates, governance allocation, resources, and enforcement and monitoring the findings highlight how fragmented responsibilities, weak monitoring systems and uneven institutional capacity undermine otherwise supportive policy commitments (O'Donnell et al., 2017). The analysis demonstrates the limits of legal reform alone. According to Awara (2025), extending statutory references to BGI does not change practice if governance systems continue to lack the necessary resources, coordination mechanisms and institutional flexibility to enable experimenting and learning. In this sense, law should not just be seen as a regulative mechanism but also a way to structurally adapt governance. This includes establishing monitoring systems that can assess the performance of BGI in flood risk mitigation and management, creating institutional pathways for learning, strengthening of effective policies, and embedding practice feedback loops into future regulatory development (Garmestani et al., 2014). In this sense, BGI provides a useful lens for assessing whether legal and policy institutions support learning, adaptation, and flexibility under conditions of climate uncertainty (De Rijke et al., 2025).

7 CONCLUSION

This paper argues that although England and Canada have increasingly referenced BGI in policy discourse, their legal and governance frameworks do not yet establish the necessary institutional conditions to enable its consistent implementation in flood risk management. The limited integration of BGI into routine flood management is impeded by a lack of cohesive governance arrangements, weak monitoring systems and inconsistent resourcing. This research proposes the use of a framework to translate principles of adaptive governance into four legal-policy dimensions:(1) the legal and policy mandates, (2) allocation of governance responsibilities, (3) resources and (4) enforcement and monitoring. The tool can help policymakers, planners and researchers to diagnose whether the legal and policy systems in place enable or constrain BGI implementation. Through the identification of gaps in these institutional dimensions, the framework can feed into policy reform, improve coordination of planning and flood governance, and support more adaptive and integrated approaches to flood resilience. The findings indicate that successful BGI implementation hinges less on the design of governance systems (centralised versus polycentric), and more on the extent that institutional arrangements facilitate coordination, effective monitoring and sustained investment in

nature-based flood management. For effective integration of BGI in flood risk management, policymakers need to prioritise a clear legal mandate, strong monitoring system, and stable long-term funding.

REFERENCES

Alexander M., Doorn N. and Priest S.J. (2018). Bridging the legitimacy gap translating theory into practical signposts for legitimate flood risk governance. Regional Environmental Change, 18(2), pp. 397–408.

Allen C., Malekpour S. and Mintrom M. (2023). Cross-scale, cross-level and multi-actor governance of transformations toward the Sustainable Development Goals: A review of common challenges and solutions. Sustainable Development, 31(3), pp. 1250–1267.

Awara R.I. (2025). An evaluation of the legislative and policy processes for blue–green infrastructure in England. Unpublished PhD thesis, Birmingham City University.

Bakker K. and Cook C. (2011). Water governance in Canada: Innovation and fragmentation. Water Resources Development, 27(2), pp. 275–289.

Curran D. (2019). The adaptation potential of water law in Canada: changing existing water use entitlements. Water International, 44(3), pp. 278–291.

Datta A.W. and Chaffin B.C. (2022). Evolving adaptive governance: challenging assumptions through an examination of fisheries law in Solomon Islands. Ecology and Society, 27(2), art. 30.

De Rijke C.A., Lim N.J., Iqbal A., Brandt S.A. and Sahlin E.A.U. (2025). A systematic review of blue-green infrastructure's role and relevance in the mitigation and management of climate-induced hazards in x-minute cities. Planning Practice & Research.

De Wee G. (2022). Comparative policy analysis and the science of conceptual systems: A candidate pathway to a common variable. Foundations of Science, 27(2), pp. 287–304.

Dong X., Guo H. and Zeng S.H. (2017). Enhancing future resilience in urban drainage system: Green versus grey infrastructure. Water Research, 124, pp. 280–289.

Garmestani A.S., Allen C.R., Arnold C.A. and Gunderson L.H. (2014). Introduction: Social-ecological resilience and law. in "Social-Ecological Resilience and Law," Garmestani A.S. and Allen C.R., Eds., Columbia University Press, New York, pp. 1–12.

Golnaraghi M., Thistlethwaite J., Henstra D. and Stewart C. (2020). Flood Risk Management in Canada. The Geneva Association, Zurich.

Grace, M., Smith, A., Mell, I., Houghton, J. and Neal, P. (2025) 'A menu of standards for green infrastructure in England', Frontiers in Environmental Science, 12, 1456519.

Hegger D.L.T., Driessen P.P.J., Dieperink C., Wiering M., Raadgever G.T. and van Rijswick H.F.M.W. (2014). Assessing stability and dynamics in flood risk governance. Water Resources Management, 28(12), pp. 4127–4142.

Henstra D. and Thistlethwaite J. (2017). Climate change, floods, and municipal risk sharing in Canada. IMFG Papers, 30. University of Toronto.

Jordan A., Huitema D., van Asselt H. and Forster J., Eds. (2018). Governing Climate Change: Polycentricity in Action? Cambridge University Press, Cambridge.

Kellner E., Petrovics D. and Huitema D. (2024). Polycentric climate governance: The state, local action, democratic preferences, and power emerging insights and a research agenda. Global Environmental Politics, 24(3), pp. 24–47.

Maloney J., Markey S., Gibson R. and Weeden S. (2024). Advancing green infrastructure solutions in rural regions: Economic impacts and capacity challenges in Southwest Ontario, Canada. Rural and Regional Development, 2, 10010.

Matthews T., Lo A.Y. and Byrne J.A. (2015). Reconceptualizing green infrastructure for climate change adaptation: Barriers to adoption and drivers for uptake by spatial planners. Landscape and Urban Planning, 138, pp. 155–163.

Mehryar S. and Surminski S. (2020). The role of national laws in managing flood risk and increasing future flood resilience. London School of Economics and Political Science.

Mell I. and Scott A. (2023). Definitions and context of blue-green infrastructure. in "ICE Manual of Blue-Green Infrastructure," Washbourne C.-L. and Wansbury C., Eds., Institution of Civil Engineers, London.
Minnes S. (2019). Watershed governance or intake governance? Implications of Ontario's Clean Water Act on collaborative watershed governance in rural areas. Canadian Water Resources Journal, 44(4), pp. 401–422.
O'Donnell E.C., Lamond J.E. and Thorne C.R. (2017). Recognising barriers to implementation of blue-green infrastructure: A Newcastle case study. Urban Water Journal, 14(9), pp. 964–972.
Scott A. and Hislop M. (2024). What does good green and blue infrastructure policy look like: A comparative assessment of UK national planning guidance. Urban Forestry & Urban Greening, 99, 128440.
Thorne C.R., Lawson E.C., Ozawa C., Hamlin S.L. and Smith L.A. (2015). Overcoming uncertainty and barriers to adoption of blue-green infrastructure for urban flood risk management. Journal of Flood Risk Management, 11(S1), pp. S960–S972.
Thornhill I., Gilchrist A., Searle B., Koksal C. and Sampson D. (2025). Using past planning practice to inform biodiversity net gain in residential developments. Ecological Solutions and Evidence, 6(1), e70021.
Wiering M., Kaufmann M., Mees H., Schellenberger T., Ganzevoort W., Hegger D.L.T., Larrue C. and Matczak P. (2017). Varieties of flood risk governance in Europe: How do countries respond to driving forces and what explains institutional change? Global Environmental Change, 44, pp. 15–26.
Zoghi A., Bilodeau É., Khaliq M.N., Kim Y., Martel J.-L. and Drake J. (2025). Nature-based solutions for flood mitigation in Canadian urban centers: A review of the state of research and practice. Journal of Hydrology: Regional Studies, 60, 102460.
zu Ermgassen S.O.S.E., Marsh S., Ryland K., Church E., Marsh R. and Bull J.W. (2021). Exploring the ecological outcomes of mandatory biodiversity net gain using evidence from early-adopter jurisdictions in England. Conservation Letters, 14(4), e12820.

Web sites:

Web-1: https://www.ciwem.org/the-environment/schedule-3-why-we-can't-afford-to-wait-for-legislation-to-catch-its-tail, consulted 2025.
Web-2: https://www.theccc.org.uk/wp-content/uploads/2018/10/Managing-the-coast-in-a-changing-climate-October-2018.pdf, consulted 2025.
Web-3: https://assets.publishing.service.gov.uk/media/5a78a61c40f0b632476990fe/pb13562-future-water-080204.pdf, consulted 2025.
Web-4: https://www.gov.uk/government/publications/national-flood-and-coastal-erosion-risk-management-strategy-for-england--2, consulted 2025.
Web-5: https://www.glc.org/wp-content/uploads/GI-policy-analysis.pdf, consulted 2025.
Web-6: https://publications.parliament.uk, consulted 2025.
Web-7: https://www.ipcc.ch/report/ar6/wg2/chapter/chapter-4/, consulted 2025.
Web-8: https://decentralization.net/2025/09/financing-green-futures-eco-fiscal-tools-in-canadian-cities/, consulted 2025.
Web-9: https://edges.sites.olt.ubc.ca/files/2018/03/Joe-et-al-2017-Perspectives_on_the_BC-1.pdf, consulted 2025.
Web-10: https://cdri.world/upload/biennial/CH3.8-INFC-ACT-SFU.pdf, consulted 2025.
Web-11: https://www.gov.uk/government/publications/green-infrastructure-framework, consulted 28 July 2025.
Web-12: https://nora.nerc.ac.uk/id/eprint/52842, consulted 2025.

ICFM 10
Adapting to Global Change:
Innovative Approaches to Flood Management and Resilience
May 20-22, 2026 | Western University, London, Ontario, Canada

A Comparative Review of Japan's Framework for Developing a Comprehensive Flood Control Master Plan

Ali Chavoshian[1], Shinji Honda[1], Yuka Sasaki[1], Shara Astillero[1]
PACIFIC CONSULTANTS CO., LTD., Kanda Nishikicho-3, Chiyoda City, Tokyo 101-0054, Japan[1]
E-mail: ali.chavoshian@tk.pacific.co.jp

ABSTRACT

Japan's river systems are characterized by steep slopes, short concentration times, and dense urbanization within flood plain. This paper provides a comparative review of the unique technical pillars within Japan's framework for developing a Comprehensive Flood Control Master Plan. Specifically, the paper clarifies two core technical elements: (i) the "stretching" approach used to develop design hyetographs from observed storm events, and (ii) the iterative High-Water Level (HWL) trial process used to finalize the vertical design datum. The Japanese approach to developing design hyetographs differs from the non-Japanese practices that are commonly used internationally. In contrast to synthetic design-storm methods (e.g., SCS-type distributions or the Alternating Block Method) that impose idealized, often symmetric temporal patterns derived from IDF relationships, the Japanese approach preserves event realism by scaling historical rainfall time series, so the basin's characteristic storm structure is retained. Moreover, the planned high-water level in Japan is set through practical trade-off analyses among channel excavation, widening, and levee height, with explicit attention to avoiding excessively elevated "ceiling river" conditions. This study highlights how Japan's framework combines historically grounded hydrology with safety-driven hydraulic design to improve robustness in urbanized basins exposed to flooding.

KEYWORDS: Ceiling Rivers, Design Hyetograph, Flood Control Master Plan, High-Water Level (HWL), River Basin Management

1 INTRODUCTION

Japan is characterized by steep mountainous terrain and short, rapid river channels that drain into densely populated alluvial plains. Unlike the continental rivers of North America or Europe, which often have longer concentration times and broader floodplains, Japanese rivers are prone to flash flood caused by destructive typhoons and active seasonal fronts (Koike, 2021). River management in Japan is governed by the River Law, which mandates a two-tiered planning structure: the long-term "Basic Policy for River Improvement" and the mid-term "River Improvement Plan" (MLIT, 2020).

Central to this framework is the determination of the Basic Flood Discharge[1], which represents the peak flow generated by a design rainfall before any regulation by facilities. While the fundamental principles of hydrology are universal, Japanese methodology differs significantly from standard practices. A key distinction lies in the construction of the Design Hyetograph. While non-Japanese approaches often utilize synthetic storm distributions (e.g., SCS Type curves or alternating block methods) derived from Intensity-Duration-Frequency (IDF) curves (Chow et al., 1988), the Japanese methodology prioritizes the use of actual observed rainfall patterns from past major floods. These historical patterns are "stretched" or

[1] The "Raw" natural peak. In Japanese, *Kihon Takamizu*

scaled to match probabilistic design rainfall volumes, ensuring the design storm reflects the specific meteorological "personality" of the basin (JICA, 2003).

Furthermore, the determination of the river's High-Water Level (HWL)[2] involves a unique iterative trial process that balances riverbed excavation against embankment height (JICA, 2002). Unlike standard approaches that may fix the design water level based solely on existing topography and peak discharge, the Japanese framework utilizes a unique, iterative trial process. This process seeks an optimal hydraulic balance among three physical variables: riverbed excavation, river widening and embankment height. By carefully weighing these factors, engineers ensure that the final HWL is set at an elevation that minimizes the risk of a catastrophic breach, preventing the creation of “ceiling rivers” where the water level significantly exceeds the elevation of the surrounding protected low-lying land.

According to Takeuchi (2022), the success of Japan’s flood control lies in its ability to treat the river basin as a holistic system where structural measures, such as dams and levees, are integrated with the "wisdom of the past." This includes analysing the actual hydro-meteorological behavior of historical floods to ensure that modern infrastructure is not merely built to a theoretical number, but is resilient against the specific, observable temporal distributions of rainfall that characterize Japanese storm events. In recent years, in response to intensifying climate change risks, Japan has transitioned from a facility-centric approach to a more holistic paradigm known as "River Basin Disaster Resilience and Sustainability by All"[3], which integrates land-use regulation and stakeholder cooperation into the master plan (MLIT, 2020).

This paper aims to elucidate these unique technical features, specifically the scaling of historical hyetographs and the setting of HWL, by providing a detailed comparison with international methods.

2 BRIEF REVIEW OF JAPANESE FLOOD CONTROL MASTER PLAN FORMULATION

The formulation of a flood control master plan in Japan is not merely a technical exercise but a legally binding process that balances hydrological theory with socio-economic reality. The methodology is designed to ensure that the river's "carrying capacity" is sufficient to convey the “design flood” safely. This relationship is anchored by the High-Water Level (HWL), which serves as the foundational vertical datum for all flood control plans and river works.

2.1 The Two-Tiered Legal and Planning Hierarchy

Following the 1997 revision of the River Law, Japan transitioned to a two-tiered planning system to improve transparency and incorporate environmental considerations alongside flood control (Takahasi, 2009):

Basic Policy for River Improvement[4]: This document establishes the long-term, fundamental goals for the entire river system. It identifies the "Design Flood" (target return period) based on the importance of the basin and determines the Basic Flood Discharge. The Basic Flood Discharge is a theoretical value representing the peak runoff generated by the design rainfall, assuming no flood control facilities (such as dams) are present. This represents the "natural" threat the basin faces.

River Improvement Plan[5]: This is a phased-based implementation plan (e.g. 20- to 30-year) focused on specific projects. It defines the Design Flood Discharge, which is the actual flow rate the river channel must safely carry after a portion of the Basic Flood Discharge has been regulated (peak-cut) by upstream dams or retention or retarding basins. This plan is developed through consultation with local stakeholders and academic experts.

[2] In Japanese, *Keikaku Kōsui*
[3] In Japanese, *Ryuiiki Chisui*
[4] In Japanese, *Kasen Seibi Kihon Houshin*
[5] In Japanese, *Kasen Seibi Keikaku*

2.2 The Technical Workflow for Plan Formulation

The transition from the "Basic Policy" to a finalized "Improvement Plan" follows a sequential six-step technical workflow as follows:

Step 1) Defining Design Conditions: The process begins by establishing the target safety level (return period) based on the river's national or regional classification. A defining characteristic of this step in Japan is the designation of "Flood Control Reference Points"[6]. These are fixed geographic locations (e.g., major confluences or urban bottlenecks) where discharge and water level targets (HWL) are legally set. These points ensure a unified, non-decentralized approach to safety across the entire river system (JICA, 2003).

Step 2) Natural Condition Hydrological Study: In this step, the Basic Flood Discharge is calculated at each flood control reference point. This represents the peak runoff generated by the design rainfall in the catchment's natural state, assuming no flood control facilities (like dams) exist. A unique Japanese feature here is the use of actual historical rainfall patterns from past major floods. These patterns are "stretched" or scaled to match the probabilistic rainfall volume, ensuring that the design hydrograph retains the realistic temporal "personality" of the basin (Takahasi, 2009). This unique Japanese technique, and how it differs from non-Japanese methodologies, will be explained in Section 3 of this paper.

Step 3) Existing Condition Hydrological Study: This step is broadly consistent with the widely used general approach, in which the model is re-run to incorporate the effects of existing and planned upstream infrastructure (e.g., dams, reservoirs, and retarding basins).

Step 4) Setting Target Discharge: The result of the previous steps is the finalization of the Design Flood Discharge. This is the specific discharge that the river channel must be physically built to convey safely after accounting for upstream regulation. These values are plotted on a Discharge Distribution Diagram, which serves as the official master document for all channel dimensions and bridge clearance requirements throughout the river system.

Step 5) Setting Tentative HWL: Using hydraulic models, planners calculate the water surface profile corresponding to the Design Flood Discharge. This determines the Tentative HWL that is the maximum expected elevation of the design flood. It is considered "tentative" because it must be cross-referenced with the surrounding ground level to ensure that the river's containment does not create an excessively high, and therefore dangerous, embankment. This step and its difference from non-Japanese methodologies, will also be explained in Section 3 of this paper.

Step 6) Adjusting and Finalizing HWL (The Trial Process): The final step is an iterative "trial" process where engineers balance riverbed excavation and river widening against embankment height (raising the levees). Multiple configurations of channel width and depth are simulated to find an optimal HWL that minimizes the risk of a catastrophic levee breach while remaining economically feasible. Once fixed, the HWL becomes the vertical datum for all future engineering works along the river.

3 REVIEW OF TECHNICAL DISTINCTIVENESS WITH NON-JAPANESE METHODLPGY

This structured workflow highlights why Japan’s flood control master planning is technically distinct from approaches commonly applied. The key pillars are Step 2, which preserves the hydro-meteorological “personality” of the basin by grounding design rainfall in observed historical events, and the safety-driven HWL finalization process in Steps 5 and 6, where iterative hydraulic trials are used to set a robust vertical design datum. Whereas many non-Japanese practices prioritize mathematical convenience through synthetic, statistically symmetric design storms and streamlined modeling assumptions (Chow et al., 1988), the Japanese framework intentionally avoids reliance on theoretical abstractions alone, emphasizing physical consistency and historical continuity. The following sections will examine the technical mechanisms underlying hyetograph scaling and the HWL trial process in Japan, highlighting their practical differences.

[6] In Japanese, *Kijun-ten*

3.1 Construction of the Design Hyetograph Based on Historical Realism

While the total rainfall depth for a target return period (e.g., 1/100 years) is determined statistically in a common way, the "shape" of the storm (its intensity over time) differs significantly in Japan. Commonly adopted approaches worldwide indicate that the design hyetograph is typically developed using synthetic distributions based on Intensity-Duration-Frequency (IDF) curves. These techniques include the Alternating Block Method or SCS Type Curves and rely on theoretical formulas to generate a "Balanced Storm" often resulting in a perfectly symmetrical hyetograph where the peak intensity is artificially cantered or fixed (Chow et al., 1988). While effective for determining a "theoretical statistical maximum", these smooth curves often fail to capture the chaotic, multi-peak nature of real weather systems.

In contrast, the Japanese methodology, as governed by the Technical Criteria for River Works (MLIT), is rooted in actual historical events and the "personality" of the basin. The procedure includes selecting a set of "Representative Disturbances" comprising significant historical flood events from the basin's recorded data (typically the five to ten largest past flood events). These observed hyetographs are subsequently scaled linearly to align with the probabilistic design rainfall volume (R_{plan}). The scaling formula is defined as:

$$r_{design}(t) = r_{obs}(t) \times \alpha \quad (1)$$

$$\alpha = R_{Plan} / R_{obs} \quad (2)$$

Where:

$r_{design}(t)$ is the design rainfall intensity at time t
$r_{obs}(t)$ is the observed historical rainfall intensity
α is the scaling factor (magnification rate)

The following outlines the scaling process in a step-by-step manner:

i. Selection of Representative Disturbances: Planners select 5 to 10 of the largest historical flood events recorded in the specific basin.
ii. Calculation of the Scaling Factor (α): The total volume of each historical storm is compared to the target probabilistic rainfall (e.g., 1/100-year).
iii. Linear Stretching: Every hourly (or sub-hourly) rainfall block in the historical record is multiplied by α.
iv. Meteorological Validation: If α exceeds 2.0, the pattern is usually discarded because the resulting intensities may exceed physical atmospheric limits.
v. Identification of the "Champion Flood" and Selecting Rainfall Hyetograph: After scaling all representative disturbances (based on the past 5-10 major floods) to the same design rainfall volume, runoff simulations are performed for each rainfall pattern. Even though the rainfall volume is identical for all these scaled storms, the peak discharge they produce will vary based on their temporal rainfall pattern (e.g., where the peak rainfall occurs in the sequence). The pattern that generates the highest peak discharge at the designated flood control reference point is identified as the the Design Hyetograph. This ensures that the infrastructure is built to survive not just a specific amount of rain, but the most dangerous arrangement of that rain ever observed in the basin.

A critical technical constraint in this method is the limit applied to the scaling factor α. If a small historical storm is "stretched" too aggressively (e.g., by a factor of 3 or 4), the resulting rainfall intensity would exceed limits, rendering the model meteorologically unrealistic. According to MLIT guidelines and practical standards, the scaling factor is generally kept within a physically plausible range (typically 1.2 to 1.5 and rarely exceeding 2.0. If a target probability requires a scaling factor ≥2.0, that specific historical pattern is often discarded as unsuitable for the design flood simulation, or a "comprehensive probability method" is employed to find a more suitable base event (JICA, 2003; MLIT, 2022).

This reflects a pragmatic engineering philosophy: rather than asking what the abstract statistical limit is, Japanese planners ask, "What would happen if this specific, catastrophic historical disaster

happened again, but with today's increased rainfall intensity?" This ensures that the resulting flood control structures are resilient against the complex, multi-peak temporal distributions, and specific storm tracks that characterize the basin's climate.

3.2 Determination of Design Flood Discharge and Iterative HWL Trials

The Design Flood Discharge[7], is the specific peak discharge that the river channel is physically designed to carry. Its determination represents the bridge between hydrological theory and structural engineering. The process begins with the Basic Flood Discharge, which is the calculated natural peak flow at a flood control point, assuming no human intervention or flood control facilities. The Design Flood Discharge is determined using the "peak-cut" volume, which refers to the amount of floodwater that upstream structures (like dams, retarding basins, or diversion channels) will divert or store. This relationship is expressed as: $Q_{design} = Q_{basic} - Q_{regulated}$

This finalized value is plotted on a Discharge Distribution Diagram, which serves as the legally binding master document for the entire river system. This diagram dictates the required capacity for every reach of the river, ensuring that downstream urban areas are protected by a coordinated system of upstream regulation and downstream channel capacity

Once the Design Flood Discharge is determined, the next step is establishing the High-Water Level (HWL). This vertical datum defines the height of levees, the clearance of bridges, and the gravity urban drainage. The methodology for setting this level reveals a sharp divergence between standard international practices and the Japanese framework.

In widely used international methodologies, such as those often employed by the USACE or for FEMA flood mapping, the determination of the flood level is primarily a hydraulic conveyance analysis. In this approach, the design discharge is routed through the existing channel topography to calculate the Water Surface Elevation (WSE). The resulting elevation dictates the necessary levee height, treating the channel geometry largely as a fixed constraint. In contrast, the Japanese methodology treats the river channel geometry not as a fixed constraint, but as a flexible design variable. The setting of the HWL is an active optimization process known as the "Trial Calculation". Rather than simply accepting the water level produced by the existing topography, Japanese approach conducts an iterative trade-off among three physical variables to force the water level down to a socially acceptable elevation: Riverbed Excavation to deepen the channel, River Widening to expand the cross-sectional width, and Embankment Height to provide the necessary safety.

The driving force behind this trial process is the strict avoidance of "Ceiling Rivers". This is a dangerous condition common in Japan where the riverbed or HWL sits significantly higher than the surrounding residential land. In Japan's densely populated flood plains, a high embankment creates immense potential energy; a breach in such a location would result in a high-velocity, destructive torrent far more lethal than a typical slow-rising inundation. Therefore, the goal of the trial process is to find the "optimal balance point" where the HWL is kept as low as possible through excavation and widening, minimizing the potential energy and the catastrophic risk of a levee breach.

4 CONCLUSIONS

Japan's approach to flood control master planning integrates hydrological science, historical evidence, and risk-averse engineering in a coherent framework. A central technical advantage is its preference for basin-specific realism over purely abstract design assumptions. In the hydrological phase, the stretching method constructs design hyetographs by scaling observed storm events, allowing the design rainfall to retain the multi-peak temporal structure typical of major typhoons and seasonal fronts. This produces runoff simulations that are often more physically consistent than results derived from synthetic, symmetric storm patterns.

[7] The "Regulated" channel peak. In Japanese, *Keikaku Takamizu*

In the hydraulic phase, the HWL finalization process for the design Flood Discharge relies on iterative trials that explicitly balance riverbed excavation, channel widening, and levee height. This shifts the objective from simple containment to reducing flood stage and limiting the potential consequences of levee breach in densely populated lowlands, while also helping to avoid excessive water levels associated with ceiling river conditions.

Under increasing climate-driven extremes, the underlying principles of this framework, namely historical continuity, physical plausibility, and safety-focused stage reduction, provide transferable insights for flood risk management in urbanized, flood-prone basins. Overall, Japan's methodology supports infrastructure design that is resilient not only to target probabilities, but also to the observed hydro-meteorological behavior that has historically produced damaging floods.

5 ACKNOWLEDGEMENTS

The author would like to express sincere gratitude to Pacific Consultants Co., Ltd. for providing the financial support necessary to conduct this research. Their commitment to advancing river engineering and flood management practices has been instrumental in the development of this study.

REFERENCES

Chow, V. T., Maidment, D. R., and Mays, L. W. (1988). *Applied Hydrology*. McGraw-Hill International Edition, New York, pp. 1-572.

JICA [Japan International Cooperation Agency] (2002). *Technical Standards and Guidelines for Planning and Design, Volume: Flood Control (Draft)*. Department of Public Works and Highways, Manila, pp. 1-144.

JICA [Japan International Cooperation Agency] (2003). *Manual on Flood Control Planning*. Department of Public Works and Highways, Manila, pp. 1-135.

Koike, T. (2021). Evolution of Japan's flood control planning and policy in response to climate change risks and social changes. *Water Policy*, 23(S1), pp. 77-93.

MLIT [Ministry of Land, Infrastructure, Transport and Tourism] (2020). *Water-related Disaster Risk Reduction Considering Climate Change: Transition to River Basin Disaster Resilience and Sustainability by All*. National Land Development Council, pp. 1-74.

Takahasi, Y. (2009). History of water management in Japan from the end of World War II. *International Journal of Water Resources Development*, 25(4), pp. 651-663.

Takeuchi, K. (2022). *Integrated Flood Risk Management: Basic Concepts and the Japanese Experience*. 1st edition, Routledge, Oxon, pp. 1-258.

ICFM 10
Adapting to Global Change:
Innovative Approaches to Flood Management and Resilience
May 20-22, 2026 | Western University, London, Ontario, Canada

Enacting Cross-Border Cooperation: Insights from Regional Flood Risk Practitioners

Anicia Touraine Andersson[1], Sean Vrielink[2], Cheryl de Boer[3], Claudia Pahl-Wostl[4] and Joanne Vinke-de Kruijf[5]

University of Twente, Enschede, 7522 NB, Netherlands[1]
E-mail: a.touraine@utwente.nl

University of Twente, Enschede, 7522 NB, Netherlands[5]
E-mail: joanne.vinke@utwente.nl

ABSTRACT

Managing flood risk in transboundary river basins requires cooperation across political borders. Such cooperation occurs across multiple governance levels, from supra-national and national to regional and local. Despite their pivotal role, regional governance actors responsible for the management of sub-basins and river systems remain underexamined in research on European water cooperation. The 2021 floods in the Benelux+ region exposed this gap, revealing breakdowns in regional cooperation and underscoring the need to understand how cooperation is interpreted and carried out by those working in regional cross-border river basins.

This study examines how regional flood risk managers perceive and enact cross-border cooperation in the Dutch-German-Belgian border area. Focusing on regional river basins where responsibilities of a variety of actors intersect, it adopts a practice-theoretical perspective that views cooperation as situated practices.

Qualitative interviews, embedded in a Q-sort exercise, explore the perceived relevance of cooperative practices. Purposive and snowball sampling identified practitioners directly involved in cross-border work, including hydrologists, flood forecasters, policy advisors, project managers, and strategic leads. Data collection is ongoing, with 11 interviews completed to date.

Emerging insights reveal differences in how cooperation is conceptualized across actors. Operational practitioners view cooperation as task-oriented and operational, while tactical and strategic actors hold broader ambitions for cooperation but struggle to translate them into concrete goals. While these differences may be a natural reflection of practitioner roles, it highlights a gaps between strategic expectations and operational realities. Strategic actors' vague goals provide limited guidance for operational implementation, and in combination with a narrow conceptualisations of cooperation among operational actors, valuable forms of cooperation may remain underexplored because they fall outside current conceptual frames of cooperation

KEYWORDS: Flood risk management, Cross-border cooperation, Regional governance, Transboundary river basins

1 INTRODUCTION

Transboundary lakes and river basins, referring to waterways that cross country borders, comprise 47% of the world's surface (McCracken and Wolf 2019). The need for cooperative governance approaches to tackle interdependent and transboundary risks in these cross-border river basins is well established in the literature (e.g. Thaler et al. 2019; Garrick et al. 2018; Clegg et al. 2021; Krishna Prabhakar 2022). This is echoed in practice, where cooperation is been formally recognized and institutionalized. Global agreements such as the 1997 UN Watercourses Convention and the EU Water Framework Directive and the EU Flood Directive set out clear expectations for cooperation in shared

river basins, requiring equitable use, integrated planning and coordinated action between countries, sectors, and governance levels (Baranyai 2019; Directive 2000). While these frameworks establish formal obligations for cooperation, they are not able to determine how to enact such cooperation in practice.

Cross-border flood risk management takes place through integrated actions across jurisdictions, often with varying institutional capacities and priorities (Pahl-Wostl, 2007). In the European context, responsibilities for cross-border cooperation are distributed across governance levels (Klein &Van den Vat 2024). National governments contribute to cross-border cooperation in major river basins through their participation in river commissions, transnational agreements and negotiations of basin-wide goals (Pfeiffer et al. 2013). In smaller transboundary tributary basins, regional authorities, such as provinces, municipalities, and subnational agencies hold primary responsibility for the enactment of operational cross-border flood-risk management, and are additionally expected to contribute to strategic planning for the region (Klein &Van den Vat 2024). This multilevel distribution of cooperation responsibilities creates a complex governance landscape in which regional actors play a pivotal yet often underexamined role in cross-border flood risk management.

The devastating floods of July 2021 in the Benelux+ region exposed the critical importance of the regional cross-border cooperation. Evaluations of the event, which caused an estimated EUR 34 billion in damages (Mohr et al. 2023) and left over 240 people dead (Hagenlocher et al. 2022), highlighted fragmented crisis governance and breakdowns in coordination among regional authorities (Hagenlocher et al. 2022). Despite their central role in implementing cross-border flood risk management, cooperation among regional practitioners have received relatively little attention in the literature (Baranyai 2019), resulting in limited understanding of how cooperation at the regional scale can best be supported.

Cross-border flood risk management in the Benelux+ regional river basins depends on a diverse set of actors, with varying mandated and responsibilities carrying out interdependent tasks, from technical data exchange and local project implementation to strategic planning and crisis coordination (Klein &Van den Vat 2024). Cooperation is shaped by how actions integrate into existing practices and roles, how practitioners conceptualise cooperation and how they understand the motivations and requirements for cooperation (Boholm et al. 2012). From this perspective, cooperation is enacted through situated practices, making practitioners' lived experiences central to understanding how cross-border collaboration actually works. Building on this perspective, the study examines how regional practitioners conceptualise and prioritise cooperation in practice. By focusing on these practical processes, the research aims to uncover the operational dynamics of cooperation and identify opportunities to strengthen cooperation across borders.

The study addresses the following questions: *How do regional practitioners conceptualise, and prioritise cross-border cooperation in regional flood risk management, and how does this influence cooperative flood risk management in cross-border regions?* To address this question, the study employs a qualitative analysis of interviews with regional flood risk managers in Germany, the Netherlands, and Belgium. The interviews were part of a Q-sort, an exercise in which participants were asked to rank the relevance of statements representing action of cross border cooperation. In doing so, the study provides an operationalisation of cooperation, providing insights into how regional practitioners conceptualise and prioritise cooperative tasks. The research identifies gaps between actor perceptions, which act as potential leverage points for strengthening cooperation in border regions. The paper proceeds with an overview of the conceptual framing, followed by the methodology, preliminary findings on practitioners' perspectives, and a reflection on potential implications for strengthening regional cross-border cooperation.

2 THEORY

To better understand how regional practitioners conceptualise and prioritise cross-border cooperation, this paper explores the conceptual landscape of cooperation. Bringing together insights from actor-layer perspectives and practice theory, it approaches cooperation as context-dependent and shaped by actors' roles, goals, and interpretations. By adopting a practice-oriented lens, the paper reframes cooperation as situated action, enabling an empirical analysis of how regional practitioners prioritise cooperative tasks and where misalignments may emerge within cross-border governance.

The interactions that make up cross-border governance are often conceptualised as collaboration, cooperation, or coordination, with these terms sometimes used interchangeably (Castañer, 2020; Morris and Miller-Stevens, 2015 Barbara Gray's (1985) foundational work defines collaboration as constructive engagement among actors with differing perspectives aimed at mutually beneficial solutions. Later work, including Morris and Miller-Stevens (2015), elaborates a spectrum of interaction types, highlighting gradations from low-intensity cooperation to high-intensity integration characterized by shared resources, negotiated goals, and joint decision-making.

While these conceptualisations strengthen our understanding of the structural features and relational ambitions of cross-border interactions, they offer limited insight into what cooperation should accomplish nnnnnnnn is achieved or what its concrete goals should be within specific management contexts. In flood risk management, these goals are not uniform: upstream and downstream actors face different risk profiles, regulatory obligations, and societal expectations, which shape what they consider meaningful or beneficial cooperation (Seher & Löschner. 2018). As a result, the aims of cooperation is situated within the frames of actors. Cooperation, then, cannot be understood simply in terms of ideal interaction types but must be explored in terms of how practitioners interpret what needs to be achieved and how they fit their tasks together across borders. To reflect the language of practitioners, this paper will use the term cooperation, not as an ideal type, but rather to describe a broad set of interactions between actors.

Research on cooperation in flood risk asset management shows that an actor's role strongly shapes both the goals of cooperation and the practices used to achieve them. Heijer et al. (2023) conceptualise these roles across three layers; strategic, tactical, and operational, each with distinct responsibilities. Each actor-layer faces unique challenges. Strategic actors are expected to hold clear or supported visions, tactical actors are asked to delineate responsibilities; and operational actors must navigate ambiguous and evolving rules and objectives.

According to Heijer et al. (2023) what constitutes meaningful cooperation vary depending on actor layers, the task, or goal to be achieved, and actors' objectives and expected benefits. Cooperation is therefore situated and adaptive. There is no central authority establishing priorities in cooperation, whether between strategic and operational goals, upstream and downstream interests, or differing organizational success indicators. Actors must deliberately negotiate, coordinate, and adapt their cooperative arrangements to align their goals and activities. Because each actor pursues distinct goals and works with different responsibilities, cooperative efforts only succeed when these goals can be meaningfully connected to the practices that make up cooperation. As a result, cross-border flood risk management hinges on deliberate, context-sensitive cooperation that aligns actors' goals with practical implementation.

Insights from research on the practice of risk governance further emphasise that governance processes unfold through the everyday activities of practitioners. Studies of risk governance highlight that actors do not simply implement predefined governance arrangements; rather, they actively interpret risk problems, negotiate responsibilities, and translate policy objectives into concrete actions within their organisational and professional contexts (Boholm et al 2012). From this perspective, governance is enacted through situated practices such as interpreting monitoring data, coordinating across organisations, and negotiating how risks should be managed in practice.

. A practice-theory perspective therefor offers an analytical lens that renders these interpretations empirically visible. It understands cooperation as a dynamic process performed through practitioners' routines, tools, and institutional contexts (Nicolini 2012; Feldman & Orlikowski 2011). Practices are socially and materially embedded ways of doing, shaped by professional norms, organisational expectations, and available technologies (Feldman & Orlikowski 2011). A practice lens therefore highlights how sociomaterial elements, such as models, monitoring systems, communication platforms, and forecasting tools, influence how actors interpret information, exchange insights, and coordinate decisions across borders (Orlikowski & Scott 2008).

Taken together, these insights suggests that cross-border flood risk management depends on how practitioners make sense of the aim of cooperation and how it should be enacted. By viewing cooperation

as situated and performed, a practice-theory lens provides a means to operationalise fit-for-purpose governance by showing where actors' understandings align or diverge, and where existing cooperative arrangements may need adjustment. This study therefore explores how diverse actors across organisations and roles conceptualise cooperation and its purpose. This forms a foundation for identifying opportunities to strengthen cross-border governance. and enables the design of context-sensitive governance aligned with the principles of fit-for-purpose governance.

3 METHOD

This study investigates how regional practitioners perceive and prioritise the enactment of cross-border cooperation in flood risk management in the Benelux+ region, focusing on sub-river basins along the borders of Germany, the Netherlands, and Belgium. It captures the perspectives of practitioners across strategic, tactical and operational roles involved in a broad range of tasks related to flood risk. The study follows an interpretivist epistemology, which views cooperation as shaped through the meanings, routines, and situated practices of practitioners. This aligns with a practice-theoretical lens, emphasizing how cooperation and knowledge practices are enacted in everyday work rather than solely in formal institutional arrangements.

Data is being collected through interviews as well as document analysis and observations conducted within the broader research context. Interviewees are identified through purposive sampling sampling identified practitioners directly involved in cross-border cooperation, including hydrologists, flood forecasters, policy advisors, project managers, and strategic leads across municipalities, counties, water authorities, and coordinating organisations. Snowball sampling is used to reach additional relevant actors within the cooperation network. To date, 11 Q-sort interviews with practitioners have been conducted, as part of an ongoing data collection effort. Participants represented a range of perspectives, including upstream (n=5) and downstream (n=6) actors, covering roles such as hydrologist, flood forecaster, policy advisor, project manager, strategic lead, and risk communication/early warning specialists. Data collection is continuing, with approximately 15 additional interviews planned to expand representation across governance levels and river basins.

Interviews are conducted online via Microsoft Teams, recorded, and transcribed verbatim. The post-sort interviews followed a Q-sort exercise in which participants order 36 statements representing cross-border knowledge management practices according to relevance from their professional perspective (Watts & Stenner 2012). The statements covered a range of cooperative practices, for example:

- co-developing basin-wide hazard maps, risk assessments, or damage models;
- conducting joint scenario exercises or cross-border crisis-response trainings;
- establishing and maintaining formal cross-border communication channels
- developing and maintaining shared digital dashboards for real-time data exchange;

During the exercise, participants reflected on their choices aloud, followed by a 20-minute debrief discussion. This study focuses on the qualitative reflections from these Q-sort interviews. A qualitative thematic analysis is used to identify recurring patterns in practitioners' accounts. The analysis is predominantly inductive, allowing themes to emerge while remaining sensitized by the practice-theoretical lens. Themes were compared across roles, organisational types, and countries to explore variation in practices and perspectives. The analysis presented in this paper reflects **preliminary qualitative patterns emerging from the current dataset**.

4 PRELIMINARY FINDINGS

The findings presented here reflect preliminary patterns from the Q-sort interviews conducted so far with regional practitioners. As data collection and analysis are ongoing, the results should be understood as early insights into how actors conceptualise and prioritise cross-border cooperation. Further analysis will refine these findings as the full dataset is completed.

While actors generally consider cross-border cooperation to be important in flood risk management, they differ in what they expect to achieve through cooperation and which practices they

consider relevant to engage in. Preliminary insights indicate that regional actors hold divergent conceptualisations and goals for cross-border cooperation, shaped by their roles, responsibilities, and tasks, as well as their perceived influence over outcomes and their attitudes towards challenges. These differences closely mirror the actor layers identified by Heijer et al. (2023), with distinct patterns emerging between operational and tactical, or strategic roles. The following sections first explore how operational actors conceptualise cooperation as addressing immediate, task-focused needs, before turning to tactical and strategic actors, who frame cooperation in terms of influence, learning, and basin-wide co-management. Together, these findings illustrate how differences across actor layers shape the translation of cooperative ambitions into practice and help explain where gaps in regional cross-border cooperation may emerge.

4.1 Task-focused cooperation anchored in immediate needs among operational actors

Operational actors involved in flood preparedness and response, including hydrologists, modelers, forecasters, and crisis response staff, describe cooperation primarily as a means to improve forecasts and gain coherent information of basin dynamics. Their main goal is reliable access to interpretable data, information, and knowledge under time pressure, enabling timely and well-informed decisions during flood events. Building cross-border relationships to support communication channels are highly valued among these actors. However, the depth of the relationship is less important than simply predictable and dependable contact in critical moments.

Operational actors describe their roles in terms of narrow, concrete, and siloed responsibilities, and as a result focus on cooperation for modular tasks, such as exchanging raw data, which provide immediate operational value. While they recognize that more systemic cooperation, with joint learning and basin-wide co-management could reduce flood risk overall, they generally do not consider such initiatives part of their scope due to limited authority, resources, and institutional support. This suggests that actors ambition in cross-border cooperation is stifled by actors perceived influence and capacity to act.

More complex cooperation, such as developing real-time cross-border forecasting dashboards, require alignment across regions with differing protocols and risk tolerances. For actors with narrower mandates, these tasks appear to be outside what whey consider their scope of work, with is used as a justification to consider such actions less relevant. As a result operational actors may be less likely to anticipate, request, or initiate cooperative practices designed to strengthen relationships, foster shared understanding or basin-wide coordination over time, which may limit the further development of more integrated forms of cross-border cooperation .

Reactions to the Q-sort statements illustrate this situated view on cooperation. Some operational actors were surprised by the range of possible enactments of cooperation, noting that joint practical training or exchanges would be interesting but are not part of current practice and not typically what they thought of as cooperation. This suggests that potentially valuable forms of cooperation remain underexplored, not due to lack of relevance, or difficulty of implementation, but because they fall outside actors' current frames. Broadening understandings of what cooperation can include may expand the repertoire of practices that support shared interpretation, trust-building, and basin-wide preparedness, beyond strategic actors and in to the operational domain.

The perceived cost of engaging in cooperation in the form of data and information exchange is low among actors, and no major differences in motivation have been observed between upstream and downstream actors so far. At the same time, it was observed that regions with longer histories of cooperation articulate higher ambitions and report fewer barriers for cooperation. This suggests that cooperation may function as a positive feedback loop in which early successes build confidence and normalise more ambitious practices over time. These differences indicate that the maturity of cooperation shapes how actors interpret what is feasible and worthwhile, influencing both the depth and scope of the cooperative practices they consider relevant.

4.2 Cooperation as influence among strategic actors

Throughout the interviews strategic and tactical actors, including policy officers, civil servants, and leadership figures in regional administrations and waterboards, frame cooperation as a means to shape basin-wide outcomes through joint learning and co-management. Their conceptualisation of cooperation extends beyond their immediate responsibilities, focusing on how upstream and downstream actions interact and how coordinated interventions can reduce flood risk at a systems level. Cooperation was expressed to rely on strong relationship building, and learning about not just technical details, but about processes and practices across different organisations. Strategic actors often described cooperation in normative terms, referring to expected indirect or long-term benefits for the basin as a whole. However, the specific outcomes they expect to achieve are frequently vague, and concrete goals are rarely articulated.

This lack of clarity regarding the goals of cooperation makes it difficult to translate strategic intentions into concrete, prioritised actions, and several actors reported uncertainty during the Q-sort exercise about which cooperative practices should be prioritised. This challenge appears to be linked to the systems perspective through which strategic actors enact their role, which emphasises steering basin-wide outcomes rather than advancing discrete actions. Tactical and strategic actors consistently emphasised the interdependence of the cooperative tasks they consider important. For example, developing a shared forecasting dashboard requires agreement on risk indicators, harmonised terminology, and a shared understanding of data interpretation. Because each task depends on the completion of several others, no single action generates meaningful effect on its own. This creates a chain-like structure of cooperation, in which progress can stall if one link is missing. This stands in contrast to the modular and immediately useful forms of cooperation described by operational actors, such as routine data exchange or updating contact networks. Recognising this interdependence helps explain why strategic ambitions tend to remain broad: achieving system-wide objectives requires coordinated movement across multiple fronts simultaneously.

Motivation to cooperate exists on both sides of the border, but the underlying drivers of cooperation and the institutional conditions under which actors operate differ. Downstream actors described strong incentives to collaborate, rooted in their dependence on upstream regions for managing flood risk. These incentives align with established roles and mandates for cross-border cooperation, which are supported by dedicated resources and organisational backing, enabling downstream actors to pursue more ambitious cooperative practices. Upstream actors also expressed motivation to cooperate, but their motivation is grounded less in direct risk dependency and more in professional responsibility and neighbourly solidarity. However, these motivations are not supported by adequate mandates, or resources. Upstream actors reported more limited formal mandates for cooperation, greater political constraints, and hierarchical decision-making structures that restrict their capacity to act on cooperative ambitions. As a result, a gap emerges between upstream actors' strategic aspirations and their ability to implement cooperative practices, posing a risk to sustained progress toward long-term, basin-wide initiatives.

4.3 IMPLICATIONS

The emerging findings suggest that differences in how cooperation is interpreted and enacted across actor layers are influenced by how practitioners situate cooperative tasks within their own professional identities and spheres of influence. Operational actors tend to anchor cooperation in concrete, time-sensitive responsibilities, prioritising data exchange and dependable communication channels. Strategic actors, by contrast, link cooperation to longer-term basin alignment and learning. This divergence is perhaps expected, yet it raises questions about how strategic agendas translate into operational practice. When operational actors face constraints such as limited mandate, budget, or tools, they may de-prioritise cooperative actions that fall outside their immediate responsibilities. This risks creating a gap between strategic aspirations for joint basin management and the operational realities that shape in particular crisis preparedness and crisis response cooperation. Strategic actors' limited ability to articulate concrete goals may reinforce this gap, as vague ambitions offer little guidance for

implementation and make it harder to connect cooperative practices to measurable outcomes. These reflections point to the importance of understanding not only what actors want from cooperation, but also what they believe they can realistically achieve.

5. CONCLUSION

This study provides initial insight into how regional practitioners conceptualise and enact cross-border cooperation in flood risk management. The preliminary findings suggest that cooperation is not uniform, but situated within actors' professional roles, responsibilities, and mandates. Divergent conceptualisations across actor layers highlight a challenge in aligning strategic ambitions with operational realities. Vague strategic goals combined with operational actors' focus on their defined tasks can make it difficult for strategic and operational layers to connect, limiting the translation of ambitions into concrete practices and the achievement of basin-wide cooperation objectives.

Understanding both what actors aim to achieve through cooperation and what they perceive themselves able to enact is therefore critical for designing fit-for-purpose governance arrangements. By focusing on cooperative practices, this study makes differences in how cooperation is conceptualised visible, helping to identify opportunities to bridge strategic and operational perspectives, expand practitioners' frames of cooperation, and strengthen context-sensitive governance in regional river basins. Further analysis of the Q-sort data will refine these insights by clarifying where cooperative efforts can be more effectively prioritised and operationalised across actor layers and borders.

1 ACKNOWLEDGEMENTS

This is an independent study, taking place within the JCAR-ATRACE project, funded by the Dutch Ministry of Infrastructure and Water Management with project no. 012215.

REFERENCES

Baranyai, Gábor. 2019. *European Water Law and Hydropolitics: An Inquiry into the Resilience of Transboundary Water Governance in the European Union*. 1st ed. Water Governance - Concepts, Methods, and Practice. Cham, Switzerland: Springer Nature.

Boholm, Åsa, Hervé Corvellec, and Marianne Karlsson. 2012. "The Practice of Risk Governance: Lessons from the Field." *Journal of Risk Research* 15 (1): 1–20.

Castañer, Xavier, and Nuno Oliveira. 2020. "Collaboration, Coordination, and Cooperation among Organizations: Establishing the Distinctive Meanings of These Terms through a Systematic Literature Review." *Journal of Management* 46 (6): 965–1001.

Clegg, G., Haigh, R., Amaratunga, D., Rahayu, H., Karunarathna, H., & Septiadi, D. (2021). A conceptual framework for flood impact mitigation through transboundary river management. *International Journal on Advanced Science, Engineering and Information Technology*, *11*(3), 880–888. https://doi.org/10.18517/ijaseit.11.3.14329

Directive 2000/60/EC of the European Parliament and of the Council of 23 October 2000 establishing a framework for Community action in the field of water policy, 2000, https://eur-lex.europa.eu/eli/dir/2000/60/oj/eng

Feldman, Martha S., and Wanda J. Orlikowski. 2011. "Theorizing Practice and Practicing Theory." *Organization Science* 22 (5): 1240–53.

Feldman, David L., and Helen M. Ingram. 2009. "Making Science Useful to Decision Makers: Climate Forecasts, Water Management, and Knowledge Networks." *Weather, Climate, and Society* 1 (1): 9–21

Heijer, Frank den, Jeroen Rijke, Marian Bosch-Rekveldt, Annemargreet de Leeuw, and María Barciela-Rial. 2023. "Asset Management of Flood Defences as a Co-production—An Analysis of

Cooperation in Five Situations in the Netherlands." *Journal of Flood Risk Management* 16 (3): e12909.

Klein, A. Van den Vat, M Lukat, E, Mueller, P. Schriewer, E. Reinert, J. Klopries, E. Kitsikoudis, V. Vinke-de Kruijf, J. et al. 2024. "Scoping Study of the Vechte, Berkel and Oude IJssel River Basins." https://www.jcar-atrace.eu/en/knowledge-base?locale=en&segment=3.

Mohr, S., Ehret, U., Kunz, M., Ludwig, P., Caldas-Alvarez, A., Daniell, J. E., Ehmele, F., Feldmann, H., Franca, M. J., Gattke, C., Hundhausen, M., Knippertz, P., Küpfer, K., Mühr, B., Pinto, J. G., Quinting, J., Schäfer, A. M., Scheibel, M., Seidel, F., & Wisotzky, C. (2023). A multi-disciplinary analysis of the exceptional flood event of July 2021 in central Europe – Part 1: Event description and analysis. *Natural Hazards and Earth System Sciences*, *23*(2), 525–551. https://doi.org/10.5194/nhess-23-525-2023

Nicolini, Davide. 2012. "Practice Theory, Work, and Organization an Introduction (Davide Nicolini) (Z-Library)."

Orlikowski, Wanda J., and Susan V. Scott. 2008. "10 Sociomateriality: Challenging the Separation of Technology, Work and Organization." *Academy of Management Annals* 2 (1): 433–74.

Pahl-Wostl, C. 2007. "The Implications of Complexity for Integrated Resources Management." *Environmental Modelling & Software: With Environment Data News* 22 (5): 561–69.

Pfeiffer, Ellen, and Jan Leentvaar. 2013. "Knowledge Leads, Policy Follows? Two Speeds of Collaboration in River Basin Management." *Water Policy* 15 (S2): 282–99.

Renner, Tobias, Sander Meijerink, and Pieter van der Zaag. 2018. "Progress beyond Policy Making? Assessing the Performance of Dutch-German Cross-Border Cooperation in Deltarhine." *Water International*, October. https://doi.org/10.1080/02508060.2018.1526562.

Seher, W., and L. Löschner. 2018. "Balancing Upstream-Downstream Interests in Flood Risk Management: Experiences from a Catchment-Based Approach in Austria: Balancing Upstream-Downstream Interests in Flood Risk Management." *Journal of Flood Risk Management* 11 (1): 56–65.

Tay, Huay Ling, Ruth Banomyong, Paitoon Varadejsatitwong, and Puthipong Julagasigorn. 2022. "Mitigating Risks in the Disaster Management Cycle." *Advances in Civil Engineering* 2022 (1): 7454760.

Thaler, T., Shively, D., Petersen-Perlman, J., Slavikova, L., & Hartmann, T. (2019, October 30). Collective Choices Affecting Natural Hazards Governance, Risk, and Vulnerability. Oxford Research Encyclopedia of Natural Hazard Science. Retrieved 30 May. 2025, from https://oxfordre.com/naturalhazardscience/view/10.1093/acrefore/9780199389407.001.0001/acrefore-9780199389407-e-142.

Watts, S., & Stenner, P. (2012). *Doing Q methodological research : theory, method and interpretation*. SAGE. http://srmo.sagepub.com/view/doing-q-methodological-research/SAGE.xml

.

Chapter 5- Governance, policy, and societal engagement

5.2 Bridging science, policy, and practice through transdisciplinary approaches

ICFM 10
Adapting to Global Change:
Innovative Approaches to Flood Management and Resilience
May 20-22, 2026 | Western University, London, Ontario, Canada

River development and risk management concept – a tool to enhance coordination on catchment scale in Austria

Clemens Neuhold[1], Martin Wenk[1], Helena Mühlmann[2], Elena Leutgöb[1], Marion Wallner[1]
[1]Flood Risk Management Directorate, Federal Ministry of Agriculture and Forestry, Climate and Environmental Protection, Regions and Water Management, Vienna, Austria
clemens.neuhold@bmluk.gv.at

[2]National and International Water Management Directorate, Federal Ministry of Agriculture and Forestry, Climate and Environmental Protection, Regions and Water Management, Vienna, Austria

ABSTRACT

The objective of the river development and risk management concept (RD-RM/GE-RM) is to enhance the coordination of measures within a river basin. To ensure efficient implementation a strategic EU project (LIFE IP IRIS) was set up to review and revise existing guidelines. Within the project, eight relevant case studies considering different river types were identified. In these regions, the RD-RM concept was applied. The planning process is based on the goals, priorities, and measures of the Flood Risk Management Plan according to the EU Floods Directive and the River Basin Management Plan according to the EU Water Framework Directive. Spatial planning, building regulations, emergency management, nature conservation, and other relevant authorities, stakeholders and affected individuals are involved in the planning process. A RD-RM concept is primarily developed where there is a need for action regarding flood risk management and ecological improvements. In addition to the hazard situation, factors such as the ecological state of the water bodies and framework conditions like land use designations, water rights, etc., are also taken into account. Based on assessments and evaluations, interdisciplinary development goals and integrative measures are determined. These form the basis for subsequent general projects, detailed planning, and ultimately, the implementation of specific measures.

One case study covers the entire course of the Lafnitz river. A special characteristic of the Lafnitz is that it forms the border between two federal provinces in Austria along large parts of its course. Therefore, the close cooperation between the two federal provinces was particularly important in the preparation of the RD-RM concept. The respective results highlighted that local measures are not sufficiently enough to reduce existing deficits (especially in context of erosion and sediment input) and, therefore, a clear need for catchment-based measures and actions. These were tested in the frame of another project called Land4Climate focussing on a close cooperation of the administration with NGOs, the agricultural chamber and private landowners. To learn from other regions in Europe the project Land4Climate was set up under the EU HORIZON funding scheme and implemented in close cooperation with LIFE IRIS project. Focus is given on the fact that climate resilience needs land. Land4Climate, aims to deploy and demonstrate the practical application of nature based solutions (NBS) on privately owned land. By specifically focusing on implementing NBS on private land, the project supports transformative efforts to increase resilience against issues caused by climate change as well as implementing and scaling innovative land policy strategies. The main output of the collaboration of the two projects is to identify options to coordinate EU legislation at one hand and to foster implementation on local level by the service of advisers by NGOs and the agricultural chamber on the other hand. Both projects clearly highlight the effort needed to coordinate on administrative level but also the benefits gained out of that process. Further, results clearly demonstrate that the service by advisors on local level is crucial for implementing measures, especially, for extensive nature-based solutions.

KEYWORDS: EU Water Framework Directive, EU Floods Directive, River development and risk management concept (RD-RM), Nature Based Solutions (NbS), LIFE IP IRIS Project, HORIZON Land4Climate project, case study Austria

1 INTRODUCTION

Water management needs to take care of different or even contradicting interests in river basins. Local, regional, national or even international interests at stake combined with increasing land use pressure on rivers and associated flood plains clearly highlight the need for a catchment-based management approach of planning and implementing measures. These water management interests are on the one hand the establishment, restoration and maintenance of riparian vegetation, riparian buffer strips and connected terrestrial and aquatic habitats and on the other hand the reduction of flood risks through flood aware land use management. Especially settlements, industry and production, energy and agriculture including associated interventions in the surrounding area and the water bodies themselves put pressure on the limited resource of land.

Additionally, issues related to agricultural practices like soil erosion and nutrient pollution need to be tackled. Sound and comprehensive planning is, therefore, needed to achieve best possible solutions by avoiding conflicts in the frame of achieving the goals set by the water policy framework. Restoration to achieve at least a good ecological status of our river systems is key to ensure a broad variety of ecosystem services. They support achieving the goals prioritised in the frame of the EU Water Framework Directive (Web-1) and EU Floods Directive (Web-2). The key objectives of the WFD are set out in Article 4 of the Directive. It requires Member States to use their River Basin Management Plans (RBMPs) and Programmes of Measures (PoMs) to protect and, where necessary, restore water bodies in order to reach good status, and to prevent deterioration. Good status means both good chemical and good ecological status. The EU Floods Directive aims to reduce and manage the risks that floods pose to human health, the environment, cultural heritage and economic activity. Both directives are implemented in 6-years cycles including a process of reviewing and, if necessary, updating all relevant steps of implementation.

To ensure best possible coordination amongst the two policies catchment-based river development and risk management concepts (RD-RM; Web-3) are implemented in Austria.

2 THE RIVER DEVELOPMENT AND RISK MANAGEMENT CONCEPT

The river development and risk management concept (RD-RM) is an overarching, integrative and catchment-based planning instrument. The aim of this administrative tool is to ensure that planning, measures and activities in the river basin, in particular with respect to flood risk management and river basin management are coordinated for achieving both, the objectives of the Water Framework Directive and the Floods Directive. The RD-RM is generally based on a compilation of existing, standardised data complemented by catchment related surveys. These surveys may focus on different aspects of water management and are agreed within the project set up. Focus might be given on ecologic and environmental aspects, sediment transport or flood risk management aspects. Therefore, the planning instrument serves flood hazard and risk management, as well as river ecology requirements and needs to define coordinated concepts of medium to long-term development goals, key measures and options. The RD-RM planning tool is to be used in Austria also as a funding prerequisite to implement structural and non-structural flood protection measures.

Inherent to the planning process is the incorporation of sectors outside water management. Part of setting up a RD-RM is to coordinate with priorities and goals of spatial planning, building regulation, emergency management, nature conservation, infrastructure, agriculture, forestry, fishery, hydropower, and also local stakeholders with a broad variety. To produce comparable concepts based on standardised data sets for different catchments in Austria the planning process for a RD-RM is standardised. It is divided into three consecutive phases with overarching activities which are shown schematically in Figure1.

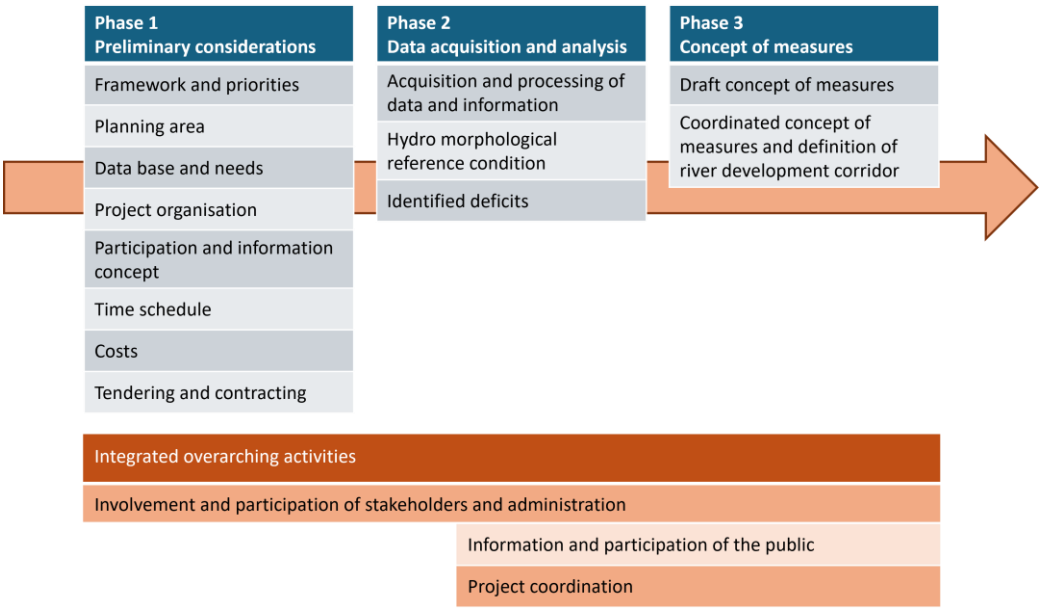

Figure 1: Processes to set up a river development and risk management concept

The three phases are structured in the (1) preliminary considerations, where – thematical – project priorities for the GE-RM are defined and a project structure is created. Missing data is collected in phase (2) data acquisition and analyses, where also the relevant deficits are identified. Finally, a (3) concept of measures is elaborated.

Project management is done by the water management administration on regional level, to ensure a transparent decision-making process in terms of both goal achievements referring to river development and flood risk management. This decision-making process is very much related to the options of measures that are agreed to be relevant, possible and feasible and the respective funding schemes that enable implementation. Thereby, the best possible results are measures serving multiple benefits such as flood retention, hydro-morphological improvement, ecological enhancement, recreation, habitat improvement, etc.

Phase 1 has substantial influence on how relevant stakeholders and affected parties are identified. Based on the thematical priorities a stakeholder analysis is done on regional level on all relevant institutions, stakeholders, NGOs and individuals are invited to participate in the planning process.

Based on preliminary considerations (phase 1) as well as the data acquisition and analysis (phase 2) the river development corridor is derived (Figure 2) as a spatial boundary for further planning. This corridor is based on recently experienced severe flood events as well as on historic data and ecological requirements combined with expert judgement for the final delineation. The corridor, further, serves as communication tool towards the public, land owners and sectors such as spatial planning and building regulation. The corridor is also applied for the delineation of areas for prioritised funding.

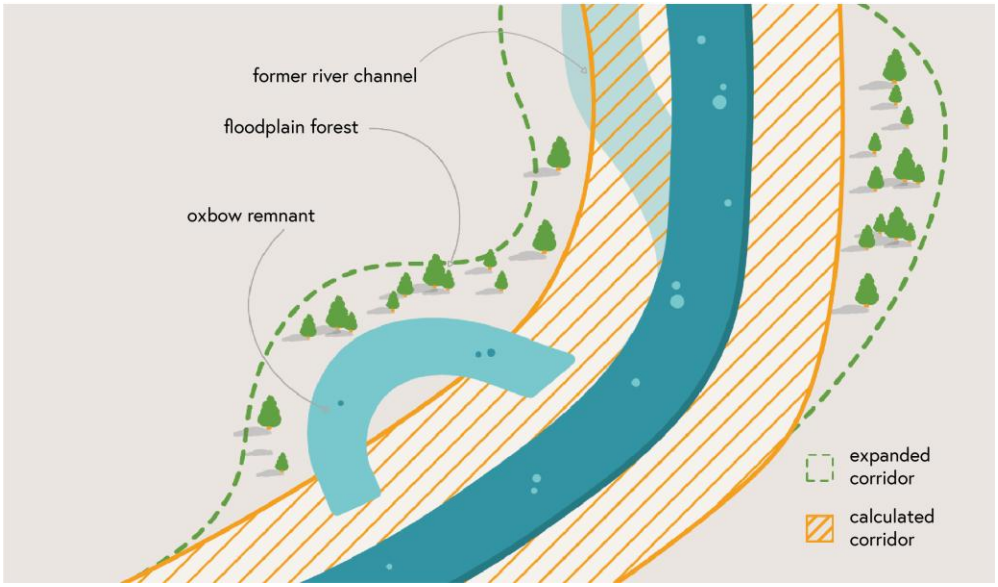

Figure 2: River development corridor as a spatial framework for planning and implementing measures

All planning phases are accompanied by integrated overarching activities to ensure involvement, information, participation and project coordination. Transparent information, communication and participation in decision-making are a central element of modern administrative understanding. For this reason, corresponding processes are also an integral obligation of the RD-RM. To ensure comparable and case-specific but comprehensive processes a guidance document (Figure 3) has been drafted and is applied in the RD-RM setup in Austria.

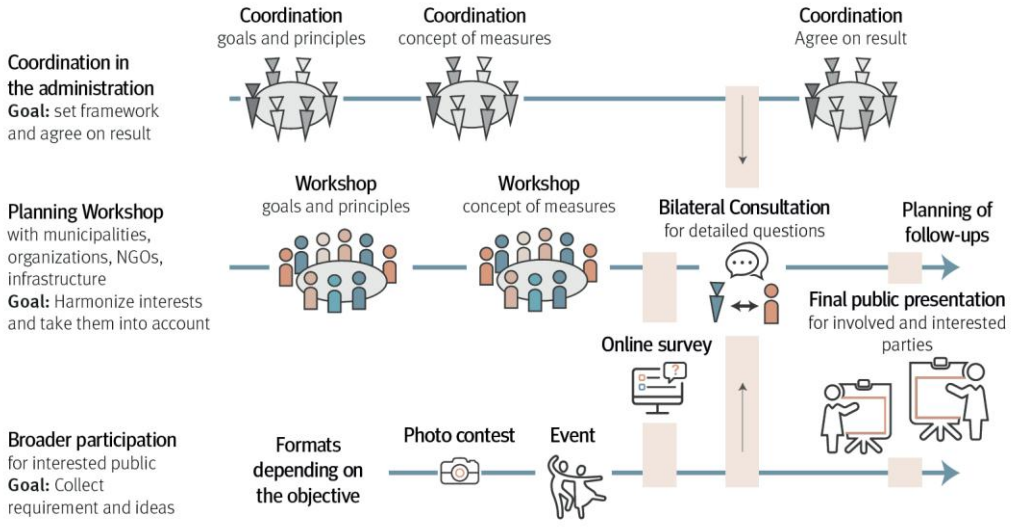

Figure 3: Roadmap for information, coordination and participation in the frame of RD-RM planning

The overall outcome of the planning procedure is a concept for measures providing an overview of measures or bundles of measures to be pursued in the future in order to best achieve the identified goals. In the process of defining relevant measures, a catalogue is used to ensure transparent and comparable planning results throughout Austria. The program of measures takes particular account of the use of synergies between measures for flood risk management and river basin management.

3 THE LIFE IP IRIS PROJECT – REVIEW AND REVISED IMPLEMENTATION OF RD-RM

LIFE IP IRIS – Integrated River Solutions in Austria project (Web-4) applied the RD-RM tool to seven pilot water bodies in Austria (Figure 3). After implementing RD-RM based on the first guidance document, a revision phase was set up to ensure efficient use of financial and human resources combined with an applicable planning tool that can be implemented in relevant catchments across Austria. Special focus was put on the share of administrative responsibilities, additional surveys and framework conditions. Additionally, the project was used to adopt governance practices in association with the RD-RM. For this review and revision phase of the first RD-RM guidance document the LIFE Integrated Project call of the European Commission proved to be the right funding schema.

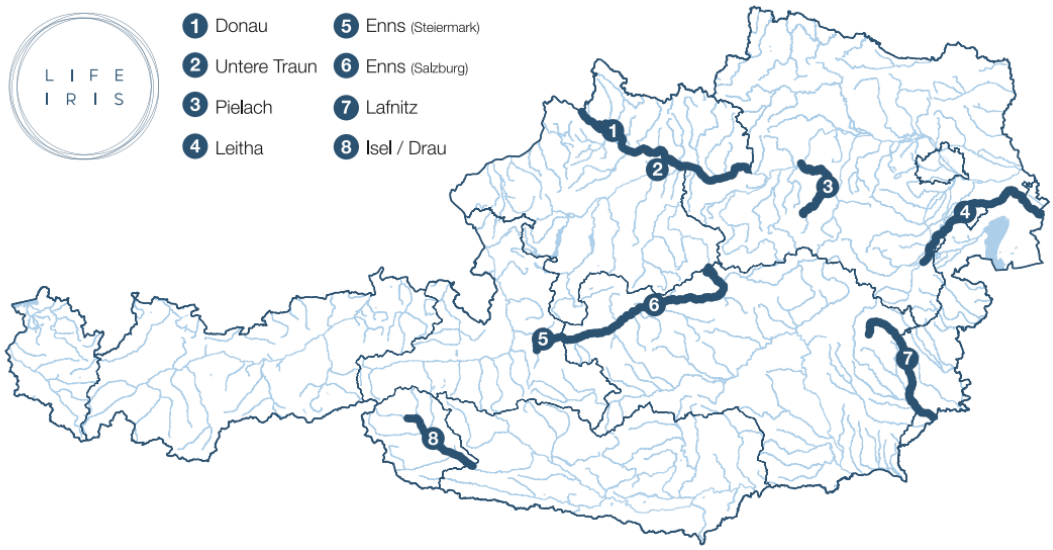

Figure 4: Case study rivers and location of measures of the LIFE IP IRIS project

The project has a total budget of 16.5 million € (EU, national and provincial funds), is being implemented by nine project partners and has a total duration of nine years (2019 to 2027). The first project phase dealt with the review and revision of the RD-RM guidance documents. In addition to strategic planning for the coordinated implementation of the National River Basin Management Plan and Flood Risk Management Plan, as well as the development of coordinated action plans for the IRIS pilot areas, the project also aims to plan and implement specific integrative river engineering projects and comprehensive monitoring of the effects of the measures.

Within the framework of the IRIS project, a monitoring concept was developed that, in addition to considering ecological and hydraulic improvements, also takes into account other effects of the measures, such as the impact on biodiversity and the water cycle and evaluates effects such as ecosystem services, impacts on terrestrial ecology, and the direct benefits that the population can derive from the implementation (sociocultural ecosystem services). Another focus of the IRIS project is capacity building. As part of the IRIS project, the necessary capacities are being developed at the federal and provincial levels. Regular networking meetings provide an opportunity to exchange information on various technical

and organizational aspects of RB-RM planning amongst the participating administrative organizations, sectors, and technical offices involved in the implementation of RB-RMs. This ongoing, open exchange of experiences enables the strengths and weaknesses of the planning instrument in its current form to be identified and solutions to be developed.

The IRIS project aims to raise public awareness that flood protection and river ecology do not have to be contradictory. The involvement of the population, stakeholders and NGOs in the planning process is intended to increase acceptance of the planning results and reduce potential conflicts in the frame of future measure implementation.

4 LAND4CLIMATE - APPLICATION OF CATCHMENT-BASED MEASURES AS A RESULT OF THE RD-RM

RD-RMs are intended to create forward-looking concepts that serve as a "roadmap" for a river basin to achieve the objectives of river basin management and flood risk management. From the perspective of flood risk management, especially under consideration of climate change impacts, the focus has to be on a broad bundle of risk management measures serving multiple benefits. The integration of the population, stakeholders and interested parties into the planning process is intended to increase acceptance for measures beyond flood protection, such as nature-based solutions (NbS, Web-5) and natural water retention measures (NWRM, Web-6), aiming at reducing flood risk and mitigate climate change at the same time. NbS and NWRM provide an important complement to technical solutions, have the potential to support other ecosystem services and promote biodiversity, therefore, having a synergistic effect on water ecology.

NbS and NWRM differ significantly from technical approaches. In many cases, the available instruments, land availability and the willingness of landowners for achieving these benefits are not yet fully developed. Further, there is still scepticism that NbS provide sufficient incentives for owners/users serving as a motivation to implement such measures. To overcome prejudice against NbS and NWRM a pilot project was implemented within the EU HORIZON program. In Austria, the LIFE IP IRIS test case of the Lafnitz river catchment (Figure 5) was chosen as implementation region for the Land4Climate project (Web-7).

Figure 5: Different sections along the River Lafnitz

In the Lafnitz river catchment, the major deficits identified by the RD-RM were related to too high sediment input from agricultural land and missing fish biomass. Thus, several stretches of the river Lafnitz fail the objective of good ecological status. While the RD-RM provides a profound planning basis for flood risk management measures within the river development corridor, the proposed measures within the catchment remain vague and require action from the local land managers. Therefore, the participation in the Land4Climate project is primarily intended to support the implementation of measures for sediment and water retention in agricultural areas outside of the river development corridor. Measures focus on reducing negative impacts of climate change. These measures are area-specific and must be aligned with

existing uses and compensated accordingly. The set of actions mainly includes adjustments in management practices and creation of landscape structural elements. Land4Climate aims to mitigate the adverse effects of flooding, drought, heat, and soil erosion while contributing to a healthy river ecosystem.

5 LESSONS LEARNT AND OUTLOOK

The river development and risk management concepts generate important stimuli for the synergistic implementation of measures in river ecology and flood risk management. The plans support the coordinated achievement of the objectives of the Water Framework Directive and the Floods Directive by tailor made measure implementation. However, after the elaboration of RD-RMs, incentives and framework conditions must be created in order to promote the implementation of the developed measurement concept in the best possible way. Lessons learnt and subjects to be tested and improved can be summarised as follows:

- The application of available legal instruments with focus on securing floodplains and floodplain areas by keeping them free from other land use needs to be strengthened and extended
- Land procurement along and near rivers needs to be done in an anticipatory way to also enable large scale Nature based Solution, Natural Water Retention Measures, restoration and renaturation measures
- Shared responsibilities amongst municipalities in the catchment area, cooperation and ownership need constant administrative support and institutionalisation by establishing water associations.
- Intersectoral coordination and implementation of measures supporting water retention as well as the reduction of sediment and contaminant input need permanent promotion and funding

Particularly with respect to climate induced changes options and measures have to be broadly discussed and evaluated together with all affected sectors and stakeholders that can contribute to achieving a broad variety of goals. Concluding, RD-RMs need to be implemented in a dynamic way to be able to react on all the external developments. Therefore, RD-RMs are set up as an forward looking planning instrument to be adapted, updated, and continued when needed, especially after the implementation of measures or a change in framework conditions.

REFERENCES

Web-1: https://environment.ec.europa.eu/topics/water/water-framework-directive_en
Web-2: https://environment.ec.europa.eu/topics/water/floods_en
Web-3: https://www.bmluk.gv.at/themen/wasser/schutz-vor-hochwasser/richtlinien-leitfaeden/leitfaden-germ-version-2024.html
Web-4: https://life-iris.at/en/
Web-5: https://research-and-innovation.ec.europa.eu/research-area/environment/nature-based-solutions_en
Web-6: https://www.nwrm.eu/
Web-7: https://land4climate.eu/

ICFM 10
Adapting to Global Change:
Innovative Approaches to Flood Management and Resilience
May 20-22, 2026 | Western University, London, Ontario, Canada

Research to Implement Policy and Operations Change: Forecast Informed Reservoir Operations within the US Army Corps of Engineers

Cary A. Talbot[1], F. Martin Ralph[2] and Cuong Ly[3]
US Army Engineer Research and Development Center, Vicksburg, MS, USA[1]
E-mail: Cary.A.Talbot@usace.army.mil

Center for Western Weather and Water Extremes, Univ. of California-San Diego, La Jolla, CA, USA[2]
E-mail: mralph@ucsd.edu

US Army Corps of Engineers South Pacific Division, Los Angeles, CA, USA[3]
E-mail: Cuong.Ly@usace.army.mil

ABSTRACT

A recent policy update within the US Army Corps of Engineers (USACE) allows forecasted conditions to be officially used in planning future water management operations. Since 2014, the USACE have been key partners with the Center for Western Weather and Water Extremes (CW3E) at the University of California-San Diego and with other federal, state and local agencies in a multi-agency, multi-disciplinary research and development effort called Forecast Informed Reservoir Operations (FIRO). FIRO has been exploring how improved forecast skill, hydrologic modeling and observations can better inform water management decisions in response to the USACE water management policy change.

FIRO viability is assessed at candidate sites using a research and operations partnership that brings scientists, engineers, regulators and reservoir operators together from across academia, federal, state and local agencies and their partners to assess the potential. FIRO implementation at pilot sites has demonstrated that implementation of FIRO can improve water availability, flood risk management and ecosystem benefits without costly infrastructure modifications.

This paper will summarize Phases I and II of the FIRO program, highlighting what was learned and accomplished in the first decade of the program; give a status update on progress with the goals of Phase III, the National Expansion Pathfinder, the current phase of the program; and share some thoughts on what's next for FIRO in the USACE and their partners. Legislative and agency changes to support FIRO both within USACE and beyond across its more than decade of history will also be presented.

The importance of the role of collaboration will be also emphasized. From partnering with academia to the FIRO viability assessment process, collaboration is at the heart of FIRO success – not just in determining how much flexibility in operations can be supported by the current science in meteorology, forecasting, hydrology and water operations, but also in building lasting relationships of institutional trust between stakeholders at any given reservoir.

KEYWORDS: water management, forecasts, reservoir operations, research and operations partnership, weather extremes

1 INTRODUCTION

The U.S. Army Corps of Engineers (USACE) has been engaged in a research and development effort called Forecast Informed Reservoir Operations (FIRO) since 2014. In late 2014, the U.S. Congress provided

additional funding to the USACE with specific direction to conduct "research into atmospheric rivers in an effort to develop and demonstrate better prediction capabilities and apply the science to improve reservoir operations to optimize multi-purpose project objectives and to meet stakeholder water needs." Additionally, in May 2016, the USACE updated a key policy regulation governing water control management that, for the first time, explicitly allows the use of forecast information in planning future water operations. In response to these events, the USACE engaged in a multi-agency, multi-discipline research and development effort to investigate how FIRO approaches might be safely and appropriately applied at a pilot reservoir, Lake Mendocino, in the Russian River watershed in northern California. This initial FIRO investigation (FIRO Phase I), carried out over a 5-year period, concluded successfully in 2020 after demonstrating substantial benefits in a severe drought year by increasing water availability for the dry summer by almost 20 percent. The investigation results motivated a 5-year deviation from the existing water control plan at Lake Mendocino to continue FIRO operations there while an update to its water control manual (WCM) was initiated to permanently incorporate FIRO.

Prior to the conclusion of Phase I, the U.S. Congress again provided funding to begin a 5-year transferability study (FIRO Phase II) focused on exploring transferability of Lake Mendocino's results across a broader range of reservoirs and watershed conditions, all within the western coastal region of the U.S. where atmospheric rivers are the dominant storm type. Through Phases I and II, FIRO has demonstrated that significant improvements in achieving a better balance between water supply, flood risk management and ecological benefits can be achieved. The improvements come at negligible negative impact to the multi-purpose objectives at reservoirs but rather provide increased benefits to all objectives simultaneously through improved efficiency in operations, as opposed to costly and lengthy infrastructure changes. The USACE has found that similar benefits can be realized at other reservoirs through execution of atmospheric and hydrologic research and exploration of FIRO applicability nationally that the FIRO Phase III workplan is currently developing and delivering. Phase III represents a National Expansion Pathfinder, as described below.

2 PREVIOUS FIRO PHASES

Brief descriptions of the objectives, goals and deliverables of FIRO Phases I and II is provided in the following sections, giving context to the objectives, goals and deliverables of FIRO Phase III, the National Expansion Pathfinder.

2.1 FIRO Phase I: Initial Pilot

FIRO Phase I was begun in 2015 and led to the development of an effective process to determine if weather forecast skill for a reservoir is adequate to safely incorporate forecast information in reservoir operations. Successful application of FIRO was demonstrated initially for a single pilot dam, Lake Mendocino, on the East Branch of the Russian River in northern California that supports a climate-change-vulnerable region, where atmospheric river-type storms are the cause of both flooding and provider of water supply. Talbot et al. (2019) describes this effort in detail along with the Final Viability Assessment (FVA) of FIRO at Lake Mendocino published by the Lake Mendocino FIRO steering committee in 2020 (Jasperse et al., 2020).

As part of the FIRO viability assessment process, major deviations, defined as plans that deviate greater than 5% from the existing water control plan contained in the WCM, were requested and FIRO scenarios were tested in water years (WY – defined as October 1 to September 30 in California) 2019 and 2020. In WY 2019, a relatively wet year, FIRO demonstrated increased flood risk management benefits while in WY 2020, the third-driest year on record at the time, nearly 20 percent more water was made available leading into the dry summer period through flexibility in operations made available to water managers through use of FIRO (Figure 1). This amount of water is roughly equivalent to the annual water use of 22,000 households. FIRO Phase I efforts concluded in 2020 and thereafter the USACE San Francisco District began a FIRO-based update to the Lake Mendocino WCM which was approved in October 2025.

The FVA-recommended plan defines a buffer zone, which is 10% of the Lake Mendocino storage volume, as flexible space available to the water manager to use to meet multipurpose objectives, based on forecasted weather, watershed and downstream conditions.

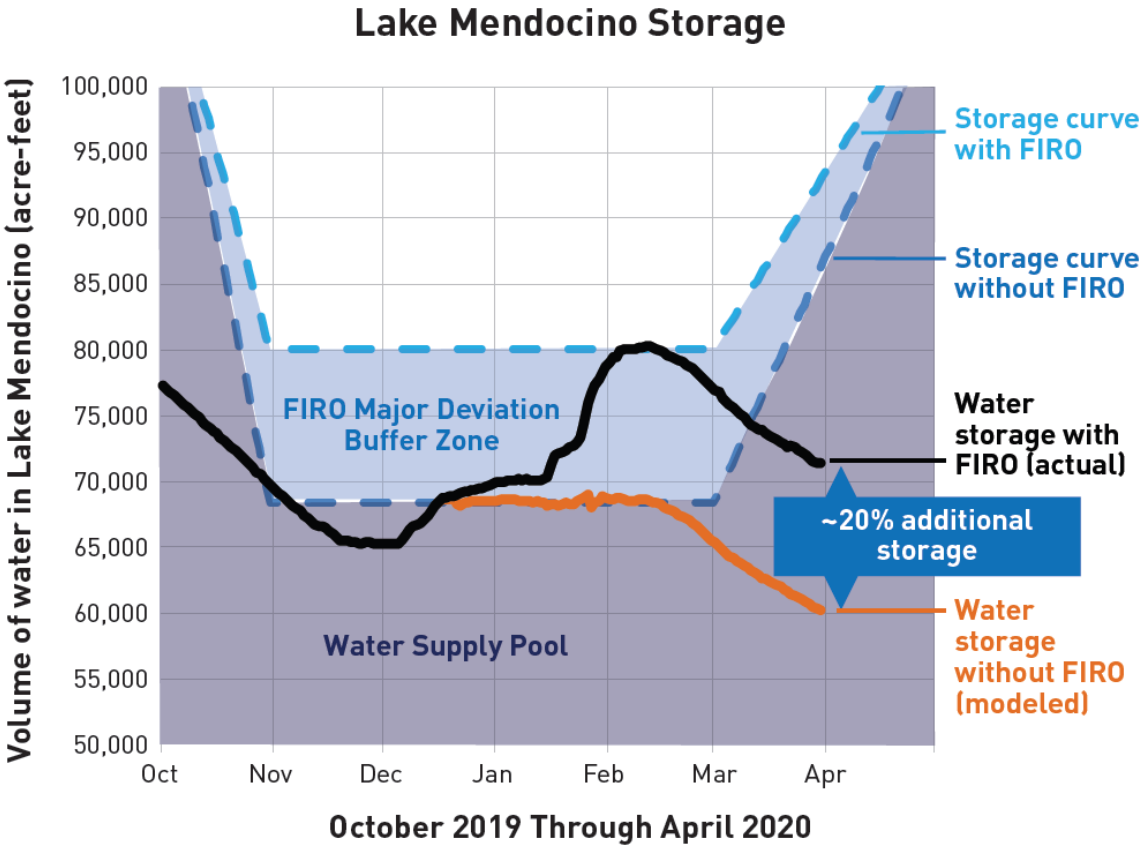

Figure 1: Lake Mendocino storage increased by ~20 percent during major deviation operations in WY 2020, compared with modeled storage without FIRO, during a year when precipitation was 38 percent of average. (figure credit: Sonoma Water)

2.2 FIRO Phase II: Transferability

Phase II, begun in 2019, explored the transferability of the findings from Phase I to other dams in the western U.S. where atmospheric rivers (ARs) are also the primary storm type, but with differing context (urban vs rural vs snow-dominated) and reservoir purposes (flood control only vs combination of supply and flood), as well as reservoir sizes and connectivity to much bigger water supply/flood control systems. These assessments are being conducted on 4 reservoirs as described in the following sections. Phase II also included development of a FIRO Screening Process – a method the USACE can use to screen the entire portfolio of USACE dams (nearly 600 with flood risk management as a purpose) to determine which dams might be suitable for further FIRO investigation and implementation. The FIRO Screening Process will also be described.

2.2.1 Prado Dam

Prado Dam, on the Santa Ana River in southern California, was built by the USACE in 1941. The Orange County Water District (OCWD) and USACE have worked together each year to maximize the capture and groundwater recharging of stormwater held behind the dam after storm events. Figure 2 shows

the elevations and volumes of the current conservation pool as well as tested FIRO elevations. USACE releases water temporarily captured at Prado Dam and OCWD recharges the water into the ground 10 miles downstream. The water conservation pool has been operated at elevations up to 505 feet based on a five-year major deviation approved by USACE in March 2018. The Prado Basin Ecosystem Restoration and Water Conservation Feasibility Study was approved in 2021 to make the 505-foot conservation pool a permanent feature within the Interim WCM (Ralph et al., 2023).

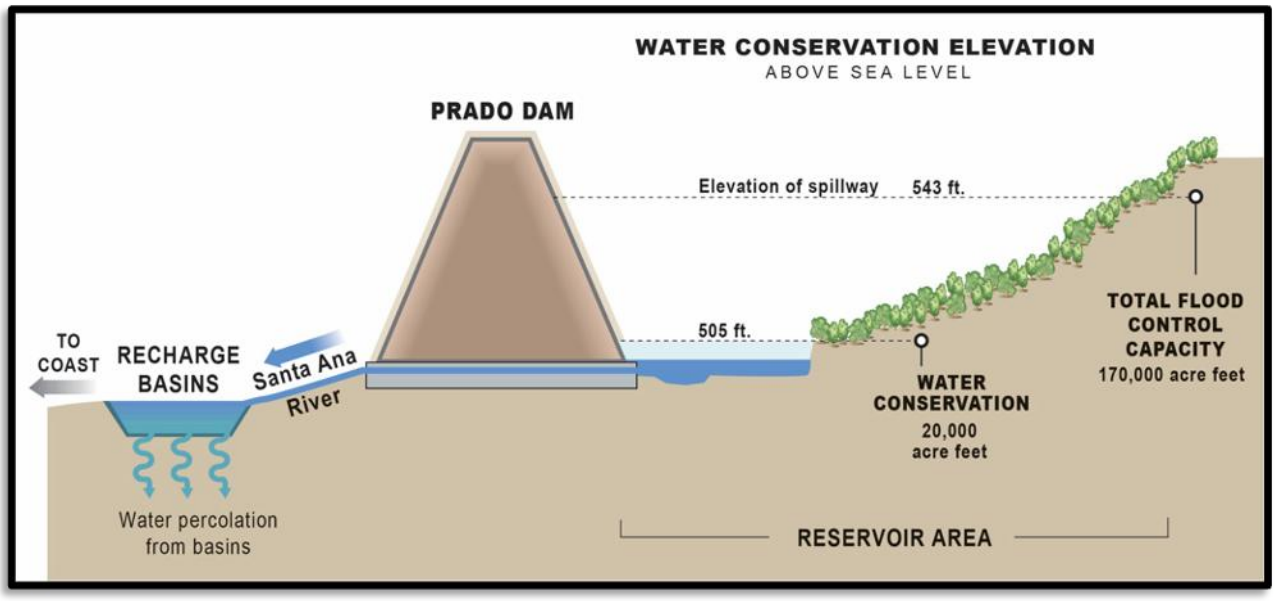

Figure 2: Schematic of Prado Dam water conservation elevation for stormwater storage and capture with tested FIRO buffer pool levels of 508 and 512 feet. (figure credit: OCWD)

Like most WCMs within the USACE, the current Prado Dam WCM does not explicitly leverage weather and water forecasts. Nonetheless, USACE water management staff consider precipitation and streamflow forecasts in their decision process while adhering to WCM guidelines and procedures. As part of the FIRO viability assessment process at this site, the Prado Dam FIRO Steering Committee conducted and published a Final Viability Assessment (PVA) in November 2023 (Ralph et al., 2023) which tested and determined the range of possible FIRO scenarios that could be supported by current operational constraints, current forecast skill and other relevant factors.

2.2.2 Yuba-Feather System

In addition to Prado Dam, a third pilot was added that consists of a two-dam system in one large watershed where snowpack is a vital water supply, and floods are strongly influenced by how much of the watershed experiences rain vs. snow in a storm. This system, the Yuba-Feather System, consists of New Bullards Bar (NBB) dam, owned and operated by the Yuba Water Agency (Yuba Water) on the Yuba River and Oroville dam (ORO), owned and operated by the California Department of Water Resources (DWR), on the Feather River (see Figure 3). By federal policy, the USACE regulates flood risk reduction operations of both reservoirs according to their respective WCMs which are written by the USACE. Releases from NBB and ORO converge in Yuba City, CA which requires that operations between these two reservoirs be coordinated. The primary objective of the Yuba-Feather FIRO project is to reduce flood risk; a secondary objective is to achieve water supply benefits where possible, while supporting environmental needs. Reducing flood risk by making reservoir releases ahead of storms creates additional temporary flood storage space for anticipated inflows but requires confidence and skill in forecasted conditions (Ralph et al., 2025).

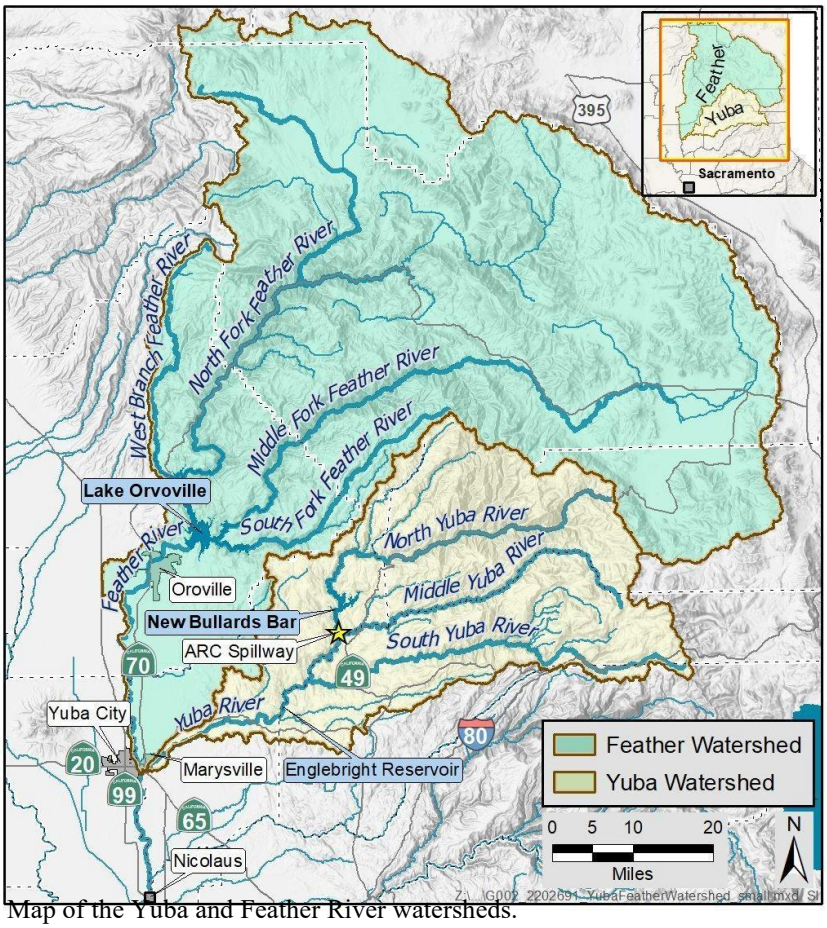

Figure 3: Map of the Yuba and Feather River watersheds.

To better leverage forecasts, Yuba Water is designing a second spillway, called the Atmospheric River Control (ARC) Spillway for NBB that allows for greater forecast-informed pre-releases at lower reservoir elevations. Using FIRO with the planned spillway will enable the management of up to an additional 117,000 acre-feet of reservoir space and the potential to reduce water levels on levees near Marysville, CA by 2 to 3 feet.

The FVA for the Yuba-Feather System, completed in February 2025, had the following key findings: 1) The FVA demonstrated that FIRO strategies combined with a planned second spillway at NBB could provide additional flood control storage capacity in the system and allow for reservoir operations flexibility to reduce downstream peak flows during major prolonged storms like 1986 and 1997 that devastated Yuba County; 2) For the scenarios tested, FIRO with the ARC spillway could provide a level of protection equivalent to the proposed (but never constructed) Marysville Reservoir, approx. 260,000 acre-feet; and 3) Post-event storages were consistently higher than pre-FIRO storages; therefore, there could be a water supply benefit, pending a full analysis in the WCM updates (Ralph et al., 2025).

2.2.3 Howard A. Hanson Dam

A fourth FIRO pilot site was selected at Howard A. Hanson Dam (HAHD) on the Green River upstream from Seattle, WA. This pilot study experienced some delays in the viability assessment process due to various factors, including the effects of the COVID-19 pandemic, but recent progress has been made that is moving this effort forward. Tacoma Water and the USACE Seattle District are collaborating with CW3E, USACE Engineer Research and Development Center, the National Weather Service (NWS), the National Marine Fisheries Service, King County River and Floodplain Management, and the Muckleshoot Indian Tribe to assess the benefits of reservoir management scenarios using forecasts at HAHD through a FIRO Viability Assessment Steering Committee. On-going construction of a downstream Fish Passage Facility plus an Additional Water Storage Project present unique opportunities to explore how FIRO at HAHD might increase the benefits of those investments through operational flexibility.

The HAHD FIRO project is investigating this key question: How can improved forecasts of landfalling ARs and associated precipitation and runoff be used to improve the reliability of spring refill to meet instream flows for fish and water supply storage objectives, improve the effectiveness of summer water management in advance of the fall flood transition period, maintain or improve operations for downstream flood risk management, and ensure forecasts and operations are flexible enough to respond to

a changing climate without impacting flood risk, water storage reliability, and flows for fish? (Ralph et al., 2024)

2.2.4 FIRO Screening Process

Using lessons learned from the transferability of FIRO to additional pilot sites in Phase II, a FIRO Screening Process was developed to scale up the implementation of FIRO. The Screening Process maintains the same level of rigor and quality to the process as demonstrated at the original pilot sites but at a screening level which can be executed more rapidly than full viability assessments.

The goal of the screening process is to employ a broadly usable tool for water management agencies to determine sites where FIRO may be appropriate, including evaluating entire portfolios of reservoirs. The Screening Process is meant to be an adaptable, easy-to-use process that empowers more local ownership over FIRO implementation.

As depicted in Figure 4, the FIRO Screening Process was designed as a three-stage process with the first Stage A being an initial screening with "weed out" criteria to eliminate dams that have little or no FIRO potential due to any one of several criteria, such as not having a controlled outlet or no WCM. Stage B delves into the specifics of each candidate site, producing a spectrum of less to more suitable for FIRO scoring. This "suitability index" can be used by a water resources agency to decide where further FIRO investigation is warranted, given limited time and resources. The third Stage C involves a more thorough assessment and dialog with the USACE District responsible for those sites that are prioritized in Stage B. As depicted in Figure 4, a variety of outcomes are possible from this Stage C assessment. Possible outcomes of Stage C are that barriers to FIRO implementation may be prohibitive, or that more research and improvements in forecast skill, for example, could be needed before FIRO could be successfully implemented. Finally, Stage C could also identify sites where all indications are that FIRO suitability is high and the recommendation is to either consider or strongly consider implementing FIRO.

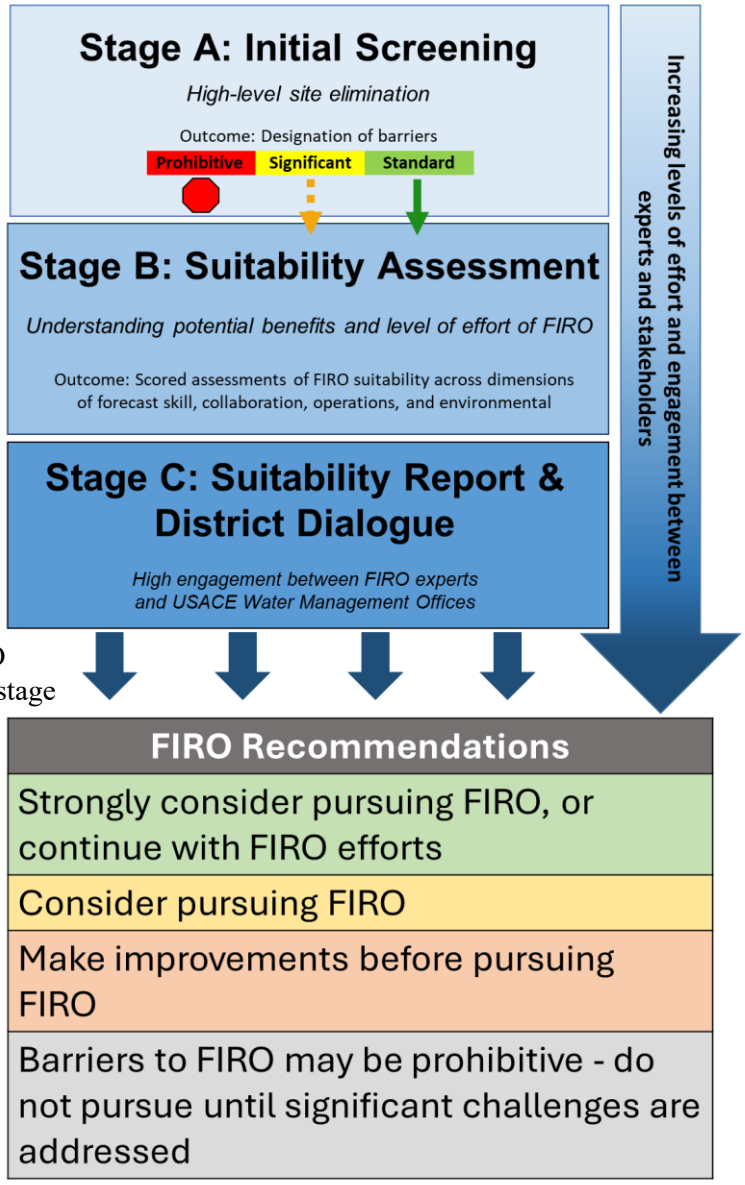

Figure 4: FIRO Screening Process stages schematic.

3 FIRO PHASE III: THE NATIONAL EXPANSION PATHFINDER

Phase III began in 2023 and accelerates FIRO assessments substantially by: expanding to systems of dams and to other regions nationally where extreme precipitation and flooding is influenced by different storm types; applying the screening process to all USACE dams; completing the FIRO viability assessments underway in Phase II; and expanding the research into improving forecast skill, particularly in areas of the U.S. that are impacted by atmospheric rivers and/or other major storm types, specifically tropical storms/hurricanes, clusters of thunderstorms, and Nor'Easters. Phase III will complete core elements of the FIRO National Expansion Pathfinder as described below.

3.1 Forecast Skill Assessment and Improvement for Multiple Types of Flooding Storms

FIRO is not viable at reservoirs where forecasts of extreme precipitation and associated floods do not have adequate skill. Although meteorology has largely struggled to improve quantitative precipitation forecasts (QPFs), FIRO Phases I and II have found that atmospheric rivers are the key storm type in the U.S. west coast flood season (fall/winter). Additionally, FIRO research has found that there is adequate skill to support FIRO operations at Lake Mendocino with additional positive results at Prado Dam, ORO and NBB. Research to improve forecasts have benefitted from focusing on the storms that predominantly produce the precipitation at these reservoirs, i.e., atmospheric rivers (ARs). FIRO viability has also been favored by the fact that watersheds along the U.S. west coast are relatively short and steep, leading to short travel times for water released from a dam to move beyond flood prone areas. AR forecast skill at lead times of even just a few days is often sufficient for FIRO to be viable at many reservoirs.

FIRO viability in other regions nationally, where different storm types dominate flooding, hinges on the forecast skill for these storms and on the watershed sizes and travel times for water released from dams. Slopes are generally much shallower and thus water travel times longer in places like much of the U.S. southeast and Great Plains. Also, convection, a frequent storm type in many parts of the country, especially in the summer, is notoriously difficult to predict accurately, while the track and intensity of landfalling tropical storms/hurricanes can also be difficult to predict, including whether they stall (e.g., hurricanes Harvey and Florence). Studies have found that forecast skill for extreme daily precipitation is best in the U.S. west (due to ARs) followed by New England and suggests the need for improvement in QPF for these storm types may be needed for FIRO to be viable.

Precipitation prediction skill is tied to the dynamical processes in the major storm types, and to the models and forecast tools that have been developed to predict them. As with atmospheric rivers in the U.S. west, a key to identifying the causes of errors in predictions of extreme precipitation in these storm types is understanding the meteorological attributes of the storms that make them capable of producing the extreme precipitation. This also leads to fruitful research pathways for improving these predictions. By analogy, the hydrologic differences in regions affected by these storms need to be considered.

3.2 Conduct Viability Assessments of Systems of Dams

Phase III will assess two major systems of dams (representing at least 8 dams in each system), for which coordination across several dams in an entire larger watershed is required. The first of these will be the Willamette Valley watershed system, with its 13 reservoirs owned and operated by the USACE, where ARs are the main drivers of floods and a leading source of water supply both for municipal, agriculture and ecological uses. The Willamette Valley FIRO Viability Assessment was initiated in 2025 with workplan development for the viability assessment across the numerous dams of the system underway. The second system of dams to be evaluated will be in a region outside of the western U.S. where non-AR storm types are a key factor and will be identified later in 2026.

3.3 Conduct FIRO Screening Process on all USACE Flood Risk Management Dams

All or parts of the western U.S. are impacted by AR events, some to greater degrees than others. The FIRO Screening Process was developed from lessons learned by applying FIRO to the initial pilot sites

described in Section 2. The screening process was then tested using all 85 USACE South Pacific Division dams, covering the states of California, Nevada, Utah, Arizona, New Mexico and parts of Colorado. Additionally, the other aspects of Phase III are exploring FIRO in regions characterized by other storm types and reservoir operations strategies, constraints and methods, allowing the systematic growth of the scientific and engineering knowledge base needed to perform well-founded future assessments of FIRO applicability across a much broader range of conditions than has been explored in the first pilot reservoir, Lake Mendocino, and the transferability study basins in the West.

In 2025 Stage A of the screening process was applied to the nationwide portfolio of USACE dams and reservoirs that have flood risk management missions. Figure 5 depicts the results of the Stage A screening for all 593 dams in the USACE portfolio. Dams depicted in red (184 or 31%) are those that did not pass Stage A of the screening due to prohibitive barriers to FIRO that were identified. Dams identified with significant barriers to FIRO are shown in yellow (299 or 50%). Dams in this category are eligible to be considered for further screening in stages B and C if the responsible USACE District indicates an interest in doing so. Dams with no significant or prohibitive barriers are shown in green (110 or 19%) and are all proceeding to stages B and C of the screening process (Yeates et al., 2026).

Stages B and C have been completed for all dams passing Stage A within the South Pacific Division and are currently being conducted for all dams passing Stage A within the Northwestern and South Atlantic Divisions (see Figure 5). Stages B and C for the dams passing Stage A in the additional USACE Divisions will be conducted later in 2026 and into 2027.

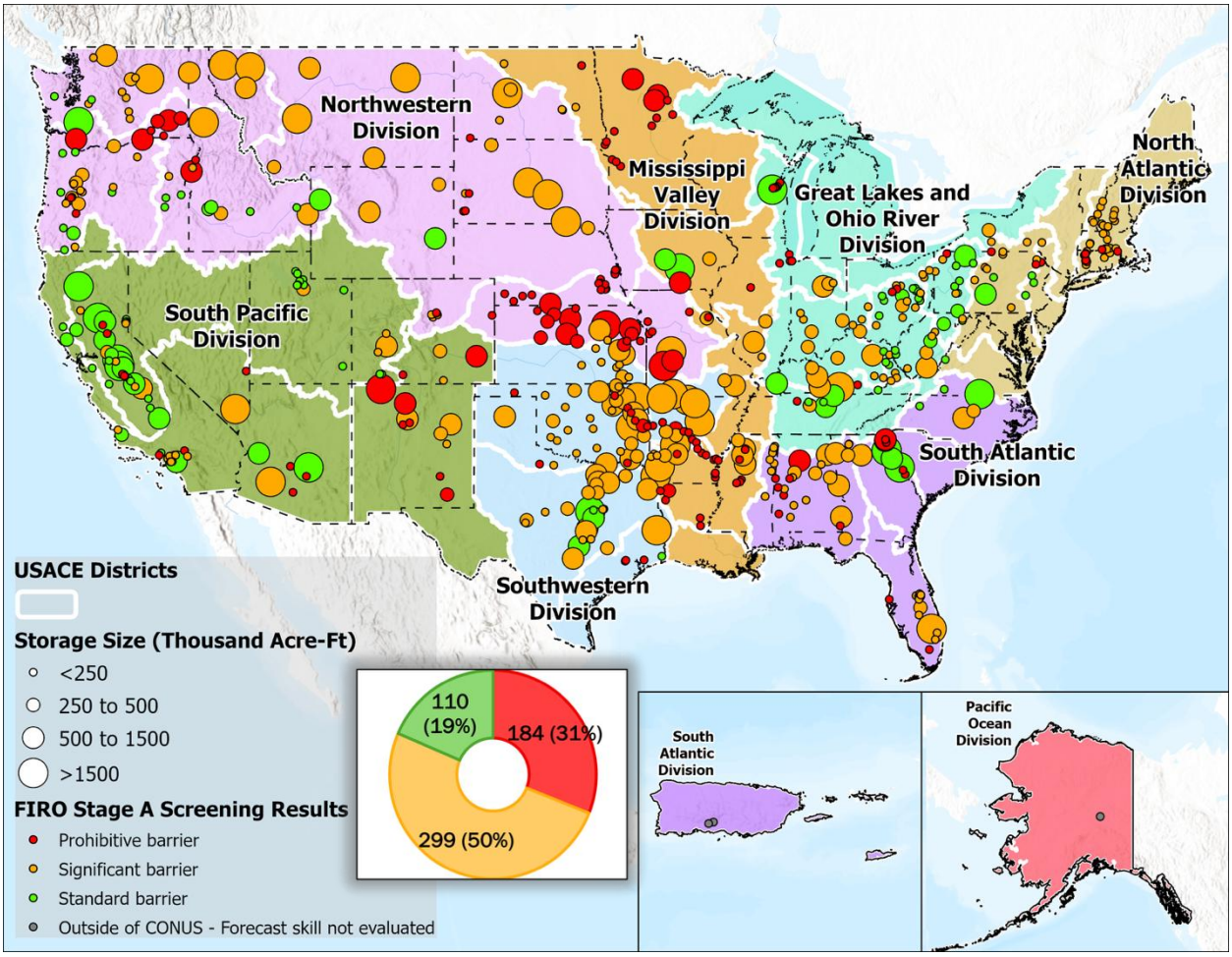

Figure 5: FIRO Screening Process Stage A results for the entire 593 dams within the USACE Flood Risk Management portfolio. An interactive version of these results can be found here: https://storymaps.arcgis.com/stories/79d51b5579ef4b0493b3c8471443bba4

3.4 Conduct Viability Assessments on Two Single Dams in Other Regions Nationally

Two additional viability assessments for single dams are to be conducted in regions of the country where extreme precipitation is dominated by weather systems other than ARs, e.g., tropical storms/hurricanes, large clusters of long-lived thunderstorms, or Nor'Easters. These dams will not be located in the same regions explored in the assessment of system of dams. Selection of these dams is underway and is being coordinated with the results of the FIRO Screening Process.

4 KEY LESSONS LEARNED AND THE PATH FORWARD

The importance of having multi-disciplinary, multi-agency steering committees, partnered together with academia, to lead the evaluation of FIRO viability through the Viability Assessment process developed in the FIRO program cannot be overstated. Having the variety of backgrounds of those with interests in water supply, flood risk management, ecological concerns, and the difference in approach between researchers and operators brings a wealth of perspective and experience that greatly enriches the experience of seeking a better balance between competing objectives in water management. A fundamental rule of engagement with each FIRO steering committee is the principle that all parties are actively engaged with the goal of finding what will the science support. This principle has the effect of making the discussion of changing water operations – often a contentious and fraught topic, particularly in the western U.S. – significantly less threatening, particularly since there isn't a specific proposed plan. The exploration of what is possible within the boundaries of each organization's constraints and the physical limitations of the existing infrastructure helps create an atmosphere of institutional trust that has, for each of the viability assessments completed to date, produced consensus proposed changes to WCMs that are universally supported through the approval and public comment process.

The River Forecast Centers (RFCs) of the NWS play a key role for USACE in providing inflow forecasts to USACE reservoirs. While USACE does have some ability to generate its own hydrologic inflow forecasts from QPFs, USACE has enjoyed a fruitful partnership with RFCs in relying on their expertise in predicting hydrologic inflows. With the advent of FIRO within USACE and other federal and state agencies, the workload for RFCs to provide more detailed and extensive forecasts, particularly ensemble forecasts, has increased. In recognition of this, NWS has embarked on a restructuring of their RFCs nationwide to better support the workload demand for supporting FIRO. USACE and other federal and state agencies view this as a very positive development that is anticipated to provide an even closer and productive collaboration between NWS and USACE in realizing maximum benefits of implementing FIRO nationwide.

The FIRO program continues to enjoy strong support from the U.S. Congress through continued appropriations as well as advocacy from within senior leadership of the USACE and current and past administrations. Looking forward beyond the completion of FIRO Phase III, the focus will be on implementing FIRO at the dams with the highest suitability scores as prioritized by the FIRO Screening Process. Accelerating the viability assessment process through streamlined and expedited pathways will be key to implementing FIRO at an increased pace to deliver the benefits of improved balance between competing reservoir operation purposes across the entire USACE portfolio of flood risk management dams.

5 CONCLUSION

With the key policy update in May 2016, the USACE has entered a new phase of water management where forecasts can be officially incorporated into WCMs and other water management practices. The FIRO research and operations partnership has defined how this can safely and effectively be done and codified in WCM updates. The viability assessment studies conducted to date indicate from 5-20% increased water availability as well as improvements in flood risk management and ecosystem benefits at the reservoirs where FIRO has been studied. The results of Phases I and II of FIRO have demonstrated the value of assessing FIRO viability at candidate reservoirs and Phase III is exploring how these benefits can

be realized in other parts of the country and at an accelerated pace. Results to date clearly indicate that FIRO provides an effective means of increasing the efficiency and resiliency of existing water resources infrastructure to achieve multi-purpose benefits and provide increased flexibility demanded by climate extremes, all without costly construction projects. FIRO viability assessments conducted by multi-disciplinary, multi-agency steering committees build institutional trust among participants that lead to increased collaboration and accelerated approval of WCM updates. Internal restructuring of NWS RFCs to support FIRO going forward will have a long-lasting positive impact on increasing the magnitude and value of FIRO benefits as it is implemented across the nation.

REFERENCES

Jasperse, J., Ralph, F. M., Anderson, M., Brekke, L., Malasavage, N., Dettinger, M. D., Forbis, J., Fuller, J., Talbot, C., Webb, R., & Haynes, A. (2020). Lake Mendocino Forecast Informed Reservoir Operations Final Viability Assessment. UC San Diego. https://escholarship.org/uc/item/3b63q04n.

Ralph, F. M., Hutchinson, A., Anderson, M., Fairbank, T., Forbis, J., Haynes, A., Sweeten, J., Talbot, C., Tyler, J., White, R. (2023). Prado Dam Forecast Informed Reservoir Operations Final Viability Assessment. UC San Diego. Retrieved from https://escholarship.org/uc/item/8rx4n0vp

Ralph, F. M., James, J., Leahigh, J., Anderson, M., Forbis, J., Haynes, A., Jasperse, J., Lindley, S., Talbot, C., White, M. (2025). Yuba-Feather Dam Forecast Informed Reservoir Operations Final Viability Assessment. UC San Diego. Retrieved from https://cw3e.ucsd.edu/FIRO_docs/Yuba-Feather_FVA/Yuba-Feather_FVA.pdf

Ralph, F. M., Talbot, C., Knickerbocker, J., Marxen, S., Intermill, J., Werner, K., Strazer, M., Warner, E., Rapin, N., Forbis, J. (2024). Work Plan for Howard A. Hanson Dam Forecast Informed Reservoir Operations. UC San Diego. Retrieved from: https://cw3e.ucsd.edu/FIRO_docs/FIRO_HowardHanson_Workplan.pdf

Talbot, C.A., M. Ralph, and J. Jasperse. (2019). Forecast-Informed Reservoir Operations: Lessons Learned from a Multi-Agency Joint Research and Operations Effort. Federal Interagency Sedimentation and Hydrologic Modeling Conference, June 25-28, Reno, Nevada. Conference Proceeding.

Yeates, E.M., Barber, C.A., Rodman, N. B., Shearer, E., Weihs, R., Forbis, J., Talbot, C. (2026). FIRO Screening Process: Stage A Development and National Results (Report No. ERDC/CHL TR-26-13). Vicksburg, MS: U.S. Army Engineer Research and Development Center.

Web sites:

Web-1: https://storymaps.arcgis.com/stories/79d51b5579ef4b0493b3c8471443bba4, consulted 12 December 2025.

ICFM 10
Adapting to Global Change:
Innovative Approaches to Flood Management and Resilience
May 20-22, 2026 | Western University, London, Ontario, Canada

Fast-tracking the Collaboration and Comprehension of Civil Engineering Structures within the Dutch Flood Protection Programme

Ellen Tromp[1], Niels Hoogendoorn[2] and Eric van der Meij[3]
Deltares, P.O. Box 177, 2600 MH Delft, The Netherlands[1]
E-mail: Ellen.Tromp@Deltares.nl

Hoogheemraadschap Hollands Noorderkwartier, P.O.Box 250, 1700 AG Heerhugowaard, The Netherlands [2]
E-mail: N.Hoogendoorn@hhnk.nl

Hoogheemraadschap Hollands Noorderkwartier, P.O.Box 250, 1700 AG Heerhugowaard, The Netherlands [3]
E-mail: E.vanderMeij@hhnk.nl

ABSTRACT

In the past years, much effort has been undertaken to gain further insight in the scope of the civil engineering structures, as part of the Dutch Flood Protection Programme (DFPP). In an innovative project, we shifted from aa flood defmount of structures to the required total investment cost to meet the statutory standards. The investment costs are considerably lower than originally thought. Here, the regional water authorities, Rijkswaterstaat, the Dutch Flood Protection Programme, research institutes and the consultancy firms joint forces. In the first phase we (1) developed a civil engineering roadmap, highlighting the different steps during the life cycle of a structure in a primary flood defence, and (2) used a framework to help identify the critical success factors.

For the second phase, allowing knowledge to flow was key. Therefore, we held several interviews to collect the available knowledge differentiating for the three phases of the hydraulic roadmap, namely (a) asset management, (b) portfolio management and (c) reinforcement projects. In our paper, we highlight the gained insights for each phase, with examples from the Dutch practice. As knowledge is situated and socially constructed, this knowledge has been actively shared and restated after each change in the group of participants.

There are two main reasons why collaboration in the civil engineering structures assignment is necessary. The limited capacity and expertise in the market requires smart and efficient cooperation. Besides this, the changing physical environment is an important reason for collaboration: climate change, technological developments and other societal challenges are the main reasons to work over one's organizational boundaries. This further enhances the collaboration between the regional water authorities and Rijkswaterstaat to ensure that their task is finished before 2050 and enhances the knowledge transfer and uptake within the triple helix.

KEYWORDS: Civil-engineering structures; flood risk management; innovation; knowledge management; Dutch Flood Protection Programme.

1 INTRODUCTION

For centuries, the Netherlands is battling with water. Approximately two-thirds of the country lies below current sea level. In recent years, the Dutch national government shifted from a reactive to a proactive approach (Delta Commission, 2008). This shift incorporates long term uncertainties—including climate

change and land subsidence—into planning and policy in order to ensure the sustainable protection of the country (Most et al., 2014). The resulting risk based approach reflects new insights into the reliability of dikes and the consequences of major flooding resulting from the failure of dikes or associated structures. Protection standards are now determined by both the probability and potential impact of flooding in 2050, taking climate and socio economic developments into account. The Dutch Environment Act establishes statutory safety standards for flood protection infrastructure, including dikes, dams, and other hydraulic structures. Every twelve years, regional water authorities (RWAs) are required to assess the condition and performance of these flood defences to verify compliance with the prescribed standards. If deficiencies are identified, the responsible authority may apply for funding through the Dutch Flood Protection Programme (DFPP) (Jorissen et al., 2017; Tromp et al., 2025). Jonkman et al. (2018) identify two major challenges in this context: first, the renewal, adaptation, or upgrading of hydraulic structures in light of evolving safety standards and functional demands (e.g., increased shipping traffic); and second, the ongoing management and maintenance of existing structures.

In 2018, representatives of Rijkswaterstaat, RWAs, knowledge institutes, and consultancy organisations jointly emphasised the need for an innovation initiative addressing the civil engineering structures that form part of the primary flood defence system (DFPP, 2018). These structures include locks, sluices, culverts, pumping stations, and storm surge barriers (Figure 1). In 2021, the regional water authority Hollands Noorderkwartier (HHNK) initiated the innovation project Working Jointly on Hydraulic Structures. Until that point, hydraulic structures had received relatively limited attention, and no systematic national approach existed. In Tromp et al. (2024), the main author presented the findings from the project's first phase, which revealed that more than 400 hydraulic structures were listed within the DFPP portfolio—implying that, on average, one structure would need strengthening every three weeks.

The DFPP continues to use the definition of hydraulic structures provided in the Dutch Environment Act (2016): a construction forming part of a flood defence that temporarily assumes the flood protection function over a limited length, but which is designed primarily to serve another utilitarian purpose crossing the flood defence (e.g., drainage or navigation). These structures typically include one or more movable components such as valves. For DFPP assessment, an additional requirement is applied: the flow area of the water retaining component must exceed 0.5 m² (DFPP, 2016). Four distinct failure mechanisms are used to assess water retaining structures: (1) Reliability of closure, expressed as the probability of non-closure per closure demand; (2) Insufficient height, expressed as the probability of excessive wave overtopping or overflow; (3) Piping, expressed as the probability of insufficient resistance to piping; and (4) Structural strength and stability, expressed as the probability of structural failure.

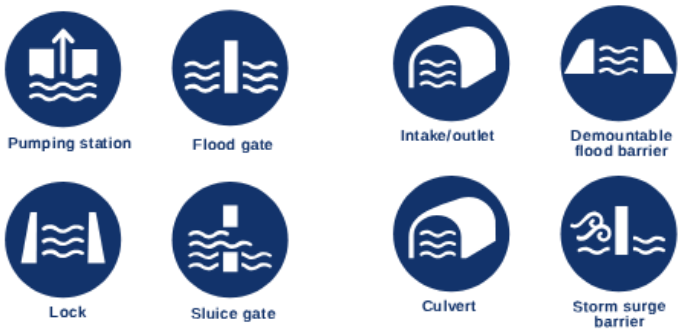

Figure 1: Hydraulic Structures within the primary flood defence of the Netherlands.

In this first phase (Tromp et al., 2024), the project team gained better understanding of the numerous obstacles that hamper the reinforcement of these civil engineering structures. To tackle these barriers, we developed a roadmap that gives more insight in the steps for strengthening these structures. Based on the first results of the statutory assessment, we updated the scope and numbers of the hydraulic structures as part of the DFPP. Phase 1, as shown in Tromp et al. (2024), concluded that a wealth of information and

knowledge needs has been identified, but as knowledge is situated and socially constructed, this knowledge must be actively shared and restated after each change in the group of participants.

In this paper, we apply the learning-while-doing approach of the DFPP (Tromp et al., 2022) to these hydraulic structures and introduce the readers to our approach and experiences so far. Here, our focus lies primarily on the hydraulic structures that often consist of a location-specific combination of components and materials and are required to perform other functions too. For these structures, multiple parties, with their own individual interests and responsibilities, play a role, and they seek to minimise trade-offs. This complexity further emphasises the importance of knowledge management and continuous learning around these structures. The paper is structured as follows: Section 2 presents the methods, looking at the Dutch Flood Protection Programme and specifically to the hydraulic structures, followed by a description of the methodology used in our study; in Section 3, we describe what insights were gained and what the lessons learned are from the second phase of the innovation project. Finally, Section 4 presents the discussion and conclusions of this paper.

2 METHODS

As phase 1 showed that knowledge transfer and uptake was key, our aim was to actively gather and share knowledge, such that project teams now and in the future will benefit from this. To acquire a better understanding of how knowledge transfer and uptake takes place in the design processes of flood defences, the first author (Tromp, 2019, Tromp et al, 2022) developed and validated a conceptual framework called the Framework for Observing, Diagnosing and Intervening in Knowledge Interaction moments (acronym: FODIKI), as depicted in Figure 2. Drawing on Vlachos (1977), we conceptualise knowledge transfer and uptake as an interaction between a knowledge supplier and knowledge user, with knowledge (K) flowing from sender (S) to receiver (R). This model retains the possibility of failure, such as semantic distortion caused by cognitive barriers. When transfer succeeds, K becomes available to R, who may then apply it. We define uptake following Knott and Wildavsky's (1980) seven-stage utilisation scale, ranging from reception and cognition to adoption, implementation, and impact.

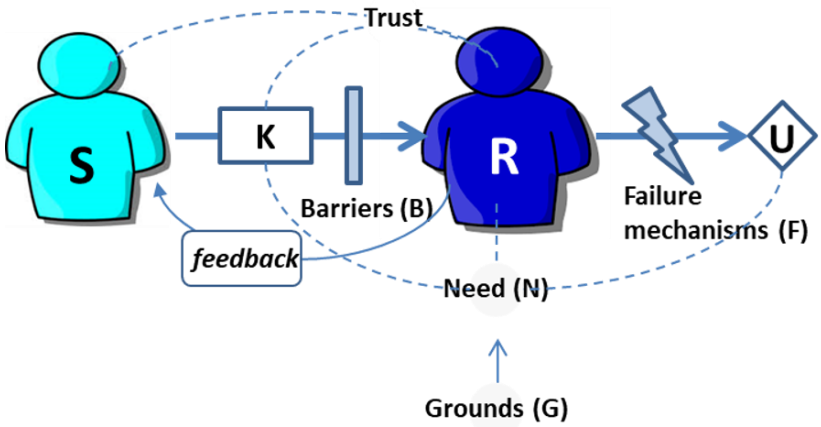

Figure 2: A sender–receiver framework for knowledge transfer and uptake (Tromp, 2019)

We identify three types of social mechanisms influencing successful transfer and uptake: preconditions, barriers, and failure mechanisms. Preconditions include a need for knowledge and mutual trust, with R trusting S's competence and intentions, and S trusting R to use K appropriately. Barriers may be: Transmission-related (e.g., physical obstacles, weak communication),Cognitive (misinterpretation of K), or Psychological (value or practice conflicts on the part of R). Even when barriers are absent or resolved, uptake can still falter through failure mechanisms, such as incorrect use (misapplication of K), diffidence (third party disqualification of K), or lack of relay (R failing to pass K to end users). We also reintroduce

feedback (fb), recognising that S and R are aware of their roles and knowledge gaps. Through feedback, R can signal understanding issues or emerging barriers, enabling S to adjust the transfer process..

We applied the FODIKI Framework during the second phase of the project to systematically collect and disseminate the knowledge acquired regarding the hydraulic framework (see Figure 2). This framework, developed in the initial project phase (Tromp et al., 2024), delineates the three principal phases in the life cycle of a hydraulic structure within a primary flood defence system. These phases comprise: (1) Asset management, involving the statutory obligation to perform routine care and maintenance. When a structure no longer meets legal performance standards, the process transitions to (2) Portfolio management, during which planning and decision-making for necessary upgrades are initiated; followed by (3) Reinforcement projects, a multistep process aimed at strengthening the hydraulic structure. Upon completion of the reinforcement phase, the life cycle returns to the asset management phase, thereby continuing the cyclical process of maintenance and renewal.

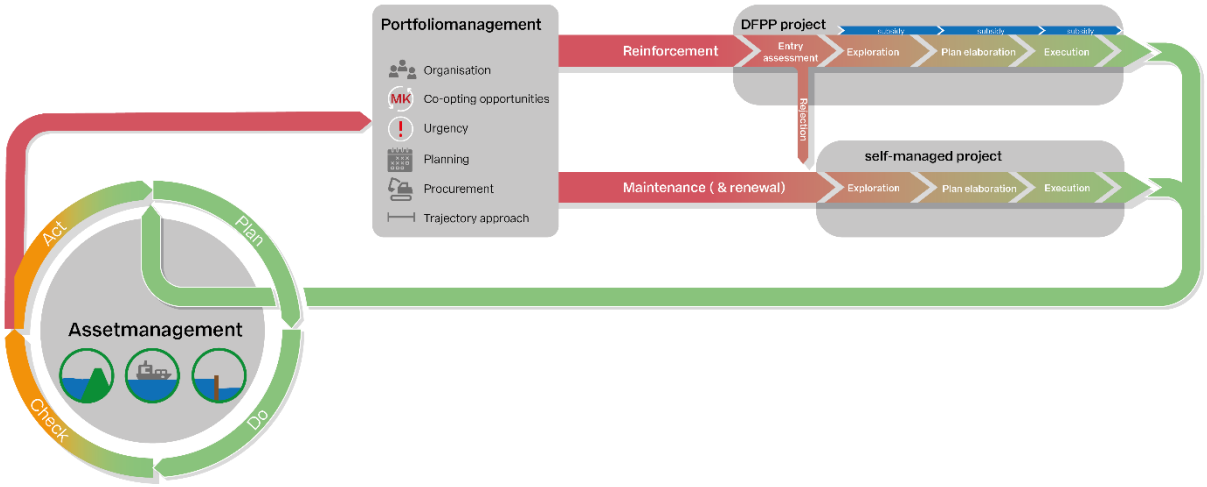

Figure 3: The Hydraulic Structures Roadmap highlighting the different phases during the life cycle of a structure in a primary flood defence.

We held multiple semi-structured interviews with different projects for each phase of the hydraulic roadmap with representatives of the RWAs. Moreover, we had meetings with the RWAs on the results of the statutory assessments and collected additional information. The results were translated into, among other things, an adjusted scope for admission to the DFPP, and the experiences gained during the projects were recorded in a repository of knowledge. We also organised meetings to enable the active sharing of knowledge and experience. Particularly one of the dominant failure mechanisms in hydraulic structures generated a great degree of interest. The following section examines the results in greater detail.

3 RESULTS

Within the DFPP project ‘Working jointly together on hydraulic structures’, further insight into the scope of the task, a uniform approach and available knowledge has been obtained. In this section, we describe these results of the research.

3.1 Scope of the hydraulic structures within the DFPP

Our project team conducted interviews with all Dutch RWAs regarding their civil engineering assets. The findings differed from initial expectations for three main reasons.

First, the scope of the task proved smaller than anticipated. This discrepancy arose from differing interpretations of assessment results between the RWAs and the DFPP. The DFPP had not fully recognized that the large number of structures, classified as non-compliant, was primarily due to limited time and data availability. The RWAs were given only six years to implement the amended statutory assessment (the risk-

based method as described in the introduction) and reassess all dike sections, including hydraulic structures. This major transition created time constraints, limiting opportunities to collect additional data for more accurate (and often safer) evaluations. Consequently, many structures were initially marked as non-compliant, even though the RWAs already were aware that most structures did not require reinforcement.

Second, the variety of reinforcement measures is considerable. The average cost per instance (financial ratio) did not provide a realistic picture of the task at hand (see Figure 4). Cost estimates for strengthening hydraulic structures were significantly overstated. In many cases, minor technical adjustments or even changes in procedures for operational closure were sufficient to restore compliance.

Third, several structures were reinforced as part of broader dike reinforcement programs, meaning they were addressed indirectly.

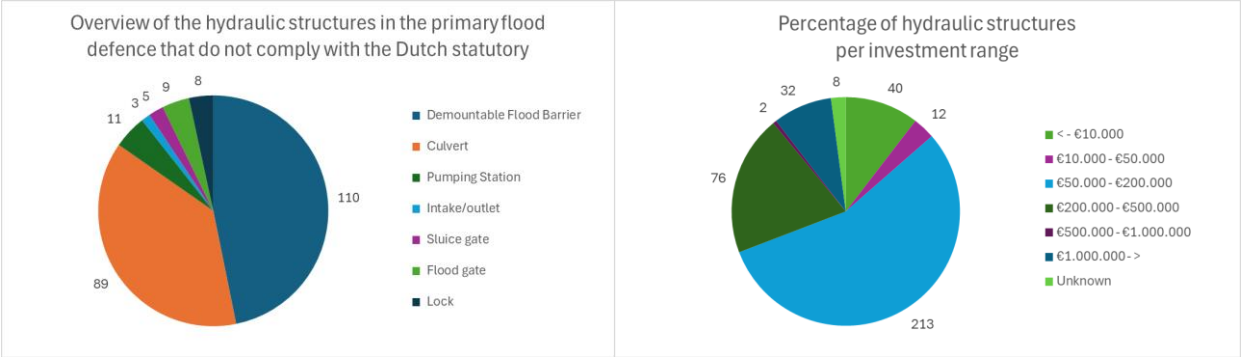

Figure 4: (a) Overview of the hydraulic structures in the primary flood defence that do not comply with the Dutch Statutory (Left). (b) Percentage of these hydraulic structures per investment range (Right).

This leads to the recommendation for the DFPP to frame the scope of the hydraulic structure within the DFPP in terms of an investment sum rather than the number of structures. Accurate estimation of this sum requires close collaboration with the RWAs, which is only possible through a strong relationship of trust and regular interaction between the DFPP and the RWAs. Based on current insights, the investment needed to ensure all civil engineering structures in the Netherlands meet flood safety standards is approximately €250 million, with an uncertainty margin of 25% (excluding economic inflation and construction material cost escalation). Adopting an investment-based approach with the current quantity of reinforcements eliminates the need for a separate programmatic strategy for structures within the DFPP.

3.2 Hydraulic Structures roadmap: Lessons learned in uniform approach

In our project, we made several key results in establishing a uniform approach for reinforcing hydraulic structures, examples are the decisions on life-cycle reliability of flood defence systems and the Roadmap for Sustainable Hydraulic Structures. A uniform approach enhances efficiency, knowledge sharing and quality across all life-cycle phases of hydraulic structures (see Figure 3).

Portfolio management: decisions on life-cycle reliability and a programmatic approach on flood defence systems

Scope definition is essential for effective portfolio management. The method of optimal marginal safety gain, as developed by Klerk (2021 & 2022), optimizes investment decisions by comparing the cost-benefit ratio of measures, expressed as risk reduction per euro spent. Originally designed for dike reinforcements, the method was successfully applied to three sluices in dike trajectory 16-1. Key findings (Deltares, 2024) indicate that investments in hydraulic structures can significantly influence dike reinforcement strategies. This interaction depends primarily on (i) the initial failure probability of the structure relative to adjacent dike sections and (ii) the cost ratio between structural and dike measures. Timing is critical: postponing structural improvements increases total costs and flood risk, while coupling

measures or advancing them can be cost-effective, especially when aligned with maintenance schedules. Importantly, optimization may deviate from strict design-level criteria, favouring solutions that balance compliance and cost-effectiveness, sometimes accepting slightly lower safety at substantially lower cost. This enables tailored strategies that reduce life-cycle costs while meeting trajectory-level standards.

Examples from Dutch RWAs have shown that adopting a programmatic approach to reinforcing hydraulic structures enhances efficiency through standardized processes, centralized design frameworks and integrated governance. For smaller portfolios, flood safety measures can be embedded within broader programs such as asset renovations or water system adaptations. Larger volumes of work strengthen collaboration with research institutes, authorities, and market partners by providing long-term visibility, which encourages investment and innovation, contributing to safer and more resilient infrastructure.

Reinforcement projects: lessons learned

Knowledge sharing between project teams is critical for improving efficiency and quality. Interviews with stakeholders revealed three key themes: technical, environmental, and contracting.

Technical**:** Early contractor involvement proved highly effective in the DFPP-project: 7 Hydraulic Structures by HHNK. Engaging the contractor during the exploration phase enabled proactive measures, such as early dewatering of sluices to assess structural condition and mitigate risks. This approach reduced uncertainty and has since been replicated in other projects, demonstrating the value of integrating contractor expertise from the outset.

Environmental**:** Reinforcement projects offer opportunities beyond local stakeholder management and cultural heritage preservation. They can contribute to (inter)national sustainability goals. The Roadmap for Sustainable Hydraulic Structures (Web-1) provides a structured framework for integrating sustainability throughout the project lifecycle. Key principles are: early scope definition to limit environmental impact, explicit governance structures with clearly defined roles and specialized expertise to ensure the translation of ambitions into concrete design criteria and the systematic embedding of sustainability in procurement and execution through functional requirements and performance indicators. Practical examples demonstrate these principles, including CO_2 reductions via optimized designs, electrification, and material reuse such as cement-free concrete and recycled steel gates.

Contracting**:** Combining hydraulic structure reinforcements together with dike projects can be efficient when the works are related to crest heights. The opposite was seen at a project in the southern part of the Netherlands (near Mook). Differences in contract forms and planning cycles often lead to misalignment. While dike projects typically require iterative detailing, reinforcement of structures is usually well-defined upfront, complicating integrated execution.

Good Conversation: empathy, respect, openness and vulnerability.

The interviews with RWAs were crucial to the findings presented in this paper. Through open dialogue, information was clarified, deepened, and enriched, fostering curiosity-driven exchanges. These conversations resulted in greater insight, trust, and a sense of ownership among the authorities. Responsibility for the hydraulic structure program lies with them, while the “conversation partner” facilitates by sharing and connecting knowledge and experiences from peer organizations.

Maintaining this constructive dialogue is essential, as shown and analyse by the FODIKI framework. It creates connection in a safe and relaxed environment, prevents barriers and failure mechanisms, keeps the hydraulic structure program clearly in focus, and reduces unnecessary administrative burdens. In addition, this enhance the ownership of RWAs. For RWAs, engaging in this dialogue annually ensures that, at the alliance level (DFPP), a current and widely supported perspective emerges, one that accurately reflects the realities and priorities of the regional authorities

4 DISCUSSION AND CONCLUSIONS

In this paper, we stressed the importance of knowledge transfer and uptake. Despite all effort, the necessity of strengthening dikes is more top of mind at the RWAs than hydraulic structures. Luckily, the required measures in the primary flood defence system are less far-reaching as originally thought. The scope of the hydraulic structures was minimised due to efforts of the project team and the RWAs who took their role of ownership. The interviews with the RWAs reveal that the importance of knowledge uptake is acknowledged, but little action is there. As a result, project teams reinvent the wheel, leading to a low degree of efficiency. The scope in the regional water system for hydraulic structures in the Netherlands is a multitude, where the question arises whether some assets continue to play a role in the near future. Learning across projects is also recognized but this is not part of the task of project teams, hampering the knowledge transfer and uptake. From our interviews, we observed several barriers and failure mechanisms occurring in the knowledge transfer and uptake, predominantly due to lack of cognitive barriers, relay of knowledge and trust.

One of the barriers mentioned is the subsidy application process. The underlying reason is the extensive administrative effort required to comply with the DFPP subsidy scheme. The cost of meeting all requirements (approximately €200,000) makes it unattractive to apply for funding for relatively small reinforcement measures, even though RWAs are formally entitled to it. As a result, hydraulic structures are predominantly included in dike reinforcement projects (where subsidies are already being requested) or addressed through regular maintenance programs, which may result in inefficient strengthening. Although a Fastlane approach already exists (combining the phases of exploration, plan elaboration and/or execution) this process must be further simplified for small-scale reinforcement measures of civil engineering structures.

Although practitioners recognise the importance of knowledge transfer and uptake, the systematic exchange of knowledge with peers—both within and beyond the RWAs—remains insufficiently utilised. Strengthening learning processes between RWAs and project teams requires a more prominent role for boundary spanners. Boundary spanners are individuals who ‘proactively scan their organisational environment, engage in activities that bridge organisational or institutional boundaries, facilitate and mediate information flows, and coordinate interactions between their home organisation and its external environment’ (Van Meerkerk & Edelenbos, 2018). They contribute substantially to processes of sense-making and framing (Carlile, 2002; Williams, 2012). In practice, such roles are typically fulfilled by staff within RWAs as well as by members of the Dutch Flood Protection Programme (DFPP) Programme Board. Positioned between RWAs and their projects, and between policy and operational practice, the DFPP increasingly needs to function as a boundary organisation (Van Meerkerk & Edelenbos, 2018), as shown by Tromp (2019).

This paper has underscored the significance of effective knowledge transfer and uptake. The Hydraulic Structures Roadmap has demonstrated its value in clarifying the steps and considerations associated with each phase of the life cycle. RWAs now possess the necessary tools to access knowledge and instruments from their counterparts. However, knowledge transfer and uptake must become an integral component of every programme or project assignment, and RWAs must treat this as a strategic priority.

Current societal challenges—such as large-scale housing development, agricultural transition, and the energy transition—are driving widespread construction activities across the Netherlands. Limited market capacity and specialised expertise highlight the need for more efficient and coordinated collaboration. In addition, the rapidly changing physical environment, driven by climate change and technological developments, reinforces the necessity of working across organisational boundaries. This imperative strengthens cooperation between regional water authorities and Rijkswaterstaat and supports timely completion of their joint objectives before 2050, while also enhancing knowledge transfer and uptake within the broader triple-helix context.

5 ACKNOWLEDGEMENTS

This text is based on the previous work of the lead author for enhancing knowledge transfer and uptake within flood risk management. In addition, we build upon the work of Phase 1 of the Innovation project 'Working jointly on hydraulic structures'. The whole project team has contributed to the overall work, as presented in this paper.

REFERENCES

Carlile, P.R. (2002). A pragmatic view of knowledge and boundaries: Boundary objects in new product development. Organization science, 13(4), 442-455.

Deltacommission (2008) Samen Werken met water, Een land dat leeft, bouwt aan zijn toekomst, report (in Dutch only).

Deltares (2024) Veiligheidsrendement voor kunstwerken, Toepassing op traject 16-1, report (in Dutch only), 11209667-010-ZWS-0003, 11December 2024

DFPP. (2016) Memo waterkerende kunstwerken binnen het HWBP: een definitie (in Dutch only), 2016

DFPP, (2008). Startnotitie POS Kunstwerken (in Dutch only), report. 2018.

Jonkman, S.N, Voortman, H.G., Klerk W.J., van Vuren, S. (2008) Developments in the management of flood defences and hydraulic infrastructure in the Netherlands, Structure and Infrastructure Engineering, 14, 7.

Jorissen, R.; Kraaij, E.; Tromp, E. (2016) Dutch flood protection policy and measures based on risk assessment, in Proc.3rd European Conference on Flood Risk Management, Lyon, France, 17–21 October 2016.

Klerk, W.J., Kanning W., Kok M., Wolfert R. (2021) Optimal planning of flood defence system reinforcements using a greedy search algorithm, Reliability Engineering & System Safety, Vol. 207, 107344, https://doi.org/10.1016/j.ress.2020.107344.

Klerk, W. J. (2022). Decisions on life-cycle reliability of flood defence systems. Ph.D. Thesis, Delft University of Technology. https://doi.org/10.4233/uuid:877bed45-d775-40bb-bde2-d2322cb334f0

Knott, J.; Wildavsky, A. (1980) If dissemination is the solution, what is the problem? Knowl. Creat. Diffus. Util. 1980, 4, 537–578.

Most, H.; van der Tánczos, I.; Bruijn, K.M.; de Wagenaar, D. (2014) New Risk-based standards for flood protection in the Netherlands, in Proc. 6th International Conference on Flood Management, Sao Paulo, Brazil, 16–18 September 2014.

Tromp, E. (2019) Enhancing Knowledge Transfer and Uptake in the Design Processes of Flood Defences. Ph.D. Thesis, Delft University of Technology, Delft, The Netherlands, 11 November 2019.

Tromp, E., Verdijck, N., Breedeveld, J., (2022) Rode Draad Waterkerende Kunstwerken. Ontwikkeling kennis en kunde voor overstromingskansanalyse waterkerende kunstwerken (in Dutch only), September 2022

Tromp, E., te Nijenhuis, A., Knoeff, H. (2022) The Dutch Flood Protection Programme: Taking Innovations to the Next Level. Water 2022, 14, 1460.

Tromp E., Breedeveld, J., Apperloo J, and Kottier, J. (2024), Working Together on Hydraulic Structures within the Dutch Flood Protection Programme: challenges and opportunities, Proc. IAHS, 386, 285–290, 2024, https://doi.org/10.5194/piahs-386-285-2024

Van Meerkerk, I. & Edelenbos, J., (2018). Boundary Spanners in Public Management and Governance: An Interdisciplinary Assessment. Edward Elgar Publishing

Vlachos, E.(1977) A conceptual model of the knowledge transfer process,in Proc.2nd International Conference on Water Resources Knowledge, Fort Collins, CO, USA, 29 June 1977.

Williams, P. (2012). Collaboration in public policy and practice: Perspectives on boundary spanners. Policy Press.

Web sites:

Web-1: https://roadmapduurzaamhwbp.nl/, consulted 10 December 2025.

Chapter 5- Governance, policy, and societal engagement

5.3 Financing flood risk reduction, insurance, and risk transfer mechanisms

ICFM 10
Adapting to Global Change:
Innovative Approaches to Flood Management and Resilience
May 20-22, 2026 | Western University, London, Ontario, Canada

Long-term Economic Analysis of Flood Protection Infrastructure: A River Basin Approach

Mikio Ishiwatari[1], Masashi Sakamoto[2], and Daisuke Sasaki[3]
Meiji University, 1-1 Kandasurugadaki, Chiyodaku, Tokyo, 1018301, Japan[1]
E-mail: ishiwatari@meiji.ac.jp
Pacific Consultants Co., Ltd, Japan[2]
E-mail: masashi.sakamoto@tk.pacific.co.jp
Tohoku University, Japan[3]
E-mail: daisuke.sasaki.b3@tohoku.ac.jp

ABSTRACT

While cost-benefit analysis is standard practice for individual flood protection projects, long-term economic analysis at the river basin scale is less common. It is vital for policymakers to have evidence that investments in flood protection contribute to regional growth. This study proposes a retrospective-prospective methodology for conducting long-term economic analysis at the basin scale. The approach integrates past observed benefits from major floods with future expected benefits derived from probabilistic simulations. The methodology is applied to the Natorigawa River basin in Japan, with an evaluation span of 118 years. The findings indicate that the investment made over the last seven decades has resulted in a benefit-to-cost ratio of 6.1. This demonstrates the investment's substantial economic efficiency. The methodology requires further simplification for application in developing countries with limited data and capacity.

KEYWORDS: investment for DRR, cost-benefit analysis, flood simulation, evidence-based policymaking, Natorigawa River, Japan

1 INTRODUCTION[1]

The Sendai Framework for Disaster Risk Reduction (2015–2030) emphasizes that disaster risk reduction budgets are investments, not expenses (UNISDR 2015). However, while individual flood protection projects are evaluated through cost-benefit analysis, comprehensive assessments of long-term investments at the river basin or regional scale remain absent. Policymakers need evidence that such investments contribute to regional growth, yet this evidence is rarely available.

Investments in flood protection serve multiple policy objectives beyond immediate disaster loss reduction (Mizutori 2020). They enable long-term regional economic planning and attract private investment. They also support urban development and enhance quality of life by reducing disaster-related anxiety. Yet without robust economic evidence demonstrating returns on investment, securing sustained funding for flood protection remains challenging, particularly in developing countries facing competing development priorities (Ishiwatari and Sasaki 2024).

This study proposes a methodology for economic analysis of long-term flood protection investments at the basin scale and applies it to the Natorigawa River basin in Japan. The methodology assesses both past

[1] The contents of this paper were released in JICA Ogata Research Institute research paper "Estimating the economic viability of long-term investment in flood protection: Case study of the Natorigawa River" (Ishiwatari, Sakamoto, and Sasaki, 2023).

benefits (from major observed floods) and future benefits (from simulated scenarios), providing comprehensive evidence of investment efficiency over decades.

2 ECONOMIC ANALYSIS OF FLOOD PROTECTION: CURRENT PRACTICE

This section reviews recent literature on the economic evaluation of flood protection measures, focusing on established methodologies and identifying limitations at the river basin scale.

2.1 Conventional Approaches and Standardization

The standard approach globally involves a cost-benefit analysis (CBA), comparing the value of investment and maintenance costs against the value of prevented flood damage benefits. Project-level evaluation is widely adopted for individual flood protection projects. Japan's Ministry of Land, Infrastructure, Transport and Tourism (MLIT) has conducted such analyses since 1957 (Takebayashi and Yasuda 1995). Similar frameworks exist in Germany (Meyer and Messner 2005) and the United States (McGee 2021). These analyses are typically based on preventing damage from a specific design flood event. The Netherlands have advanced beyond simple CBA to adopt comprehensive risk-based approaches. These methodologies integrate probabilistic modelling to set tolerable death risk thresholds and inform social cost-benefit analysis for long-term planning (Tomura et al. 2018).

2.2 Fundamental Challenges in Damage Assessment

While the CBA framework is established, its accuracy is constrained by several fundamental challenges in quantifying both the risk and the resulting damages. Merz et al. (2010) identified key difficulties, including limited historical damage data and a lack of standardized, region-specific damage estimation methods. Reliable damage functions correlate asset damage ratios to inundation depth and asset type. However, these functions remain underdeveloped or inconsistent across many regions, hindering accurate loss estimation. Conventional methods often struggle to capture indirect economic damages (e.g., business interruption, supply chain disruption) and non-monetary damages (e.g., mental health impacts, loss of life).

2.3 Defining the Research Gap

Project-level and risk-based CBAs have become increasingly sophisticated. Nevertheless, few studies systematically evaluate the accumulated economic efficiency of multiple flood protection projects at the river basin scale over several decades. Conventional analyses fail to provide evidence for policymakers that addresses two critical needs: (i) Demonstrating the aggregated economic returns (B/C ratio) across multiple generations of projects, particularly by integrating the retrospective benefits derived from existing infrastructure during past observed floods. (ii) Assessing the cumulative economic value of protection across an entire system, which is necessary to link investment to regional economic planning and sustainable growth objectives.

This study addresses this gap by proposing and applying a basin-scale methodology that integrates observed past benefits with projected future benefits to provide a comprehensive, long-term economic assessment.

3 METHODOLOGY

The study estimates benefits by calculating the difference between damage with and without flood protection structures (Figure 1). Past benefits are calculated as: estimated damage without structures minus actual damage for observed major floods. This retrospective approach is justified when major protective structures predate the flood events analysed, ensuring structures provided protection for identified risk areas.

To accurately calculate historical flood protection benefits, the estimated damage requires adjustment. Present-day asset values are scaled downward based on the ratio of residential area at the time of the flood to the present day. This prevents overestimation of benefits by recognizing that asset concentration was lower historically.

Future benefits are estimated by calculating expected annual damage (EAD) reduction over a 50-year evaluation period. Damage is estimated using asset values (housing, infrastructure, crops) multiplied by damage ratios based on inundation depth, business interruption, and costs for emergency response (MLIT 2020). Inundation depths are determined through flood simulations conducted per the MLIT manual (MLIT 2015).

Past costs include river improvement and dam construction expenses. Construction costs are allocated across the construction period to establish annual costs. Future costs are operation and maintenance expenses over 50 years.

Costs and benefits are converted to present values using a 4% social discount rate and deflators. This 4% rate is consistent with Japan's standard methodology for infrastructure project evaluation (MLIT 2020). Deflators are applied only to past costs; past benefits use current asset values to reflect protection value at present time. This treatment ensures consistency between the cost stream (historical expenditures) and benefit stream (current asset values protected).

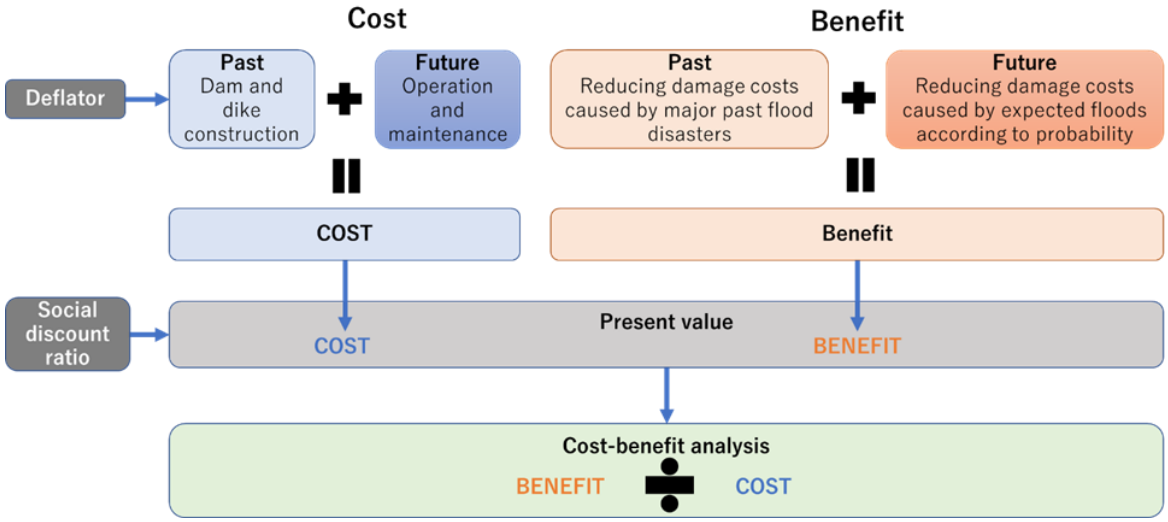

Figure 1: Concept of economic analysis in flood protection at the river basin scale

4 CASE STUDY: NATORIGAWA RIVER BASIN

4.1 Basin Characteristics

The Natorigawa River is designated as a first-class river under the Japan's River Law. This classification applies to rivers of significant national importance for land conservation and the national economy. First-class rivers are managed directly by MLIT, in contrast to second-class rivers, which are managed by prefectural governments.

The river has a main channel length of 55 km and a watershed area of 939 km². The river originates at the Miyagi-Yamagata prefectural border, merges with the Hirose River and other tributaries, and flows through Sendai City. It empties into the Pacific Ocean at Yuriage, Natori City.

The basin comprises Sendai, Natori, Iwanuma, Kawasaki, and Murata cities. Land use is approximately 76% mountain forests, 12% agricultural land (rice paddies and farmland), and 12% urban areas. Significant urbanization has occurred: the basin population increased from approximately 0.8 million (1960) to 1.1 million (2000). By 2010, the basin contained about 50% of Miyagi Prefecture's total population, demonstrating intense population concentration in this flood-prone corridor (Tohoku Regional Development Bureau 2012).

Population concentration reflects the basin's economic importance. Sendai City serves as the regional economic centre for the Tohoku region. It hosts diversified manufacturing, service industries, and administrative functions. The basin's low elevation and proximity to the river historically provided advantages for transportation and water supply. However, these same features now create elevated flood risk for the concentrated populations and infrastructure.

The risk areas are divided to three blocks. Block R1 (right bank), located in rapidly developing areas of Natori and Sendai cities, showed particularly high asset concentration, with modern residential developments and commercial facilities. Block L1 (left bank) was restricted as a disaster risk zone following the 2011 Great East Japan Earthquake and Tsunami. Since this disaster caused land subsidence and tsunami inundation, block L1 is preserved agricultural land. Block L2, proximal to downtown Sendai, concentrated office and commercial facilities representing high-value business assets.

4.2 Flood Protection Investment

The basin experienced catastrophic floods in 1947, 1948, and 1950. In response, MLIT commenced dike construction in 1951 and formulated the first formal flood protection plan in 1954. Major construction works were substantially completed by 1985, with subsequent modifications made following the 2011 Great East Japan Earthquake to address land subsidence.

Two major multi-purpose dams serve flood control and water supply functions. The Kamafusa Dam is a 45.5 m high gravity concrete dam constructed in 1971 on the Goishigawa River, with a total project cost of JPY 8.72 billion. The Okura Dam is an 82 m high arch-type concrete dam constructed in 1961 on the Okuragawa River, with a total project cost of JPY 2.76 billion.

The evaluation period spanned 118 years: 67 years of past investment (1951–2018) and 50 years of future projection (2018–2068). Total past costs, converted to present value using a 4% social discount rate and appropriate deflators, were JPY 624.6 billion (approximately $4.16 billion). Future operation and maintenance costs for structure completed totalled JPY 1.5 billion (approximately $10 million) in present value terms.

4.3 Benefit Estimation

Past benefits were calculated using Typhoon Hagibis (October 2019)—the largest recorded flood in the basin with a flow volume of 3,300 m³/s—as the base case. This typhoon caused the highest flood damage ever recorded in Japan (approximately 1.86 trillion yen nationwide, or approximately $12.4 billion). The typhoon resulted in 87 deaths or missing persons, 21,000 destroyed houses, and 60,000 flooded houses nationally (Ishiwatari 2022).

Under the scenario of no flood protection structures in the Natorigawa basin, estimated damage was JPY 350 billion (approximately $2.33 billion) (Figure 2 (a)). This damage was distributed as follows: general assets (houses, offices, factories) 36% (JPY 126 billion, or $840 million), public facilities 60% (JPY 210 billion, or $1.40 billion), and emergency measures 4% (JPY 14 billion, or $93 million).

Damage varied significantly by location: Block R1 experienced potential damage of JPY 240 billion (approximately $1.60 billion), representing 69% of total basin damage. Blocks L1 and L2 combined faced JPY 109 billion (approximately $727 million), representing 31% of total. This distribution reflected the

concentration of modern development in Block R1, which contains newly developed residents and extensive commercial-industrial infrastructure in Natori and Sendai City.

Six major historical floods (August 1986, August 1989, September 1994, July 2002, September 2007, September 2011) were analysed. Damage for each event was scaled proportionally to Typhoon Hagibis using a linear relationship between flood volume ratios and damage ratios. This simplified approach reduced computational requirements while maintaining reasonable accuracy. For example, the August 1986 flood (2,690 m^3/s, 0.82 of Hagibis volume) was estimated to cause damage of approximately JPY 284 billion (approximately $1.89 billion) without protection structures.

Total past benefits from structures protecting against these major flood events were JPY 3.7 trillion (approximately $24.67 billion). This figure represents the cumulative protection value provided by dikes, dams, and channel improvements completed by 1985, protecting residents and assets during seven decades of flood events.

The future benefits were calculated based on a target flood magnitude of a 1/150-year return period for the ongoing programme's safety level over a 50-year evaluation period. This safety level represents the target design flood magnitude for protecting the river basin. Damage from a 1/150-year flood without protection structures was estimated at JPY 1.3 trillion (approximately $8.67 billion) (Figure 2 (b)). With existing and planned structures in place, this damage would be reduced to JPY 260 billion (approximately $1.73 billion), yielding a baseline benefit of JPY 1.05 trillion (approximately $7.00 billion).

Expected annual damage (EAD) reduction was calculated across ten flood probability scales: 1/10, 1/20, 1/30, 1/40, 1/50, 1/60, 1/70, 1/80, 1/100, and 1/150 years. The calculation used a linear damage scaling model weighted by interval probabilities. This probabilistic approach captures flood risk across the full distribution of possible magnitudes, rather than focusing on single design events. The average annual EAD reduction totalled JPY 4.998 billion (approximately $33.32 million). Accumulated over 50 years and discounted to present value at 4%, future benefits totalled JPY 112 billion (approximately $747 million).

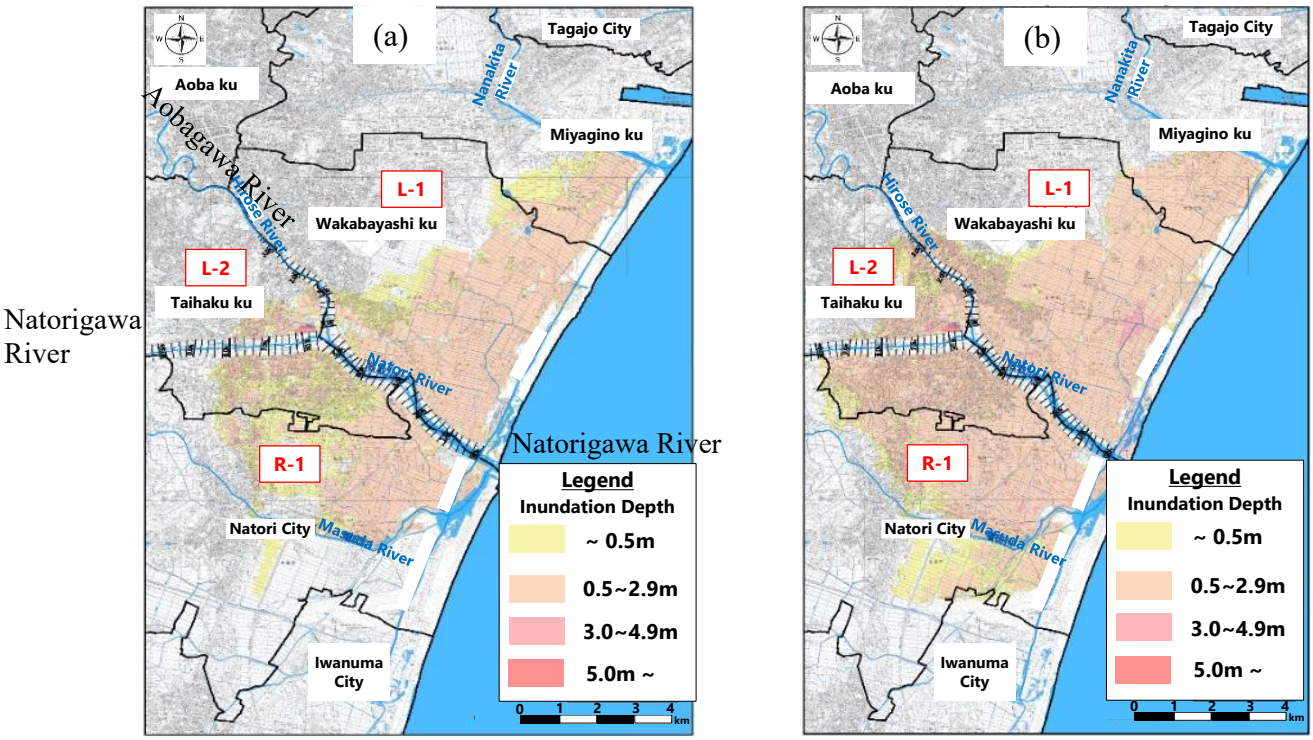

Figure 2: Inundation simulation map (a)Typhoon Hagibis in 2019, (b) 1/150-year flood)

5 Results

Total costs: JPY 626 billion (approximately $4.17 billion)

Total benefits: JPY 3.81 trillion (approximately $25.4 billion)
Net Present Value: JPY 3.2 trillion (approximately $21.3 billion)
Benefit-cost ratio: 6.1

The analysis demonstrates that flood protection investment in the Natorigawa basin generated substantial returns, with each yen invested producing approximately 6.1 yen in benefits. The net present value of JPY 3.2 trillion (approximately $21.3 billion) indicates that after accounting for all costs, society received a significant net benefit from flood protection investments.

6 DISCUSSION AND LIMITATIONS

6.1 Methodological Contributions

The proposed methodology is a significant improvement on the conventional approach of conducting cost-benefit analyses on an individual project basis. By integrating past investments and their observed protective effects with future projections, it provides a more comprehensive view of the long-term efficiency of flood protection measures. The basin-scale approach considers the cumulative impact of various projects, including embankments and dams, over several decades. This gives policymakers stronger evidence on which to base decisions on investment prioritisation and budget allocation.

The use of a linear damage scaling model simplified computational requirements. For practitioners in resource-constrained environments, this simplified approach provides workable alternative to computationally intensive full-physics simulations.

The methodology explicitly accounts for urbanization effects by adjusting past benefits based on residential land area changes. Ignoring urbanization would substantially overestimate damage—the Natorigawa basin experienced development of residential area.

6.2 Policy recommendations

This methodology provides practical tools for evidence-based decision-making. Its retrospective element provides compelling evidence to support the need for sustained flood control funding. By demonstrating the measurable benefits of past investments during actual flood events, policymakers can strengthen their case for continued budget allocation. This is particularly valuable when competing for limited public funds against other infrastructure sectors.

The 118-year evaluation period used in this study reflects the true lifespan of major flood control infrastructure. Similarly, policymakers should adopt a long-term perspective when evaluating flood control investments. Short-term evaluation periods systematically undervalue flood control because its major benefits only become apparent over decades.

Authorities should conduct comprehensive economic evaluations every 10 to 15 years, incorporating new flood events and updated climate projections. The results should be communicated in an accessible format to promote public understanding and support.

While this methodology requires extensive data, a simplified version can be used in developing countries where data is limited. Assessments can estimate values using globally available satellite flood mapping, satellite-observed topography and rainfall data, population datasets, publicly available flood simulation models, and simplified damage functions. Key simplification techniques include focusing on major historical floods, applying linear damage scaling and using regional damage functions. Pilot applications in basins with recent flood events and planned investments can demonstrate value and promote broader adoption.

6.3 Limitations and Future Research Needs

This study has several limitations. Each limitation also suggests directions for future research.

The analysis excludes facility replacement costs, a significant limitation given the 100-year evaluation period. Dams and major structures typically have 50-year design lives in asset management guidelines, yet some Japanese structures have functioned for over 100 years. The Kamafusa Dam (built 1971) and Okura Dam (built 1961) are now 50+ years old, approaching potential replacement periods. Future research needs to develop standardized cost estimation methods for aging flood infrastructure, including maintenance, rehabilitation, and replacement scenarios.

The study used current flood probability relationships. Future flood risk assessments must incorporate climate change effects. MLIT projects that rainfall will increase by 10% and flood volumes by 20% nationally under representative concentration pathway 2.6 scenario (consistent with Paris Agreement 2°C target) (MLIT 2021). Future research should integrate climate-adjusted flood frequency curves and damage functions into basin-scale economic analysis.

A fundamental conceptual issue arises from feedback between flood protection and development. Because flood protection investments enhanced perceived safety, urbanization accelerated in protected areas. Without such investments, assets would not have accumulated at current levels. The relationship is complex: investments enabled development, but development also justified further investments. Separating induced development effects from pure risk reduction remains methodologically challenging. Future research must develop counterfactual scenario modelling techniques. These methods would estimate the level of development that would have occurred without flood protection. Such approaches would enable a more precise separation of induced development effects from pure risk reduction benefits.

The analysis excludes several important benefit categories, such as supply chain disruption, mental health impacts from flood anxiety, and mortality reduction. Typhoon Hagibis caused 87 deaths nationally—a toll that would have been higher without flood protection. Including these benefits would strengthen the economic case for investment. Human life is not monetized due to ethical concerns, yet flood fatalities represent one of the most important benefit measure. Systematic inclusion of mortality reduction in future analyses would strengthen the case for flood protection investment, particularly for urban basins with high population density.

7 CONCLUSIONS

Flood protection investment in the Natorigawa River basin proved highly economically efficient. The benefit-cost ratio of 6.1 indicates that each yen invested generated over six yen in societal benefits. The net present value of JPY 3.2 trillion (approximately $21.3 billion) confirms substantial net gains from seven decades of sustained investment.

Three key findings emerge from this analysis. First, retrospective assessment of actual flood events provides compelling evidence that complements traditional prospective analysis. Second, basin-scale analysis captures cumulative benefits that project-level evaluations miss. Third, the methodology demonstrates that flood protection enables regional development, as evidenced by the 32% increase in residential area within protected zones.

These findings carry important policy implications. Flood protection should be framed as economic investment rather than defensive expenditure. Budget decisions should adopt evaluation horizons matching infrastructure lifespans. Periodic reassessment incorporating new flood events strengthens the evidence base over time.

The methodology offers a replicable framework for other river basins. With appropriate simplification using satellite data and global datasets, the approach can inform investment decisions in developing countries where such evidence is urgently needed.

8 ACKNOWLEDGEMENTS

Financial support for this research has been provided by the FRICS Research Grant.

REFERENCES

Ishiwatari, M. (2022). “Effectiveness of investing in flood protection in metropolitan areas: lessons from 2019 Typhoon Hagibis in Japan”. International journal of disaster resilience in the built environment, 13(1), 89-98.

Ishiwatari, M., & Sasaki, D. (2024). “Investing in Resilience: Estimating Financial Needs and Benefits of Flood Protection in Developing Asian Countries.” Proceedings of IAHS, 386, 87-93.

McGee, K. (2021). “A Place Worth Protecting: Rethinking Cost-Benefit Analysis Under FEMA's Flood-Mitigation Programs.” University of Chicago Law Review 88 (8): 1925–70.

Merz, B., H. Kreibich, R. Schwarze, and A. Thieken. (2010). “Review Article: ‘Assessment of Economic Flood Damage’.” Natural Hazards and Earth Systems Sciences 10: 1697–1724, https://doi.org/10.5194/nhess-10-1697-2010.

Meyer, V. and F. Messner. (2005) . “National Flood Damage Evaluation Methods A Review of Applied Methods in England, the Netherlands, the Czech Republic and Germany.”, UFZ Discussion Papers 21/2005, Helmholtz Centre for Environmental Research: Leipzig.

Ministry of Land, Infrastructure, Transport and Tourism (MLIT), (2015). “Manual for Drawing Flood Inundation Assumption Area Maps (4th Edition)” (in Japanese). MLIT: Tokyo.

———. (2020). “Manual for Economic Evaluation of Flood Protection Investment (Draft)” (in Japanese). MLIT: Tokyo, https://www.mlit.go.jp/river/basic_info/seisaku_hyouka/gaiyou/hyouka/r204/chisui.pdf.

———. (2021). “Proposal for Flood Protection Planning Based on Climate Change” (in Japanese). MLIT: Tokyo.

Mizutori, M. (2020). "Reflections on the Sendai Framework for Disaster Risk Reduction Five Years Since Its Adoption.” International Journal of Disaster Risk Science 11: 147–51.

Takebayashi S., and G. Yasuda. (1995). “Status Quo of Economic Appraisal Methods for Rivers in Japan and Their Future Prospects.” Journal of Japan Society of Hydrology and Water Resources 8 (1), 19–37.

Tohoku Regional Development Bureau. (2012). “River Improvement Plan for Natorigawa River” (in Japanese). http://www.thr.mlit.go.jp/sendai/kasen_kaigan/nahi/pdf/12112002.pdf.

Tomura S., M. Nakatsugawa, T. Yamamoto, M. Chiba, T. Yamada, and T. Hoshino. (2018). “The Point on Risk-based Flood Management Plan in the Netherlands.” (in Japanese), Proceedings of Hokkaido Branch of Japan Society of Civil Engineers 75. https://www.ric.or.jp/gyoumu/data/ric_paper/20191210/201901_B-22.pdf.

United Nations Office for Disaster Risk Reduction (UNISDR). 2015. “Sendai Framework for Disaster Risk Reduction 2015-2030”. UNISDR: Geneva.

ICFM 10
Adapting to Global Change:
Innovative Approaches to Flood Management and Resilience
May 20-22, 2026 | Western University, London, Ontario, Canada

Financing Flood Protection in Archipelagic Asia: A Comparative Analysis of Indonesia, Japan, and the Philippines

Mikio Ishiwatari[1] and Akiyuki Kawasaki[2,3,4]

Meiji University, 1-1 Kandasurugadaki, Chiyodaku, Tokyo, 1018301, Japan[1]
E-mail: ishiwatari@meiji.ac.jp
Institute for Future Initiatives, The University of Tokyo,7-3-1 Hongo, Bunkyo-ku, Tokyo 113-8654, Japan[2]
Department of Civil Engineering, The University of Tokyo[3]
Institute for Digital Observatory, The University of Tokyo[4]
E-mail: kawasaki@ifi.u-tokyo.ac.jp

ABSTRACT

Flood-prone countries need to invest in flood protection measures to safeguard populations and economic assets in an era of climate change and societal transformation. This study aims to propose policies and approaches to financial mobilization for flood protection. It examines flood protection investments and resulting damage in Indonesia, Japan, and the Philippines over the past two decades. While various financing mechanisms have been proposed for disaster risk reduction, empirical analysis of cost-sharing policies using actual budget and damage data remains limited. Through analysis of budget allocation trends, damage patterns, and financing mechanisms, this research reveals varying approaches to flood protection investment and their effectiveness. The study highlights the importance of cost-sharing among national governments, local governments, and local communities, offering insights into effective strategies for flood risk management in diverse economic and geographical contexts. Key findings indicate that the Philippines has increased investment following major disasters as predicted by earlier models, while Indonesia has not consistently increased budgets despite economic growth. Japan shows a recent increase after a period of decline. Policy recommendations include implementing cost-sharing mechanisms, providing financial incentives for local governments, and enhancing community engagement.

KEYWORDS: cost-sharing, financial mechanism, disaster risk reduction, climate change adaptation

1 INTRODUCTION[1]

Flood protection remains a critical issue for many countries as climate change increases the frequency and intensity of extreme weather events (Wasko et al. 2021). In particular, developing countries that are experiencing urbanisation and development need to invest effectively in flood protection measures to safeguard populations and economic assets. (Dottore et al. 2023; Rentscheler et al 2022).

The study aims to identify effective strategies and potential areas for improvement in flood risk management by comparing approaches to flood protection investments and resulting flood damages. It focuses on three archipelago countries in the Asian monsoon area with significant flood risks: Indonesia,

[1] The contents of this paper were released in JICA Ogata Research Instituter Discussion Paper "Flood Protection Investments in Indonesia, Japan, and the Philippines: A Comparative Analysis" (Ishiwatari and Kawasaki, 2025)

Japan, and the Philippines. These nations share common challenges related to their geographical characteristics—extensive coastlines, densely populated low-lying areas, and exposure to typhoons and monsoon rainfall. The diverse economic and geographic characteristics provide a rich context for understanding the challenges and opportunities associated with investing in flood protection.

2 MOBILIZING FINANCING FOR FLOOD PROTECTION

This section revies recent studies, focusing on the challenges of maintaining long-term investment, the potential of various funding sources and innovative financing strategies. There is limited literature examining practical data on investment and damage or cost-sharing policies between different levels of government.

Research has shown that while national authorities often increase flood protection funding in the aftermath of major flood events, maintaining high levels of investment over time proves challenging. Ishiwatari and Sasaki (2022) identified cyclical patterns in flood protection investments, where the ratios of flood budgets and damages to GDP form distinct investment cycles. They observed five such cycles in Japan over almost 150 years. This cyclical nature highlights the need for strategies to sustain funding beyond immediate post-disaster periods.

Recent trends point towards a more diverse approach to flood protection financing. Driessen et al. (2018) noted an increasing involvement of local governments, private companies including insurance firms, municipalities, and property owners in flood protection efforts. This expands financial resources, allows for a community-based approach, and strengthens capacity to prepare for and respond to disasters. The challenge, however, is that financial resources and expertise are not always available at the community level.

Various financing mechanisms have been proposed for disaster risk reduction and climate change adaptation. Kunreuther and Linnerooth-Bayer (2003) studied pre-disaster hedging instruments such as insurance and catastrophe bonds in emerging economies, finding that these instruments can effectively channel funds from international capital markets to support post-disaster recovery. Brugmann (2012) proposed a paradigm shift in viewing investments in disaster risk reduction and climate change adaptation, arguing that investing in resilience can increase investment returns and confidence in asset values. Kok et al. (2021) proposed mechanisms for leveraging public investments in nature-based flood defense projects through value capture and co-investment approaches.

Most existing research focuses on theoretical frameworks or case studies of individual countries, with limited comparative analysis using actual budget allocation and damage data across multiple nations. This study addresses this gap by analysing practical investment data and financing mechanisms in three countries over two decades.

3 METHODOLOGY

This study utilizes a mixed-methods approach, combining quantitative analysis of historical data with qualitative assessment of policy documents and expert interviews. Data collection involved gathering budgetary and damage data from government statistics, the EM-DAT database, and interviews with officials and experts. Semi-structured interviews were conducted with Indonesian officers in January and June 2024, Filipino officers in March 2024, and experts in international organizations and aid agencies.

The budget data includes expenditure on flood, landslide and coastal hazard protection works. There is no common definition of flood protection budgets among the three countries, and the data are not clearly differentiated. Japanese data include local government budgets, whereas Indonesian and Philippine data primarily reflect national government spending. Budget data from the Indonesian provinces of Jakarta, West Java and Bandung were collected to understand local government investment. The difficulty of collecting standardised data is a limitation of budget analysis studies in disaster risk reduction.

To ensure comparability across different economies and time periods, all financial data has been converted to 2015 USD. Analysis considers both absolute values and percentages of GDP to account for economic differences between countries.

4 RESULTS

This section examines investments in flood protection and flood damage in three countries (Table 1). Indonesia has not increased its budget as a percentage of GDP. The Philippines increased its budget following major disasters. Japan decreased its budget due to a stagnating economy but started to increase it again after a series of disasters.

Table 1. Summary of Flood Protection Investment Characteristics

Indicator	Indonesia	Philippines	Japan
Avg. Annual Damage	~$500M (0.06% GDP)	~$670M (0.3% GDP)	<0.2% GDP
Budget Trend	Stagnant (0.03-0.07%)	Increasing (0.3→0.7%)	Recovering (0.9→0.3→0.5%)

4.1 Indonesia

Indonesia comprises over 17,000 islands stretching along the equator with a population exceeding 270 million. The country's major cities, including the Jakarta metropolitan area, were developed in low-lying coastal areas, making them particularly vulnerable to flooding from both heavy rainfall and sea-level rise.

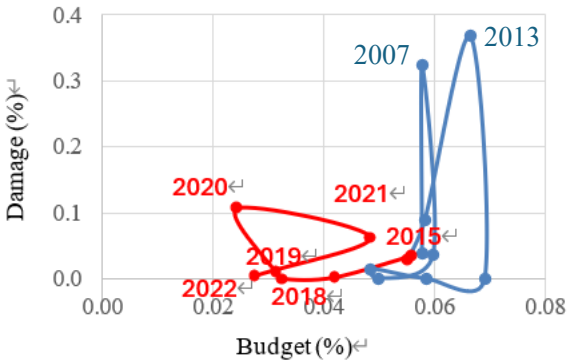

Figure 1 Flood protection budget and flood damage in Indonesia (Ratio to GDP)

Damage: From 2006 to 2023, the country suffered flood damages amounting to USD 8.6 billion in 2015 prices, averaging about USD 500 million per year (0.06% of GDP) (Figure 1). Damage in Jakarta is increasing because of population migration, climate change, land subsidence, and land use change (Budiyono et al. 2016). The 2007 flood inundated 340,000 people in 35% of the city and closed the Jakarta international airport for three days (World Bank 2019). The 2013 flood damaged the capital region with about USD 3 billion (0.37% of GDP), and the 2020 flood caused USD 1.2 billion in damage (0.11% of GDP).

Investment: Flood protection budgets of the Ministry of Public Works and Housing (MPWH) have varied over time, often fluctuating rather than consistently increasing. The budget was around 300 million USD in 2015 prices until 2010, increasing 260-570 million USD from 2010 to 2022. Over nearly two decades, the budget remained in the range of 0.03-0.07% of GDP (Figure1). The budgets did not increase according to the country's growth, creating expanding gaps with estimated needs. The Asian Development Bank (2023) estimated that 1.6 billion USD/year is needed for the coming two decades. The MPWH implements the DKA subsidy programme to sub-national governments (valued at 9 million USD) on a small scale, which is one-hundredth the size of national projects.

Local Government Investment: The Special Capital Region of Jakarta allocated a budget for flood protection of 160 million USD in 2023, accounting for one-third of the flood protection budget in MPWH and some 3% of the total regional budget. This demonstrates the potential for subnational entities to take leadership roles. The financial sources are regional funds (30%) and interest-free loans from the central government (70%), repayable over 18 years. The operation and maintenance budget reaches 37 million USD, accounting for 20% of the total flood protection budget—relatively high because the capital

region operates large-scale facilities of diversion channels and pumping stations constructed by the central government. The regional government allocates operation and maintenance funds to the five districts. The districts then hire community members to operate and maintain pumping stations, gates, and cleaning facilities. These employees are known as the 'blue troops' and the 'green troops'.

Bandung City, the 4th largest city with 2.5 million population, allocated 8 million USD, 1.5% of the total city budget, while West Java Province allocated 1.2 million USD. The city identified 12 flood-prone locations and formulated a mitigation plan, currently operating 10 retention ponds with depths of 1.5-4 meters. The City government enforces infiltration wells as approval conditions for construction and provides financial support for their installation.

4.2 Philippines

The Philippines, consisting of over 7,000 islands with a population exceeding 100 million, is particularly vulnerable to natural disasters, especially typhoons and consequent flooding. A significant portion of the population lives in coastal areas, creating substantial challenges for protection.

Damage: From 2006 to 2023, the country suffered flood damages amounting to USD 12 billion in 2015 prices, averaging about USD 670 million per year (0.3% of GDP). Typhoons Ondoy and Pepeng caused severe floods and landslides in Metro Manila and Luzon Island in September and October 2009, with total economic damage estimated at 1.1 billion USD (0.5% of GDP). Typhoon Yolanda caused a high tide disaster in Leyte Island in 2013, with economic damage estimated at 2.3 billion USD (0.8% of GDP) (Figure 2). In 2020 and 2021, typhoons also caused damage of approximately 1 billion USD (Figure 3).

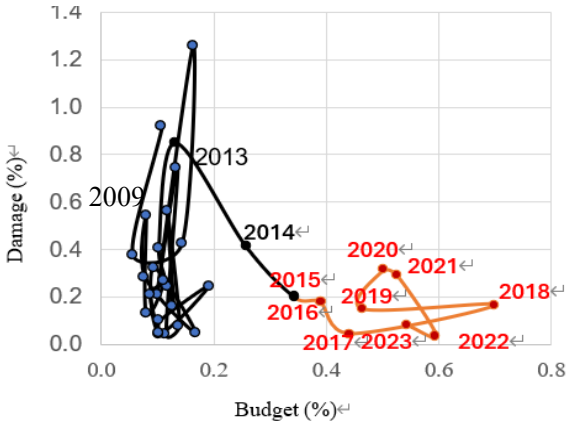

Figure 2 Flood protection budget and flood damage in the Philippines (Ratio to GDP)

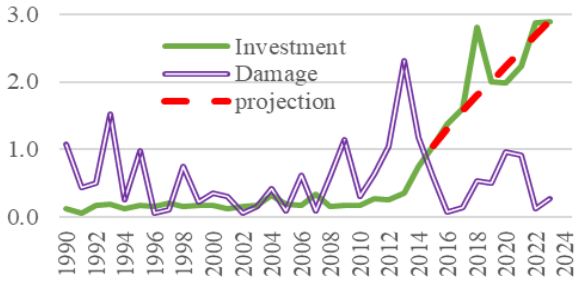

Figure 3 Flood protection budget and flood damage in Philippines (Billion USD)

Investment: The Philippines started to increase flood protection budgets following the 2013 Typhoon Yolanda disaster. The budget in 2023 became more than 8 times that of 2013 (Figure 3). Moreover, the country increased the budget in excess of the country's growth—fluctuating at less than 0.2% of GDP until 2013, then increasing to over 0.5% in the 2020s, reaching 0.7% in 2018 (Figure 2). GDP per capita reached USD 2,000 in the late 2000s, providing room to increase budgets for flood protection. This trend aligns with predictions by Ishiwatari and Sasaki (2020), validating their investment model (Figure 3).

The Department of Public Works and Highway (DPWH) implements most flood protection projects, prioritizing 18 major river basins and implementing projects in 12 river basins. The Metro Manila Development Agency, the national agency administrating Metro Manila Region, is responsible for managing flood protection facilities such as weirs, gates, and pumping stations. In addition, the government allocates the National disaster risk reduction and management fund to mainly response and rehabilitation work following disasters, with budgets of 680 million USD in 2024.

4.3 Japan

Japan, with most of its population concentrated in flood-prone coastal areas and river basins, has developed flood risk management systems over centuries.

Damage: Japan succeeded in decreasing flood damage to less than 0.5% of GDP from 1962 and further decreased damage to less than 0.2% from 1984 except 2004. However, damage recorded 0.25% (12 billion USD) in 2018 and 0.39% (18 billion USD) in 2019 (Figure 4), the figure in 2019 as a record high.

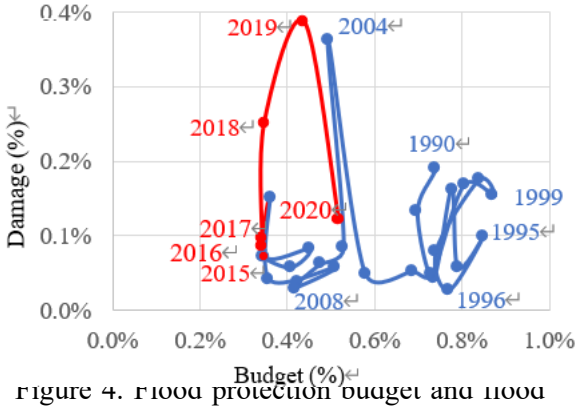

Figure 4. Flood protection budget and flood damage in Japan (Ratio to GDP)

Investment: Japan invested more than 0.9% of GDP in flood protection in the late 1970s and early 1980s, but this fell to less than 0.4% in the early 2010s (Figure 4). The country had halved investment in flood protection from 2000 to the 2010s due to a stagnant economy and tight fiscal situation. Following a series of severe flood disasters, Japan began to increase investment from 2019, reaching over 0.50% of GDP in 2020.

Japan enacted the River Law in 1896, and the national government began national flood protection projects on major rivers. Local governments contributed one-third of these national projects—a ratio maintained to the present day (Ishiwatari and Aldrich 2024). Japan started a subsidy program for medium and small rivers in 1932, where the national government subsidizes 50% of local government programs.

Local communities have been historically engaged in financial mobilization for structure measures as well as operation and maintenance work in their communities. Before the subsidy program, local communities shared some costs of local projects. For example, communities covered 30% in Saitama Prefecture and 50% in Niigata Prefecture. Even today, this community participation remains an essential component of flood management system, such as operating gates and cleaning rivers. This has fostered local ownership and rapid response capabilities during flood events.

5 Discussion

5.1 Investment Trends Analysis

The analysis reveals divergent trends in flood protection investment across the three countries. The Philippines is increasing flood protection budgets following major typhoon disasters in the 2010s. Japan's investment pattern shows a recent increase after a period of decline, reflecting renewed focus on flood protection in response to severe events.

Indonesia has not constantly increased the budget against predictions. Indonesia's failure to consistently increase its budget highlights the challenges of maintaining flood protection as a priority in the face of competing national interests. The overall budget for water resources has remained largely unchanged, with priority given to dam construction and water resource development in the new capital.

While the national government in Indonesia has not increased flood protection budgets, the Special Capital Region of Jakarta invested with a scale of one-third of the national budget. This demonstrates the potential for subnational entities to take leadership roles in addressing localized flood risks. The Jakarta region can afford to cover the cost because of its strong economic and budgetary situation.

5.2 Financing Mechanisms Comparison

The financing mechanisms employed by each country offer insights into potential strategies for sustainable flood protection investment (Table 2). Indonesia and the Philippines rely primarily on national

government funding, while Japan's model of cost-sharing among national, prefectural, and municipal governments presents an alternative approach.

In Indonesia, state-owned enterprises (PJT: Perum Jasa Tirta) conduct operation and maintenance of facilities in some river basins. PJT I manages facilities in Brantas River and expanded functions to Bengawan Solo and other river basins. PJT II manages the Jatiluhur dam and Citarum River Basin. These enterprises collect water tariffs from water supply utilities and the private sector for operation and maintenance.

In the Philippines, DPWH implements most flood protection projects, usually covering all costs without contribution from local governments. DPWH prioritized 18 major river basins and is implementing projects in 12 river basins. While the 1976 Water Act provides for local governments to take over facilities built by DPWH, in reality DPWH continues to operate and maintain the facilities following construction.

Table 2 Comparison of financial mechanisms

	Central	Local government	Community
Indonesia National project	✓		
Subsidy/ DKA	✓		
PJT		✓ Water tariff	✓
Local govt. project		✓	✓ Troops (JKT)
Philippines National project	✓		
Local govt. project		✓	
Japan National project	✓	✓ (33%)	✓
Local (Subsidy)	✓(50%)	✓(50%)	✓
Local govt. project		✓	✓

5.3 Historical and Cultural Context

The millennia-long history of cost-sharing for flood protection in Japan highlights the importance of cultural and historical factors in shaping effective flood management strategies. Japan has a history of sharing costs among national government, local government, communities, and the private sector for over a thousand years.

In Indonesia and the Philippines, the current centralized approach can be explained by the loss of traditional community-based water management practices during the colonial period and the centralized development approach after independence (Henley 2008; Tamaki 2002). As archipelagic nations, these countries have traditionally employed region-specific management mechanisms. Building on this historical foundation, traditional water management practices should be revitalized and integrated into modern contexts.

5.4 Policy Recommendations

Based on the analysis, the following policy recommendations are proposed for enhanced flood protection investment:

Cost-Sharing with Local Government: Implementing a robust cost-sharing mechanism between national and local governments can boost investment. For Indonesia and the Philippines, extending the cost-sharing model implemented in Jakarta to other provinces is recommended. Local governments should contribute to operation and maintenance costs of national projects. A tiered system should consider differences in financial capacity of local governments.

Financial Incentives for Local Governments: Establishing a system of subsidies and grants for local governments can initiate flood protection projects at the local level as Japanese case shows. A matching fund system where national contributions are tied to local investments would encourage greater commitment.

Expansion of Water Agency Financing: Expanding the role and financing capabilities of water agencies like PJT in Indonesia is recommended. Mechanisms should be developed for these agencies to reinvest a portion of their water user fees into flood protection infrastructure. This could include broadening their mandate to manage flood protection facilities and allowing them to contribute financially to construction projects.

Community Engagement and Contribution: It is essential to develop programmes that facilitate community contributions, whether in the form of cash or in-kind donations. The historical involvement of communities in Japan, and the success of the 'blue troops' and 'green troops' in Jakarta, demonstrate the potential of this approach. A framework should be created to recognise and integrate in-kind community contributions, such as labour and local knowledge, into flood protection projects. Traditional water management practices should be revitalised and integrated into modern contexts.

Long-term Financial Planning: Developing comprehensive, long-term financial plans incorporating climate change scenarios is crucial. Flood protection financing should be integrated into national development plans and climate change adaptation strategies. Regular national assessments of long-term flood protection needs should be conducted.

6 CONCLUSION

This comparative analysis of flood protection investments and financing mechanisms in Indonesia, the Philippines, and Japan has revealed the complex relationships between economic development, historical practices, governance structures, and effective flood protection. While each nation grapples with its unique set of challenges, several overarching conclusions emerge from this study.

A key finding is the critical importance of engaging multiple stakeholders—national governments, local governments, and communities—in both financing and management of flood protection initiatives. From national governments to local governments and communities, the involvement of diverse actors can lead to more comprehensive and sustainable approaches. This multi-stakeholder engagement not only enhances the financial base for flood protection but also fosters a sense of shared responsibility and ownership, which is crucial for long-term success.

The study validates the investment prediction model for the Philippines while highlighting Indonesia's challenge in maintaining flood protection as a national priority. The Philippines' trajectory demonstrates that economic growth can enable increased flood protection investment when coupled with appropriate policy responses to major disaster events. Conversely, Indonesia's experience shows that economic growth alone does not guarantee increased investment without deliberate policy prioritization.

Japan's long history of cost-sharing provides valuable lessons for developing countries, though its approach reflects unique cultural and historical factors that have evolved over more than a millennium. The influence of colonial history on current centralized approaches in Indonesia and the Philippines underscores the need for strategies that are not only technologically sound but also culturally appropriate and aligned with local traditions and practices.The study also underscores the significant influence of historical and cultural contexts on current flood protection strategies. Each country's approach is deeply rooted in its unique water management practices, which have evolved over time. Traditional water management practices should be revitalized and integrated into modern contexts.

This study has several limitations. The lack of standardized budget definitions across countries makes direct comparison challenging, as Indonesian and Philippine data primarily reflect national spending while Japanese data include local government budgets. Additionally, the analysis relies on budget allocations rather than actual expenditures. Despite these limitations, the comparative framework provides a useful foundation for understanding financing mechanisms and flood protection outcome.

Future research should explore quantitative analysis of long-term benefits of different financing approaches, including poverty alleviation and inequality reduction effects. Such research could analyse the socioeconomic impacts of flood protection investments and provide valuable data to support policy decisions and investment strategies. Additionally, studies should examine how emerging technologies such as green infrastructure and advanced risk assessment can be appropriately integrated into planning and investment frameworks.

This analysis underscores the complex and dynamic nature of flood protection in an era of climate change and societal transformation. It highlights the need for adaptive, multi-faceted approaches that combine robust financing mechanisms, stakeholder engagement, and flexible policy frameworks. As countries around the world grapple with increasing flood risks under climate change, the lessons drawn from Indonesia, Japan, and the Philippines offer valuable insights for developing resilient and sustainable flood protection strategies.

7 ACKNOWLEDGEMENTS

Financial support for this research has been provided by the FRICS Research Grant.

REFERENCES

Asian Development Bank (ADB). (2016). River basin management planning in Indonesia: Policy and practice. Mandaluyong City, Philippines: Asian Development Bank.

ADB. (2023). Proposed Loan and Administration of Loan Republic of Indonesia: Flood Management in North Java Project. Asian Development Bank.

Brugmann, J. (2012). Financing the resilient city. Environment and Urbanization, 24(1), 215-232.

Budiyono, Y., Aerts, J.C.J.H., Tollenaar, D., and Ward, P.J. (2016). River flood risk in Jakarta under scenarios of future change. Nat. Hazards Earth Syst. Sci., 16, 757-774.

Dottori, F., Mentaschi, L., Bianchi, A., Alfieri, L., & Feyen, L. (2023). Cost-effective adaptation strategies to rising river flood risk in Europe. Nature Climate Change, 13(2), 196-202.

Driessen, P.P. et al. (2018). Governance strategies for improving flood resilience in the face of climate change. Water, 10(11), 1595.

Girishankar, N. (2009). Innovating development finance-from financing sources to financial solutions. World Bank Policy Research Working Paper, (5111).

Henley, D. (2008). Natural resource management: historical lessons from Indonesia. Human Ecology, 36, 273-290.

Ishiwatari M., Aldrich D.P. (2024). Transforming Water Resources Management Investment: The Evolution of Cost Sharing among Local Communities, Governments, and the Private Sector in Japan. In Sociocultural Dimensions in Water Resources Management, Asian Development Bank Institute, Tokyo.

Ishiwatari, M., Sasaki, D. (2022). Disaster Risk Reduction Funding: Investment Cycle for Flood Protection in Japan. Int. J. Environ. Res. Public Health, 19, 3346.

Ishiwatari, M., Sasaki, D. (2020). Bridging the gaps in infrastructure investment for flood protection in Asia. JICA Research Institute: Tokyo.

Kok, S., Bisaro, A., de Bel, M., Hinkel, J., & Bouwer, L.M. (2021). The potential of nature-based flood defences to leverage public investment in coastal adaptation. Ecological Economics, 179, 106828.

Kunreuther, H.C., & Linnerooth-Bayer, J. (2003). The financial management of catastrophic flood risks in emerging-economy countries. Risk Analysis: An International Journal, 23(3), 627-639.

Rentschler, J., Salhab, M., & Jafino, B. A. (2022). Flood exposure and poverty in 188 countries. Nature communications, 13(1), 3527.

Tamaki A. (2002). Economics of Climate and Culture: Beyond the Western Model. Shinhyoron: Tokyo.

Wasko, C., Nathan, R., Stein, L., & O'Shea, D. (2021). Evidence of shorter more extreme rainfalls and increased flood variability under climate change. Journal of Hydrology, 603, 126994.

World Bank. (2019). Strengthening the disaster resilience of Indonesian cities: a policy note. World Bank: Washington DC.

World Bank. (2015). Toward Efficient and Sustainable River Basin Operational Services in Indonesia. Washington DC: World Bank.

ICFM 10
Adapting to Global Change:
Innovative Approaches to Flood Management and Resilience
May 20-22, 2026 | Western University, London, Ontario, Canada

Resilience Bonds as a Public-Private Partnership for Managing Increasing Risks of Climate Change

David Casagrande, John Roper, and Paolo Bocchini
Center for Catastrophe Modeling and Resilience, Lehigh University, Bethlehem, PA, USA
E-mail: dac511@lehigh.edu

ABSTRACT

Private insurance is a major mechanism for managing natural disaster risk in the U.S. We argue that public programs cannot provide sufficient levels of financial protection to homes and businesses and that private insurance is necessary. Research indicates that increasing disaster impacts due to climate change and building in high-risk areas are undermining current methods used by the insurance and reinsurance industries to spread financial risk, including premium pricing and catastrophe bonds. A potential strategy to enhance financial sustainability is to expand business-interruption loss coverage to vulnerable populations by investing in resilience and reducing community recovery times. This would be especially effective in disadvantaged communities where slower recovery prolongs business interruption losses. Public collaboration with private industry using tools like resilience bonds would benefit both the public sector and private insurance industry as well as homeowners and businesses.

KEYWORDS: catastrophe bonds, climate change, disaster, equity, insurance, resilience, sustainability, vulnerability

1 INTRODUCTION

Private insurance is the primary method for risk management within the United States and is necessary for any business or homeowner seeking financial protection from natural disasters. To remain financially solvent, an insurance company must maintain access to enough capital to pay its claims from a large disaster. Climate change has increased the severity and frequency of weather-related disasters (Adler et al., 2019; Jay et al., 2023). Concentration of high-value assets in risky areas combined with increasing damage has caused the insurance industry to incur significantly higher claim costs (Collier et al., 2021; Web-1, 2024). Many insurers who cover property damage caused by natural disasters purchase reinsurance to maintain financial solvency (Web-2). Increases in the frequency and severity of storms and floods have caused the insurance and reinsurance industries to abandon markets in states where they are losing their ability to spread risk effectively (Charpentier, 2007; Web-1).

The cost of business interruption resulting from a weather-related disaster is often significantly higher than the cost of physical damages (Dormady et al., 2022). Demand for business interruption loss insurance has risen with the increasing frequency of disasters (Dormady et al., 2022). If resilience is defined as time required for recovery, then public policies that promote private investments in resilience could help make business interruption loss insurance more affordable to a broader market. Investing in resilience and resilient infrastructure is economically beneficial because it reduces the costs associated with both damage and business interruption losses (Dormady et al., 2022; Hallegatte, 2019; Sun et al.,

2021). Through investments in resilience, private insurers can enhance their financial sustainability by expanding business interruption loss insurance into vulnerable and marginalized populations that bear disproportionate impacts compared to the rest of the population (SAMHSA, 2017; Hallegatte et al., 2016). Reducing the potential for physical impacts on infrastructure will speed recovery times and reduce resources that are spent on disaster aid and rebuilding (Sun et al., 2020). Therefore, investment in resilience presents an opportunity for the public and private sectors to collaborate and invest in economic growth while reducing community downtime and protecting against business interruption losses due to disasters.

To contextualize the current state of the industry and risk management options, we used Google Scholar and Claude AI Professional to conduct a literature review of peer-reviewed articles, grey literature, and industry news published between 2000 and 2024 by searching for overlapping themes of climate change, insurance, finance, pricing, resilience, and risk. We read 67 articles and determined that current industry methods for spreading risk, including premium pricing and catastrophe bonds, are threatened by climate change. We describe resilience bonds as one way to enhance financial sustainability by investing in resilience and reducing community recovery time to expand property damage and business interruption coverage to vulnerable populations. We conclude by describing how public collaboration with private industry using tools like resilience bonds would benefit both the public and private sectors. Catastrophe modeling simulations could be used to optimize investments and maximize cost reduction and financial security for consumers, governments, and private insurers.

2 CHALLENGES TO INSURANCE INDUSTRY SOLVENCY

The financial strain on the insurance industry results, in part, from increasing damage costs because of climate change (Charpentier, 2007; NCSL, 2023; Web-3). The trend of increasing costs of disasters was made salient with Hurricane Andrew in 1992, which cost insurers $16 billion at the time and caused nine insurance companies in Florida to become insolvent (Charpentier, 2007; Web-3). According to Charpentier (2007) at the beginning of this century, the frequency of category 4 and 5 hurricanes had doubled compared to 35 years prior. In addition, 6 out of 10 of the most expensive disasters up until that point had occurred in the 56 years prior to 2007 (Charpentier, 2007). This is because of the increased frequency of weather-related events in addition to the increased concentration of wealth and insured assets in risky areas such as Florida, California, and Japan (Charpentier, 2007; Collier et al., 2021). Every peril from drought, wildfires, floods, hail, winter storms, freezes, severe storms, and tropical cyclones have been on the rise over the past few decades (Web-4). The cost of these disasters has reached a magnitude that is equivalent to fighting a war domestically and permanently (Bilal and Känzig, 2024). In 2022, only $140 billion of the $360 billion in direct global economic costs due to weather events were covered by insurance with $125 billion coming from private insurers and $15 billion being covered by public insurers (Web-5). Additionally, U.S. property-casualty insurers suffered $32.2 billion in net underwriting losses in the first nine months of 2023 (Web-1). This trend of debt and loss caused by disasters has precluded reinsurers globally from being unable to earn back their cost of capital in 5 of the 6 years from 2017-2022 (Web-3).

Publicly financed programs are unlikely to perform better. The National Flood Insurance Program (NFIP) is the primary form of flood insurance for people living in flood zones within the U.S. This program has been in debt of around $20 billion since 2013, reaching a high of around $30 billion in 2017 (Web-6). In October 2017, Congress cancelled $16 billion of NFIP debt, making it possible for the program to pay claims for Hurricanes Harvey, Irma, and Maria (Web-6). The NFIP currently owes $20.5 billion to the U.S.

Treasury, leaving $9.9 billion in borrowing authority from a $30.4 billion limit by law. Meanwhile, more people and properties are experiencing increased flood risk. Between 1970 and 2010 there was a 114% increase in the population living in flood zones (UNISDR, 2011).

An important tool that insurance and reinsurance companies use to spread risk and reduce financial vulnerability to disasters is catastrophe bonds (Charpentier, 2007). Catastrophe bonds are short-term investments issued by the reinsurance industry to pool capital in case policies get triggered. Catastrophe bonds are purchased and used to cover a predefined disaster risk at a set monetary threshold (Polacek, 2018). If the disaster occurs and the conditions are met, the bond capital will be used to help mitigate losses and insolvency via policy payout, but the investor forfeits the principal and interest on the bond (Charpentier, 2007; Polacek, 2018). Catastrophe bonds have the effect of keeping reinsurance prices and volatility low while allowing for the transfer of insurance risks to the bond market (Polacek, 2018). The bonds themselves are issued by insurance companies, reinsurers, and state catastrophe funds, and payouts are dependent upon several triggers including indemnity, industry loss, and parametric (Polacek, 2018). Indemnity triggers pay out based on the insurance losses experienced by the insurer, industry loss triggers pay out based on aggregate losses that are often calculated by a third party, and parametric triggers pay out based on the intensity of the catastrophe being covered (Polacek, 2018). Insurance companies are the largest issuer of catastrophe bonds, with reinsurance companies being the next largest issuers (Polacek, 2018). The associated increase in frequency and magnitude of weather-related perils due to climate change may render the traditionally safe catastrophe bonds too risky an investment for many investors (Charpentier, 2007; Morana and Sbrana, 2019). Nevertheless, we describe below how catastrophe bonds could provide a model for public-private partnership resilience bonds.

3 WHY DO WE NEED PRIVATE INSURANCE?

It was predicted in 2007 that financial pressure caused by the uncertainty of climate change would lead to a rapid increase in premiums (Charpentier, 2007). This rise in premiums can be seen in home insurance where double-digit percentage increases have been common for the past few years (Web-7). The combination of inflation, increased property damage from storms, increased challenges in assessing risk due to climate change, and excess litigation has caused some insurers to pull out of high-risk states such as California and Florida, leaving only last-resort, state-created options funded by taxpayers (Collier et al., 2021; Web-1; Web-7). In some states where insurers continue to offer disaster policies, premiums are being raised at rates that consumers cannot sustainably afford (Web-1).

Unaffordable premiums or complete exit from markets by the private insurance industry has economic consequences. The inability for real estate buyers to obtain insurance required for mortgages will create regional declines in property values and equity. If premiums increase to a threshold where the market lacks the financial capital to adapt, then it could lead to widespread displacement and a sudden decline in property values, which would have cascading impacts on other aspects of the U.S. and global economies. The ability of the government to insure the escalating risk resulting from climate change is limited, as evidenced by the financial insolvency of the NFIP (Adler et al., 2019). Efforts to restore solvency by raising premiums through legislation in 2012 were repealed due to public pressure (Horn and Webel, 2023). If last-resort, state-created insurance models become the norm in high-risk states, then the catastrophe losses previously incurred by private insurers will be passed on to the public (Web-8), most likely through repetitive and contentious legislative appropriations. Public safety nets are not meant to be the primary form

of insurance in areas of high risk (Web-8). Private investment enables companies to leverage significantly greater amounts of capital by promising returns to investors (Mauboussin and Callahan, 2020). The reinsurance industry can leverage billions of dollars globally. It is also argued that privatization should lead to cost-cutting and greater attention to customer satisfaction (Goodman and Loveman, 1991).

Some insurers are encouraging climate mitigation to decrease risk (Collier et al., 2021). Other actions that can be taken to reduce the impacts of climate change include being more proactive in explaining how mitigation actions can lead to policy discounts, lobbying for higher performance requirements in building codes, and investing more in risk assessment. We propose an additional strategy, which is to partner with public institutions to invest directly in resilience.

4 WHY INVEST IN VULNERABLE POPULATIONS?

When a large area is designated as uninsurable, it is referred to as being "blue lined" (Montgomery and Palmeira, 2023). While blue lining reduces the industry's financial risk, it establishes areas where people either must be willing to cover damages out-of-pocket or leave and live elsewhere. Within the United States, there are often social factors that contribute to inequalities in outcomes and systems that perpetuate disparities. Many blue-lined areas overlap with previously redlined areas, where racially discriminatory practices were used to consolidate minority populations and conditions that contribute to poverty (Montgomery and Palmeira, 2023). Areas with high concentrations of minorities were deemed 'undesirable' for investment by the Homeowners Loan Corporation in the 1930s (Web-9). Previously redlined areas were shown to have 25% higher flood risk when compared with areas that were not redlined (Web-9).). A total of $107 billion worth of homes exists in previously redlined areas that are at risk of flooding (Web-9).

Research on the current observable impacts of redlining and disaster response has found that historically redlined communities have higher levels of social, evacuation, and preparedness vulnerabilities when compared to communities that never experienced redlining (Dugan et al., 2022). The Dugan et al. (2022) study was conducted on the relationship between redlining, social vulnerability, and impacts during power outages, which can occur during flood events and natural disasters. Poor urban households are more exposed to floods, more likely to incur moderate to more severe levels of damage during a flood, more likely to have the bulk of their savings concentrated in their homes, and more likely to live in vulnerable housing (Hallegatte et al., 2016; SAMHSA, 2017). Low-income households also tend to take 2-3 times longer to recover financially after a disaster, which can decrease their ability to participate in the local economy and contribute to longer business recovery times (Hallegette et al., 2016; Peacock et al., 2014; Tasri et al., 2022). This has the effect of decreasing the economic capacity of disadvantaged communities, further cementing inequalities (Tasri et al., 2022). Research by Xiao and Van Zandt (2012) showed that the rapid return of households in a market area will increase the chances for businesses to return. When a disaster strikes, low-income households have the most to lose and the businesses that serve them experience longer business interruption losses.

On average, the cost of business interruption is 900% higher than that of business property damage loss during a natural catastrophe (Dormady et al., 2022). Investing in resilient infrastructure has been shown to yield economic benefits that greatly exceed costs (Multi-Hazard Mitigation Council, 2019), including significant reductions in losses due to business interruption (Dormady et al., 2022). Private investments in resilience can help to shift the insurance industry to a return-on-place model where consumers and insurers are better insulated from catastrophic losses. Historic disinvestment in socially

vulnerable populations has concentrated social, natural, infrastructural, preparedness, and evacuation vulnerability and limited access to resources within these communities (Dugan et al., 2022; SAMHSA, 2017). On the other hand, it has concentrated opportunities for the largest return on investment in resilience. This is especially true when dealing with investments in housing (Walker, 2014) and infrastructure (Pereira, 2001).

For every dollar invested in resilient infrastructure, $4.57 is saved in business interruption costs and $6 is saved in structural damage loss (Dormady et al., 2022; FEMA, 2018). Federal, state, and local governments all have an incentive to invest in resilient infrastructure to reduce overall financial and structural losses in communities. Local governments rely on property taxes for up to 61% of their tax revenue (Web-10). Suspending insurance coverage in high-risk markets threatens local tax bases as communities are less able to recover after disaster. Long-term returns on investing in resilience through updating building codes can reduce the total value of insurance claims by 70% over a ten-year period with income and employment rates rising 9% over this timeframe (Obama White House, 2016; Walker, 2014). For example, specific actions like installing green roofs on homes have been shown to reduce peak flood runoff by 65%, which reduces localized flood impacts (GSA, 2011; Web-11). While many resilience-based solutions cost more upfront, the long-term savings and financial security they provide would benefit public and private insurers. It has been shown that wealthier communities tend to be more resilient in that they recover faster (Flanagan et al., 2011). Investing the same amount of money to increase resilience in a wealthy community would have less impact than investing it in a marginalized community. This is because low-income households must spend a larger proportion of their wealth to recover than wealthier households (Hallegatte et al., 2016). The best opportunities for public-private partnerships (PPP) that help foster resilience in communities are in vulnerable areas that have historic underinvestment in infrastructure.

5 PUBLIC-PRIVATE RESILIENCE BONDS

Considering the high returns from investments in infrastructure resilience, private investors and insurers could work with federal, state, and local governments to invest in resilient infrastructure that can be maintained with tax revenues to reduce claims and allow for affordable premiums. Resilience bonds are one method for promoting resilience already used in reinsurance and insurance (Web-12). Resilience bonds are a form of catastrophe bond "that link insurance premiums to resilience projects in order to monetize [future] avoided losses through a rebate structure" (Vaijhala and Rhodes, 2018). The initial idea was proposed in 2015 as a guide for public entities looking to build and monetize resilience through risk reduction programs in their communities (Motlagh et al., 2024). The intention was to develop "integrated resilience solutions and innovative public-private partnerships for vulnerable communities" (Motlagh et al., 2024; Web-13). To illustrate how public-private resilience bonds can be leveraged to develop such solutions and partnerships, it is important to explain how they work and who is involved.

There are three primary parties involved with these types of resilience bonds: sponsors, issuers, and investors. The sponsor is the party in need of natural catastrophe insurance and investments to finance disaster resilience projects (Web-13). The issuer is a third-party that brings the resilience bond to the market, sells the bond to investors to raise capital, and manages the funds in a collateral account (Vaijhala and Rhodes, 2017). This party is also responsible for ensuring that any resilience impacts and goals are clearly defined and that appropriate investment boundaries are set (Motlagh et al., 2024). The final party is the investor who buys and holds the resilience bond until it reaches bond maturity by a specified date

(Vaijhala and Rhodes, 2017). Investors accept lower rates of return in exchange for a lower investment risk (Kunreuther et al., 2016). Ideally, public-private resilience bonds would create win-win-win scenarios for all parties involved. Unfortunately, there is no current example of implementation. However, that does not minimize their potential feasibility or importance (Motlagh et al., 2024). We believe an impediment may be lack of access to high quality catastrophe modeling needed to confidently estimate future risk reductions.

The following hypothetical scenario illustrates how a public-private resilience bond would function to finance a coastal resilience project in Miami-Dade County, Florida. Miami-Dade County will serve as the sponsor for the project. The fictitious private Florida Insurance Company (FIC) who is motivated to expand business interruption loss coverage serves as the issuer. Investors Inc. serves as the investor. Miami-Dade County is interested in constructing a comprehensive coastal flood protection system protecting 25 miles of coastline that includes economically vulnerable communities with potentially longer recovery times. Currently, the county pays $50 million in annual public infrastructure flood insurance costs and is looking to reduce a potential $2 billion in flood damages over the next 20 years. FIC is interested in issuing a resilience bond to help finance the project that will cost an estimated $500 million. Through catastrophe modeling, FIC determines that the coastal resilience project will reduce Miami-Dade's hurricane and flood losses by 60% upon completion. FIC issues the bond for $500 million with a 4% coupon rate and a $1 billion regional economic loss trigger threshold for a named storm. Investors Inc. invests $500 million from pension funds into the bond with an expected 4% annual return that drops to 2.5% upon project completion to reflect the lower risk provided by the resilience project.

Miami-Dade would pay $25 million in annual premiums to FIC, the issuer of the bond, and the funds from the premium are used to pay investors their 4% coupon payments which would be $20 million annually. The capital provided by Investors Inc. is used to construct the project while FIC monitors and reports on project milestones. Once the project is complete, Miami-Dade's flood insurance premiums drop from $50 million to $30 million annually, representing a 40% reduction in costs. The reduced risk and completion of the project lead to the investor coupons dropping to 2.5% which is equivalent to $12.5 million. The combined savings of $20 million in flood insurance premiums and $7.5 million from the coupon discount results in a $27.5 million annual resilience rebate to the county that they can use to finance additional infrastructure projects or find additional ways to invest in community resilience at their discretion.

With public-private resilience bonds, sponsors are only responsible for paying the premium to the issuer rather than repaying the principle to investors as with conventional bonds (Vaijhala and Rhodes, 2019). If a hurricane occurs during the bond period and exceeds the trigger threshold, the bond is used to cover the county's losses, resulting in a partial loss of the principal for investors, but the county itself avoids catastrophic financial loss. In this hypothetical scenario, Miami-Dade county saves millions of dollars between annual insurance savings and the resilience rebates, investors receive a stable 2.5% return with lower risks than traditional catastrophe bonds, and the community sees increased insurability, enhanced property values, and a reduced risk of displacement. Expected losses are reduced, leading to a win-win-win scenario for the county, insurer, and investor.

6 CONCLUSION

While climate change will continue to progress and cause increased weather-related damages, its impact on the economy can be mitigated with preventative measures such as investing in resilient infrastructure in vulnerable communities. The financial sustainability of public and private property-casualty insurers overburdened by damage costs could benefit from greater cooperation. An option for reducing the risk faced by insurers is to promote resilient infrastructure to decrease incurred damages and increase how quickly vulnerable communities can recover, which will minimize business interruption losses, and allow for private insurers to expand business interruption coverage. Building on pre-existing public-private insurance relationships through targeted investments in resilient infrastructure in vulnerable areas has the potential to transform communities while protecting and improving returns on private investments. More precise effects on community recovery times after a natural disaster and the return on investments in resilience can be estimated using catastrophe modeling. Catastrophe models that can calculate the mitigative effects of investing in resilient infrastructure and expanding insurance markets to previously red-lined areas could increase the adaptive capacity of communities while also contributing to the financial sustainability of the insurance industry.

7 ACKNOWLEDGMENTS

The authors thank the Lehigh University Provost's Office for supporting this research through a Research Futures grant awarded to the Center for Catastrophe Modeling and Resilience and the Center's members who provided insights and inspiration.

REFERENCES

Adler D., Burger M., Moore R. and Scata J. (2019). Changing the National Flood Insurance Program for a Changing Climate. Envtl. L. Rep., 49, 10320.

Bilal A. and Känzig D.R. (2024). The Macroeconomic Impact of Climate Change: Global vs. Local Temperature. Working Paper 32450. National Bureau of Economic Research, Cambridge, MA

Charpentier A. (2007). Insurability of Climate Risks. The Geneva Papers on Risk and Insurance - Issues and Practice, 33(1), 91–109.

Collier S.J., Elliott R. and Lehtonen T.K. (2021). Climate change and insurance. Economy and Society, 50(2), 158–172.

Dormady N.C., Rose A., Roa-Henriquez A. and Morin B. (2022). The Cost-Effectiveness of Economic Resilience. International Journal of Production Economics 244: 108371.

Dugan J., Byles D. and Mohagheghi S. (2022). Social Vulnerability to Long-Duration Power Outages. SSRN Electronic Journal.

FEMA. (2018). Fact Sheet: Federal Insurance and Mitigation Administration Natural Hazard Mitigation Saves Interim Report. Federal Emergency Management Agency, Washington, DC.

Flanagan B., Gregory E., Hallisey E., Heitgerd J. and Lewis B. (2011). A Social Vulnerability Index for Disaster Management. Journal of Homeland Security and Emergency Management, 8(1), Article 3.

GSA. (2011). The Benefits and Challenges of Green Roofs on Public and Commercial Buildings. General Services Administration, Washington, DC.

Goodman J.B. and Loveman G.W. (1991). Does Privatization Serve the Public Interest? Harvard Business Review. November-December.

Hallegatte S., Vogt-Schilb A., Bangalore M. and Rozenberg J. (2016). Unbreakable: Building the Resilience of the Poor in the Face of Natural Disasters. World Bank Group, Washington, DC.

Hallegatte S., Rentschler J. and Rozenberg J. (2019). Lifelines: The Resilient Infrastructure Opportunity. World Bank Group, Washington, DC.

Horn, D.P. and Webel B. (2023). Introduction to the National Flood Insurance Program (NFIP). Congressional Research Service, Washington, DC.

Jay A.K., Crimmins A.R., Avery C.W., Dahl T.A., Dodder R.S., Hamlington B.D., Lustig A., Marvel K., Méndez-Lazaro P.A., Osler M.S., Terando A., Weeks E.S. and Zycherman A. (2023). Fifth National Climate Assessment. Global Change Research Program, Washington, DC.

Kunreuther H., Michel-Kerjan E. and Tonn G. (2016). Insurance, Economic Incentives and Other Policy Tools for Strengthening Critical Infrastructure Resilience: 20 Proposals for Action. Center for Risk Management and Decision Processes, The Wharton School, University of Pennsylvania.

Mauboussin M. and Callahan D. (2020). Public to Private Equity in the United States: A Long-Term Look. Morgan Stanley, New York, NY.

Montgomery B. and Palmeira M. (2023). Bluelining: Climate Financial Discrimination on the Horizon. The Greenlining Institute, Oakland, CA.

Morana C. and Sbrana G. (2019). Climate change implications for the catastrophe bonds market: An empirical analysis. Economic Modelling, 81, 274–294.

Motlagh F., Hamideh S., Gallagher M., Yan G. and van de Lindt J.W. (2024). Bonds for Disaster Resilience: A Review of Literature and Practice. International Journal of Disaster Risk Reduction, 104, 104318.

Multi-Hazard Mitigation Council. (2019). "Natural Hazard Mitigation Saves: 2018 Interim Report." National Institute of Building Sciences, Washington, DC.

NCSL. (2023). State Policy Considerations for Disaster Risk and Resilience. National Conference of State Legislatures, Washington, DC.

Obama White House. (2016). Standards and Finance to Support Community Resilience. National Archives, Washington, DC.

Peacock W.G., Van Zandt S., Zhang Y. and Highfield W.E. (2014). Inequities in Long-Term Housing Recovery After Disasters. Journal of the American Planning Association, 80(4), 356–371.

Pereira A.M. (2001). On the Effects of Public Investment on Private Investment: What Crowds in What? Public Finance Review, 29(1), 3–25.

Polacek, A. (2018). Catastrophe Bonds: A Primer and Retrospective. Federal Reserve Bank of Chicago.

SAMHSA. (2017). Greater Impact: How Disasters Affect People of Low Socioeconomic Status. SAMHSA Disaster Technical Assistance Center Supplemental Research Bulletin. Substance Abuse and Mental Health Services Administration, Washington, DC.

Sun W., Bocchini P. and Davison B.D. (2020) Model for estimating the impact of interdependencies on system recovery. Journal of Infrastructure Systems, 26(3).

Sun, W., Bocchini, P., & Davison, B. D. (2021). Policy-based disaster recovery planning model for interdependent infrastructure systems under uncertainty. Structure and Infrastructure Engineering, 17(4), 555–578.

Tasri E.S., Karimi K. and Muslim I. (2022). The effect of economic variables on natural disasters and the impact of disasters on economic variables. Heliyon, 8(1), e08678.

UNISDR (2011). Global Assessment Report on Disaster Risk Reduction. UNISDR, Geneva.

Vaijhala S. and Rhodes J. (2017). A Guide for Public-Sector Resilience Bond Sponsorship. Re:focus partners, LLC.

Vaijhala S. and Rhodes J. (2018). Resilience Bonds: A Business-Model for Resilient Infrastructure. The Journal of Field Actions, Special Issue 18, 58–63.

Vaijhala S. and Rhodes J. (2019). Conservation Investment Blueprint: Resilience Bonds. Coalition for Private Investment in Conservation.

Walker C. (2014). Building Sustainable Communities: Initial Research Results. Local Initiatives Support Corporation. New York.

Xiao Y. and Van Zandt S. (2012). Building Community Resiliency: Spatial Links Between Household and Business Post-Disaster Return. Urban Studies, 49(11), 2523–2542.

Web Sites:

Web-1: https://www.wsj.com/business/insurance-home-auto-rate-increases-climate-change-03b806f3?gaa_at=eafs&gaa_n=AWEtsqcUlJE7OSW2lvTft2ATDeTGDatFqoEXUqNvNHfH1309iLbr3oTZCf3bIuIbrg%3D%3D&gaa_ts=69c9fcdc&gaa_sig=XHgR2fTTHUn2jqxt6cWPZLNrE30lW6CDTdle7NgBEfHKLK02SraHXG6NFO-Udl3CijFh3exfpE_Jgn5435C1tg%3D%3D, consulted 15 July 2025.

Web-2: https://www.investopedia.com/terms/r/reinsurance.asp, consulted 29 March 2026.

Web-3: https://www.wsj.com/finance/insurance-catastrophe-reinsurance-hurricane-77a69eab?gaa_at=eafs&gaa_n=AWEtsqdhwAPGw6CSQwzNPdS1vXnH0EzleTlBBEjtpwWIxgp87knlB3vLgJp0vhpjsg%3D%3D&gaa_ts=69c9fa8a&gaa_sig=zendOMDGrHSczuz4c9quWm8U5KODZSCJe6v8GHl76UbZzRvMILoCt2MkL9qDhzZXcSU9VFd4TiIdVArdcIF1Kg%3D%3D, consulted 30 March 2026.

Web-4: https://www.climate.gov/news-features/blogs/beyond-data/2022-us-billion-dollar-weather-and-climate-disasters-historical, consulted 12 July 2025.

Web-5: https://www.reuters.com/business/environment/less-than-half-global-cost-climate-disasters-insured-broker-gallagher-re-says-2023-01-30/, consulted 28 June 2025.

Web-6: https://www.congress.gov/crs-product/IN10784, consulted 29 June 2025.

Web-7: https://www.wsj.com/economy/housing/home-insurers-are-charging-more-and-insuring-less-9e948113?gaa_at=eafs&gaa_n=AWEtsqfuAF06TiGtA_OLO5A18EEmnEvYfgm5s9S2Fzbj8aXkZkhVa_5q5QxBEc3hdA%3D%3D&gaa_ts=69c9fc49&gaa_sig=PrlzCd02mo7dmY9SyHLFw5AZCX173_ITN0h2xZCVLWC6b7TL0Wq3XsDHZiIcJFQbTaS0Re-E_w-MRc_g7DMJPA%3D%3D, consulted 13 July 2025.

Web-8: https://calmatters.org/environment/wildfires/2020/05/states-insurer-of-last-resort-should-not-become-the-primary-insurance-market/, consulted 2 August 2025.

Web-9: https://www.redfin.com/news/redlining-flood-risk/, consulted 20 July 2025

Web-10: https://rmi.org/supporting-local-governments-as-climate-change-threatens-their-communities/, consulted 12 May 2025.

Web-11: https://cfpub.epa.gov/si/si_public_record_report.cfm?Lab=NRMRL&dirEntryId=20 5444, consulted 13 July 2025.

Web-12: https://www.bbc.com/future/article/20170515-resilience-bonds-a-secret-weapon-against-catastrophe, consulted 8 July 2025.

Web-13: https://www.refocuspartners.com/wp-content/uploads/2017/02/RE.bound-Program-Report-December-2015.pdf, consulted 15 May 2025.

ICFM 10
Adapting to Global Change:
Innovative Approaches to Flood Management and Resilience
May 20-22, 2026 | Western University, London, Ontario, Canada

International approaches to flood risk management: the role of insurance, maps and regulations. Comparing the United States, the European Union and Canada

Anna Serra-Llobet[1,2], Clemens Neuhold[3], Francisco Espejo-Gil[4], Robin Bourke[5]
Center for Catastrophic Risk Management, Institute of Governmental Studies, 109 Philosophy Hall, University of California Berkeley, California 94720, United States[1]
Berkeley Center for Smart Infrastructure, Department of Civil and Environmental Engineering, Davis Hall, University of California Berkeley, California 94720, United States[2]
E-mail: annaserrallobet@berkeley.edu

Austrian Federal Ministry of Agriculture and Forestry, Climate and Environmental Protection, Regions and Water Management, Marxergasse 2, 1030 Vienna, Austria[3]
E-mail: Clemens.NEUHOLD@bmluk.gv.at

Consorcio de Compensación de Seguros, Paseo de la Castellana, 32, 28046 Madrid, Spain[4]
E-mail: fespejo@consorseguros.es

Public Safety Canada | Sécurité publique Canada, 269 Laurier Ave W, Ottawa, Ontario, Canada[5]
E-mail: Robin.Bourke@ps-sp.gc.ca

ABSTRACT

Flood losses are increasing worldwide because of expanding urbanization in flood-prone lands and flood peaks super-charged by climate change. Across the globe, countries struggle to manage flood risk, drawing upon insurance, structural measures, and land-use regulations. Canada is now creating its first federal flood insurance program while reinventing its flood mapping guidelines after two decades without a federally-supported flood mapping program. Recent changes in the current U.S. administration have put on the table two options for the future of flood risk management in the country: "shutting down" the Federal Emergency Management Agency or a massive reform of the National Flood Insurance Program. While these unprecedented situations have created big uncertainty on the future of flood policy in the United States and Canada, it can also create an opportunity to reimagine flood risk management in the 21st century. What can we learn from international experiences to inform strategies in North America? In this paper we summarize the results of a recent workshop hosted by the University of California Berkeley, where a group of researchers, practitioners and policy-makers from the United States, Canada, and the European Union reviewed the state of the art in flood risk management with emphasis on the interface between insurance, mapping, and land use planning regulations.

Our results show that there is no perfect insurance scheme. Some European countries such as Austria and Spain employ universal multi-peril insurance models. These systems have proven to be more sustainable financially. In contrast, the United States' National Flood Insurance Program, which is characterized by an adverse selection model, has experienced persistent financial deficits since Hurricane Katrina in 2005. The "moral hazard" – the fact that flood insurance can encourage exposure in high hazard zones - is a big challenge in all the countries analyzed. There are no agreed methods on how to assess risk reduction indication. Exposure in high hazard zones is increasing in all these countries. However, land use regulations in these zones are more restringing in Austria, Spain and some regions of Canada (e.g., Quebec) than in the United States. Currently, regulatory flood mapping – "official flood maps"- is more advanced and holistic in Europe, which aims at integrating flood risk management and nature protection (e.g., areas for groundwater recharge, habitat connectivity, etc.), although there are no harmonized European or other international standards for flood mapping.

KEYWORDS: Flood risk management, insurance, mapping, regulations, international approaches.

1 INTRODUCTION

Insurance relies on the law of large numbers — pooling many independent (non-correlated) risks to make losses predictable on average. If risks are "non-correlated", losses occur randomly and independently, what allows the insurer predict total losses more accurately to set fair premiums. Insurance also relies on the principle of "randomness", which refers to the idea that losses should occur by accident or chance, not by intention or certainty (Borch 1967). For example, a fire caused by accident is insurable while arson by the owner is not. Insurance also relies on the principle of "ease to estimate", what means that the amount of potential loss must be measurable or capable of being estimated accurately (Berliner, 1982).

However, if risks are highly correlated, what happens with extreme events, many losses might happen at the same time (e.g., flood disasters) (Jarzabkowski et al., 2023). This increases systemic or catastrophic risk. Catastrophe risk violates these principles for insuring risks: non-correlation, randomness, ease to estimate, etc. Therefore, catastrophe risk has to be insured with specific mechanisms such as "coinsurance", which is the percentage of costs that the policyholder and the insurer share after any deductible has been met, "reinsurance", a financial arrangement where an insurance company (the "ceding company") transfers part of its risk to another insurance company (the "reinsurer") in exchange for a share of the premiums, "Public–Private Partnership" (PPP), which is a structural partnership between public and private sectors to manage disaster risk, or "Insurance-Linked Securities" (ILS), a financial mechanism connecting insurance and capital markets to expand risk-bearing capacity, etc.

Different countries arrange solutions to address catastrophic risk based on their socio-economic and also their cultural contexts. However, the main problem is to conciliate three key issues: *availability*, *affordability* and *risk reduction indication*. Solutions have generally to choose between two of them, as meeting the three at the same time is really complicated. For example, providing subsidized insurance can encourage exposure in high hazard zones because there is a reduced incentive to prevent or minimize flood risk because someone else (like the government or an insurer) will bear the cost of the loss. In economy, this is known as "the moral hazard" (Pauly 1968).

Not meeting these three points – *availability*, *affordability* and *risk reduction indication*- usually conducts to a wider "insurance protection gap", which is the difference between economic losses from disasters and the portion of those losses that are insured. This gap is a matter of particular global concern with current urbanization trends in high hazard zones and climate change exacerbated hazards and therefore, loss. To fill this gap some countries have created what Jarzabkowski et al. call "Protection Gap Entities" (PGE) to cope with uninsurable risk. PGE are public insurance mechanisms that address the gap between the total risk of a disaster and the insurance covered.

In this paper we compare three protection gap entities: the National Flood Insurance Program in the US, the Consorcio de Compensación de Seguros in Spain and the Catastrophe Funds in Austria. We also analyse regulatory flood mapping systems used to inform land use planning decisions in these three countries to understand how each country balance the moral hazard. Our goal is to find insights from international approaches that can inform ongoing policy changes in Canada and the United Stated.

1.1 Methods and study areas

The comparative analysis presented in this paper draws primarily on the outcomes of the workshop *"Managing Flood Risk: The Role of Insurance, Maps, and Regulations—International Approaches,"* organized by the University of California, Berkeley's Center for Catastrophic Risk Management. The workshop, held on the UC Berkeley campus, convened scientists, policy-makers, industry representatives, and officials from state and federal agencies to identify potential directions for flood insurance, mapping, and regulatory frameworks across North America, with particular attention to Canada, which is currently in the process of developing a national flood insurance system.

2 THE ROLE OF INSURANCE, MAPS AND LAND-USE REGULATIONS IN REDUCING FLOOD RISK: COMPARING INTERNATIONAL APPROACHES

2.1 Flood risk management in Spain: the Consorcio de Compensación de Seguros and the EU Floods Directive's Flood Maps

Spain has a bold and comprehensive approach to insuring certain catastrophic perils. The Extraordinary Risk Insurance Scheme has been in place since 1954, and by law, it is compulsory to extend the coverage of most property damage policies (including business interruption) and all personal injury policies sold in the Spanish market to include a list of extraordinary perils. These perils encompass all types of floods (riverine, pluvial, and coastal), as well as windstorms, earthquakes, volcanic eruptions, and other events, including human-made hazards such as terrorism (Sanabria-García and Torres-Sempere, 2025).

To fund this coverage, a surcharge is applied to policies sold by every insurer operating in the Spanish market. The surcharge depends only on the type of line and property insured (taxes vary for dwellings, shops, factories, motor vehicles, or infrastructure) and the sum insured. For instance, for residential properties, the surcharge is 0.07‰ of the insured capital. These surcharges are transferred to a public insurer, the Consorcio de Compensación de Seguros (CCS), which establishes equalization reserve with these funds to indemnify losses caused by extraordinary perils. CCS manages the entire process of claim filing, loss assessment, and compensation as a direct insurer under the same policies issued by private insurers.

This system exemplifies a public-private partnership: nearly all policies in Spain are dual, with one component covered by the private market—responsible for selling policies, selecting risks, and setting premiums freely—and the other by CCS, which charges a flat rate and covers extraordinary perils. In practice, this means the insurance protection gap against events such as flooding is virtually zero in Spain, as all insured properties are covered for flood risks. At a national level, approximately 80% of residences are insured. While insurance itself is not mandatory, extending coverage for extraordinary perils to insured properties is compulsory. This universal approach applies to both privately and publicly owned assets and prevents adverse selection, reduces premiums, and ensures the long-term sustainability of the insurance scheme.

CCS possesses a wealth of data. In the case of flooding, CCS holds all insured flood loss data in the country with high granularity and long-term series. These data are shared with different levels of government and academia to inform risk prevention measures and serve as a baseline for risk reduction and climate change adaptation policies.

For risk reduction and adaptation, both susceptibility reduction and exposure control are essential, with land use planning serving as the key mechanism to implement these measures. In Spain, this is regulated through the national transposition of the EU Floods Directive (2007/60/CE), via Royal Decree 903/2010 on the Assessment and Management of Flood Risks. This decree modifies the Water Act and the Public Water Domain Regulation, defining different areas associated with river courses and their uses. The main areas include the "Floodable Zone" (zona inundable), defined by the 500-year return-period flood, and the "Frequent Discharge Zones" (zona de flujo preferente), affected by the 100-year return-period flood. Within the frequent discharge zones, a more severely affected area—the "Intense Drainage Channel" (vía de intenso desagüe)—is delineated. Most uses, such as schools, hospitals, nursery homes, malls, and potentially polluting industries, are prohibited within the frequent discharge zones. Residential and certain other uses are permitted only with safety measures adapted to cope with 500-year return-period floods. Uses in the rest of the Floodable Zone (between the 100-year and 500-year floods) are allowed provided the design is adapted to flood risk.

Insurance loss data is crucial for calibrating flood models used to create these flood maps, which must be updated every six years as mandated by the EU Floods Directive.

2.2 Flood risk management in the United States: The National Flood Insurance Program

The National Flood Insurance Program (NFIP) was created by the National Flood Insurance Act of 1968, enacted by the U.S. Congress, with the goal of reducing the economic impact of flooding in the United States. It does so by providing affordable (frequently subsidized) insurance, encouraging communities to adopt floodplain management regulations, and reducing the need for post-disaster federal aid. Now administered by the Federal Emergency Management Agency (FEMA), the NFIP operates through a partnership among the federal government, local communities, and private insurers (Congressional Research Service 2025). Its structure combines risk-mitigation policy with an insurance mechanism, to make coverage available to property owners who might otherwise be unable to obtain it.

This link—local compliance with development criteria in exchange for access to federal flood insurance—is central to the program's design. Communities that participate are required to adopt and enforce floodplain management ordinances that meet FEMA standards. These local regulations govern development in high-risk areas, ensuring that new construction and substantial improvements are built in accordance with FEMA's development criteria[1] to withstand specific flooding events. Participation in the NFIP is voluntary, but for participating communities, NFIP flood insurance is available to homeowners, renters, and business owners. When properly implemented, it can help reduce future flood damage, thereby lowering insurance payouts and federal disaster spending.

In parallel with the development criteria established under the NFIP, another influential set of standards in the United States is the American Society of Civil Engineers' (ASCE) "Flood Resistant Design and Construction" standards, known as ASCE 24. ASCE 24 standards set minimum requirements for designing and constructing buildings and structures to resist flood damage. Although the NFIP minimums are an improvement over earlier requirements, they are still far below the standards of ASCE 24-24, the 2024 edition of the ASCE 24.

ASCE 24-24 is anticipated to be adopted into the next International Code Council (ICC) model codes (2027 cycle). ICC develops a set of model codes, including the International Residential Code (IRC) – which apply to small residential buildings-, International Building Code (IBC) - which applies to all other buildings including larger commercial buildings or more complex residential (e.g., apartments, condos), and the International Mechanical, Plumbing, and Energy Codes. These are model codes, meaning they don't have legal force until a state, city, or county officially adopts them. Whether IRC might treat ASCE 24-24 differently from the IBC is still unclear. Historically, the IRC does reference ASCE 24 flood provisions, but often in a more limited way than the IBC. In states such as California, state-adopted provisions such as ASCE 24 flood requirements can take precedence over NFIP development criteria since ASCE24 is often more stringent or detailed than NFIP minimums.

The NFIP produces and maintains Flood Insurance Rate Maps (FIRMs), which delineate "Special Flood Hazard Areas" (SFHAs)—zones with at least a 1% annual chance of flooding (100-year return period flood). While properties with federally backed mortgages in SFHAs are required to carry flood insurance, flood insurance is only encouraged for all other properties both in and out of the SHFA. This results in an overall low insurance take-up rate, particularly in areas outside of the SFHA where the perceived risk is lower.

The low overall take-up rate contributes to a phenomenon known as "adverse selection," where individuals with a higher likelihood of experiencing a loss are more likely to purchase insurance. In flood insurance, those in "official" flood-prone areas are more inclined to buy coverage, leading to an unequal distribution of risk among policyholders. This can result in increased claim costs and financial strain on the insurer and the government (through taxpayers), as evidenced by estimates suggesting that between 2015 and 2019, 40% of all NFIP claims came from outside of the SFHA (Federal Emergency Management

[1] Under FEMA's 44 CFR § 59.1, "development" is defined as: "Any man-made change to improved or unimproved real estate, including but not limited to buildings or other structures, mining, dredging, filling, grading, paving, excavation or drilling operations, or storage of equipment or materials."

Agency, 2024). The age of the FEMA maps and the lack of pluvial mapping contributes to adverse selection, as the Flood Insurance Rate Maps may not identify areas of known localized flooding.

Insurance premiums under the NFIP are based on several factors, including property location, building characteristics, elevation relative to the base flood elevation, and flood risk as mapped by FEMA and as identified by commercial catastrophe models. For decades, rates were partially subsidized and did not fully reflect actuarial flood risk, leading to financial instability in the NFIP. The Biggert-Waters Flood Insurance Reform Act of 2012 (BW-12) required FEMA to move the National Flood Insurance Program (NFIP) toward actuarially sound, risk-based rates and to reduce or eliminate long-standing subsidies. Thus, BW-12 created the legal and policy foundation that pushed FEMA to modernize its pricing methodology, called "current pricing approach" (informally known as "Risk Rating 2.0"). Under this system, properties with higher flood risk pay higher rates, while many lower-risk properties benefit from reduced premiums. Although rate changes are capped annually to ease the transition, the shift aims to build long-term financial resilience for the program. However, the lack of gradual implementation and insufficient support mechanisms for affected homeowners whose insurance premiums skyrocket made the policy politically and socially contentious, highlighting the tension between risk-based pricing and affordability in flood insurance.

Claims under the NFIP are paid even when catastrophic events cause widespread damage, because the program has federal backing. However, repeated major disasters have often forced the NFIP to borrow from the U.S. Treasury (over $23 billion as of December 2025), highlighting the tension between individual affordability and the financial sustainability of the insurance scheme. Reforms over the years have aimed to reduce repetitive-loss properties, improve flood mapping technology, and strengthen mitigation grants that help elevate structures, buy out high-risk homes, or enhance community resilience. However, increased exposure in high-hazard zones remains the biggest driver of rising flood risk in the United States (Wing et al. 2022).

Recent changes in the current U.S. administration have raised discussions about potentially abolishing FEMA or drastically reducing its functions (Pinter et al. 2025). As of June 1, 2025, 2,446 FEMA employees have either been dismissed or taken buyout offers since the new administration took office in January, 2025 (U.S. Government Accountability Office, 2025). As a result, the future of the NFIP remains uncertain. Some states are preparing to strengthen their own roles in flood risk management in anticipation of further downsizing of FEMA or major reforms to the NFIP (Pinter et al. 2025).

2.3 Flood risk management in Austria: the catastrophe funds and the flood maps included in the Hazard Zone Plans

Every private property owner in Austria is required to have household insurance that includes coverage for natural hazards. However, this natural hazard coverage is capped, generally in the range of €10,000–15,000. There is also an option for voluntary insurance against additional risks, such as flooding. The premiums for these extra policies are calculated with support from the HORA system (www.hora.gv.at), a public-private partnership between the Austrian Association of Insurance Companies and the Austrian Federal Ministry for Agriculture, Forestry, Climate and Environmental Protection, Regions, and Water Management.

In addition to insurance, damage compensation in Austria follows the "solidarity principle." In the event of a catastrophe—which, depending on the spatial extent of the flood, must be declared by the municipality, district, federal province, or federal government—direct tangible damages are compensated through national catastrophe funds. The compensation rate typically amounts to up to 40% of eligible direct tangible damages, while luxury goods are excluded. For extreme events, such as the 2002 flood along the Danube and its tributaries, compensation rates may be higher.

For the agricultural sector, natural hazard insurance is available, with premiums partially subsidized. In cases of flooding, hail, or similar events, 100% of losses are compensated for insured properties. For industry and trade, individual or facility-specific insurance solutions are available and often mandatory.

To raise awareness and support the insurance sector, Austria provides various tailor-made maps for different target groups and purposes. Austria has approximately 100,000 km of river courses, of which 25,000 km along major urban areas and infrastructures are mapped with Hazard Zone Plans based on 2D hydrodynamic modelling. These maps are also used to implement the EU Floods Directive, which requires preparing flood hazard and risk maps.

These detailed maps are complemented by the HORA system, which provides simplified mapping to cover most areas in Austria and raise public awareness of flood risks. Established in 2005, the HORA system is an open-access tool that allows users to locate hazards by address and includes downloadable PDF reports. A login area for insurers supports the determination of policy premiums.

Two types of maps are available: flood hazard and risk maps according to the EU Floods Directive, and HORA system maps at approximately 1:6,000 scale. For local decision-making, property-level information at 1:2,000 scale is provided by Hazard Zone Plans (Neuhold, 2026). These plans delineate two zones: the "Yellow Zone," based on a 100-year flood scenario, and the "Red Zone," based on flood intensity (a function of water depth and flow velocity), representing areas of higher conveyance within the 100-year flood. These zones serve as advisory assessments for local spatial planning and building regulations. Hazard Zone Plans also define "functional areas" based on a 300-year flood scenario, intended for water retention, conveyance, and the prevention of increased flood risk. Public participation is mandatory in creating Hazard Zone Plans. Thus, these maps also help raise flood risk awareness among citizens.

Zoning restrictions and flood-related building codes for hazard zones and functional areas are defined in national spatial planning laws and local building regulations. New developments are prohibited in "Red Zones," though some exemptions exist for expansions of existing buildings or urban areas under high land-use pressure. In "Yellow Zones," development is discouraged and restricted according to the legal framework; new structures are permitted if elevated at least 50 cm above the 100-year flood level. However, raising terrain by filling is prohibited to prevent adverse effects upstream or downstream. "Functional areas" must remain free of new developments to ensure safe water retention and conveyance during 300-year flood events. Functional areas and related regulations are currently under discussion concerning urban development, pluvial flooding, and zoning. Finally, the "residual flood risk" beyond the 100-year flood prone area, including residual risk behind levees (dikes), is also communicated to the public in these maps by highlighting 300-year flood scenarios.

In summary, Austria uses four types of flood maps to inform flood risk reduction measures at different scales: (1) Hazard Zone Plans (1:2,000): Highest resolution maps including expert judgment, providing recommendations for spatial planning and building regulations at the local level, (2) Flood Conveyance Maps (1:5,000): High-resolution maps based on 2D models, used as a basis for Hazard Zone Plans, (3) Flood Hazard and Risk Maps (EU Floods Directive): Incorporating Hazard Zone Plans and flood conveyance maps, (4) HORA System Maps: Simplified 2D models complementing flood risk information beyond areas covered by Flood Directive maps.

3 CONCLUSION

Our results show that while the United States was ahead of Europe as a whole in floodplain mapping through the 20th century, flood mapping has evolved enormously in Europe since the implementation of the Floods Directive in 2007. However, there are no harmonized European or other international standards for flood mapping. In the US, mapping is only mandatory for communities that want to participate in the NFIP and is generally restricted to the 100-year flood hazard zone, (the Special Flood Hazard Area, SFHA). The SFHA is the area where floodplain management regulations must be enforced and where the mandatory flood insurance purchase requirement applies. Recent federal flood initiatives in Canada include Natural Resources Canada's guidelines and mapping programs, and several major programs at Public Safety Canada focusing on flood risk quantification, Disaster Assistance, Flood Insurance costing, and flood risk communication. However, at the provincial and territorial levels of government, approaches to flood hazard identification and mapping are not consistent.

The EU has a more integrated, holistic and forward-looking flood risk management approach that strengthens coordination and collaboration between different sectors beyond water management, especially civil protection, spatial planning and nature conservation.

Public consultation has become the norm in all EU Member States leading to improved awareness of flood risk by citizens and stakeholders. However, there are still major challenges to be tackled such as the consideration of climate change on a long-term perspective, pluvial flooding as a local process and vulnerability assessment. Flood hazard and risk maps are required in all Member States under the Floods Directive but, unlike the US, flood maps are not systematically linked to the flood insurance system, which can be public, private or a public-private partnership, depending on each country. The increasing uninsurability of flood disasters is a global concern.

4 ACKNOWLEDGEMENTS

The international workshop *"Managing Flood Risk: The Role of Insurance, Maps, and Regulations—International Approaches"* organized at UC Berkeley in November 2023 was hosted by the UC Berkeley Center for Catastrophic Risk Management and the Institute of Governmental Studies, in collaboration with the Association of State Floodplain Managers (ASFPM) International Committee. This workshop was supported by the Jean Monnet Center of Excellence Seed Grant, the UC Berkeley Institute of European Studies (IES) European Union Center (Jean Monnet Center of Excellence), and the UC Berkeley French-Berkeley Fund (FBF), and benefited from the collaboration of the UC Berkeley Canadian Studies Program. We want to thank all the participants for their contributions to the workshop. We also thank Eric Simmons, FEMA Region IX (retired) currently HDR and Kathleen Schaefer, FEMA Region IX (retired) currently UC Davis for their comments on earlier drafts of the manuscript.

REFERENCES

Berliner, B. (1982). Limits of insurability of risks. Englewood Cliffs, NJ: Prentice-Hall.

Borch, K. (1967). The Theory of Risk, Journal of the Royal Statistical Society Series B, 29 (3), pp. 432-452. https://doi.org/10.1111/j.2517-6161.1967.tb00707.x

Congressional Research Service. (2025, April 22). Introduction to the National Flood Insurance Program (NFIP). Congressional Research Service.

Federal Emergency Management Agency. (2024). Technical Mapping Advisory Council 2023 Annual Report.

Jarzabkowski, P., Chalkias, K., Cacciatori, E., and Bednarek, R. (2023). Disaster Insurance Reimagined: Protection in a Time of Increasing Risk. Oxford University Press. https://doi.org/10.1093/oso/9780192865168.001.0001

Neuhold, C.: Hazard zone planning in Austria – a tool to link flood risk management and settlement development (2026 ICFM10 Conference proceedings)

Pauly, M. V. (1968). The Economics of Moral Hazard: Comment. *The American Economic Review*, 58(3), 531–537. http://www.jstor.org/stable/1813785

Pinter, N., Kousky, C., Conrad, D., Fugate, C., Ghilarducci, M., Neal, A., Serra-Llobet, A., Watkins, N. [Expert panel] (2025). Securing California's Flood Future: In a time of national policy turbulence [White paper]. University of California, Davis - Flood Risk and Policy Research Group.

Sanabria-Garcia, S., Torres-Sempere, J. (2025). Two-Level System for Optimal Flood Risk Coverage in Spain. Water 2025, 17, 1997. https://doi.org/10.3390w17131997

U.S. Government Accountability Office. (2025). Disaster assistance high-risk series: Federal response workforce readiness (GAO-25-108598).

Wing, O.E.J., Lehman, W., Bates, P.D. et al. (2022). Inequitable patterns of US flood risk in the Anthropocene. *Nat. Clim. Chang.* 12, 156–162. https://doi.org/10.1038/s41558-021-01265-6

Chapter 5- Governance, policy, and societal engagement

5.4 Role of communities, citizen science, and non-traditional actors in flood risk management

ICFM 10
Adapting to Global Change:
Innovative Approaches to Flood Management and Resilience
May 20-22, 2026 | Western University, London, Ontario, Canada

Integrated Analysis of Flooding and Waterlogging Risks in New Urban Development: A Case Study of Jinan Start-up District, China

Benyou Jia[1,2], Yixin Jing[1], Haochuan Hong[1], Jingxiu Wu[1], Shujuan Cai[1], Ziwu Fan[1]
Hydraulic Engineering Department, Nanjing Hydraulic Research Institute, Nanjing, 210029, China[1]
E-mail: byjia@nhri.cn
National Key Laboratory of Water Disaster Prevention, Nanjing, 210029, China[2]
E-mail: zwfan@nhri.cn

ABSTRACT

The development of new urban areas involves complex subsurface modifications through concurrent construction of critical infrastructure systems. These include flood control structures, drainage networks, transportation corridors, utility pipelines, and urban facilities spanning governmental, residential, educational, and industrial functions. Effective flood risk management in such developments requires comprehensive assessment of both external flood inundation and internal waterlogging hazards to inform resilient urban planning. This study presents a multi-model integration framework combining: 1) rainfall-runoff generation modeling, 2) 1D hydrodynamic simulations for river networks and drainage systems, 3) 2D surface inundation modeling, and 4) hydraulic structure operation protocols for sluice gates and pumping stations. The coupled modeling system enables holistic simulation of complete flood processes from precipitation through runoff generation, surface flow propagation, and water recession.Using Jinan Start-up District as a demonstration case, we developed a flood integration model evaluating 17 computational schemes across two rainfall scenarios. Spatial risk patterns were analyzed through flood depth and duration parameters, with hazard levels classified into four tiers (very high, high, medium, low). The assessment incorporates critical urban assets including completed infrastructure and population centers. Our findings reveal key vulnerabilities and support proposed mitigation strategies: 1) Upgrading drainage channels and pipe networks, 2) Developing park-integrated detention basins, 3) Implementing risk-adaptive measures (population evacuation protocols, temporary flood barriers), and 4) Coordinated watershed-level flood management. The methodology provides a technical foundation for resilient urban planning, emphasizing integrated structural and non-structural flood prevention measures.

KEYWORDS: Resilient Cities; Urban Flood Modeling; Multi-risk Assessment; Extreme Rainfall; Urban Flood Management Strategies

1 INTRODUCTION

In recent years, influenced by climate change, China has experienced increasingly frequent and severe hazardous weather events, with urban rainstorm-induced flooding being particularly prominent in northern regions. The extreme rainfall event that occurred in Zhengzhou, Henan Province, on July 20, 2021, triggered catastrophic urban flooding, leading to cascading disasters such as subway inundation, damage to roads and bridges, and widespread disruption of daily life and economic activities. This event resulted in more than 300 fatalities and direct economic losses amounting to 53.2 billion CNY, causing extraordinarily severe human and property losses and offering profound lessons. Urban flood disasters induced by extreme rainfall are typically characterized by sudden onset, concealed risk points, wide impact ranges, compound flooding processes, diverse secondary hazards, and substantial losses. These features pose complex and formidable challenges to urban flood prevention and mitigation in China (Zhang et al., 2025; Ahmad & Simonovic, 2013). Consequently, promoting the development of sponge cities and resilient cities has become an inevitable choice. On the one hand, such initiatives help enhance the capacity of built-up urban areas to prevent and respond to rainstorm-induced flooding. On the other

hand, in the construction of new urban districts, it is necessary to coordinate the relationship between flood control infrastructure and rapid urban spatial development, so as to achieve an organic integration of disaster prevention and urban construction (Ma et al., 2021; Yang et al., 2025).

Over the years, numerous scholars both domestically and internationally have conducted extensive research on urban flood risk assessment and management, forming a comprehensive research chain from risk identification and process simulation to decision-making and response, and yielding abundant (Hou et al., 2025). In terms of risk assessment, early studies predominantly adopted indicator-based approaches, such as the hazard-exposure-vulnerability framework, to perform static evaluations. With technological advancement, scenario-based simulation has become the mainstream approach, in which rainfall–flood modeling is coupled with loss assessment models to quantify risks under multiple climate and land-use scenarios. This approach has progressively evolved from regional-scale analyses toward refined assessments at the street and community levels, and has begun to address the risk characteristics and evaluation models of cascading rainstorm events, such as subway inundation and building damage (Ming et al., 2020; Lin et al., 2023; Chen et al., 2012). In terms of simulation and scenario deduction, which constitute the core technologies for risk assessment and early warning, traditional hydrological and hydraulic models, such as SWMM, HEC-RAS, and MIKE, have been widely applied in urban flood modeling. The current trend is to couple physical-process-based models with data-driven models in order to balance accuracy and computational efficiency (Lu et al., 2024; Dazzi et al., 2024; Romana et al., 2015). In emergency management, the focus has shifted from an emphasis on engineering defenses toward comprehensive process-oriented management and the coordination of socio-technical systems. Complex network theory has been employed to analyze disaster-chain propagation and emergency resource allocation. Meanwhile, emerging information technologies, including media data mining, artificial neural networks, and unmanned aerial vehicle remote sensing, have demonstrated increasing effectiveness in emergency response (Yang & Yeh, 2014; Li et al., 2023; Konapala et al., 2020). In summary, risk assessment provides risk scenarios and vulnerability parameters of exposed elements for simulation, while simulation generates dynamic inundation extents, depths, velocities, and early-warning information for risk assessment. Emergency management, in turn, utilizes the warning outputs from simulations and the vulnerability analyses from risk assessment to optimize resource allocation and implement targeted interventions. These three components are mutually reinforcing and form a closed-loop framework, constituting a core technical pathway for urban flood risk governance.

This study selects the Jinan Start-up District, a rapidly developing urban new area, as the research object. Based on the construction tasks defined in the flood control and drainage master plan, the dimensions and anticipated parameters of engineering infrastructure are preset. A coupled hydrological-hydrodynamic model is then constructed. Multiple rainfall scenarios are assumed to analyze river water level processes and the spatial distribution of surface inundation risk. The impacts of inundation risk factors on planned urban spatial elements are systematically evaluated. On this basis, recommendations are proposed for the optimization and adjustment of planned infrastructure as well as for the prevention and response of key urban protection targets under extreme rainfall conditions. The study aims to provide effective technical support for the development and construction of urban new districts.

2 METHEDOLOGY

2.1 Jinan Start-up District Overview

Jinan is one of China's key flood-prone cities. It is located with Mount Tai to the south and the Yellow River to the north, situated at the transitional zone between the central-southern Shandong mountainous region and the northwestern Shandong alluvial plain. The terrain is characterized by higher elevations in the south and lower elevations in the north, with pronounced intra-annual and inter-annual variability in precipitation. The long-term mean annual rainfall is approximately 670 mm, with most precipitation concentrated during the flood season from June to September. Under extreme weather conditions, the city is highly susceptible to flood disasters. The Jinan New and Old Kinetic Energy Conversion Start-up District (hereinafter referred to as the Start-up District) is a national-level strategic

new area. Its directly administered area includes four subdistricts: Daqiao, Cuizhai, Sungeng, and Taiping. The total area is approximately 450 km². According to statistics in 2020, the district contained 308 villages and nearly 400,000 mu of cultivated land, and is currently undergoing a rapid process of urbanization. According to the flood control and drainage special plan for the Start-up District, by 2035, a "safe and resilient" flood control and drainage disaster reduction system will be established through a combination of engineering and non-engineering measures. This system is intended to safeguard the sustainable socio-economic development of the Start-up District. The 2020 satellite imagery of the Start-up District and the planned river system and concentrated urban areas for 2035 are shown in Figure 1.

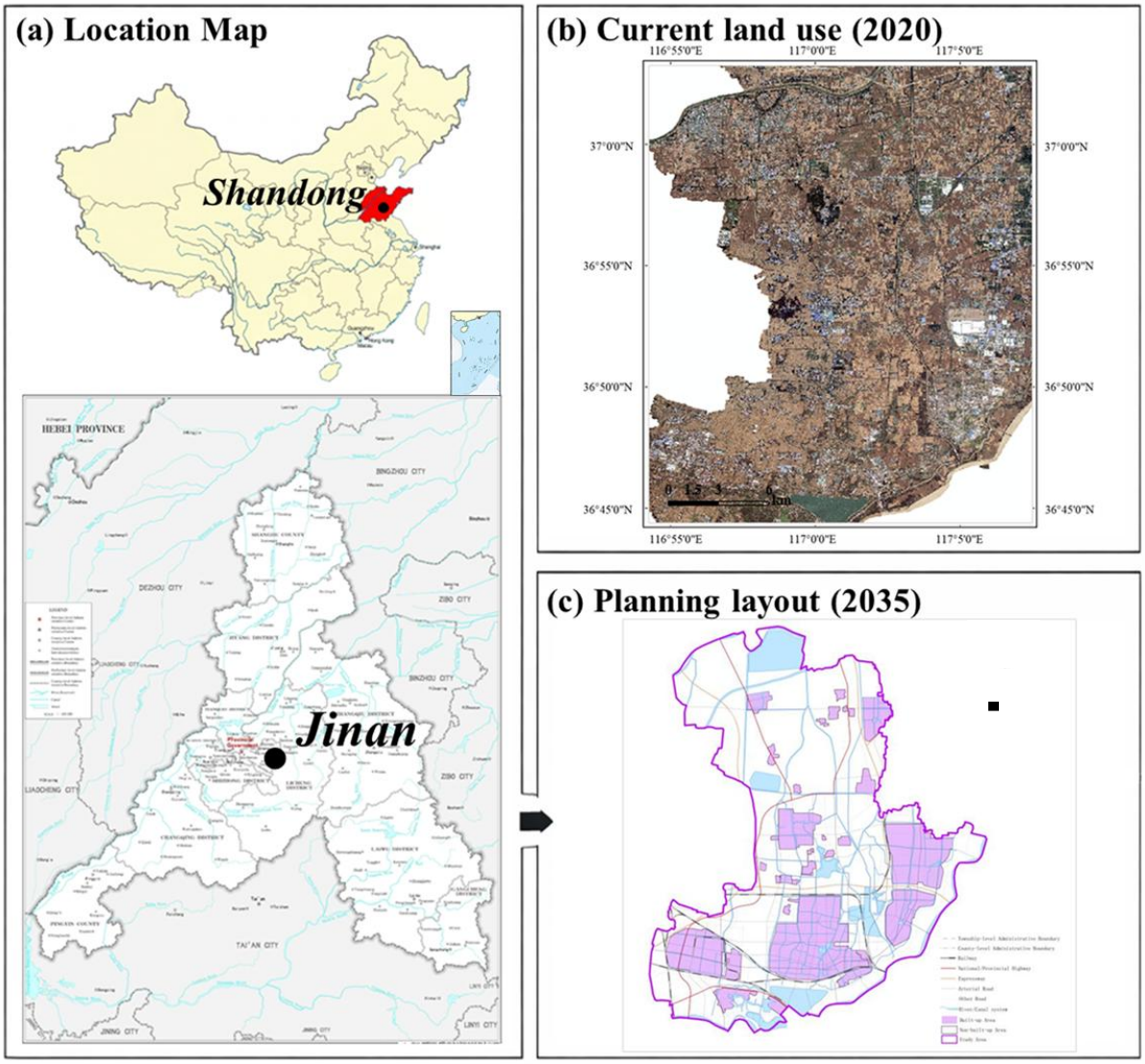

Figure 1. Location and planning layout of the study area (a) Geographic location of the study area within Jinan City, Shandong Province, China. (b) Curent land useconditions in 2020. (c) Planned urban layout in 2035. Major rivers, urban areas, and planning boundaries are ill.

2.2 Integrated Analysis Process

Based on the fundamental parameters of flood control and drainage infrastructure at the planning stage, and incorporating key geographical attributes such as the construction targets in urban areas and their parcel elevations, this study constructs an integrated flood simulation model. The model is employed to evaluate inundation risk factors under both design rainfall and extreme rainfall scenarios. Flood impact

assessment criteria are established accordingly. Using GIS-based spatial overlay analysis, the flooding risk levels of urban construction targets are identified. Targeted long-term flood risk prevention and response strategies for urban new district development are then proposed. The results provide technical support for improving the flood control and drainage master plan of the Start-up District, enhancing flood resilience, and informing safety-oriented decision-making.

2.3 Hydrology and Hydrodynamic Model

The integrated flood simulation model which is conducted by Infoworks ICM for the Start-up District mainly incorporates hydrological and hydrodynamic processes, including rainfall generation, surface runoff formation, drainage network convergence, and river network routing. A basin-scale integrated urban flood modeling software is employed to construct the model framework and support flood inundation simulations under multiple analytical scenarios. The flood inundation simulation adopts a coupled one-dimensional and two-dimensional hydraulic computation approach. The one-dimensional unsteady flow simulation in rivers is based on the Saint-Venant equations. Model construction primarily involves establishing river cross-sections, hydraulic structures, and their operational rules. The two-dimensional overland flow simulation is based on the shallow water assumption. Under this assumption, the fundamental conservation equations are simplified and solved using grid-based numerical computation. The key components of model construction are illustrated in Figure 2.

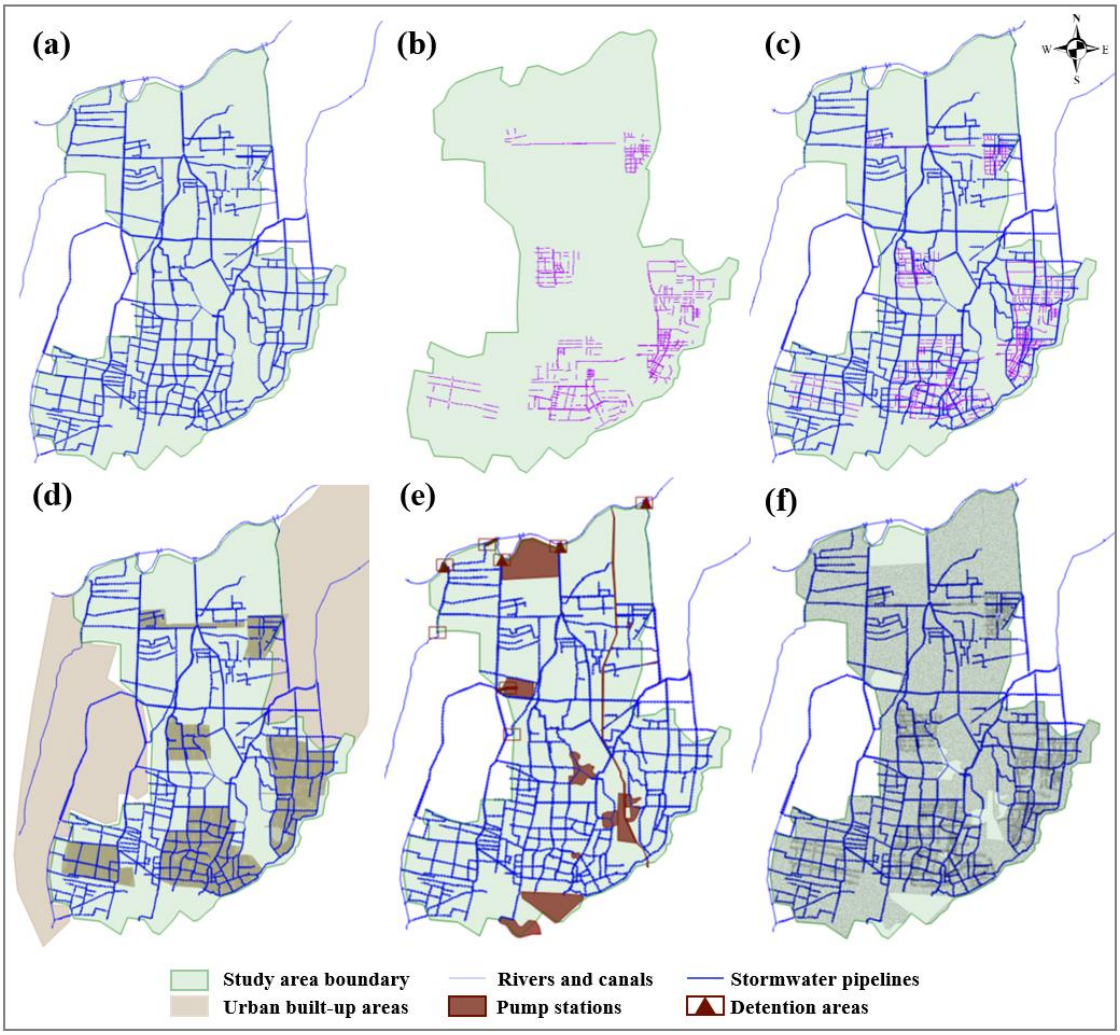

Figure 2. Schematic diagram of key components of hydrology & hydrodynamic model construction ((a) River and canal network, (b) Stormwater pipelines network, (c) Integrated rivers and pipelines, (d) Urban built-up areas, (e) Pump stations & Flooding detention areas, (f) Computational grid)

2.4 Integrated Analysis Scheme

Flood risk is often the result of the superposition of multiple adverse factors, and it is therefore necessary to first clarify the composition of floodwater sources responsible for inundation. This step is essential for identifying the flood-generating mechanisms considered in the risk analysis. According to the actual conditions of the Start-up District, under regional heavy rainfall events, the main flood sources considered in this study include three types: (1) inundation caused by the overtopping of internal trunk drainage rivers due to backwater effects from high water levels in external rivers, representing flood-induced waterlogging; (2) waterlogging caused by insufficient drainage capacity of urban stormwater pipelines due to backwater effects from high water levels in internal trunk rivers, representing capacity-limited waterlogging; (3) waterlogging caused by rainfall accumulation in locally low-lying areas. The computational schemes for different scenario combinations are presented in Table 1.

Table 1. Computational schemes under different scenarios

Scenario Design	Scheme Combination	No.	Rainfall (mm)	Rainfall Return Period (a)	Initial Water Depth (m)
Design Rainfall	Short-duration (3h) combined with high / low inner river water depth	1	85.7	3	0.1, 1.2
		2	98.0	5	0.1, 1.2
		3	114.6	10	0.1, 1.2
		4	131.3	20	0.1, 1.2
	Long-duration (24h) combined with outer river flood control / drainage water depth	5	199.0	20	3.0, 5.0
		6	219.8	30	3.0, 5.0
		7	246.0	50	3.0, 5.0
		8	281.3	100	3.0, 5.0
Extreme Rainfall	Short-duration (1h) combined with low inner river water depth	9	100	50	0.1
	Short-duration (6h) combined with low inner river water depth	10	200	/	0.1
	Long-duration (24h) combined with outer river drainage water depth	11	250	50	3.0
		12	280	100	3.0
		13	350	/	3.0
		14	450	/	3.0
		15	550	/	3.0
		16	650	/	3.0
	Zhengzhou 7·20 Rainstorm (72h)	17	201.9 645.6 789.1	1000	3.0

2.5 Flooding Risk Classification Criteria

Studies by Xu Zongxue and colleagues on human and vehicle vulnerability indicate that the risk of human sliding and falling instability is determined by water depth. When the overturning moment generated by the drag force of flowing water equals the resisting moment produced by the effective body weight, a person will topple. The Guidelines for Flood Risk Mapping provide explicit indicators and standards for flood risk classification. By synthesizing existing academic findings and industry standards, this study classifies flood disaster risk levels based on the maximum inundation depth. Five risk levels are defined, as presented in Table 2.

Table 2 Flooding Risk Level Classification Criteria

Risk Level	Inundation Depth (m)	Impact Severity	Distinguishing Color
No Risk	≤0.15	Minimal impact on production and daily life	White
Low Risk	0.15~0.30	Significant impact on travel	Green

Medium Risk	0.30~0.60	Travel safety for children is threatened	Yellow
High Risk	0.60~1.00	Life safety of minors cannot be guaranteed	Orange
Extremely High Risk	≥1.00	Movement is threatened for everyone	Red

3 RESULT AND DISCUSSION

3.1 Design Rainfall Scenario

(1) Short-duration rainfall

Comparisons between high and low initial inner-river water levels indicate that the differences in the total inundation extent across the Start-up District are negligible. The differences in the total inundated area within the concentrated urban zones are 0 km^2, 0.01 km^2, 0 km^2, and 0.02 km^2, respectively. This demonstrates that, during short-duration rainfall events, the drainage performance of the concentrated urban areas is only weakly influenced by the initial river water level. For short-duration design rainfall events at different return periods, most of the concentrated urban areas fall within the no-risk category, with a small proportion classified as low risk. The proportion of areas with high risk or above (inundation depth $\geqslant$ 0.6 m) is 0.24%, 0.35%, 0.40%, and 0.54%, respectively. These inundated locations are primarily distributed in locally low-lying zones. The results indicate that, by 2035, the planned stormwater drainage network will significantly enhance the drainage capacity of urban areas.

(2) Long-duration rainfall

Different combinations of the initial drainage and flood-control water levels of external rivers are employed to comprehensively evaluate the potential inundation-prone areas, inundation severity, and the accumulation and recession processes of floodwater under various design frequencies. Under low external river water levels, when the concentrated urban areas encounter 20-, 30-, 50-, and 100-year return period design rainstorms, the total inundated areas (water depth > 0.15 m) are 5.33 km^2, 5.97 km^2, 6.80 km^2, and 8.15 km^2, accounting for 4.38%, 4.91%, 5.59%, and 6.70% of their respective areas. In the non-concentrated urban areas, the corresponding inundated areas are 77.84 km^2, 83.53 km^2, 90.73 km^2, and 98.92 km^2, representing 20.69%, 22.28%, 24.42%, and 26.92% of their total extents. Under high external river water levels, when the concentrated urban areas experience 20-, 30-, 50-, and 100-year return period design rainstorms, the total inundated areas are 5.34 km^2, 6.02 km^2, 6.91 km^2, and 8.31 km^2, accounting for 4.38%, 4.91%, 5.59%, and 6.70% of their areas. In the non-concentrated urban areas, the corresponding inundated areas are 81.57 km^2, 87.86 km^2, 96.30 km^2, and 106.17 km^2, representing 19.74%, 21.18%, 23.01%, and 25.08% of their extents. These results indicate that, by 2035, owing to the planned river widening, dredging, and water system connectivity projects, the river water level hydrographs under long-duration rainfall events exhibit limited variation. The trunk rivers are capable of maintaining effective drainage performance. However, downstream areas remain affected by backwater effects from the Tuhai River.

3.2 Extreme Rainfall Scenario

(1) 24-hours Extreme Rainstorm

Taking the 250 mm rainfall event as an example, the total inundated area reaches 99.99 km^2, accounting for 19.38% of the district. The inundated area within the concentrated urban zones is 7.01 km^2, representing 5.76% of their total area. Compared with the 6-hour 200 mm rainfall scenario, the inundation extent in the concentrated urban zones is slightly reduced. Only a very small number of medium- to high-risk areas (inundation depth > 0.3 m) are observed. This indicates that, although the total rainfall amount increases, its temporal concentration decreases. Meanwhile, the planned drainage network operates over a longer discharge duration, resulting in a reduced inundation extent.

(2) Zhengzhou 7 • 20 Rainstorm

The total inundated area reaches 243.4 km², accounting for 47.2% of the Start-up District. Within the concentrated urban zones, the inundated area accounts for 25.45% of their total extent. Areas classified as high risk or above constitute 9.08% of the concentrated urban zones. Regarding urban waterlogging, the peak rainfall of the Zhengzhou “7 • 20” event occurred at 17:00 on July 20, with a maximum single-station intensity of 201.9 mm/h. After the peak, rainfall persisted until 12:00 on July 21. When this event is transposed to the Start-up District for simulation, the peak inundation depths in the concentrated urban zones mostly occur between 21:00 on July 20 and 06:00 on July 21, corresponding to 2-11 hours after the rainfall peak. Urban waterlogging is primarily caused by overtopping of secondary rivers and surcharging of stormwater pipelines. In terms of river drainage, the water level hydrographs at representative cross-sections exhibit a pattern of rapid rising and slow recession. By 2035, although the river drainage capacity will be enhanced, overtopping still occurs, indicating that the Zhengzhou “7 • 20 ” rainstorm exceeds the planned design standards.

3.3 Flooding Risk Impact Assessment

Based on the attribute information of planned urban spatial elements in the Start-up District, this study focuses on two categories of objects: urban lifeline infrastructures and key flood-protection targets. A total of 150 urban lifeline infrastructure objects and 665 key flood-protection objects are involved. By integrating the model-derived inundation risk results, flood risk hotspots for different urban objects under various rainfall scenarios are identified. The flooding impacts on representative objects, including power infrastructure and primary and secondary schools, are illustrated in Figure 3.

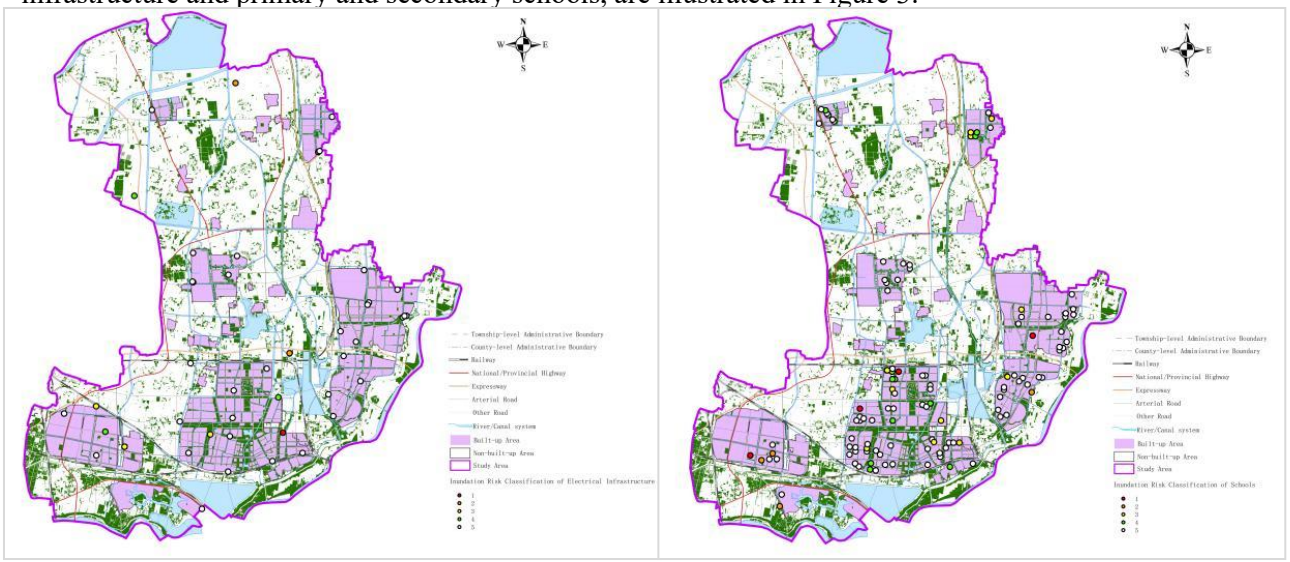

Figure 3. Illustration of flood impacts on planned power infrastructure and primary & secondary schools

4 CONCLUSION

Based on the 2035 urban development layout and the flood control and drainage construction tasks of the Jinan Start-up District, this study proposes a planning-level coupled flood simulation framework. The framework is applied to analyze flood inundation risks under both design rainfall and extreme rainfall scenarios, and refined assessments of inundation risk impacts are conducted. The main conclusions are summarized as follows.1) Under short-duration design rainstorms, the inundation extent within concentrated urban zones shows negligible differences under different initial river water levels, and urban waterlogging is primarily controlled by the intake capacity of the stormwater drainage network. 2) Under long-duration design rainstorms, the overall drainage performance generally meets the 50-year return period design standard. The inundation extent within concentrated urban zones increases with rainfall magnitude, while being only weakly affected by the backwater effects of external rivers. 3) Under the Zhengzhou “7 • 20” extreme rainstorm scenario, the inundation extent in the Start-up District becomes

extensive. The rainfall amount is approximately 2.6 times that of the 50-year design rainfall, far exceeding the response capacity of the planned 2035 flood control and drainage system of the Start-up District. Future research should prioritize optimizing the spatial layout of planned engineering measures, exploring the potential of coordinated flood control operations at both watershed and regional scales, and strengthening flood emergency management measures.

5 ACKNOWLEDGEMENTS

This work was jointly funded by the Basic Research Foundation of Central-Level Research Institutions (No. Y125001), the Frontier Science and Technology Special Program of Guangxi (No. AA23062053), the Water Science and Technology Program of Jiangsu (No. 2021001; No. 2021048) and the National Natural Science Foundation of China (No. 51709178).

REFERENCES

Ahmad S S. Simonovic P S. (2013). Spatial and temporal analysis of urban flood risk assessment. Urban Water Journal, 10(1), 26 – 49.

Zhang J Y. Song X M. He R M. (2025). Thoughts on urban flood disaster prevention and control in large cities in the new era. China Water Resources, (17), 15 – 21. (in Chinese)

Ma S Q. Lyu S R. Zhang Y D. et al. (2021). Weighted clustering-based risk assessment on urban rainstorm and flood disaster. Urban Climate, 39(9), 100974.

Yang F. Li X D. Song L X. et al. (2025). Risk assessment methodology for rainstorm induced ur ban flood disaster chain. Water Resources Protection, 41(05), 52 – 60. (in Chinese)

Hou J M. Wang T. Li D L. et al. (2025). Efficient simulation and prediction method for extreme rainfall-induced flooding processes in ultralarge cities. China Water Resources, (18), 19 – 28. (in Chinese)

Ming X, Liang Q, Xia X, et al. (2020). Real‐time flood forecasting based on a high performance 2D hydrodynamic model and numerical weather predictions. Water resources research, 56(7), e2019WR025583.

Lin L, Tang C Q, Liang Q H, et al. (2023). Rapid urban flood risk mapping for data-scarce environments using social sensing and region-stable deep neural network. Journal of Hydrology, 617.

Chen A S. Evans B. Djordjevics. et al. (2012). A coarse-grid approach to representing building blockage effects in 2D urban flood modelling. Journal of Hydrology, (426), 1 – 16.

Lu X C. Xu Z X. Li Y K. et al. (2024). Assessment on dynamic risk of urban flooding and waterlogging disaster based on multi-agent models. Water Resources Protection, 40(04), 36 – 47. (in Chinese)

Dazzi S. (2024). Physics-Informed Neural Networks for the Augmented System of Shallow Water Equations With Topography. Water Resources Research, 60(10), 036589.

Romana. Berariu. Christian. et al. (2015). Understanding the impact of cascade effects of natural disasters on disaster relief operations. International Journal of Disaster Risk Reduction, 12, 350 – 356.

Yang C C. Yeh C H. (2014). Application of system dynamics in environmental risk management of project management for external stakeholders. Systemic Practice and Action Research, 27(3), 211 – 225.

Li G Y. Liu J H. Shao W W. et al. (2023). Research Progress in Flood Disaster Risk Assessment and Zoning. Journal of China Hydrology, 43(04), 15 – 20. (in Chinese)

Konapala G. Mishra A K. Wada Y. et al. (2020). Climate change will affect global water availability through compounding changes in seasonal precipitation and evaporation. Nature Communications, 11(1), 30 – 44.

ICFM 10
Adapting to Global Change:
Innovative Approaches to Flood Management and Resilience
May 20-22, 2026 | Western University, London, Ontario, Canada

Sensitivity-Driven Log-Linear Modelling of Time-to-Peak for Enhanced Flood Forecasting in Heterogeneous Canadian Catchments

Vinay Kumar Chukka[1] and Tirupati Bolisetti[2]
Department of Civil and Environmental Engineering, University of Windsor, Windsor, Ontario, Canada[1]
E-mail: vinaykumarchukka05@gmail.com

Department of Civil and Environmental Engineering, University of Windsor, Windsor, Ontario, Canada[2]
E-mail: tirupati@uwindsor.ca

ABSTRACT

Accurate estimation of the time-to-peak (T_p) of a synthetic unit hydrograph (SUH) is essential for flood routing, urban drainage design, and real-time hydrological forecasting. Classical SUH approaches, such as Snyder and Taylor-Schwarz (TS), primarily rely on watershed geomorphology and neglect rainfall variability and catchment-specific heterogeneity. This limitation can lead to large prediction errors under diverse hydrological conditions, particularly in rapidly urbanizing or variable-slope catchments. This study develops and evaluates a data-driven empirical model for T_p that explicitly integrates catchment characteristics (main channel length (L), centroidal length (L_c), slope (S), roughness (n), and imperviousness (U)) and event-specific inputs (storm duration (D) and intensity (I)). A dataset of 69 rainfall-runoff events from seven Canadian catchments was compiled and analyzed to derive a multi-parameter formulation using least squares nonlinear regression. Model sensitivity was assessed using perturbation and exponent-based elasticity analyses to quantify the influence of geomorphic and rainfall parameters. The proposed model achieved strong predictive capability (Calibration: $R^2 = 0.745$, NSE = 0.742; Validation: $R^2 = 0.876$, NSE = 0.85) and demonstrated balanced performance for a wide range of catchment scales and land-use conditions. In contrast, Snyder's method showed moderate correlation but poor efficiency ($R^2 = 0.4$, NSE = -0.98), while the TS model exhibited extremely weak predictive skill ($R^2 = 0.024$, NSE = -24.215), often overestimating T_p by more than 100-500%. Sensitivity analysis revealed that channel roughness and storm duration exert the strongest influence on T_p, whereas rainfall intensity has a relatively weak impact. The findings confirm that coupling geomorphic indices with rainfall event properties yields substantially improved T_p estimation for SUH applications. The proposed model provides a robust tool for flood forecasting and urban drainage planning, particularly in data-rich regions where traditional SUH methods are insufficient. This enhanced responsiveness makes the model directly applicable to real-time flood-forecasting frameworks.

KEYWORDS: Synthetic Unit Hydrograph; Time-to-Peak; Parameter Estimation, Log-Linear Optimization, Local One-at-a-Time (OAT) Sensitivity Analysis, Snyder's Time-to-Peak, Flood Forecasting.

1 INTRODUCTION

The reliable prediction of hydrological response to rainfall remains fundamental to flood estimation, stormwater design, reservoir operation, and real-time flood forecasting. One of the most enduring methods used for this purpose is the synthetic unit hydrograph (SUH), a conceptual representation of runoff produced by a unit depth of effective rainfall over a watershed. Among its parameters, the time-to-peak (T_p) is particularly crucial because it governs peak discharge timing, affects flood routing, and dictates infrastructure design capacity. Despite recent advancements in physically distributed and high-resolution modelling frameworks, SUH remains widely practiced due to its simplicity, low data demand, and adaptability to ungauged conditions (Sarangi et al., 2006). However, classical SUH derivations such as Snyder's method, developed in the 1930s, rely almost entirely on watershed geomorphology and do not account for rainfall dynamics or catchment heterogeneity (Paquet, 2019). This neglect has been questioned in modern hydrology, especially at a time when rapid urbanization and erratic climate-driven precipitation patterns strongly influence watershed response, as discussed by Acanal (2021). Snyder's method assumes that T_p can be expressed using empirical constants that represent basin shape and response time; however, several studies indicate that regional calibration limits its applicability beyond the region in which its constants were developed. In particular, regions experiencing increased imperviousness, land-use shifts, and nonlinear rainfall intensities tend to show hydrograph responses that diverge significantly from Snyder-based predictions (Bhunya et al., 2007; Chothe & Devappa, 2023). Although the Taylor-Schwarz (TS) model attempted to integrate geomorphology more explicitly into hydrograph prediction, it remained rooted in the assumption that channel networks alone dictate response time, disregarding rainfall variability, infiltration, storage, and storm characteristics. In contemporary studies, the TS model has repeatedly been shown to substantially overpredict T_p, especially in small, steep, or urban-influenced watersheds, causing errors that can reach several hundred percent (Tunas et al., 2017; Zhu et al., 2025). As climate variability increases short-duration intense storms, hydrologists have emphasized that relying solely on morphometric parameters is increasingly inadequate. A growing body of research supports integrating rainfall intensity, storm duration, and anthropogenic modifications such as imperviousness into empirical hydrograph models to enhance predictive performance (Adib et al., 2019; Ewea et al., 2016). With improvements in rainfall measurement networks, high-resolution geospatial data, and computational analytics, data-driven hydrology has emerged as a bridge between classical empirical approaches and modern physically-based modelling. Unlike purely machine-learning hydrographs, which often lack physical interpretability and are difficult to standardize into engineering practice, hybrid empirical models can combine statistical calibration with mechanistic understanding (Ajami et al., 2016; Singh, 2019). Notwithstanding these advancements, most existing data-driven SUH studies remain limited by small sample sizes, omission of key rainfall variables, weak sensitivity evaluation, or excessive regionalization that restricts broader application (Ghorbani et al., 2019). Moreover, the influence of urban imperviousness and channel roughness, two parameters known to significantly alter runoff concentration time, remains largely underexplored in SUH formulations (Chothe & Devappa, 2023). The absence of these parameters in conventional models leads to systematic biases, particularly for contemporary basins that are no longer purely natural systems. As cities continue to expand and rainfall intensities become more erratic, the need for a transferable, physically interpretable, and data-driven SUH T_p formulation becomes increasingly evident.

The research presented in this paper aims to fill this research gap by developing a multi-parameter empirical model that integrates both morphometric and rainfall-dependent variables to

estimate T_p. Based on data collected from seven diverse Canadian watersheds, the model employs nonlinear regression to relate T_p with the main channel length (L), centroidal length (L_c), slope (S), surface roughness (n), fractional imperviousness (U), storm duration (D), and rainfall intensity (I). Unlike classical SUH models that treat hydrographs as physiographic products, this model considers runoff as a dynamic outcome of both landscape structure and storm forcing. The inclusion of dual sensitivity diagnostics, consisting of perturbation-based and elasticity-based analyses, enhances transparency by quantifying relative contributions of each parameter. In order to maintain physical consistency and interpretability of the model, we introduce two sensitivity diagnostics that can assess the effect of each parameter using perturbation-based and elasticity-based approaches. In general, the proposed formulation is conceived to be a physically based and more flexible alternative compared with traditional SUH methods for advancing stormwater design, flood-risk assessment, and infrastructure planning in the face of evolving land-use and climate patterns. Although the primary contribution of this research lies in advancing the empirical estimation of T_p, the implications extend far beyond hydrograph characterization. Time-to-peak is a foundational predictor for short-term flood forecasting because it governs the lead time available for emergency response, real-time reservoir regulation, and anticipatory operation of stormwater infrastructure. By explicitly incorporating the parameters L, L_c, S, n, U, D, and I, the proposed model produces T_p estimates that are dynamically responsive to event-scale hydrometeorological forcing.

2 TEST CATCHMENTS AND DATA

The analysis was carried out using seven contrasting watersheds across Canada (refer to Figure 1), representing a wide range of hydrogeomorphic and land-use conditions, from predominantly natural basins to highly urbanized systems. Geomorphic attributes were extracted through a GIS-based watershed delineation workflow using high-resolution DEMs, from which drainage boundaries, L, and L_c were determined using flow direction and accumulation algorithms.

National Geographic, Esri, Garmin, HERE, UNEP-WCMC, USGS, NASA, ESA, METI, NRCAN, GEBCO, NOAA, increment P Corp.

Figure1: Location of the seven study catchments.

Slope (S) was calculated as an area-weighted average of local slopes derived from the DEM, while n was assigned using land-cover classifications that translated surface characteristics into Manning's coefficients. Fractional imperviousness (U) was quantified as the ratio of paved and built-up area to total watershed area, obtained from land-use data and validated through high-resolution imagery (see Table 1).

Table 1 Watershed characteristics of the seven Canadian catchments used for T_p model evaluation.

Catchment	L (Km)	Lc (Km)	S (m/m)	n	U (0-1)
A	22.87	12.48	0.00025	0.13	0.16
B	9.64	4.97	0.00025	0.17	0.31
C	26.58	10.79	0.00083	0.13	0.42
D	6.04	4.22	0.00035	0.10	0.61
E	13.25	12.82	0.00347	0.11	0.39
F	10.68	5.78	0.00290	0.19	0.21
G	16.59	11.09	0.00240	0.25	0.12

The selected watersheds display substantial variability in geomorphic and surface properties. Catchments A and C contain long natural channels; Catchment B has short and steep flow paths;

Catchments D and E exhibit urban drainage influence; Catchment F reflects mixed agricultural and natural characteristics; and Catchment G combines moderate imperviousness with steeper slopes. This diversity in L, Lc, S, n, and U provides a robust basis for evaluating T_p generation under varying runoff conditions. The compiled geospatial database and delineated drainage maps, therefore, supply the necessary physical descriptors to support empirical model development for T_p estimation.

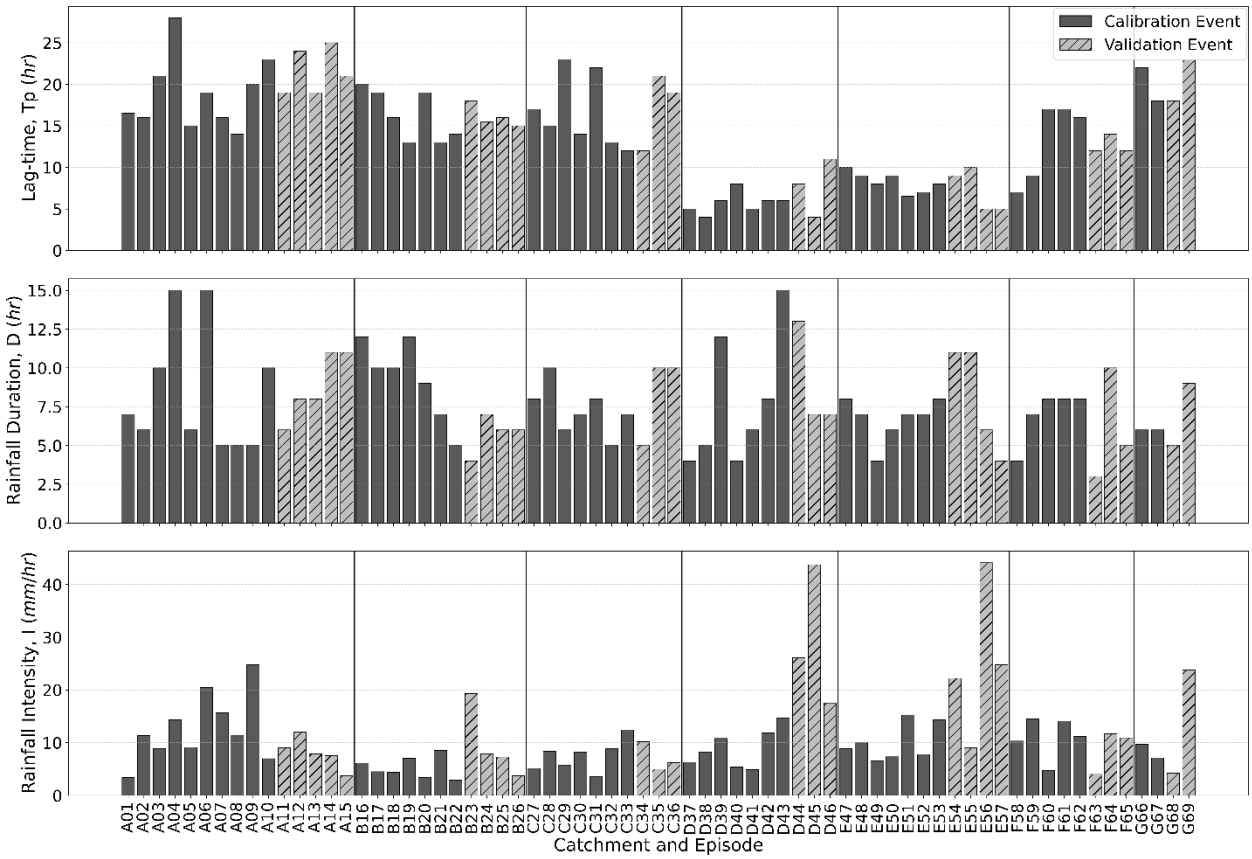

Figure 2: Rainfall-runoff event characteristics (T_p, D, I)

A total of 69 rainfall-runoff events were extracted from hydrographs for the seven study watersheds as shown in Figure 2, representing a wide range of storm characteristics from short-duration convective bursts to medium- and long-duration stratiform systems. Rainfall data were obtained from the NASA POWER website, from which mean rainfall intensity (I) and storm duration (D) were derived after aggregating sub-hourly records to the event scale. To ensure physical consistency, only events exhibiting a single, distinct hydrograph peak were retained, and each event was screened to avoid periods with antecedent or trailing rainfall, thereby isolating runoff response to a single storm without carryover effects. Additional quality checks included exclusion of snowmelt-driven events, verification against backwater or storage impacts, and cross-validation of cumulative rainfall depths with station totals. This rigorous filtering ensured that extracted T_p values reflect direct rainfall-driven hydrologic response, yielding a reliable dataset for empirical model calibration and sensitivity analysis.

3 TRADITIONAL SUH METHODS

3.1 Snyder's Method

Snyder proposed one of the earliest SUH methods, in which the T_p is estimated using basin geomorphology (Snyder, 1935). The relationship assumes that runoff travel time increases with stream length and basin shape and is calibrated using a regional coefficient C_t (see Eqs. 1) that reflects watershed characteristics such as slope, storage, and channel configuration. The simplified formulation is:

$$T_p = C_t(LL_c)^{0.3} \tag{1}$$

where C_t is a nondimensional constant and in general varies from 1.8 to 2.2, L is the length of the main channel, and L_c is the distance between the centroid of the catchment and the outlet.

3.2 Taylor and Schwarz (TS) Model

The TS model (Taylor & Schwarz, 1952) is another classical synthetic hydrograph method built on geomorphic controls, but unlike Snyder's formulation, it emphasizes the structure of the drainage network. The method assumes that the basin response time is primarily governed by the channel system and expresses the T_p as a function of L and S, accounting for regional channel geometry. The simplified expression is:

$$S_e = [\frac{N}{\sum_{i=1}^{N}\left(\frac{1}{S_i}\right)^{0.5}}]^2 \tag{2}$$

$$T_p = (\frac{0.6}{S_e{}^{0.5}})e^{(m_1 D)} \tag{3}$$

$$m_1 = 0.212(LL_c)^{-0.36} \tag{4}$$

where S_e is the average slope of the main channel, S_i is the slope of the i^{th} reach of the main channel, and N is the total number of reaches. In Eqs. (3) - (4), T_p, L, and L_c are the same as Snyder's method, for D-hour rainfall in Unit Hydrograph duration.

4 PARAMETERS AND DEVELOPMENT OF THE PROPOSED MODEL

4.1 Model Parameters

Parameter selection was guided by the need to represent both the physical structure of the watershed and the variability of individual rainfall events in a hydrologically meaningful way. Four geomorphic descriptors were incorporated as determinants of flow routing and travel time: L, L_c, S, and n. These descriptors together characterize the spatial distribution of the drainage network and

the resistance offered by catchment surfaces, thereby influencing the velocity and timing of runoff concentration. Basin imperviousness (*U*) was introduced as a surface characteristic reflecting the degree of land sealing, which affects infiltration reduction, storage loss, and acceleration of overland flow generation, particularly in urbanizing watersheds.

To represent storm-driven variability, two event-based parameters were included: *D* and *I*. These rainfall descriptors capture the persistence and volume-loading rate of precipitation, which determine excess rainfall availability and the buildup of runoff over the catchment. The response variable, T_p, expressed in hours, was manually extracted from observed hydrographs by identifying the elapsed time between the onset of effective rainfall and the peak of direct runoff. To estimate T_p using combined watershed and storm controls, a nonlinear empirical model was developed as shown in Eqs. (6).

$$T_p = f(L, L_c, S, n, U, D, I) \tag{5}$$

$$T_p = K(LL_c)^{\delta} S^{\alpha} n^{\beta} U^{\gamma} D^{\phi} I^{\eta} \tag{6}$$

Where T_p is lag-time (*hr*), *L* is main channel length (*km*), L_c is centroidal channel length (*km*), *S* is basin slope, *n* is Manning's roughness coefficient (-), *U* is fractional imperviousness (0-1), *D* is rainfall duration (*hr*), *I* is mean rainfall intensity (*mm/hr*) and $(K, \delta, \alpha, \beta, \gamma, \phi, \eta)$ are empirical coefficients or exponents.

The combined use of geomorphic, land-surface, and rainfall characteristics allows for a physically interpretable representation of watershed response while maintaining sensitivity to event-specific forcing. Collectively, these eight variables provide a robust foundation for developing a transferable empirical formulation for T_p that can account for hydrologic variability across diverse catchment types and storm conditions.

4.2 Model Development

The empirical model for estimating T_p was formulated using a nonlinear multiplicative structure to preserve hydrologic interpretability and reflect the scaling behaviour inherent in watershed response. A power-law representation was selected to relate T_p to geomorphic attributes, land-surface characteristics, and storm controls as shown in Eqs. (6). The formulation consists of a dimensionless constant and elasticity-type exponents associated with model parameters

presented in subchapter 4.1. The nonlinear least-squares optimization was conducted, minimizing squared deviations between observed and simulated T_p while retaining physically meaningful exponent signs to avoid unrealistic influences on routing time.

To avoid model overfitting and evaluate predictive transferability, the dataset of 69 rainfall-runoff events was split into calibration (70%) and validation (30%) subsets for each catchment (as shown in Figure 2). The first subset was used to optimize the empirical coefficients, and the resulting calibrated model was then applied to the remaining events without further adjustment. Predictive skill was assessed through the coefficient of determination (R^2) and Nash–Sutcliffe Efficiency (NSE), ensuring that both correlation strength and magnitude-based agreement were quantified.

To examine the influence of individual predictors and validate the physical plausibility of calibrated exponents, a Local one-at-a-time (OAT) sensitivity assessment was performed. Perturbation diagnostics quantified the change in T_p under ±10% variations in each input, while log-elasticity inspection exploited the exponent structure of the power-law form to interpret proportional response sensitivities. Together, these diagnostics provided a consistent sensitivity hierarchy and confirmed that the calibrated model responds to contour length, roughness, storm duration, and imperviousness in agreement with expected hydrological behaviour.

5 RESULTS AND DISCUSSION

After nonlinear optimization, the regression procedure yielded the calibrated coefficients for both catchment-scale and rainfall-driven parameters, which are presented in Eqs. (7).

$$T_p = 7.16(LL_c)^{0.311} S^{-0.169} n^{1.205} U^{0.04} D^{0.246} I^{-0.08} \quad (7)$$

5.1 Performance of Proposed Model

The proposed empirical formulation demonstrated strong predictive capability across both calibration and validation datasets. During calibration, the model achieved $R^2 = 0.745$ and NSE $= 0.742$, indicating that the simulated T_p closely reproduced the observed temporal patterns without structural bias. Validation confirmed even higher skill, yielding $R^2 = 0.876$ and NSE $= 0.85$, showing that the optimized coefficients generalized well to independent events without recalibration, as shown in Figure 3.

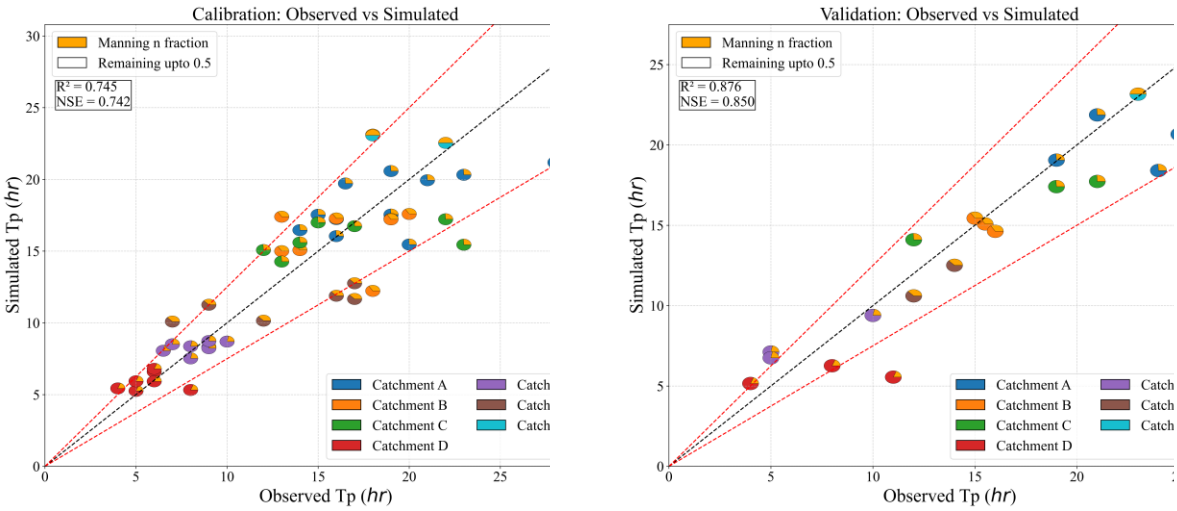

Figure 3: Observed vs simulated T_p for calibration and validation datasets.

Observed versus modeled scatter plots clustered tightly around the 1:1 line, and a majority of points fell within the ±25% acceptance bounds, demonstrating stability across a wide range of watershed sizes and storm conditions. Error statistics further support the robustness of the proposed formulation. In calibration, the percent error ranged between 0.28% and 44.13%, with a mean absolute error of ≈17.2%.

Validation showed even smaller deviations, which ranged from 0.29% up to 49.52%, with a lower average of about 14.4% (refer to Figure 3). The largest discrepancies were concentrated in small, rapid-response systems (e.g., Catchment D), where even minute uncertainties in rainfall onset, sensor latency, or temporal aggregation disproportionately distort hydrograph rise and peak timing. Runoff translation in these basins is dominated by super-concentrated travel times, low levels of surface storage and channel attenuation, resulting in an abrupt change to the T_p with relatively small changes to storm duration or intensity. Consequently, the model's continuous empirical scaling, although robust for moderate and large basins, becomes more sensitive in these highly reactive hydrologic regimes, where T_p exhibits threshold-like behavior rather than gradual scaling. In these rapid-response systems, model bias remained lower than benchmark methods, highlighting improved temporal accuracy in routing estimation.

5.2 Comparison with Standard Models

For benchmarking, the proposed formulation was compared against Snyder's and the TS model,

both of which rely solely on geomorphologic scaling and omit rainfall and land-surface variability. Each model was executed using the same input dataset, allowing differences in performance to be attributed solely to structural modelling assumptions rather than data inconsistency. Evaluation metrics included R^2, NSE, and relative T_p prediction error, thus quantifying both bias and statistical fidelity.

To evaluate the limits of the Snyder method, a "Land-Use Adapted" approach was also tested, wherein the C_t coefficient was step-wise reduced from 2.0 to 1.1 based on catchment imperviousness. Despite this adaptive parameterization intended to capture urban flow acceleration, the method yielded an NSE of -0.98, confirming that coefficient calibration alone cannot compensate for the omission of rainfall dynamics. Benchmark comparisons against Snyder's and TS models showed substantial performance limitations in classical SUH formulations. Snyder's method produced $R^2 = 0.4$, whereas the TS model performed even worse, with $R^2 = 0.024$ and NSE $= -24.21$. These negative NSE values indicate that both traditional models predict T_p less accurately than the mean of observed values, signifying strong systematic bias. Snyder's approach is primarily based on watershed geometry, which results in approximately the invariant T_p predictions; the points are projected onto a single line (see Figure 4). On the other hand, the TS method is considered more dynamic as well as diverse rainfall and consequently shows an even greater scatter with higher deviation when different rainfall inputs are used for different events.

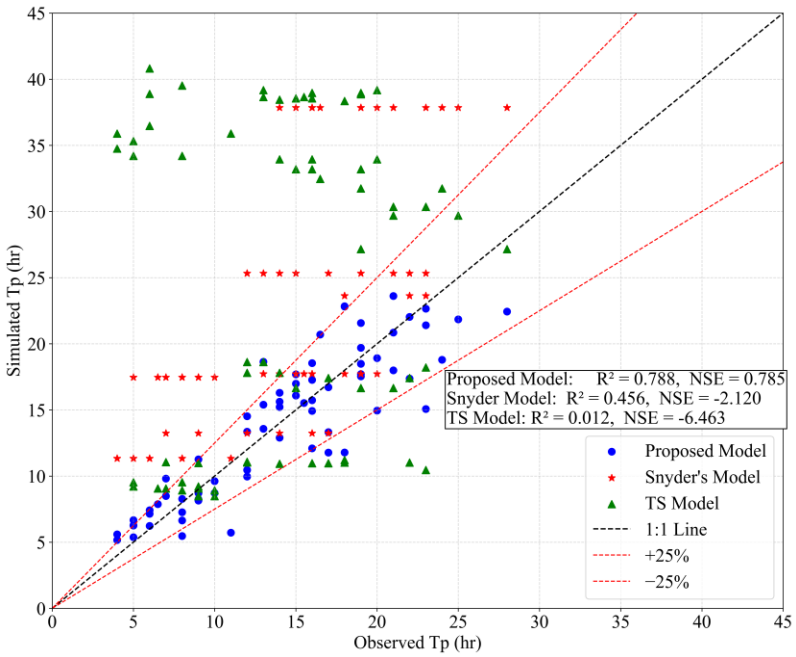

Figure 4: Performance comparison of the proposed T_p model with standard prediction models against observations.

Across all catchments, Snyder's and TS formulations consistently overestimated T_p values, frequently by **100-500%**, particularly in highly impervious or fast-draining basins. For example, Catchment D (urbanized channelized basin), which has observed T_p values of 4-11 hours, was predicted to be 11-40 hours by benchmark models. This overestimation stems from an exclusive reliance on geomorphology-based scaling, without accounting for the rapid storm-runoff acceleration caused by urban surfaces, rainfall duration, or direct channel roughness effects. The results clearly indicate that traditional SUH methods are insufficient for contemporary stormwater-dominated landscapes where precipitation dynamics and land-use alterations significantly alter hydrograph response.

5.3 Sensitivity Analysis Findings

Sensitivity diagnostics indicate that T_p is controlled predominantly by n, with D and L exerting secondary influence, whereas U, S, and I display comparatively minor effects. The primacy of n reflects its role in hydraulic retardation and momentum dissipation, elongating travel time even under small perturbations, while D governs temporal runoff accumulation, aligning peak timing with rainfall persistence rather than intensity. Incremental increases in U accelerate hydrograph response by reducing infiltration losses, whereas the weak sensitivity of I confirms that peak timing is a routing-dominated process rather than an intensity-driven phenomenon.

Accordingly, calibration and validation scatterplots were rendered with pie-fractional markers (0-0.5 range) to explicitly encode the spatial variability of n (see Figure 3), emphasizing its disproportionate leverage in controlling hydrograph timing. These findings affirm that urban flood timing is governed primarily by frictional impedance and storm persistence, highlighting the inadequacy of classical SUH models that ignore these controls and consequently distort peak discharge estimation in stormwater design (refer to Figure 5).

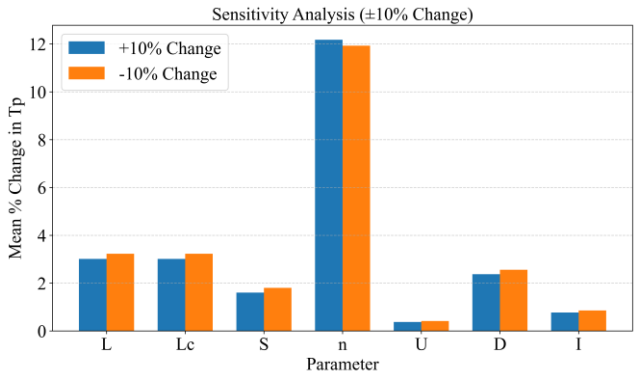

Figure 5: Sensitivity of T_p to ±10% perturbations in model parameters.

5.4 Application of the Proposed Model to Flood Forecasting

The proposed T_p formulation provides immediate value for flood-forecasting systems by enabling rapid, event-responsive estimation of hydrograph timing. Unlike traditional SUH parameters that assume static watershed behavior, the model incorporates rainfall persistence, U, and n, allowing T_p predictions to adjust dynamically to evolving storm characteristics. Its elasticity-based structure enables forecasters to infer how changes in D or watershed conditions will shift T_p, supporting proactive reservoir operation and urban drainage management.

Because the model captures travel-time compression in highly impervious or fast-responding basins, it delivers more realistic T_p than classical SUH methods, especially during short, intense events. When coupled with radar rainfall or ensemble precipitation forecasts, it can generate continuously updated T_p estimates suitable for real-time decision-support tools and early-warning platforms. Thus, beyond enhancing SUH parameterization, the model functions as a computationally efficient component for operational flood forecasting in rapidly changing and urbanized watersheds.

6 CONCLUSIONS

This investigation demonstrates that T_p estimation in Canadian watersheds cannot be credibly represented using traditional geomorpho-centric SUH formulations that disregard rainfall controls and land-surface heterogeneity. The proposed nonlinear, multi-parameter T_p model, calibrated across seven hydroclimatically contrasting basins, substantially outperforms canonical approaches (e.g., Snyder; TS), which exhibited systematic bias and overprediction stemming from their exclusion of storm persistence and imperviousness. The newly derived exponent structure and sensitivity hierarchy reveal that routing resistance, particularly manifest through n, is the paramount regulator of hydrograph temporal translation, while D and L impose secondary constraints, thereby confirming that fluvial impedance and rainfall temporal load supersede instantaneous rainfall rate in peak-timing control. By integrating geomorphic resistance, storm structure, and anthropogenic surface alteration into a single transferable formulation, this model delivers a physically interpretable and computationally efficient tool adaptable to evolving Canadian hydroscapes under urbanization and climatic intensification. Consequently, the model enables superior prediction of hydrograph lag, reduces structural underdesign risks, and provides a defensible basis for flood-routing design, low-impact drainage planning, and real-time peak-flow forecasting within a broad spectrum of Canadian watershed typologies. By providing a dynamically responsive and computationally lightweight formulation for T_p, the model is readily deployable within early-warning systems, real-time hydrograph generation modules, and event-based flood-forecasting platforms where accurate T_p prediction is indispensable.

REFERENCES

Acanal, N. (2021). Snyder-gamma synthetic unit hydrograph. *Arabian Journal of Geosciences*, *14*(4), 271-. https://doi.org/10.1007/S12517-021-06531-7

Adib, A., Lotfirad, M., & Haghighi, A. (2019). Using uncertainty and sensitivity analysis for finding the best rainfall-runoff model in mountainous watersheds (Case study: the Navrood watershed in Iran). *Journal of Mountain Science*, *16*(3), 529–541. https://doi.org/10.1007/S11629-018-5010-6

Ajami, H., Khan, U., Tuteja, N. K., & Sharma, A. (2016). Development of a computationally efficient semi-distributed hydrologic modeling application for soil moisture, lateral flow and runoff simulation. *Environmental Modelling & Software*, *85*, 319–331. https://doi.org/10.1016/J.ENVSOFT.2016.09.002

Bhunya, P. K., Berndtsson, R., Ojha, C. S. P., & Mishra, S. K. (2007). Suitability of Gamma, Chi-square, Weibull, and Beta distributions as synthetic unit hydrographs. *Journal of Hydrology*, *334*(1–2), 28–38. https://doi.org/10.1016/J.JHYDROL.2006.09.022

Chothe, O. K., & Devappa, V. (2023). Synthetic unit hydrograph for ungauged basin using Synder, Taylor- Schwarz model, SCS method by GIS techniques. *Materials Today: Proceedings*, *77*, 855–859. https://doi.org/10.1016/J.MATPR.2022.11.505

Ewea, H. A., Elfeki, A. M. M., Bahrawi, J. A., & Al-Amri, N. S. (2016). Sensitivity analysis of runoff hydrographs due to temporal rainfall patterns in Makkah Al-Mukkramah region, Saudi Arabia. *Arabian Journal of Geosciences*, *9*(5), 424-. https://doi.org/10.1007/S12517-016-2443-5

Gede Tunas, I., Anwar, N., & Lasminto, U. (2017). Parameters Estimation of Synthetic Unit Hydrograph Model Using Multiple Linear and Non-linear Regressions. *2nd International Conference on Applied Mathematics*.

Ghorbani, K., Salarijazi, M., Abdolhosseini, M., Eslamian, S., & Ahmadianfar, I. (2019). Evaluation of Clark IUH in rainfall-runoff modelling (case study: Amameh Basin). *International Journal of Hydrology Science and Technology*, *9*(2), 137–153. https://doi.org/10.1504/IJHST.2019.098131

Paquet, E. (2019). Synthetic hydrograph generation by hydrological donors. *Hydrological Sciences Journal*, *64*(5), 570–586. https://doi.org/10.1080/02626667.2019.1593418

Sarangi, A., Madramootoo, C. A., Enright, P., & Prasher, S. O. (2006). Evaluation of three unit hydrograph models to predict the surface runoff from a Canadian watershed. *Water Resources Management*, *21*(7), 1127–1143. https://doi.org/10.1007/S11269-006-9072-9

Singh, S. K. (2019). Dynamic parameter estimation for hydrological model. *International Journal of Hydrology Science and Technology*, *9*(2), 124–136. https://doi.org/10.1504/IJHST.2019.098159

Snyder, F. F. (1935). Synthetic Unit Hydrograph. *Trans Am Geophysical Union*, *19*, 447–454.

Taylor, A. B., & Schwarz, H. E. (1952). Unit hydrograph lag and peak flow related to basin characteristics. *Trans Am Geophys Union*, *33*, 235–246.

Zhu, W., Ianculescu, D., & Anghel, C. G. (2025). Synthetic Hydrograph Estimation for Ungauged Basins: Exploring the Role of Statistical Distributions. *Stats*, *8*(4), 100. https://doi.org/10.3390/STATS8040100

Websites:
Web-1: https://power.larc.nasa.gov/
Web-1: https://wateroffice.ec.gc.ca/mainmenu/real_time_data_index_e.html

ICFM 10
Adapting to Global Change:
Innovative Approaches to Flood Management and Resilience
May 20-22, 2026 | Western University, London, Ontario, Canada

Establishing Resilient Community Flood Groups to Reduce Flood Impacts in England and Wales

Sophie Laidlaw[1], Sarah Percival[1], Neil Simcock[1], Patrick Byrne[1] and Tracy Garrett[2]
[1]Liverpool John Moores University, City Campus, Byrom Street, Liverpool, England, L3 3AF
Email: S.M.Laidlaw@2017.ljmu.ac.uk

[2]National Flood Forum, Bewdley, England, DY12 9BL.

ABSTRACT

Flooding is one of the most common natural hazards within England and Wales. Previously, the flooding sector focused on reducing flood risk and exposure through the construction of flood defences; however, a more progressive approach is required to reduce flood impacts through improving flood resilience. Community Flood Groups (CFGs) are one way of improving this, through representing community requirements and improving resilience. These grassroot community groups provide a platform for flood-affected communities with Key Flood Actors (KFAs) and potential policy changes. However, the sustainability of these groups is precarious, with many becoming dormant or disbanded over time. To address this issue, this project aims to develop a CFG sustainability framework that will identify key areas for groups to improve. As part of this wider research project, this paper identifies initial factors that can influence CFG sustainability through an online survey distributed to flood group members, asking questions regarding the group's demographics, practices and relationships with KFAs. 132 responses were collected from 102 groups in England and Wales. Reflective thematic analysis was used to identify recurring themes within responses, which were then used to identify initial CFG sustainability factors. A range of both positive and negative factors were identified, such as age of group members, which can be detrimental to group longevity if younger generations are not involved, which is the case in many groups. Other factors include communication methods, being able to reach residents in time of need and use of social media, perceived active status of the group, and relationships with key flood actors. These are all determined as factors that may affect group sustainability. These preliminary factors will be taken forward to phase 2 of the research, where further methods, including interviews and workshops, will be used to confirm and identify further factors, ultimately resulting in development of a CFG Sustainability Framework.

KEYWORDS: Community Flood Groups, Resilience, Sustainability Model, Factor Identification

1 INTRODUCTION

Flooding is one of the most common natural hazards globally, with data suggesting that floods account for around 35-40% of weather-related disaster occurrences (Web-1), as well as being the costliest in terms of damage (Whitfield, 2012, Web-2). Flooding is expected to increase, driven by climate change and rapid urbanisation rates. With 55% of the world residing in urban areas (Web-3), increasing to 94.9% and 88% in England and Wales respectively (Web-4), the impacts of flooding can be devastating to many.

With an increase in both flood events and flood impacts, we need to ensure that the communities who are the greatest risk of flooding are not forgotten about, particularly those in rural areas. Previously, flood management in England and Wales has centred around reducing flood risk, focusing on an 'engineered' approach (sea walls, flood defences) designed to 'keep water out' (Web-5). More recently, this has shifted towards a more integrated approach, including flood resilience practices (i.e. 'learning to

live with water' or Natural Flood Management), encompassing community-level actions, to help try and reduce the impacts of flooding.

It is important that all communities are represented within flood resilience, ensuring that the previous inequalities, such as flood exposure and funding can be reduced. Therefore, allowing communities to have a voice within flood risk management practices is important and vital. One way to achieve this is through Community Flood Groups (CFGs), including Flood Action Groups and flood wardens. There are over 400 of these grassroot groups in England and Wales; they act as the voice of the local community.. Forrest *et al.,* (2017) described CFGs as 'groups of people who have an interest in flood issues and meet to discuss them' whilst providing advocacy for the local community and aid in times of need. Many groups are formed following a major flood event within their local area, to try and address immediate concerns and reduce potential future impacts. To contribute to long-term flood resilience, they are required to persist over time to maintain their active status; if they become dormant or disband the area is left undefended once again.

Many CFGs are assisted by the National Flood Forum (NFF), who are the main charity that are dedicated to assisting communities prior to, during and after flood events in England and Wales. The help of the NFF can be vital in CFGs forming a strong, beneficial relationship with Key Flood Actors (KFAs) (i.e. the Environment Agency, councils, utility companies, emergency services). This is important as the groups can provide them with vital lay knowledge, that may be missed if they are not consulted, allowing the complexity of local flooding to be captured (McEwen et al., 2012); which is key in enhancing local flood resilience and helping future flood risk management plans in the local area.

Expanding and safeguarding the CFG network is therefore critical and is part of the new Environment Agency Flood and Coastal Erosion Risk Management (FCERM) Strategy Action Plan 2021 (Web-6). A key directive of this strategy is to support vulnerable communities and develop community led flood response plans, elements CFGs can assist in delivering if effective. It is also included in the UK Government Resilience Framework, where it is set out that the Voluntary and Community Sector (VCS) plays a key role in improving the UK's resilience (Web-7). However, the sustainability of these groups (including their functionality and practices) is precarious. Over time, some groups become dormant, ineffective, or disband and dissipate. It is key that CFGs are ultimately sustainable, as a loss of functionality can negatively impact recovery during disasters (Irawan et al., 2021). Ensuring the longevity and sustainability of local CFGs is therefore key to ensure that flood impacts are reduced in vulnerable communities.

The aim of this paper is to identify preliminary key factors that determine the sustainability of CFGs, which can ultimately contribute to the development of a CFG Sustainability model. Such a model could then help improve the longevity and impact of these key groups. This is achieved through the following objectives:

- Conduct CFG questionnaire assessing group members opinions on the group's functionality and practices, inclusive of strengths, weaknesses and relationships with KFAs
- Conduct thematic analysis of survey results, identifying potential baseline CFG sustainability factors to be further analysed.

2 METHODOLOGY

2.1 Survey design and distribution

A survey was designed in three sections, to utilise the views of CFG members, and opinions of their group dynamics and relationships. Section 1 focused on the collection of demographic data (age, gender, location) as well data on the number of members, age of the group, group affiliation and active status of the group. Section 2 focused on the perceived strengths and weaknesses of the CFGs. Section 3 focused on the group's relationships with KFAs, as well asking what makes a CFG effective.

These surveys were designed using a mix of open and closed questions. Whilst closed questions provided structure and comparable data (Patel and Joseph, 2016), open questions allowed a depth of data

to be collected, allowing the respondents to express their opinions freely and thereby reduce researcher bias (Jenn, 2006).

The surveys were distributed online, using a targeted sampling method, via the NFF who acted as a gatekeeper. Surveys were sent out via email, Facebook, LinkedIn and X to over 400 CFGs. These were also shared by the research team as well as the Environment Agency, resulting in 132 answers from 102 different CFGs across England and Wales.

2.2 Thematic analysis

Reflective thematic analysis (TA) was conducted on the open-ended questions, following Braun and Clarke's (2006) 6 stage approach. Themes were identified through extensive analysis of each response, identifying commonalities and coding these to identify key themes. This process ensured that all answers were analysed in a consistent way, whilst still allowing flexibility for themes to be identified from the data, without being decided beforehand. Computer-assisted qualitative data analysis software (CAQDAS) NVivo was used to help organise codes and themes identified during TA.

3 RESULTS AND DISCUSSION

Numerous themes and potential CFG sustainability factors were identified from the survey results, including group dynamics, ensuring increased collaboration and knowledge sharing, and having the knowledge, skills and training to make the groups effective. The main factors drawn from the survey results are discussed in more detail below.

3.1 Age of members

Whilst gender was split relatively even between male and female (55% and 43% respectively), with 2% preferring not to say, age appeared to be increasingly disproportionate, with 95% of responses falling in the age categories of 41+. This was also a factor that had been discussed with preliminary meetings with NFF staff and had been identified as a potential issue prior to the data collection. Similar findings have been identified by Nakamura *et al.,* (2025) when assessing demographic variations in volunteering, with 66% of identified volunteers from the UK being over the age of 40. Exploring this further, the average age of participants in this study was between 61-80, which is predominantly around retirement age within England and Wales. This aging demographic of the CFGs can be a benefit, as these are likely the demographic that have the most free time for volunteering. However, this is indicates challenges relating to inclusion, as younger demographics are impeded from participating due to work, caring or other commitments.

This ageing demographic is also a downfall of the groups, due to a higher possibility of health decline (Tang *et al.,* 2010), that can cause older volunteers to step away. This was also identified by participants as one of the weaknesses of the group, with one participant stating: "*I'm 74 and am concerned that if I become unwell, the group will fold. I try to keep records in order. We would like more young people involved.*" As we are moving towards an increasingly individualised society, encouraging younger generations to become volunteers can be met with increasing difficulty, even though these are the people that will be most affected by change (Jardim and Marques de Silva, 2018). However, the participation of younger volunteers is important for the long-term sustainability and success of CFGs.

3.2 Group active state and mindsets

For any volunteer group, especially CFGs, to be successful, they need to remain active within the community they serve. However, it is becoming increasingly difficult for this to remain the case, due to several factors. Whilst over 65% of survey participants were part of CFGs that were perceived to be either "Very active" or "Active", data provided by the NFF suggests that 46% of known CFGs have disbanded. This can prove problematic, especially if the area continues to flood or experiences severe flooding in the future, due a loss in the local knowledge or emergency response and support networks.

Assessing participants' perceptions of what doesn't work well in CFGs can help enhance understanding of why some of groups become dormant or disband. One of the most frequently mentioned themes was the internal dynamics and experiences of the groups. This included subthemes such as member engagement and participation, as well as leadership and governance. As the members of the groups are ultimately what keeps them running, ensuring volunteer retention and motivation is vital. This can be difficult due to the demands of the group, who tend to have limited resources and sometimes experience little to no progress (e.g. limited actions taken by KFAs, lack of funding or lack of defined roles within the group), resulting in volunteer turnover. This has been identified in other research, including Holtrop *et al*., (2024), who also identified factors such as poor communication and poor leadership.

Focusing on the existing dynamics of not only the groups that are dormant or disbanded, but also those groups that consider themselves as active is important as many of the groups also stated group dynamics as something that works *well* within the group. However, these mostly focused on the mindset of the group members and emotions such as "passion", "persistence" and "enthusiasm". Ensuring that CFG members keep these high spirits and motivations is important, particularly due to the emotionally challenging situations that members encounter which can lead to despondence or volunteer burnout (Allen and Mueller, 2013). This is therefore considered another important factor that will be taken forward to further analysis, particularly to understand potential methods of maintaining motivation within CFGs (such as training or group maintenance activities).

3.3 Locality and frequency of flood events

The type, frequency, locality and intensity of flooding CFGs experience can also influence a group's longevity and sustainability. Many of the CFG members experience repeated flooding. Experiencing a "*constantly occurring problem*" was identified by group members as a factor that can make a CFG effective, due to constant exposure improving the desire to continue working on a solution. For example, one participant suggested the group is "*Most effective (unfortunately) when there is a local flooding issue- often difficult to maintain continuity and interest when things are normal/ stable*". This allows the group members to build knowledge through active remembering, creating 'sustainable flood memories' (McEwen *et al.,* 2016), that can be shared within the group for support, or with the KFAs as a tool to help them understand the impacts of previous flood events. This is also a factor that is expected to influence the active state of the group, as if flooding is perceived as no longer a relevant issue this may encourage groups to disband or become dormant. This was most commonly mentioned when the area a CFG was based in had received a "scheme" (i.e. flood defences, sustainable urban drainage systems or property level resilience) and had not experienced any flooding since. However, this can lead to a 'safe development paradox', which can result in more severe consequences if a severe flood does occur yet the community are not prepared (Haer *et al.,* 2020). Therefore, a consideration needs to be given to the experience of the groups, and if they have received a scheme.

Even if they 'no longer' experience flooding, there is still a depth of knowledge stored within the communities that can be useful in flood risk management practices. This was also identified in the survey, with a sub theme of *'local knowledge and experience'* being identified by many as something that works well within their CFG. This local, lay knowledge can be vital, not only in the recovery stage after a flood,

but also in planning and preparation stages. Therefore, ensuring that this knowledge is used proactively is key in reducing the risk and impacts of future flooding and increasing the resilience of the area. This has been reiterated in the Pitt Review, published in 2008 (Web-8), which in turn led to the Department for Environment, Food and Rural Affairs (DEFRA) to acknowledge the inclusion of lay community knowledge within flood risk management is vital (McEwen *et al.,* 2016). However, it is important to consider how this knowledge is not only gathered, but also used by KFAs, to ensure that it is effectively considered in future planning for the area.

3.4 Communication strategies

Communication was identified as a factor that influences not only what works well within the groups, but also what does not work so well. This is a vital skill for developments within communities (Adedokin, Adeyemo and Olorunsola, 2010), especially those advocating for change, like CFGs. This communication is not one dimensional but works in many ways and with many different demographics of people, including other group members, the wider community, KFAs and agencies. Each of these actors require a different form of communication, therefore a 'one size fits all' method is inadequate (Bourne, 2015). However, this is not as simple as it may seem, especially when communicating with the wider community and KFAs.

When communicating with the wider community, it appears that many of the groups rely on social media (i.e. Facebook and WhatsApp). Whilst social media can help build online communities, which may in turn form social systems (Mauriner and Heudorfer, 2016), this is only possible if residents have an active platform, which many may not. This was an issue identified by the participants, for example one participant identified issues in '*Trying to reach vulnerable residents who are not online, on Facebook'*. Ensuring that the community is adequately informed as quickly as possible during possible flood events is key in assisting increase the resilience of the area (Nicholls, 2012). Therefore, a diversification of communication is required by the groups to ensure that the whole community is informed. <add sentence here on investigating which platforms CFGs are using and the importance of these being diverse – see reviewer comment>

Furthermore, a different approach is required in the communication strategies when it comes to KFAs. Whilst communication with these actors was considered by many of the participants to be key in making a CFG effective, it was also seen as something that could be better. However, many of the responses indicated that the issue may come from the KFAs themselves, and not from the groups. This included communication between the KFAs and a lack of information sharing. Having good relationships with the KFAs is crucial for the groups, and so this is a factor that needs investigating further.

3.5 Relationships with Key Flood Actors

Whilst communication is a key part of successful relationships with KFAs (such as flood action plans, multi-agency meetings and reporting issues), there are numerous other aspects to this, many of which appear to be challenges faced by the CFGs with KFAs.

With over 70 KFAs being identified from the survey, these relationships can be difficult to manage, especially when each KFAs all have different requirements from the group alongside different focuses. This can have an impact on the effectiveness of a community group and their relationships with KFAs (Balser and McCluskey, 2005). Ensuring these relationships are as advantageous as possible to both parties is essential.

One way of managing this is through using an intermediatory party, such as the NFF, to assist and represent the CFGs. They can act as a mediator, assisting with the communication and relationships between the CFGs and KFAs, which can be effective in ensuring that goals are met and any challenges faced can be addressed (Dragomir *et al.,* 2020). However, there are some cases where this is not possible (i.e. a group has stepped away from the intermediatory or cuts in funding), therefore, it is important to ensure that this

is something that both the CFG and KFAs can be given guidance on, to help ensure a uniform approach. This is a factor that needs taking forward to future stages.

4 CONCLUSION

As flood frequency and impacts increase, the focus of policy, practice and research need to shift towards those communities who are most at risk. Investing in these communities and groups they form can assist in improving the flood resilience of an area, complementing the traditional engineering focus that has previously been adopted within England and Wales. Focusing on CFGs can help not only provide communities with help during a flood even, but also allow them to have a voice, especially with KFAs. Whilst there are currently over 400 groups within England and Wales, many of the group's struggle with their longevity and sustainability. Therefore, research is required into the difficulties of these groups and how we can make them more sustainable.

To do this, this paper aimed to provide group members with the opportunity to voice their opinions of how their groups work, their strengths, weaknesses and finally their relationships with KFAs. This was assessed through surveys with a mix of open and closed questions, to determine preliminary factors that are important for the sustainability of these key groups.

Whilst many preliminary factors were identified from the survey results, this paper discusses some of the key findings and the CFG sustainability factors that will be taken through to the next stage of the research. One of the biggest challenges faced by the groups was the ageing membership and the worries of continuity that come along with this. This is a factor that was also determined from conversations with NFF staff prior to the start of data collection, therefore was predicted to be mentioned by many of the respondents. Furthermore, other factors including local knowledge and frequency of flood events appear to be important in keeping the momentum of the CFG going, whilst also allowing informed decisions and a voice for the group. These are also important when it comes to the communication strategies of the groups, which allow successful relationships to be built with KFAs and the wider local community. Building these relationships with KFAs is also important in ensuring CFG sustainability. However, sometimes this may not be straightforward, and so having an individual third party to act as a mediator can be beneficial in ensuring these relationships.

These results will now be taken forward to the next stage of research, where considerations from interviews with the NFF and KFAs will be integrated to identify any further key CFG sustainability factors. These will then be presented to CFGs through a workshop, that will be ran in 4 areas around England and Wales, to gather their opinions and explore potential weightings of the factors. This will then result in a decision of the final CFG sustainability factors and the creation of a CFG sustainability model that incorporates these corresponding factors, as well as guides of best practice for CFG members and KFAs. This will create a deeper understanding of these vital groups, ensuring their longevity and impact within the flood risk management and resilience sectors.

5 ACKNOWLEDGEMENTS

We would like to thank Liverpool John Moores University for the funding a PhD Scholarship for Sophie Laidlaw. Further we would like to acknowledge the staff at the National Flood Forum for assisting in recruitment of research participants.

REFERENCES

Adedeji, T. Proverbs, D.G. Xiao, H. and Oladokun, V.O. (2024). Measuring property flood resilience (PFR) in UK homes. International Journal of Building Pathology and Adaptation, 42(6), 1328-1349.

Adedokun, M.O., Adeyemo, C.W., and Olorunsola, E.O., (2010) The impact of communication on community development. J. Communication, 1(2) 101-105.

Allen, J.A., and Mueller, S.L., (2013) The revolving door: A closer look at major factors in volunteers intentions to quit. Journal of Community Psychology, 41(2), 139-155

Balser, D., and McClusky, J., (2005) Managing stakeholder relationships and nonprofit organisation effectiveness Nonprofit Management and leadership, 15(3), 295-315

Bourne, L (2015) "Targeted communication: the key to effective stakeholder engagement" in 29th World Congress International Project Management Association (IPMA) 2015, IPMA WC 2015, 28-30 September – 1 October 2015, Westin Playa Bonita, Panama, 431-438.

Braun, V. and Clarke, V., (2006). Using thematic analysis in psychology. Qualitative research in psychology, 3(2), 77-101.

Dragomir, C.C., Foriş, D., Ţîţu, A.M. and Foriş, T., (2020). The role of intermediaries in supporting collaboration for sustainability: A model of commissioning intervention in the multi-stakeholder collaboration for sustainable territorial development. Sustainability, 12(17), 6769-6783.

Fenn, T. Clarke, C. Burgess-Gamble, L. Harding, E. Ogunyoye, F. Hick, F. Dawks, S. Morris, J. and Chatterton, J (2016) The costs and impacts of the winter 2013/14 floods in England and Wales, in E3S web of conferences (Vol. 7, p. 05004). EDP Sciences

Forrest, S. Trell, E.M. and Woltjer, J. (2019). Civil society contributions to local level flood resilience: Before, during and after the 2015 Boxing Day floods in the Upper Calder Valley. Transactions of the institute of British geographers, 44(2), 422-436.

Haer, T. Husby, T.G. Wouter Botzen, W.J. and Aerts, J.C.J.H., (2020) The safe development paradox: an agent-based model for flood risk under climate change in the European Union. *Global Environment Change*, 60, 102009

Holtrop, D. Soo, C. Gagne. M. Kragt, D. Dunlop, P. and Luksyte, A., (2024) Exploring volunteer turnover reasons, intentions and behaviour. Group and Organisation Management, 0, 1-45

Irwan, D., Prabowo, H., Kuncoro, E.A., and Thoha, N., (2021) Operational resilience and human capital toward corporate sustainability longevity in Indonesian. *The Journal of Asian Finance, Economics and Business, 8(3),* 1035-1044.

Jardim, C., and Marques de Silva, S., (2018) Young People Engaging in Volunteering: Questioning a Generational Trend in an Individualized Society. Societies, 8(1), 8-20.

Jenn, N.C., (2006). Designing a questionnaire. Malaysian family physician: the official journal of the Academy of Family Physicians of Malaysia, 1(1), 32.

Laidlaw, S. and Percival, S. (2024) Flood resilience: A review of evolving definitions. Nat. hazards, *120*(12) 10773-10784

Mauriner, O. and Heudorfer, A., (2016) Social media in disaster management: How social media impact the work of volunteer groups and aid organisations in disaster preparation and response International Journal Emergency Management, 12(2), 196-217.

McEwen, L. Garde-Hansen, J. Holmes, A. Jones, O. and Krause, F. (2016). Sustainable flood memories, lay knowledges and the development of community resilience to future flood risk. Transactions of the Institute of British Geographers, 42(1), 14-28.

Nakamura, J.S., Gibson, C.B. Woodberry, R.D. Lee, M.T. Kim, Y. Shiba, K. Padgett, N. Johnson, B.R. and VanderWeele, T.J., (2025) Understanding who volunteers globally through an examination of demographic variation in volunteering across 22 countries. Scientific Reports. 15(1) 25299-25321

Nicholls, S., (2012) The resilient community and communication practice. Australian Journal of Emergency Management, *27*(1), 46-51.

Patel, H.R. and Joseph, J.M., (2016). Questionnaire designing process: A review. Journal of Clinical Trials, 6(2), 2-7.

Rose, C. Lamond, J. Dhonau, M. Joseph, R. and Proverbs, D. (2016). Improving the uptake of flood resilience at the individual property level. Flood Risk Management and Response, 6(3), 153-162.
Tang, F. Morrow-Howell, N. and Choi, E., (2010) Why do older adult volunteers stop volunteering? Ageing and Society, 30, 859-878.
Whitfield, P.H. (2012) Floods in future climates: a review. Journal of Flood Risk Management, 5(4), 336-365.

Web sites:
Web-1: https://www.undrr.org/gar/gar2025/hazard-exploration/floods
Web-2: https://www.jbarisk.com/knowledge-hub/insights/a-picture-of-future-flood-risk-in-europe/
Web-3: https://www.un.org/uk/desa/68-world-population-projected-live-urban-areas-2050-says-un
Web-4:
https://www.ons.gov.uk/peoplepopulationandcommunity/housing/articles/townsandcitiescharacteristicsofbuiltupareasenglandandwales/census2021
Web-5: https://nationalinfrastructurecommission.wales/2025/06/30/toolkit-community-engagement/
Web-6:
https://assets.publishing.service.gov.uk/media/5f6b6da6e90e076c182d508d/023_15482_Environment_agency_digitalAW_Strategy.pdf
Web-7:
https://assets.publishing.service.gov.uk/media/63cff056e90e071ba7b41d54/UKG_Resilience_Framework_FINAL_v2.pdf
Web-8:
https://webarchive.nationalarchives.gov.uk/ukgwa/20100807034701/http:/archive.cabinetoffice.gov.uk/pittreview/_/media/assets/www.cabinetoffice.gov.uk/flooding_review/pitt_review_full%20pdf.pdf